

# PROCEEDINGS

## HARMO'17

17th International Conference on  
Harmonisation within Atmospheric  
Dispersion Modelling  
for Regulatory Purposes

9-12 May 2016, Budapest, Hungary  
Danubius Health Spa Resort Margitsziget

Organized by  
Hungarian Meteorological Service  
[www.met.hu](http://www.met.hu)

# **HARMO 17**

**17th International Conference on  
Harmonisation within Atmospheric Dispersion Modelling  
for Regulatory Purposes  
9-12 May 2016, Budapest, Hungary**

# **PROCEEDINGS**

**Edited by**

**László Bozó**

**Zita Ferenczi**

**Márta T. Puskás**

ISBN 978-963-9931-10-7

**Hungarian Meteorological Service**



**Budapest, 2016**

## PREFACE

The 17<sup>th</sup> International Conference on Harmonisation within Atmospheric Dispersion Modelling for Regulatory Purposes (Harmo 17) continues the activities of the International Initiative on this topic, which started in 1991. Detailed and extensive scientific, practical and historical information can be found at the web site of the Harmo Initiative: [www.harmo.org](http://www.harmo.org).

The original focus of the workshops on harmonisation was on the development of dispersion models for regulatory purposes and for real-time applications in Europe, in such a way, that latest scientific achievements are used, but also the specific demands of society and regulators are met. These meetings developed further into a series of high-level scientific conferences, motivated by the idea to apply in a better and harmonised way the meteorological and air quality sciences to serve the needs of European citizens.

Dispersion modelling is a tool to assess the actual or future impact of air pollution sources on environment and human health. Studying dispersion needs interdisciplinary approach, namely reliable meteorological forecast (including for complex terrain, plant-canopy and urban areas); proved parametrizations of the atmospheric boundary layer and exchange with surface processes; precise description of the variety of sources (such as transport sector releases, industrial releases, accidental releases, deliberate releases, natural releases, etc.); proved parametrizations of all physical and chemical processes in the atmosphere. In addition, the real time data assimilation, the evaluation of model performance and the presentation of results to public and managers are now disciplines of their own.

It has been proven through the success of the Harmo conferences by now, that this forum is needed to allow scientists focusing on one or several of these different topics, to work together and come up with improved and harmonised solutions. There is a variety of models – simple or complex – covering different space and time scales and different areas of applicability. The user needs to select a fit-for-purpose dispersion model that produces reliable results for a given task and also to know the uncertainties associated with the model results.

There are many requirements to models for regulatory purposes. These models should be scientifically sound; validated against observations; accompanied by clear guidelines and support to ensure proper use. Constant efforts are needed to promote the good practices and eliminate the bad practices; to assure quality with respect to model development; to establish reference problems; to exchange of experiences.

The Harmo Conferences are directed towards model developers, model users, environmental protection agencies, and environmental legislation experts. This series of conferences is different from other scientific fora, because it focuses on common tools and methodologies in a broad interdisciplinary field. These conferences are natural forum for discussing modelling issues related to the European Union air quality directives. European networks such as the FAIRMODE network use the Harmo conferences to expose their work to a broader audience. Harmo 17 also provides an opportunity to present results from MODITIC project. The Harmo conferences have a role as a forum where users and decision-makers can bring their requirements to the attention of scientists.

More than 150 participants from 29 countries – including Europe, North and South America, Asia and Australia - attended the 17<sup>th</sup> International Conference on Harmonisation within Atmospheric Dispersion Modelling for Regulatory Purposes , 9–12 May 2016, Thermal Hotel Margitsziget, Budapest, Hungary, organized by the Hungarian Meteorological Service.

**History of the Harmonisation Workshop/Conference:**

- 1st Harmo workshop, Risø National Laboratory, Denmark, 1992
- 2nd Harmo workshop, Manno, Switzerland 1993
- 3rd Harmo workshop, Mol, Belgium, 1994
- 4th Harmo workshop, Oostende, Belgium, 1996
- 5th Harmo conference, Rodos, Greece, 1998
- 6th Harmo conference, Rouen, France, 1999
- 7th Harmo conference, Belgirate, Italy, 2001
- 8th Harmo conference, Sofia, Bulgaria, 2002
- 9th Harmo conference, Garmisch-Partenkirchen, Germany, 2004
- 10th Harmo conference, Crete, Greece, 2005
- 11th Harmo conference, Cambridge, UK, 2007
- 12th Harmo conference, Cavtat, Croatia, 2008
- 13th Harmo conference, Paris, France, 2010
- 14th Harmo conference, Kos, Greece, 2011
- 15th Harmo conference, Madrid, Spain, 2013
- 16th Harmo conference, Varna, Bulgaria, 2014

**The scientific focus of Harmo 17 is on the following topics:**

- Model evaluation and quality assurance – model validation, model intercomparisons, model uncertainties and model sensitivities
- Environmental impact assessment: Air pollution management and decision support systems
- Use of modelling in support of EU air quality directives, including FAIRMODE
- Parametrization of physical processes in mesoscale meteorology relevant for air quality modelling
- Urban scale and street canyon modelling: Meteorology and air quality
- Use of modelling in health and exposure assessments
- Inverse dispersion modelling and source identification
- Modelling air dispersion and exposure to accidental releases
- Mathematical problems in air quality modelling
- Highlights of past work. Session devoted to reviews and to prominent scientists and ‘golden papers’ of the past, which have still relevance and should not be forgotten.

### **Steering Committee**

Dr. D. Anfossi, CNR, Torino, Italy  
Prof. J. Bartzis, University of West Macedonia, Greece  
Prof. E. Batchvarova, NIMH, Sofia, Bulgaria  
Prof. C. Borrego, University of Aveiro, Portugal  
Prof. L. Bozó, HMS, Budapest, Hungary  
Dr. B. Carissimo, EdF R&D, Chatou, France  
Dr. D. Carruthers, CERC, Cambridge, UK  
Dr. F. Martin, Ciemat, Spain  
Dr. C. Mensink, VITO, Mol, Belgium  
Prof. N. Moussiopoulos, Univ. Of Thessaloniki, Greece  
Dr. H. Olesen, Aarhus University, Denmark (Chairman)  
Dr. A. Skouloudis, JRC Ispra, Italy  
Dr. P. Suppan, KIT/IMK-IFU, Garmisch-Partenkirchen, Germany  
Dr. P. Thunis, JRC, Ispra, Italy  
Dr. S. Vidič, Meteorological and Hydrological Service of Croatia

### **Scientific Committee**

Dr. A. Albergel, Aria Technologies, France  
Dr. D. Anfossi, CNR, Torino, Italy.  
Prof. J. Bartzis, University of West Macedonia, Greece  
Prof. E. Batchvarova, NIMH, Sofia, Bulgaria  
Prof. C. Borrego, University of Aveiro, Portugal  
Prof. L. Bozó, HMS, Budapest, Hungary  
Dr. B. Carissimo, EdF R&D, Chatou, France  
Dr. D. Carruthers, CERC, Cambridge, UK  
Dr. C. Cuvelier, JRC, Ispra, Italy  
Prof. I. Faragó, ELTE, Budapest, Hungary  
Dr. Z. Ferenczi, HMS, Budapest, Hungary  
Prof. R. S. Jose, Technical Univ. of Madrid, Spain  
Dr. A. Jeričević, CCAA, Croatia.  
Dr. G. Kallos, Univ. of Athens, Greece  
Dr. P. Kassomenos, Univ. of Ioannina, Greece  
Dr. D. Maro, Inst. for Radioprotection and Nuclear Safety, France  
Dr. F. Martin, CIEMAT, Spain  
Dr. C. Mensink, VITO, Mol, Belgium  
Dr. P. Mestayer,IRSTV, CNRS, Nantes, France  
Prof. N. Moussiopoulos, Univ. Of Thessaloniki, Greece  
Dr. H. Olesen, Aarhus University, Denmark  
Prof. M. Schatzmann, Met. Inst., Univ. Hamburg, Germany  
Dr. J.F. Sini, Ecole Centrale, Nantes, France  
Dr. A. Skouloudis, JRC Ispra, Italy  
Dr. P. Suppan, KIT/IMK-IFU, Garmisch-Partenkirchen, Germany  
Prof. D. Syrakov, NIMH, Sofia, Bulgaria  
Dr. D. Thomson, The Met Office, Exeter, UK  
Dr. P. Thunis, JRC, Ispra, Italy

### **Local Organizing Committee:**

Prof. László Bozó (Hungarian Meteorological Service)  
Dr. Zita Ferenczi (Hungarian Meteorological Service)

Ms. Judit Stefkó (Congress Kft.)  
Ms. Roni Szekely (Congress Kft.)

**Harmo 17 Organising Institution:**  
Hungarian Meteorological Service

**Wishing to all participants successful and fruitful conference and enjoyable stay at capitol of Hungary.**

**Budapest,  
May, 2016**

**Sincerely yours,**

A handwritten signature in black ink, appearing to read 'László Bozó', written in a cursive style.

**Professor László Bozó**  
**On behalf of the Local Organising Committee**

# CONTENTS

<b>TOPIC 1: MODEL EVALUATION AND QUALITY ASSURANCE – MODEL VALIDATION, MODEL INTERCOMPARISONS, MODEL UNCERTAINTIES AND MODEL SENSITIVITIES</b> .....	1
COMPARING DISPERSION MODELLING AND FIELD INSPECTION FOR ODOUR IMPACT ASSESSMENT IN THE VICINITY OF TWO ANIMAL HUSBANDRY FARMS.....	2
Dietmar Oetl and Stefan Oitzl	
EDMS MODEL VERIFICATION CONSIDERING REMARKABLE CHANGES IN AIRPORT TRAFFIC SYSTEM.....	7
Veronika Groma, Zita Ferenczi, Bálint Alföldy, János Osán, Szabina Török and Roland Steib	
VALIDATION OF PANACHE CFD POLLUTION DISPERSION MODELLING WITH DENSE GAS EXPERIMENTS .....	13
Liyang Chen and Malo Le Guellec	
AN AIR QUALITY CFD MODEL PERFORMANCE IN COMPLEX ENVIRONMENT WITH EMU OBSERVATIONS.....	20
Liyang Chen, Pramod Kumar, Malo Leguellec, Amir-Ali Feiz	
ROADSIDE HOT-SPOT ANALYSIS IN URBAN AREA .....	26
Weiping Dai, Qiguo Jing, Tiffany Stefanescu, and Brian Holland	
VALIDATION OF THE PERFORMANCE OF METEOROLOGICAL FORECASTS IN FINE SPATIAL AND TEMPORAL RESOLUTION DESIGNED AS AN INPUT FOR DISPERSION MODELS .....	30
Primož Mlakar, Dragana Kokal, Boštjan Grašič, Marija Zlata Božnar, Dejan Gradišar and Juš Kocijan	
SENSITIVITY OF MODELLED URBAN BACKGROUND OZONE CONCENTRATIONS TO UNCERTAINTIES IN THE GRS INPUT VARIABLES.....	36
Andrea L. Pineda Rojas and Nicolás A. Mazzeo	
FIELD DATA VERSUS WIND TUNNEL DATA: THE ART OF VALIDATING URBAN FLOW AND DISPERSION MODELS.....	41
Bernd Leitl, Frank Harms, Denise Hertwig, and Michael Schatzmann	
WRF SURFACE AND UPPER AIR VALIDATION OVER CENTRAL CHILE DURING LA NIÑA-EL NIÑO TRANSITION .....	46
F. Carrera-Chapela, G. Ruiz-Filippi, J.A. González, G. Yarwood, J. Johnson	
FLOW SIMULATIONS FOR THE ASSESSMENT OF SMALL WIND TURBINES IN URBAN AREAS.....	51
Sirma Stenzel , Kathrin Baumann-Stanzersen, Gabriele Rau, Renate Teppner, Kurt Leonhartsberger	
VALIDATION OF THE ATMOSPHERIC DISPERSION MODEL NAME AGAINST LONG-RANGE TRACER RELEASE EXPERIMENTS.....	56
Vibha Selvaratnam, David Thomson and Helen Webster	

IMPACT OF ALTERNATIVE DISPERSION MODEL VALIDATION METHODS: A CASE STUDY ON THE LNG MODEL VALIDATION DATABASE USING DRIFT .....	61
Simon Gant, Simon Coldrick, Graham Tickle and Harvey Tucker	
A VALIDATION STUDY OF THE ADMS PLUME CHEMISTRY SCHEMES .....	66
Stephen E. Smith, Jenny Stocker, Martin Seaton and David Carruthers	
A REVIEW OF DISPERSION MODELLING OF AGRICULTURAL AND BIOAEROSOL EMISSIONS WITH NON-POINT SOURCES .....	71
Jenny Stocker, Andrew Ellis, Steve Smith, David Carruthers, Akula Venkatram, William Dale and Mark Attree	
VALIDATION OF A LPDM AGAINST THE CUTE EXPERIMENTS OF THE COST ES1006 ACTION – COMPARISON OF THE RESULTS OBTAINED WITH THE DIAGNOSTIC AND RANS VERSIONS OF THE MODELS.....	76
Christophe Duchenne, Patrick Armand, Maxime Nibart, and Virginie Hergault	
EFFECT OF THE TERRAIN FEATURES ON THE ACCURACY OF CALMET. A COMPLEX TERRAIN CASE STUDY .....	81
A. Hernandez, J.A. Gonzalez, J.J. Casares	
USING METEOROLOGICAL ENSEMBLES FOR ATMOSPHERIC DISPERSION MODELING OF THE FUKUSHIMA NUCLEAR ACCIDENT.....	86
Raphaël Périllat, Irène Korsakissok, Vivien Mallet , Anne Mathieu , Thomas Sekiyama , Mizuo Kajino, Kouji Adachi, Yasuhito Igarashi, Takashi Maki, Damien Didier	
VALIDATION OF THE GAUSSIAN PUFF MODEL PX USING NEAR-FIELD KRYPTON-85 MEASUREMENTS AROUND THE AREVA NC LA HAGUE REPROCESSING PLANT: COMPARISON OF DISPERSION SCHEMES .....	91
Irène Korsakissok, Mathieu Contu, Olivier Connan, Anne Mathieu and Damien Didier	
UDINEE PROJECT: INTERNATIONAL PLATFORM TO EVALUATE URBAN DISPERSION MODELS' CAPABILITIES TO SIMULATE RADIOLOGICAL DISPERSION DEVICE.....	96
Miguel A. Hernández-Ceballos, Stefano Galmarini, Steven Hanna, Thomas Mazzola, Joseph Chang, Roberto Bianconi, Roberto Bellasio	
ASSESSING THE PERFORMANCE OF ATMOSPHERIC DISPERSION MODELS .....	101
Steven Herring and Pablo Huq	
WIND PROFILES FOR THE ATMOSPHERIC BOUNDARY LAYER IN DIFFERENT STABILITY CONDITIONS .....	106
Ana Graciela Ulke	
CMAQ (COMMUNITY MULTI-SCALE AIR QUALITY) ATMOSPHERIC DISPERSION MODEL ADAPTATION FOR HUNGARY.....	110
Dora Lazar and Tamas Weidinger	
EMISSION PROCESSOR FOR AIR QUALITY MODELS UTILIZING NEWLY AVAILABLE DATA....	117
Pavel Juruš, Jan Karel, Radek Jareš, Josef Martinovský, Václav Píša, Robert Polák, Eva Smolová, Emil Pelikán, Marek Brabec, Ondřej Konár, Viktor Fuglík, Kryštof Eben, Jaroslav Resler, Ondřej Vlček, Pavel Machálek, Miloslav Modlík, Helena Hnilicová, Nina Benešová, Daša Srbová, Miloš Zapletal, Radek Kadlubiec, Pavla Škarková, Jiří Barnet	
WRF-CAMX APPLICATION TO THE PEARL RIVER DELTA REGION.....	121
Diogo Lopes, Joana Ferreira, Ka In Hoi, Kai Meng Mok, Ana I. Miranda and Ka Veng Yuen	

EVALUATION OF MODEL PERFORMANCE USING NEW DEPOSITION SCHEMES IN THE RANDOM DISPLACEMENT PARTICLE MODEL PELLO USING FUKUSHIMA POWER PLANT ACCIDENT DATA.....	126
Pontus von Schoenberg, Håkan Grahn and Peter Tunved	
IMPACT OF BIOGENIC EMISSION MODEL AND LANDUSE ON ISOPRENE AND OZONE CONCENTRATIONS FROM A CHEMICAL TRANSPORT MODEL.....	130
Kinga Wałaszek, Małgorzata Werner, Maciej Kryza and Carsten Ambelas Skjøth	
SIMULATING LARGE EMITTERS USING CMAQ AND A LOCAL SCALE FINITE ELEMENT MODEL. ANALYSIS IN THE SURROUNDINGS OF BARCELONA.....	135
Albert Oliver, Raúl Arasa, Agustí Pérez-Foguet, and M <sup>a</sup> Ángeles González	
VALIDATION OF GAUSSIAN PLUME MODEL AEROPOL AGAINST CABAUW FIELD EXPERIMENT.....	140
Marko Kaasik , Gertie Geertsema and Rinus Scheele	
ASSESSING AIR QUALITY IMPACTS OF AIRPORT EMISSIONS AT THE LOS ANGELES INTERNATIONAL AIRPORT USING AN INTEGRATED MODELING AND MEASUREMENT APPROACH.....	145
Saravanan Arunachalam, Alejandro Valencia, Philip Soucacos, Jeffrey Wei	
LAGRANGIAN SIMULATIONS OF THE PLUME RISE IN STRONG CAPPING INVERSION .....	150
Enrico Ferrero, Stefano Alessandrini, Domenico Anfossi	
MODEL CHAIN FOR BUOYANT PLUME DISPERSION.....	155
Andrea Bisignano, Luca Mortarini and Enrico Ferrero	
PRELIMINARY POLLUTANT DISPERSION MODELLING WITH CALMET AND CALPUFF OVER COMPLEX TERRAIN IN THE BOLZANO BASIN (IT).....	160
Elena Tomasi, Lorenzo Giovannini, Marco Falocchi, Dino Zardi, Gianluca Antonacci	
<b>TOPIC 2: ENVIRONMENTAL IMPACT ASSESSMENT: AIR POLLUTION MANAGEMENT AND DECISION SUPPORT SYSTEMS.....</b>	<b>165</b>
EFFECT OF THE LONG-RANGE TRANSPORT ON THE AIR QUALITY OF BUDAPEST .....	166
Zita Ferenczi and László Bozó	
ANALYSIS OF THE DAILY CYCLES IN THE DATA ON AIR POLLUTION THROUGH THE USE OF ADVANCED ANALYTICAL TOOLS.....	171
Marija Zlata Božnar, Boštjan Grašič, Primož Mlakar, Dejan Gradišar and Juš Kocijan	
JRODOS FOR NUCLEAR EMERGENCIES: IMPLEMENTATION IN SWITZERLAND AND FURTHER DEVELOPMENTS .....	177
Markus Oberle and Cyrill von Arx	
IMPROVING URBAN AIR QUALITY USING A COST-EFFICIENCY AND HEALTH BENEFIT APPROACH.....	180
A.I. Miranda, J. Ferreira, C. Silveira, H. Relvas, M. Lopes, P. Roebeling, A. Monteiro, E. Sá, C. Gama, S. Costa, J.P. Teixeira and C. Borrego	
DISPERSION MODELING UNCERTAINTIES IN DISPERSION ENGINE (DE).....	186
Robert Sigg, Håkan Grahn, Jan Burman, Niklas Brännström, Oscar Björnham, Petter Lindgren, Leif Å Persson, Pontus Von Schoenberg and Lennart Thaning	

ESTIMATION OF SHORT ODOR EVENTS BY USING CHEMICALLY REACTIVE ODORANTS ATMOSPHERIC DISPERSION MODELLING AROUND A PULP PAPER MILL .....	191
D. Cartelle, J.M. Vellón, A. Rodríguez, D. Valiño, J.A. González, M. Bao, C. Casas	
REAL SCALE DEMONSTRATION OF THE DEPOLLUTING CAPABILITIES OF A PHOTOCATALYTIC PAVEMENT IN A REAL URBAN AREA .....	197
M. Pujadas, M. Palacios, L. Núñez, M. Germán, J. Fernández-Pampillón, J. D. Iglesias, J. L. Santiago	
INVESTIGATION OF ATMOSPHERIC DISPERSION OF GAS COMPOUNDS FROM AN INDUSTRIAL INSTALLATION OVER A REALISTIC TOPOGRAPHY .....	202
Diamando Vlachogiannis, Athanasios Sfetsos, Nikolaos Gounaris and Athanasios Papadopoulos	
A NUMERICAL STUDY OF AIR-POLLUTION AND ATMOSPHERIC FINE-SCALE FLOW OVER THE COASTAL COMPLEX TERRAIN OF MT. CARMEL .....	208
N. Haikin, P. Alpert, Y. Mahrer	
CHALLENGES IN ASSESSING AIR POLLUTION FROM RESIDENTIAL WOOD COMBUSTION.....	212
Helge R. Olesen	
AIR QUALITY FORECASTS FOR POLAND - APPLICATION OF THE WRF-CHEM MODEL WITHIN THE LIFE/APIs PROJECT.....	217
Małgorzata Werner, Maciej Kryza, Hanna Ojrzyńska, Kinga Wałaszek, Anetta Drzeniecka-Osiadacz	
DYNAMIC-STATISTICAL ODOUR DISPERSION MODEL USING THE CALPUFF MODEL AND GEOSTATISTICAL ANALYSIS .....	222
Maria Skrętowicz and Jerzy Zwoździak	
INVESTIGATION OF THE TRANSPORT OF POLLUTANTS FROM THE METROPOLITAN AREA OF SÃO PAULO AND FROM THE INDUSTRIAL CITY OF CUBATÃO TO NEARBY AREAS.....	227
Atenágoras Souza Silva, Américo A F S Kerr, Simone Gioia and Marly Babinskky	
FAR-FIELD EFFECT OF A TALL BUILDING ON THE SHEAR LAYER ABOVE STREET CANYONS.....	232
Árpád Varga	
APPLICATION OF DISPERSION MODELS FOR DEVELOPMENT OF ATMOSPHERIC POLLUTION MANAGEMENT ZONES IN RIGA AGGLOMERATION .....	237
Iveta Steinberga, Janis Bikse Jr, Janis Kleperis, Janis Bikse	
SENSITIVITY ANALYSIS OF A METEOROLOGICAL PRE-PROCESSOR USING ALGORITHMIC DIFFERENTIATION .....	242
John Backman, Curtis Wood, Mikko Auvinen, Leena Kangas, Ari Karppinen, Jaakko Kukkonen	
<b>TOPIC 3: USE OF MODELLING IN SUPPORT OF EU AIR QUALITY DIRECTIVES, INCLUDING FAIRMODE.....</b>	<b>247</b>
EXCEEDING THE EUROPEAN NO <sub>2</sub> -LIMIT VALUE IN BELGIUM: CAN WE SOLVE THE PROBLEM IN A SHORT TO MEDIUM TIME FRAME? .....	248
Wouter Lefebvre, Hans Hooyberghs, Felix Deutsch, Sandy Adriaenssens, Frans Fierens	

AIR QUALITY MODELING OF NON-ATTAINMENT AREAS AS A BASIS FOR AIR QUALITY PLANS.....	252
Jana Krajčovičová, Jana Matejovičová, Martin Kremler, Vladimír Nemček	
TESTING THE SHERPA TOOL TO SUPPORT AIR QUALITY PLANS OVER PORTUGAL .....	256
Alexandra Monteiro, Carla Gama, Alain Clappier, Philippe Thunis, Ana Isabel Miranda	
APPLICATION OF A PHOTOCHEMICAL MODEL TO THE ASSESSMENT OF REGIONAL AIR QUALITY LEVELS IN SOUTHERN ITALY: PROCEDURES AND RESULTS.....	262
R. Giua, A. Morabito, I. Schipa, A. Tanzarella, C. Silibello and G. Assennato	
URBAN TRAFFIC EMISSION MODELLING FOR POLICY-RELATED APPLICATIONS.....	267
Oxana Tchepel and Daniela Dias	
FAIRMODE'S EU COMPOSITE MAPPING EXERCISE.....	272
Stijn Janssen and Philippe Thunis	
COMPARING AIR QUALITY MODEL PERFORMANCE FOR PLANNING APPLICATIONS.....	277
Michel Vedrenne, Julio Lumbreras, Rafael Borge, Alain Clappier, Philippe Thunis, and M <sup>a</sup> Encarnación Rodríguez	
<b>TOPIC 4: PARAMETRIZATION OF PHYSICAL PROCESSES IN MESOSCALE METEOROLOGY RELEVANT FOR AIR QUALITY MODELLING .....</b>	<b>282</b>
A SENSITIVITY ANALYSIS FOR DETERMINING OPTIMUM WRF AND CALPUFF CONFIGURATION FOR OPERATIONAL AIR QUALITY FORECAST: APPLICATION TO A CASE STUDY IN THE PORT OF HUELVA (SOUTHERN SPAIN).....	283
M <sup>a</sup> Ángeles González, Raúl Arasa, Anna Domingo-Dalmau, Ignasi Porras, Miquel Picanyol, Bernat Codina, Jesica Piñón	
IMPACT OF WRF URBAN PARAMETERIZATIONS IN THE PERFORMANCE OF CMAQ ON 1 KM RESOLUTION ANNUAL RUNS IN MADRID (SPAIN).....	289
David de la Paz, Rafael Borge, Alberto Martilli	
ANALYSIS OF THE INTERNAL BOUNDARY LAYER FORMATION ON TROPICAL COASTAL REGIONS USING SODAR DATA IN SANTA CRUZ REGION OF MRRJ .....	294
Leonardo Aragão Ferreira da Silva, Silvana Di Sabatino, Luiz Claudio Gomes Pimentel and Fernando Pereira Duda	
<b>TOPIC 5: URBAN SCALE AND STREET CANYON MODELLING: METEOROLOGY AND AIR QUALITY .....</b>	<b>299</b>
MODELLING ULTRAFINE PARTICLE CONCENTRATIONS AT STREET-LEVEL SCALE FOR THE ENTIRE CITY OF ANTWERP.....	300
Hans Hooyberghs, Wouter Lefebvre, Felix Deutsch, Sandy Adriaenssens, Elke Trimpeneers, Frans Fierens, Stijn Janssen	
EVALUATION AND DEVELOPMENT OF TOOLS TO QUANTIFY THE IMPACTS OF ROADSIDE VEGETATION BARRIERS ON NEAR-ROAD AIR QUALITY .....	306
Vlad Isakov, Akula Venkatram, Richard Baldauf, Parik Deshmukh, Max Zhang	
A HYBRID APPROACH FOR THE NUMERICAL SIMULATION OF FLOWS IN URBAN ENVIRONMENT.....	311
Bence Hermann and Miklós Balogh	

REDUCED-FORM AIR QUALITY MODELING FOR COMMUNITY-SCALE APPLICATIONS ....	316
Vlad Isakov, Timothy Barzyk, Saravanan Arunachalam	
MODELLING THE RECIRCULATION ZONE IN STREET CANYONS WITH DIFFERENT ASPECT RATIOS, USING CFD SIMULATION .....	319
Arsenios Chatzimichailidis, Marc Assael, Matthias Ketzel and Konstantinos E Kakosimos	
WATER CHANNEL INVESTIGATION OF FLOW AND DISPERSION IN STREET CANYONS ...	324
Annalisa Di Bernardino, Paolo Monti, Giovanni Leuzzi and Giorgio Querzoli	
IMPACTS OF GLOBAL CLIMATE SCENARIOS OVER THREE EUROPEAN CITIES USING MESOSCALE AND CFD SIMULATIONS WITH VERY HIGH RESOLUTION .....	329
Roberto San José Juan L. Pérez, Libia Pérez, Julia Pecci, Antonio Garzón and Marino Palacios	
DEVELOPMENT OF THE PARALLEL VERSION OF A CFD – RANS FLOW MODEL ADAPTED TO THE FAST RESPONSE IN BUILT-UP ENVIRONMENTS .....	334
O. Oldrini, M. Nibart, P. Armand, J. Moussafir and C. Duchenne	
MICROSCALE SIMULATION OF ROAD TRAFFIC EMISSIONS FROM VEHICULAR FLOW AUTOMATIC SURVEYS AND COMPARISON WITH MEASURED CONCENTRATION DATA.....	340
Grazia Ghermandi, Sara Fabbi, Alessandro Bigi, Sergio Teggi and Luca Torreggiani	
NEW INFLOW BOUNDARY CONDITIONS FOR HOMOGENEOUS ATMOSPHERIC BOUNDARY LAYER UNDER THE POWER LAW FOR STREET SCALE MODELLING.....	346
Vasilis Akylas, Fotios Barmpas, Nicolas Moussiopoulos, and George Tsegas	
THE AIR QUALITY IN TWO-DIMENSIONAL URBAN CANYONS WITH GABLE ROOF BUILDINGS: A NUMERICAL AND LABORATORY INVESTIGATION .....	351
Simone Ferrari, Maria Grazia Badas, Michela Garau, Alessandro Seoni and Giorgio Querzoli	
LES STUDY OF UNSTEADY FLOW PHENOMENA IN AN URBAN GEOMETRY – THE NEED FOR SPECIAL EVALUATION METHODS .....	357
Nektarios Koutsourakis, John G. Bartzis, George C. Efthimiou, Alexandros G. Venetsanos, Ilias C. Tolias, Nicolas C. Markatos, Denise Hertwig and Bernd Leitl	
STREET-LEVEL MODELLING OF THE EFFECT OF CLIMATE ADAPTATION MEASURES ON AIR QUALITY.....	362
Jaroslav Resler, Pavel Krč, Michal Belda, Pavel Juruš, Kryštof Eben, Nina Benešová, Daša Srbová, Přemysl Derbek, Pavel Hrubeš, Jan Lopata, Ondřej Vlček, Jana Blumelová, Mária Kazmuková, Petra Bauerová	
AIR POLLUTION MODELING IN URBAN ENVIRONMENT USING WRF-CHEM MODEL.....	367
Attila Kovács, Róbert Mészáros, Ádám Leelőssy, István Lagzi	
SIMULATIONS OF TRAFFIC RELATED POLLUTANTS IN A MAIN STREET OF RIO DE JANEIRO CITY (BRAZIL) USING COMPUTATIONAL FLUID DYNAMICS MODELLING .....	371
Roseane A.S. Albani Beatrice Pulvirenti and Silvana di Sabatino	
MODELLING NO <sub>x</sub> AND NO <sub>2</sub> IN TWO STREET CANYONS IN COPENHAGEN USING AN IMPROVED VERSION OF OSPM.....	376
Thor-Bjørn Ottosen, Matthias Ketzel, Ole Hertel, Jørgen Brandt, Henrik Skov, and Konstantinos E. Kakosimos	

DRY DEPOSITION ONTO VERTICAL SURFACES IN THE URBAN ENVIRONMENT .....	381
Patrick Conry, Silvana Di Sabatino, Francesca Di Nicola, Maria Lisa Vincenti, Riccardo Buccolieri, Pierina Ielpo, Livia Giotta, Alessandra Genga, Ludovico Valli, Gennaro Rispoli and H. J. S. Fernando	
THE ROLE OF SURFACE BUILDING MATERIALS IN AIR QUALITY APPLICATIONS .....	388
Francesca Di Nicola, Maria Lisa Vincenti, Patrick Conry, Riccardo Buccolieri, Piera Ielpo, Alessandra Genga, Livia Giotta, Harindra J. S. Fernando, Silvana Di Sabatino	
VEHICLE INDUCED TURBULENCE AS KEY FACTOR INFLUENCING POLLUTANT DISPERSION IN CLOSE VICINITY OF TRAFFIC PATHS.....	395
Jiri Pospisil and Miroslav Jicha	
SIMULATING TURBULENT AIR FLOWS IN CENTRAL LONDON AND STUDYING EFFECT OF TALL BUILDINGS .....	400
Elsa Aristodemou , Luz Maria Boganegra, Christopher Pain, and Alan Robins	
FLOW AND DISPERSION MODELLING STUDY AT ONE OF DENMARKS TRAFFIC HOT-SPOTS.....	406
Matthias Ketznel, Konstantinos E. Kakosimos, Ulas Im, Thor-Bjørn Ottosen, Jørgen Brandt, Steen S. Jensen,Thomas Ellermann, Maria B. Poulsen and Ole Hertel	
INTEGRATED URBAN AIR POLLUTION DISPERSION MODELLING FRAMEWORK AND APPLICATION IN AIR QUALITY PREDICTION OF THE CITY OF GYŐR .....	410
Zoltán Horváth Bence Liszcai, György Istenes, Péter Zsebők, Balázs Szintai, Éva V.P. Rác, László Környei and István Harmati	
GRAMM/GRAL: COMPUTING AIR QUALITY MAPS AT THE URBAN SCALE .....	415
K. Zink , A. Berchet , D. Brunner , J. Brunner and L. Emmenegger	
<b>TOPIC 6: USE OF MODELLING IN HEALTH AND EXPOSURE ASSESSMENTS.....</b>	<b>420</b>
DYNAMIC URBAN POPULATION SIMULATOR.....	421
Oscar Björnham and Håkan Grahn	
EXPLOSION DAMAGE AND INJURY ASSESSMENT MODELLING: BALANCING MODEL SOPHISTICATION WITH FINITE RESOURCES.....	427
Brian Holland, Qiguo Jing, Weiping Dai, Tiffany Stefanescu	
REAL-TIME USE OF A CFD MODELLING SYSTEM IN THE FRAMEWORK OF “TOXIC 2014”, A MAJOR CIVILIAN SECURITY EXERCISE AT A VERY COMPLEX URBAN SITE IN PARIS.....	432
Patrick Armand, Christophe Duchenne, Yasmine Benamrane, Sébastien Gouillat, Nadège Cabibel, Bertrand Masselin, and Thomas Bineau	
THE INFLUENCE OF THE HOLUHRAUN ERUPTION SO <sub>2</sub> EMISSIONS ON THE AUSTRIAN AIR QUALITY .....	438
Christian Maurer, Delia Arnold, Florian Geyer, Claudia Flandorfer, Marcus Hirtl, Sabine Eckhardt, Thomas Krennert and Gerhard Wotawa	
EVALUATION OF EXPOSURE TO AIR POLLUTION THROUGH MOBILE PHONE DATA IN THE CITY OF MADRID (SPAIN).....	441
M. Picornell, T.Ruiz, R. Borge, P.García, D. de la Paz and J. Lumbreras	

ARE TOXIC LOAD-BASED TOXICITY MODELS CONSISTENT WITH EXPERIMENTAL OBSERVATIONS? INDEPENDENT ANALYSIS OF TIME-VARYING EXPOSURE DATA FROM THE 2012–2013 ECBC/NAMRU-D TOXICOLOGICAL EXPERIMENTS .....	446
Alexander Slawik, James Silva , Kevin Axelrod , Jeffry T. Urban, Nathan Platt	
ESTIMATING AMBIENT CONCENTRATIONS OF BENZO(A)PYRENE IN EUROPE – POPULATION EXPOSURE AND HEALTH EFFECTS .....	452
Cristina Guerreiro, Jan Horálek, Frank de Leeuw, and Florian Couvidat	
ARE TOXIC LOAD-BASED TOXICITY MODELS CONSISTENT WITH EXPERIMENTAL OBSERVATIONS? INDEPENDENT ANALYSIS OF STEADY-EXPOSURE DATA FROM THE 2012–2013 ECBC/NAMRU-D TOXICOLOGICAL EXPERIMENTS .....	453
Alexander J. Slawik, Kevin C. Axelrod, James B. Silva, Ivo K. Dimitrov, Jeffry T. Urban, and Nathan Platt	
BEST PRACTICE GUIDELINES FOR THE USE OF ATMOSPHERIC DISPERSION MODELS AT LOCAL SCALE IN CASE OF HAZMAT RELEASES INTO THE AIR .....	459
Patrick Armand, Kathrin Baumann-Stanzer, E. Bemporad, Claudio Gariazzo, Marko Gerbec, Steven Herring, Ari Karpinnen, Bernd Leitl, Tamir G. Reisin, Gianni Tinarelli, and Silvia Trini Castelli	
COMBINING METEOROLOGICAL MODELS AND DISPERSION MODELS ON LARGESCALE AND MESOSCALE, IMPLEMENTED AS AN AIR QUALITY FORECAST MODEL SYSTEM IN IRAN .....	466
Lorentz, Helmut, Hermann Jakobs, Thomas Flassak, Abbas Ranjbar, Majid Azadi	
<b>TOPIC 7: INVERSE DISPERSION MODELLING AND SOURCE IDENTIFICATION .....</b>	<b>471</b>
TIME-REVERSIBILITY IN ATMOSPHERIC DISPERSION .....	472
Timea Haszpra	
UNCERTAINTY ESTIMATION IN THE RECONSTRUCTION OF ATMOSPHERIC TRACER SOURCE EMISSIONS .....	477
Sarvesh Kumar Singh, Gregory Turbelin, Pramod Kumar, Raj Rani, Amir-Ali Feiz, Pierre Ngae	
INVERSE DISPERSION MODELLING FOR IDENTIFICATION OF MULTIPLE-POINT SOURCE EMISSIONS IN ATMOSPHERE.....	482
Raj Rani, Sarvesh Kumar Singh, Gregory Turbelin, Pramod Kumar, Amir-Ali Feiz, Pierre Ngae	
SOURCE RECONSTRUCTION IN URBAN AND NON-URBAN ENVIRONMENTS USING AN INVERSION METHODOLOGY COUPLED WITH A CFD APPROACH .....	487
Pramod Kumar, Amir-Ali Feiz, Sarvesh Kumar Singh, Pierre Ngae, Raj Rani, Emerson Barbosa, Grégory Turbelin, Jean-Pierre Issartel, Nadir Bekka	
A BAYESIAN APPROACH OF THE SOURCE TERM ESTIMATE COUPLING RETRO-DISPERSION COMPUTATIONS WITH A LAGRANGIAN PARTICLE DISPERSION MODEL AND THE ADAPTIVE MULTIPLE IMPORTANCE SAMPLING .....	492
Harizo Rajaona, François Septier, Yves Delignon, Patrick Armand, Laurent Makke, Christophe Olry, and Armand Albergel	
A CFD MODELING APPROACH FOR A CONTAMINANT RELEASED IN A CITY .....	498
Nadir Bekka, Pramod Kumar, Amir-Ali Feiz, Sarvesh Singh, Mohamed Sellam, Emerson Barbosa, Pierre Ngae, Grégory Turbelin, Amer Chpoun	

MODIFICATION AND VALIDATION OF A METHOD FOR ESTIMATING THE LOCATION OF A POINT STATIONARY SOURCE OF PASSIVE NON-REACTIVE POLLUTANT IN AN URBAN ENVIRONMENT.....	504
George C. Efthimiou, Spyros Andronopoulos, Alexandros Venetsanos, Ivan V. Kovalets, Konstantinos Kakosimos and Christos D. Argyropoulos	
AEROSOL TRANSPORT MODELLING OVER DEBRECEN, HUNGARY .....	509
Zsófia Török, Zoltán Szoboszlai, Enikő Furu, Anikó Angyal, Rostislav Kouznetsov, Mikhail Sofiev, Zsófia Kertész	
METEOROLOGICAL ANALYSIS OF SAHARAN DUST TRANSPORT TO SONNBLICK.....	513
Kathrin Baumann-Stanzer, Sirma Stenzel, Claudia Flandorfer, Gerhard Schauer, Anne Kasper-Gieb	
IMPROVEMENTS TO AN OPERATIONAL INVERSION METHOD FOR ESTIMATING VOLCANIC ASH SOURCE PARAMETERS USING SATELLITE RETRIEVALS .....	518
Helen N. Webster, David J. Thomson, Michael C. Cooke and Rachel E. Pelley	
ON THE EXPLOITATION OF DOSE-RESPONSE INFORMATION FOR THE SOURCE-RECONSTRUCTION IN THE CASE OF ATMOSPHERIC HAZARDOUS MATERIAL RELEASES .....	523
Samar Elkhalfa, Christos D. Argyropoulos, George C. Efthimiou, Spyros Andronopoulos, Alexandros G. Venetsanos, Ivan V. Kovalets and Konstantinos E. Kakosimos	
A NEW PERSPECTIVE ON THE FUKUSHIMA RELEASES BROUGHT BY NEWLY AVAILABLE <sup>137</sup> CS AIR CONCENTRATION OBSERVATIONS AND RELIABLE METEOROLOGICAL FIELDS.....	528
O. Saunier , A. Mathieu , T. Sekiyama, M. Kajino, K. Adachi, M. Bocquet, Y. Igarashi, T. Maki, D. Didier	
APPLICATION OF INVERSE DISPERSION MODELLING FOR THE DETERMINATION OF PM EMISSION FACTORS FROM FUGITIVE DUST SOURCES IN OPEN-PIT LIGNITE MINES..	536
Athanasios Triantafyllou, Nicolas Moussiopoulos, Athina Krestou, George Tsegas, and Melina Andreadou	
OPTIMIZING INITIAL VALUES AND EMISSION FACTORS ON MESOSCALE AIR QUALITY MODELLING USING 4D-VAR DATA ASSIMILATION.....	541
Isabel Ribeiro, Zoi Paschalidi and Hendrik Elbern	
SOURCE REGIONS OF BIOGENIC AEROSOLS IN WROCLAW (POLAND) AND THE INFLUENCE OF METEOROLOGICAL DATA ON THE HYSPLIT MODEL RESULTS .....	546
Daria Bilińska, Carsten Ambelas Skjøth, Małgorzata Werner, Maciej Kryza, Małgorzata Malkiewicz, Justyna Krynicka, Anetta Drzeniecka-Osiadacz	
PRELIMINARY ANALYSIS OF OBSERVATIONS FROM THE JACK RABBIT II–2015 FIELD EXPERIMENT ON DENSE GAS DISPERSION IN A BUILT ENVIRONMENT .....	551
Steven Hanna, Joseph Chang, Thomas Spicer, Michael D. Sohn, Shannon Fox, Mark Whitmire, Leo Stockham, Damon Nicholson, Thomas Mazzola	
<b>TOPIC 8: MODELLING AIR DISPERSION AND EXPOSURE TO ACCIDENTAL RELEASES .....</b>	<b>557</b>
RADON-BASED ASSESSMENT OF STABILITY EFFECTS ON POTENTIAL RADIOLOGICAL RELEASES .....	558
Scott Chambers, Alastair Williams, Dan Galeriu, Anca Melintescu and Marin Duma	

NAME-EPS: DEVELOPING A DISPERSION MODELLING CAPABILITY UTILISING ENSEMBLE WEATHER FORECASTS FOR EMERGENCY-RESPONSE APPLICATIONS .....	564
Andrew R. Jones, Ayoe B. Hansen and Susan J. Leadbetter	
SIMULATION OF EXPLOSIVE EVENTS IN THE URBAN ENVIRONMENT COUPLING A FAST DYNAMICS CFD MODEL WITH LOW MACH NUMBER DISPERSION SOLVERS IN CERES® CBRN-E.....	569
Luc Patryl, Emmanuel Lapébie, and Patrick Armand	
PROBABILISTIC ASSESSMENT OF DANGER ZONES ASSOCIATED WITH A HYPOTHETICAL ACCIDENT IN A MAJOR FRENCH PORT USING A SURROGATE MODEL OF CFD SIMULATIONS .....	576
Felipe Aguirre Martinez, Yann Caniou, Christophe Duchenne, Patrick Armand, and Thierry Yalamas	
CFD-RANS PREDICTION OF INDIVIDUAL EXPOSURE FROM CONTINUOUS RELEASE OF HAZARDOUS AIRBORNE MATERIALS .....	581
George C. Efthimiou, Spyros Andronopoulos, John G. Bartzis	
CFD MODELLING OF DISPERSION IN NEUTRAL AND STABLE ATMOSPHERIC BOUNDARY LAYERS: RESULTS FOR PRAIRIE GRASS AND THORNEY ISLAND.....	582
Rachel Batt, Simon Gant, Jean-Marc Lacomme, Benjamin Truchot and Harvey Tucker	
CONCLUSIONS AND REFLECTIONS FROM COST ACTION ES1006 ACTIVITY: WHAT DO WE MISS FOR THE APPLICATIONS OF MODELS IN LOCAL-SCALE EMERGENCY RESPONSE IN BUILT ENVIRONMENTS? .....	588
Trini Castelli S., Leiti B., Baumann-Stanzer K., Reisin T.G., Armand P., Andronopoulos S., and all COST ES1006 Members	
EFFECTS FROM URBAN STRUCTURES TO ATMOSPHERIC DISPERSION MODELS IN DECISION SUPPORT SYSTEMS FOR NUCLEAR EMERGENCIES.....	593
Hartmut Walter and Gerhard Heinrich	
IMPACT OF CHANGING THE WET DEPOSITION SCHEMES IN LDX ON 137-CS ATMOSPHERIC DEPOSITS AFTER THE FUKUSHIMA ACCIDENT .....	598
Arnaud Quérel, Denis Quélo, Yelva Roustan, Anne Mathieu, Mizuo Kajino, Thomas Sekiyama, Kouji Adachi, Damien Didier, Yasuhito Igarashi, Takashi Maki	
PROJECT SAGEBRUSH: A NEW LOOK AT PLUME DISPERSION.....	603
Kirk L. Clawson, Richard M. Eckman, Dennis D. Finn	
FLOW AND DISPERSION MODELLING IN A COMPLEX URBAN DISTRICT TAKING ACCOUNT OF THE UNDERGROUND ROADS CONNECTIONS.....	608
Maxime Nibart, Patrick Armand, Christophe Duchenne, Christophe Olry, Armand Albergel, Jacques Moussafir, Olivier Oldrini	
EMERGENCIES – A MODELING AND DECISION-SUPPORT PROJECT FOR THE GREAT PARIS IN CASE OF AN ACCIDENTAL OR MALICIOUS CBRN-E DISPERSION .....	613
O. Oldrini, S. Perdriel, M. Nibart, P. Armand, C. Duchenne and J. Moussafir	
BEST PRACTICE IN APPLYING EMERGENCY RESPONSE TOOLS TO LOCAL-SCALE HAZMAT INCIDENTS.....	618
Steven Herring, Patrick Armand <sup>2</sup> and Claudio Gariazzo	
VALIDATION OF THE GAMMA SUBMERSION CALCULATION OF THE REMOTE POWER PLANT MONITORING SYSTEM OF THE FEDERAL STATE OF BADEN-WÜRTTEMBERG .....	623
Janis Lapins, Wolfgang Bernnat, Walter Scheuermann	

SPATIAL AND TEMPORAL CONCENTRATION DISTRIBUTIONS IN URBAN AREAS.....	628
Eva Berbekar, Frank Harms, Bernd Leidl	
HARMONIZATION IN CFD APPROACHES TO ASSESS TOXIC CONSEQUENCES OF AMMONIA RELEASES .....	633
Guillaume Leroy, Jean-Marc Lacomme, Benjamin Truchot, Lauris Joubert	
A SENSITIVITY ANALYSIS FOR A LAGRANGIAN PARTICLE DISPERSION MODEL IN EMERGENCY-RESPONSE TEST CASES .....	640
Gianni Tinarelli, Maxime Nibart, Patrick Armand, Silvia Trini Castelli	
<b>TOPIC 9: MATHEMATICAL PROBLEMS IN AIR QUALITY MODELLING .....</b>	<b>646</b>
ANALYSIS OF SIMULATION RESULTS ISSUED BY A LATTICE BOLTZMANN METHOD IN COMPLEX URBAN ENVIRONMENTS – APPLICATIONS TO PARIS AND HAMBURG.....	647
Fabrice Boisseranc, Patrick Armand, Christophe Duchenne, and Guillaume Douarre	
IMPROVEMENT OF ATMOSPHERIC DISPERSION SIMULATIONS IN CASE OF AN ACCIDENT OR A MALEVOLENT ACTION USING DATA ASSIMILATION METHODS IN CERES® CBRN-E.....	652
Robin Locatelli, Vivien Mallet and Patrick Armand	
EFFICIENT NUMERICAL METHODS IN AIR POLLUTION TRANSPORT MODELLING: OPERATOR SPLITTING AND RICHARDON EXTRAPOLATION.....	658
Ágnes Havasi, István Faragó and Zahari Zlatev	
AN APPLICATION OF THE SCHAAKE SHUFFLE TECHNIQUE TO GENERATE SPACE-TIME CONSISTENT AQ PREDICTIONS .....	663
S. Alessandrini, L. Delle Monache, Irina Djalalova, Jim Wilczak	
<b>MODITIC: MODELLING THE DISPERSION OF TOXIC INDUSTRIAL CHEMICALS.....</b>	<b>666</b>
MODITIC - MODELLING THE DISPERSION OF TOXIC INDUSTRIAL CHEMICALS IN URBAN ENVIRONMENTS.....	667
Monica Endregard, Stephane Burkhart, Jan Burman, Olivier Gentilhomme, Alan Robins, Emma M. M. Wingstedt, B. Anders Pettersson Reif, Leif Persson, Niklas Brännström, Oskar Parmhed, Oscar Björnham, Guillaume Leroy, Daniel Eriksson, Thomas Vik, John Aa. Tørnes and Jean-Pierre Issartel	
MODITIC WIND TUNNEL EXPERIMENTS.....	672
Alan Robins, Matteo Carpentieri, Paul Hayden, Joseph Batten, Jack Benson and Ashley Nunn	
MODITIC WIND TUNNEL EXPERIMENTS NEUTRAL AND HEAVY GAS SIMULATION USING RANS .....	677
Stéphane Burkhart Jan Burman	
MODITIC INVERSE MODELLING IN URBAN ENVIRONMENTS .....	683
Niklas Brännström, Tobias Brännvall, Stéphane Burkhart, Jan Burman, Xavier Busch, Jean-Pierre Issartel, Leif Å. Persson	
MODITIC - LARGE EDDY SIMULATIONS OF DISPERSION OF NEUTRAL AND NON-NEUTRAL SCALAR FIELDS IN COMPLEX URBAN-LIKE GEOMETRIES.....	688
E. M. M. Wingstedt, D. Eriksson, O. Parmhed, G. Leroy, A. N. Osnes, B. A. Pettersson Reif <sup>3</sup> and J. Burman	

MODITIC- ON THE GENERATION OF INFLOW BOUNDARY CONDITIONS FOR DISPERSION SIMULATIONS USING LARGE EDDY SIMULATIONS.....	694
Andreas N. Osnes, P. Daniel Eriksson and B. Anders Pettersson Reif	
MODITIC OPERATIONAL MODELS.....	699
Oscar Björnham, Arnaud Gousseff, John Tørnes and Stephane Burkhart	
AUTHOR INDEX.....	704
HARMO 17 PROGRAMME: ORAL PRESENTATIONS.....	709
HARMO 17 PROGRAMME: POSTER PRESENTATIONS.....	718

## **TOPIC 1**

**MODEL EVALUATION AND QUALITY ASSURANCE –  
MODEL VALIDATION, MODEL INTERCOMPARISONS,  
MODEL UNCERTAINTIES AND MODEL SENSITIVITIES**

**17th International Conference on  
Harmonisation within Atmospheric Dispersion Modelling for Regulatory Purposes  
9-12 May 2016, Budapest, Hungary**

---

**COMPARING DISPERSION MODELLING AND FIELD INSPECTION FOR ODOUR IMPACT  
ASSESSMENT IN THE VICINITY OF TWO ANIMAL HUSBANDRY FARMS**

*Dietmar Oettl<sup>1</sup> and Stefan Oitzl<sup>2</sup>*

<sup>1</sup>Government of Styria, Air Quality Control, Graz, Austria

<sup>2</sup>Government of Upper Austria, Environment Protection, Linz, Austria

**Abstract:** For two cases odour frequencies obtained by dispersion modelling and field inspections were compared. The GRAL model has been used for modelling. In fact, GRAL is a hybrid model where the dispersion is computed via the Lagrangian approach, while the necessary flow fields in built-up areas are computed with an inherent Eulerian microscale, prognostic flow field model. The German guideline VDI 3940-1 prescribes a method to assess ambient odour frequencies by a group of trained persons. It should be noted that the minimum number of panellists is 10, whereas in the two case studies presented in this work only two persons carried out the field inspections on a fixed grid. While in the first case good agreement was found between modelled and observed odour frequencies, these were overestimated by about a factor of 2-3 in the second case by the simulations. Several tracer dispersion studies gave evidence that modelled mean concentrations with the GRAL model typically do not deviate from average observed concentrations by more than  $\pm 30\%$ . Thus, model uncertainties can be clearly excluded as possible cause for the huge discrepancies. Based on only two case studies conclusive reasons for the differences cannot be drawn. However, possible causes, which are discussed in more detail, might be: (i) different average (over the two testers) olfactory sensibilities of the persons in each case study, (ii) and/or problems linked with odour adaptation especially in areas affected by high odour concentrations. Not further analysed in this work but also conceivable would be (iii) uncertainties of the emission factors for fattening pigs, (iv) statistical uncertainties in the field study due to the limited number of visits (approx. 100 visits in each case), and (v) errors arising from the assumption of a constant ratio between the 90 percentile and hourly average odour concentration in the simulations.

**Key words:** *Odour dispersion modelling, Odour hours, GRAL, Odour field inspections*

## **INTRODUCTION**

In practice either field inspections (e.g. VDI, 2006) and/or dispersion modelling (e.g. GIRL, 2009) is used to assess odour impact. Both methods shall provide congruent results within the uncertainty range inherent in each method. From a legal point of view the differences between results should not lead to different conclusions e.g. with regard to the necessity of taking abatement measures or not. In this study results of both methods are investigated on the basis of two case studies, which are described in detail in the following chapter.

## **DATA SETS**

### **Data set A**

Panel field inspections to assess the odour burden were carried out in the vicinity of a farm for 1,600 fattening pigs and 17,000 broilers. Further odour sources at the farm were an open liquid manure storage and a partly open corn silage. As multi-phase feeding for the fattening pigs is applied, odour emissions given by VDI (2009) were cut by 20 %, while for all other sources the emission factors as suggested by VDI (2009) were utilized. In total, 55 MOU h<sup>-1</sup> resulted for the site. The pig stable was ventilated via several stacks mounted at the roof, while the broiler stables were ventilated through horizontal openings in the building. With one exception all points for the field inspection were located at distances several hundreds of metres away from the livestock buildings (Figure 1). The area is characterized by softly rolling terrain, small forests, which are treated as obstacles in the dispersion modelling.

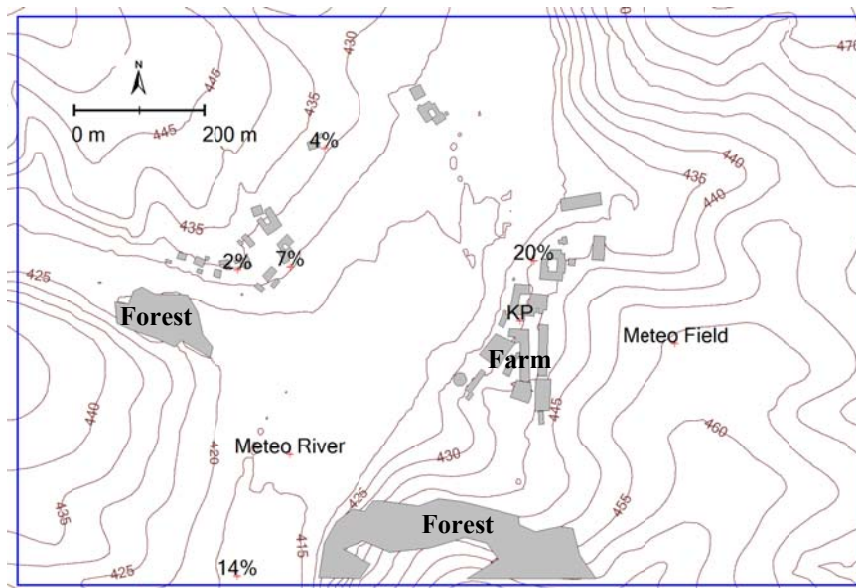


**Figure 1.** Model domain for dispersion modelling, orography, buildings, forests, and position of the meteorological stations as well as the inspection points for the panel field study. Numbers indicate the observed frequency of odour hours.

#### Data set B

In this case several farms for fattening pigs were situated within a small village. All receptor points of the panel field study were placed within the village (Figure 2).

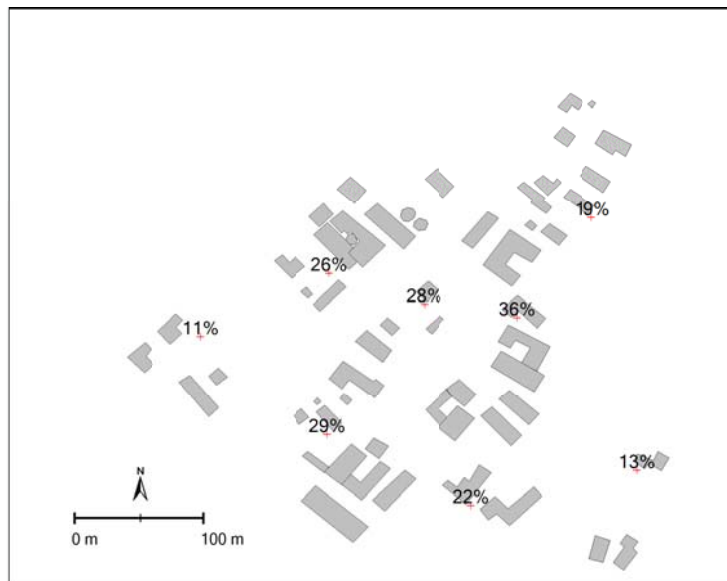


**Figure 2.** Model domain for dispersion modelling, buildings, and position of the inspection points for the panel field study. Numbers indicate the observed frequency of odour hours. The meteorological site was slightly outside the domain.

Terrain is quite flat and was therefore not taken into account in the dispersion simulations. All in all 2,000 fattening pigs, some 600 piglets, and about 150 breeding sows were present in the livestock buildings. Some of the stables were ventilated via stacks at roof top level, while others had no ventilation, i.e. air exchange was managed by keeping windows open.

Basically, emission factors provided by VDI (2009) were applied. However, in case of the non-artificially ventilated stables emissions were reduced by 50 %. Jeppsson (2003) found a strong positive correlation of

ammonia emission rates in  $[\text{kg h}^{-1}]$  on ventilation rates in fattening pig stables. It is assumed that the non-forced ventilated stables owe rather low ventilation rates of about 10 % of those being artificially ventilated. KTBL (2012) provides the following relationship between normalized volume flux  $V_n$  and emission factor  $e$ :

$$e = e_0 V_n^{c_V} \quad (1)$$

In equation (1)  $e_0$  is the basic emission factor taken from VDI (2009), which is only valid for stables with forced ventilation and not representative for non-ventilated stables. Schaubberger et al. (2012) found for the empirical constant  $c_V$  a value of 0.32 in case of odour. Inserting these values results in  $e/e_0 = 0.5$ . As for data set A, in total 55 MOU  $\text{h}^{-1}$  were released from the livestock buildings.

## METHODS

### Panel field studies

The field inspections were carried out on the bases of VDI (2006) with the exception of some minor and one major issue: instead of having a panel of at least ten persons, only two people took part in each of the assessments (note: the two persons were not the same in both studies). Both panellists were tested for their olfactory sensibility with regard to n-Butanol, which, according to VDI (2006), shall fall within 64 and 256  $\mu\text{g m}^{-3}$ . In case of data set A, the average sensibility for the two persons was 84  $\mu\text{g m}^{-3}$ , and in case of data set B it was 189  $\mu\text{g m}^{-3}$ .

### Dispersion modelling

The Lagrangian particle model GRAL (Oetl, 2014) has been used for the dispersion modelling. In case of data set A, where orographical effects had to be taken into account, the non-hydrostatic prognostic mesoscale model GRAMM (Oetl, 2016) was used to simulate 3D wind-fields. Grid resolution was 100 m x 100 m x 10 m with increasing vertical grid cells by a factor of 1.4. Buildings were accounted for by utilizing the non-hydrostatic prognostic microscale model implemented in GRAL (Oetl, 2015). Grid size was 3 m x 3 m x 1.5 m in this case. GRAL allows for the definition of various kinds of sources (line, area, volume, point) including plume rise modelling due to momentum and/or excess temperature. The GRAL model provides hourly mean odour concentrations, but the field inspections give (annual) frequencies of odour hours, which is defined by an odour perception of at least 6 minutes (= 90 percentile) within one hour. Therefore, a relationship is needed between the 90 percentile of odour concentrations within one hour and the corresponding average. Mostly, in Austria and Germany a ratio of 4/1 (Janicke and Janicke, 2004) is applied and also used in this study. The GRAMM and GRAL models were driven by locally observed meteorological data 10 m above ground level. It should be noted that both the field inspections and the modelling covered the same time period, which was March – September (data set A) and March – October (data set B).

## RESULTS

Based on a threshold value of 1 OU  $\text{m}^{-3}$  in the GRAL model, modelled and observed odour frequencies are listed in Table 1 and Table 2 for the two data sets (see also Figure 3). While for data set A reasonable agreement was found, larger deviations between the two methods are visible in case of the data set B. In the latter case, GRAL overestimates odour hours significantly.

**Table 1.** Observed and modelled frequencies of odour hours for a threshold in the modelling of 1 OU  $\text{m}^{-3}$ . Data set A

Location	1	2	3	4	5
Field inspection	14%	2%	7%	4%	20%
GRAL	13%	2%	5%	4%	25%

**Table 2.** Same as Table 1, but for data set B

Location	1	2	3	4	5	6	7	8
Field inspection	13%	22%	29%	11%	26%	28%	36%	19%
GRAL	23%	30%	38%	30%	32%	58%	60%	37%

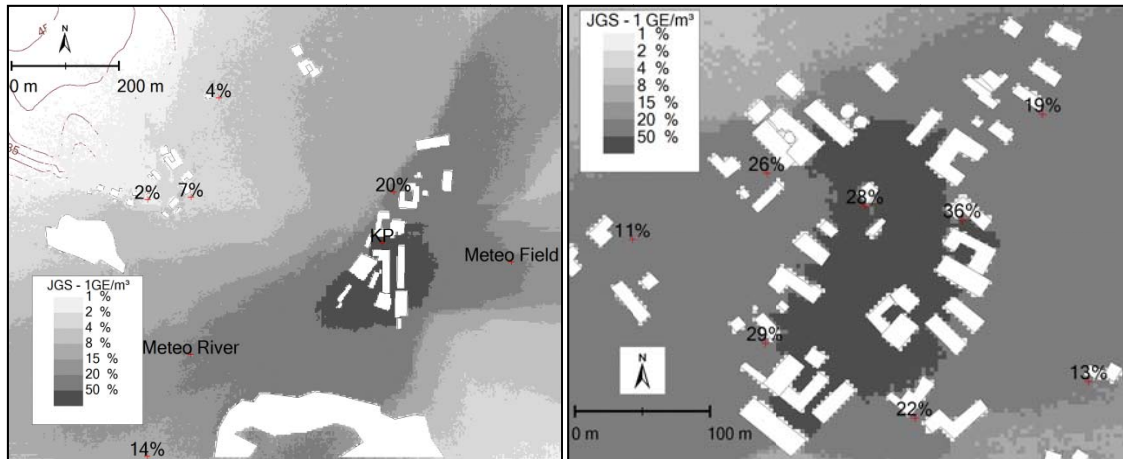


**Figure 3.** Simulated odour hour frequencies for data set A (left) and data set B (right). Odour threshold:  $1 \text{ OU m}^{-3}$

In the following it is investigated how the different olfactory sensibilities of the panellists might have influenced the results of the field inspections. As already outlined, the average detected concentration of n-Butanol for data set B was by a factor of 2.3 higher than that for data set A. That means that the persons involved in data set B were much more sensible and thus, would detect a higher frequency of odour hours than did the participants in data set A. Increasing the odour threshold in the modelling for data set B to  $2.3 \text{ OU m}^{-3}$  results in far better agreement between modelled and observed odour frequencies (Table 3). Nevertheless, it should be stressed that the average sensibility of the participants in data set B is much closer to the average concentration of n-Butanol of  $160 \mu\text{g m}^{-3}$ , which is to be the expected average sensibility if only enough (at least 10) persons had taken part in the field studies.

**Table 3.** Observed and modelled frequencies of odour hours for a threshold in the modelling of  $2.3 \text{ OU m}^{-3}$ .

Location	Data set B							
	1	2	3	4	5	6	7	8
Field inspection	13%	22%	29%	11%	26%	28%	36%	19%
GRAL	11%	19%	27%	17%	22%	23%	23%	23%

BMWFJ (2009) states that odour is not perceivable outdoors below thresholds of about  $2 - 5 \text{ OU m}^{-3}$ . Field inspections as described in VDI (2006) foresee a 10 minutes sniffing interval for each location. Especially in areas with constant odour concentrations adaptation cannot be avoided, resulting in lower sensibility and lower observed odour frequencies. However, the German guideline GIRL (2009) fixes the odour threshold for modelling with  $1 \text{ OU m}^{-3}$ . Hence, in general one would expect a model to overestimate observed odour frequencies. Indeed there exist several studies revealing such overestimations (e.g. Müller and Riesewick, 2013; Grotz and Zimmermann, 2015; Hartmann and Borchering). In the following, new simulations have been carried out setting the threshold to  $2 \text{ OU m}^{-3}$ . In addition, the different average sensibilities of the panellists have been taken into account (assuming that the correct average odour sensibility over all panellists would be  $160 \mu\text{g m}^{-3}$  for n-Butanol if only enough participants would take part in an investigation) by applying the following correction factors  $c$  to the modelled odour concentrations:

$$\text{data set A: } c = 84/160 = 0.53$$

$$\text{data set B: } c = 189/160 = 1.18$$

In the modelling, the effect of increasing the odour threshold from  $1$  to  $2 \text{ OU m}^{-3}$  is the same as if concentrations were corrected by a factor of 0.5. Hence, considering the sensibility of the participants in data set A in combination with an increased threshold in the modelling of  $2 \text{ OU m}^{-3}$  results in an effective odour threshold of  $2 \text{ OU m}^{-3} * 0.53 = 1.05 \text{ OU m}^{-3}$ . For data set B an effective threshold for odour of  $2 \text{ OU m}^{-3} * 1.18 = 2.4 \text{ OU m}^{-3}$  can be established in this way. The new results for data sets A and B do not

differ from those presented in Table 1 (data set A and 1 OU m<sup>-3</sup>) and Table 3 (data set B and 2 OU m<sup>-3</sup>), which show in general a good agreement between field inspection and modelling.

## CONCLUSIONS

Panel field investigations based on the German guideline VDI (2006) might give quite different odour hour frequencies than obtained by dispersion modelling, if an odour threshold of 1 OU m<sup>-3</sup> is applied in the simulations. Several studies as well as the comparisons presented in this work indicate that dispersion modelling provides in general significant higher odour hour frequencies than field inspections. The reason is probably that odour cannot be detected by panellists at the theoretical threshold of 1 OU m<sup>-3</sup> in an outdoor environment. Indeed, for the two cases herein a threshold of 2 OU m<sup>-3</sup> leads to a significant better agreement of modelled and observed odour hour frequencies.

## ACKNOWLEDGEMENT

The provision of activity, meteorological, and field inspection data by the Environmental Advocacy of Upper Austria is greatly acknowledged.

## REFERENCES

- BMWFJ, 2009: Technische Grundlage für die Beurteilung von Einwirkungen, die beim Betrieb von Koch-, Selch-, Brat- und Backanlagen auftreten können und Abhilfemaßnahmen (Technical Guide for Odours). Austrian Ministry for Economy, Research, and Youth., Vienna, 137 pp.
- GIRL, 2009: Feststellung und Beurteilung von Geruchsimmissionen (Geruchsimmissions-Richtlinie – GIRL) in der Fassung vom 5. November 2009 mit Begründung und Auslegungshinweisen, Ministerium für Umwelt und Naturschutz, Landwirtschaft und Verbraucherschutz Nordrhein-Westfalen, Düsseldorf, 37 pp.
- Grotz, W., and B. Zimmermann, 2015: Vergleich Rasterbegehung – Immissionsprognose. Beispiele aus der Papierindustrie. VDI Report **2252**, 81-94.
- Hartmann, U., and N. Borchering, 2015: Emissionsmessungen, Ausbreitungsrechnungen und Rasterbegehungen – Vergleich berechneter und gemessener Geruchsstundenhäufigkeiten anhand verschiedener Anwendungsfälle, VDI Report **2252**, 95-104.
- Janicke, L. and U. Janicke, 2004: Development of the dispersion model AUSTAL2000G. Berichte zur Umweltphysik, **5**, Ingenieurbüro Janicke, Dunum, 122 pp.
- Jeppsson, K.H., 2003: Diurnal variation in ammonia, carbon dioxide and water vapour emissions from a deep litter house for fattening pigs. Int. Symp. on Gaseous and Odour Emissions from Animal Production Facilities, Horsens 1-4 June 2003, 131-139.
- KTBL, 2012: Emissionen und Immissionen von Tierhaltungsanlagen – Handhabung der Richtlinie VDI 3894. KTBL-Schrift **494**, Darmstadt, 216 pp.
- Müller, F. and H. Riesewick, 2013: Geruchsproblematik im Rahmen der Bauleitplanung im ländlichen Raum. VDI Report **2195**, 137-148.
- Oettl, D., 2014a: Documentation of the Lagrangian Particle Model GRAL (Graz Lagrangian Model) Vs. 14.8, Government of Styria, Rep. Nr. LU-08-14, Graz, 139 pp.
- Oettl, D., 2015: Quality assurance of the prognostic, microscale wind-field model GRAL 14.8 using wind-tunnel data provided by the German VDI guideline 3783-9. *J. Wind Eng. Ind. Aerod.*, **145**, 104-110.
- Oettl, D., 2016: Documentation of the prognostic mesoscale model GRAMM (Graz Mesoscale Model) Vs. 15.12, Government of Styria, Rep. Nr. LU-05-16, Graz, 118 pp.
- Schauberger, G., T.T. Lim, J.Q. Ni, D.S. Bundy, B.L. Haymore, C.A. Diehl, R.K. Duggirala, A.J. Heber, 2012: Empirical model of odor emission from deep-pit swine finishing barns to derive a standardized odor emission factor. *Atmos. Environ.*, 84-90.
- VDI 3894-1, 2009: Emissions and immissions from animal husbandry – Housing systems and emissions – Pigs, cattle, poultry, horses. Düsseldorf, 84 pp.
- VDI 3940-1, 2006: Measurement of odour impact by field inspection – Measurement of the impact frequency of recognizable odours – Grid measurements. Düsseldorf, 44 pp.

**17th International Conference on  
Harmonisation within Atmospheric Dispersion Modelling for Regulatory Purposes  
9-12 May 2016, Budapest, Hungary**

---

**EDMS MODEL VERIFICATION CONSIDERING REMARKABLE CHANGES IN AIRPORT  
TRAFFIC SYSTEM**

*Veronika Groma<sup>1</sup>, Zita Ferenczi<sup>2</sup>, Bálint Alföldy<sup>1,3</sup>, János Osán<sup>1</sup>, Szabina Török<sup>1</sup> and Roland Steib<sup>2</sup>*

<sup>1</sup>Hungarian Academy of Sciences, Centre for Energy research, Budapest, Hungary

<sup>2</sup>Hungarian Meteorological Service, Budapest, Hungary

<sup>3</sup>Air Quality Environmental Research Center, Qatar University, Doha, Qatar

**Abstract:** This paper presents the verification process of the Emission and Dispersion Modeling System adapted to evaluate the air quality of Liszt Ferenc International Airport. One receptor point was selected at the Airport, at Terminal Building 2 for the analysis, where an air quality monitoring station has been operating. Modeling results completed with background concentrations generated from another suburban monitoring station were compared with measured hourly concentrations using statistical indicators for three compounds (CO, NO<sub>x</sub> and PM<sub>10</sub>). Acceptable correlation coefficients (0.53-0.76) were obtained, however modeled PM<sub>10</sub> concentrations were significantly underestimated. Pollution roses were generated that highlighted the areal distribution of the pollution sources influencing air quality at the receptor point. The contribution of aircraft movement and apron area emission was found to be well rated, but in case of CO and NO<sub>x</sub> small (17%) deficiency was found for ground vehicles emission, moreover a much higher (65%) difference was obtained for PM<sub>10</sub>.

**Key words:** *airport air quality, dispersion modeling, EDMS modeling system*

## **INTRODUCTION**

Airport air pollution related early mortality is not negligible. One of the most important topics of health effect studies is a suitable dispersion model combined with a detailed emission inventory. Numerical modeling tools give the opportunity to forecast and plan air quality supporting decision making. There are a number of dispersion models, some of which are investigated in detail in case studies and compared at specific airport sites.

This paper presents a verification study of EDMS (Version 4.5) adapted to Liszt Ferenc International Airport (Budapest, Hungary), by comparing simulation results with air quality monitoring data. The EDMS system is a combined emission and dispersion model, which can be used to produce an inventory of emission generated at airport site, as well as to calculate pollutant dispersion inside and around the airport. Steib et al. (2008) showed that meteorological situation intensively affects air quality at airport region, the influence of distant sources can be commensurable with the contribution of local sources depending on wind direction.

The traffic at Budapest Airport show significant activity growth in accordance with global trends, thus developments connected to airport service were realized. Furthermore, due to economic crisis, the Hungarian Airlines (MALÉV) became bankrupt in 2011 that again entailed changes in airport operation. As a result, the operational principles changed notably, especially the traffic at terminal buildings (T1 and T2) at Budapest Airport: Terminal Building 1 (T1) was closed in 2012 so that all aircraft traffic is transferred to Terminal Building 2 (T2), which was rebuilt to be able to serve even more passengers. This also means that the route of the passenger related cars and the use of parking facilities have been changed significantly. Furthermore, the section of city close to the Airport showed remarkable developments, which infers the growth of vehicle traffic. Therefore, our first aim was to study long term datasets to find out the contribution of the airport related emission sources to overall air quality situations and follow the changes in air quality due to Airport operational alteration. Secondly, the applicability of default emission parameters is studied in order to verify the assumptions made for the time and spatial description of relevant pollution sources.

## EXPERIMENTAL

For our selected model EDMS, the system architecture and input data requirements were already described in detail in our previous article (Steib et al., 2008). Since the emission factors vary in a wide range, especially for ground vehicles, where the vehicle types are very diverse, mostly EDMS default values were used. The runway usage of aircrafts is registered by the operators, so that the timing and aircraft type of landing and takeoff operations could be simulated in accordance with the reality. All other aircraft movement (taxiing, Auxiliary Power Unit - APU) and aircraft operation related vehicle traffic were chosen as the default values from EDMS. Taxiing time was set to 12 minutes. Aircraft types were divided into three categories, for each of them a representative aircraft was chosen in order to simplify input data generation: Heavy - Boeing 767, Medium - Boeing 737, Light - Citation I. Simulations were made for daily averages on an 8,000 m × 8,000 m grid, with 200 m spatial resolution, for compounds CO, NO<sub>x</sub> and PM<sub>10</sub>. Emissions of significant point sources were also taken into account.

In 2008, a monitoring station was installed on the terrace of T2, since then it has been continuously measuring hourly average concentrations of various compounds (CO, NO<sub>x</sub>, PM<sub>10</sub>, SO<sub>2</sub>, O<sub>3</sub>, CH<sub>4</sub>). These data are used to verify model results for statistically acceptable periods. On the area of T2 apron, emissions of aircrafts APU and taxi of Ground Support Equipment (hereafter GSE) and ground supporting vehicles (catering, passenger transporting buses), and of employees cars should be taken into account as well. In addition Airport operation related emission sources positioned far from T2 (like takeoff, point sources) can have demonstrable effect depending on the meteorological situation.

Since EDMS calculates the concentration distribution of specified compounds originating only from sources defined by the Airport, one has to determine background concentrations to be able to compare measurement and modeling results. Determination of the background concentrations is not straightforward, since due to the closeness of the city, it can be supposed that the urban pollution plume might also affect the air quality of the airport. To overcome this, a dataset of a nearby monitoring station was used. The closest station of the Hungarian Air Quality Network is located ca. 3 km west from the Airport at Gilice tér (hereafter GT). The station registers hourly average concentrations of all three compounds (CO, NO<sub>x</sub>, PM<sub>10</sub>) chosen for the model verification study. However, this station is at a suburban location, the effect of local sources must be taken into account. There exists a road with important traffic, but the measured concentration data shows characteristic daily and weekly time structure. Beside this, point sources can be found in the vicinity of GT (like Budapest Power Plant and smaller workshops), which have significant effect on local air quality. Therefore, background concentrations at the Airport were determined in two steps. First, because the tendency of the minimum values of 00h-06h periods (when vehicle and aircraft traffic is negligible) during the entire year showed great similarity but significantly higher at GT than at the Airport, an  $f_k$  (where  $k$  stands for the given pollutant) linear regression factor was calculated. This significant difference can be explained on one hand with the unbuilt environment at Airport, which ensures favorable conditions for pollutants dilution. On the other hand, it is due to the influence of local sources (power plant, households, etc.). The obtained factors are  $f_{CO}=0.7$ ,  $f_{NOX}=0.6$ , and  $f_{PM10}=0.4$ .

In the second step, our aim was to remove the effect of emissions related to local traffic, for which a method introduced by Balczó et al. (2011) was used with small modifications. The principle of this method is that components calculated with Fourier analysis of the dataset are filtered above a frequency threshold ( $\nu > 0.056 \text{ h}^{-1}$ ). In our case the Fourier spectra of the day-of-week averaged hourly concentrations were calculated for every pollutant. The results confirm the previously expected trends, that beside the daily cycle, a significant component with 12 h periodic time is detectable for CO and NO<sub>x</sub> pollutants, which can be identified with the effect of typical suburban vehicle traffic. The correction is defined by the ratio of the 12 h Fourier component amplitude and the averaged measured maximum daily difference in the concentration time series. As the traffic is much lower at weekends, the contribution of vehicle sources can be neglected for these days. Therefore, weekdays and weekends were treated separately, so that on weekends no corrections were done. Daily averaged corrected background concentrations for a certain  $k$  pollutant for the  $i$ -th day ( $c_{bg,k}^i$ ) could be calculated from  $c_{l,k}^i$  hourly averaged measured concentrations as

$$c_{bg,k}^i = \begin{cases} f_k \frac{1}{24} \left[ \sum_{l \in \bar{H}} c_{l,k}^i + \sum_{l \in H} \left( 1 - \frac{A_k}{\frac{1}{7} \sum_{j=1}^7 \overline{c(\max)_{j,k}} - \overline{c(\min)_{j,k}}} \right) c_{l,k}^i \right] & \text{if weekday} \\ f_k \frac{1}{24} \sum_{l=1}^{24} c_{l,k}^i & \text{if weekend} \end{cases} \quad (1)$$

where  $A_k$  is the amplitude of the Fourier component with 12h periodic time ( $A_{CO}=78.29 \mu\text{gm}^{-3}$ ,  $A_{NOX}=17.32 \mu\text{gm}^{-3}$ ,  $A_{PM10}=1.04 \mu\text{gm}^{-3}$ ),  $\overline{c(\max)_{j,k}}$  and  $\overline{c(\min)_{j,k}}$  are the averages of the  $j$ -th day minimum and maximum concentrations ( $j=1 \dots 7$ ).  $H$  is the set of peak hours:  $H = \{7, 8, 9, 18, 19, 20\}$ .

Modeled concentrations at the defined receptor point were added to background values determined using the method described above. As a consequence, measured concentrations close to the receptor point were expected to be comparable with these values. An example period of measured versus the sum of modeled and background concentration time trend of  $\text{NO}_x$  is presented in Figure 1.

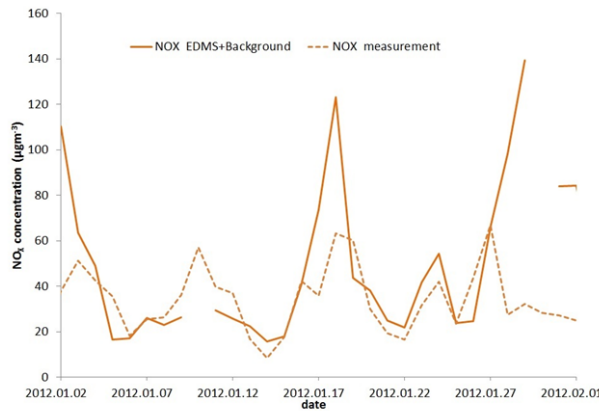


**Figure 1.** Daily averages of measured and simulated  $\text{NO}_x$  concentrations at T2 site in January 2012

## RESULTS

Emission and meteorological input files were generated based on data of on-site measurements. The simulation process consists of two parts, first a preprocessor (EDMS) generates emission values for the different sources, then the second part (AERMOD system) calculates dispersion. As a result, concentration fields for daily averages on a certain domain for the selected compounds as well as meteorological parameters are calculated. Two periods were chosen for the analysis: years 2006 and 2012. The obtained distributional difference for  $\text{NO}_x$  in annual averages (grid values for 2012 were subtracted from the ones calculated for 2006) is presented in Figure 2.

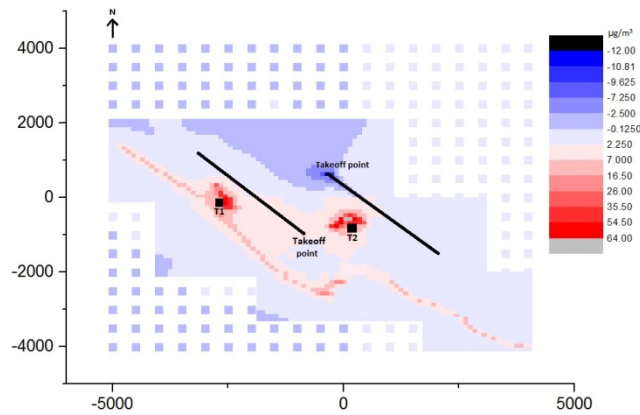


**Figure 2.** Difference between yearly average of  $\text{NO}_x$  concentration distribution for 2006 and 2012

Previous concentration distribution results showed that areas of T2 and roadways beside Airport area have highest concentration (Steib et al., 2008). Due to the decrease of aircraft traffic annual average CO and PM<sub>10</sub> concentrations were lower in 2012 at the entire Airport area. Though CO emissions of point sources showed a great increase in some cases, the annual quantities were orders of magnitude less than aircraft LTO emissions. A notable difference could be found for NO<sub>x</sub> concentrations at takeoff starting points, northern takeoff point showed remarkable NO<sub>x</sub> contribution in 2012. This was due to meteorological and operational causes. For situations with no wind, Airport operators directed the aircrafts to closer takeoff point to reduce taxiing time. In 2006, Terminal Building 1 (T1) was in operation during the total period, so that starting point between the Terminal buildings was used dominantly, resulting in much lower NO<sub>x</sub> load at the northern takeoff point. After the closure of T1, the usage of starting points was changed, thus the ratio between the two takeoff starting points have been equalized. As it is shown later, it has had significant effect on T2 apron air quality.

Long term monitoring data gives us the opportunity to verify modeling results. Though EDMS predict concentrations for every grid point of the Airport, only one receptor point could be used for the verification due to availability of air quality monitoring site. Concentration monitoring was performed at the most contaminated area of Airport, where the considerable emission sources are the most diverse (APU, GSE, handling and passenger related cars and buses, etc.). Our aim was to study the accuracy of modeling results at this point, principally focusing on the time tendencies of pollutant concentrations that were compared for daily averages of measured and simulated results for the closest receptor point. Background values, which were the corrected values of GT site using the method described above, were added to the output values of EDMS. Statistical indicators (correlation coefficient, BIAS, relative BIAS, root-mean-square error (RMSE)) were calculated to check the quality of simulation results. The joint analysis of these markers can show the accuracy of modeling output values added to background values. Statistical indicators of this comparison (for year 2012) are presented in Table 1.

**Table 1.** Statistical indicators of the difference between measured and modeled daily average CO, NO<sub>x</sub> and PM<sub>10</sub> concentrations for 2012

	<b>Correlation coefficient</b>	<b>BIAS</b>	<b>Relative BIAS</b>	<b>RMSE</b>	<b>Concentration span (µg/m<sup>3</sup>)</b>
CO	0.71	-0.29	-8.38×10 <sup>-4</sup>	142.16	1234
NO <sub>x</sub>	0.53	13.73	0.555	24.59	103
PM <sub>10</sub>	0.76	-2.31	-0.44	5.11	43

The best agreement was found for CO, only the negative value of BIAS indicate that a small but significant underestimation exists. Modeling of PM<sub>10</sub> concentration is usually a weak point of air quality models. Our data have shown surprisingly good agreement, however BIAS and RMSE values indicate incompleteness in EDMS results or/and in background determination. The correlation between measured and modeled NO<sub>x</sub> concentrations is the weakest. Since background values are typically small compared to daily average values, the discrepancy should originate from modeling. This can be partly due to the fact that no chemical reaction or sink of NO<sub>x</sub> is considered during the dispersion calculation.

Beside time trend analysis bivariate pollution roses were drawn to identify emission sources which affect local air quality at a certain point. Bivariate pollution rose is a graphical data analysis technique, where concentration distribution is shown in the function of wind vector on radar chart. Bivariate pollution roses were generated for (i) EDMS results added to corrected background concentrations, (ii) measured concentrations and (iii) EDMS results only. Our aim was to identify the sources responsible for the extreme discrepancies in time series.

As a result of comparing the bivariate pollution roses for CO generated from measurement and EDMS + background results it was found that emissions originating from the apron area are slightly underestimated. Remarkable difference occurs in the direction of south from receptor point, which area contains the parking places for passenger cars. This amount of shortcoming can be partly explained with the incomplete data of parking usage (only those cars were registered, which entered into the parking

area, those passed through, or stopped for few minutes were not taken into account). Previous studies (Celikel et al., 2005) showed the weakness of EDMS built-in emission parameters for passenger cars, since they are characteristic for operations in the USA, but do not reflect the conditions of European airports, which should be present in our case as well. To quantify this effect, we need to have detailed information about the actual vehicle fleet parameters (types, age, etc.).

For  $\text{NO}_x$ , similar effects can be identified (see Figure 3). The apron and the passenger parking area's emission is underestimated by a factor of 0.3. At the same time, the influence of aircraft emission during takeoff is demonstrable (segment from north to northeast), since concentration distribution shows local maximum in that direction as well. It is important to note, that the clear appearance of runway emission is not expected, since takeoff time is a short part of an hour, whereupon takeoff emission contribution might not be detectable in all cases. Increasing the time resolution of EDMS results could correct this effect, but this high time resolved analysis exceeds our purposes.

In case of  $\text{PM}_{10}$ , whereas correlation coefficient show good agreement, a significant underestimation is demonstrated from statistical indicators, however apron area and passenger parking emission shows similar magnitude of emission in EDMS results, which corresponds to the reality. Although background values are determined with assumable uncertainty, the magnitude of  $\text{PM}_{10}$  concentrations is certainly underestimated by EDMS.

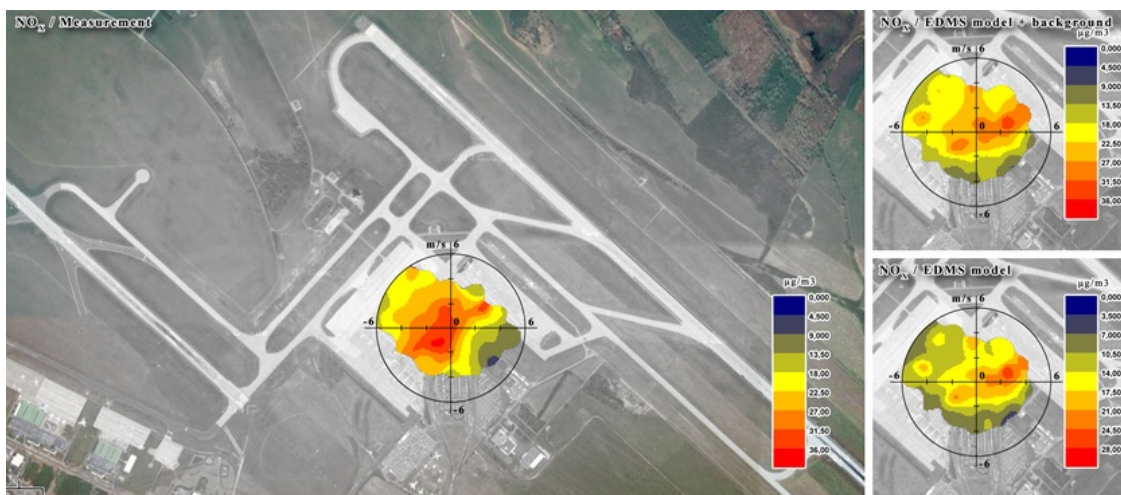


**Figure 3.** Pollution roses for measurement (left), EDMS + background (up, right) and EDMS (down, right) results of daily average  $\text{NO}_x$  concentration, at T2 site in 2012

In general, air quality at Airport area became better between the period of 2006 and 2012, while the number of passengers slightly increased, which means that the operational optimization was successful from the environmental aspects. However, as a result of rearrangement of aircraft movements, the effect of  $\text{NO}_x$  contribution due to takeoff emission at Terminal Building 2 depending on meteorological situation can be detectable.

## CONCLUSION

In this study, a comparison of measured data and modeled concentration distribution calculated by EDMS for three compounds ( $\text{CO}$ ,  $\text{NO}_x$  and  $\text{PM}_{10}$ ) was presented. A statistically acceptable 1-year (2012) period was studied to analyze the accuracy of input data, and to study the effect of change in aircraft traffic on local air quality. A monitoring site was operated continuously during this period, which was chosen as the nearest receptor point of the model for comparison. Background values were generated from the closest air quality measurement station (Gilice tér), which was found to be expressive in case of  $\text{CO}$  and especially  $\text{PM}_{10}$ . Statistical indicators and pollution roses were generated to analyze the accuracy and weaknesses of emission parameters.

EDMS gives reliable and realistic results for long term data and applicable for air quality management for Budapest Airport. Correlation between measurement and simulation values were acceptable for all 3 compounds, however a slight underestimation is noticeable, especially in case of PM<sub>10</sub>. This is basically due to the uncertain determination of ground vehicle emissions since at present such data are only available for the registered cars. These observed discrepancies should be corrected by a more precise determination of ground vehicle traffic.

In general, air quality at Airport area became better between the period of 2006 and 2012, while the number of passengers slightly increased, which means that the operational optimization was successful from the environmental aspects. However, as a result of rearrangement of aircraft movements, the effect of NO<sub>x</sub> contribution due to takeoff emission at Terminal Building 2 depending on meteorological situation can be detectable. Taking these findings into consideration, the contribution to Budapest city contamination can be determined by EDMS, especially in critical meteorological situations, when Airport operation related emission cannot be neglected.

#### REFERENCES

- Balczo, M., Balogh, M., Goricsan, I., Nagel, T., Suda, J., Lajos, T., 2011: Air quality around motorway tunnels in complex terrain - computational fluid dynamics modeling and comparison to wind tunnel data. *Időjárás* **115**, 179-204.
- Celikel, A., Duchene, N., Fuller, I., Fleuti, E., Hofmann, P., 2005: Airport local air quality modelling: Zurich Airport emissions inventory using three methodologies. [https://www.eurocontrol.int/eec/gallery/content/public/document/eec/conference/paper/2005/007\\_Zurich\\_Airport\\_emissions.pdf](https://www.eurocontrol.int/eec/gallery/content/public/document/eec/conference/paper/2005/007_Zurich_Airport_emissions.pdf).
- Steib, R., Labancz, K., Ferenczi, Z., Alföldy, B., 2008: Airport (Budapest Ferihegy – Hungary) air quality analysis using EDMS modeling system. Part I. Model development and testing. *Időjárás* **112**, 99-112.

**17th International Conference on  
Harmonisation within Atmospheric Dispersion Modelling for Regulatory Purposes  
9-12 May 2016, Budapest, Hungary**

---

**VALIDATION OF PANACHE CFD POLLUTION DISPERSION  
MODELLING WITH DENSE GAS EXPERIMENTS**

*Liyang Chen and Malo Le Guellec*

Fluidyn, 7 boulevard de la libération, 93200, Saint-Denis, France

**Abstract:** The prediction of atmospheric pollution dispersion is now one of the first concerns for emergency response and risk assessment. With rapid advances in computer hardware and numerical methods, the computational fluid dynamic (CFD) technology is often applied to determine the consequences of accidental releases of hazardous or toxic materials. The current paper concerns the Fluidyn-PANACHE CFD model evaluation with regard of dense gases dispersion. The CFD model has been evaluated here with four experimental data series for dense gases releases: Desert Tortoise series (4 trials with steady horizontal releases of large scale pressurized liquid ammonia over water surfaces and dry ground), Burro series (4 trials with a liquefied natural gas (LNG) release on a water pool), CO2PIPETRANS series (5 trials with steady and transient leakages of liquid and supercritical CO<sub>2</sub> in a test site), and Porton down series (2 trials with transient releases of a mixture of air and Freon over a flat grassland). The numerical results are analyzed by maximum arc-wise concentration and BOOT criteria for the four experiments. All the simulations of Desert tortoise meet the criteria calculated from the maximum arc-wise concentrations while they have the slight under-prediction tendency far away from the source. Regarding the BURRO series, The BOOT criterion calculated for shortest averaging is met for all the trials in case of flat terrain approach. In the frame of CO2PIPETRANS data series, the comparison of concentration and temperature profiles are in good agreement with the experimental measurements. Concentration time series comparison plots for Porton down series show the good performance of CFD model, with 88% of prediction within a FAC2 of the observations. This detailed analysis with statistical criteria shows that the performance of Fluidyn-PANACHE model versus these four dense gas experimental data series is well within the acceptable range for air quality applications.

**Key words:** *atmospheric pollution dispersion, CFD model evaluation, emergency response, dense gas dispersion*

## **INTRODUCTION**

The pollution dispersion models have been used initially in risk assessment for safety reports in environmental problem and industrial programme since 1970s. The quality of consequence model, especially dense gas dispersion models may be therefore very important to make some decisions for industrial programme.

Until now, many dense gas dispersion models have been developed, which range from simple box model through more sophisticated integral models like DEGADIS, SLAB, (Touma et al, 1995) to 3D CFD model (Duijm and Carissimo, 2001). Models for simulating dense gas releases need to account for the source term, initial gravitational spreading of a heavy gas cloud and the downwind dispersion of the cloud in air. With the rapid development of computer hardware and numerical methods, CFD model is becoming increasingly important in this field. Since 1990s, the dense gas CFD models were evaluated by the dense gas release field measurements (Mohan & al., 1995; Duijm et al., 1997; Sklavounos and Rigas, 2004).

The current paper concerns the Fluidyn-PANACHE CFD model evaluation. PANACHE uses physical models and deterministic solutions that are adapted to any kind of release scenarios, complex environments and pollutant characteristics. To demonstrate the CFD model's capabilities with regard of dense gases dispersion in different accidental conditions even in the most extreme conditions, four field measurements have been selected: Desert Tortoise series, Burro series, CO2PIPETRANS series, and Porton down series. Indeed, evaluation of gas dispersion models need fundamentally to be performed on full-scale releases especially of dense gases to check out the prediction ability.

## DESCRIPTION OF THE CFD MODEL

### Governing Equations

The Fluidyn-PANACHE solves the Navier-Stokes equations along with the equations describing conservation of species concentration, mass, and energy for a mixture of ideal gases. The model solves the Reynolds averaged forms of these equations for turbulent flow. The Reynolds stresses are modeled using the linear eddy viscosity model (LEVM) (Ferziger and Peric, 2002). Ideal gas law is used for the thermodynamic model of mixture of gases. Air is modeled as compressible, moist with effective properties of the mixture of dry air and water vapor.

Density difference in the vertical direction drives the body force. This model is suitable for flows where density of air changes significantly.

The accuracy of the results produced by a numerical solution procedure in solving the above type of governing equation directly depends on the discretization schemes employed. Accuracy is expressed in terms of the order of a Taylor series expansion used in the discretization of the differential operators in the governing equation.

The TVD (Total Variation Diminishing) scheme is a 2nd order scheme used in the present study.

### Turbulence Model

Fluidyn-PANACHE uses a modified standard  $k$ - $\epsilon$  turbulence model to solve the turbulence structures within the domain. The  $k$ - $\epsilon$  model is a two-equation linear eddy viscosity model. Fluidyn-PANACHE implementation of this model is derived from the standard high- $Re$  form with corrections for buoyancy and compressibility (Hanjalic, 2005). It solves the transport equations for turbulent kinetic energy,  $k$  and its dissipation rate,  $\epsilon$ .

### Boundary Conditions

Boundary conditions are required on the main domain boundary, the ground, and on obstacles. The top boundary is treated as an outflow boundary. The lateral boundaries of the domain are treated as inflow and outflow boundaries based on the direction of the wind with respect to the domain boundary. At the inflow boundary, velocity, temperature and turbulence vertical profiles are specified. Pressure is extrapolated from inside the domain. Species concentrations are set according to the specified background concentrations.

### Wind profile

The vertical wind profile is an important choice for the Atmospheric Boundary Layer definition. In this study, a log-law profile based on Monin–Obukhov (M–O) similarity theory has been used to parametrize the inflow boundary condition representative of the atmospheric stability condition: unstable, neutral and stable.

### Turbulence profile

Fluidyn-PANACHE has many parametrizations for inlet turbulence profiles. The profile selected for this study is a semi-empirical model based on similarity theory and measurements (Han & al., 2000).

## STATISTICAL MODEL PERFORMANCE EVALUATION METHODS

The performance of the CFD model Fluidyn-PANACHE against experimental data is evaluated both qualitatively by results analysis and quantitatively using the standard statistical measures (Chang and Hanna, 2004) such as, Normalized Mean Square Error (NMSE), Fractional Bias (FB), Geometric Mean bias (MG), Geometric Variance (VG) and Factor of Two (FAC2).

For an acceptable model performance, the values of the statistical measures must be in the following bounds.

**Table 1.** BOOT statistical parameters

Parameter	Interval of acceptance	Ideal value
FB	[-0.3 ; 0.3]	0
MG	[0.7 ; 1.3]	1
NMSE	<4	0
VG	<1.6	1
FAC2	Above 50%	100%

## RESULTS AND PERFORMANCE EVALUATIONS

### Desert Tortoise series 1, 2, 3, and 4

Four large scale pressurized liquid ammonia experiments were conducted during the Desert Tortoise Series in 1983 at the Liquefied Gaseous Spill Test Facility in Nevada (Hanna & al., 1993 and the REDIPHEM database package, 1995).

The experiments were carried out with an 81 to 133 kg sec<sup>-1</sup> horizontal flash boiling jet source and the duration was from 1 to 8 minutes. The wind speeds were fairly strong from 4.5 to 7.4 m.s<sup>-1</sup>, and the air was dry and hot with 30 –33 °C and 10 –21% relative humidity.

The release configuration for the data assumes a gaseous release, with specific release geometry and flow outlet estimated for a fully expanded virtual jet source at sonic speed. To stay inside the usual practice in industrial assessment cases, the mesh was not further refined.

The maximum experimental concentrations at each range in the downwind direction are considered for the model evaluation.

The table below shows the comparison for each measurement point in volume mass fraction with respect to the numerical results. In most of the cases, the results are in good agreement with experimental results. The results at 100 m are close to experimental while at 800 m they are slightly under predicted at the ground level.

**Table 2.** Comparison of numerical data with experimental data for Desert Tortoise series (Vol %)

Distance (m)	Z (m)	DT1		DT2		DT3		DT4	
		Exp.	Num.	Exp.	Num.	Exp.	Num.	Exp.	Num.
100	1.0	6.33	6.11	10.958	7.50	9.72	7.75	8.43	7.99
100	2.5	4.78	5.17	7.12	6.54	7.98	6.71	7.09	6.85
100	6.0	-	2.99	3.78	4.31	4.03	4.37	3.89	4.54
800	1.0	1.1	1.09	1.86	1.42	1.56	1.46	2.09	0.96
800	3.5	0.96	0.96	1.71	1.39	1.31	1.31	1.42	0.99
800	8.5	0.29	0.67	0.40	1.20	0.22	0.96		

All the values of FB, MG, NMSE and VG are within the acceptable range as defined in Table 1 and the CFD model predicts respectively 80%, 83%, 83% and 67% points within a FAC2 for the four tests DT1, 2, 3 and 4.

### Burro series 3 and 5

The Burro Series of liquefied Natural Gas (LNG) spill experiments were performed at the Naval Weapons Center, China Lake, California during the summer and fall of 1981 (Hanna & al., 1993). Figure 1 represents the computational domain considered Burro tests 3 and 5. First, the undulations near the source are considered.

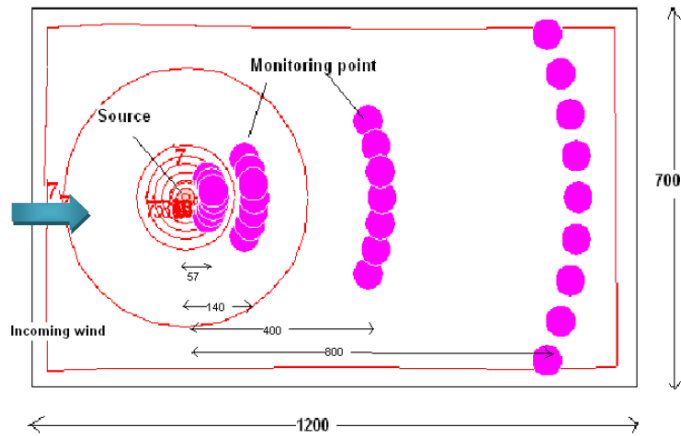


**Figure 1.** Site features and dimensions for Burro series (m)

Concentration measuring devices are located at 57, 140, 400 and 800 m distance from the source. The meteorological data included wind, turbulence and temperature measurements to describe the turbulent atmospheric boundary layer. For modelling purposes, total mass flow rate from the pool is assumed to be equal to release rate as pool spreading and vaporization reach equilibrium with the release rate.

The following figures show the area occupied by instantaneous cloud contours with the scale of 1%, 2%, 5%, 10% and 15% over the domain at 1m height. These areas are calculated at 50s and 190s and are compared to the experiment data (area of cloud contour). The modelled results are slightly under-predicting for 1% and 2% and over predicting for 5%, 10% and 15%.

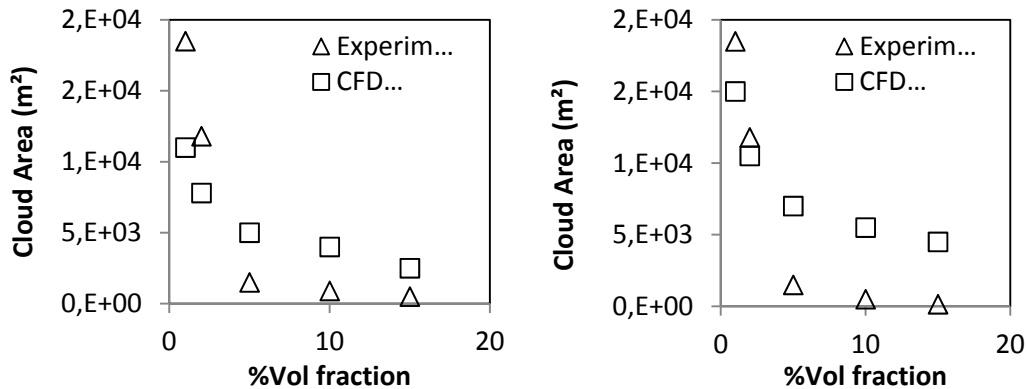


**Figure 2.** Comparison of surface area with experimental results at 50 secs (left) and at 190 secs (right) of BU5 case

The comparison of modeled and experimental results of shortest (1s) and longest averaging time for BU3 (100s) and BU5 (130s) is shown in Table 3. The shortest averaging time results are under-predicted because of the RANS model used in the CFD model while the longest averaging time results are over-predicted at 57 m and slightly under-predicted at 140 m. The longest averaging time results at 140 m for BU5 experiment shows very good agreement. The unsteady solution predicts more than 50% points within factor of two for the both experiments.

**Table 3.** Comparison for maximum arc-wise LNG concentration (ppm) for shortest and longest averaging from different downwind distances at 1m height

Distance (m)	BU3				BU5			
	Longest (100s)		Shortest		Longest (130s)		Shortest	
	Exp.	Mod.	Exp.	Mod.	Exp.	Mod.	Exp.	Mod.
57	79053	125363	224380	126245	68925	137401	190410	137854
140	63731	33581	8 9850	33749	49913	47174	96000	47377

**CO2PIPETRANS series T5DS1, T8 DS1, T11DS1 and T14DS2**

To investigate and fill the identified knowledge gaps and to validate computer dispersion models for liquid and supercritical CO2 releases, BP set up a research project in 2006. This section covers the validation of dispersion results obtained by PANACHE against the experimental results for both high-pressure cold release and high-pressure supercritical release.

**Table 3.** Discharge data for T5DS1 and T11DS1 cases

Discharge data	T5	T11
Inlet pressure (bar)	156.9	82.2
Inlet temperature (°C)	12.5	18.4
Orifice diameter (mm)	25.4	12.7
Steady/transient	steady	steady
Mean mass flow rate (kg/s)	40.7	7.1

In the frame of this validation case, source term was modeled as Pseudo source (temperature, pressure, velocity...).

For many sensors, concentrations levels are not constant but vary significantly with time over the period of CO2 injection. Steady state simulations with RANS approach gives unique value at converged state.

**Steady cases T5DS1 and T11DS1**

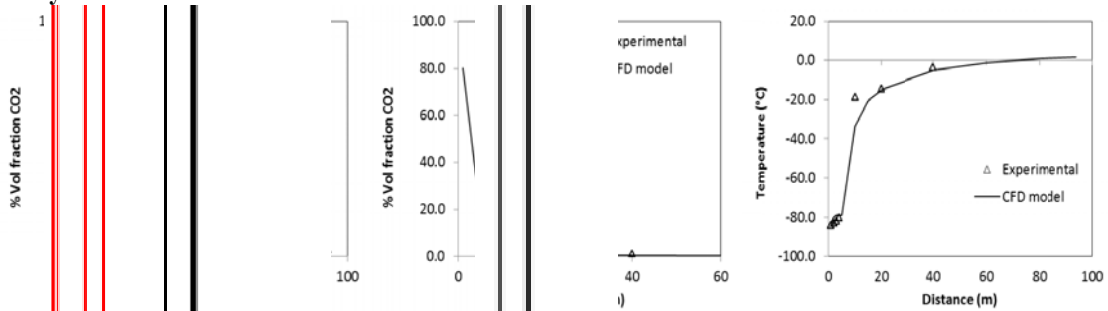


**Figure 3.** Concentration of CO2 at 1m height from the ground along the axis of leak at different downwind distances from the source for T5DS1 (left) and T11DS1 (center) (sensors accuracy ±1%) - Temperature at 1m height from the ground along the axis of leak at different downwind distance from the source for T5DS1 (right)

The CO2 concentration is well predicted in the near and far field from the release section.

**Transient cases T8DS1 and T14DS2**

Time varying mass flow rate at the source point has been modelled. The results obtained for hot T08DS1 and cold T14DS2 releases are shown in Figure 4 for concentration comparison with the experimental results.

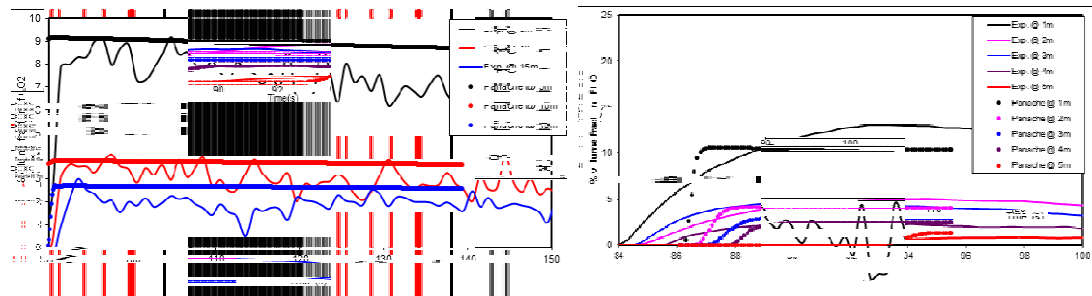


**Figure 4.** Temporal concentration of CO2 at 1m height along the axis of leak at different downwind distances from the source for T8DS1 (left) and T14DS2 (right) (sensors accuracy ±1%)

### Porton down series 26 and 29

Forty two moderate scale ( $40 \text{ m}^3$ ) Freon ( $\text{CCl}_2\text{F}_2$ ) dispersion experiments “Porton Down Series” were conducted in 1976 at the Chemical Defence Establishment in Porton Down (Picknett Report, 1978). The simulation results for trial No. 26 are compared with field trials and the results of No. 29 are compared with wind tunnel results trials (Hall et al, 1982).

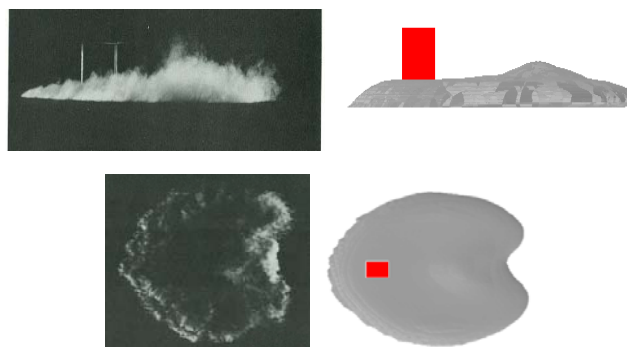


Figure 5. CFD modeled and wind tunnel modeled top view visualisation comparison for trial 29 at 4.3 sec

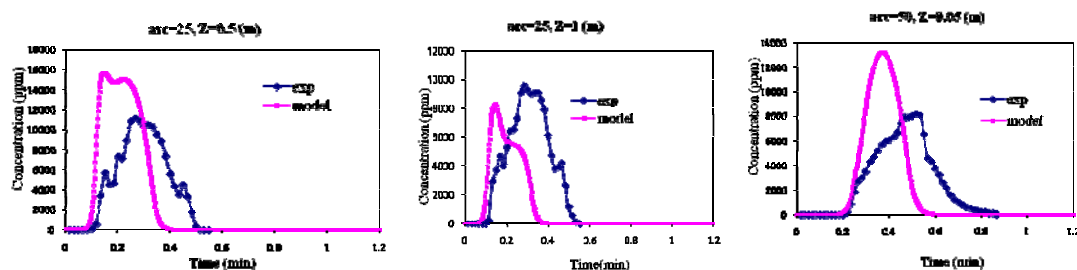


Figure 6. Concentration time series comparison plot for trial no 26

In general, the simulations results show good agreement with field trials at the different sensor locations. The cloud arrival times are also in very good agreement but cloud departure times are slightly under-predicted.

### CONCLUSION

The present paper shows the CFD model Fluidyn-PANACHE evaluation in four dense gases releases experiments: Desert Tortoise series, Burro series, CO2PIPETRANS series, and Porton down series. The results are analyzed for maximum arc-wise concentration and standard statistical criterion.

For these experiments, the CFD model has shown good performance for all the cases. It can be used with confidence in contexts of various dense gas accidental releases.

### REFERENCES

- Duijm, N.J. and B. Carissimo, 2001: Evaluation methodologies for dense gas dispersion models. In: (ed.: M. Fingas) The handbook hazardous materials spills technology. Mc Graw-Hill, New York.
- Duijm, N.J., B. Carissimo, A. Mercer, C. Bartholome and H. Giesbrecht, 1997: Development and test of an evaluation protocol for heavy gas dispersion models. *J. Hazard. Mater.*, **56**, 273-285.
- Ferziger, J.H. and M. Perić, 2002: Computational Methods for Fluid Dynamics. Springer.
- Hall, D.J., E.J. Hollis and H. Ishaq, 1984: A wind tunnel model of the porton dense gas spill. In: (eds: Ooms, G. and Tennekes H.) Atmospheric Dispersion of Heavy Gases and Small Particles. Symposium, Delft, The Netherlands August 29 – September 2, 1983. Springer.
- Han, J., S.P. Arya, S. Shen, and Y-L Lin, 2000: An Estimation of Turbulent Kinetic Energy and Energy Dissipation Rate Based on Atmospheric Boundary Layer Similarity Theory. NASA/CR-2000-210298.

- Hanjalic, K., 2005: Turbulence And Transport Phenomena: Modelling and Simulation. Turbulence Modeling and Simulation (TMS) Workshop, Technische Universität Darmstadt.
- Hanna, S.R., D.G. Strimaitis and J.C. Chang, 1993: Hazard Response Modeling Uncertainty (A Quantitative Method). Volume 2. Evaluation of Commonly Used Hazardous Gas Dispersion Models. SIGMA RESEARCH CORP WESTFORD MA.
- Kohout, A. J., 2011: Evaluation of fire dynamics simulator for liquefied natural gas vapor dispersion hazards (Doctoral dissertation).
- Mohan, M., T.S. Panwar and M.P. Singh, 1995: Development of dense gas dispersion model for emergency preparedness. *Atmos. Environ.*, **29**, 2075-2087.
- Picknett, R.G., 1978: Field Experiments On The Behaviour Of dense clouds, main report. Report 1 and 2 (d), 3(b),(c), Chemical Defence Establishment.
- Rediphem database, 1995: A Collection of Data from Dense Gas Experiments. Morten Nielsen and Søren Ott, Risø Laboratory Report: Risø-R-845(EN), ISBN 87-550-2113-1.
- Sklavounos, S. and F. Rigas, 2004: Validation of turbulence models in heavy gas dispersion over obstacles. *J. Hazard. Mater.*, **208**, 9-20.
- Touma, J.S., W.M. Cox, H. Thistle, J.G. Zapert, 1995: Performance Evaluation of Gas Dispersion Models, *J. Appl. Meteorol.*, **34**, 603-615.

**17th International Conference on  
Harmonisation within Atmospheric Dispersion Modelling for Regulatory Purposes  
9-12 May 2016, Budapest, Hungary**

---

**AN AIR QUALITY CFD MODEL PERFORMANCE IN COMPLEX ENVIRONMENT  
WITH EMU OBSERVATIONS**

*Liying Chen<sup>1</sup>, Pramod Kumar<sup>2</sup>, Malo Leguellec<sup>1</sup>, Amir-Ali Feiz<sup>2</sup>*

<sup>1</sup> Fluidyn France, 7 boulevard de la Libération, 93200 Paris, France

<sup>2</sup> Université d'Evry-Val d'Essonne, LMEE, 40 rue du Pelvoux, 91020 Evry, France

**Abstract:** In the frame of this work, the three-dimensional (3-D) computational fluid dynamic (CFD) model fluidyn-Panache dedicated to the dispersion of toxic and hazardous gases around buildings and in geometrically complex chemical sites has been evaluated. The evaluation exercise is based on the following wind tunnel experiments and tracer data from the EMU project (Evaluation of Modelling Uncertainty): A1 (a release from an open door in the courtyard area of a simple L-shaped building on a flat ground) and C1 (a continuous, release over larger distances around an industrial site featuring numerous buildings and complex local topography). A detailed analysis with statistical measures shows that the performance of the fluidyn-PANACHE model against wind tunnel observations with both cases of EMU project is well within the acceptable bounds of statistical measures for air quality applications. The CFD model with three cases A1 and C1 predicts respectively 66% and 67% of the total concentrations within a factor of two and shows the over-prediction tendency at the receptors near to the source but under-prediction at far away from the source. This study critically examines the real predictive capability of the CFD model fluidyn-PANACHE to apply it in emergency contexts of an accidental or deliberate airborne release in complex environments.

**Keywords:** *CFD modeling, EMU experiment, fluidyn-PANACHE, Model evaluation, Urban dispersion modelling*

## **INTRODUCTION**

In industrial safety and environment programme, near-field (<10km) dispersion of toxic and hazardous gases near buildings and in a complex chemical site are often predicted with CFD dynamic codes. A CFD model solves the Navier–Stokes equations using a small grid size (of the order 1m or even less) (Hanna et al., 2004) over complex terrain. With rapid advances in computer hardware and methods, CFD models provide now accurate wind flow and dispersion modelling around buildings and other structures in urban areas or industrial areas for any kind of release scenarios. Compared with simple Gaussian dispersion model or other analytical approximations, the CFD model efficiently predict the obstacles influence on wind patterns and cloud shapes (Kumar et al., 2015). Nevertheless, the CFD model evaluation against experimental datasets is one critical point to estimate its capability to provide reliable and valuable informations in emergency planning or chronic impact assessment. Many CFD results were successfully validated against experimental field data (Hanna et al., 2004; Milliez and Carissimo, 2007; Labovský and Jelemenský, 2010). The current paper concerns the fluidyn-PANACHE CFD model evaluation. PANACHE uses physical models and deterministic solutions that are adapted to any kind of release scenarios, complex environments and pollutant characteristics. Here, the evaluation is based on extensive field observations involving tracer gas releases in a wind tunnel from the ‘Evaluation of Modelling Uncertainty’ (EMU) project. EMU provides an unique dataset for evaluation of dispersion models around buildings and over complex topography (Hall, 1997). To demonstrate the PANACHE model’s capabilities to simulate the flow and dispersion patterns in the near field but also at larger distances, the single L-shaped building case and the real industrial site case have been selected.

## **DESCRIPTION OF THE EMU EXPERIMENT**

The ‘Evaluation of Modelling Uncertainty’ (EMU) project funded by the European Commission involves the evaluation of the spread in results due to the way that CFD codes are used and the accuracy of such codes in complex gas dispersion situations. The project consisted in 14 test cases of industrial scenarios were chosen, which ranged from single building on flat terrain scenarios right through to cases associated with a specific, complex topography industrial site. Stage A comprised three cases, A1 to A3, involving a

simple building on flat ground, neutral atmosphere and isothermal conditions were considered. Stage B incorporated increases in complexity of the geometry (i.e. terrain, obstacles and number of buildings), release conditions (i.e. two-phase and non-isothermal releases) and meteorology (i.e. stability and wind speed). Stage C concerned an actual industrial site, featuring numerous buildings and complex local topography. Experiments were performed at the University of Surrey (Cowan, Castro et Robins, 1995) in a large stratified wind tunnel (20m x 3.5m x 1.5m) at a model scales between 1/133 and 1/250. Continuous jet releases of dense, buoyant and neutrally-buoyant gases have been simulated in neutral or stable atmospheres. In the present work, two test cases A1 and C1 of EMU project have been simulated using commercial software package fluidyn-PANACHE.

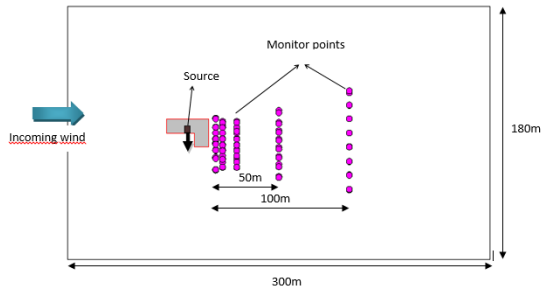


Figure 1. Site features and dimension (Case A1)

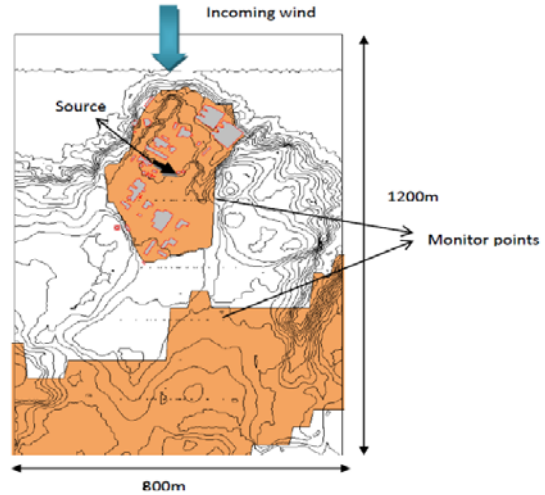


Figure 2. The site features and dimension (Case C1)

## SOLUTION AND RESULTS OF EVALUATIONS

### EMU project simulation, Case A, Phase I (Case A1)

Case A1 of EMU project entailed the numerical simulation of a passive release from an L-shaped building (see Figure 1) located on a flat surface into an atmospheric boundary layer flow. Neutral ambient conditions were assumed and the EnFlo wind-tunnel was modelled at the University of Surrey. In this case, the concentration predictions at a few cross-wind locations on the cross-section at five distances downwind of the lee edge of the L-shaped building were compared ( $x_1/H = 0.5, 1, 2, 5, 10$ ;  $H$  is the height of the building), corresponding to the numerical simulation sensor positions, are compared with the experimental data. Also, the approximate dimensions of the predicted recirculation zones are compared with observations. Figure 1 represents the computational domain considered for EMU project Case A1. The dimensions have been set as follows: 300 m long, 180 m wide and 120 m high. The distance between the source and the inlet flow boundary condition is 85m and the source is located in the middle of the width of the domain. A mixture of 2.96% ethylene ( $C_2H_4$ ) in a nitrogen balance was used for the source gas, and was essentially neutrally stable. The properties of the source are listed in Table 1.

Table 1. Source data for the EMU project: Case A1

Type of source	Exit velocity (m/s)	Chemical species	Source surface (m <sup>2</sup> )	Height of source (m)	Mass flux (kg/s)	Temperature (°C)	Release duration (s)
General	1.0	C <sub>2</sub> H <sub>4</sub> (2.96%) N <sub>2</sub> (97.04%)	20	2.5	23.68	25	Continuous

The Table 2 contains the comparison of the maximum concentrations for each measurement cross-section in volume fraction with respect to the numerical results. In general, the results are in good agreement with tunnel observations. They are slightly over-predicted where the heights are less than 10m, but slightly under-predicted at the heights more than 10m. The prediction may be assessed, which plot the simulated data against the experimental profiles at  $x_1/H=1, 2, 5$  and 10 (not represented here). Close to the building

( $x_1/H \leq 2$ ,  $z/H \leq 1$ ), the CFD plume is slightly shallower than its experimental counterpart. However, agreement between the simulated and experimental data at sensor positions is very good at a given distance from the source. Figures 3 show the predicted and observed average concentrations comparison for 256 measurement points of case A1 shows good agreement with the wind tunnel observations. One can observe a slight over-prediction tendency in the near field of the release at some locations. The overall simulated concentration predicts 66% of points within FAC2 (Case A1). Also, values of FB, MG, NMSE, NAD and FAC2 are within the acceptable range for each vertical plan.

**Table 2.** Comparison of modeled and experimental results of ground-level maximum concentration (Case A1) ( $C/C^*$ )

$x1/H$	$z/H$	Exp./Num.
0.50	0.13	4.10E-01
0.50	0.33	4.33E-01
0.50	1.03	6.79E-01
0.50	1.45	1.67E+00
0.50	1.93	1.67E+00
1.00	0.16	4.08E-01
1.00	0.67	6.24E-01
1.00	1.02	8.10E-01
1.00	1.99	1.81E+00
2.00	0.11	4.45E-01
2.00	0.66	5.96E-01
2.00	1.03	9.71E-01
2.00	1.99	1.77E+00
5.00	0.34	6.80E-01
5.00	0.98	9.66E-01
5.00	1.97	1.66E+00
10.00	0.16	9.31E-01
10.00	0.98	1.64E+00
10.00	3.00	1.26E+00

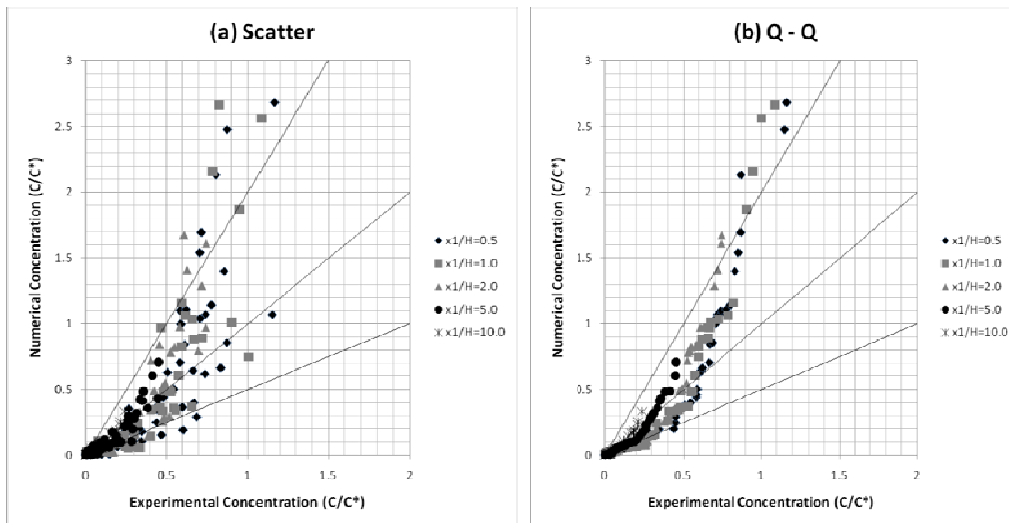


**Figure 3.** (a) Scatter and (b) quantile-quantile (Q-Q) plots between the predicted and observed average concentrations for 256 points of Case A1. The middle solid line is one-to-one line between observed and simulated concentrations whereas the dotted lines correspond to factor of two.

### EMU project simulation, Case C, Phase I (Case C1)

Case C1 of EMU project entails a continuous, passive jet release from the side of a building within a real chemical site. The surrounding terrain is complex, with steep hills, trench-like features and cliffs at the edge of the sea. The site comprises a large number of irregularly shaped buildings, most of which however are conveniently aligned with each other. Cowan (1996) reported the 4 categories of roughness in the domain: sea, land, village/town and industrial site. The atmospheric stability classes encountered are neutral and stable. In this case, we take our origin to be at sea-level, directly below the source position. The source is thus centred on (0, 0, 18.7) m. Three types of concentration data (126 observations) were recorded: cross-stream profiles at ground-level and at  $(Z-Z_g)/H \sim 2-3$  ( $Z_g$  is the height of ground-level), and vertical profiles through the ground-level maxima. A number of other ground-level concentration measurements were also made.

**Table 3.** Statistical performances measures of the average concentrations for each vertical plan (Case A1)

Criteria	FB	MG	NMSE	NAD	FAC2
<b>Ideal value</b>	0	1	0	0	100%
<b>Acceptable interval</b>	[-0.3 ; 0.3]	[0.7 ; 1.3]	<4	<0.3	>50%
$x_1/H = 0.5$	-0.26	1.22	1.19	0.27	64%
$x_1/H = 1.0$	-0.25	1.21	1.11	0.28	69%
$x_1/H = 2.0$	-0.15	1.29	0.72	0.26	69%
$x_1/H = 5.0$	0.05	1.38	0.21	0.16	63%
$x_1/H = 10.0$	0.13	1.63	0.17	0.14	65%

Figure 2 represents the computational domain of EMU project Case C1. The domain dimensions have been set as 800m long, 1200m wide and 200m high.

**Table 4.** Source data for the EMU project: Case C1

Type of source	Exit velocity (m/s)	Chemical species	Height of source (m)	Mass flux (kg/s)	Temperature (°C)	Jet direction
Point	7.5	C2H4 (77.3%) N2 (22.7%)	2.0	5.46	15	Horizontal 327.5°

The product released of Case C1 is a mixture of 77.3% by volume C2H4 in N2, giving a mixture density ratio of  $\alpha = 1.0$ . The release of C1 is modelled as four point sources. Mass flux, release temperature, release duration, exit velocity and emission direction have been considered as inputs for point model and assumed constant for the release duration. The source characteristics are tabulated on Table 4. Table 5 shows the comparison of modeled and experimental results of ground-level concentration maximum. It is observed that it shows a good comparison with experimental results. The experimental and numerical results for cross-stream profile at ground-level and at  $(Z-Z_g)/H = 3.6$  are slightly over-predicted at ground-level while they are slightly under-predicted at  $(Z-Z_g)/H = 3.6$  (not represented here). The vertical concentration profiles in the near-field and in the far-field for  $Y/H = 6.3$  and  $5.0$  have over-prediction tendency at receptors near to the ground-level, however, they are under-predicted at the higher height (not represented here). Accordingly, all performance measures are calculated for each cross-stream profile and each vertical profile separately. The computed statistical indices at each profile are given in Table 6. The variation of FB shows that the extent of under-prediction for each profile and ground-level maxima. Case C1 predicts 66%, 56%, 69%, 75% and 100% points within a FAC2 for cross-profile ground-level and  $(Z-Z_g)/H = 3.6$ , vertical profile  $Y/H = 6.3$  and  $5.0$  and ground-level maxima respectively. Also, it predicts 67% of points within FAC2 for the overall simulated concentrations. The simulated averaged concentrations for all 126 observations are presented in form of a scatter plots (Figure 4(a)) and a Q - Q plot (Figure

4(b)). In the scatter plot (Figure 4(a)), it is observed that the simulated averaged concentrations by the CFD model have good agreement with the observations. The simulated higher averaged concentrations at the receptors near to the source are close to one-to-one line; however, comparably more scatter is observed for lower concentrations at far away from the source. This trend of the predicted averaged concentrations is more visible in Q-Q plot (Figure 4(b)) that shows a comparison of the concentration distributions of simulated and observed concentrations.

## CONCLUSIONS

This work presents the 3-D CFD simulations for near-field dispersion of toxic and hazardous gases near buildings and in a geometrically complex chemical site. A CFD model fluidyn-PANACHE is evaluated using two case tests of EMU project: A1 and C1, which ranged from single building on flat terrains right through to case associated with a specific, complex topography industrial site. The simulation was performed in a neutrally stable atmosphere. Quantitative performance measures are used to analyze the performance of the CFD model simulations in 2 cases of EMU project. The overall simulated concentration of case A1 predicts 66% of points within FAC2 for 256 observations. The scatter plots show also good agreement with the wind tunnel observations but the over-prediction tendency at the heights close to ground level. The values of FB, MG, NMSE and VG are within the acceptable range for each vertical plan  $x_i/H=0.5, 1.0, 2.0, 3.0, 5.0$  and  $10.0$ . The simulated results of case C1 shows 100% points within a FAC2 for the ground-level maximum concentrations. Comparison of measured and simulated concentrations for cross-profiles and vertical profiles in the near-field and in the far-field shows the over-prediction tendency at the receptors near to the source but slight under-prediction at far away from the source.

**Table 5.** Comparison of modelled and experimental results of ground-level maximum concentration (Case C1) (C/C\*)

<b>X/H</b>	<b>(Z-Zg)/H</b>	<b>Exp./Num.</b>
5.5	5.0	0.769
11.0	5.6	0.764
11.0	5.1	0.581
19.5	6.0	0.646
30.0	6.3	0.733
30.0	7.0	0.906
37.5	7.0	1.008
45.0	6.8	0.878
45.0	7.0	1.019
56.3	7.0	1.017
67.5	6.8	0.931
67.5	7.0	1.079

**Table 6.** Statistical performances measures of the average concentrations for each profile (Case C1)

<b>Criteria</b>	<b>FB</b>	<b>MG</b>	<b>NMSE</b>	<b>NAD</b>	<b>FAC2</b>
<b>Ideal value</b>	0	1	0	1	100%
<b>Acceptable interval</b>	[-0.3 ; 0.3]	[0.7 ; 1.3]	<4	<1.6	>50%
<b>(Z-Zg)/H=0 (ground level)</b>	-0.24	3.11	0.59	0.21	66%
<b>(Z-Zg)/H=3.6</b>	0.46	2.12	0.62	1.02	56%
<b>Y/H=6.3</b>	0.05	1.67	0.12	0.12	69%
<b>Y/H=5.0</b>	-0.14	1.32	0.21	0.17	75%
<b>Ground level maxima</b>	-0.27	0.81	-0.20	0.13	100%

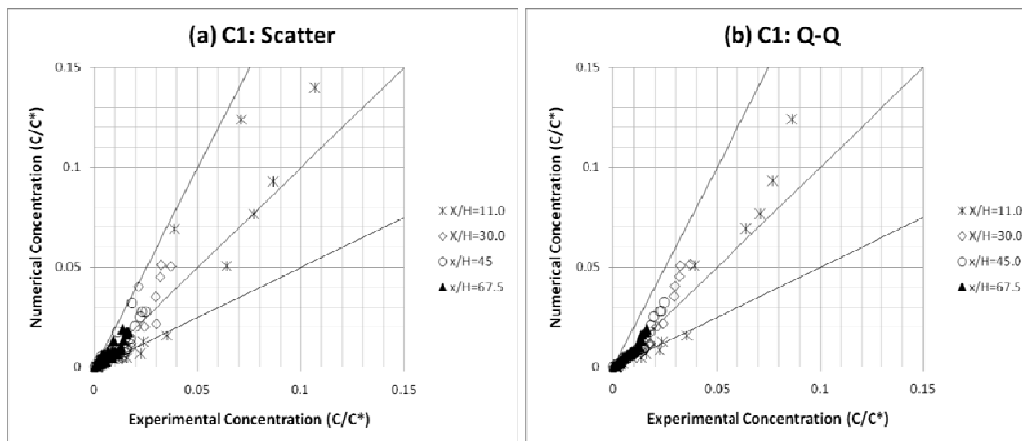


**Figure 4:** (a) Scatter and (b) quantile-quantile (Q-Q) plots between the predicted and observed average concentrations for 126 points (Case C1). The middle solid line is one-to-one line between observed and simulated concentrations whereas the dotted lines correspond to factor of two.

The values of FB, NMSE, NAD and FAC2 are within the acceptable range for each profile of case C1. Also, it predicts 67% of points within FAC2 for the overall simulated concentrations. The statistical evaluation results show an overall good performance of the CFD model in such complex environment. The CFD model fluidyn-PANACHE used in this study is well suited for the air pollution and emergency planning in industrial or urban areas. This paper is also hoped to share methodologies, contribute to CFD model comparison by collaborative efforts and improve the CFD approaches.

## REFERENCES

- Cowan, I. R., 1996. Project EMU Simulations, Stage C. Tech. rep., EnFlo Research Centre, Department of Mechanical Engineering, University of Surrey, Guildford, Surrey GU2 5XH, UK.
- Cowan, I. R., Robins, A. G., Castro, I. P., 1995. Project EMU Experimental data, Case A, Release 1; Case B, Release 3 and Case C, Release 1. Tech. rep., EnFlo Research Centre, Department of Mechanical Engineering, University of Surrey, Guildford, Surrey GU2 5XH, UK.
- Fluidyn-PANACHE, 2010. User Manual. FLUIDYN France / TRANSOFT International, version 4.0.7 Edition.
- Hall, R. C., 1997. Evaluation of Model Uncertainty (EMU)-CFD modelling of near-field atmospheric dispersion. Project EMU Final Report. Tech. Rep. WS Atkins Doc No. WSA/AM5017/R7, European Commission, WS Atkins, Woodcote Grove, Ashley Road, Epsom, Surrey KT18 5BW, UK.
- Hanna, S. R., Hansen, O. R., Dharmavaram, S., 2004. FLACS CFD air quality model performance evaluation with kit fox, must, prairie grass, and EMU observations. *Atmospheric Environment* **38**, 4675-4687.
- Kumar, P., Feiz, A.-A., Ngae, P., Singh, S. K., Issartel, J.-P., 2015. CFD simulation of short-range plume dispersion from a point release in an urban like environment. *Atmospheric Environment* **122**, 645-656.
- Labovský, J., Jelemenský, L., 2010. CFD simulations of ammonia dispersion using “dynamic” boundary conditions. *Process Safety and Environmental Protection*, **88**, 243-252.
- Milliez, M., Carissimo, B., 2007. Numerical simulations of pollutant dispersion in an idealized urban area, for different meteorological conditions. *Boundary-Layer Meteorology* **122**, 321-342.

**17th International Conference on  
Harmonisation within Atmospheric Dispersion Modelling for Regulatory Purposes  
9-12 May 2016, Budapest, Hungary**

---

**ROADSIDE HOT-SPOT ANALYSIS IN URBAN AREA**

*Weiping Dai<sup>1</sup>, Qiguo Jing<sup>1</sup>, Tiffany Stefanescu<sup>2</sup>, and Brian Holland<sup>1</sup>*

<sup>1</sup>Trinity Consultants Inc., Dallas, Texas, U.S.A.

<sup>2</sup>Trinity Consultants Inc., Charlotte, North Carolina, U.S.A.

**Abstract:** CALINE3-based models (CALINE4, CAL3QHC, and CAL3QHCR) are currently recommended by U. S. EPA for roadside hot-spot analysis. Recently, U. S. EPA proposes to remove CALINE3-based models for mobile source applications and replace it with AERMOD. We evaluate air dispersion models, AERMOD, CALINE4, and RLINE, to estimate concentrations of PM<sub>2.5</sub> for such analysis in downtown Los Angeles with high-rise buildings. The model performance indicates that AERMOD and RLINE provides an adequate description of roadside PM<sub>2.5</sub> concentrations, while CALINE3 generally overestimates the concentrations of PM<sub>2.5</sub>.

**Key words:** *Roadside Hot-Spot Analysis, AERMOD, Caline3, Urban Area*

## **INTRODUCTION**

Roadside hot-spot analysis assesses impacts of transportation emissions from mobile sources on local air quality of carbon monoxide (CO), lead (Pb), nitrogen dioxide (NO<sub>2</sub>) and particulate matter (PM). Potential hot-spot analysis is one aspect of the State Implementation Plan (SIP) project-level conformity determinations, which is required by the Clean Air Act (ACC) in nonattainment or maintenance areas. It is also required for regional transportation plans (RTP), transportation improvement programs (TIP) and transportation project development/modification by transportation conformity rules and National Environmental Policy Act (NEPA) process.

The current version of U. S. EPA's Guideline on Air Quality Models, published as Appendix W to 40 CFR Part 51 (Appendix W) in 2005, addresses modelling mobile sources, with specific recommendations for each criteria pollutant. For CO, CAL3QHC (U. S. EPA, 1995) is recommended for screening and CALINE3 (Benson, 1984) for free flow situations. For Pb, CALINE3 and CAL3QHCR (Eckhoff and Braverman, 1995) are identified for highway emissions, while for NO<sub>2</sub>, CAL3QHCR is listed as an option. No models for mobile emissions are explicitly identified for PM or SO<sub>2</sub>, though CALINE3 is listed in Appendix A as appropriate for highway sources for averaging times of 1-24 hours. CALINE3 was developed in the late 1970's using P-G stability classes as the basis for the dispersion algorithms. CALINE3-based models used in quantitative hot-spot analyses have not undergone major updates since 1995 and have limitations in simulating air quality impacts of complex urban roadway networks. Zhang and Gao (2009) shows the increased turbulence due to vehicles and roads; Schulte and Venkatram (2013) shows that infinitely long roadside sound barriers increase vertical dispersion, induce vertical mixing and loft the emissions above the barrier, and Schulte et al. (2015) indicates the rapid vertical dispersion due to the presence of roadside buildings.

The recent proposed revisions to Appendix W include the proposal to remove CALINE3 for mobile source applications and replace it with AERMOD (Cimorelli et al., 2005), which incorporates air dispersion based on planetary boundary layer turbulence structure and scaling concepts, and includes treatment of both surface and elevated sources, and both simple and complex terrain. In addition, the LINE and AREA source options in AERMOD implement a full numerical integration of emissions across the LINE and AREA sources. This proposed replacement is supported by two model performance comparison studies conducted by U. S. EPA (2015). One evaluates the CALTRANS 99 field study conducted along Highway 99 outside Sacramento, CA; the other evaluates the Idaho Falls, ID, field study conducted in an open field with a barrier between the line source and receptors. Both evaluations indicate

that AERMOD performs better than CALINE4. However, both field studies do not represent either a suburban area with low building density or deep urban canyons with dense urban environments.

This paper compares AERMOD with CALINE3-based models (CALINE4) and RLINE (Snyder and Heist, 2013) using a field study conducted in downtown Los Angeles in 2008. The evaluation supports the proposed replacement when AERMOD is executed with onsite meteorological data.

**DESCRIPTION OF FIELD STUDY**

Figure 1 refers to a 400 m × 350 m area in downtown Los Angeles (LA) covering high-rise buildings and skyscrapers. The heights of the buildings vary from 5 to 187 m. The streets are three-lane one-way roadways. There are two street parking lanes on both sides. The street width is about 13 m. The field measurements were conducted during the weekdays from June 19, 2008 to August 1, 2008. Experiments were conducted for three days. Meteorological measurements lasted 12 hours for each day from morning (about 7:00 a.m.) to late afternoon (about 7:00 p.m.). DustTraks covered the morning (7:00 a.m. ~ 9:00 a.m. local time), evening (5:00 p.m. ~ 7:00 p.m. local time) commute and lighter mid-day (11:00 a.m. ~ 1:00 p.m. local time) traffic. DustTraks collected 1 Hz PM<sub>2.5</sub> for 6 hours. Traffic flows were recorded using digital cameras and manually counted afterwards (Pan et al., 2013). The averaged vehicle PM<sub>2.5</sub> emission rate among different fleet mixes was calculated based on EMFAC 2014 (CARB, 2014a). The fugitive PM<sub>2.5</sub> emission rate from paved roads was calculated based on CARB’s miscellaneous process methodology 7.9 (CARB, 2014b). The resulting PM<sub>2.5</sub> emission rate is 0.16 g/km.

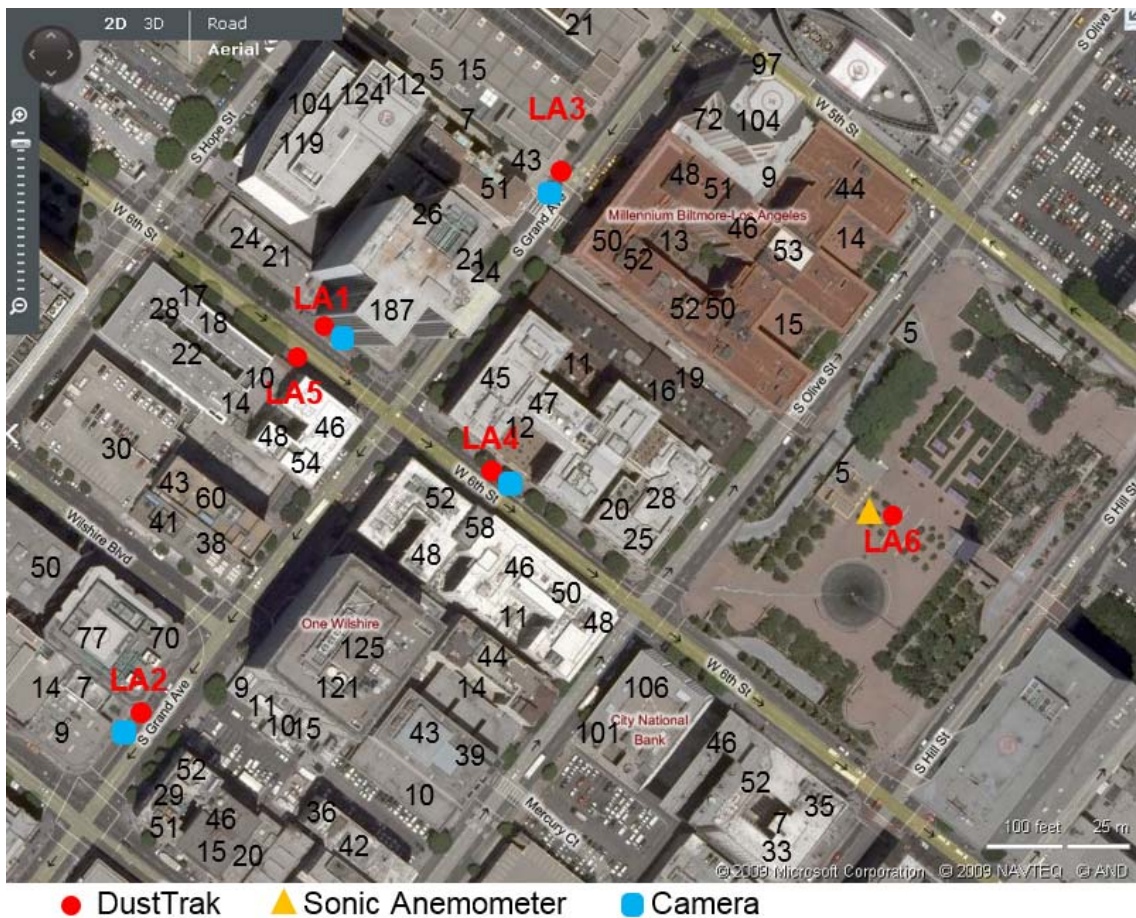


**Figure 1.** Site distribution in high-rise settlement-Los Angeles. The numbers marked on buildings show height in meters (Pan et al., 2013)

## MODEL EVALUATION

Figure 2 shows the Quantile-Quantile (Q-Q) plot for the downtown LA field study. Q-Q plots are typically used to show model performance for ranked concentrations, which do not pair in time and location. It can be seen from Figure 2 that CALINE4 with onsite meteorological data generally overestimates the PM<sub>2.5</sub> concentrations for all concentrations ranges. This could be an indication that CALINE4 does not provide enough vertical mixing since CALINE4 does not require an input for standard deviation of vertical wind speed ( $\sigma_w$ ). AERMOD with onsite meteorological data, especially the measured  $\sigma_w$ , appears to perform the best of all the dispersion models, being closest to the 1:1 line. AERMOD with nearby airport (LAX) meteorological data, however, has the worst performance over all concentration ranges. RLINE with onsite meteorological data has similar performance to AERMOD with onsite data, but it overestimates the highest concentration substantially. All dispersion models with onsite data tend to overestimate the high-end concentrations.

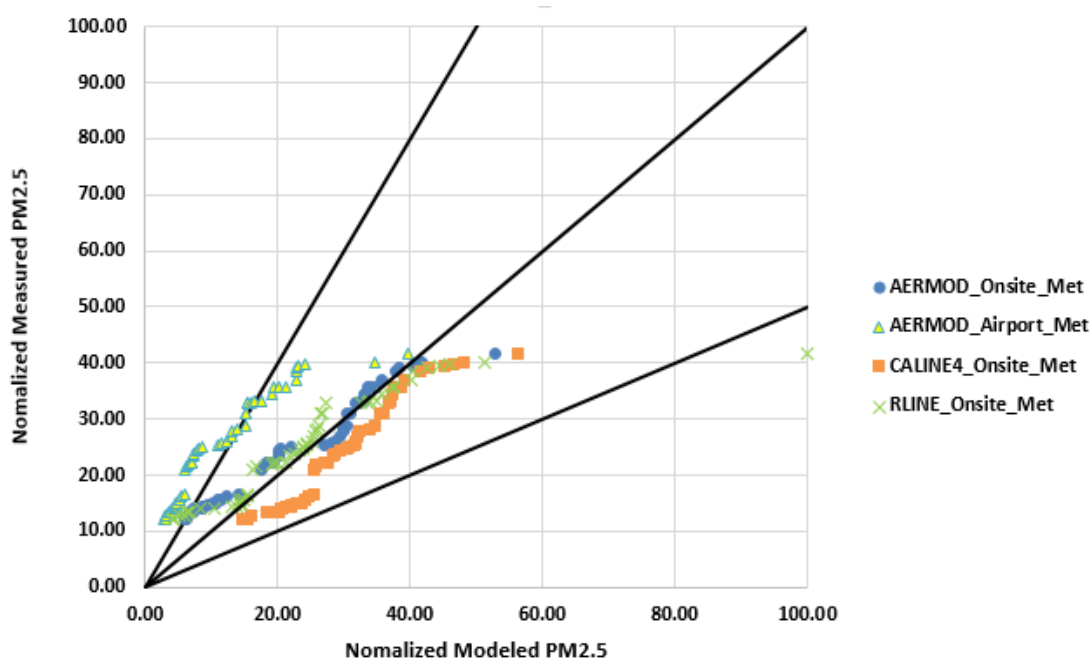


Figure 2. Q-Q Plot for Downtown LA Field Study

## SUMMARY

In response to the proposed replacement of CALINE3 with AERMOD in Appendix W, this paper compares air dispersion models' performance using a field study conducted in downtown LA, a typical high-rise urban environment. The results support the proposed replacement when onsite meteorological data is used as inputs to AERMOD.

## ACKNOWLEDGEMENTS

We thank Professor Marko Princevac and his research team for providing us with the data collected in downtown LA.

## REFERENCES

- Benson, P, 1984: CALINE4--a dispersion model for predicting air pollutant concentrations near roadways, California Department of Transportation, Sacramento, CA, FHWA-CA-TL-84-15.
- CARB, 2014a: EMFAC 2014 User Guide; Mobile Source Analysis Branch, Air Quality Planning & Science Division.
- CARB, 2014b: Miscellaneous Process Methodology 7.9 – Entrained Road Travel, Paved Road Dust.

- Cimorelli, A. J, S. G. Perry, A. Venkatram, J. C. Weil, R. Paine, R. B. Wilson, R. F. Lee, W. D. Peters, R. W. Brode, 2005: AERMOD: A Dispersion Model for Industrial Source Applications. Part I: General Model Formulation and Boundary Layer Characterization. *J. Appl. Meteorol.*, **44**, 682-693.
- Eckhoff, P. and T. Braverman, 1995: Addendum to the User's Guide to CAL3QHC Version 2.0 (CAL3QHCR User's Guide), OAQPS, RTP, NC.
- Pan, H, C. Bartolome, E. Gutierrez, M. Princevac, R. Edwards, M. G. Boarnet, D. Houston, 2013: Investigation of roadside fine particulate matter concentration surrounding major arterials in five Southern Californian cities. *J. Air Waste Manage. Assoc.*, **63**, 482-498.
- Schulte, N. and A. Venkatram, 2013: Effects of Sound Barriers on Dispersion from Roadways, South Coast Air Quality Management District.
- Schulte, N, S. Tan, and A. Venkatram, 2015: The ratio of effective building height to street width governs dispersion of local vehicle emissions. *Atmos. Environ.*, **112**, 54-63.
- Snyder, M. G. and D. K. Heist, 2013: User's Guide for R-Line Model Version 1.2: A Research Line Source Model for Near-Surface Releases, U. S. EPA/ORD/NERL, RTP, NC, MD-81.
- U. S. EPA, 1995: User's guide to CAL3QHC version 2.0: A modeling methodology for predicting pollutant concentrations near roadway intersections (revised), OAQPS, RTP, NC, EPA-454/R-92-006R.
- U. S. EPA, 2015: Technical Support Document (TSD) for Replacement of CALINE3 with AERMOD for Transportation Related Air Quality Analyses, OAQPS, RTP, NC, 2015: EPA- 454/B-15-002.
- Zhang, K. M. and H. O. Gao, 2009: Development of Advanced Modeling Tools for Hotspot Analysis of Transportation Emissions, University Transportation Research Center, Region 2, Report No. 49777-22-19.

**17th International Conference on  
Harmonisation within Atmospheric Dispersion Modelling for Regulatory Purposes  
9-12 May 2016, Budapest, Hungary**

---

**VALIDATION OF THE PERFORMANCE OF METEOROLOGICAL FORECASTS IN FINE  
SPATIAL AND TEMPORAL RESOLUTION DESIGNED AS AN INPUT FOR DISPERSION  
MODELS**

*Primož Mlakar<sup>1</sup>, Dragana Kokal<sup>1</sup>, Boštjan Grašič<sup>1</sup>, Marija Zlata Božnar<sup>1</sup>,  
Dejan Gradišar<sup>2</sup> and Juš Kocijan<sup>2,3</sup>*

<sup>1</sup>MEIS d.o.o., Mali Vrh pri Šmarju, Slovenija

<sup>2</sup>Jožef Stefan Institute, Ljubljana, Slovenija,

<sup>3</sup>University of Nova Gorica, Nova Gorica, Slovenija,

**Abstract:** In conditions of complex terrain, modelling of air pollutant dispersion is a very demanding task, which still has a number of scientific challenges. Ideally, appropriate meteorological data should be available for modelling, which should include the measurements of vertical profiles of wind and temperature, and not just ground-based meteorological information. Unfortunately, for many purposes, such as for example for studies of the impact of industrial plants to the surrounding atmosphere, where it is necessary to analyse the data for at least one year, there is no time to carry out suitable measuring campaigns.

Therefore, instead of measuring the profile and ground-level meteorological parameters, the results of prognostic weather forecasts (NWP models) are being widely used. However, these models still have quite a few disadvantages when their results are used as input for dispersion models over complex terrain.

The study presents the validation of the quality of the weather forecasts in surroundings of Nuclear Power Plant Krško in Slovenia, an area with highly complex terrain and the resulting complex meteorological characteristics.

For air pollution dispersion models, we have developed specially for Slovenia a dedicated forecast of meteorological parameters with the NWP model of WRF and the use of GFS global input data. The forecast takes place in real time and is intended for real-time use for several areas in Slovenia as well as the use of historical data for different studies. For different areas of Slovenia, the forecast takes place in different temporal and spatial resolutions, whereby the finest is available for horizontal resolution of 2 km and half hour temporal interval and seven days in advance.

The predicted meteorological parameters, which are key for the models of air pollutant dispersion, will be validated using the measured meteorological parameters. The quality of the forecasts will be analysed both qualitatively and quantitatively with the relevant indexes.

**Key words:** *validation, weather forecast, fine spatial and temporal resolution, complex terrain*

## **INTRODUCTION**

In conditions of complex terrain, modelling of air pollutant dispersion is a very demanding task, which still has a number of scientific challenges. Ideally, appropriate meteorological data should be available for modelling, which should include the measurements of vertical profiles of wind and temperature, and not just ground-based meteorological information. Unfortunately, for many purposes, such as for example for studies of the impact of industrial plants to the surrounding atmosphere, where it is necessary to analyse the data for at least one year, there is no time to carry out suitable measuring campaigns.

Therefore, instead of measuring the profile and ground-level meteorological parameters, the results of prognostic weather forecasts (NWP models) are being widely used. However, these models still have quite a few disadvantages when their results are used as input for dispersion models over complex terrain.

This paper dedicates special attention to a qualitative wind forecast, which is a basic parameter in pollution modelling. An additional parameter, which can lead to an incorrect assessment of the stability of the atmosphere with the wrong forecast, is the forecast of global solar radiation.

The aim of this paper is to demonstrate the quality of the forecast of meteorological parameters, which are important for modelling air pollutants expansion, on an actual example of Slovenia, which is a country with a very complex terrain in the slipstream on the sunny side of the Alps.

Our final goal is that on harmonization initiative we should harmonize criteria how well should be prognostic meteorology prepared when it is used for air pollution dispersion modelling.

## **METHODOLOGY**

When modelling the meteorological parameters above a complex terrain, we must be aware in the first place that the modelled meteorological description of the atmosphere must be a good match with the actual description in all three spatial dimensions, namely also vertically. Therefore, we are required to use an area where we dispose the quality measurements of meteorological parameters in the higher layers of the atmosphere in order to validate the modelled meteorological parameters.

Thus, we chose the area in Slovenia in the vicinity of the town of Krško because the Krško Nuclear Power Plant is located there, which takes exemplary care of its meteorological measuring system. This measuring system includes four ground level meteorological stations at the bottom of a half-open basin, and an additional SODAR station, which provides quality measurements of the wind directions and speed up to 500m above the ground. A MEIS weather forecast system, which gives the forecast for Slovenia for 7 days ahead in half-hour steps, and with a cell sized to 14km, and subsequently it gives the forecast for seven days ahead in half-hour steps with a cell sized to 2km horizontally for a narrower area in the vicinity of Krško is validated. The forecast has been compared to the forecast of the MEIS Kooreg model, which gives the forecast for the entire Slovenia for 2 days ahead with a cell sized to 4km horizontally. The forecasts in all the examples is performed with the WRF model and global American input GFS data. (Mlakar et al., 2014, Mlakar et al., 2015).

We focused on the first day of the forecast in the validation for all three modules. However, we are of course aware that in the event of the validation of the forecast for several days ahead, the quality of the forecast would diminish. According to our opinion, the forecast validation for the first day is also a solid assessment for the validation of reanalyses. Reanalyses in general may provide better results than the real forecasts, however, they are important because they are a traditional source of meteorological data for the events, when the atmospheric dispersion modelling is performed for a period that has already passed (and not in a continuous on-line mode, as is the case at the Krško Nuclear Power Plant).

We used one a year of forecasts and one year of measured data from the meteorological station at the location of the Krško Nuclear Power Plant, SODAR provided data only for six months within the chosen one-year-period interval due to a breakdown. Firstly, we validated the forecasts of the basic meteorological quantities for the bottom layer of the atmosphere. Validation of precipitation is a particular problem. Validation concluded with the validation of wind at higher altitudes. We use the traditional numeric estimators: RMSE (root-mean-square error), PCC (Pearson's correlation coefficient), MFB (mean fractional bias), FAC2 (The factor of the modelled values within a factor of two of the observations) and SMSE (standardized mean-squared error) as defined in the paper by Kocijan et al. (2016).

## **RESULTS**

In Tables 1–12, we firstly gathered the values for the basic meteorological parameters, predicted with three different configurations of the WRF model (configurations are marked based on the horizontal size of the cells, and additionally with an internal code of the WRF configuration).

**Table 1.** Temperature validation results at 2m

MODEL	PCC	RMSE	MFB	FAC 2	SMSE
WRF04 – 4km	0.97	2.38	0.047	0.87	0.07
WRF26 – 2km	0.97	2.52	0.073	0.86	0.08
WRF31 – 14km	0.97	2.75	0.127	0.85	0.09

**Table 2.** Temperature validation results at 10m

MODEL	PCC	RMSE	MFB	FAC 2	SMSE
WRF04 – 4km	0.97	2.55	0.042	0.87	0.08
WRF26 – 2km	0.96	2.77	0.114	0.86	0.10
WRF31 – 14km	0.97	3.01	0.198	0.84	0.12

**Table 3.** Relative air humidity validation results at 2m

MODEL	PCC	RMSE	MFB	FAC 2	SMSE
WRF04 – 4km	0.68	15.86	0.065	0.99	0.65
WRF26 – 2km	0.71	14.61	0.034	0.99	0.55
WRF31 – 14km	0.72	13.91	0.010	0.99	0.50

**Table 4.** Air pressure validation results

MODEL	PCC	RMSE	MFB	FAC 2	SMSE
WRF04 – 4km	0.994	2.09	0.002	1.00	0.08
WRF26 – 2km	0.991	4.42	0.004	1.00	0.37
WRF31 – 14km	0.918	18.63	0.019	1.00	6.52

**Table 5.** Global solar radiation validation results

MODEL	PCC	RMSE	MFB	FAC 2	SMSE
WRF04 – 4km	0.92	111.87	0.945	0.69	0.20
WRF26 – 2km	0.92	113.83	0.974	0.68	0.21
WRF31 – 14km	0.92	113.11	0.945	0.69	0.21

**Table 6.** Precipitation validation results

MODEL	PCC	RMSE	MFB	FAC 2	SMSE
WRF04 – 4km	0.20	0.43	0.017	0.30	1.21
WRF26 – 2km	0.18	0.44	0.019	0.34	1.25
WRF31 – 14km	0.30	0.39	-0.056	0.26	1.00

**Table 7.** Wind velocity validation results at the height of 10m

MODEL	PCC	RMSE	MFB	FAC 2	SMSE
WRF04 – 4km	0.58	1.50	-0.305	0.60	1.88
WRF26 – 2km	0.52	1.44	-0.234	0.58	1.74
WRF31 – 14km	0.54	1.66	-0.507	0.56	2.30

**Table 8.** Wind direction validation results at the height of 10m

MODEL	PCC	RMSE	MFB	FAC 2	SMSE
WRF04 – 4km	0.45	104.85	0.101	0.71	1.16
WRF26 – 2km	0.41	110.76	0.056	0.71	1.29
WRF31 – 14km	0.41	115.41	0.153	0.67	1.41

**Table 9.** Wind velocity validation results at the height of 220m (SODAR measurements)

MODEL	PCC	RMSE	MFB	FAC 2	SMSE
WRF04 – 4km	0.65	3.99	-0.507	0.57	2.04
WRF26 – 2km	0.64	4.76	-0.628	0.49	2.90
WRF31 – 14km	0.65	3.89	-0.476	0.57	1.94

**Table 10.** Wind direction validation results at the height of 220m (SODAR measurements)

<b>MODEL</b>	<b>PCC</b>	<b>RMSE</b>	<b>MFB</b>	<b>FAC 2</b>	<b>SMSE</b>
<b>WRF04 – 4km</b>	0.62	89.35	0.021	0.77	0.78
<b>WRF26 – 2km</b>	0.60	91.57	0.006	0.78	0.82
<b>WRF31 – 14km</b>	0.60	91.35	0.030	0.77	0.81

**Table 11.** Wind velocity validation results at the height of 440m (SODAR measurements)

<b>MODEL</b>	<b>PCC</b>	<b>RMSE</b>	<b>MFB</b>	<b>FAC 2</b>	<b>SMSE</b>
<b>WRF04 – 4km</b>	0.65	4.78	-0.303	0.71	1.56
<b>WRF26 – 2km</b>	0.70	4.94	-0.371	0.68	1.67
<b>WRF31 – 14km</b>	0.71	4.36	-0.287	0.72	1.30

**Table 12.** Wind direction validation results at the height of 440m (SODAR measurements)

<b>MODEL</b>	<b>PCC</b>	<b>RMSE</b>	<b>MFB</b>	<b>FAC 2</b>	<b>SMSE</b>
<b>WRF04 – 4km</b>	0.71	61.31	0.026	0.83	0.34
<b>WRF26 – 2km</b>	0.72	59.11	0.015	0.83	0.32
<b>WRF31 – 14km</b>	0.71	59.81	0.017	0.82	0.33

For the parameters: air temperature at 2m and 10m above the ground, relative air humidity at 2m, air pressure and global solar radiation, which are relatively easy to predict, we may see that the WRF 2km and WRF 4km configurations are very similar, and that they both achieved extremely good values. There are major discrepancies with the WRF 14km configuration, as a 14km large cell in the horizontal direction is substantially a too homogeneous area at the ground, which does not see the proper characteristics of the atmosphere over highly complex terrain. The values of the estimator in the precipitation analysis are bad, but for the proper validation, we would have to analyse, for example, radar measurements and compare them with the forecast models. In our case, we validated the model by a spot metering of the precipitation at the location of the Krško Nuclear Power Plant. The problem with the precipitation is the extremely stochastic nature of storms, and additionally there is also some shift in space and time even between forecasts and the actual front passage. Due to averaging through a larger cell, the WRF 14km configuration is better than the other two with precipitation. In the analysis of the ground wind for the wind speed at the location of the Krško Nuclear Power Plant, the WRF 2km and WRF 4km configurations are again more successful, and they are exchanging the title as the best configuration based on the estimator. Thus, Figure 1 additionally also displays a scatter plot for all three configurations. It is evident from this chart that the WRF 2km makes less exaggerations than the WRF 4km. A forecast of a too strong ground wind over a complex terrain is a known issue of our NWP models. This issue is very disturbing for atmospheric dispersion modelling as a stronger wind means better dispersion in general. Therefore, the WRF 2km is the best configuration for atmospheric dispersion modelling. We only took into consideration the values expressed in angle degrees for the verification of the wind direction, and we did not perform special analyses of the circular nature of the wind direction. The verification of the forecast of wind at higher altitudes of 220m and 440m respectively with the SODAR measurements (as shown in Figures 2 and 3) has shown that matching the forecasts of wind improves with height, which confirms the usefulness of forecasts of wind in the higher layers for the purpose of air pollution modelling. With the altitude, also the difference between the success of an individual WRF configuration decreases, where we are able to achieve good results even with the use of a lower spatial resolution.

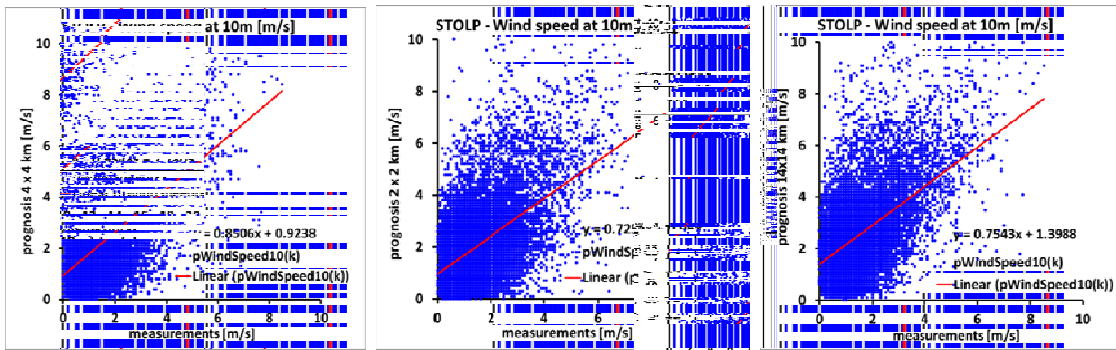


Figure 1. Scatter plot for ground wind speed at 10m

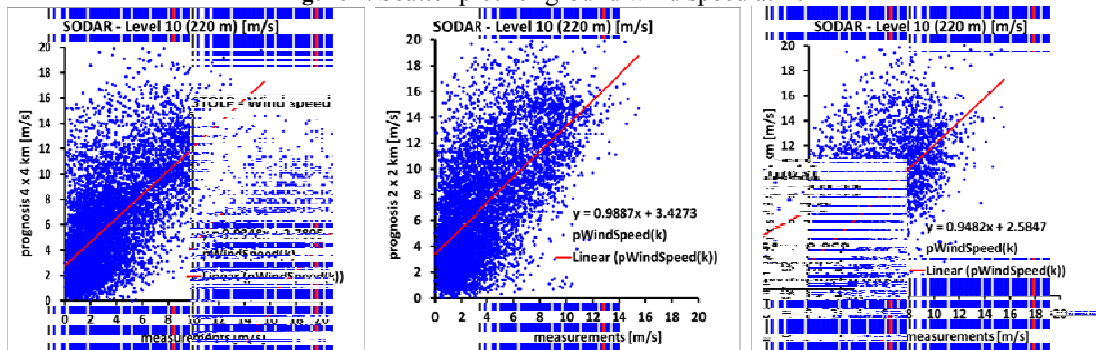


Figure 2. Scatter plot for wind speed at 220m (SODAR measurements)

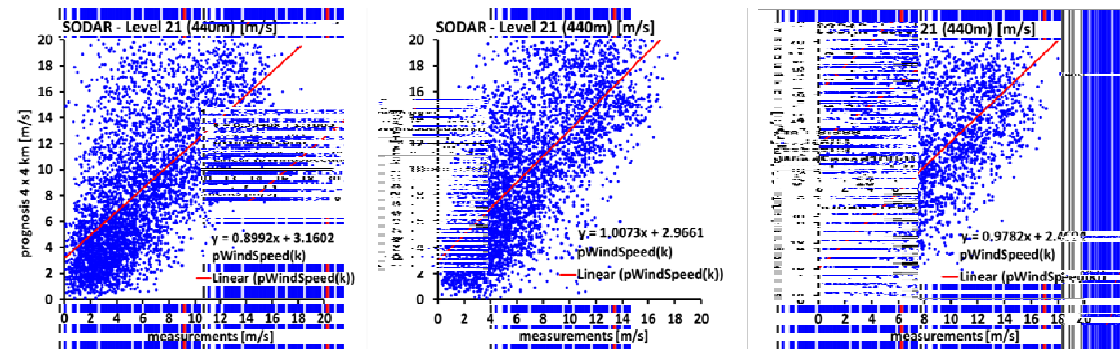


Figure 3. Scatter plot for wind speed at 440m (SODAR measurements)

## CONCLUSION

This paper presents the validation of forecasting the basic meteorological parameters, used for atmospheric dispersion modelling. Validation has been carried out with the measured data at the location of the Krško Nuclear Power Plant in Slovenia with a very complex terrain, which makes the modelling much more difficult. Both ground measurements and also SODAR measurements of the vertical profile of the wind were used for the validation. The values for the first day of forecast are subject to validation. We have shown that the forecasts are very good most of the time, we only have to be slightly more careful in the interpretation of the wind direction, and the speed of the ground wind, and also with the interpretation of precipitation, which is generally still a major challenge for the NWP models.

## ACKNOWLEDGEMENT

This research was supported by the Slovenian Research Agency Projects No. L1-4154(A), L2—5475(C) and L2—6762(B). We are grateful to Nuclear Power Plant Krško for meteorological data.

## REFERENCES

- Mlakar, P., M.Z. Božnar and B. Breznik, 2014: Operational air pollution prediction and doses calculation in case of nuclear emergency at Krško Nuclear Power Plant. *Int.l J. Environ. Pollut.*, **54**, 175-183, doi: 10.1504/IJEP.2014.065118.
- Mlakar, P., B. Grašič, M. Z. Božnar and B. Breznik, 2015: Online relative air dispersion concentrations one week forecast for Krško NPP prepared for routine and emergency use. 24th International Conference Nuclear Energy for New Europe - NENE 2015, Portorož, Slovenia, September 14-17. Proceedings. Ljubljana: Nuclear Society of Slovenia, pp. 602-1-602-8.
- Kocijan, J., D. Gradišar, M. Z. Božnar, B. Grašič, and P. Mlakar, 2016: On-line algorithm for ground-level ozone prediction with a mobile station. *Atmos. Environ.*, **131**, 326-333, doi: 10.1016/j.atmosenv.2016.02.012.

**17th International Conference on  
Harmonisation within Atmospheric Dispersion Modelling for Regulatory Purposes  
9-12 May 2016, Budapest, Hungary**

---

**SENSITIVITY OF MODELLED URBAN BACKGROUND OZONE CONCENTRATIONS TO  
UNCERTAINTIES IN THE GRS INPUT VARIABLES**

*Andrea L. Pineda Rojas<sup>1,2</sup> and Nicolás A. Mazzeo<sup>1,3</sup>*

<sup>1</sup>National Scientific and Technological Research Council (CONICET), Argentina

<sup>2</sup>Centro de Investigaciones del Mar y la Atmósfera (CIMA/CONICET-UBA), DCAO/FCEN, UMI-  
IFAECI/CNRS, Buenos Aires, Argentina

<sup>3</sup>Department of Chemical Engineering, Avellaneda Regional Faculty, National Technological University,  
Buenos Aires, Argentina

**Abstract:** In this work, we apply the Monte Carlo analysis to evaluate the uncertainty of modelled summer maximum ozone diurnal peak concentrations ( $C_{\max}$ ) in the Metropolitan Area of Buenos Aires (MABA), Argentina resulting from uncertainties in the Generic Reaction Set (GRS) input variables, using the DAUMOD-GRS model. Values of  $C_{\max}$  occurring at early morning or late evening hours present greater uncertainties than those occurring around midday hours. Uncertainty of  $C_{\max}$  is dominated by that in the GRS ozone initial concentration at all analysed receptors, with relative contributions varying between 67.5-89.8%. The second most important variable is the nitrogen oxides initial concentration, whose relative contribution may increase (in our experiments up to 11.7%) depending on the uncertainties of the GRS input variables.

**Key words:** DAUMOD-GRS, Monte Carlo method, ozone, sensitivity, uncertainty.

## INTRODUCTION

The Generic Reaction Set (GRS) (Azzi et al., 1992) is a simplified photochemical scheme which represents the interactions between nitrogen oxides ( $\text{NO}_x$ ), reactive organic compounds (ROC) and ozone ( $\text{O}_3$ ). It is included in the algorithms of several air quality models (e.g., ADMS-Urban, TAPM, SOMS) and despite of its simplicity it has proved a good ability to simulate ground-level  $\text{O}_3$  concentrations at urban scale (e.g., Hurley et al., 2005; Kim et al., 2005). The DAUMOD-GRS model (Pineda Rojas and Venegas, 2013a) has also shown an acceptable performance when tested against concentrations observed at the Metropolitan Area of Buenos Aires (MABA), Argentina (Pineda Rojas, 2014). In a recent work (Pineda Rojas et al., 2016), an uncertainty analysis of modelled summer maximum  $\text{O}_3$  peak 1 h-concentrations ( $C_{\max}$ ) due to uncertainties in the model input variables showed that despite being mostly influence by that in the regional background  $\text{O}_3$  concentration (which is well known to be a key input variable for the GRS), other variables can also make important contributions. In order to better understand these results, in this work we assess the uncertainty of  $C_{\max}$  that is introduced by uncertainties in the GRS input variables, and their relative contributions. Since errors in such variables are not really known, the sensitivity of  $C_{\max}$  uncertainty to them is also analysed.

## METHODOLOGY

The DAUMOD-GRS model allows the estimation of ground-level urban background  $\text{O}_3$  concentrations, resulting from area source emissions of  $\text{NO}_x$  and ROC. In the coupling, the DAUMOD model (Mazzeo and Venegas, 1991) feeds the GRS. A detailed description of the coupled model can be found in Pineda Rojas and Venegas (2013a).

The GRS input variables that can be affected by errors in the model input variables are: the reaction constant rates ( $k_1$ - $k_4$ ) which depend on the air temperature and the solar radiation; the initial concentrations of nitrogen oxides ( $C_i\text{NO}_x$ ) and reactive organic compounds ( $C_i\text{ROC}$ ), that are controlled by their respective emissions and the atmospheric transport and dispersion; and the initial concentration of ozone ( $C_i\text{O}_3$ ) which depends on the regional background  $\text{O}_3$  concentration and on the remaining concentration from the hour before (i.e., the “memory effect”).

In order to evaluate the uncertainty of  $C_{\max}$  that is introduced by the uncertainties in these seven variables, the Monte Carlo (MC) analysis (Moore and Londergan, 2001; Hanna et al., 2007) is applied. Since the probability density functions for such internal variables are not known, we design three experiments considering log-normal distributions for all variables and different combinations of their possible errors (see Table 1) which are based on values published in the literature (e.g., Hanna et al., 1998). Simple random sampling (Moore and Londergan, 2001) is used to obtain sets of  $N=100$  perturbations for each variable and experiment. The relatively simple coupling between the DAUMOD and the GRS models allows a few code modifications so that the GRS input variables can be perturbed during each simulation. The MC runs are performed for eight selected receptors shown in Figure 1 (see Pineda Rojas et al., 2016), obtaining a set of 100 possible results of  $C_{\max}$ , from which uncertainty is estimated. On the other hand, these results are also used to perform Multiple Linear Regression Analysis in order to assess the relative contribution from each variable to the estimated  $C_{\max}$  uncertainty.

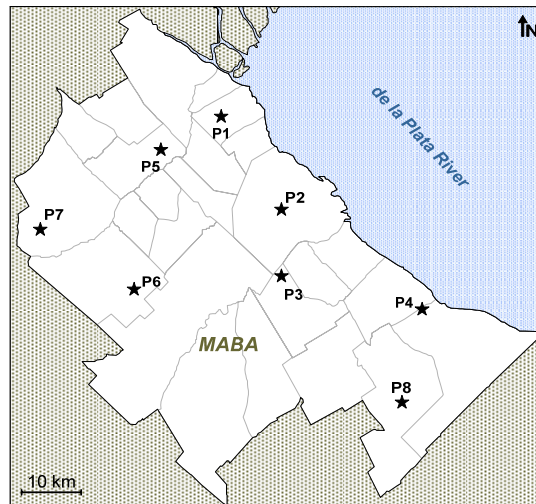


**Figure 1.** The Metropolitan Area of Buenos Aires (MABA) and selected receptors presenting different emission and atmospheric conditions at the time of occurrence of  $C_{\max}(ZU)$ .

The model input data for the zero-uncertainty (ZU) simulation conditions are the following: surface hourly meteorological information registered at the domestic airport during the 2007 summer, sounding data from the station located at the international airport, high-resolution ( $1 \text{ km}^2$ , 1 h) area source emissions of nitrogen oxides and volatile organic compounds from the emissions inventory developed for the MABA (Venegas et al., 2011), and clean air regional background concentrations for all species (see Pineda Rojas, 2014). The performance of the DAUMOD-GRS to simulate peak  $O_3$  concentrations in the MABA under such conditions has been discussed in Pineda Rojas and Venegas (2013b).

**Table 1.** Considered errors for the GRS input variables in each experiment

Input variable	Exp-1	Exp-2	Exp-3
$k_1, k_4$	30%	30%	30%
$C_iNO_x$	30%	50%	80%
$C_iROC$	30%	50%	80%
$C_iO_3$	30%	30%	40%

In this work, at each of the eight selected receptors, the uncertainty of  $C_{\max}$  (taken as the 95% confidence interval) is approximated by that of  $O_3$  hourly concentration at the time (day of summer and hour) of occurrence of  $C_{\max}(ZU)$ .

## RESULTS

The eight selected receptors (Figure 1) present a wide range of atmospheric and emission conditions at the time of occurrence of  $C_{\max}(ZU)$ , with varying wind speed and direction, air temperature, sky cover, atmospheric stability class, solar radiation, and  $NO_x$  and ROC emission rates. The order of the receptors is

in the direction of decreasing emission rates. The wide range of atmospheric conditions is related to the varying hour of occurrence of  $C_{\max}(ZU)$ : around midday hours at receptors P1-P5, and in the early morning or late evening at receptors P6-P8.  $C_{\max}(ZU)$  values simulated at these receptors are in the range 16.3-26.2 ppb (see Pineda Rojas et al., 2016).

### Variation of $C_{\max}$ uncertainty among selected receptors

In order to analyse the  $C_{\max}$  uncertainty under such different environmental conditions, we first consider the results obtained in the Experiment 2 (Exp-2) whose uncertainties values are commonly found in the literature (e.g., Hanna et al., 1998) and because they represent a kind of average between the three experiments.

Mean  $C_{\max}$  values obtained from the MC runs under conditions of Exp-2 vary between 16.4-26.1 ppb and tend to those of  $C_{\max}(ZU)$ , indicating that convergence is achieved for  $N=100$  simulations. On the other hand, the coefficient of variation ( $\sigma \times 100/\text{mean}$ ) of  $C_{\max}$  varies between 14.5-28.5%, being consistent with results obtained in other places (e.g., Bergin et al., 1999; Hanna et al., 2005).

Figure 2 shows the 95% confidence range of  $C_{\max}$  obtained at each receptor under conditions of Exp-2. A great difference of the uncertainty is observed between receptors P1-P5 (10.6-12.1 ppb) and P6-P8 (19.0-22.2 ppb), which shows that the uncertainty of  $C_{\max}$  at receptors where the  $O_3$  peaks occur during early morning or late evening hours is almost twice that obtained at receptors where the peaks present around midday hours.

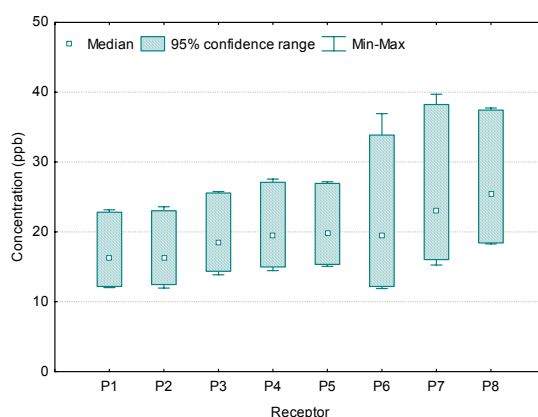


**Figure 2.** Uncertainty of  $C_{\max}$  at each selected receptor, under conditions of Experiment 2

At all receptors, the uncertainty in  $C_iO_3$  is the main contributing source to  $C_{\max}$  uncertainty (67.5-89.8%); the second most important variable is  $C_iNO_x$  (0.2-5.0%); while the reaction constant rates  $k_1-k_4$  (k's) represents the lowest contribution (up to 3.1%) (see Table 2). By comparing these contributions in ppb, it is observed that that of  $C_iO_3$  varies between 7.7 ppb (at P1 and P2) and 17.4 ppb (at P7).

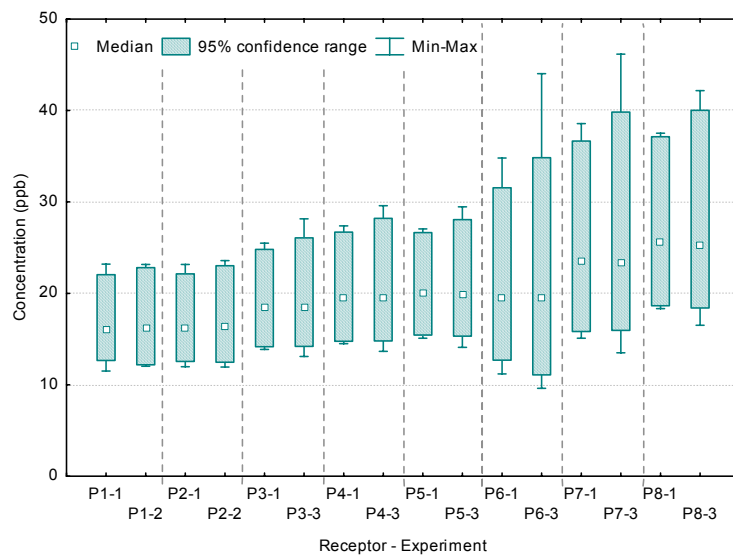
**Table 2.** Uncertainty contribution [in % and ppb] of the GRS input variables to  $C_{\max}$  uncertainty at each receptor, under conditions of Experiment 2. k's denotes the sum of  $k_1$  to  $k_4$ .

Receptor	k's		$C_iNO_x$		$C_iO_3$	
	%	ppb	%	ppb	%	ppb
P1	3.1	0.3	4.7	0.5	72.7	7.7
P2	2.7	0.3	5.0	0.5	73.2	7.7
P3	0.5	0.1	1.2	0.1	84.7	9.5
P4	0.4	0.1	1.1	0.1	85.5	10.4
P5	0.2	<0.1	0.4	<0.1	88.5	10.2
P6	0.2	0.1	4.2	0.9	67.5	14.6
P7	0.2	<0.1	2.7	0.6	78.6	17.4
P8	<0.1	<0.1	0.2	<0.1	89.8	17.1

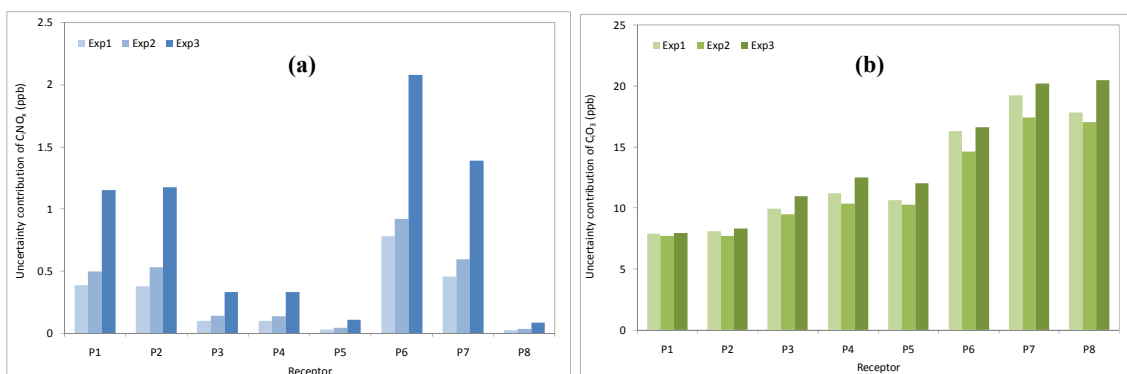
### Sensitivity of $C_{\max}$ uncertainty to the GRS input variables' uncertainties

Figure 3 presents the greatest difference of  $C_{\max}$  uncertainty obtained among the three experiments. At all receptors, the lowest  $C_{\max}$  uncertainty is obtained under conditions of Exp-1. The greatest difference of the 95% confidence range at receptors P1 and P2 is found between Exp-1 and Exp-2 (1.0-1.5 ppb). At receptors P3-P8, the greatest differences occur with Exp-3 and vary between 3.1-5.0 ppb.

The comparison of the relative contributions from the uncertainties in  $C_iNO_x$  and  $C_iO_3$  to  $C_{\max}$  uncertainty between the three experiments is shown in Figure 4. The contribution of the  $k$ 's is not shown because it varies in its second decimal. The contribution from  $C_iNO_x$  increases from Exp-1 to Exp-3 as long as its uncertainty does, with a maximum-to-minimum ratio varying between 2.7 (P6) and 3.8 (P8) (i.e., greater than the variation of its uncertainty). The uncertainty contribution of  $C_iO_3$  is lower in Exp-2 and greater in Exp-3, at all receptors. The maximum-to-minimum ratio varies between 1.0 (P1) and 1.2 (P4), indicating that the uncertainty contribution of  $C_iO_3$  is less sensitive to changes in its uncertainty range than that of  $C_iNO_x$ .



**Figure 3.** Uncertainty of  $C_{\max}$  at each selected receptor, under conditions of the two experiments presenting the greatest difference



**Figure 4.** Uncertainty contribution (ppb) of  $C_iNO_x$  (a) and  $C_iO_3$  (b) to  $C_{\max}$  uncertainty at each selected receptor obtained under conditions of experiments 1, 2 and 3

## CONCLUSIONS

An uncertainty and sensitivity analysis of the summer maximum O<sub>3</sub> peak concentrations (C<sub>max</sub>) simulated with the DAUMOD-GRS model to uncertainties in the GRS input variables shows that, under the environmental conditions of the Metropolitan Area of Buenos Aires (MABA):

- Uncertainty of C<sub>max</sub> (taken as its 95% confidence range) varies spatially, being greater at receptors where C<sub>max</sub> occurs in the early morning or late evening than where peaks occur around midday hours.
- The relative contributions from the GRS input variables vary spatially also, although the initial concentration of ozone dominates at all analysed receptors.
- The sensitivity of C<sub>max</sub> uncertainty to the input variables' uncertainty varies among the selected receptors between 1.0 ppb (10%) and 5.0 ppb (26%). The relative contribution of NO<sub>x</sub> initial concentration is more sensitive to its uncertainty than that of O<sub>3</sub>.

## REFERENCES

- Azzi, M., Johnson, G., Cope, M., 1992: An introduction to the generic reaction set photochemical smog model. In: Proc. 11th Int. Clean Air Conf., pp. 451-462.
- Bergin, M.S., Noblet, G.S., Petrini, K., Dhieux, J.R., Milford, J.B., Harley, R.A. 1999: Formal uncertainty analysis of a Lagrangian photochemical air pollution model. *Environ. Sci. Technol.*, **33**, 1116-1126.
- Hanna, S.R., Chang, J.C., Fernau, M.E. 1998: Monte Carlo estimates of uncertainties in predictions by a photochemical grid model (UAM-IV) due to uncertainties in input variables. *Atmos. Environ.*, **32**, 21, 3619-3628.
- Hanna, S.R., Paine, R., Heinold, D., Kintigh, E., Baker, D. 2007: Uncertainties in Air Toxics Calculated by the Dispersion Models AERMOD and ISCST3 in the Houston Ship Channel Area. *J. Appl. Meteorol. Climatol.*, **46**, 1372-1382.
- Hanna, S.R., Russell, A.G., Wilkinson, J.G., Vukovich, J., Hansen, D.A. 2005: Monte Carlo estimation of uncertainties in BEIS3 emission outputs and their effects on uncertainties in chemical transport model predictions, *J. Geophys. Res.*, **110**, D01302.
- Hurley, P.J., Physick, W.L., Luhar, A.K. 2005: TAPM: a practical approach to prognostic meteorological and air pollution modelling. *Environ. Model. and Softw.*, **20**, 737-752.
- Kim, C.-H., Park, S.-U., Song, C.-K., 2005: A simple semi-empirical photochemical model for the simulation of ozone concentration in the Seoul metropolitan area in Korea. *Atmos. Environ.*, **39**, 5597-5607.
- Mazzeo, N.A., Venegas, L.E. 1991: Air pollution model for an urban area. *Atmos. Res.*, **26**, 165-179.
- Moore, G.E., Londergan, R.J. 2001. Sampled Monte Carlo uncertainty analysis for photochemical grid models. *Atmos. Environ.*, **35**, 4863-4876.
- Pineda Rojas, A.L. 2014: Simple atmospheric dispersion model to estimate hourly ground-level nitrogen dioxide and ozone concentrations at urban scale. *Environ. Model. and Softw.*, **59**, 127-134.
- Pineda Rojas, A.L.; Venegas, L.E. 2013a: Upgrade of the DAUMOD atmospheric dispersion model to estimate urban background NO<sub>2</sub> concentrations. *Atmos. Res.*, **120-121**, 147-154.
- Pineda Rojas, A.L.; Venegas, L.E. 2013b: Spatial distribution of ground-level urban background O<sub>3</sub> concentrations in the Metropolitan Area of Buenos Aires, Argentina. *Environ. Pollut.*, **183**, 159-165.
- Pineda Rojas A.L., Venegas, L.E., Mazzeo, N.A. 2016: Uncertainty of modelled urban background O<sub>3</sub> peak concentrations and its sensitivity to input data perturbations based on the Monte Carlo analysis. Submitted to *Atmos. Environ.* Under review.
- Venegas, L.E., Mazzeo, N.A., Pineda Rojas, A.L. 2011: Chapter 14: Evaluation of an emission inventory and air pollution in the Metropolitan Area of Buenos Aires. In: D. Popovic (ed.) *Air Quality-Models and applications*, Editorial In-Tech, 261-288.

**17th International Conference on  
Harmonisation within Atmospheric Dispersion Modelling for Regulatory Purposes  
9-12 May 2016, Budapest, Hungary**

---

**FIELD DATA VERSUS WIND TUNNEL DATA: THE ART OF VALIDATING URBAN FLOW  
AND DISPERSION MODELS**

*Bernd Leitl, Frank Harms, Denise Hertwig, and Michael Schatzmann*

Meteorological Institute, University of Hamburg, Germany

**Abstract:** When a numerical model has the potential to simulate flow and dispersion episodes in complex urban terrain, it does not mean that the model is actually able to do this in a proper way. Whether the model output is in agreement with observation has to be proven in model validation exercises.

The backbone of any validation work is the existence of data which have sufficient quality and detail that they can be regarded as a standard. Due to the variability of the atmosphere it seems to be hardly feasible to obtain such data in urban field experiments. This shifts the focus to wind tunnel modelling. In the talk it will be reported how such data can be generated in the laboratory and how wind tunnel data compare with those from corresponding field tests.

**Key words:** *Model validation strategies, Field measurements, Wind tunnel measurements, Dispersion in urban terrain*

**VALIDATION OF NUMERICAL MODELS**

Validating models is not a trivial task. In urban environments it is much more difficult to generate reliable validation data than for many technical applications. The urban geometry is heterogeneous and so are the properties of the urban boundary layer flow. Due to the generally complex geometrical structure of urban sites a variety of time and space scales are involved.

Above the buildings but still within the roughness layer the flow is continuously adjusting to the ever changing surface conditions, never reaching equilibrium. Consequently, the laws known from established flows over homogeneous roughness elements (constant fluxes, logarithmic profiles etc.) are not applicable here.

The situation is even worse within the canopy layer. Here the flow is sort of channeled by the street canyons which, at least in Europe, have many different orientations with respect to the wind direction. It is trivial to note that measured values heavily depend on where the probes are located. Since the gradients of flow properties are considerable within the urban canopy layer (UCL), measurements taken a few meter apart from each other might show largely different results (Repschies et al, 2007).

The lack of spatial representativeness is accompanied by a lack of representativeness with respect to time. As will be subsequently shown, even within more or less regular arrays of obstacles and under steady ambient conditions, flow and dispersion properties measured within the UCL are difficult to interpret. Averages over 10 min or even 30 min are usually not ergodic, i.e. repeating an experiment under identical conditions would not lead to the same result. As smoke experiments within the UCL reveal, this is caused by low frequency turbulent variations of the flow which make the plume meander. Results from single measurements are highly uncertain and usually not representative. The degree of uncertainty can be large and must be known before the data can be used for model validation purposes.

As meteorologists would prefer to use full-scale field data for model validation, Schatzmann and Leitl (2011) raised the question whether field data do represent the truth, particularly in urban flow and air

quality modelling. In order to decide how close models should get to measured field data, the representativeness of them needs to be evaluated carefully. Often it must be stated that a perfect match of reference data from field experiments and simulation results is not proving a successful model validation rather than providing an example for successfully tuning simulation results. The variability inherently present in field data sets results in a large degree of freedom with respect to interpretation of measured values and assumed boundary conditions. Obviously, there is a gap between what can be observed and measured at full scale and the well-defined world of a numerical model.

## FIELD EXPERIMENTS

In recent years, Hamburg University participated in a number of field experiments in urban or industrial landscapes. With VALIUM in Hanover, BUBBLE in Basel, JOINT URBAN 2003 in Oklahoma City, the Mock Urban Setting Tests (MUST) at Dugway Proving Ground (Utah) or the CT\_ANALYST flow and dispersion experiments in the city of Hamburg only the most important are mentioned here. All these field experiments were either prepared or replicated in Hamburg University's large boundary layer wind tunnel facility, so that data sets from both, the field and laboratory are available and can be compared with each other.

The scope and focus of these experiments was, of course, different from case to case, but nevertheless some general conclusions can be drawn. Due to space restrictions this will be done here solely at the example of the Hamburg case.

### The Hamburg field experiment

To perform measurements in a vibrant metropolitan area is subject to many restrictions, above all when dispersion experiments are on the agenda. Although we were tasked by the Hamburg State government and had full support from police and fire fighters, permission for carrying out such experiments was granted only for a few early Sunday morning hours at 2 weekends. In order to gain flexibility we planned to position the source on a boat on river Elbe and to select wind directions from the river to the inner city area. This strategy proved to be reasonably successful. As tracer gas SF<sub>6</sub> was chosen, but despite the fact that this is a nearly inert gas, we were allowed to release only a few g/s. In consequence, since the expected concentrations were very small, we had to use bag samplers and to analyse the probes subsequently by using gas chromatography. About 20 automated bag samplers (Figure 1a) were distributed over the inner city area (Figure 1b). This was done in cooperation with scientists from the Forschungszentrum Jülich.



**Figure 1.** (a) Picture of an automated bag sampler rig in front of the Hamburg town hall.  
(b) Measurement positions during the field experiments.

Early morning observations are always somewhat of a problem. During the first observational period at April 16, 2011, there was high pressure over Hamburg with clear skies and large radiative cooling of the surface. Such weather situations are subject to stratification and inversion layers, and this was indeed the

case as the measurements at the 300m Hamburg TV-Mast approximately 10 km apart from the site clearly indicated. As becomes evident from Figure 2a, there was a strong inversion above the 110 m measurement platform although the wind speed at higher altitudes was quite strong (Figure 2b). As smoke experiments carried out at the end of the intensive operation period evidenced, there were even more inversions near to the ground. None of the altogether 8 ultra-sonic-anemometers which were operated simultaneously at different locations around the test site provided a wind speed and direction which matched the movement of the cloud.

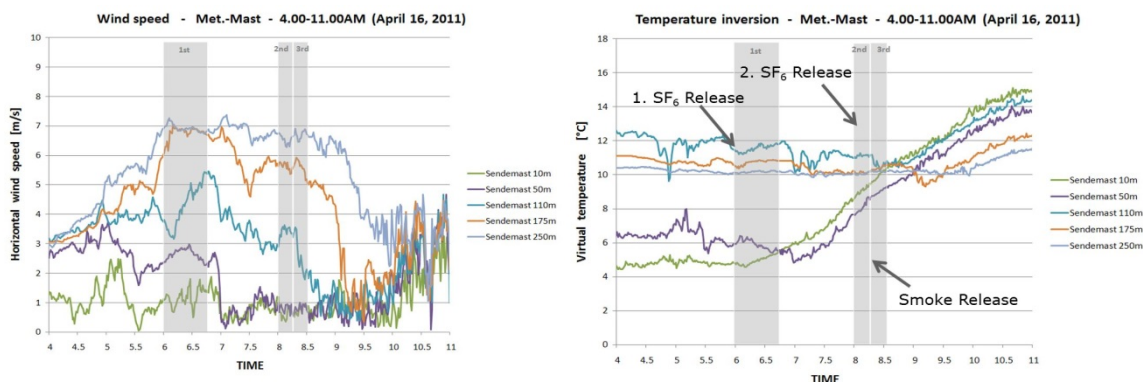


**Figure 2.** Wind velocities (a) and virtual potential temperatures (b) measured during the first experimental period at 5 different height levels at a TV mast located about 10 km apart from the test site at the eastern edge of Hamburg.

With the second field experiment we waited until a weekend with sufficient wind from the favored directional sector arrived. Although highly fluctuating with time, wind speed and direction were much more uniform compared to the first campaign (Figure 3b). This finding was fully corroborated by the measurements performed at different height levels at the Hamburg TV mast. In contrast to Figure 2, in the second phase the boundary layer was well mixed. The wind directions in the lowest 250 m above ground were always around  $220^\circ$ , independent of height and time, and the velocity profile only slightly increased with height.

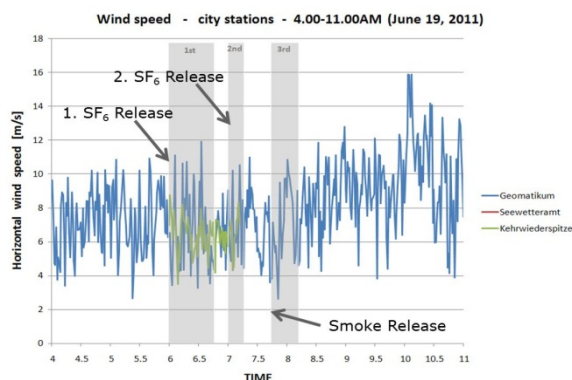


**Figure 3.** Second campaign at June 19, 2011: (a) Picture from the highly meandering smoke plume and from the ultra-sonic anemometer located at 'Kehrwiederspitze'. (b) Wind velocity versus time trace measured simultaneously at 2 different stations during the intensive operation period

The automated samplers were spread over an area much wider than the expected cloud width in order to identify not only polluted but unpolluted areas as well. Figure. 4 shows a few results. Shown are estimated cloud contours together with arrival times and time averaged cloud concentrations. All care was taken to secure the quality of the data. However it must be clear that the time resolution of the measurements was insufficient. Since the bag samplers average over an intermittently fluctuating contaminant supply rate, large variability bars would have to be added to the measured values since it is to be expected that repeats of the experiments under seemingly identical ambient conditions would show largely different results. The magnitude of these bars indicating the natural variability of the atmosphere

(and not the error of the instruments!) remains unknown since short-time experiments do not provide the information necessary for statistical analyses of the data (see Schatzmann and Leitl, 2011). Such analyses, however, would be necessary in order to quantify the representativeness of the data which is of utmost importance for any validation data set.

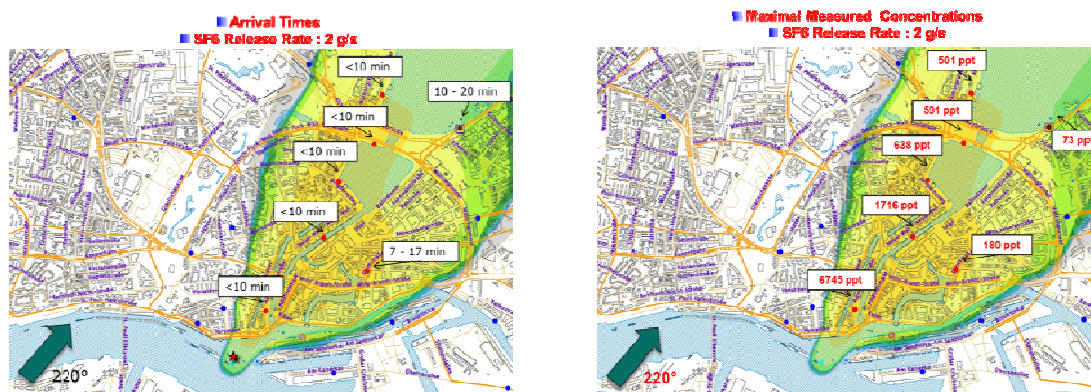


**Figure 4.** Second campaign at June 19, 2011. Bag sampler positions are shown with red dots polluted and blue dots unpolluted. The bag-samplers operated time-staggered with suction intervals of 10 min. Shown are arrival times (a) and concentration averages of the cloud (b)

### The Hamburg wind tunnel experiment

In order to enhance the data, wind tunnel experiments were carried out in the large boundary layer wind tunnel ‘Wotan’ of Hamburg University. This tunnel has a total length of 25 m with a test section which is 4 m wide and 2.75 m high and contains a flow establishment section of about 18 m length. The wind tunnel is equipped with an adjustable ceiling allowing 0.5 m height extension of the test section. An approach flow boundary layer matching the scale of the Hamburg model (1:350) was generated. The size of the test section allowed the reproduction of turbulence with length scales of more than 1 km in full scale.

The boundary layer properties were controlled and documented similarly as described in Schatzmann and Leitl (2011) for another wind tunnel investigation. Non-intrusive flow measurements were carried out with an optical LDA fibre probe with a focal length of 800 mm. To measure high resolution concentration time series a fast flame ionisation detector was used. Figure. 5 shows a sector of the (in full scale) 3700m long and 1400m wide physical model in the wind tunnel. Under steady-state mean flow conditions numerous instantaneous and continuous clouds were released at multiple positions and time series of the resulting velocity and concentration fields were monitored. Details of the comparison between wind tunnel and numerical model results cannot be given here due to space limitations, it is mentioned only that the field data very satisfyingly matched the variability range found in the wind tunnel data.

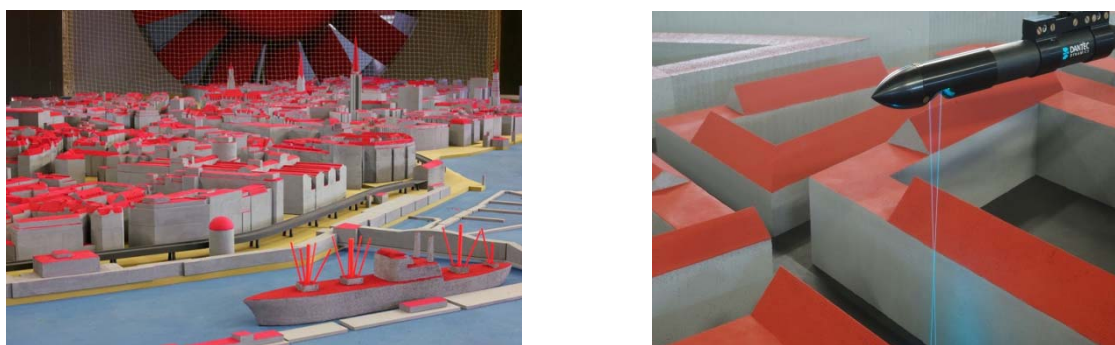


**Figure 5.** Physical model of the site in Hamburg University’s large boundary layer wind tunnel (a) and non-intrusive flow measurements with Laser-Doppler-Anemometry (b)

## CONCLUSIONS

Validation data for numerical models are not just any experimental data; they must fulfill certain requirements with respect to completeness, spatial and temporal resolution, accuracy, representativeness and documentation of the measured results (Schatzmann and Leidl, 2002). If these requirements are not met, too many degrees of freedom remain to set-up numerical model runs. A wide variety of numerical results can be generated with reasonable assumptions for the input data, with the consequence that a solid conclusion concerning the model quality cannot be reached. Hence validation datasets that match the complexity of specific groups of models are needed.

In order to validate urban RANS or LES models validation data are required that contain flow and concentration fields measured with high resolution in space and time. Field measurements usually do not fulfil these high validation requirements. Under certain limiting conditions, such datasets can be generated under carefully controlled conditions in well-equipped boundary layer wind tunnels.

In the present example two short field campaigns were carried out in addition to wind tunnel experiments. Such field tests are always limited in scope. As was described in more detail in Schatzmann and Leidl (2011) for another combined data set, it is nearly impossible gaining reliable test data for complex CFD models in such experiments. The atmosphere is intrinsically time dependent and never steady state. The commonly assumed 15 min or 30 min quasi-steady episodes exhibit a large inherent variability. Data obtained over such short periods of time are not representative for the assumed mean wind velocity and direction. And even worse, in urban canopy layers it occurs to be nearly impossible to determine positions at which a wind vector representative for the dispersion of the cloud could be measured. Nevertheless comparisons with field data are vital for building confidence in the quality of numerical and physical model predictions; whenever possible they should be carried out.

The dispersion process in complex geometries is driven by complex wind flows and turbulent diffusion. From a strict physical point of view, the source sizes, release rates or (mostly short time) durations of release events often restrict the use of tools which are based on mean flow and dispersion modelling because in the atmosphere the assumed mean conditions do not exist for relevant time periods less than many hours of constant weather.

Therefore it is necessary to move forward to advanced modelling technics which have the potential to deal with the unsteady behaviour of local scale dispersion in complex geometries in a more consistent way.

## REFERENCES

- Allwine, K.J., Leach, M.J., Stockham, L.W., Shinn, J.S., Hosker, R.P., Bowers, J.F., Pace, J.C., 2004: Overview of JOINT URBAN 2003: An atmospheric dispersion study in Oklahoma City. Symposium on Planning, Nowcasting, and Forecasting in the Urban Zone, January 11-15, WA. Amer. Meteor. Soc. J7.1, Seattle.
- Biltoft, C.A., 2001: Customer report For Mock Urban Setting Test, DTC Project no. 8-CO-160-000-052, DPG Document No. WDTC-FR-01-121
- Repschies, D., Schatzmann, M., Leidl, B., 2007: How dense is dense enough? – Systematic evaluation of the spatial representativeness of flow measurements in urban areas. Proceedings International Workshop on Physical Modelling of Flow and Dispersion Phenomena, Orleans, France, Aug. 28-31.
- Rotach, M., Vogt, R., Bernhofer, C., Batchvarova, E., Christen, A., Clappier, A., Feddersen, B., Gryning, S.E., Martucci, G., Mayer, H., Mitev, V., Oke, T.R., Parlow, E., Richner, H., Roth, M., Roulet, Y.A., Ruffieux, D., Salmond, J.A., Schatzmann, M., Voogt, J.A., 2005: BUBBLE- An urban boundary layer meteorology project. *Theor. Appl. Climatol.*, **81**. 231-261.
- Schatzmann, M., and Leidl, B., 2002: Validation and application of obstacle resolving urban dispersion models. *Atmos. Environ.*, **36**, 4811-4821.
- Schatzmann, M., Bächlin, W., Emeis, S., Kühlwein, J., Leidl, B., Müller, W.J., Schäfer, K., Schlünzen, H., 2006: Development and Validation of Tools for the Implementation of European Air Quality Policy in Germany (Project VALIUM). *Atmos. Chemist. Phys.*, **6**, 3077-3083.
- Schatzmann, M. and Leidl, B. (2011) Issues with validation of urban flow and dispersion CFD models. *J. Wind Engineer. Indust. Aerodynam.*, **99**, 169-186.

**17th International Conference on  
Harmonisation within Atmospheric Dispersion Modelling for Regulatory Purposes  
9-12 May 2016, Budapest, Hungary**

---

**WRF SURFACE AND UPPER AIR VALIDATION OVER CENTRAL CHILE DURING LA NIÑA-EL NIÑO TRANSITION**

*F. Carrera-Chapela<sup>1,2</sup>, G. Ruiz-Filippi<sup>2</sup>, J.A. González<sup>1</sup>, G. Yarwood<sup>3</sup>, J. Johnson<sup>3</sup>*

<sup>1</sup> Department of Chemical Engineering; University of Santiago de Compostela;  
15782 Santiago de Compostela, Spain

<sup>2</sup> School of Biochemical Engineering, Pontificia Universidad Católica Valparaíso, Chile

<sup>3</sup> Ramboll Environ, Novato, California, USA

**Abstract:** Pacific Ocean suffers El Niño-La Niña sea surface oscillations which influences regional meteorological variables as surface temperature, wind fields and the diurnal development of the planetary boundary layer (PBL). In this work, we used WRF in order to evaluate its performance during the transition from weak La Niña to moderate El Niño phenomena, against surface observations and upper air measurements. Surface 2-m temperature was better described during moderate El Niño than weak La Niña event for selected settings. 10-m wind surface have not highlighted any influence. Upper air WRF validation was well described using PBL height estimations from LIDAR observations for comparison. Also, upper air WRF validation was considered against PBL height estimations based in bulk Richardson number from synoptic rawinsonde observations; however, these synoptic rawinsonde measurements usually failed in the estimation of the PBL height.

**Key words:** *WRF model validation, Niño-Niña, surface, LIDAR and rawinsonde data*

## **INTRODUCTION**

It is well known that air quality models require high quality mass consistent meteorological fields from prognostic meteorological models. While these meteorological models have demonstrated increasing forecast skill over North America and Western Europe, few studies have focused on model validation in the Southern Cone of South America (Falvey and Garreaud 2002; Saide et al., 2011). Furthermore, this region suffers sea surface temperature (SST) oscillations due to El Niño and La Niña phenomena, producing changes in the surface weather conditions over Central Chile. In addition, this Southern mid-latitude location is affected by synoptic subsidence of subtropical Pacific anticyclone, limiting the vertical development of the planetary boundary layer height (PBLH) and promoting air pollution episodes (Garreaud et al., 2002; Saide et al., 2011).

In this work, we used Weather Research Forecast Model v3.6 (WRF) in order to evaluate its performance during the transition from weak La Niña to moderate El Niño phenomena, against surface observations and upper air measurements. Upper air WRF validation is focused in the PBL and model results are compared to estimated PBLH values from either synoptic rawinsonde or LIDAR ceilometer datasets.

## **STUDY AREA AND EVALUATION PERIOD**

The study area covers 150x150 km<sup>2</sup> over Central Chile, around Santiago de Chile (33° 27'S 70°40'W), centered in the Metropolitan Region inside the Central Valley, surrounded on the east by the Andes Mountains with altitudes over 4000 asl-m, on the west by the Coastal Range over 1500 asl-m, and hilly chains partially blocking the north and south faces (Figure 1a). In this work, we apply the WRF meteorological model for an annual 2009 simulation using three telescoping one-way nested grids (Figure 1b) with a maximum 2x2 km<sup>2</sup> horizontal resolution in the innermost grid.

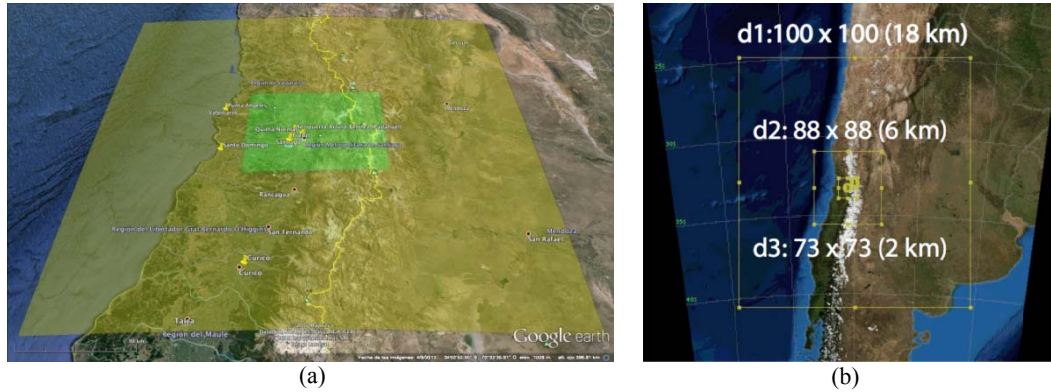


**Figure 1.** Study area: (a) Location and physical geography of the D2 and D3 WRF simulation domains, also with the location of the meteorological surface stations and the upper-air site at Santo Domingo; (b) WRF nested domains.

About the WRF model settings selected, they include: Kain-Fritsch cumulus scheme (outer and medium domain), WSM 3-class microphysics scheme, RRTM longwave and Dudhia shortwave radiation schemes, and a 5-layer soil model. About PBL physics, Yonsei University-Pleim-Chang (YSU) scheme was applied. NCEP reanalysis fields supplied initial and boundary conditions.

About the study period, the beginning of 2009 marked the end of a weak La Niña event that transitioned into a moderate El Niño event by the last quarter of 2009 (Table 1).

**Table 1.** Sea surface temperature, 3 months running mean (Huang et al., 2015).

	DJF	JFM	FMA	MAM	AMJ	MJJ	JJA	JAS	ASO	SON	OND	NDJ
<b>2009</b>	<b>-0.8</b>	<b>-0.7</b>	<b>-0.4</b>	-0.1	0.2	0.4	<b>0.5</b>	<b>0.6</b>	<b>0.7</b>	<b>1.0</b>	<b>1.2</b>	<b>1.3</b>

For model validation, we applied the DS-3505 global surface hourly observational database along 2009 year in order to compare wind speed and temperature over six stations: two stations are located along the coast (D-F) and the remaining four stations (A,B,C,E) are located in Central Valley surrounded by complex terrain composed by the Andes Mountains to the East and Chilean Coastal Range to the West (Figure 1a). Surface validation performance was based on the criteria reported by Emery et al. (2001).

Upper air validation was focused in 1-12 June period against rawinsonde (as its available dataset) and in 1-30 June period (against ceilometer dataset), as during this period national air quality government authority warned Santiago de Chile citizens about air pollution risks due to strong atmospheric stability.

To validate upper air model performance, two different approaches were considered: (a) Observations from Santo Domingo synoptic rawinsonde launched twice daily near the coast (Figure 1a: D site) were used to estimate PBLH by means of the bulk Richardson number (Holtslag and van Ulden, 1983; González et al., 2015); this approach is very feasible, as almost every National Meteorological Office provides these data. (b) Estimation of PBLH from an algorithm based on aerosol concentration measurements provided by a ceilometer installed at inner Santiago de Chile; these PBLH estimations were supplied by Muñoz et al. (2010).

## RESULTS

During the first quarter of 2009 the transition from weak La Niña to moderate El Niño event was observed (Table 1). This phenomenon has an impact in the 2-m temperature surface WRF performance (Table 2): systematic, random and gross errors are usually lower during El Niño than La Niña event. Also, YSU PBL scheme produces higher sensible heat flux than other schemes during nighttime, which can result in an increase in 2-m temperature (Kleczek et al., 2014). In addition, this systematic error can be influenced by the thermal 5-layer thermal diffusion (TD) soil model, which also increases the sensible heat flux compared to the Noah parametrization (Kleczek et al., 2014); this effect is noted on the surface stations. Particularly, coastal observations presented higher bias, reflecting the overestimation of the heat transfer by coupling YSU-TD, with a higher deviation along cold sea surface episodes, i.e., at the beginning of 2009 with the final weak La Niña. Surface stations located far from sea breeze effect are better described by this model configuration. About inner/inland sites results, they changed from overestimation to underestimation; negative bias is in agreement with previous results from Kleczek et al. (2014).

**Table 2.** Statistics for 2-m temperature: blue cells corresponds to January-June and red cells to July-December

Station	BIAS (°C)	Gross Error	IOA (°C)	RMSE (°C)	BIAS (°C)	Gross Error	IOA (°C)	RMSE (°C)
A	1.73	3.87	0.53	4.69	1.43	4.57	0.81	5.30
B	1.57	2.83	0.92	3.68	-0.75	2.39	0.93	3.04
C	0.85	2.14	0.95	2.82	-1.22	2.11	0.95	2.74
D	2.70	2.92	0.81	3.47	1.89	2.25	0.85	2.80
E	1.02	2.88	0.90	3.65	-0.06	2.11	0.94	2.67
F	1.97	2.49	0.61	2.98	1.09	2.08	0.65	2.56

10-m wind speed is generally overestimated independently of the PBL scheme used, as WRF trends to force non-local synoptic patterns instead of local effects. On the other hand, YSU scheme usually produces slightly lower wind speed during daytime; at the opposite, after sunset higher values are predicted. Against coastal observations higher positive is achieved bias due to more influence of oversea geostrophic winds on the computation of inland winds. There is no clear pattern about the influence of La Niña-El Niño on the prediction of 10-m wind speed, highlighting the capability of WRF to properly represent both events.

**Table 3.** Statistics for 10-m wind speed: blue cells corresponds to January-June and red cells to July-December

Station	BIAS (m s <sup>-1</sup> )	Gross Error	IOA (m s <sup>-1</sup> )	RMSE (m s <sup>-1</sup> )	BIAS (m s <sup>-1</sup> )	Gross Error	IOA (m s <sup>-1</sup> )	RMSE (m s <sup>-1</sup> )
A	0.63	1.46	0.44	1.94	0.53	1.67	0.61	2.06
B	-0.35	1.19	0.83	1.58	-0.51	1.44	0.69	1.96
C	0.86	1.00	0.77	1.19	0.65	0.92	0.69	1.14
D	1.11	1.48	0.74	1.89	0.93	1.50	0.80	1.93
E	-0.54	1.18	0.74	1.45	-0.81	1.30	0.68	1.65
F	2.44	3.00	0.51	3.69	2.99	3.47	0.59	4.19

About upper air WRF validation, the PBLH WRF parameter was extracted at the two specific locations where either rawinsonde (Figure 3) or ceilometer (Figure 4) were launched/located. For the rawinsonde selected episode (1-12 June) the maximum PBL height occurs at 1500 LT over both locations, and it never exceeds 500 m. Coastal PBL height dynamics are more unstable before sunrise and after sunset due to sea breeze influence. On average, it is noted the very low PBL height during winter over the Chilean central zone, no matter onshore or inland location.

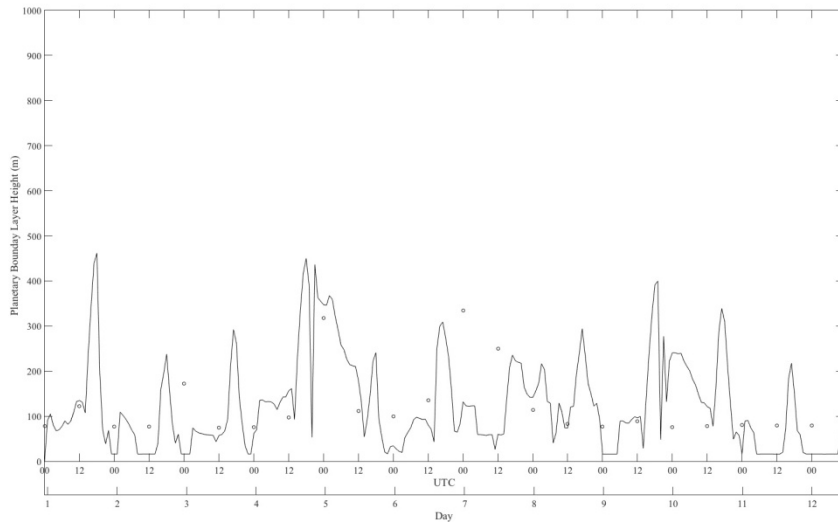


**Figure 3.** Evolution of the planetary boundary layer height along 1-12 June: (-) WRF, (○) rawinsonde

In this work, the available rawinsonde data do not represent properly the daily fluctuations and the diurnal development of the PBL height: this fact points out the low frequency of these measurements in the PBL (just 3-4 levels), as this rawinsonde is focused on synoptic patterns rather than the physics of the lowest layer. However, this approach of using synoptic rawinsonde to estimate PBL height could be feasible if the location presents a more convective behavior, as convection increases the PBL height and more upper air observations are included in this layer.

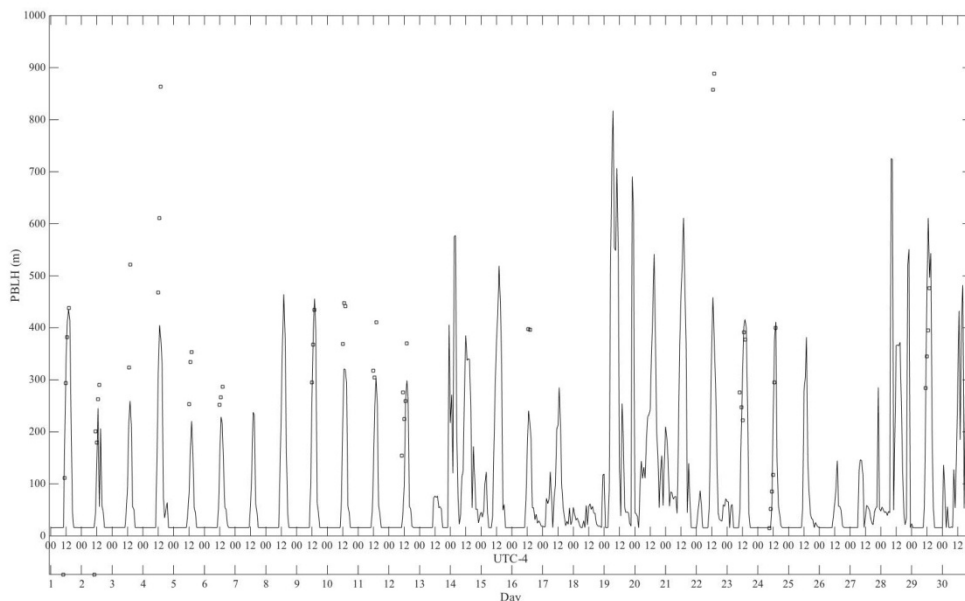


**Figure 4.** Evolution of the planetary boundary layer height along June 2009: (-) WRF, (□) ceilometer

In contrast with rawinsonde observations, ceilometer dataset provides a good representation of the diurnal dynamic development of the PBLH along June 2009 (Figure 4): At 1100 LT, mixing starts to increase, until it reaches its maximum at 1500 LT. The dynamic diurnal cycle predicted by WRF in inner Santiago de Chile is in agreement with ceilometer data. On some days the WRF model underestimates PBLH, also following the 2-m temperature underestimation during wintertime, lower heat transfer is predicted by WRF, affecting both parameters

## CONCLUSIONS

Both ENSO (El Niño Southern Oscillation) and topographic conditions of Central Chile provide a singular influence to the meteorological conditions over this region; which also affect to the PBL structure. In this work, WRF model validation at PBL over Central Chile was done during the El Niño-La Niña transition period, covering the whole 2009 year. About surface temperature, a positive bias in coastal model results was observed, especially during cold sea surface episodes along La Niña period; this result can be related to the overestimation of surface heat flux using YSU PBL scheme and 5-layer thermal diffusion soil model, combined to the sea breeze effect. In fact, inland sites model results show an underestimation of surface temperature. Better results were achieved for surface wind speed, with similar statistics in both El Niño and La Niña periods.

Specific conditions over Central Chile are favorable to low PBL height periods, producing poor air quality events over Santiago de Chile. Therefore, validation of PBL height calculated by WRF model was done along June 2009 period when air quality warnings were announced in that city. PBL height estimations from LIDAR observations are comparable to WRF model predictions, showing the capability of this model to represent this PBL parameter; only some differences arise when surface temperature bias is higher. Also, PBL estimations from synoptic rawinsonde datasets were done but, because of the low number of observations at the PBL, these estimations are not realistic. As synoptic rawinsondes are launched everyday all over the world, it should be highly recommended to increase these rawinsondes vertical resolution at the lowest layer, so they can be applied not only as synoptic observations, but also as PBL observations closely related to poor air quality episodes.

## ACKNOWLEDGMENTS

This paper/work was partially supported by CONICYT PAI/ Concurso Nacional Tesis de Doctorado en la Empresa, convocatoria 2014, 781413011 and CIRIC - INRIA-Chile (EP BIONATURE) through Innova Chile Project Code: 10CE11-9157.

## REFERENCES

- Emery, C., E. Tai and G. Yarwood, 2001: Enhanced Meteorological Modeling and Performance Evaluation for Two Texas Ozone Episodes. Environ International Corporation.
- Falvey, M. and R.D. Garreaud, 2005: A numerical case study of an orographically enhanced frontal system in central Chile. *Croat. Meteor. J.*, **40**, 486–489.
- Garreaud, R., J. Rutllant and H. Fuenzalida, 2002: Coastal Lows along the Subtropical West Coast of South America: Mean Structure and Evolution. *Monthly Weather Review*, **130**, 75–88.
- Gonzalez, J. A., A. Hernandez-Garces, A. Rodriguez, S. Saavedra and J.J. Casares, 2015: Surface and upper-air WRF-CALMET simulations assessment over a coastal and complex terrain area. *Int. J. Environ. Pollut.*, **57**, 249–260.
- Holtzlag, A.A.M. and van Ulden, A.P., 1983: A simple scheme for daytime estimates of the surface fluxes from routine weather data. *J. Clim. Appl. Meteor.*, **22**, 517–529.
- Huang, B., V. F. Banzon, E. Freeman, J. Lawrimore, W. Liu, T. C. Peterson, T. M. Smith, P. W. Thorne, S. D. Woodruff and H.-M. Zhang, 2015: Extended Reconstructed Sea Surface Temperature Version 4 (ERSST.v4). Part I: Upgrades and Intercomparisons. *J. Climate*, **28**, 911–930.
- Kleczek, M. A., G. J. Steeneveld, and A. Holtzlag, 2014: Evaluation of the Weather Research and Forecasting Mesoscale Model for GABLS3: Impact of Boundary-Layer Schemes, Boundary Conditions and Spin-Up. *Bound.-Lay. Meteorol.*, **152**, 213–243.
- Muñoz, R. C. and A. Undurraga, 2010: Daytime Mixed Layer over the Santiago Basin: Description of Two Years of Observations with a Lidar Ceilometer. *J. Appl. Meteorol. Climatol.*, **49**, 1728–1741.
- Saide, P., G. Carmichael, S. Spak, L. Gallardo, A. Osses, M. Mena-Carrasco and M. Pagowski, 2011: Forecasting urban PM10 and PM2.5 pollution episodes in very stable nocturnal conditions and complex terrain using WRF–Chem CO tracer model. *Atmos. Environ.*, **45**, 2769–2780.

**FLOW SIMULATIONS FOR THE ASSESSMENT OF SMALL WIND TURBINES  
IN URBAN AREAS**

*Sirma Stenzel<sup>1</sup>, Kathrin Baumann-Stanzersen<sup>1</sup>, Gabriele Rau<sup>1</sup>, Renate Teppner<sup>2</sup>, Kurt Leonhartsberger<sup>3</sup>*

<sup>1</sup>Central Institute for Meteorology and Geodynamic (ZAMG), Vienna, Austria

<sup>2</sup>AIT, Vienna, Austria

<sup>3</sup>Technikum Wien, Vienna, Austria

**Abstract:** In the frame of a national research project, as a part of the “City of future” program of the Austrian Research Promotion Agency, the potential and applicability of Small Wind Turbines (SWTs) in urban areas is investigated. The wind profile within the urban boundary layer is observed continuously for two years with a METEK SODAR in an industrial area in the northern part of Vienna. Close to the SODAR site, two types of SWTs are operated, one after another, on top of a building. Additionally, ultrasonic measurements are undertaken at two masts on the roof-top.

Focus of the presentation is stationary and non-stationary simulations of the wind field at roof-level of a building in an urban area with the models MISKAM, FLUENT and OpenFOAM. Differences and agreements between the model first results are discussed. The results are evaluated in comparison to ultrasonic and SODAR measurements. Main purpose of the project is the investigation of the capability of SWTs in an urban area and giving recommendations for site assessment of SWTs in a building environment.

**Key words:** *Small Wind Turbines, wind field simulations, SODAR measurements, CFD, MISKAM, FLUENT, OpenFOAM*

## INTRODUCTION

Small Wind Turbines (SWTs) are getting more popular when dealing with renewable energy. The practical application of the SWT is a big challenge, since the site assessment for them is quite complex and a rather unclear situation concerning certifications and laws exist up to now. In the following work the potential and the capability for SMTs in urban area are investigated. For this purpose measurements with METEK SODAR are conducted in an industrial area, near to the building of interest on the top of which the two SWTs will be operated (see Figure 1 and Figure 2).



**Figure 1.** Picture of the SWT (left) and one of the masts with ultrasonics in 3m and 6m above roof level and a sonic at 9m above roof level for site calibration at the SWT mast (right) on the top of the roof of the Energy Base building in the northern part of Vienna.

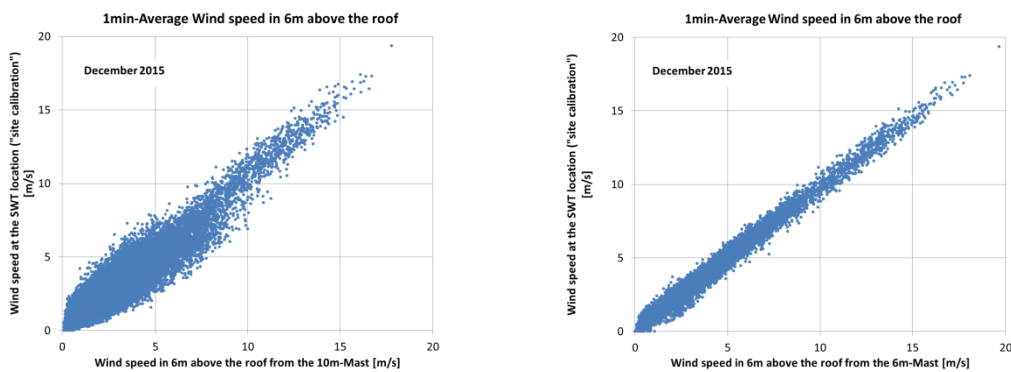


**Figure 2.** Location of the METEK SODAR east of the Energy Base building (left) and SODAR antenna array (right)

Additionally, ultrasonic measurements are undertaken at one 6m, one 10m mast and at the SWT mast (for site calibration) on the same roof.

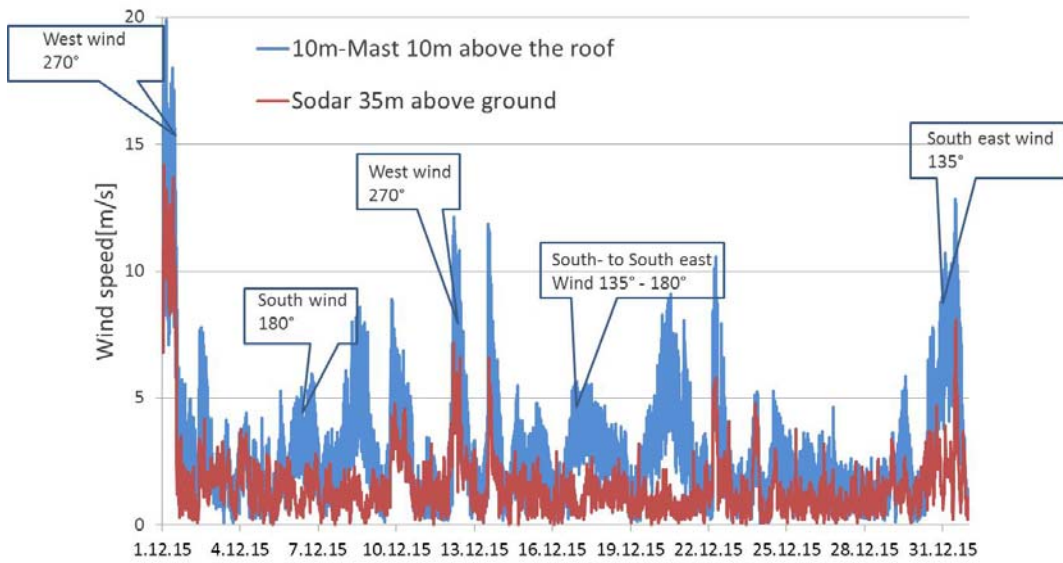
## RESULTS

Figure 3 shows 1min wind speed measurements from December 2015 at the masts in 6 m and 10 m above roof level compared to the site calibration data recorded in 9 m above roof level at the SWT mast. The wind speed measurements at the 6m are in good agreement with the site calibration measurement (Figure 3 right).



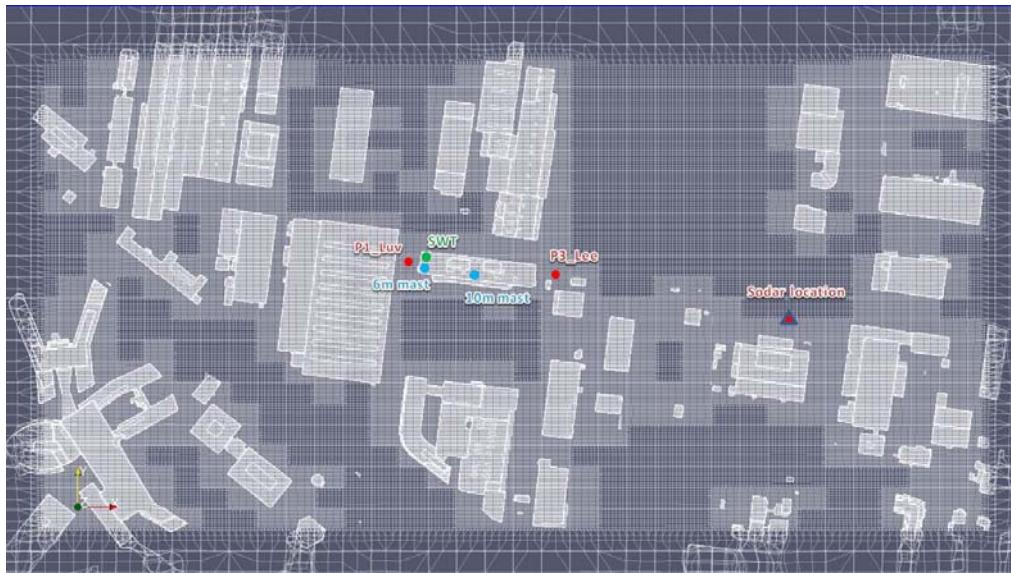
**Figure 3.** Example of the wind speed measurement on the roof of the building

Wind speed measurements for some selected days in December 2015 are depicted in Figure 4. Due to the deflection of the flow, as expected, wind speeds above the building tend to be higher than at the same height in the relatively undisturbed area where the SODAR is located. A good agreement between these wind measurements is found in days with prevailing westerly flow (e.g. 1.12.2015 and 13.12.2015). During southerly (e.g. 7.12.2015) or south-easterly flow (31.12.2015), the wind speeds measured with the SODAR are up to  $6 \text{ ms}^{-1}$  lower than at the same height above the Energy Base building as the flow at the SODAR site is obviously influenced by the one-storied building situated south of the SODAR, which is visible in Figure 2.



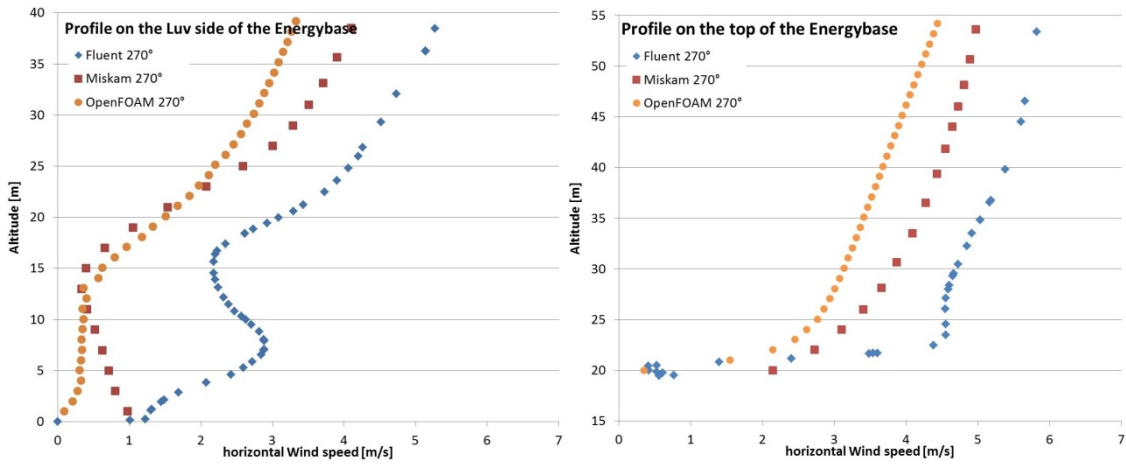
**Figure 4.** Time-series of SODAR wind speeds at 35m above ground and wind speeds measured with sonic at the 10m mast above roof for December 2015. The building is 25 m high. Main wind directions are depicted for selected episodes with good/poor agreement between the wind flow above roof and at the SODAR site.

A main focus of the project is the proceeding of stationary and non-stationary simulations of the wind field at the roof of the building with the models FLUENT, MISKAM and OpenFOAM. The input data for all the models are kept as identical as possible, nevertheless general differences in the models mesh, boundary conditions, solver etc. are to be kept in mind by the interpretation of the results. The turbulence models in FLUENT is the RSM (Reynolds Stress model) and MISKAM and OpenFOAM are conducted with RANs, where for OpenFOAM the standard k-ε turbulence model (Hargreaves and Wright, 2007) and the SIMPLE solver method for velocity-pressure coupling were applied. An example of the mesh generated with SnappyHexMesh in OpenFOAM is shown in Figure 5.



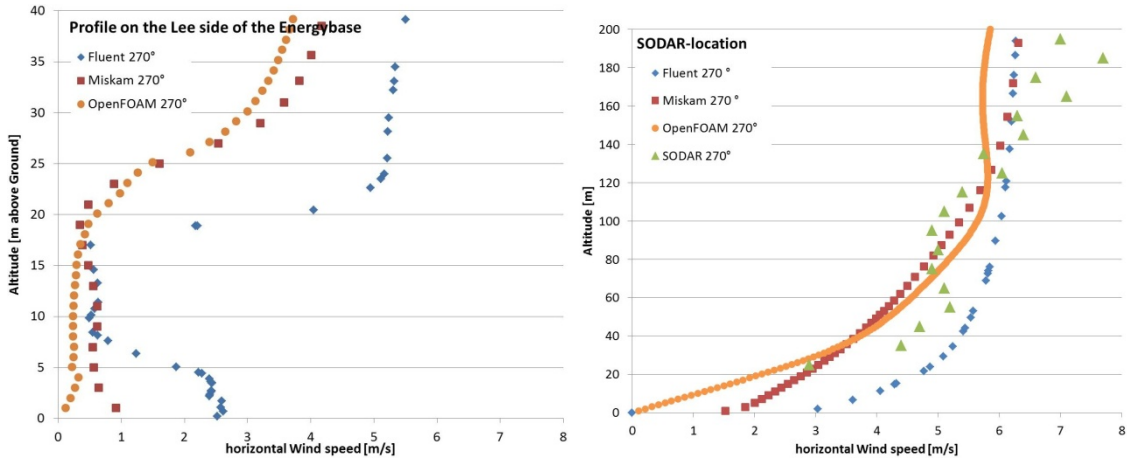
**Figure 5.** Mesh in OpenFOAM with ENERGY Base building in the centre of the model domain. Red points depict model grid points luv and lee of the building for model comparison (for 270° case), the red triangle indicates the SODAR site, green point the SWT site and blue points depict the 6m and 10m wind masts.

Figure 6 and Figure 7 depict the RANS model simulations for a  $270^\circ$  flow. There is a good agreement among the models on the top of the building (SWT location), but some differences are found for the model simulation for the selected luv and lee points near the building.



**Figure 6.** Profiles of the horizontal wind speed on the luv side (left) and at the SWT site on top of the Energy Base building (right) simulated with FLUENT, MISKAM and OpenFOAM for the  $270^\circ$  flow case.

Model simulations for a  $270^\circ$  case and SODAR measurements averaged over a period with nearly homogeneous upper level westerly winds (06.07.2015 from 7:00 am to 8:00 pm) are compared in the following. The models and the SODAR show similar profiles.



**Figure 7.** Profiles of the horizontal wind speed on the lee side of the building (left) and at the SODAR site (right) simulated with FLUENT, MISKAM and OpenFOAM for the  $270^\circ$  flow case compared to SODAR wind measurements averaged for a period with nearly homogeneous westerly flow (06.07.2015 from 7:00 am to 8:00 pm).

## CONCLUSIONS

First analyses of wind measurements at three masts on top of a building and from SODAR nearby as well as from RANS model simulations with MISKAM, FLUENT and OpenFOAM conducted in the frame of a national research project on site assessment for roof-mounted small wind turbines in urban areas are presented. The wind measurements at the different sites reveal clearly that the winds in the first ten meters above the building are accelerated due to the deflection of the flow. Small building structures on top of the roof have a visible impact on the winds at the 10m mast site. The wind profiles measured by the SODAR are clearly influenced by a nearby one-storied building during southerly flow. The RANS model

simulations for a 270 ° flow render similar profiles on top of the building and at the SODAR site while relatively large differences are found in the luv and lee of the building. Some of these differences may be explained by differences in the models inputs (boundary conditions, mesh etc.). Main output of the project will be a report on the capability of different types of SWTs at an urban site and recommendations for measurements and model simulations for site assessment of SWTs in a building environment.

## REFERENCES

- Ansys,2009: Ansys Fluent 14. 0Theory Guide, Canonsburg, Pa, USA.
- D.M. Hargreaves and N.G. Wright, 2007:On the use of the k-epsilon model in commercial CFD software to model the neutral atmospheric boundary layer. *J.Wind Engineer. Industrial Aerodynam.* **95**, 355-369.
- Eichhorn, J., 2010: MISKAM – Handbuch zu Version 6. giese-eichhorn umweltmeteorologische software, 2010.
- OpenCFD Limited, OpenFOAM User Guide—Version 2.3.1,OpenCFD Limited, December 2014.

**17th International Conference on  
Harmonisation within Atmospheric Dispersion Modelling for Regulatory Purposes  
9-12 May 2016, Budapest, Hungary**

---

**VALIDATION OF THE ATMOSPHERIC DISPERSION MODEL NAME AGAINST LONG-RANGE TRACER RELEASE EXPERIMENTS**

*Vibha Selvaratnam, David Thomson and Helen Webster*

Met Office, UK

**Abstract:** The Met Office's atmospheric dispersion model NAME has been validated against the long-range controlled tracer-release experiments CAPTEX and ANATEX. The model is driven by different sources of meteorology obtained from WRF and from ERA-Interim by ECMWF. The performance of NAME is assessed and compared with the validation of other Lagrangian particle dispersion models against the same experiments.

**Key words:** *model validation, model comparison, dispersion experiments*

## **INTRODUCTION**

Validating dispersion models against controlled experiments gives the advantage of having more information about the releases than with ad-hoc events. This more accurate information about the releases along with the systematic measurements taken throughout the course of the experiments makes this data ideal for assessing how well the model is performing. It also gives the opportunity to consider how different sources of meteorological data used to drive the models might affect their performance.

The Met Office's atmospheric dispersion model NAME (Numerical Atmospheric-dispersion Modelling Environment) (Jones et al., 2007) is validated against controlled tracer release experiments conducted in North America. Here we will consider two long-range experiments that have also been used to validate other dispersion models (Hegarty et al., 2013). This will give the opportunity for both evaluating against the observations and comparing with the performance of other models.

## **EXPERIMENTAL DATA**

The Cross-Appalachian Tracer Experiment (CAPTEX) and the Across North America Tracer Experiment (ANATEX) were controlled tracer-release experiments conducted in the North American region in the 1980's (Draxler and Heffter, 1989, Ferber et al., 1986).

CAPTEX consisted of seven releases (referred to as CAPTEX-1 through to CAPTEX-7) from 18 September to 29 October 1983. CAPTEX-6 was a short release of 30 minutes from Dayton, Ohio which has been omitted for this comparison to be consistent with the work done by Hegarty et al. (2013). Each of the others was a 3 hour release of perfluoromonomethylcyclohexane (PMCH), the first four of which were from Dayton, Ohio and the last two (CAPTEX-5 and CAPTEX-7) from Sudbury, Ontario, Canada. Each release was separated by a few days so each release is treated as a separate experiment. A sampling network of 84 sites 300-800km from the source collected samples of the tracers at ground level. 3 and 6 hour averages were retrieved for 48-60 hours after each release over the period from 19 September to 30 October.

ANATEX consisted of 66 3 hour releases from 5 January to 26 March 1987. Half were releases of perfluorotrimethylcyclohexane (PTCH) from Glasgow, Montana (GGW) and the other half were releases of perfluorodimethylcyclohexane (PDCH) from St. Cloud, Minnesota (STC). The releases from St. Cloud included releases of PMCH but these were not included in the comparison by Hegarty et al. (2013) as they were coincident with the PDCH releases. As such, they are not included in this validation of NAME to be consistent with the validation of the other models. As each site released a different tracer, releases

from each were treated as separate experiments (called ANATEX-GGW and ANATEX-STC). The releases were at 2.5 day intervals to alternate between afternoon and nighttime. The sampling network consisted of 75 sites over the eastern United States and southeastern Canada reaching up to about 3000km from the sources. Air samples averaged over 24 hours were collected at ground level from 5 January through to 29 March.

For this comparison, only the first 10 releases (spanning 5-16 January) from ANATEX are included to make it comparable in length to CAPTEX and to use the same period used in previous validations of particle dispersion models (Hegarty et al., 2013). This period at the start of the experiment also gives the contrast of winter conditions compared to the summer like conditions during CAPTEX. Each CAPTEX release was represented by 50,000 particles and the ANATEX releases by 25,000 particles which is consistent with the number of particles released by other model runs. Increasing the number of particles seems to have little to no effect on the analyses and the fewer particles released for the ANATEX releases is compensated for by the longer averaging time for calculating the air concentrations.

### **DISPERSION MODELS**

All the models discussed here are Lagrangian particle dispersion models. Particles are released from a source location and are advected by the mean winds obtained from input meteorological data and a random component added by the model to represent turbulence.

#### **Numerical Atmospheric-dispersion Modelling Environment (NAME)**

The NAME output is given on a 0.25 x 0.25 degree grid in the lat-long coordinate system and concentrations are calculated over the lowest 100m agl. The meteorological data was used on its native horizontal grid with the vertical grid being interpolated and the model time-step was set to 15 minutes. Dispersion due to both turbulence and unresolved mesoscale motions were represented while convection above the boundary layer was not.

#### **Hybrid Single-Particle Lagrangian Integrated Trajectory (HYSPLIT)**

The dispersion calculations in HYSPLIT conducted by Hegarty et al. (2013) were made on the same horizontal grid as the meteorological data. HYSPLIT uses an internal terrain following vertical coordinate so the meteorological fields are linearly interpolated to this grid. The lowest vertical grid level was at approximately 10m above ground level and the resolution decreases with height. The resolution of the output grid and the number of particles representing each release are the same as in the NAME runs and the time-step was 1 minute (Hegarty et al., 2013).

#### **Stochastic Time-Inverted Lagrangian Transport (STILT)**

STILT is built upon HYSPLIT and so has many of the same features such as the mean advection scheme and the calculation grid. Although STILT is primarily used in backward mode, for this comparison only the performance of the model run forward in time has been considered. The configuration used is the same as HYSPLIT (for example output concentration grid and number of particles released) but STILT simulates turbulence differently (Hegarty et al., 2013).

#### **Flexible Particle (FLEXPART)**

The version of FLEXPART used by Hegarty et al. (2013) is one modified to use meteorological data from WRF. It uses the native horizontal grid of WRF and the vertical levels are interpolated to an internal terrain following coordinate. The output concentrations were given on a 25km x 25km horizontal grid using the same projection as the meteorological data which is similar to the 0.25 degree grid used for the other models. As with the other models, output concentrations were given over the lowest 100m agl. The time-step was calculated dynamically with a maximum of 90 seconds and each release was represented by 100,000 particles in both CAPTEX and ANATEX (Hegarty et al, 2013).

### **METEOROLOGICAL DATA**

The models are run using reanalysed meteorological data from different sources and in some cases, different configurations of the same numerical weather prediction model. The meteorological data used for the two sets of comparisons are detailed below.

The ERA-Interim meteorological fields are from ECMWF. ERA-Interim is a global atmospheric reanalysis starting from 1979 produced with a 2006 version of the IFS (Integrated Forecast System). The spatial resolution is approximately 80km with 60 vertical levels and output is given every 3 hours.

The North American Regional Reanalysis (NARR) is an extension of the NCEP/NCAR (National Centers for Environmental Prediction/National Center for Atmospheric Research) Global Reanalysis which has been run over the North American region. The reanalysis was run from 1979 to 2014 and is on a Lambert Conformal grid of approximately 32km and 45 vertical levels with output every 3 hours. This data is used to drive the WRF data used.

The Advanced Research version of the WRF (Weather Research and Forecasting) model (ARW) is used and the initial and boundary conditions are obtained from NARR. The configuration of ARW used is on a Lambert Conformal horizontal grid and uses a terrain-following hydrostatic-pressure vertical coordinate system of 43 levels, with the lowest approximately 33m thick. The model was configured with two nested horizontal resolutions of 30km and 10km with one way boundary conditions between the two and 3 hourly output. Output from the ARW model with wind nudging towards NARR in the boundary layer both turned on and off are used to run the dispersion models.

### STATISTICAL MEASURES

Assessing the accuracy of a dispersion model is difficult due to having both temporal and spatial variations. Each statistical parameter has different sensitivities to these variations. We use the same system of ranking used by Hegarty et al. (2013) which combines four statistical parameters to obtain an overall rank. The software used for the calculations is detailed in Draxler et al. (2001) and provided by NOAA Air Resources Laboratory.

The correlation coefficient (R) ranges from -1 to 1 where 1 is a perfect (positive) correlation between measured and predicted concentrations. The normalised sum of  $R^2$  ranging from 0 to 1 is the value that contributes to the final rank. The fractional bias (FB) is a fraction of the average between paired predicted and measured values and ranges from -2 to 2. The values are paired in both space and time. A positive value indicates an overprediction by the model and a negative value an underprediction. The figure of merit in space (FMS) is a percentage overlap between measured and predicted areas at a fixed time. A fixed significant concentration level is set (although here a value of  $0 \text{ g m}^{-3}$  is used) and the percentage is the proportion of sites that agree to be either above or below this level. Because it is evaluated at a fixed time, although a high FMS indicates a good prediction, a low value does not necessarily imply a bad prediction as the plume could have the correct shape but slightly shifted in space or time. This bias is particularly pronounced with narrow plumes. The Kolmogorov-Smirnov parameter (KSP) is the maximum absolute difference between two cumulative distributions (expressed as percentages), so a smaller value implies a better prediction (Mosca et al. 1998).

These four parameters are equally weighted so that each can contribute a maximum value of one to the final rank, which ranges from 0 to 4 and a higher rank implies a better prediction. The formula used is

$$Rank = R^2 + (1 - |FB / 2|) + FMS / 100 + (1 - KSP / 100). \quad (1)$$

### RESULTS

Table 1 and Figure 1 show how well NAME performs when being driven by different meteorological data. The three sources of driving fields are from WRF, both with wind nudging towards NARR switched on (V1) and with it switched off (V2) and from ERA-Interim. Figure 1 shows how each of the statistical parameters contributes to the final rank given for each simulation as well as averages for each of the sources of meteorological data. We see that NAME driven by WRF generally performs better when the wind nudging towards NARR is switched on compared to when it is switched off. We also see that NAME seems to perform best when run with the ERA-Interim meteorology despite the lower resolution of the data.

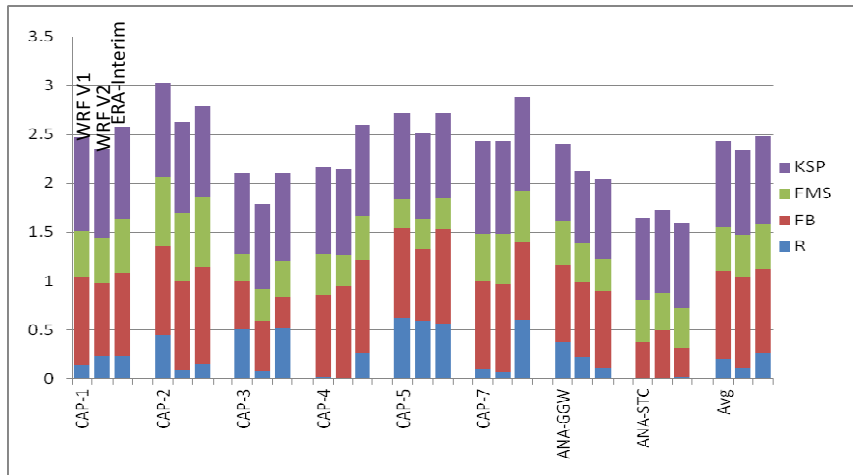


**Figure 1.** Bar plots of the normalised statistical parameters contributing to the rank as calculated in Eq. (1) for NAME driven by meteorological fields from WRF V1 (column 1), WRF V2 (column 2) and ERA-Interim (column 3).

The two cases where the model performs noticeably better when driven by ERA-Interim rather than with the WRF are for CAPTEX-4 and CAPTEX-7. In both of these experiments we see that the difference in the contribution from the correlation coefficient appears to make the most difference in the overall rank as it is almost zero for both the WRF driven simulations. The other statistical parameters seem to be largely the same for all three runs. However, the correlation coefficient does not always give an indication of the final rank, for example for ANATEX-STC where the correlation coefficient is almost zero for all of the runs but the final rank does differ. This reiterates the fact that a single statistical parameter may not give an accurate representation of how well the model is performing overall due to different biases but in combining the four, this should give a more robust indication.

**Table 1.** Rank results from the NAME model evaluation. Simulations are driven by WRF time-averaged fields with grid nudging of winds towards NARR either turned on (V1) or off (V2), and ERA-Interim fields.

Experiment	WRF V1	WRF V2	ERA-Interim
CAPTEX-1	2.47	2.35	2.58
CAPTEX-2	3.02	2.63	2.79
CAPTEX-3	2.11	1.79	2.12
CAPTEX-4	2.17	2.15	2.60
CAPTEX-5	2.73	2.51	2.72
CAPTEX-7	2.43	2.43	2.89
ANATEX-GGW	2.40	2.12	2.04
ANATEX-STC	1.65	1.73	1.59
Avg	2.37	2.21	2.42

Figure 2 shows how all the dispersion models perform being driven by both versions of the WRF meteorological data with the ranks for HYSPLIT, STILT and FLEXPART from Hegarty et al. (2013). In all cases except ANATEX-STC, NAME and FLEXPART perform better with WRF V1 data where the wind nudging towards NARR is turned on compared to that when there is no wind nudging. HYSPLIT and STILT however do not seem to have a preference for one set of WRF meteorology over the other and on average there is little difference between the two. As STILT is built upon the HYSPLIT model, it is unsurprising that they react to a change in driving meteorology in a similar way and, for each experiment, they both show a similar difference in performance using one set of meteorology over the other.

On average, the performances of each of the models are relatively similar. It can be seen that FLEXPART driven by WRF V2 meteorological data generally has a slightly lower ranking than the other three models apart from for the CAPTEX-7 experiment where it noticeably performs better than all the other models. It is also clear that the ANATEX-STC experiment seems to have been the most difficult to predict as this is the

experiment that all the models had the weakest performance for. Although this could be due to the WRF data having errors, we see in Figure 1 that NAME runs driven by ERA-Interim shows the same low ranking for this experiment so it is likely that there were some difficult conditions to predict over this time and location.

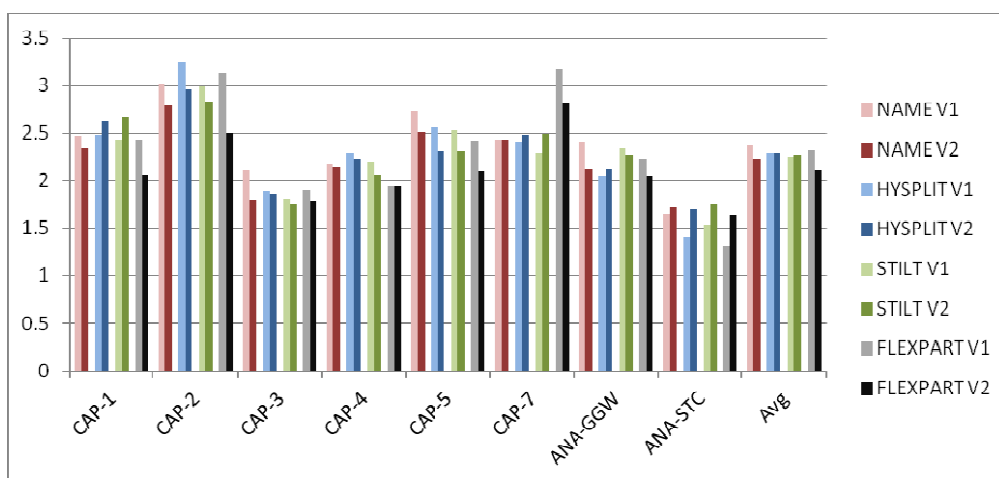


**Figure 2.** Bar plot of the rank for NAME, HYSPLIT, STILT and FLEXPART driven by meteorological fields from WRF with wind nudging on (V1) and WRF without wind nudging (V2).

## CONCLUSIONS

The Lagrangian particle dispersion model NAME was run to simulate controlled tracer-release experiments and the performance evaluated when driven by different meteorological fields as well as comparing the performance with other dispersion models. The assessment used a system of ranking consisting of four statistical parameters to be consistent with the validation of the other models (Hegarty et al., 2013).

It was found that the different models responded in a similar way to differences in driving meteorology, in particular a tendency to perform better with WRF winds nudged towards NARR. NAME simulations were also conducted using ERA-Interim meteorology which generally performed better than the WRF driven runs despite the lower resolution. There was no distinctive difference in performance for a particular model and differences in model performance over the different experiments were generally consistent, for example all the models achieved lower ranks for the ANATEX-STC experiment.

## REFERENCES

- Draxler, R.R. and J.L. Heffer, 1989: Across North America Tracer Experiment (ANATEX) Volume I: Description, ground-level sampling at primary sites and meteorology. *NOAA Tech. Memo. ERL ARL-167*, 83 pp.
- Ferber, G.J., J.L. Heffer, R.R. Draxler, R.J. Lagomarsino, F.L. Thomas, and R.N. Dietz, 1986: Cross-Appalachian Tracer Experiment (CAPTEX '3) final report. *NOAA Tech. Memo. ERL ARL-142*, 60 pp.
- Hegarty, J., R.R. Draxler, A.F. Stein, J. Brioude, M. Mountain, J. Eluszkiewicz, T. Nehr Korn, F. Ngan and A. Andrews, 2013: Evaluation of Lagrangian Particle Dispersion Models with Measurements from Controlled Tracer Releases. *J. Appl. Meteor. Climatol.*, **52**, 2623-2637.
- Mosca, S., G. Graziani, W. Kulg, R. Bellasio and R. Bianconi, 1998: A statistical methodology for the evaluation of long-range dispersion models: An application to the ETEX exercise. *Atmos. Environ.*, **32**, 4307-4324.
- Draxler, R.R., J. L. Heffer, G. D. Rolph, 2001: Data Archive of Tracer Experiments and Meteorology. [Available online at <http://www.arl.noaa.gov/documents/datem/document/datem.pdf>].
- Jones A.R., Thomson D.J., Hort M. and Devenish B., 2007: The U.K. Met Office's next-generation atmospheric dispersion model, NAME III. Borrego C. and Norman A.-L. (Eds) *Air Pollution Modeling and its Application XVII (Proceedings of the 27th NATO/CCMS International Technical Meeting on Air Pollution Modelling and its Application)*, Springer, 580-589.

**17th International Conference on  
Harmonisation within Atmospheric Dispersion Modelling for Regulatory Purposes  
9-12 May 2016, Budapest, Hungary**

---

**IMPACT OF ALTERNATIVE DISPERSION MODEL VALIDATION METHODS: A CASE  
STUDY ON THE LNG MODEL VALIDATION DATABASE USING DRIFT**

*Simon Gant<sup>1</sup>, Simon Coldrick<sup>1</sup>, Graham Tickle<sup>2</sup> and Harvey Tucker<sup>1</sup>*

<sup>1</sup>Health and Safety Executive (HSE), Buxton, UK

<sup>2</sup>GT Science and Software Ltd.

© British Crown Copyright, 2016

**Abstract:** This paper assesses the impact of using different methods to compare dense-gas dispersion model predictions to experimental data, using the DRIFT integral model and the field-scale experimental data presented in the Liquefied Natural Gas (LNG) Model Validation Database. Three different model comparison methods are tested, which relate to different interpretations of the predicted maximum arc-wise concentration. Method 1 takes the predicted maximum arc-wise concentration to be the maximum concentration at any radial position and any height on a given arc. Method 2 takes it to be the maximum at any radial position but at the height of the sensors in the experiments. Method 3 takes it to be the maximum of the predicted concentrations at the sensors positions (at both their radial position and height). The motivation for this work is that Method 3 is adopted in the LNG Model Evaluation Protocol used by the US Pipelines and Hazardous Materials Safety Administration to approve models for use in LNG siting studies. Methods 1 and 2 have been used in other model assessment exercises.

The results show that the choice of method has a significant effect on the outcome of the model evaluation exercise. Method 1 makes it appear that DRIFT over-predicts the measured concentrations on average, whereas Method 2 and (more so) Method 3 make it appear that the model under-predicts the concentrations. One of the difficulties in applying Method 3 is that narrow plumes sometimes miss all of the sensors on an arc, which causes problems in calculating the geometric mean and variance. Results from a modified wind-meandering model in DRIFT are also presented, which gives improved agreement with the data when using Method 3.

**Key words:** *Dense-gas dispersion, LNG, model evaluation, validation, DRIFT, arc-wise maximum concentration*

## **INTRODUCTION**

It is important to have a consistent approach to validation within the context of the regulatory use of dispersion models to ensure that models are evaluated on a common basis. If different models are evaluated using different approaches (e.g. by outputting the predicted concentrations at different locations) then this could bias the results of the validation exercise and defeat the purpose of a standardised validation procedure.

The use of dispersion models to determine the size of exclusion zones around Liquefied Natural Gas (LNG) facilities in the US is regulated by the Pipeline and Hazardous Materials Safety Administration (PHMSA), who require models to be approved using the procedure defined in the LNG Model Evaluation Protocol (Ivings *et al.*, 2007). An important part of this approval process involves the comparison of dispersion model predictions to experimental data given in the National Fire Protection Association's (NFPA) LNG Model Validation Database (Coldrick *et al.*, 2010) and the calculation of Statistical Performance Measures (SPMs). The experimental data consist of maximum concentrations at sensors on each downstream measurement arc (i.e. maximum arc-wise concentrations), plume widths and maximum concentrations at individual sensors in 33 dispersion experiments. These include field-scale experiments from the Burro, Coyote, Falcon, Maplin Sands and Thorney Island trials and wind-tunnel experiments from the BA-Hamburg, BA-TNO and CHRC experiments. Three dispersion models have been subject to this approval process to date (FLACS, PHAST and DEGADIS) and other model developers have expressed an interest in seeking approval for their models following this process.

A consistent methodology for comparing models to measurements has been applied by PHMSA in evaluating models, but other dispersion modellers have adopted different methods when they have independently tested their models against the LNG Model Validation Database. Specifically, the way in which maximum arc-wise concentrations have been output from models has differed. Previous dense-gas dispersion model evaluation exercises (e.g. Havens, 1992) have suggested that these different approaches could have a significant effect on the outcome of the model evaluation exercise.

To investigate this matter, the present work compares three different methods to calculate the arc-wise maxima using the DRIFT integral dispersion model. The analysis only considers the experimental data from four of the field-scale tests in the LNG Model Validation Database (Burro, Coyote, Falcon and Maplin Sands). The wind-tunnel tests are not considered because the three different methods would give identical results in those cases. Only short-time-averaged concentrations are examined, since the primary interest is in assessing the flammable hazard.

### METHODS FOR DETERMINING ARC-WISE MAXIMUM CONCENTRATIONS

The different methods used to determine the maximum arc-wise concentrations are summarised in Figure 1. The experimental data in the LNG Model Validation Database was processed by first taking the maximum of the time-varying concentrations at each of the sensors along the arc. The highest of these maximum concentrations was then taken as the measured maximum arc-wise concentration (i.e. from any of the sensors along the arc, at any radial position or height). For the unobstructed field-scale tests, the highest concentrations were nearly always measured at the sensors nearest to the ground, typically at a height of 1.0 m.

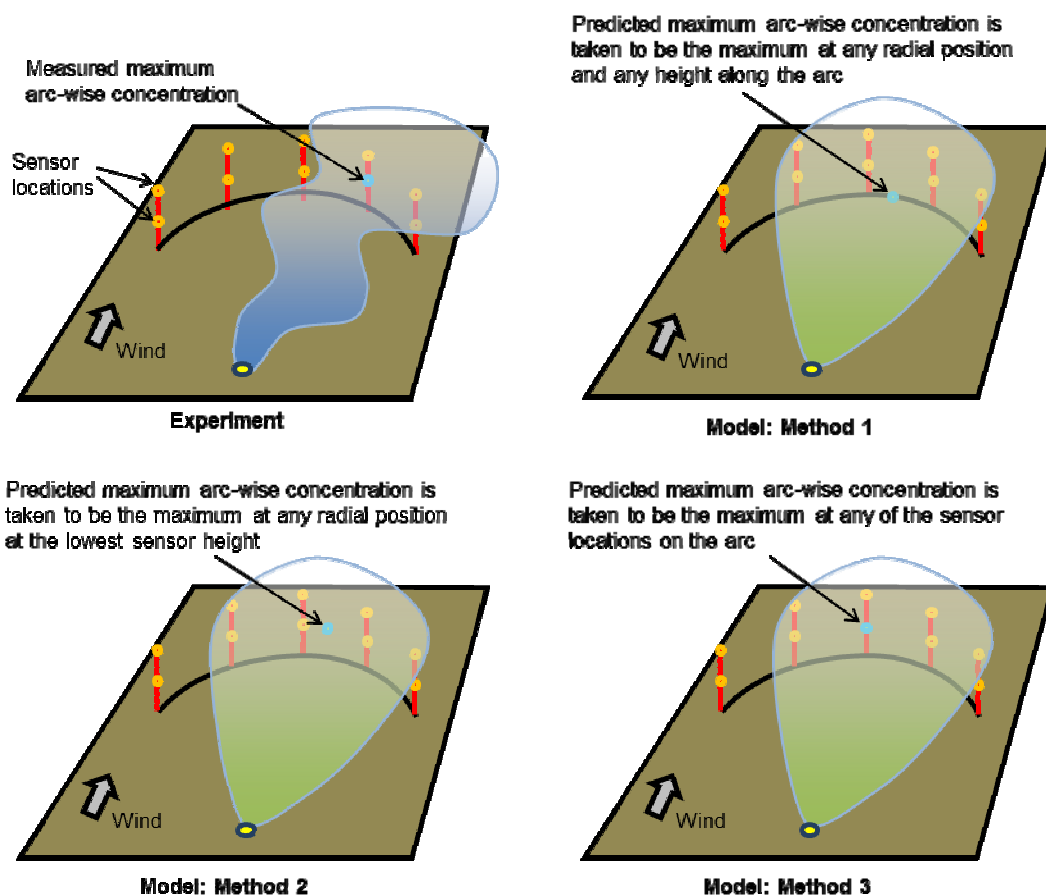


Figure 1. Illustration of methods for determining the predicted arc-wise maximum concentration

The three methods shown in Figure 1 for determining the predicted maximum arc-wise concentration are:

- **Method 1:** which takes the “absolute” maximum concentration at any radial location and height. Typically, this will be at ground level on the centreline of the cloud.
- **Method 2:** which takes it to be the maximum concentration at any radial position but at the height of the lowest sensors in the experiments.
- **Method 3:** which takes it to be the maximum of the predicted concentrations at the sensors positions (at both their radial position and height). This is the method used by PHMSA.

#### DRIFT INTEGRAL DISPERSION MODEL

DRIFT (Dispersion of Releases Involving Flammables or Toxics) is an integral model for dispersion of dense, passive or buoyant gas clouds produced from instantaneous, time-varying or continuous releases (Tickle and Carlisle, 2008), which is currently developed by ESR Technology and GT Science and Software, and used by HSE for land-use planning purposes in the UK. To model evaporating pools of LNG, the model uses the GASP source model (Webber, 1990). Details of the configuration of DRIFT for the cases considered here can be found in the report by Coldrick (2014).

The effect of lateral plume meandering is accounted for in DRIFT by making the plume width a function of the averaging time and plume travel time. For a given release (at a fixed distance downwind), the model predicts a narrower plume with a higher peak concentration for a shorter averaging time (see Figure 2a). The predicted concentrations are ensemble-mean values, i.e. an average over multiple “snapshots” of the meandering plume, not a single snapshot in time.

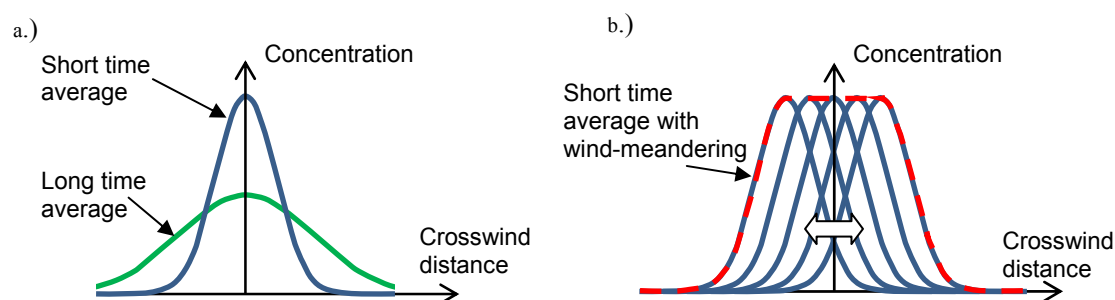


**Figure 2.** Typical lateral profiles of the plume concentration using: a.) short and long averaging times; b.) short averaging time with wind-meandering

In contrast to these notions of ensemble mean concentrations, the measured maximum arc-wise concentrations in the LNG Model Validation Database are taken as the highest concentration measured at any of the sensors across the arc at any point in time as the cloud passes the sensors. The measured maximum arc-wise concentrations are not determined from an ensemble mean. Lateral meandering of the plume causes high instantaneous concentrations to be distributed across the plume width in the experiments, producing a more flat-topped profile for the short time-averaged peak concentrations than that produced by an ensemble mean (as shown in Figure 2b).

These differences between the quantities output by DRIFT and those measured in the experiments has a significant impact on the model evaluation results when Method 3 is used to determine maximum arc-wise concentrations. Method 3 relies on the location of individual sensors and the DRIFT model with short time averaging and no meander produces a relatively narrow plume that sometimes misses the sensors, whereas the measured meandering plume is more likely to pass through the sensors. To compare to the experiments on a more like-for-like basis, DRIFT’s plume meandering model has been used to produce results denoted “**Method 3a**”. These results are based on meandering the short time-averaged concentrations, replicating the process used to produce the dashed red line shown in Figure 2b. Formally,

Method 3a calculates the new concentration profile by laterally displacing the short time averaged plume up to a maximum distance corresponding to the 5% level of DRIFT's cumulative probability distribution for plume meander, i.e. the centreline is predicted to be displaced by this lateral distance 5% of the time.

## RESULTS

Sample results are presented from DRIFT in Figure 3 for the Maplin Sands 27 experiment, which involved a continuous spill of LNG onto the surface of the sea with a wind speed of 5.5 m/s. The four different methods for determining the predicted maximum arc-wise concentration all produce different results for this case. Close to the source, the vertical gradient in concentration is such that the concentrations predicted at the sea surface (Method 1) were roughly twice as high as those predicted at 1.0 m height (Method 2). The narrow plume predicted by DRIFT missed most of the sensors and so Method 3 gave practically zero concentrations at most of the measurement arcs. Using the meandering model (Method 3a), DRIFT predicted a wider plume and therefore higher concentrations at the sensor positions, but the measurements were still under-predicted by around a factor of three.

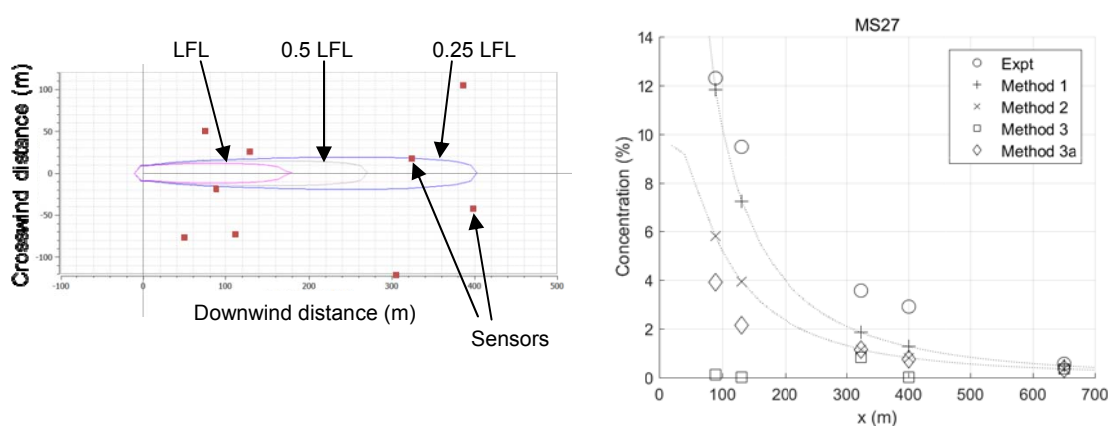


**Figure 3.** Maplin Sands 27 results showing contours of predicted Lower Flammability Limit (LFL) concentration on a horizontal slice at a height of 1.0 m (left) and comparison of predicted and measured maximum arc-wise concentration (right)

Table 1 and Figure 4 present a summary of the results for all four of the field-scale tests (Burro, Coyote, Falcon and Maplin Sands) in terms of predicted versus measured maximum arc-wise concentrations and the SPMs (for the definition of the SPMs, see Ivings *et al.*, 2007). These show that Method 1 makes DRIFT appear to over-predict the measurements on average (MRB < 0), whilst Methods 2, 3 and 3a make it appear that DRIFT under-predicts the measurements on average, by varying degrees. Using Methods 1 and 2, DRIFT falls within the bounds of what is considered “acceptable” model performance according to the LNG Model Evaluation Protocol (MEP) (Ivings *et al.*, 2007). Method 3 gives very large values for the MG and VG, since they are calculated from the ratio of measured to predicted concentrations, and the predicted concentrations are close to zero in some cases. Method 3a suffers less from these problems, but low concentrations in the Maplin Sands and Coyote 3 experiments still produce very high values of MG and VG.

**Table 1.** Statistical Performance Measures for Methods 1, 2, 3 and 3a and their acceptable limits as specified in the LNG MEP (Ivings *et al.*, 2007). Unacceptable values are highlighted in bold.

Method	Mean Relative Bias (MRB)	Mean Relative Square Error (MRSE)	Geometric Mean (MG)	Geometric Variance (VG)	Factor of Two (FAC2)
Acceptable	-0.4 < MRB < 0.4	MRSE < 2.3	0.67 < MG < 1.5	VG < 3.3	FAC2 > 50%
1	-0.21	0.34	0.79	1.5	78%
2	0.31	0.38	1.4	1.6	61%
3	<b>0.59</b>	1.1	<b>6.6</b>	<b>1.8 × 10<sup>13</sup></b>	54%
3a	<b>0.41</b>	0.59	<b>1.9</b>	<b>15</b>	56%

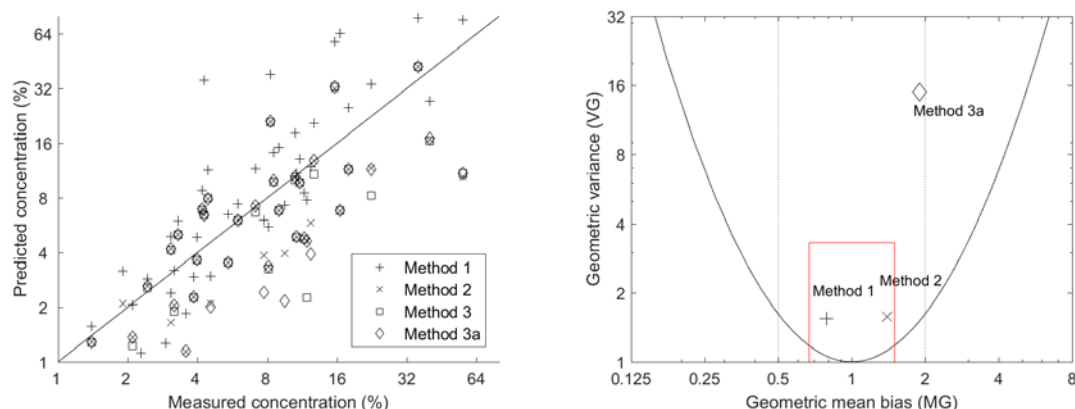


**Figure 4.** Scatter plot of predicted versus measured concentrations (left) and geometric mean versus geometric variance (right). Some points fall outside the bounds of the plots

## DISCUSSION AND CONCLUSIONS

This work has shown that the choice of method used to output predicted maximum arc-wise concentrations can have a strong effect on the conclusions of a dense-gas model validation exercise. Depending on the method used, DRIFT was found to either under-predict or over-predict the measurements on average. The method used by PHMSA (Method 3) made it appear that DRIFT significantly under-predicted the measurements. This behaviour was mainly due to DRIFT producing a narrow plume for a short averaging time that sometimes missed all of the sensors on a given arc, whereas the way in which the measurements were processed produced a wider plume which was more likely to pass through the sensors. As a refinement, DRIFT's plume meandering model was used to output a quantity from the model that more closely matched the type of quantity measured in the experiments. This refined output (Method 3a) showed improved agreement with the measurements. Further work is needed to assess this approach in more detail.

## ACKNOWLEDGEMENTS AND DISCLAIMER

The authors would like to thank Julie Halliday (PHMSA), Simon Rose (Oak Ridge National Laboratory) and Andrew Kohout (US Federal Energy Regulatory Commission) for their support in producing this work. This publication and the work it describes were funded by the Health and Safety Executive (HSE). Its contents, including any opinions and/or conclusions expressed, are those of the authors alone and do not necessarily reflect HSE policy.

## REFERENCES

- Coldrick, S., C.J. Lea and M.J. Ivings, 2010: Guide to the LNG Model Validation Database, Version 11.0, 17<sup>th</sup> May 2010. Available from: [http://www.nfpa.org/~media/files/research/research-foundation/research-foundation-reports/hazardous-materials/lng\\_database\\_guide.pdf?la=en](http://www.nfpa.org/~media/files/research/research-foundation/research-foundation-reports/hazardous-materials/lng_database_guide.pdf?la=en), accessed 8 February 2016.
- Coldrick, S., 2014: Review of DRIFT version 3.6.4, Health and Safety Laboratory (HSL) Report MSU/2012/11. Available from HSL: Buxton, UK.
- Havens, J., 1992: An evaluation of the DEGADIS dense gas (atmospheric) dispersion model with recommendations for a model evaluation protocol, South Coast Air Quality Management District, Diamond Bar, California 91765, USA.
- Ivings, M.J., S.F. Jagger, C.J. Lea and D.M Webber, 2007: Evaluating vapor dispersion models for safety analysis of LNG facilities, Fire Protection Research Foundation Report, National Fire Protection Association (NFPA), Quincy, MA, USA
- Tickle, G.A. and J.E. Carlisle, 2008: Extension of the dense gas dispersion model DRIFT to include buoyant lift-off and buoyant rise, HSE research report RR629. Available from: <http://www.hse.gov.uk/research/rrhtm/rr629.htm>, accessed 8 February 2016.
- Webber, D.M., 1990: A model for pool spreading and vaporisation and its implementation in the computer code GASP, UKAEA Report SRD R507.

**17th International Conference on  
Harmonisation within Atmospheric Dispersion Modelling for Regulatory Purposes  
9-12 May 2016, Budapest, Hungary**

---

**A VALIDATION STUDY OF THE ADMS PLUME CHEMISTRY SCHEMES**

*Stephen E. Smith<sup>1</sup>, Jenny Stocker<sup>1</sup>, Martin Seaton<sup>1</sup> and David Carruthers<sup>1</sup>*

<sup>1</sup>Cambridge Environmental Research Consultants, Cambridge, UK

**Abstract:** The paper presents validation, from two sites in Alaska, of two ADMS chemistry schemes for the prediction of in-plume NO<sub>2</sub> concentrations. Both the standard scheme, which assumes instantaneous mixing of ambient O<sub>3</sub> into the plume at source, and the dilution and entrainment scheme which takes account rate of the entrainment of O<sub>3</sub> into the plume, show good performance. A novel methodology comprising a scatter plot of the ratio of modelled to observed NO<sub>2</sub> vs. modelled to observed NO<sub>x</sub> is used to distinguish errors in the chemistry schemes from errors in the prediction of NO<sub>x</sub>. This shows the dilution and entrainment model has superior performance.

**Key words:** *plume chemistry, nitrogen dioxide, ADMS, validation*

## INTRODUCTION

Combustion sources emit a combination of oxides of nitrogen (NO<sub>x</sub>), but air quality standards are generally expressed in terms of one component of NO<sub>x</sub>, nitrogen dioxide (NO<sub>2</sub>). For example the EU imposes limit values for annual and hourly average concentrations of NO<sub>2</sub>. As the components of NO<sub>x</sub> are chemically reactive in the atmosphere it is necessary to model this conversion to predict concentrations of NO<sub>2</sub> for comparison with the standards. The simplest models assume a fixed conversion rate, empirically based formulae (e.g. Carslaw *et al.*, 2013), or use an ozone limiting method in which all available ozone is used to oxidize NO to NO<sub>2</sub> (Cole and Summerhays, 1979). A more advanced plume based chemical scheme, PVMRM, is available in AERMOD (Hanrahan, 1999). The Atmospheric Dispersion Modelling System ADMS 5 (Carruthers *et al.*, 1994, Carruthers *et al.*, 2003) includes two plume based schemes for predicting NO<sub>2</sub>, a standard chemistry scheme and a newly developed scheme that takes account of the rate of entrainment of air into the plume and its dilution as it travels downstream.

This paper presents validation of both the ADMS 5 chemistry schemes and includes a new graphical method which allows the performance of a chemistry scheme to be considered in isolation from a model's performance in predicting NO<sub>x</sub>. An ideal validation dataset for NO<sub>2</sub> would include observations of NO<sub>2</sub>, NO<sub>x</sub> (total NO and NO<sub>2</sub>) and O<sub>3</sub> concentrations from several monitors around an emission source with well quantified emissions and appropriate meteorological observations. Such a dataset does not exist, but two adequate datasets were identified, in Wainwright and Prudhoe Bay, both of which are in Alaska.

## ADMS CHEMISTRY SCHEMES

Both chemical reaction schemes within ADMS consider the two reactions which take place over short timescales:



where the photochemical reaction (2) may only take place during daylight. In the standard scheme, concentrations of primary NO and NO<sub>2</sub> within the plume are first calculated using the standard dispersion algorithms. The background concentrations of NO<sub>x</sub>, NO<sub>2</sub> and O<sub>3</sub> are assumed to be well-mixed into this 'primary' plume at the source; to calculate in-plume concentrations of NO<sub>2</sub> and O<sub>3</sub>, reactions (1) and (2) take place for a 'reaction time' calculated as the concentration-weighted average of the travel time from

the sources to a receptor. In the dilution and entrainment scheme, rather than full entrainment of the background at source, background pollutants are entrained into the plume at a rate determined by the rate of entrainment of ambient air into the instantaneous plume, as given by the concentration fluctuation module of ADMS (Davies *et al.*, 1998). It is to be anticipated that the dilution and entrainment scheme will better reflect the mixing processes in the plume and therefore more accurately predict concentrations of NO<sub>2</sub>; the standard scheme would be expected to be conservative in NO<sub>2</sub> since entrainment of ozone into the plume is effectively assumed to be instantaneous.

### VALIDATION CASES

The two validation sites that were used in this study are from Wainwright and Prudhoe Bay, both in Alaska. ADMS version 5.0.2.0 was used throughout.

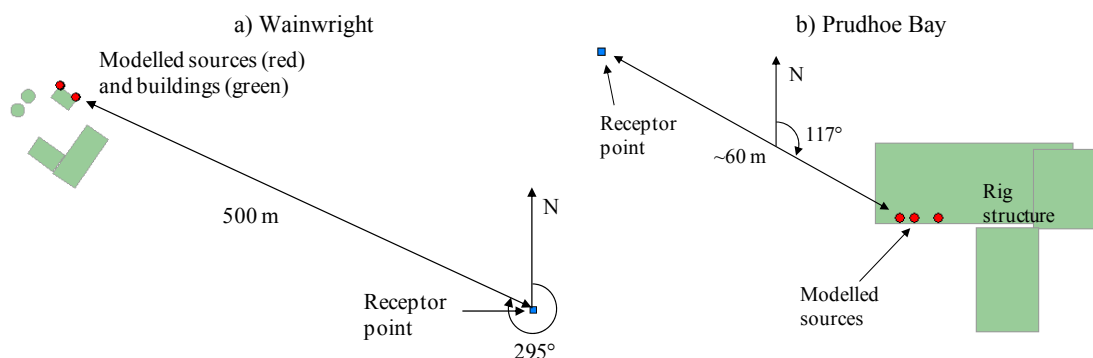


**Figure 1.** Diagram of the study area for a) Wainwright and b) Prudhoe Bay

At Wainwright the NO<sub>x</sub> emissions source is a power plant on edge of the small town of Wainwright (Hendrick *et al.*, 2013). It consists of five diesel generators with exhaust stacks located on two corners of the power plant building. Concentrations of NO, NO<sub>2</sub> and O<sub>3</sub> and the meteorological parameters of wind speed, wind direction, temperature and solar radiation were measured at a single location 500 m to the east, as shown in Figure 1a. Modelling using both the standard and dilution and entrainment ADMS chemistry schemes was conducted for the period September 2009 to September 2010. At Prudhoe Bay the NO<sub>x</sub> emissions source consists of a drilling rig on an oil well; of the considerable number of sources only three were significant. Concentrations of NO, NO<sub>2</sub>, and O<sub>3</sub> and meteorological parameters including wind speed, wind direction, rms vertical velocity ( $\sigma_w$ ), temperature and solar radiation were measured at a single monitoring station approximately 60 m away from the rig, as shown in Figure 1b. Modelling was conducted for the first 40 days of 2007 using only the standard ADMS chemistry scheme, as the dilution and entrainment scheme has not yet been implemented for multiple sources. As the drilling rig was large and close to the monitor, its effect on airflow and hence dispersion has been included in the modelling. Rather than use the ADMS meteorological pre-processor to estimate the Monin Obukhov length ( $L_{MO}$ ), which is likely to be subject to significant error in the very stable conditions prevailing at Prudhoe Bay in January and February, the measured  $\sigma_w$  was used to estimate  $L_{MO}$  using an approximate relationship for the wind speed in stable conditions:

$$u(z) = \frac{u_*}{\kappa} \left( \ln \left( \frac{z+z_0}{z_0} \right) + \frac{5z}{L_{MO}} \right) \quad (3)$$

where  $u_* \sim \frac{\sigma_w}{1.3}$ ,  $z$  is the height above ground,  $z_0$  is the surface roughness and  $\kappa$  ( $\approx 0.4$ ) is von Karman's constant. As there were no measured upstream values of pollutant concentrations in either study, it was necessary to estimate background values of NO<sub>x</sub>, NO<sub>2</sub> and O<sub>3</sub> from the single receptor in each. NO<sub>x</sub> and NO<sub>2</sub> background concentrations were estimated from time periods that were not included in the model analysis. At Wainwright these values were found to be negligible so were set to zero. At Prudhoe Bay, an average diurnal, wind direction dependent background was used. The O<sub>3</sub> background was then estimated assuming conservation of oxidant (NO<sub>2</sub> + O<sub>3</sub>).

## RESULTS AND DISCUSSION

Tables 1 and 2 show the model validation statistics for Wainwright and Prudhoe Bay respectively. Figure 2 shows, for Wainwright, the quantile-quantile plots for NO<sub>x</sub> (a) and NO<sub>2</sub> (b), the scatter plots of modelled vs. observed ratios NO<sub>2</sub>/NO<sub>x</sub> for standard chemistry (c) and the dilution and entrainment chemistry (d), and the scatter plots of modelled to observed ratios of NO<sub>2</sub> vs. modelled to observed ratios of NO<sub>x</sub> for standard chemistry (e) and the dilution and entrainment chemistry (f). Figure 3 shows the equivalent plots for Prudhoe Bay, without those for dilution and entrainment chemistry which was not modelled at Prudhoe Bay.

The focus of this validation is on the performance of the chemical reaction schemes, so the discussion highlights the insight that the tables and graphs provide about this. We first note for Wainwright that NO<sub>x</sub> is underestimated although the correlation is high, and both the standard and dilution and entrainment schemes underestimate NO<sub>2</sub>, with a greater underestimate for the dilution and entrainment chemistry; ratios of NO<sub>2</sub> to NO<sub>x</sub> are overpredicted for the standard scheme but well predicted for the dilution and entrainment scheme. At Prudhoe Bay both NO<sub>x</sub> and NO<sub>2</sub> are underestimated for low observed concentrations but well predicted for higher levels; there is wide scatter in the ratios of NO<sub>2</sub> to NO<sub>x</sub>. However, to assess the performance of the reaction schemes it is necessary to distinguish the errors in NO<sub>x</sub> from errors in NO to NO<sub>2</sub> conversion. This is achieved by the scatter plots of ratios of modelled to observed NO<sub>2</sub> vs. ratios of modelled to observed NO<sub>x</sub> (Figures 2(e,f) and 3(d)). When NO<sub>x</sub> is overpredicted then NO<sub>2</sub> should be overpredicted but the ratio of NO<sub>2</sub> to NO<sub>x</sub> underpredicted as it must decrease with increasing NO<sub>x</sub>, and conversely for underprediction of NO<sub>x</sub>; when NO<sub>x</sub> is well predicted then NO<sub>2</sub> should also be well predicted. This means that the points should lie between the diagonal and horizontal blue lines on the plots and the line of best fit should pass through (1,1). This is indeed, in the main, the case for the dilution and entrainment scheme for Wainwright (Figure 2(e)), which therefore has very good performance and somewhat better performance than the standard scheme. In the case of Prudhoe Bay, Figure 3 (d) shows that the standard chemistry performs well, just slightly overestimating the conversion to NO<sub>2</sub>. Such good performance may be a consequence of the large buildings resulting in rapid mixing into the plume so that the instantaneous mixing assumption is good in this case.

**Table 1.** Statistics for modelled NO<sub>x</sub> and NO<sub>2</sub> concentrations for Wainwright. Includes observed and modelled means, correlation coefficient, fraction of modelled values within a factor of 2 of the observed values, fractional bias, and observed and modelled maximum values.

Run summary		Statistical summary						
Pollutant	NO <sub>x</sub> chemistry method	Obs Mean	Mod Mean	R	Fac2	Fb	Obs Max	Mod Max
NO <sub>x</sub>	N/A	43.2	27.4	0.780	0.423	-0.447	369	145
NO <sub>2</sub>	Standard chemistry	12.7	10.9	0.671	0.517	-0.148	72.5	66.7
NO <sub>2</sub>	Dilution and entrainment chemistry	12.7	8.68	0.682	0.520	-0.374	72.5	49.1

**Table 2.** Statistics for modelled NO<sub>x</sub> and NO<sub>2</sub> concentrations for Prudhoe Bay. Same statistics as shown in Table 1.

Run summary		Statistical summary						
Pollutant	NO <sub>x</sub> chemistry method	Obs Mean	Mod Mean	R	Fac2	Fb	Obs Max	Mod Max
NO <sub>x</sub>	N/A	192	145	0.688	0.515	-0.279	845	498
NO <sub>2</sub>	Standard chemistry	57.9	37.8	0.683	0.627	-0.420	246	170

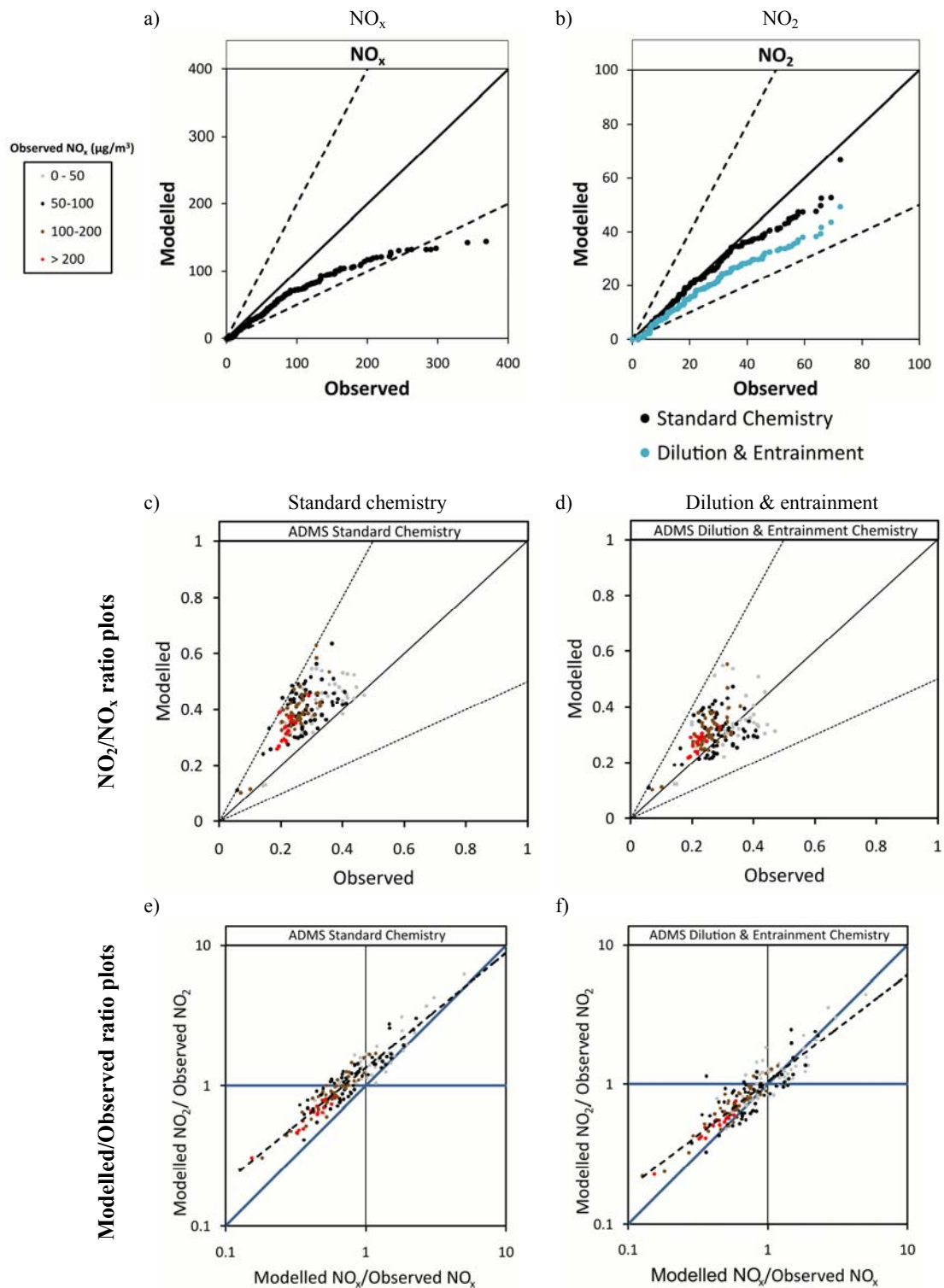


**Figure 2.** Quantile-quantile plots of modelled against observed a)  $\text{NO}_x$  concentrations and b)  $\text{NO}_2$  concentrations. Scatter plots of  $\text{NO}_2/\text{NO}_x$  ratio for c) standard chemistry and d) dilution & entrainment. Scatter plots of modelled/observed ratio of  $\text{NO}_2$  against the ratio for  $\text{NO}_x$  for e) standard chemistry and f) dilution & entrainment with a dashed line of best fit. Points in c) – f) are coloured by  $\text{NO}_x$  concentration. All at Wainwright.

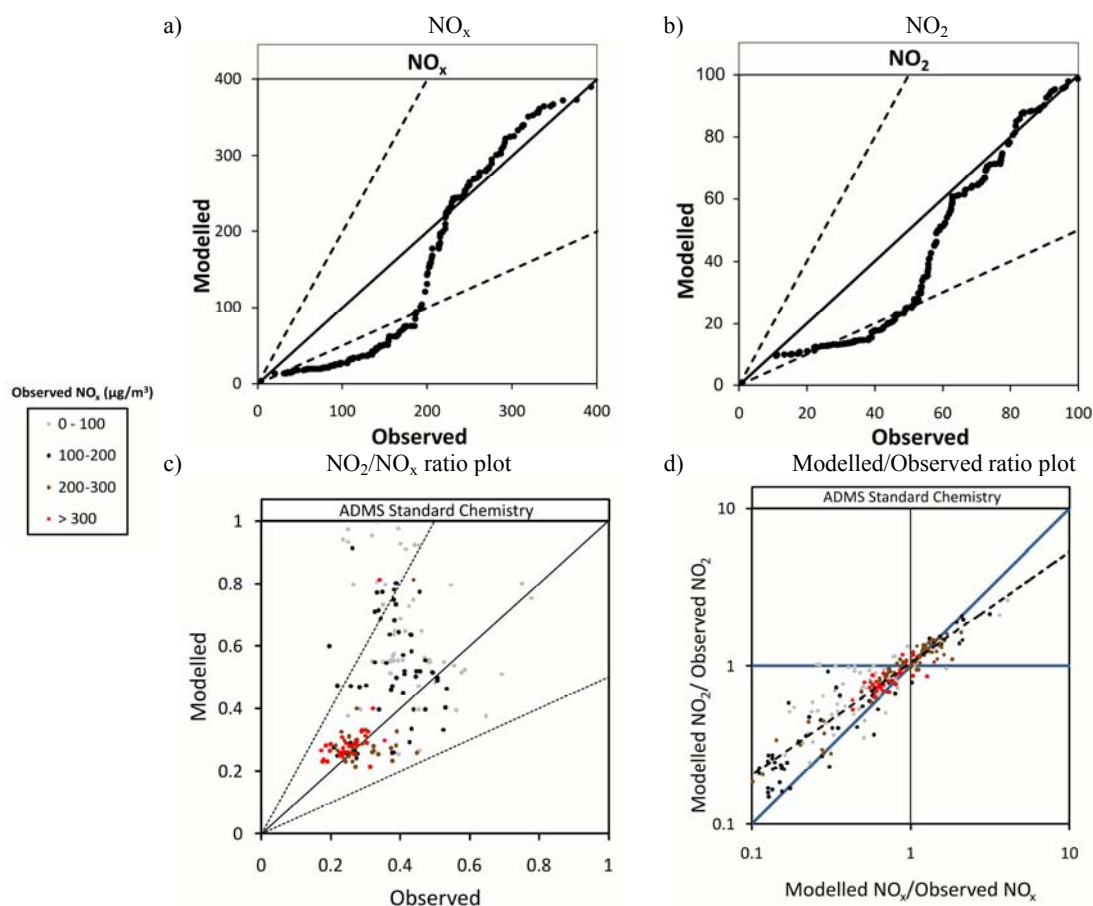


**Figure 3.** Quantile-quantile plots of modelled against observed a) NO<sub>x</sub> concentrations and b) NO<sub>2</sub> concentrations. Scatter plots of c) NO<sub>2</sub>/NO<sub>x</sub> ratio and d) modelled/observed ratio of NO<sub>2</sub> against the ratio for NO<sub>x</sub> for standard chemistry with a dashed line of best fit. Points in c) and d) are coloured by NO<sub>x</sub> concentration. All at Prudhoe Bay.

#### ACKNOWLEDGEMENTS

We should like to acknowledge BP International Limited for their support of this study.

#### REFERENCES

- Carruthers, D. J., R. J. Holroyd, J. C. R. Hunt, W-S. Weng, A. G. Robins, D. D. Apsley, D. J. Thompson and F. B. Smith, 1994: UK-ADMS: A new approach to modelling dispersion in the earth's atmospheric boundary layer. *J. of Wind Engineering and Industrial Aerodynamics*, **52**, 139-153.
- Carruthers, D. J., S. J. Dyster and C. A. McHugh, 2003: Factors affecting inter-annual variability of NO<sub>x</sub> and NO<sub>2</sub> concentrations from single point sources. *Clean Air & Environ. Protection*, **33**, 15-20.
- Carshaw, D., H. ApSimon, S. Beevers, D. Brookes, D. Carruthers, S. Cooke, N. Kitwiroon, T. Oxley, J. Stedman and J. Stocker, 2013: Defra Phase 2 urban model evaluation, KCL.
- Cole, H. S. and J. E. Summerhays, 1979: A review of techniques available for estimating short-term NO<sub>2</sub> concentrations. *J. Air Pollut. Control Assoc.*, **29**(8), 812-817.
- Davies, B. M., C. D. Jones, A. J. Manning and D. J. Thomson, 1998: Some field experiments on the interaction of plumes from two sources. Internal Met Office Note TDN 252. *Quarterly J. of Royal Met. Soc.*, **126**(565), 1343-1366.
- Hanrahan, P. L., 1999: The plume volume molar ratio method for determining NO<sub>2</sub>/NO<sub>x</sub> ratios in modeling. Part I: Methodology. *J. Air & Waste Manage. Assoc.*, **49**, 1324-1331.
- Hendrick, E. M., V. R. Tino, S. R. Hanna and B. A. Egan, 2013: Evaluation of NO<sub>2</sub> predictions by the plume volume molar ratio method (PVMRM) and ozone limiting method (OLM) in AERMOD using new field observations. *J. Air & Waste Manage. Assoc.*, **63**(7), 844-854.

**17th International Conference on  
Harmonisation within Atmospheric Dispersion Modelling for Regulatory Purposes  
9-12 May 2016, Budapest, Hungary**

---

**A REVIEW OF DISPERSION MODELLING OF AGRICULTURAL AND BIOAEROSOL  
EMISSIONS WITH NON-POINT SOURCES**

*Jenny Stocker<sup>1</sup>, Andrew Ellis<sup>1</sup>, Steve Smith<sup>2</sup>, David Carruthers<sup>1</sup>, Akula Venkatram<sup>3</sup>, William Dale<sup>1</sup> and  
Mark Attree<sup>1</sup>*

<sup>1</sup>Cambridge Environmental Research Consultants, Cambridge, UK

<sup>2</sup>A S Modelling & Data Ltd, UK

<sup>3</sup>University of California, CA, US

**Abstract:** This paper presents some key aspects of a review of limitations and uncertainties associated with modelling pollutant dispersion from non-point sources, focussed on emissions from agricultural and bioaerosol sources. The plume dispersion models ADMS and AERMOD were used to represent releases from four sheds housing intensively farmed poultry. When the emission and volume flow rates used in the modelling were derived from measurements, the models give reasonably accurate predictions for the period average near-source NH<sub>3</sub> concentrations. However for releases with non-negligible efflux, modelling using non-point sources allowing for the momentum and buoyancy of the release (line, point and area sources in ADMS; buoyant line source in AERMOD) has much better agreement with observations than those that do not (volume sources in ADMS; volume, area and default line source in AERMOD); in these cases, neglecting plume rise results in an overestimate of both period average and maximum concentrations.

**Key words:** *Dispersion, ammonia, odour, non-point sources, agriculture, poultry*

## **INTRODUCTION**

There are many regulated sources of pollution which have complex geometries near or at ground level. These include pig and poultry farms which may have high emissions of ammonia (NH<sub>3</sub>) and particulates from sheds of intensively farmed animals, from litter and manure storage, and land spreading, and also composting sites, where bio-waste such as that contained within windrows emits fungi and bacteria. In environmental impact assessments such sources are often represented using 'non-point source' configurations i.e. line, area, jet or volume sources. In contrast to point sources, for which extensive model validation has been conducted, the use of non-point sources to model agricultural and bioaerosol emissions is relatively poorly quantified. This is both because the sources usually have crudely defined physical characteristics and because the emissions are often highly uncertain.

A review of approaches to modelling pollutant dispersion from non-point sources was recently undertaken for the particular case of agricultural and bioaerosol sources (Stocker *et al.* 2016). Part of the review involved collating a parameter space of values used to characterise non-point source types. This was then used to formulate idealised modelling scenarios, where concentration outputs from the ADMS (Carruthers *et al.*, 1994) and AERMOD (Cimorelli *et al.*, 2005) models were compared for the different non-point source types. The review also involved using ADMS and AERMOD for three agricultural and one bioaerosol real-world case studies; model predictions were compared with observations to assess the suitability of each source type and model for each case. Overall the review has led to a number of conclusions on the best approach to modelling agricultural and bioaerosol sources. The current paper focuses on presenting results from the most robust study, that for Whitelees Farm (Hill *et al.*, 2014), where continuous monitoring of NH<sub>3</sub> concentrations was undertaken close (60 m) to four poultry sheds. The results from two other studies involving particulate emissions from poultry housing and one of the dispersion of bioaerosols from a small UK composting site are not discussed further in this paper.

## CASE STUDY DESCRIPTION

Whitelees Farm is located in South Lanarkshire, Scotland. The site houses approximately 37,000 laying hens housed in four identical rectangular sheds, closely spaced and aligned parallel to each other. Each shed is divided into two buildings ventilated through a series of ten fan-assisted cowls pointing upwards at a 45° angle on each long side, giving a total of 80 vents. Meteorological data from an onsite automatic weather station were recorded at 30 minute intervals and then averaged to derive hourly values for modelling. Data were available for the period between 14<sup>th</sup> August 2013 and 4<sup>th</sup> November 2013. Three datasets were used for model validation: continuous NH<sub>3</sub> monitoring from a single station approximately 60 m to the north of the farm (co-located with the meteorological measurements); two sets of fixed-period NH<sub>3</sub> measurements recorded using Alpha Samplers at 9 locations surrounding the farm; and odour measurements from transects on the 19<sup>th</sup> of September ('sniffers' measured odour levels for a ten minute period within each hour at each location). Volume flow rates, NH<sub>3</sub> and odour concentrations were measured at a number of vents across the site during two days of the campaign; on these two days, a maximum of 4 vents operated per building. These measurement data were used to estimate average flow rates and emissions and are summarised in Table 1. Figure 1 a) shows the locations of the NH<sub>3</sub> monitors and meteorological station and Figure 1 b) indicates where the odour measurements were recorded.

**Table 1.** Calculated emissions parameters for the Whitelees farm site

Modelling period	Volume flow rate (m <sup>3</sup> /s)	NH <sub>3</sub> emission rate (g/s)	Odour emission rate (ou <sub>F</sub> /s)
19/09/2013	55.8	0.86	14740
Whole period	52.7	0.98	14470

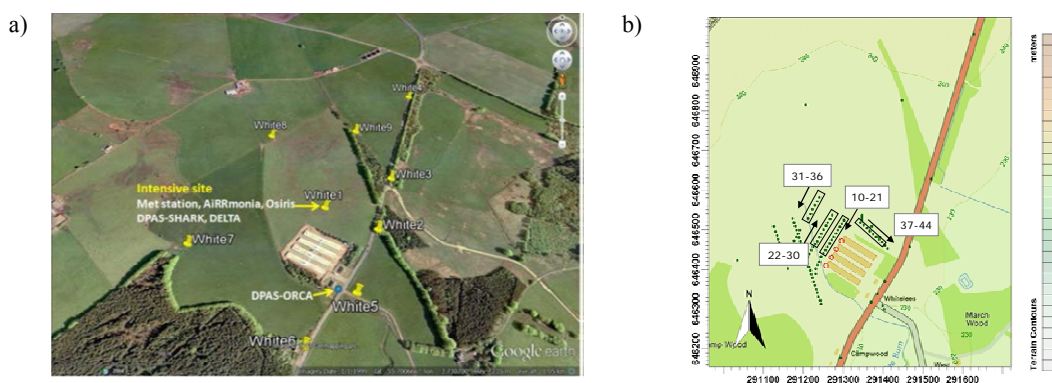


**Figure 1.** a) Aerial photograph of the location of the onsite meteorological station (White 1) co-located with continuous ammonia monitoring equipment; White 2 to White 9 indicate the locations of additional ammonia measurements; figure taken from Hill *et al.* (2014), reproduced here with permission from Sniffer. b) Whitelees Farm showing buildings (orange rectangles) and receptors (dark green dots); receptor numbers and arrows of locations of odour measurements on Sept 19<sup>th</sup>; background map courtesy of ©Crown copyright and database right, 2015.

## MODEL CONFIGURATION

When modelling dispersion from a poultry house, it is standard practice to model a representative subset of sources on the building as, typically, release data are not available on a vent-by-vent basis. This was the approach taken for the current study. Figure 2 shows the horizontal representation for each source type (point, jet, volume, area and line) used to model the release. Single area and volume sources were used to model all four sheds and the line sources located to approximate the position of the side vents on of the sheds. Four vents were assumed per building, with two vents evenly spaced along each side. In order to model the odour emissions, average emissions and volume flow rates were used for the day when odour concentrations were measured. For modelling longer periods (i.e. to predict NH<sub>3</sub> concentrations), the average parameters measured across the campaign were used. For point, line, and area sources, the vertical component of the calculated exit velocity was used as the modelled exit velocity. Source dimensions and exit parameters are given in Table 2; note that ADMS volume and AERMOD volume,

area and default line source types do not allow for plume rise in the dispersion calculations. The surface roughness length was taken as 0.2 m to represent the mainly open area around the site. Receptors were 1.5 m above ground. Versions 5.1 (ADMS) and 15181(AERMOD) were used throughout.

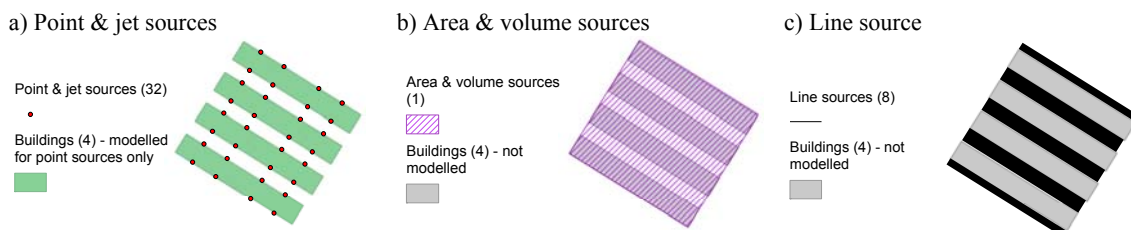


**Figure 2.** Source representations for Whitelees Farm; buildings explicitly modelled with point sources only

**Table 2.** Whitelees farm source parameter ranges; \*ADMS only, AERMOD jet sources are wind aligned; †AERMOD area and default line source do not account for plume rise

Idealised source type	Source dimensions (m)			Efflux parameters	
	Height (m)	Diameter (m) / Dimensions: Length (m) x Width (m) x Depth (m)	Elevation angle to horizontal*	Temperature (°C)	Ammonia / odour velocity (m/s)
Point	2	0.72	n/a	17.4	2.8 / 3.0
Jet*	2	0.72	45°	17.4	4.0 / 4.2
Volume	2	94 x 90 ( x 2 )	n/a	n/a	n/a
Area <sup>†</sup>	2	94 x 90	n/a	17.4	0.0062 / 0.0066
Line <sup>†</sup>	2	94 x 5	n/a	17.4	2.8 / 3.0

## RESULTS

Tables 3 and 4 present the model evaluation statistics relating to the continuous monitor for both ADMS and AERMOD. These comprise: period averages (mean); normalised mean square error (NMSE); correlation (R); the number of modelled values within a factor of two of the observed (Fac2); the index of agreement (IoA), used to represent overall model performance (spans between -1 and +1, with values approaching +1 representing better performance); and maximum concentrations. Model performance is quite variable depending on model and source type, but of note is that modelled means are within a factor of two of the observed for all cases, suggesting that the simplifications regarding the emission and volume flow rates are appropriate. For ADMS, NMSE, R and IoA indicate generally good model performance for all sources except the volume source, for which concentrations are overestimated. For AERMOD, the statistics indicate that model performance is good for the point and buoyant line sources, but limited for the area, default line and volume sources. In addition these cases exhibit very large overestimates of maximum values. The conclusion is that the source types which take into account the initial plume momentum and buoyancy perform significantly better than those which are assumed to be passive. Comparing ADMS and AERMOD, we conclude that AERMOD has a tendency to predict higher concentrations than ADMS, with the notable exception of the buoyant line source which gives the lowest model predictions over all source types. The plot of NMSE against fractional bias, Figure 3, summarises the models' performance; the most accurate models have symbols that are closest to (0,0). Figure 4 presents a selection of ADMS and AERMOD contour plots of modelled concentrations for one of the fixed periods (27 days), with the measurements overlaid using the same colour scale. For ADMS, the jet source model configuration has been presented alongside the volume source results. The jet source gives a good representation of the spatial variation of the observations, both near and far from the source, whereas, as we would anticipate from the previous discussion, the volume source overpredicts ground level concentrations at all locations. The AERMOD point source slightly overpredicts the concentrations and the volume source significantly overpredicts. Figure 5 presents comparisons between the measured and modelled odour concentrations for the single day considered. Observed odour concentrations are reasonably well predicted by the ADMS jet and AERMOD point source types; the AERMOD buoyant line source follows a similar trend to the other source types, but exhibits a large underprediction.

**Table 3.** ADMS Model evaluation statistics for Whitelees; ‘best’ values are in bold

Idealised source type	Average statistics						Maximum statistics	
	Obs. Mean ( $\mu\text{g}/\text{m}^3$ )	Mod. mean ( $\mu\text{g}/\text{m}^3$ )	NMSE	R	Fac2	IoA	Obs. maximum	Mod. maximum
Area	119	67	0.97	<b>0.66</b>	0.41	0.61	362	<b>388</b>
Jet	119	96	<b>0.60</b>	0.63	<b>0.53</b>	<b>0.65</b>	362	445
Line	119	<b>104</b>	0.90	0.52	0.52	0.60	362	961
Point	119	87	1.07	0.47	0.41	0.57	362	872
Volume	119	163	7.54	0.18	0.48	0.26	362	3997

**Table 4.** AERMOD Model evaluation statistics for Whitelees: ‘best’ values are in bold

Idealised source type	Average statistics						Maximum statistics	
	Obs. Mean ( $\mu\text{g}/\text{m}^3$ )	Mod. mean ( $\mu\text{g}/\text{m}^3$ )	NMSE	R	Fac2	IoA	Obs. maximum	Mod. maximum
Area	119	196	13.3	0.14	<b>0.44</b>	0.04	362	5736
Default line	119	200	13.3	0.14	<b>0.44</b>	0.02	362	5750
Buoyant line	119	64	<b>1.2</b>	<b>0.60</b>	0.33	<b>0.58</b>	362	<b>198</b>
Point	119	<b>151</b>	1.9	0.48	0.43	0.46	362	1789
Volume	119	<b>151</b>	9.8	0.15	0.35	0.19	362	4860

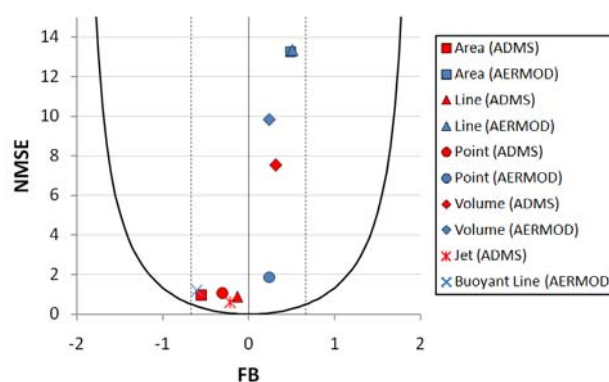


**Figure 3.** NMSE against fractional bias (FB) for all source types; buildings explicitly modelled with point sources only. Black line indicates minimum NMSE possible for FB.

## DISCUSSION

This model evaluation study demonstrates that when accurate estimates (or measurements) of emission and volume flow rates are available, the dispersion models ADMS and AERMOD are able to predict average near-source concentrations within a factor of two of the measured values when non-point source types are used to represent the release. Using source types for which models allow for initial plume momentum and buoyancy leads to much better model performance. As the sources at Whitelees are jets at a 45° angle, it is unsurprising that this source type performs best in ADMS. For AERMOD, where the jet source type could not be used due to the source type restrictions (wind alignment), the new buoyant line source gives the best correlation with measurements, however concentrations are underpredicted. Although the non-point source types considered neglect building effects, predicted model concentrations are comparable to those from point source configurations where the effect of buildings are included. This suggests that the impact on dispersion of low-level agricultural sheds and buildings at waste sites may be unimportant. Possible explanations for this are the limited downwash resulting from the low buildings and the limited impact of building-induced turbulence because the sources are already spread out.

## ACKNOWLEDGEMENTS

The authors gratefully acknowledge the UK Atmospheric Dispersion Modelling Liaison Committee who funded this study and to Sniffer who provided the Whitelees dataset.

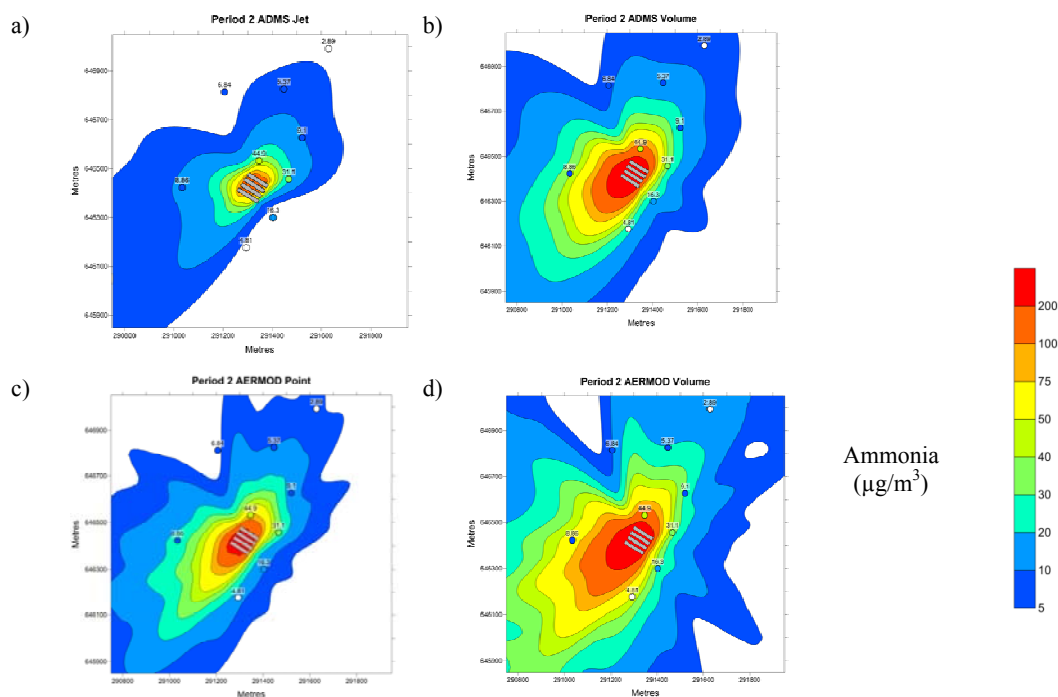


**Figure 4.** Period average  $\text{NH}_3$  for Whitelees ‘Run 2’: a) ADMS jet, b) ADMS volume, c) AERMOD point and d) AERMOD volume. Observations shown by the circles, the buildings are shown in grey (modelled in c).

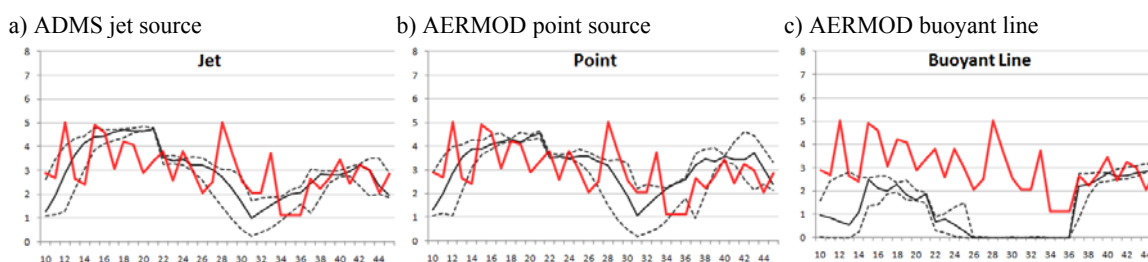


**Figure 5.** Short-term odour results for Whitelees a) ADMS jet, b) AERMOD point and c) AERMOD buoyant line sources; observations shown in red, minimum, median and maximum modelled values shown in black, where range of modelled values corresponds to wind direction adjustments of  $\pm 15^\circ$ . Horizontal axis shows transect receptor number, as shown in Figure 1b).

## REFERENCES

- Carruthers, D. J., R. J. Holroyd, J. C. R. Hunt, W-S. Weng, A. G. Robins, D. D. Apsley, D. J. Thompson and F. B. Smith, 1994: UK-ADMS: A new approach to modelling dispersion in the earth's atmospheric boundary layer. *J. of Wind Engineering and Industrial Aerodynamics*, **52**, 139-153.
- Cimorelli, A. J., S. G. Perry, A. Venkatram, J. C. Weil, R. J. Paine, R. B. Wilson, R. F. Lee, W. D. Peters and R. W. Brode, 2005: AERMOD: a dispersion model for industrial source applications. Part I: general model formulation and boundary layer characterization. *J. Appl. Meteorol.*, **44**, 682–693.
- Hill, R., B. Bealey, C. Johnson, A. Ball, K. Simpson, A. Smith, M. Theobald, C. Braban, I. Magaz and T. Curran, 2014. SCAIL Agriculture. Sniffer ER26 Final Report. <http://www.scail.ceh.ac.uk/agriculture>
- Stocker, J., A. Ellis, S. Smith, D. Carruthers, A. Venkatram, W. Dale and M. Attree, 2016: A review of the limitations and uncertainties of modelling pollutant dispersion from non-point sources. Report for the UK Atmospheric Dispersion Modelling Liaison Committee.

**17th International Conference on  
Harmonisation within Atmospheric Dispersion Modelling for Regulatory Purposes  
9-12 May 2016, Budapest, Hungary**

---

**VALIDATION OF A LPDM AGAINST THE CUTE EXPERIMENTS  
OF THE COST ES1006 ACTION – COMPARISON OF THE RESULTS OBTAINED  
WITH THE DIAGNOSTIC AND RANS VERSIONS OF THE MODELS**

*Christophe Duchenne<sup>1</sup>, Patrick Armand<sup>1</sup>, Maxime Nibart<sup>2</sup>, and Virginie Hergault<sup>3</sup>*

<sup>1</sup>CEA, DAM, DIF, F-91297 Arpajon, France

<sup>2</sup>Aria Technologies, F-92100 Boulogne-Billancourt, France

<sup>3</sup>Alten, F-92100 Boulogne-Billancourt, France

**Abstract:** In the frame of the European COST Action ES1006, this paper presents the comparison of PMSS diagnostic, PMSS momentum, and Code\_SATURNE results with trials carried out in the city of Hamburg and in its mock-up. The results comparison highlights the impact of the modelling approaches on the atmospheric dispersion and the importance of taking into account the momentum equation. For the field experiment, some of the statistical measures are larger than the acceptance limits due to the low values of the concentrations and the high degree of variability and uncertainty of the real field data. The metrics for the wind tunnel experiment are better and meet the acceptance limits. Finally, the sensitivity tests show the importance of having access to appropriate meteorological input data for modelling in order to achieve more reliable simulations of accidental releases.

**Key words:** *Diagnostic flow, momentum equation, LPDM, COST ES1006, CUTE experiments, validation.*

## **INTRODUCTION**

Numerous accidental situations as malevolent activities imply the atmospheric release of hazardous materials. Even if all events are not as serious as Chernobyl or Fukushima nuclear accidents and Seveso or Bhopal chemical disasters, consequences on health and environment of all kinds of incidents on industrial sites or during transport operations have to be assessed making use of modelling and simulation. Several models are available from the simplest to the most advanced and detailed ones with very different computational resources requested. If the Gaussian approach seems definitely not adapted to complex environments such as urban districts and industrial sites, simplified CFD models offer an alternative approach to full CFD which is in principle the reference solution. Thus, it is essential to compare the advantages and drawbacks of existing models, especially in the case of well-documented experimental campaigns like the Complex Urban Test Experiment (CUTE). The CUTE dataset includes results from field and wind tunnel measurement, carried out in the downtown area of the city of Hamburg and in its mock-up, reproduced in the wind tunnel of the Hamburg University. Measurements of concentration resulting from continuous or short tracer releases were utilized in 2014 as a test-bed for modellers involved in the European COST Action ES1006. In this respect, two codes were used: Parallel-Micro-SWIFT-SPRAY (PMSS), a simplified CFD model combined with a Lagrangian Particle Dispersion Model PSPRAY, and Code\_SATURNE, a full CFD code with a RANS k- $\epsilon$  turbulent flow model also combined with PSPRAY. A comparison of PMSS results, obtained on one hand with the diagnostic fast-response version of the flow model (PMSS diagnostic) and with its RANS version on another (PMSS momentum), has been performed. Results of the codes are compared together and with the experiments using the methods and metrics proposed in the frame of the project. This paper presents the CUTE experimental trials, a short description of codes, atmospheric dispersion results which are compared to measurements, and finally, a sensitivity analysis on the initial conditions.

## **DESCRIPTION OF THE CUTE EXPERIMENTAL TRIALS**

In order to provide data for the validation of local scale emergency response models in the frame of COST Action ES1006, the CUTE dataset includes results from field and wind tunnel measurement, carried out in the downtown area of the city of Hamburg and in its mock-up at 1:350 scale, reproduced in the WOTAN atmospheric boundary layer wind tunnel at the Environmental Wind Tunnel Laboratory in Hamburg (see Figure 1). For the field trial, the source was located on a boat and the tracer (SF6) was

released continuously for 45 minutes with a constant flow rate of 2g/s. The tracer was detected by 20 measurement devices and each recorded concentration represents a 10-minute average concentration. For the wind tunnel dataset, concentration time series of tracer from continuous and puff releases were measured with fast Flame Ionization Detector (FID). The source was located in the city center. Firstly, the tracer was released continuously with a constant flow rate of 0.5kg/s and detected by 34 sensors. Then, 50kg of tracer were released during 31s and detected by 17 sensors.

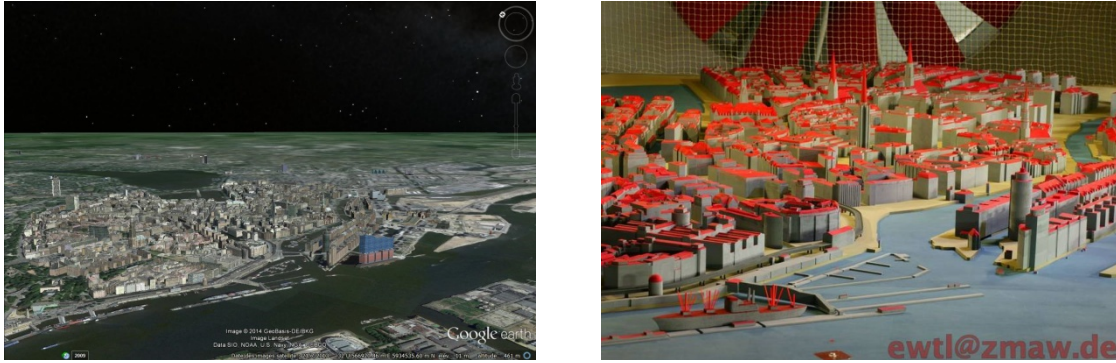


**Figure 1.** City centre of Hamburg (left) and its mock-up in the WOTAN wind tunnel (right)

### MODELS DESCRIPTION

The Parallel-Micro-SWIFT-SPRAY (PMSS) modelling system (Tinarelli et al., 2013; Oldrini et al., 2011) includes parallelized models PSWIFT and PSPRAY. PSWIFT is an analytically modified mass consistent interpolator over complex terrain and urban areas. Given topography, meteorological data and building geometry, a mass consistent 3D wind field is generated. It is also able to derive diagnostic turbulence parameters (namely the Turbulent Kinetic Energy, TKE, and its dissipation rate) to be used by PSPRAY especially inside the flow zones modified by obstacles. PSPRAY is a Lagrangian Particle Dispersion Model (LPDM) able to take into account the presence of obstacles. It is directly derived from the SPRAY code (Tinarelli et al., 1994 and 2007). It is based on a 3D form of the Langevin equation for the random velocity (Thomson, 1987).

A simplified model of momentum equation has been introduced as an option in PMSS and this RANS version of the flow uses a zero equation turbulence model with a mixing-length-based closure.

Code\_SATURNE (Archembeau et al., 2004) is a three-dimensional CFD model adapted to atmospheric flow and pollutant dispersion, which can handle complex geometry and complex physics. The numerical model is based on a finite-volume approach for co-located variables on an unstructured grid. Time discretization of the Navier-Stokes equations is achieved through a fractional step scheme, with a prediction-correction step. In Code\_SATURNE, two approaches can be used to deal with turbulent flows: the Reynolds averaged Navier–Stokes method (RANS) with the choice between two closure models, as well as the large-eddy simulation (LES) method. In the present paper, we use a RANS approach with a  $k-\epsilon$  turbulence closure. The turbulence model can take into account the stratification of the atmosphere through the production or destruction rate due to buoyancy. In this paper, Code\_SATURNE is combined with PSPRAY to model atmospheric dispersion.

### COMPUTATIONAL PARAMETERS

Wind tunnel measurements have been converted to full scale using similarity laws. For calculations, we consider that we are at the full scale and digital mock-ups are built at this scale. PMSS (diagnostic and momentum) and Code\_SATURNE work on a structured mesh with a regular horizontal grid of 625x525 nodes and a 4-meters resolution, and a vertical grid of 26 nodes, from the ground to a height of 200 meters, with a regular grid inside the urban canopy and a logarithmic progression above. It leads to a computational grid with about 8.7 million nodes.

Input data consist of an experimental inflow vertical profile. A standard deviation is associated with each wind component. We consider an isotherm profile for temperature and therefore, neutral conditions. In PMSS diagnostic model, turbulence is diagnosed using parameterizations. We consider turbulence as the sum of the local turbulence due to the presence of buildings, evaluated with a mixing length method depending on the distance to the nearest building, and the background turbulence depending on the atmospheric conditions we have supposed (here, neutral). Background turbulence is estimated with Hanna parameterization (Hanna et al., 1982) and depends, among others, on surface stress  $u^*$ . PMSS computes  $u^*$  from roughness  $z_0$  and wind speed near the ground. We decide to fix  $z_0$  in order to keep the same surface stress between the value computed by PMSS and the value deduced from the standard deviation measurements using Stull formula.

Unlike Code\_SATURNE, where turbulence is performed with the  $k-\epsilon$  model, PMSS momentum model uses a zero equation turbulence model with a mixing-length-based closure.

For the Lagrangian model PSPRAY, we deal with about 2000 numerical particles per second, so that we can describe low concentrations with a sufficient number of numerical particles.

All cases were run as blind tests, having minimum input information available for the model simulations, as it would be the case during a real accident.

## RESULTS

Figure 2 and Figure 3 show concentrations near the ground obtained with PSPRAY from the three flow models (PMSS diagnostic, PMSS momentum and Code\_SATURNE) for the field and wind tunnel experiment respectively. Some areas of the plume obtained with PMSS diagnostic present null or low concentrations contrary to models resolving momentum conservation (PMSS momentum and Code\_SATURNE). Furthermore, there is a significant channeling effect towards the east for models with momentum resolution. Indeed, momentum enables to take into account global effects due to obstacles like channeling or Venturi effects. Besides, the plume modelled with Code\_SATURNE is shorter than those obtained with both PMSS versions (diagnostic and momentum) due to stronger wind fields calculated with Code\_SATURNE and a stronger turbulence in the case of the field experiment.

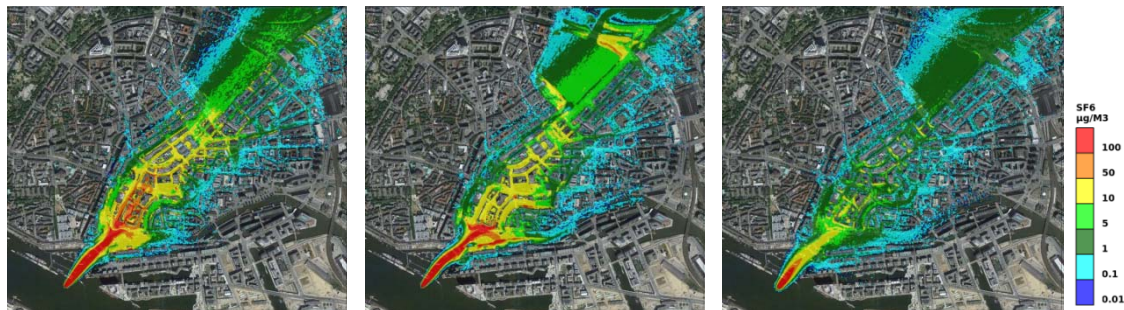


**Figure 2.** Field experiment / continuous release – Concentration field – Cross-section near the ground  
PMSS diagnostic (left) / PMSS momentum (centre) / Code\_SATURNE (right)

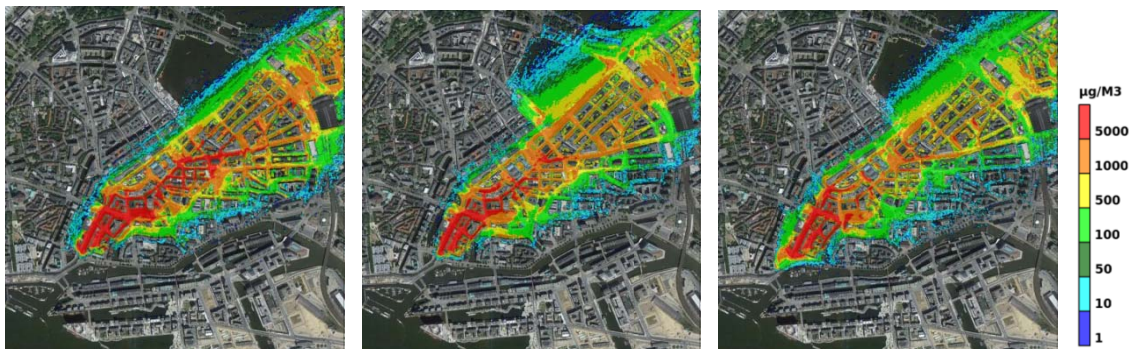


**Figure 3.** Wind tunnel experiment / continuous release – Concentration field – Cross-section near the ground  
PMSS diagnostic (left) / PMSS momentum (centre) / Code\_SATURNE (right)

In order to evaluate the predictions of models (here, PMSS and Code\_SATURNE) against observations, Chang et al. (2004) recommend the use of statistical performance measures, which include the fractional bias (FB), the normalized mean square error (NMSE), and the fraction of predictions within a factor of two of the observations (FAC2). These statistical measures have to be compared with the following criteria to assess if there is a good agreement between computational results and observations for the concentrations.

$$-0,67 < FB < 0,67 \quad ; \quad NMSE < 6 \quad ; \quad FAC2 > 0,3$$

For the field-experiment, the continuous release results are shown considering ten-minute averaged concentration and for the wind tunnel experiment, five-minute averaged concentration.

In Table 1, the summarized statistics for continuous and puff releases are reported. In the case of the field experiment, the statistical measures indicate biased FB and NMSE, larger than the acceptance limits. In contrast, a FAC2 within the 0.3 acceptance criterion can be noticed. Observations and predictions mainly show small concentration values, in a range from  $10^{-6}$  to  $10^{-2}$  ppmv. Consequently, the comparison of concentration values is quite severe since even small differences between the paired values produce a relatively large scatter. The metrics for wind tunnel experiment are better and meet the acceptance limits.

**Table 1.** Statistical performance measures for mean concentrations

Results	Model	FB	NMSE	FAC2
Field experiment / Continuous release	PMSS diagnostic	0.03	6	0.35
	PMSS momentum	-1.08	23	0.31
	Code_SATURNE	1.43	40	0.31
Wind tunnel experiment / Continuous release	PMSS diagnostic	-0.35	1.9	0.38
	PMSS momentum	-0.10	2.2	0.47
Wind tunnel experiment / Puff release	PMSS diagnostic	-0.42	2.6	0.38

The initial conditions and input data are among the key items, and their related uncertainty which is assumed to be relatively high in case of accidental release, strongly controls the model results. Sensitivity analysis was run for different turbulence conditions and wind data needed as input for models (see the companion paper by Tinarelli et al., 2016).

A sensitivity test was performed to verify the change in model output to different driving wind data. Two different simulations were carried out. In the first one, a vertical wind profile was calculated starting from the only available measurement at 175 m. The wind direction was kept constant with height. In the second one, the data measured at a weather mast 8 km away was used to build a wind profile with wind directions varying with height by following the available measurements.

In Figure 4, the effect of the different wind input conditions is visible as the plume disperses in slightly different directions and the affected areas are substantially different. The sensitivity test highlights the importance of having access to appropriate meteorological input data for modelling, characterizing, for example, the vertical variability of wind direction, in order to achieve more reliable simulations of accidental releases. While, in general, it is not easy to provide such kind of observed data, in case of known sensitive sites such as for instance industrial plants, a proper planning of a net of sensors becomes essential for optimum support in the use of emergency response tools.

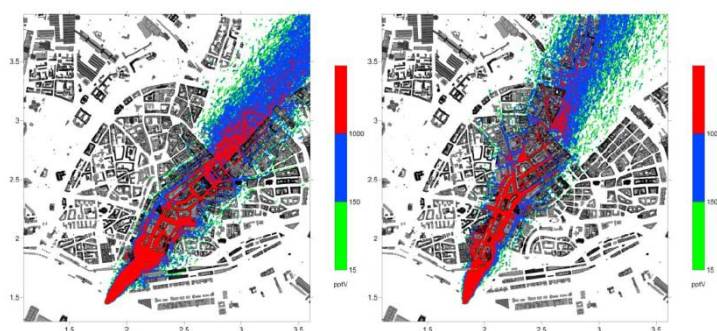


**Figure 4.** Field experiment / continuous release – Cross-section near the ground (PMSS diagnostic)  
Comparison of concentration field with two wind inlet profiles

## CONCLUSIONS

In the frame of the COST Action ES1006, atmospheric dispersion of continuous and puff releases experiments and modelling were carried out in the downtown area of the city of Hamburg and its mock-up, reproduced in the wind tunnel of the Hamburg University. Simulations to reproduce flow were performed using PMSS with a mass-consistent diagnostic flow model, PMSS with the RANS version of the flow model, and Code\_SATURNE, a finite volume CFD code with a RANS k-epsilon turbulent flow model. The three flow models are combined with a Lagrangian Particle Dispersion Model. A comparison of results highlights the impact of the flow model on the atmospheric dispersion and the importance of taking into account the momentum equation.

Methods and metrics (FB, NMSE, FAC2) proposed in the frame of the project, were used to compare results of codes with field and wind tunnel experiments. In the case of the field experiment, the statistical measures indicate biased FB and NMSE, larger than the acceptance limits, but a FAC2 within the 0.3 acceptance criterion. Given the low absolute values of the concentrations characterizing this case, the differences between observed and predicted data are small, but they have a large relative importance. Moreover, real field data are characterized by a much higher degree of variability and uncertainty with respect to the carefully controlled, quasi-stationary wind tunnel conditions, and this has a consequence in evaluating the performances of the models. Results for the wind tunnel experiment are in a good agreement with measures, as all metrics satisfy defined criteria.

Compared with the results of other modellers involved in the COST Action ES 1006, performances of PMSS and Code\_SATURNE are similar to equivalent models in their categories.

Finally, the sensitivity tests highlight the importance of having access to appropriate meteorological input data for modelling in order to achieve more reliable simulations of accidental releases. In case of known sensitive sites, a proper planning of a net of sensors becomes essential for optimum support in the use of emergency response tools.

## REFERENCES

- Archambeau F, N. Mechtoua and M. Sakiz, 2004: Code\_SATURNE: a finite volume code for the computation of turbulent incompressible flows - industrial applications. *Int. Journal on Finite Volumes*, **1**, 1-62
- Chang J. C. and S. R. Hanna, 2004: Air quality model performance evaluation. *Meteorology and Atmospheric Physics*, **87**, 167-196
- Hanna, S. R., G. A. Briggs and R. P. Hosker Jr: 1982, 'Handbook on Atmospheric Division', *U.S. Dept. of Energy report DOE/TIC-11223*, Washington, DC.
- Oldrini O., C. Olry, J. Moussafir, P. Armand and C. Duchenne, 2011: Development of PMSS, the parallel version of Micro-SWIFT-SPRAY, 14th International Conference on Harmonisation within Atmospheric Dispersion Modelling for Regulatory Purposes, Harmo'14, Kos (Greece), Oct. 2-6, 2011.
- Thomson D.J., 1987: Criteria for the selection of stochastic models of particle trajectories in turbulent flows. *J. Fluid Mech.*, **180**, 529-556
- Tinarelli G., D. Anfossi, G. Brusasca, E. Ferrero, U. Giostra, M.G. Morselli, J. Moussafir, F. Tampieri and F. Trombetti, 1994: Lagrangian particle simulation of tracer dispersion in the lee of a schematic two-dimensional hill. *Journal of Applied Meteorology*, **33**, N. 6, 744-756
- Tinarelli G., G. Brusasca, O. Oldrini, D. Anfossi, S. Trini Castelli and J. Moussafir, 2007: "Micro-Swift-Spray (MSS) a new modelling system for the simulation of dispersion at microscale. General description and validation". *Air Pollution Modelling and its Applications XVII*, C. Borrego and A.N. Norman eds., Springer, 449-458
- Tinarelli, G., L. Mortarini, S. Trini-Castelli, G. Carlino, J. Moussafir, C. Olry, P. Armand, and D. Anfossi, 2013: Review and validation of Micro-SPRAY, a Lagrangian particle model of turbulent dispersion. *Lagrangian Modeling of the Atmosphere, Geophysical Monograph, Volume 200, AGU*, pp. 311-327, May 2013.
- Tinarelli G., M. Nibart, P. Armand and S. Trini Castelli, 2016: A sensitivity analysis for a Lagrangian particle dispersion model in emergency-response test cases, 17th International Conference on Harmonisation within Atmospheric Dispersion Modelling for Regulatory Purposes, Harmo'17, Budapest (Hungary), May 9-12, 2016. To be published.

**17th International Conference on  
Harmonisation within Atmospheric Dispersion Modelling for Regulatory Purposes  
9-12 May 2016, Budapest, Hungary**

---

**EFFECT OF THE TERRAIN FEATURES ON THE ACCURACY OF CALMET.  
A COMPLEX TERRAIN CASE STUDY**

*A. Hernandez<sup>1</sup>, J.A. Gonzalez<sup>2</sup>, J.J. Casares<sup>2</sup>*

<sup>1</sup>Centro de Estudios de Ingeniería de Procesos (CIPRO), Facultad de Ingeniería Química, Instituto Superior Politécnico José Antonio Echeverría (CUJAE), Havana, Cuba

<sup>2</sup>Department of Chemical Engineering; University of Santiago de Compostela; 15782 Santiago de Compostela, Spain

**Abstract:** Accurate and high resolution meteorological fields are critical to obtain good air quality modelling results, a common tool in air quality management. CALMET diagnostic model is a good solution to obtain high resolution meteorological fields, but its setup includes a wide number of schemes and parameters which should be selected on the specific environment where the model is applied. Particularly, the parameter TERRAD takes into account the influence of the terrain features in CALMET results. In this work, CALMET outputs using different TERRAD values were tested over a complex terrain and coastal environment at the NW of the Iberian Peninsula. Surface wind and temperature results from CALMET were compared to hourly observations from eleven surface stations. As a result, the lowest wind speed RMSE ( $2.51\text{m}\cdot\text{s}^{-1}$ ) was achieved using a TERRAD value of 6 km. No significant differences in CALMET surface temperature performance using different TERRAD values were found.

**Key words:** *CALMET, model calibration, terrain features, complex terrain.*

## **INTRODUCTION**

The management of air quality requires previous knowledge of atmospheric processes, and air quality modelling is currently an important tool to achieve it. However, accurate and high resolution meteorological fields are critical to obtain good air quality modelling results.

CALMET diagnostic model (Scire et al., 2000) is a widespread solution for getting high resolution meteorological fields, using different meteorological inputs (observations, weather forecast models, or both). In CALMET, a large number of calculation options and parameters can be selected, and this selection depends on the specific environment where the model is applied. In a previous experience, Lee et al. (2003) performed a sensitivity study of R1 CALMET parameter for several MM5-CALMET system setups.

Particularly, TERRAD is an empirical parameter that takes into account the effect of the radius of influence of terrain features on meteorological fields; that is, how far is affected the meteorology by valleys, hills, etc. TERRAD value is highly dependent on each specific domain topographic dataset; therefore, testing of different TERRAD values over a specific environment is recommended in order to calibrate it to get a more accurate CALMET simulation. The US Interagency Workgroup on Air Quality Modelling (IWAQM) outlined a list of recommendations for many CALMET settings, and set 15 km as default recommended TERRAD value (Fox, 2009). Moreover, Lakes Environmental (2011) suggested three different criteria to be considered for TERRAD setting: from 4 to 10 grid cells length, ridge to ridge distance, and size of the terrain features needed to be captured. Because of this variety of criteria, statistical assessment of CALMET output over a specific environment is highly recommended.

In the past, several statistical methods were used in meteorological models assessment. The advantages of using RMSE rather than other statistics to evaluate meteorological models output were showed for Willmott (1981), as other statistics generate either overestimation of large errors or masking small ones.

Also, other parameters as BIAS, MGE, etc (Emery et al., 2001; Chang and Hanna, 2004; Mohan and Sati, 2016), are commonly used in many meteorological model evaluations.

In this work, outputs from CALMET diagnostic model were tested using different TERRAD values over a complex terrain and coastal environment at the NW of the Iberian Peninsula, using the same WRF model simulations as CALMET input.

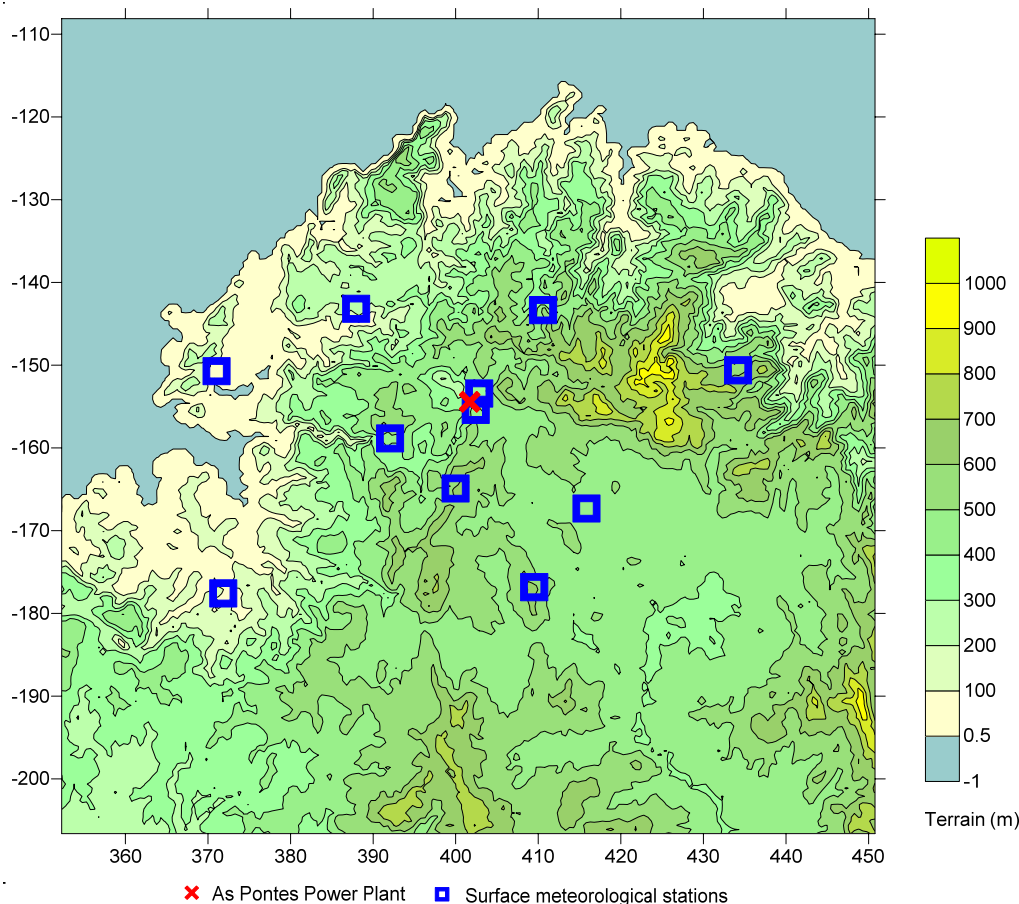


**Figure 1.** Location (UTM coordinates) and digital elevation model (asl-m) of the CALMET simulation domain inside the D3 domain (Northwestern Galicia), with the location of meteorological surface sites for model assessment. Terrain values [-1,0.5] correspond to sea level.

### STUDY AREA AND EVALUATION PERIODS

Galicia is a region located in the northwest corner of the Iberian Peninsula, between 42° and 44° N and 7° and 9°30' W, with complex terrain and land use, and sea influence. In this work, a study area around As Pontes 1400 MW coal fired power plant with a 356.5 m stack was considered (Figure 1), because of the interest in the application of CALPUFF system to evaluate that power plant plume diffusion (Souto et al., 2014). This study area is centred at As Pontes valley, covering the roughly E-W oriented lowlands around the River Eume (including two large dams as inland surface waters) with the following surrounding geographic features: to the East, two mountain ranges up to 1000 asl-m; to the North, a series of hills running roughly N-S from the coast, with maximum altitudes of 550-750 asl-m; to the West, low coastal hills (< 200 asl-m) bordering the Atlantic coast; to the South, to mountain ranges, with maximum altitudes of 750-850 asl-m; and to the SE, an elevated plain. Consequently, it is a complex terrain, with some granitic mountains, valleys, water surfaces, and a narrow coastal line, all mixed in the same environment.

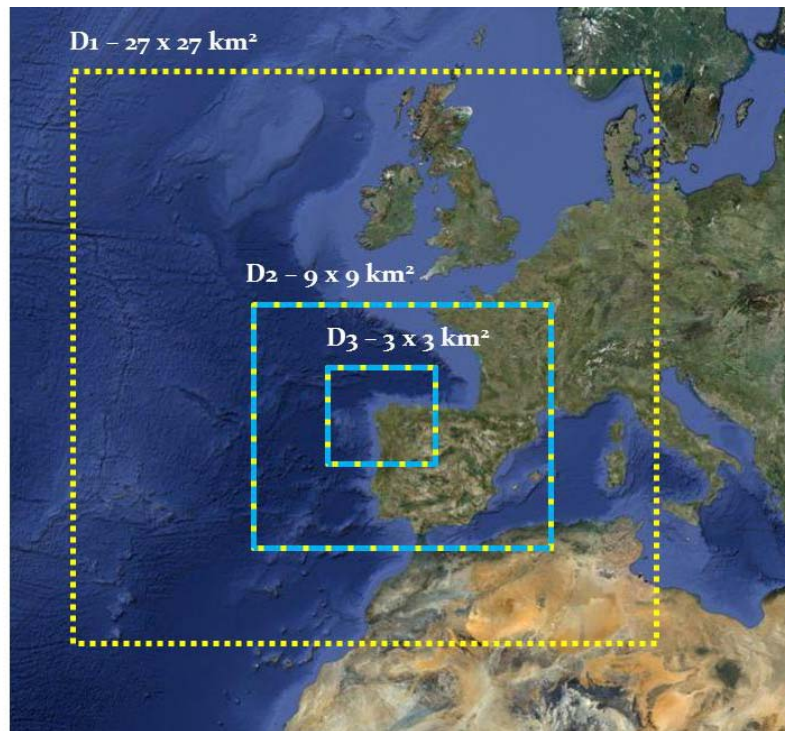


**Figure 2.** WRF nested domains, including D3 domain that provides the meteorological input to CALMET simulations.

In order to compare to previously CALMET simulations over the same environment (Gonzalez et al., 2015) the following testing period was considered: June 1<sup>st</sup>, 2006 – June 3<sup>rd</sup>, 2006. This period corresponds to anticyclonic and stable conditions, which are typical in this region during the synoptic pattern High Pressure over Atlantic and Europe (HPAE) (Saavedra et al., 2012).

#### **METEOROLOGICAL MODELING**

Simulation domain (Figure 1) covers 99x99 km<sup>2</sup> and a CALMET 0.5 km horizontal resolution grid was set in all simulations. Also, 14 vertical layers were set in order to get a good representation of the PBL vertical structure, with reasonable computational time effort (Gonzalez et al. 2015). About CALMET settings, default values were applied except to the parameter TERRAD.

As CALMET meteorological input, WRF model simulations using three one-way nested grids were done (Figure 2), with a 3x3 km<sup>2</sup> horizontal resolution in the innermost grid. US NCEP GFS reanalysis fields supplied initial and boundary conditions. WRF model settings include: Kain-Fritsch cumulus scheme (outer and medium domain), WSM 3-class microphysics scheme, a RRTM long wave and Dudhia shortwave radiation scheme, 5-layer soil model, and Yonsei University-Pleim-Chang (YSU) PBL scheme (Souto et al., 2013).

Considering Lakes Environmental (2011) criteria, four different TERRAD values from 1 to 10 times the horizontal grid resolution (0.5 km) were initially selected: 0.5, 1, 3 and 5 km. After that, TERRAD value was increased in order to check its performance: 6, 7, 9, 15, 20, and 30 km. Surface wind and temperature CALMET results for every TERRAD value were compared to hourly observations from eleven surface stations located at the simulation domain (see Figure 1) during the same period.

## RESULTS

Following Willmott (1981), RMSE statistics were considered to measure the different CALMET simulations performance. Regarding wind speed, every CALMET simulations provide lower RMSE (see Figure 3) than WRF 3x3 km<sup>2</sup> resolution results (2.58 m·s<sup>-1</sup>); also lower RMSE values are obtained with CALMET around the TERRAD range recommended by Lakes Environment (2011), that is, 0.5-5 km. However, the lowest RMSE value (2.51 m·s<sup>-1</sup>) is achieved with TERRAD=6 km, close to the maximum recommended value. This result can be derived by the quite complex topography in this domain that requires taking into account terrain features influence over the wind flow a bit further than usual.

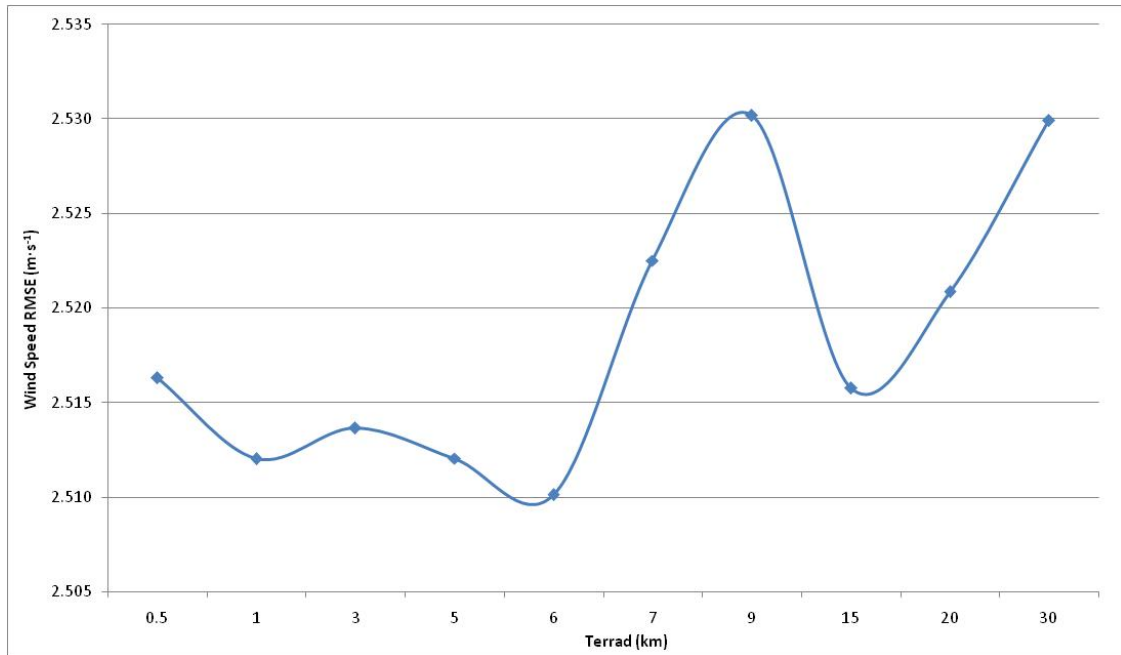


**Figure 3.** Wind speed RMSE variation from CALMET simulations using with different TERRAD values

About surface temperature, RMSE values are very similar using different TERRAD values (Table 1); although land uses could affect to the surface temperature, actually CALMET results are derived from WRF output, which is the same for every CALMET simulation; therefore, any surface temperature improvement requires either better WRF simulations or surface temperature measurements as additional input.

**Table 1.** Temperature RMSE results from CALMET simulations using different TERRAD values

TERRAD (km)	Temperature RMSE (°C)
0.5	2.2941
1	2.2939
3	2.2931
6	2.2928
9	2.2927
15	2.2926
20	2.2926
30	2.2925

## CONCLUSIONS

The influence of complex terrain features in CALMET requires the calibration of different parameters and model options. In this work, TERRAD empirical parameter shows its influence over surface wind speed results in a complex terrain and coastal environment. Although every CALMET simulations provide lower wind speed RMSE than WRF (3x3 km<sup>2</sup> resolution) simulation, RMSE differences using different TERRAD values simulations are small, because of the higher influence of that same WRF output applied as CALMET input. However, an improvement (lowest RMSE) using TERRAD=6 km is obtained, which is a bit higher than the maximum TERRAD recommended value (5 km). This can be related to the complex terrain features, as higher complexity can require higher TERRAD values, in order to consider the influence of further topographic features over the wind flow. On the other hand, no influence of TERRAD value is observed in surface temperature performance, as temperature has a lower sensitivity to the topographic features.

## ACKNOWLEDGEMENTS

Anel Hernandez's research stages at the University of Santiago de Compostela were supported by USC-Santander Bank PhD Programme for Latinoamerican university lecturers. Meteorological observations provided by As Pontes Power Plant and MeteoGalicia (Galician Regional Meteorological Office) are acknowledged.

## REFERENCES

- Chang, J.C. and Hanna, S.R., 2004: Air quality model performance evaluation, *Meteorology and Atmospheric Physics*, **87**, 167-196.
- Emery, C., E. Tai and G. Yarwood, 2001: *Enhanced Meteorological Modeling and Performance Evaluation for Two Texas Ozone Episodes*, Environ International Corporation.
- Fox, T., 2009: *Memorandum: Clarification on EPA-FLM Recommended Settings for CALMET*, August 31<sup>st</sup>, 2009.
- Gonzalez, J. A., A. Hernandez-Garces, A. Rodriguez, S. Saavedra and J.J. Casares, 2015: Surface and upper-air WRF-CALMET simulations assessment over a coastal and complex terrain area. *International Journal of Environment and Pollution*, **57**, 249–260.
- Lakes Environmental, 2011: CALPUFF Air Dispersion Modeling Workshop: Course Slides, Barcelona, Spain, Oct 19-21, 2011.
- Lee, R.F. and Thé, J.L., 2003: The effect of CALMET surface layer weighting parameter R1 on the accuracy of CALMET at other nearby sites: a case study. In: *Guideline on Air Quality Models: The Path Forward*, October 22-24, 2003, Mystic, CT, no. 03-A-32.
- Mohan, M. and Sati, A. P., 2016): WRF model performance analysis for a suite of simulation design. *Atmospheric Research*, **169**, 280-291.
- Saavedra, S., Rodríguez, A., Taboada, J.J., Souto, J.A. and Casares, J.J., 2012: Synoptic patterns and air mass transport during ozone episodes. *Science of the Total Environment*, **441**, 97–110.
- Scire, J.S., Robe, F.R., Fernau, M.E. and Yamartino, R.J., 2000: *A User's Guide for the CALMET Meteorological Model (Version 5)*, Earth Tech, Concord, MA.
- Souto, J.A., Saavedra, S., Rodriguez, A., Dios, M., Cartelle, D. and Vellon, J.M., 2013: Evaluation of the PRESAXIO air quality forecasting system: PBL schemes WRF comparison and air quality modeling validation. In: *15<sup>th</sup> International Conference on Harmonisation within Atmospheric Dispersion Modelling for Regulatory Purposes (HARMO15)*, Madrid, May 6-9 2013.
- Souto, J.A., Moral, C., Rodríguez, A., Saavedra, S., Casares, J.J. and Hernández-Garces, A., 2014: Simulation of plume dispersion using different stack configurations and meteorological inputs. *International Journal of Environment and Pollution*, **55**, 139-147.
- Willmott, C.J., 1981: On the validation of models. *Physical Geography*, **2**, 184–194.

**17th International Conference on  
Harmonisation within Atmospheric Dispersion Modelling for Regulatory Purposes  
9-12 May 2016, Budapest, Hungary**

---

**USING METEOROLOGICAL ENSEMBLES FOR ATMOSPHERIC DISPERSION MODELING  
OF THE FUKUSHIMA NUCLEAR ACCIDENT**

*Raphaël Périllat<sup>1,2</sup>, Irène Korsakissok<sup>1</sup>, Vivien Mallet<sup>3</sup>, Anne Mathieu<sup>1</sup>, Thomas Sekiyama<sup>4</sup>,  
Mizuo Kajino<sup>4</sup>, Kouji Adachi<sup>4</sup>, Yasuhito Igarashi<sup>4</sup>, Takashi Maki<sup>4</sup>, Damien Didier<sup>1</sup>*

<sup>1</sup> IRSN - Institute of Radiation Protection and Nuclear Safety, Fontenay-aux-roses (France).

<sup>2</sup> BERTIN Technologie, Saint-Aubin (France).

<sup>3</sup> INRIA, Paris (France).

<sup>4</sup> Japan Meteorological Agency, Meteorological Research Institute,  
Tsukuba (Japan).

**Abstract:** Dispersion models are used in response to an accidental release of radionuclides of the atmosphere, to infer mitigation actions, and complement field measurements for the assessment of short and long term environmental and sanitary impacts. However, the predictions of these models are subject to important uncertainties, especially due to input data, such as meteorological fields or source terms (Korsakissok et al. (2013), Girard et al. (2014), ).

In the framework of the SAKURA project, an MRI-IRSN collaboration, a meteorological ensemble of 20 members designed by MRI (Sekiyama et al. (2013)) was used with IRSN's atmospheric dispersion models. Another ensemble, retrieved from ECMWF and comprising 50 members, was also used for comparison. The MRI ensemble is assimilated every 3 hours, with a 3-kilometer resolution, designed to reduce the meteorological uncertainty in the Fukushima case. The ECMWF is a 24-hour forecast with a coarser grid, and is supposed to be representative of the uncertainty of the data available in a crisis context.

First, it was necessary to assess the quality of the ensembles for our purpose, i.e. to ensure that their spread was representative of the uncertainty of the meteorological fields. Using meteorological observations allowed characterizing the ensembles' spreads, with tools such as rank histograms. Then, the ensemble simulations were carried out with atmospheric dispersion models. The underlying question is whether the output spread is larger than the input spread, that is, whether small uncertainties in meteorological fields can produce large differences in atmospheric dispersion results. Here again, the use of field observations was crucial, in order to characterize the spread of the ensemble of atmospheric dispersion simulations. In the case of the Fukushima accident, ambient gamma dose rates, air activities and deposition data were available. Based on these data, selection criteria for the ensemble members were designed. Finally, the total uncertainty, including from the source term and the model formulation, was propagated in time. The results were compared with the meteorological-induced uncertainty, and between the two sets of meteorological data.

**Key words:** *Uncertainty, Fukushima, Monte Carlo, meteorological ensemble*

## **INTRODUCTION**

Atmospheric dispersion simulations made in case of nuclear accidents rely on meteorological fields provided by meteorological models. The strong uncertainties in these data have an impact on the computed plume's trajectory. A good knowledge of this uncertainty is necessary for a good decision making in case of an emergency. Since meteorological data are 2D or 3D-fields varying in time and space, perturbing them in a physically consistent way is not trivial. Using meteorological ensembles seems therefore a good alternative to coarse perturbation, as homogeneous additive or multiplicative perturbations. A meteorological ensemble is constituted of several equiprobable forecasts on the same region and on the same period of time. It is evaluated for meteorological forecasts, and the spread of the members is supposed to represent the forecast uncertainty.

The aim of this study is to evaluate the use of meteorological ensembles for uncertainty studies in the case of the Fukushima disaster. The two ensembles used are presented and compared to meteorological

observations. Then, dispersion results at local scale are shown with a set of source terms, using the meteorological ensembles with and without an additional perturbation.

### METEOROLOGICAL ENSEMBLES

In this study, we use two meteorological ensembles. The first one is from the Meteorological Research Institute (MRI) of the Japan Meteorological Agency (Sekiyama et al. (2013), Sekiyama et al. (2015)). It is built with 20 members on a 3-km horizontal resolution with an hourly time step. These data come from a posteriori assimilation of the AMeDAS<sup>1</sup> observations of the wind and temperature, every three hours. This ensemble is representative of the a posteriori analysis error, i.e. the meteorological uncertainty with our best knowledge of the target times on forecast. The second meteorological ensemble used here is from the European Centre for Medium-Range Weather Forecasts (ECMWF). It is built with 50 members on a horizontal resolution of 0.25°, with a three-hour time step. These data come from 24-hour forecasts and are representative of the uncertainty of data available during a crisis. These two ensembles were available on pressure levels and were interpolated on vertical levels.

**Table 1.** Property of the meteorological ensembles

Ensemble	Spatial resolution	Time resolution	Vertical levels (m)	Assimilation frequency	Domain
MRI	3 km	1h	10, 20, 50, 100, 120, 250, 500, 1000	3h	207km x 207km
ECMWF	0.25°	3h	10, 100, 250, 500, 1000	24h	300km x 300km

To study the behaviour of the two meteorological ensembles, we compared them to AMeDAS observations of the wind, the rain precipitation and the temperature, available at more than 60 stations in our simulation domain. The model-to-data comparison was carried out using time series of each variable, scores and rank histograms.

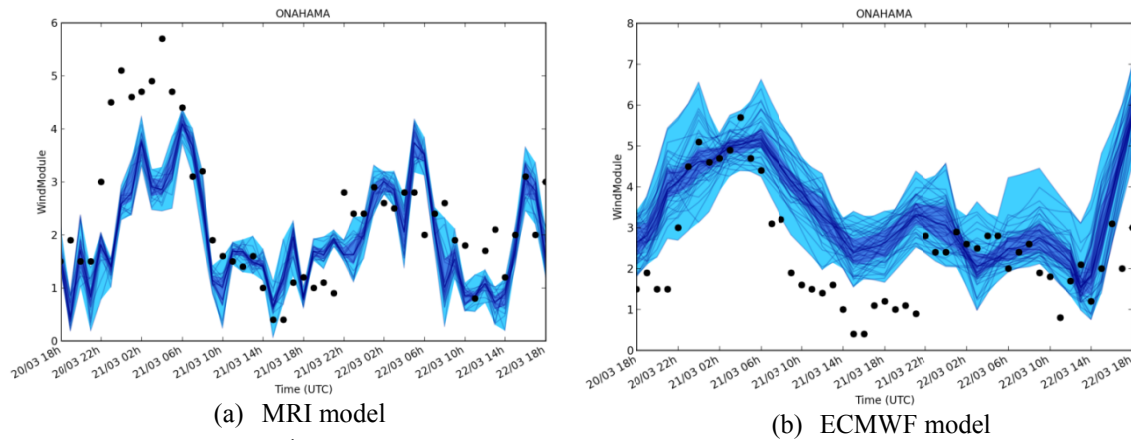


**Figure 1.** Wind module ( $\text{m}\cdot\text{s}^{-1}$ ) of the meteorological ensembles (in blue) compared to the AMeDAS observations (in black) for the Onahama station.

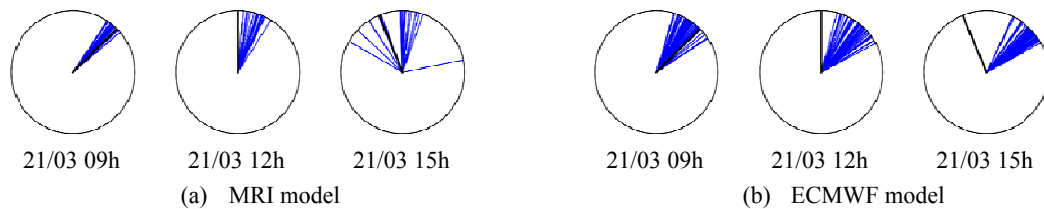


**Figure 2.** Wind direction of the meteorological ensembles (in blue) compared to the AMeDAS observation (in black) for the Onahama station.

<sup>1</sup> Automated Meteorological Data Acquisition System (<http://www.jma.go.jp/en/amedas/>)

It appears on Figures 1 and 2 that the members of the ECMWF ensemble are more spread compared to the MRI ensemble, which is consistent with the larger assimilation time. According to the scores, the MRI members are closer to the observations, with a root mean square error (RMSE) around  $1.5 \text{ m.s}^{-1}$  for the wind module of MRI against  $2.1 \text{ m.s}^{-1}$  for ECMWF. For the rain precipitation, the RMSE is around  $0.68 \text{ mm.h}^{-1}$  for all the members of the MRI ensemble against  $0.71 \text{ mm.h}^{-1}$  for the ECMWF. However, these two ensembles are not spread enough to encompass the observations. In a lot of cases, the AMeDAS observations are above or under all the members, which leads to a rank histogram in U-shape. A rank histogram is a way to assess an ensemble spread using a set of observations. For each observation we compute the rank which is the number of ensemble members that forecast less than the observation. The rank histogram shows the total number of observations of a given rank against the rank. If the ensemble is representative of the uncertainty, the rank histogram tends to be flat. The U-shaped rank histogram found for the two ensembles means that they underestimate the meteorological uncertainty. They were built to represent the uncertainty of large-scale variables that are used for meteorological forecast. The 10 meters variables are not considered for the construction of the ensemble, while the forecast error in the boundary layer is much more important than in the large scale variables, because of the direct interactions with the ground.

Therefore, we decided to apply an additional perturbation on wind and rain fields, to expand the spread of the ensembles and better represent the amplitude of the uncertainty on 10-meters variables. For that, we added a homogeneous, time-dependent, perturbation to each ensemble's member. The perturbation was chosen so as to obtain a flat rank diagram of these fields, compared to AMeDAS observations, while keeping the same ensemble mean (see Figure 3). While the physical consistency of the resulting fields can be questioned, this allowed us to verify whether a wider meteorological ensemble was sufficient to represent the output uncertainty. A better approach, in the future, would be to construct adequate meteorological ensembles, representative of the boundary layer uncertainties.

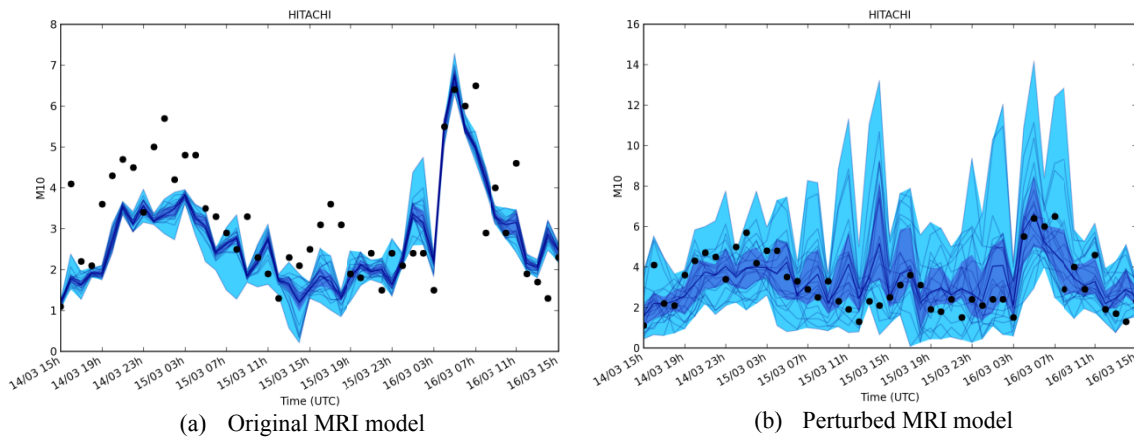


**Figure 3.** Wind module ( $\text{m.s}^{-1}$ ) of the meteorological ensemble (in blue) compared to the AMeDAS observations (in black) for the Hitachi station.

### SIMULATION OF THE DISPERSION

For atmospheric dispersion computation at local scale, we used the pX model, which is a Gaussian puff model developed and used in the IRSN (Korsakissok et al. (2013)). In order to add more variability to the computation, we used the meteorological ensemble in the pX model with different source terms. The five source terms used are those from Mathieu et al. (2012), Saunier et al. (2013), Terada et al. (2012), Katata et al. (2015), and a new IRSN source term that was evaluated with inverse modelling, using the same methodology as in Saunier et al. (2013), with IRSN's large scale model and MRI's deterministic meteorological fields. As we expected, the results are really different depending on the source term.

Comparing the results with the ambient gamma dose rate observations available in the Fukushima prefecture, the two ensembles do not embrace the observations, even if we include all source terms for

more variability. The rank histograms are in U-shape, which means that in a lot of cases the observations are above or under all the simulations. The results are shown for MRI ensemble (Figure 4(a)), but are similar when using ECMWF ensemble, even though the ensemble's spread was larger. When using the additional perturbation on meteorological fields, the rank diagram of the simulation outputs is greatly improved (Figure 4(b)). There is still not enough spread in the simulations, but they clearly embrace the observations much more. This kind of perturbations creates more variability on the simulations and can, for instance, allow representing a peak that the previous meteorological data missed (see Figure 5).

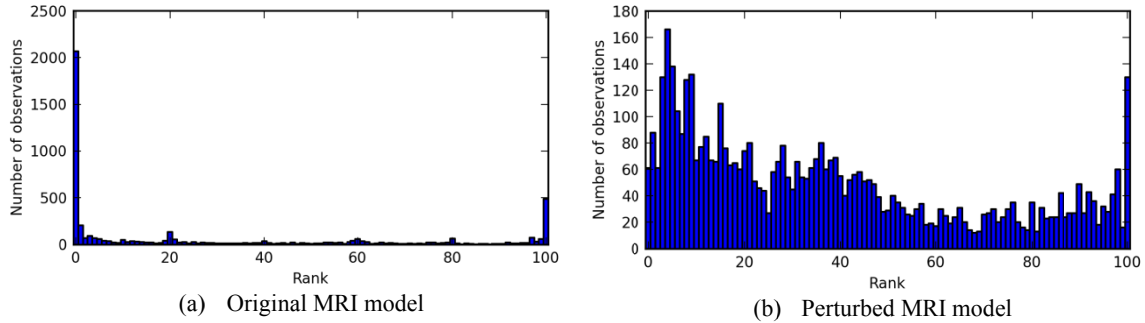


**Figure 4.** Rank histograms of the ambient gamma dose rate for the pX out, calculated with all source terms, compared to the observations.

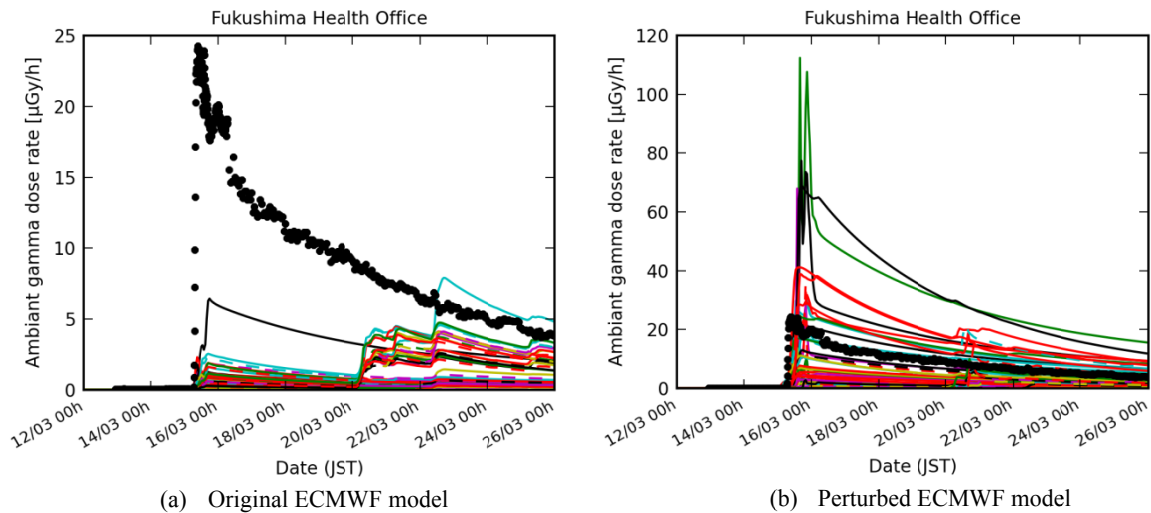


**Figure 5.** Gamma dose rate of each outputs of the meteorological ensemble compared to the observation for the Fukushima Health Office station.

## CONCLUSION

Two meteorological ensembles were used for atmospheric dispersion computations in the Fukushima case, along with five up-to-date source terms. The aim was to propagate the input's uncertainties through the model, and evaluate their impact on dispersion results. The resulting ensemble simulations were compared to gamma dose rate observations. When using a non-perturbed meteorological ensemble, the output spread is not sufficient to encompass the observations. If an additional perturbation is added to the input fields, so as to be better representative of the 10-meter variables' uncertainty, the dispersion results are much better in terms of rank histogram.

However, the physical consistency of this perturbation is questionable. A more satisfactory approach, in the future, would be to construct adequate meteorological ensembles, representative of the boundary layer uncertainties.

Other uncertain parameters will also be perturbed. First, the source term uncertainty is also underestimated when using only five of them, and additional perturbations on the release times, the source altitude and the amplitude of the release should be applied. The modelling parameters are also uncertain, and deposition parameters such as the scavenging coefficient and the deposition velocity will be included in future uncertainty propagation study.

## REFERENCES

- Girard, S., Korsakissok, I. and Mallet, V. (2014): Screening sensitivity analysis of a radionuclides atmospheric dispersion model applied to the Fukushima disaster. *Atmospheric Environment* **95**(0): 490-500.
- Katata, G., Chino, M., Kobayashi, T., Terada, H., Ota, M., Nagai, H., Kajino, M., Draxler, R., Hort, M. C., Malo, A., Torii, T. and Sanada, Y. (2015): Detailed source term estimation of the atmospheric release for the Fukushima Daiichi Nuclear Power Station accident by coupling simulations of an atmospheric dispersion model with an improved deposition scheme and oceanic dispersion model. *Atmos. Chem. Phys.* **15**(2): 1029-1070.
- Korsakissok, I., Mathieu, A. and Didier, D. (2013): Atmospheric dispersion and ground deposition induced by the Fukushima Nuclear power plant accident : a local-scale simulation and sensitivity study. *Atmospheric Environment* **70**: 267-279.
- Mathieu, A., Korsakissok, I., Quélo, D., Groëll, J., Tombette, M., Didier, D., Quentric, E., Saunier, O. and Benoit, J.-P. (2012): Assessment of atmospheric dispersion for the Fukushima Dai-ichi Nuclear Power Plant accident. 13th International Congress of the International Radiation Protection Association, Glasgow, 14-18 May, 2012.
- Saunier, O., Mathieu, A., Didier, D., Tombette, M., Quélo, D., Winiarek, V. and Bocquet, M. (2013): An inverse modeling method to assess the source term of the Fukushima Nuclear Power Plant accident using gamma dose rate observations. *Atmos. Chem. Phys.* **13**(22): 11403-11421.
- Sekiyama, T., Kajino, M. and Kunii, M. (2013): Ensemble simulation of the atmospheric radionuclides discharged by the Fukushima nuclear accident. EGU General Assembly C1 - Vienne.
- Sekiyama, T. T., Kunii, M., Kajino, M. and Shimbori, T. (2015): Horizontal Resolution Dependence of Atmospheric Simulations of the Fukushima Nuclear Accident Using 15-km, 3-km, and 500-m Grid Models. *Journal of the Meteorological Society of Japan. Ser. II* **93**(1): 49-64.
- Terada, H., Katata, G., Chino, M. and Nagai, H. (2012): Atmospheric discharge and dispersion of radionuclides during the Fukushima Dai-ichi Nuclear Power Plant accident. Part II: verification of the source term and analysis of regional-scale atmospheric dispersion. *Journal of Environmental Radioactivity* **112**: 141-154.

**17th International Conference on  
Harmonisation within Atmospheric Dispersion Modelling for Regulatory Purposes  
9-12 May 2016, Budapest, Hungary**

---

**VALIDATION OF THE GAUSSIAN PUFF MODEL pX USING NEAR-FIELD KRYPTON-85  
MEASUREMENTS AROUND THE AREVA NC LA HAGUE REPROCESSING PLANT:  
COMPARISON OF DISPERSION SCHEMES**

*Irène Korsakissok<sup>1</sup>, Mathieu Contu<sup>1</sup>, Olivier Connan<sup>2</sup>, Anne Mathieu<sup>1</sup> and Damien Didier<sup>1</sup>*

<sup>1</sup> IRSN - Institute of Radiation Protection and Nuclear Safety - PRP-CRI, SESUC, BMCA,  
Fontenay-aux-Roses, France

<sup>2</sup> IRSN - Institute of Radiation Protection and Nuclear Safety - PRP-ENV, SERIS, LRC,  
Cherbourg, France

**Abstract:** In case of an accidental release of radionuclides in the atmosphere, atmospheric dispersion models are used by IRSN to assess the sanitary and environmental consequences, and infer mitigation actions. Several tools are comprised in the C3X operational platform (Tombette et al. (2014)), including various models and levels of complexity. Among them, the Gaussian puff model pX is used for local scale. Gaussian models are indeed widely used in a crisis context, due to their simple approach, low computational burden, and fair performance at short distance in most situations. However, many dispersion schemes can be used, from a crude, discrete representation of the atmospheric stability, to more physical parameterizations. Besides, most schemes are not well adapted to very stable situations. Thus, model-to-data validation is crucial to determine the model's performance and limitations, and the best dispersion scheme for each meteorological situation.

The AREVA NC La Hague site is one of the world's largest fuel reprocessing plant. During reprocessing operations, the plant's 100-m height stacks emit krypton-85 that can be measured in the environment. IRSN carried out several experimental campaigns, measuring <sup>85</sup>Kr air concentration activities (Connan et al, 2013, Connan et al, 2014). A fixed measurement device is now continuously registering air concentrations in the courtyard of IRSN's laboratory of Cherbourg (LRC), 18 kilometers from the source. These measurements were used with the pX model, along with near-field measurements (1-5 km) conducted during stable situations. These field data are particularly relevant for studying local-scale dispersion from an elevated release, in a topographically complex area (near the ocean and cliffs). In particular, near-field measurements raise the matter of effective release height, taking into account the effect of neighboring buildings. Several dispersion schemes and ways of determining atmospheric stability were compared. Various meteorological data were also used (10-m and 30-m on-site anemometers, 100-m measurements from SODAR profiles), highlighting the complexity of wind fields in this area, and the issue of measurement representativeness.

**Key words:** *Gaussian model, model validation, Kr-85, atmospheric dispersion, stable cases, elevated release*

## **INTRODUCTION**

The Gaussian puff model pX is used at IRSN (the French Institute of Radiation Protection and Nuclear Safety) to model dispersion up to a few tens of kilometers in case of an accidental release of radionuclides in the atmosphere. The results are then used to infer mitigation actions, to take countermeasures for the protection of populations, and to help design measurement strategies. Thus, model-to-data validation is crucial to determine the model's performance and limitations. The pX model was already validated on classic field experiments with passive tracers, such as those contained in the Model Validation Kit (Olesen (2001), Olesen (2005)), or the Prairie Grass experiment. However, there is a need for more experiments in very stable, low-wind conditions, where models are less accurate.

While local-scale (up to a few kilometers) or large scale (from 100 to 1000 km) field experiments have been conducted in the past, there is clearly a gap in the literature, between 10 to 50 kilometers, which are the distances of interest for our applications. At such distances, <sup>85</sup>Kr can be used as a tracer. Krypton-85 (<sup>85</sup>Kr) is a  $\beta^-$  and  $\gamma$  emitting radioactive noble gas with a half-life of 10.7 year. As such, it is particularly interesting for tracer experiments, since it does not undergo deposition processes, and its half-life is large

enough for radioactive decay to be neglected during the experiment. Its main source of emission is anthropogenic, mainly from the reprocessing of spent nuclear fuel.

Here, IRSN's field measurements of  $^{85}\text{Kr}$  around AREVA NC La Hague, one of the world's largest reprocessing plants, are used. Two case studies are shown:

- Continuous measurements of  $^{85}\text{Kr}$  in the courtyard of IRSN's laboratory of Cherbourg (LRC), 18 kilometers from the source (Connan et al. (2013)),
- Near-field (1-5 km) measurements in stable situations (Connan et al. (2014)).

### FIELD EXPERIMENTS

The releases of  $^{85}\text{Kr}$  occur at the site of AREVA NC La Hague, from the 100-m high stack of the production unit. The plant is located in a coastal area, near cliffs. It contains two production units with high stacks and many buildings (Figure 1). The time series of the release were provided by AREVA NC.



**Figure 1.** Aerial view of the AREVA NC La Hague reprocessing plant (left), geographical situation of the plant and IRSN's laboratory (LRC) (right).

The meteorological observations were obtained from several sources: (1) 30-meters wind measurements (sonic anemometer) located on AREVA NC site, near the release point (for 2012-2013 cases), (2) 6-meters wind measurements at a site located 2 kilometers from AREVA NC (available since 2014), (3) SODAR wind profile measurements at the AREVA NC site. In addition, meteorological measurements were also available at IRSN's laboratory. The meteorological measurement frequency is 1 minute, and variables are then averaged over 10 minutes. The wind standard deviations ( $\sigma_v$ ,  $\sigma_w$ ) are also calculated, so as to induce stability parameters, such as Monin-Obukhov length or Pasquill stability class.



**Figure 2.** Beta counting proportional counter (Berthold-LB123) (left), air sampler VEGA (middle), and 6-m sonic anemometer for wind measurement (right).

Close to the discharge point i.e. less than 20 km,  $^{85}\text{Kr}$  concentrations are usually sufficiently high to allow real-time measurements (Figure 2). In these conditions, the activity concentration in the air sample may be determined by  $\beta$  counting in a Berthold-LB123 gas proportional counter (Connan et al. (2013)). The

detection limit is about  $500 \text{ Bq.m}^3$ . In addition, for integrated measurement, air samples are collected in tedlar bag (20-L) and measured by  $\gamma$  spectrometry. Then, the detection limit depends on the counting time duration.

## RESULTS AT LRC

Continuous measurements of  $^{85}\text{Kr}$  are made in LRC's courtyard. Each time the wind direction is such that peaks are detected, the corresponding release amounts are given by AREVA to IRSN and simulations are made. Here, six one-month periods between 2012 and 2014 were studied. Each time, several peaks were detected, of relatively short duration (Figure 3). The simulations were carried out with pX, using several meteorological data, and three Gaussian standard deviations: Pasquill (1978), Doury (1976) and formulas based on similarity theory (Hanna et al. (1982), Hanna and Paine (1989), Irwin (1979)).

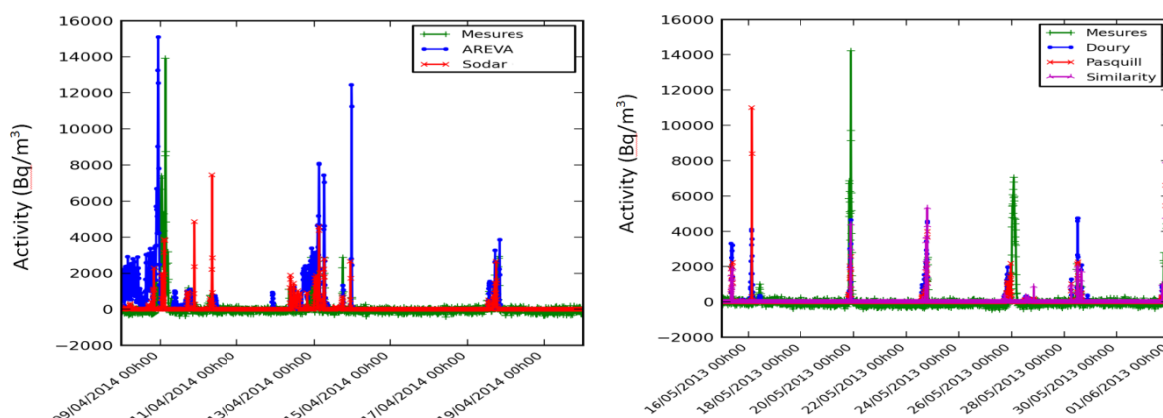


**Figure 3.** Examples of  $^{85}\text{Kr}$  measurements at LRC site, for April, 2014 (left) and May, 2013 (right). Observations are in green. On the left, results with Pasquill parameterization are compared using two different wind data: 6-m anemometer observations (blue) and 100-m SODAR data (red). On the right, 3 Gaussian standard deviations are shown (Doury, Pasquill and Similarity) with 6-m wind data.

Contrary to usual dispersion experiments, which include several measurement points recording time-averaged values, here, the measurement frequency is high (1 minute) but we only have a single measurement point. Thus, results are very sensitive to wind direction measurements uncertainties: even at this distance, a shift of a few degrees in wind direction can result in a missing peak, or a false alarm. Since the stack is 100-meter high, and the measurement device is a few meters above the ground, it is difficult to determine the adequate wind measurement height. In Figure 3 (left), for instance, the 6-meter wind measurement (in blue) shows a lot of peaks at the beginning of the time series (on April 8<sup>th</sup>), whereas the SODAR and measurements don't. This comes from the wind direction, which blows towards LRC according to the 6-m anemometer, while the 100-m direction differs by a few degrees. Besides, the source and receptors are 18 kilometers apart, in a complex orography, and the representativeness of meteorological observations can be questioned.

To get an overview of the model's performance, statistical indicators were designed. Traditional indicators used in dispersion validation, such as bias or correlation, did not seem well adapted to this kind of measurements. Instead, we decided to use indicators based on peak detection: a peak is detected each time a value (observed or simulated) is above a given threshold. If both observations and simulations detect a peak at the same time, it is a *hit*. If the peak is observed, but not simulated, it is a *miss*, and the reverse is a *false alarm*. Then, three indicators can be based on the number of *hit*, *miss* and *fa*:

- The probability of detection:  $pod = hit / (hit + miss)$
- The false alarm rate:  $far = fa / (fa + hit)$
- The measure of effectiveness:  $moe = hit / (hit + 1.5*miss + 0.5*fa)$

**Table 1:** Statistical indicators (POD, FAR and MOE) computed over the six case studies at LRC for several configurations: 3 Gaussian standard deviations (Pasquill, Doury, Similarity) and two meteorological data (AREVA anemometer and wind at 100-m from SODAR profile).

Configuration (1-h average, threshold 200 Bq/m <sup>3</sup> )	Probability of detection (POD)	False alarm rate (FAR)	Measure of effectiveness (MOE)
Pasquill – AREVA anemometer	0.83	0.30	0.66
Doury – AREVA anemometer	0.80	0.34	0.61
Similarity – AREVA anemometer	0.78	0.36	0.59
Pasquill – SODAR 100m	0.72	0.37	0.53
Doury – SODAR 100m	0.69	0.41	0.50
Similarity – SODAR 100m	0.72	0.40	0.52

A perfect model would have  $pod = 1$ ,  $far = 0$  and  $moe = 1$ . The  $moe$  is designed so as to be more penalizing for a model that would miss a peak than for one that would falsely detect one. Table 1 summarizes the model's performance with several configurations. Between 70 and 80% of the observed peaks are detected, but about 30 to 40% of simulated peaks are false alarm. The  $moe$  is between 50% and 66%. Results are clearly better when using the 6-m wind measurements than using 100-m SODAR data. However, for some cases, 100-m observations give better results, as shown Figure 3. Results in terms of peak detection are not very sensitive to standard deviations, but the Pasquill parameterization gives the best performance. The peak intensities, however, are clearly dependent on the chosen parameterization and on the stability diagnosis (Figure 3, right).

#### NEAR-FIELD MEASUREMENTS IN STABLE SITUATIONS

Twenty-two measurement campaigns were conducted in stable situations, during nighttime, between 2010 and 2013 (Connan et al. (2014)). Sensors were positioned downwind from the source, at distances varying from 1 to 5 kilometers. Results were integrated over 30 minutes. In this preliminary study, eight cases have been simulated with the pX model, using on-site meteorological measurements (30-meter sonic anemometer). Simulations were made with three Gaussian standard deviations (Doury, Pasquill and similarity) and three release heights: 100 meters (stack height), 50 meters and ground release, in order to take into account building downwash due to the high number of buildings close to the source (Figure 1, left).

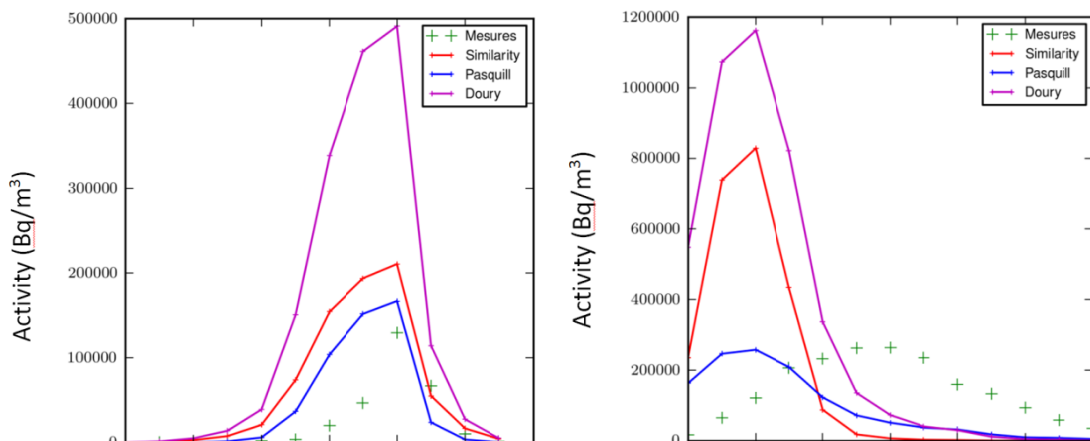


**Figure 4.** Crosswind <sup>85</sup>Kr activity for two cases (February, 19<sup>th</sup> and 20<sup>th</sup>, 2013). Simulations are made with a ground release, and 3 Gaussian standard deviations are shown (Doury, Pasquill and Similarity).

Figure 4 shows two examples of crosswind concentrations obtained for a ground release. While there is an overestimation with some parameterizations, simulations are in good agreement with observations, especially with Pasquill standard deviations. However, with 50-m and 100-m releases, which are more

realistic, concentrations are highly underestimated, and there is often no simulated plume close to the ground at these distances. This shows the crucial importance of taking into account the effect of buildings in the simulations. Also, in several cases, there is no simulated plume at all, no matter the source height or the parameterization. This comes from a discrepancy between the wind direction used in the model and the “real” wind direction responsible for the plume transport.

## CONCLUSION

We presented model-to-data comparisons to  $^{85}\text{Kr}$  measurements in the vicinity of AREVA NC La Hague reprocessing plants. The continuous measurements at the LRC laboratory, located 18 kilometers from the plant, allowed us to carry out comparisons between several configurations and meteorological data. They raised the issue of meteorological representativeness in such a complex area, with a 100-m release and several surrounding buildings. The near-field measurements in stable situations highlighted the issue of building downwash, and the difficulty to model dispersion in some cases. Again, the question of meteorological data representativeness was raised. In the future, more experiments will be added to our dataset, and 3D meteorological fields at fine resolutions will be tested, and compared to observations.

## ACKNOWLEDGEMENTS

We would like to thank the Environment Laboratory at the AREVA NC La Hague plant for their contribution to the successful performance of the experimental campaigns and for making the meteorological and emission parameters data available.

## REFERENCES

- Connan, O., Smith, K., Organo, C., Solier, L., Maro, D. and Hébert, D. (2013): Comparison of RIMPUFF, HYSPLIT, ADMS atmospheric dispersion model outputs, using emergency response procedures, with  $^{85}\text{Kr}$  measurements made in the vicinity of nuclear reprocessing plant. *Journal of Environmental Radioactivity* **124**: 266-277.
- Connan, O., Solier, L., Hébert, D., Maro, D., Lamotte, M., Voiseux, C., Laguionie, P., Cazimajou, O., Le Cavelier, S., Godinot, C., Morillon, M., Thomas, L. and Percot, S. (2014): Near-field krypton-85 measurements in stable meteorological conditions around the AREVA NC La Hague reprocessing plant: estimation of atmospheric transfer coefficients. *Journal of Environmental Radioactivity* **137**: 142-149.
- Doury, A. (1976). Une méthode de calcul pratique et générale pour la prévision numérique des pollutions véhiculées dans l'atmosphère. CEA. Rapport.
- Hanna, S. and Paine, R. (1989): Hybrid plume dispersion model (HPDM) development and evaluation. *Journal of applied meteorology* **28**: 206-224.
- Hanna, S. R., Briggs G.A. and Hosker, R. P. (1982). Handbook on Atmospheric Diffusion, U.S. Department of Energy.
- Irwin, J. (1979). Estimating plume dispersion. A recommended generalized scheme. 4th AMS Symposium on Turbulence and Diffusion. Reno, Nevada, USA.
- Olesen, H. (2001): A platform for model evaluation. 7th International Conference on Harmonisation within Atmospheric Dispersion Modelling for Regulatory Purposes, Belgirate, May 2001.
- Olesen, H. (2005). User's Guide to the Model Validation Kit. NERI. Rapport n°226.
- Pasquill, F. (1978). Dispersion from individual sources. Philadelphia, PA, ETATS-UNIS, American Society for Testing and Materials.
- Tombette, M., Quentric, E., Quélo, D., Benoit, J.-p., Mathieu, A., Korsakissok, I. and Didier, D. (2014): C3X : A software platform for assessing the consequences of an accidental release of radioactivity into the atmosphere. International Radiation Protection Association congress, Geneva.

**17th International Conference on  
Harmonisation within Atmospheric Dispersion Modelling for Regulatory Purposes  
9-12 May 2016, Budapest, Hungary**

---

**UDINEE PROJECT: INTERNATIONAL PLATFORM TO EVALUATE URBAN DISPERSION  
MODELS' CAPABILITIES TO SIMULATE RADIOLOGICAL DISPERSION DEVICE**

*Miguel A. Hernández-Ceballos<sup>1</sup>, Stefano Galmarini<sup>2</sup>, Steven Hanna<sup>3</sup>, Thomas Mazzola<sup>4</sup>, Joseph Chang<sup>5</sup>,  
Roberto Bianconi<sup>6</sup>, Roberto Bellasio<sup>6</sup>*

<sup>1</sup> European Commission, Joint Research Centre (JRC), Institute for Transuranium Elements (ITU), Ispra  
VA, Italy

<sup>2</sup> European Commission, Joint Research Centre (JRC), Institute for Environmental Sustainability (IES),  
Ispra VA, Italy

<sup>3</sup>Hanna Consultants, Kennebunkport, ME USA

<sup>4</sup>Engility, Lorton, VA, USA

<sup>5</sup>Homeland Security Studies and Analysis Institute, Falls Church, VA

<sup>6</sup>Enviroware srl

**Abstract:** Since the mid-1980s, the European Commission Joint Research Centre (EC-JRC) has carried out a series of studies to compare and evaluate atmospheric dispersion models (ADMs) for specific source scenarios. This kind of evaluation has contributed to assess the real capacity of these systems to respond to emergency under many aspects such as timeliness of the prediction and accuracy of the predictions. Considering the features of the urban environment, these would be likely to be major targets of a Radiological Dispersive Device (RDD) event, as high numbers of people and important infrastructural elements could be affected. In this environment, the meteorological and concentration fields can be very inhomogeneous in space and can vary rapidly with time, leading to challenges concerning accurate temporal and spatial simulation with current modelling capabilities. In this context, the EC-JRC with the support of the U.S. Defense Threat Reduction Agency (DTRA) launched, in December 2014, the “Urban Dispersion International Evaluation Exercise” (UDINEE) project, with the purpose to create a framework to evaluate the atmospheric dispersion models’ capabilities to simulate RDD events in an urban environment. Currently, 9 institutions from Europe, U.S. and Canada, are participating in the project, simulating the transport and dispersion of the set of puff releases carried out (by popping a balloon containing SF<sub>6</sub> tracer) during the Joint Urban 2003 (JU2003) field experiment in Oklahoma City. The detailed data collected during this campaign are available and, currently, are being used to evaluate the modelling results. The project is described in the present work.

**Key words:** *UDINEE, urban dispersion model, JU2003, ENSEMBLE.*

## **INTRODUCTION**

The potential use of a Radiological Dispersal Device (RDD), often called “dirty nuke” or “dirty bomb”, and which combines a conventional explosive device with radioactive material to scatter the latter over a targeted area, is considered one of the most likely malevolent acts (Medalia, 2011). The RDD is much less powerful than a nuclear bomb, and the extent of the affected area is also much less (from hundreds of meters to few kilometers). The RDD is not a nuclear explosion and it is unlikely to deliver radiation doses high enough to cause immediate fatalities to a large number of people. However, the RDD would have the capacity to contaminate facilities or places where people live and work for a very long time, and above all, to create panic and chaos in the population during the potential evacuation associated with the psychological fear over radioactivity.

These impacts would be maximized whenever the RDD event occurs in urban areas, as high numbers of people and important infrastructures could be affected. In the urban scenario, the transport and dispersion and the effects would depend on the meteorological conditions (e.g., wind speed and direction, stability, and turbulence intensity) and the configuration of the city (e.g., sizes of buildings and overall morphology, distribution of streets, total dimension of urban area). If models can simulate accurately the transport and dispersion of the radioactivity plume, then the models could be useful in helping to prevent

and minimize the potential impact of the RDD and would support decision making and other aspects of the management of the emergency.

The main challenge of modelling atmospheric transport and dispersion consists of understanding how materials are mixed by turbulence and are transported from the release point (Fernando et al., 2010). In the specific case of the dispersion in urban areas, a wide range of approaches to including urban characteristics and the subsequent simulation of air motions in and around the urban area have resulted in a wide range of models and consequently variability in outputs (see Britter and Hanna, 2003).

Because there are several types of Atmospheric Dispersion Models (ADM) that can be applied to RDDs, it is important that the scientific and quantitative differences be assessed, since they may lead to different conclusions and decisions. In this context, the “Urban Dispersion International Evaluation Exercise” (UDINEE) is the first multi-model urban dispersion model comparison for RDD releases. The project, led by the EC-Joint Research Centre (DG-JRC) with the support of the U.S. Defense Threat Reduction Agency (DTRA), was launched in December 2014, and 9 modelling groups from Europe, U.S. and Canada are participating in this first phase that will end in November 2016.

As part of the North American-European collaboration, standardized meteorological-tracer observations generated in the Joint Urban 2003 Oklahoma City (JU2003) campaign (Allwine et al., 2004) and model outputs have been made available. The observations and model outputs are on the ENSEMBLE system (<http://ensemble.jrc.ec.europa.eu/>) hosted at the JRC (Galmarini et al, 2004a,b; Galmarini et al., 2012). This web-based platform allows temporal and spatial analyses of individual models, as well as comparisons among models, and allows use of multiple models in an ensemble approach. This phase of the project is focused on the evaluation of model outputs against a large set of monitoring observations collected following instantaneous puff releases of SF<sub>6</sub> (by popping a balloon at a height of about 1.5 m) carried out during JU2003.

The use of this large and comprehensive database will allow the assessment of model performance and the identification of model deficiencies, which are key aspects needed to achieve the specific objectives of UDINEE:

- to assess the real capacity of these systems to respond to an emergency under many aspects such as, timeliness of the prediction, accuracy of the prediction, also in presence of limited inputs;
- to support the use of local models for decision making and policy development;
- to improve and develop common model formats for the rapid and coherent exchange of information across countries and produced by different modelling systems;
- to define under what circumstances (e.g., urban characteristics, meteorological conditions, horizontal and vertical resolution), given the current state of the science, it would be optimum in an emergency situation to use ADMs, and what other methods should be envisaged to complement missing aspects not yet covered by currently available modelling systems.

## **MATERIAL AND METHODS**

### **Joint Urban 2003 database**

The JU2003 urban field experiment (Allwine et al., 2004; Allwine and Flaherty, 2006), carried out from June 28 to July 31, 2003, is one of the most comprehensive field campaigns in an urban environment. It was designed with the goal of collecting meteorological and tracer data at several different scales, going from the scale of individual city blocks (<100 m and their street canyons and specific buildings), to the scale of the central business district (CBD) (<1000 m), up to scales of a few kilometres downwind of the CBD of Oklahoma City.

The selection of the JU2003 data set in UDINEE is based on the availability of a large amount of tracer and meteorology information recorded during ten Intensive Operational Periods (IOPs). The sampling duration of each IOP was 8-hours, during which there were three to six instantaneous puff SF<sub>6</sub> releases performed near street level within or just upwind of the built-up city centre. In UDINEE, measurements

from the surface monitoring network, consisting of nine real-time fast-response (0.5 sec) SF<sub>6</sub> samplers placed at downwind distances ranging from about 100 m to 1000 m, were used as reference.

Based on an analysis of the JU2003 puff observations by Zhou and Hanna (2007) a total of 167 concentration times series were suitable for analysis. In UDINEE, a set of puff data is used only if the quality control (QC) flag was 0 (meaning good data) or 5 (the analyser was in position and operating correctly and no SF<sub>6</sub> was found). Clawson et al. (2005) and Hanna et al. (2007) provide more detailed descriptions of JU2003.

### Ensemble system

ENSEMBLE is a web-based platform for the inter-comparison and evaluation of atmospheric chemistry transport and dispersion models. The real advantage of a system like ENSEMBLE is the possibility of easily performing the evaluation of several model predictions against measurements and against other model predictions. With the present capabilities of this system, it can be applied to a wide variety of scenarios and models. For example, it can be applied to domains that could range from small to global scale and with any grid resolution. It is also possible to work with unlimited time periods and resolutions of the observations and simulations. ENSEMBLE has been proven as a suitable system to host this multi-model urban dispersion model comparison. For more information on the ENSEMBLE system, we refer to Bianconi et al., 2004; Galmarini et al., 2004a,b; Galmarini et al., 2012.

### Participants

Table 1 summarises the models and their sponsors who are participating in the UDINEE project. UDINEE includes six modelling groups from Europe and three modelling groups from North America. The models have been applied retrospectively to simulate the transport and dispersion of the set of instantaneous puff trials carried out during JU2003. The models participating in the exercise are all well-documented in the scientific literature. Among all participants, only one group from EU applied the same model system (NAME) but with different settings (NAME and NAME URBAN).

**Table 1.** Modelling institutions and systems participated to UDINEE

Code	Institution	Model
SK1	ABmerit	ESTE CBRN
CA1	Meteorological Service of Canada	Canadian Urban Dispersion Modelling System
FR1	CEA	Parallel-Micro-SWIFT-SPRAY (PMSS)
IT1	CNR-ISAC	microRMS / MSS
UK1	Met Office	NAME
US1	NARAC	Aeolus
PL1	National centre for Nuclear Research	EULAG / QUIC
GR1	National Centre for Scientific Research "Demokritos"	ADREA-HF
US2	DTRA	HPAC-UDM
UK2	Met Office	NAME Urban

### Domain and grid specifications – Modelling outputs

The information on each release (including the location, starting time, duration and rate), meteorological (time series from one anemometer and 4-km MM5 outputs) and 3D building data (geographic information system (GIS) shapefiles) were provided to the modelling community via the UDINEE website.

The modellers are free to determine the way in which their model results of the dispersion of the tracer gas were be projected onto the spatial domain defined for UDINEE. For this exercise, we prescribed a horizontal resolution of 5 m (1.6 x 1.4 km) and 57 vertical levels (from 0 to 402 m). Each group produced the following results for the selected IOPs: 1) 0.5 sec instantaneous concentrations of SF<sub>6</sub> at each one of the nine sampling sites for each one of the nine IOPs, and 2) 1-minute averaged concentrations of SF<sub>6</sub> over the whole domain at all vertical levels.

### PRELIMINARY RESULTS

Quantitative and qualitative analyses are planned in the project. As an example, several parameters used to characterize the concentration time series have been calculated to compare and evaluate the model results. Parameters such as, the travel time (the difference between the time when the Cmax is reached and the release time), the peak concentration, the time duration of concentrations above 0.1\* Cmax, or the cloud speed were calculated and compared. For more information about these and other parameters, we refer to Doran et al., 2007 and Zhou and Hanna (2007).

As an example of the results that are being obtained, Figure 1 displays the scatter plot between observed and simulated results of two models for the travel time, and for all puffs in each IOP. The figure clearly shows the differences between models to follow the observations, and how the model results depend on the IOP and puff simulated and on the sampling site location.

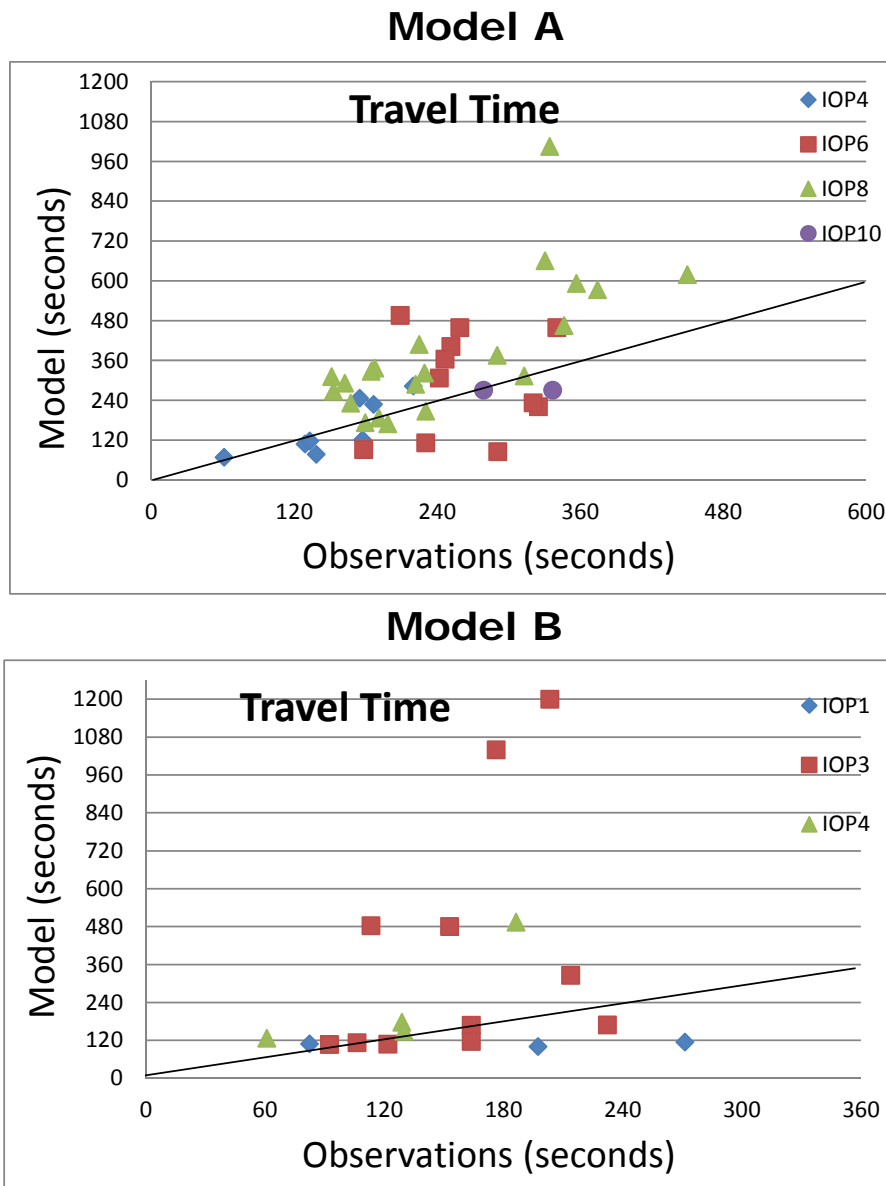


**Figure 1.** Scatter plot between observations and model results for travel time for several IOPs. The line represents the perfect agreement between observations and model results

## ACKNOWLEDGEMENT

We gratefully acknowledge the contribution of all of the participating groups to the UDINEE project.

## REFERENCES

- Allwine, K.J. et al., 2004: Overview of Joint Urban 2003-An atmospheric Dispersion Study in Oklahoma City. *Preprints, Symposium on Planning, Nowcasting and Forecasting in the Urban Zone*, American Meteorological Society available at. [www.ametsoc.org](http://www.ametsoc.org)
- Allwine, K.J. and Flaherty, J.E., 2006. Joint Urban 2003: Study Overview and Instrument Locations. Prepared for the U.S. Department of Homeland Security under a Related Services Agreement with the U.S. Department of Energy under contract DE-AC05-76RL01830.
- Bianconi, R., et al., 2004. Web-based system for decision support in case of emergency: ensemble modelling of long-range atmospheric dispersion of radionuclides. *Environ. Model. Soft*, **19**, 401-411.
- Britter ,R.E., Hanna, S.R., 2003: Flow and dispersion in urban areas. *Annu. Rev. Fluid. Mech*, **35**, 469–496.
- Clawson, K.L, Carter, R.G, Lacroix, D.J, Biltoft, C.A, Hukari, N.F, Johnson, R.C, Rich, J.D, 2005: Joint Urban 2003 (JU03) SF6 atmospheric tracer field tests. *NOAA Technical Memorandum OARARL-254, Air Resources Lab*
- Doran, J.C., et al., 2007: Characteristics of puff dispersion in an urban environment. *Atmos. Environ*, **41**, 3340-3452.
- Fernando, H.J.S, 2010: Fluid dynamics of urban atmospheres in complex terrain. *Annu. Rev. Fluid Mech.*, **42**, 365–389.
- Galmarini, S., et al., 2004. Ensemble dispersion forecasting—Part I: concept, approach and indicators. *Atmos. Environ*, **38**, 4607–4617.
- Galmarini, S., et al., 2004. Ensemble dispersion forecasting—Part II: Application and evaluation. *Atmos. Environ* **38**, 4619–4632.
- Galmarini, S., et al., 2012. ENSEMBLE and AMET: Two systems and approaches to a harmonized, simplified and efficient facility for air quality models development and evaluation. *Atmos. Environ*, **53**, 51-59.
- Hanna, S.R, White, J, Zhou, Y., 2007: Observed winds, turbulence, and dispersion in built-up downtown areas in Oklahoma city and Manhattan. *Boundary-Layer Meteorol*, **125**, 441–468
- Medalia, J, 2011: "Dirty Bombs": Background in Brief. *Congressional Research Service*, 7-5700. [www.crs.gov](http://www.crs.gov). R41891.
- Zhou, Y., Hanna, S.R., 2007. Along-wind dispersion of puffs released in a built-up urban area. *Boundary Layer Meteorol*, **125**, 469-486.

**17th International Conference on  
Harmonisation within Atmospheric Dispersion Modelling for Regulatory Purposes  
9-12 May 2016, Budapest, Hungary**

---

**ASSESSING THE PERFORMANCE OF ATMOSPHERIC DISPERSION MODELS**

*Steven Herring<sup>1</sup> and Pablo Huq<sup>2</sup>*

<sup>1</sup>CBR Advice Group, Defence Science and Technology Laboratory, Porton Down, Salisbury, England

<sup>2</sup>College of Earth, Ocean and Environment, University of Delaware, USA

**Abstract:** There are a large number of models and tools available for predicting the dispersion of material released into the atmosphere. These take many forms, ranging from simple models that execute in a fraction of a second to complex models requiring weeks of computational time. The primary purpose of many of these models is to predict the hazard resulting from releases of hazardous materials, and so it is critical to understand the level of predictive accuracy that might be expected from them. However, this is not easily determined from comparisons with experimental measurements for a number of reasons which include: the limited number of releases typically made, limited range of meteorological conditions, limited range of test environments and the arrangement and number of sensors used. In addition, the results of a comparison may be significantly influenced by practical decisions relating to what data to include and exclude, and the approach adopted to temporal and spatial averaging of the data. Given these factors, it is difficult to understand how the performance of one model relates to another.

The paper presents the issues involved in comparing model predictive performance to experimental data by reference to a number of comparison exercises against experimental data sets. It then presents an approach which is designed to make the performance of atmospheric dispersion models (of whatever type) more transparent. This involves clearly defining the basis on which the comparison is made, the use of the widely accepted BOOT software for generating quantitative measures and comparing the performance of the chosen model to the performance of a simple analytic model for the same experimental data. A simple analytical model is adopted as it is easily understood, and provides a clear baseline performance against which the performance benefits of more sophisticated models may be easily assessed.

**Key words:** *dispersion modelling, validation*

## **INTRODUCTION**

A wide range of models have been developed for predicting the transport and dispersion of material released into the atmosphere. These range from simple analytic or empirical Gaussian plume models defined by a single equation, to models based on complex Computational Fluid Dynamics (CFD) simulations. Whereas the former will execute in a fraction of a second on standard desktop computer, the latter may require weeks of computational time on a High Performance Computing (HPC) facility. Independent of the method that is used to predict the dispersion, there is a need for the end user to be able to readily assess how good any particular model is, and what its limitations are. Thus there is considerable interest in methodologies for comparing the performance of different dispersion models (Warner et al., 2001), and also the development of automated tools to facilitate such comparisons (Andronopoulos et al., 2015).

It is very difficult to describe the performance of a dispersion model in terms of a single metric. Although most studies utilise a number of generally recognised statistical parameters, researchers and organisations have developed their own favoured metrics on which they place particular emphasis. For example, some researchers favour the 2-D Measure of Effectiveness (2-D MOE) and Normalised Absolute Difference (NAD) parameters (Warner et al., 2001), while others look at the Cumulative Factor (Tull and Suden, 2014). However, when authors wish to compare their results to those of others they will generally relate them to the bounds for an acceptable model suggested by Hanna and Chang (2012). While these criteria may provide a reasonable basis for evaluating the performance of a dispersion model, examination of the process reveals that the values of the metrics are highly dependent on the way in which the comparison is

made. This being so, it may be difficult for a third party to fully appreciate the performance of a model without access to full details of the comparison process. The purpose of this paper is to propose a way by which the performance of models may be made more transparent.

### **ISSUES IN VALIDATING DISPERSION MODELS**

The acquisition of sufficient dispersion data from field trials to validate models involves the deployment of a large amount of instrumentation and a large number of releases. This is complex and costly even for open terrain experiments, and the complexity and costs increase substantially for urban experiments. It is important to appreciate that even the biggest datasets consist of only a limited number of releases at a limited range of conditions. A consequence of this is that they invariably represent statistically small samples which limit the degree of confidence that can be obtained from comparing model predictions against a single data set.

Although field trials may involve releases made at a range of different times during the day and at night, they are generally conducted over a few days or weeks. This inevitably limits the range of meteorological conditions covered by the dataset. The environment is obviously fixed by the location of the trial, while the amount of data obtained is governed by the numbers of sensors that are available, their spatial distribution and sampling periods. To illustrate the difficulties we note that even though a large number of samplers (600 in all) were used in the Prairie Grass open terrain experiment (Haugen and Barad, 1958), the number that recorded data was limited to a fraction of these. The complexity of the urban wind field suggests that an even larger number of samplers are required to obtain good coverage, however, this is prohibitively expensive, and only 130 samplers were deployed in the Joint Urban 2003 experiment (Allwine and Flaherty, 2006). In addition, although the dispersion of a plume is three dimensional, most sampling is restricted to a horizontal plane close to the ground, with only small numbers of measurements in the vertical dimension. This means that even in large experiments, such as those referred to above, the data is likely to be sparse, and of low fidelity.

The accuracy of any dispersion prediction is fundamentally linked to the accuracy of the meteorological data that is input to the model. The need for accurate meteorological data is typically addressed in research experiments by deploying a range of instrumentation at a number of locations, and at a range of heights. Nevertheless, it not obvious how this data should be consolidated to derive the most appropriate wind field information for input into a dispersion model. In addition to the meteorological uncertainties above, there are also typically smaller uncertainties relating to the definition of the source and release conditions which may introduce systematic errors that are important in assessing accuracy in the near-field

Some of the limitations associated with conducting field trials can be overcome by the use of wind and water tunnel experiments, which provide well-defined, constant, meteorological conditions that support repeatable measurements. In addition, the constant conditions and reduction in scale permit the acquisition of large statistical samples (Harms et al., 2011). However, the walls of the tunnel physically limit the maximum dimensions of the turbulence scales, and although Reynolds number independent flows can be achieved, there is a limit to the detail that can be represented (e.g. roof top geometries are generally simplified and trees omitted). It is also difficult to vary stability conditions, and most data from wind and water tunnel experiments are restricted to neutral buoyancy conditions, although stability effects are of great importance.

### **APPROACHES TO MODEL VALIDATION**

A wide range of statistical metrics have been used by researchers in conducting dispersion model validation exercises. These include the Normalised Mean Square Error (NMSE), geometric mean, coefficient of correlation and percentage of observations and predictions within factors of two or ten (FAC2 and FAC10). Many are incorporated in the widely used BOOT statistical package (Chang and Hanna, 2005), but other measures and tools exist. In addition to the choice of metrics, the results of a validation exercise depends upon decisions made by the analyst regarding the basis on which the comparison is made. Consider the design of field studies involving arc maximum concentration values. This depends on the samplers being deployed on arcs, but even if there are a large number of samplers,

such an approach is problematic. This is because the plume is only likely to cover a small number of samplers on a given arc and not provide a well-defined distribution (particularly in urban areas) which makes evaluation of the arc maximum difficult.

Once the performance metrics have been chosen, the resulting values are highly dependent on the criterion used for determining the data that should be included in the comparison. After defining the threshold at which a sampler reading is taken to be zero, there are then three options for filtering the observed and predicted data pairs (Boubert and Herring, 2015): 1) accept all, 2) accept if both above threshold 3) accept if one above threshold. It is important to note that the application of strategy (3) to a spatially and temporally correlated comparison will likely lead to significantly poorer performance metrics than if strategies (1) or (2) are adopted. In addition, the performance metrics can generally be improved by adopting longer averaging times if a series of samples are taken at each location.

### **MAKING MODEL PERFORMANCE TRANSPARENT**

The combination of factors described in the preceding sections, mean that if the results of a model comparison are presented in isolation without a detailed description of the analysis process, then it is difficult for a third party to evaluate how good the model is. It may perform well for a particular data set, or may appear to perform well because of the particular validation strategy adopted. In order to address the problem of making the results of model comparisons more transparent, we propose that as well as presenting the results for the chosen model further effort should also be made to include a comparison with a standard reference model whose details are freely available. The utility and acceptance of such a standard model is greatly increased if it is based on well-founded understanding and physical principles, and can account for a range of conditions.

### **A REFERENCE MODEL**

One possible candidate for a standard reference model for continuous ground level releases is the analytical model developed by Franzese and Huq (2011) which has been validated against data from urban experiments conducted in Oklahoma City, Salt Lake City, London, and St. Louis.

The model is based on a standard Gaussian formulation, in which the mean concentration  $c$  is predicted by equation (1), in which  $y$  indicates the crosswind direction,  $z$  the vertical direction,  $\sigma_y$  and  $\sigma_z$  are the standard deviations of the crosswind and vertical distributions of concentration, respectively and  $U$  is the reference wind speed and  $Q$  the mass release rate.

$$c = \frac{Q}{\pi U \sigma_y \sigma_z} \exp\left(-\frac{y^2}{2\sigma_y^2} - \frac{z^2}{2\sigma_z^2}\right) \quad (1)$$

In contrast to other simple urban dispersion models which are based solely on implementing empirical relationships derived from particular experiments, this model is based on fundamental dispersion theory. This means that the horizontal and vertical diffusion coefficients are determined according to the theories of Taylor (1921) and Hunt and Weber (1979) respectively as discussed in Franzese and Huq (2011).

The validation conducted by Franzese and Huq (2011) showed that model predicted the existence of near and far field urban dispersion regimes, and suggested that urban dispersion was governed by the characteristic length scales of atmospheric boundary layer turbulence, rather than urban canopy length scales which were more likely to affect dispersion only in the vicinity of the source. The model predictions demonstrated a convincing collapse of data for both daytime and nighttime conditions as shown in Figure 1.

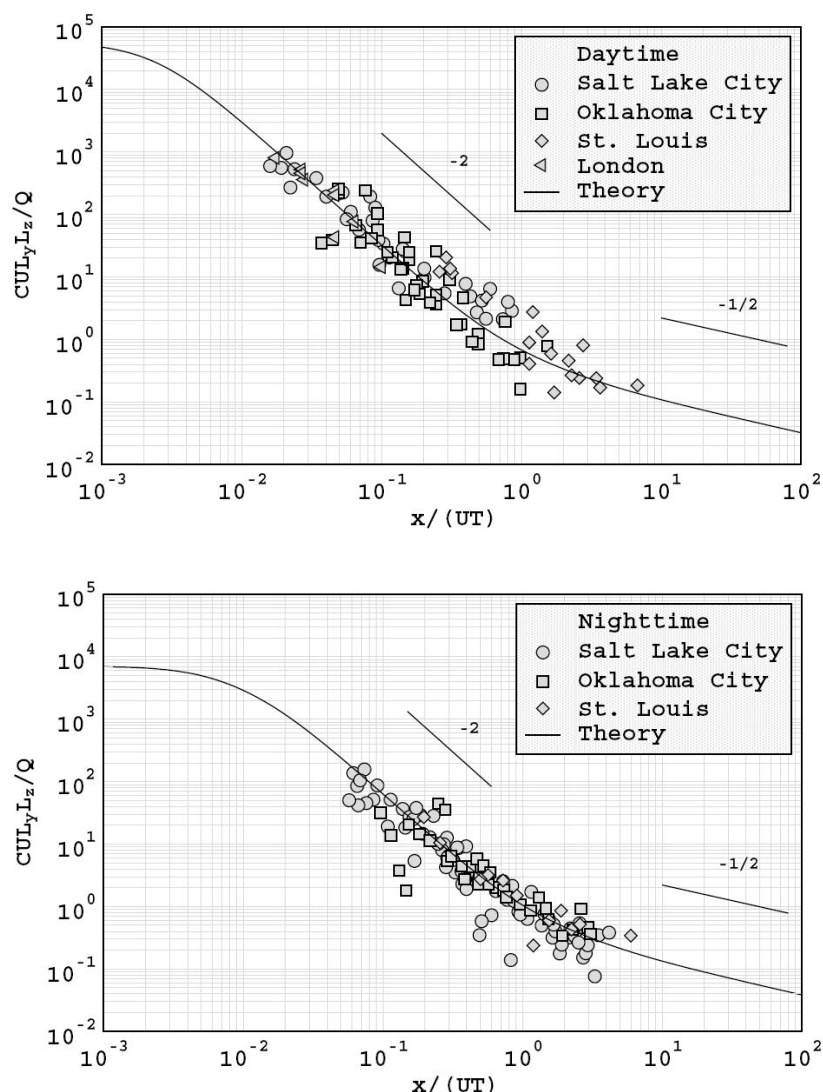


**Figure 1.** Comparisons between observed daytime and nighttime data and analytical model predictions.

The results therefore suggest that the model may be used to obtain realistic predictions of atmospheric dispersion in urban areas in both daytime and nighttime conditions, but has the advantage of being simple in formulation and applicable to a wide range of conditions. The authors therefore propose to undertake work to demonstrate how this model may be used as a reference model for quantifying the performance benefits of more sophisticated methods.

## CONCLUSIONS

An examination of the literature shows that there is a lack of consistency in the approaches adopted to validating dispersion models in terms of the metrics used to assess performance. In addition, the wide variety of experimental arrangements and relatively limited data typically available, coupled with the large effect of subjective decisions on the inclusion or exclusion of data, mean that it is often difficult to establish the true performance of a model. One way of alleviating this is to always include a comparison against a reference model. It is suggested that the simple analytic plume model for ground-based releases developed by Franzese and Huq (2011) provides a suitable starting point for such an approach which the authors intend to develop.

## REFERENCES

- Allwine, K.J. and J.E. Flaherty 2006: Joint Urban 2003: Study Overview and Instrument Locations, Technical Report PNNL-15967, Pacific Northwest National Laboratory.
- Andronopoulos, S. and F. Barmpas, J.G. Bartzis, K. Baumann-Stanzer, E. Berbekar, G. Efthimiou, C. Gariazzo, F. Harms, A. Hellsten, S. Herring, K. Jurcakova, B. Leidl, S. Trini-Castelli 2015: COST ES1006 Model Evaluation Protocol. ISBN 987-3-9817334-1-9.
- Boubert, B. and S. Herring 2015: Validation of UDM Against Data from the MUST Experiment, Dstl/84143.
- Chang, J.C. and Hanna, S.R. 2005: Technical Descriptions and User's Guide for the BOOT Statistical Model Evaluation Software Package, Version 2.0, Technical report.
- Franzese, P. and P. Huq, 2011: Urban dispersion modeling and experiments in daytime and nighttime atmosphere. *Boundary Layer Meteorology*, **139**, 395-409.
- Hanna, S.R. and J. Chang (2012): Acceptance criteria for urban dispersion model evaluation, *Meteorology and Atmospheric Physics*, 116 (3-4), 133-146.
- Harms, F. and Leidl, B., Schatzman, M., Patnaik, G. 2011: Validating LES-based flow and dispersion models, *Journal of Wind Engineering and Industrial Aerodynamics*, pp 289-295.
- Haugen, D. and M.L. Barad, 1958: Project Prairie Grass, a field program in diffusion, Volume 1. Air Force Cambridge Research Center.
- Haugen, D. and M.L. Barad, 1958: Project Prairie Grass, a field program in diffusion, Volume 2. Air Force Cambridge Research Center.
- Hunt J.C.R. and Weber A.H. 1979: A Lagrangian statistical analysis of diffusion from a ground-level source in a turbulent boundary layer. *Quart J Roy Meteor Soc* 105(444):423-443.
- Taylor, G.I. 1921: Diffusion by continuous movements. *Proc Lond Math Soc* 20:196-211.
- Tull, B. and P. Suden 2014: Urban Dispersion Model Evaluation of the QUIC and HPAC Models Using the DAPPLE Dataset. 16th International Conference on Harmonisation within Atmospheric Dispersion Modelling for Regulatory Purposes 8-11 September 2014, Varna, Bulgaria.
- Storwold, D.P., 2007: Detailed Test Plan for the Fusing Sensor Information from Observing Networks (FUSION) Field Trial 2007 (FFT 07), Meteorology Division, West Desert Test Center, U.S. Army Dugway Proving Ground.
- Warner, S., and N. Platt, J. F. Heagy, S. Bradley, G. Bieberbach G. Sugiyama, J. S. Nasstrom, K.T. Foster, D. Larson User-Oriented Measures of Effectiveness for the Evaluation of Transport and Dispersion Models, Institute for Defense Analyses Alexandria, Virginia Paper P-3554, Jan 2001.

Content includes material subject to © Crown copyright (2016), Dstl. This material is licensed under the terms of the Open Government Licence except where otherwise stated. To view this licence, visit <http://www.nationalarchives.gov.uk/doc/open-government-licence/version/3> or write to the Information Policy Team, The National Archives, Kew, London TW9 4DU, or email: [psi@nationalarchives.gsi.gov.uk](mailto:psi@nationalarchives.gsi.gov.uk).

**17th International Conference on  
Harmonisation within Atmospheric Dispersion Modelling for Regulatory Purposes  
9-12 May 2016, Budapest, Hungary**

---

**WIND PROFILES FOR THE ATMOSPHERIC BOUNDARY LAYER IN DIFFERENT  
STABILITY CONDITIONS**

*Ana Graciela Ulke*

Universidad de Buenos Aires, Facultad de Ciencias Exactas y Naturales, Departamento de Ciencias de la  
Atmósfera y los Océanos; UMI-IFAECI-CNRS-3351, Buenos Aires, Argentina

**Abstract:** A formulation for the wind speed profile in the atmospheric boundary layer in neutral and diabatic conditions is evaluated. The proposed vertical variations depend on the turbulent state of the atmospheric boundary layer described in terms of the friction velocity and the stability conditions. The availability of tower data as well as published results from tall masts allowed the evaluation of the performance of the proposed formulation for a variety of conditions. The wind speed profiles compare adequately with the observational data.

**Key words:** *Boundary-layer wind profile, atmospheric stability, wind speed measurements, atmospheric turbulence*

#### **INTRODUCTION**

Currently, there is an increasing need for expressions for the wind speed variation in the atmospheric boundary layer, for a variety of applied research as well as modelling studies. In addition to pollution dispersion modelling and scalar transport, analysis of wind power generation or loading on buildings and bridges might be mentioned.

In this contribution, a wind speed formulation based on the observed turbulence structure and behaviour in the boundary layer under steady and horizontally homogeneous conditions is evaluated. The functional forms were developed as part of a modelling approach for the dispersion of pollutants released in the atmospheric boundary layer and was evaluated against data from different diffusion experiments (Ulke, 2000).

Gryning et al. (2007) analyzed measurements from tall masts at Høvsøre (Denmark) and at Hamburg (Germany) and evaluated the performance of an extension of the wind profiles beyond the atmospheric surface layer with satisfactory results and much better agreement with the data than the predictions of the Monin-Obukhov similarity profiles.

#### **DATA AND METHODOLOGY**

The detailed information about the measurements and analysis procedures can be found in Gryning et al. (2007). One measurement site is the testing station for wind turbines at Høvsøre (Denmark), and the second one is located near Hamburg (Germany). Høvsøre measurements (rural area) were made on a 116m meteorological mast and at 160m at a nearby light-mast. The Hamburg measurements were obtained at 50, 110, 175 and 250m height on a TV tower and at 12m height on a small mast nearby and are representative of residential and urban areas of the city.

Table 1 presents the information that is needed for the wind profile calculations, which was obtained from Gryning et al. (2007) and is organized for each of the stability classes they defined:  $10 < L < 50$  (very stable);  $50 < L < 200$  (Stable);  $200 < L < 500$  (near neutral/stable);  $L > 500$  or  $L < -500$  (neutral);  $-500 < L < -200$  (near neutral/unstable);  $-200 < L < -100$  (unstable) and  $-100 < L < -50$  (very unstable). The classes were assigned a number as included in Table 1 in order to facilitate the interpretation of the Figures.

**Table 1.** Parameters used in the wind profile calculations

Stability class	Range of L (m)	Mean L (m)	$z_0$ (m)	$U_{*0}$ (m/s)	h (m)
<i>Høvsøre</i>					
1	-100 to -50	-71	0.018	0.340	500
2	-200 to -100	-142	0.013	0.367	500
3	-500 to -200	-275	0.012	0.405	500
n	L>500; L<-500	neutral	0.014	0.388	320
4	200 to 500	323	0.013	0.358	280
5	50 to 200	108	0.008	0.249	200
6	10 to 50	24	0.0013	0.152	200
<i>Hamburg - urban</i>					
2	-200 to -100	-148	0.45	0.553	570
3	-500 to -200	-322	0.55	0.659	600
n	L>500; L<-500	neutral	0.65	0.671	800
4	200 to 50	349	0.43	0.436	1000

Although the derivation and evaluation of the wind profiles are fully described in Ulke (2000), a brief explanation along with the expressions is included. The profiles of wind speed are functions of the relative height ( $z/h$ , where  $h$  is the atmospheric boundary layer height), the friction velocity ( $u_*$ ) and the stability parameter ( $h/L$ , where  $L$  is the Obukhov length).

The expressions are the following:

For stable conditions ( $h/L > 0$ ):

$$\bar{u}(z) = \frac{u_{*0}}{k} \left\{ \ln \frac{z}{z_0} - \left[ 1 - 6.9 \frac{h}{L} \right] \left[ \frac{z-z_0}{h} \right] - \frac{6.9}{2} \frac{h}{L} \left[ \frac{z^2}{h^2} - \frac{z_0^2}{h^2} \right] \right\} \quad (1)$$

For unstable conditions ( $h/L < 0$ ):

$$\bar{u}(z) = \frac{u_{*0}}{k} \left\{ \ln \frac{z}{z_0} + \ln \left[ \frac{(1+\mu_0^2)(1+\mu_0)^2}{(1+\mu^2)(1+\mu)^2} \right] + 2 \left[ \tan^{-1} \mu - \tan^{-1} \mu_0 \right] + \frac{2L}{33h} \left[ \mu^3 - \mu_0^3 \right] \right\} \quad (2)$$

with

$$\mu = \left( 1 - 22 \frac{h}{L} \frac{z}{h} \right)^{1/4} \quad \text{and} \quad \mu_0 = \left( 1 - 22 \frac{h}{L} \frac{z_0}{h} \right)^{1/4}$$

where  $u_{*0}$  is the surface friction velocity,  $z_0$  is the surface roughness length,  $k$  is the von Karman's constant and the coefficients of the atmospheric stability factors are from Wieringa (1980).

The profiles include shear and buoyancy-induced turbulence and conform a continuous description for the entire atmospheric boundary layer, from stable to unstable conditions. Near the surface, they tend to the classic surface layer Monin-Obukhov similarity functions expressions. In addition, for small  $h/L$ , tend to the functional form valid on neutral conditions. It is important to remark that, as the model parameterizations are based on the gradient transfer theory, its applicability gives adequate estimates for atmospheric stability ranging from stable to slightly unstable. During strong unstable conditions the model presented poorer performance in previous evaluations when the stability parameter was near the lower theoretical limit for free-convection conditions.

## RESULTS AND DISCUSSION

Figure 1 illustrates the comparison between the measurements and the calculated wind speeds for both measurement sites.

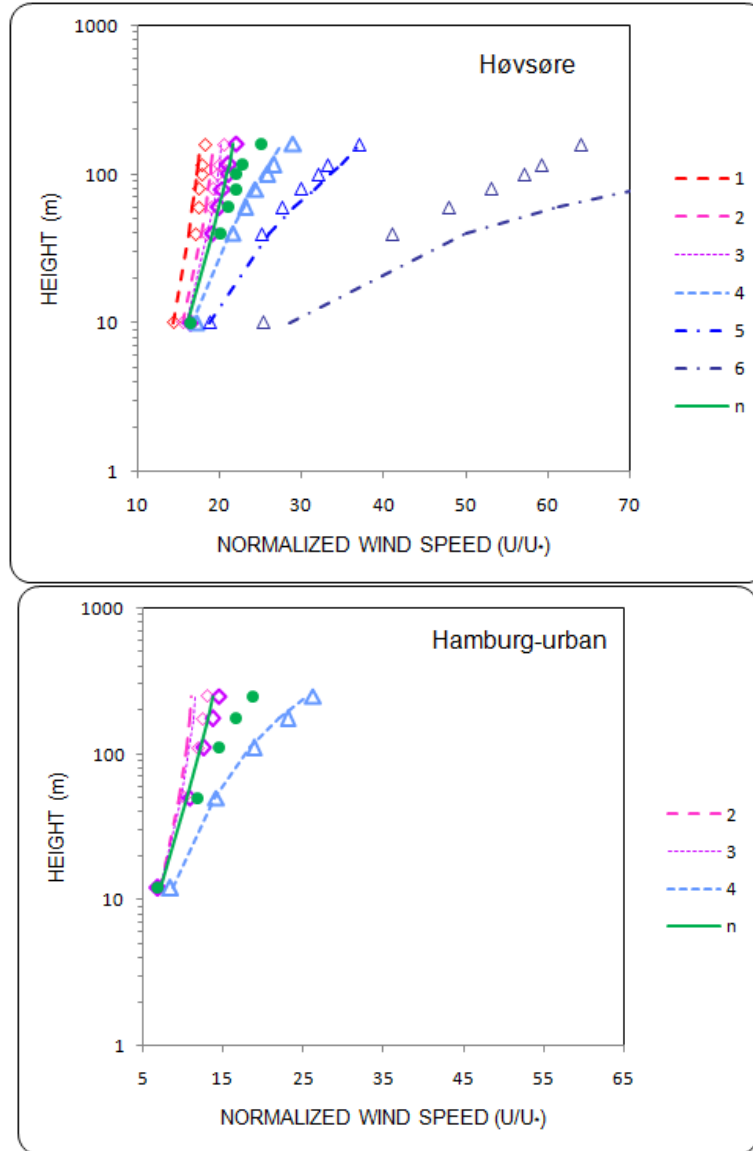


**Figure 1.** Comparison of normalized wind profiles (lines) with measurements (symbols) as a function of stability for Høvsøre (upper panel) and Hamburg (bottom panel)

In general, the measurements are slightly underpredicted with the applied wind profile formulation under most of the stability conditions at both sites. During strong stable conditions at the rural site, the opposite behaviour is observed.

The dispersion plots (Figure 2) depict the comparison of the estimated normalized wind speeds with the measured wind speeds and a very satisfactory agreement is observed. The slight underestimation appears more evident at the urban location. The departure from the best fit on neutral conditions might be related to the assumption of null buoyancy flux in the whole atmospheric boundary layer instead of the actual stability condition.

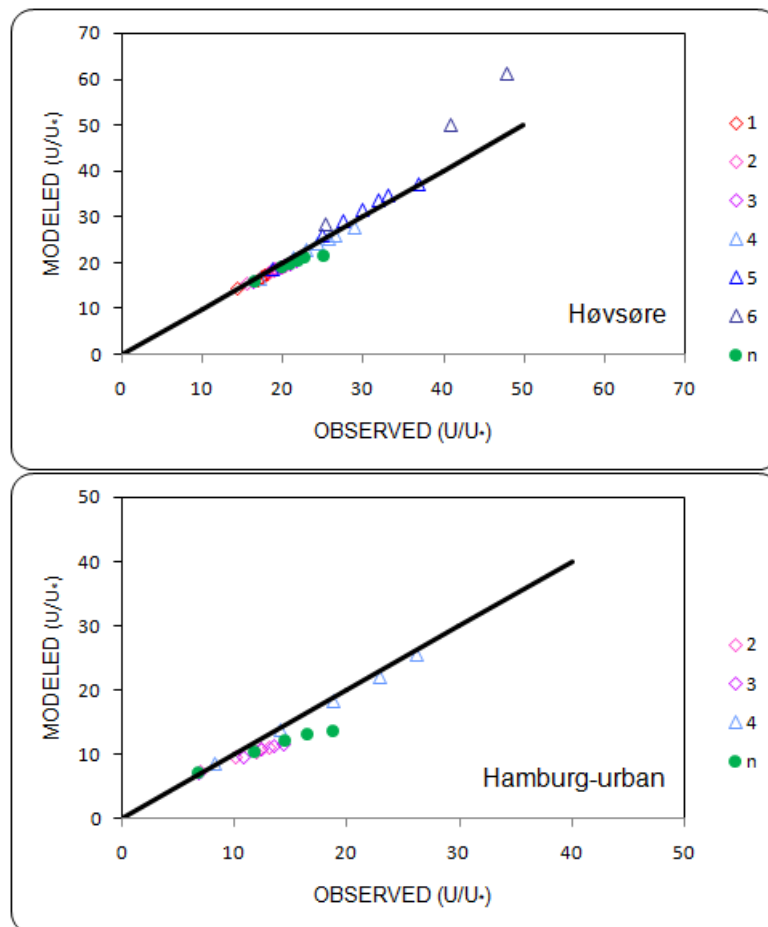


**Figure 2.** Comparison of modeled normalized wind profiles with measurements as a function of stability (symbols) for Høvsøre (upper panel) and Hamburg (bottom panel). The line indicates the best fit.

Under the constraints of the considered measurements and related assumptions, the parameterizations presented here can be considered as an alternative to the power law profile or the frequent extension of the Monin-Obukhov logarithmic profile beyond the surface layer.

#### Acknowledgments

The financial support of the projects UBACyT 20020130100771 by the University of Buenos Aires, Argentina and AO-LEFE-CHAT 875064 from CNRS, France is acknowledged.

#### REFERENCES

- Gryning, S-E., E. Batchvarova, B. Brümmer, H. Jørgensen and S. Larsen, 2007: On the extension of the wind profile over homogeneous terrain beyond the surface boundary layer. *Boundary-Layer Meteorol.*, **124**, 251-268.
- Ulke, A. G., 2000: New turbulent parameterization for a dispersion model in the atmospheric boundary layer. *Atmospheric Environment*, **34**, 1029-1042.
- Wieringa, J., 1980: A reevaluation of the Kansas mast influence on measurements of stress and cup-anemometer overspeeding. *Boundary-Layer Meteorol.*, **18**, 411-430.

**17th International Conference on  
Harmonisation within Atmospheric Dispersion Modelling for Regulatory Purposes  
9-12 May 2016, Budapest, Hungary**

---

**CMAQ (COMMUNITY MULTI-SCALE AIR QUALITY) ATMOSPHERIC DISPERSION  
MODEL ADAPTATION FOR HUNGARY**

*Dora Lazar and Tamas Weidinger*

Department of Meteorology, Institute of Geography and Earth Sciences, Eötvös Loránd University,  
Budapest, Hungary

**Abstract:** Up to our days it has become more important to measure and predict the concentration of atmospheric pollutants – harmful contaminants such as dust, aerosol particles of different sizes, nitrogen compounds, and ozone. The Weather Research and Forecasting (WRF) model has been applied at the Department of Meteorology at Eötvös Loránd University for several years now. This model is suitable for weather forecasting purpose and may also provide input data for various environmental simulation softwares (e.g. DNDC, AERMOD). By adapting the CMAQ (Community Multi-scale Air Quality) model we have implemented a coupled air-quality – meteorological environmental model system, primarily for the representation of atmospheric ozone. The modular structure of the CMAQ allows successful and fast simulations with different scales from global to local. In our present investigation it is important to apply different scale emission databases and describe the initial distribution of pollutants using a background model. We are going to adapt CMAQ model to Hungary. The meteorological parameters are the primary physical forces in the atmosphere. We used WRF model in order to generate the meteorological driver database and the so-called SMOKE model for the generation of the input emission database. WRF/CMAQ model system has been run on a three-level one-way nested grid of 108/36/12 km grid spacing, covering Central Europe, the Carpathian Basin and Hungary, respectively. We used the CMAQ 5.0.1 version which includes i) an updated version of the carbon bond “CB05” gas-phase mechanism (with active chlorine chemistry and updated toluene mechanism), ii) sixth-generation aerosol mechanism (with sea salt and specialized PM among others), iii) Cloud module, etc. For better quality simulations we used the Geos-Chem model results as initial and boundary conditions. We studied ozone forecasts for Hungary based on different model settings and transition time using several verification methods. This paper presents the outline of the project work and the first results of concentration calculations compared to the national ambient air stations data.

**Key words:** *air-quality modelling, ozone, CMAQ, SMOKE, WRF, emission, model adaptation*

## **INTRODUCTION**

In discussions about the forecast of ozone concentrations e.g. during summer smog episodes, relative importance of horizontal advection, vertical mixing, and chemical production is still an unsolved problem. The solution of this problem probably lies in sensitivity studies with complex numerical models including both meteorology and chemistry (Neu et al., 1994). The forecasts of ozone concentration are important by reason of the harmful effects of ozone (O<sub>3</sub>) on both human health and the environment (McDonnell et al., 2002; Colette et al., 2012). Breathing ozone may trigger several health problems including chest pain, coughing, throat irritation, and congestion (Gryparis, 2004; Amann et al., 2011). It may worsen bronchitis, emphysema, and asthma (McDonnell et al., 2002; Holicska, 2008). Ground-level ozone also may reduce lung function and inflame the linings of the lungs. Repeated exposure may permanently scar lung tissue. In the US the human exposure to high concentration of ground level ozone continues to bother many areas in spite of the implementation of government-mandated emissions control strategies (Finlayson et al., 2000). This is because the control of ground level ozone is more difficult than for many other primary pollutants because ozone is a secondary pollutant. In case of other primary pollutants, a reduction in emissions results approximately proportional reduction of pollutants. However, as a secondary pollutant that is formed from primary pollutants and other chemical species in the atmosphere, ozone does not necessarily respond in a proportional manner to reductions in precursor emissions. Air quality modelling provides a good alternative to study the physical and chemical mechanism of ozone formation because modelling can provide good temporal and spatial resolution for a

wide variety of pollutants (Bozó, 2005; Leelóssy et al., 2014). For instance, regional air quality models such as the US EPA's Community Multiscale Air Quality model (CMAQ/Models-3) can be used to generate hourly ambient concentration fields for ozone, PM<sub>10</sub>, PM<sub>2.5</sub>, and many other pollutants, which allows researchers to study the relationship between pollution and health outcomes for times, locations, and pollutants for which monitoring data are not available (Lu et al., 2008; Pay et al., 2010).

In this work, an air quality modelling system was applied to PhD thesis to adaptation and study ozone concentration and relationship between other chemical substances (eg. NO<sub>x</sub>, VOCs, HAPs) for Hungary. Some studies have been conducted to investigate ozone and other pollutant emission concentration with different areas, model domain and chemical mechanism. In USA the model system has been configured and studied up-to-date, e.g. Wong et al. (2012) studied WRF – CMAQ model with two-way coupled system with some pollutant (ozone, PM<sub>10</sub>, PM<sub>2.5</sub>). They concluded that ozone has absorption bands in the long wave radiation bands and can thus absorb outgoing radiation. Efforts are underway to implement ozone feedback in the coupled WRF-CMAQ system and study the impact of ozone on long wave radiation using the RRTMG long wave radiation scheme. Boulton et al. (2012) studied the 2012 year emissions in Toronto. This was a multi-year project, which has been concluded with assessing behaviour of the model for ozone and PM<sub>2.5</sub>. In Europe WRF-CMAQ model system has been applied for research goals in many institutes e.g. in Scotland (Pederzoli, 2008) and in Bulgaria with cb04 mechanism and on 14 vertical levels (Syrakov et al., 2015).

In this article we represent the model attributes and the selected case of our studies, then we examine the first model forecast results and conclude the attribute of the model. The main goal is we understand the model attitude in the area of the Europe and Carpathian Basin.

#### **CASE SELECTED AND MODEL CONFIGURATION**

In this chapter the model inputs, the weather situation for the case simulation, selected chemical mechanisms and design of numerical simulations will be presented.

We used 3 different model input for the applied model system, i) the meteorology input has been utilised by WRF model outputs and MCIP (Meteorology-Chemistry Interface Processor) to create netCDF-formatted input meteorology files that are used by the emissions model (SMOKE) that computes emissions inputs to CMAQ. ii) For the emission database we applied EMEP (European Monitoring and Evaluation Programme) ASCII files and recalculate with SMOKE for the CMAQ emissions, iii) for construction of initial and boundary conditions we run GEOS (Goddard Earth Observing System) – Chem model system and used PseudoNetCDF python script. The model system settings was Single-moment 3-class in WRF model, Nei2005 (National Emissions Inventory) CB05 with SOA (secondary organic aerosol) in SMOKE model, tropospheric chemistry mechanisms (aka "Full-chemistry") with 47 levels in GEOS-Chem model system. In SMOKE model we used this chemical mechanism, for the reason that we could use and compare 2 different chemical mechanism in CMAQ model, as Carbon Bond version 5 chemical mechanism (cb05tucl\_ae6\_aq, TUCL (toluene and chlorine mechanism)) and explicit air toxics chemistry (cb05tump\_ae6\_aq, TUMP (Multi-pollutant mechanism)).

The CB05 mechanism includes updates in toluene chemistry, in homogeneous hydrolysis rate constants for dinitrogen pentoxide (N<sub>2</sub>O<sub>5</sub>), and in chlorine chemistry. Whitten et al. (2010) developed new condensed toluene chemistry for the CB05 mechanism. The International Union of Pure and Applied Chemistry (IUPAC) now suggest using only the bimolecular homogeneous hydrolysis of N<sub>2</sub>O<sub>5</sub> and also recommend a lower rate constant for the reaction. The existing chlorine chemistry contains 21 reactions involving chlorine. The cb05tump\_ae6\_aq mechanism predicts criteria air pollutants and several hazardous (toxic) air pollutants based on the 5.1 version of the cb05tucl\_ae6\_aq mechanism. The cb05tump\_ae6\_aq mechanism modifies the cb05tucl\_ae6\_aq mechanism (Sarwar et al., 2008; Whitten et al., 2010) to predict several Hazardous Air Pollutants (HAPs). It accomplishes the goal by adding mercury compounds, acrolein, 1,3-butadiene and reactive tracers to the cb05tucl\_ae6\_aq mechanism. The first three HAPs require adding complex chemical kinetics to the original photochemical mechanism. The reactions involving mercury do not alter predictions from the cb05tucl\_ae6\_aq mechanism because elemental mercury is treated as a reactive tracer with inert daughter products.

In our case study we selected an anticyclone weather situation in Europe at 3th decade of September 2012. The weather of the Carpathian Basin had been developed by the above-mentioned anticyclone, which was placed to the east on Saturday (22<sup>th</sup> September 2012), and faintly more humid air had been flown over Hungary. In the verification study we used several measurements from air-quality monitoring stations in 4 different countries (Austria, Hungary, Romania, and Slovakia). We selected Győr (47°40'40.8"N 17°39'26.6"E), Budapest (47°28'33.0"N 19°02'24.8"E) and K-pusztá (46°58'00.0"N 19°35'00.0"E) in Hungary, Ilmitz (47°46'00.0"N 16°46'00.0"E) and Masenberg (47°20'53.0"N 15°52'56.0"E), in Austria. We used data from Poiana Stampei (47°19'29.2"N 25°08'04.8"E) in Romania and from Chopok (48°56'00.0"N 19°35'00.0"E) and Topolniky (47°57'36.0"N 17°51'38.0"E) in Slovakia. All observation points (except Győr and Budapest) are EMEP stations; the databases are free of charge on the official EMEP website (<http://emep.int>).

As it was mentioned in the abstract earlier 3 model domains covering Europe, the Carpathian Basin and Hungary separately using one-way nested grid with horizontal resolution of 108, 36 and 12 km (Figure 1). The 36 km model domain covers the Carpathian Basin, and the 12-km domain covers Hungary. All nested domains have 43 vertical layers, and the model top is set at 50 hPa. The lowest 17 model sigma levels are among 1.0 and 0.80.

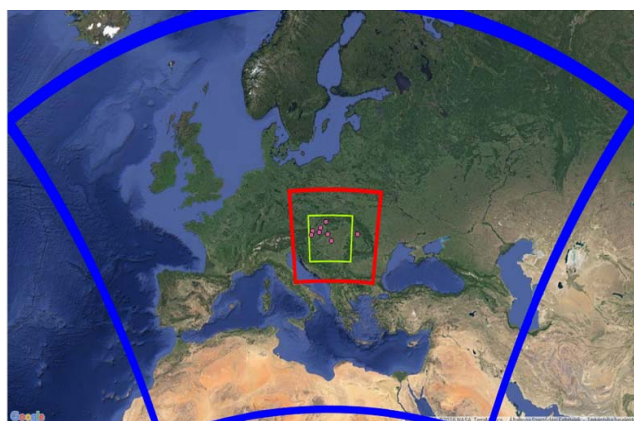


**Figure 1.** Nested domains employed by WRF – CMAQ – SMOKE model system, a) blue domain: 108 km grid (Europe), b) 36 km grid (Carpathian Basin), c) 12 km (Hungary), d) pink point: air-quality monitoring stations for verification study

### STRUCTURE OF THE MODEL SYSTEM

The CMAQ – WRF – SMOKE model system has a complex model structure (Figure 2). As it can be seen in the left side of the picture are the system models which gave the input files for the system. The WRF model makes the meteorological datasets with GFS data, which had to be modified to the system formats for SMOKE and CMAQ model. This task made the MCIP processor.

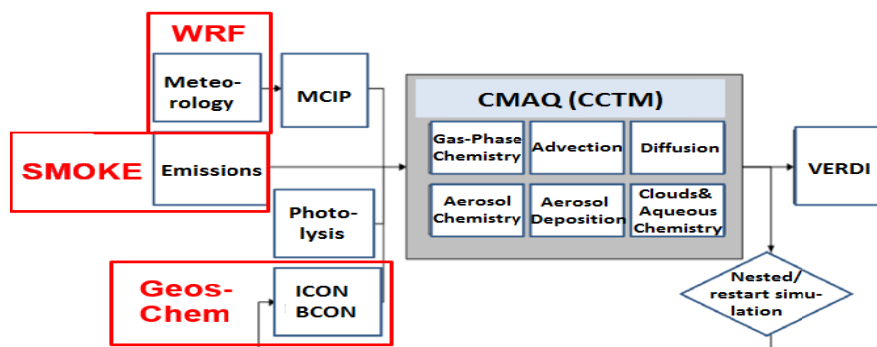


**Figure 2.** Sematic picture of the WRF – CMAQ – SMOKE model system. Black arrow shows the direction of the construction of the model system. Red box are optional model within the system, blue box is the sub processors in the CMAQ model

The emission dataset was constructed by SMOKE with meteorological data files, all emission sources (point, area, mobil or road) were in ASCII files. The boundary and initial concentration files were calculated by the GEOS-Chem model, which were put the CMAQ model inputs with PseudoNetCDF python scripts. After we had the input files for the CMAQ, we could run the forecast in our grid area. The outputs of the system were NetCDF files which we could visualise with VERDI program. The CMAQ, SMOKE models and VERDI program were made by CMAS centre (<http://cmascenter.org>), the applied GEOS-chem model is managed by the GEOS-Chem Support Team, based at Harvard University and Dalhousie University with support from the US NASA Earth Science Division and the Canadian National and Engineering Research Council (<http://www.geos-chem.org/index.html>). All models and programs are available free of charge. The model system is running at ELTE ATLASZ server.

### CASE STUDY

In this section we represent the first results of our complex model for Hungary between 19<sup>th</sup> September 2012 and 27<sup>th</sup> September 2012. We would have liked to examine the model system quality with ozone datasets in the first place. Relationship between measurements and calculated concentrations had been studied, and after that the behaviour of each station with the modelled values was determined. First, we examined at 108 km grid how the model behaves in correlation with the data of the measurements. O<sub>3</sub> values were examined with both (TUCL and TUMP) chemical mechanisms thus we could decide which mechanism can be advantageous for forecasts of the Carpathian Basin.

In Figure 3. the correlation of measurements and forecasted concentrations were examined in K-pusztá at 108 km grid. The model system was run with different start dates in order to estimate the time gap after that fairly good concentration results can be yielded from a 7-day-long forecast in comparison with the measurement data. Forasmuch as at 108 km grid the model system did not forecast the measured small concentration values at 21<sup>st</sup>, 22<sup>nd</sup> and 23<sup>rd</sup>, the values of 21<sup>st</sup> and 25<sup>th</sup> September 2012 were examined at 108 km, 36 km, 12 km grids in one point (K-pusztá) separately. In the case of 25<sup>th</sup> September 2012 each the 108 km, 36 km and 12 km grid values were higher than the measurement data but morning and evening differences were smaller than forecast-measurement differences of 21<sup>st</sup> September 2012.

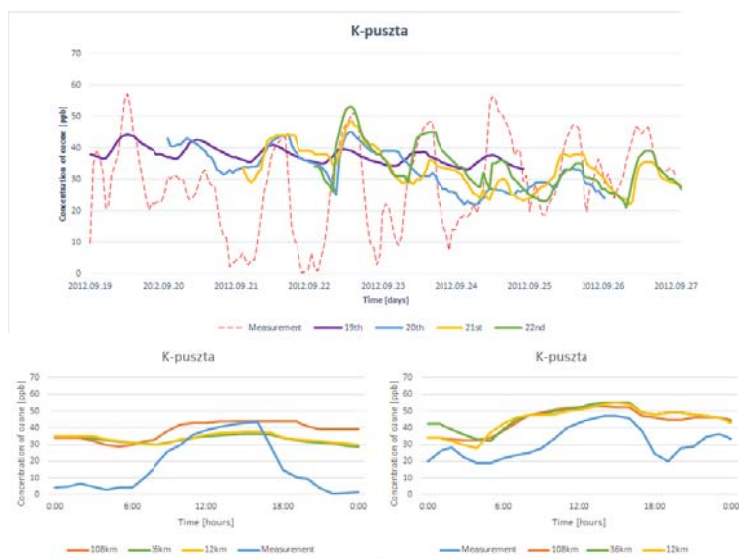


**Figure 3.** Concentration of ozone (O<sub>3</sub>) on K-pusztá. a.) eight-day ozone forecasts with different start time at 108 km grid (red:measurements, violet: 19<sup>th</sup>, blue: 20<sup>th</sup>, yellow: 21<sup>st</sup>, green: 22<sup>nd</sup>), b.) concentration of ozone at 21<sup>st</sup> September 2012. (blue: measurement, yellow: 12 km, green: 36 km, orange: 108km grid, 24-hour run) c.) concentration of ozone at 25<sup>th</sup> September 2012. (blue: measurement, yellow: 12 km, green: 36 km, orange: 108 km grid, 24-hour run)

Figure 4. shows the temporal changes of ozone concentration in the Carpathian Basin at 22<sup>nd</sup> September 2012. Spatial differences between the measurement data and the forecast values were studied. Figure 4. represents the above mentioned observation stations of the Carpathian Basin. The colour of each station

shall be interpreted according to the same ozone map scale. To study the temporal changes two stations (K-pusztta and Chopok) were chosen where the results of the observations and the model system values were compared at 22<sup>nd</sup> September 2012. In the case of K-pusztta the system values were higher than the measurement data. We assumed that these differences were due to initial concentrations presumably generated by an anticyclone weather situation. In the case of Chopok differences between the measurement data and the model values were smaller, presumably due to the location of the observation station (hilly region in a national park).

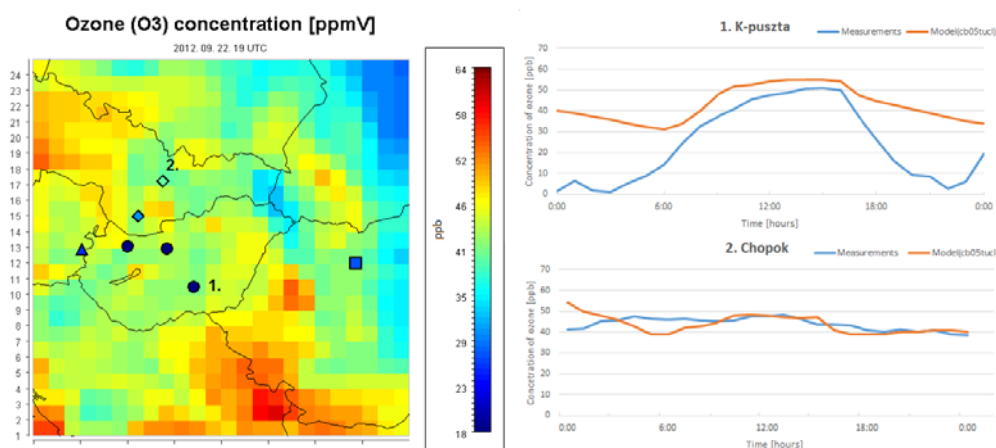


**Figure 4.** Ozone concentration forecast in the Carpathian Basin [ppb] a.) concentration values separately marked at the observation stations (19 UTC) (circle: Hungarian stations; triangle: Austrian stations; diamond: Slovakian stations; square: Romanian station) b.) measurements (blue line) and forecast values (orange line) for K-pusztta (Dot 1.) and Chopok (Dot 2.) at 22<sup>th</sup> September 2012.

As it was mentioned above, in the Fig 5. the differences of the cb05 tucl and cb05tump chemical mechanism are shown with different visualisation methods. On the map of the spatial differences (a) there are chiefly small negative values, but in Romania and on the Great Plain (mostly in Eastern Hungary) higher positive difference values may appear. On the temporal change plot (b) and on the scatter plot (c) can be noticed that differences are particularly typical in the afternoon.

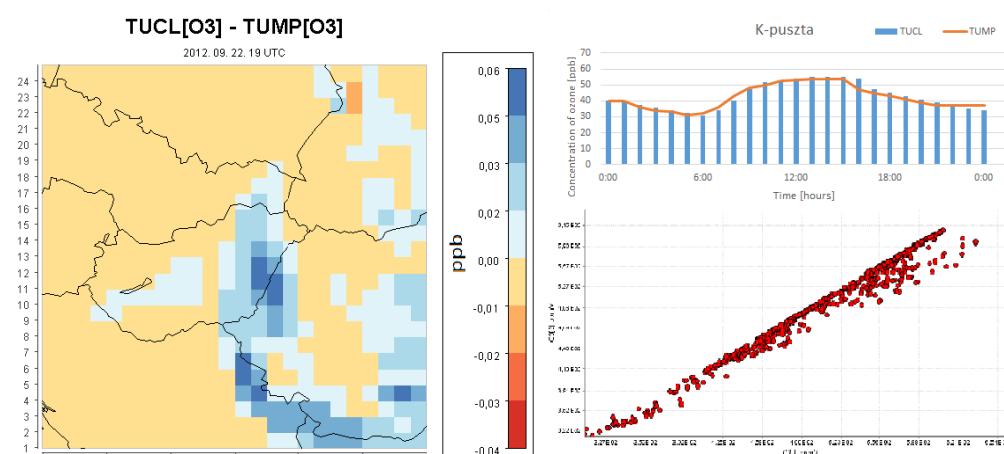


**Figure 5.** Differences of the two chemical mechanism ozone forecasts in the Carpathian Basin at 22th September 2012 at 36 km grid. a.) differences of ozone forecasts shown on map at 17 UTC 22<sup>nd</sup> September 2012 (brown: negative; beige and blue: positive) [ppb], b.) temporal change of O<sub>3</sub> concentration forecasted by two chemical mechanism on a one-day interval (orange: TUMP, blue: TUCL) [ppb], c.) scatter plot of the ozone concentration [ppmV] (x: TUCL, y: TUMP)

## CONCLUSION

In this paper we introduced our adaptation of CMAQ – SMOKE – WRF model system on Europe and the Carpathian Basin in forecasting ozone concentration. After comparing the forecast values with the observation values we have concluded that a.) the model system shall be run about 3 days before fairly good forecast results can be yielded, b.) the forecast values depend on the initial and boundary values of the O<sub>3</sub> concentration, c.) the cb05 TUMP chemical mechanism produces typically lower forecast values than cb05 TUCL mechanism in the afternoon.

Our further plan is i) to configure a more detailed emission dataset for Europe and Hungary, ii) to examine the air pollution concentration forecasts for a full-year period, iii) to test the model sensitivity with other air-quality models (e.g. WRF-Chem) and iv) to build up an ensemble ozone forecast.

## REFERENCES

- Amann, M., I. Bertok, J. Borken-Kleefeld, J. Cofala, C. Heyes, L. Höglund-Isaksson, Z. Klimont, B. Nguyen, M. Posch, P. Rafaj, R. Sandler, W. Schöpp, F. Wagner, and W. Winiwarter, 2011: Cost-effective control of air quality and greenhouse gases in Europe: Modeling and policy applications. *Environmental Modelling & Software* **26**, 1489–1501.
- Boulton, W., J. Lundgren, G. Conley, M. Gauthier, A. Wolfe, C. McClellan, M. Moran, J. Zhang, Q. Zheng, Z. Adelman, M. Omary, L. Aubin, and K. McAdam, 2012: Emissions Inventory Preparation in Support of High - Resolution CMAQ Modelling Applications. [https://www3.epa.gov/ttn/chief/conference/ei21/session1/jboulton\\_pres.pdf](https://www3.epa.gov/ttn/chief/conference/ei21/session1/jboulton_pres.pdf)
- Bozó, L., 2005: Assessment of air quality and atmospheric deposition in Hungary. *WIT Transactions on Ecology and the Environment* **82**, Air pollution XIII, 187–193. [www.witpress.com](http://www.witpress.com).
- Colette, A., C. Granier, Ø. Hodnebrog, H. Jakobs, A. Maurizi, A. Nyiri, S. Rao, A. Amann, B. Bessagnet, A. D'Angiola, M. Gauss, C. Heyes, Z. Klimont, F. Meleux, M. Memmesheimer, A. Mieville, L. Rouil, F. Russo, S. Schucht, D. Simpson, F. Stordal, F. Tampieri, and M. Vrac, 2012: Future air quality in Europe: a multi-model assessment of projected exposure to ozone. *Atmospheric Chemistry and Physics* **12**, 10613–10630.
- Finlayson-Pitts B. J., and J. N. Pitts, 2000: Chemistry of the Upper and Lower Atmosphere. Academic press, New York, USA.
- Gryparis, A., B. Forsberg, K. Katsouyanni, A. Analitis, G. Touloumi, J. Schwartz, E. Samoli, S. Medina, H. R. Anderson, E. M. Niciu, H.-E. Wichmann, B. Kriz, M. Kosnik, J. Skorkovsky, J. M. Vonk, and Z. Dörtludak, 2004: Acute Effects of Ozone on Mortality from the “Air Pollution and Health”. *American Journal of Respiratory and Critical Care Medicine* **170**, 1080–1087.
- Holicska, Sz. (ed.), 2008: Man trying Weather – Medical meteorology for everyone (in Hungarian). OMSz, Athenaeum Kiadó Kft., 256 pp.
- Leelőssy, Á., F. Molnár, F. Izsák, Á. Havasi, I. Lagzi, and R. Mészáros, 2014: Dispersion modeling of air pollutants in the atmosphere: a review. *Open Geosciences* **6**, 257–278.
- Lu, D., R. S. Reddy, R. F. Fitzgerald, W. R. Stockwell, Q. R. Williams, and P. B. Tchounwou, 2008: Sensitivity Modelling Study for an Ozone Occurrence during the 1996 Paso Del Norte Ozone Campaign. *International Journal of Environmental Research and Public Health* **5**, 181–203.
- McDonnell, W. F., J. A. Raub, D. C. Spencer, S. L. Stone, J. Brown, and E. Wildermann, 2002: Health Effects of Ozone in Patients with Asthma and Other Chronic Respiratory Disease. EPA webpage course: <https://www3.epa.gov/apti/ozonehealth/effects.html>
- Neu, U., T. Künzle, and H. Wanner, 1994: On the relation between ozone storage in the residual layer and daily variation in near-surface ozone concentration — A case study, *Boundary-Layer Meteorology* **69**, 221–247.
- Pay, M. T., M. Piot, O. Jorba, S. Gassó, M. Gonçalves, S. Basart, D. Dabdub, P. Jiménez-Guerrero, and J. M. Baldasano, 2010: A full year evaluation of the CALIOPE-EU air quality modeling system over Europe for 2004. *Atmospheric Environment* **44**, 3322–3342.
- Pederzoli, A., 2008: The application of an Eulerian chemical and transport model (CMAQ) at fine scale resolution to the UK. PhD thesis, pp 232.
- Roselle, S. J, T. E. Pierce, and K. L. Schere, 1991: The sensitivity of regional ozone modelling to biogenic hydrocarbons. *Journal of Geophysical Research* **96**, 7371–7394.

- Sarwar, G., D. Luecken, G. Yarwood, G. Whitten, and B. Carter, 2008. Impact of an updated Carbon Bond mechanism on air quality using the Community Multiscale Air Quality modeling system: preliminary assessment. *Journal of Applied Meteorology and Climatology* **47**, 3–14.
- Syrakov, D., M. Prodanova, E. Georgieva, and K. Slavov, 2015: Air Quality Modelling with WRF-CMAQ over Europe – Focus on Ozone and Particulate Matter. EMS 12, EMS2015-410.
- Whitten, G. Z., G. Heo, Y. Kimura, E. McDonald-Buller, D. T. Allen, W. P. L. Carter, and G. Yarwood, 2010. A new condensed toluene mechanism for Carbon Bond: CB05-TU. *Atmospheric Environment* **44**, 5346–5355.
- Wong, D. C., J. Pleim, R. Mathur, F. Binkowski, T. Ottel, R. Gilliam, G. Pouliot, A. Xiu, J. O. Young, and D. Kang, 2012: WRF-CMAQ two-way coupled system with aerosol feedback: software development and preliminary results. *Geoscientific Model Development* **5**, 299–312.

**17th International Conference on  
Harmonisation within Atmospheric Dispersion Modelling for Regulatory Purposes  
9-12 May 2016, Budapest, Hungary**

---

**EMISSION PROCESSOR FOR AIR QUALITY MODELS UTILIZING NEWLY AVAILABLE  
DATA**

*Pavel Juruš<sup>1,3</sup>, Jan Karel<sup>4</sup>, Radek Jareš<sup>4</sup>, Josef Martinovský<sup>4</sup>, Václav Piša<sup>4</sup>, Robert Polák<sup>4</sup>, Eva Smolová<sup>4</sup>, Emil Pelikán<sup>2,3</sup>, Marek Brabec<sup>1,3</sup>, Ondřej Konár<sup>1,2</sup>, Viktor Fuglik<sup>1,3</sup>, Kryštof Eben<sup>2,3</sup>, Jaroslav Resler<sup>2,3</sup>, Ondřej Vlček<sup>5</sup>, Pavel Machálek<sup>5</sup>, Miloslav Modlík<sup>5</sup>, Helena Hnilicová<sup>5</sup>, Nina Benešová<sup>5</sup>, Daša Srbová<sup>5,8</sup>, Miloš Zapletal<sup>6</sup>, Radek Kadlubiec<sup>6</sup>, Pavla Škarková<sup>6</sup>, Jiří Barnet<sup>7</sup>*

<sup>1</sup>Faculty of Transportation Sciences, Czech Technical University in Prague, Czech Republic

<sup>2</sup>Czech Institute of Informatics, Robotics and Cybernetics, Czech Technical University in Prague,  
Czech Republic

<sup>3</sup>Institute of Computer Science, Czech Academy of Sciences, Prague, Czech Republic

<sup>4</sup>ATEM – Studio of Ecological Models Ltd., Czech Republic

<sup>5</sup>Czech Hydrometeorological Institute, Czech Republic

<sup>6</sup>EKOTOXA Ltd., Czech Republic

<sup>7</sup>SHERLOG TRACE Ltd., Czech Republic

<sup>8</sup>Czech University of Life Sciences Prague, Czech Republic

**Abstract:** High-quality emission data are of utmost importance for the reliable outputs of air quality models. AQ models require speciated hourly emissions, whereas emission inventories are constructed on annual basis and include only main pollutants. For the time disaggregation simple and constant monthly, daily, and hourly factors are usually used. Likewise, chemical speciations are usually based on outputs of very few and sometimes quite old reports and do not necessarily correspond to the situation in the country of interest. For the emission processing itself many scientific groups use SMOKE pre-processor, due its availability and since it is fitted for the WRF and CMAQ models. Nevertheless, its application for non-US countries can be quite complicated due to different data and metadata structure. Our project focusses on two aims:

- 1) The derivation of the time and speciation profiles specific for the Czech Republic. For this purpose, we analyse continuous emission measurements from the large stationary sources, temperature and behaviour dependency of the household heating emission, and the data available in the extensive Czech emission database REZZO. For the transport we managed to access data from the Electronic Control Units (ECU) of the vehicular fleet maintained by the SHERLOG company. These unique data give us information on engine state, fuel consumption, and driving styles from the real traffic flow.
- 2) The construction of a flexible emission processor for AQ models based on the freely available software.

**Key words:** *Emission processor, air quality modelling, chemical transport models, air pollution*

## INTRODUCTION

Emission rates (typically, hourly emissions of given species for point sources or for the cells of a model grid) represent one of the basic inputs of air quality models. Accuracy and fidelity of emission inputs are among the most important factors affecting any modelling results. It is not possible to do realistic air quality simulations without reliable emission inputs. On the other hand, the process of transformation of emissions, starting from primary emission data and ending with emission inputs to chemical transport model, can be quite intricate. The complexity of the emission processing lies in a number of factors:

1. Emissions enter the atmosphere from a number of sources of different type and a number of heterogeneous mechanisms is involved (physical, chemical, biological, societal etc.).
2. Most of the emission sources is not measured directly. This means that we have to model and estimate emission sources behaviour. Even in the rare cases when we have direct measurements (e.g. some large point sources with continuous measurement), we have to estimate their emissions in case of forecasts or scenarios. The methods for modelling and estimation range from statistical analysis,

laboratory measurements, physical and chemical process modelling, demographical and sociological knowledge up to all kinds of qualified estimates based on domain knowledge.

3. Some of the more detailed inputs for emission modelling are not accessible. Reasons may vary from the lack of centralized gathering of emission data in some countries to various security or business concerns. Although the availability of primary data is generally getting better, there can be still a number of constraints which have to be worked around.

The emission processor is a complex heterogeneous system consisting of a number of parts dealing with particular aspects of various emission data and transforming them to consistent form usable for further processing – typically by chemical transport models.

Our design goal for the emission processor is to have the largest possible part of the processor generic and independent on particular use case (e.g. the type of primary emission data or type and format of outputs). The processor is modular and its input, output and configuration can use the same emission processing core.

This also means that emission consolidation and further manipulation is not tied to any particular spatial grid or point sources structure. The design of the processor allows for using of original primary data spatial segmentation (often given by GIS polygons, polylines and points).

Any system for realistic modelling of air quality has to contain an emission processor. It could be expected that the emission processor would be a standard part of coupled models in the same fashion as is the coupling of publicly available numerical weather models (e.g. MM5, WRF) and chemical transport models (e.g. CMAQ, CAMx, CHIMERE). This role is fulfilled by the SMOKE model (Coats and Houyoux, 1996) which is the part of MODELS-3 framework (Byun and Schere, 2006). Unfortunately, the same solution is not satisfactory for the modelling of emissions outside of USA. Particularly in Europe, the differences in legislation, emission reporting, information gathering and regulatory practise make adaptation of SMOKE model very difficult. Nevertheless, the SMOKE model have been used for emission modelling in Europe after some modifications (for examples, see Bieser et al. (2011), Borge et al. (2008) or Yu et al. (2008)). The previous attempts to adapt and extend SMOKE have shown that the design of a new emission processor may be easier way and may also include updates in emission modelling, data management and processing, and software engineering. Many of the SMOKE approaches are nevertheless worthwhile inspiration for any emerging emission processor.

## **EMISSION PROCESSOR**

Structure of the emission processor can be divided into three main layers which corresponds to three phases of emission processing: 1) inputs preprocessing and preparation, 2) emission processor core, 3) outputs postprocessing. Figure 1 shows the schematic structure of the emission processor indicating the basic data flow and modules dependency of the processor.

### **Preprocessing, transformations, scenario setup**

Emission processor has to ingest heterogeneous primary information about the emissions. The role of this phase is to consolidate and unify the structure and format of emission inputs. An important part of preprocessing is also the work with meteorological data, preparation of the grid and construction of spatial factors for the cases when they are not dependent on time. The grid can be created on-the-fly based on configuration of the particular task or scenario. Another possibility is to use already precomputed data (e.g. as a GIS shapefile) from previous tasks with the same grid configuration.

### **Emission processor core**

Emission processor core is a key part of the toolchain where the disaggregation of emission totals takes place. The central task is the processing of spatiotemporal factors for the disaggregation and consequent chemical speciation. The factors range from static profiles stored in database to less or more dynamic profiles which can be computed by complex models (e.g. for biogenic emissions or emissions from lightning). The emission processor should be also able to encapsulate external sub-models for the calculation of emission factors.

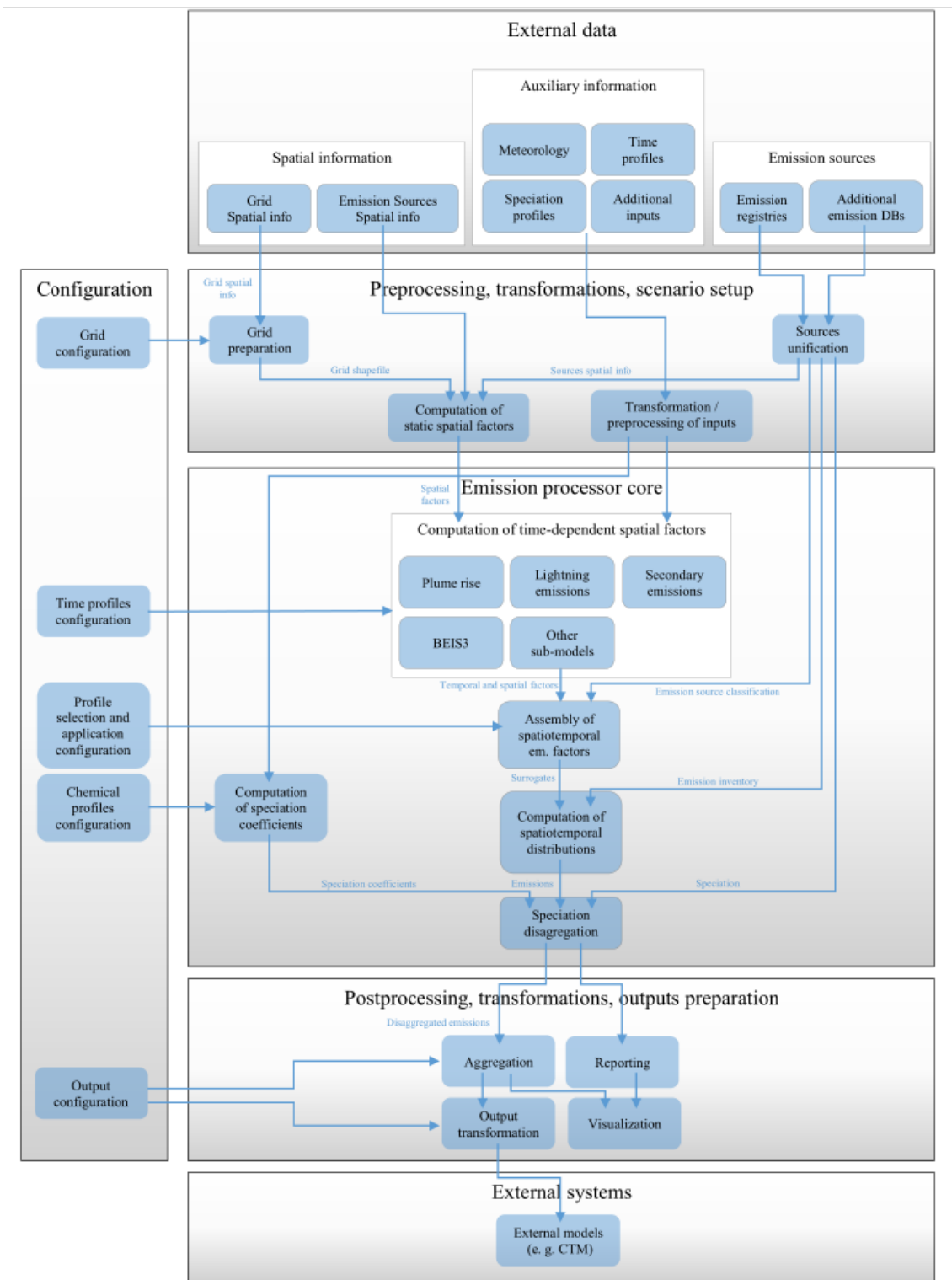


**Figure 1.** Structure of the new emission processor. The scheme shows basic layers of the processor, flow of the data and modules dependency.

The steps of emission processor core are:

- Computation of time dependent spatial factors – based on static time profiles, meteorology, mathematical models, GIS data etc.
- Assembly of spatiotemporal emission factors – the factors are consolidated and adjusted according to scenario setup.
- Computation of spatiotemporal distributions – the factors are applied to emission sources which results in the set of emissions properly distributed in time and space.
- Speciation disaggregation – the emission data are recalculated into modelled species or groups based on speciation coefficients.

### **Postprocessing, transformations, outputs preparation**

The resulting raw data containing disaggregated emissions from emission processor core are aggregated based on the requirements. The results are then transformed to desired data format which is used by external systems – typically by chemical transport models. Various visualizations and reports are also the part of this phase.

### **Configuration**

Configuration of the whole toolchain is an important part of the emission processor. One of the tasks solved by configuration is the setup of particular modules and adjustments to emission data based on simulation scenario. Configuration also decides which module implementation will be used in case of multiple implementations of particular submodule – e.g. different calculations of plume rise based on availability of e.g. meteorological data or stack gas temperature and velocity.

### **ACKNOWLEDGEMENTS**

The work reported in this submission is supported by the project “TA04020797 – Emission processor of the new generation utilizing newly available sources of data” granted by Technology Agency of the Czech Republic - programme ALFA.

### **REFERENCES**

- Bieser, J., A. Aulinger, V. Matthias, M. Quante and P. Builtjes, 2011: SMOKE for Europe–adaptation, modification and evaluation of a comprehensive emission model for Europe. *Geoscientific Model Development*, **4**, 47-68.
- Borge, R., J. Lumberras and E. Rodríguez, 2008: Development of a high-resolution emission inventory for Spain using the SMOKE modelling system: a case study for the years 2000 and 2010. *Environmental Modelling & Software*, **23**, 1026-1044.
- Byun, D. and K. L. Schere, 2006: Review of the governing equations, computational algorithms, and other components of the Models-3 Community Multiscale Air Quality (CMAQ) modeling system. *Applied Mechanics Reviews*, **59**, 51-77.
- Coats Jr, C. J. and M. R. Houyoux, 1996: Fast Emissions Modeling with the Sparse Matrix Operator Kernel Emissions (SMOKE) Modeling System. No. CONF-9609223--. Air & Waste Management Association, Pittsburgh, PA (United States).
- Yu, Y., R. S. Sokhi, N. Kitwiroon, D. R. Middleton and B. Fisher, 2008: Performance characteristics of MM5–SMOKE–CMAQ for a summer photochemical episode in southeast England, United Kingdom. *Atmospheric Environment*, **42**, 4870-4883.

**17th International Conference on  
Harmonisation within Atmospheric Dispersion Modelling for Regulatory Purposes  
9-12 May 2016, Budapest, Hungary**

---

**WRF-CAMX APPLICATION TO THE PEARL RIVER DELTA REGION**

*Diogo Lopes<sup>1</sup>, Joana Ferreira<sup>2</sup>, Ka In Hoi<sup>1</sup>, Kai Meng Mok<sup>1</sup>, Ana I. Miranda<sup>2</sup> and Ka Veng Yuen<sup>1</sup>*

<sup>1</sup>Department of Civil & Environmental Engineering, Faculty of Science and Technology,  
University of Macau, Macau SAR, China

<sup>2</sup>CESAM & Department of Environmental and Planning, University of Aveiro, Aveiro, Portugal

**Abstract:** The Pearl River Delta (PRD) is located in the southern coast of China and it is the second largest delta of the country. In 2014, several exceedances to the Chinese limit-values, for nitrogen dioxide (NO<sub>2</sub>) and ozone (O<sub>3</sub>), were recorded in the PRD. To implement measures for air quality improvement in this region, it is necessary to understand the spatial distribution of air pollution. Therefore, the present work aims to study air pollution patterns, focusing on O<sub>3</sub> and NO<sub>2</sub>, over the PRD region by the application of the WRF-CAMx regional air quality modelling system. The WRF-CAMx system was applied, with its nesting capabilities, to one winter and one summer 7-day periods of the year 2014 and was validated with data from several air quality monitoring stations distributed along the southern coast of China. The results for the higher resolution domain showed a reasonable performance of the model. The WRF-CAMx tends to overestimate and underestimate the O<sub>3</sub> and NO<sub>2</sub> concentrations, respectively. The analysis of temporal and spatial variability of simulated concentrations pointed to the need to improve the emission inventory with further information on the temporal and spatial distribution of local sources.

**Key words:** *Pearl River Delta, WRF-CAMx, NO<sub>2</sub>, O<sub>3</sub>.*

## **INTRODUCTION**

The Pearl River Delta (PRD) is one of the largest industrialized regions in China. It is located in the southern coast and it comprises nine municipalities (Guangdong province) and two special administrative regions (Macao and Hong Kong). In the last decades, the region recorded a rapid development resulting in the increase of the energy consumption, atmospheric emissions and degradation of the air quality. Guangdong province and Hong Kong have implemented measures to reduce the air pollution. Between 2006 and 2014, the annual averaged NO<sub>2</sub> and O<sub>3</sub> concentrations changed from 46 to 37 and 48 to 57 µg.m<sup>-3</sup>, respectively. According to “Pearl River Delta Regional Air Quality Monitoring Network” for 2014, this region continues to record several exceedances for NO<sub>2</sub> and O<sub>3</sub>. Except ozone which is formed through photochemical reactions enhanced by solar radiation, the highest pollution concentrations are recorded in winter (SO<sub>2</sub>, PM10, PM2.5, NO<sub>2</sub> and CO) and are associated with the northeast air mass trajectories crossing the China-Taiwan strait region. Therefore, the PRD region may be affected by the transboundary pollution besides its local emissions. Typically O<sub>3</sub> concentrations are higher in summer months (May, June, July, August and September) and minimum in winter months (November, December, January and February). Chemical transport modelling could be a useful tool to provide scientific advice on emission reduction strategies and air quality management.

Wu et al. (2012) evaluated the performance of three air quality models (including CAMx) over PRD for November 2006. The authors concluded that models have different behaviours at different spatial locations. Lu et al. (2016) applied CAMx and ozone source apportionment techniques to several months of 2011 to study the NO<sub>x</sub> different emissions source contributions over southern China, and observed that heavy duty diesel vehicles, light duty gasoline vehicle, industrial and marine sources are the main sources of NO<sub>x</sub> emissions.

In this work, the performance of WRF-CAMx was evaluated for two seasons (winter and summer) in PRD, by its application to two 7 day episodes. The selection of the episodes was based on the analysis of air pollution concentrations recorded at different air quality monitoring stations across PRD. In 2014, the highest and lowest concentrations for almost all pollutants (excluding ozone) were observed in winter and

summer season, respectively. The WRF-CAMx capability to simulate NO<sub>2</sub> and O<sub>3</sub> air pollution levels was based on data from 11 air quality monitoring stations selected by their location (spread over the study region) and type. The pollutants - NO<sub>2</sub> and O<sub>3</sub> - were chosen as they are the most concerned in terms of air quality in the region.

### MODELLING SETUP AND CONFIGURATION

The WRF-CAMx modelling system, composed by the Advanced Research Weather Research and Forecasting (WRF-ARW) and the Comprehensive Air quality Model with extensions (CAMx), was selected to study the air pollution patterns that characterize the PRD by its application over the southeast coast of China. The WRF-ARW (version 3.6.1) (Skamarock et al., 2008) was built over a coarse domain covering east Asia, Indian subcontinent, part of the southeastern Asia and middle east (at 81 km<sup>2</sup> horizontal resolution) and three nested domains with resolutions of 27×27 km<sup>2</sup>, 9×9 km<sup>2</sup> (southeast coast of China) and 3×3 km<sup>2</sup> (over the PRD region). The global meteorological fields from the National Centre for Environmental Prediction, with 1° by 1° spatial resolution and 6 hours temporal resolution, were used to initialize the meteorological simulation. The WRF-ARW simulation considered the following physical options: Ferrier scheme, rapid radiative transfer model, Goddard shortwave, Monin-Obukhov similarity scheme, Noah land surface model, Kain-Fritsch scheme and Yonsei University scheme. WRF results were validated against observation at 27 meteorological stations, selected according to their spatial distribution, revealing a good performance for temperature and a reasonable agreement for wind speed and direction.

CAMx is a 3D Eulerian photochemical dispersion model that can be applied for different scales ranging from sub-urban to global. It simulates the emissions, dispersion, chemical reactions and removal of pollutants in the troposphere by solving the Eulerian continuity equation for each chemical species on a system of nested three-dimensional grids (ENVIRON, 2015). CAMx (version 6.20) was applied to the two smaller WRF domains - a coarse domain covering southeast coast of China (9 km<sup>2</sup> horizontal resolution) and a nested domain with 3×3 km<sup>2</sup> resolution (over the PRD region) (Figure 1. Simulation domains used by CAMx: parent grid (D1, 9×9km<sup>2</sup> resol) and nested domain (D2, 3×3km<sup>2</sup> resol).). The horizontal diffusion and chemistry were calculated using Piecewise Parabolic Method (PPM) and Euler Backward Iterative (EBI) method, respectively. The WESELY89 dry deposition option was used to define surface ultraviolet albedo, surface resistances for dry deposition calculations, and to set seasonal default surface roughness lengths and leaf area index values. For more information about CAMx see (ENVIRON, 2015).

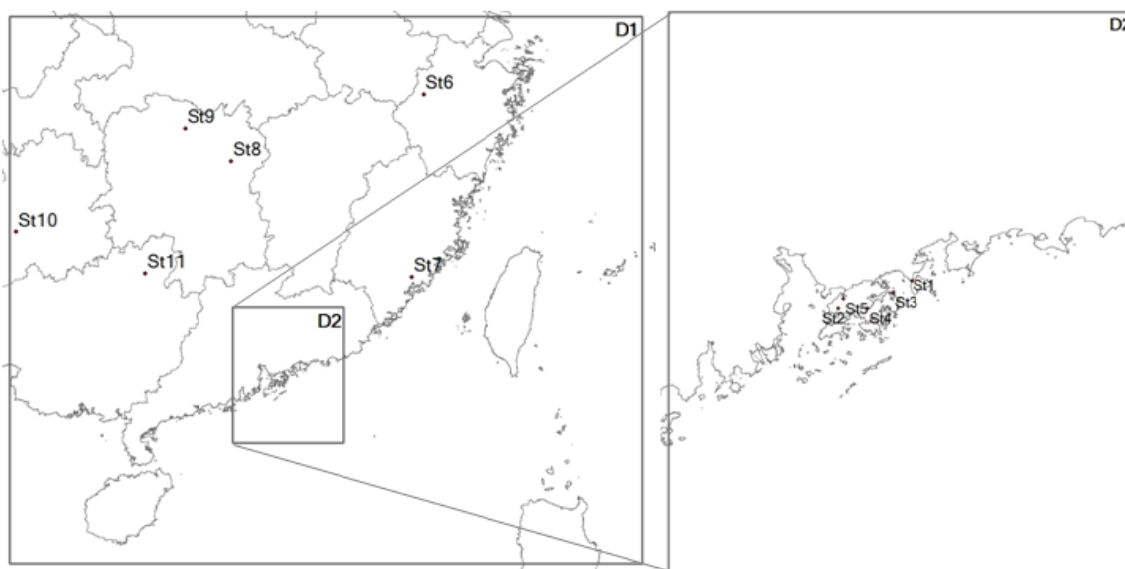


**Figure 1.** Simulation domains used by CAMx: parent grid (D1, 9×9km<sup>2</sup> resol) and nested domain (D2, 3×3km<sup>2</sup> resol).

The initial and boundary conditions were taken from the MOZART4 model outputs at every 6 hours. Regarding anthropogenic emissions, the 2008 Regional Emission inventory for Asia was adapted to generate temporally and spatially disaggregated emissions to the CAMx coarser domain (D1). This inventory includes monthly emissions at 0.25 degrees horizontal resolution for several pollutants (PM, SO<sub>2</sub>, NO<sub>2</sub>, etc.) distinguishing the activity sectors road transport, domestic, industrial sources, power plants, etc. (Kurokawa et al., 2013). A literature review was performed aiming to find the most suitable speciation and temporal profiles for China and Chinese chemical speciation profiles were used for road transport (Cai and Xie, 2009; Dai et al., 2015; Li et al., 2011), domestic (He et al., 2004) and solvents (Yuan et al., 2010). For the remaining sectors, the SPECIATE database from the United States Environmental Protection Agency was used. Monthly, weekly and daily variability of emissions was also considered. For road transport, temporal profiles were derived from the hourly variation of carbon monoxide concentrations at 4 urban air quality monitoring stations (1 in Macao and 3 in Hong Kong). The daily profile for the domestic sector was based on the author's living experience. For the other sectors, the European temporal profiles were considered (Gon et al., 2011). Gridded emissions for the CAMx smaller domain (D2) were interpolated from D1 emissions using the flexi nesting CAMx capability.

## AIR POLLUTION MODELLING EVALUATION

The WRF-CAMx system was applied to one winter (20 to 26 January) and one summer (10 to 16 July) 7-day periods and was validated with data from 11 air quality monitoring stations over the simulation domains (Figure 1). The evaluation of the WRF-CAMx performance for NO<sub>2</sub> and O<sub>3</sub> was done by computing the following statistical parameters: correlation coefficient (r), BIAS and root mean squared error (RMSE) (Borrego et al., 2008). Table 1 and Table 2 present the statistical analysis results for O<sub>3</sub> and NO<sub>2</sub> respectively. Simulated concentrations for CAMx D1 (9 km resolution) and D2 (3 km resolution) were compared with observations from St1 to St11 stations, as indicated in the tables.

**Table 1.** Statistical parameters obtained for ozone at the 11 selected air quality monitoring stations.

Stations	Domain	winter episode			summer episode			
		r (-)	BIAS (µg/m <sup>3</sup> )	RMSE (µg/m <sup>3</sup> )	r (-)	BIAS (µg/m <sup>3</sup> )	RMSE (µg/m <sup>3</sup> )	
Guangdong province	St1	D1	0.31	-44.02	54.88	0.64	51.72	58.66
		D2	0.34	-0.26	25.89	0.08	77.30	84.33
Hong Kong	St2	D1	0.21	15.64	41.42	0.50	51.49	65.93
		D2	0.39	36.18	43.09	0.16	54.94	54.94
	St3	D1	0.35	-54.36	58.44	0.72	41.20	46.12
		D2	0.46	-11.56	27.98	0.15	69.73	69.86
St4	D1	0.50	-24.11	40.28	0.49	51.46	56.92	
	D2	0.63	11.60	33.12	0.04	70.01	70.85	
St5	D1	0.27	-12.36	39.75	0.64	58.18	63.43	
	D2	0.53	26.24	35.04	0.14	72.10	72.97	
Zhejiang province	St6	D1	0.64	34.83	45.59	0.56	19.93	41.18
Fujian province	St7	D1	0.66	6.68	17.51	0.54	78.91	128.05
Hunan province	St8	D1	0.35	40.04	45.11	0.38	68.87	86.31
	St9	D1	0.49	83.54	101.70	0.06	79.89	89.50
Guizhou province	St10	D1	0.53	15.66	36.13	0.36	17.50	30.69
Guangxi province	St11	D1	0.17	1.15	40.97	0.43	23.18	32.74

Globally, for the correlation coefficient a better agreement between O<sub>3</sub> observed and simulated concentrations was obtained for the winter period (higher correlation coefficients). Furthermore, the winter episode simulation led to lower biases and RMSE at almost all the stations. Comparing the results for D1 and D2 for the station St1 to St5, it is noticeable a better performance of the model for D2 with higher resolution, in the winter period, and in summer the opposite is verified. For D1, the correlation coefficient ranges between 0.17-0.66 in winter and 0.06-0.72 and in summer episodes. In general, the stations located in the south (St1-St2-St3-St5-St8-St11) returned the highest correlation coefficients in summer and the ones in southeast of China (St6-St7) the best correlations in winter. The BIAS range between -54.36 and 83.54 and 17.50 to 79.89  $\mu\text{g}/\text{m}^3$  in winter and summer episodes, respectively. The magnitude errors range between 17.51 and 101.70 in the winter episode and 30.69 to 128.05  $\mu\text{g}/\text{m}^3$  in the summer episode. In general, the highest magnitude errors are recorded in the summer episode. All stations, except St1 to St5 in winter episode, tend to overestimate the O<sub>3</sub> concentrations (positive biases). These results, together with the analysis of the spatial and temporal variations of simulated concentrations (not presented) revealed that, in summer, the model reproduces reasonably well the O<sub>3</sub> concentration variability and magnitude, for the lower resolution simulation domain but not for the higher resolution. For the winter period, characterized by lower O<sub>3</sub> levels, the model performance is generally higher at higher resolution.

**Table 2.** Statistical parameters obtained for nitrogen dioxide at the 11 selected air quality monitoring stations.

Stations	Domain	winter episode			summer episode			
		r (-)	BIAS ( $\mu\text{g}/\text{m}^3$ )	RMSE ( $\mu\text{g}/\text{m}^3$ )	r (-)	BIAS ( $\mu\text{g}/\text{m}^3$ )	RMSE ( $\mu\text{g}/\text{m}^3$ )	
Guangdong province	St1	D1	-0.02	14.14	21.27	0.01	15.09	19.90
		D2	0.26	-8.97	9.61	0.24	-6.85	7.49
Hong Kong	St2	D1	0.23	-50.11	55.73	0.11	15.07	33.41
		D2	0.22	-80.93	80.93	0.04	-25.90	26.05
	St3	D1	-0.17	21.50	23.88	0.08	32.47	32.78
		D2	0.08	-6.06	6.42	0.12	-0.55	1.91
St4	D1	0.40	-21.17	33.84	0.25	15.20	28.75	
	D2	0.50	-54.92	54.92	0.11	-33.79	33.99	
St5	D1	0.18	-20.42	40.76	0.12	18.48	36.78	
	D2	0.26	-66.11	68.98	0.06	-32.40	32.79	
Zhejiang province	St6	D1	0.35	-4.95	6.87	0.04	-0.38	4.80
Fujian province	St7	D1	0.58	-1.76	7.92	0.15	7.04	13.76
Hunan province	St8	D1	0.07	-51.37	59.52	0.06	-7.80	11.38
	St9	D1	0.40	-0.18	2.56	0.23	-12.46	13.86
Guizhou province	St10	D1	0.03	-15.79	23.17	0.20	3.52	9.77
Guangxi province	St11	D1	0.11	-9.63	12.29	0.00	2.20	4.70

The overall performance of the model for NO<sub>2</sub> is much lower than for O<sub>3</sub>, with a maximum correlation coefficient of 0.58 in the winter episode. Notwithstanding, slightly better results are obtained for the summer period (lower biases and RMSE). For St1 and St3, in the winter episode, a negative correlation coefficient was obtained, revealing the inability of the model to reproduce NO<sub>2</sub> variability at these stations. In general, the model tends to underestimate the NO<sub>2</sub> concentrations. In general, the highest magnitude errors are recorded in winter episode. However, there is not clear evidence of a better performance of the model for one of the domains (Table 2).

## CONCLUSIONS

The model exhibited a reasonable performance for both pollutants. For ozone, the WRF-CAMx showed a better performance in the winter episode. However, the model tends to overestimate the O<sub>3</sub> concentrations. For nitrogen dioxide, the WRF-CAMx results revealed a lower performance for this pollutant, with a better agreement between observations and modelled concentration in winter and an overall better performance for summer (lower biases and error). This preliminary analysis of the WRF-CAMx capacity to simulate the air pollution patterns in the region revealed some weaknesses of the global modelling setup, namely regarding emissions temporal and spatial allocation. The results pointed to the need to improve the NO<sub>2</sub> emission inventory, focusing on the temporal and spatial distribution of local sources.

## ACKNOWLEDGEMENTS

This study is supported by the Science and Technology Development Fund of the Macau SAR government under grant no. 079/2013/A3, the university multi-year research grant MYRG2014-00038-FST of the research committee of University of Macau and the university postgraduate studentship. The authors wish to thank the National Center for Atmospheric Research and ENVIRON Corp for their free open-source WRF and CAMx modelling system, respectively. This work was performed in part at the High Performance Computing Cluster which is supported by Information and Communication Technology Office at University of Macau.

## REFERENCES

- Borrego, C., Monteiro, A., Ferreira, J., Miranda, A.I., Costa, A.M., Carvalho, A.C., Lopes, M., 2008: *Procedures for estimation of modelling uncertainty in air quality assessment* **34**, 613–620. doi:10.1016/j.envint.2007.12.005
- Cai, H., Xie, S.D., 2009: Tempo-spatial variation of emission inventories of speciated volatile organic compounds from on-road vehicles in China. *Atmos. Chem. Phys. Discuss.* **9**, 11051–11085. doi:10.5194/acpd-9-11051-2009
- Dai, S., Bi, X., Chan, L.Y., He, J., Wang, B., Wang, X., Peng, P., Sheng, G., Fu, J., 2015: Chemical and stable carbon isotopic composition of PM<sub>2.5</sub> from on-road vehicle emissions in the PRD region and implications for vehicle emission control policy. *Atmos. Chem. Phys.* **15**, 3097–3108. doi:10.5194/acp-15-3097-2015
- ENVIRON, 2015: CAMx User's Guide Version 6.2 User's Guide COMPREHENSIVE AIR QUALITY MODEL.
- Gon, H.D. van der, Hendriks, C., Kuenen, J., Segers, A., Visschedijk, A., 2011: TNO Report Description of current temporal emission patterns and sensitivity of predicted AQ for temporal emission patterns.
- He, L.Y., Hu, M., Huang, X.F., Yu, B. De, Zhang, Y.H., Liu, D.Q., 2004: Measurement of emissions of fine particulate organic matter from Chinese cooking. *Atmos. Environ.* **38**, 6557–6564. doi:10.1016/j.atmosenv.2004.08.034
- Kurokawa, J., Ohara, T., Morikawa, T., Hanayama, S., Janssens-Maenhout, G., Fukui, T., Kawashima, K., Akimoto, H., 2013: Emissions of air pollutants and greenhouse gases over Asian regions during 2000–2008: Regional Emission inventory in ASia (REAS) version 2. *Atmos. Chem. Phys.* **13**, 11019–11058. doi:10.5194/acp-13-11019-2013
- Li, H., Chen, K.S., Lai, C.H., Wang, H., 2011: Measurements of Gaseous Pollutant Concentrations in the Hsuehshan Traffic Tunnel of Northern Taiwan. *Aerosol Air Qual. Res.* **11**, 776–782. doi:10.4209/aaqr.2011.02.0009
- Lu, X., Yao, T., Li, Y., Fung, J.C.H., Lau, A.K.H., 2016: Source apportionment and health effect of NO<sub>x</sub> over the Pearl River Delta region in southern China. *Environ. Pollut.* **212**, 135–146. doi:10.1016/j.envpol.2016.01.056
- Skamarock, W.C., Klemp, J.B., Dudhi, J., Gill, D.O., Barker, D.M., Duda, M.G., Huang, X.-Y., Wang, W., Powers, J.G., 2008: A Description of the Advanced Research WRF Version 3, Technical Report. doi:10.5065/D6DZ069T
- Wu, Q., Wang, Z., Chen, H., Zhou, W., Wenig, M., 2012: An evaluation of air quality modeling over the Pearl River Delta during November 2006. *Meteorol. Atmos. Phys.* **116**, 113–132. doi:10.1007/s00703-011-0179-z
- Yuan, B., Shao, M., Lu, S., Wang, B., 2010: Source profiles of volatile organic compounds associated with solvent use in Beijing, China. *Atmos. Environ.* **44**, 1919–1926. doi:10.1016/j.atmosenv.2010.02.014

**17th International Conference on  
Harmonisation within Atmospheric Dispersion Modelling for Regulatory Purposes  
9-12 May 2016, Budapest, Hungary**

---

**EVALUATION OF MODEL PERFORMANCE USING NEW DEPOSITION SCHEMES IN THE  
RANDOM DISPLACEMENT PARTICLE MODEL PELLO USING FUKUSHIMA POWER  
PLANT ACCIDENT DATA**

*Pontus von Schoenberg<sup>1</sup>, Håkan Grahn<sup>1</sup> and Peter Tunved<sup>2</sup>*

<sup>1</sup>Dispersion modelling group, CBRN Environment and protection, Swedish Defence Research Agency,  
FOI, Sweden

<sup>2</sup>Department of Environmental Science and Analytical Chemistry, ACES, Stockholm University, Sweden

**Abstract:** The nuclear power plant accident in Fukushima 2011 emitted large quantities of radioactive nuclides into the atmosphere. This accident stimulated extensive measurement efforts using different techniques all over the globe, especially in Japan and in the northern hemisphere. This data is highly valuable for testing the performance of dispersion models. In this study, the performance of a random displacement particle model PELLO, Particle model in an Etha Lat Long coordinate system, (Lindqvist, 1999), has been evaluated against this data. The radionuclide Xenon, Xe, has been continuously observed within the CTBTO network, Comprehensive Nuclear-Test-Ban Treaty Organization, (CTBTO, 2016) especially on the northern hemisphere since 1996. The radioactive decay of Xenon is well known and other atmospheric sinks are of small importance, which means that Xe may be used as an inert tracer in dispersion models, allowing for evaluation of applied transport schemes. Conjointly released cesium-137, <sup>137</sup>Cs, is however assumed to attach on ambient aerosols during and after release. On contrary to Xe and other noble gases, particles are not stable in the atmosphere, but instead subjected to aerosol dynamical ageing as well as wet and dry deposition. While comparison of modelled and measured Xenon suggest that the dispersion across the northern hemisphere is satisfactory described in terms of order of magnitude and timing of the plume arrival to the different locations (P. von Schoenberg & Grahn, 2013), modelled <sup>137</sup>Cs calculations offers a larger challenge. This highlights the requirement of more detailed representation of dominating sinks, i.e. wet and dry deposition. First steps in this direction have been taken, and this presentation explores more in depth the role of these two processes. The results presented suggest a need of more rigorous treatment of dominant aerosol sinks in the atmosphere to be represented in dispersion models, and different approaches to make such implementations are discussed.

**Key words:** *Wet deposition, deposition, precipitation, dispersion modelling, PELLO, CALM.*

## **INTRODUCTION**

Dispersion modelling constitutes a powerful tool to study the fate of emitted radioactive nuclides during and after a radiological event (e.g. after releases from nuclear power plant accidents, radiological dispersion devices and fallout after nuclear detonations).

In order to accurately describe transport and dispersion of different pollutants and hazardous substances in the atmosphere, meteorological aspects as well as compound specific dynamical processes must be taken into account. On one hand, temporal and spatial variability of wind and turbulence is responsible for the actual transport of the tracer (the substance of interest that undergoes atmospheric processes), while on the other hand the tracer itself is subjected to dynamical processes acting on its chemical and physical properties. The approach in modeling these two different aspects, however, is fundamentally different.

While the actual transport requires knowledge about boundary layer dynamics, turbulence and wind, the dynamical processes do require a broad physical and chemical knowledge and a firm understanding of the importance of different processes in different environments. To complicate matters these two aspects of transport and dispersion are largely entwined. The dynamical processes strongly determine the transport efficiency (e.g. wet removal), while at the same time the dynamical processes are influenced by meteorology and boundary layer processes.

Today, a wide range of different models addressing either of these aspects exist. However, models describing actual transport and dispersion (e.g. a Lagrangian dispersion model) usually, due to computational limitations, put less effort in describing dynamical processes affecting the tracer (may it be in aerosol or gaseous form) while detailed dynamical process models for the same reason simplify the horizontal and vertical dispersion.

At the Swedish defence research Institute (FOI), scientists have for a long period of time used Lagrangian dispersion models, e.g. PELLO (Lindqvist, 1999), as part of the work with accident preparedness and basic research. The model is implemented together with the Swedish meteorological and hydrological institute (SMHI) in the radiological emergency preparedness system at the Swedish radiation authority (SSM). This regional to global, high resolution, random displacement particle model solves the equations governing atmospheric transport of different tracers in the atmosphere. The model can be applied to study transport and dispersion of gaseous emissions, radionuclides from nuclear accidents, radioactive material from nuclear explosions as well as other, accidental, releases of toxic compounds.

Today, the model PELLO does not address aerosol dynamical processes sufficiently. Instead, the aerosol is assumed to be static, which may both underestimate or overestimate aerosol sinks, depending on transport conditions. Since the Fukushima accident in 2011 the dispersion model PELLO has been evaluated towards observations of nuclides performed during the time around the accident. These comparisons has been published in FOI reports (P. von Schoenberg & Grahn, 2013, 2014) and in conference proceedings (Pontus von Schoenberg et al., 2014). The results show that the model has good possibilities to calculate the horizontal dispersion of an aerosol in relative terms and that the magnitude of concentration and deposition is much more difficult to get accurate. To include aerosol processes during the transport is an important next step to improve model behavior.

## **METHOD**

A first step to improve the aerosol dynamic processes is to look in to the wet deposition parameterisations. The efficiency of wet deposition of particles is depending on the size, concentration and composition of the particle. The current wet deposition parameterization in PELLO only considers washout (i.e. below cloud scavenging) of aerosol particles as outlined in (Baklanov & Sørensen, 2001). Furthermore, this parameterisation considers only size dependent scavenging efficiency for different particles with diameter above 2.8µm, while being held constant for particles smaller than 2.8 µm in diameter. Thus, the current treatment overestimates below scavenging in the accumulation mode size range, while at the same time neglects in-cloud scavenging. In this study we test the sensitivity to the washout parameterisation by comparing the current one with a more rigorous but computationally more heavy deposition parameterization comes from (Seinfeld & Pandis, 1997).

To evaluate the different routines in PELLO the Fukushima nuclear power plant accident was used as a scenario. The release of <sup>137</sup>Cs from the power plant was assumed to be spherically attached to the surrounding aerosol, i.e. the activity size distribution is equal to a surface size distribution of spherical aerosols.

## **RESULT**

In Figure 1 the variation of <sup>137</sup>Cs activity in Swedish filter measurements after the Fukushima NPP accident is visualized. The measurements are compared with PELLO simulations with the two different washout parameterizations.

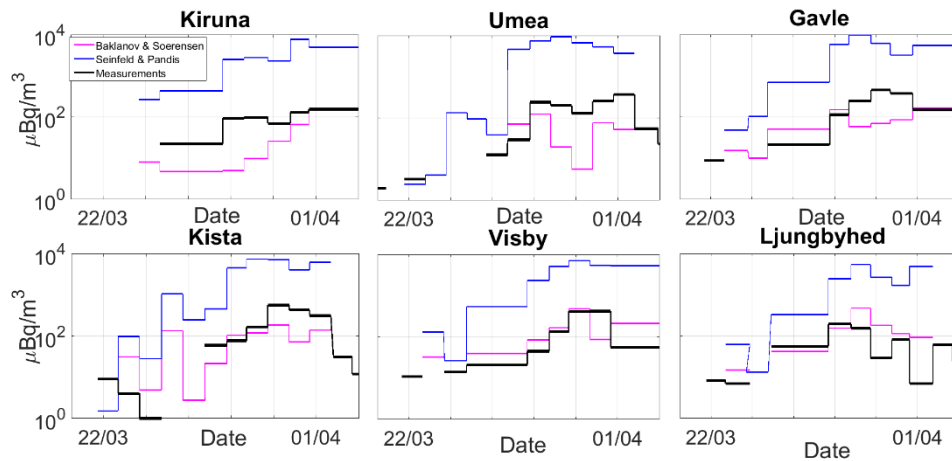


**Figure 1.** Radioactivity variation in time in Sweden after the Fukushima NPP accident. Comparison between measurements (black line) and model calculations with PELLO for the old wet deposition parameterization by Baklanov and Sørensen (purple line) and the new parameterization by Seinfeld and Pandis (blue line).

Figure 2 shows the ground level deposition patterns from wet deposition with the two different parameterization schemes. It is visible that the new wet deposition scheme gives lower deposition resulting in substantially overestimated air concentrations in Sweden. As the new scheme better captures the size dependence of scavenging efficiency for accumulation mode particles, a lower washout is to be expected. The result also highlight that there is a strong need to implement a physically based representation of in-cloud scavenging, which in turn is the most efficient removal mechanism for the rather persistent accumulation mode.

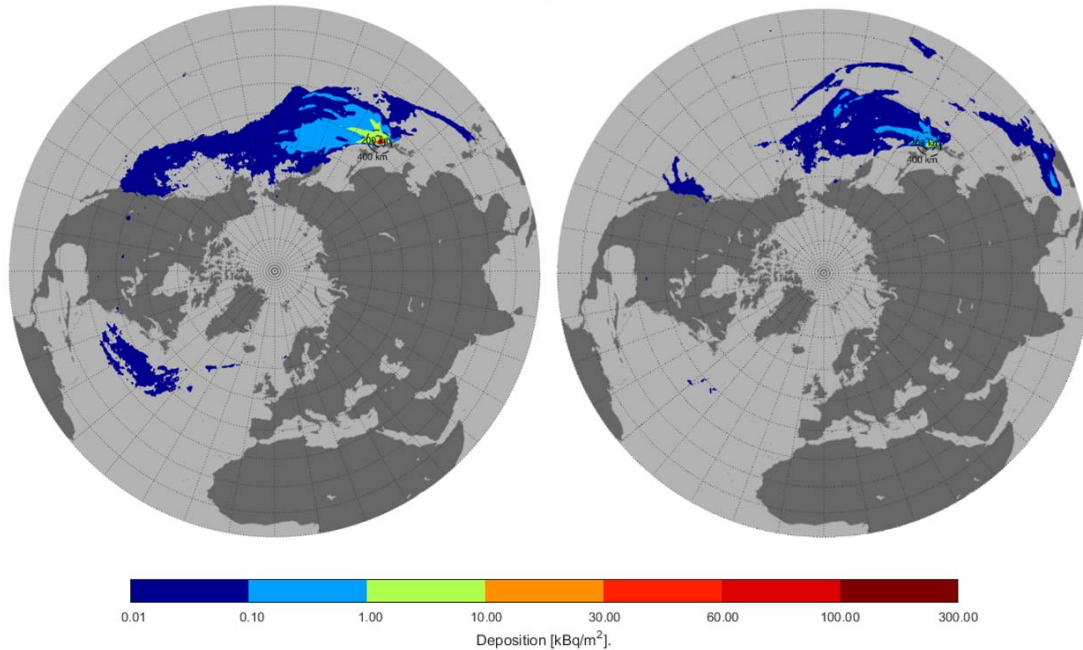


**Figure 2.** Wet deposition of  $^{137}\text{Cs}$  from the Fukushima Daiichi Nuclear power plant accident. To the left the Baklanov Sørensen parameterization and to the right the Seinfeld Pandis parameterization.

## CONCLUSIONS

As has been known for a long time accurate parameterization of wet deposition (both in-cloud and below cloud scavenging) is crucial for describing the long range transport since it is the major sink for these particles. It looks like the new scheme for the PELLO model over predicts the concentrations in Sweden

compared to measurements and compared to the old parameterization. However there are many assumptions that are not studied here that will be the purpose of future studies. The result also highlight that in-cloud scavenging is missing in the current model setup. In the old parameterization this was partially worked around by assuming unrealistically high scavenging efficiency in the accumulation mode size range, again highlighting the need for a more rigorous treatment of aerosol processes in the atmosphere. Other questions recently actualized relates to how to best use the limited amount of precipitation parameters in the numerical weather prediction model (NWP) that PELLO uses. For example to correctly separate large scale and small scale precipitation or to separate precipitation as rain and as snow.

## REFERENCES

- Baklanov, A., & Sørensen, J. H. (2001). Parameterisation of radionuclide deposition in atmospheric long-range transport modelling. *Physics and Chemistry of the Earth Part B-Hydrology Oceans and Atmosphere*, **26**, 787-799. doi:Doi 10.1016/S1464-1909(01)00087-9
- CTBTO. (2016). CTBTO, Preparatory Commission for the Comprehensive Nuclear-Test-Ban Treaty Organization. <http://www.ctbto.org/>
- Seinfeld, J. H., & Pandis, S. N. (1997). *Atmospheric Chemistry and Physics From Air Pollution to Climate Change*: John Wiley & Sons.
- von Schoenberg, P., Boson, J., Grahn, H., Nylén, T., Ramebäck, H., & Thaning, L. (2014). Atmospheric Dispersion of Radioactive Material from the Fukushima Daiichi NuclearPower Plant. *Air Pollution Modeling & its Application XXII*, 345. Retrieved from <https://ezp.sub.su.se/login?url=http://search.ebscohost.com/login.aspx?direct=true&db=edb&AN=94129118&site=eds-live&scope=site>
- von Schoenberg, P., & Grahn, H. (2013). Dispersion of radioactive material across the northern hemisphere from Fukushima Daiichi Power Plant accident modeled with a random displacement stochastic particle model (FOI-R--3746--SE).
- von Schoenberg, P., & Grahn, H. (2014). Våtdeposition av radioaktiva partiklar. Del 2. Implementation (FOI-R--3972--SE).

**17th International Conference on  
Harmonisation within Atmospheric Dispersion Modelling for Regulatory Purposes  
9-12 May 2016, Budapest, Hungary**

---

**IMPACT OF BIOGENIC EMISSION MODEL AND LANDUSE ON ISOPRENE AND OZONE  
CONCENTRATIONS FROM A CHEMICAL TRANSPORT MODEL**

*Kinga Walaszek<sup>1</sup>, Małgorzata Werner<sup>1</sup>, Maciej Kryza<sup>1</sup> and Carsten Ambelas Skjøth<sup>2</sup>*

<sup>1</sup>Department of Climatology and Atmosphere Protection, University of Wrocław, Wrocław, Poland

<sup>2</sup>National Pollen and Aerobiology Research Unit, University of Worcester, Worcester, United Kingdom

**Abstract:** Information about isoprene emissions is important for calculating ozone concentrations, but it is difficult to estimate because of its short atmospheric lifetime. Many factors affect isoprene production in emission models, including forest area and tree species composition. Here, the Weather Research and Forecasting model with Chemistry (WRF-Chem) is applied for three spatial domains, covering the area of Europe and Poland, for a high ozone episode of July 2010. Four simulations were run, two with Guenther biogenic emission model and two with Model of Emissions of Gases and Aerosols from Nature (MEGAN). WRF-Chem simulations for the same emission model differ in land use – one was run with US Geological Survey Land Cover (USGS) data as input and one with CORINE Land Cover, merged with USGS for areas where CORINE was not available. All model runs use the same configuration, including time-dependent TNO MACC II anthropogenic emission data. Modelled isoprene concentrations were evaluated with data from the EMEP measurement sites for the outermost domain, whereas ozone concentrations were evaluated for all three domains with measurements from rural and urban background stations from the AirBase database. The results show that both the land use and biogenic emission model impact ozone and isoprene concentrations, however the role of the emission model is more significant.

**Key words:** *isoprene, ozone, air quality model, landuse, biogenic emission, Poland.*

## **INTRODUCTION**

Ozone (O<sub>3</sub>) is one of the most problematic summertime air pollutants in Central Europe from a health perspective. It is a secondary air pollutant and its concentration depend on meteorological conditions causing large variation in time and space. Another important factor determining ozone formation is emission of its precursors, mainly nitrous oxides (NO<sub>x</sub>) and volatile organic compounds (VOC; Atkinson and Arey, 2003; Karl et al., 2009). The primary source of NO<sub>x</sub> is human activity (road transport and combustion processes in industry), while the picture is much more complicated with VOCs. They are produced by industry and emitted from plants, so called biogenic VOCs or BVOCs (Steinbrecher et al., 2009). The role of BVOC sources becomes more important on sites distant from anthropogenic emission sources (i.e. regional background stations), because their atmospheric lifetime is too short for them to be transported on long distances (Simpson et al., 1995; Vogel et al., 1995). One of the most reactive natural VOC is isoprene, which is emitted mainly by broadleaf trees. Each tree species has a specific emission rate, which also depends on air temperature and amount of sunlight reaching the canopy. Because it is difficult to measure natural emissions and the complexity of biological systems is high, there are multiple BVOC emission models available. These models can be used as standalone products (e.g. Arneth et al., 2011) or applied by chemical transport models to estimate emission of natural VOC based on meteorology and land use. The quality of the results depends on algorithms estimating emission rates and on the accuracy of meteorological input data, the detail of the land use maps (e.g. Arneth et al., 2011) and how many tree species or plant functional types are described by the emission model (Zare et al., 2012). Two of such emission models are used in this study together with the Weather Research and Forecasting model with Chemistry (WRF-Chem; Grell et al., 2005) to evaluate their ability to estimate isoprene and ozone concentrations in different environments during a high ozone episode.

## DATA AND METHODS

This study focuses on a high ozone episode of July 2010 in Poland, during which hourly O<sub>3</sub> concentrations reached 180 µgm<sup>-3</sup> on 12 measurement sites in Poland and the peak value reaching 218 µg m<sup>-3</sup> in Zabrze (South-West Poland) located in a highly populated and industrialized area. All isoprene measurements from the EMEP network were available, which includes 5 sites in Europe, which are all analysed. It should be noted that there was missing data in four of them. All ozone observations from the airbase network that are within the entire WRF-Chem model domain included XX sites are all analysed.

The WRF-Chem model version 3.6 is used to simulate weather and air pollution during July 2010. Three one-way nested domains are used, the outer domain (d01) with 36 km x 36 km grid covering the entire Europe, an intermediate domain (d02) with 12 km x 12 km for Central Europe and inner domain (d03) with a 4 km x 4 km mesh covering Poland. Four monthly simulations are performed, using two different biogenic emission models and two different land use data sets. All other physical and chemical parameterizations are the same for all simulations and the description is given e.g. in Wałaszek et al. (2016). The first biogenic emission model is the online Guenther et al. (1994) scheme. In this model isoprene is a function of temperature and photosynthetically active radiation (PAR) for forests (divided into coniferous, mixed and deciduous). Isoprene is in the Guenther scheme only temperature dependent for agricultural and grassland areas. Similarly, then other VOCs only depend on temperature. This module allows for a rough estimation of biogenic emission and usually underestimates isoprene emissions (Peckham, 2012). The second biogenic emission model is MEGAN (Model of Emissions of Gases and Aerosols from Nature; Guenther et al. 2006). It is based on a 30 s latitude by 30 s longitude resolution global dataset containing leaf area index (LAI) and plant functional types (PFT), which allows it to be applied both in global and regional studies. Two different land cover data were used for the WRF-Chem simulations: 1. The standard USGS land cover in WRF-Chem and 2. A data set where the USGS data has been replaced with the Corine Land Cover 2006 (reclassified into 24 USGS land cover classes according to Pineda et al, 2004) whenever possible. Four simulations in total were therefore conducted: two with the Guenther et al. emission model and using USGS land cover (gu) and Corine Land Cover (gc), and the MEGAN emission model with USGS land cover (mu) and Corine Land Cover (mc).

Evaluation of the model simulations was based on statistical comparison with hourly concentrations of ozone from AirBase v7 measurement sites. These sites were divided into four environment categories (Figure 1): three types with background stations (urban, suburban, rural) and one with urban traffic sites and also handled as an entire group (Table 2). Model simulations of isoprene were evaluated for the entire group (Table 1). Four error statistics are calculated for both pollutants: Mean Error, Root Mean Square Error, Index of Agreement, and Factor of Two. The differences in these indices between simulations are compared for isoprene and ozone. Additionally, the effect of the spatial resolution on the simulations of ozone, is explored by comparing the results from all three domains. Selected sites with observations of both isoprene and ozone were evaluated using time series (Figure 2) of the results from d01.

## RESULTS AND DISCUSSION

Differences in isoprene concentrations between each simulation and measurements are shown in Table 1. The presented statistics confirm that the MEGAN model is better at modelling isoprene emissions, as errors are smaller and model-measurements agreement, represented by IOA and FAC2, is more than twice higher than for Guenther et al. scheme. The impact of changing the land use is minimal where the detected differences are highest for the Guenther scheme due to slightly better statistics for Corine Land Cover data set. Nevertheless, the best simulation (mu) gives poor model-measurements agreement, with less than a half of simulated isoprene concentrations being within a factor of two from the measurements.

**Table 1.** Error statistics for isoprene concentrations for d01 domain

simulation	n	ME [µgm <sup>-3</sup> ]	RMSE [µgm <sup>-3</sup> ]	IOA	FAC2
gu	1359	-0.20	1.32	0.21	0.10
gc	1359	-0.22	1.28	0.24	0.12
mu	1359	-0.11	0.56	0.60	0.48
mc	1359	-0.11	0.56	0.60	0.49

For ozone, results from all three domains and all simulations are presented in Table 2. The WRF-Chem model results using the MEGAN emission model underestimates ozone concentrations, whereas for Guenther et al. overestimates ozone concentrations, with the smallest ME for the coarse domain (d01). The differences for other indices are very small, with lowest RMSE for Guenther et al. simulations and IOA and FAC2 on a similar level. However, FAC2 values show good model-measurements agreement – in every case more than 85% of modelled data points are within a factor of two from the measurements.

**Table 2.** Error statistic for ozone concentrations for all model domains.

		<b>n</b>	<b>MB</b>	<b>RMSE</b>	<b>IOA</b>	<b>FAC2</b>
gu		29415	3.29	23.88	<b>0.67</b>	0.85
gc	d01	29415	3.39	<b>23.61</b>	<b>0.67</b>	0.85
mu		29415	-1.76	24.00	0.66	<b>0.86</b>
mc		29415	<b>-1.61</b>	23.93	0.66	<b>0.86</b>
gu		29415	2.97	<b>24.32</b>	<b>0.66</b>	0.85
gc	d02	29415	4.72	24.68	0.65	0.85
mu		29415	-2.60	24.78	0.65	<b>0.87</b>
mc		29415	<b>-1.20</b>	24.98	0.64	0.86
gu		29415	2.38	<b>23.73</b>	<b>0.67</b>	0.86
gc	d03	29415	5.07	23.92	<b>0.67</b>	0.86
mu		29415	-4.45	25.17	0.64	<b>0.87</b>
mc		29415	<b>-2.30</b>	24.96	0.65	<b>0.87</b>

Figure 1 presents average ozone concentrations for all available European measurement sites within the d01 domain for two simulations – Guenther et al. with USGS landuse and MEGAN with Corine landuse. The figures show the measurement sites located in the four different environments. There are very small differences between the simulations, as in both cases ozone concentrations at urban and traffic sites are generally overestimated, particularly low values. At suburban background stations high concentrations have tendency for underestimation, whereas there is no pattern for rural sites. Overall, there is a good model-measurements agreement, with the exception of a few outliers.

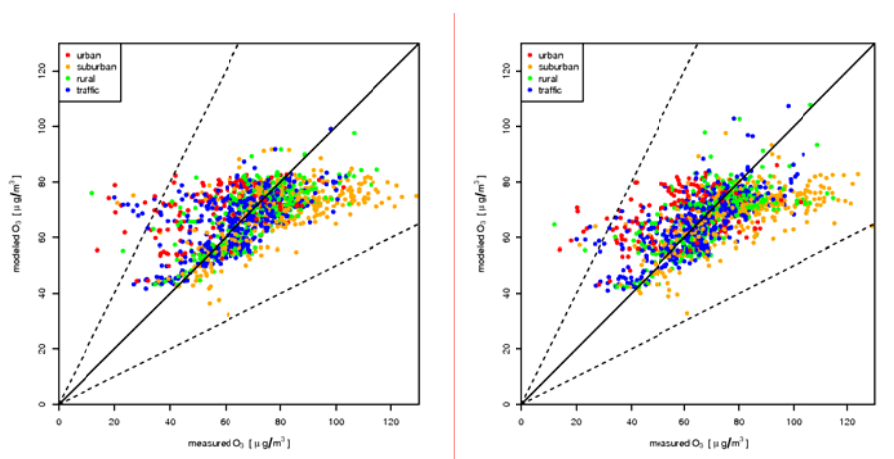


**Figure 1.** Average ozone concentrations on all European measurement sites for gu and mc simulations. Dotted lines denote 2:1 and 1:2 ratios

Time series of isoprene concentrations, shown in Figure 2, present much more variability in the simulations running with the MEGAN model compared to the Guenther scheme. However, modelled

ozone concentrations are very similar for both the urban background site and for the rural site simulations running with the Guenther et al. scheme, thereby giving higher daily maxima of ozone.

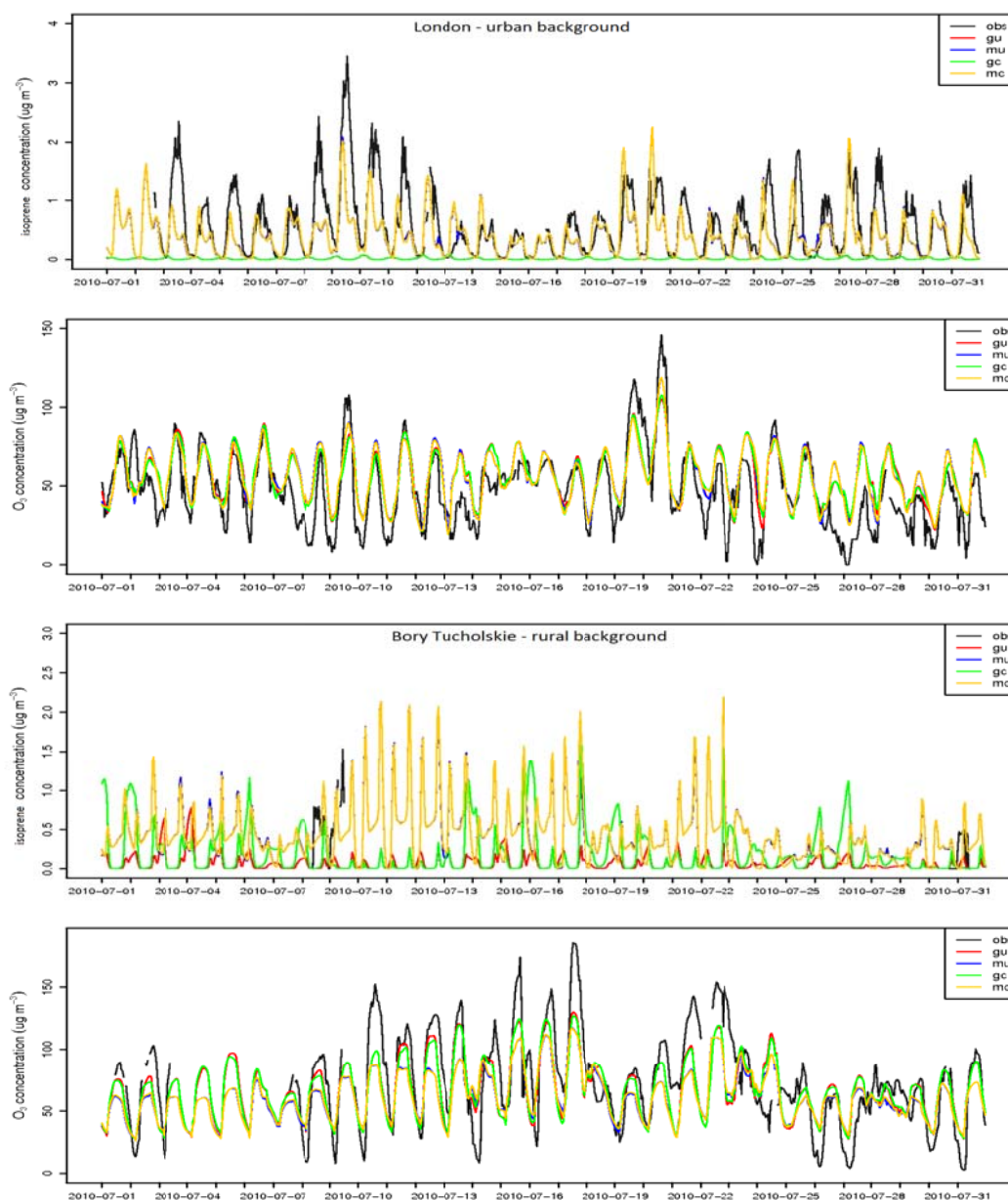


**Figure 2.** Hourly ozone and isoprene concentrations at urban background station in London, UK and rural station in Bory Tucholskie, Poland, during the study period

One potential explanation to this could be that both Poland and England have relatively limited isoprene emission from trees compared to other regions, where emission of monoterpenes and oxygenated volatile organic compounds are considered to be higher in these areas (Oderbolz et al., 2013). These other BVOCs have a more complex description in the MEGAN model.

## CONCLUSIONS

The model does not represent isoprene concentrations well – this is most likely due to high temporal and spatial variability of isoprene and its high chemical reactivity, as well as many simplifications in estimating emission rates from both models. However, despite large uncertainties in isoprene, it is still possible to

accurately estimate ozone concentrations on multiple spatial scales. The results show that better model performance for isoprene concentrations does not always implicate better ozone concentrations – in this case MEGAN biogenic emissions model gives more accurate isoprene predictions, but at the same time produces larger uncertainties in ozone concentrations. One possible reason for this may be inaccurate emission of other ozone precursors, which results in different model sensitivity to changes in isoprene emissions. The results of isoprene concentrations should be analysed carefully, because there were only 5 measurement sites available for the whole Europe and there was a lot of missing data. The only site with a complete dataset for the study period is urban background station in London, UK.

#### ACKNOWLEDGEMENTS

The project was supported by the Polish National Science Centre project no. UMO-2013/09/B/ST10/00594 and by European Union and co-financed by NFOSiGW within LIFE+ Program, Project: LIFE-APIS/PL - Air Pollution and Biometeorological Forecast and Information System. LIFE12 ENV/PL/000056.

#### REFERENCES

- Arneth, A., G. Schurgers, J. Lathiere, T. Duhl, D. J. Beerling, C. N. Hewitt, M. Martin, and A. Guenther, 2011: Global terrestrial isoprene emission models: sensitivity to variability in climate and vegetation. *Atmospheric Chemistry and Physics*, **11(15)**, 8037–8052.
- Atkinson, R. and J. Arey, 2003: Gas-phase tropospheric chemistry of biogenic volatile organic compounds: a review. *Atmospheric Environment*, **37**, 197–219.
- Grell, G., S. Peckham, and R. Schmitz, 2005: Fully coupled “online” chemistry within the WRF model. *Atmospheric Environment*, **39**, 6957–6975.
- Guenther, A., T. Karl, P. Harley, C. Wiedinmyer, P. I. Palmer, and C. Geron, 2006: Estimates of global terrestrial isoprene emissions using MEGAN (Model of Emissions of Gases and Aerosols from Nature). *Atmospheric Chemistry and Physics*, **6(11)**, 3181–3210.
- Guenther, A., P. Zimmerman, and M. Wildermuth, 1994: Natural volatile organic compound emission rate estimates for U.S. woodland landscapes. *Atmospheric Environment*, **28(6)**, 1197–1210.
- Karl, M., A. Guenther, R. Köble, A. Leip, and G. Seufert, 2009: A new European plant-specific emission inventory of biogenic volatile organic compounds for use in atmospheric transport models. *Biogeosciences*, **6(6)**, 1059–1087.
- Oderbolz, D.C., S. Aksoyoglu, J. Keller, I. Barmpadimos, R. Steinbrecher, C. A. Skjøth, C. Plaß-Dülmer, and A. S. H. Prévôt, 2013: A comprehensive emission inventory of biogenic volatile organic compounds in Europe: improved seasonality and land-cover. *Atmospheric Chemistry and Physics*, **13(4)**, 1689–1712.
- Peckham, S.E., 2012: *WRF/Chem Version 3.3 User's Guide*, U.S. Department of Commerce, National Oceanic and Atmospheric Administration, Oceanic and Atmospheric Research Laboratories, Global Systems Division.
- Pineda, N., O. Jorbab, J. Jorgea, and J. M. Baldasano, 2004: Using NOAA AVHRR and SPOT VGT data to estimate surface parameters: application to a mesoscale meteorological model. *International Journal of Remote Sensing*, **25(1)**, 129–143.
- Simpson, D., A. Guenther, C. N. Hewitt, and R. Steinbrecher, 1995: Biogenic emissions in Europe: 1. Estimates and uncertainties. *Journal of Geophysical Research: Atmospheres*, **100(D11)**, 22875–22890.
- Steinbrecher, R., G. Smiatek, R. Köble, G. Seufert, J. Theloke, K. Hauff, P. Ciccioli, R. Vautard, and G. Curci, 2009: Intra- and inter-annual variability of VOC emissions from natural and semi-natural vegetation in Europe and neighbouring countries. *Atmospheric Environment*, **43(7)**, 1380–1391.
- Vogel, B., F. Fiedler, and H. Vogel, 1995: Influence of topography and biogenic volatile organic compounds emission in the state of Baden-Württemberg on ozone concentrations during episodes of high air temperatures. *Journal of Geophysical Research: Atmospheres*, **100(D11)**, 22907–22928.
- Wałaszek, K., M. Kryza, M. Werner, and H. Ojrzńska, 2016: Sensitivity of ground-level ozone to NOx emission during a high ozone episode in SW Poland. *Air Pollution Modelling and its Applications XXIV*, 339–343.
- Zare, A. J. H. Christensen, P. Irannejad, and J. Brandt, 2012: Evaluation of two isoprene emission models for use in a long-range air pollution model. *Atmospheric Chemistry and Physics*, **12(16)**, 7399–7412.

**17th International Conference on  
Harmonisation within Atmospheric Dispersion Modelling for Regulatory Purposes  
9-12 May 2016, Budapest, Hungary**

---

**SIMULATING LARGE EMITTERS USING CMAQ AND A LOCAL SCALE FINITE ELEMENT  
MODEL. ANALYSIS IN THE SURROUNDINGS OF BARCELONA**

*Albert Oliver<sup>1</sup>, Raúl Arasa<sup>2</sup>, Agustí Pérez-Foguet<sup>3</sup>, and M<sup>a</sup> Ángeles González<sup>2</sup>*

<sup>1</sup>University Institute for Intelligent Systems and Numerical Applications in Engineering (SIANI),  
University of Las Palmas de Gran Canaria (ULPGC), Las Palmas de Gran Canaria, Spain

<sup>2</sup>Technical Department, Meteosim S.L., Barcelona, Spain

<sup>3</sup>Engineering Sciences & Global Development (EScGD), University Research Institute for Sustainability  
Science and Technology (IS.UPC), Department of Civil and Environmental Engineering, ETSECCPB,  
Universitat Politècnica de Catalunya (UPC), Barcelona, Spain

**Abstract:** In this work, we compare two state of the art models to simulate large emitters in the local scale. The area of study is in the surroundings of Barcelona, where an important contributor to the SO<sub>2</sub> levels is considered. The first modelling system uses the mesoscale meteorological model WRF-ARW, the Air Emission Model of Meteosim, AEMM, and the air quality model CMAQ. The second model is a one way nesting of the results from the first system in a subgrid Finite Element model; the results from the CMAQ simulation are used as initial and boundary conditions. The simulations have been carried out for two episodes. We have chosen an episode with high levels of SO<sub>2</sub>, and another day with atmospheric stability. The time period of the simulations is of 48h with a 24h spin-up.

**Key words:** *Local scale, Air Quality Modelling, Large Emitters, WRF-CMAQ, Finite Element Method.*

## **INTRODUCTION**

Air quality is an environmental issue that affects directly to the population. According to the World Health Organization, it is estimated that air pollution affects much of the population, with 2.4 million deaths annually (EEA, 2007). For this reason the study of its impact, specially in urban areas is of vital importance.

Mesoscale air quality models are not enough to calculate the concentrations in the local scale that affect the health. For this reason efforts have been made to simulate the local scale using different techniques (Karamchandani et al. 2011). The most commonly used approaches are the nested grid, Plume-in-Grid (PinG), and hybrid models. The nested grid modelling is used in the U.S. Environmental Protection Agency models-3/CMAQ model (Byun et al. 2006). It uses grids with fine resolution in small domains within the larger domain, sometimes with more than one level of refinement. The Plume-in-Grid (PinG) model uses a puff or plume model in the grid model. The plume model simulates the subgrid scale processes and returns the solution to the grid model. So this technique is two-way. SCICHEM uses this technique and can be coupled to CMAQ (Karamchandani et al 2002, 2008). The hybrid models combines the solution from a coarse grid model and a local plume model. It is being used to model the population exposure to hazardous air pollutants, e.g. using CMAQ and the Hazardous Air Pollutant Exposure Model HAPEM (Rosenbaum 2005) to predict the exposure estimates (Isakov et al. 2007). This technique combines both solutions in a one-way approach, being this one the main difference with PinG.

In this work we propose two different sub-grid strategies and compare their results. The first strategy is an Eulerian coupled modelling system using the meteorological model WRF-ARW (Skamarock 2008), an emission model developed by Meteosim AEMM (Arasa 2013, 2014, 2016) and CMAQ. The other strategy is an adaptive, Eulerian, non-steady finite element model that uses the photochemical model of CMAQ (Oliver 2013).

## METHODOLOGY

In the following sections we show a more detailed description of the studied areas as well as the simulation domains and periods analysed and the modelling approach.

### Studied area

The area of interest is in the surrounding of Barcelona. We will study the emission of a large emitter of SO<sub>2</sub> in the atmosphere. In Figure 1 we show the simulation domains used by the CMAQ modelling system. In Figure 2 you can see a zoom of the smaller domain, and the location of the emitter, and the domain of the finite element method. The domain of the finite element model is smaller due to the computational cost.

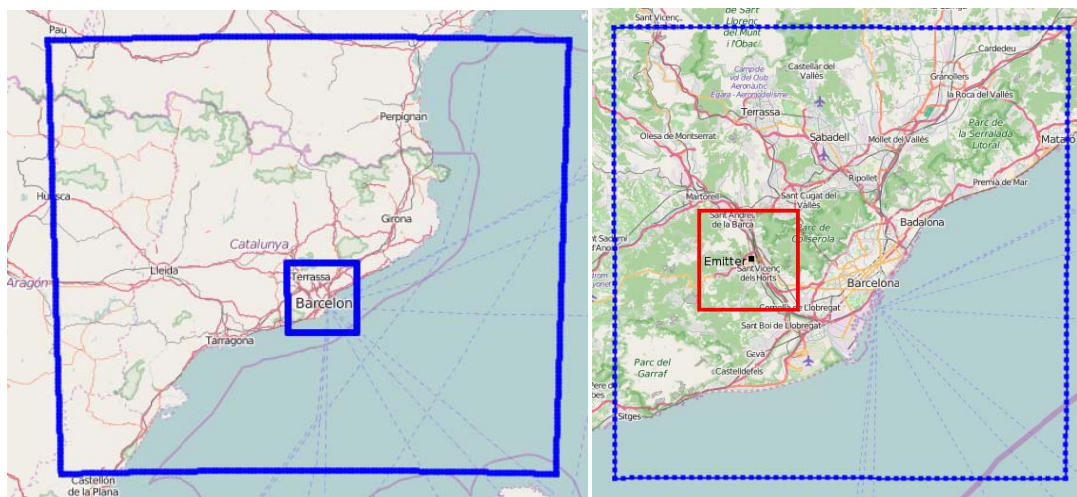


**Figure 1.** Models domains for simulation (left). Zoom of the inner domain. The red domain is the one used in the finite element model with the emitter position (right)

### Emitter characteristics

The emitter is located at position 416442m, 4584580m (UTM 31N). It has a height of 125m, and a diameter of 4.25m. The emission of SO<sub>2</sub> is 105t year<sup>-1</sup> with a velocity of 10.33m s<sup>-1</sup>.

### Modelling episodes

The simulations have been carried out on two different days with different characteristics. The criteria to choose the days, were to have a day with a high concentration of SO<sub>2</sub> and another day with atmospheric stability. These criteria have been selected to test the finite element model with different conditions, and to compare the results with the CMAQ system and determine in which scenarios works better.

The chosen days are the second of December, 2013 for the day with high concentration levels, and the fourth of December, 2015 for the day with atmospheric stability.

### Modelling approach

Next, we outline the main feature of the two models presented in this work.

#### WRF-ARW/AEMM/CMAQ

We have used an Eulerian coupled modeling system (WRF-ARW/AEMM/CMAQ). The mesoscale meteorological model used is Weather Research and Forecasting—Advanced Research (WRF-ARW) version 3.6.1.(Skamarock, 2008), Air Emission Model of Meteosim (AEMM v3.0) is a numerical, deterministic, Eulerian, local-scale model developed by Meteosim S.L. It allows to obtain the intensity of emissions in different areas, either anthropogenic (traffic, industry, residential, etc.) or natural (emissions caused by vegetation or erosion dust) for the area of interest. And the U.S. Environmental Protection Agency models-3/CMAQ model is the one used to simulate the physical and chemical processes into the atmosphere. CMAQ is an open-source photochemical model which is updated periodically by the research community. In this contribution we use CMAQ v5.0.1, considering CB-5 chemical mechanism and associated EBI solver (Yarwood, 2005), and AERO5 aerosol module (Carlton, 2010).

For each of the selected days we have run numerical simulations for 48 hours, leaving the first 24 hours as a spin-up to minimize the consequences of taking into account the initial conditions for the start of simulation. The vertical structure of the model includes 32 vertical layers.

#### Finite Element model

The finite element model is composed by a mesh generator, a wind mass-consistent model, a plume-rise model, and finally the transport and reaction of pollutants is performed with a finite element method stabilized with Least Squares. The model is coupled with the CMAQ system model in a one-way nesting, i.e. the results from the CMAQ system are used as boundary and initial conditions in the finite element model.

A tetrahedral mesh adapted to the terrain is constructed using the Delaunay-based tetrahedral mesh generator Tetgen (Si, 2015). The mesh incorporates some layers to emulate those in CMAQ.

The wind field is computed interpolating the results from the WRF-ARW simulation, and using a mass-consistent model (Oliver, 2015). Once the wind field is computed the plume rise has to be taken into account. Using the Briggs formulation a three-dimensional trajectory of the plume is computed, and the wind field is perturbed so that the pollutants that are emitted follow the trajectory of the plume.

The transport and reaction of pollutants is simulated splitting the transport and the chemistry. The transport is solved using a finite element method stabilized with Least Squares. To solve the system an incomplete Cholesky factorization has been used. The chemical mechanism used is the same used by the CMAQ system. To improve the accuracy of the results and the computational cost an adaptive technique is used. It has been proven for various convection-diffusion problems (Monforte, 2014). To improve the computational cost the model has been parallelized using a multimesh strategy (Monforte, 2013).

### PRELIMINARY RESULTS

In the following sections we describe the results that have been obtained with the two strategies.

#### WRF-ARW/AEMM/CMAQ model

The first step to simulate the air quality has been the meteorological simulation using the WRF-ARW. We have simulated the meteorological situation using the two nested domains show in Figure 1. The result from the simulation has been used to feed the CMAQ simulation. CMAQ uses the same configuration as the WRF simulation. Initial and boundary conditions for the nested domain are provided by the results of the larger domain. Meteorology-Chemistry Interface Processor (MCIP) version 4.1 is used to prepare WRF output to CMAQ model. And AEMM model prepares emissions as AERO5 and CB5 modules require.

The two episodes selected have been simulated. Figure 2 represents the maximum concentration of SO<sub>2</sub> for the selected days.

#### Finite element model

To simulate the air pollution using the finite element model we need to generate a tetrahedral mesh adapted to the terrain. The discretization of the terrain that we have used is from the shuttle radar topography mission (Farr et al., 2007), specifically the SRTM3 version defined over an uniform grid of 3" × 3" (approximately 90 m × 90 m). The resulting mesh element size ranges from tens of centimeters to hundreds of meters. In Figure 3 you can see a detail of the terrain discretization.

With this mesh, the wind field is simulated, and the transport and reactions of pollutants is computed using the results from the CMAQ system modelling as boundary and initial conditions as a one-way nesting.

With the results of the air quality using the finite element method, a comparison between the results of both methods against measured data will be carried.

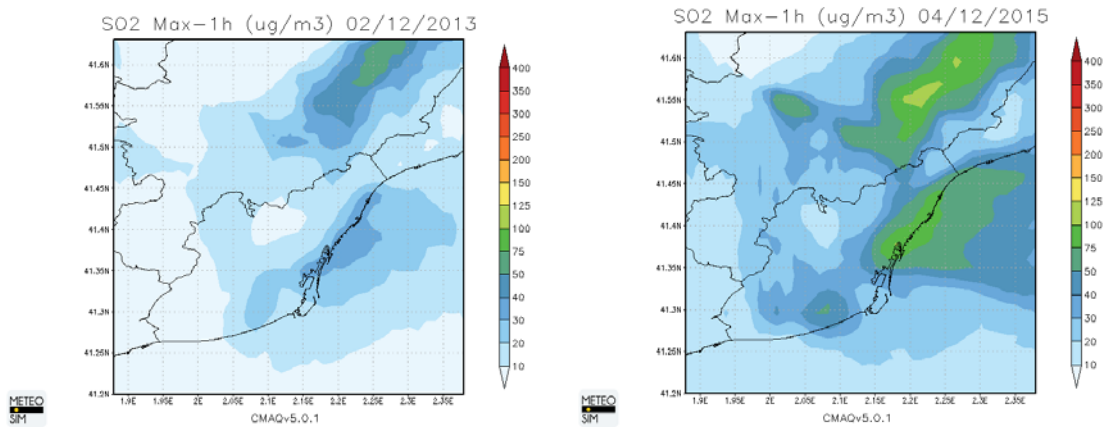


**Figure 2.** Results from CMAQ system simulation. Max. SO<sub>2</sub> concentration for 2013 episode (left) and 2015 episode (right)

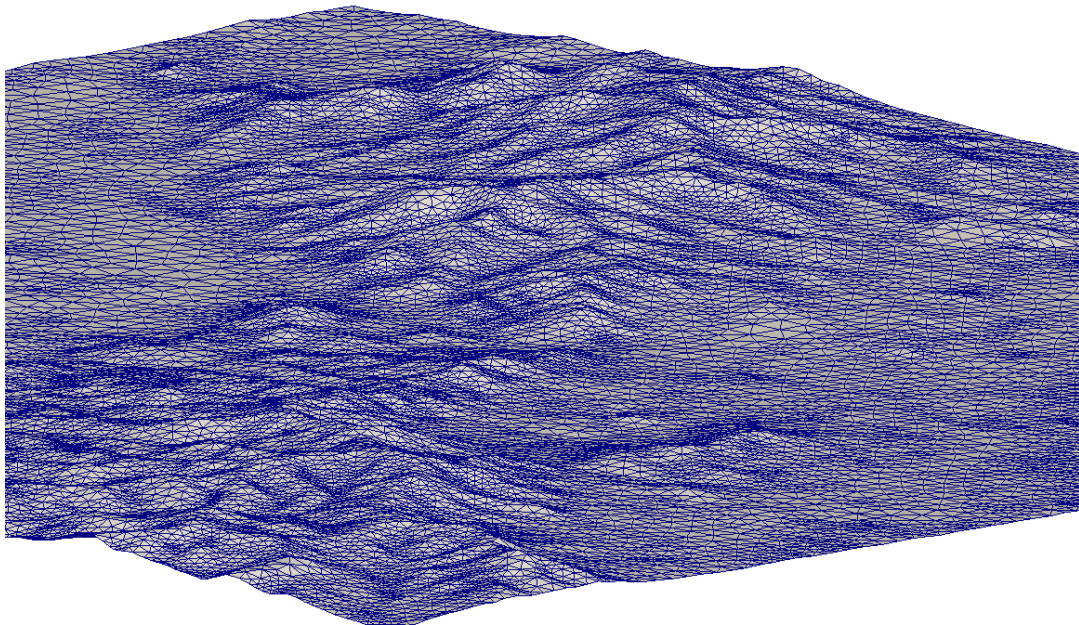


**Figure 3.** Detail of the tetrahedral mesh with the terrain discretization

## REFERENCES

- Arasa, R., Picanyol, M., and Solé, J.M., 2013. Analysis of the Integrated Environmental and Meteorological Forecasting and Alert System (SIAM) for Air Quality Applications over Different Regions of the Iberian Peninsula. <http://www.harmo.org/Conferences/Proceedings/Madrid/publishedSections/H15-70.pdf>
- Arasa, R., Lozano-García, A. & Codina, B., 2014. Evaluating Mitigation Plans over Traffic Sector to Improve NO<sub>2</sub> Levels in Andalusia (Spain) Using a Regional-Local Scale Photochemical Modelling System. OJAP, 03(03). <http://dx.doi.org/10.4236/ojap.2014.33008>
- Arasa, R., Domingo-Dalmau, A. and Vargas, R., 2016. Using a Coupled Air Quality Modeling System for the Development of an Air Quality Plan in Madrid (Spain): Source Apportionment and Analysis Evaluation of Mitigation Measures. Journal of Geoscience and Environment Protection, 04(03). <http://dx.doi.org/10.4236/gep.2016.43005>
- Byun, D. and Schere, K.L., 2006. Review of the Governing Equations, Computational Algorithms, and Other Components of the Models-3 Community Multiscale Air Quality (CMAQ) Modeling System. Appl. Mech. Rev., 59(2). <http://dx.doi.org/10.1115/1.2128636>

- Carlton, A.G. Bhawe PV., Napelenok, S.L., Edney, E.O., Sarwar, G., Pinder, R.W., Pouliot, G.A., and Houyoux, M., 2010. Model Representation of Secondary Organic Aerosol in CMAQv4.7. *Environ. Sci. Technol.*, 44(22). <http://dx.doi.org/10.1021/es100636q>
- EEA, 2007. Air Pollution in Europe 1990–2004. EEA Report No2/2007. European Environment Agency, Copenhagen
- Farr, T.G., Rosen, P.A., Caro, E., Crippen, R., Duren, R., Hensley, S., Kobrick, M., Paller, M., Rodriguez, E., Roth, L., Seal, D., Shaffer, S., Shimada, J., Umland, J., Werner, M., Oskin, M., Burbank, D., and Alsdorf, D., 2007. The Shuttle Radar Topography Mission. *Reviews of Geophysics*, 45(2). <http://dx.doi.org/10.1029/2005rg000183>
- Isakov, V., Irwin, J.S., and Ching, J., 2007. Using CMAQ for Exposure Modeling and Characterizing the Subgrid Variability for Exposure Estimates. *Journal of Applied Meteorology and Climatology*, 46(9). <http://dx.doi.org/10.1175/jam2538.1>
- Karamchandani, P., 2002. Development and application of a state-of-the-science plume-in-grid model. *Journal of Geophysical Research*, 107(D19). <http://dx.doi.org/10.1029/2002jd002123>
- Karamchandani, P., Lohman, K., and Seigneur, C., 2008. Using a sub-grid scale modeling approach to simulate the transport and fate of toxic air pollutants. *Environ Fluid Mech*, 9(1). <http://dx.doi.org/10.1007/s10652-008-9097-0>
- Karamchandani, P., Vijayaraghavan, K., and Yarwood, G., 2011. Sub-Grid Scale Plume Modeling. *Atmosphere*, 2(4). <http://dx.doi.org/10.3390/atmos2030389>
- Monforte, L. and Pérez-Foguet, A., 2013. A multimesh adaptive scheme for air quality modeling with the finite element method. *Int. J. Numer. Meth. Fluids*, 74(6). <http://dx.doi.org/10.1002/flid.3855>
- Monforte, L. and Pérez-Foguet, A., 2014. Esquema adaptativo para problemas tridimensionales de convección-difusión. *Revista Internacional de Métodos Numéricos para Cálculo y Diseño en Ingeniería*, 30(1). <http://dx.doi.org/10.1016/j.rimni.2012.11.003>
- Oliver, A., Montero G., Montenegro R., Rodríguez E., Escobar J.M., Pérez-Foguet A., 2013. Adaptive finite element simulation of stack pollutant emissions over complex terrains. *Energy*, 49. <http://dx.doi.org/10.1016/j.energy.2012.10.051>
- Oliver, A., Rodríguez, E., Escobar, J.M., Montero, G., Hortal, M., Calvo, J., Cascón, J.M., and Montenegro, R., 2015. Wind Forecasting Based on the HARMONIE Model and Adaptive Finite Elements. *Pure Appl. Geophys.*, 172(1). <http://dx.doi.org/10.1007/s00024-014-0913-9>
- Si, H., 2015. TetGen, a Delaunay-Based Quality Tetrahedral Mesh Generator. *TOMS*, 41(2). <http://dx.doi.org/10.1145/2629697>
- Rosenbaum, A. The HAPEM5 User's Guide, Hazardous Air Pollutant Exposure Model, Version 5. [https://www.epa.gov/sites/production/files/2013-08/documents/hapem5\\_guide.pdf](https://www.epa.gov/sites/production/files/2013-08/documents/hapem5_guide.pdf)
- Skamarock, W.C. and Klemp, J.B., 2008. A time-split nonhydrostatic atmospheric model for weather research and forecasting applications. *Journal of Computational Physics*, 227(7). <http://dx.doi.org/10.1016/j.jcp.2007.01.037>
- Yarwood, G., Rao, S., Yocke, M., and Whitten, G.Z., 2005. Updates to the Carbon Bond Chemical Mechanism: CB05. Final Report Prepared for US EPA. [http://www.camx.com/publ/pdfs/CB05\\_Final\\_Report\\_120805.pdf](http://www.camx.com/publ/pdfs/CB05_Final_Report_120805.pdf)

**17th International Conference on  
Harmonisation within Atmospheric Dispersion Modelling for Regulatory Purposes  
9-12 May 2016, Budapest, Hungary**

---

**VALIDATION OF GAUSSIAN PLUME MODEL AEROPOL AGAINST CABAUW FIELD  
EXPERIMENT**

*Marko Kaasik<sup>1</sup>, Gertie Geertsema<sup>2</sup> and Rinus Scheele<sup>2</sup>*

<sup>1</sup>Institute of Physics, University of Tartu, Tartu, Estonia

<sup>2</sup>Royal Dutch Meteorological Institute, De Bilt, Netherlands

**Abstract:** The Gaussian dispersion model AEROPOL is validated against Cabauw (1977 – 1978) data set, applying the parameters and rules described in the Model Validation Kit. The purpose to revisit this classical experiment is preparation for fast response to elevated (buoyant) accidental releases. In AEROPOL model (Kaasik & Kimmel, 2003) two alternatives for dispersion parameterisations are used: (i) classical Pasquill-Gifford stability and (ii) a scheme based on Lagrangian time scales by Gryning *et al.* (1987). Validation is based on correlation, fractional bias, fractional sigma, NMSE and fraction in factor 2, applying these statistics to maximal arc-wise, near-centreline and cross-wind integrated concentrations. Both parameterisations are found fairly adequate. Pasquill-Gifford parameterisation performs somewhat better, except for correlations, which exceed even 0,9 with Gryning scheme. Gryning scheme results in too wide Gaussian spread and thus, lower maxima compared to measurements, whereas the Pasquill parameterisation gives sharper maxima, which makes the statistics more sensitive to the small discrepancies in plume position. The average wind speed and direction between the lowest measurement level and release level was found a good approximation for effective wind according to position of Gaussian plume.

**Key words:** *Gaussian plume, dispersion experiment, Cabauw, AEROPOL, HARMONIE, Model Validation Kit.*

## **INTRODUCTION**

The purpose of revisiting the classical dispersion experiment in Cabauw (Agterberg *et al.*, 1983) is a better understanding of dispersion from elevated (buoyant) accidental releases, such as 2011 in Moerdijk, and preparation for fast response.

A fire at the chemical plant Chemie-Pack on January the 5th of 2011 resulted in a large-scale accident with the release of many different hazardous materials. The accident lasted almost a day, though the fire was under control after some ten hours. Due to the enormous heat the hazardous material was ejected into the atmosphere at heights of several tens of meters to hundreds of meters, where the wind direction was more easterly (veered) with respect to the wind at lower heights. Moerdijk is about 40 km south of the port of Rotterdam and even closer to the cities Dordrecht and Rotterdam, which are part of the densely populated western parts of the Netherlands which include The Hague and Amsterdam, and the impact could have been disastrous. Luckily the weather situation was such that the hazardous material was dispersed at higher altitudes. Due to vertical shear the plume was essentially split over two heights. The lower plume moved towards the city of Dordrecht. Shipping traffic towards the Moerdijk area was halted and the motorway was closed. The upper plume was advected in the direction of Flevoland where much of the food for the citizens is grown, resulting in another concern for public health.

Extensive evaluation of the accident showed the need for mesoscale dispersion models capable of capturing vertical wind shear and precipitation. Dispersion models available to assist the emergency responders were either appropriate for short range and short-lived accidents or for long range accidents. The Moerdijk accident showed the need for high-resolution dispersion models using numerical weather forecasts up to a distance of several tens of kilometers. A project to implement a mesoscale dispersion model for the Dutch emergency response has since been launched. In this report we investigate the validation and verification of the dispersion model the experiments at the Cabauw mast. Two questions

have to be answered: (1) is the quality of these older measurements up to par for the present state-of-art dispersion models and (2) is it possible to reconstruct the weather with the latest high-resolution numerical weather prediction models. The first question is tested using the dispersion model AEROPOL with two different parameter schemes. The second question is answered by a reconstruction of the weather in 1977 and 1978 using HARMONIE v.38 (<http://www.hirlam.org>) nested in ERA40 (<http://www.ecmwf.int>).

### CABAUW DATASET

The dispersion experiment was carried out in Cabauw atmospheric measurement site in 1977-1978, using the facilities of a 213 m high mast (<http://www.cesar-observatory.nl>). The data set consists of 28 half-hourly runs – two sequent half hours per day, thus 14 days in total. The SF<sub>6</sub> tracer was released from the height either at 80 or 200 m depending on pre-estimated dispersion conditions, and measured at surface level on an arc 2 – 5 km downwind. As during two half-hours the arc-wise maximal concentration was obviously out of the arc, these experiments were excluded from the comparison. The comparison is made on hourly basis, except these two days, when one of half-hours was excluded. Thus, number of valid cases is 14. The data set includes on-site evaluated meteorological parameters, which were used for modelling: temperature, wind speed and direction at different heights in the mast, surface turbulent heat flux. More detail parameters included in the data, such as standard deviations of wind speed and direction, are not used, as the minimalistic application-oriented AEROPOL model does not need them.

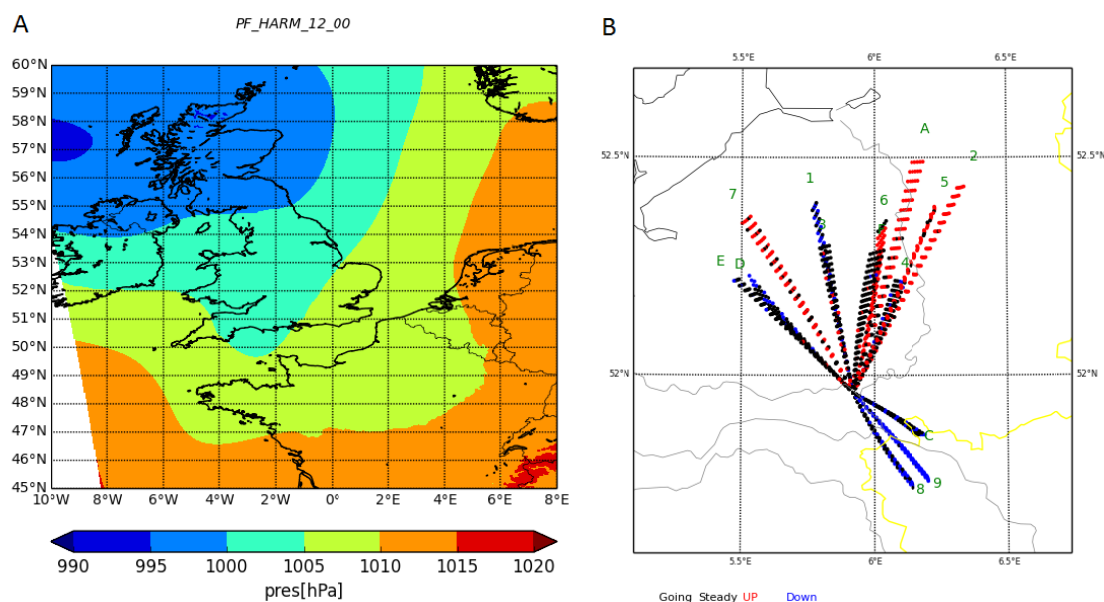


**Figure 1.** The panel A shows the pressure at mean sea level at 1977042812 UTC calculated by HARMONIE. The panel B shows trajectories with a colour code for a constant height (black), an upward movement (red) or a downward movement (blue) for all experiments. For each experiment a trajectory is calculated every 15 minutes and the location is plotted every 5 minutes. A vertical displacement upward larger than 1 meter per 5 minutes is defined as an ascending trajectory (red). Descending is defined as a vertical displacement downward of more than 1 meter per 5 minutes. The numbers denote the experiments 1-9, the letters represent experiments 10-15, with A for the 10<sup>th</sup> experiment.

### MODELS AND METHODS

The data from this dispersion experiment is downloaded from <http://www.jsirwin.com/>. The synoptic weather charts for the 14 different cases are provided in Agterberg et al (1983). We analysed the synoptic weather using the ERA40 reanalysis dataset. Based on the 3D-wind information from the ERA40 reanalysis dataset, the trajectory model TRAJKS (Stohl et al., 2001) calculated the advection of the centre of the plume. Figure 1 shows whether the trajectories are ascending (in red), descending (in blue) or move at a constant height (in black). In experiments 1 and 3 the trajectories coincide, in both experiments the

centre of the plume is advected towards NNW. In experiment 1 the centre of the plume ascends in the first kilometres and descends afterwards. Trajectories are calculated starting at the source location every 15 minutes and from the spread in the trajectories it can be seen that the wind direction did not change significantly during the release period. In the third experiment the spread in the horizontal location of the plume is larger whereas the spread in the vertical is small and the trajectories stay at the same height.

AEROPOL (basic features, see Kaasik & Kimmel, 2003) is a stationary Gaussian plume model developed in University of Tartu, Estonia. AEROPOL 5.2, applied in this study, enables two alternative parameterisations for dispersion parameters:

- classical Pasquill-Gifford stability classification (further referred as Pasquill scheme);
- a scheme based on Lagrangian time scales, developed by Gryning et al. (1987) and validated against the Copenhagen dispersion experiment (further referred as Gryning scheme).

Both the parametrisation schemes apply the wind speed and surface heat flux as key input parameters, whereas Pasquill classes are evaluated as a discrete empirical function of surface roughness and Monin-Obukhov length, applying the approach by Myrup & Ranzieri (1976). The detail description of the method is given by Kaasik & Kerner (2010).

The model vs. measurement intercomparison follows the standard of the Model Validation Kit of the HARMO initiative. The validated output parameters are cross-wind integrated, maximal arc-wise and near-centreline concentrations. Validation is based on correlation (COR), fractional bias (FB), fractional sigma (FS), normalised mean square error (NMSE) and fraction of measured vs. modelled values in factor of two (FA2). The near-centreline concentration is defined as average of concentrations between  $-0.67\sigma_y$  and  $0.67\sigma_y$ , where  $\sigma_y$  is the horizontal standard deviation of the plume in Gaussian approximation (Olesen, 2000).

## RESULTS

### Wind correction

As the AEROPOL model can use only single-point meteorological data and wind from maximum two levels (standard 10 m height and another arbitrarily chosen level higher up), the most straightforward way would be to take the higher level exactly at source height, thus giving to the plume the direction and speed at the release level. However, comparison of these initial results gave unsatisfactory match of modelled plumes with measured ones – too high wind speeds and wrong directions were obvious in vast majority of runs. Then, repeating the model runs with average wind speed between the standard level and the source height, the consistent results were achieved. Keeping in mind that the downward-dispersed tracer starts to move with local wind, the gradual dispersion in line with downwind transport should result in an intermediate transport speed and direction – thus, this approach is theoretically sound as a first approximation. All the model results presented this point forward, are computed with wind data averaged between the estimated (extrapolated, when needed) 10 m level and actual wind at release height.

### Summary statistics

The summary statistics for cross-wind integrated, arc-wise maximum and near-centreline concentrations is given in Table 1.

**Table 1.** Summary statistics for cross-wind integrated, arc-wise maximum and near-centreline concentrations. Statistics are given separately for model runs with the Pasquill and the Gryning parameterisation schemes (see Models and Methods)

	Cross-wind integrated		Maximum arc-wise		Near-centreline	
	Gryning	Pasquill	Gryning	Pasquill	Gryning	Pasquill
CORR	0,92	0,79	0,94	0,74	0,83	0,79
FB	-0,13	-0,25	0,65	0,03	0,46	-0,12
FS	-0,03	-0,07	0,83	0,06	0,75	0,05
NMSE	0,08	0,22	0,65	0,22	0,51	0,18
FA2	0,86	0,86	0,50	0,71	0,71	0,79

As seen from Table 1, the conservative Pasquill-Gifford parameterisation performs somewhat better, except for correlations, which exceed even 0,9 with Gryning scheme for cross-wind integrated and maximal arc-wise concentrations. In most cases, the Gryning scheme results in too wide spread and thus, lower maxima compared to measurements, whereas the Pasquill parameterisation gives sharper maxima, which makes the statistics more sensitive to the small discrepancies in plume position.

### Modelled vs. measured data plots

The plots of cross-wind integrated, maximum arc-wise and near-centreline concentrations are given in Figures 2, 3 and 4 respectively. All these concentrations are normalised with source release rate.

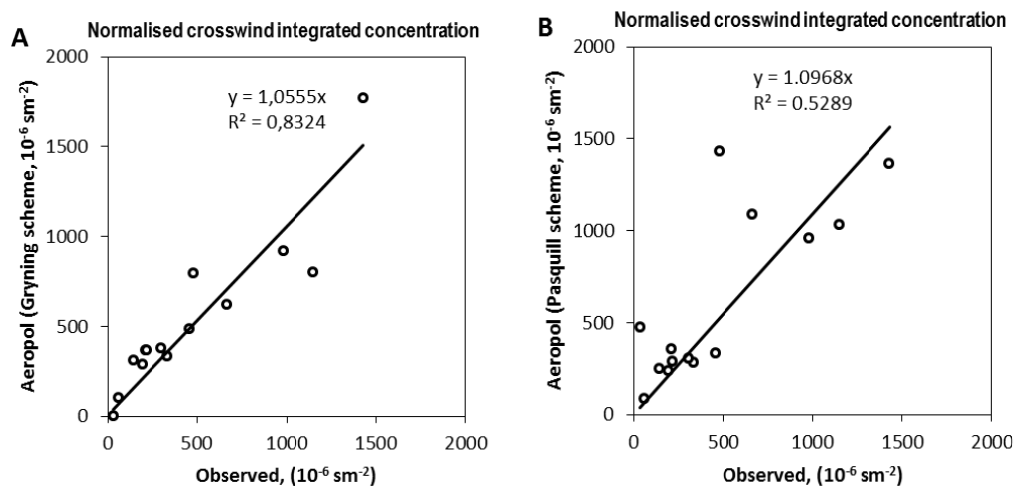


**Figure 2.** Plots of modelled *versus* measured normalised cross-wind integrated concentrations. Modelled concentrations are computed with the Gryning (A) and the Pasquill-Gifford (B) parameterisations

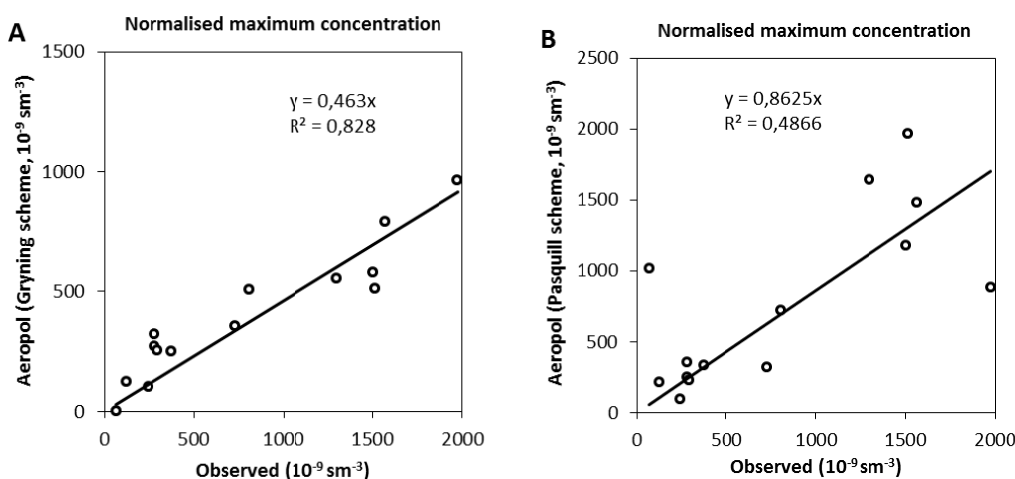


**Figure 3.** Plots of modelled *versus* measured normalised arc-wise maximum concentrations. Modelled concentrations are computed with the Gryning (A) and the Pasquill-Gifford (B) parameterisations

The effect of too wide Gaussian spread of Gryning scheme is seen in plots of the arc-wise maximum and the near-centreline concentrations, as the reason of serious underestimation. On the other hand, the wider spread makes the fit less sensitive to the exact position of the Gaussian peak and thus, the scatter of data points is much lower than with Pasquill-Gifford scheme. In contrary, the fit of arc-wise integrated concentrations is almost perfect with Gryning scheme and much looser with Pasquill-Gifford scheme, i.e. the latter one is not that precise to reproduce the vertical transport of the tracer. However, both schemes are within 10% range from one-to-one relation by trendline, thus handling the vertical dispersion rather well.

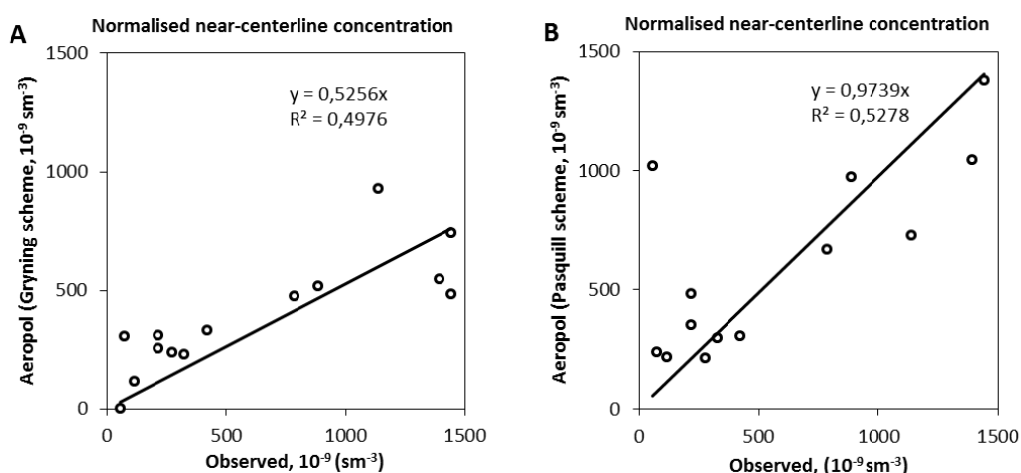


**Figure 4.** Plots of modelled *versus* measured normalised near-centreline concentrations. Modelled concentrations are computed with Gryning (A) and Pasquill-Gifford (B) parameterisation

## CONCLUSIONS

The first question posed in Introduction above got a positive answer: the AEROPOL model reproduced the measured concentrations rather consistently, thus both *Cabauw* data set is still useful for model validation, and *vice versa*: AEROPOL is a useful tool for predicting the dispersion of pollutants from elevated releases. As a supplement to earlier validation studies (e.g. Kaasik & Kimmel, 2003), the advantages and disadvantages of newer Gryning parameterisation scheme are clarified. Based on this validation study the Pasquill-Gifford scheme seems better for predicting the highest concentrations near the surface, but key issue for exact matching is the proper wind direction. On the other hand, the Gryning scheme is somewhat more accurate in predicting the cross-wind integrated concentrations. To match these two advantages together, more research is needed.

To answer the second question, the next stage of research consisting of the AEROPOL runs based on HARMONIE meteorological re-analysis, is in progress.

## ACKNOWLEDGEMENTS

This study was funded by Estonian Ministry of Education and Research, institutional research funding IUT20-11.

## REFERENCES

- Agterberg, R., Nieuwstadt, F.T.M., Duuren, van H., Hasseltn, A.J. and Krijt, G.D., 1983: Dispersion experiments with Sulphur Hexafluoride from the 213m high meteorological mast at Cabauw in The Netherlands. Royal Netherlands Meteorological Institute, De Bilt, The Netherlands, WR83-04 (<http://www.jsirwin.com/Cabauw1983JanuaryReport.pdf>).
- Gryning, S.E., Holtslag, A.A.M., Irwin, J.S., Siverson, B., 1987: Applied dispersion modelling based on meteorological scaling parameters. *Atmospheric Environment*, **21**, 1, 79-89.
- Kaasik, M.; Kerner, E.-S., 2010: An updated method for estimating of surface-layer scaling parameters from routine ground-based meteorological data. In: Rao, S.T.; Steyn, D. (Ed.). *Air Pollution Modelling and its Application XX* (105–108). Springer.
- Kaasik, M., Kimmel, V., 2003: Validation of the improved AEROPOL model against the Copenhagen data set. *Int. J. of Environment and Pollution*, **20**, 1-6, 114-120, doi: 10.1504/IJEP.2003.004256.
- Myrup, L.O., Ranzieri, A.J., 1976: A consistent scheme for estimating diffusivities to be used in air quality models. Caltrans, FHWA-CA-TL-7169-76-32.
- Olesen, H.R., 2000: The Model Validation Kit-status and outlook. *Int. J. of Environment and Pollution*, **14**, 1-6, 65-76, doi: 10.1504/IJEP.2000.000527
- Stohl, A., Haimberger, L., Scheele, M.P., Wernli, H., 2001: An intercomparison of results from three trajectory models. *Meteorol. Appl.*, **8**, 127-135.

**17th International Conference on  
Harmonisation within Atmospheric Dispersion Modelling for Regulatory Purposes  
9-12 May 2016, Budapest, Hungary**

---

**ASSESSING AIR QUALITY IMPACTS OF AIRPORT EMISSIONS AT THE LOS ANGELES  
INTERNATIONAL AIRPORT USING AN INTEGRATED MODELING AND MEASUREMENT  
APPROACH**

*Saravanan Arunachalam<sup>1</sup>, Alejandro Valencia<sup>1</sup>, Philip Soucacos<sup>2</sup> and Jeffrey Weil<sup>3</sup>*

<sup>1</sup>Institute for the Environment, University of North Carolina at Chapel Hill, USA

<sup>2</sup>Booz Allen and Hamilton, Inc., USA

<sup>3</sup>Cooperative Institute for Research in Environmental Sciences, University of Colorado at Boulder, USA

**Abstract:** Aircraft emissions affect local air quality as well as public health during multiple modes of operation in the vicinity of the airport – including startup, taxi, takeoff and landing. The FAA’s Emissions Dispersion Modeling System (EDMS) coupled with the EPA’s AERMOD modeling system is the required model to study airport local air quality in the U.S. However, given the unique nature of aircraft sources during LTO activity, it is not clear if AERMOD can accurately model these sources, and there is a lack of consistent practice for on use of dispersion models for airport local air quality for addressing public health risk issues. The objective of this study is to apply multiple local-scale dispersion models for a large airport and assess the strengths and weaknesses of these models in the context of modeling airport sources. We chose the Los Angeles International airport (LAX) in Southern California as the study airport to apply four different models (two Gaussian plume and two Lagrangian puff models) – AERMOD, ADMS-Airport, SCICHEM, and CALPUFF. The LAX airport was chosen to leverage the intense measurements during the Air Quality Source Apportionment Study (AQSAS) Phase III for two different seasons during Winter and Summer of 2012, when multiple pollutants including NO<sub>x</sub>, CO, SO<sub>2</sub>, BC, PM<sub>2.5</sub>, UFP, and various VOCs were measured at 17 different locations (4 core, 4 satellite and 9 gradient sites) in and around the airport. We processed emissions using EDMS to prepare hourly emissions inventories for the study region, and which included all airport-related sources as well as few other key emissions sources in the vicinity of the airport. We present results from this multi-model study for the LAX airport, and present model evaluation at these 17 locations as well as at a few other routine AQS sites in the Los Angeles basin. Specific focus will be on the ability of each model to characterize aircraft sources during the landing and takeoff cycles adequately, and being able to reproduce the observed concentrations at various locations in and around the airport.

**Key words:** *Aircraft Emissions, Dispersion, Landing and Takeoff, AERMOD, ADMS-Airport, SCICHEM, CALPUFF, Air Quality*

**17th International Conference on  
Harmonisation within Atmospheric Dispersion Modelling for Regulatory Purposes  
9-12 May 2016, Budapest, Hungary**

---

**LAGRANGIAN SIMULATIONS OF THE PLUME RISE IN STRONG CAPPING INVERSION**

*Enrico Ferrero<sup>1,3</sup>, Stefano Alessandrini<sup>2</sup>, Domenico Anfossi<sup>3</sup>*

<sup>1</sup>Università del Piemonte Orientale, Torino, Italy

<sup>2</sup>NCAR, RAL, Boulder (Colorado), USA

<sup>3</sup>CNR, ISAC, Torino, Italy

**Abstract:** In this work we have performed new investigations applying our Lagrangian algorithm described by Alessandrini et al. (2013) to simulate the plume rise in a convective boundary layer, capped with a strong inversion layer. We tested our model with the results of a water tank experiment (Weil et al. 2002). For each case we compare the simulated and measured mean height, horizontal and vertical plume standard deviation and the entrainment, the fraction of the plume that remains captured above the inversion respect to the whole mass of the plume. The model is able to correctly reproduce the main characteristics of the plume.

**Key words:** *Lagrangian Model, Plume Rise, Entrainment.*

## INTRODUCTION

The correct simulation of plume rise is of basic importance for a correct estimation of the transport and dispersion of airborne pollutants and for the evaluation of their ground level concentration. A buoyant plume rises because of its initial momentum and buoyancy. In the first stage one has also to account for the action of the buoyancy-generated turbulence. However, progressively the effect of ambient turbulence becomes predominant. The rising plume experiences a shear force at its perimeter, where momentum is transferred from the plume to the surrounding air, and ambient air is entrained into the plume. This phenomenon, called entrainment, is responsible for the plume diameter increase and for the decrease of both its mean velocity and the average air-plume temperature difference. In the Eulerian dispersion models, the calculation of the plume rise is based on the fluid dynamic equations, namely on the mass, momentum and energy conservation equations. Since a complete theory is not yet available, these equations generally assume that the rate at which ambient air is entrained into the plume is proportional to the mean local rise velocity. This assumption was generally used in semi-empirical formulations (Briggs, 1975) but more complex three-dimensional expressions are inserted in the integral models. In Lagrangian Particle Models (LPM) plume rise can be dynamically computed, i.e. each particle, at each time step, can respond to local conditions: wind speed and direction, ambient stability and turbulence (both the self-generated and ambient ones). This allows obtaining a high degree of resolution. In particular, with a reference to the present work, it allows simulating the interaction of a plume with a capping inversion layer in a "natural" way. In this paper the method proposed by Alessandrini et al. (2013) is considered. It makes use of two scalars transported by the particles. They represent the temperature and vertical velocity difference between the plume and the environment. The entrainment is properly simulated and the plume rise is calculated from the local property of the flow. In that paper, concerning controlled conditions, the algorithm was tested only in neutral and stable boundary layers both in water tank and ideal experiment showing good results. In the present work we have performed new investigations applying the algorithm in a convective boundary layer (CBL) capped with a strong inversion layer. We considered the laboratory water tank experiment carried out by Weil et al. (2002). The focus of the experiment is on highly buoyant plumes that loft near or become trapped in the CBL capping inversion and resist downward mixing. Such plumes can be defined by a dimensionless buoyancy flux,  $F_{b,*}$  (which depends on the stack buoyancy flux, the mean wind speed, the convective velocity scale and the CBL depth) and the dimensionless down-wind distance  $X$  (which depends on the distance, the mean wind speed, the convective velocity scale and the CBL depth). By comparing the simulated and measured plume rise characteristics as a function of  $F_{b,*}$  and the dimensionless down-wind distance  $X$ , we verified that the plume rise model is able to fulfil the experiment results.

### THE PLUME RISE MODEL

The Lagrangian plume rise module was introduced in the Lagrangian stochastic particle model SPRAY (Tinarelli et al., 2000, Alessandrini and Ferrero, 2009). Each particle carries two quantities that specify the difference between the temperature and the momentum of the plume air and the environment. To this aim we assign to any  $i$ -th emitted particle in the time interval the “temperature mass”  $m_T$ , defined as follows:

$$m_{T_i} = \frac{[T_{pinit} - T_a(H_s)]w_u A \Delta t}{N_p} \quad (1)$$

where  $T_{pinit}$  is the initial plume temperature,  $T_a(H_s)$  is the environment air temperature at the stack height,  $A$  is the stack exit section and  $N_p$  is the total number of particles released in the time interval  $\Delta t$  and  $w_u$  the plume exit velocity. Note that  $m_T$  does not have the dimension of a mass but can be considered a “mass” when the temperature difference is considered a density. Considering the domain divided in fixed regular cubic cells, the air-plume temperature difference for the generic cell,  $\Delta T_c$ , is:

$$\Delta T_c(t_0) = \frac{\sum_M m_{T_i}(t_0)}{V_c} \quad (2)$$

where  $M$  is the number of particles in the cell  $c$  and  $V_c$  is the cell volume. In order to take into account the momentum flux we define the momentum mass  $m_{w_i}$ , which is assigned to each particle. At the beginning of the simulation we have:

$$m_{w_i} = \frac{[W_{pinit}]w_u A \Delta t}{N_p} \quad (3)$$

where  $W_{pinit}$  is the stack exit vertical velocity of the plume. Also in this case,  $m_{w_i}$  has not the dimension of a mass but it can be considered so when  $W_{pinit}$  is considered a density. Then the cell vertical velocity  $w_c(t_0)$  at the time  $t_0$  is computed as

$$w_c(t_0) = \frac{\sum_i^M m_{w_i}(t_0)}{V_c} \quad (4)$$

The new temperature difference  $\Delta T_c(t_1)$  at the time  $t_1$  (where  $t_1 = t_0 + \Delta t$ ) is calculated by the equation:

$$\Delta T_c(t_1) = \Delta T_c(t_0) + \Gamma(z_c) \cdot w_c(t_0) \cdot \Delta t - 0.0098 w_c(t_0) \cdot \Delta t \quad (5)$$

where  $z_c$  is the cell height and  $\Gamma(z_c)$  is the lapse rate of the ambient air at cell height  $z_c$ . The second term on the right side updates the temperature difference between the cell and the ambient considering the vertical inhomogeneity of the atmosphere temperature. The third term on the right takes into account the adiabatic expansion due to the plume ascending motion. Clearly, in case of neutral temperature profile, these two terms delete each other. Equation 5 aims to simulate the variation in time of plume-ambient air temperature difference due to the ascending motion.

Afterwards, the value of  $w_c$  at the time  $t_1$  is computed for every cell using the following equation:

$$w_c(t_1) = w_c(t_0) + \frac{\Delta T_c(t_0)}{T_a(z_c) + \Delta T_c(t_0)} g \Delta t - \frac{0.5 \cdot c_D \cdot S \cdot w_c^2(t_0) \cdot \rho_a \cdot \Delta t}{\rho_p \cdot V_c} \quad (6)$$

where  $T_a(z_c)$  is the ambient air temperature at the same cell height  $z_c$ ,  $S$  the cell horizontal surface area,  $c_D$  the drag coefficient,  $\rho_a$  and  $\rho_p$  are the ambient air and plume density, respectively. The second term on the right represents the buoyancy vertical acceleration while the last term on the right represents the aerodynamic drag. Equation 6 simulates the plume vertical ascending velocity variation in time due to the buoyancy acceleration and the aerodynamic drag. Then, the “temperature difference and velocity masses” at the time  $t_1$ ,  $m_{T_i}(t_1)$  and  $m_{w_i}(t_1)$  are computed for each particle following the two equations:

$$m_{T_i}(t_1) = \frac{m_{T_i}(t_0) \Delta T_c(t_1)}{\Delta T_c(t_0)}; \quad m_{w_i}(t_1) = \frac{m_{w_i}(t_0) \Delta T_c(t_1)}{\Delta T_c(t_0)} \quad (7)$$

This method was proposed by Chock and Winkler (1994 a,b) and applied for a different purpose. In fact, in their papers, the masses were representing the actual masses of different substances carried by the particles in a chemically reactive plume. In our algorithm they carry the information, for each particle, relative to the two scalars introduced, the difference between the plume and environment temperatures and the vertical momentum.

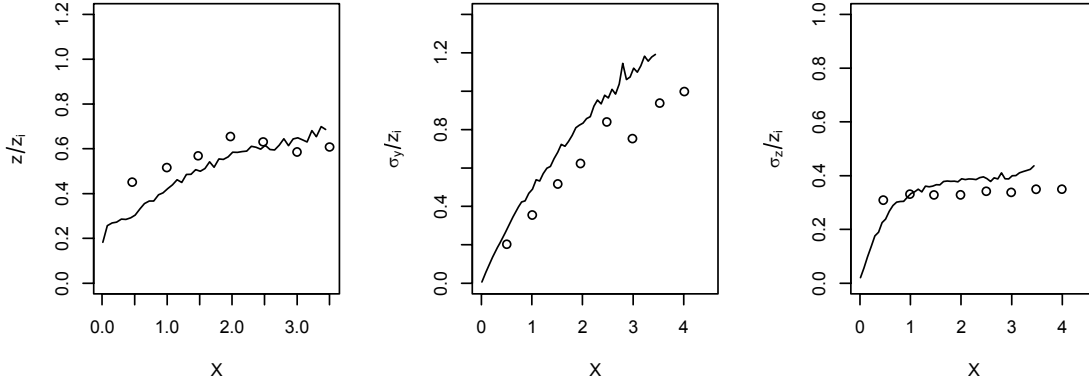


**Figure 1.** Comparison between model results (lines) and measured data (circles) for  $F_{b^*}=0.0$  as a function of the dimensionless downwind distance. From left to right the plots refer to the dimensionless mean plume height and to the dimensionless crosswind and vertical concentration standard deviations, respectively

### THE CASE STUDY

We considered the Weil et al. (2002) experiment, which reproduced, in a water tank, the dispersion of a plume emitted from an elevated source in a convective boundary layer with a strong inversion at the top. It is important to mention that in the experiment there was no mean flow (and, hence, no environment turbulence) and the mean wind, constant with the height, was simulated by towing a model stack along the tank centreplane. The experiments are characterized by four different values of the normalized stack buoyancy flux

$$F_{b^*} = \frac{F_b}{W_s^3 z_i} \quad \text{with} \quad F_b = w_s r_s^2 g \frac{\rho_a - \rho_s}{\rho_a} = w_s r_s^2 g \frac{T_s - T_a}{T_s} \quad (8)$$

where  $F_b$  is stack buoyancy flux,  $z_i$  the mixing height,  $w_s$  the convective velocity scale,  $\rho$  the density,  $T$  the temperature,  $r$  is the source radius,  $W_s$  the plume velocity at the source, and  $g$  the gravitational acceleration. ‘s’ stands for stack values and ‘a’ for ambient air values. In order to perform the simulation we reported the experiments to typical atmospheric conditions. The scaling factor for the lengths, velocity and buoyancy were based on the Froude number similarity:  $L_m = 5000L_v$ ,  $V_m = 200V_v$ ,  $\Delta_m = 8\Delta_v$ ; where ‘m’ indicates the numerical model and ‘v’ the experiment. Furthermore,  $\Delta_v = \frac{\rho_a - \rho_s}{\rho_a}$  and  $\Delta_m = \frac{T_s - T_a}{T_s}$ .

Using these scaling factors we calculated the values for the simulation parameters. In the simulations  $u$  was kept constant with height as was in the experiment. The potential temperature profiles were set constant from 0 to  $z_i$  and increasing above  $z_i$  up to the top of the domain with the value of the vertical gradient corresponding to that of the experiment.

### RESULTS

We present the results of the simulation performed with  $c_D=0.3$ , which we considered the best choice for this parameter. We compare the simulated and measured mean height, horizontal and vertical plume standard deviations and the entrainment, the fraction of the plume that remains captured above the inversion with respect to the whole mass of the plume. The Figures 1 – 4 indicate that the overall simulation results are good, even if there are some deviations between predictions and observations. The model is able to correctly reproduce the basic characteristics of the plume rise phenomenon in convective conditions. This is interesting because the emission conditions cover a large scale of buoyancies: from a neutral emission (no buoyancy,  $F_{b^*}=0.0$ ) to very high buoyancy ( $F_{b^*}=0.4$ ). We have also to mention that

the absence of environmental turbulence in the experiment limits somehow the accuracy of our simulations. For instance, the plots of dimensionless crosswind standard deviation versus X show a slight overestimation at the furthest distances for the first three  $F_{b^*}$  values and a perfect agreement for the highest buoyancy.

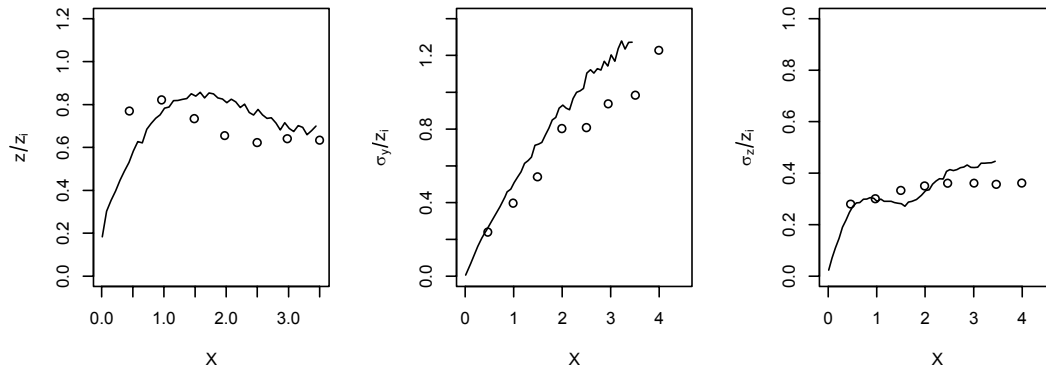


**Figure 2.** As in Figure 1 but for for  $F_{b^*}=0.1$

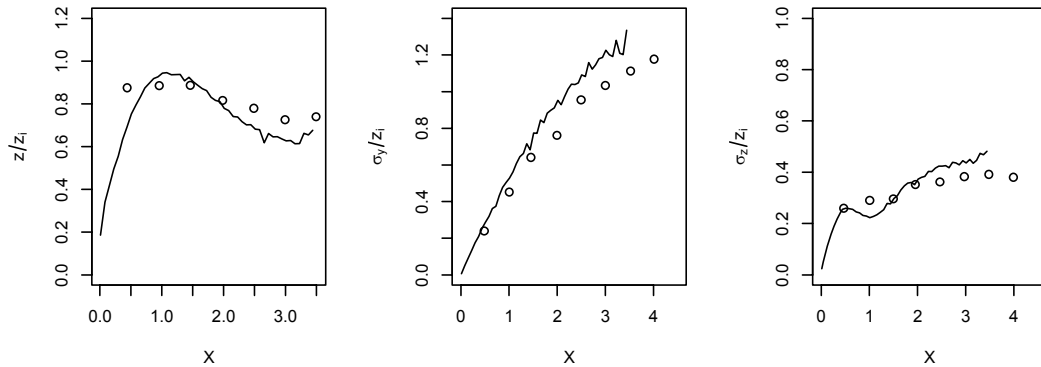


**Figure 3.** As in Figure 1 but for for  $F_{b^*}=0.2$

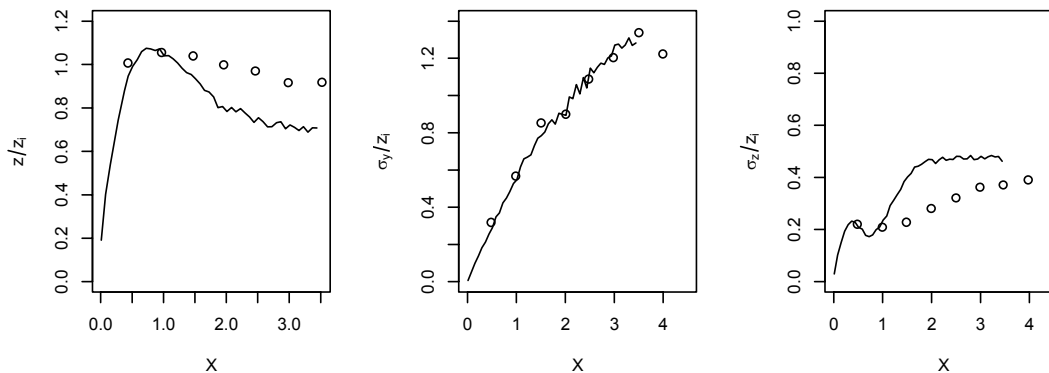


**Figure 4.** As in Figure 1 but for for  $F_{b^*}=0.4$

Figure 5 shows the mean plume entrainment as a function of the dimensionless distance for the four buoyancy cases. The model predictions are better close to the source while the model slightly overestimates for  $X > 3$ . Furthermore, for  $X > 1$  simulations results underestimates the measured data in the cases with  $F_{b^*}=0.2$  and  $F_{b^*}=0.4$ . We add that the simulation with different  $c_d$  perform almost in the same way in the case of  $F_{b^*}=0$  and that in the other cases the lower is the value of  $c_d$  and the higher is the entrainment, as it can be expected.

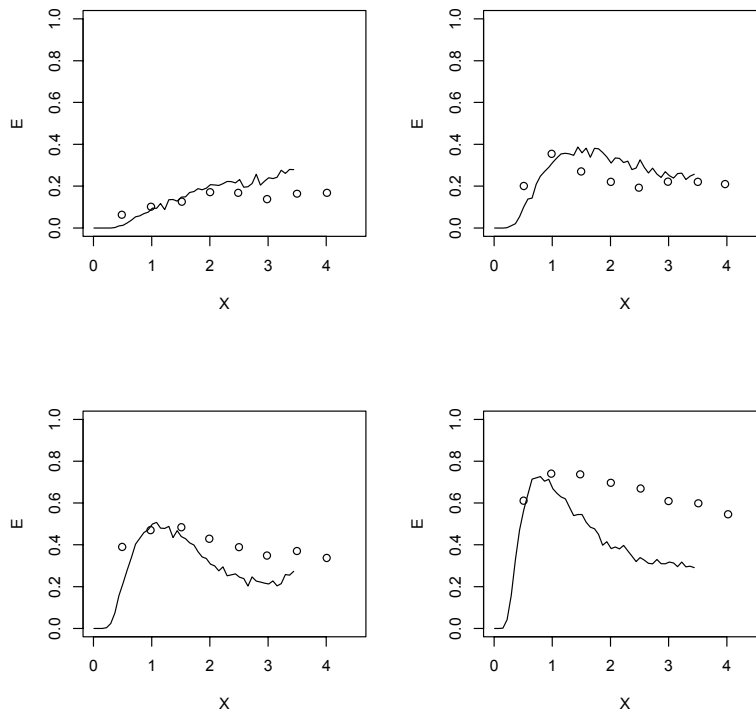


**Figure 5.** Comparison of the simulated (lines) and measured (circles) entrainment. From left to right and from top to bottom: for  $F_{b^*}=0.0$ , for  $F_{b^*}=0.1$ , for  $F_{b^*}=0.2$ , for  $F_{b^*}=0.4$

## REFERENCES

- Alessandrini S. and Ferrero E. (2009). A hybrid Lagrangian-Eulerian particle model for reacting pollutant dispersion in non-homogeneous non-isotropic turbulence. *PHYSICA A*, ISSN: 0378-4371, 388, **8**, 1375-1387
- Alessandrini S., Ferrero F., Anfossi D., (2013), A new Lagrangian method for modelling the buoyant plume rise, *Atmos. Environ.*, **77**, 239-249
- Anfossi, D., Ferrero E., Brusasca G., Marzorati A., Tinarelli G. (1993) A simple way of computing buoyant plume rise in a Lagrangian stochastic model for airborne dispersion, *Atmospheric Environment*, **27A**, 1443-1451
- Anfossi D., G. Tinarelli, S. Trini Castelli, M. Nibart, C. Olry and J. Commanay (2010): A new Lagrangian particle model for the simulation of dense gas dispersion, *Atmospheric Environment*, **44**, 753-762
- Briggs, G.A. (1975): Plume rise predictions. In: Lectures on air pollution and environmental impact analyses, D. Haugen (editor). Workshop proceedings, Boston, Massachusetts, September 29 – October 3, pp. 59-111, American Meteorological Society, Boston, Massachusetts, USA.
- Chock, D.P. and Winkler, S.L. (1994a) ‘A particle grid air quality modeling approach, 1. Dispersion aspect’, *Journal of Geophysical Research*, **99**, D1, pp.1019–1031.
- Chock, D.P. and Winkler, S.L. (1994b) ‘A particle grid air quality modeling approach, 2. Coupling with Chemistry’, *Journal of Geophysical Research*, **99**, D1, pp.1033–1041.
- Hoult, D.P., and J.C. Weil (1972): A turbulent plume in a laminar crossflow. *Atmos. Environ.*, **6**:513-531
- Morton, B.R., G.I. Taylor, and J.S. Turner (1956): Turbulent gravitational convection from maintained and instantaneous sources. *Proc. Roy. Soc. London*, **A234**, 1-23.
- Tinarelli, G., Anfossi, D., Bider, M., Ferrero, E., & Trini Castelli, S. (2000). A new high performance version of the Lagrangian particle dispersion model SPRAY, some case studies. In S. E. Gryning & E. Batchvarova (Eds.), *Air pollution modelling and its applications XIII* (pp. 499– 507). New York: Plenum Press.
- Weil C. J., Snyder W. H., Lawson R. E. JR. and Shipman M. S. (2002) Experiments on buoyant plume dispersion in a laboratory convection tank, *Bound.-Layer Meteor.*, **102**, 367–414.

**17th International Conference on  
Harmonisation within Atmospheric Dispersion Modelling for Regulatory Purposes  
9-12 May 2016, Budapest, Hungary**

---

**MODEL CHAIN FOR BUOYANT PLUME DISPERSION**

*Andrea Bisignano<sup>1</sup>, Luca Mortarini<sup>2</sup> and Enrico Ferrero<sup>1</sup>*

<sup>1</sup>Università del Piemonte Orientale, Dipartimento di Scienze e Innovazione Tecnologica, Alessandria, Italy

<sup>2</sup>Institute of Atmospheric Sciences and Climate, National Research Council (ISAC-CNR), Torino, Italy

**Abstract:** The model chain is aimed to simulate high buoyant plume and can be applied in case of risk assessment and emergency response. It consists of the WRF mesoscale meteorological model and the SPRAYWEB dispersion model. The novelty lies in the new interface linking the two models. We use the Bull-Run data-set from the model evaluation kit in order to compare our results.

**Key words:** *Lagrangian model, pollution dispersion, plume rise*

## INTRODUCTION

Emissions from many natural and anthropogenic hot sources are compared with the surrounding ambient air. Buoyancy effects cause the emitted plume to rise, increasing the effective source height and significantly decreasing the maximum ground level concentrations. A major aspect that distinguishes buoyant and passive dispersion is that buoyant fluid particles create their own turbulence and hence exchange processes between the plume and its environment need to be accounted for. The inclusion of plume rise in Lagrangian stochastic models of turbulent dispersion has been considered by many authors (i.e. Anfossi et al. 1993, Bisignano and Devenish 2015) but the interaction of the buoyant plume with the environment through the entrainment phenomenon is difficult to be modelled in a Lagrangian framework. In this work we develop a model chain for the dispersion of buoyant plumes. The meteorological input to the dispersion model is provided by the WRF (Weather Research and Forecasting) model in term of mean flow, temperature and wind profiles. Then a Lagrangian stochastic model that satisfies the well-mixed condition calculates the pollutant concentrations. In order to verify our model chain we simulate the EPRI Bull Run experiments, which were conducted in moderately complex terrain. The plume was very buoyant, and the wind was often light and variable (Model Evaluation Kit, Olesen and Chang 2010). The results in term of statical analysis as indexes are presented.

## THE DISPERSION MODEL

SPRAYWEB (Tinarelli et al, 1994; Alessandrini and Ferrero, 2009; Alessandrini et al. 2013) is a Lagrangian stochastic particle model designed to study the pollutants dispersion in complex terrain. It is based on the Langevin equation for the turbulent velocities (Thomson, 1987), whose coefficients depend on a solution of the Fokker-Planck equation for a given Eulerian probability density function (PDF) of the turbulent velocity and on the inertial range turbulence theory respectively. In the two horizontal directions the PDF is assumed to be Gaussian. In the vertical direction the PDF is assumed to be non-Gaussian, so to deal with convective conditions. The equations prescribing the evolution of the vertical velocity fluctuation  $w$  and the displacement  $z$  are the following:

$$\begin{aligned}dw &= a(z, w)dt + \sqrt{C_0} dW \\ dz &= wdt\end{aligned}\tag{1}$$

where  $dW$  is a Wiener process with zero mean and unit variance,  $C_0$  is a constant and  $\varepsilon$  is the dissipation rate of turbulent kinetic energy.  $a(z, w)$  must be determined by solving the Fokker-Planck equation, obtaining:

$$a(z, w) = \frac{1}{P} \left( B_0 \frac{\partial P}{\partial w} + \Phi \right) \quad (2)$$

with  $B_0 = \frac{1}{2} C_0$  and, as suggested by Thomson (1987):

$$\Phi = - \frac{\partial}{\partial z} \int_{-\infty}^w w P(z, w) dw \quad (3)$$

where  $P(z, w)$  is the PDF that must be prescribed from the available measurements or parameterizations. In the present work, we used the Gram-Charlier PDF (Ferrero and Anfossi, 1998). Furthermore SPRAYWEB includes the method for the buoyant plume rise simulation proposed by Anfossi et al. (1993). The dispersion model is coupled to the circulation model WRF, which provides the mean flow and from which the turbulence parameters are evaluated.

#### THE NUMERICAL WEATHER PREDICTION MODEL

WRF (Weather Research and Forecasting, <http://www.wrf-model.org>) modeling system is used for various forecast and analysis applications, from the microscale to the synoptic and even global scales. WRF includes dozens of parameterizations for boundary layer processes, convection, microphysics, radiation, and land surface processes, and several options for numerical schemes (Skamarock et al., 2008). In the following we list the choice for some physics parameter. The WRF pre-processing module, WRF Preprocessing System (WPS), sets the computational domain, the geographical projection, and the resolutions both in the horizontal and in the vertical, and interpolates the meteorological fields used as initial and boundary conditions. In order to simulate the EPRI Bull Run experiments we used the NNRP data, that is the NCEP/NCAR reanalysis with a resolution of 2.5 deg, a six hours output frequency, 17 pressure levels. In the WRF simulation we used WSM 5-class scheme as microphysics option, the RRTM scheme for the longwave radiation, the MM5 (Dudhia) scheme for the shortwave radiation, the Monin-Obukhov similarity theory as surface scheme, the Noah Land Surface Model (Unified ARW/NMM version in Version 3) for the surface physics, the YSU PBL scheme (Hong, Noh and Dudhia 2006) for the PBL parameterization, the Kain-Fritsch as cumulus scheme, and a 2<sup>nd</sup> order diffusion on model levels with constant  $k$ .

#### WRF-SPRAYWEB INTERFACE

The most inherent difficulty in interfacing WRF and SPRAYWEB lies in the different coordinates used to formulate the equations. SPRAYWEB uses terrain-following coordinates  $(x, y, s)$  to express the orography that are related to the cartesian coordinates  $(x, y, z)$  as:

$$x = x \quad y = y \quad s = \frac{z - z_g(x, y)}{z_t - z_g(x, y)} \quad (4)$$

where  $z_t$  is the top of the domain and  $z_g(x, y)$  is the orography. Hence  $s = 1$  for  $z = z_t$  and  $s = 0$  for  $z = z_g(x, y)$  so that  $s = 0$  is not a horizontal plane but the orographic surface.

In WRF the vertical coordinates are terrain-following as well, but they are expressed as terrain-following hydrostatic-pressure (Laprise 1992) coordinates defined as:

$$\eta = \frac{P_h - P_{ht}}{P_{hs} - P_{ht}} \quad (5)$$

where  $P_h$  is the hydrostatic component of the pressure,  $P_{hs}$  and  $P_{ht}$  refer to the values along the surface and top boundaries respectively. This coordinate definition is analogous to the traditional  $\sigma$  coordinate use in many hydrostatic models but  $\eta$  varies from a value of 1 at the surface to a value of 0 at the upper boundary.  $\eta$  are also called vertical mass coordinate and they are time-dependent. Hence we need a time independent mapping from  $\eta$  to  $s$  in order to match the WRF output with the SPRAYWEB input. In particular we choose  $s$  to be equivalent to a certain  $\eta$  at fixed time and then we interpolate all the time-dependent WRF output variables on this given  $\eta$ . Then we use the Hanna (1982) parameterisation in order to evaluate the turbulence parameters.

### BULL RUN DATA SET

The models have been applied to the Bull Run experiment (Hanna and Paine 1989). Hourly ground level concentrations due to SF6 emissions from a 244 m stack at Bull Run, a moderately hilly site near Oak Ridge, Tennessee, were observed by a network of about 200 monitors, spaced on arcs at downwind distances ranging from 0.5 to 50 km during convective conditions. In Figure 1 the topography from WRF simulation, the receptors and the source position are shown. Generally, about 5 arcs of monitors were operating. The monitoring arcs extended completely around the stack, since the winds were often light and variable at that site during the field study period of August-October 1982. In particular we choose for the simulations the day 5 October 1982 when the tracer was released for 12 hours starting at 9 LST (Local Standard Time) and the hourly measurements have been performed for 9 hours since 11 LST. In Figure 2 we plot the wind speed and the temperature of air evaluated from WRF showing that October 5th 1982 was a sunny day with low winds.

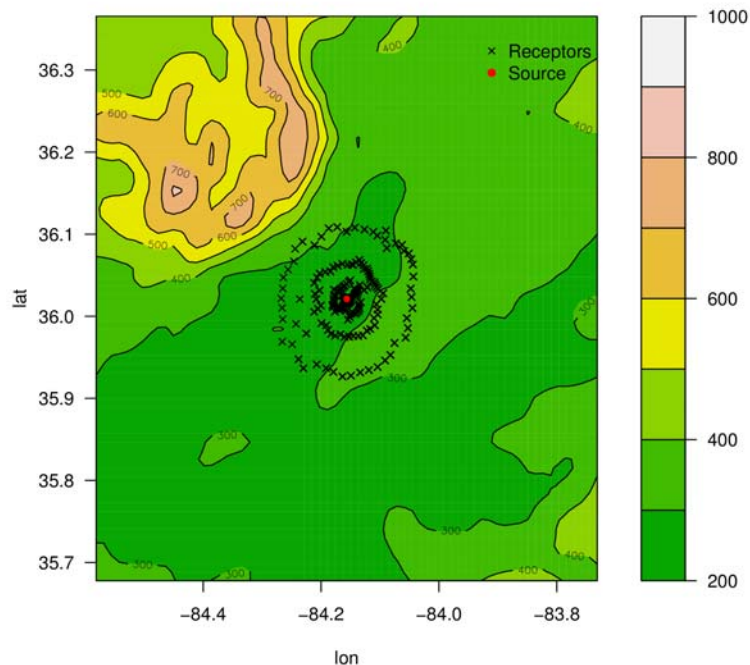


**Figure 1.** Topography, receptors positions on 4 arcs and source position (centre of the figure).

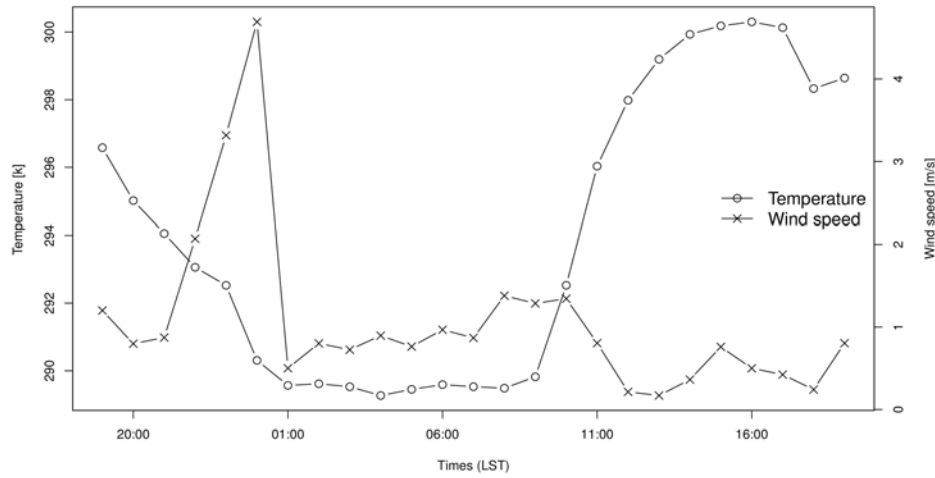


**Figure 2.** Wind speed and temperature measured near the surface by the WRF simulation during 5 October 1982.

### SIMULATION AND RESULTS.

WRF was run using for horizontal nested grids corresponding to domains of extension 3960 km, 1320 km, 440 km and 73 km with horizontal resolution equal to 30000 m, 10000 m, 3333 m and 1111 m respectively. In the vertical direction a stretched grid of 38 levels from  $\eta=1$  to  $\eta=0$ . The integration time steps for the three grids were 90 s, 30 s, 10 s and 3 s, respectively. The WRF simulation was carried out for a period of 24 hours from 5 October 00 UTC until 6 October 00 UTC. The initial and boundary conditions were provided by the NNRP data from NCEP/NCAR analysis. The results of the SPRAYWEB simulation evaluation are presented in Table 1 for the maximum of concentration at ground, and in Table 2 for the crosswind integrated concentrations. Following Hanna and Paine (1987), we considered the ground level concentrations measured at three arcs with radius 2, 5, 10 km. The comparison is performed in terms of maximum of concentration and cross wind integrated concentrations on the three arcs. The SPRAYWEB simulation refers to time period 15-18 (LST). We compared the obtained results with the measurements, in term of the following statistical indexes: mean, correlation coefficient (COR), normalised mean square error (NMSE) and fractional bias (FB). The first line indicates the expected value for a “perfect model” where mean and standard deviation are calculated from the measured data provided in the Bull Run data set.

**Table 1.** Maximum of ground level concentration

	Mean ( $\mu\text{g}/\text{m}^2$ )	CORR	NMSE	FB
Measured	256.333	1.000	0.000	0.000
Simulated	288.714	0.928	0.017	0.119

**Table 2.** Crosswind integrated concentration

	Mean ( $\mu\text{g}/\text{m}^2$ )	CORR	NMSE	FB
Measured	6625.421	1.000	0.000	0.000
Simulated	5149.403	0.903	0.219	-0.250

### CONCLUSION

The statistical indexes presented in Table 1 and Table 2 exhibit a good agreement between the measures and the simulation results. The correlation is very high both for the maximum of concentration at ground and the crosswind integrated concentration. The normalised mean square error is smaller for the

maximum of ground level concentration but the value for the crosswind integrated concentration is acceptable as well. The fractional bias shows a slight overestimation for the maximum and an underestimation for the crosswind integrated concentration.

Future developments would include the following features:

- several PBL schemes available in WRF will be tested in order to understand which one is the most appropriated to build the model chain with SPRAYWEB
- different turbulence parameterisation will be implemented in the interface code.
- new plume rise schemes (Alessandrini et al., 2013; Bisignano and Devenish, 2015) will be developed in SPRAYWEB.

## REFERENCES

- Alessandrini, S., Ferrero, E., 2011, A Lagrangian particle model with chemical reactions: application in real atmosphere, *Int. J. Environ. Pollut.* **47** (1e4), 97e107.
- Alessandrini, S., Ferrero, E., Anfossi, D., 2012. A new method for buoyant plume rise computation in lagrangian particle models. *Air Pollut. Model. Its Appl.* XXI NATO Sci. Peace Security Ser. C: Environ. Security 4, 45e50.
- Anfossi, D., Ferrero, E., Brusasca, G., Marzorati, A., Tinarelli, G., 1993. A simple way of computing buoyant plume rise in a lagrangian stochastic model for airborne dispersion. *Atmos. Environ.* **27A** (9), 1443e1451.
- Bisignano, A., Devenish, B., 2015, A model for temperature fluctuations in a buoyant plume. *Boundary-Layer Meteorology*, **57**, 2, p157
- Hanna S.R., 1982. Applications in air pollution modelling. In *Atmospheric Turbulence and Air Pollution Modelling*, Nieuwstadt F, Van Dop H (eds). Reidel: Dordrecht, Netherlands; 275–310.
- Hanna, S.R., Paine, R.J., 1987. Convective scaling applied to diffusion of buoyant lumes from tall stacks. *Atmos. Environ.* **21** (10), 2153e2162.
- Hanna, S.R., Paine, R.J., 1989. Hybrid plume dispersion model (HPDM) development and evaluation. *J. Appl. Meteorol.* **28**, 206e224.
- Laprise, R., 1992. The Euler Equations of Motion with Hydrostatic Pressure as an Independent Variable, *Monthly Weather Review*, American Meteorological Society, 120, 187-207.
- Olesen. H.R. and J.C Chang, 2010. Consolidating tools for model evaluation, *Int. J. Environ.Pollut.*, **40**, 1/2/3, 175–183.
- Skamarock, W. C., Klemp, J. B., Dudhia, J., Gill, D. O., Barker, D. M., Duda, M. G., Huang, X. Y., Wang, W., and Powers, J. G., 2008:A description of the advanced research WRF version 3, Tech. Note, NCAR/TN 475+STR, 125 pp., Natl. Cent. for Atmos.Res., Boulder, Colo., USA.
- Thomson, D.: Criteria for the selection of stochastic models of particle trajectories in turbulent flows, 1987, *J. Fluid Mech.*, **180**, 529–556.
- Tinarelli, G., Anfossi, D., Bider, M., Ferrero, E., Trini Castelli, S., 2000. A new high performance version of the Lagrangian particle dispersion model SPRAY, some case studies. In: Gryning, S.E., Batchvarova, E. (Eds.), *Air Pollution Modelling and its Applications XIII*. Plenum Press, New York, pp. 499e507.
- Trini Castelli, S., 2000. Mirs: a Turbulence Parameterisation Model Interfacing RAMS and SPRAY in a Transport and Diffusion Modelling System. Rap. Int. ICGF/C.N.R. No 412/2000.

**17th International Conference on  
Harmonisation within Atmospheric Dispersion Modelling for Regulatory Purposes  
9-12 May 2016, Budapest, Hungary**

---

**PRELIMINARY POLLUTANT DISPERSION MODELLING WITH CALMET AND CALPUFF  
OVER COMPLEX TERRAIN IN THE BOLZANO BASIN (IT)**

*Elena Tomasi<sup>1</sup>, Lorenzo Giovannini<sup>1</sup>, Marco Falocchi<sup>1</sup>, Dino Zardi<sup>1</sup>, Gianluca Antonacci<sup>2</sup>*

<sup>1</sup>Atmospheric Physics Group, Department of Civil, Environmental and Mechanical Engineering,  
University of Trento, Italy

<sup>2</sup>CISMA - Centro di Ingegneria e Sviluppo Modelli per l'Ambiente, Bolzano, Italy

**Abstract:** The assessment of the impact on air quality of a new waste incinerator for the city of Bolzano (Central Italian Alps) required to improve the forecast of dispersion processes within the Bolzano basin, especially in critical weather conditions (e.g. wintertime ground-based inversions under calm conditions). This led to test the CALMET and CALPUFF modelling chain performance in such a complex terrain. CALMET was used for the diagnostic reconstruction of meteorological fields, the input data being provided by a variety of in-situ measurements: surface temperature and wind (speed and direction) from eight different weather stations, wind profiles from a SODAR, and temperature profiles from a thermal profiler. Simulations performed with a prognostic approach (WRF model) showed that the strong complexity of the area affects the development of ground-based thermal inversions, as well as alternating up- and down-valley winds in the valleys merging into the basin. The simulation of such a complex pattern of meteorological fields is a challenging goal for the diagnostic pre-processor CALMET. Indeed in such a complex domain it is very difficult for CALMET to spatialize appropriately meteorological variables, such as surface temperature and wind speed and direction, strongly affecting the transport of pollutants. Therefore efforts were made to understand the causes of these deficiencies. In particular the operations of CALMET pre-processor were examined, and effects of different meteorological input passed to CALPUFF were analysed, to ascertain their impact on dispersion patterns.

**Key words:** CALMET, CALPUFF, WRF, Alps, Bolzano basin, complex terrain

## INTRODUCTION

Air quality scenarios provided by coupled meteorological and dispersion models can play a key role in supporting policies for monitoring pollutant dispersion and reducing health risks. However, air quality modelling in complex terrain still pose many challenges, due to the inherent difficulties in accurately reproducing both the atmospheric and the dispersion processes. Here we present some preliminary evidences from a project carried out in the Bolzano basin, in the Central Italian Alps. In July 2013, a new waste incinerator became operative 2 km Southwest of the city centre of Bolzano, the most populated town (about 106000 inhabitants) of South Tyrol. This new plant, with a maximum waste treatment capacity of 130000 t y<sup>-1</sup> and a flow rate of 85000 Nm<sup>3</sup> h<sup>-1</sup> released at 60 m a.g.l. at 413 K, required policy makers to improve the forecast of dispersion processes in the area (Ragazzi et al., 2013), with the aid of both atmospheric and dispersion modelling. A dedicated project was therefore set up to provide a technically-sound support for the design of a permanent air-quality station network monitoring the effects of pollutants from the incinerator. Accordingly, a trustful modelling chain, able to provide emission-impact scenarios with yearly-based numerical simulations, was needed. To assess the appropriateness of the CALMET/CALPUFF modelling chain (Scire et al., 2000) for application over such a complex terrain, these modelling instruments were tested, by means of short-term (7 h) simulations in diagnostic mode, feeding them with all the available atmospheric measurements in the Bolzano basin. Testing and evaluation were performed under meteorological situations conducive to critical air pollution episodes, e.g. strong ground-based thermal inversion and calm conditions. Attention is focused on the reconstruction of meteorological fields, which are qualitatively compared with prognostic numerical simulations run with the Weather Research and Forecasting (WRF) model (Skamarock et al., 2008). As to

the dispersion modelling, the release of a tracer from the chimney is going to be simulated, in order to appreciate the effects on pollutant transport of different meteorological input into CALPUFF.

## CASE STUDY

### Bolzano basin

The city of Bolzano lies at 262 m a.s.l. on the floor of a wide basin at the junction of the Isarco Valley (East) and of the Sarentino Valley (North) with the Adige Valley (South and Northwest) (Figure 1). The climate of Bolzano is continental, characterized by warm summers and cold winters. Wind regimes are dominated by terrain effects (Dosio et al. 2001), developing thermally-driven winds (de Franceschi et al. 2009), which however are mostly absent or very weak during wintertime (de Franceschi and Zardi 2009). This aspect, in connection with the frequent occurrence of ground-based inversions at the valley floor, determines frequent critical conditions for air quality. Figure 1 shows the study area in the Bolzano basin and its tributary valleys.

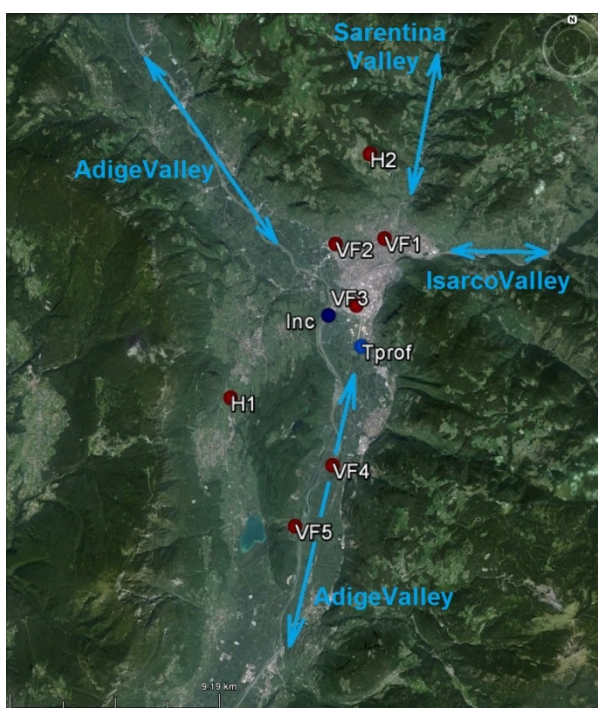


**Figure 1.** Bolzano basin with its tributary valleys. Locations of the available weather stations are also highlighted: “Inc” corresponds to the incinerator plant position; “Tprof” to the thermal profiler; “VF#” to the valley floor permanent stations and “H#” to the permanent stations on the sidewalls (background map from GoogleEarth).

### Period of study: meteorological conditions

The 27<sup>th</sup> of January 2016 was chosen as the reference day for the simulations, covering a period of 7 hours, from 04 to 10 LST (UTC+1). Indeed January 27<sup>th</sup> 2016 presented most of the typical wintertime meteorological conditions relevant for the stagnation of locally emitted atmospheric pollutants. Data from measurements showed a strong ground-based thermal inversion, developing up to 700 m above the valley floor, and relatively weak wind speeds at the valley floor. Figure 2 shows measurements from a vertical temperature profiler (“Tprof” in Figure 1) and from surface weather stations located both on the valley floor (“VF#” in Figure 1) and at various heights along the sidewalls (“H1”, 500 m, and “H2”, 1000 m, in Figure 1).

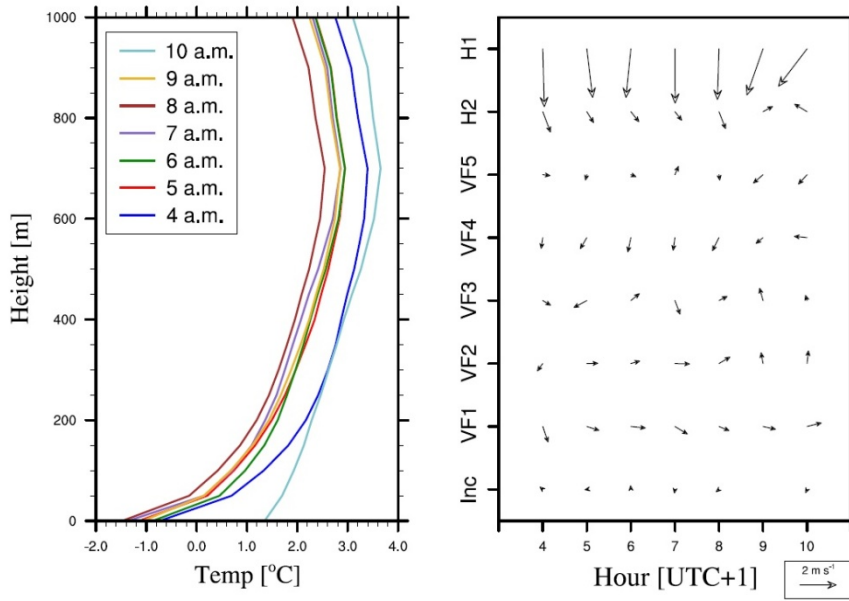


**Figure 2.** Observations of the vertical temperature profile in the morning (from “Tprof” in Figure 1) up to 1000 m a.g.l. (left) and wind speed and direction measured at 10 m a.g.l. at various weather stations (right).

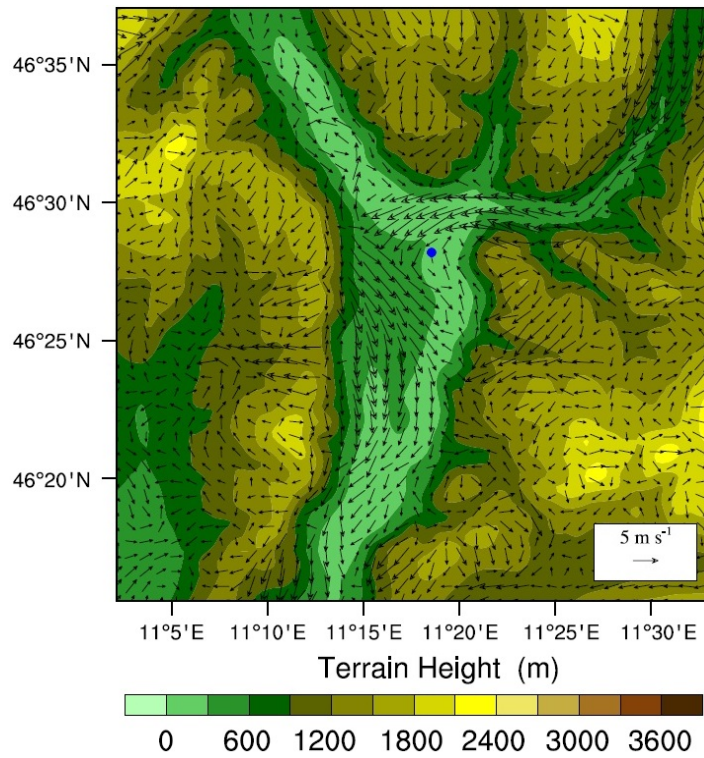


**Figure 3.** Topography of the inner domain of WRF simulations and simulated wind field at 10 m a.g.l. at 5 LST. The blue dot represents the incinerator location.

For a more detailed overview of the meteorological situation occurring on January 27<sup>th</sup>, high-resolution numerical simulations were run with a prognostic approach, with the WRF model. Simulations with the

WRF model were performed with four nested domains, up to an horizontal resolution of 333 m over the Bolzano basin. A 30-m resolved Digital Terrain Model and a 100-m land use map were used in order to properly describe the characteristics of the inner domain (Figure 3 shows the inner domain topography).

WRF simulations highlighted that the flow field in the Bolzano basin is very complex, due to alternating up- and down-valley winds flowing in the valleys which merge into the basin. In particular, a low-level nocturnal jet at the exit of the narrow canyon-like Isarco Valley adds complexity to the wind field and results to be relevant for the releases from the incinerator, as it flows exactly over the plant. As an example, a screenshot of simulated wind field at 10 m a.g.l. is shown in Figure 3. It is clear that the simulation of the interaction between these different local circulations, including their correct evolution in space and time, represents a very challenging task for a diagnostic model as CALMET, but their correct reconstruction is of fundamental importance for dispersion issues.

#### DIAGNOSTIC NUMERICAL SIMULATIONS WITH CALMET/CALPUFF

Simulations with the CALMET/CALPUFF model are run in diagnostic mode with a horizontal resolution of 200 m over a 20x20km<sup>2</sup> domain. The dispersion module is set up to simulate a tracer release from the incinerator chimney starting at 7 LST and lasting 40 minutes. Nevertheless, the focus of the present work is on the reconstruction of the meteorological fields provided by CALMET. The pre-processor is fed with different observations, both conventional and non-conventional. Indeed the following input data were provided to the model: wind speed and direction, temperature, relative humidity and atmospheric pressure from eight permanent stations, six distributed on the valley floor and two along the sidewalls (300 m and 700 m above the valley floor, respectively); vertical profiles of wind speed and direction from a SODAR, set up on the roof of the incinerator, reaching heights of 400 m; and a temperature vertical profile up to 1000 m measured in the centre of the Adige Valley. The vertical profiles of both temperature and wind, observed within the domain of interest, are uncommon data and should act as a relevant resource to guide the meteorological pre-processor to properly reconstruct meteorological fields, especially when run over complex terrain.

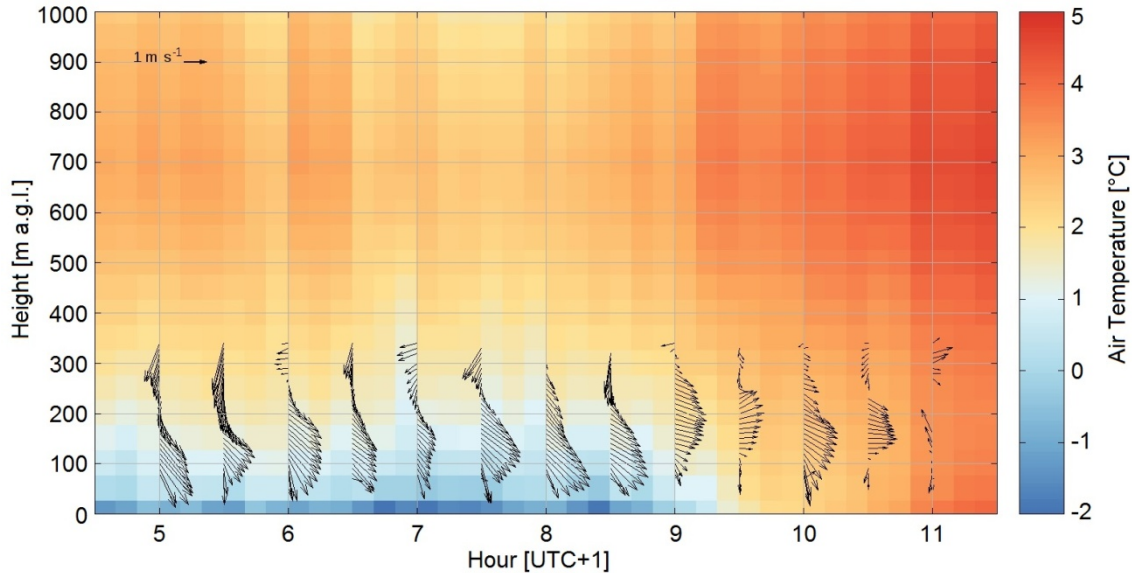


**Figure 4.** Observed vertical temperature and wind profiles measured from the thermal profiler and the SODAR, respectively.

Figure 4 summarizes the vertical input data provided to CALMET: the temperature profile has a 10-min temporal resolution and is vertically 50 m spaced, while the wind profile has a 30-min temporal resolution and is vertically 20 m spaced. Observations clearly show the ground-based thermal inversion and also catch the presence of the above-mentioned north-easterly jet starting from 200 m above the valley floor.



## **TOPIC 2**

### **ENVIRONMENTAL IMPACT ASSESSMENT: AIR POLLUTION MANAGEMENT AND DECISION SUPPORT SYSTEMS**

**17th International Conference on  
Harmonisation within Atmospheric Dispersion Modelling for Regulatory Purposes  
9-12 May 2016, Budapest, Hungary**

---

**EFFECT OF THE LONG-RANGE TRANSPORT ON THE AIR QUALITY OF BUDAPEST**

*Zita Ferenczi and László Bozó*

Hungarian Meteorological Service, Budapest, Hungary

**Abstract:** SO<sub>2</sub>, NO<sub>2</sub> and Particulate Matter (PM) are air pollutants, generated by a variety of human activities and can travel long distances in the atmosphere and cause a wide range of air quality problems in Europe. The influence of transboundary and national contributions in PM concentrations in Central-European cities could be dominant, and only a little improvement can be expected from local control policies. The air quality of Budapest is determined mainly by the local residential heating and traffic emissions combined with the meteorological conditions. Sometimes the impact of the transboundary sources can be negligible especially under special meteorological conditions when the local effects determine the air quality of Budapest, but sometimes it could be responsible for the formation of air pollution episodes. In this research the effect of long-range transport on the air quality of Budapest was analyzed in details, using the outputs of EMEP chemical transport model.

**Key words:** long-range transport, EMEP chemical transport model, urban air quality, emission

## INTRODUCTION

Many types of air pollutants have been observed to travel far from their sources causing air quality problems. The potential of a pollution for long-range transport, sometimes referred to as its characteristic travel distance or spatial range, depends not only on its real physico-chemical properties, but also on its mode and point of release to the environment. This process becomes relevant only when the transported chemical material has some harmful effect on human health or on ecosystems far from its source.

Atmospheric emissions of SO<sub>2</sub> result mainly from the combustion of sulphur containing coal and other fossil fuels, but the contributions from volcanoes and the biogenic precursor dimethyl sulphide are non-negligible (Benkovitz, et al, 2004) either. Air pollution by long-range transported SO<sub>2</sub> globally is not a recent problem, but locally it can cause serious trouble. Long-range transport of SO<sub>2</sub> from east Asia to the Pacific have been most intense during springtime because of strong westerly winds (Tu, Fang Huang, et al. 2004).

The dominant sources of nitrogen oxides are anthropogenic emissions from combustion processes in transportation, power plants, industry and agricultural biomass burning, as well as natural sources such as lightning emissions, natural biomass burning and microbial soil emissions. The lifetime of NO<sub>2</sub> in the planetary boundary layer amounts to a few hours, depending on the strength of solar irradiation and on the available radical species. This, combined with low wind speeds near the surface, makes long-range transport of anthropogenic NO<sub>2</sub> in the planetary boundary layer very unlikely. However its lifetime is up to a week in the middle and upper troposphere. More and larger plumes are emitted in winter, when the lifetime of NO<sub>2</sub> is long, anthropogenic emission rates are especially high and meteorological conditions are favorable with frequent cold fronts and cyclones. Arctic is likely to be one of the most sensitive regions to the effects of altered atmospheric and oceanic chemistry due to NO<sub>2</sub> long-range transports (Zien, et al. 2014).

PM<sub>10</sub> particles mainly originate from sea salt, soil dust resuspension, construction/demolition, non-exhaust vehicle emissions, and industrial fugitives, whereas PM<sub>2.5</sub> and PM<sub>0.1</sub> particles are mainly produced by combustion processes, forest fires and transformation of gaseous species. The lifetime of smaller size particles can range from days to weeks, while bigger particles have a lifetime of hours to days. This is the reason while there has been certain evidence that long-range transport of fine aerosol particles over distances crossing national borders and could have essential effect on air quality in urban areas in Europe (Moreno, et al., 2005). Many scientific articles described the long-range transport of

particulate matter which have a significant impact on PM<sub>10</sub> levels in big European cities while strong local sources could tend to mask long-range transport influences (Borge, et al. 2007).

In Central Europe the effect of the long range transport determine the air quality of the big cities like Budapest. The location of Budapest is not favorable, since polluted air arrive from any direction by the wind. There are some notable industrial areas like Po valley and the south part of Poland which play critical role in the air quality of Budapest. These facts portend that the qualitative analysis of the long range transport is essential in order to distinguish the effect of the local and distant sources, and to create effective air quality plan to make the air quality of the capital of Hungary healthier.

In this work, the effect of the long-range transport of SO<sub>2</sub>, NO<sub>2</sub> and Particulate Matter (PM) was analyzed in detail using the results of EMEP chemical transport model. The results will show how important this effect is and how we will able to put this information into an air quality forecasting system.

## **METHOD**

Based on scientific results mentioned above, it was very important to begin the development of chemical transport models with investigating the long-range transport of the air pollutants. A representative of these types of models is the EMEP Eulerian long-range transport model (Simpson, et al. 2012). The model is an important tool to analyze both acidification and photo-oxidant activities in the air. Determining the effect of the long range transport of different hazardous materials on the air quality of Budapest the EMEP chemical transport model was used. Applying the results of this chemical transport model only the yearly average of this effect could be analyzed. The results will show how this effect is important and how we will able to put this information into an air quality forecasting system.

The current version of the EMEP model working on a polar-stereographic projection, true at 60 N, has commonly been used, with grid-size of 50 km×50 km at 60 N. The standard domain has changed somewhat over the years, and was enlarged towards Eurasia in 2007. The model currently uses 20 vertical levels from the surface to the top of the model domain (currently: 100 hPa, 15 km). The 15 km high air column is divided into 20 levels in a form that the lower layer (3 km), which is relevant in the mixture of air pollutants, includes 10 levels, allowing the detailed examination of this air layer. The EMEP model uses a chemical pre-processor to convert lists of input chemical species and reactions to differential equations in Fortran code. The default chemical scheme, which is used in the open source version of the EMEP model, is the EmChem09. This chemical scheme describes 137 reactions and 26 photochemical reactions between 72 chemical species. The model calculates the dry and wet deposition of the chemistry substances. The dry deposition flux is determined by using the deposition velocity, while the wet deposition processes include both in-cloud and sub-cloud scavenging of gases and particles.

The standard emissions input required by EMEP model consists of gridded annual national emissions of sulphur dioxide (SO<sub>2</sub>), nitrogen oxides (NO<sub>x</sub> =NO+NO<sub>2</sub>), ammonia (NH<sub>3</sub>), non-methane volatile organic compounds (NMVOC), carbon monoxide (CO), and particulates (PM<sub>2.5</sub>, and PM<sub>coarse</sub>, the latter being the coarse aerosol fraction, PM<sub>10</sub>-PM<sub>2.5</sub>). The particulate matter categories can be further divided into elemental carbon, organic matter, and other compounds as required. Emissions can be from anthropogenic sources (burning of fossil and biomass based fuels, solvent release, etc.), or from natural sources such as foliar VOC emissions or volcanoes.

The EMEP model has been adapted to run with meteorological fields calculated by a number of numerical weather prediction models, like the ECMWF IFS. Beginning from 2001, the data of the ECMWF IFS are available for forecasts with 0.125° × 0.125° horizontal grid length and 137 vertical levels, and this model became the default meteorological driver.

## **RESULTS**

The amount of pollutants emitted in one location and the fraction that finally reaches a certain downwind location depends on three factors: (i) the quantity of the pollutant emitted or produced at the source, (ii) the meteorological conditions that transport the pollution from one continent to another, and (iii) the physical and chemical transformation processes that modify the quantity and composition of the pollution during transport that lasts from days to weeks. The aim of our work was determining the effect of the long

range transport on the air quality of Budapest. This information could be very important when an air quality forecast system is being developed. Without these information the forecasted values of different pollutants could be underestimated. The special output of the EMEP chemical transport model was used: the yearly grid-to-grid source-receptor calculations by country for deposition of sulphur and nitrogen, and concentrations of particulate matter (PM). To evaluate the year to year temporal variability of the long range transport the model results between 2000 and 2013 were analyzed.

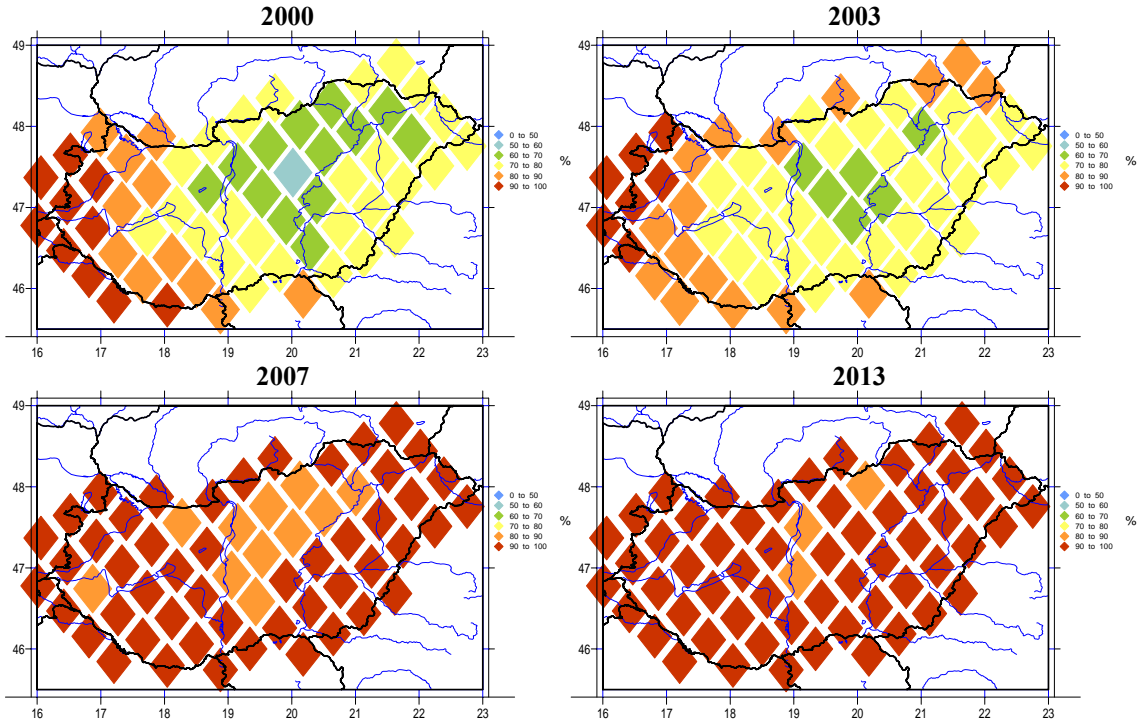


Figure 1. Fraction of transboundary contribution to  $SO_x$  deposition in Hungary (unit %)

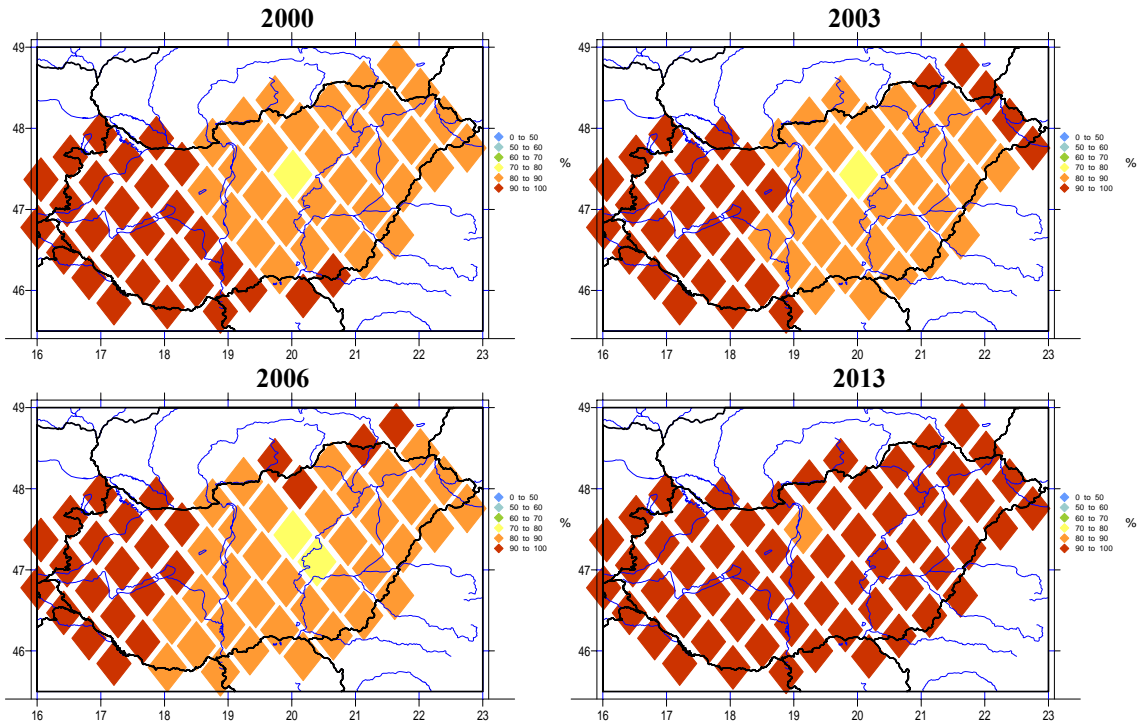
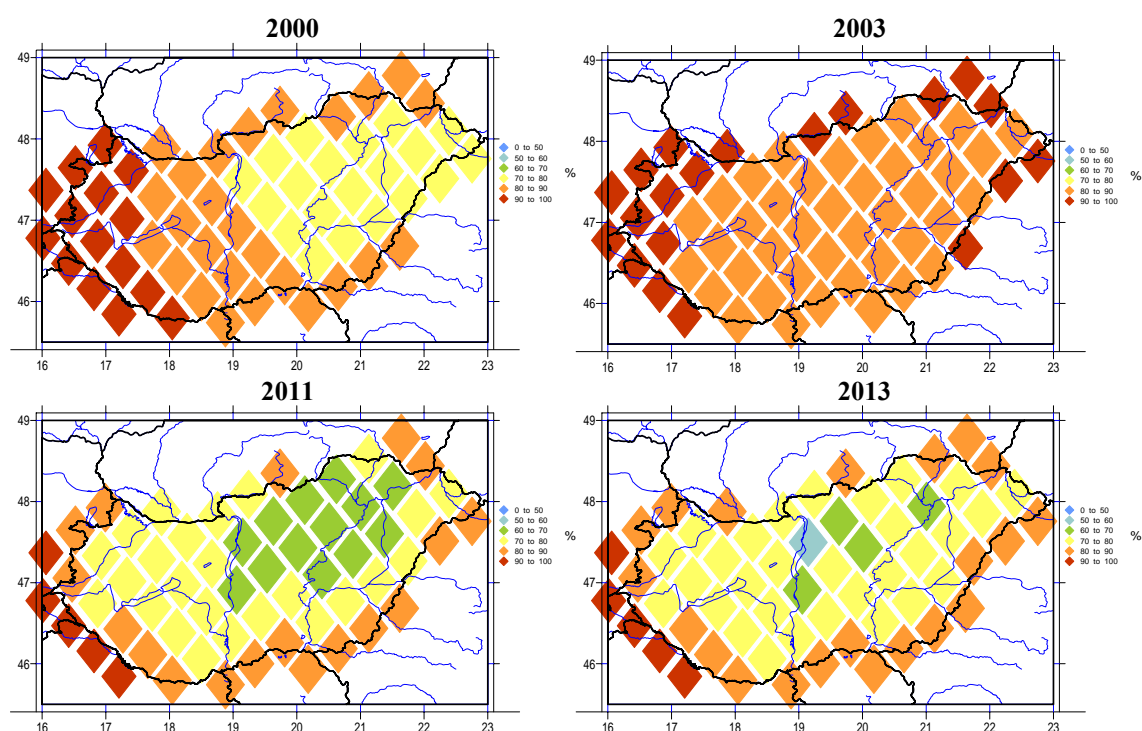


Figure 2. Fraction of transboundary contribution to  $NO_x$  deposition in Hungary (unit %)

In Figures 1-3. the results of model calculations are shown in mapped format, indicating the fractions of transboundary contributions to sulphur and nitrogen deposition, as well as PM<sub>10</sub> concentration, respectively. The effect of the long-range transport shows significant spatial variability, the most important part is at the western frontier of Hungary, and the smallest one is in the central part of the country.

Considering the deposition of SO<sub>x</sub> and NO<sub>x</sub> the picture was changed remarkably in the last 14 years. After 2007, the deposition of oxidised sulphur and nitrogen in Hungary are determined mainly by the transboundary sources. The quantity of this effect is larger than 90%, and it is smaller only in the surrounding area of Budapest.

In case of PM<sub>10</sub> the situation is somewhat different, as the effect of the long range transport shows a continuously decreasing tendency. The multiyear variation is mainly explained by changes in the PM<sub>10</sub> emission of Hungary. In the years when the emission of Hungary was decreased significantly the proportion of the long-range transport increased slightly. Unfortunately, the emission of PM<sub>10</sub> was not decreased in Hungary as much as it decreased in Europe.



**Figure 3.** Fraction of transboundary contribution to PM<sub>10</sub> concentration in Hungary (unit %)

In Figure 4, the temporal variation of fractions of transboundary contribution to SO<sub>x</sub> and NO<sub>x</sub> deposition and PM<sub>10</sub> concentration in Budapest is presented. Based on the results gained from model calculations, it can be stated, that a significant increase of transboundary contribution can be seen for sulphur, while transboundary contribution to PM<sub>10</sub> concentration in Budapest tended to decrease during 2000-2013.

The temporal variation can mainly be explained by changes in the rate of emission in Hungary, especially in the surrounding area of Budapest and in Europe. During the period, when the emission of Hungary decreased significantly, the proportion of the long-range transport increased slightly.

The emission of SO<sub>x</sub> dramatically decreased in Hungary until 2005, then there was a gradual decline. Parallel to this, the emission of SO<sub>x</sub> in Europe decreased continuously. This is the reason why the effect of the long-range transport increased significantly until 2005, and then it was changed only slightly.

The situation in case of  $\text{NO}_x$  is different, because the emission of  $\text{NO}_x$  continuously decreased both in Hungary and in Europe. This is the reason why the fractions of transboundary contribution to  $\text{NO}_x$  deposition is around 85% during the 14 years investigated.

In the last decade the emission of the  $\text{PM}_{10}$  in Europe continuously decreased while in case of Hungary the emission was rather stagnant with a fluctuation of  $\pm 20\%$ . This situation explains, that the fraction of transboundary contribution to  $\text{PM}_{10}$  concentration in Budapest continuously decreases.

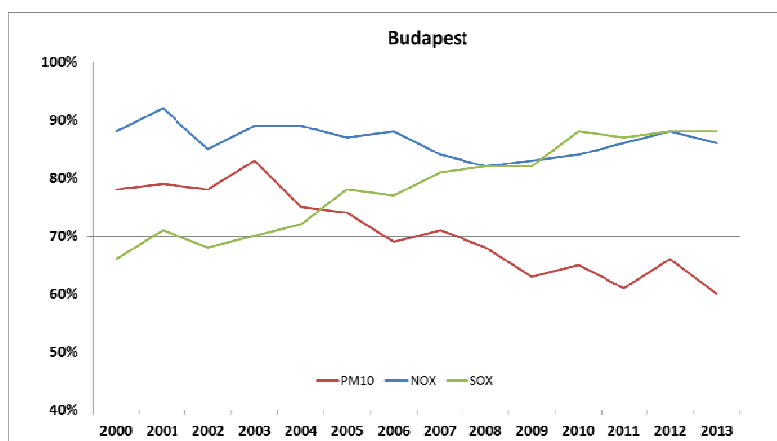


**Figure 4.** Fraction of transboundary contribution to  $\text{SO}_x$  and  $\text{NO}_x$  deposition and  $\text{PM}_{10}$  concentration in Budapest (unit %)

## CONCLUSION

In this work the effect of the long range transport on the air quality of Budapest and surrounding area was determined using the outputs of EMEP chemical transport model. It was determined that the effect of the transboundary sources on the air quality of Budapest is essential, its fraction is higher than 60% in all three pollutants' cases. These results are proving, that without boundary conditions calculated by a global chemical transport model, an air quality forecasting model is unable to produce realistic air quality forecasts for the area of Budapest.

## REFERENCES

- Benkovitz, C. M., Schwartz, S. E., Jensen, M. P., Miller, M. A., Easter, R. C., & Bates, T. S., 2004: Modeling atmospheric sulfur over the Northern Hemisphere during the Aerosol Characterization Experiment 2 experimental period. *J Geophys Res: Atmos* **109**. D22207, doi:10.1029/2004JD004939.
- Tu, F. H., Thornton, D. C., Bandy, A. R., Carmichael, G. R., Tang, Y., Thornhill, K. L., ... & Blake, D. R., 2004. Long-range transport of sulfur dioxide in the central Pacific. *J Geophys Res: Atmos* **109**. D15S08, doi:10.1029/2003JD004309.
- Simpson, D., Benedictow, A., Berge, H., Bergström, R., Emberson, L. D., Fagerli, H., Flechard, C. R., Hayman, G. D., Gauss, M., Jonson, J. E., Jenkin, M. E., Nyíri, A., Richter, C., Semeena, V. S., Tsyro, S., Tuovinen, J.-P., Valdebenito, Á., and Wind, P., 2012.: The EMEP MSC-W chemical transport model – technical description, *Atmos. Chem. Phys.*, **12**, 7825-7865.
- Zien, A. W., Richter, A., Hilboll, A., Blechschmidt, A. M., & Burrows, J. P., 2014: Systematic analysis of tropospheric  $\text{NO}_2$  long-range transport events detected in GOME-2 satellite data. *Atmos Chem Phys*, **14**, 7367–7396.
- Borge, R., Lumberras, J., Vardoulakis, S., Kassomenos, P., & Rodríguez, E., 2007: Analysis of long-range transport influences on urban  $\text{PM}_{10}$  using two-stage atmospheric trajectory clusters. *Atmos Environ*, **41**, 4434-4450.
- Donnelly, A. A., Broderick, B. M., & Misstear, B. D. (2015). The effect of long-range air mass transport pathways on  $\text{PM}_{10}$  and  $\text{NO}_2$  concentrations at urban and rural background sites in Ireland: Quantification using clustering techniques. *J Environ Sci Health, Part A*, **50**, 647-658.
- Moreno, T., Querol, X., Alastuey, A., Viana, M., Gibbons, W., 2005. Exotic dust incursions into central Spain: implications for legislative controls on atmospheric particulates. *Atmos Environ* **39**, 6109-6120.

**17th International Conference on  
Harmonisation within Atmospheric Dispersion Modelling for Regulatory Purposes  
9-12 May 2016, Budapest, Hungary**

---

**ANALYSIS OF THE DAILY CYCLES IN THE DATA ON AIR POLLUTION THROUGH THE  
USE OF ADVANCED ANALYTICAL TOOLS**

*Marija Zlata Božnar<sup>1</sup>, Boštjan Grašič<sup>1</sup>, Primož Mlakar<sup>1</sup>,  
Dejan Gradišar<sup>2</sup> and Juš Kocijan<sup>2,3</sup>*

<sup>1</sup>MEIS d.o.o., Mali Vrh pri Šmarju, Slovenija

<sup>2</sup>Jožef Stefan Institute, Ljubljana, Slovenija,

<sup>3</sup>University of Nova Gorica, Nova Gorica, Slovenija,

**Abstract:** From a temporal viewpoint, air pollution has significant daily patterns/cycles of behaviour. Daily patterns are highly expressed especially in case of ground-level ozone pollution, pollution caused by the domestic heating with solid fuels (in particular in the event of the exploitation of wood biomass in various forms), and in case of pollution caused by traffic, when it comes to traffic due to commuters.

These cycles are partly conditioned by anthropogenic reasons as is the case with traffic and domestic heating systems, and partly by natural phenomena. In both cases, a detailed observation and an understanding the daily cycles rules or daily patterns of air pollution can be significant and at the same time can contribute to more effective measures to reduce the harmful impact of air pollution on human health. The measures are more effective when they are designed more targeted to specific parts of the population and for concrete measures of avoiding the harmful effects of air pollution.

In this article, we will first present the advanced analytical tools, the “sunflower” graph, which was developed for the analysis of the characteristics of the daily cycles of meteorological data, data on air pollution and other related content. The “sunflower” graph is a double radial frequency diagram, which allows the plotting of samples for analysed time periods of different lengths. The key advantage is the ease of understanding the result and the ability to present information in the form of a graphic pattern, allowing the user to quickly understand the content that would otherwise be required to be represented by a plurality of unclear numerical data.

Using the “sunflower” tool, we will present an analysis of the meteorological parameters that are important for the understanding of air pollution and air pollution data for different locations in Slovenia.

**Key words:** *daily cycles, analysis tool, sunflower, air pollution flower, weather flower, wind flower*

## **INTRODUCTION**

Numerous processes in nature have a diurnal cycle. Firstly, this applies to basic meteorological processes that describe the processes in the atmosphere. These processes subsequently also affect the processes of atmospheric pollution. When exploring the entire atmospheric pollution cycle, many emissions already have a distinctive diurnal cycle (such as emissions from traffic and domestic heating sources). Moreover, everyone is already familiar with the diurnal cycle of the ozone, when we speak about the concentrations in the lower atmosphere. In order to understand, and subsequently reduce the bad influence of pollutants on the health of people, it is necessary to recognize such diurnal cycles with concentrations in the atmosphere, and to present them in a manner which is easily understandable to the lay public. An understandable presentation of atmospheric pollution is one of the preconditions for people to be able to organize their daily activities in a way to minimize our exposure to polluted air, if we cannot eliminate the pollution entirely.

Researchers of atmospheric pollution usually dedicate too much attention to the aspect which is interesting merely to us, namely the statistical analysis and the presentation of the concentration of pollutants in the atmosphere. This aspect is mainly dictated by regulatory requirements (e.g. EU directives), and we keep forgetting the aspect of presenting the statistics to the final users (exposed population). Thus, MEIS has defined a new way of a graphical method of analysis, which is suitable for a statistical analysis of diurnal cycles. We called the basic graph the “sunflower”. In this paper, we will firstly present this graph, and subsequently demonstrate a few cases, how this graph may be useful in statistical analysing, and for the presentation of the data about the concentration of pollutants in selected locations.

## METHODOLOGY

We firstly encountered the problem, i.e. seeking an appropriate presentation of diurnal cycles, when we studied the meteorological variables – global solar radiation. We defined a new way of a graphical method of analysis, which we called the “sunflower”. A detailed definition of the method is available in the paper (Božnar et al., 2015). The objective of this chart is an explicit graphical presentation of the characteristics of the diurnal cycle of the observed environmental parameter. A graphical display of the characteristics allows a quick perception of the information. It is even more important that people are mainly trained in a way that they are able to easily find both similarities and differences in the details between two more or less similar images. Such similarities and differences are of course noticed much faster on an image than in a numerical table chart.

The example of two sunflower graphs is presented in Figure 1. On the left, we can see the analysis of the measured half-hour data for January 2015, for the global solar radiation at the Pustice station in the continental part of Slovenia. On the right, we can see the same analysis for July 2015. The sunflower is actually a double circular histogram. The course of preparation of this chart will be presented with the case of global solar radiation measurements. Firstly, we have to sort all the measurement values into groups for each hour of the day, namely into groups from 1 to 24, whereby a measurement must be sorted in the interval (each interval is independent), when the measurements were actually taken, and the interval mark is the full hour mark at the end of the interval. Each given group is then separately presented in the form of a spike (segment) on the sunflower graph in the direction from the centre towards the appropriate time. Measurements performed within one class for each individual hour are subsequently sorted into classes by values. We selected 8 value classes with solar radiation, which are presented on the graphical legend besides the graph. The boundaries between the classes are chosen so that they are reasonably adapted to the problem under consideration. In this case the values under  $5\text{W/m}^2$  are sorted in the class “darkness”, which is presented in the centre of the diagram as a share in %. This central class consists of all the values which are not interesting for the analysis of the daily cycle (darkness in this case, when there is no solar radiation). In the other classes, which are presented on a spike, we sort out the values on a scale from the lowest borderline to the highest expected value, however, the last class may be left open in the upward direction (as is the case in the figure for the values above  $1,100\text{W/m}^2$ ), when we expect only a few very large values. Each individual value class on the figure is presented as a spike section of a clock in its own time class. Hereby, all the individual spike parts are aligned on a virtual radial line running from the centre point to the mark of the corresponding time on the outer circle of a circular graph. Each value class has its own codifying colour, in the event potentially black/white image reproductions, we present the values also with the width of the spike section. The length of the spike section is proportional to the percentage of the class in comparison to the whole. The whole is identified as a number of all (mark besides the graph: “all”) measurement intervals, which occur from the beginning of the statistical interval until the end. This interval for the statistical treatment is written beside the graph in the form of a date. Specifically, it makes sense to also write how many of the used measurement values were useful (“good”) and how many of them were unknown and incorrect (“unknown”).

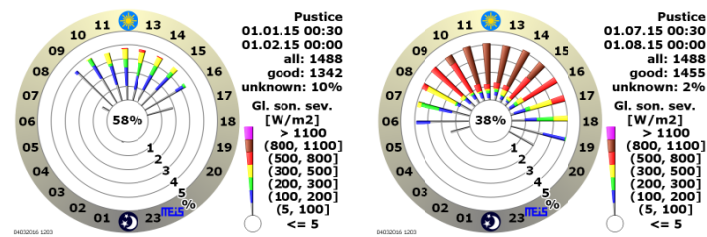


**Figure 1.** On the left, we can see the analysis of the measured half-hour data for January 2015, for the global solar radiation at the Pustice station in the continental part of Slovenia. On the right, we can see the same analysis for July 2015.

In the final figure (case of the left or right image in Figure 1) we may clearly see the representation of individual global solar radiation value classes by the hours of the day. In the winter month of January, we have a relatively short period of the light of the day (from 7 a.m. to 5 p.m.), thus interesting value classes are visible only in these hours. We do not indicate clock spikes during the night time, but present their measurement values together for all the hours as a part of the whole, indicated in the centre of the graph. However, the bright part of the day in the July sunflower is evidently longer, according to the colour scale, we can also see the highest values. The representation of the value classes by individual hours determines the natural course of the global solar radiation deviations from the theoretically expected course. It indicates when on average a cloud or fog reduces the global solar radiation, which penetrates to the ground. On the way, as we have just described the presentation of the global solar radiation on the “sunflower” graph, we can introduce other variables. Unlike traditional wind rose, with the help of this wind flower we are able to give the wind speed (i.e. categorization of absolute speed in classes and by hours without considering the direction of the wind) or any other data on the concentration of atmospheric pollutants for the chosen location and the pollutant. It is also important that the statistical interval expressed with the sunflower is at least a day long if possible, but it does not have any limitations regarding the duration (day, week, month, quarter as a season, year, several years etc.). The sunflower graph and the air pollution flowers are very appropriate for the comparison of the daily statistics not only between various periods of time but also between various locations (e.g. for the same month between various locations across the country). Such cases will be shown below.

## RESULTS

In Figure 2 we present an analysis of the PM<sub>10</sub> measured values for the town of Zagorje on a complex terrain in central Slovenia. The analysis comprises daily cycles which were measured every 30 minutes for a period of one year. We created air pollution flowers for each individual month. Thus, we are able to quickly determine the information on various daily pollution patterns for various parts of the year. Zagorje is a place in a narrow half-closed valley, which partly expands to a basin, the winds are weak and thermal inversions are common during the winter. Particle pollution comes from the traffic, local heating sources, and the production of lime (Božnar et al., 2014, Mlakar et al., 2012). The figures show in a very clear and graphical way the following information about typical daily air pollution regimes with PM<sub>10</sub>: Firstly, the yellow and brown spikes present relatively high concentrations; green, blue and grey spices consequentially show more and more clean air. Very clean air as a share in every interval is also presented in the centre of each air pollution flower. Firstly, we see that during the winter months from December to February inclusively, the pollution is pronounced during the entire day, the highest values in December and January occur in the late afternoon and last until midnight, or an hour longer, which indicates that they are most likely due to heating (people start the heating when they return home from work). The opposite of this are the months of June, July and August, when the air is more or less clear for the major part of the day, a few higher concentrations may be noticed in the late afternoon, from 3 p.m. to 8 p.m., which indicates the influence of the traffic (the station is located very close to the main road through the town). In the spring and autumn, we can notice the transition from one described daily pollution pattern to another. Figure 3 presents the measurements for 8 individual consecutive days for PM<sub>10</sub> in the town of Celje, which also lies in central Slovenia. If we use the air pollution flower graph for individual days, we are able to monitor very precisely when in a day and in a week, high and low concentrations occurred, and are thus more able to find the reasons for them (or confirm the hypotheses about their origin when we do not have a spatial model in a sufficiently precise spatial and

time resolution). The lay public may use it for planning when to let fresh air into their houses, and outdoor activities.

Figure 4 presents the air pollution flower graph for ozone and NO<sub>2</sub> for two selected months; both graphs indicate these two pollutants in Celje, where the station is located in the centre of the town, where the impact of urban transport is felt. The scales on the display for ozone and NO<sub>2</sub> are chosen in a way that we notice only increased concentrations. A daily pollution with NO<sub>2</sub> is clearly visible both for April and September, and the elevated values follow the expected increase in the urban traffic during rush hours both in the morning and late afternoon. However, the picture is complementary with the ozone, as is apparent from the well-known cycle of formation and decomposition of ozone due to solar radiation and ozone precursors, among which, NO and NO<sub>2</sub> are also very important. The two graphs for ozone and NO<sub>2</sub> for the same month show the complementarity between the ozone and NO<sub>2</sub>. Exceedingly high concentrations of both are not present together at the same time. The air pollution flower graph for NO<sub>2</sub> and ozone vary from the PM<sub>10</sub> air pollution flower graphs, indicating that the elevated concentrations hardly occur during some hours of the day, which is clearly visible by the fact that the spikes at these hours are significantly shorter than those when the pollution is significant (if the concentrations occur in the clean air class, their presence on the graph is indicated in the numerically written share in the middle of the circle, however, they are not present as parts of the spikes).

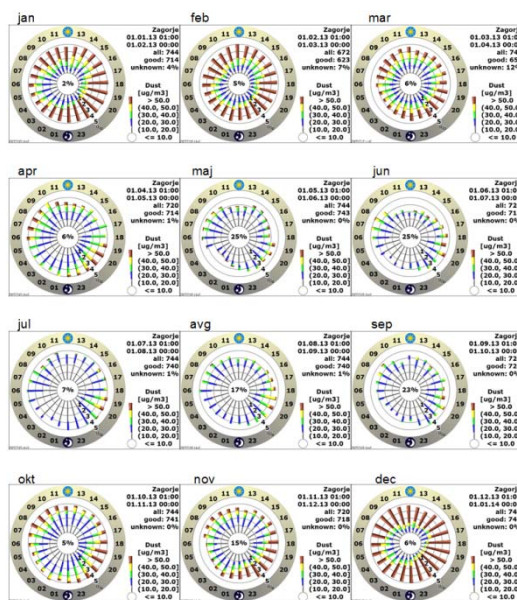


**Figure 2.** Analysis PM<sub>10</sub> measured values (dust) for Zagorje on a complex terrain in central Slovenia. The analysis comprises the daily cycles which were measured every 30 minutes for a period of one year (2013). We created air pollution flowers for each individual month.

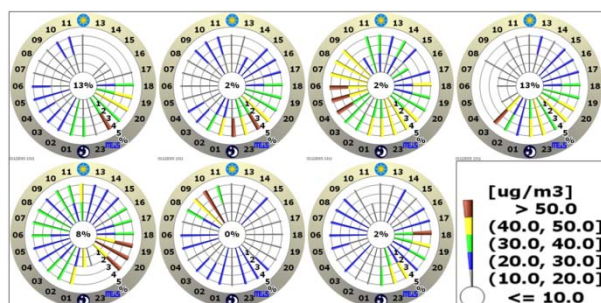


**Figure 3.** Measurement for 8 individual consecutive days for PM<sub>10</sub> in the town of Celje (22–29 November 2015), also in central Slovenia.

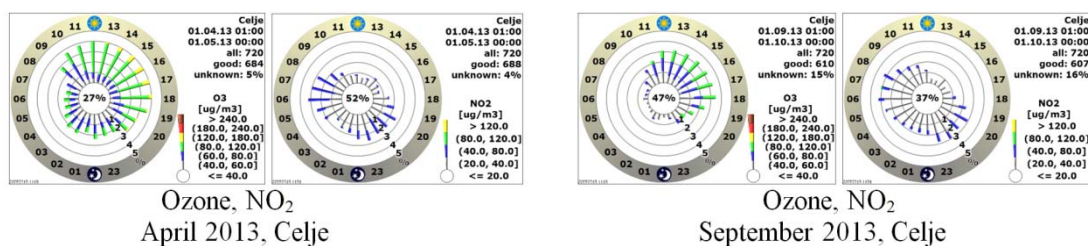


**Figure 4.** Presents the air pollution graph for ozone and NO<sub>2</sub> for two selected months, both graphs indicate these two pollutants in Celje, where the station is located in the centre of the town, and you can feel the impact of urban transport.

To conclude the presentation of the broad possibilities of using the sunflower graph, we present a weather flower graph in Figure 5, which is slightly modified version of sunflowers. This graph presents three main parameters of weather forecast, namely one individual day on each separate graph. These concentric rings indicate the forecast for cloudiness, which is the nearest to the centre of the graph, the following ring indicates solar radiation, and the last ring indicates the predicted precipitation based on the same principle as the sunflower graph. Figure 5 shows an example of the use with a pictorial legend. With such a presentation, we are able to show a much more detailed weather forecast without using numerous pictograms or line charts, which are not close to all the lay public.

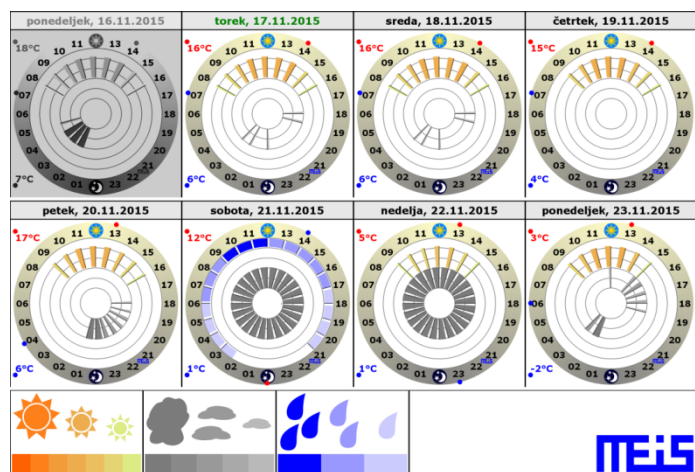


**Figure 5.** Example of a weather flower graph, presentation example of a selected location at Krško for eight days (previous day, current day, following 6 days)

## CONCLUSION

The paper presents our new analytical tool, the “sunflower” graph, which is suitable both for basic meteorological parameters, as well as an analysis of daily concentrations of air pollutants. Some of possible examples of the application are defined in detail in the Results, however, they are not only limited to these kinds of application, a few additional options are described in the paper Božnar et al. 2015.

## ACKNOWLEDGEMENT

This research was supported by the Slovenian Research Agency Projects No. L1-4154(A), L2—5475(C) and L2—6762(B). We are grateful to Slovenian Environment Agency for measured data from Zagorje and Celje.

## REFERENCES

- Božnar, M. Z., B. Grašič, P. Mlakar, J. R. Soares, A. P. de Oliveira and T. S. Costa, 2015: Radial frequency diagram (sunflower) for the analysis of diurnal cycle parameters: solar energy application. *Applied energy*, **154**, 592-602, doi: 10.1016/j.apenergy.2015.05.055.
- Božnar, M. Z., B. Grašič and P. Mlakar, 2014: The problem of limit values exceedances detection in complex terrain using measurement and models. *16th International Conference on Harmonisation within Atmospheric Dispersion Modelling for Regulatory Purposes*, 8-11 September 2014, Varna, Bulgaria. BATCHVAROVA, Ekaterina (ur.), KIROVA, Hristina (ur.), HRISTOVA, Elena (ur.). HARMO 16: proceedings. [Sofia]: National Institute of Meteorology and Hydrology, Bulgarian Academy of Sciences, 5 pages
- Mlakar, P., M. Z. Božnar, B. Grašič, and G. Tinarelli, Gianni, 2012: Zasavje canyon regional online air pollution modelling system in highly complex terrain - description and validation. *International Journal of Environment and Pollution*, **50**,. 22-30.

**17th International Conference on  
Harmonisation within Atmospheric Dispersion Modelling for Regulatory Purposes  
9-12 May 2016, Budapest, Hungary**

---

**JRODOS FOR NUCLEAR EMERGENCIES:  
IMPLEMENTATION IN SWITZERLAND AND FURTHER DEVELOPMENTS**

*Markus Oberle and Cyrill von Arx*

Swiss Federal Nuclear Safety Inspectorate ENSI, Industriestrasse 19, CH-5200 Brugg, Switzerland

**Abstract:** JRODOS stands for Java Real-time Online DecisiOn Support system and is a modular programme intended for use in radiological emergency protection. Switzerland has implemented this software as primary prognosis tool for the impact assessment of radiological emergencies in nuclear installations. As a result, Switzerland has become a major promoter of this system and has been instrumental in furthering its development.

**Key words:** *JRODOS, decision support system, emergency protection, dose calculation, system development*

## **INTRODUCTION**

Providing prognostic assessment of the radiological situation in case of a nuclear accident and suggesting appropriate emergency protection measures to the decision makers is one of the key tasks of the Swiss Federal Nuclear Safety Inspectorate ENSI, as stipulated by law. From the year 2000 until 2015, the code ADPIC was used to achieve this goal. However, in 2010 a project was launched to find a suitable successor for the ageing program and from 2012 onwards JRodos was the preferred solution. As a consequence, ENSI has invested greatly in further developing the abilities and functions of JRODOS as well as increasing its stability.

## **DEVELOPMENTS**

To provide at least the same level of quality and detail as the previous system, advanced requirements for JRODOS were defined and the development of the software was fostered in these directions. The first among these was the use of meteorological data from the COSMO-2 model with its native time step of 10 minutes as provided by the Swiss Federal Office of Meteorology and Climatology MeteoSwiss. This in turn led to the possibility of calculating with a time resolution of 10 minutes (compared to the hourly resolution before).

Next came the request for a fivefold nested grid with selectable number of 'rings' and selectable innermost horizontal grid resolution. This grid is composed of approximately 30'000 grid cells per ring, totalling approximately 150'000 grid cells. The horizontal resolution is reduced by half from one ring to the next; combined with the fixed number of cells per ring and a selectable innermost grid resolution, this leads to a configuration where the downwind distance can be doubled by adding another ring. The values currently available for the innermost grid resolution are 50 m, 125 m, 250 m, 500 m, and 1 km.

A further development was the incorporation of approximately 140 nuclides (compared to the 25 nuclides available before) to cover regulatory requirements and the automatic inclusion of the most important mother or daughter nuclides if not already present in the source term nuclide list. As a consequence in the next release, the developers will include completely new dose conversion factors (according to ICRP119 and corresponding calculations performed by Public Health England) to provide a state-of-the-art dose calculation methodology.

Another new feature requested was a method for defining periodically recurrent jobs which run independently of any client GUI. This last request is intended, e.g., for hourly dispersion simulations for all nuclear installations of a certain country based on the most recent meteorological forecast.

Last but not least, we have been instrumental in the parallelisation and implementation of the Lagrangian dispersion model LASAT as a sub-module. LASAT (LAGrange Simulation of Aerosol Transport) is a

dispersion model developed by Janicke consulting (Janicke, 2011) and incorporates state-of-the-art methods for the treatment of physical processes. It conforms to the VDI guideline 3945 part 3 and was the basis for the development of the German regulatory model AUSTAL2000, the official reference model of the Technical Instruction on Air Quality Control (*TA Luft*).

Parallelisation has been a major topic because speed is essential in case of a nuclear emergency. The requirements of ENSI's emergency organisation demand the availability of simulation results within 15 minutes at most, for a clearly defined benchmark configuration. This configuration mirrors a typical emergency calculation: a simulation domain of 24 km radius (approximate size of the UPZ in Switzerland), prognostic time span of 24 hrs, horizontal resolution of 250 m, time resolution of 10 min, and a source term consisting of approximately 100 nuclides. Thus, JRodos and LASAT had to be adapted to make sure multiple simulations started from one client run in parallel on the available sockets and cores. Research by the Ingolstadt University of Applied Sciences together with Janicke Consulting helped pave the way for a sufficient parallelisation of LASAT (Meyer *et al.*, 2012).

On a more general basis, ENSI has pushed for an increase in stability and reliability of the system. This includes a test suite designed by the developer and executed by himself before all releases, intended to ensure that no bugs are (re-)introduced into productive versions. All users are invited to provide test cases for this suite such that the range of possible applications of the system is eventually covered. Overall, JRODOS has matured significantly and became suitable for continuous operation as decision support tool in an emergency organisation environment.

#### **IMPLEMENTATION**

Since JRodos is intended as tool for the emergency organisation staff, it must be running on reliable and suitable hardware and of course be constantly available. The hardware layout chosen by ENSI is quite simple: two identical and parallel machines with JRodos server running on both, using completely independent databases. Thus, we have an operational system and a test system. The hardware chosen consists of two IBM X3850 X5 systems with four sockets of ten cores each, Xeon E7-8870 2.4 GHz processor cores, 256 GB RAM, and eight 280 GB SAS disks. Although this is very modest in comparison to the system required by ADPIC, JRodos runs suitably fast and provides results within a timespan acceptable for the emergency organisation.

The client runs on the workstations locally and connects primarily to the operational system but can be changed to address the test system. For training purposes, we provide the client as Windows 'Work Resource.' In this way, we set up the client on an in-house server and define which Windows users are permitted to access the program from their desktop or portable machines. A 'Work Resource' behaves similar to a Remote Desktop connection with only the program window being transmitted. This has the advantage of requiring only one centralised client instance to be updated and maintained.

At the National Emergency Operations Centre NEOC, another server-client combination is set up, with comparable configuration and hardware but a different operating system. Our aim is to connect these two systems in such a way that at login time the JRodos user can specify which of the three servers (in total) will be accessed. This will provide not only redundancy but also diversity to the two organisations.

#### **HANDLING OF METEOROLOGICAL FORECAST DATA**

Atmospheric dispersion simulations are based on numerical weather prediction (NWP) data. At ENSI (and NEOC), we use the forecast of COSMO-2, which is provided by MeteoSwiss every three hours for a prognosis time span of 24 hrs. To manage incoming data, we have set up two virtual SFTP servers and two virtual 'meteo' servers, connected as two parallel branches. The datasets are sent in parallel to both SFTP servers and stored on disks mounted from the 'meteo' servers. From there, the data sets are transferred to the operational and the test system, respectively. In addition, a daily backup of the forecast data is made. In case one of the SFTP or 'meteo' servers fails, the other transfer branch will provide both machines with data. This way, we have achieved redundancy in the delivery process to ENSI as well as within our data handling system. At NEOC, one train of SFTP and 'meteo' servers is set up to handle NWP data.

## **OUTLOOK**

All the software developments detailed above lead to a simulation time of about 15 minutes for a typical calculation and about 30 minutes for the benchmark configuration on our hardware. Whilst this is sufficient for application within our emergency organisation, we envision further developments to enable speedier and more versatile calculations. Paramount amongst these is the further parallelisation of JRodos, its modules, and sub-modules as well as the interaction between them to achieve an extended and architecture-independent use of the available processor power.

## **REFERENCES**

Janicke Consulting, 2011: Dispersion Model LASAT Version 3.2 Reference Book.  
Meyer, Facchi, and Pichler, 2012: Performance Analysis and Optimization of the LASAT Dispersion Model. Final Report to ENSI.

**17th International Conference on  
Harmonisation within Atmospheric Dispersion Modelling for Regulatory Purposes  
9-12 May 2016, Budapest, Hungary**

---

**IMPROVING URBAN AIR QUALITY USING A COST-EFFICIENCY AND HEALTH BENEFIT  
APPROACH**

*A.I. Miranda<sup>1</sup>, J. Ferreira<sup>1</sup>, C. Silveira<sup>1</sup>, H. Relvas<sup>1</sup>, M. Lopes<sup>1</sup>, P. Roebeling<sup>1</sup>, A. Monteiro<sup>1</sup>, E. Sá<sup>1</sup>,  
C. Gama<sup>1</sup>, S. Costa<sup>2,3</sup>, J.P. Teixeira<sup>2,3</sup> and C. Borrego<sup>1</sup>*

<sup>1</sup>CESAM & Dep Environment and Planning, University of Aveiro, Portugal

<sup>2</sup>EPIUnit- Institute of Public Health, University of Porto, Portugal

<sup>3</sup>National Institute of Public Health, Environmental Health Department, Porto, Portugal

**Abstract:** Notwithstanding the achievements in emission reductions and air quality improvement in some European urban agglomerations like Grande Porto (Portugal), additional efforts have to be undertaken to improve air quality in a cost-efficient way. This work focuses on the definition and assessment of emission abatement measures and their associated costs, air quality and health impacts and benefits by means of air quality modelling and cost-benefit analysis tools. The MAPLIA modelling system was applied to the Grande Porto urban area, addressing (particulate matter) PM10 and (nitrogen oxides) NOx, which are the most pertinent pollutants in the region. Four different measures to reduce PM10 and NOx emissions were defined and characterized in terms of emissions and implementation costs, and combined into 15 emission scenarios simulated by an air quality model (TAPM). Air quality concentration fields were then used to estimate health benefits in terms of avoided costs (external costs), using dose-response health impact functions per pollutant for different health indicators (morbidity and mortality). Results revealed that the resulting scenario including all 4 measures lead to a total benefit of 0.3 M€/yr. Among the 15 scenarios analysed, the largest benefit is obtained for the scenario considering the conversion of 50% of open wood stoves into heat recovery wood stoves. Although the implementation costs of this measure are high, the benefits outweigh the costs. The most cost-efficient scenario is the one that combines the heat recovery wood stove measure and the replacement of 10% of passenger cars below EURO3 by hybrid vehicles.

**Key words:** *Emission abatement measures, air quality modelling, health impact functions, cost-benefit.*

## **INTRODUCTION**

Urban areas are still facing air pollution problems. The European Commission air quality standards (EU Directive 2008/50/EC) have been exceeded and Members States are obliged to develop and implement Air Quality Plans (AQP) to improve air quality and health (EEA, 2015).

Together with air quality assessment, quantifying the impact of air pollution on the public's health is an important component for the design and evaluation of effective local and regional AQP. The health impact assessment provides an objective estimate of the influence of the mitigation measures in air quality on a given population's health. It uses available epidemiological studies together with routine environmental and health data to evaluate the potential effects of a policy, programme or project on the health of a population, including how those effects are distributed across the population, thus helping decision makers to plan and implement measures to protect public health more effectively. Exposure-response function (ERF) can be used to estimate the risk of developing a disease due to exposure to agents with different levels of intensity and duration (Smith et al., 1999). Hence, an ERF links the concentration of pollutants to which a population is exposed with the number of health events occurring in that population. The appropriate selection of adverse health outcomes and ERF is a critical step. The impact is determined by the relation of two variables: exposure and effect. One or more indicators are used to express the change in population health status due to exposure to an air pollutant. Most health-based indicators are, or derive from, mortality and morbidity endpoints. Thus, to evaluate the health impacts arising from air pollution, the following aspects can be considered: (i) involved pollutants and their air concentration levels; (ii) health indicators analysed in terms of morbidity and mortality; (iii)

affected age groups; and (iv) exposure time. These data are used to quantify the extent of these impacts, evaluated through ERFs and health outcome frequencies, which combined with the population exposure to air pollution provides the number of attributable cases/days (Equation 1) (EC, 2005).

$$\Delta R_i = I_{ref} \times CRF_{i,p} \times \Delta C_p \times pop \quad (1)$$

where:

$\Delta R_i$  – Response as a function of nr of unfavourable implications (cases, days or episodes) over all health indicators ( $i = 1, \dots, n$ ) avoided or not;

$I_{ref}$  – Baseline morbidity/mortality annual rate;

$pop$  – Population units exposed to pollutant  $p$ ;

$CRF_{i,p}$  – Correlation coefficient between pollutant  $p$ 's concentration variation and probability of experiencing or avoiding a specific health indicator  $i$  (i.e. Relative Risk - RR);

$\Delta C_p$  – Change in pollutant  $p$ 's concentration after adoption of abatement measures (emission scenarios).

When economic values are applied to health endpoints, the monetary costs and benefits of different options can be directly compared (O'Connell and Hurley, 2009). The World Health Organization (WHO) has recently published a set of recommendations for ERF and cost-benefit analysis of key pollutants in support of the European Union's air quality policy revision (WHO, 2013). This report recommends ERF and associated background information for several mortality and morbidity effects associated with short and long-term exposure to particular air pollutants such as PM, ozone (O<sub>3</sub>) and nitrogen dioxide (NO<sub>2</sub>). The resulting health impacts are translated into monetary values (i.e. external costs), in order to be properly considered as economic costs. In the recent years, Integrated Assessment Models (IAM) for air quality planning (encompassing health impact assessment) have already been formulated and implemented at the continental and country scales (e.g. Carnevale et al., 2012; Amann et al., 2011). However, they are not specifically addressing the sub-national scale, particularly urban areas where a major share of the European population lives and where health impacts are more pertinent.

This work is focused on the definition and assessment of emission abatement measures and their associated costs, air quality and health impacts and benefits by means of air quality modelling tools and cost-benefit analysis, specifically developed for urban areas in the scope of the recently concluded MAPLIA project "Moving from Air Pollution to Local Integrated Assessment".

### THE MAPLIA SYSTEM

The MAPLIA system was designed to support the development of AQP requiring the definition and testing of local/regional abatement measures. It is based on a scenario analysis, which starts with the identification of control strategies/measures as a result of air quality exceedances. These measures have to be translated into emission reductions and their impacts on air quality quantified using modelling tools. Policy implications, technical feasibility, resulting costs and health impacts are evaluated, but not in a fully integrated perspective.

The MAPLIA system allows, therefore, evaluating the effects of previously selected measures in terms of costs, emissions, air quality, health impacts, and associated monetary benefits (i.e. avoided external costs). For this purpose, scenarios including different emission abatement measures are defined and their implementation costs are estimated. A reference scenario reflecting the emissions of a base year, for which only the influence of imposed/implemented measures in accordance with the legal framework is evaluated (CLE – Current Legislation Emissions), is the basis for the assessment. Reduction scenarios are established to cover non-compliance situations to the air quality limit values defined on the air quality Directive (2008/50/EC), aiming to act in an efficient and incisive way on the major emission sources in order to achieve significant benefits comparatively with the reference scenario. Based on the pre-defined emission scenarios, resulting emissions and air quality have to be quantified. The concentration values estimated by an air quality model, jointly with population data and morbidity and mortality indicators, expressed as health impact functions, allow calculating the number of attributable cases/days according to Equation 1. The number of cases is then transposed in monetary values allowing for the estimation of the avoided external costs per emission scenario. These costs are compared with the internal/implementation

costs of the respective scenario (cost-benefit analysis), constituting an added value in the decision-making process to identify the best policies to adopt for air quality management.

The MAPLIA system was adapted to Portuguese needs and a set of input information was prepared, including: a detailed emission inventory, emission scenarios, reduction measures and related costs, population distribution by age, air pollution based health indicators, and source-receptor relationships.

#### APPLICATION TO A CASE STUDY

The Grande Porto area (11 municipalities) was selected for the application of the MAPLIA system for the reference year 2012. This region of Portugal is one of the several EU zones that had to develop and implement air quality plans (AQP) to reduce PM10 and NO<sub>2</sub> concentrations (e.g. Miranda et al., 2015). This case study selection is based on the registered exceedances to the air quality limit values and on the available AQP. According to the national emission inventory, the share of NO<sub>x</sub> and PM10 emissions per activity sector for the Grande Porto area allows identifying industrial combustion, residential combustion and road traffic as the most relevant emission sectors.

The MAPLIA application to Grande Porto consisted of an emissions, air quality, health and cost-benefit analysis for a set of 15 scenarios based on combinations of the following 4 emission reduction measures: 1) Replacing 10% of light vehicles below EURO3 by hybrids (HYB); 2) Introducing a Low Emission Zone in the Porto city banning vehicles below Euro 3 (LEZ); 3) Replacing/reconverting 50% of the conventional fireplaces by more efficient equipment (FIR); and 4) Application of particle reduction technologies allowing reducing 10% of PM10 emissions from industrial combustion and production processes (IND) (more details in Duque et al., 2016). These measures to reduce PM10 and NO<sub>2</sub> concentrations were characterized in terms of emissions, and their impacts on air quality were evaluated by the application of the TAPM (The Air Pollution Model) to the 15 scenarios defined, along the meteorological 2012 year conditions. The TAPM applied at 1km/1h horizontal and temporal resolutions allowed assessing air quality improvements based on the reference scenario, with no reduction measures.

Based on the achieved air quality state for the different reduction scenarios, human health impacts were quantified using the Equation 1. These impacts were analysed through morbidity and mortality indicators associated to PM10 and NO<sub>2</sub> concentrations due to short and long-term exposure. Additionally, for each health indicator a survey of the associated external costs per case/day was carried out. In terms of long-term exposure, the costs were expressed as annual average costs taking into account the duration and chronic effects of the disease. Table 1 gathers the information used in the reduction scenarios to estimate health impacts (ERF recommended in WHO, 2013) and subsequent external costs (Pervin et al., 2008) updated to the base year 2012.

**Table 1.** Input dataset used for quantifying health impacts and external costs assigned to the PM10 reduction scenarios.

Health effect	Age group	Study design	Relative risk (%)	Baseline annual rate (%)	Cost (€)	Unit
Asthma	5 - 19 yr	Short-term	0.28	17	115	Day
Heart failure	> 65 yr	Short-term	1.85E-05	Included in RR	18,538	Case
Chronic bronchitis (incidence)	>18 yr	Long-term	1.17	0.39	18,970	Year
Chronic bronchitis (prevalence)	6-18 yr	Long-term	0.8	18.6	18,970	Year
Total mortality	< 1 yr	Long-term	0.4	0.163	1,844	YOLL

Once determined the number of cases and known the annual costs per health indicator, the benefits (or avoided external costs) to human health resulting from the application of the reduction scenarios were estimated. There is a strong positive correlation between the spatial patterns of population density and health benefits associated to the reduction scenarios. It means, therefore, that in densely populated areas,

normally with higher anthropic activity, and where the air pollution problems are more alarming, the potential health benefits of the reduction scenarios are larger than in rural areas. Furthermore, these abatement measures are focused on the main activity sources, mostly concentrated in urban centers, and so, air quality improvements in relation to the reference scenario are more significant on these air pollution hotspots. As an example, Figure 1 presents the spatial distribution of annual concentration averages ( $\mu\text{g}\cdot\text{m}^{-3}$ ) obtained for the reference case and for the scenario considering all emission reduction measures (in terms of percentage) and the human health benefits or avoided external costs ( $\text{€}\cdot\text{y}^{-1}$ ) for this total reduction scenario, for PM10.

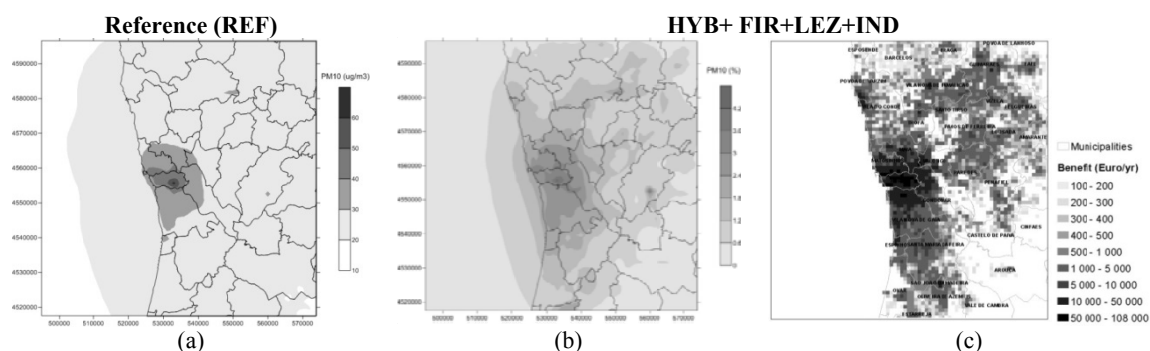


**Figure 1.** Modelling results (annual averages): (a) PM10 concentration ( $\mu\text{g}\cdot\text{m}^{-3}$ ) for the REF scenario; (b) percentage reduction of PM10 concentrations between the REF and the scenario including all the reduction measures; (c) human health benefits ( $\text{€}\cdot\text{y}^{-1}$ ) for the total reduction scenario.

Model simulation results for the reference scenario showed higher annual averages ( $>30 \mu\text{g}\cdot\text{m}^{-3}$ ) over Porto and the surrounding area mainly, where concentrations exceeding the legislated limit values are expected (Figure 1a). The remaining domain is characterized by low annual concentrations ( $\approx 15\text{-}20 \mu\text{g}\cdot\text{m}^{-3}$ ). The largest reductions in PM10 annual concentration are obtained for the application of FIR and IND measures and a combination of them. More details can be found in Duque et al. (2016). The combination of all referred measures (HYB+FIR+LEZ+IND) indicates a total reduction of 4.5% in PM10 concentrations mainly over Porto, which corresponds to reductions of up to  $2.8 \mu\text{g}\cdot\text{m}^{-3}$ . The spatial pattern of the human health benefits (Figure 1c) shows that in densely populated areas the potential health benefits of the reduction scenarios are larger than in suburban/rural areas. The largest contribution for health benefits derives from the reduction in PM10 concentrations in the Grande Porto municipalities

The application of the MAPLIA system was completed with the balance between the internal/implementation costs and health benefits (or avoided external costs) allocated to each scenario, taking as basis the year 2012. Table 2 summarizes the estimated values (in  $\text{M€}\cdot\text{y}^{-1}$ ) of internal costs and external benefits, for the most relevant reduction scenarios tested and considering the aggregate effect of PM10 and NOx pollutants.

**Table2.** Cost-benefit analysis of the reduction scenarios.

Reduction scenario	Implementation costs ( $\text{M€}\cdot\text{y}^{-1}$ )	Health benefits ( $\text{M€}\cdot\text{y}^{-1}$ )	Net benefit ( $\text{M€}\cdot\text{y}^{-1}$ )	Benefit-cost ratio (BCR)
HYB	2.0	1.5	- 0.5	0.75
FIR	0.8	1.8	1.0	2.25
LEZ	3.8E-2	3.9E-2	1.0E-3	1.03
IND	5.8	5.6	- 0.2	0.97
HYB + FIR	2.8	3.3	0.5	1.18
FIR + IND	6.5	7.4	0.9	1.14
HYB+FIR+LEZ+IND	8.6	8.9	0.3	1.03

The net benefit (i.e. benefits minus costs) per reduction scenario corresponds to the difference between the total health benefits (for NO<sub>x</sub> and PM<sub>10</sub> and considering both short and long-term effects) and the implementation costs (in M €/year). Table 2 shows that the fireplaces' scenario (FIR) is probably the best strategic option to improve the air quality reducing negative impacts on health, as this abatement measure provides largest net benefits (1.0 M €/year) and with a benefit-cost ratio of 2.25. Furthermore, the significant influence of this scenario when combined with other measures is notable.

It should be mentioned that this cost-benefit analysis did not consider all air pollution related health impacts and associated benefits. Moreover, environmental impacts and benefits were also not taken into account in this analysis.

## CONCLUSIONS

An Integrated Assessment Modelling system specifically adapted to urban areas was developed (the MAPLIA system) following a scenario analysis approach and applied to a Portuguese urban region – Grande Porto Area. A group of 15 emission reduction scenarios was defined based on combinations of 4 emission reduction measures. All these scenarios were evaluated in terms of an emissions, air quality, health and cost-benefit analysis. Results revealed that, among the 15 scenarios analysed, the resulting scenario including all 4 measures lead to a total net benefit of 0.3 M€.y<sup>-1</sup>. The largest benefit is obtained for the scenario considering the conversion of 50% of open wood stoves into heat recovery wood stoves. Although the implementation costs of this measure are high, the benefits outweigh the costs. The most cost-efficient scenario is the one that combines the heat recovery wood stove measure and the replacement of 10% of passenger cars below EURO 3 by hybrid vehicles.

The MAPLIA system is a useful tool for policy decision support for air quality improvement strategies, since it covers both air quality and health impacts and costs, and could be applied to other urban areas where AQP need to be implemented and monitored.

## ACKNOWLEDGEMENTS

The authors would like to acknowledge the financial support of FEDER through the COMPETE Programme and the national funds from FCT - Science and Technology Portuguese Foundation within project PEST-C/MAR/LA0017/2013 for the MAPLIA Project (PTDC/AAG-MAA/4077/2012), and also the PhD grants of C. Silveira (SFRH/BD/112343/2015), H. Relvas (SFRH/BD/101660/2014) and C. Gama (SFRH/BD/87468/2012), and the post-doc grant of J. Ferreira (SFRH/BPD/100346/2014). Thanks are also due, for the financial support to CESAM (UID/AMB/50017), to FCT/MEC through national funds, and the co-funding by the FEDER, within the PT2020 Partnership Agreement and Compete 2020.

## REFERENCES

- Amann, M., Bertok, I., Borken-Kleefeld, J., Cofala, J., Heyes, C., et al., 2011: Cost-effective control of air quality and greenhouse gases in Europe: Modeling and policy applications. *Environ. Model. Softw.*, **26**, 1489-1501.
- Carnevale, C., Finzi, G., Pisoni, E., Volta, M., Guariso, G., Gianfreda, R., Maffei, G., Thunis, P., White, L., Triacchini, G., 2012: An integrated assessment tool to define effective air quality policies at regional scale. *Environ. Model. Softw.*, **38**, 306-315.
- Duque, L., Relvas, H., Silveira, C., Ferreira, J., Monteiro, A., Gama, C., Rafael, S., Borrego, C., Miranda, A.I., 2016: Evaluating strategies to reduce urban air pollution. *Atmos. Environ.*, **127**, 196-204.
- EC (European Commission), 2005: ExternE Externalities of Energy - Methodology 2005 Update, Office for Official Publications of the European Communities, Edited by Peter Bickel and Rainer Friedrich, EUR 21951 EN.
- EEA (European Environment Agency), 2015: Air quality in Europe - 2015 Report, EEA Report. No.5/2015, Copenhagen, ISSN 1977-8449, 64 pp.
- Miranda, A.I., Silveira, C., Ferreira, J., Monteiro, A., Lopes, D., Relvas, H., Borrego, C., Roebeling P., 2015: Current air quality plans in Europe designed to support air quality management policies. *Atmos. Pollut. Res.*, **6**, 434-443.
- O'Connell E. and Hurley F., 2009: A review of the strengths and weaknesses of quantitative methods used in health impact assessment. *Public Health*, **123**, 306-310.

- Pervin, T., Gerdtham, Ulf-G, Lyttkens, C.H., 2008: Societal costs of air pollution-related health hazards: A review of methods and results. *Cost. Eff. Resour. Alloc.*, **6**, 22 pp.
- Smith, K.R., Corvalán, C.F., Kjellström, T., 1999: How much global ill health is attributable to environmental factors? *Epidemiology*, **10**, 573-584.
- WHO, 2013: Recommendations for concentration–response functions for cost–benefit analysis of particulate matter, ozone and nitrogen dioxide. Health risks of air pollution in Europe – HRAPIE project, WHO Regional Office for Europe, Copenhagen, Denmark, 54 pp.

**17th International Conference on  
Harmonisation within Atmospheric Dispersion Modelling for Regulatory Purposes  
9-12 May 2016, Budapest, Hungary**

---

**DISPERSION MODELING UNCERTAINTIES IN DISPERSION ENGINE (DE)**

*Robert Sigg, Håkan Grahn, Jan Burman, Niklas Brännström, Oscar Björnham, Petter Lindgren,  
Leif Å Persson, Pontus Von Schoenberg and Lennart Thaning*

The Swedish Defence Research Agency, Umeå, Sweden.

**Abstract:** We have used a method called Latin Hypercube Sampling (LHS) to study uncertainties in dispersion modeling. The strength of the method is that it reduces the number of runs needed to estimate the uncertainties. Input to the dispersion runs are based on probability distributions. Most of them are set through expert judgement but for wind direction, weather prediction ensemble runs can be used to add information to the distribution. Individual weather prediction runs have forecast errors and here we suggest a way to combine information on ensembles and wind direction error distributions via the LHS approach. Results show that the ensembles perturbed with the error distribution seem to give a better representation of the uncertainties from a probabilistic point of view. However, in directions with few ensembles represented, the approach with one perturbation per one ensemble member gives too much of a plume-like behaviour. Further improvements of the approach involve studies of a correct sampling approach to handle both a cluster of ensemble runs and single outliers. Also, it remains to study the stability of the LHS-approach.

**Key words:** *LHS, ensembles, probability distributions, dispersion modeling*

## **INTRODUCTION**

Uncertainties in dispersion modeling may sometimes be quite large, both concerning source terms and parameters controlling the dispersion itself. However, for decision makers it is becoming more and more important to also understand the uncertainties in relation to CBRN-releases. We have studied and implemented a method called Latin Hypercube Sampling (LHS) in order to reduce the number of numerical runs needed to estimate the uncertainties (Burman et al 2013, only in Swedish). In this stage of the implementation we have focused on developing the uncertainty calculations. One important part is however to suggest how the uncertainty calculations should be presented. Many times decision makers would like to have yes and no answers but uncertainties based on probability distributions only give solutions which are related to levels of probability. In this work we do not aim to develop presentation methods even though we have recognized that this is an important part if a decision maker should take full use of the calculations. Our goal is rather to explore how sensitive the solution is to different parameters and if there are any combinations which we need to pay extra attention to. Two of these parameters are wind speed and wind direction which determine the speed of the dispersed cloud and the main transport axis. The specific goal of this study is thus to investigate how the information of ensemble weather prediction runs can be combined with forecast error probability distributions in order to better describe the distributions of wind direction. The main scenario that we visualize is an accident where a release of a CBRN-substance may happen but does not occur immediately. Then decision makers may be interested in what happens if the release takes place now, in a couple of days or in five days. Information from an ensemble weather prediction system could be helpful in such a situation.

## **THE LHS METHOD**

The LHS method requires knowledge about the probability distributions for the parameters used as input data to dispersion runs. The number of runs in this approach is independent of the number of input parameters and only determined by how many subintervals of the probability distributions are used. The main rule is to never use the same subinterval twice. We typically use 50 subintervals which also coincides with the number of ensemble runs in many numerical weather prediction systems.

The LHS approach is implemented in a framework called Dispersion Engine (DE) which is used by the Swedish rescue services for example. The DE framework takes care of source descriptions, dispersion calculations and effect calculations. It runs in a .NET environment with all the dispersion models set up as separate executables. DE was originally designed for training and simulation environments and is also currently used in a simulation tool for the Swedish armed forces stand-off detection instrument RAPID.

## ENSEMBLES

Since the motions in the atmosphere are a part of a chaotic system the solutions are sensitive to the initial conditions. Therefore, a numerical weather prediction system is built-up both with so-called deterministic runs and runs where the initial conditions are perturbed (see for example Toth and Kalnay 1993). The runs using a perturbed initial condition defines the ensemble weather prediction solutions. Basically, for a specified location at a specified time we obtain approximately 50 different solutions which can be used to estimate the uncertainty of the deterministic weather forecast. Each ensemble run is said to be equally probable. The difference between the deterministic run and the ensemble runs is mainly that a lower resolution is used in the ensemble runs. Therefore, a control run is performed which is a part of the ensemble but with the same initial conditions as the high resolution deterministic run. The ensemble runs often coincides with the deterministic run the first days and it is not until day three into the forecast that you usually notice differences. At day five into the forecast and onward the differences are clearly seen. In this study we have not analyzed real ensemble weather forecasts but instead defined two academic realizations corresponding to how day three and five may behave in a weather prediction system. In summary, first a smaller spread is considered and then one where significant jumps consist in the ensemble solutions.

## PROBABILITY DISTRIBUTIONS

Here, we have studied LHS-runs in DE where probability distributions are set for a number of parameters: wind direction, roughness, friction velocity, Brunt-Vaisala frequency (stability) and vertical velocity. All other parameters in this study, also those coupled to the source are set to specific values. The runs are based on an event where an accident with a train filled with Chlorine occurred. A release never took place but the Swedish rescue service needed to decide the best time to empty the tanks. Here, uncertainty runs could be an important input to decide the right time when to do this. The ensemble itself describes a distribution of likely parameter settings. However, wind direction is not easy to forecast and comparisons with observations show that a 3 day forecast has a mean error (bias) of approximately 5-10 degrees and a standard deviation of 50 degrees. This is the case for every individual forecast, both the deterministic as well as the ensemble runs. However, when using the ensemble to describe a distribution we argue that an overlap exist between information from the ensemble and the existing forecast errors. Therefore, it is reasonable to believe that a distribution described by the ensemble should employ an error distribution different from the individual one. We suggest that the error distribution for the whole ensemble is set to a mean error of zero degrees and a standard deviation of 10 degrees. However, wind direction errors are allowed out to 40 degrees when sampling is done from the distribution.

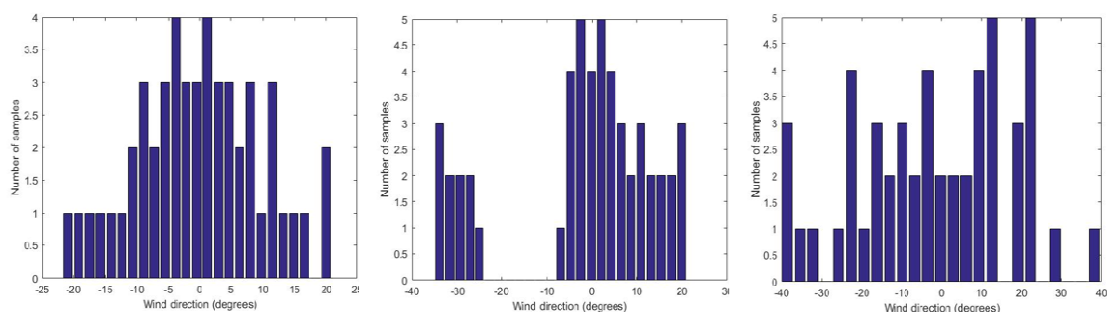


**Figure 1.** From left we have the error distribution, ensemble wind directions and the perturbed ensemble wind directions. Notice how the “hole” in the ensemble is filled with information when applying LHS sampling.

An example of the error distribution, ensembles and the resulting wind directions distribution is seen in Figure 1. In our approach we take one sample from the wind error distribution and add to one of the wind directions from the ensemble. The process is then repeated for every wind direction in the ensemble. This means that a broadening of the ensemble distribution takes place in a random procedure specified by the LHS-method. In this way we believe that we cover the wind direction parameter space more realistically. In summary, the input data to the runs consists of fixed (known) variables and the five parameters mentioned above are given uncertainties according to probability distributions. Roughness and Brunt-Vaisala frequency are sampled from uniform distributions while all the other parameters are sampled from normal distributions.

## RESULTS

The runs are performed in DE with a lagrangian particle model. The results are presented using the dose calculations. All grid points which have a dose larger than zero are set to one. Then all dose fields are added and divided by the number of runs (fifty). Finally, we take the logarithm in order to easier visualize the features of the calculations. Thus, we get a probability of passage in all grid points and in grid points where all plumes passes the probability is of course hundred percent. We have done calculations using only the information from the ensemble and when the ensemble wind directions have been perturbed with the LHS error distribution as well. First, we consider the case with a smaller spread, corresponding to day three. The results from the idealized ensembles without any perturbations show a plume-like behavior, especially in one direction (Figure 2). This corresponds to the “hole” in the ensemble seen in Figure 1. Such a behavior could mislead a decision maker to believe that there is no risk in certain directions. When using ensemble information perturbed according to LHS we avoid this behavior and a more smooth transition is seen (Figure 3) which also reflect the forecast error better. In this case a decision makers can get a more realistic situational awareness

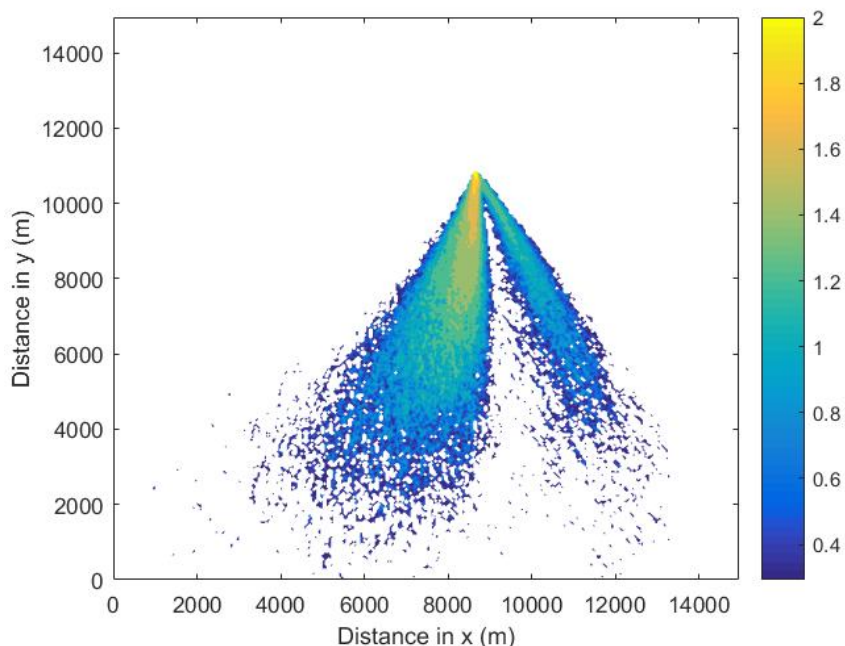


**Figure 2.** The probability in space of the plume-passage for the ensemble only plotted in a logarithmic scale. Hundred percent corresponds to 2 and ten percent to 1.

For the situation corresponding to day five we have set fifteen ensembles with a shifted wind direction to around 180 degrees. As seen in Figure 4 we will then get two main areas potentially influenced by a release. Clearly, when the ensembles are fewer a more plume-like behavior is present especially near the edges of the main probability area. However, this is usually the case in reality also. We also reduced the number of ensembles at the shifted direction to five (Figure 5). Then, we can almost identify every single run and this points out the weakness of the method that we have implemented so far. In directions with

few ensembles we have to add more samples from the error distribution to the ensemble wind direction in order to represent the dispersion from a probabilistic view. This of course means more runs. However, in directions where many ensembles are present we can probably reduce the number of runs. We are therefore hopeful that by analyzing the ensemble and make a clever design of the distributions the number runs can stay at approximately fifty.

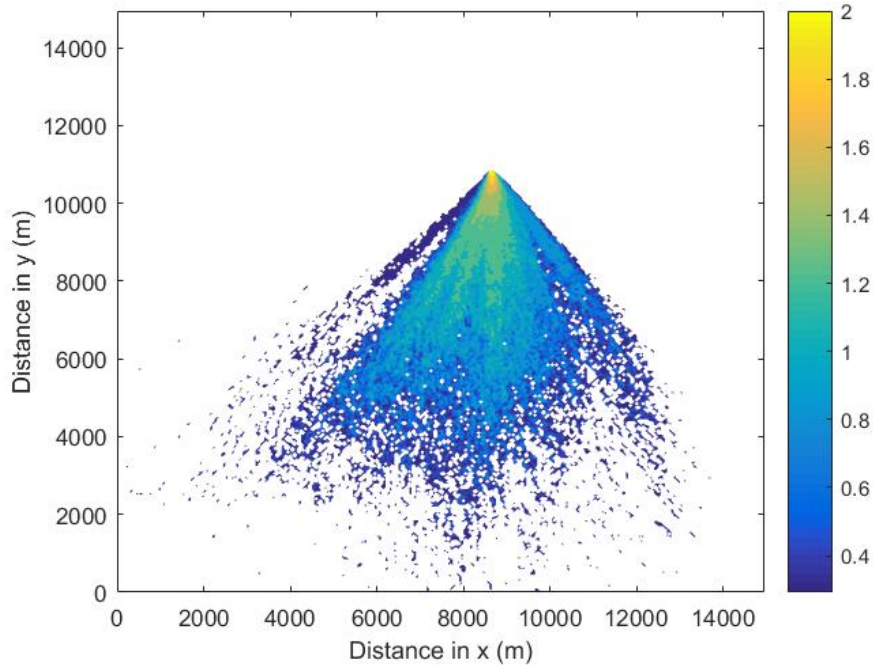


**Figure 3.** The probability in space of the plume-passage for the LHS-perturbed ensemble plotted in a logarithmic scale. Hundred percent corresponds to 2 and ten percent to 1.

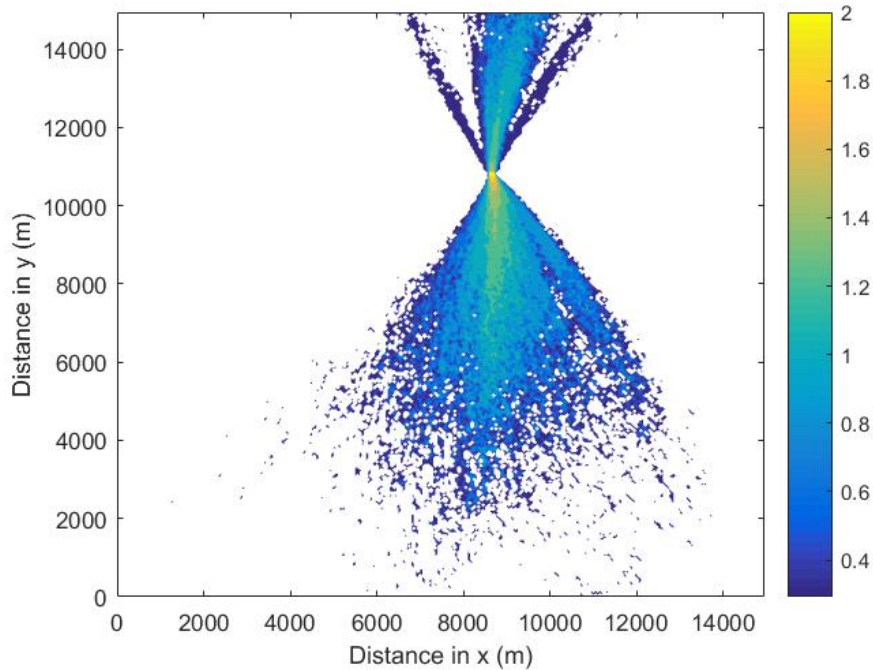


**Figure 4.** The probability in space of the plume-passage for the shifted LHS-perturbed ensemble plotted in a logarithmic scale. Hundred percent corresponds to 2 and ten percent to 1.

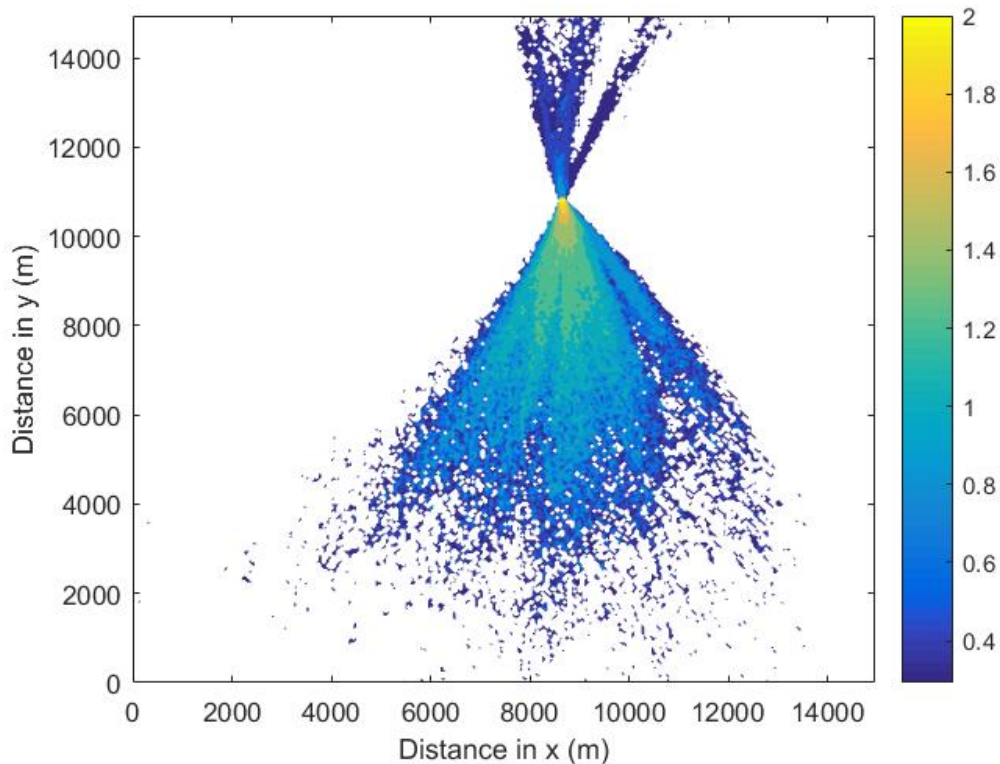


**Figure 5.** The probability in space of the plume-passage for the single-shifted LHS-perturbed ensemble plotted in a logarithmic scale. Hundred percent corresponds to 2 and ten percent to 1.

## CONCLUSIONS

So far we have been working with idealized ensemble distributions and therefore analysis of real weather situations are necessary. Especially, we need to study the ensemble wind direction distributions in order to understand how to set appropriate error distributions. Initial runs with the LHS methodology show that the suggested error distribution together with the ensemble information seem to produce realistic results as we could anticipate the real world to look like from a probabilistic view. However, if only a few number of the ensembles have different main wind directions there is a need to add a proper amount of samples (more than one) from the error distribution to be able to reproduce real world uncertainties. Otherwise one can end up with too much of a plume behavior. Thus, the suggested one-sampling approach from the error distribution can fully work only where the overlap between ensemble information and the forecast error for one forecast is large enough. Thus, the error distribution depends on the behavior of the ensemble and we also have to choose a correct sampling approach to handle both a cluster of ensemble runs and single outliers. Also, it remains to study the stability of the LHS-approach. One should of course get more or less the same behavior if we design a new LHS-distribution. By using a multi-processor approach we could speed up the calculations and therefore we believe that uncertainty calculations could be a standard tool of rescue services in the future in the view of local scale dispersion.

## REFERENCES

- Burman j., Brännström N., Björnham O., Lindgren P., Persson L., Von Schoenberg P., and L. Thaning, 2013: Osäkerheter i observationer och beräkningar. *FOI report*, FOI-R—3764—SE.
- Toth, Z., and E. Kalnay, 1993: Ensemble forecasting at NMC. The generation of perturbations. *Bull. Amer. Meteor. Soc.*, **74**, 2317-2330.

**17th International Conference on  
Harmonisation within Atmospheric Dispersion Modelling for Regulatory Purposes  
9-12 May 2016, Budapest, Hungary**

---

**ESTIMATION OF SHORT ODOR EVENTS BY USING CHEMICALLY REACTIVE  
ODORANTS ATMOSPHERIC DISPERSION MODELLING AROUND A PULP PAPER MILL**

*D. Cartelle<sup>1</sup>, J.M. Vellón<sup>1</sup>, A. Rodríguez<sup>1,2</sup>, D. Valiño<sup>1,2</sup>, J.A. González<sup>2</sup>, M. Bao<sup>2</sup>, C. Casas<sup>3</sup>*

<sup>1</sup>Troposfera Soluciones Sostenibles, S.L. Real St., 217, 15401 Ferrol, A Coruña, Spain.

david.cartelle@troposfera.es

<sup>2</sup>Department of Chemical Engineering, Universidade de Santiago de Compostela, 15782 Santiago de

Compostela, Spain. ja.souto@usc.es

<sup>3</sup>ENCE-Pontevedra, Marin Av., Pontevedra, Spain

*Corresponding author(s): J.A. Souto-Gonzalez, ja.souto@usc.es*

**Abstract:** Odor episodes control due to low threshold perception odorants, as H<sub>2</sub>S, is extremely difficult, as they are detected in very low concentrations. Traditionally, pulp paper mills using Kraft process produce TRS (Total Reduced Sulphur) odorants emissions, so their environment can be affected by odors. A model-based operational odor forecast system, namely *PrOlor*, was developed, tested and applied around ENCE-Pontevedra paper pulp mill in order to prevent any short odor event (less than 1 hour). This system includes WRF model coupled to CALMET model, to provide meteorological inputs to CALPUFF model. Both surface wind and temperature WRF and CALMET models outputs were validated against surface measurements, and statistics calculated by Openair software usually accomplished valid ranges. About CALPUFF performance, estimated odorant ground level concentrations were converted to short odor event intensity applying both peak-to-mean approach and Steven's Law. When forecast short odor events were compared to the 34 short odor events registered, 32 of them were caught by *PrOlor*.

**Key words:** *Odorants, Total Reduced Sulphur (TRS), Pulp Paper Mill, WRF, CALMET/CALPUFF*

## **INTRODUCTION**

The use of atmospheric models to prevent odor events around wastewater treatment and industrial plants is increasing and improving nowadays (Carrera-Chapela et al., 2014) ENCE-Pontevedra paper pulp mill developed along the last six years several investments in order to reduce systematically its TRS emissions, to avoid persistent odor around it. However, due to the changeable conditions of its environment, the possibility of short and sporadic odor events (from seconds to minutes) remains.

In this work, *PrOlor* system is presented as an odor forecast system to prevent short odor events, based in WRF and CALMET/CALPUFF modelling systems. Models results were tested against meteorological measurements and qualitative environmental odor observations.

## **MATERIALS AND METHODS**

*PrOlor* is a software system based in different atmospheric models running on Linux systems. For its feasible application, *PrOlor* includes a web-based interface for data analysis, daily odor forecast e-mail reports to the paper pulp mill staff by e-mail, back trajectory analysis and, also an app for mobile devices to check the zones where the odor thresholds should be superseded.

About the mathematical models and datasets applied, Figure 1 shows a flow diagram of *PrOlor* system. GFS model from US NCEP daily provides the input dataset to WRF (Weather Research & Forecast) model (Skamarock and Klemp, 2008), with the following physics parameterizations: Longwave RRTM (Radiation), MM5-Dudhia (Shortwave), YSU (with sfclay: Monin-Obukhov from MM5 MRF) for PBL, 5 layer MM5 LSM (Surface), Kain-Fritsch (Cumulus), and WSM6 for Microphysics. WRF is applied over four nested domains (Figure 2a) around the study area, with different horizontal resolutions: D1 (36x36 km<sup>2</sup>), D2 (12x12 km<sup>2</sup>), D3 (4x4 km<sup>2</sup>), and D4 (study area, 1.3x1.3 km<sup>2</sup>).

Using CALWRF interface (Figure 1), WRF forecast is applied as input dataset to CALMET (v. 6.334) meteorological diagnostic model (Scire et al., 2000a), to get hourly meteorological fields over the study area (D4 domain) with  $250 \times 250 \text{ m}^2$ . This CALMET setup includes IKINE (kinematic module) and IOBR (procedure for adjusting vertical velocity) options. As Digital Elevation Model (DEM), Spanish Geographic Centre (CNIG) LIDAR  $5 \times 5 \text{ m}^2$  resolution elevation dataset is applied; 22 different land use categories, following the Land Cover Classification System (LCCS), are considered from the Global Cover Characterization (GLCC) dataset with  $300 \times 300 \text{ m}^2$  resolution. Also, 12 vertical layers up to 4000 m are applied, with a telescopic distribution (thinner layers close to the surface) (Gonzalez et al., 2015).

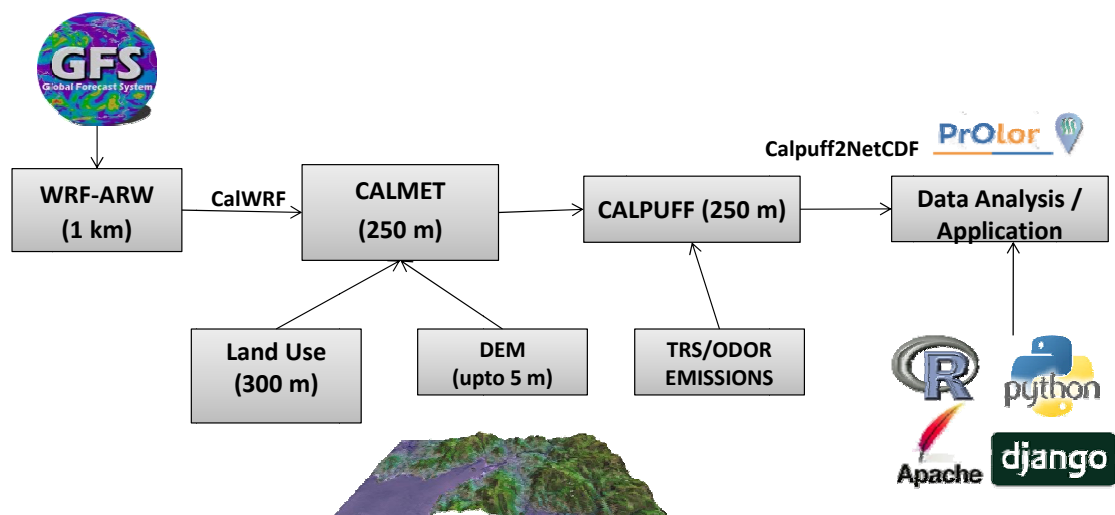


**Figure 1.** General scheme of PrOlor system, showing the models, input dataset, and data analysis and application modules.

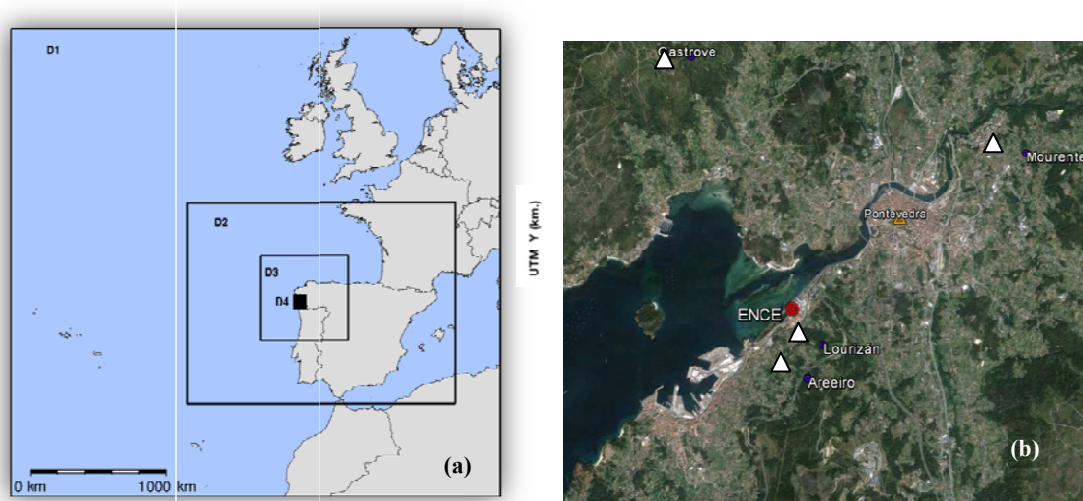


**Figure 2.** (a) WRF model nested domains at four different horizontal resolutions to achieve up to  $1.3 \times 1.3 \text{ km}^2$  resolution over the innermost D4 domain; (b) study area (D4 domain), with location of the ENCE paper pulp mill, the four surface meteorological stations, and Pontevedra town urban area.

CALPUFF (v. 6.42) (Scire et al., 2000b) Lagrangian dispersion model setup default options are selected, except for chemistry. First order chemical decay of each odorant is calculated during the CALPUFF simulation, considering typical atmospheric average lifetimes per odorant (Liang, 2008). As CALPUFF input, mean steady state TRS chemical emissions measurements from 3 point sources (stacks) and 4 area sources (water treatment plant) at the paper pulp mill were measured by using a Chromatech MEDOR

TRS model C51000 chromatograph. In these measurements H<sub>2</sub>S and DMS were detected; otherwise, none significant DMDS and Methyl-SH emissions were observed.

As its main output, CALPUFF produces hourly odorants concentrations and odor levels are obtained over the same 3-dimensional grid applied in CALMET. These concentrations are applied as input dataset to estimate hourly odor levels by using the Stevens' Law (Gostelow et al., 2001). Also, as CALPUFF outputs are obtained in hourly-basis, short odor events (less than 1 hour) are estimated by using the peak-to-mean ratio, Eq (1) (Smith, 1973; Piringer et al., 2012),

$$\frac{C_p}{C_m} = \left( \frac{T_m}{T_p} \right)^U \quad (1)$$

where  $C_p$  is the mean odorant concentration over the  $T_m$  integration time (typically, 1 hour),  $C_m$  is the peak (short) concentration,  $T_p$  is the integration time for  $C_p$  (typically, 30 seconds), and  $U$  depends on the atmospheric Pasquill stability (Piringer et al., 2012).

Finally, TRAJ2D back-trajectory module is applied to analyze the origin of odor events, by using CALMET output and WIND2D processor.

## RESULTS

*PrOlor* system runs every day to obtain an odor forecast 72 h in advance, and both average and peak hourly odorants concentrations ( $\mu\text{g}/\text{m}^3$ ) and odor levels ( $\text{OU}/\text{m}^3$ ) are predicted.

Both WRF and CALMET meteorological validations were done, from April, 1st 2014 to August, 31st 2014, against four surface meteorological stations measurements at the study area (Figure 2b); also, CALPUFF odor levels are validated against short odor events olfactometric observations (qualitative) at the study area.

About meteorological validations, hourly average wind speed and direction, temperature and relative humidity surface measurements were compared to both forecast results from WRF inner domain (D4) and from CALMET domain in "NOOBS" mode using WRF-D4 domain as CALMET input. Unfortunately, from the four meteorological surface stations available, only Castrove site provides valid wind measurements during this period; as other sites are affected by obstacles and they don't accomplished criteria for a valid winds validation.

**Table 1.** Statistics of hourly surface wind speed of WRF and CALMET results against measurements at Castrove site, 04/01/2014-08/31/2014. Green: pass benchmark; red: does not pass benchmarks. Absolute statistics in  $\text{m}\cdot\text{s}^{-1}$ .

Model	n	FAC2	MB	MGE	NMB	NMGE	RMSE	r	COE	IOA
WRF	3672	0.60	-0.25	2.15	-0.07	0.57	2.96	0.32	0.03	0.52
CALMET	3672	0.77	-0.37	1.46	-0.10	0.39	2.03	0.73	0.34	0.67

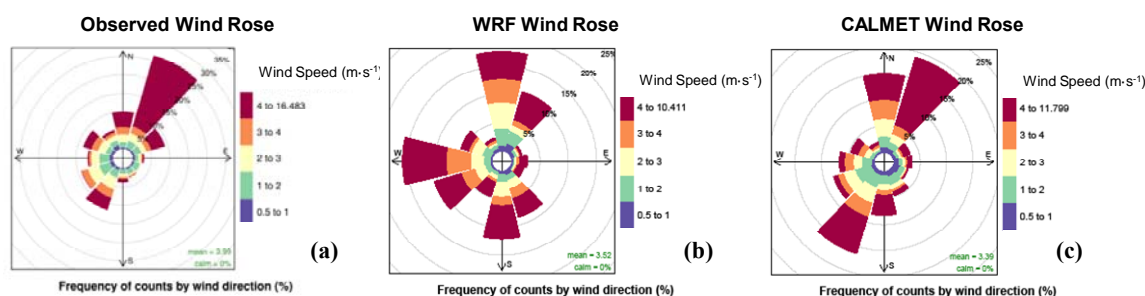


**Figure 3.** Wind roses at Castrove site: (a) observed, (b) WRF model, and (c) CALMET model, 04/01/2014-08/31/2014

Validation dataset was calculated by using Openair module of R freeware software (Carslaw and Ropkins, 2012). The different statistics were recommended by Chang and Hanna (2004) and Emery et al. (2001) for the validation of meteorological models (to be applied as input to air quality models). Table 1 shows WRF and CALMET wind speed outputs statistics against Castrove site measurements: considering Emery et al. (2001) benchmarks, that is, IOA>0.6, RMSE<2.0 m·s<sup>-1</sup> CALMET output is practically in agreement to measurements (just CALMET RMSE 2.03 m·s<sup>-1</sup>, a bit out of range); and, CALMET statistics always improve WRF statistics. Only WRF MB and NMB are lower than CALMET statistics, but all values are very low, so differences are not significant.

About wind direction, Emery et al. (2001) consider a more liberal benchmark, as low wind speeds can produce unrealistic wind directions. Therefore, a qualitative wind roses comparison is shown in Figure 3 at the Castrove site: again CALMET wind direction frequencies are more similar to the observed wind rose than WRF output, showing the necessity of applying CALMET model with higher horizontal resolution to achieve accurate meteorological fields as CALPUFF input. However, CALMET seems to overestimate northern and southwestern wind speed at this site: these differences also increases the wind speed CALMET RMSE (Table 1), but they can be explained by some barriers around Castrove meteorological tower (mainly, trees), that cannot be considered by CALMET.

Taylor diagrams (Figure 4) also shows the improvement of wind speed CALMET output at Castrove site over WRF output, as a graphical combination of RMSE, standard deviation, and Pearson product moment correlation coefficient (r).

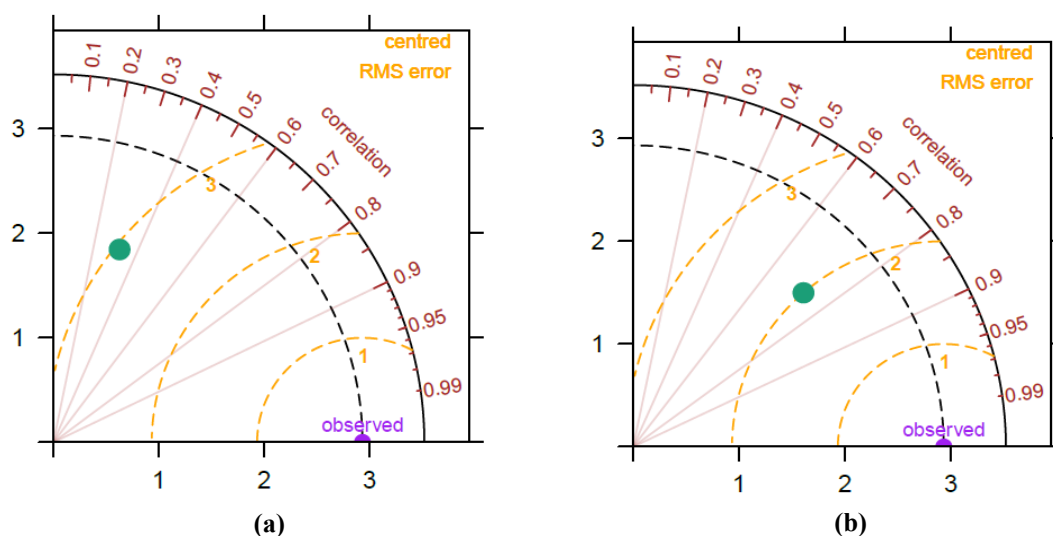


**Figure 4.** Taylor Diagrams of wind speed at Castrove site: (a) WRF output and (b) CALMET output, against hourly measurements along 04/01/2014-08/31/2014 period.

**Table 2.** Statistics of hourly surface temperature of WRF and CALMET results against measurements at the four sites, 04/01/2014-08/31/2014. Green: pass benchmark; red: does not pass benchmarks. Absolute statistics in °C.

SITE	WRF					CALMET				
	MB	MGE	IOA	RMSE	R	MB	MGE	IOA	RMSE	R
Areiro	0.68	1.48	0.80	1.99	0.91	-0.02	1.61	0.78	2.07	0.89
Castrove	1.68	2.04	0.73	2.37	0.94	0.02	1.18	0.85	1.49	0.95
Lourizán	0.30	1.80	0.77	2.38	0.87	-0.03	1.89	0.76	2.42	0.87
Mourente	-0.85	1.76	0.76	2.09	0.91	0.00	1.33	0.82	1.79	0.92

About surface temperature (Table 2), again CALMET provides better statistics than WRF at the four sites, achieving all the statistical benchmarks suggested by Emery et al. (2001):  $MB \leq \pm 0.5$  °C,  $MGE < 2$  °C, and  $IOA > 0.7$ .

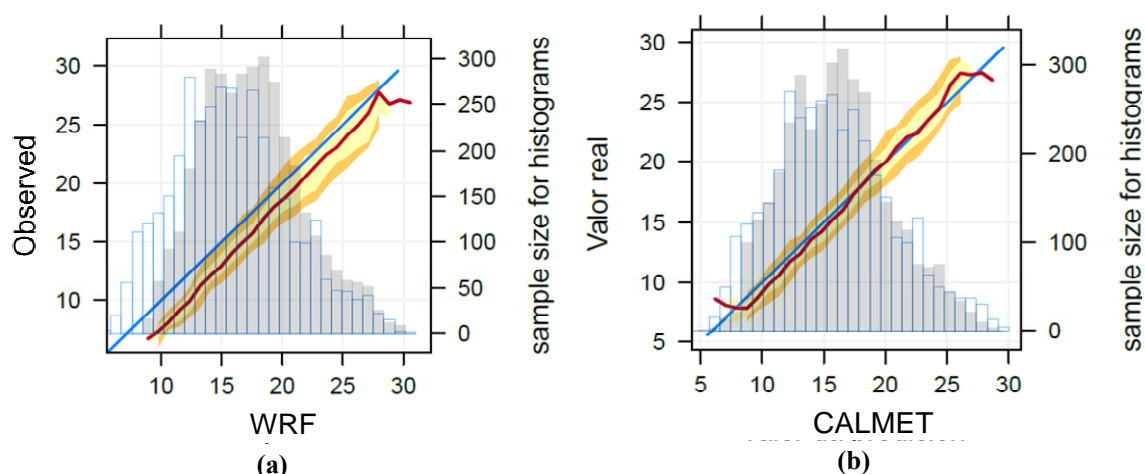


**Figure 5.** Quantile diagrams of surface temperature at Castrove site: (a) WRF output and (b) CALMET output, against hourly measurements along 04/01/2014-08/31/2014 period.

As an example, Figure 5 shows surface temperature quantile diagrams at Castrove site. CALMET output histogram (Figure 5b, gray bars) and observed data histogram (blue bars) are more similar than WRF output histogram (Figure 5a, gray bars); also CALMET median (red line), 25/75 percentile (yellow area), and 10/90 percentile (orange area) in Figure 5b are very close to the perfect model (blue line), and closer than WRF results (Figure 5a).

About the odor forecast validation, as odorants ambient concentrations observations are not available, a register of short odor events based in olfactometric qualitative observations from the paper pulp mill staff was set. Every observed odor event was reported to a database using a Smartphone app, to register its time and location. 34 short odor events were reported during the validation period; and, 32 of those events were forecast by PrOlor, near to the reported location and at the same daily period (morning, afternoon, night). For the remaining 2 events, one of them was caused by an accidental increase in H<sub>2</sub>S emissions at stripping process.

## CONCLUSIONS

Operational ambient odor PrOlor system for the simulation and forecast of short odor events around a pulp paper mill, based in meteorological models (WRF, CALMET) and a CALPUFF Lagrangian dispersion model, was developed and validated around ENCE-Pontevedra paper pulp mill. About meteorological forecast validation, CALMET output (with WRF output as meteorological input) passed the statistical benchmarks for wind and temperature by Emery et al. (2001). About ambient odor validation, 34 short events were registered along 5 months by the paper pulp mill staff outside its plant; CALPUFF in PrOlor agreed in 32 of those events; and, one of failed event was due to a fugitive H<sub>2</sub>S emission from the paper pulp mill, as PrOlor forecast is based in mean historical emissions measurements. Although no explanation was found for another failed event, it could be related to the mixing layer depth estimation, as it is a significant parameter in the short term plume dispersion at the PBL.

## ACKNOWLEDGMENTS

Meteorological measurements for validation were provided by Galician Regional Meteorological Office (MeteoGalicia) and Spanish Meteorological Office (AEMET).

## REFERENCES

- Carrera-Chapela, F., Donoso-Bravo, A., Souto, J.A. and Ruiz-Filippi, G., 2014: Modeling the Odor Generation in WWTP: An Integrated Approach Review, *Water Air Soil Pollut.*, **225**, 1932-1947.
- Carslaw, D.C. and Ropkins, K., 2012: Openair — an R package for air quality data analysis, *Environ. Model. Softw.*, **27-28**, 52-61.
- Chang, J.C. and Hanna, S.R., 2004: Air quality model performance evaluation, *Meteorol. Atmos. Phys.*, **87**, 167-196.
- Emery, C.A., Tai, E. and Yarwood, G., 2001: Enhanced Meteorological Modeling and Performance Evaluation for Two Texas Ozone Episodes, ENVIRON International Corp., Novato, CA.
- Gonzalez, J.A., Hernandez-Garces, A., Rodriguez, A., Saavedra, S. and Casares, J.J., 2015: Surface and upper-air WRF-CALMET simulations assessment over a coastal and complex terrain area. *Int. J. Environment and Pollution*, **57**, 249-260.
- Gostelow, P., Parsons, S.A. and Stuetz, R.M., 2001: Odour measurements for sewage treatmentworks, *Water Res.*, **35**, 579-597.
- Liang, C.C.V., 2008: Reduced sulphur compounds in ambient air and in emissions from wastewater clarifiers at a kraft pulp mill, MSc Thesis in Applied Science, University of Toronto, Canada.
- Piringer, M., Werner, K., Petz, E. and Knauder, W., 2012: Comparison of two peak-to-mean approaches for use in odour dispersion models, *Water Sci. Technol.*, **66**, 1498-1501.
- Scire, J.S., Robe, F.R., Fernau, M.E. and Yamartino, R.J., 2000a: A User's Guide for the CALMET meteorological model, Earth Tech Inc., Concord, MA, USA.
- Scire, J.S., Strimaitis, D.G., Fernau, M.E. and Yamartino, R.J., 2000b: A User's Guide for the CALPUFF dispersion model, Earth Tech Inc., Concord, MA, USA.
- Skamarock, W.C. and Klemp, J.B., 2008: A time-split nonhydrostatic atmospheric model for weather research and forecasting applications, *J. Comput. Phys.*, **227**, 3465-3485.
- Smith, M.E., 1973: Recommended Guide for the Prediction of the Dispersion of Airborne Effluents, ASME, NY, USA.

**17th International Conference on  
Harmonisation within Atmospheric Dispersion Modelling for Regulatory Purposes  
9-12 May 2016, Budapest, Hungary**

---

**REAL SCALE DEMONSTRATION OF THE DEPOLLUTING CAPABILITIES OF A  
PHOTOCATALYTIC PAVEMENT IN A REAL URBAN AREA**

*M. Pujadas<sup>1</sup>, M. Palacios<sup>1</sup>, L. Núñez<sup>1</sup>, M. Germán<sup>1</sup>, J. Fernández-Pampillón<sup>2</sup>, J. D. Iglesias<sup>3</sup>,  
J. L. Santiago<sup>1</sup>*

<sup>1</sup>Department of Environment, Research Center for Energy, Environment and Technology (CIEMAT),  
Madrid, Spain

<sup>2</sup>National University of Distance Education (UNED), Madrid, Spain

<sup>3</sup>Alcobendas City Council, Madrid, Spain

**Abstract:** In the framework of the LIFE MINOX-STREET European project (co-financed by the EU), once a variety of commercial photocatalytic products have been subjected to rigorous laboratory essays, one of them has been selected and implemented in a main road of the Municipality of Alcobendas (Madrid, Spain) in order to evaluate its depolluting effect. After a first phase of monitoring meteorological parameters and air quality conducted in the selected street, the photocatalytic coating has been applied on the road, covering an area of approximately one thousand square meters both ways. The designed and installed experimental system has allowed the continuous measurement of the ambient concentration of NO<sub>x</sub> at several different points located along the longitudinal axis of the road, both inside and outside the treated area with photocatalytic material, allowing experimentally evaluate the ability of this decontaminating photocatalytic coating under different climatic and weather conditions. All the collected data have given valuable information for the development and evaluation of a mathematical model capable of simulating microscale by calculating the dispersion of air pollutants at urban scale.

**Key words:** *Photocatalytic pavement, TiO<sub>2</sub>, air pollution abatement*

## **INTRODUCTION**

The lessening of pollutants as nitrogen oxides (NO<sub>x</sub>) constitutes one of worrying challenges in densely populated areas, where atmospheric pollution problems are mainly caused by road traffic emissions. As a consequence, the development of emerging abatement techniques, as those based on photocatalytic oxidation, is nowadays being fostered. Applying titanium dioxide (TiO<sub>2</sub>)-modified coatings or cementitious materials onto the external covering of buildings or roads might be a supplement to conventional technologies, such as catalytic converters fitted on the vehicles, for mitigating air pollution. Nevertheless, although some photocatalytic materials have been deeply studied in laboratory, their efficiency as sink of NO<sub>x</sub> at real scale is still matter of debate.

In the framework of LIFE MINOX-STREET European project, a variety of commercial TiO<sub>2</sub> based photocatalytic building materials have been subjected to rigorous laboratory essays in order to study, on one hand, their mechanical and physical properties, operation-induced changes and durability, and, on the other, their photoactivation and air-purifying capacity, chemical and structural properties, and the changes induced by ageing and regeneration processes (Palacios et al, 2015a). Then, the most promising materials have been selected and essayed by means of both outdoor experiments and controlled essays under ambient conditions (German et al, 2015, Palacios et al, 2015b). The selected photocatalytic coating designed for use on bituminous mixtures has been implemented in a real urban scenario in Alcobendas, Madrid, and the assessment of its effect on the degradation of atmospheric nitrogen compounds is presented here.

## **EXPERIMENTAL**

The photocatalytic coating was implemented in the road of Paseo de la Chopera, a main street of the Municipality of Alcobendas (Madrid), consisted of two lanes in each traffic direction and a median strip. The street has an east-west orientation that assured enough solar irradiation of the bituminous pavement

from 7 to 16 UTC. An area of about one thousand square meters (sixty meters along the road) was covered by means a distributor truck with a spray bar with nozzles fitted on the back. The application was done after the roadway was cleared of any debris. Traffic was reopened on September, 25<sup>th</sup> 2015, two days after the product application.

The air quality monitoring started on September, 11<sup>th</sup> 2015, two weeks before the implementation of the photocatalytic coating to obtained background information and continued till October, 25<sup>th</sup> 2015. Ambient concentrations of NO<sub>x</sub> (NO and NO<sub>2</sub>) were measured continuously at six different points located along the longitudinal axis of the road, two inside and four outside the treated area with the photocatalytic material (Figure 1). The air sampling lines consisted in perfluoroalkoxy (PFA) tubing with 0.4 cm inner diameter and 53 m (lines 1 to 4) and 12 m (lines 5 and 6) long (Figure 1). They were properly protected and buried under the asphalt surface to prevent damage from road traffic. Sampling points were located at 40 cm high in the middle of the road and protected with a meshed cages anchored to the pavement. Particulate filters (cut-off diameter of 15 μm) were placed at the beginning of the sample lines. The sampling height has been selected taking into account the results obtained from previous measurements of NO<sub>x</sub> concentration vertical gradients over a similar photocatalytic coating in a suburban area (German et al, 2015).

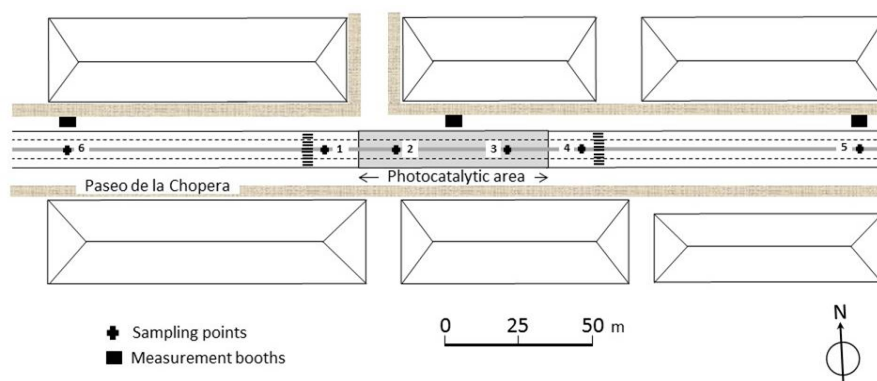


**Figure 1.** Schematic overview of the experimental set up in Paseo de la Chopera.

Apart from measurements at ground level, ambient NO<sub>x</sub>, ozone (O<sub>3</sub>) and meteorological parameters (air temperature, solar radiation, relative humidity, wind speed and direction) were measured continuously at a height of 15 m from September, 15<sup>th</sup> 2015 to October, 25<sup>th</sup> 2015. Meteorological sensors and gas analyzers were deployed at the roof of a building located near the Paseo de la Chopera in order to characterize the general air dynamics of this area.

NO<sub>x</sub> concentration measurements were done by applying the chemiluminescence technique. Thermo Scientific NO<sub>x</sub> analyzers were used in five lines, Model 42i for sampling lines 1 to 4 and Model 42iTL for line 5, and two Teledyne API 200 A for both line 6 and at roof level. Ozone concentrations were measured with a UV absorption ozone analyzer (Teledyne API 400 A). The gas analyzers were calibrated before the beginning of the experimental campaign. All the instruments were located in temperature controlled rooms or booths.

An automatic switching system was developed for consecutive 1-minute averaged NO<sub>x</sub> measurements from sampling points corresponding to lines 1 to 4 (see figure 1). An external pump maintained a constant flow for all the lines, and a system of four solenoid valves which were switched every two minutes allowed the NO<sub>x</sub> analyzer performs alternating measurements associated to each valve. Only the data associated to the second minute of the cycle were taken into account in order to assure that the sampling was not affected by the measurement with the previous line.

Additionally, intensive measurement campaigns were performed during four days in which stagnant meteorological conditions occurred that favored the accumulation of air pollutants. In those occasions volatile organic compounds, particulate matter and road traffic were characterized during the diurnal

periods. Moreover, UVA radiation across the street and temperature of facades, sidewalks and bituminous photocatalytic pavement were also registered.

Part of the collected data have been used as inputs to evaluate a mathematical model capable of simulating microscale by calculating the dispersion of air pollutants at urban scale.

## RESULTS

The overall NO<sub>x</sub> concentration results obtained from the measurements along the road (sampling lines 1 to 4) are presented in Figure 2. Maximum values were registered during traffic rush hours in the morning and in the late afternoon. The evolution of NO<sub>x</sub> concentrations profiles correlated quite well with the traffic patterns observed during selected days. The cadence of one minute averaged measurements allowed to detect the influence of almost every vehicle emissions in this road as it is shown in Figure 2. It is noticeable the presence of a large amount of peaks superimposed to a NO and NO<sub>2</sub> background level. This fact has hampered the assessment of the NO<sub>x</sub> depolluting ability of the photocatalytic road pavement.

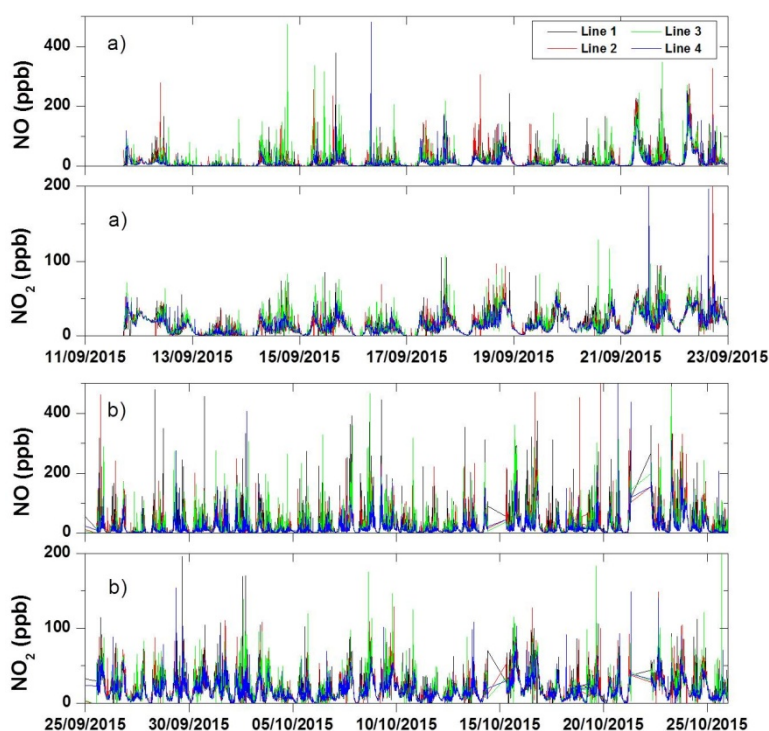


**Figure 2.** One minute averaged NO and NO<sub>2</sub> concentrations measured during the periods without (a) and with (b) the photocatalytic coating over the bituminous pavement.

Meteorological variables registered during the campaign are shown in Figure 3. During this time, anticyclonic stagnant conditions have occurred in three distinct periods (from September, 18<sup>th</sup> to 22<sup>nd</sup> 2015, from October, 8<sup>th</sup> to 9<sup>th</sup> 2015, and from October 15<sup>th</sup> to 16<sup>th</sup> 2015). Under this kind of meteorological conditions, the development of a consistent urban plume is very fast (in 1-2 days) and the limit values for NO<sub>2</sub> ambient concentrations are usually exceeded after few days of stability when the ventilation conditions of the air basin is poorer than normally.

The air depolluting capability of a photocatalytic material, obtained from laboratory essays, depends not only on the active product itself and its photocatalytic properties, but also on several parameters of the own test (Sikkema et al, 2015). The photocatalytic activity of the photocatalytic coating over a similar bituminous pavement of Paseo de la Chopera was essayed under the ISO international standard (ISO, 2007) giving a NO depolluting efficiency of 45%. After varying the test conditions (NO inlet concentration, irradiance intensity, relative humidity and flow rate), the amount of NO removed from the gas phase by photocatalytic oxidation was strongly affected by changes of the light intensity as well as of

the relative humidity (Palacios et al, 2015d). This dependence has also been observed in measurements of NO<sub>x</sub> concentration gradients made in a suburban area (German et al, 2015).

Taking into account these results, the effect of the presence of the photocatalytic pavement on the NO concentration has been studied for specific meteorological conditions: solar radiation (SR) higher than 400 Wm<sup>-2</sup>, relative humidity (RH) lower than 65 %, and wind speed (WS) lower than 5 m s<sup>-1</sup>. A comparison of the wind speed registered at roof level with the wind speed monitored in a near meteorological station of the Alcobendas municipality at ground level indicates that the selected value of 5 m s<sup>-1</sup> corresponds to approximately 2 m s<sup>-1</sup> in the street. Moreover, in order to avoid the influence of instantaneous NO emissions from traffic, only NO concentration values lower than 20 ppb has been considered. The wind direction was also included in the analysis to distinguish between east and west sectors. These wind directions were the most favorable for observing the effect of the photocatalytic pavement in reducing the concentration of NO because they were parallel to the street axis and thus to the sampling points on the road median strip.

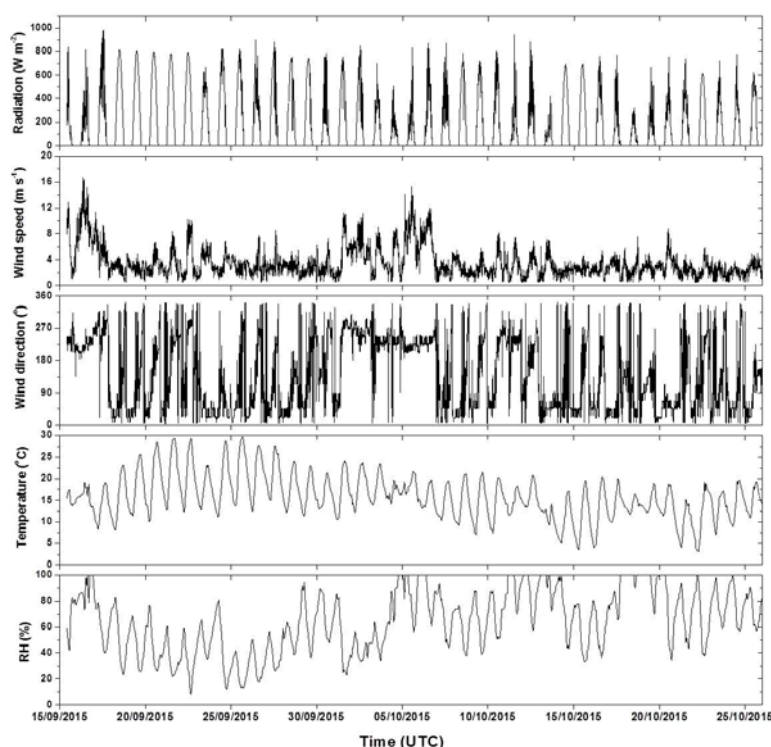


**Figure 3.** Meteorological variables registered at roof level during the measurement campaign in Paseo de la Chopera

The NO concentrations registered from the sampling lines 2, 3 and 4 were correlated against the corresponding values from the line 1. It was expected that before implementing the photocatalytic coating on the bituminous pavement the concentration of NO measured in the four sampling points were quite similar among them. In the NO selected data set that similarity would disappear from the time the photocatalytic coating was implemented. A summary of the obtained results are shown in Table 1.

**Table 1.** Slopes from the correlation of sampling lines 2 to 4 against line 1 for NO concentration before and after the implementation of the photocatalytic coating (SR>400 Wm<sup>-2</sup>, RH<65%, WS<5ms<sup>-1</sup>)

Sampling lines	Before application of photocatalytic coating (E direction)	After application of photocatalytic coating (E direction)	Before application of photocatalytic coating (W direction)	After application of photocatalytic coating (W direction)
2	0.77±0.03	0.73±0.03	1.05±0.08	1.07±0.08
3	0.73±0.05	0.74±0.03	1.41±0.17	1.03±0.06
4	0.64±0.03	0.70±0.03	0.89±0.06	0.90±0.07

The remediation of NO cannot be distinguished from zero as the slopes values for the two distinct periods are almost very similar. Moreover, although there is a tendency of a lower slope value for the line 4 it happens not only when the road was photoactive but also when there were no photocatalytic coating.

In order to ascertain if there were a bias due to an instrumental systematic problem of the sampling line 4, the nocturnal NO concentration values (from 00:00 to 04:00 UTC) were analysed. During that period there were almost no traffic emissions, preventing the point effect of individual vehicles, and the absence of solar light avoids the potential photocatalytic activity of the treated pavement. Under these conditions only an instrumental problem could produce different NO concentration measurements among the four lines. The values obtained for nocturnal conditions (Table 2) reflect that the correlation between the sampling lines is approximately the unity, thus there is not a bias due to any systematic instrumental error, so the deviation of the individual slopes from unity presented in Table 1 may result from general differences in the pollution levels between both ends of the street and along it.

**Table 2.** Slopes from the correlation of sampling lines 2 to 4 against line 1 for NO concentration before and after the implementation of the photocatalytic coating (00:00 to 00:04 UTC)

Sampling lines	Before application of photocatalytic coating	After application of photocatalytic coating
2	1.014±0.005	0.983±0.004
3	0.977±0.005	0.915±0.004
4	0.985±0.005	0.946±0.025

Therefore, the results obtained during the selected optimal measurement periods indicate that NO photocatalytic remediation has not been observed.

## CONCLUSIONS

The depolluting capability of a selected TiO<sub>2</sub>-based photocatalytic material applied over a bituminous pavement has been evaluated in an urban scenario with real traffic. Despite a) having used a product with good performance according to the results of laboratory ISO tests, b) NO measurements were performed low over the treated surface and c) the data evaluated were selected according to the optimal weather conditions under which potentially the sink effect of the photocatalytic material on the NO should have produced measurable horizontal concentration gradients, the application of the photocatalytic product to an important section of the road did not allow to detect any improvement effect on NO concentrations detected in the median strip directly attributable to the presence of such material.

## REFERENCES

- Germán M., M. Palacios, M. Pujadas, L. Núñez and J. Fernández-Pampillón, 2015: Experimental study of NO<sub>x</sub> depolluting capabilities of a photocatalytic coating tested under suburban ambient conditions. 12<sup>th</sup> Urban Environmental Symposium–Urban Futures for a Sustainable World. Oslo, (Norway), 01 - 03 June 2015. Book of Abstracts, 37-44.
- International standard ISO 22197-1:2007, 2007, ISO, Geneva.
- Palacios M., L. Núñez, M. Pujadas, J. Fernández-Pampillón, M. Germán, B. S. Sánchez, J. L. Santiago, A. Martilli, S. Suárez and B. S. Cabrero, 2015a: Estimation of NO<sub>x</sub> deposition velocities for selected commercial photocatalytic products. *WIT Transactions on The Built Environment*, **168**, 12.
- Palacios M., S. Suárez, L. Núñez, B. Sánchez, M. Pujadas and J. Fernández-Pampillón, 2015b: Influence of parameters on the photocatalytic oxidation of nitric oxide at the surface of titanium dioxide-modified concrete materials. International Conference on Chemical and Biochemical Engineering, Paris, France, July 20-22. ISBN: 978-84-944311-1.
- Sikkema J.K., S.K. Ong and J.E. Alleman, 2015: Photocatalytic concrete pavements: Laboratory investigation of NO oxidation rate under varied environmental conditions. *Construction and Building Materials*, **100**, 305-314.

**17th International Conference on  
Harmonisation within Atmospheric Dispersion Modelling for Regulatory Purposes  
9-12 May 2016, Budapest, Hungary**

---

**INVESTIGATION OF ATMOSPHERIC DISPERSION OF GAS COMPOUNDS FROM AN  
INDUSTRIAL INSTALLATION OVER A REALISTIC TOPOGRAPHY**

*Diamando Vlachogiannis<sup>1</sup>, Athanasios Sfetsos<sup>1</sup>, Nikolaos Gounaris<sup>1</sup> and Athanasios Papadopoulos<sup>2</sup>*

<sup>1</sup>Environmental Research Laboratory

<sup>2</sup>Bio-molecular Physics Laboratory, INRASTES, National Centre for Scientific Research “Demokritos”,  
Agia-Paraskevi, 15310, Attiki, Greece

**Abstract:** The aim of the work was to compile a methodology using appropriate modelling tools for the study of the dispersion of gas pollutants from a fictitious industrial site over a realistic complex topography, treated as a point source, in a region of varying climate conditions, for regulatory purposes. To calculate the average levels and the maximum values of the pollutant concentrations in the atmosphere on an annual, daily and hourly basis, the procedure of identifying the characteristic weather types or weather days of the area of interest was followed. For the current study, meteorological files were extracted from the National Centres for Environmental Prediction (NCEP / USA) Global Forecasting System (GFS) available on a 6-hour temporal resolution from a planetary model of 1 degree horizontal resolution for a five-year period. The prevailing meteorological conditions or in other words characteristic weather types were obtained using these files and by applying a specific methodology based on Principal Components Analysis. The simulation of the 3-d meteorological fields was carried out for the characteristic weather types or days for the area of interest (computational domain extent 20x20 km<sup>2</sup>) with 3 × 3 km<sup>2</sup> horizontal and 1-hour temporal resolution. The air dispersion simulations have been performed with the WRF-HYSPLIT modelling system. Modelled pollutants ground concentrations have been compared against European air quality standards (2008/50/EC), adopted by Greek legislation, considering potential receivers (residential places).

**Key words:** *Atmospheric dispersion, air pollutants, fictitious industrial source, complex terrain*

## INTRODUCTION

Air dispersion and air quality modelling are unique tools for evaluating the impacts of air pollutant emission sources on the concentration fields in a region and assessing the compliance with existing air quality control legislation. Given the fact that such models incorporate the most updated progress in knowledge of atmospheric dynamics, chemical transformations and pollutant deposition, they become indispensable tools particularly in the case of investigating the impact of emission sources from future installations (Zaneti, 1990). The dispersion patterns of air pollutants can be very complex particularly over irregular topographies and where there are large number and / or different types of emission sources. Numerous studies have been carried out using Gaussian, Lagrangian, Eulerian and Computational Fluid Dynamics (CFD) dispersion models to understand and predict the concentration fields of air pollutants in various environments for impact assessment and human exposure purposes. A review of such models can be found in e.g. Holmes and Morawska (2006) and in Leelocly et al., (2014).

The integrated study presented in this paper addresses the calculation of the concentration fields of air pollutants Nitrogen Oxides (NO<sub>x</sub>), Non-Methane Hydrocarbons (HC), Carbon Monoxide (CO) and Particulate Matter (PM<sub>10</sub>) emitted from a fictitious installation of multi stack industrial combustion source with realistic data, in a mountainous region with varying meteorological conditions throughout the year. The study included the effect of varying the height of the emission stacks as well. In the following sections the methodology compiled, which includes appropriate modelling tools and data, and the results achieved are discussed in detail.

## METHODOLOGY

The aim of this work was to study the impact of the dispersion of  $\text{NO}_x$ , HC, CO and PM10 on the atmosphere from an industrial source (type of compression station of natural gas), located at a mountainous region of northwest Greece (region of Epirus), using appropriate 3-dimensional computer modelling. The work included also the investigation of varying the height of the emission stacks. The region of interest has peculiarities as regards to its topographical features and varying climatic conditions throughout the year. The climate conditions in Epirus are varying depending on the part of the region. The coastal areas experience moderate temperatures, which rarely fall below zero in winter. The summer months are typical Mediterranean and rather hot with frequent precipitation events. The inland mountainous parts of the region are characterised by heavy winters with snow and rain and rather cool summers. The computer modelling system included the Weather Research Forecasting (WRF-ARW) version 3.6.1 (Skamarock et al., 2008) and the atmospheric dispersion model Hybrid Single Particle Lagrangian Integrated Trajectory Model (HYSPPLIT) (Stein et al., 2015). The position and geometry of the source as well as the necessary data on stacks, emission rates of  $\text{NO}_x$ , HC, CO and PM10 were based on construction information. The basic computational steps followed are discussed below.

### Topography and Meteorological Data Processing

For the specific study, the necessary data for input to the atmospheric dispersion model included the topography and meteorological fields. The computational domain for the atmospheric modelling calculations was constructed in a way so as to include at its centre the fictitious installation. The domain size was set to  $20 \text{ km} \times 20 \text{ km}$  to include all the neighbouring urbanised areas with a minimum population of 50 residents (Figure 1). In the west, the domain included the coastline with some plains of rather limited area extent. The original topographical data used were of 100 m resolution. The topography of the area revealed a non uniform terrain with ridges (up to a height of 1000 m) alternating with valleys running in a northwest to southeast direction.

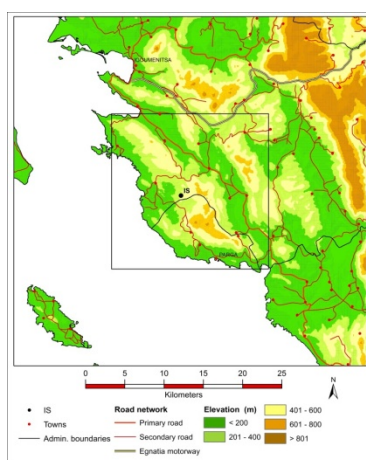


**Figure 1.** Topography map of the computational domain of size  $20 \times 20 \text{ km}^2$  (contour interval 200 m). The (fictitious) industrial source of emission is located in the centre of the domain denoted as IS.

The meteorological data (vertical distribution of wind speed and direction, temperature, mixing layer height, humidity, precipitation, cloud cover etc) were extracted from the National Centres for Environmental Prediction (NCEP / USA) Global Forecasting System (GFS) available on a 6-hour temporal resolution from a planetary model of 1 degree horizontal resolution. To calculate the average levels and the maximum values of the pollutant concentrations in the atmosphere on an annual, daily and hourly basis, the procedure of identifying the characteristic weather types of the area of interest was followed, addressing the varying climate over those temporal scales. The prevailing meteorological conditions or in other words characteristic weather types of the region were obtained by applying the methodology of Sfetsos et al. (2005), which is based on Principal Components Analysis (PCA). The specific methodology was applied on the GFS meteorological data of large scale, as referenced above,

covering a five year period (2006-2010). The analysis revealed the prevailing weather conditions in the defined computational domain and the corresponding frequency of their occurrence (in percentage) per year. Each weather condition was assigned a characteristic or else typical day (24-hour).

The results showed that the area of study was characterised by 7 in total weather types, WT (Table 1). The meteorological conditions from the planetary scale model, which characterise each typical weather day of the region were returned by the applied methodology in terms of WS wind speed (m/s), WD wind direction (deg.) (at 850 mbar and 10 m above sea level), T temperature (K) (at 2 m above ground level), MLH mixing layer height (m above ground level). As an example here (due to limited space), the values of the calculated variables are shown for 12:00 hrs of the typical day identified (Table 1).

**Table 1.** Characteristic weather types/typical days, frequency of their occurrence (in %) in the area of study and calculated prevailing meteorological conditions during each typical day at 12:00 hrs.

Typical day & ( % ) of occurrence	WS (m/s) (850 mb)	WD (deg.) (850 mb)	T (K) (2 m)	MLH (m)	WS (m/s) (10 m)	WD (deg.) (10 m)
1 (9)	17.77653	15.254	286.0511	790.3441	9.746546	16.65174
2 (11)	12.36237	28.25053	293.3918	1199.438	10.22959	7.142796
3 (23)	7.064888	16.18699	293.8235	1223.496	7.889754	18.88497
4 (10)	2.157312	278.7621	291.4452	1090.954	4.904919	19.34661
5 (13)	9.192361	218.6249	287.7477	884.8964	4.322308	60.41888
6 (13)	4.06865	26.30287	284.3701	696.6619	10.16672	43.70327
7 (21)	4.782067	356.4973	286.0512	790.3529	6.125416	15.5691

Once the typical weather days were identified, the data from the planetary model for the characteristic days were used as initial and boundary conditions to the WRF model. The model has been extensively tested, appropriately parameterised and validated in the Environmental Research Laboratory for a number of applications (e.g. Emmanouil et al., 2015, Vlachogiannis et al., 2013). The WRF model calculated the 3-d meteorological fields of the region of interest, in a horizontal and temporal resolution of  $3 \times 3 \text{ km}^2$  and 1-hour, respectively.

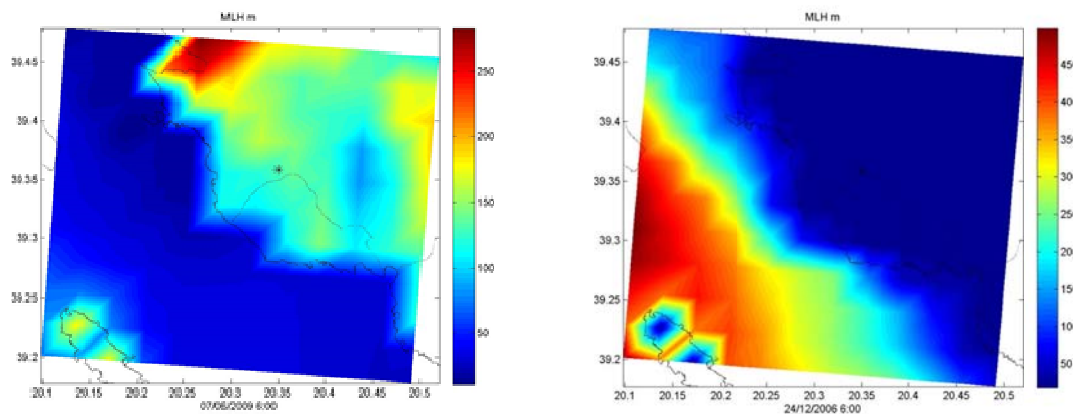


**Figure 2.** WRF calculated Mixing Layer Height above sea level (m) at 6:00 hours, during (a) WT4 and (b) WT6.

The meteorological calculations showed that the weather types 4 and 6 exhibited rather low values of the Mixing Layer Height (MLH) during early morning hours compared to the rest of the characteristic types

(Figure 2 (a) and (b)). Moreover, those days were characterised by calm conditions with very low winds between the ground surface and 50 meters height. Such stagnant atmospheric conditions favour the formulation of air pollution events, as pollutants are trapped. The meteorological data files obtained were used subsequently as input to the air dispersion model.

### Dispersion Model calculations

This section presents the preparation of the input data for the dispersion model HYSPLIT and describes the results obtained, for each characteristic weather type. The installation was assumed to comprise four Compressors of 30MW each, in full annual operation (24 hours x 365 days) and one Back-up Generator (Gas turbine exhaust) of 3.5 MW, operating 350 days per year. The computational study investigated the effect of varying the height of the stacks of the compressors (19 m or 25 m) on the concentration fields of the pollutants. The data on emissions sources and the pollutant composition in the exhaust gases were realistic and those were provided by the constructor (Table 2). The modelling approach was performed without the inclusion of the photochemical reactions and background air quality concentrations. The modelled calculated concentrations of the pollutants were compared against the respective air quality limits as set by the legislation in force (Directive 2008/50/EC).

**Table 2.** Data on emission sources from the fictitious installation.

Number of stacks	Stack Geometric characteristics		Exit gas Temperature (°C)	Exhaust gas flow rate (kg/h)	Exhaust gas flow volume rate (Nm <sup>3</sup> /h)	Exit gas velocity (m/s)
	Height (m)	Diameter (m)				
4	19 or 25	3.5	528	338400	254492	21.7
1	19 or 25	5	445	68365	51274	

The analysis of the results showed that the maximum hourly average values of NO<sub>x</sub> concentrations from the installation did not to exceed the air quality limit of 200 µg/m<sup>3</sup> for any assumed height of the stacks and during any weather type in the region even during those (WT4 and WT6) characterised by high stability in atmospheric masses and low wind speeds. The maximum hourly average NO<sub>x</sub> concentrations remained low and well below the air quality limit even in the vicinity of the stacks. In fact, the highest maximum hourly NO<sub>x</sub> concentrations values were found to be equal to 106 µg/m<sup>3</sup> and 104 µg/m<sup>3</sup> for stack height of 19m and 25m, respectively during WT4. Additionally, the annual average values of NO<sub>x</sub> did not exceed the respective air quality limit (40 µg/m<sup>3</sup>) as very low values had been calculated for the two stack heights and weather types. The maximum 8-hour value of CO concentration was calculated to be equal to 4.2 µg/m<sup>3</sup> and 4.0 µg/m<sup>3</sup> during WT4. The CO values were calculated to remain very low compared to the legislative limit everywhere in the domain and no exceedances occurred. Similarly, no exceedances in the PM10 hourly maximum and annual concentrations of the respective air quality limits were calculated for both stack heights and weather types. The PM10 calculated concentrations were found to be very low everywhere in the area of study. Finally, an inspection of the values yielded that overall the HC concentrations were low. Even in the case of the average annual total HC concentrations, the values remained well below the level of 5 µg/m<sup>3</sup>, which was the air quality limit of Benzene. Due to the limited space of the paper, examples only of the maximum hourly NO<sub>x</sub> for the 7 weather types and the average annual PM10 near ground concentration values are shown for the 19 m and 25 m stack heights (Figure 3 (a) and (b); Figure 4 (a) and (b)).

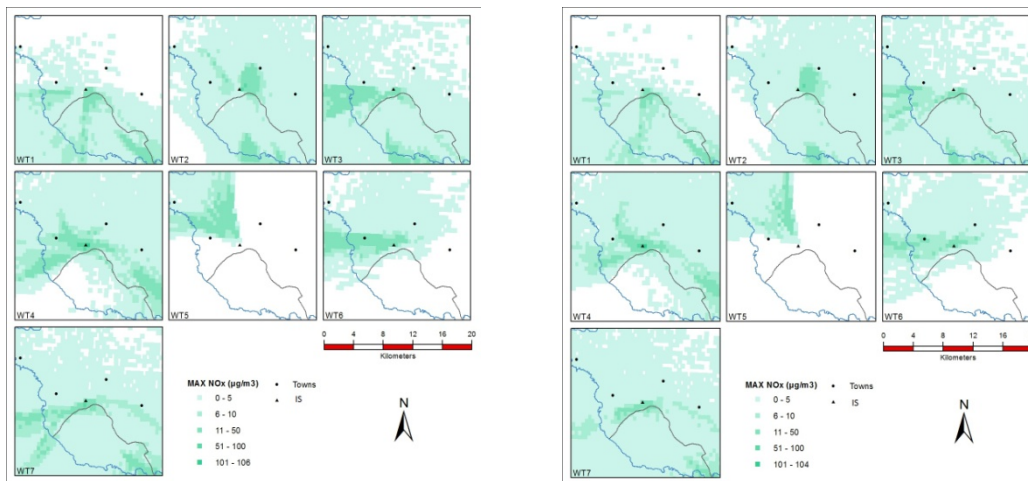


**Figure 3.** Maximum average hourly concentrations of NO<sub>x</sub> for (a) 19 m and (b) 25 m stack heights near the ground for the 7 weather types (WT). Black dots indicate residential areas. (Air quality limit value for hourly concentration of NO<sub>2</sub>: 200 (µg/m<sup>3</sup>)).

## CONCLUSIONS

This work presented an integrated computational methodology to derive concentration values of pollutants emitted from a number of stacks of two different heights of a fictitious industrial combustion source.

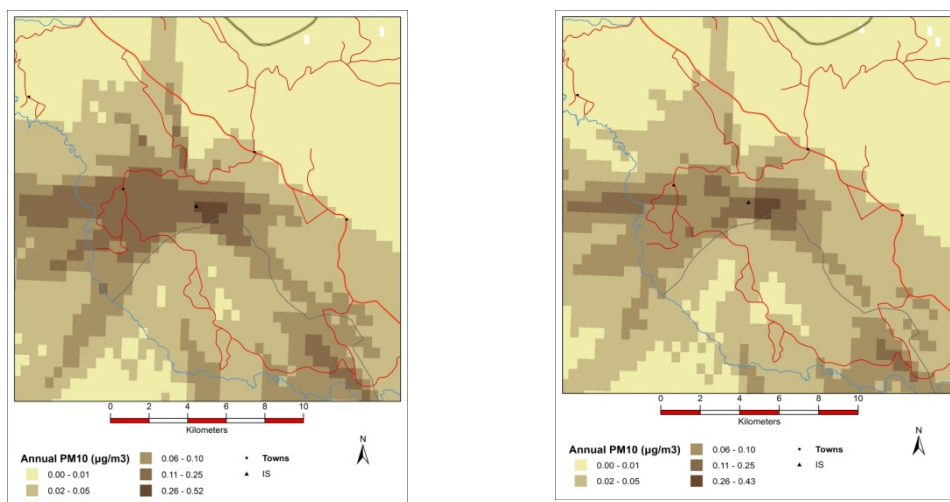


**Figure 4.** Average annual PM10 concentration contours (in µg/m<sup>3</sup>) for a) 19 m and b) 25 m stack heights. (Annual Air Quality Limit for PM10: 40 µg/m<sup>3</sup>).

The source was assumed to be located in a region of complex terrain and with varying climate throughout the year. To account for the varying climate conditions, data from the Global Forecast System covering a 5 year period were analysed to obtain the characteristic weather types of the area. The meteorological model WRF-ARW and the HYSPLIT dispersion model were set up and parameterized to calculate the concentration fields of the pollutants. The investigation of the effect of varying the height of the emission stacks showed that the differences in the concentration values were found to be small. For the particular emission source, there were no exceedances found of the pollutants averaged over the time scales defined by the air quality limits of the legislation in force (Directive 2008/50/EC).

## REFERENCES

- Emmanouil, G., D. Vlachogiannis, A. Sfetsos, S., N. Karozis, 2015: Climate Change and Extreme Weather Events in Mediterranean Sea: Studies with the WRF model, Our Common Future Under Climate Change 2015, International Scientific Conference, Paris, 07-10 July 2015.
- Holmes, N.S., and L. Morawska, 2006: A Review of Dispersion Modelling and its application to the dispersion of particles: An overview of different dispersion models available. *Atmospheric Environment*, **40**, 5902-5928.
- Leelossy, A., F. Molnár Jr., F. Izsák, A. Havasl, I. Lagzl, R. Mészáros, 2014: Dispersion modelling of air pollutants in the atmosphere: a Review. *Central European Journal of Geosciences*, **6**, 257–278.
- Sfetsos, A., D. Vlachogiannis, N. Gounaris, and A. K. Stubos, 2005: On the identification of representative samples from large data sets with application to synoptic climatology, *Theor. Appl. Climatol.* **82**, 177–182.
- Skamarock, W. C., J. B. Klemp, J. Dudhia, D. O. Gill, D. M. Barker, M. G. Duda, X.-Y. Huang, W. Wang, and J. G. Powers, 2008: A description of the Advanced Research WRF version 3. NCAR Technical Note 475, [http://www.mmm.ucar.edu/wrf/users/docs/arw\\_v3.pdf](http://www.mmm.ucar.edu/wrf/users/docs/arw_v3.pdf).
- Stein, A.F., R.R. Draxler, G.D. Rolph, B.J.B. Stunder, M.D. Cohen and F. Ngan, 2015: NOAA's HYSPLIT atmospheric transport and dispersion modeling system, *Bull. Amer. Meteor. Soc.*, **96**, 2059-2077, <http://dx.doi.org/10.1175/BAMS-D-14-00110.1> 
- Vlachogiannis, D., A. Sfetsos, S. N. Karozis, N. Gounaris and C., Mita, 2013: Mesoscale Simulation of Hot Weather Events during August 2012 in Greece, HARMO15 Conference, Madrid May, 6-9, 2013.
- Zanetti, P., 1990: Air Pollution Modeling: Theories, Computational Methods and Available Software, ISBN 978-1-4757-4465-1, Southampton: Computational Mechanics and New York: Van Nostrand Reinhold, pp 443.

**17th International Conference on  
Harmonisation within Atmospheric Dispersion Modelling for Regulatory Purposes  
9-12 May 2016, Budapest, Hungary**

---

**A NUMERICAL STUDY OF AIR-POLLUTION AND ATMOSPHERIC FINE-SCALE FLOW  
OVER THE COASTAL COMPLEX TERRAIN OF MT. CARMEL**

*N. Haikin<sup>1,2</sup>, P. Alpert<sup>1</sup>, Y. Mahrer<sup>3</sup>*

<sup>1</sup>Department of Earth sciences, Tel-Aviv University, Ramat-Aviv, Tel Aviv 69978, Israel

<sup>2</sup>NRCN, POB 9001 Beer Sheva 84190, Israel

<sup>3</sup>Hebrew University, Soil and Water Dept., Rehovot, Israel (Emeritus)

**Abstract:** Haifa Bay, located on the Eastern Mediterranean, is densely populated by industrial facilities alongside inhabitants. The area is characterized by a complex terrain, mainly due to Mt. Carmel which rises up to 450 - 500 m (asl) over a short distance from the coast. The atmospheric models RAMS and HYPACT were employed with 0.5 km resolution on an air pollution episode over the domain. Simulated data of surface and upper air concentration profiles revealed a significant spatial and temporal variability over the domain, more complex than could be captured by the monitoring network.

## **INTRODUCTION**

Haifa is a densely populated and industrialized region, located on the Eastern Mediterranean coast. In recent years the region has been under focus of the public and the authorities (Israel MoEP, 2016), both struggle against air pollution sources and hazards. Researchers have long been studying the health effects which potentially were caused by exposure to excess concentrations of air pollutants in the region (Goren et al., 1991; Paz et al., 2009; Eitan et al., 2010). Although long term emissions and ambient observed data present a decreasing trend of air pollution over the last decade, due to stricter regulation and enforcing, the debate about the actual effects and potential risks is up front publically. Haifa region is densely monitored, with more than 20 monitoring stations within a 15 x 15 km<sup>2</sup> domain. The monitoring devices are stationed on sites with a potential of high air pollution and/or in populated neighborhoods, in order to continually evaluate the air quality there. The monitoring stations are aimed to represent the air quality in their surroundings. However, in the complex environment of the study regime micrometeorology may cause very high variability of pollution patterns over short time and distance, with higher resolution than can be monitored. Moreover, multi-pollutant environment can never be completely monitored for all components. Atmospheric models may support spatial and temporal analysis of pollution dispersion and risk management, where they may supply additional unique information, especially in complex domain (e.g. Pielke et al, 1983; Schmitz R, 2005). In the current work, the models RAMS and HYPACT were employed on an air pollution episode which occurred in the region. Based on the simulations results, we analyzed the sensitivity of monitoring locations to plume variations, and to spatial variability of plumes in the study domain.

## **RESULTS AND DISCUSSION**

The atmospheric models RAMS and HYPACT were employed on the Haifa domain, where several monitoring stations locations were selected for analysis of the pollutants plumes (Figure 1). The sites were chosen to represent the mountainous part of the region, the bay, and the eastern foothills of Mt. Carmel. Meteorological data extracted from RAMS simulation demonstrated significant variability of which an example is presented in Figure 2. Temperature profiles were extracted for sites 1 and 6, less than 5 km apart from each other (horizontal distance). The simulated profiles over the bay (site 1 in Figure 1) present evolution of low level inversion along the day, while over the mountainous site (site 6, in Figure 1) only a mild inversion appears in the morning. However, the 1300 UTC profile presents a similar inversion over both sites, where over site 6 it is almost ground inversion, and over site 1 it appears at an elevation of almost 400 m which is close to the elevation of the ridge top. These profiles suggest this

midday inversion layer is leveled over the domain at that time. Surface temperatures differences between the two sites are up to 10°C along the episode.

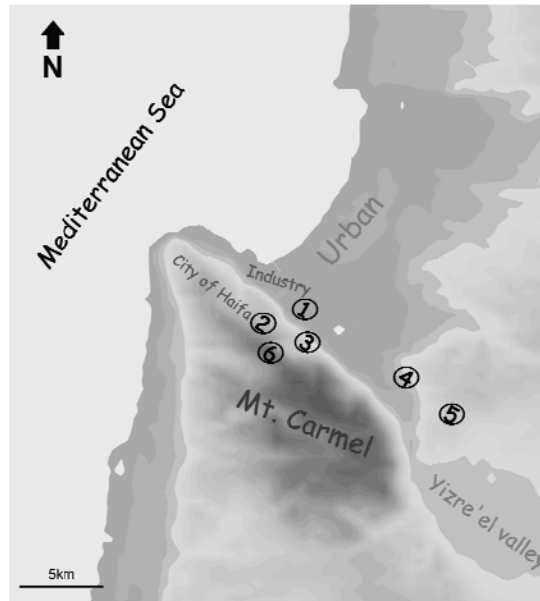


**Figure 1.** Haifa domain with selected monitoring (marked 1-5) and meteorological (marked 6) sites. Site 1 represents the bay, sites 2, 3, 6 are mountainous and sites 4, 5 represent the eastern foothills of Mt. Carmel.

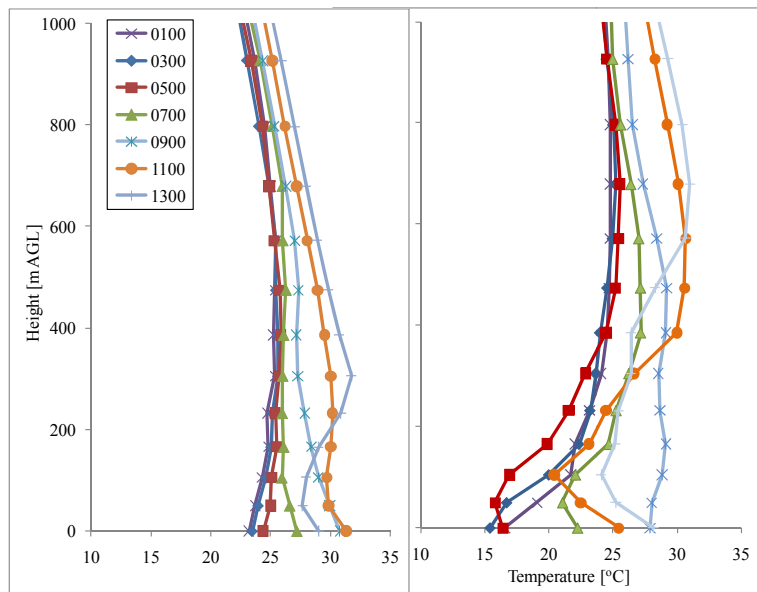


**Figure 2.** Simulated temperature profiles over Mt. Carmel, at about 450 m (asl) elevation (left) and over the bay (right); each line represents a different hour (UTC). Over the bay the profiles show evolution of surface and elevated inversion, of which only traces are seen over the mountainous site.

Air pollution concentrations along the case study episode show an early morning peak observed over the mountainous site, and later that day it shows high concentrations which were observed over the eastern foothills (Figure 3 (a)). While the morning simulated peak agree with the observed one by means of location, time and intensity, the afternoon simulated peak appeared both over the foothills and the

mountainous sites (Figure 3 (b)), with higher peaks than the observed ones. Another morning peak was also simulated over the foothills, below the mountainous sites (not shown here). Both observed and simulated concentrations were compared over point sites, hence, the variations between the observed and simulated locations may strongly be effected by westerly shift of the simulated plume towards the mountain, or by monitors' under detection of the plume. It is suggested that in this case the plume may have missed monitoring sites by only short horizontal or vertical distance (Haikin et al, 2016).

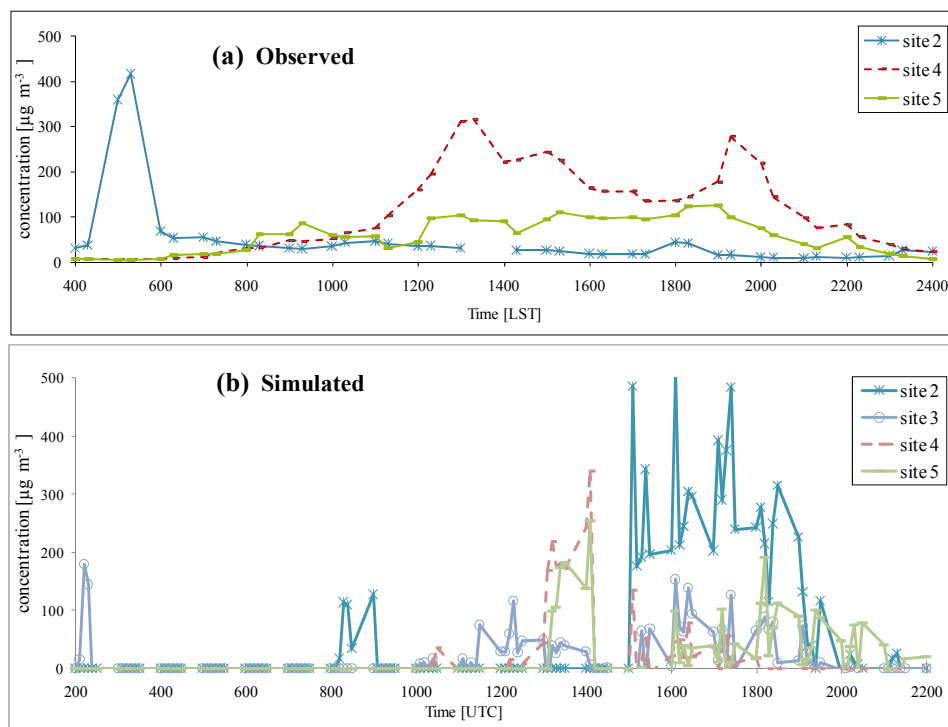


**Figure 3.** Observed (a) and simulated (b) concentrations along the case study episode: morning peak was observed over mountainous site and the later ones over the valley, while the afternoon and evening highest simulated peaks appear over the mountainous site.

## CONCLUSION

An air pollution episode was used to study the variability of pollution dispersion in a complex domain, where the models added unique information of the spatial temporal evolution of the plume. Monitoring network density is restricted by costs and available locations. On the other hand, atmospheric models have their limits of sensitivity and ability to capture reality correctly. In order to gain sufficient knowledge for air pollution and risk management a combination of observations and simulations should be used.

## REFERENCES

- Eitan O., Yuval, Barchana M., Dubnov J., Linn S., Carmeli Y., Broday D.M, 2010, Spatial Analysis of air pollution and cancer rates in Haifa Bay, Israel. *Science of the total Environ.* **408**, 4429-4439.
- Goren A I, Hellman S, Brener S, Egoz N, Rishpon S, 1990: Prevalence of Respiratory Conditions among Schoolchildren Exposed to Different Levels of Air Pollutants in the Haifa Bay Area, Israel. *Environ Health Perspect.* **89**, 225-231.
- Haikin n., Alpert P., Mahrer Y, 2016: Why a dense network of air pollution monitoring stations is not sufficient over highly complex terrain? Mt. Carmel high-resolution modeling study. *Submitted.*
- Israel Ministry of Environmental protection (MoEP), 2016 (English)  
<http://israelforeignaffairs.com/2016/03/moep-increasing-air-quality-monitoring-and-enforcement-in-haifa-bay/>

- Paz S, Linn S, Portnov B A, Lazimi A, Futerman B, Barchana M, 2008: Non-Hodgkin Lymphoma (NHL) linkage with residence near heavy roads—A case study from Haifa Bay, Israel. *Health and Place*, **15**, 636-641. doi:10.1016/j.healthplace.2008.10.004
- Pielke, R.A., Cotton, C.J., Walko, R.L., Tremback, C.J., Lyons, W.A., Grasso, L.D., Nicholls, M.E., McNider R.T., Segal M., Mahrer Y, 1983, The use of a mesoscale numerical model for evaluation of pollutant transport and diffusion in coastal regions and over irregular terrain. *Bull. American Meteorol Soc.* **64**, 243-249.
- Schmitz R 2005, Modelling of air pollution dispersion in Santiago de Chile. *Atmospheric environ*, **39**, 2035-2047.

**17th International Conference on  
Harmonisation within Atmospheric Dispersion Modelling for Regulatory Purposes  
9-12 May 2016, Budapest, Hungary**

---

**CHALLENGES IN ASSESSING AIR POLLUTION FROM RESIDENTIAL WOOD  
COMBUSTION**

*Helge R. Olesen*

Department of Environmental Science, Aarhus University, Roskilde, Denmark

**Abstract:** The paper highlights a number of important challenges in quantifying the impact of residential wood combustion on air quality. The fact that real life emissions are controlled by the behaviour of the users makes it a challenge to determine representative emission factors. Further, in respect to determination of particle emissions factors, there are inconsistencies between countries due to different handling of condensable gases released from wood combustion. These and other challenges are discussed in the paper.

**Key words:** *residential wood combustion, wood stoves, emission factors.*

#### **INTRODUCTION**

Residential wood combustion is an important sector when it comes to air pollution, both in Europe and worldwide. Therefore, it is a common task for dispersion modellers to conduct assessments of the impact of residential wood combustion on air quality.

The large impact of residential wood combustion was recently quantified in an assessment of health costs associated with residential wood combustion in Denmark (Economic Council, 2016; Brandt et. al, 2016). The study estimated the health costs of using a wood stove for one hour at various locations in Denmark. According to the study, the health cost amounted to 5.5 Euro/hour for use of an old wood stove in Copenhagen, while it was less than 1 Euro/hour for a modern stove. In less populated regions the cost was smaller – e.g., 0.13 Eurocents/hour for a modern stove on the island of Bornholm. If a user were compelled to pay such costs, it would have dramatic influence on the use of residential wood combustion.

Results such as these demonstrate the importance of residential wood combustion as a source of pollution. However, it should be recognized that the estimates are also quite uncertain because they are based on many simplifying assumptions. The purpose of the present paper is to take a modeller's perspective and highlight important challenges in quantifying the impact of residential wood combustion on air quality. Modellers should be aware of the challenges to avoid misleading conclusions.

#### **THE CHALLENGE OF REPRESENTATIVE EMISSION FACTORS**

A major challenge is that for residential wood combustion, *test bench emissions cannot simply be considered representative of real-world emissions*. Figure 1 serves to illustrate this. It shows real world emission factors for particles from wood stoves measured at 12 houses on up to four days (over two winters). The data are from Glasius et al. (2005; 2007).

Each column represents one measurement period with duration 5-10 hours from ignition until fire is extinguished. The columns are grouped by house (ID). All wood stoves on the graph were classified as belonging to the same emission category (classified by age). During measurements the residents were instructed to use their stove as usual. For one user this implied that during one measurement period (5B) he included some painted wood for feeding his stove. The graph illustrates clearly that there is an enormous variability in emissions from house to house and from day to day.

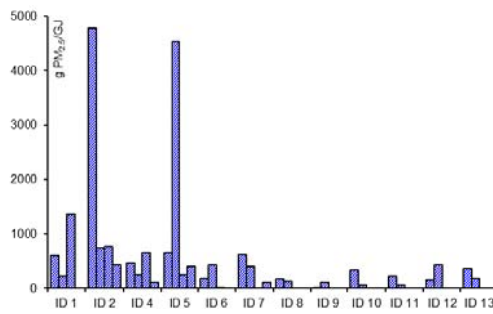


**Figure 1.** Emission factors for PM<sub>2.5</sub> for 12 houses with wood stoves. There are up to 4 measurements (bars) for each house. The graph includes data from two winter seasons and is based on data from Glasius et al. (2005; 2007).

When considering additional pollutants, there are further complications. Figure 2 is similar to Figure 1, but displays results for, respectively, particles, PAH and dioxin. The figure includes some of the data from Figure 1, but it is based on data from only one winter season. When comparing the patterns for the three substances in Figure 2 it is clear that the patterns are very dissimilar. Thus, a large emitter of particles is not a large emitter of PAH, and large emitters of dioxin are not large emitters of the other substances.

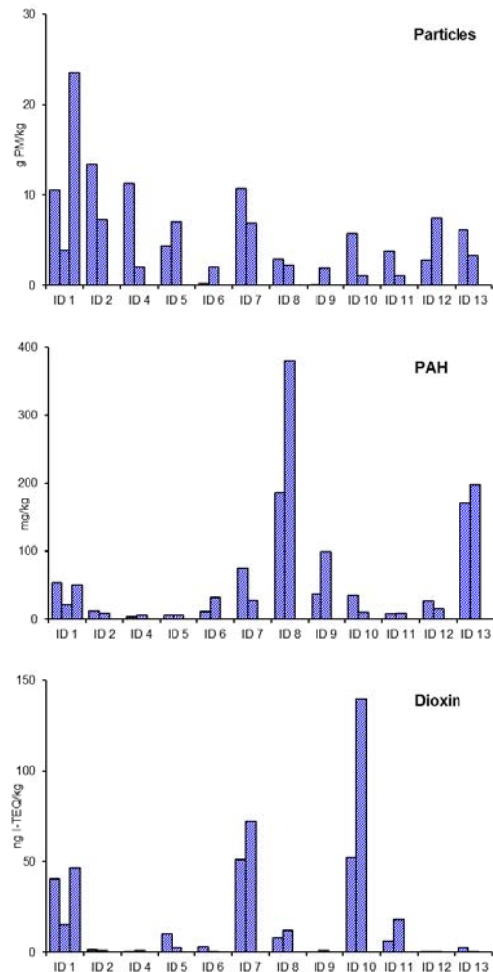


**Figure 2.** Emission factors for three pollutants – particles, PAH and dioxin – for 12 houses with wood stoves with up to 3 measurements (bars) for each house. There is data from one winter season only. The unit is pollutant mass per kg firewood. Data from Glasius et al. (2007).

The dissimilar patterns are a result of the fact that different processes are responsible for generation of, respectively, particles, PAH and dioxin. The graph demonstrates clearly that it is a gross simplification to assume that for a given stove technology emissions are simply proportional to the amount of wood burned.

The examples show that it is a major challenge to determine representative emission factors for a population of stoves. The fundamental reason behind this challenge is that residential wood combustion is a technology where the behaviour of the user plays a dominant role.

### **THE CHALLENGE OF COMBUSTION CONDITIONS**

In all emission inventories, it is recognized that the type of combustion device is an important parameter. However, many other factors play a decisive role, but are not taken explicitly into account in emission inventories. Most of these factors relate to combustion conditions. A wealth of studies exist on the influence of combustion conditions on emission of air pollutants. Here, we will briefly recapitulate some important findings.

Insufficient oxygen supply provokes large particle emissions. Overload works in a similar manner. In a study of the effect of combustion conditions Klippel et al. (2007) found that compared to optimal combustion conditions (small load, completely dry wood), more typical conditions (moderate load, 20% moisture content in wood) resulted in 14 times higher particle concentrations. Moreover, very bad combustion conditions (filled stove, insufficient oxygen supply) resulted in a difference of more than a factor 300 compared to optimum conditions. (These particle measurements included condensables, see later.)

Moisture content in the wood is a further important factor. It should not exceed 20%, and preferably be less.

The type of firewood matters; in different regions, there are different favourite wood types.

Further, log size should not be too large, neither too small. One study where 'logs' had a quadratic cross-section found a dimension of 7 by 7 cm to be optimal, whereas larger and smaller dimensions increased particle pollution considerably. This result cannot immediately be generalized, as logs seldom are quadratic, and the result is presumably sensitive to the specific stove. However, it illustrates that changes in user behaviour can influence pollution.

When operating wood stoves in real life a large part of the total particle mass is emitted during the initial ignition period. Experiments have shown that generally the method of "ignition from above" (Nussbaumer et. al, 2008a) is to be recommended. It was found that in some cases cumulated particle pollution over an entire period of stove use could be reduced by as much as 80% by ignition from above.

Furthermore, chimney construction, ventilation of the house and the resulting draft are important factors.

When considering the above list of important factors it comes as no surprise that results such as those in Figure 1 and 2 can be found in practice. The whole range of challenges outlined are too many to take explicitly into account in modelling, but some understanding of them is important to avoid misleading conclusions. Neglecting the challenges may have as a consequence that focus is not on the most appropriate measures to reduce harmful air pollution from residential wood combustion

### **THE CHALLENGE OF CONDENSABLE GASES**

An important challenge that modellers should be aware of is that emission factors are based on laboratory measurements according to standards, which vary from country to country. Different standards are a major reason why particle emission factors for wood stoves vary considerably between countries.

An all-important issue is whether particle mass measurement are performed on hot gas close to the stove, or whether the gas has been diluted and cooled. The first method (e.g. the German standard EN 13240

DIN+ HF.) will *not* include the mass of condensable gases which form particles when leaving the stack, whereas the second method (e.g. Norwegian standard NS 3058) will.

For optimal combustion conditions, the difference between the two approaches is not so large, but for less ideal conditions, it is of extreme importance. In a review of studies from many countries and combustion conditions (Nussbaumer et al., 2008b) found a factor between 2.5 and 10 between results from the two methodologies when conditions were not optimal.

This issue and its implication for modelling was addressed in a recent study by Denier van der Gon et al. (2015), where the authors compiled an emission inventory for Europe that used a new and more harmonised approach to residential wood combustion. The results suggest that the contribution to particle pollution in terms of OC (organic carbon) from residential wood combustion should be augmented by a factor of 2-3 in most European countries, implying an increase of total European PM<sub>2.5</sub> emission by about 20%.

### **THE CHALLENGE OF ACTIVITY DATA**

In all countries, it represents a challenge to compile realistic activity data for the consumption of firewood. Such inventories are best acquired through a combination of surveys among residents and registries of combustion appliances. Use of improved methods for compiling activity data can dramatically change the result of inventories. Thus, Lefebvre et al. (2014) reported that an improved methodology resulted in a 13-fold increase in particle emission from residential wood combustion in Flanders. A factor of 3.4 could be ascribed to wood consumption, and a factor of 4 to more realistic emission factors.

### **HOW TO MEET THE CHALLENGES**

The sections above have outlined a number of challenges. These challenges inevitably have as consequence that modelling results for residential wood combustion will be more uncertain than modelling results for most other emission sectors. As modellers we should pay critical attention to the way emission inventories for residential wood combustion are compiled, having the considerable challenges in mind.

When considering standards for quantifying pollution from wood stoves the question of condensables is extremely important. However, there are also other important features that cause a variation between standards, such as differences in how the combustion cycle is defined. In response to these challenges, as well as the set of other challenges involved in reflecting real-world operating conditions, an EU project was initiated in 2013. It is the beReal project (Advanced Testing Methods for Better Real Life Performance of Biomass Heating Appliances; URL 1), which works with testing procedures, and can result in more harmonised and realistic inventories. At a recent international seminar with focus on the question of real world emissions from residential wood combustion some beReal project participants gave presentations; these can be found through URL 2.

There is formal standardisation work ongoing in the standardisation committee CEN/TC 295 (Residential solid fuel burning appliances). The outcome of that work is important because it deals with the crucial question on the choice between standards which do, respectively, do not, include condensable gases when measuring particle mass.

No matter what standard come out of that work modellers will need to take into account the effect of condensables in order to produce realistic results, as pointed out by Denier van der Gon et al. (2016).

The fact that the user has so much influence on the pollution from his wood stove has a positive side: There is potential for a dramatic reduction of pollution from wood stoves.

Much can be achieved by educating users. In Denmark, public campaigns during many years have gradually led to general changes in behaviour, which have supposedly led to reduced emission factors. However, this effect cannot be objectively quantified.

In order to minimize pollution from wood stoves there is one measure which may be efficient, but which presumably can only be applied locally or in limited periods: Banning their user. Disregarding that option, the optimum solution would be to eliminate the influence of the user. This can be achieved by automatic solutions that use sensor technology and have features such as automatic regulation of air supply for wood stoves. Such systems are a reality today, and e.g. in Denmark there is a commercial market for these modern, hi-tech woodstoves.

## REFERENCES

- URL 1: <http://www.bereal-project.eu/> beReal project on advanced testing methods for better real life performance of biomass heating appliances.
- URL 2: <https://woodburningstovesblog.wordpress.com/presentations/> Seminar “Real-world emissions from residential wood combustion” held in Copenhagen, December 3, 2015.
- Brandt, J., S.S. Jensen, M.S. Andersen, M.S. Plejdrup, O.K. Nielsen, 2016: Helbredseffekter og helbredsomkostninger fra emissionssektorer i Danmark. Aarhus Universitet, DCE – Nationalt Center for Miljø og Energi, 47 s. - Videnskabelig rapport fra DCE - Nationalt Center for Miljø og Energi nr. 182. <http://dce2.au.dk/pub/SR182.pdf>
- Denier van der Gon, H.A.C., R. Bergström, C. Fountoukis, C. Johansson, S.N. Pandis, D. Simpson, A. Visschedijk, 2015: Particulate emissions from residential wood combustion in Europe – revised estimates and an evaluation. *Atmos. Chem. Phys.* **15**, 6503-6519.
- Economic Councils in Denmark: Discussion paper for meeting in Council for Environmental Economy. March 1, 2016. Air pollution. [http://www.dors.dk/files/media/rapporter/2016/M16/m16\\_disk.pdf](http://www.dors.dk/files/media/rapporter/2016/M16/m16_disk.pdf)  
English summary: [http://www.dors.dk/files/media/rapporter/2016/M16/m16\\_disk\\_summary.pdf](http://www.dors.dk/files/media/rapporter/2016/M16/m16_disk_summary.pdf)
- Glasius, M., P. Konggaard, J. Stubkjær, R. Bossi, O. Hertel, M. Ketzler, P. Wählin, O. Schleicher, & F. Palmgren, 2007): Partikler og organiske forbindelser fra træfyring – nye undersøgelser af udslip og koncentrationer. Arbejdsrapport fra DMU, nr. 235. 42 s. <http://www.dmu.dk/Pub/AR235.pdf>
- Glasius, M., J. Vikelsøe, R. Bossi, H.V. Andersen, J. Holst, E. Johansen & O. Schleicher: 2005: Dioxin, PAH og partikler fra Brændeovne. Danmarks Miljøundersøgelser. Arbejdsrapport fra DMU, nr. 212. 27 s. [http://www2.dmu.dk/1\\_viden/2\\_Publikationer/3\\_arbrapporter/rapporter/AR212.pdf](http://www2.dmu.dk/1_viden/2_Publikationer/3_arbrapporter/rapporter/AR212.pdf)
- Klippel, N. and, T. Nussbaumer, 2007: Einfluss der Betriebsweise auf die Partikelemissionen von Holzöfen. Bundesamt fuer Energie, Bern, Switzerland, 63 p. [www.verenum.ch/Publikationen/SBOfenmessun.pdf](http://www.verenum.ch/Publikationen/SBOfenmessun.pdf)
- Lefebvre, W., F. Fierens, C. Vanpoucke, N. Renders, K. Jespers, J. Vercauteren, F. Deutsch, S. Janssen, 2014: The effect of wood burning on particulate matter concentrations in Flanders, Belgium. 16th International Conference on Harmonisation within Atmospheric Dispersion Modelling for Regulatory Purposes, 8-11 September 2014, Varna, Bulgaria.
- Nussbaumer, T., A. Doberer, N. Klippel, R. Bühler, W. Vock, 2008a: Influence of ignition and operation type on particle emissions from residential wood combustion. 16th European Biomass Conference and Exhibition, 2–6 June 2008, Valencia, Spain. <http://www.verenum.ch/Publikationen/Biomass-Conf9.5.pdf>
- Nussbaumer, T., C. Czasch, N. Klippel, L. Johansson, C. Tullin, 2008b: Particulate emissions from biomass combustion in IEA countries. Survey on measurements and emission factors. 40 pp. Report on behalf of International Energy Agency (IEA) Bioenergy Task 32. [http://www.ieabcc.nl/publications/Nussbaumer\\_et\\_al\\_IEA\\_Report\\_PM10\\_Jan\\_2008.pdf](http://www.ieabcc.nl/publications/Nussbaumer_et_al_IEA_Report_PM10_Jan_2008.pdf)

**17th International Conference on  
Harmonisation within Atmospheric Dispersion Modelling for Regulatory Purposes  
9-12 May 2016, Budapest, Hungary**

---

**AIR QUALITY FORECASTS FOR POLAND - APPLICATION OF THE WRF-CHEM MODEL  
WITHIN THE LIFE/APIs PROJECT**

*Małgorzata Werner, Maciej Kryza, Hanna Ojrzyńska, Kinga Walaszek, Anetta Drzeniecka-Osiadacz*

Wrocław University, Department of Climatology and Atmosphere Protection, Wrocław, Poland

**Abstract:** In this work we present the air quality forecasting system which is running operationally for the area of Poland since December 2015. The system is based on the online WRF-Chem model, which is configured using two nested domains covering Europe (12km x 12km grid mesh) and Poland (4km x 4km grid mesh). For meteorology, the system uses GFS forecasts as boundary and initial conditions. TNO-MACC 3 emission inventory for the year 2011 is used for both domains. The system calculates hourly emissions taking into account country and SNAP sector dependent emission factors, bank holidays and winter/summer time. During the post-processing of the forecasts, the Air Quality Indices are calculated. The results are disseminated using the OGC services. The comparison of the WRF-Chem forecasts with hourly measurements of PM<sub>10</sub> and NO<sub>2</sub> for the heating season on December 2015-February 2016 shows that there is a large underestimation of PM<sub>10</sub>, and the model resolves well temporal changes in NO<sub>2</sub> concentrations.

**Key words:** *air quality, forecasting, WRF-Chem, Poland*

## **INTRODUCTION**

Despite a significant reduction of pollutant emissions in past years, many European regions still touch problems in complying with the European Union's (EU) air quality directive (European Commission (EC), 2008). It also concerns one of the biggest European countries – Poland, for which the air quality is especially problematic in winter seasons. During winter months, episodes of poor air quality, related to e.g. high concentrations of particulate matter (PM) are frequent in Poland. These episodes are due to both high coal consumption used for residential heating and meteorological conditions preventing mixing and dilution of air pollutants.

Poor air quality has an adverse impact on human health (Pope et al., 2002), ecosystems (Serengil et al., 2011) and climate (Menon et al., 2008). A constant finding is that air pollutants contribute to increased mortality and hospital admissions (Brunekreef and Holgate, 2002). The different composition of air pollutants, the dose and time of exposure and the fact that humans are exposed to pollutant mixtures can lead to diverse impacts on human health. Human health effects can range from nausea and difficulty in breathing or skin irritation to cancer (Kampa and Castanas, 2008). Atmospheric aerosols are currently a subject of extensive research and from an environmental standpoint, aerosols constitute an important policy issue in air quality and climate science. Particulate matter pollution is one of the most pressing issue in air quality regulation, and at the same time it represents one of the biggest sources of uncertainty in chemical transport model simulations. Besides PM, nitrogen dioxide (NO<sub>2</sub>) has also received a special attention due to several reasons – it acts as a precursor of both particulate matter and tropospheric ozone (Beelen et al., 2014) as well as has an adverse respiratory effects (WHO 2013).

Nitrogen oxides are emitted as NO, which reacts rapidly with ozone or free radicals in the atmosphere forming NO<sub>2</sub>. The main anthropogenic sources are mobile and stationary combustion sources. Particulate matter consists of complex mixtures of particles suspended in the air, which vary in size and composition, and are produced by a variety of natural and anthropogenic activities. Major sources of PM are combustion processes in power plants, households, factories, motor vehicles, as well as construction activity, fire and natural sources of aerosols (wind blown dust and sea salt).

The ability to forecast regional and local air pollution events is challenging since the processes governing the production and accumulation of pollutants are complex and nonlinear. Comprehensive atmospheric models, by representing in as much detail as possible the various dynamical, physical, and chemical processes regulating the atmospheric fate of pollutants, provide a scientifically sound tool for providing air quality forecast guidance (Mathur et al., 2008).

The air pollution forecasting in Poland is still limited and in this work we present the air quality forecasting system which is developed within the LIFE/APIIS (<http://life-apis.meteo.uni.wroc.pl/>) project and is running operationally for the area of Poland since the 1st of December 2015. The system is based on the online WRF-Chem model, which is configured using two nested domains covering Europe (12km x 12km grid mesh) and Poland (4km x 4km grid mesh) with the main focus on the south-west Poland (Lower Silesia). Within this first stage of the system existence the forecasts are not presented to the public but the main effort is towards evaluation of the results. Here, we used the air pollution concentrations (PM10 and NO<sub>2</sub>) measured at the Lower Silesia stations and evaluated the model results for the first 3 months of the forecasts (December 2015 – February 2016).

## **DATA AND METHODS**

The WRF-Chem model version 3.5.1 is used with the configuration similar to Werner et al. (2016). These include the Noah Land Surface Model (Chen and Dudhia, 2001), YSU boundary layer physics (Hong et al., 2006), RRTMG long and short wave radiation scheme (Iacono et al., 2008), Grell 3D parameterisation with radiative feedback and shallow convection (Grell, 2002), the Lin microphysics scheme (Lin et al., 1983). The simulations are driven by the GFS meteorological data, available every 3h, at a 0.5° x 0.5° spatial resolution. Previous work of Werner et al. (2016) has shown the performance of the forecasting system with a flat emission inventory and TNO MACC II emission data. Here, we used the newest TNO MACC III emission inventory for the year 2011 and included hourly emission profiles taking into account country and SNAP sector dependent emission, bank holidays and winter/summer time. The first 48-h forecasting cycle on the 1st of December uses a 2-week spin-up, with the model simulations initialized with the GFS FNL meteorology for initial and boundary conditions. From the 2nd day of December, the model uses chemistry cycling, and the WRF-Chem run from the last hour on the previous day are used to initialize the next day's forecasting simulation.

The PM10 and NO<sub>2</sub> concentrations' forecasts were compared with hourly observations gathered by the Voivodeship Inspectorate of Environmental Protection at 16 stations in the Lower Silesia region in SW Poland. We used here basic error statistics to summarize the system performance for the 16 December 2015 - 28 February 2016. It included: bias (BIAS), mean absolute error (MAE) and index of agreement (IOA). For NO<sub>2</sub>, data from 13 measuring sites and for PM10 7 measuring sites were available. Forecasts are compared with the measurements separately for the <24h and 48-72h lead time. For February 2016, the measurements were used with no detailed quality control.

## **RESULTS**

Examples of PM10 and NO<sub>2</sub> forecasts are presented in Figure 1 for the SW Poland (Dolnośląskie province). Both maps show the highest concentrations of atmospheric pollutants for the emission source areas. These are both the main cities (e.g. Wrocław) or the large industrial or energy production sites (e.g. Turoszów at the SW boundary of Poland). Modelled atmospheric concentrations in the closest vicinity of the large point sources are too high if compared with the measurements. This should be linked with a lack of vertical emission profile, which is currently under the development for the LIFE/APIIS forecasting system.

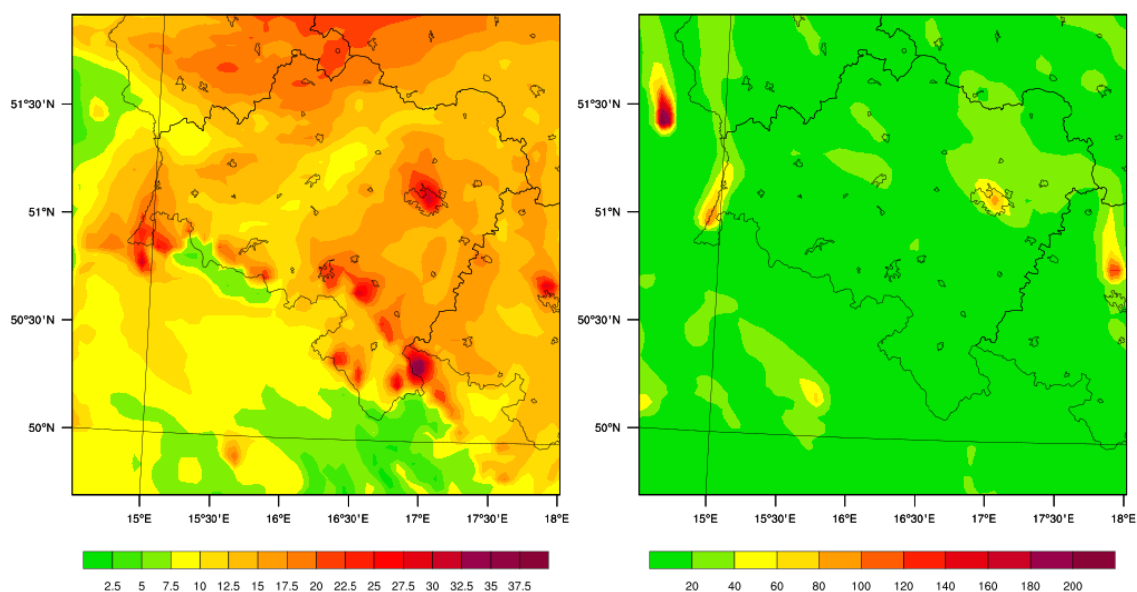


**Figure 1.** Examples of PM10 (left, time valid 06.01.2016 13:00 UTC) and NO2 (right, time valid 11.01.2016 07:00 UTC). Units are  $\mu\text{g m}^{-3}$

The PM10 concentrations are to the large extent underestimated for the majority of the measuring sites. Especially the peaks, which are of a large concern in terms of human health, are underestimated. This is shown with the example of the Działoszyn station (Figure 2). Temporal variability of the observed PM10 concentrations is well resolved, but the measured values, and especially the peaks, are underestimated. This is also shown in Table 1. The bias for hourly PM10 concentrations, calculated for all the stations for the period of December 2015 – February 2016 is  $-26.7 \mu\text{g m}^{-3}$ .

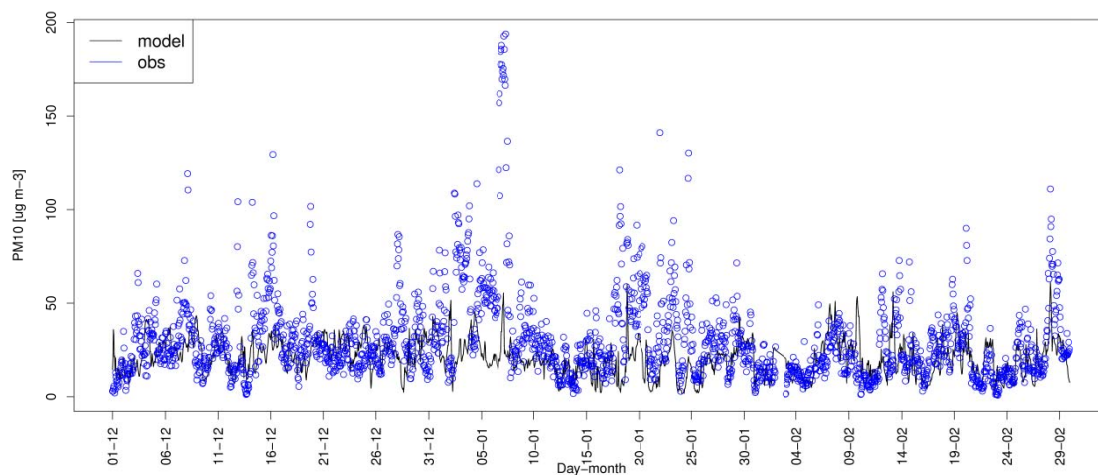


**Figure 2.** Modelled and measured hourly PM10 concentrations at rural station (Działoszyn), lead time  $<24\text{h}$

The forecasting system was able to reproduce the observed NO2 air concentrations during the analysed period. The bias is relatively small, concerning the absolute values of measured NO2, and the temporal variability of modelled NO2 is similar to the measurements, as shown in Figure 3 at Legnica station as an example.

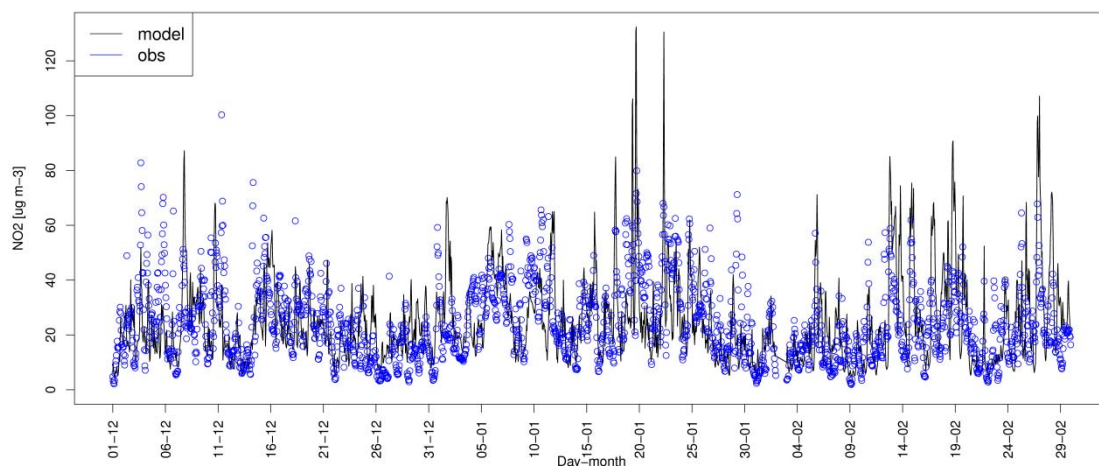


**Figure 3.** Modelled and measured hourly NO<sub>2</sub> concentrations at suburban station (Legnica), lead time <24h

The error statistics, calculated for the entire period and all the available stations, are summarized in Table 1 for two lead times: <24h and >48h. The results confirm large underestimation by the model of the measured PM<sub>10</sub> values. NO<sub>2</sub> is also underestimated. There are relatively small changes in the model performance if the two lead times are compared.

**Table 1.** Error statistics for PM<sub>10</sub> and NO<sub>2</sub>, lead time <24h and lead time>48h, all stations

	PM <sub>10</sub> LT<24h	PM <sub>10</sub> LT>48h	NO <sub>2</sub> LT<24h	NO <sub>2</sub> LT>48h
BIAS [ $\mu\text{g m}^{-3}$ ]	-26.7	-27.2	-19.6	-19.8
MAE [ $\mu\text{g m}^{-3}$ ]	31.9	32.5	20.0	20.0
IOA	0.36	0.36	0.42	0.43

## SUMMARY AND CONCLUSIONS

We have presented here the results of the improved version of the air pollution forecasting system for SW Poland developed within the LIFE/APIS project. In comparison to the first version of the system (Werner et al. 2016), the main change includes the application of the hourly temporal emission profile, which vary between weekday, weekend and holidays and is SNAP sector dependent. This change improved temporal and spatial variability of modelled NO<sub>2</sub> concentrations, which are related, in a high degree, with emissions from road transport. The bias is relatively small and the temporal variability of modelled NO<sub>2</sub> is similar to the measurements. The improvement for PM<sub>10</sub> concentrations is not so clear as for NO<sub>2</sub>. In fact temporal variability of the observed PM<sub>10</sub> concentrations is well resolved, but the measured values, and especially the peaks, are underestimated. The underestimation of the PM<sub>10</sub> concentrations might be linked with the uncertainty in primary particulates emission inventory. National emission database, developed for the year 2015 by the Chief Inspectorate of Environment Protection, shows that the PM<sub>10</sub> emission from residential combustion is c.a. two times higher if compared with TNO MACC III data.

Moreover, for both pollutants modelled concentrations in the closest vicinity of the large point sources are too high if compared with the measurements. We link this with a lack of vertical emission profile, which is currently under the development for the LIFE/APIS forecasting system.

## ACKNOWLEDGEMENTS

The project was partially financed by European Union and co-financed by NFOSiGW within LIFE+ Program, Project: LIFE-APIS/PL - Air Pollution and biometeorological forecast and Information System. LIFE12 ENV/PL/000056. Calculations have been carried out using resources provided by Wrocław Centre for Networking and Supercomputing (<http://wcss.pl>).

## REFERENCES

- Beelen, R., Raaschou-Nielsen, O., Stafoggia, M., Andersen, Z. J., Weinmayr, G., Hoffmann, B., Wolf, K., Samoli, E., Fischer, P., Nieuwenhuijsen, M., Vineis, P., Xun, W. W., Katsouyanni, K., Dimakopoulou, K., Oudin, A., Forsberg, B., Modig, L., Havulinna, A. S., Lanki, T., Turunen, A., Oftedal, B., Nystad, W., Nafstad, P., De Faire, U., Pedersen, N. L., Östenson, C.-G., Fratiglioni, L., Penell, J., Korek, M., Pershagen, G., Eriksen, K. T., Overvad, K., Ellermann, T., Eeftens, M., Peeters, P. H., Meliefste, K., Wang, M., Bueno-de-Mesquita, B., Sugiri, D., Krämer, U., Heinrich, J., de Hoogh, K., Key, T., Peters, A., Hampel, R., Concin, H., Nagel, G., Ineichen, A., Schaffner, E., Probst-Hensch, N., Künzli, N., Schindler, C., Schikowski, T., Adam, M., Phuleria, H., Vilier, A., Clavel-Chapelon, F., Declercq, C., Grioni, S., Krogh, V., Tsai, M.-Y., Ricceri, F., Sacerdote, C., Galassi, C., Migliore, E., Ranzi, A., Cesaroni, G., Badaloni, C., Forastiere, F., Tamayo, I., Amiano, P., Dorronsoro, M., Katsoulis, M., Trichopoulou, A., Brunekreef, B. and Hoek, G.: Effects of long-term exposure to air pollution on natural-cause mortality: an analysis of 22 European cohorts within the multicentre ESCAPE project., *Lancet* (London, England), **383**(9919), 785–95, doi:10.1016/S0140-6736(13)62158-3, 2014.
- Brunekreef, B. and Holgate, S. T.: Air pollution and health., *Lancet*, **360**(9341), 1233–42, doi:10.1016/S0140-6736(02)11274-8, 2002.
- Chen, F. and Dudhia, J.: Coupling an Advanced Land Surface–Hydrology Model with the Penn State–NCAR MM5 Modeling System. Part I: Model Implementation and Sensitivity, *Monthly Weather Review*, **129**, 569–585, doi:10.1175/1520-0493(2001)129<0569:CAALSH>2.0.CO;2, 2001.
- Grell, G. A.: A generalized approach to parameterizing convection combining ensemble and data assimilation techniques, *Geophysical Research Letters*, **29**, 1693, doi:10.1029/2002GL015311, 2002.
- Hong, S.-Y., Noh, Y. and Dudhia, J.: A New Vertical Diffusion Package with an Explicit Treatment of Entrainment Processes, *Monthly Weather Review*, **134**, 2318–2341, doi:10.1175/MWR3199.1, 2006.
- Iacono, M. J., Delamere, J. S., Mlawer, E. J., Shephard, M. W., Clough, S. A. and Collins, W. D.: Radiative forcing by long-lived greenhouse gases: Calculations with the AER radiative transfer models, *Journal of Geophysical Research*, **113**(D13), D13103, doi:10.1029/2008JD009944, 2008.
- Kampa, M. and Castanas, E.: Human health effects of air pollution., *Environmental pollution* (Barking, Essex : 1987), **151**(2), 362–7, doi:10.1016/j.envpol.2007.06.012, 2008.
- Lin, Y.-L., Farley, R. D. and Orville, H. D.: Bulk Parameterization of the Snow Field in a Cloud Model, *Journal of Climate and Applied Meteorology*, **22**, 1065–1092, doi:10.1175/1520-0450(1983)022<1065:BPOTSF>2.0.CO;2, 1983.
- Mathur, R., Yu, S., Kang, D. and Schere, K. L.: Assessment of the wintertime performance of developmental particulate matter forecasts with the Eta-Community Multiscale Air Quality modeling system, *Journal of Geophysical Research D: Atmospheres*, **113**, doi:10.1029/2007JD008580, 2008.
- Menon, S., Unger, N., Koch, D., Francis, J., Garrett, T., Sednev, I., Shindell, D. and Streets, D.: Aerosol climate effects and air quality impacts from 1980 to 2030, *Environmental Research Letters*, **3**(2), 024004, doi:10.1088/1748-9326/3/2/024004, 2008.
- Pope, C. A., Burnett, R. T., Thun, M. J., Calle, E. E., Krewski, D., Ito, K. and Thurston, G. D.: Lung cancer, cardiopulmonary mortality, and long-term exposure to fine particulate air pollution., *JAMA*, **287**(9), 1132–41 [online] Available from: <http://www.pubmedcentral.nih.gov/articlerender.fcgi?artid=4037163&tool=pmcentrez&rendertype=abstract> (Accessed 21 October 2014), 2002.
- Serengil, Y., Augustaitis, A., Bytnerowicz, A., Grulke, N., Kozovitz, A., Matyssek, R., Müller-Starck, G., Schaub, M., Wieser, G., Coskun, A. and Paoletti, E.: Adaptation of forest ecosystems to air pollution and climate change: a global assessment on research priorities, *iForest - Biogeosciences and Forestry*, **4**(2), 44–48, doi:10.3832/ifor0566-004, 2011.
- Werner, M., Kryza, M., Ojrzyńska, H., Skjøth, C. A., Wałaszek, K. and Dore, A. J.: Application of WRF-Chem to forecasting PM10 concentration over Poland, *Int. J. Environ. Pollut.*, in press, 2016.

**17th International Conference on  
Harmonisation within Atmospheric Dispersion Modelling for Regulatory Purposes  
9-12 May 2016, Budapest, Hungary**

---

**DYNAMIC-STATISTICAL ODOUR DISPERSION MODEL USING THE CALPUFF MODEL  
AND GEOSTATISTICAL ANALYSIS**

*Maria Skrętowicz<sup>1</sup> and Jerzy Zwoździak<sup>2</sup>*

<sup>1</sup> Division of Automotive Engineering, Faculty of Mechanical Engineering, Wrocław University of Technology (WUT), Wrocław, Poland

<sup>2</sup> Institute of Meteorology and Water Management, National Research Institute, Warsaw, Poland

**Abstract:** Reliable researches of odours are very difficult to perform due to the characteristics of these pollutants. Except that the sensing odours is a subjective for each person, with odours researches are also many technical and chemical problems. The odours appearance in the area is incidental and depends mainly on weather conditions. So it is important to use models which are 'sensitive' to temporary change meteorological parameters. In addition, it should be recognized that odours occurring in atmospheric air are usually a mixture of chemical gases. These substances can often interact: one substance can enhance, change or neutralize the smell of another substance, and hence the whole mixtures of odorants. That is the reason why chemical analysis of odorants make no sense. For these reasons, in order to achieve reliable results of researches of odours, there is often necessary to use more than one research tool.

In the paper dynamic-statistical odour dispersion model, consist of CALPUFF model and geostatistical analysis was be presented. Using of these two mathematical tools allowed for reliably evaluate odour impact of the analysed object causing the odour nuisance. Emission used in the CALPUFF model was calculated on the basis of measured odour concentration by dynamic olfactometry method. Data for geostatistical analysis have been obtained in field inspections in the plume according to VDI guidelines. The results of the field inspections was odour intensity. Odour intensity values have been converted into odour concentrations values with using Weber-Fechner law. As a result of the model and geostatistical analysis obtained a raster presented a distribution of odour's concentrations in the study area. Connections that two rasters in GIS software allowed for verification both of used tools and getting verified and reliable results of odour nuisance researches.

**Key words:** *mathematic modelling, method uncertainty, odour nuisance, air pollution, odours*

## **INTRODUCTION**

Mathematical air pollution dispersion modelling is one of basic tools used for air quality evaluation in the vicinity of air pollution sources. Almost all of air pollutants could be modelled with using single dispersion model. However, there are types of air pollutants for which using single model gives not enough reliable results. Such pollutants are odours, which, due to their specific nature, are pollutants causing a lot of controversy. In many European countries and throughout the world relevant legislation has been established obligating abatement emission of odours for odour emission sources. These are such countries as Germany, Netherlands, United Kingdom, Denmark, the United States or Australia. In Poland in recent years there were also attempts to impose a duty on facilities owners to limit odour emission, by introducing into Polish law the relevant legislation acts.

For odour dispersion modelling purposes models with very advanced description of the meteorological processes in the atmosphere should be used. Previous studies show that wind velocity, wind direction, temperature and humidity are meteorological parameters that have the greatest impact on odours dispersion. While the temperature and humidity influence mainly the long-term odour immission concentrations (seasonal changes), wind velocity affect the instantaneous change (Nagaraj & Sattler, 2005), (Sówka et al., 2013). According to the German VDI guideline (VDI 3788-1:2000) it is recommended to consider any mixture of odours as individual air pollutant, without analysing chemical composition of the mixture. Therefore, it is not justified to use chemical models in terms of odour dispersion modelling. Additionally, in Danish and German VDI guidelines it is suggested not to use only

one tool in odour measurements (Olesen et al., 2005), (VDI 3788-1:2000). When selecting odour dispersion model it is crucial to choose a model with detailed description of meteorological processes in the atmosphere. The model used for odour dispersion calculations due to the incidental occurrence of odour should be able to calculate the instantaneous odour concentration, for example averaged to several or dozen minutes.

There is a lot of dispersion models extra dedicated for odour dispersion modelling, eg. AUSTAL2000G, NaSt3D or AODM (Austrian Odour dispersion Model), which is the reference odours dispersion model in Austria (Piringer et al., 2007). But also the other models which meet the requirements concerned the odours could be used. One of them is CALPUFF model. It could be used as a simple tool and also in connection with the other such as field inspections. Sironi et al. (2010) applied the CALPUFF model to determine the maximum odour immission concentrations from four animal waste facilities located in Italy. There is also a lot of researches in which two or more models were compared. Dourado et al. proposed a FPM-PRIME model as a useful tool in odour dispersion modelling based on a comparison of this model with AERMOD and CALPUFF (Dourado et al., 2014). Piringer et al. compared Gaussian Austrian Odour Dispersion Model AODM and the Lagrange particle diffusion model LASAT used for short-term peak odour concentrations (Piringer et al., 2015).

Eusebio et al. in Italy investigated an odour impact from composting sludge heaps on the nearby area using field inspections and mathematical dispersion modelling (CALPUFF model) (Eusebio et al., 2013). But nobody have done physically connection of two different tools as a one, compact model yet. In this paper the model developed by physically connection of two different, but consistent tools: CALPUFF model and geostatistical analysis based on field inspections are presented.

## MATERIAL AND METHODS

In the study a distillery situated in the south-west of Poland was analysed. A plant is located in small town, abutting with a city with population above 500 thousand, in the industrial-service area. The nearest residential buildings are located about 1500 meters south from the plant and these are low buildings. The distillery produces ethanol and gluten for food industrial purposes. Three characteristic smells emitted by distillery were identified: smell of ‘a baked bread’ (from the gluten drying process), smell of ‘a cooked pasta’ (from the feeding stuff drying process) and smell of ‘an alcohol’ (from fermentation process).

The model was built based on two tools: odour dispersion calculations using a mathematical model CALPUFF and geostatistical analysis (ordinary kriging) carried out using spatial data obtained during field measurement of odour intensity in the plume (VDI 3940-2:2006). So, the model is based on two spatial meshes: fixed mesh for deterministic model and variable in space and time measurement mesh prepared as a result of geostatistical calculations. Both of the meshes after imposition on each other provide a coherent tool, which aim is to improve the reliability and accuracy of odour research. Model diagram shown in Figure 1.

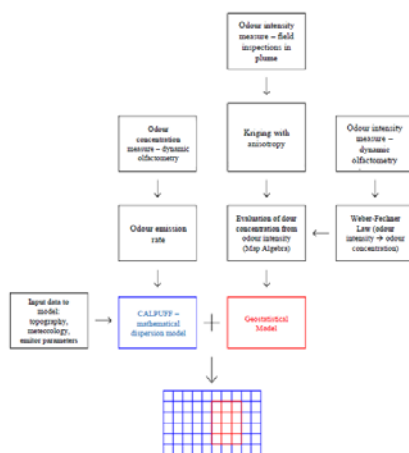


Figure 1. The model conception scheme

Odour emission values used as input data for CALPUFF model are obtained by laboratory odour concentration analysis using dynamic olfactometry (according to EN 13725:2003). Kriging geostatistical analysis method is carried out based on the results field odour intensity measurements in plume (according to VDI 3940-2:2006). Through statistical analysis odour intensity spatial distribution is obtained from discrete (point) data. What is important, the term of odour dispersion calculations using CALPUFF model was the same as term of field inspections. It means that the date inserted into the CALPUFF model (and the date of meteorological data) corresponded to date of field inspections execution. Totally, 9 measurement series have been receiving for 2 years (2011/2012).

Data obtained in olfactometry measurements was odour concentrations in European odour units per cubic meter ( $ou_E/m^3$ ). Data collected in field measurements was odour intensity on a scale from 0 to 6, where 0 means no odour and 6 0 extremely strong odour. To calculate odour intensity from field inspections to odour concentration with using Weber-Fechner law it was necessary to conducted additional measurements of odour intensity using dynamic olfactometry (according to VDI 3882-1:1992).

Samples to olfactometry were collected from emitters which emit characteristic for the distillery smells: E-14, E-22, E-24, hall ventilation, fermenters and CO<sub>2</sub> scrubber. Analysed emitters covered all of the processes conducted in the plant. In addition, for field inspections, characteristic smells have been marked by letters symbols. In table 1 all of information refer to emitters and emitted odours were compared.

**Table 1.** Comparison of emitters and odours emitted from the distillery

<b>Process</b>	<b>Smell description</b>	<b>Emitters</b>	<b>Odour symbol in field inspections</b>
gluten drying	a baked bread	E-22, E-24	L
feeding stuff drying	a cooked pasta	E-14, hall ventilation	M
fermentation	an alcohol	fermenters, CO <sub>2</sub> scrubber	N

## THE MODEL BUILD AND THE RESULTS

According to the German VDI guideline (VDI 3788-1:2000) any mixture of odours were treated as individual air pollutant. It means that each of smell emitted from the distillery ('L', 'M' and 'N') were three different pollutants. As a results of calculations of odour dispersion using CALPUFF model were spatial distributions of odour concentration as a raster in the Geographic Information System (GIS) software ArcGIS 10.1 ESRI. Odour intensity (immission) obtained from field inspections were as discreet data (points). These discreet data of odour intensity were used in geostatistical analysis conducted using ordinary kriging. As a results of the estimation were spatial distributions of odour intensity also in GIS software as a raster. Values of odour intensity were converted in ArcGIS (using Map Algebra tool) to odour concentrations using Weber-Fechner law:

$$I = k_1 \cdot \log C + k_2 \quad (1)$$

where: I – odour intensity  
 C – odour concentration (in  $ou_E/m^3$ )  
 k<sub>1</sub>, k<sub>2</sub> – constance

As it was said, the mesh for all calculations using CALPUFF model was fixed, while the mesh for kriging was variable (always smaller than for model) and depended on the area of each of field inspection series. Example of results of odour dispersion modelling and the corresponding geostatistical analysis in Figure 2 were presented.

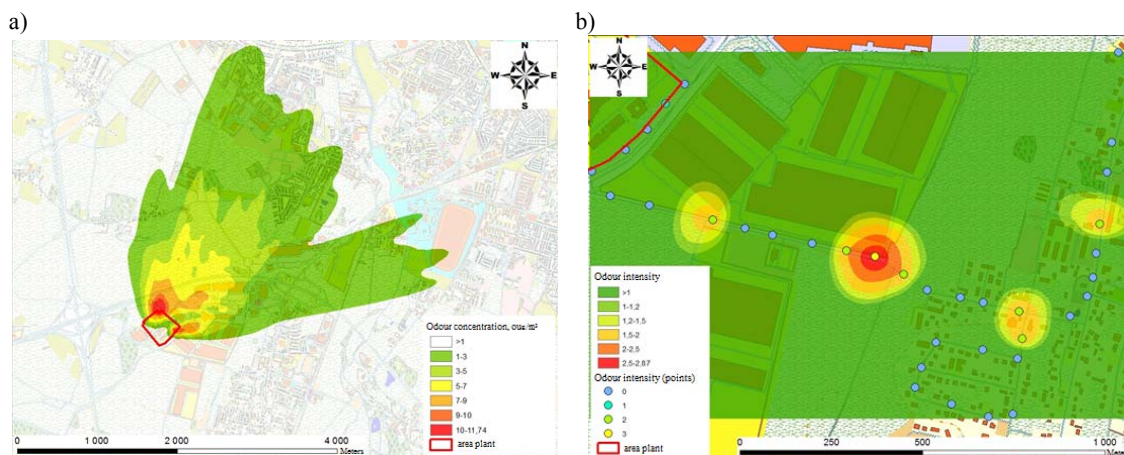


**Figure 2.** Results of calculations for series 6 (25.06.2012): a) spatial distribution of 'M' odour concentration calculated with CALPUFF model; b) spatial distribution of 'M' odour intensity estimated with ordinary kriging

Model was developed by physical connection in GIS software using Arc Toolbox application in ArcGIS 10.1 ESRI. Connection of the two rasters (from CALPUFF and from kriging) was done using raster mosaic process (with Mosaic To New Raster tool). Every new raster was created in PUWG 1992 coordinate system (applicable in Poland) and with resolution 10 meters. The new rasters were created in such a way that in the places, where surface of two rasters overlapped, the values of odour concentration to new raster were taken from raster made of kriging. It allowed the evaluation the modelling results.

In Figures 3a and 3b two examples of created models for two different measurement series are presented. Built models allow to identify differences between results of simulations made in CALPUFF model and estimation of odour concentrations measured as odour intensity in the field. In the Figures the occurrence of odour 'L' in series 3 (Figure 4) and 'M' in series 6 (Figure 5) measured in the field inspections in some places overlap with occurrence of odours calculated using CALPUFF model. However, we have got an information, that in places not covered by the CALPUFF model, the odours also were perceptible. It means that CALPUFF model in both examples underestimated range of the odours impact. But, on the other side, the model complements the range of the odours in other areas, where at the same time field measurements were not possible to do, because of time and human restrictions. CALPUFF model extends the range of occurrence of odour plume.

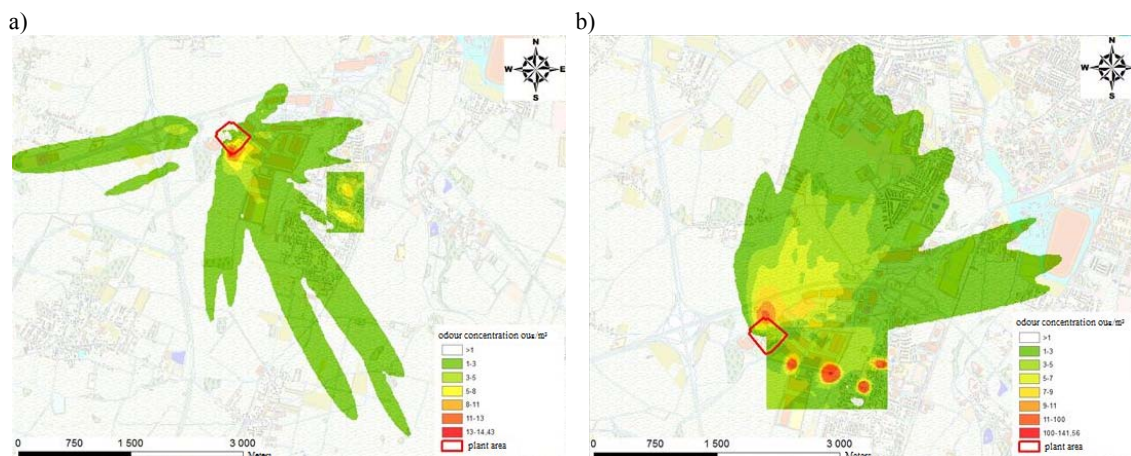


**Figure 3.** Dynamic-statistical odour dispersion model built a) for odour 'L' in series 3 (8.07.2011); b) for odour 'M' in series 6 (25.06.2012)

## SUMMARY

The dynamic-statistical model was built by physical connection of two rasters as the results of the modelling simulates based on emission measures and geostatistical analysis based on field inspections. It is a very good tool for assessment of odour nuisance because of its reliability. In this way both of the methods verify and complement each other. It creates the new, reliable tool to evaluate odour impact on the analysed area. The developed model can be used in researches of the odour impact evaluation for every object which emits odours: agricultural, municipal economy or industrial plant.

## REFERENCES

- Dourado H., Santos J.M., Reis N.C, Jr., Mavroidis I., 2014: Development of a fluctuating plume model for odour dispersion around buildings, *Atmospheric Environment*, **89**, 148-157
- EN 13725:2003: Air quality. Determination of odour concentration by dynamic olfactometry
- Eusebio L., Dentoni L., Capelli L., Sironi S., Rossi A.N., Bonati S., 2013: Odour impact assessment in the field: the plume method, 2013, *Environmental Engineering and Management Journal*, **12**, S11, Supplement, 193-196, <http://omicron.ch.tuiasi.ro/EEMJ/>
- Nagaraj A., Sattler M.L., 2005: Correlating Emissions with Time and Temperature to Predict Worst-Case Emissions from Open Liquid Area Sources, *Journal of the Air & Waste Management Association*, **55** (8), 1077-1084
- Olesen H.R., Løfstrøm P., Berkowicz R., Ketzel M., 2005: Regulatory odour model development: Survey of modelling tools and datasets with focus on building effects, National Environmental Research Institute, Technical Report No. 541, Denmark
- Piringer M., Petz E., Groehn I., Schaubberger G., 2007: „A sensitivity study of separation distances calculated with the Austrian Odour Dispersion Model (AODM)”, *Atmospheric Environment*, **41**, 1725–1735
- Piringer M., Knauder W., Petz E., Schaubberger G., 2015: “A comparison of separation distances against odour annoyance calculated with two models”, *Atmospheric Environment*, **116**, 22-35
- Sironi S., Capelli L., Centola P., Del Rosso R., Pierucci S., 2010: „Odour impact assessment by means of dynamic olfactometry, dispersion modelling and social participation”, *Atmospheric Environment*, **44**, 354-360
- Sówka I., Skrętowicz M., Sobczyński P., Zwoździak J., 2013: Estimating odour impact range of selected wastewater treatment plant for winter and summer seasons in Polish conditions using CALPUFF model, HARMO'15 Proceedings, 15th Conference on Harmonisation within Atmospheric Dispersion Modelling for Regulatory Purposes HARMO 15, Madrid, Spain
- VDI guidelines – 3788 part 1, 2000: Environmental meteorology - Dispersion of odorants in the atmosphere – Fundamentals
- VDI 3882 part 1, 1992: Olfactometry; determination of odour intensity
- VDI guidelines – 3940 part 2, 2006: Measurement of odour impact by field inspection - Measurement of the impact frequency of recognizable odours - Plume measurement

**17th International Conference on  
Harmonisation within Atmospheric Dispersion Modelling for Regulatory Purposes  
9-12 May 2016, Budapest, Hungary**

---

**INVESTIGATION OF THE TRANSPORT OF POLLUTANTS FROM THE METROPOLITAN  
AREA OF SÃO PAULO AND FROM THE INDUSTRIAL CITY OF CUBATÃO TO NEARBY  
AREAS**

*Atenágoras Souza Silva<sup>1</sup>, Américo A F S Kerr<sup>1</sup>, Simone Gioia<sup>2</sup> and Marly Babinsky<sup>3</sup>*

<sup>1</sup>Instituto de Física, Universidade de São Paulo (USP), São Paulo, Brazil

<sup>2</sup>Centro Tecnológico da Marinha de São Paulo, São Paulo, Brazil

<sup>3</sup>Centro de Pesquisas Geocronológicas, Instituto de Geociências, Universidade de São Paulo,  
São Paulo, Brazil

**Abstract:** The mesoscale meteorological model BRAMS and the Lagrangian dispersion model SPRAY were used to discuss the transport of pollutant inside, between, and nearby the Metropolitan Area of São Paulo and Mogi Valley, at an industrial town from Cubatão city. The acceptable agreement between simulated and measured data showed the models skill to represent meteorology and air pollution dispersion in these areas. Two winter episodes were studied and, in general, the local emissions dominated the local air quality levels, although transport was significant to some localized places.

**Key words:** *São Paulo air Pollution, Cubatão air pollution, Dispersion Modeling, SPRAY, BRAMS*

## **INTRODUCTION**

The Metropolitan Area of São Paulo (MASP) has more than 20 million inhabitants and above 7 million vehicles. In the coast, 40 km farther, there are a strong industrial city, named Cubatão, with 23 big industrial plants and tenths of small and middle size ones. In the winter of 2006 an experiment was conducted in these areas, collecting the fine and coarse atmospheric aerosol in four stations, every 12h, for one week (Gioia, S., 2006). One stations was in a small city, Juquitiba, a remote border area of the MASP, rounded by native vegetation, other was slightly more inside the MASP area, another in an almost central point of the MASP, and the last one at the industrial area of Cubatão. Samples was analyzed by PIXE and ID-TIMS, respectively to identify chemical elements (atomic number>10) and Pb isotopes concentrations and ratios, to characterize the aerosol, to study they sources and to get some information of pollutant transport among the sampled areas. In the present work, we used the mesoscale atmospheric model BRAMS and SPRAY, a Lagrangian Stochastic Model (LSM), to improve the discussion about pollutant dispersion in and around the area of this experiment. An inventory of the particulate emitted by five fertilizer plants from Cubatão, and, of the CO emitted by the vehicular fleet from MASP, was used in the simulations, providing reliable concentrations values and images for the pollutant transport during two winter episodes for PM<sub>10</sub>.

## **METHODS**

### **The modeling system BRAMS & SPRAY**

The LSM SPRAY basis and development (ENEL, ICG/CNR, and Ariantet) are described by Tinarelli et al. 1994 and 2000, among other references. It uses the generalized Langevin equation to simulate the dispersion of inert gases; the key input is the Eulerian PDF of the turbulent velocities, used in the corresponding Fokker-Planck equation to determine the value of the drift coefficient of the Langevin equation. In this work, for instance, the Gram-Charlier PDF truncated to the third order moment was used in the vertical, and in the horizontal direction the PDF was Gaussian.

The meteorological parameters needed by SPRAY were provided by BRAMS (Brazilian developments on the Regional Atmospheric Modelling System-RAMS), version 4.2 (Fazenda et al. 2007). It is a shared development of ATMET, IME/USP, IAG/USP, and CPTEC/INPE, with the aims of provide a new RAMS version, improved for tropics. Historical development and theoretical basis for BRAMS is well described in BRAMS, 2013.

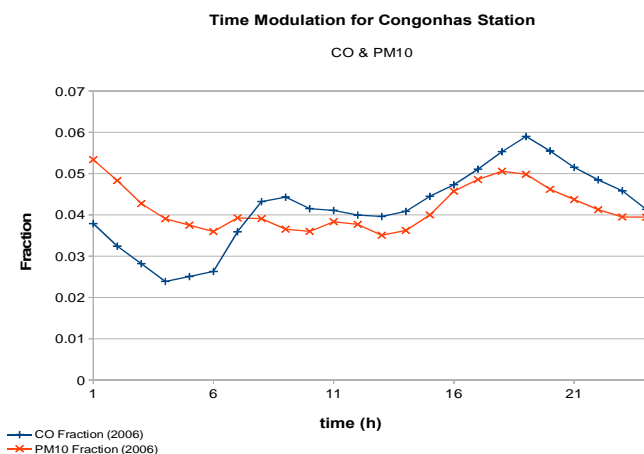


**Figure 1.** Time modulation for CO and PM<sub>10</sub> concentrations at Congonhas' Station in 2006. They showed a good correlation. An assumption used in the work was that CO to PM<sub>10</sub> ratio at Congonhas (40.7) was a first approximation of this vehicular emission ratio at MASP.

**Table 1.** Resolution and boundary conditions for simulation areas

Grid	Grid center (lat/Lon)	Grid resolution (m)	Grid area (Km x Km)	Latitude limits (deg)	Longitude limits (deg)
1	23.077°S / 46.345°E	12000	456 x 456	20.985°S - 25.141°S	48.579°W - 44.049°W
2	23.293°S / 46.342°E	3000	403 x 360	22.231°S - 24.344°S	47.713°W - 44.949°W
3	23.714°S / 46.615°E	1000	346 x 267	23.284°S - 24.143°S	47.199°W - 46.028°W

**Table 2.** Meteorological and/or CO measuring Stations

Station Number	Station Name	Latitude (S, Degree)	Longitude (W, Degree)
1	Ibirapuera	23.591	46.629
2	Cubatão Centro	23.879	46.418
3	Cubatão Vale do Mogi	23.832	46.37
4	Cubatão Vila Parisi	23.849	46.388
5	Pinheiros	23.561	46.702
6	Santo Amaro	23.655	46.71
7	São Caetano	23.617	46.556
8	São José dos Campos	23.187	45.871
9	Osasco	23.527	46.792
10	Sorocaba	23.502	47.479
11	Santo André	23.646	46.536
12	Pedro II	23.544	46.66
13	Taboão da Serra	23.609	46.758
14	IAG	23.649	46.625

BRAMS uses a two ways nesting procedure, allowing coherence between large to small grids data processing. Three nested grids were used in this case (Table-1) to simulate meteorological parameters in the areas studied, between days 23 and 29 August 2006. The model was initialized with CPTEC (Centro de Previsão de Tempo e Estudos Climáticos, a Brazilian Weather Forecast Center) global files (time resolution of 12h, and Lat-Lon resolution of 0.9375°, with 28 vertical levels).

SPRAY simulated the dispersion of the CO emitted by the MASP's vehicular fleet using the meteorological data from Grid-2 (3 km resolution). In the other hand, the transport of PM<sub>10</sub> emitted by 5 Fertilizer Plants at Cubatão, a complex terrain area, was analyzed using the better resolution (1 km) of Grid-1 (sources' position and emission rates at Kerr et al., 2000). The CO vehicular area emission at MASP, with 5 km<sup>2</sup> resolution, was estimated considering the fleet composition and traffic flow, estimated by Kerr, A., et al., 2005, for the year 2000 at MASP (a total of 1.69x10<sup>6</sup> t.y<sup>-1</sup>). A reduction factor of 1.5 was applied considering 2000 to 2006 CO concentrations ratio at Congonhas' station (CETESB, 2001 and 2007). The time modulation of CO concentrations was also associated to the pattern observed at this station in the year 2006 (Figure 1). An assumption was that this station is representative of the vehicular CO emission, because it is very close to a typical high traffic MASP avenue. In the same way, the CO to PM<sub>10</sub> average ratio at this station in 2006 (40.7) was taken as representing, in a first approximation, the vehicular CO to PM<sub>10</sub> concentration ratio at MASP in this year.

Arianet provided GAP (Grid Adaptator) and SurfPro softwares to adapt the simulated BRAMS' meteorological data grid for SPRAY and, added to USGS landuse data, evaluate also the turbulence information to be used by SPRAY

## RESULTS AND ANALYSIS

### Statistical comparisons for Meteorological and Pollutants dispersion simulations

Table 2 shows the position of 13 stations from the São Paulo State environmental agency (CETESB, 2007), measuring air pollutants and/or meteorological parameters, and one meteorological station from the Institute of Astronomy, Geophysics and Atmospheric Sciences of the University of São Paulo – IAG. Meteorological and/or CO data comparisons were performed in every station where these data are available with acceptable number of miss values.

Tables 3 to 5 show the comparisons between observed and simulated values for wind, temperature, and relative humidity. The columns “r” report the observed to simulated data correlation (index “u” and “v” indicate the two horizontal wind components) and “P” is the significance level of the correlation; the  $\sigma$  are standard deviations (index “o” and “s”, refer to observed and simulated data, respectively), and  $\sigma(u,v)$  is equal to  $(\sigma_u^2 + \sigma_v^2)^{0.5}$ , accounting for both, u and v, standard deviations; RMSE is the Root Mean Square Error (RMSVE is used for vector variables); N is the number of compared points.

**Table 3.** Comparisons between observed and simulated horizontal wind at 10 m (N from 120 to 167)

Station	$\sigma_s(u,v)$ (m.s <sup>-1</sup> )	$\sigma_o(u,v)$ (m.s <sup>-1</sup> )	RMSVE (m.s <sup>-1</sup> )	r <sub>u</sub>	r <sub>v</sub>	P (for the worse r)
1	2.25	1.90	1.65	0.5590	0.8214	<0.001
3	2.98	3.16	3.12	0.2317	0.7439	<0.005
4	2.57	2.54	2.73	0.2448	0.6354	<0.005
5	2.29	2.18	1.61	0.6739	0.8279	<0.001
6	2.49	2.42	1.43	0.7896	0.8667	<0.001
7	2.64	1.95	2.10	0.6968	0.7640	<0.001
8	2.25	1.90	1.65	0.5590	0.8214	<0.001
9	2.75	2.12	1.66	0.7359	0.8595	<0.001
10	2.37	2.11	1.93	0.5099	0.8006	<0.001
14	2.60	2.46	2.79	0.4452	0.4608	<0.001

**Table 4.** Relative Humidity – Comparison between measured and simulated values (N=167)

Station	$\sigma_s$ (%)	$\sigma_o$ (%)	RMSE (%)	r	P	$\langle RH \rangle_o$ (%)	$\langle RH \rangle_s$ (%)
1	28	20	17	0.81	<0.001	72.4	67.3
2	17	11	30	0.43	<0.001	86.2	61.1
5	28	21	19	0.85	<0.001	58.0	67.0
7	26	22	17	0.88	<0.001	71.4	66.9
14	26	24	16	0.77	<0.001	71.0	67.8

**Table 5.** Air Temperature - Comparison between measured and simulated values (N=167)

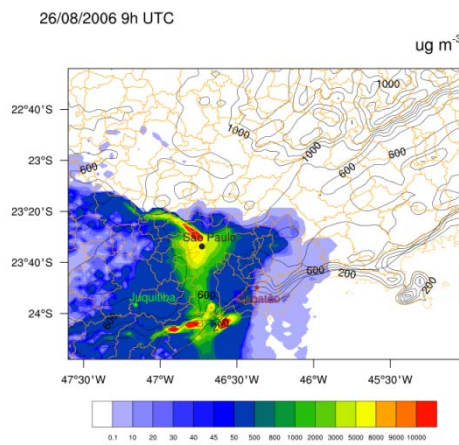
Station	$\sigma_s$ (°C)	$\sigma_o$ (°C)	RMSE (°C)	r	P	$\langle T \rangle_o$ (°C)	$\langle T \rangle_s$ (°C)
1	7.1	5.3	3.8	0.86	<0.001	18.9	17.4
2	6.6	6.6	3.6	0.78	<0.001	17.4	17.2
5	7.3	6.8	3.7	0.87	<0.001	18.8	17.6
7	4.3	4.8	3.0	0.8	<0.001	17.4	17.2
14	6.5	7.1	3.4	0.89	<0.001	18.9	17.3

Horizontal wind at 10 m are correlated at high level of significance, while RMSVE and  $\sigma_s(\mathbf{u},\mathbf{v})$  values are lower or similar to the observed  $\sigma_s(\mathbf{u},\mathbf{v})$ , all indicating a good BRAMS skill for simulating the 10 m wind. The same could be inferred for humidity and temperature in tables 4 and 5, except for humidity at station 2, probably because this station is settled at the ground of the Mogi Valley, which walls are steep, and fast growing from sea level till 600 to 1200 m heights, limiting the Model’s ability to capture such variability.

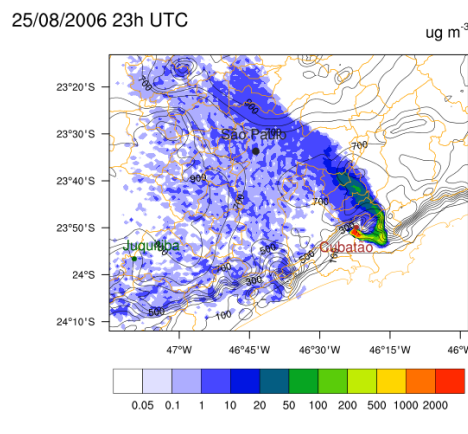
Comparisons between simulated and observed CO concentrations (Table 6) show correlations with good significance level (stations 5, 7, 11 and 13), while RMSE and  $\sigma_s$  are less or not much higher than  $\sigma_o$  for stations 7, 11 and 13. Finally, the ratio of simulated to observed CO averages in the last stations differs by less than 37%, corroborating to qualify their good data agreement. Stations 5 and 12 showed acceptable significance level for the data correlation, although the other parameters do not show fair results. Data for station 1, otherwise, showed high discrepancies, being the simulated average CO concentration 3.51 times greater than the observed values, probably because this station is settled in a large park inside the MASP, and the model resolution was not able to capture the dilution produced by the park.

The two selected images of simulations at Figure 2 show the significative amount of pollutant transported down (from São Paulo), and up the mountain range (from Cubatão) following the shore line.

**CO Concentration for MASP and Nearby Areas**



**MP10 Concentration for MASP and Nearby Areas**



CONTOUR FROM 100 TO 1200 BY 100

**Figure 2.** CO transport and concentration related with two episodes.

Although not exceeding the 8h standard ( $10 \times 10^3 \mu\text{g.m}^{-3}$  or 9.0 ppm) the CO plume contours show the CO transport, with 1 h values relatively high in remote and forested areas of the MASP.

**Table 6.** CO concentrations - Comparison between observed and simulated values (N from 53 to 93)

Station	$\sigma_s$ ( $\times 10^2 \mu\text{g.m}^{-3}$ )	$\sigma_o$ ( $\times 10^2 \mu\text{g.m}^{-3}$ )	RMSE	r	P	$\langle \text{CO} \rangle_o$ ( $\times 10^2 \mu\text{g.m}^{-3}$ )	$\langle \text{CO} \rangle_s$ ( $\times 10^2 \mu\text{g.m}^{-3}$ )	N	s/o
1	35.4	7.81	45.5	0.30	<0,002	13.4	46.9	91	3.51
5	36.7	14.0	42.2	0.37	<0,001	22.7	49.9	93	2.2
7	12.6	17.1	11.8	0.77	<0,001	19.9	17.0	53	0.86
11	7.7	8.90	8.7	0.54	<0,001	13.8	10.7	91	0.78
12	48.3	11.8	68.5	0.27	<0,01	15.2	65.2	75	4.28
13	25.7	19.6	27.5	0.30	<0,01	22.8	31.4	84	1.37

**Table 7.** PM<sub>10</sub> exceedance of World Health Organization daily guide lines ( $50 \mu\text{g.m}^{-3}$ , WHO, 2005).

City	Measure period	Start date	Finish date	$\langle \text{PM}_{10} \rangle$ ( $\mu\text{g.m}^{-3}$ )
Cubatão	daytime	25/08/2006	25/08/2006	107
São Paulo	daytime	25/08/2006	25/08/2006	57
Cubatão	night time	25/08/2006	26/08/2006	73
Juquitiba	night time	25/08/2006	26/08/2006	81
São Paulo	night time	25/08/2006	26/08/2006	84

## CONCLUSION

The Couple BRAMS/SPRAY meteorological and diffusion simulation modeling systems was able to simulate reliable concentration fields for vehicular CO emitted in the MASP, as well as the PM<sub>10</sub> emitted by fertilizer plants at Cubatão. Pollutant transport between some zones of these areas, highly populated and comprising forested reserves may arrive to significant intensity.

In the next steps of this work, this dispersion simulations system, chemical analysis of the measured PM<sub>10</sub>, and receptor modeling will be put together to better understand the sources' role and air pollution transport among these areas.

## REFERENCES

- BRAMS, 2013, CPTEC, [http://www.cptec.inpe.br/brams/f\\_time.shtml](http://www.cptec.inpe.br/brams/f_time.shtml), visited in 03/28/2013.
- CETESB, 2001 and 2007: Relatório de Qualidade do Ar no Estado de São Paulo. Secretaria de Estado de Meio Ambiente. São Paulo, SP, Brazil, <http://ar.cetesb.sp.gov.br/publicacoes-relatorios/>, visited in 03/20/2006.
- Fazenda, L. A., D.S. Moreira, E.H. Enari, J. Panetta, L.F. Rodrigues, 2007: First Time User's Guide, (BRAMS Version 4.0), CPTEC, [http://www.cptec.inpe.br/brams/f\\_time.shtml](http://www.cptec.inpe.br/brams/f_time.shtml), visited in 03/28/2013.
- Gioia, S., 2006: Estudo da Composição dos Aerossóis e da assinatura isotópica de Pb como traçador das fontes da poluição atmosférica da cidade de São Paulo., post-doc work.
- Kerr, A. A. F. S., ANFOSSI, Domenico, CASTELLI, Silvia Trini, NASCIMENTO, S. A., 2000. Investigation of Inhalable Aerossol at Cubatão by means of a Modeling System for Complex Terrain, *Hybrid Methods in Engineering*, **2**, 389-407.
- Kerr, A., Landmann, M. C., Carvalho, J., 2005: Investigation of CO dispersion from São Paulo Metropolis by means of modelling system for complex terrain. 9<sup>th</sup> Harmonisation, 2005.
- Tinarelli, G., D. Anfossi, G. Brusasca, E. Ferreiro, Giostra U., M.G. Morselli, Moussafir J., Tampieri F., Trombetti F., 1994: Lagrangian Particle Simulation of Tracer Dispersion in the Lee of a schematic Two-Dimensional Hill. *Journal of Applied Meteorology*, **33**, 744-756.
- Tinarelli, G., D. Anfossi, M. Bider, E. Ferrero, S. Trini Castelli, 2000: A new high performance version of the Lagrangian particle dispersion dispersion model SPRAY, some case studies. Air Pollution Modelling and its Applications XII, S.E. Gryning and E. Batchvarova, eds, Kluwer Academic/Plenum Press. New York, 499-507.
- WHO - World Health Organization, 2005. Air quality guidelines for particulate matter, ozone, nitrogen dioxide and sulfur dioxide.

**FAR-FIELD EFFECT OF A TALL BUILDING ON THE SHEAR LAYER ABOVE STREET  
CANYONS**

*Árpád Varga*

Theodore von Kármán Wind Tunnel Laboratory, Department of Fluid Mechanics, Budapest University of  
Technology and Economics (BME), Budapest, Hungary

**Abstract:** It was shown by several previous studies that tall buildings improve ventilation in their immediate neighbourhood by the frontal downwash effect and the vertical velocity directed upwards in the separation zone on their backward side (Brixey et al., 2009). These effects improve local air quality near the ground. On the upwind side the downwash transports clean air to the ground. On the backward side of the building, polluted air is elevated to larger heights, thus local ground level concentrations decrease. However, there is no clear understanding in the literature what is the far field effect of a single tall building.

To develop tangible guidelines for urban planners, how and where to place tall buildings in a low-rise urban area in order to avoid the increase of local pollutant concentrations or even to utilise them in reducing the air pollution at pedestrian level, a series of wind tunnel tests is planned, the first of which is presented in this paper.

**Key words:** *Street canyon, urban flow, wind tunnel, quadrant analysis*

**INTRODUCTION**

Significant amount of human population lives in urban areas, where one of the major problems is atmospheric pollution. The air quality is mainly influenced by the mixing and propagation of pollutants, driven by the complex turbulent atmospheric flow structures above the urban environment. To understand the basics of these complex flow patterns, both experimental and computational fluid dynamics (CFD) studies use strongly idealized, simplified geometries which represent simplified urban architectural environments (Kastner-Klein et al. 2004). One of these simplified geometries is the row of street-canyons, in which the long, continuous building blocks are followed by empty spaces, corresponding the streets of the city. In the most basic, fundamental case the main flow direction is perpendicular to the streets, the roofs of the building blocks are flat, the height, width of the building blocks and the width of the streets are equal (distance  $H$ , Figure 1.). Based on these considerations, wind tunnel model was constructed and placed in to the test section of the Large Wind Tunnel of the Theodore von Kármán Wind Tunnel Laboratory, containing 22 street canyons. with height of 0.1 m and with width of 1.25 m. The scale of the model was 1:300.

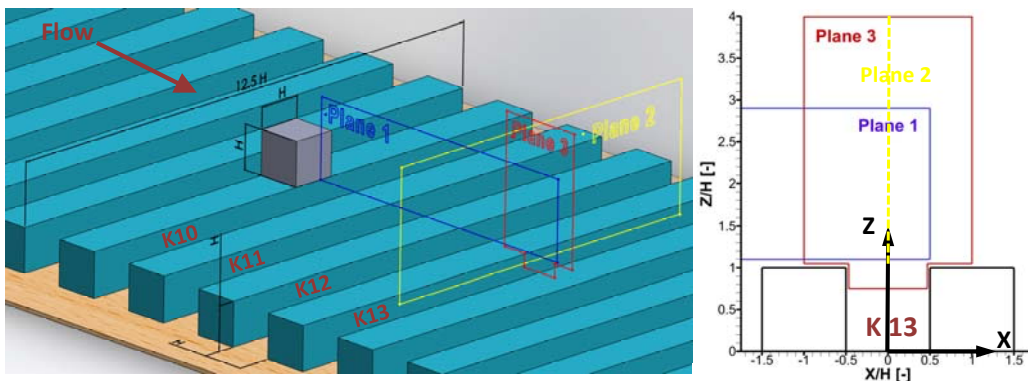


**Figure 1.** Scheme of the wind tunnel model with the cubic tall building, the measurement planes and the used coordinate system

## MEASUREMENT TECHNIQUE AND BOUNDARY LAYER CHARACTERISTICS ABOVE THE WIND TUNNEL MODEL

During the measurements presented in this paper a 55P51 type two-component constant temperature hot-wire anemometer was used, manufactured by DANTEC. This instruments consist of two 9  $\mu\text{m}$  thick, gold-coated electrically heated tungsten wire, suitable for measuring two velocity components simultaneously, if the flow angle does not exceeds  $+45^\circ$  or  $-45^\circ$ . The width of the anemometer was 2.5 mm. Calibration of the instrument was carried out in a blower-type open test section wind tunnel. The flow angle was varied by rotating the probe support relative to the incoming flow. During the calibration process the velocity of the incoming flow (measured by a TSI Pitot-static-tube as a reference) varied between  $1\text{--}16\text{ ms}^{-1}$  in  $0.6\text{ ms}^{-1}$  steps and the flow angle between  $-40^\circ$  to  $+40^\circ$  in  $4^\circ$  steps. According to the control measurements, the error of the device for the velocity measurement is less than  $0.05\text{ ms}^{-1}$  and  $0.8^\circ$  for the angle. After the calibration the support of the anemometer was mounted on the probe holding arm of the traversing system, integrated into the test section of the Large Wind Tunnel.

Above the series of street canyons a boundary layer develops the depth of which is increasing into the main flow direction. In case of the first experiment series vertical profiles was measured in the vertical symmetry plane of the model parallel to the main flow direction at the centreline of each second canyon (K1-3-5-7-9-11-13-15-17). The sampling time at each point was 25 s, the sampling rate was 500 Hz and the measurements were carried out at reference velocity  $U_{Pr,ref}=10.5\text{--}11.5\text{ [ms}^{-1}\text{]}$ , measured by a Pitot-static-tube, placed in an undisturbed flow above the model (10-12 H). The dimensionless velocity ( $U$ ) profiles are rapidly changing in case of K1-5, showing rapidly thickening boundary layer, but after K9 the profiles are the same in the shear layer at  $Z_{fs}\approx 30\text{ m}$  and in the lower part of the external flow region up to  $Z_{fs}=60\text{ m}$  (Figure 2.). In case of the  $I_u$  and  $I_w$  longitudinal and vertical turbulent-intensity profiles the differences are larger, but the profiles are still nearly the same in the shear layer up to  $Z_{fs}\approx 40\text{ m}$ . For further investigations the K13 was chosen, as the flow in the shear layer of this canyon is similar to any other subsequent canyons. The atmospheric boundary layer above K13 can be characterised with  $\alpha=0.18$  power-law exponent, which corresponds to moderately rough terrain, the profile is elevated with  $d_f=30\text{ m}$ . The longitudinal and vertical turbulent intensities are also compared to the limits recommended by VDI (2000) guidelines for the atmospheric boundary layer above moderately rough and rough terrains. The values of  $I_u$  are inside the band for moderately rough terrains, while the  $I_w$  values mainly in the domain recommended for rough terrains. Here can be noticed, that during the experiments there were no additional turbulence-generating elements (spires, roughness elements etc.) involved. In a selected point ( $Z_{fs}=57\text{ m}$  at K13) a measurement was carried out with 100 s sampling time and the dimensionless spectral power density distribution was determined and compared with the theoretical von Kármán spectral distribution function, showing a reasonable correspondence.

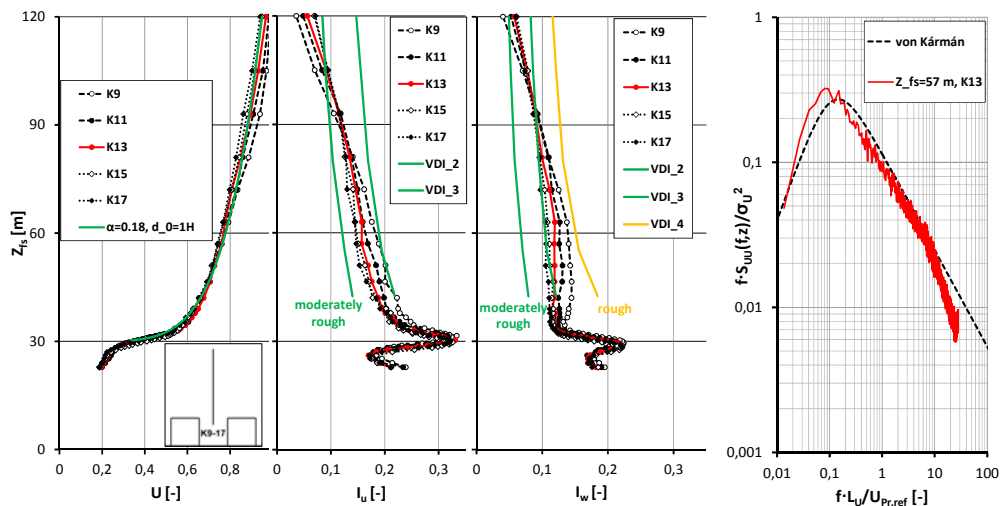


**Figure 2.** Dimensionless velocity ( $U$ ), longitudinal ( $I_u$ ) and vertical ( $I_w$ ) turbulent intensity profiles at the centreline of canyons K9-17 (the height above the surface is expressed in full scale, therefore the top of the building blocks are at  $Z_{fs}=30\text{ m}$ ). Left: dimensionless power spectral density of the longitudinal velocity fluctuations at height  $Z_{fs}=57\text{ m}$  (K13) compared to the theoretical von Kármán spectrum.

### GLOBAL EFFECTS OF AN OBSTACLE ON A FLOW FIELD ABOVE THE URBAN CANOPY

To simulate the effect of a tall building on the flow above the idealized urban canopy a cubic body was mounted at the top of the building block located directly in front of K10. The height, width and the length of the body was 1 H, the total height of the obstacle therefore was 2H. Then measurements were carried out in measurement Planes 1, 2 and 3. (depicted with blue, yellow and red in Figure 1., they contained 350, 403 and 502 single measurement points). Then, the obstacle was removed and the whole measurement campaign for Plane 1, 2, 3 was repeated for the basic, non-disturbed idealized urban canopy configuration, which was handled as the reference case. In the measurement points of Plane 1 and 2 the sampling time was 25 s, which was not enough to record fully statistically representative time series for the longitudinal and vertical velocity ( $u$  and  $w$ ), but still was enough to map and explore the changes caused by the obstacle, relative to the reference case. In case of Plane 3 (located at K13) the sampling time was raised to 100 s, which is already provided statistically representative data set. In case of Plane 3 measurement points with the lowest  $Z/H$  coordinate value were below the roof level of the building blocks, and their dense distribution allow to resolve spatially rapidly changing quantities in the shear layer at the top of the canyon. The measurement campaigns with and without the obstacle altogether required approximately 45-50 measurement hour in the Large Wind Tunnel. The measurements were carried out at reference velocity  $U_{Pr,ref} = 10.5-11.5$  [ms<sup>-1</sup>], as in the case of the boundary layer measurements.

After measurements in Plane 1 and 3 the dimensionless mean velocity absolute values (relative to the reference Pitot-static-tube) were determined both for the reference case and for the measurement arrangement with the obstacle. The distribution of the difference in the dimensionless velocity absolute value between the two arrangements relative to the initial state (in percent) in Plane 1, 2 are presented on Figure 3-4. The same procedure was carried out for the dimensionless turbulent kinetic energy ( $TKE_d = 0.5 \cdot \sigma_{|U|}^2 / U_{Pr,ref}^2$ ) for the “disturbed” case (with building) and the reference state.

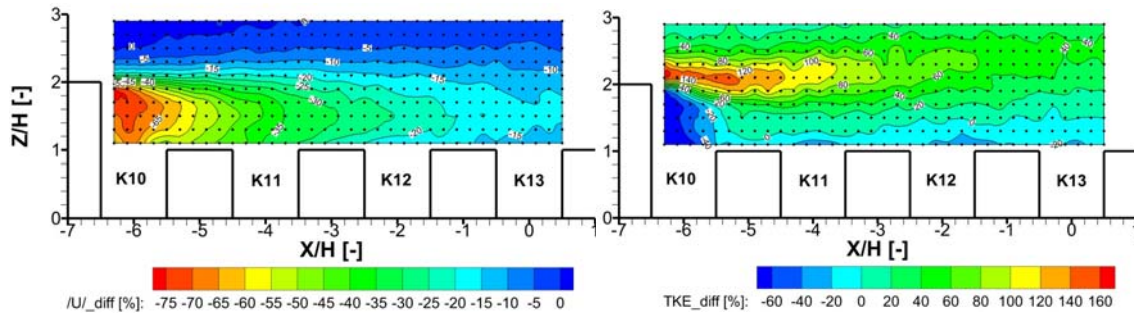


**Figure 3.** Distribution of the velocity-absolute value and turbulent kinetic energy difference between the reference case and the arrangement with the obstacle, relative to the initial state (in percent) in Plane 1

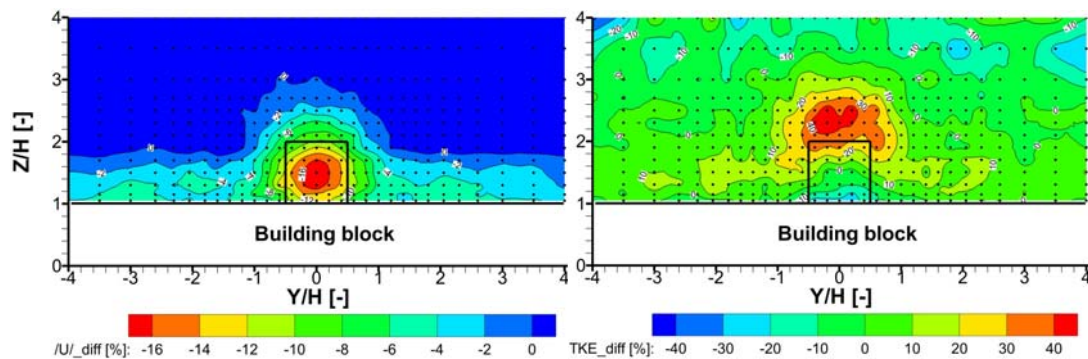


**Figure 4.** Distribution of the velocity-absolute value and turbulent kinetic energy difference between the reference case and the arrangement with the obstacle, relative to the initial state (in percent) in Plane 2.

The velocity deficit caused by the building model is the largest directly behind the obstacle (more than 50%), and directly above K13 the velocity is still smaller by 5-15% than in the reference case. Significant rise in turbulent kinetic energy (30-40% relative to the reference case) can be observed at the height of the roof of the high-rise building ( $Z/H \approx 2-2.5$ ), caused by probably the strong vortices, which are generated on the shear layer, developing above the obstacle. Close to the rooftop level ( $Z/H=1-1.5$ ) TKE level is smaller than in the reference case, the difference directly above K13 is about -20%.

Based on the difference distributions on Plane 2 can be noted, that the “shading” effect of the high-rise building is the strongest behind the projection of its contour lines, the velocity deficit is -16% at  $Y/H=0$  and  $Z/H=1.5$ . Although, it is worth to appreciate, that the effect of the building can be detected at the whole width of the street at the height close to the rooftop level (-12% near  $Y/H=0$  and -5% at  $Y/H=4$  or -4). The turbulent kinetic energy rises by 30-40% in the vicinity of the upper edge of the obstacle. Near the lower part of the building above the canyon at height  $Z/H=1$  from  $Y/H=-0.5$  to  $Y/H=0.5$  reduction can be observed in the level of the turbulent kinetic energy (-10-20%).

### QUADRANT ANALYSIS ON SHEAR LAYER FLOW ABOVE K13

Several contemporary full scale and wind tunnel measurements use the quadrant analysis method to study the turbulent mass and impulse exchange process between the lower and upper regions of the urban canopy. Based on the sign of the fluctuation of the instantaneously measured longitudinal and vertical velocity component relative to the mean values ( $u'$  and  $w'$ ), four different event types can be distinguished (Figure 5., left). In case of a sweep event relatively fast air particles are transported downwards, while during an ejection a small package of medium with lower momentum moving temporarily upwards. During outward interactions air with relatively higher impulse is moving upwards, and inward interaction indicate movement of medium towards the ground with smaller momentum. From the viewpoint of the turbulent impulse transfer the sweep and ejection events are more favourable, hence they assist the mixing between the low speed air closer to the ground and the air with higher moment at the upper part of the urban canopy.

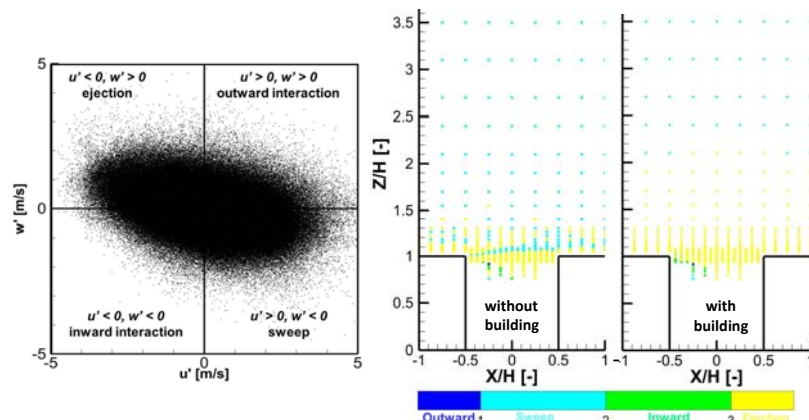


**Figure 5.** Left: Scheme of the quadrants and scatter plot of the measured velocity fluctuations in a point at  $Z/H=1.1$  (at  $X/H=0$ , without building). Right: distribution of the dominant event in a measurement points at K13 in Plane 3.

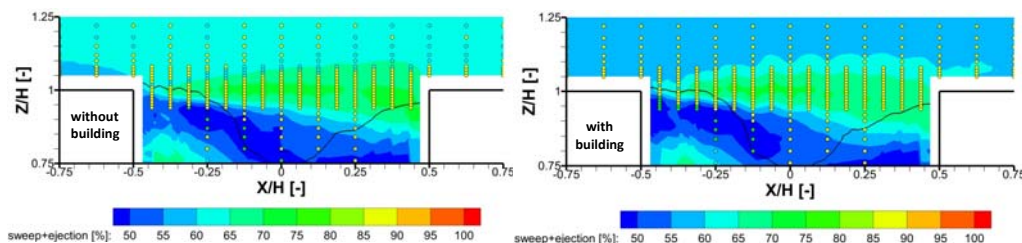


**Figure 6.** The proportion of sweep and ejection events at the lower part of Plane 3 measured without and with building. The colouring of the discrete measurement points refers to the dominant event according to the colour scheme as on Figure 5. Below the solid black line the proportion of out-of-range incoming hot-wire-probe samples (flow angle is larger than  $40^\circ$  or smaller than  $-40^\circ$ ) were larger than 5%

Contemporary wind tunnel investigation techniques allow simultaneous point measurements of two velocity components ( $u$  and  $w$ ) and the concentration of the pollution ( $c$ ), which is usually modelled with a tracer gas. In a recent wind tunnel study (Nosek et al., 2016) a quadrant analysis method was also employed to the concentration fluctuations and the vertical velocity ( $c'$ ,  $w'$ ) above three-dimensional, more realistic street canyon model. It was found, that there is strong correlation between entrainment of clean air ( $c' < 0$ ,  $w' < 0$ ) and the sweep event, and also between venting of polluted air ( $c' > 0$ ,  $w' > 0$ ) and ejection events. The correlation coefficient reached the highest values (0.7-0.8) near the rooftop level of the modelled canyons. It can be assumed, that the incidence of the sweep and ejection events can forecast the efficiency of the ventilation process of the polluted air released at the bottom of the urban canopy.

Based on the velocity time series measured in plane 3 instantaneous value of velocity fluctuations were calculated and categorized as events corresponding to the quadrant analysis. The most incidentally occurred or dominant event is determined in every spatial measurement point. As the plots on the right side of Figure 5. shows, sweep and ejection were the dominant events in case of both measurement configuration (without and with building), which is typical in case of atmospheric flows, a typical scatter plot depicting the measured velocity fluctuations is also shown on Figure 5. Near the rooftop level ( $Z/H=1-1.5$ ) in case of reference measurement configuration the sweep and ejection dominant spatial points occur miscellaneously, while arrangement with building has only ejection dominant points at this level. Above  $Z/H=1.5$  only sweep dominant points can be found in both cases. Enlarging the environment of the rooftop level (Figure 6.), it can be seen, that in case of the reference arrangement the sweep dominant points forming a continuous stripe above the street canyon, starting from the upper streamwise edge of the building block.

The proportion of the favourable ejection and sweep events shows a significant rise in both cases in the vicinity of the shear layer above K13 (Figure 6.). Here 75-85% of the events can be categorized as a sweep or an ejection. However, when the “disturbing” building was mounted, the proportion of the sweep and ejection events decreased by 10-15% directly above the shear layer (from 65% to 50%).

## CONCLUSIONS AND FUTURE OUTLOOK

The effects of a 2H tall building is significant, even it is situated 7H distance before the investigated street canyon in upstream direction, causing velocity deficit and change the level and distribution of the turbulent kinetic energy. Moreover, according to the quadrant analysis, it can be assumed, that there are also demonstrable changes in the transport process in the shear layer above the canyon. To prove it unambiguously, simultaneous concentration measurements are planned in the future, using an FFID (Fast Flame Ionization Detector) device.

## ACKNOWLEDGEMENTS

The scientific work presented in this paper was supported by the project K 108936 “Flow and dispersion phenomena in urban environment” of the Hungarian Scientific Research Fund and the New Széchenyi Plan project TÁMOP-4.2.1/B-09/1/KMR-2010-0002 “Development of quality-oriented and harmonized R+D+I strategy and functional model at BME”.

Spetial thanks to Dr. Tamás KALMÁR-NAGY for his inspirations in the field of quadrant analysis.

## REFERENCES

- Brixey L. A., D. K. Heist, J. Richmond-Bryant, G. E. Bowker, S. G. Perry and R. W. Wienere, 2009: The effect of a tall tower on flow and dispersion through a model urban neighbourhood. *Journal of Environmental Monitoring*, **11**, 2171–2179.
- Kastner-Klein P., R. Berkowicz, and R. Britter, 2004: The influence of street architecture on flow and dispersion in street canyons. *Meteorology and Atmospheric Physics*, **87**, 121-131.
- Nosek Š., L. Kukačka, R. Kellnerová, K. Jurčáková. and Z. Jaňour, 2016: Ventilation processes in a three-dimensional street canyon. *Boundary-Layer Meteorol.*, 10.1007/s10546-016-0132-2, 1-26.
- VDI 3783 PART 12 (2000): Environmental meteorology, Physical modelling of flow and dispersion processes in the atmospheric boundary layer, Application of wind tunnels, VDI/DIN-Handbuch Reinhaltung der Luft, Band 1b

**17th International Conference on  
Harmonisation within Atmospheric Dispersion Modelling for Regulatory Purposes  
9-12 May 2016, Budapest, Hungary**

---

**APPLICATION OF DISPERSION MODELS FOR DEVELOPMENT OF ATMOSPHERIC  
POLLUTION MANAGEMENT ZONES IN RIGA AGGLOMERATION**

*Iveta Steinberga<sup>1</sup>, Janis Bikse Jr<sup>1</sup>, Janis Kleperis<sup>2</sup>, Janis Bikse<sup>3</sup>*

<sup>1</sup>Faculty of Geography and Earth Sciences, University of Latvia, Riga, Latvia

<sup>2</sup>Riga City Council, Riga, Latvia

<sup>3</sup>Vidzeme University of Applied Sciences, Valmiera, Latvia

**Abstract:** Almost in all European countries air quality models are used for regulatory purposes - issuing emission permits, cases studies for environmental impact assessment, analysis of future development and planning. Directive 2008/50/EC (into force from 11 June 2008) regulate that air quality status should be maintained where it is good and improved if necessary. Riga municipality has monitored air pollution in Riga and nearby areas for more than 10 years and results showed necessity to regulate pollution, particular nitrogen dioxide (NO<sub>2</sub>), particulate matter (PM<sub>10</sub>) and benzene because of too high concentration. Air dispersion model was applied to develop atmospheric pollution management zones for NO<sub>2</sub>, PM<sub>10</sub> and benzene. This was 4th time when NO<sub>2</sub> zoning is applied for Riga (previous in years 2004, 2007, 2010), but first time for PM<sub>10</sub> and benzene. One of the actions showing roadmap for air quality improvement consist of revision of emission data and sources data base, and further modelling in order to identify hot spots for further actions.

**Key words:** *air quality management; urban air pollution control; modelling*

## **INTRODUCTION**

Numerous investigations in Europe, USA and rest of the world shows diverse impact of air pollution in many fields causing climate change, impact on biodiversity, disrupting photosynthesis, reducing crop harvests, massive impact on human health causing various types of allergies, circulatory problems, respiratory diseases, disturbances of central nervous system, etc. (Afroz et al., 2003; Brunekreef and Holgate, 2002; Paoletti et al., 2010; Sunyer et al., 1993; Svartengren et al., 2000;) Poor air quality especially in urban areas mainly is determined by high pollution level with nitrogen oxides, particulates and benzene consequential of the human activities. To avoid worsening of situation, the European Commission establishes a legal instruments to improve the air quality. One of the management actions consist of air quality plans development for zones and agglomerations where air quality limit values are exceeded with a further strategical aim to find and implement control pollution actions. Effective air pollution management planning is essential in several meanings: (1) most appropriate instruments leading to air quality improvement; (2) any air quality improvement gives positive feedback in health, morbidity and mortality aspects. Actions what could be applied varies very much from strategical to site specific restrictions, but one of most popular instruments in order to identify high pollution zones and effective actions are modelling. In most European member states modelling as a tool is used for emissions and dispersion modelling for further decision making process. The main objective of this study is to identify high pollution zones in Riga agglomeration by using Gaussian dispersion model. Air pollution dispersion modelling has been performed by AERMOD for nitrogen dioxide, particulate matter (PM<sub>10</sub>) and benzene dispersion.

## **METHODOLOGY**

### **Study area**

The Riga city (capital of Latvia) is located in Northeast Europe close to Baltic Sea Gulf. This is mostly economically developed center in Latvia. Riga is located in a temperate climate zone and weather conditions are determined by the Atlantic air masses, the Baltic Sea and the Riga Sea Gulf stretching deep

into the country. The temperature during the year typically varies from  $-7^{\circ}\text{C}$  to  $24^{\circ}\text{C}$ , occurrence of precipitation closely correlate to season – most likely precipitations is observed in January nor in May. The most common forms of precipitation are light rain, moderate snow, light snow, and thunderstorms. The relative humidity typically ranges from 45% (comfortable) to 97% (very humid), rarely dropping below 28% (dry). Typical wind speeds vary from 0 m/s to 6 m/s (calm to moderate breeze), rarely exceeding 9 m/s (fresh breeze). The wind is most often out of the south (24% of the time), south west (13% of the time), north (12% of the time), and south east (11% of the time).

### Model configuration

In order to perform concentration calculations at receptors, database of sources (physical description) with emission spectral and volumetric data were prepared. Emissions of nitrogen dioxide varies from year to year, but overall there is rather week correlation between number of sources and emission amounts; situation  $\text{PM}_{10}$  case is slightly different – for the period until 2009 there are rather opposite fluctuations of number of sources and emissions what seems unbelievable, but actually could be explained by changes in national legislation. The issued air pollution permits were revised and emissions were recalculated according to European methodology, and since 2010 there is growing trend of  $\text{PM}_{10}$  emission sources and emission amounts as well. Situation with benzene ( $\text{C}_6\text{H}_6$ ) is quite similar to  $\text{PM}_{10}$ , only source typology is different, while main sources of  $\text{PM}_{10}$  are coal processing and industrial heat processing (burning of heavy fuels, coal), benzene sources are mainly located in Riga Freeport territory and connected to oil products storage and processing. Variability of sources and annual emissions are shown in Figure 1.

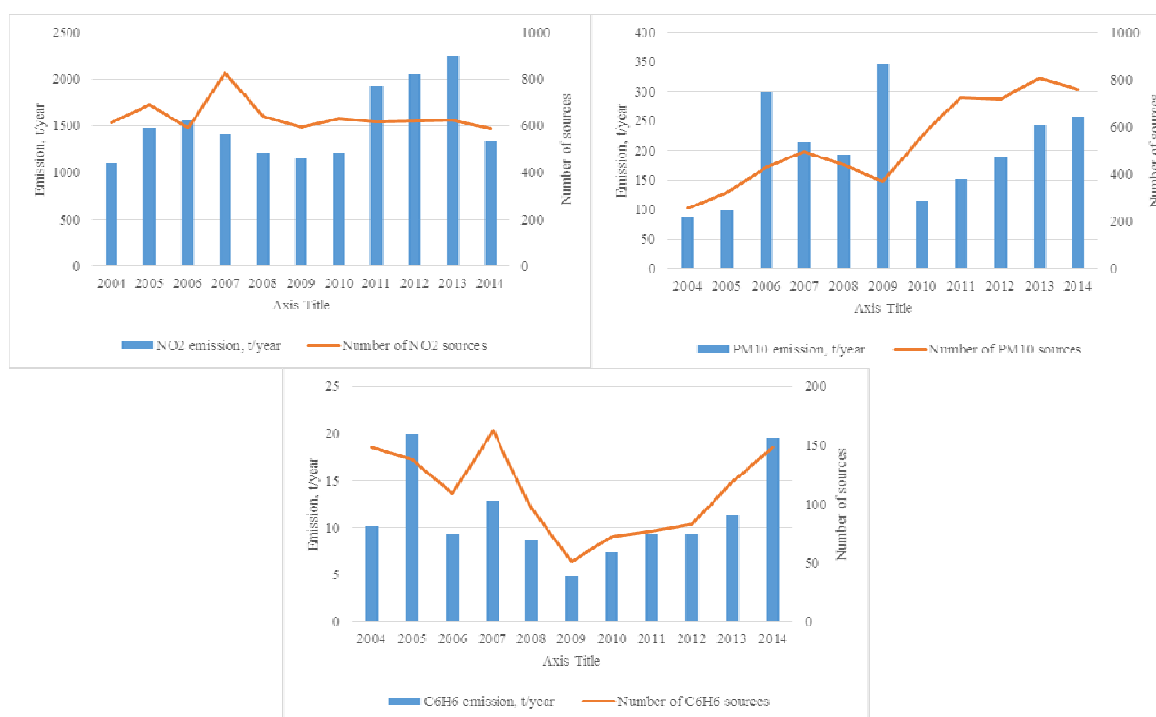


**Figure 1.** Variability of number of stationary sources and annual emissions in Riga agglomeration, 2004-2014

All necessary ground level meteorological data (air temperature at 2 m height, wind speed and wind direction at 10 m height, global radiation at 2 m height) from Riga meteorological station (N 56.9506; E 24.1161) was obtained for meteorological inputs for AERMET data pre-processor what was used to calculate boundary layer parameters, such as the Monin-Obukhov length, convective velocity scale, temperature scale, mixing height, and surface heat flux.

## Monitoring results

Air quality monitoring at national level were performed at background, industrial and traffic sites in Riga agglomeration. Measurements were done continuously by differential optical absorption (DOAS) method for nitrogen dioxide and benzene, but PM<sub>10</sub> concentrations were obtained gravimetrically on daily basis. Monitoring results show some indications: (1) at traffic monitoring sites substantial decreasing trend for PM<sub>10</sub> and benzene were identified; (2) at industrial sites and background level substantial changes didn't detected. Long-term results were shown in Figure 2.

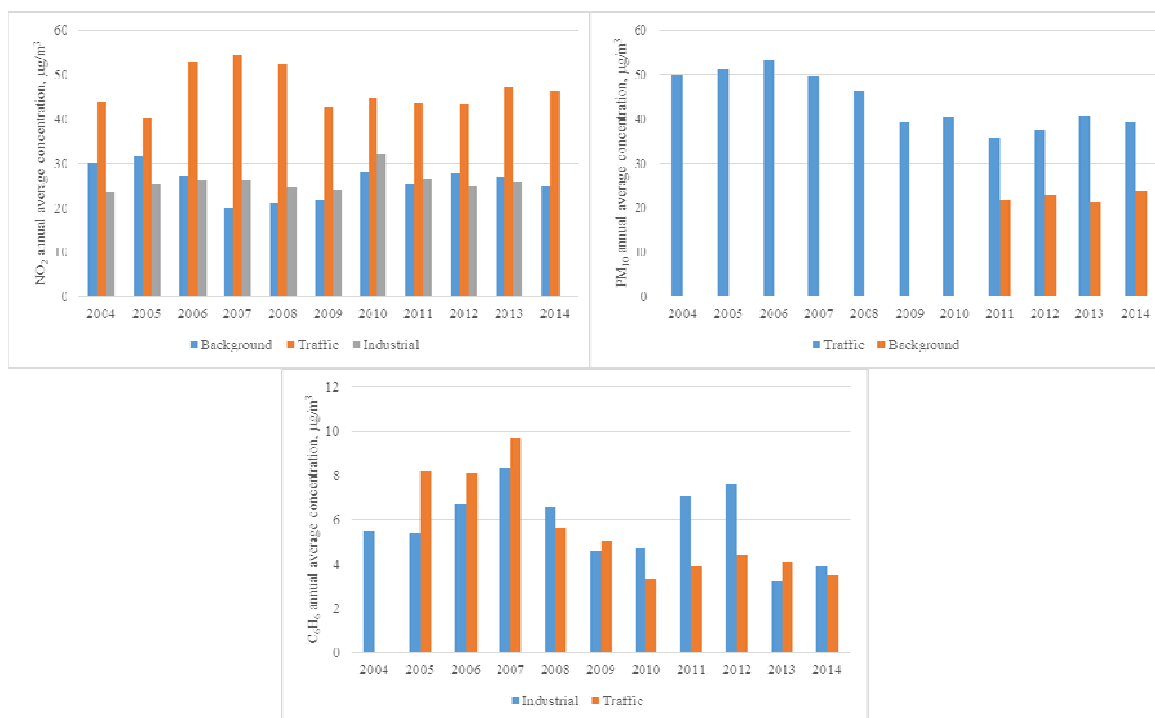


Figure 2. Long-term monitoring results in Riga agglomeration, 2004-2014

Correlation analysis of monitoring results shows very strong correlation ( $r = 0,9$ ;  $p < 0,05$ ) between PM<sub>10</sub> and benzene concentrations in city central part indicating massive impact of mobile sources.

## MODELLING RESULTS

Simulation results for NO<sub>2</sub> didn't show any substantial changes for 10 years period, higher pollution zones strongly correlate with traffic flow, indicating high pollution zones (above determined annual limit value 40 µg/m<sup>3</sup>) in street canyons. In case of particulate matter PM<sub>10</sub> dispersion high pollution zones are dissipated and associated with traffic jams, specific hot spots (coal storage and processing enterprises, welding operations, metal and steel works). Benzene spatial distribution were modelled for strictly defined pollution zones which are associated with limit values, lower and upper assessment levels. Maps of benzene pollution were elaborated for following pollution zones: I zone – benzene annual concentration exceeds limit value 5,0 µg/m<sup>3</sup>; II zone – benzene annual concentration varies between 3,5 and 5,0 µg/m<sup>3</sup>; III zone – benzene annual concentration varies between 2,0 and 3,5 µg/m<sup>3</sup>; IV zone – benzene annual concentration is less than 2,0 µg/m<sup>3</sup>. According to EK regulations and local legislation rules particular zones could be associated with further development plans, while in high pollution zone any additional pollution sources are prohibited, in less polluted zones (e.g. 2,0 - 3,5 µg/m<sup>3</sup>) there is strong need for further monitoring in order to inform habitats and air quality managers about air pollution condition. According to modelling results, benzene pollution zones are very closely connected to city traffic, traffic jams and Riga Sea Port activities. Source-receptor modelling of benzene shows how important is source geometry and working regime; while in 2014 69 % of benzene emissions comes from

industry including volatile organic compound sources only 29 % of benzene concentrations at receptor level gives this type of source. As most significant source in case of benzene pollution within all city is traffic. Map of benzene pollution zones were given in Figure 3.

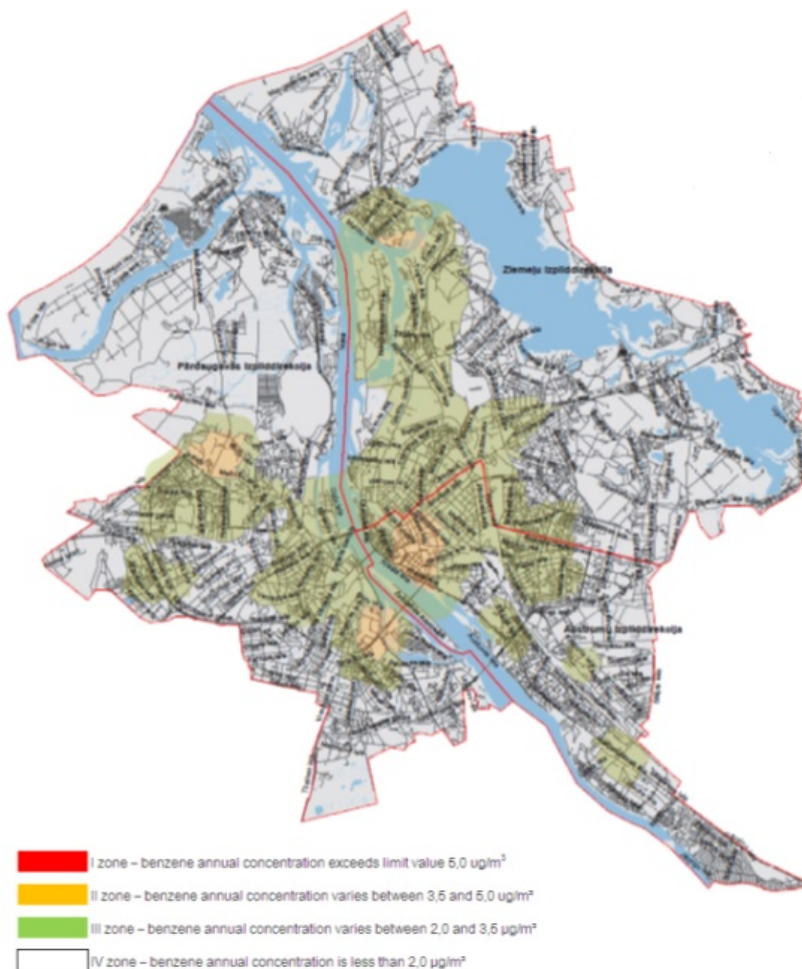


**Figure 3.** Benzene modelling results, annual average concentrations ( $\mu\text{g}/\text{m}^3$ )

Additionally, in order to evaluate modelling results, these results were checked according to data quality objective criteria what is set to 50%. This quality procedure were successfully performed for three monitoring points, results are given in Table 1.

**Table 1.** Evaluation of benzene modelling results

Monitoring point type	Monitoring results, $\mu\text{g}/\text{m}^3$	Lower assessment level, $\mu\text{g}/\text{m}^3$	Upper assessment level, $\mu\text{g}/\text{m}^3$	Modelling results, $\mu\text{g}/\text{m}^3$
Industrial	3.90	1.95	5.85	2.35
Traffic	3.48	1.74	5.22	3.79
Background	3.31	1.66	4.97	1.96

## CONCLUSIONS

- (1) Dispersion model is very usable tool for modelling of zonation of atmospheric pollutants and zoning for NO<sub>2</sub>, PM<sub>10</sub> and benzene has been accomplished;
- (2) NO<sub>2</sub> pollution in city centre closely correlate with traffic flow and future actions for improvement are necessary;
- (3) Modelling results showed highest concentrations of PM<sub>10</sub> in relation to traffic impact and in Riga Sea Port territory where activities are conducted to coal handling and processing;
- (4) Main benzene pollution sources in Riga are traffic and volatile organic compound sources located in Riga Freeport territory;
- (5) Growing tendency of volatile organic sources could rise benzene pollution level in Riga central and North part, but connection between number of sources, emissions and ground level concentrations is quite complex. While in 2014 69 % of benzene emissions comes from industry including volatile organic compound sources only 29 % of benzene concentrations at receptor level gives this type of source;
- (6) Modelling results of benzene shows evidences of further monitoring necessity in city center and other territories where benzene pollution levels varies between 3,5 µg/m<sup>3</sup> – 5 µg/m<sup>3</sup>.

## ACKNOWLEDGEMENTS

This work was supported by Riga City Council and the authors appreciate support of Ms. Aiva Eindorfa, Latvian Environment, Geology and Meteorology Centre.

## REFERENCES

- Afroz, R., Hassan, M.N. and N.A. Ibrahim, 2003: Review of air pollution and health impacts in Malaysia. *Environmental Research*, **92**, 71–77.
- Brunekreef, B. and S.T. Holgate, 2002: Air pollution and health. *Lancet*, **360**, 1233–1242.
- Paoletti, E., Schaub, M., Matyssek, R., Wieser, G., Augustaitis, A., Bastrup-Birk, A.M., Bytnerowicz, A., Gunthardt-Goerg, M.S., Muller-Starck, G. and Y. Serengil, 2010: Advances of air pollution science: From forest decline to multiple-stress effects on forest ecosystem services. *Environmental Pollution*, **158**, 1986–1989.
- Svartengren, M., Strand, V., Bylin, G., Jarup, L. and G. Pershagen, 2000: Short-term exposure to air pollution in a road tunnel enhances the asthmatic response to allergen. *European Respiratory Journal*, **15**, 716–724.
- Sunyer, J., Saez, M., Murillo, C., Castellsague, J., Martinez, F. and J.M. Anto, 1993: Air-pollution and emergency room admissions for chronic obstructive pulmonary-disease – A 5-year study. *American Journal of Epidemiology*, **137**, 701–705.

**SENSITIVITY ANALYSIS OF A METEOROLOGICAL PRE-PROCESSOR USING  
ALGORITHMIC DIFFERENTIATION**

*John Backman<sup>1</sup>, Curtis Wood<sup>1</sup>, Mikko Auvinen<sup>1,2</sup>, Leena Kangas<sup>1</sup>, Ari Karppinen<sup>1</sup>, Jaakko Kukkonen<sup>1</sup>*

<sup>1</sup>Atmospheric Composition Research, Finnish Meteorological Institute, Helsinki, Finland

<sup>2</sup>Department of Physics, Division of Atmospheric Sciences, University of Helsinki, Helsinki, Finland

**Abstract:** For the roadside dispersion model CAR-FMI, information about the state of the atmospheric boundary layer is provided by a meteorological pre-processor called MPP-FMI. The meteorological pre-processor uses basic meteorological observations to derive the necessary quantities describing the atmospheric state required by CAR-FMI. The sensitivity of this meteorological pre-processor has not previously been investigated, which is the focus of this work. The sensitivity analysis of the pre-processor parametrisation is studied using an algorithmic differentiation (AD). In brief, AD is a branch of computer science that deals with numerical evaluation of derivatives for functions that are implemented in a computer program. The study of these derivatives is the foundation of the sensitivity study. Here we restrict the study to the estimated Obukhov length obtained using MPP-FMI with regard to different atmospheric states represented by the range of input parameters which is a part of a broader study of the pre-processor. The study shows that the MPP-FMI estimated Obukhov length is most sensitive to wind speed. This is most pronounced at low wind speeds.

**Key words:** *meteorological pre-processor, Monin-Obukhov similarity, algorithmic differentiation, sensitivity analysis, fluxes, micro meteorology, urban climate*

## INTRODUCTION

A model developed at the Finnish Meteorological Institute to model the emissions, and the dispersion and transformation of pollution from an open road network (CAR-FMI) is used for such purposes (Kauhaniemi et al., 2008; Kukkonen et al., 2001). The model is a Gaussian finite line source model where the road network comprises the emission sources (Kukkonen et al., 2001). Like any short-range urban dispersion model, CAR-FMI requires that information about the state of the atmospheric boundary layer is provided to it externally. This information is generated by a meteorological pre-processor MPP-FMI (Karppinen et al., 1997, 2000), which uses basic meteorological observations (such as 30-min-averaged temperature, wind speed, etc) to derive the necessary quantities describing the atmospheric state required by CAR-FMI (such as Obukhov length and friction velocity). These evaluations are done by applying an energy-flux method that estimates turbulent heat and momentum fluxes in the boundary layer.

MPP-FMI is based on the work by (Van Ulden and Holtslag, 1985) with modifications that makes the parametrisation more suitable for high latitudes. The core of the method is the surface heat budget equation

$$Q^* - Q_G = Q_H + Q_E. \quad (1)$$

In Eq. (1),  $Q^*$  is the surface net radiation,  $Q_G$  is the soil heat flux,  $Q_H$  is the sensible heat flux, and  $Q_E$  is the latent heat flux.

First, the pre-processor estimates the sign of the  $Q_H$  by decomposing the surface heat budget equation into components. This determines if the subsequent calculations are performed using stability functions for stable or unstable conditions (Karppinen et al., 1997, 2000). Initially,  $Q^*$  is broken into short-wave and long-wave components. Latent heat flux ( $Q_E$ ) is estimated using a empirical saturation enthalpy curve as a

function of temperature and a estimated ground moisture parameter from meteorological data. Furthermore, the friction velocity ( $u_*$ ) is also first estimated without stability functions since the stability is not yet known. Depending on the atmospheric stability, different stability profiles are used for  $u_*$  and temperature scale ( $\theta_*$ ). Then, through iteration, the Obukhov length ( $L$ ) is changed. During the iterations, the temperature scale is calculated using stability profiles and using the estimated  $Q_H$  obtained during the iteration. The iteration stops when these two temperature scales match.

The sensitivity of this meteorological pre-processor has not previously been investigated, which is the focus of this work. The sensitivity analysis of the pre-processor parametrisation is studied using an algorithmic differentiation tool called TAPENADE (Hascoet and Pascual, 2013). The differentiated code will, in addition to the original output, also yield the partial derivatives of the output. The sensitivity of the energy-flux method is of interest because we want to evaluate the performance of the pre-processor, and investigate its sensitivity to the input data, in order to find ways in which it can be improved. For this purpose a state-of-the-art meteorological observational network in Helsinki, Finland (<http://urban.fmi.fi>) will serve as a benchmark.

### ALGORITHMIC DIFFERENTIATION

Algorithmic differentiation (AD) is a branch of computer science that deals with the numerical evaluation of derivatives of functions that are implemented in a computer programme, in this case MPP-FMI. Any computer program, no matter how complex, performs a sequence arithmetic operations (+, -, /, ...) or elementary functions (*exp, sin, log, ...*) whose derivatives are known. AD exploits this fact by applying the chain rule of differentiation to the entire sequence of operations within the program (Griewank and Walther, 2008). This systematic approach yields numerical derivative values at machine-precision, which describe how the program's results (i.e. outputs) depend on its input parameters. It is important to note that AD carries out each differentiation operation exactly and does not employ approximate techniques involving finite differences. For this reason AD does not suffer from truncation or round off errors.

AD is further separated into two modes, a forward mode or a reverse mode (Griewank and Walther, 2008). Here the discussion will be limited to the forward mode, which has been employed in this study. As a starting point, consider an arbitrary computer program that takes  $n$  input variables and returns  $m$  outputs. It can be described as a vector-valued function

$$\mathbf{y} = F(\mathbf{x}) \quad (2)$$

such that, the function  $F$  maps  $\mathbb{R}^n \rightarrow \mathbb{R}^m$  where  $\mathbf{x} \in \mathbb{R}^n$  defines the input and  $\mathbf{y} \in \mathbb{R}^m$  the output vectors.

Application of the forward mode AD to (2) yields a new implementation of the program, which, in addition to the original function evaluation, evaluates its differential

$$\dot{\mathbf{y}}_k = F'(\mathbf{x})\dot{\mathbf{x}}_k \quad (3)$$

where  $F'(\mathbf{x}) \in \mathbb{R}^{m \times n}$  defines the Jacobian matrix, which contains the all first-order partial derivatives  $\delta \mathbf{y} / \delta \mathbf{x}$  and  $\dot{\mathbf{x}}_k = (\delta x_1 / \delta x_k, \dots, \delta x_k / \delta x_k, \dots, \delta x_n / \delta x_k)^T$  is the seeding vector, which can be viewed as the  $k^{\text{th}}$  unit vector that operates on the Jacobian. The result is the  $k^{\text{th}}$  column from the Jacobian matrix  $\dot{\mathbf{y}}_k = (\delta y_1 / \delta y_k, \dots, \delta y_k / \delta y_k, \dots, \delta y_n / \delta y_k)^T$  which yields the dependency of all outputs with respect to the user-specified  $x_k$  input parameter. In the forward mode differentiated computer program, the chain rule-based derivative evaluations contained in (3) are carried out following the same order as the associated operations in (2), but always such that the derivative operations are executed after their corresponding step in the original program have completed.

A typical goal in sensitivity analysis is to obtain the full Jacobian. Utilizing forward mode AD, this is achieved by repeating the computation of Eq.(3)  $n$  times to yield all the columns from the Jacobian matrix. This is best illustrated with an example matrix (Eq. (4)), where the first column of the Jacobian is chosen. Thus, for a given input  $\mathbf{x}$  one can construct the Jacobian using AD and extract the derivatives of the output of interest at that point. This procedure can then be repeated for any number of points.

$$\dot{\mathbf{y}}_1 = \underbrace{\begin{bmatrix} \frac{\partial y_1}{\partial x_1} \\ \frac{\partial y_2}{\partial x_1} \\ \vdots \\ \frac{\partial y_m}{\partial x_1} \end{bmatrix}}_{\dot{\mathbf{y}}_{k=1} \in \mathbb{R}^m} = \underbrace{\begin{bmatrix} \frac{\partial y_1}{\partial x_1} & \frac{\partial y_1}{\partial x_2} & \cdots & \frac{\partial y_1}{\partial x_n} \\ \frac{\partial y_2}{\partial x_1} & \frac{\partial y_2}{\partial x_2} & \cdots & \frac{\partial y_2}{\partial x_n} \\ \vdots & \vdots & \ddots & \vdots \\ \frac{\partial y_m}{\partial x_1} & \cdots & \cdots & \frac{\partial y_m}{\partial x_n} \end{bmatrix}}_{F'(\mathbf{x}) \in \mathbb{R}^{m \times n}} \underbrace{\begin{bmatrix} 1 \\ 0 \\ \vdots \\ 0 \end{bmatrix}}_{\dot{\mathbf{x}}_{k=1} \in \mathbb{R}^n} \quad (4)$$

The reverse mode of AD is not applied in this work because the number of input variables are roughly the same as the number of output variables ( $m \approx n$ ). The reverse mode should be favoured when  $n \gg m$  (Griewank and Walther, 2008). In this work, the differentiation was performed using the AD tool called TAPENADE (Hascoet and Pascual, 2013). TAPENADE has been developed by the French National Institute for computer science and applied mathematics (Inria) and is free of charge as an online service.

## RESULTS AND DISCUSSION

The meteorological pre-processor is used to estimate turbulent fluxes and atmospheric stability and makes use of routinely observed meteorological observations (Karppinen et al., 1997, 2000). These meteorological observations include temperature ( $T_2$ ), wind speed ( $U$ ) at 10 meters, amount of predominant clouds ( $C_C$ ), cloud height ( $C_Z$ ), incoming short-wave solar radiation ( $R_S$ ), and the state of the ground (wet, dry, snow, ice etc.). Additional input variables are surface roughness length ( $z_0$ ) and a list of surface albedo ( $r$ ) values. These input data are then used to estimate the Priestly-Taylor moisture-parameter ( $\alpha$ ), Obukhov length ( $L$ ), temperature scale ( $\theta_*$ ), friction velocity ( $u_*$ ), sensible heat flux ( $Q_H$ ), latent heat flux ( $Q_E$ ), surface albedo ( $r$ ) and net radiation ( $Q^*$ ). In addition, radiosondes are used to determine the height of the mixing layer. The part of the MPP-FMI that deals with radiosonde data is omitted in this work. Here, we focus on the sensitivity of the energy-budget method implemented into MPP-FMI, which is based on the work by (Van Ulden and Holtslag, 1985) The sensitivity study was performed using artificial data for the various input variables for the pre-processor.

Outside of this work, some parameters in the MPP-FMI that are used in the calculations get their values through a table lookup. For example, precipitation and state of the ground input data are used in a table lookup to estimate a value for  $\alpha$ . From a sensitivity study point-of-view, it makes more intuitive sense to be able to assess the sensitivity to  $\alpha$  directly rather than the sensitivity of the table lookup procedure. Therefore, in this work, the table lookup variables  $r$  and  $\alpha$  are included as inputs to the MPP-FMI which reduces the number of input variables to be analysed. Therefore, this sensitivity study becomes more straightforward to interpret because inherent step-functions of a table lookup is avoided. Table 1 summarises the range of input variables that was used in the sensitivity study.

**Table 1.** Range of parameters used in the sensitivity study. For each range, six points were linearly spaced within the range. This amounts to  $6^8$  (roughly  $1.7 \cdot 10^6$ ) combinations of input variables to be evaluated

Inputs	$z_0$	$r$	$T_2$ [C]	$C_C$	$C_Z$ [m]	$U$ [ $\text{ms}^{-1}$ ]	$\alpha$	$R_S$ [ $\text{Wm}^{-2}$ ]
Range	0.3 – 1.3	0.05 – 0.7	-20 – 30	0 – 1	30 – 6000	1 – 20	0.5 – 1.0	0 – 900

The values in Table 1 were then used to construct the Jacobian (Eq. 4) for every combination of the input variables. The columns of interest for this work are those columns in the Jacobian containing the sensitivity information of  $L$  and  $u_*$  since these are further needed in CAR-FMI. In addition to  $L$  and  $u_*$ , the Jacobian comprise sensitivity information for  $Q_H$ ,  $Q_E$ ,  $Q^*$ , and  $\theta_*$ .

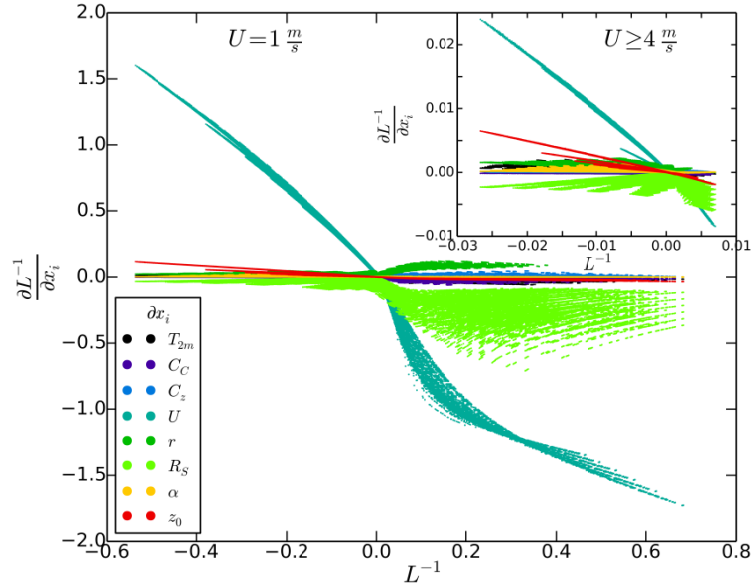


**Figure 1.** Sensitivity of inverse Obukhov length ( $L^{-1}$ ) with respect to input variables of MPP-FMI. The main figure shows sensitivities to the input variables at a wind speed  $U$  of  $1 \text{ ms}^{-1}$ . The insert shows sensitivities for wind speeds in the range of  $4 - 20 \text{ ms}^{-1}$ . In the figure, the derivatives have been normalised by the range of the input parameters described in Table 1 in order to make them inter-comparable.

In Figure 1, the sensitivity of the inverse Obukhov length ( $L^{-1}$ ) is shown for all combinations of the input parameters listed in Table 1.  $L^{-1}$  describes the atmospheric stability. For neutral conditions  $L^{-1} \approx 0$ . When  $L^{-1} \ll 0$  the atmosphere is unstable, and when  $L^{-1} \gg 0$  the atmosphere is stable. The figure serves as an illustrative example of the study. For clarity, Figure 1 is further separated into a low wind speed situation with all other input variables varied (the main figure). The insert figure contains all combinations of input parameters associated with wind speeds in the range of  $4 - 20 \text{ ms}^{-1}$ . The figure is separated into a low and high wind speed situation because the model is so much more sensitive at low wind speeds.

As can be seen from Figure (1),  $L^{-1}$  is most sensitive to a change in  $U$ . When compared to the insert ( $4 \leq U \leq 20 \text{ ms}^{-1}$ ), the sensitivity to a change in wind speed is more pronounced at low wind speeds. First, let us consider the situation when  $L^{-1}$  is negative at low wind speeds. When  $L^{-1}$  is negative, which is the case for unstable and neutral conditions, the derivative  $\partial L^{-1}/\partial U$  is positive. That means that an increase in  $U$ , when  $L^{-1} < 0$ , will always tend to favour the estimate of the stability to become more neutral. That is, a negative  $L^{-1}$  and a positive derivative  $\partial L^{-1}/\partial U$  will therefore move  $L^{-1}$  towards neutral should  $U$  increase.

On the opposite, when  $L^{-1} > 0$  (i.e. stable or neutral), then  $\partial L^{-1}/\partial U$  is always negative. That implies that a increase in  $U$  will therefore, again, tend to make  $L^{-1}$  move towards neutral. This is in agreement with what one would expect in nature since an increase in  $U$  will induce mechanical turbulence regardless of the initial stability and hence favour neutral conditions. At higher values of  $U$ , seen in the insert of Figure 1, the  $L^{-1}$  range is now restricted to roughly the range of  $-0.03 - 0.01$  (i.e. neutral).

The second most important input variable for the MPP-FMI with regard to  $L^{-1}$  is  $R_S$ . Since the derivative  $\partial L^{-1}/\partial R_S$  of in all combination of inputs considered is always negative, and even more so when  $L^{-1} > 0$ , this implies that an increase in  $R_S$  will always move the stability towards unstable. This follows the intuition that an increase in  $R_S$  will increase turbulence due to buoyancy induced turbulence, and therefore favour unstable conditions. At low wind speeds, it has to be noted, that the spread in the sensitivity of  $L^{-1}$  to  $R_S$ , is an indication that other meteorological input variables influence the results, especially when  $L^{-1} > 0$ . This is evident from the fact that the sensitivity to  $R_S$  does not follow a single line, but is spread out. For example when  $L^{-1} = 0.3$ , then  $\partial L^{-1}/\partial R_S$  is in the range of  $-0.1 - 0.6$ . The highest sensitivity to a change in  $R_S$ , at low wind speeds, is when  $R_S$  is close to zero and the surface albedo ( $r$ ) is low. This information is, however, not colour coded into the figure not to degenerate the clarity of the figure.

## CONCLUSIONS

Future work will be to study the whole chain from input into MPP-FMI through CAR-FMI. Since it is being investigated if the output of MPP-FMI can be replaced by other models, or the model itself being improved, the sensitivity of the model is of particular interest. Consequently, the sensitivity study of MPP-FMI would need to succeed with a sensitivity study of CAR-FMI. This will be the next step for this research.

## REFERENCES

- Griewank, A. and Walther, A. 2008: Evaluating Derivatives Principles and Techniques of Algorithmic Differentiation, 2<sup>nd</sup> Edition, Society for Industrial and Applied Mathematics, USA, pp 461.
- Hascoet, L. and Pascual, V., 2013: The Tapenade Automatic Differentiation Tool: Principles, Model, and Specification, *ACM Trans. Math. Softw.*, **39(3)**, 20:1–20:43, doi:10.1145/2450153.2450158.
- Karppinen, A., Joffre, S. M. and Vaajama, P., 1997: Boundary-layer parameterization for Finnish regulatory dispersion models, *Int. J. Environ. Pollut.*, **8**, 3–6.
- Karppinen, A., Joffre, S. M. . and Kukkonen, J., 2000: The refinement of a meteorological preprocessor for the urban environment, *Int. J. Environ. Pollut.*, **14(1-6)**, 1–9.
- Kauhaniemi, M., Karppinen, A., Härkönen, J., Kousa, A., Alaviippola, B., Koskentalo, T., Aarnio, P., Elolähde, T. and Kukkonen, J., 2008: Evaluation of a modelling system for predicting the concentrations of PM<sub>2.5</sub> in an urban area, *Atmos. Environ.*, **42**, 4517–4529, doi:10.1016/j.atmosenv.2008.01.071.
- Kukkonen, J., Härkönen, J., Walden, J., Karppinen, A. and Lusa, K., 2001: Validation of the dispersion model CAR-FMI against measurements near a major road, *Atmos. Environ.*, **35(5)**, 949–960, doi:doi:10.1016/S1352-2310(00)00337-X.
- Van Ulden, A. P. and Holtslag, A. A. M., 1985: Estimation of Atmospheric Boundary Layer Parameters for Diffusion Applications, *J. Clim. Appl. Meteorol.*, **24(11)**, 1196–1207, doi:10.1175/1520-0450(1985)024<1196:EOABLP>2.0.CO;2.

## **TOPIC 3**

### **USE OF MODELLING IN SUPPORT OF EU AIR QUALITY DIRECTIVES, INCLUDING FAIRMODE**

**17th International Conference on  
Harmonisation within Atmospheric Dispersion Modelling for Regulatory Purposes  
9-12 May 2016, Budapest, Hungary**

---

**EXCEEDING THE EUROPEAN NO<sub>2</sub>-LIMIT VALUE IN BELGIUM: CAN WE SOLVE THE  
PROBLEM IN A SHORT TO MEDIUM TIME FRAME?**

*Wouter Lefebvre<sup>1</sup>, Hans Hooyberghs<sup>1</sup>, Felix Deutsch<sup>1</sup>, Sandy Adriaenssens<sup>2</sup>, Frans Fierens<sup>2</sup>*

<sup>1</sup>VITO, Flemish Institute for Technological Research, Unit Environmental Modelling. Boeretang 200, B-2400 Mol, Belgium.

<sup>2</sup>Belgian Interregional Environment Agency (IRCEL-CELINE), Kunstlaan 10-11, 1210 Brussels, Belgium

**Abstract:** The European Directive on Air Quality (2008/50/EC) states that annual average NO<sub>2</sub>-concentrations should be below 40 µg/m<sup>3</sup> at every location from 2010 onwards. However, it was possible to get time extension till 2015. In the meantime, it became clear that the limit values were exceeded in 2015 at three different monitoring sites: one in Flanders and two in the Brussels Capital region. This abstract examines the causes of this compliance failure and assesses which measures are needed in order to be compliant with the European limit value within the shortest possible time frame.

While the European limit value is, in general, assessed at monitoring locations, compliance should be reached also at locations where no measurements are available. Therefore, we apply the RIO-IFDM-model, an extensively validated combination of an intelligent interpolation tool and a local scale bi-gaussian dispersion model. With this model, it was estimated that in 2020 the NO<sub>2</sub> annual mean concentrations will still be exceeded in a very densely populated region of 5.41 km<sup>2</sup> (0.018% of Belgium). We assume a worst case scenario for EURO 6 conformance in real world driving situations. The effect of street canyons is not taken into account, hence the limit value will be exceeded even more frequently. As the regions with exceedances of the NO<sub>2</sub> limit value are closely linked to major roads, a backcast simulation was performed in order to calculate the appropriate emission reductions necessary to be in compliance on these roads. It was estimated that emission reductions up to 80% are needed in order to be in compliance with the annual mean limit value. When areas close to tunnel exits are excluded, emission reductions of more than 50% are still needed at some locations. Therefore, it can be concluded that only harsh measures, such as a complete shift of passenger cars from diesel to less NO<sub>x</sub> emitting vehicles (gasoline, CNG, EV, ...) combined with significant traffic volume and emission reductions in other sectors, will be needed to be in compliance in the short to medium time frame. Quick win measures, likespeed limit reductions on highways will not be sufficient.

**Key words:** NO<sub>2</sub> limit, deadline extension

## **INTRODUCTION**

The European Directive on Air Quality (2008/50/EC) states that annual average NO<sub>2</sub>-concentrations should be below 40 µg/m<sup>3</sup> at almost every location from 2010 onwards. However, it was possible to demand an extension of this deadline to 2015. In the meantime, it became clear that the limit values were exceeded during the year 2015 at three different measurement locations in Belgium, one in Flanders and two in the Brussels. This abstract examines the causes of this failure and assesses which measures are needed in order to be compliant with the European limit value as quickly as possible.

## **MODEL DESCRIPTION**

An integrated model chain has been set up to assess the air quality at the local scale, including both regional variability as well as local variation in sources of air pollution. The MIMOSA4.3 emission model (Mensink et al., 2000; Vankerkom et al., 2009) is used to calculate local traffic emissions. In order to take into account the new findings of Ligterink et al. (2013), for NO<sub>x</sub>, the CAR EURO6-emissions of diesels

are taken to be equal to the CAR EURO4-emissions of diesels. The resulting spatially and temporally distributed emissions are used in the bi-Gaussian model IFDM (Lefebvre et al., 2011a; 2011b). These results are coupled to the background concentrations. The background concentrations for 2020 are obtained by rescaling the RIO-background (Hooyberghs et al., 2006; Janssen et al., 2008) for 2009 using the evolution of the Chimere data. More in detail, the background for 2020 is obtained by applying the relative difference observed in the Chimere data between 2009 and 2020 to the 2009 RIO-data using an exponential trend (Veldeman et al., 2015). A method to avoid double counting of the (local) emissions by the different models is applied (Lefebvre et al., 2011b).

To describe the local weather parameters correctly on a national level, we use hourly assimilated meteorological data, with total spatial coverage at a 1x1 km<sup>2</sup> resolution for 2009. No street canyons are taken into account.

### BASECASE 2020

The highest concentrations of the highly traffic-dependent pollutant NO<sub>2</sub> is found close to the main city centers and close to the main highways. Especially around Brussels, Antwerp and Ghent high concentrations are observed, but also all other regions in the vicinity of major highways show significant increases compared to their surroundings.

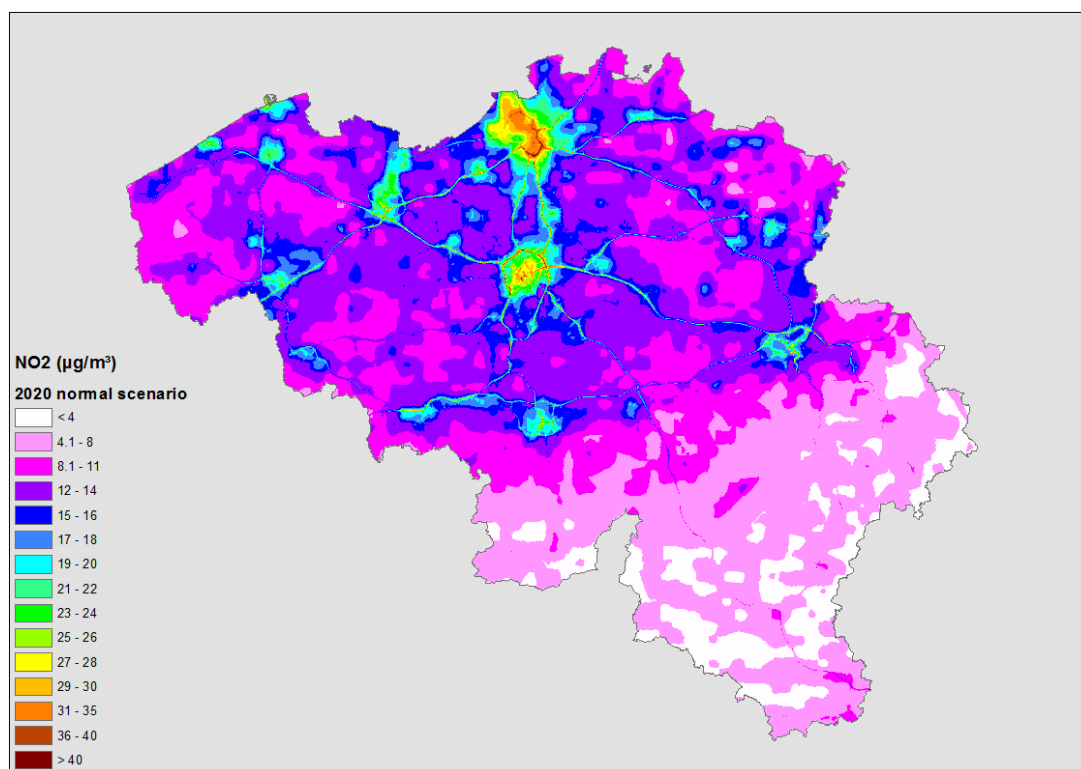


**Figure 1:** Annual averaged concentrations of NO<sub>2</sub> for 2020 in µg/m<sup>3</sup>.

There remain a small number of spots at which the yearly threshold of 40 µg/m<sup>3</sup> is exceeded. These exceedances are, of course, observed at the locations with the highest NO<sub>2</sub>-concentrations, i.e. close to the major highways and roads. In total, the threshold is exceeded in 0.18 % (5.41 km<sup>2</sup>) of the grid cells, hence only a very small part of the area is exposed to values larger than the EU-standard. Nevertheless, these areas are in some cases densely populated.

The major regions with exceedances, amongst other, include

- A series of major tunnel exists
- Major parts of the Antwerp and the Brussels Ring Roads and their immediate surroundings
- Parts of the Brussels city center.

It should be noted that the exceedance of the limit value in 2015 was measured only at three locations. This shows both the strength and drawbacks of using only measurements or only model values in order to test the exceedance of the limit values. Indeed, the measurement location in Flanders where exceedances of the European limit values are still measured is located in a street canyon, which have not been taken into account in this modelling exercise. On the other hand, no measurement locations in the Flanders region are currently located close to a major highway.

### BACKCASTING

The emission reductions are obtained using a backcasting procedure. In a first step, the grid cells for which the concentrations are too high are appointed and binned into several zones based on the magnitude of the exceedance. For these zones, the base case concentration is split into a share related to the background concentrations and a share related to the local traffic. Thereafter, we determine the reduction needed in the latter share such that the total concentrations are below the EU-standards. The traffic emissions for all pollutants for the road segments in and close to the zones are subsequently reduced in the equivalent way and the new emissions are used as input for new IFDM-simulations. The whole procedure is repeated iteratively (using the results of the simulations with the reduced and the total emissions as input) until the intended concentrations have been reached.

The emission reductions for the different road segments of this scenario are shown in Figure 2. The four road segments with the highest reductions are all linked to tunnel exits with four tunnels between 83 and 67%. The most important non-tunnel exit road segments are all highways or major roads in the Antwerp or Brussels area with reductions of more than 50% (and up to more than 60%).

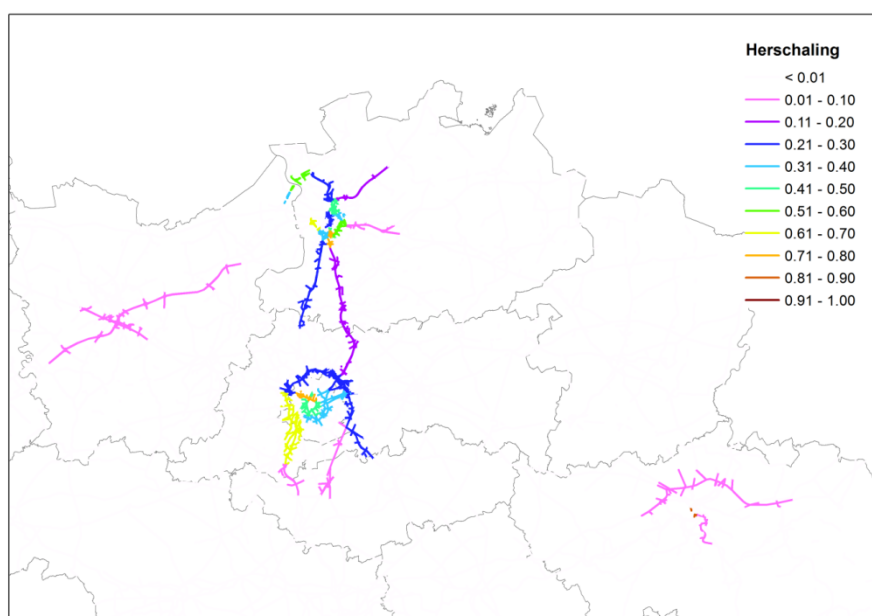


**Figure 2:** Needed local emission decreases (in %) in order to reduce the annually averaged NO<sub>2</sub>-concentrations in 2020 below the 40 µg/m<sup>3</sup> limit.

### CONCLUSIONS

It is shown that very large reductions of traffic emissions are needed if the European NO<sub>2</sub>-limit is to be met at all locations in Belgium, despite the relatively small area at which it is still exceeded at the moment. Therefore, it can be concluded that only harsh measures, such as a complete shift for passenger cars from diesel to less NO<sub>x</sub> emitting cars (gasoline, CNG, ...) combined with strong traffic reductions and emission reductions in other sectors, will be needed if the limit values are to be reached in a short to medium time frame. Quick win measures, such as reductions of speed limits on highways will not be sufficient.

## ACKNOWLEDGEMENTS

The authors want to acknowledge the VMM (Vlaamse MilieuMaatschappij) who financed this study in the framework of the INTERREG IV-B NWE Joaquin project.

## REFERENCES

- Hooyberghs, J., Mensink, C., Dumont, G., Fierens F., 2006. Spatial interpolation of ambient ozone concentrations from sparse monitoring points in Belgium, *Journal of Environmental Monitoring*, **8**, 1129-1135, doi: 10.1039/b612607n.
- Janssen, S., Dumont, G., Fierens, F., Mensink, C., 2008. Spatial interpolation of air pollution measurements using CORINE land cover data, *Atmospheric Environment*, **42**, 20, 4884-4903, doi: 10.1016/j.atmosenv.2008.02.043.
- Lefebvre, W., Fierens, F., Trimpeners, E., Janssen, S., Van de Vel, K., Deutsch, F., Viaene, P., Vankerkom, J., Dumont, G., Vanpoucke, C., Mensink, C., Peelaerts, W., Vliegen, J., 2011a. Modeling the effects of a speed limit reduction on traffic-related elemental carbon (EC) concentrations and population exposure to EC, *Atmospheric Environment*, **45**, 197-207, doi: 10.1016/j.atmosenv.2010.09.026
- Lefebvre, W., Vercauteren, J., Schrooten, L., Janssen, S., Degraeuwe, B., Maenhaut, W., de Vlieger, I., Vankerkom, J., Cosemans, G., Mensink, C., Veldeman, N., Deutsch, F., Van Looy, S., Peelaerts, W., Lefebvre, F., 2011b. Validation of the MIMOSA-AURORA-IFDM model chain for policy support: modeling concentrations of elemental carbon in Flanders, *Atmospheric Environment*, **45**/37, 6705-6713., doi: 10.1016/j.atmosenv.2011.08.033
- Ligterink N., Kadijk G., van Mensch P., Hausberger S., Rexeis M., 2013. Investigations and real world emission performance of Euro 6 light-duty vehicles, TNO report, TNO 2013 R11891, [https://www.tno.nl/downloads/investigations\\_emission\\_factors\\_euro\\_6\\_ld\\_vehicles\\_tno\\_2013\\_r11891.pdf](https://www.tno.nl/downloads/investigations_emission_factors_euro_6_ld_vehicles_tno_2013_r11891.pdf).
- Mensink, C., De Vlieger, I., Nys, J., 2000. An urban transport emission model for the Antwerp area, *Atmospheric Environment*, **34**, 4595-4602.
- Vankerkom, J., De Vlieger, I., Schrooten, L., Vliegen, J., Styns, K., 2009. Beleidsondersteunend onderzoek: Aanpassingen aan het emissiemodel voor wegtransport MIMOSA. Studie uitgevoerd in opdracht van VMM - MIRA, 2009/TEM/R/084.
- Veldeman N., Maiheu B., Lefebvre W., Viaene P., Janssen L., Deutsch F., Vankerkom J., Van Looy S., Driesen G., Peelaerts W., Janssen S., Rapport activiteiten in 2014 uitgevoerd in kader van de referentietaak 12 “Kenniscentrum Luchtkwaliteitmodellering”, VITO-rapport 2015/RMA/R/5, Februari 2015.

**17th International Conference on  
Harmonization within Atmospheric Dispersion Modelling for Regulatory Purposes  
9-12 May 2016, Budapest, Hungary**

---

**AIR QUALITY MODELING OF NON-ATTAINMENT AREAS  
AS A BASIS FOR AIR QUALITY PLANS**

*Jana Krajčovičová, Jana Matejovičová, Martin Kremler, Vladimír Nemček*

Slovak Hydrometeorological Institute, Jeséniova 17, Bratislava, Slovakia

**Abstract:** Directive 2008/50/EC requires preparation and implementation of the air quality plans for zones and agglomerations where one or more limit values have been exceeded. The air quality plans should be based on source apportionment, so that the measures are targeted effectively.

In 2010 a method has been developed at SHMI, implementing CALPUFF modeling system in order to carry out high resolution modelling and source apportionment of PM<sub>10</sub> in the non-attainment areas in Slovakia, using routinely available data. The method has been gradually applied to the total of 18 areas over the period of the last 5 years. The results were presented at Harmo 15 (Krajčovičová et al, 2014), since then it has been subject to several improvements and upgrades. This paper presents recent implementation of the upgraded methodology for the air quality management area of Prievidza region. It includes modeling of PM<sub>10</sub> and PM<sub>2,5</sub>, NO<sub>2</sub>, SO<sub>2</sub> and benzo(a)pyrene (BaP). Whole year of 2013 is modeled and the results are compared to the available air quality monitoring data.

**Key words:** *air quality modeling, CALPUFF, source apportionment, PM<sub>10</sub>, PM<sub>2,5</sub>, NO<sub>2</sub>, SO<sub>2</sub>, benzo(a)pyrene*

## **INTRODUCTION**

High concentrations of PM<sub>10</sub> and PM<sub>2,5</sub> have been a major problem in most regions of Slovakia for a long time. In addition, exceedances of NO<sub>2</sub> and BaP limit values has been observed in some monitoring locations. Currently, there are 17 so called air quality management areas in Slovakia, which are areas where a limit value of one or more pollutants has been exceeded. Air quality plans has had to be prepared for all such areas and for most of them the plans are regularly revised and updated as the problems with high concentrations persist. Air quality management of Prievidza region is an example. It covers an industrialized district of the size of 960 km<sup>2</sup>, with the population of 136 500 inhabitants. The district capital is Prievidza located in the NW. Handlová, located in a narrow valley in the NE is a smaller mining town. Bystričany is a village in the SW, where third monitoring station is located, due to its vicinity to a large chemical plant in Nováky and coal power station in Zemianske Kostol'any. The population density of the district is 142 people per km<sup>2</sup>. It has been historically one of the most polluted regions, hosting some heavy chemical and energy production industry and several coal mines producing low quality coal. Today, due to technological advances, the emissions from industry has been continuously decreasing. However, due to increasing costs, local heating has been shifting from natural gas to wood burning, with the emissions replacing in their importance those of the industry.

Slovak Hydrometeorological Institute is responsible for carrying out air quality analyses as a basis for Air quality plans. We carried out an air quality study for Prievidza in 2008 for the first time. It was focused on mainly on PM<sub>10</sub>. This year we have updated the modeling taking 2013 as a basis. Besides PM<sub>10</sub>, other pollutants has been included, such as PM<sub>10</sub> and PM<sub>2,5</sub>, NO<sub>2</sub>, SO<sub>2</sub> and BaP.

## **EMISSION SOURCES**

The following source groups have been included in the simulations:

- Large and medium sources from National Emission Information System (NEIS) database
- Seasonal sources of residential heating
- Road transport

Besides these, there are of course other sources, e.g., nearby agricultural activities, temporary construction sites, occasional fires or accidents which can have impact on the PM<sub>10</sub> concentrations

during a limited time. As we are not able to quantify their emissions, they are not included in our modelling. Fortunately, they do not have a substantial influence in the long-time perspective.

### **Large and medium sources from NEIS database**

They comprise of seasonal point sources (centralized heating), non-seasonal point sources (industrial stacks), and fugitive industrial sources, represented as volume sources in the simulations.

### **Seasonal sources of residential heating**

Emissions from residential heating are based on the statistical census data (ŠÚSR, 2011), containing number of households using solid fuels for heating, sizes, age and insulation status of houses and other useful parameters for each census element (element being of a size of a small municipality or several streets of a city). Climatological parameters of local heating season have also been included in the model, which computed amount of combusted wood. Consequently emission factors for each pollutant in question have been applied. These emissions has been geographically allocated to residential areas identified using Google Earth.

### **Road transport**

Exhaust and non-exhaust vehicle emissions were calculated using a top-down method from the total national emissions (COPERT 4), based on the ratio of road network length inside the domain to the total road network length. Consequently, the emissions were distributed throughout the roads in the domain based on the road category and length, vehicle counts and categories.

Resuspension of dust was estimated based on the AP 42 (US EPA, 2011) methodology using bottom-up approach.

## **MODELING TOOLS AND SETUP**

As the district of Prievidza is a mountainous region, CALPUFF model (Scire et al., 2000b) was used as our modelling tool, driven by diagnostic meteorological model CALMET (Scire et al., 2000a). The terrain model (SRTM – Farr et al., 2007) and landuse (CORINE – Bossard et al., 2000) together with full year of 2013 meteorological data from three surface meteorological stations within the domain and three upper air sounding stations outside the domain were input to CALMET model, which calculated high resolution three dimensional wind fields reflecting local orography and circulation systems.

The size of the modelling area is 33.5 x 27.5 km, horizontal resolution is 500 m (meteorological fields). There are 10 vertical layers with top at 3000 m. Industrial sources from NEIS database were modeled as point sources (part of them seasonal), residential heating sources were modeled as grids of volume sources with the horizontal resolution of 20 m, and road emissions were modeled as segments consisting of volume sources. As CALPUFF only takes into account emission sources located within the modeling domain, a regional background (nearest available EMEP station has been used) was added to the contributions of the above mentioned source groups in order to compute totals.

## **RESULTS**

Table 1 shows the contributions of different source groups to the total concentrations at the locations of the air quality monitoring stations, compared to measured values. However, some of the pollutants, such as NO<sub>2</sub>, are not monitored at any of the stations, while other, such as BaP, are monitored only in one of them. In those locations where comparison is possible, the results are rather encouraging.

Although NO<sub>2</sub> measurements are not available, the modeling results suggest that the annual mean limit value might be exceeded at Prievidza monitoring stations. This should be investigated further, using better resolution, as the monitoring station is located rather near a major road (cca 40 m), where the concentration gradients are high.

Figure 1 shows the maps of total annual concentrations for different pollutants. High concentrations of PM<sub>10</sub> and PM<sub>2.5</sub> are concentrated in and around residential areas with local heating in Handlová and Bystričany. Prievidza is a larger town where wood combustion does not occur as frequently as in the

previous two cities. As expected, NO<sub>2</sub> is concentrated along the roads, with very small contribution from residential heating. SO<sub>2</sub> is emitted from high industrial stacks and therefore has much more regional character. As it dilutes sufficiently, the total SO<sub>2</sub> values are well under the legislative limits for vegetation protection. Modeling results seem to underestimate SO<sub>2</sub> concentrations.

**Table 1.** Annual mean values of pollutants as modelled by CALPUFF, compared to measurements at three monitoring stations.

Station	Point ( $\mu\text{g}\cdot\text{m}^{-3}$ )	Road ( $\mu\text{g}\cdot\text{m}^{-3}$ )	Residential heating ( $\mu\text{g}\cdot\text{m}^{-3}$ )	Regional background ( $\mu\text{g}\cdot\text{m}^{-3}$ )	Total ( $\mu\text{g}\cdot\text{m}^{-3}$ )	Measured ( $\mu\text{g}\cdot\text{m}^{-3}$ )
<b>NO<sub>2</sub></b>						
Prievidza	0.6	50.3	0.3	4.3	55.5	-
Bystričany	2.6	14.3	2.2	4.3	23.4	-
Handlová	0.7	22.3	1.5	4.3	28.8	-
<b>SO<sub>2</sub></b>						
Prievidza	1.6	0.1	0.0	1.5	3.1	10.7
Bystričany	9.1	0.0	0.0	1.5	10.6	17.4
Handlová	0.7	0.0	0.0	1.5	2.2	8.3
<b>PM<sub>10</sub></b>						
Prievidza	0.5	6.4	1.4	18.1	26.4	32
Bystričany	1.1	2.6	10.8	18.1	32.6	35
Handlová	0.1	3.1	7.5	18.1	28.9	24
<b>PM<sub>2.5</sub></b>						
Prievidza	0.4	3.2	1.3	11.8	16.7	25
Bystričany	0.7	1.1	10.2	11.8	23.8	22
Handlová	0.1	1.5	7.1	11.8	20.5	16
<b>BaP<sup>1</sup></b>						
Prievidza	0.0	0.0	0.3	0.7	1.0	1.8
Bystričany	0.0	0.0	2.2	0.7	2.9	-
Handlová	0.0	0.0	1.5	0.7	2.2	-

## CONCLUSIONS

Although the modeling results are quite encouraging, it is necessary to make further simulations on smaller domains with higher resolution. We are planning to set three additional smaller domains around Prievidza city, Handlová and Bystričany, and use better resolution of road segments. In the current simulation, we used emission factors for residential wood combustion identical with those used for national emission reporting in Slovakia (MoE, 2008). However, these emission factors are extremely high (all countries around use much lower values) and need to be reevaluated. We also need to improve the road emission data by introducing daily and weekly variability.

<sup>1</sup> BaP values are in  $\text{ng}\cdot\text{m}^{-2}$

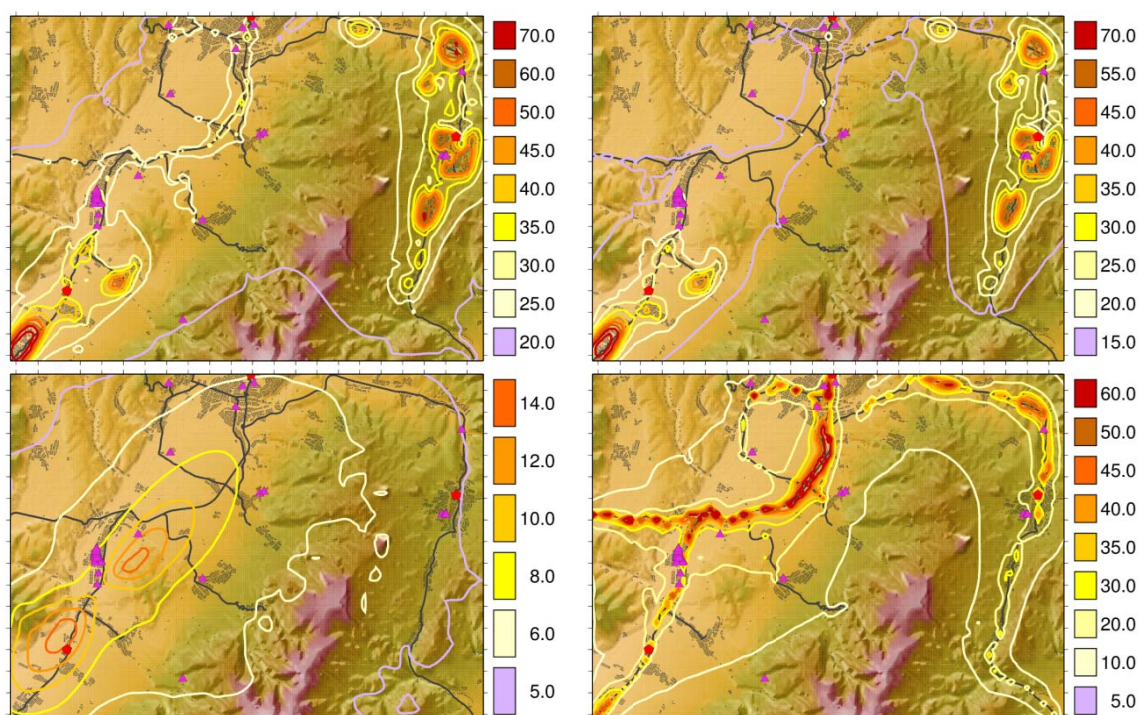


**Figure 1.** Annual concentrations of PM<sub>10</sub> (upper left), PM<sub>2.5</sub> (upper right), SO<sub>2</sub> (lower left) and NO<sub>2</sub> (lower right) modeled by CALPUFF. Red pentagons are monitoring stations, pink triangles are industrial point sources and black lines are major roads.

## REFERENCES

- Bossard, M. et al. (2000) CORINE Land Cover Technical Guide – Addendum 2000, European Environment Agency, Copenhagen.
- Farr, T.G. et al. (2007) ‘The shuttle radar topography mission’, *Rev. Geophys.*, Vol. 45, RG2004, doi: 10.1029/2005RG000183.
- Krajčovičová, J., Kremler, M., Matejovičová, J. (2014) Local PM<sub>10</sub> source apportionment for non-attainment areas in Slovakia. *Int. J. of Environment and Pollution*, **54**, 166-174.
- Ministry of the Environment (2008) Všeobecné emisné závislosti a všeobecné emisné faktory pre vybrané technológie a zariadenia podľa § 2 ods. 3 písm. f) a g) vyhlášky MŽP SR č. 408/2003 Z. z., *Bulletin of the Ministry of the Environment SR*, **XVI**, No. 5.
- Pay, M.T., Jiménez-Guerrero, P. and Baldasano, J.M. (2011) ‘Implementation of resuspension from paved roads for the improvement’, *Atmospheric Environment*, **45**, 802–807.
- Scire, J.S., Robe, F.R., Fernau, M.E. and Yamartino, R.J. (2000a) *A User’s Guide for the CALMET Meteorological Model*, Earth Tech, Inc., Concord, MA.
- Scire, J.S., Strimaitis, D.G. and Yamartino, R.J. (2000b) *A User’s Guide for the CALPUFF Dispersion Model*, Earth Tech, Inc., Concord, MA.
- ŠÚSR (2011) Sčítanie obyvateľov, domov a bytov. Statistical Office of the Slovak Republic. [www.statistics.sk](http://www.statistics.sk).
- US EPA (2011) Compilation of Air Pollutant Emission Factors, 5th ed., AP 42 [online]

**17th International Conference on  
Harmonisation within Atmospheric Dispersion Modelling for Regulatory Purposes  
9-12 May 2016, Budapest, Hungary**

---

**TESTING THE SHERPA TOOL TO SUPPORT AIR QUALITY PLANS OVER PORTUGAL**

*Alexandra Monteiro<sup>1</sup>, Carla Gama<sup>1</sup>, Alain Clappier<sup>2</sup>, Philippe Thunis<sup>3</sup>, Ana Isabel Miranda<sup>1</sup>*

<sup>1</sup>CESAM, Department of Environment, University of Aveiro, 3810-193 Aveiro, Portugal

<sup>2</sup>Université de Strasbourg, Laboratoire Image Ville Environnement, 67000 Strasbourg, France

<sup>3</sup>European Commission, JRC, Institute for Environment and Sustainability, Air and Climate Unit, Via E. Fermi 2749, 21027 Ispra, VA, Italy

**Abstract:** During the last years, air quality problems have been detected in the urban area of Porto (Portugal), mainly regarding PM10 concentration levels. Limit values have been surpassed in some air quality monitoring stations and, following the European legislation requirements, an Air Quality Plan was designed and implemented to reduce PM10 levels. In this sense, measures to decrease PM10 emissions have been selected and their impact assessed with a numerical modelling tool (The Air Pollution Model - TAPM). These measures are mainly related to the industrial and residential combustion sectors and also, in minority, to the road traffic sector. The main objective of this study is to investigate the efficiency of these reduction measures, with regards to the improvement of PM10 concentration levels over the Porto region, using the new SHERPA tool. SHERPA was designed, in the scope of the FAIRMODE initiative, to provide potencies for all kind of reduction over Europe, and is particularly useful to identify the feasibility and priority of a given action. The impacts arising from different factors (different precursors) are quantified, together with the magnitude of the locally produced impacts of emission reductions on concentrations with respect to the “external to the domain” contribution. A major contribution of non-controllable sources for PM10 levels was found and the application also allowed identifying PM2.5 as the main precursor. Besides that, emission reduction scenarios should be focused on Porto urban area where potency is higher.

**Key words:** *emissions reduction; air quality; model; plans; SHERPA tool*

## **INTRODUCTION**

Air quality is one of the environmental areas in which the European Union (EU) has been most active, in particular designing and implementing legislation on air quality and on the restriction of pollutant emissions to the atmosphere. The Directive on Ambient Air Quality and Cleaner Air for Europe (Directive 2008/50/EC), published in May 2008, reinforces the obligation of EU member states to elaborate and implement Air Quality Plans (AQP) to improve air quality when standards are not fulfilled. The Directive also highlights modelling as a fundamental tool to improve air quality assessment and management (Ribeiro et al., 2014). Due to their ability in assessing the efficiency of distinct emission reduction measures air quality numerical models are useful tools to support the design of an AQP (Nagl et al., 2007). Eulerian Chemical Transport Models (CTM) are the most frequently used (APPRAISAL, 2013), requiring the emissions for several activity sectors, meteorological variables and initial and boundary conditions as input data. Exceedances of the thresholds of particulate matter (PM10) have been reported in the urban agglomeration of Porto Litoral, where human exposure is also high (Monteiro et al., 2007; Miranda et al., 2014; 2015). Air Quality Plans were developed for this pollutant for the period 2005-2008 (Borrego et al., 2012). Despite improvements in air quality, verified after the 2008-2010 period, some of the legislated limits continue to be exceeded every year in particular monitoring sites. In the framework of the EU Thematic Strategy for air quality (COM 2005 446) and the EU Directive 2008/50/EC, the JRC decided to develop a screening software based on relationships between emissions and concentration levels. The SHERPA (Screening for High Emission Reduction Potential on Air) tool aims at identifying the key activity sectors and pollutants on which to focus an AQP for an improved efficiency. It also delivers information on the area (region, province, country...) on which these actions should be applied and coordinated to be optimal. More generally it assesses the impact of local emission abatements in a given region.

The main objective of this study is to investigate the aptness of the AQP defined for the Great Porto area and the respective measures to reduce PM10 concentration levels using the the SHERPA tool. This will allow supporting future additional mitigation measures and policy maker’s decisions for the air quality management over this particular region.

### THE AIR QUALITY PLANS OVER PORTO REGION

With a total area of 1024 km<sup>2</sup> and a total population of more than 1.2 million inhabitants the Great Porto Area (11 municipalities) was selected as study case. . Figure 1a shows the location of the Great Porto Area in the northern region of Portugal. This region of Portugal is one of the several EU zones that had to develop and implement air quality plans (AQP) to reduce PM10 (Borrego et al., 2012; Miranda et al., 2015). Figure 1b shows the exceedances to the daily limit value for PM10 along the period 2004-2013.

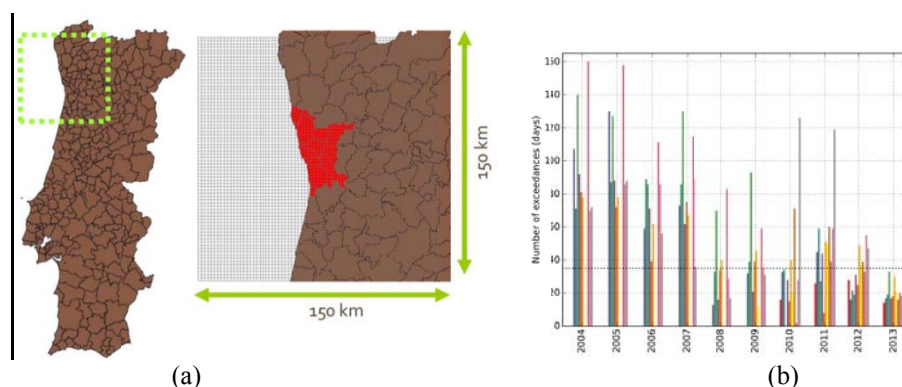


**Figure 1.** (a) Location of the Great Porto Area in Portugal and in the Northern Region of Portugal; (b) Number of exceedances to the PM10 daily limit value ( $50 \mu\text{g}\cdot\text{m}^{-3}$ ), obtained in the air quality monitoring stations of Northern Region for the period 2004 to 2013 (different colours relate to different stations).

The analysis of PM10 measured values at the air monitoring stations of the Great Porto Area for the period 2004 – 2013 confirms the several exceedances to the PM10 daily limit value, mainly before 2008. This may be due not only to the AQP that have been developed and implemented and their potential effect on air quality improvement, but also to the economic crises that Portugal has been facing. Figure 3 presents the share of PM10 emissions per activity sector for the Great Porto Area, according to the national emission inventory (APA, 2014). The most relevant identified emission sectors were industrial combustion, residential combustion and also, in minor part, road traffic.

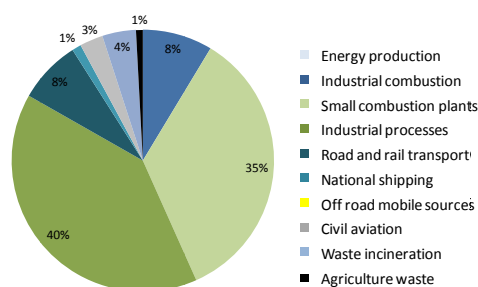


**Figure 2.** PM10 emissions per activity sector for the Great Porto area.

The measures to reduce the PM10 concentrations and decrease the exceedances to the legislated limits, were selected and tested with the TAPM modelling system (see Borrego et al., 2012). The Air Pollution Model (TAPM) (Hurley et al., 2005) is particularly suited to evaluate the impact of emission reduction strategies due to its flexibility, user friendly environment and short time demands in terms of computational efforts for long term simulations (1 year) compared to other CTM models. For this reason,

TAPM, which was previously applied and validated over several Portuguese areas (Borrego et al., 2010). The criteria used for the selection of the measures included: (i) relative contributions of each activity sector to the total pollutant emissions; (ii) types of exceedances (annual/daily) and the monitoring sites where they were registered; (iii) actions already planned by municipalities authorities. Following these criteria, and knowing that the main contributing sectors are residential combustion, industry and traffic, and that the monitoring sites with higher concentrations are located in urban and traffic sites, a group of measures were defined (Borrego et al., 2012), which includes: (i) reconversion of conventional fireplaces by more efficient equipment for residential combustion; (ii) promotion of industrial air cleaners and enhanced surveillance of stationary sources; (iii) promotion of hybrid model vehicles, design of a Low Emission Zone (LEZ), improvement of public transport network, renewal of the fleet of taxis and vehicles for waste collection, promotion of car sharing; (iv) educational actions. Duque et al. (2016) further describe some of these defined measures.

### **THE SHERPA TOOL AND ITS APPLICATION FOR GREAT PORTO AREA**

SHERPA is made up of graphical user interfaces and operation processes and some fundamental pre- and post-processors. SHERPA is entirely open-source with an interface that includes seven main modules accessible from the main screen, namely:

(1) *Scenario Assessment (NUTS)*: to assess the impact of a given emission reduction scenario (e.g. a specific air quality plan) on air quality in one region. Based on a user selected control area where specific emission reductions are applied, SHERPA produces an air quality impact map over the selected region and surrounding areas. Emission reduction percentages can freely be introduced by the user in terms of sectors and precursors.

(2) *Scenario Assessment (ATLAS)*: the same as previous option but in this case the impact of a given emission reduction scenario is assessed in all European regions.

(3) *Source apportionment*: to assess the relative contribution of the various emission sectors/precursors to the overall impact of an emission reduction strategy. Based on a user selected control area where emission reductions are applied, SHERPA produces source apportionment estimates in terms of sectors and/or precursors.

(4) *Potency/Potential (NUTS)*: to estimate the potential air quality improvement in a region when emissions (all or selected sectors) are switched off. Based on a user selected control area where emission reductions are applied and on a selection of precursor/sectors to be reduced, SHERPA produces a gridded map of potential improvements in the control region and surrounding areas.

(5) *Potency/Potential (ATLAS)*: the same as previous option but for all European domain. SHERPA produces a gridded map of potential improvements in the each NUTS control region.

(6) *Governance control area*: to assess the extension the control domain should have to optimize air quality improvements. Based on a selection of precursor/sectors to be reduced and a given NUTS level for the analysis, SHERPA produces a map where NUTS entities are grouped in such a way to optimize the improvements in terms of air quality.

(7) *RIAT+ first guess*: SHERPA allows also to downloading the data required for a RIAT+ application over a specified NUTS area using the “first guess data” contained in SHERPA (<http://www.operatool.eu>). Figure 3 shows the interface of SHERPA and a scheme of its implementation (see more detail at <http://fairmode.jrc.ec.europa.eu/>).

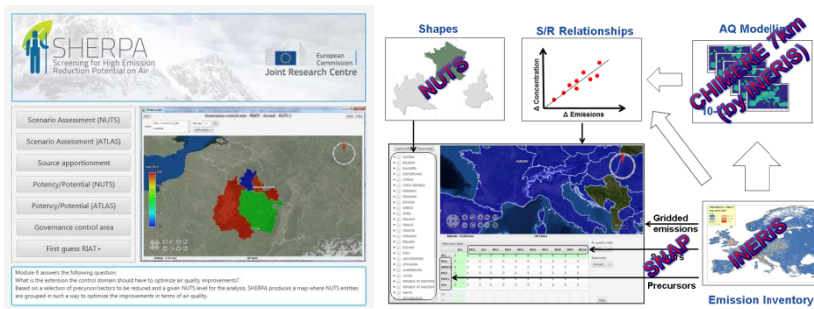


Figure 3. (a) SHERPA interface and (b) implementation process of SHERPA.

SHERPA was applied to the Great Porto area. The entire year of 2012 was set as the base year for the analysis of the impacts of the previously selected measures. The MACC emission inventory and the CTM model CHIMERE were used. The simulation domain covered Europe with a spatial resolution of 7x7 km<sup>2</sup>. The source apportionment option was used to estimate the relative contribution of the various emission sectors/precursors to the overall impact of a PM10 emission reduction strategy, selecting the NUT2, which corresponds to the Northern region of Portugal (study area). Figure 4 presents the SHERPA results per sector and for different precursors (a) PM2.5, b) NOx, c) NH<sub>3</sub> and d) SOx).



Figure 4. SHERPA source apportionment results per sector and for different precursors (a,b,c,d).

Figure 5 shows the gridded map of potential improvements in the study region produced by SHERPA tool (Potency/potential (NUTS)) considering that all emissions are switched off (Figure 5a) and only emissions from residential combustion are removed (Figure 5b).

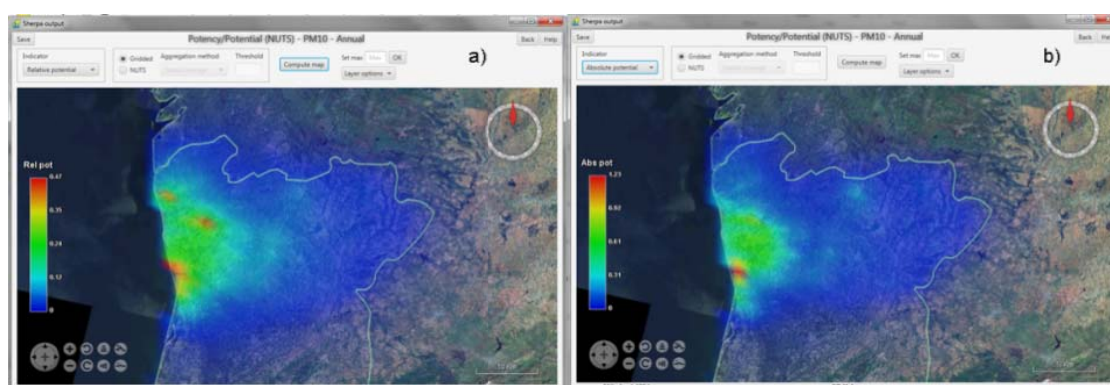


**Figure 5.** Potency/potential considering all the sectors (a) and only SNAP2/residential combustion (b).

## DISCUSSION AND CONCLUSIONS

The source apportionment results reveal, first of all, that there is a very high fraction, superior to 85%, of non-controllable sources (external and natural sources) for all the studied precursors, which is particularly critical when the purpose is to develop and establish air quality plans. The small percentage of controllable sources is dominated by different sectors depending on the pollutant/precursor. Nevertheless, strategies should focus on the mitigation of PM<sub>2.5</sub>, precursor with major contribution to PM<sub>10</sub> levels, followed by NO<sub>x</sub>. The contribution of SO<sub>x</sub> and NMVOC (not shown) to PM<sub>10</sub> concentration is negligible. The absolute potential diagram (left diagram of Figure 4) suggest that mitigation measures should give priority to the residential and industrial combustion sectors (for PM<sub>2.5</sub>) and traffic (for NO<sub>x</sub> precursor), which is in agreement to what was defined in the previous AQP.

Regarding the spatial analysis where emission reduction measures should take place, the analysis of the gridded map of potential improvements in the control region and surrounding areas indicates that there is high potential air quality improvement if control actions focus on the Porto urban area and also over two municipalities located on the north metropolitan area (Viana and Braga). For the particular case of residential sector (SNAP2, see Figure 5b), measures should focus on Porto area, where the potency is higher, which was already pointed out in previous works (Borrego et al., 2010; Gonçalves et al. 2012).

## ACKNOWLEDGMENTS

Thanks are due, for the financial support to CESAM (UID/AMB/50017), to FCT/MEC through national funds, and the co-funding by the FEDER, within the PT2020 Partnership Agreement and Compete 2020, and also for the PhD grant of C. Gama (SFRH/BD/87468/2012).

## REFERENCES

- APA (Portuguese Environmental Agency), 2014: Portuguese informative inventory report 1990-2012. Submitted under the UNECE convention on longrange transboundary air pollution. Agência Portuguesa do Ambiente (Ed.), Amadora, Portugal, March 2014.
- APPRAISAL (project on Air Pollution Policies foR Assessment of Integrated Strategies At regional and Local scales), 2013: Air quality assessment and planning, including modelling and measurement, Report No. D2.3, 49 pages.
- Borrego, C., Valente, J., Carvalho, A., Sá, E., Lopes, M., Miranda, A.I., 2010: Contribution of residential wood combustion to PM<sub>10</sub> levels in Portugal. *Atmos Environ*, **44**, 642-651.
- Borrego, C., Sá, E., Carvalho, A., Sousa, S., Miranda, A.I., 2012: Plans and Programmes to Improve Air Quality over Portugal: A Numerical Modelling Approach. *Int J Envir and Pollut* **48** (1-4), 60-68.
- Duque, L., Relvas, H., Silveira, C., Ferreira, J., Monteiro, A., Gama, C., Rafael, S., Freitas, S., Borrego, C., Miranda, A.I., 2016: Evaluating strategies to reduce urban air pollution. *Atmos Environ*, **127**, 196-204.
- Gonçalves, C., Alves, C., Pio, C., 2012: Inventory of fine particulate organic compound emissions from residential wood combustion in Portugal. *Atmos Environ*, **50**, 297-306.

- Hurley, P., Physick, W., Luhar, K., 2005. TAPM: a practical approach to prognostic meteorological and air pollution modelling. *Environ Model Softw*, **20**, 737-752.
- Miranda, A.I., Relvas, H., Turrini, E., Lopes, D., Silveira, C., Ferreira, J., Lopes, M., Sá, E., Borrego, C., Volta, M., 2014: Urban Air Quality Plans and Integrated Assessment Methodologies. *J Env Science and Engineering B*, **3**, 70-78.
- Miranda, A., Silveira, C., Ferreira, J., Monteiro, A., Lopes, D., Relvas, H., Borrego, C., Roebeling, P., Turrini, E., Volta, M., 2015: Current air quality plans in Europe designed to support air quality management policies. *Atmos Pol Res*, **6**, 434-443.
- Monteiro, A., Miranda, A.I., Borrego, C., Vautard, R., 2007: Air quality assessment for Portugal. *Sci Total Environ*, **373**, 22-31.
- Nagl, C., Moosmann, L., Schneider, J., 2007: Assessment of plans and programmes reported under 1996/62/EC - final report, Report No. 0079, Vienna, 139 pages.
- Ribeiro, I., Monteiro, A., Fernandes, A.P., Monteiro, A.C., Lopes, M., Borrego, C., Miranda, A.I.: 2014. Air quality modelling as a supplementary assessment method in the framework of the European Air Quality Directive. *Int J Environ Pollut*, **54**, 262-270.

**17th International Conference on  
Harmonisation within Atmospheric Dispersion Modelling for Regulatory Purposes  
9-12 May 2016, Budapest, Hungary**

---

**APPLICATION OF A PHOTOCHEMICAL MODEL TO THE ASSESSMENT OF REGIONAL  
AIR QUALITY LEVELS IN SOUTHERN ITALY: PROCEDURES AND RESULTS**

*R. Giua<sup>1</sup>, A. Morabito<sup>1</sup>, I. Schipa<sup>1</sup>, A. Tanzarella<sup>1</sup>, C. Silibello<sup>2</sup> and G. Assennato<sup>1</sup>*

<sup>1</sup>Regional Environment Protection Agency (ARPA) Puglia, Bari, Italy

<sup>2</sup>ARIANET Srl, via Gilino 9, Milan, Italy

**Abstract:** A modelling system based on FARM photochemical model was applied to assess the air quality (AQ) levels over the Apulia region (Southern Italy) for the 2013 year. FARM implements the SAPRC99 gas-phase chemical mechanism and the AERO3 aerosol module, derived from CMAQ model. Simulations were performed on a 316 km x 248 km domain, covering the entire region with 4 km grid spacing. The meteorological fields necessary for dispersion simulations came from the meteorological model RAMS. Emission data were derived from the regional INEMAR inventory, updated to the year 2013, while the emissions from the neighbouring regions were taken from the Italian national emission inventory. Initial and boundary conditions were provided by a national-scale simulation performed by the Air Quality Forecasting System QualeAria. According to the INEMAR emission inventory, the most relevant pollutant sources in the region are a steel plant, the largest in Europe (in Taranto area), a coal fired plant, the second most powerful in Italy (in Brindisi area) and biomass burning for residential heating. Simulation results evidenced exceedances for PM<sub>10</sub> daily limit value and BaP annual limit values occurring at some areas. To evaluate the model performance, hourly and daily data, measured by the 35 monitoring stations belonging to the regional air-monitoring network, were compared with the simulation results, for the main pollutants regulated by the European Directive 2008/50/EC. The comparison between simulated and experimental data evidenced a good capability of the modelling system to reproduce the spatial distribution and the temporal variability of the observations. Some exceptions occurred, probably due to the adopted model spatial resolution, the uncertainties in emission inventories and the spatial representativeness of air quality monitoring stations. The interesting results obtained suggest the use of this modelling strategy for further source apportionment studies, in order to identify and to implement proper emission control strategies.

**Key words:** *air quality assessment, photochemical model, model evaluation tool.*

## **INTRODUCTION**

Humans can be adversely affected by exposure to air pollutants in ambient air. In response, the European Union has developed an extensive body of legislation which establishes health based standards and objectives for a number of pollutants in the air. These standards and objectives are considered by the Italian Legislative Decree 155/2010, which adopted the European Directive 2008/50/EC.

The application of numerical models for air quality assessment is allowed by the legislation of European Community (EU) that establishes the possibility of using modelling techniques in combination with air quality observations. This work showed the air quality modelling assessment results over the Apulia region with 4 km grid spacing for the year 2013; for this purpose, the three-dimensional Eulerian model FARM (Mircea et al., 2015) was applied and evaluated. The modelled concentrations obtained by the simulations, were also compared with the threshold limit values. Finally, the model performances were analysed by using the DELTA Tool, an Interactive Data Language-based evaluation software, developed within FAIRMODE as support in the application of the EU Air Quality Directive. Such tool was helpful among the modellers community in fast identifying problems with model performance and indicating potential weaknesses (Georgieva et al., 2015).

## **MODEL DESCRIPTION, SIMULATION SETUP AND EMISSION DATA**

A modelling system, based on FARM model, was applied to a domain covering an area of 316x248 km<sup>2</sup>, including the entire Puglia region (Southern Italy) with a grid spacing of 4 km and a vertical extent of

5330 km. Initial and boundary conditions were provided by the national-scale Air Quality Forecasting System (AQFS) “QualeAria” (<http://www.aria-net.it/qualearia/en/>).

FARM was configured with an updated version of SAPRC99 gas-phase chemical mechanism (Carter, 2000), that includes PAHs and Hg chemistry, and the Aero3 modal aerosol module, implemented in CMAQ model (Binkowski, 1999). Aero3 aerosol module includes ISORROPIA (Nenes et al., 1998) and SORGAM (Schell et al., 2001) models for the calculation of secondary inorganic and organic aerosols. Input meteorological fields for all 2013 have been generated by the prognostic, non-hydrostatic model RAMS (Cotton et al., 2003), applied over three nested grids covering the whole Europe, Italy and the Apulia region, with spatial resolution of 60, 20 and 4km respectively.

Emission data were derived from the regional INEMAR inventory (<http://www.inemar.arpa.puglia.it/>), updated to the 2013, while the emissions from the neighbouring regions were taken from the Italian national emission inventory. The regional INEMAR inventory is a database developed in order to estimate on municipality level the emissions of different pollutants, grouped for activities (heating, road transport, agriculture, industry, etc.) according to the SNAP nomenclature adopted in the EMEP - CORINAIR inventory. The most relevant pollutant industrial sources in the region are the steel plant, located in Taranto area and the coal fired power plant in Brindisi area (2640 MWe). In particular regarding to the total INEMAR emissions these sources contribute respectively by 72% for SO<sub>2</sub>, 27% for NO<sub>x</sub> and 13% for primary PM<sub>10</sub>. To reconstruct accurately with INEMAR the emissions from the biomass residential heating, it was carried out a specific survey on the biomass consumption for the residential heating in Apulia. For primary PM<sub>10</sub> the total emission from this activity accounts for 30% with respect to the total regional emissions. Biogenic emissions (VOC from vegetation, soil dust, sea salts and heavy metals from soil and sea) were computed by applying the MEGAN emission model (Guenther et al., 2006) and the SURFPRO model. The contribution of Saharan dust was not modelled and no assimilation data was performed.

#### MONITORING DATA AND MODEL EVALUATION

The regional air-monitoring network, managed by the Regional Environmental Protection Agency (ARPA), is equipped with 71 stations of different type, all active in the year 2013. In order to evaluate the performances of the adopted modeling system, the NO<sub>2</sub>, O<sub>3</sub>, BaP, PM<sub>10</sub> and PM<sub>2.5</sub> predictions were compared with the observation satisfying following requirements: the stations should have a spatial representativeness similar to the model horizontal resolution and a data availability greater than 75%. Table 1 shows the number of stations, distinguished for type, as defined by conventional classification established by the Italian regulation.

**Table 1.** Number of stations per type and pollutant for 2013

<b>Number of Stations</b>	<b>NO<sub>2</sub> hourly</b>	<b>O<sub>3</sub> hourly</b>	<b>PM<sub>10</sub> daily</b>	<b>PM<sub>2.5</sub> daily</b>	<b>BaP monthly</b>
Urban-background	3	1	2	-	6
Suburban	25	11	19	3	4
Rural	7	4	7	3	2
Number of stations with more than 75% of available data	32	16	28	6	12

Delta Tool was used to compute the following statistical indicators: root mean square error (RMSE), correlation coefficient (R), mean bias (Bias), mean standard deviation (SD) and centred root mean square error (CRMSE). These statistics have the peculiarity in DELTA to be normalised by the observations uncertainty U(O<sub>i</sub>) (Thunis et al., 2013; Pernigotti et al, 2013), in particular by the quadratic mean of measurement uncertainty, defined as:

$$RMS_U = \sqrt{\frac{1}{N} \sum_{i=1}^N (U(O_i))^2} \quad (1)$$

With the simple principle of allowing the same margin of tolerance to both model and observations, the Model Quality Objective (MQO) is defined by comparing the error between observed and modelled values to the absolute measured uncertainty:

$$MQO = \frac{1}{2} \frac{RMSE}{RMS_U} = \frac{\sqrt{\frac{1}{N} \sum_{i=1}^N (O_i - M_i)^2}}{2RMS_U} \leq 1 \quad (2)$$

If  $MQO \leq 0.5$  the model results are within the range of  $U(O_i)$ , if  $0.5 < MQO \leq 1$  RMSE is larger than  $RMS_U$ , but model results could still be closer to the true value than the observations; if  $MQO > 1$  the observation and model uncertainty ranges do not overlap and model and observation are more than  $2 RMS_U$  apart.

To identify the fulfilment of the performance criteria, MQO can be visualized for every monitoring stations on an adapted target diagram, named target plot, where X and Y axes represent CRMSE and BIAS, normalised by observation uncertainty.

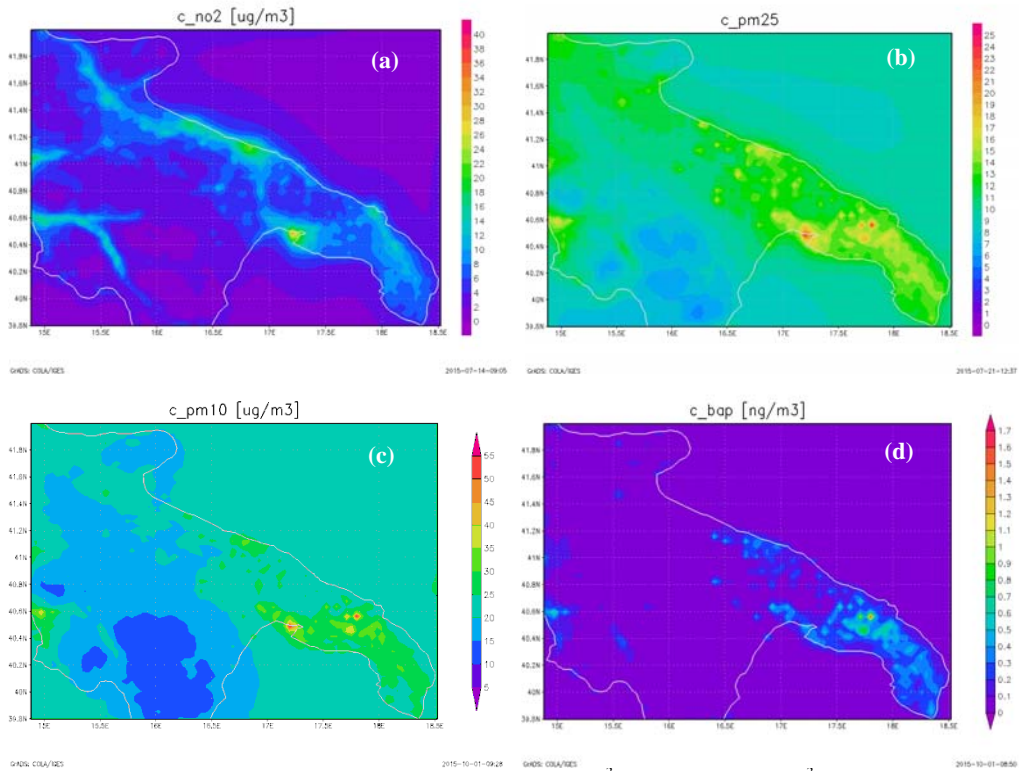
## RESULTS AND DISCUSSION

Figure 1(a-d) show the predicted  $NO_2$ ,  $PM_{2.5}$  and BaP annual averaged concentration maps and the 90.4° percentile of  $PM_{10}$  daily means. As for  $NO_2$  (Fig. 1a), higher levels were estimated in correspondence of larger urban areas and major traffic roads. The predicted values were, however, relevantly lower than the prescribed thresholds. As for  $PM_{2.5}$ ,  $PM_{10}$  and BaP, the highest predicted concentrations were estimate in the Taranto industrial area and in the central southern part of the peninsula, where the biomass burning emissions due to agricultural activities and (especially) to residential heating by fireplaces are relevant. Regarding  $PM_{10}$ , a number of daily exceedances greater than that the value allowed by the air quality directive (equal to 35) were estimated in both areas, while exceedances of the BaP annual limit value were predicted only in the central southern part of peninsula.

The model concentrations were compared with hourly and daily observed data to evaluate the modelling system performance. The statistical indicators were summarized in Table 2. Results showed a general good performance of the model in comparison with the acceptance criteria included in Delta Tool. The bias indicated an underestimation for almost all the locations and pollutants, maybe due to deficiencies in local emission estimation and in boundary conditions. The worst correlation was calculated for summer ozone in correspondence of the urban-background monitoring stations. The FA2 was greater than 50% for all pollutants, while IOA is greater than 0.5 except for  $O_3$ .

Figure 2 (a-b) gives an overview of model performance in terms of the target diagram for hourly  $NO_2$  and daily  $PM_{10}$  concentrations. Each symbol refers to a single station, while the colours represent rural stations (orange), suburban stations (red) and urban-background stations (blue). The MQO was fulfilled for more than 90% of the stations for all these pollutants. The green area circle identifies the fulfilment of the performance criteria. The negative and positive sides of Y axis identify negative and positive biases, while the left and right zone identify errors dominated by correlation or standard deviation.

The symbols were located on the left side of diagram, except for one station for  $NO_2$ , indicating that the error for all pollutants was dominated by correlation. The bias for  $NO_2$  was both positive and negative, while for  $PM_{10}$  daily mean concentrations the underestimation was more evident for all the stations.



**Figure 1.** Annual mean concentrations for (a) NO<sub>2</sub>, (b) PM<sub>2.5</sub> ( $\mu\text{g}/\text{m}^3$ ) and (d) BaP ( $\text{ng}/\text{m}^3$ ) and (c) 90.4<sup>th</sup> percentile for PM<sub>10</sub> ( $\mu\text{g}/\text{m}^3$ )

**Table 2.** Statistical indicators

Station	Mean obs. ( $\mu\text{g m}^{-3}$ )	Mean mod. ( $\mu\text{g m}^{-3}$ )	BIAS ( $\mu\text{g m}^{-3}$ )	RMSE ( $\mu\text{g m}^{-3}$ )	R	FA2 (%)	IOA
<b>NO<sub>2</sub> hourly (year)</b>							
<i>rural</i>	9.5	9.4	-0.12	10.0	0.33	56	0.55
<i>suburban</i>	13.9	12.0	-1.9	14.7	0.47	57	0.63
<i>urban-background</i>	19.2	20.3	1.14	15.0	0.58	72	0.75
<b>8hDMax O<sub>3</sub> (summer)</b>							
<i>rural</i>	82.9	70.3	-25.8	31.2	0.24	99	0.43
<i>suburban</i>	87.7	71.4	-23.0	28.0	0.38	100	0.46
<i>urban-background</i>	75.3	67.3	-16.2	20.0	0.17	100	0.38
<b>PM<sub>10</sub> daily (year)</b>							
<i>rural</i>	19.3	15.8	-3.5	11.8	0.32	80	0.51
<i>suburban</i>	19.7	17.2	-2.6	8.5	0.43	88	0.68
<i>urban-background</i>	19.4	17.3	-2.1	8.4	0.46	89	0.65
<b>PM<sub>2.5</sub> daily (year)</b>							
<i>rural</i>	11.4	13.5	2.1	7.3	0.55	80	0.64
<i>suburban</i>	14.9	14.0	-0.9	6.6	0.69	89	0.81
<i>urban-background</i>	-	-	-	-	-	-	-

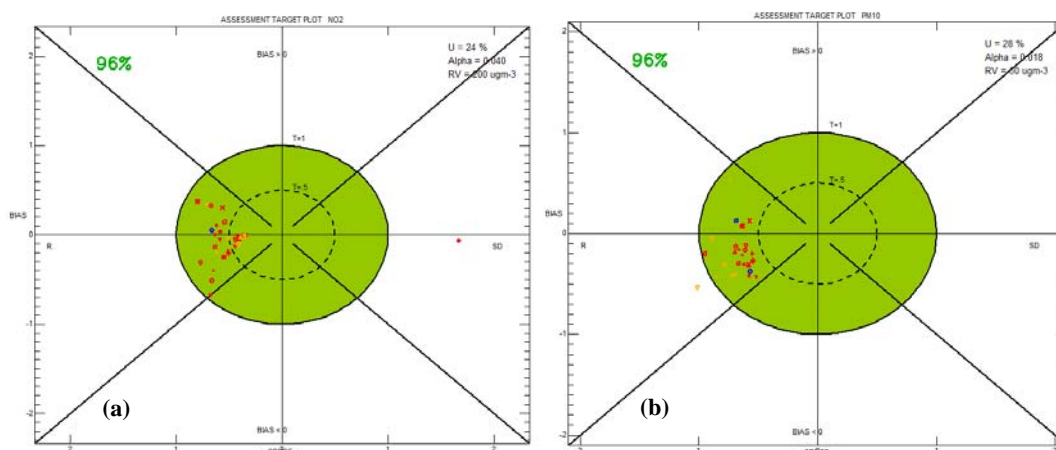


**Figure 2.** Target plot for NO<sub>2</sub> hourly values (a) and (b) daily mean PM<sub>10</sub> concentrations.

## CONCLUSIONS

A modelling system was applied to assess the air quality levels over the Apulia region. The simulations were performed for the year 2013, allowing the comparison between modelled data and the reference values set in the regulations. The results showed some exceeding of the limit values as regard the PM<sub>10</sub> and BaP species; some of these exceeding occurred in areas where the observations are not yet available. These results suggest the need to improve the monitoring network by locating some stations in such areas. The model performance was estimated by using the DELTA software package, showing a good behaviour of the model, with a tendency to underestimate the PM<sub>10</sub> levels. Future improvements will consider the application of data assimilation/fusion techniques and source apportionment studies to better analyse the influence of different sources on air quality levels.

## REFERENCES

- Binkowsky, 1999 The aerosol portion of Models-3 CMAQ. In Science Algorithms of the EPA Models-3 Community Multiscale Air Quality (CMAQ) Modeling System. Part II: Chapters 9-18. EPA-600/R-99/030, D.W. Byuan and J.K.S. Ching (Eds). National Exposure Research Laboratory, US. Environmental Protection Agency.
- Georgieva, E., Syrakov, D., Prodanova, M., Etropolecka, I. and Slavov, K., 2015: Evaluating the performance of WRF-CMAQ air quality modelling system in Bulgaria by means of the DELTA tool, *Int. J. Environment and Pollution*, **57**, 272-282.
- Guenther, A, Karl, T, Harley, P, Wiedinmyer, C, Palmer, PI, Geron, C (2006) Estimates of global terrestrial isoprene emissions using MEGAN (Model of Emissions of Gases and Aerosols from Nature), *Atmos. Chem. Phys.*, **6**, 3181-3210.
- Mircea, M., Ciancarella, L., Briganti, G., Calori, G., Cappelletti, A., Cionni, I. Costa, M., Cremona, G., D'Isidoro, M., Finardi, S., Pace, G., Piersanti, A., Righini, G., Silibello, C., Vitali, L., Zanini, G. (2014) Assessment of the AMS-MINNI system capabilities to predict air quality over Italy for the calendar year 2005. *Atmospheric Environment*, **84**, 178-188.
- Pernigotti, D., Gerboles M., Belis, C.A. and Thunis, P., 2013: Model quality objectives based on measurement uncertainty. Part II: NO<sub>2</sub> and PM<sub>10</sub>, *Atmospheric Environment*, November, **79**, 869-878.
- Schell, B., Ackermann, I.J., Hass, H., Binkowski, F.S. and Ebel, A. (2001). Modeling the formation of secondary organic aerosol within a comprehensive air quality model system. *Journal of Geophysical Research* **106**
- Thunis, P., Pernigotti, D. and Gerboles M., 2013: Model quality objectives based on measurement uncertainty. Part I: Ozone, *Atmospheric Environment*, November, **59**, 476-482.

**17th International Conference on  
Harmonisation within Atmospheric Dispersion Modelling for Regulatory Purposes  
9-12 May 2016, Budapest, Hungary**

---

**URBAN TRAFFIC EMISSION MODELLING FOR POLICY-RELATED APPLICATIONS**

*Oxana Tchepele and Daniela Dias*

CITTA, Department of Civil Engineering, University of Coimbra, Pólo II, 3030-788, Portugal

**Abstract:** The prime objective of the current work is evaluation of traffic related emission inventory based on inter-comparison of bottom-up and top-down methodologies. For this purpose, FAIRMODE emission benchmarking tool was applied for Coimbra city at local and regional scales. Additionally, a policy-related application comprising the potential implementation of a Low Emission Zone in historic city centre is evaluated.

**Key words:** urban area, road traffic, emission modelling, DELTA-tool, bottom-up inventory

## **INTRODUCTION**

Given the widespread exceedances of air quality limits observed in European cities (EEA, 2012), the reliable characterization of key pollution sources is an urgent task. Therefore, the development of accurate atmospheric emission inventory is recognized as an important step in an air quality management process, especially when it is used to design effective control measures to mitigate the adverse impact of air pollution and to track the success of implemented policies (ETC/ACM, 2013).

Emission inventories are typically developed based on two different methodological concepts often referred to as “top-down” and “bottom-up” approach. Overall, the main difference between both approaches relies on the specificity of the emission factor selected and the spatial and temporal data aggregation level. However, developing an accurate emission inventory for urban areas, which are characterized by high spatial and temporal variability in air pollution levels, poses a very challenging task. Despite much work has been performed towards to improve the methodologies used for quantification of atmospheric emissions in urban areas, the reliability and accuracy of the emission data is still of great concern (Davison et al., 2011).

The prime objective of the current work is evaluation of traffic related emission inventory based on inter-comparison of bottom-up and top-down methodologies. For this purpose, FAIRMODE DELTA-tool for emissions was applied at local scale for Coimbra, a midsize Portuguese city, and for the Coimbra Region. The bottom-up estimates are obtained by using transportation and emission modelling. For this purpose, the new plug-in QTraffic developed in open-source QGIS environment is used to quantify atmospheric emissions for the study area with high spatial resolution using traffic flow at road segment level and updated European emission factors based on average-speed approach. The bottom-up inventory is compared with spatially disaggregated emission data set from TNO-MACC3. As an example of policy-related application, influence of traffic restrictions for private cars related with potential implementation of a Low Emission Zone in historic city centre is evaluated additionally to the baseline emission scenario.

## **STUDY DOMAIN**

Coimbra, selected in this study, is the third-largest urban centre in Portugal, after Lisbon and Porto. Two different domains were defined (Figure 1) to analyse traffic related emissions: (i) Coimbra Region with area of 5835 km<sup>2</sup> and total population of 576 506 inhabitants; (ii) Coimbra urban area of 57.8 km<sup>2</sup> with population of 115 022 inhabitants. The reference year for the statistical data and for the emission inventory is 2011.

In the purpose of the current study, a policy-related application comprising the potential implementation of a Low Emission Zone in historic city centre is evaluated additionally to the baseline emission scenario. The zone classified as LEZ was designed to cover the Coimbra's city centre presenting the same geographical delimitation as the cultural heritage protection zone. It was assumed that the LEZ operates 24 hours per day, and the entry restriction was applied to private vehicles that do not meet for Pre-Euro, Euro 1 and Euro 2 emission standards, constituting 47% of Coimbra's car fleet (ACAP, 2011).

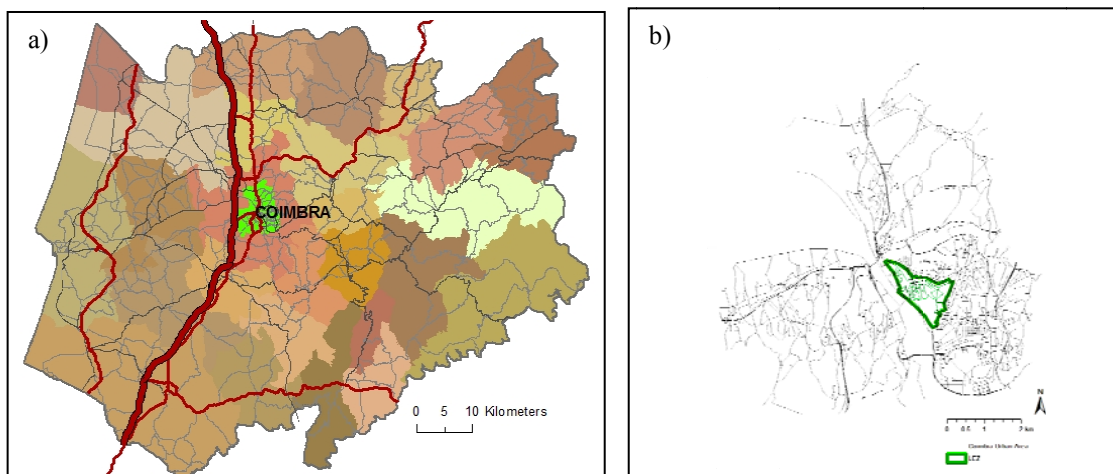


**Figure 1.** Two study domains considered in the study: a) Coimbra Region and b) Coimbra urban area with LEZ.

## METHODOLOGY

The main steps of methodological framework implemented in this study for evaluation of traffic related emissions are schematically shown in Figure 2. The evaluation and comparison of different types of emissions inventories was performed by using the FAIRMODE emission benchmarking tool (Cuvelier, 2015). This tool, commonly denominated as the “ $\Delta$ -Emission Tool”, has been developed in the framework of FAIRMODE, and it is designed to screen and benchmark emission inventories, especially to compare bottom-up and top-down estimates at the country, regional and city scale. The main details of bottom-up and top-down approaches used in this inter-comparison exercise are presented in the following sections.

### Bottom-up approach

The bottom-up estimates are obtained for the road network by using transportation (VISUM) and emission modelling (QTraffic -Traffic Emission and Energy Consumption Model for open-source QGIS), as schematically shown in Figure 2.

Firstly, traffic volume for each road segment is estimated by the four-step transportation model VISUM using detailed data on Origin-Destination of daily journeys. The modelled traffic volumes for private vehicles were used to characterize the baseline scenario and estimated changes in traffic after the introduction of the LEZ were modelled considering that restricted vehicles move to alternate routes outside the LEZ. The only exemption is residents within LEZ. The outputs of this model were used as inputs in the new plug-in QTraffic model to quantify the emission amounts with high temporal and spatial resolution. Additionally to private passenger cars, Heavy Duty vehicles (outside of urban area) and Urban Buses are considered in the data. The results from transportation modelling, comprising traffic flows for each road segment by transport mode and the average traffic speed for each segment, yielded significant data to fill in the subsequent emissions modelling.

The QTraffic model is particularly designed for emission estimations at urban scale with hourly resolution and at road segment level. The model is developed based on the updated European guidelines (EMEP/EEA, 2014) for emission factors and a novel technology for producing dynamic interactive data

visualization. Also, it is implemented as a plug-in for open-source QGIS environment and integrates D3.js library with the Python programming. The road traffic emissions are estimated individually for each road segment based on an average speed approach. Several vehicle categories are distinguished by the model. The current version of QTraffic is prepared to calculate road traffic hot emissions for several pollutants including ozone precursors; greenhouse gases; acidifying substances; particulate matter; carcinogenic species. For the inter-comparison purpose of the current study, exhaust emissions from gasoline, diesel and LPG vehicles are estimated separately.

### **Top-down approach**

A top-down methodology was applied to disaggregate the anthropogenic emissions, using the European top-down emission inventory TNO-MACC3 (Kuenen et al., 2014) available in the FAIRMODE  $\Delta$ -Emission Tool. This inventory is defined on a regular grid with resolution of  $0.125^\circ \times 0.0625^\circ$ . Quantitative information is provided for the main atmospheric pollutants: CO<sub>2</sub>, CO, NH<sub>3</sub>, VOC, NO<sub>x</sub>, PM<sub>10</sub>, PM<sub>2.5</sub>, SO<sub>2</sub>, CH<sub>4</sub>, which are classified according to the Selected Nomenclature for sources of Air Pollution (SNAP). Road transport emissions (SNAP 7) are distinguished between: 5 subsectors: exhaust emissions of gasoline road transport (SNAP 7.1); exhaust emissions of diesel road transport (SNAP 7.2), exhaust emissions of LPG road transport (SNAP 7.3), non-exhaust volatilization (only VOC emissions) (SNAP 7.4) and non-Exhaust brake wear, tire wear, road wear (SNAP 7.5).

The computation of top-down emissions over the study domain was performed by using FAIRMODE  $\Delta$ -Emission Tool. For this purpose, the annual emissions from road transport for each pollutant are spatially disaggregated from the top-down cell in the inventory into sub-cells of  $1 \times 1 \text{ km}^2$ . The contribution of emissions on a sub-cell to the top-down total is considered by the  $\Delta$ -Emission Tool only if the center of the sub-cell is located within the domain. Therefore, despite the top-down spatial resolution of 1 km is considered for the inter-comparison, the top-down emissions are uniformly distributed over the emission cell. In order to maintain a consistency with road traffic emissions obtained by the bottom-up approach for both scenarios analyzed, the most recent emission inventory TNO-MACC3 available, corresponding to 2011, has been used.

**Figure 2.** Methodological simulation framework.

## **RESULTS AND DISCUSSION**

The results for Coimbra are analysed at local and regional scales for SNAP 7, SNAP 7.1 and SNAP 7.2. Statistical parameters provided for the study area by the benchmarking tool are presented in Figure 3 and Figure 4. Thus, emissions ratio obtained from Bottom-Up (BUP) versus Top-Down (TOD) inventory (Figure 3) shows underestimation of the user defined emissions in comparison with the MACC inventory

at regional scale, while urban inventory reveal higher values from the Bottom-Up estimates for almost all the pollutants of SNAP7 (S7). However, emissions from gasoline (S7.1) and diesel (S7.2) subsectors contribute differently to the total values. In general, gasoline exhaust emissions are higher from BUP for both, regional and local scales, with biggest discrepancy for NOx achieving the ratios of about 3.7 and 8.8 respectively.

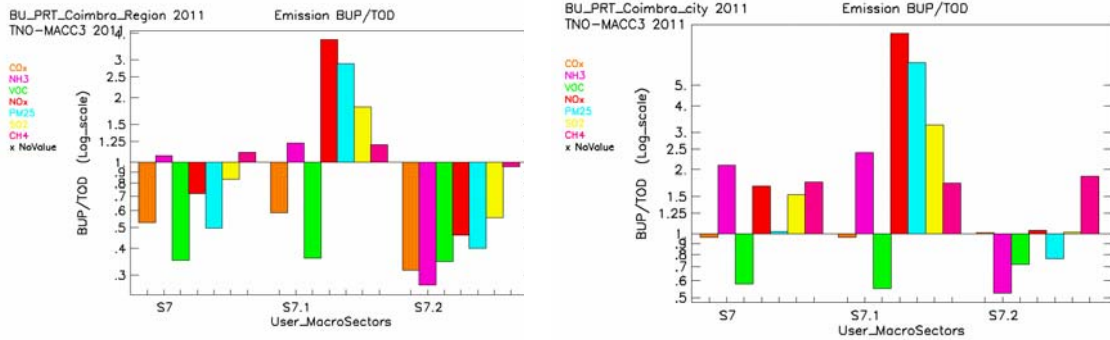


Figure 3. Emission ratio between BottomUp and TopDown inventories.

The differences between the inventories allocated in terms of activity data and emission factors are presented in Figure 4 using the Diamond diagram. Better agreement between the inventories is verified for local scale data with most of the points positioned inside of the red diamond shape (factor 2). The main outliers are associated with SNAP 7.1 showing underestimations for the emission factors and overestimation for the activity data. These problems may be related with different issues. Thus, higher proportion of gasoline vs diesel vehicles considered in the user-defined dataset may be associated with higher activity data for SNAP 7.1 and lower values for SNAP 7.2. On the other hand, simplified methodology implemented to estimate regional traffic flow for Heavy Duty vehicles may lead to significant underestimation of diesel-related emissions. The discrepancy in the emission factors is probably related with the vehicle age distribution considered in BUP inventory. Additionally, it should be stressed that only hot-engine emissions are included in the user-defined inventory. This fact should result in a discrepancy between the two inventories at local scale only. However, it is not clear how cold-start emissions are processed during the TOD disaggregation process.

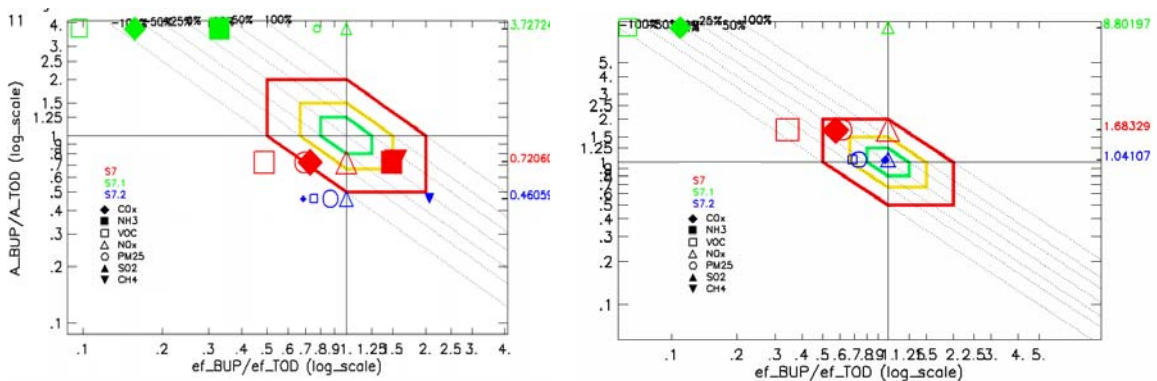


Figure 4. Diamond diagram corresponding to a) regional and b) local inventories for Coimbra.

As an example of policy related application, potential implementation of Low Emission Zone (LEZ) in Coimbra historic centre is considered additionally to the baseline scenario at city scale. The main result of this application was that PM10 and NO2 emissions from private cars would decrease significantly inside the LEZ (63% and 52%, respectively). However, total emissions for the urban area will increase of about

1.2% and 1.5% respectively in the PM10 and NOx due to longer alternative routes generated by LEZ entrance restrictions. Also, spatial distribution of these emissions within the urban area will change significantly. The inter-comparison of the inventories based on total emission values is not sensitive for the such scenarios.

## **CONCLUSIONS**

In this work the methodology developed within FAIRMODE project for inter-comparison of Bottom-Up and Top-Down emission inventories is implemented for different scales and scenarios. The benchmarking tool provide an important insight on potential sources of inconsistency presented in the inventories in terms of the emission factors and activity data. However, DELTA-tool is not sensitive to the changes related with spatial redistribution of the emissions if total urban emissions are not affected as could occur in policy relevant scenarios at urban-scale (e.g. Low Emission Zones). For this purpose, an additional set of parameters will be required for the spatial analysis. Adopting an inter-comparison approach, this study provides insight on potential improvement of urban scale inventories for road traffic emissions to be used in policy-related applications.

## **ACKNOWLEDGMENTS**

This research was carried out within the framework of projects EMSURE (CENTRO-07-0224-FEDER-002004) and TRAPHIC (PTDC/ECM-URB/3329/2014).

## **REFERENCES**

- ACAP, 2011: Estatísticas do Sector Automóvel.
- Cuvelier, C, 2015: Users manual Delta\_Emis Tool V2.0
- Davison, S., van den Elshout, S., Wester, B., 2011: Integrated Urban Emission Inventories, CiteAIRII, Common Information to European Air, Interreg IVC Programme.
- EEA, 2012: Indicator: Exceedance of Air Quality Limit Values in Urban Areas. European Environment Agency, Copenhagen, Denmark.
- EMEP/EEA, 2014: Exhaust emissions from road transport. Passenger Cars, Light-Duty Trucks, Heavy-Duty Vehicles Including Buses and Motor Cycles. European Monitoring and Evaluation Programme (EMEP) Air Pollutant Emission Inventory Guidebook 2013, updated July 2014, Technical report No 12/2013, 146 pp.
- ETC/ACM, 2013. How to start with PM modelling for air quality assessment and planning relevant to the Air Quality Directive, ETC/ACM Technical Paper 2013/11.

**17th International Conference on  
Harmonisation within Atmospheric Dispersion Modelling for Regulatory Purposes  
9-12 May 2016, Budapest, Hungary**

---

**FAIRMODE'S EU COMPOSITE MAPPING EXERCISE**

*Stijn Janssen<sup>1</sup> and Philippe Thunis<sup>2</sup>*

<sup>1</sup> Unit Environmental Modelling, VITO, Boeretang 200, 2400 Mol, Belgium.

<sup>2</sup> Directorate-General Joint research Centre, Institute for Environment and Sustainability,  
Ispra, Italy

**Abstract:** Within the context of FAIRMODE's Working Group 1 on Assessment, an exercise is setup in which national, regional or local air quality maps are collected and compiled into a so called "EU Composite Air Quality Map". The objective of the initiative is to gain further insight in air quality mapping for policy support in European Member States, regions and cities and to use the composite map and the lessons learnt during the process to provide further guidance for air quality model applications. The first prototype is made up out of 47 contributions and covers a large part of Europe. FAIRMODE is currently organising follow-up actions to collect feedback and lessons learnt.

**Key words:** FAIRMODE, air quality assessment

## **INTRODUCTION**

One of the aims of FAIRMODE is to harmonize modelling practices and provide guidance to EU Member States on the use of models in the framework of the Air Quality Directive. A recent survey completed by the National Contact Points pointed out that modelling activities have a clear added value to the policy making process but there is still a lack of clarity in legislation and a lack of common guidance on how to apply models in support of the implementation of the Air Quality Directive.

Over the last couple of years FAIRMODE-WG1 has focused on a QA/QC methodology (Model Quality Objectives, DELTA) and a Benchmarking process for air quality assessment. There is more and more consensus within the community on the proposed methodologies and first steps towards a CEN standardization process have been made.

Although tackling the QA/QC problem is for sure a big step in the right direction to provide common guidance, it is not sufficient. Remaining open questions within the modelling community are for example: what is the appropriate model setting (adequate resolution, adequate assumptions...)? how best to combine modelling results with monitoring data...? Providing answers to those questions is seen as the next challenge for WG1.

## **METHODOLOGY**

In order to open the discussion on the questions mentioned above, FAIRMODE-WG1 initiated an activity aiming at collecting and assembling modelled air quality maps, following the work initiated in the ETC/ACM pilot study (de Smet et al, 2013). The objective is to create a bottom-up composition map of air quality over Europe. National, regional or urban agencies or modelling teams were encouraged to provide their best available air quality map for their particular region. In the first phase, it was decided to limit the exercise to NO<sub>2</sub> and PM<sub>10</sub> annual averaged maps.

The first data collection started in Autumn 2015. In order to collect the maps, a dedicated upload webpage was setup within the FAIRMODE website. Interested parties were able to upload their air quality maps and provide essential meta information such as model name and version, projection system, reference year, contact details of the modelling team etc. By the end of 2015, 47 unique contributions were collected. Detailed information about those individual contributions can be found in Table 1.

**Table 1.** Overview of all contributions in the first prototype of the EU Composite Mapping Exercise. Per contribution, the country, region or city, contributing institute, contact person and model applied are given

Country	Region/City	Institute	Contact person	Model
<b>Austria</b>	Austria	ZAMG	Hirtl Marcus	WRF-Chem
	Styria	Federal state government of Styria	Payer Ingrid	Gral-Graz2
	Linz	Linz - Amt der OöLandesreg.	Oitzl Stefan	GRAL-Linz
<b>Belgium</b>	Belgium	IRCEL	Fierens Frans	RIO
	Flanders	IRCEL	Fierens Frans	RIO-IFDM
	Antwerp	VITO	Lefebvre Wouter	RIO-IFDM- OSPM
<b>Croatia</b>	Croatia	DHZ	Sonja Vidic	EMEP
<b>Cyprus</b>	Cyprus	University Thessaloniki	Tsegas Georgios	MARS-aero
	Nicosia	University Thessaloniki	Tsegas Georgios	MARS-aero
	Famagusta	University Thessaloniki	Tsegas Georgios	MARS-aero
	Limassol	University Thessaloniki	Tsegas Georgios	MARS-aero
	Larnaca	University Thessaloniki	Tsegas Georgios	MARS-aero
	Paphos	University Thessaloniki	Tsegas Georgios	MARS-aero
<b>Czech Republic</b>	Czech Republic	CHMI	Benešová Nina	RIMM
<b>Denmark</b>	Denmark	Ahrus University	Jesper Heile Christensen	DEHM
<b>Estonia</b>	Estonia	KLAB	Erik Teinemaa	SMHI Grid model
<b>Finland</b>	Finland	Finnish Meteorological Institute	Karppinen Ari	SILAM
<b>France</b>	France	INERIS	MELEUX Frederik	CHIMERE
<b>Germany</b>	Germany	Umweltbundesamt	Nordmann Stephan	RCG
	Germany	Research Center Juelich	Krajsek Kai	EURAD_IM
<b>Italy</b>	Italy	ENEA	Ciucci Alessandra	AMS-MINNI
	Emila Romagna	ARPA Emilia Romagna	Stortini Michele	NINFAPESCO
<b>Netherlands</b>	Netherlands	RIVM	Joost Wesseling	NL-OPS
<b>Norway</b>	Norway	NILU	Vogt Matthias	Basemap
	Oslo	NILU	Vogt Matthias	Episode
<b>Poland</b>	Poland	Ekometria	Malgorzata Paciorek	CAMx
	Dolnoslaskie Voivodship	Ekometria	Malgorzata Paciorek	CALPUFF
	Lodzkie Voivodship	Ekometria	Malgorzata Paciorek	CALPUFF
	Mazowieckie Voiv.	Ekometria	Malgorzata Paciorek	CALPUFF
	Opolskie Voivodship	Ekometria	Malgorzata Paciorek	CALPUFF
	Podlaskie Voivodship	Ekometria	Malgorzata Paciorek	CALPUFF
	Pomorskie Voivodship	Ekometria	Malgorzata Paciorek	CALPUFF
	Warminsko-mazurskie Voivodship	Ekometria	Malgorzata Paciorek	CALPUFF
	Zachodniopomorskie Voivodship	Ekometria	Malgorzata Paciorek	CALPUFF
<b>Portugal</b>	Portugal	Universidade de Aveiro	Monteiro Alexandra	CHIMERE
<b>Slovakia</b>	Slovakia	SHMU	Matejovicova Jana	IDWA
	Slovakia	SHMU	Matejovicova Jana	CEMOD
<b>Spain</b>	Mainland Spain and the Balearic Islands	CIEMAT	Theobald Mark	CHIMERE
	Canary Islands	Barcelona Supercomputing Cent.	Pay Maria Teresa	CALIOPE
	Iberian Peninsula and Balearic Islands	Barcelona Supercomputing Cent.	Pay Maria Teresa	CALIOPE
	Madrid	Barcelona Supercomputing Cent.	Pay Maria Teresa	CALIOPE
	Andalucia	Barcelona Supercomputing Cent.	Pay Maria Teresa	CALIOPE
	Catalonia	Barcelona Supercomputing Cent.	Pay Maria Teresa	CALIOPE
	Spain	Technical Univ. Madrid (UPM)	Borge Rafael	CMAQ
<b>Sweden</b>	Sweden	SMHI	Backstrom Hans	SIMAIR
<b>UK</b>	UK	Ricardo-AEA	Brookes Daniel	PCMBK
	London	CERC	Kate Johnson	ADMS-Urban

All the individual maps were assembled into the first prototype of the EU Composite Map. The result for the annual averaged  $PM_{10}$  maps is given in Figure 1. During the process, the individual maps were not resampled or interpolated to a standard grid and care was taken to maintain the data sets as provided by the participant. As can be observed from the figure below, a large part of Europe<sup>2</sup> is already covered in this first prototype. The contributions can be classified according to their spatial coverage ranging from the national down to the local level. A segregation into national, regional and urban scale maps is presented in Figure 2.

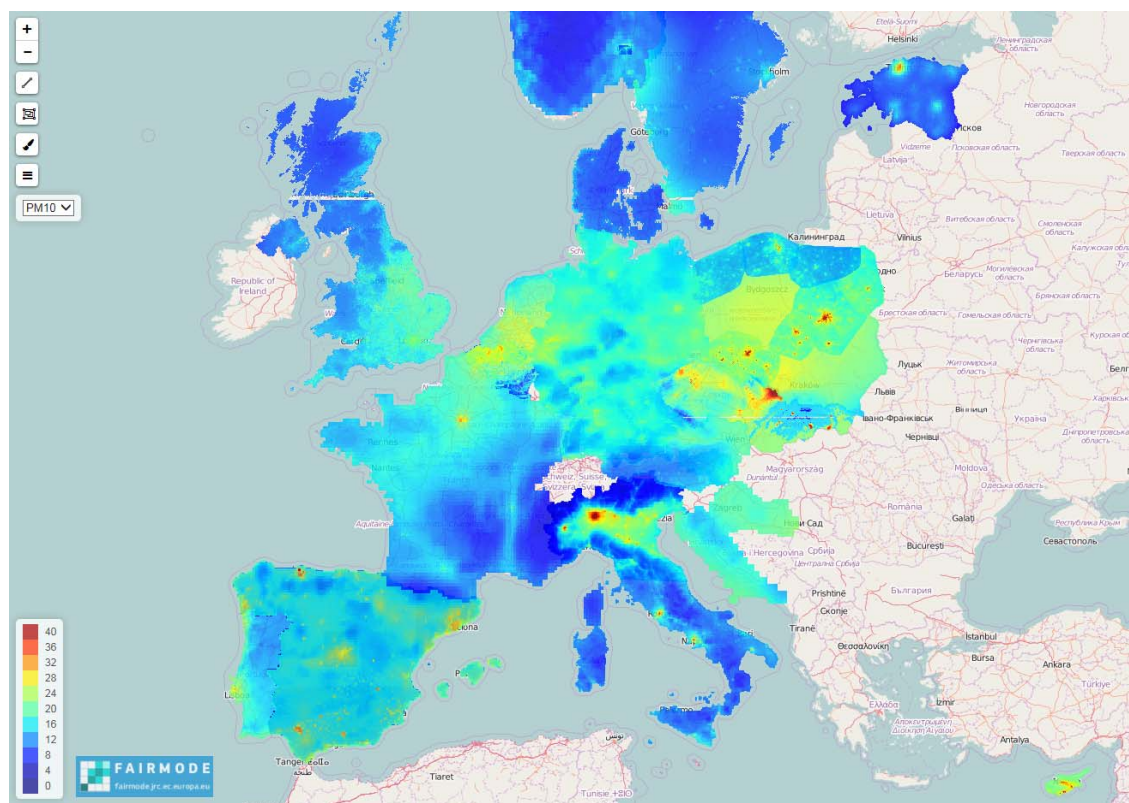


**Figure 1.** EU Composite Map for  $PM_{10}$  for the year 2012. The map is composed out of 47 individual contributions as detailed in Table 1.

<sup>2</sup> Note that the FMI and UMP contribution were delivered but not uploaded in the final system due to data format reasons. This shortcoming will be solved in the next update.

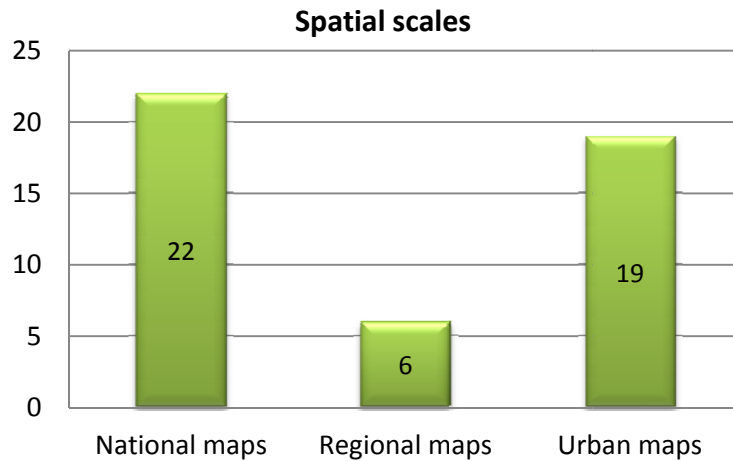


**Figure 2.** Contributions classified according to their spatial scales. Note that regional maps refer to maps produced by regional authorities and covering sub-national domains.

In order to support the analysis of the maps, a web based visualization platform was setup and made available via the FAIRMODE website. The platform allows zooming into a specific domain of interest, to enable or disable individual maps, to modify the colour legend and to draw a concentration profile along a user defined transect. An example of such a concentration profile is given in Figure 3. The concentration profile turns out to be a useful instrument to explore for example concentration differences at inter-regional or inter-national borders.

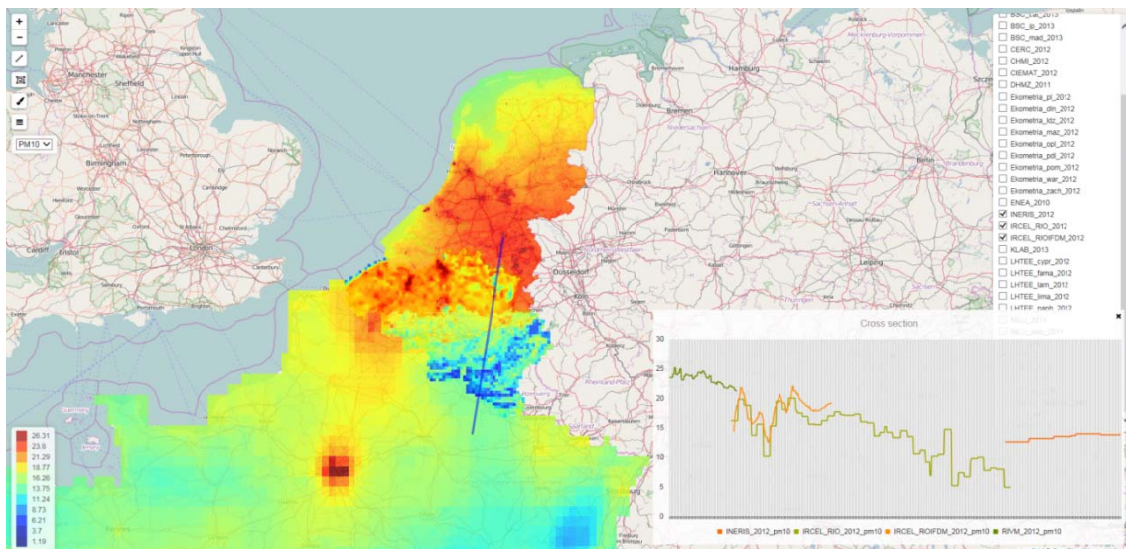


**Figure 3:** Concentration profile (right bottom) along a user defined transect (blue line). PM<sub>10</sub> concentration maps are visible for the Netherlands, Belgium and France.

## **DISCUSSION AND OUTLOOK**

The first prototype of the EU Composite Mapping clearly demonstrates the potential of such an European wide initiative. The mapping exercise will be used as common platform within FAIRMODE as a catalyst to trigger discussions on:

- Border effects which are visible between neighbouring regions or countries
- Use of data assimilation or data fusion techniques to produce air quality maps
- Quality and consistency of underlying emission inventories
- Choice of an adequate spatial resolution for a particular application
- ...

Furthermore, the exercise can also be used to convince countries or regions that are not yet using models on a regular basis to participate in the process.

In summary, the objective of this exercise is in the first place capacity building. The platform will improve comparability of assessment methodologies and will make it easier to learn from each other. Therefore, the platform is hosted in a “safe space” (the FAIRMODE website) without any link to the formal compliance checking processes.

However, a long term objective of the initiative is to contribute also to the e-Reporting process. Some Member States are already reporting modelling data in the official data flows and more Member States are expected to do so in the future. However, also here is a clear lack of guidelines on the use of models and reporting formats. It is not the objective of this initiative to deliver model data for the e-Reporting process but it is obvious that FAIRMODE can prepare the ground for a possible harmonized approach and contribute to reporting guidelines.

## **REFERENCES**

de Smet Peter, de Leeuw Frank, Horálek, Jan, Kurfürst Pavel, (2013) A European compilation of national air quality maps based on modelling, ETC/ACM Technical Paper 2013/3.

**17th International Conference on  
Harmonisation within Atmospheric Dispersion Modelling for Regulatory Purposes  
9-12 May 2016, Budapest, Hungary**

---

**COMPARING AIR QUALITY MODEL PERFORMANCE FOR PLANNING APPLICATIONS**

*Michel Vedrenne<sup>1,2</sup>, Julio Lumbreras<sup>1</sup>, Rafael Borge<sup>1</sup>, Alain Clappier<sup>3</sup>, Philippe Thunis<sup>4</sup>,  
and M<sup>a</sup> Encarnación Rodríguez<sup>1</sup>*

<sup>1</sup>Department of Chemical & Environmental Engineering, Technical University of Madrid (UPM),  
Madrid, Spain

<sup>2</sup>Air & Environmental Quality, Ricardo Energy & Environment, London, United Kingdom

<sup>3</sup>Laboratoire Image Ville Environnement, Strasbourg University, Strasbourg, France

<sup>4</sup>Joint Research Centre, European Commission, Ispra, Italy

**Abstract:** The current policy making needs for emission abatement of air pollutants in Europe call for having simple yet robust tools that allow evaluating the effect of measures and sorting those that produce the most significant effects. As a result, the FAIRMODE Planning Working Group (WG4) seeks to develop a consistent framework for streamlining the understanding of models in order to identify more efficiently the relationship between changes in emissions and their effect in ambient concentration through a series of indicators or potencies. The comparison of sector-specific potencies was carried out using the Delta Tool for the AERIS integrated assessment model for the Iberian Peninsula and the SERCA modelling system, on which it is based. Air quality observations from 11 monitoring stations located in Spain and Portugal were used as independent comparison dataset, focusing on a winter and summer month (January and August), as well as on an annual basis. The comparison revealed that the main difference between AERIS and SERCA is the description of the non-linear relationship between changes in emissions and the formation of secondary pollutants (e.g. secondary particles, ground-level ozone). This is a consequence of the linear simplification that was used to construct AERIS, as opposed to the deterministic formulation that is contained in SERCA and is basically composed of the WRF-CMAQ ensemble. The comparison also suggested differences in the ability to reproduce seasonal variations of pollutants, something which is a consequence of the annual character of AERIS. However, AERIS is able to reproduce its parent air quality model (SERCA) and complies with the general modelling performance requirements stipulated under FAIRMODE. Moreover, its simplified approach, as evidenced by the values of the potencies allows identifying the interactions between emissions and concentrations, facilitating choosing mitigation measures depending on the abatement needs. Additionally, the ability of AERIS to reproduce ambient concentrations under a simplified approach makes it a robust alternative to SERCA for informing policy making and planning in Spain.

**Key words:** *Integrated Assessment Modelling, Air Quality Planning, Policy Making, Model Evaluation, FAIRMODE*

## **INTRODUCTION**

The use of air quality models for supporting the selection of cost-effective measures to reduce air pollution has been an essential part of environmental policy planning in Europe, in order to assess compliance with the targets of Directive 2008/50/EC and to ensure that the associated impacts are kept at a minimum (EEA, 2011). While reducing ambient levels of airborne pollutants is often the objective of the process, decision makers are only able of acting on a given number of emission sources and are limited by technical or financial constraints. Although the ownership of air pollution models traditionally lies within the scientific community, the fact that policy makers are evermore requiring their use for the appraisal of abatement policies highlights the need of constructing simplified yet robust tools that simplify the dialogue at the “science-policy” interface (Carnevale et al., 2016).

The Forum for Air Quality Modelling (FAIRMODE) initiative aims for the establishment of a conceptual framework that illustrates the complex relationships between emissions and concentrations, in order to increase the transparency of a model and easily identify the abatement potential of measures without the need of configuring and running the model itself (Thunis et al., 2015). An essential part in the construction of policy-tailored air quality modelling tools is evaluating against a deterministic model

(usually its originating “parent” model) in order to demonstrate that the difference in performance is minimal or at least that there is a balance between the loss of performance and the gain in swiftness in the policy-science interaction.

The AERIS integrated assessment model was designed to provide national-level policy support for Spain and Portugal relying on parameterisations based on source-receptor matrices of the SERCA modelling system, composed by the WRF-SMOKE-CMAQ models. In previous studies the performance of AERIS was contrasted against that of SERCA in (i) reproducing average concentrations of airborne pollutants and (ii) in responding to individual and simultaneous changes of emission sectors (Vedrenne et al., 2013; 2014). In this work however, an evaluation of the response of ambient concentrations as a result of variation in emissions is carried out at specific receptors throughout the Iberian Peninsula (e.g. monitoring locations). The results from this evaluation will allow identifying performance differences associated with the simplifications of AERIS with respect to SERCA and will illustrate the dependency degree of the concentrations of specific airborne pollutants with variations in the emissions of precursors. This evaluation is especially useful for differentiating the interplay of the emissions of specific precursors in the formation of secondary pollutants.

To this respect, the methodology for dynamic evaluation proposed within WG4 of FAIRMODE allows quantifying these dependencies in the form of potencies, which is defined as the elasticity of the change of emissions of one or more precursors to the change in concentration of a given pollutant (Thunis et al., 2015). The FAIRMODE methodological framework for dynamic evaluation allows carrying out these model comparisons with the Planning version of the Delta Tool, which provides the output in a graphical and comprehensive format. The details of the comparison of AERIS against SERCA are described in the following sections.

## MATERIALS AND METHODS

### Description of Models

The AERIS model is an integrated assessment model conceived for Spain and the Iberian Peninsula, which addresses air quality variations as a function of percentual variations of emissions against a reference scenario. The model also allows assessing the effect of policy on the air quality metrics defined by Directive 2008/50/EC for numerous pollutants (SO<sub>2</sub>, NO<sub>2</sub>, NH<sub>3</sub>, PM<sub>10</sub>, PM<sub>2.5</sub> and O<sub>3</sub>). The model is also able to determine the impacts on human health, ecosystems and vegetation produced by the concentrations of these pollutants (Vedrenne et al., 2015). AERIS was built by parameterising the response of the SERCA model.

The SERCA model is a multi-scale air quality model composed of the Weather Research and Forecast (WRF) model for the determination of meteorology, the SMOKE emissions processor and the Community Multiscale Air Quality (CMAQ) model for modelling atmospheric chemistry and transport. The SERCA model has been especially configured to provide concentration of pollutants for the Iberian Peninsula and the city of Madrid and has been thoroughly used for policy support purposes at the national and local level (Borge et al., 2008; 2014).

### Description of Methodology

The comparison of the performance of AERIS against its parent air quality model (SERCA) was carried out following the FAIRMODE Working Group 4 methodology for the assessment of models used for planning applications and specified in Thunis and Clappier (2014) and Thunis et al., (2015). This methodology relies on the concept of potency which is an indicator of the elasticity of concentration changes as a function of variation in emissions. The absolute potency is defined as in equation (1).

$$P_{\alpha}^k = \frac{\Delta C_{\alpha}^k}{\alpha E^k} \quad (1)$$

Where  $\Delta C_{\alpha}^k$  is the concentration change between the base case and the emission reduction scenario concentration,  $\alpha$  is the reduction ratio of emissions and  $E^k$  are the emissions of precursor k over the area

A. To carry out the evaluation, a series of independent simulations in which the emissions of precursors are reduced either independently or contemporarily was required. Simulations with changing precursor emissions for the whole of Spain were carried out for the month of January 2007 with both SERCA and AERIS, with the objective of identifying the interactions between emissions and air quality levels.

These simulations consisted of:

- A base case simulation.
- Five simulations where the following precursors were decreased by 50%: nitrogen oxides (NO<sub>x</sub>), sulphur dioxide (SO<sub>2</sub>), ammonia (NH<sub>3</sub>), primary particulate matter (PPM) and volatile organic compounds (VOC).
- Five simulations where the before mentioned precursors were decreased by 90%.
- Two simulations in which all 5 precursor emissions were reduced contemporarily by 50% and 90%.

The evaluation of these potencies was carried out for ground-level ozone (O<sub>3</sub>) and fine particulate matter (PM<sub>2.5</sub>) measured at 11 background monitoring locations in Spain from the EMEP network (Table 1). These stations were selected as their measurements are representative of the concentration values at the resolution of SERCA and AERIS (16 km). The analysis of absolute potencies and the output diagrams in this work was carried out using the Dynamic Evaluation function of the JRC Delta Tool. The total emissions for the determination of the potency for each of the precursors in Spain were obtained from the National Emissions Inventory for 2007.

**Table 1.** Selected monitoring stations for potency analysis

Station	Name	Latitude	Longitude
ES0011R	Barcarrota	38°28'22''N	6°55'14''W
ES0010R	Cabo de Creus	42°19'09''N	3°18'56''E
ES0009R	Campisábalos	41°16'27''N	3°08'33''W
ES0017R	Doñana	37°03'06''N	6°33'19''W
ES0014R	Els Torms	41°23'38''N	0°44'04''E
ES0008R	Niembro	43°26'21''N	4°50'60''E
ES0016R	O Saviñao	42°38'14''N	7°42'16''W
ES0013R	Peñausende	41°14'20''N	5°53'51''W
ES0015R	Risco Llano	39°31'15''N	4°21'11''W
ES0007R	Víznar	37°14'13''N	6°32'03''W
ES0012R	Zarra	39°04'58''N	1°06'03''W

## RESULTS AND DISCUSSION

The results of the analysis explained in the sections above is presented in Figure 1 for fine particulate matter concentrations (PM<sub>2.5</sub>) and in Figure 2 for ground-level ozone (O<sub>3</sub>). In the case of PM<sub>2.5</sub>, model responses in SERCA are heavily dominated by the emissions of PPM and followed by the emissions of NO<sub>x</sub>. In the case of the emissions of PPM, its dominance is significantly higher for episodes than for the average response. The rest of precursors do not show a substantial influence to PM<sub>2.5</sub> according to the model. In the case of AERIS, the resulting PM<sub>2.5</sub> concentrations are also influenced by PPM emissions,

and to a greater extent by the emissions of the rest of precursors ( $\text{NH}_x$  and  $\text{NO}_x$ ). While in the case of AERIS the modelling response is more linear as represented by the coincidence between both lines and central circles for both 50% and 90% variations, SERCA exhibits variations.

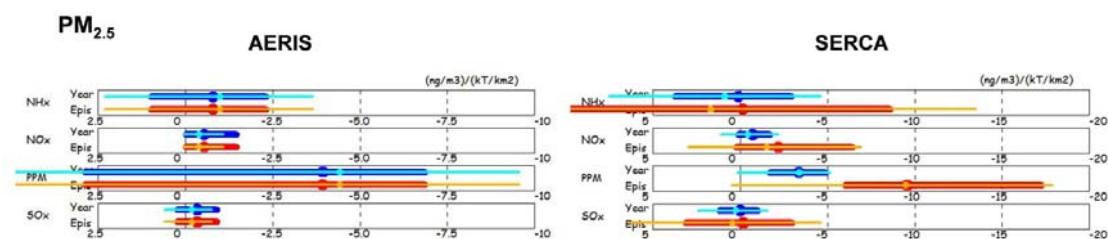


**Figure 1.** Comparison of  $\text{PM}_{2.5}$  absolute potencies from AERIS and SERCA for Spain.

In the case of episodic events, and in particular for SERCA, the potencies obtained indicate the larger control that is available on abating high  $\text{PM}_{2.5}$  episodes rather than average concentrations. When the objective of measures is controlling  $\text{O}_3$ , its levels are conditioned by  $\text{NO}_x$  emissions principally, but the influence of VOC emission controls is also visible (Figure 2). The response of  $\text{O}_3$  to other precursors different to  $\text{NO}_x$  or VOC was not studied due to the negligible effect that was reported in Thunis et al., (2015).

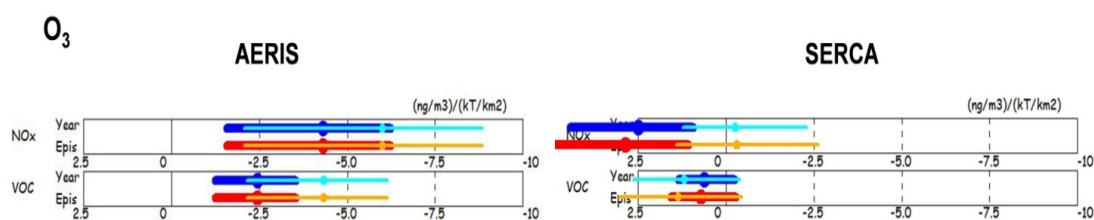


**Figure 2.** Comparison of  $\text{O}_3$  absolute potencies from AERIS and SERCA for Spain.

The summary diagrams presented in Figures 1 and 2 show that there is a different degree of response to emission controls (variations) between the models despite the fact that AERIS is derived from SERCA. The main reasons for the observed discrepancies are the following:

1. Temporal resolutions. AERIS is an “annual model”, which means that it cannot produce hourly outputs in the way that a deterministic model such as SERCA does. In the case of this work and for the month of January, only one value (the monthly average concentration of  $\text{O}_3$ ,  $\text{PM}_{2.5}$ ) was produced; this is the reason why there are no differences between the average and the episodic lines in the diagrams.
2. Statistical parameterisations. AERIS has been developed through a series of source-receptor matrices that provide a shortcut for estimating air pollutant concentrations as a function of changes in emissions. These parameterisations have been developed individually for a number of sectors which correspond to the majority of emissions (and whose sectors are more likely of being affected by policy) in the domain and there is an accumulation of accuracy loss associated with their simultaneous variation. In the case of SERCA, variations are applied on all sources across the domain irrespectively. Additionally, AERIS considers that the relationships between the changes in emissions of  $\text{NO}_x$  and the resulting concentrations of  $\text{NO}_2$  are linear.

## CONCLUSIONS

The dynamic evaluation of the model outputs of AERIS and SERCA has allowed identifying the differences in the dependencies that exist between the concentrations of PM<sub>2.5</sub> and O<sub>3</sub> and the emissions of precursors. In both cases, similarities in the dominance of changes in the emissions of precursors can be seen; in particular, PPM and NO<sub>x</sub> seem to play a substantial role in the formation of PM<sub>2.5</sub> and O<sub>3</sub> respectively for both models. Differences have been seen in the way both models deal with episodic and average behaviours, being this a limitation of AERIS as it has been built as an annual model. The other sources of observed differences are related with modelling assumptions, with the statistical parameterisations and with the fact that AERIS does not consider the totality of the emissions of a specific precursor across the entire domain.

## REFERENCES

- Borge, R., Lumbreras, J., Rodríguez, M.E., 2008. Development of a high-resolution emission inventory for Spain using the SMOKE modelling system: a case study for the years 2000 and 2010. *Environmental Modelling & Software* **23**, 1026-1044.
- Borge, R., Lumbreras, J., Pérez, J., de la Paz, D., Vedrenne, M., de Andrés, J.M., Rodríguez, M.E., 2014. Emission inventories and modeling requirements for the development of air quality plans. Application to Madrid (Spain). *Science of the Total Environment* **466-467**, 809-819.
- Carnevale, C., Douros, J., Finzi, G., Graff, A., Guariso, G., Nahorski, Z., Pisoni, E., Ponche, J.L., Real, E., Turrini, E., Vlachokostas, Ch., 2016. Uncertainty evaluation in air quality planning decisions: a case study for Northern Italy. *Environmental Science & Policy*. In Press. Corrected Proof.
- EEA, 2011. The Application of Models under the European Union's Air Quality Directive: a Technical Reference Guide. Technical report No 10/2011.
- Thunis, P., Pisoni, E., Degraeuwe, B., Kranenburg, R., Schaap, M., Clappier, A., 2015. Dynamic evaluation of air quality models over European regions. *Atmospheric Environment* **111**, 185-194.
- Thunis, P. and Clappier, A., 2014. Indicators to support the dynamic evaluation of air quality models. *Atmospheric Environment* **98**, 402-409.
- Vedrenne, M., Borge, R., Lumbreras, J., de la Paz, D., Rodríguez, M.E., 2013. Development and implementation of an air quality integrated assessment model for the Iberian Peninsula. In: R. San José, J.L. Pérez (Eds.), Proceedings of the 15th International Conference on Harmonisation Within Atmospheric Dispersion Modelling for Regulatory Purposes (HARMO) (2013) ISBN 978-84-695-7353-5
- Vedrenne, M., Borge, R., Lumbreras, J., Rodríguez, M.E., 2014. Advancements in the design and validation of an air pollution integrated assessment model for Spain. *Environmental Modelling & Software* **57**, 177-191.
- Vedrenne, M., Borge, R., Lumbreras, J., Conlan, B., Rodríguez, M.E., de Andrés, J.M., de la Paz, D., Pérez, J., Narros, A., 2015. An integrated assessment of two decades of air pollution policy making in Spain: Impacts, costs and improvements. *Science of the Total Environment* **527-528**, 351-361.

## **TOPIC 4**

# **PARAMETRIZATION OF PHYSICAL PROCESSES IN MESOSCALE METEOROLOGY RELEVANT FOR AIR QUALITY MODELLING**

**17th International Conference on  
Harmonisation within Atmospheric Dispersion Modelling for Regulatory Purposes  
9-12 May 2016, Budapest, Hungary**

---

**A SENSITIVITY ANALYSIS FOR DETERMINING OPTIMUM WRF AND CALPUFF  
CONFIGURATION FOR OPERATIONAL AIR QUALITY FORECAST: APPLICATION TO A  
CASE STUDY IN THE PORT OF HUELVA (SOUTHERN SPAIN)**

*M<sup>a</sup> Ángeles González<sup>1</sup>, Raúl Arasa<sup>1</sup>, Anna Domingo-Dalmau<sup>1</sup>, Ignasi Porras<sup>1</sup>, Miquel Picanyol<sup>1</sup>, Bernat Codina<sup>1,2</sup>, Jesica Piñón*

<sup>1</sup> Technical Department, Meteosim S.L., Barcelona, Spain

<sup>2</sup> Department of Astronomy and Meteorology, University of Barcelona, Barcelona, Spain

**Abstract:** Meteorological inputs are of great importance when implementing an air quality modelling system. The aim of this study is to define a standardized methodology to determine the best meteorological configuration to reduce the uncertainty of the model predictions. To do this, a detailed sensitivity analysis to different parameterizations and schemes of the Weather Research and Forecast (WRF-ARW) model has been realized. The sensitivity of the model to different options: physical and dynamical configurations, different vertical levels distribution, and the impact of the high resolution topography and land use data have been evaluated. A sensitive analysis was done in order to evaluate some simulated meteorological variables (temperature, relative humidity, wind velocity and wind direction) and achieve the optimum WRF configuration. Since the better options for WRF simulations were chosen, a new sensitivity analysis was done to determine the optimum CALPUFF-CALMET configuration for air quality forecasting. Changes in number of vertical levels and physical options were done in this analysis.

The study has been realized in a coastal region of Andalusia, in the South of Spain. A period of 4 months for different climatic seasons was used to calibrate adequately the WRF model. Moreover, 2-year period (2012 and 2013) with the optimum configuration from the previous calibration was validated. Numerical deterministic comparison between observed and modelled data has been the methodology analysis used.

Results show a moderate improvement of meteorological predictions when comparing meteorological forecasts using default WRF model options and forecasts using the optimum WRF model configuration over the region of interest. The same is shown for CALPUFF sensitive analysis, where parameters such wind direction achieved better results when optimum CALMET configuration was selected.

**Key words:** *WRF, CALPUFF, CALMET, Sensitive Analysis, Meteorological Modelling, Air Quality Modelling, Physical options, High Resolution*

## **INTRODUCTION**

The goal of this paper is to achieve the optimum configuration of meteorological model WRF and dispersion model CALPUFF in order to obtain better results in air quality forecasts (Warner, 2011; Stensrud, 2007; Reboredo et al., 2015). A region in Southern Spain, Huelva, was selected for the development of this work. Industrial and port activities, especially aggregate handling and storage piles, are responsible of major of atmospheric pollution existing in this area. An operating prediction system will be used as early warning system and will allow improving the air pollution and risk management associated to the Port of Huelva. The methodology used for sensitive analysis and configurations here defined can be extrapolated to other interesting regions. Meteorological forecasting system developed increases the resolution and the accuracy, not only for meteorological results, but also for air quality and risk management in the zone.

## **METHODOLOGY**

The Port of Huelva is one of the most important industrial sources in the South of Spain. Moreover, this area coexists with the city of Huelva, greenhouse zones and some nature reserves like Doñana Park. Meteorology can greatly affect the atmospheric pollution generated by the Port, because the activities here carried out (loading and unloading operations and material handling) are mainly an important source

of particles; meteorological parameters, such as wind speed and wind direction, are highly significant in dispersion of these particles. In this sense, the meteorology influence the atmospheric pollution generated by port activities, in it-self, is conditioned by the meteorological conditions.

### **Meteorological model**

Air quality levels achieved and the risk management in a complex harbour located very near of metropolitan and protected nature areas made important the implementation of a very accuracy meteorological model in the zone. Also, better results in meteorological modelling will lead more accurate results in air quality modelling. Here is defined the methodology to obtain the optimum WRF configuration, and then it was applied over the Port of Huelva and surroundings.

In Figure 1 modeling domains used in simulations are shown. The WRF model is built over a mother domain (called d01) with 9 km spatial resolution, with three nested domains: d02, with a spatial resolution of 3 km, d03, with 1 km of spatial resolution covering Huelva, and d04, with a spatial resolution of 0.333 km covering the Port of Huelva.



**Figure 1.** Modeling domains for simulations. [Images generated using Google Earth]

Simulations were executed for 30 hours in different periods between 01/01/2012 and 12/31/2013, taking the first 6 hours as spin-up time to minimize the effects of initial conditions. The regional and mesoscale meteorological model used for the study has been the Weather Research and Forecasting - Advanced Research (WRF-ARW) version 3.7 (Skamarock et al., 2008), developed by the National Center of Atmospheric Research (NCAR). The initial and boundary conditions for the operational configuration over domain d01 were supplied by the National Centers for Environmental Prediction (NCEP). For model configuration, calibration and validation, two-way nesting was used for the external domains (d00, d01, d02 and d03) and one-way nesting for d04 innermost domain. Also, in d04 Large-Eddy-Simulation (LES) technique has been applied, which is considered relevant when the horizontal resolution meteorological model works is below 500 m (Dudhia and Wang, 2015).

18 experiments modifying physical options (compared with WRF default configuration), 4 experiments modifying dynamical options, 2 experiments modifying the number and density of vertical levels, 2 experiments modifying land use and topography databases, and 5 experiments applying grid and observational nudging. A sensitivity analysis was done considering the full set of experiments, modifying only one configuration option each time, and holding all else constant. This analysis is going to be the best way to know the optimum configuration for modelling.

### **Air quality dispersion model**

As said before, the coastal region of Huelva is characterized by atmospheric pollution generated as consequence of industrial and port activities among others. Meteorological fields calculated before can be used for air quality and risk management. For this purpose, CALPUFF model was considered; CALPUFF (Scire et al., 2000) is an advanced, integrated gaussian puff modeling system, developed by Atmospheric Studies Group (ASG) and recommended by the United States Environmental Protection Agency (EPA) for atmospheric pollution dispersion studies. This model is appropriated for areas with complex topography and coastal zones like the Port of Huelva.

Domain used in CALPUFF simulation was designed similar to d04 WRF domain, covering the Port of Huelva and surroundings. Horizontal resolution was set in 100 m, in order to achieve reproduce the complex terrain of this area. WRF meteorological fields were adapted by CALWRF model, and then processed by CALMET, taking into account topography information and land use cover. 10 experiments were developed for identifying the better CALMET configuration: changes in number of vertical levels and physical options, such kinematic effects, the O'Brien vertical velocity adjustment, or the diagnostic wind module. Better configuration for the model was selected according to best statistics (Mean Bias, MB, Mean Absolute Gross Error, MAGE, Root-Mean-Square Error, RMSE, and the Index of Agreement, IOA), calculated for each experiment.

Apart from meteorological information, CALPUFF model needs emissions inputs, provided by AEMM (Air Emission Model of Meteosim, Arasa et al., 2013; 2016). Emissions are calculated by the model after taking information of the Integration Platform Operations Authority of Port of Huelva. This platform includes data about emission types, emission sources and their physical characteristics, handled materials stored, and emission process times. With this information and specific emission factors for different materials, AEMM gives emission predictions for TSP, PM<sub>10</sub> and PM<sub>2.5</sub>. Simultaneously, emissions are also estimated considering some mitigation measures: water sprays, cleaning programmes, or aestivation good practices. The last step, postprocessing, is done with CALPOST module. Analysis of dispersion results and statistics are calculated by CALPOST with the purpose of compare with legislated values.

## RESULTS

A sensitive analysis was done in order to determine the optimum configuration for WRF model. Physical options, dynamical options and physiographic databases were manipulated and tested. Some meteorological parameters were modelled and compared with observed values, specifically temperature, wind speed, wind direction and relative humidity in high resolution domains (d03 and d04). Results obtained by the whole group of experiments were compared individually with an experiment done with WRF default configuration. A local meteorological station inside the Port of Huelva (37.20°N, 6.93°W) was incorporated to compare the performance obtained in these high resolution domains. A statistical evaluation (Denby et al., 2008) was done for each experiment; metrics have been calculated from hourly data of the model and observations. For summarize the sensitive analysis, in Table 1 are shown all the selected options for that configuration whose statistical evaluation was the best. This configuration showed the best results for temperature, wind speed, wind direction and relative humidity predictions.

**Table 1.** Configuration options selected as optimum for meteorological forecast over the coastal region of Huelva

Scheme or parameterization	Selected option
Initialization	GFS 0.25°
Microphysics	SBU-Lin
Longwave radiation	RRTMG
Shortwave radiation	Dudhia
Cumulus	Kain-Fritsch
Surface Layer	MM5 similarity
Planetary Boundary Layer	YSU (9, 3 and 1 km) / LES (0,333 km)
Vertical levels number	36
Diffusion 6th order option	Knierel
Diffusion 6th order factor	0.36 (d03)
Damping	Rayleigh
Topography	GTOPO30 (9 and 3 km) / ASTER (1 and 0,333 km)
Land Uses	GLC (9 and 3 km) / CLC2006 (1 and 0,333 km)
Nudging	Grid nudging (9 km) / Observational nudging (3 and 1 km)

Statistical evaluation is also was done for air quality forecast, taking into account some meteorological parameters, by comparing the modelled parameters to the meteorological station observations of

temperature at 2 m, wind speed at 10 m, wind direction at 10 m and relative humidity at 2 m. Options that provided better results, and therefore, were selected, are listed in Table 2; also, metrics obtained for this configuration are shown and compared with benchmarks (Emery and Tai, 2001; Tesche et al., 2002; Arasa et al., 2012) in Table 3. Slight improvement was achieved in wind speed RMSE, and also in wind direction better metrics were obtained, with MB values from 3.73° to 3.20° and MAGE values from 20.18° to 18.86°.

**Table 2.** Configuration options selected as optimum for meteorological forecast over the coastal region of Huelva

Scheme or parameterization	Selected option
Kinematics effects	IKINE Activated
O'Brien vertical velocity adjustment	IOBR Activated
Diagnostic wind module	IWF COD Activated
Vertical levels number	20
Topography	ASTER 1s
Land Uses	CLC2006 100m

**Table 3.** Comparison between modelled and observed values in CALPUFF calibration experiments

Meteorological parameter (reference height)	Statistic	Benchmark	Statistic values for optimum WRF configuration and CALMET default configuration	Statistic values for optimum WRF configuration and CALMET optimum configuration
Temperature (2 m)	MB	< ±0.50 K	0.58	0.58
	MAGE	< 2.00 K	1.19	1.19
	IOA	≥ 0.80	0.98	0.98
Wind speed (10 m)	MB	±0.50 ms <sup>-1</sup>	-1.64	-1.64
	RMSE	< 2.00 ms <sup>-1</sup>	2.26	<b>2.13</b>
Wind direction (10 m)	MB	< ±10.00°	3.73	<b>3.20</b>
	MAGE	< 30.00°	20.18	<b>18.86</b>
Relative humidity (2 m)	MB	< 10.00%	0.89	0.89
	MAGE	< 20.00%	6.29	6.29
	IOA	≥ 0.60	0.93	0.93

An operating prediction system was developed for the Port of Huelva. Meteorological and air quality forecasting had been integrated in a platform which allows visualize all the predictions. Prediction system is actualized four times a day, and various types of air quality forecasting are shown. First, dispersion of each pollutant is calculated without considering mitigation measures in emission estimation. Then, three different mitigation measures (cited above) are added, and therefore three new air quality forecasting are obtained for each pollutant (one with each mitigation measure). This methodology lets the user to compare and to know the differences between different air quality predictions, when mitigation measures in industrial and port activities are considered or not.

Apart from hourly meteorological variables and fields, multiple maps and tables for atmospheric pollution are included in operating prediction system, and they are actualized each six hours in order to obtain the highest accuracy in air quality forecasting. Daily statistics maps for each prediction and pollutant (TSP, PM<sub>10</sub> and PM<sub>2.5</sub>), time series of selected points of interest near the Port of Huelva, windroses and trajectories calculated with HYSPLIT model (Stein et al., 2015) are displayed. As an example, Figure 2 shows some maps for air quality predictions, calculated with CALPUFF model with 100 metres of horizontal resolution, with and without consider mitigation measures.

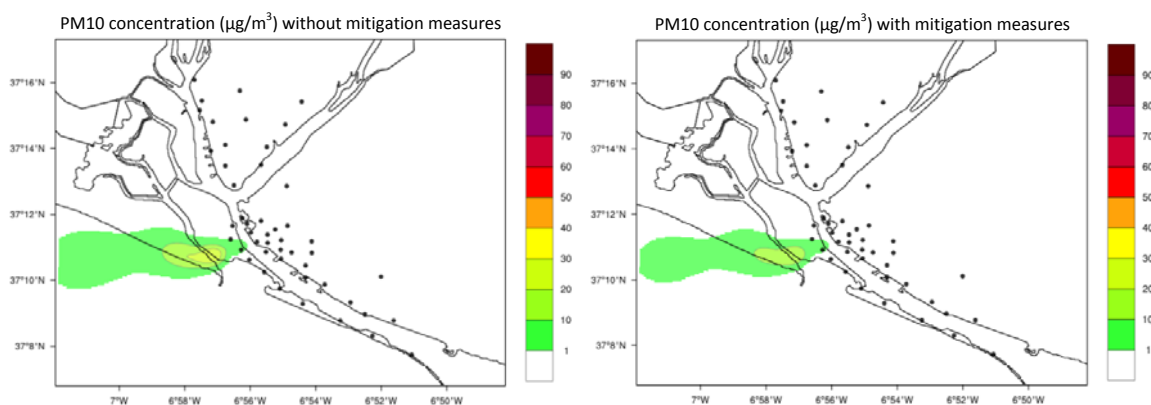


**Figure 2.** Some examples for air quality forecasting for PM<sub>10</sub>.

## CONCLUSIONS

To improve air quality and to manage more efficiently the daily activity of the Port of Huelva, an air quality modelling system has been developed. A standard methodology to select the optimum meteorological and air quality configuration in any region has been defined. Some experiments modifying parameters such physical options, dynamical options, number of vertical levels, or land use and topography databases were carried out. First, a sensitivity analysis was done for WRF model with the purpose of obtain its optimum configuration; then, a similar methodology was developed for CALPUFF model. Both analyses were useful for determining the best options for modelling air quality in the Port of Huelva. Anyway, this meteorological and air quality prediction system could be developed in any complex region of interest.

## ACKNOWLEDGMENTS

This work has been developed within the framework of the contract SAFE AND GREEN PORT funded by FEDER Investigación, Desarrollo e Innovación para el Desarrollo de las empresas Fondo Tecnológico 2007-2013 and partly funded by the Spanish Government through PTQ-12-05244. The authors gratefully acknowledge Port of Huelva and GTD System & Software Engineering for their support and collaboration, and AEMET, EUMETSAT, ESA, NASA and USGS institutions through which it was possible to obtain data used in this paper.

## REFERENCES

- Arasa, R., Soler, M.R. and Olid, M. (2012) Evaluating the performance of a regional-scale photochemical modelling system: Part I ozone predictions. *ISRN Meteorology*, Article ID 860234.
- Arasa, R., Picanyol, M., Porrás, I., Solé, J.M. (2013). Integrated environmental and meteorological forecasting and alert system (SIAM): Air quality and meteorological application for the mining sector. Proceedings to the 3rd International Seminar on Environmental Issues in Mining. 4-6 December 2013, Santiago, Chile.
- Arasa, R., Domingo, A., Vargas, R., 2016. Using a coupled air quality modelling system for the development of an air quality plan in Madrid (Spain). Source apportionment analysis, evaluation of mitigation measures and emission projections. In press.
- Dudhia, J. and Wang, J. (2015) WRF Advanced Usage and Best Practices. 16th WRF Annual Workshop, Boulder, Colorado, USA.
- Denby, B., Larssen, S., Guerreiro, C., Douros, J., Moussiopoulos, N., Fragkou, L., Gauss, M., Olesen, H. and Miranda, A.I. (2008). Guidance on the use of models for the European Air Quality Directive. ETC/ACC Report.
- Emery, C., Tai, E. (2001) Enhanced Meteorological Modeling and Performance Evaluation for Two Texas Ozone Episodes. Final report submitted to Texas Natural Resources Conservation Commission, prepared by ENVIRON, International Corp, Novato, CA.
- Reboredo, B., Arasa, R. and Codina, B. (2015) Evaluating Sensitivity to Different Options and Parameterizations of a Coupled Air Quality Modelling System over Bogotá, Colombia. Part I: WRF Model Configuration. *Open Journal of Air Pollution*, **4**, 47-64.

- Scire, J.S., Strimaitis, D.G., Yamartino, R.J. (2000). A User's Guide for the CALPUFF Dispersion Model. Earth Tech, Inc, 196 Baker Avenue, Concord, MA 01742 USA.
- Skamarock, W. C., Klemp, J.B., Dudhia, J., Gill, D.O., Barker, D.M., Duda, M.G., Huang, X.Y., Wang, W., Powers, J.G. (2008). A description of Advanced Research WRF V3. NCAR Tech. Note 475.
- Stein, A.F., Draxler, R.R., Rolph, G.D., Stunder, B.J.B., Cohen, M.D., Ngan, F. (2015). NOAA's HYSPLIT Atmospheric Transport and Dispersion Modeling System. *Bulletin of the American Meteorological Society*, **96**, 2059–2077.
- Stensrud, D.J. (2007). Parameterization schemes: keys to understanding numerical weather prediction models. Cambridge University Press, 459pp.
- Tesche, T.W., McNally, D.E. and Tremback, C. (2002). Operational Evaluation of the MM5 Meteorological Model Over the Continental United States: Protocol for Annual and Episodic Evaluation. Prepared for US EPA by Alpine Geophysics, LLC, Ft. Wright, KY, and ATMET, Inc., Boulder, CO.
- Warner, T. (2011). Quality Assurance in Atmospheric Modeling. *Bulletin of the American Meteorological Society*, **92**, 1601-1610.

**17th International Conference on  
Harmonisation within Atmospheric Dispersion Modelling for Regulatory Purposes  
9-12 May 2016, Budapest, Hungary**

---

**IMPACT OF WRF URBAN PARAMETERIZATIONS IN THE PERFORMANCE OF CMAQ ON  
1 KM<sup>2</sup> RESOLUTION ANNUAL RUNS IN MADRID (SPAIN)**

*David de la Paz<sup>1</sup>, Rafael Borge<sup>1</sup>, Alberto Martilli<sup>2</sup>*

<sup>1</sup> Laboratory of Environmental Modelling, Department of Chemical & Environmental Engineering,  
Technical University of Madrid, (UPM), c/ José Gutiérrez Abascal 2, 28006 Madrid,  
Spain Madrid, Spain

<sup>2</sup> CIEMAT (Research Centre for Energy, Environment and Technology), Av. Complutense, 40, 28040  
Madrid, Spain

**Abstract:** Eulerian 3D mesoscale models can consistently describe a wide range of spatial scales. However, urban areas present features that are usually missed by land-surface and PBL modules commonly implemented in such models. The Weather Research and Forecasting model (WRF) incorporates urban parameterizations to take into account changes in albedo, roughness length and thermal properties imposed by buildings. In this study the multi-layer Building Energy Parameterization (BEP) scheme is tested over the Madrid city with the primary aim of understanding the effect that the use of the scheme may have on routinely (annual) air quality modelling activities in this urban area using the Community Multiscale Air Quality (CMAQ) model. The results for the main meteorological variables are compared with those from the WRF reference configuration, based on the BULK simple scheme included in the Noah Land Surface Model. It was found that the BEP-based configuration improved significantly wind speed results over built areas, with an annual average bias of  $-0.3 \text{ m s}^{-1}$  in comparison with the  $1.6 \text{ m s}^{-1}$  yielded by the reference WRF run. Meteorological outputs from the two alternative configurations were used to feed the CMAQ model to assess the influence of this urban parameterization on air quality predictions. The effect was a clear improvement of the model performance regarding the most relevant pollutants, reducing  $\text{NO}_2$  underestimation to only  $1.6 \mu\text{g m}^{-3}$ . Model skills to reproduce  $\text{O}_3$  and  $\text{PM}_{2.5}$  ground-level concentration were also substantially improved.

**Key words:** *Air quality modelling, urban parameterization, WRF, BEP, CMAQ, Madrid*

## **INTRODUCTION**

Given that the biggest impacts of air pollution on human health occur in cities (Dockery and Pope, 1994), poor urban air quality has become one of the main environmental concerns worldwide. According to the World Health Organization (WHO) outdoor air pollution caused 3.7 million premature deaths in 2012, most of them in urban areas where both, emission sources and population concentrate. Concentration levels are strongly influenced by meteorological features at different scales that determine how the emitted pollutants are dispersed within and above the urban canopy. The presence of the buildings generate complex flow and turbulence patterns that induce strong spatial heterogeneity in the concentration fields. A better understanding of the factors involved in the city-atmosphere interactions may help improving the estimation of the pollutant concentration at street level and consequently help to define more effective abatement strategies.

Multi-scale Eulerian models can provide a satisfactory description of air quality dynamics from the continental to the urban scale with a typical maximum horizontal resolution of about 1 km (Borge et al., 2014). However microscale processes cannot be dealt with explicitly at this resolution, since microscale phenomena in the canopy layer occur at a scale of few meters. This has been the motivation for the development in the last couple of decades of urban canopy parameterizations that have been integrated in mesoscale models. In the Weather Research and Forecasting (WRF) model (Skamarock and Klemp, 2008) several have been implemented, with the aim of reproducing the effects of the urban canopy on the urban boundary layer (UBL) dynamics (Chen and Dudhia, 2001) and therefore can be used for a better simulation of urban air quality at mesoscale.

The simplest approach (BULK scheme) (Liu et al., 2006) modifies several parameters such as the roughness length, the albedo and the thermal capacity and diffusivity without any other modification. SLUCM scheme (Single Layer Urban Canopy Model) (Kusaka et al., 2001) that takes into account buildings geometry to compute the exchange of momentum and heat fluxes between the city and the atmosphere. The BEP scheme (Building Energy Parameterization) (Martilli et al., 2002) is a multi-layer canopy model that represents the direct interaction of the buildings with the atmosphere through geometric, thermal and aerodynamic properties of different urban land uses. The BEP+BEM scheme (Building Energy Model) (Salamanca et al., 2010) is an evolution of BEP that takes into account the energy consumption of buildings due to air conditioning and its effect on urban heat budget. The main aim of the study is to understand the effect that the use of the multilayer urban parameterization BEP to produce the meteorological fields with WRF has on routinely air quality modelling activities in Madrid using CMAQ.

## METHODOLOGY

### Experimental setup

This paper assess the impact of the BEP multi-layer canopy model in comparison with the configuration based on the BULK scheme used for air quality modelling in Madrid in recent studies (Borge et al., (2014) and references within). BEP parameterization was selected as an optimum compromise between computational cost, input data requirements and model performance according to de la Paz et al. (2014) where several options were tested specifically for Madrid under typical winter and summer conditions. A complete meteorological year (2007) was run and the outputs were used to feed the CMAQ air quality model keeping constant all other model inputs such as emissions, chemical boundary conditions, etc. The simulation of a whole year provides interesting information on how the CMAQ model performance to depict policy-relevant air quality indexes (NO<sub>2</sub>, PM<sub>2.5</sub> annual means or relevant hourly or daily percentiles) is affected by BEP.

### Modelling system and domains

The air quality modelling system used in this study is based on the Community Multiscale Air Quality modeling system version 4.6 (CMAQv4.6) (Byun and Schere, 2006), the Sparse Matrix Operator Kernel Emissions modelling system (SMOKE, Version 2.7) (UNC Carolina Environmental Program, 2009) and the Weather Research and Forecasting (WRF, Version 3.3.1) (Skamarock and Klemp, 2008). Four nested domains were used in this study (Figure 1). The mother domain (D1) has a spatial resolution of 48 km and it is centred at 51°18'N, 20°25'E, covering Europe and Northern Africa. The first nested domain includes the Iberian Peninsula with a horizontal resolution of 16 km (D2) while the third (D3) and fourth (D4) modelling domains are centred over the Madrid Greater Region and the Madrid metropolitan area with a grid cell size of 4 km and 1 km respectively.

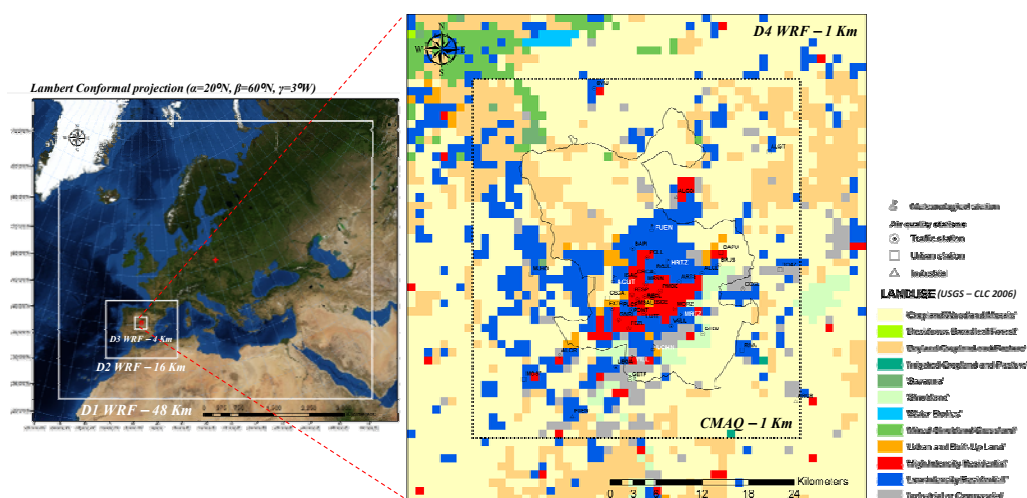


**Figure 1.** Modelling domains and land uses considered in the innermost nested domain for the BEP run.

**WRF model configuration**

General model setup is based on (Borge et al., 2008). The model is initialized from global reanalysis from the National Centers for Environmental Prediction (NCEP) Global Forecast System (GFS). Terrain elevation and land uses are taken from USGS global land cover data with a spatial resolution of 10' (D1), 2' (D2) y 30" (D3 and D4). Urban parameterizations were applied in the 1 km<sup>2</sup> resolution innermost domain (D4) so finer information regarding urban surfaces was provided. The implementation of BEP in WRF considers three urban classes (Low intensity Residential “L”, High intensity Residential “H”, Industrial or Commercial “IC”) that assume different built and vegetation area fractions with different average building height, street direction and width as well as specific albedo, thermal properties and roughness length. The distribution of these urban classes within D4, shown in Figure 1, is based on the Corine Land Cover (CLC 2006) database.

**Assessment methodology and observational data**

The methodology for model assessment is twofold: first maps showing the outputs from both model runs are compared to understand the changes associated to meteorological patterns (WRF<sub>BEP</sub>-WRF<sub>BULK</sub>) and pollution distribution within the modelling domain (CMAQ<sub>BEP</sub>-CMAQ<sub>BULK</sub>). And secondly, model outputs are compared with observations to assess to what extent the urban parameterization impacts model performance. Hourly data from 6 meteorological stations and 36 from air quality monitoring stations were compared with WRF and CMAQ model outputs respectively.

**RESULTS**

**Meteorology**

Figure 2 shows the spatial distribution of the annual-averaged differences of ground-level temperature (T2m) and wind speed (WSPEED). It is remarkable that WRF<sub>BEP</sub> temperature predictions are 0.7 °C higher than those of WRF<sub>BULK</sub> (Figure 2a) as an annual average over the modelling domain.

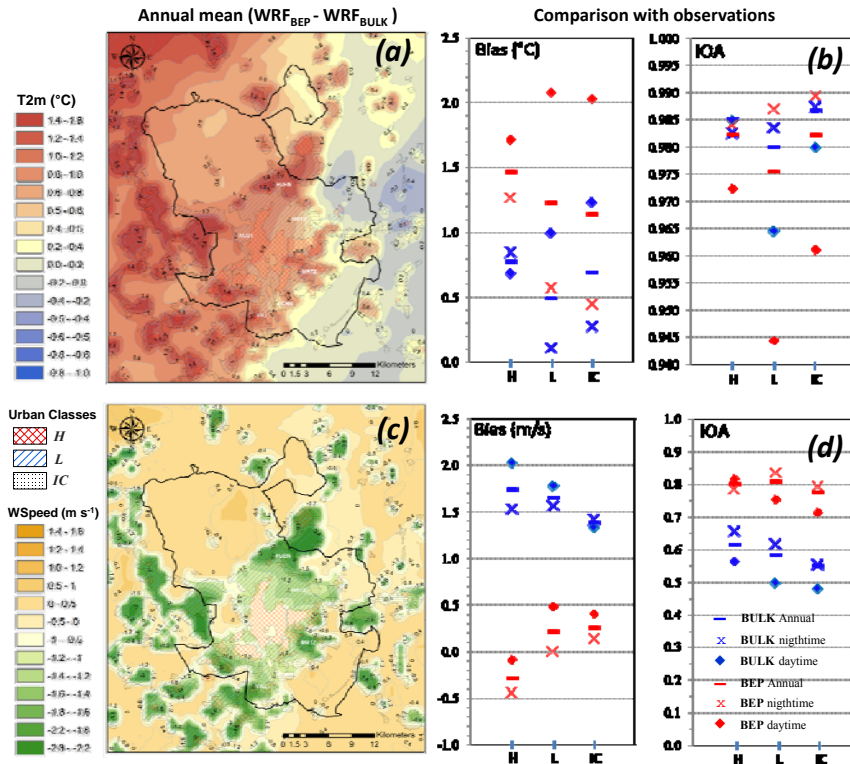


**Figure 2.** Left. Differences between BEP and BULK annual mean for (a) ground level temperature, (c) wind speed. Right. Comparison with observations Temperature (b) and wind speed (d) (2<sup>nd</sup> vertical level) bias and index of agreement for the two parameterizations compared by land use.

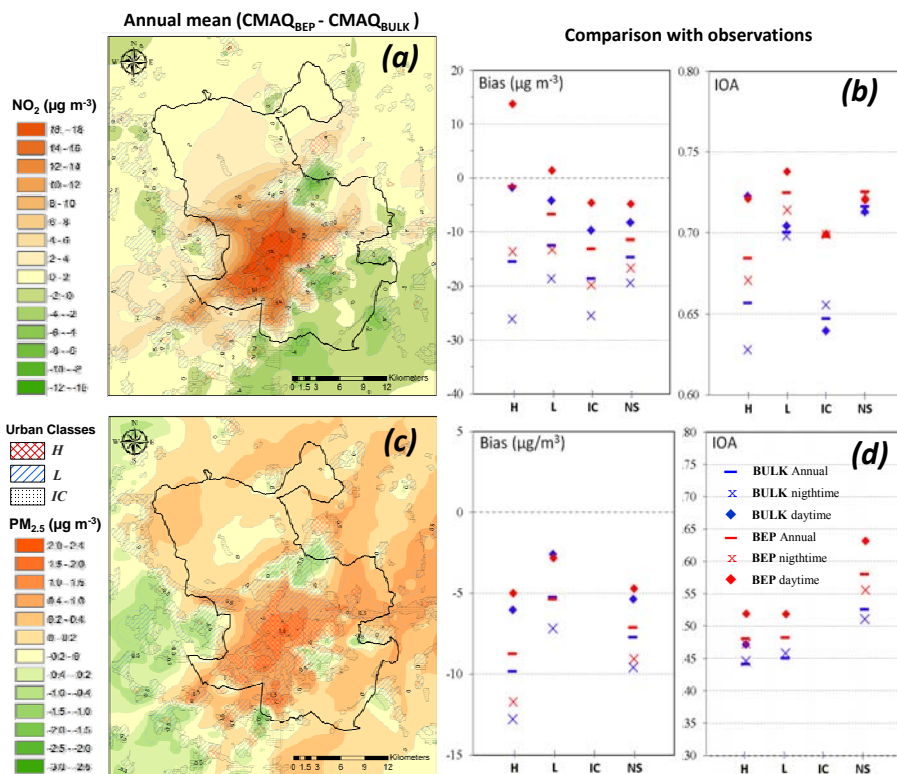
It can be seen that both model configurations overestimate ground level temperature, especially WRF<sub>BEP</sub>, with an average overestimation of approximately 1.3 °C and a maximum departure from observations for L urban class during night-time (Figure 2b). From the results of IOA it can be deduced that not only WRF<sub>BULK</sub> brings about smaller error but it also describes better temperature trends than WRF<sub>BEP</sub>.

Figure 2c shows the differences obtained for wind speed, one of the most influential variables on air quality since it is strongly related to advection, usually the dominant process in pollution transport. It is clear that BEP urban parameterization substantially reduces wind predictions for urban land uses. In the centremost area of Madrid a general reduction of 0.8 m s<sup>-1</sup> is observed. It can be seen that the BEP parameterization produces a slight underestimation for high intensity (H) urban classes (-0.3 m s<sup>-1</sup>) and a similar overestimation (0.2-0.3 m s<sup>-1</sup>) for the other urban classes. WRF<sub>BEP</sub> IOA for wind is also better globally than that of WRF<sub>BULK</sub> (0.80 Vs 0.55)

### Air quality

The results for NO<sub>2</sub>, one of the main concerns in urban areas nowadays, are shown in Figure 3a. It can be seen that predicted NO<sub>2</sub> concentrations by CMAQ<sub>BEP</sub> in the city centre are considerably higher than those of CMAQ<sub>BULK</sub> (up to 41 % higher). In absolute terms this implies a global difference of 10 µg m<sup>-3</sup> for the annual average, with maximum increments up to 18 µg m<sup>-3</sup> inside Madrid.

Annual mean NO<sub>2</sub> concentration for those air quality monitoring stations located in high intensity residential areas (H) is 59.9 µg m<sup>-3</sup>, very close to the corresponding prediction of CMAQ<sub>BEP</sub> (58.3 µg m<sup>-3</sup>) and considerably higher than that of CMAQ<sub>BULK</sub> (44.4 µg m<sup>-3</sup>). Therefore, BEP substantially improves CMAQ performance reducing NO<sub>2</sub> underestimation to only 1.6 µg m<sup>-3</sup> (Figure 3b). BEP clearly improves CMAQ skills providing better IOA scores, especially for L class (0.72 for the annual run).



**Figure 3.** Left. Differences between BEP and BULK results for (a) NO<sub>2</sub>, (c) PM<sub>2.5</sub> annual mean. Right. Comparison with observations NO<sub>2</sub> (b) and PM<sub>2.5</sub> (d) bias and index of agreement for the two parameterizations compared by land use. Figure 3c illustrates the differences obtained between CMAQ<sub>BEP</sub> and CMAQ<sub>BULK</sub> for PM<sub>2.5</sub>. The net effect of the urban parameterization is a moderate increment of PM<sub>2.5</sub> concentration. BEP helps reducing CMAQ underestimation, especially in densely urbanized areas where the annual PM<sub>2.5</sub> concentration predicted by CMAQ<sub>BEP</sub> is 0.5 µg m<sup>-3</sup> higher than that of CMAQ<sub>BULK</sub> (1 µg m<sup>-3</sup> as an average of the two monitoring stations located in H areas).

## CONCLUSIONS

It can be concluded that BEP substantially improved CMAQ performance and therefore it should be implemented for routinely modelling exercises (AQ limit values compliance assessment, plans and measures evaluation, etc.). This study also demonstrates that the effects of urban parameterizations may considerably change on different areas of the modelling domain that correspond to different urban typologies. The study indicates that wind speed is the most relevant meteorological variable air quality-wise. Despite improving energy balances within BEP during stable conditions (where errors concentrate), future efforts should be aimed at developing methods to provide better land-use information and more detailed characteristics regarding building configuration and other relevant properties.

## ACKNOWLEDGEMENTS

This study was carried out within the TECNAIRE-CM (innovative technologies for the assessment and improvement of urban air quality) scientific programme funded by the Directorate General for Universities and Research of the Greater Madrid Region (S2013/MAE-2972).

## REFERENCES

- Borge, R., Alexandrov, V., Del Vas, J.J., Lumberras, J., Rodríguez, E., A comprehensive sensitivity analysis of the WRF model for air quality applications over the Iberian Peninsula, *Atmospheric Environment* **42**(2008), pp. 8560-8574.
- Borge, R. et al., Emission inventories and modeling requirements for the development of air quality plans. Application to Madrid (Spain), *Science of the Total Environment* **466**(2014), pp. 809-819.
- Byun, D., Schere, K.L., Review of the governing equations, computational algorithms, and other components of the Models-3 Community Multiscale Air Quality (CMAQ) modeling system, *Applied Mechanics Reviews* **59**(2006), pp. 51-77.
- Chen, F., Dudhia, J., Coupling an advanced land surface-hydrology model with the Penn State-NCAR MM5 modeling system. Part I: Model implementation and sensitivity, *Monthly Weather Review* **129**(2001), pp. 569-585.
- Ching, J., Byun, D., Introduction to the Models-3 framework and the Community Multiscale Air Quality model (CMAQ), *Science Algorithms of the EPA Models-3 Community Multiscale Air Quality (CMAQ) Modeling System*(1999).
- Dockery, D.W., Pope, C.A., Acute respiratory effects of particulate air pollution, *Annual review of public health* **15**(1994), pp. 107-132.
- Kusaka, H., Kondo, H., Kikegawa, Y., Kimura, F., A simple single-layer urban canopy model for atmospheric models: Comparison with multi-layer and slab models, *Boundary-Layer Meteorology* **101**(2001), pp. 329-358.
- Liu, Y., Chen, F., Warner, T., Basara, J., Verification of a mesoscale data-assimilation and forecasting system for the Oklahoma City area during the Joint Urban 2003 field project, *Journal of applied meteorology and climatology* **45**(2006), pp. 912-929.
- Martilli, A., Clappier, A., Rotach, M.W., An urban surface exchange parameterisation for mesoscale models, *Boundary-Layer Meteorology* **104**(2002), pp. 261-304.
- de la Paz, D. et al., Assessment of urban parameterizations in the WRF model for air quality modelling purposes in Madrid (Spain), (2014).
- Salamanca, F., Krpo, A., Martilli, A., Clappier, A., A new building energy model coupled with an urban canopy parameterization for urban climate simulations—part I. formulation, verification, and sensitivity analysis of the model, *Theoretical and applied climatology* **99**(2010), pp. 331-344.
- Skamarock, W.C., Klemp, J.B., A time-split nonhydrostatic atmospheric model for weather research and forecasting applications, *Journal of Computational Physics* **227**(2008), pp. 3465-3485.

**17th International Conference on  
Harmonisation within Atmospheric Dispersion Modelling for Regulatory Purposes  
9-12 May 2016, Budapest, Hungary**

---

**ANALYSIS OF THE INTERNAL BOUNDARY LAYER FORMATION ON TROPICAL  
COASTAL REGIONS USING SODAR DATA IN SANTA CRUZ REGION OF MRRJ**

*Leonardo Aragão Ferreira da Silva<sup>1,2</sup>, Silvana Di Sabatino<sup>2</sup>, Luiz Claudio Gomes Pimentel<sup>3</sup> and  
Fernando Pereira Duda<sup>1</sup>*

<sup>1</sup>Department of Mechanical Engineering, Federal University of Rio de Janeiro (UFRJ),  
Rio de Janeiro, Brazil.

<sup>2</sup>Department of Physics and Astronomy, University of Bologna (UniBO), Bologna, Italy.

<sup>3</sup>Department of Meteorology, Federal University of Rio de Janeiro (UFRJ), Rio de Janeiro, Brazil.

**Abstract:** This paper investigates local circulation features in the industrialized coastal region of Santa Cruz given the close relevance to recent air quality problems. The topographic characteristics and the variety of micro and mesoscale phenomena acting over the area suggest the formation of Internal Boundary Layers (IBLs) during cold front and bay breeze flows, whose parameterization is often employed in air quality modeling. Preliminary results using data from acoustic atmospheric profilers shows a frequent occurrence of the IBL formation during bay breeze periods, coinciding with flow direction upstream of the major industries and having an impact on the most populated area of this region. Vertical profiles of main meteorological variables are evaluated together with surface weather station and satellite data to derive a detailed physics-based description of the various stages of bay breeze in terms of the main forces, duration and atmospheric stabilities. It is found that the development phase exhibits the largest bay/land differences and, consequently, it is the strongest condition to observe the IBL formation.

**Key words:** *Sea Breeze, Acoustic Soundings, Vertical Profiles, Internal Boundary Layer*

## **INTRODUCTION**

According to Garratt (1990), the internal boundary layer (IBL) formation is associated with air mass horizontal advection over any discontinuity of surface property. Several studies interpret this surface forcing as an abrupt change of surface roughness, temperature, humidity, or surface fluxes of heat or humidity. The mechanical forcing that produces IBL derives from a shear stress change found on coastlines due of an abrupt change in roughness. Usually, the IBL height exhibits a 1 to 10 growth rate relative to the distance that the flow covers over the roughness surface (Elliott, 1958), and this height is usually dominated by the thermal forcing at surface (Raynor et al., 1979).

Propitious conditions for IBL formation are always available during sea-breeze fronts, where a simple land-water temperature difference induces a flow crossing a coastline, generated by thermal forces ranging from mesoscale to micro-scale (Leo et al., 2015). Therefore, to identify the main physical mechanisms acting over each stage of sea breeze (Cuxart et al., 2014) becomes the key to recognize IBL formation process. The main target in this work is to understand how bay breeze acts over tropical regions where the land-bay temperature gradient is not as large as expected, and to describe the effect on IBL evolution.

## **METHOD AND MATERIALS**

### **Site Characteristics**

The region of Santa Cruz is part of the Metropolitan area of Rio de Janeiro city where rural characteristics can be found inside the second largest metropolitan area of Brazil with a population around 12 million. Situated over a flat lowland, this region is surrounded by several mountains with a complex topography and a coastal area delimited by the Sepetiba Bay (Figure 1).

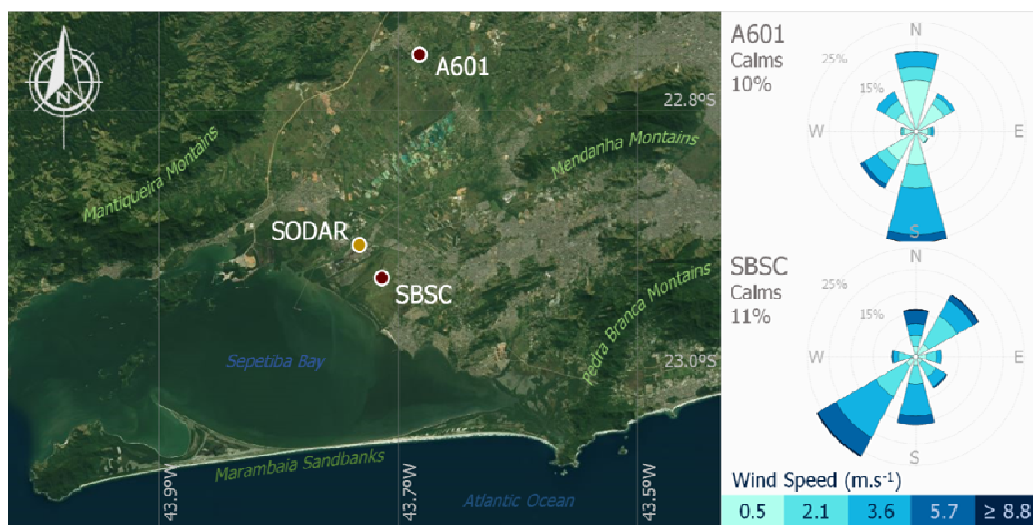


**Figure 1.** Satellite image of the study area highlighting the main regional topography, water bodies, and meteorological monitoring stations, and wind roses for the coastal (SBSC) and the inland (A601) surface weather stations pointing the presence of the land/bay breeze over the region of interest.

At synoptic scale, the region of interest is usually influenced by the South Atlantic Subtropical Anticyclone (SASA) and low frontal pressure systems (cold fronts), besides breeze systems on meso and local scales (sea/bay–land and valley–mountain) (Paiva, et al., 2014). The latter becomes specifically relevant considering the features of the surrounding region that is characterized by nonhomogeneous land-use and land-cover, and has the borders delimited by water bodies such as the Sepetiba Bay, and the Atlantic Ocean (Zeri, et al., 2011). On the other hand, the SASA is a semi-permanent high-pressure system (counterclockwise in South Hemisphere) with vertical subsidence winds that generates divergence at surface level and, consequently, favors calm weather and clear sky conditions over a influence area. In addition, SASA contributes to inhibit cloudiness and the advancement of frontal systems in the region of interest.

### Meteorological Data

As show on Figure 1, the present study uses data from two surface weather stations (SWS). The first one is located inside an airport area named Station Base of Santa Cruz (SBSC), controlled by the National Army and positioned at 3 km from the coastline (22.93°S and 43.72°W) with 3 m of ground elevation and hourly measurements of wind at 10 m and air temperature at 2m. The second station, A601 Seropédica, belongs to the National Institute of Meteorology (INMET) and it is located about 20 km from the coastline (22.76°S and 43.68°W) at 35 m height over a very gentle slope, with hourly measurements at the same levels of SBSC. Both stations follows the World Meteorological Organization (WMO) standard and integrate the main global atmospheric monitoring systems with station codes 83115 and 86878, respectively.

An acoustic sounding profiler SODAR (SOmatic Detection And Ranging) equipped with a windRASS extension (Radio Acoustic Sounding System) was used to acquire measurements of the atmospheric column over the study region. The instrument installed at the end of 2013 attend to a local government request for air quality controlling purposes, once that an important global mineral industry was established acting as the main source of pollutant emissions in the region. The SODAR model MFAS WindRASS (Scintec) is located 5 km from the coastline (22.90°S and 43.73°W) at 4 m above sea level, and operates in a range from 40 m up to 800 m above the ground level with 10 m of vertical spatial resolution and time integration of 10 minutes.

In order to evaluate near surface temperature gradients between bay and land, a time-compositing approach for Sea Surface Temperature (SST) was built using satellite products from Aqua MODIS. This

compositing have been used to make a comparison with the land surface temperature (LST) and evaluate the diurnal cycle of the bay breeze as detailed below.

### **Period of Interest**

The selected period for the analyses includes 72 hours starting at 00:00 (LT) of December 26 and finishing at 00:00 (LT) of December 29, 2013, where three entire and consecutive cycles of bay/land breezes circulation were observed. During these three days, air temperature oscillates between 22 and 35°C, relative humidity between 43 and 94%, maximum wind velocities around 7 m.s<sup>-1</sup>, no precipitation, and clear sky condition with the exception of few scattered clouds at some hours. This period was selected within 92 days between October 1<sup>st</sup> and December 31, 2013 using as criteria the simultaneous availability of data on both surface weather stations and SODAR data for, at least, three consecutive days of bay/land breezes events.

### **Synoptic Condition**

The selected period occurs after a long period of the South Atlantic Convergence Zone (SACZ) governing the synoptic circulation over a major part of the South America between December 11 and 27, 2013. This event promoted an increase of precipitation outside of region of interest, but close enough to avoid the influence of other synoptic systems (as cold fronts, for example). Despite the SASA position was not relevant in this case, migratory high-pressure systems have influenced the region of interest during the selected period, favoring the local circulation and, consequently, the bay/land breeze evolution.

### **Land/Bay Breeze circulation**

The region of interest present a wind field pattern well defined blowing from northeast to southwest directions, strictly perpendicular aligned to the coastline (see SBSC wind rose at Figure 2). Generally, southwest winds are associated to the bay breeze beginning close to midday (10:00-12:00 LT) with maximum wind velocities around 10 m.s<sup>-1</sup>. On the other hand, the land breeze starts close to midnight (22:00-00:00 LT) with northeast winds and velocities up to 7 m/s. According to Pimentel et al (2014), in some occasions land breeze displays a north direction pointing out to a possible interaction with the mountain nocturnal circulation (katabatic winds). In other situations the bay breeze can be hidden by the northeast winds of SASA circulation depending of its positioning and intensity (Paiva, et al., 2014). However, it is important mention that during 92 days evaluated on the present study, 65 showed a land/bay breeze circulation (~70%), reinforcing the hypothesis of its relevance in the local circulation over the region.

## **RESULTS**

### **Bay Breeze Circulation**

In general terms, the time evolution of the bay breeze (Figure 2) follows a sequence of previous, preparatory, development, mature and decay phases, each one with specific patterns and duration ruled by a specific dynamics. The first phase of the bay breeze begins with sunrise, when LST is significantly colder than sea surface temperature (SST), lasting between 2 (tropics) and 4 hour (mid-latitudes) depending on solar radiation intensity. In our case, bay breeze began around 6:00LT and lasted until the previous nocturnal inversion layer break-up (between 7:30 and 8:00LT). It coincides with a land breeze intensity decreasing (NE winds) and finally suppressed by convection starting as result of land surface warming. At this point, the preparatory phase starts with LST-SST becoming positive, convective boundary layer beginning to build, and wind shifting on SW direction just near to the coastline (normal aligned). As observed of Figure1, this last condition shows a delay at Dec 27 and 28, indicating that land breeze intensity has not decreased enough to obtain a convective condition over the region.

Further, around 11:00LT the development phase starts which usually last for 3 hours. The critical period of bay breeze have the greatest temperature and pressure gradients, providing all conditions for the front breeze (wind  $\geq 3$  m s<sup>-1</sup>) as well as the maximum turbulence (indicated by TKE on Figure2) and maximum LST-SST difference. The maximum wind speed of the evaluated period always occurs during this phase, suggesting the appropriated time to observe the IBL building up (discussed later). Close to 14:00LT it is possible to observe the bay breeze arriving at the inland station (~1 hour delayed in relation to the coast station), with an increase of wind speed and a decrease of air temperature. This is the mature phase, when

the vertical circulation cell between bay and land is established with convergence winds inland. This configuration remains for 3 or 4 hours with wind speed, LST-SST difference and turbulence nearly constant, with only a slow temperature decrease. Finally, the last one called decay phase starts near to sunset (after 18:00LT) and makes the transition to the land breeze circulation. During this period, all the evaluated parameters decrease slowly until sunset, when wind speed reduces to calm winds and LST-SST difference become negative, providing the conditions for land breeze initiation.

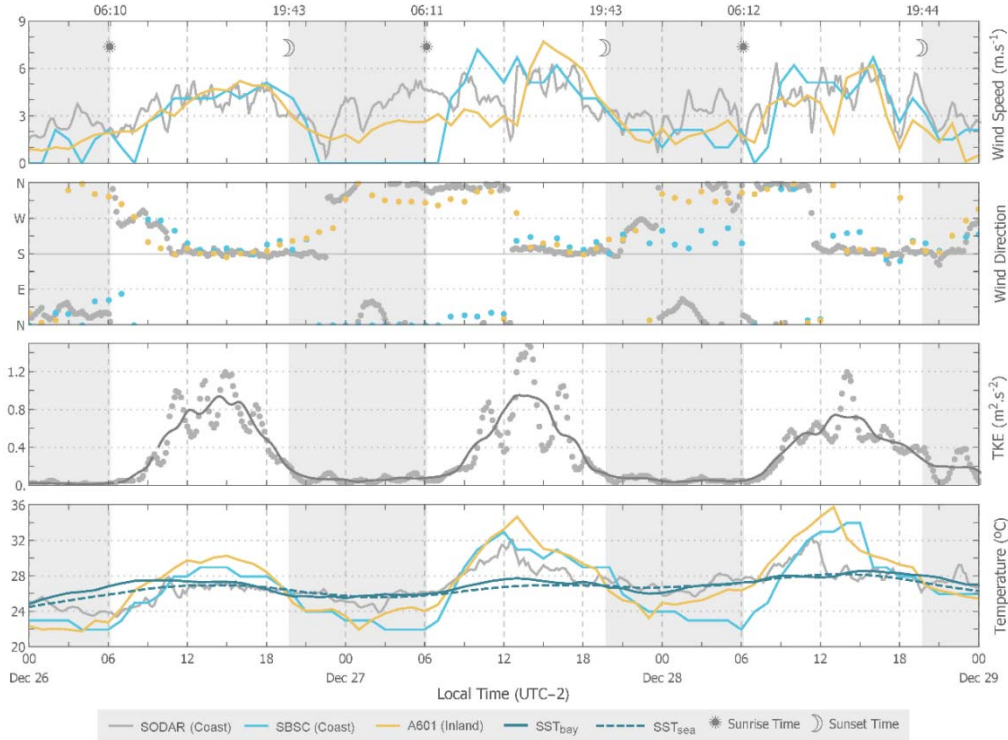


**Figure 2.** Meteorological data for the region of interest between 26 and 29 December 2013. Wind speed, wind direction, and air temperature measurements recorded at 10 m by surface stations. SODAR measurements are presented only for the first level (40 m), except for TKE which integrates all column (smoothed data – solid line). SST data show averages of specific areas over the Sepetiba Bay and Atlantic Ocean.

### IBL Building

Despite SODAR limitation to observe the atmospheric boundary layer height under convective condition, acoustic soundings proved to be adequate to detect the inversion height  $z_i$  (m) since it occurs inside the measurement range, for example, during nocturnal boundary layer or IBL cases (Mellas, 1993). SODAR data for the study period had  $z_i$  observations only during nighttime (stable conditions), except on Dec 26 and Dec 28, when inversions were observed for few minutes on vertical temperature profiles with heights up to 130 m (Figure 3). Both episodes occur during the development phase of the bay breeze, when the wind speed, turbulence intensity, and LST-SST reaches their maximum values, providing all the minimal conditions for a IBL building up along the coastline.

Two simple analytical formulations were applied to estimate IBL heights  $h_i$  (m) when front breezes crosses the coastline: Weisman (1976) which uses the surface heat flux  $H_0$  ( $\text{W m}^{-2}$ ) as the main term (Eq.1), and Raynor et al. (1979) which consider LST-SST  $\Delta T_{L-B}$  ( $^{\circ}\text{C}$ ) as principal on formulation (Eq.2).

$$h_w = \left( \frac{2 H_0 x}{\rho c_p |\gamma| U} \right)^{1/2} \quad (1)$$

$$h_r = \frac{u_*}{U} \left( \frac{x |\Delta T_{L-B}|}{|\gamma|} \right)^{1/2} \quad (2)$$

where  $x$  is crosswind distance from the coastline (m),  $\rho$  is air density ( $1.225 \text{ kg m}^{-3}$ ),  $c_p$  specific heat at constant pressure ( $1004.67 \text{ m}^2 \text{ s}^{-2} \text{ K}^{-2}$ ),  $\gamma$  is the vertical gradient of temperature ( $^\circ\text{C m}^{-1}$ ),  $u_*$  is friction velocity ( $\text{m s}^{-1}$ ) and  $U$  is mean wind ( $\text{m s}^{-1}$ ). The results presented in Figure 3 shows a good estimative for IBL height at 5 km (SODAR position) for both days using both models. The smaller  $\Delta T_{L-B}$  on Dec 26 (1) explains the underestimation of Eq.2. Considering the wind speed during these cases ( $3.1$  and  $5.1 \text{ m s}^{-1}$ , respectively) blowing for approximately 40 minutes, a possible IBL fetch for the region under this atmospheric conditions varies between 8 and 12 km from the coastline, impacting severely over the main emission areas suggesting a potential increase of pollutant concentration during these periods.

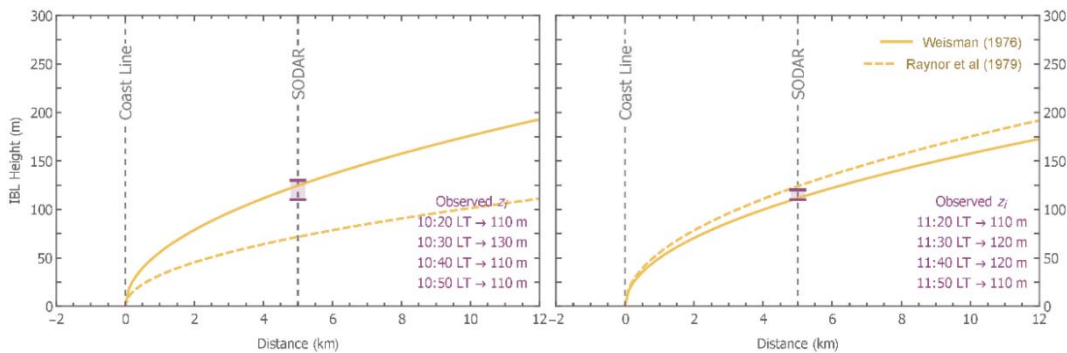


**Figure 3.** IBL height estimative at crosswind direction for 26 Dec 2013 at 10:00LT (left) and 28 Dec 2013 at 11:00LT (right) using Weisman (1976) and Raynor et al. (1979) formulations. Positioned 5 km from coastline, these measurements are the only one available during daytime (convective) on the study period, and both were recorded during the development phase of the bay breeze.

## CONCLUSIONS

A thorough analysis over three consecutive and entire cycles of bay-land breeze was presented with a focus on the evaluation for onset of IBL and its evolution in time. The results of our analyses shows that the development phase is the critical period of bay breeze due the highest differences between air mass properties over bay and land. Furthermore, available parameterizations for IBL height estimations were tested showing good results in comparison with SODAR measurements, even when considering different approaches on formulations.

## REFERENCES

- Cuxart, J, M. A. Jiménez, M. T. Prtenjak, and B. Grisogono, 2014: Study of a Sea-Breeze Case through Momentum, Temperature, and Turbulence Budgets. *J. Appl. Meteor. Climatol.*, **53**, 2589-2609.
- Elliott, W. P., 1958: The growth of the atmospheric internal boundary layer. *EOS Trans. Amer. Geoph. Union.* **39**, 1048-1054.
- Garratt, J. R., 1990: The internal boundary layer - a review. *Boundary-Layer Meteorol.*, **50**, 171-203.
- Leo, L. S, H. J. S. Fernando, S. Di Sabatino, 2015: Near-surface flow in complex terrain with coastal and urban influence. *Environ. Fluid. Mech.*, **2**, 349-372.
- Melas, D., 1993: Similarity methods to derive turbulence quantities and mixed-layer depth from SODAR measurements in the convective boundary layer: a review. *Applied Physics B*, **57**, 11-17.
- Paiva, L.M.S, G.C.R. Bodstein and L.C.G. Pimentel, 2014: Influence of high-resolution surface databases on the modeling of local atmospheric circulation systems. *Geosci. Model Dev.*, **7**, 1641-1659.
- Pimentel, L.C.G, E. Marton, M. Soares da Silva, and P. Jourdan, 2014: Caracterização do regime de vento em superfície na Região Metropolitana do Rio de Janeiro. *Eng. Sanit. Ambient.*, **19**, 121-132.
- Raynor, G. S., Sethuraman, S. and Brown, R. M., 1979: Formation and characteristics of coastal internal boundary layers during onshore flows. *Boundary-Layer Meteorol.*, **16**, 487-514.
- Weisman, B. 1976: On the criteria for the occurrence of fumigation inland from a large lake - A Reply. *Atmos. Environ.*, **10**, 172-173.
- Zeri, M., Oliveira-Júnior, J. F. and Lyra, G. B., 2011: Spatiotemporal analysis of particulate matter, sulfur dioxide and carbon monoxide concentrations over the city of Rio de Janeiro, Brazil. *Meteorol. Atmos. Phys.*, **113**, 139-152.

## **TOPIC 5**

### **URBAN SCALE AND STREET CANYON MODELLING: METEOROLOGY AND AIR QUALITY**

**17th International Conference on  
Harmonisation within Atmospheric Dispersion Modelling for Regulatory Purposes  
9-12 May 2016, Budapest, Hungary**

---

**MODELLING ULTRAFINE PARTICLE CONCENTRATIONS AT STREET-LEVEL SCALE  
FOR THE ENTIRE CITY OF ANTWERP**

*Hans Hooyberghs<sup>1</sup>, Wouter Lefebvre<sup>1</sup>, Felix Deutsch<sup>1</sup>, Sandy Adriaenssens<sup>2</sup>, Elke Trimpeneers<sup>2</sup>,  
Frans Fierens<sup>2</sup>, Stijn Janssen<sup>1</sup>*

<sup>1</sup>VITO, Flemish Institute for Technological Research, Unit Environmental Modelling,  
Boeretang 200, B-2400 Mol, Belgium.

<sup>2</sup>Belgian Interregional Environment Agency (IRCEL-CELINE), Kunstlaan 10-11, 1210 Brussels,  
Belgium

*Contact: hans.hooyberghs@vito.be*

**Abstract:** In this study, an integrated model chain has been set up to assess the concentration of ultrafine particles at the local (street level) scale for an entire city, including both regional variability as well as local variation in sources of air pollution. The model chain starts from spatially and temporally distributed traffic emissions based on the HBeFa-methodology. These traffic emissions are subsequently used in IFDM, a bi-Gaussian plume model designed to simulate non-reactive pollutant dispersion at a local scale. The effects of street-canyons are added using the OSPM-module, which takes into account the specific dispersion characteristics in the street canyon. The model is subsequently successfully validated using a measurement campaign carried out in the city of Antwerp in 2013. This modelling exercise and the subsequent successful validation confirm the hypothesis that dynamical processes do not play a major role in the dispersion of ultrafine particles at the local and urban scale.

**Key words:** *Urban air quality, Ultrafine particles, Dispersion modelling*

## **INTRODUCTION**

In recent years, the fraction of particulate matter with a diameter smaller than 0.1µg, more commonly known as ultrafine particles (UFPs), has gained a lot of attention. Given their small size, UFPs contribute little to the mass of particulate matter in ambient air, but they are the dominant contributors to the total particle number. Concern about the toxicity of UFPs arose since animal and in-vitro studies suggest that the ultrafine particles could be inhaled much further into the lungs, and that they may be translocated into the blood (HEI, 2013).

Currently there is no limit value to control the UFP-concentration, but if a policy for ultrafine particles is to be introduced in the future, performance evaluation of new and existing models against measured data in various conditions will be needed. In this study, an integrated model chain has been set up to assess the concentrations of ultrafine particles at the local (street level) scale for the entire city of Antwerp. The model is subsequently successfully validated using a measurement campaign carried out in the city of Antwerp in 2013. In the remainder of this extended abstract we first focus on the model chain and the measurement campaigns, and thereafter provide the detailed results of the validation.

## **MODEL CHAIN**

The model chain consists of several models coupled to each other. The different components are discussed one by one in the next paragraphs.

The MIMOSA4.3 emission model (Mensink et al., 2000) is used to calculate local traffic emissions based on the HBeFa emission factors (Hausberger et al., 2009). However, the original emissions have been multiplied by ten in our methodology. The choice of multiplying the emissions with such a high factor is an important decision. There were, nevertheless, sufficient arguments to make this assumption reasonable. When the first simulations were performed, excluding this factor, it was clear that something

was wrong. The resulting concentrations were too low, although the spatial correlation factor was very high. Furthermore, the UFP concentration maps were mainly dominated by the background coming from LOTOS-EUROS, although UFP in cities is mainly driven by local traffic. Moreover, other studies indicate much higher emission factors than those contained in the HBeFa-database, see for instance Nikolova et al. (2011). Finally, the underestimation in HBefa v3.1 is probably related to differences in emissions between test cycles and real driving conditions. Although HBefa uses the CADC-cycle, it is probable that real-world driving conditions are still different from this cycle.

The resulting spatially and temporally distributed emissions are used in the bi-Gaussian model IFDM (Lefebvre et al., 2011a; 2011b). IFDM (Immission Frequency Distribution Model) model is a bi-Gaussian plume model, designed to simulate non-reactive pollutant dispersion at a local scale. Apart from diffusion, all other dynamical specific UFP-processes, such as, i.e. nucleation, condensation, coagulation and deposition, are not represented.

To incorporate regional scale background concentrations, these results are coupled to output of the LOTOS-EUROS regional air quality model. A method to avoid double counting of the (local) emissions by the different models is applied (Lefebvre et al., 2011b). The street canyon contribution to the concentrations is calculated by using the IFDM output as boundary conditions to a street canyon module, OSPM, which takes into account the specific dispersion characteristics in the street canyon (Berkowicz, 1997). The results of the IFDM model and OSPM are subsequently combined using a post processing tool, so that the street canyon concentrations are confined to the street canyons, and the IFDM roof top concentrations are used outside of the canyons. The final output are (annual) average maps and time series at selected locations.

This model chain (also known as the IFDM-OSPM model) has previously been used at VITO to successfully model the concentrations of nitrogen dioxide, ozone, particulate matter, elemental and black carbon, and has now, within the scope of the INTERREG IVB Joaquin project, been adapted to model the concentrations of (total number of) ultrafine particles. The resulting annual mean concentration in Antwerp in 2013 is shown in Figure 1.

## **MEASUREMENTS**

The methodology is validated over the city of Antwerp using two short-term measurement campaigns carried out during February and October 2013. The measurement data is described in detail in Frijns et al. (2013; 2014). Table 1 provides a list of the different stations and the naming convention applied in the following paragraphs, Figure 1 locates the measuring stations on a map of Antwerp.

During February, UFP-concentrations were measured at 7 diverse locations: three locations close to the busy Plantin-Moretuslei (at distances varying from 10m over 30m to 55m from the center of the road), at the suburban location at Linkeroever, at a station close to the busiest highway in Belgium (Ring of Antwerp), in the public park “Stadspark” and in a street canyon (Turnhoutsebaan). During October, measurements have been carried out at 4 locations: the station located at 30m of the Plantin-Moretuslei, at Linkeroever, in the public park and close to the Ring.

**Table 1:** Overview of the measurement locations and time frames. The number in the third column refers to the locations shown in Figure 1.

Official name	Location	Location on map (see Figure 1)	Type	Period
R801 Borgerhout	Telemetric monitoring station situated at approx. 30m from a busy road (Plantin-Moretus lei)	1	Urban background	February and October
Borgerhout 10m	Trailer at approx. 10m from a busy road (Plantin-Moretus lei)	1	Urban background	February
Borgerhout 55m	Trailer at approx. 10m from a busy road (Plantin-Moretus lei)	1	Urban background	February
Linkeroever	Linkeroever	5	Suburban	February and October
Ring	Near the busiest highway in Belgium	3	Roadside	February and October
Stadspark	In the city park	4	Public park	February and October
Turnhoutsebaan	Roadside of a busy road (Turnhoutsebaan)	2	Street canyon	February

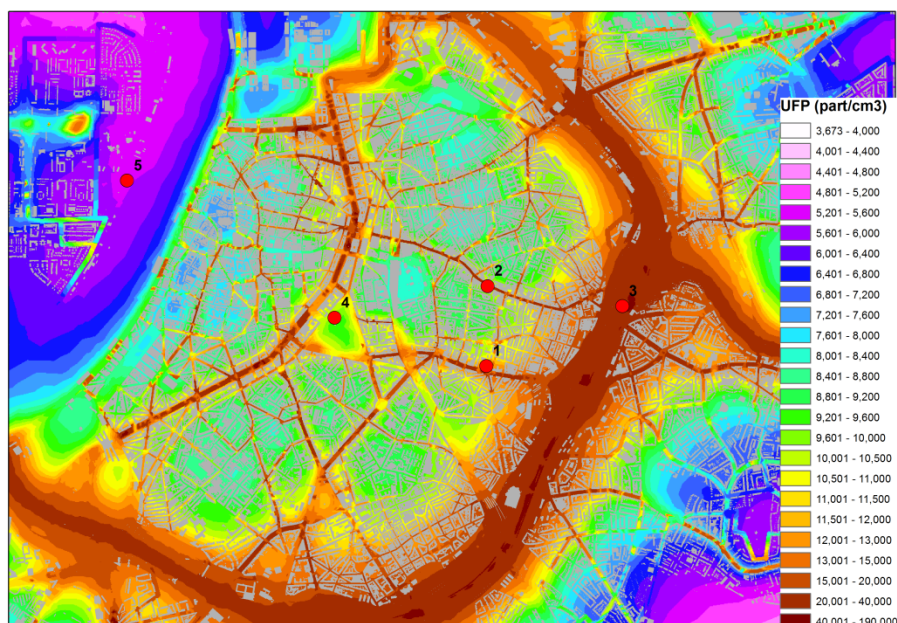


**Figure 1:** Annual mean UFP-concentration (in  $\text{part}/\text{cm}^3$ ) in Antwerp in 2013. The map also shows the location of the measurement sites as indicated in Table 1.

## VALIDATION

Within this extended abstract, we focus on two types of validations. Firstly, we assess the spatial pattern simulated by the model chain by comparing the mean values for the measurement periods with the

modelled values. Secondly, we perform a spatio-temporal validation by focusing on 24h-averaged values. More details on the validation are reported in Hooyberghs et al. (2015).

Figure 2 shows the validation of the spatial pattern. We find a good agreement between the modelled data and the measurements. There is a slight underestimation of the concentrations (bias = -18%), some scatter (RMSE = 25%) and a high correlation ( $R^2=0.93$ ). In the validation plot, the strong underestimation of the concentrations at the Turnhoutsebaan is clear. Without this location, the spatial validation parameters improve significantly (BIAS = -15%, RMSE = 17%,  $R^2 = 0.98$ ). A comparison of the input traffic dataset with actual countings during the UFP-measurement campaign and with information on the website of the public transport company suggests that the number of heavy duty vehicles (and especially public busses) in the dataset is significantly underestimated at this location, which could explain the discrepancy. This situation illustrates the importance of getting good traffic data, since deficiencies in the traffic data (both in locations and in number of vehicles) can have a large influence on the final results.

Also the validation for 24h-averaged values is quite good, as can be seen in Figure 3. We find a slight underestimation of the concentrations (bias = -12%), some scatter (RMSE = 41%) and a reasonable high correlation ( $R^2 = 0.70$ ). Studying the results in more detail, they point to a large underestimation at the Turnhoutsebaan, which is in line with the discrepancy observed for in the spatial validation. At most other locations, a small underestimation is found, except for the location near the Ring Road, where only a very slight negative bias is found.

In sum, both the spatial and the spatio-temporal validation are successful, indicating that, although assumptions have been made, the modelling chain provides accurate results for the UFP-concentration in the city of Antwerp. The success of the modelling chain moreover indicates that the dispersion of ultrafine particles at the local and urban scale is mainly governed by the dilution process, while other dynamical processes can be neglected.

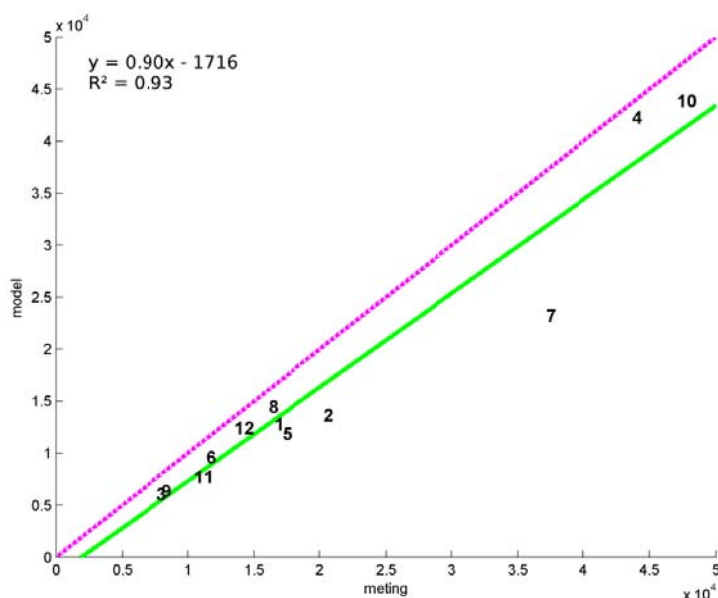


**Figure 2:** Spatial validation. The plot shows the average values for the different measurement campaigns for UFP (in particles/cm<sup>3</sup>). Every number denotes a measurement-model combination of averages at one location over the complete measurement campaign. Numbers 1 to 7 denote February values (VMM R801 (1), Borgerhout 10m (5) and Borgerhout 55m (2), at Linkeroever (3), close to the Ring Road (4), at the city park (6) and in the street canyon of the Turnhoutsebaan (7)). Numbers 8 to 11 are respectively measurements at R801 (8), at Linkeroever (9), close to the

Ring Road (10) and at the city park (11) during October. Number 12 is the annual mean value at the R801 location. The (full) green line is the regression of the model on the measurements, while the (dotted) purple line is the 1:1-line.

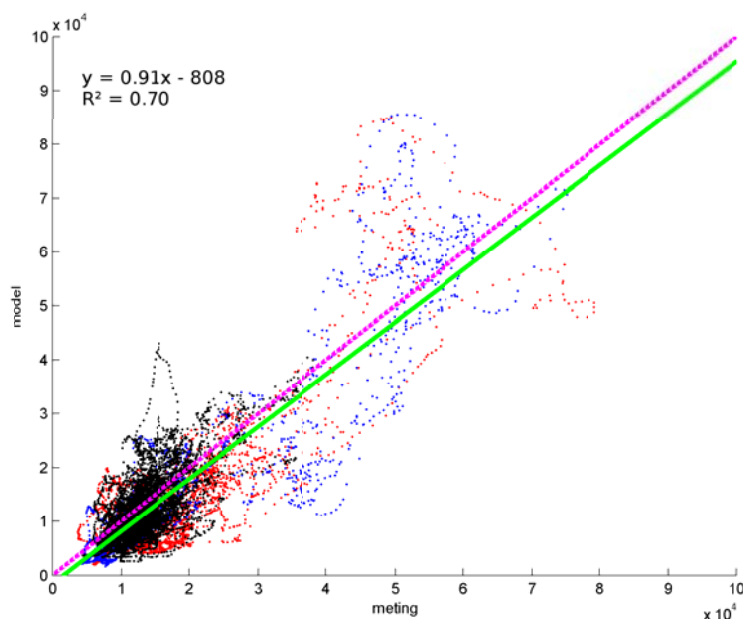


**Figure 3** :Spatio-temporal validation. The UFP-validation plot (24h averages, in particles/cm<sup>3</sup>), for all measurement locations and periods (4 weeks) combined. Every dot is a corresponding measurement-model combination (blue = October, red = February, black = annual values at R801). The (full) green line is the regression of the model on the measurements, while the (dotted) purple line is the 1:1-line.

## CONCLUSIONS

We have introduced an integrated model chain, the IFDM-OSPM model, to assess the concentration of ultrafine particles at the local (street level) scale for the entire city of Antwerp. The methodology is validated using measurement campaigns carried out in 2013. Although dynamical processes such as nucleation and coagulation are neglected in the local scale IFDM-OSPM model, in general, there is a very good agreement between the measurements and the model output. Especially the spatial validation is highly successful, and thus the model is certainly suitable to compose maps of annual mean ultrafine particle concentrations and to identify hotspots on a local and regional scale.

This modelling exercise and the subsequent successful validation confirms the hypothesis that dynamical processes do not play a major role in the dispersion of ultrafine particles at the local and urban scale. Here the dispersion pattern is mainly governed by the dilution process which is well simulated by the IFDM-OSPM model chain. Furthermore, the validation illustrates the importance of good traffic data, since deficiencies in the traffic data (both in locations and in number of vehicles) can have a large influence on the final results.

## ACKNOWLEDGEMENTS

The research presented in this extended abstract was funded by the INTERREG IVB Joint Air Quality Initiative (Joaquin) project. The authors gratefully acknowledge TNO for the use of the LOTOS-EUROS background concentrations.

## REFERENCES

- Berkowicz, R., Hertel, O., Larsen, S.E., Sørensen, N.N., Nielsen, M., 1997. Modelling traffic pollution in streets.
- Frijns E., Van Laer J., Berghmans P., 2013. Short-term intra-urban variability of UFP number concentration and size distribution, 2013/MRG/R/173.
- Frijns E., Van Laer J., Berghmans P., 2014. Short-term intra-urban variability of UFP number concentration and size distribution – October 2013 campaign, 2014/MRG/R/59.
- Hausberger S., Rexeis M., Zallinger M., Luz R., 2009. Emission Factors from the Model PHEM for the HBEFA Version 3, Report Nr. I-20/2009 Haus-Em 33/08/679
- HEI, Understanding the Health Effects of Ambient Ultrafine Particles, 2013
- Hooyberghs H., Lefebvre W., Deutsch F., 2015. Evaluation of local and regional measures in order to improve the air quality in the framework of the Interreg IV-B JOAQUIN project.
- Lefebvre, W., Fierens, F., Trimpeneers, E., Janssen, S., Van de Vel, K., Deutsch, F., Viaene, P., Vankerkom, J., Dumont, G., Vanpoucke, C., Mensink, C., Peelaerts, W., Vliegen, J., 2011a. Modeling the effects of a speed limit reduction on traffic-related elemental carbon (EC) concentrations and population exposure to EC, *Atmospheric Environment*, **45**, 197-207, doi: 10.1016/j.atmosenv.2010.09.026
- Lefebvre, W., Vercauteren, J., Schrooten, L., Janssen, S., Degrauwe, B., Maenhaut, W., de Vlieger, I., Vankerkom, J., Cosemans, G., Mensink, C., Veldeman, N., Deutsch, F., Van Looy, S., Peelaerts, W., Lefebvre, F., 2011b. Validation of the MIMOSA-AURORA-IFDM model chain for policy support: modeling concentrations of elemental carbon in Flanders, *Atmospheric Environment*, **45** 6705-6713., doi: 10.1016/j.atmosenv.2011.08.033
- Mensink, C., De Vlieger, I., Nys, J., 2000. An urban transport emission model for the Antwerp area, *Atmospheric Environment*, **34**, 4595-4602.
- Nikolova I., Janssen S., Vrancken K., Vos P., Mishra V., Berghmans P., 2011. Size resolved ultrafine particles emission model – a continuous size distribution approach, *Science of the Total Environment*, **409**, 6492-3499, doi:10.1016/j.scitotenv.2011.05.015

**17th International Conference on  
Harmonisation within Atmospheric Dispersion Modelling for Regulatory Purposes  
9-12 May 2016, Budapest, Hungary**

---

**EVALUATION AND DEVELOPMENT OF TOOLS TO QUANTIFY THE IMPACTS OF  
ROADSIDE VEGETATION BARRIERS ON NEAR-ROAD AIR QUALITY**

*Vlad Isakov<sup>1</sup>, Akula Venkatram<sup>2</sup>, Richard Baldauf<sup>3</sup>, Parik Deshmukh<sup>4</sup>, Max Zhang<sup>5</sup>*

<sup>1</sup>U.S. EPA, Office of Research and Development, National Exposure Research Laboratory,  
Computational Exposure Division, Research Triangle Park, North Carolina, USA

<sup>2</sup>University of California, Riverside, California, USA

<sup>3</sup>U.S. EPA, Office of Research and Development, National Risk Management Research Laboratory,  
Research Triangle Park, North Carolina, USA

<sup>4</sup>Jacobs Technologies, Research Triangle Park, North Carolina, USA

<sup>5</sup>Sibley School of Mechanical and Aerospace Engineering, Cornell University, Ithaca, New York, USA

**Abstract:** Regulatory and urban planning programs require an accurate evaluation of how traffic emissions transport and disperse from roads to fully determine exposures and health risks. Roadside vegetation barriers have shown the potential to reduce near-road air pollution concentrations; however, the characteristics of these barriers needed to ensure pollution reductions are not well understood. U.S. EPA conducted several field experiments to understand the effects of vegetation barriers on dispersion of pollutants near roadways (e.g. 2008 mobile monitoring study in Chapel Hill, North Carolina and 2014 mobile monitoring study in San Francisco Bay Area, California). The results of these field studies were used to evaluate dispersion models in simulating the effects of near road barriers and to develop recommendations for model improvements. The improved models can be used for evaluating the effectiveness of vegetation barriers as a potential mitigation strategy to reduce exposure to traffic-related pollutants and their associated adverse health effects. This paper presents the results of the analysis of the field studies and discusses the applicability of dispersion models to simulate the impacts of vegetation barriers.

**Key words:** *Roadways, Barriers, Vegetation, Dispersion, Models*

## **INTRODUCTION**

There is a strong international consensus on elevated health risks for populations living, working, or going to school near large roadways. The health concerns have been linked to elevated levels of air pollution caused by traffic emissions. Public health concerns have raised interest in methods to mitigate these traffic emission impacts. Traditionally, transportation and land use planning options have been focusing on vehicle emission standards and reduction in vehicle activity, and also establishing buffer or exclusion zones. These options are typically “long-term” since emission reductions take long to implement and planning and zoning is involved in rerouting and vehicle miles travelled reduction programs. Other options to mitigate the impacts of traffic emission focus on roadway design and urban planning that includes road location and configuration, and roadside noise barriers and vegetation. The advantage of the roadside barriers option is that it provides an opportunity for a “short-term” solution and also because roadside features may already be present. Also, the roadside barriers often have other positive benefits. Thus, appropriately selected and planted roadside vegetation may reduce traffic-related air pollution concentrations by providing a way of reducing exposures to traffic emissions. While roadside vegetation barriers have shown the potential to reduce near-road air pollution concentrations, the characteristics of these barriers needed to ensure pollution reductions are not well understood. Therefore, models and more supporting field measurement data are needed to fully assess these impacts. U.S. EPA has initiated studies to examine how roadside vegetation barriers affect near-road air pollutant exposures. The studies used a combination of modeling and monitoring to characterize the impact of roadway features on near-road air quality. The 2008 mobile monitoring study Chapel Hill, North Carolina and 2014 mobile monitoring study in Woodside, California provided data to evaluate dispersion models in simulating the effects of near road barriers and to develop recommendations for model improvements.

### CHAPEL HILL ROADSIDE BARRIER FIELD STUDY

The Chapel Hill, North Carolina field study was conducted in fall of 2008 along U.S. Route 15–501. The Geospatial Monitoring of Air Pollution (GMAP) electric car provided real-time mapping of PM, NO<sub>2</sub>, and CO by repeatedly driving a specified route at each study site. Thus, mobile monitoring provided spatially-resolved air quality data behind the barrier in the clearing. Details of the experimental setup can be found in (Hagler et al., 2012). The vegetation barrier consists around 10% of deciduous trees (Maple tree), and 90% of coniferous trees (Leyland Cypress and Morella cerifera) approximately 4-8 m in height and 2-5 meters thick (Figure 1). A four lane highway, US 15-501, passed next to the vegetation barrier.



**Figure 1.** Pictures of vegetation barriers in Chapel Hill, NC next to highway (left) and behind the barrier (right)

We used a combination of measurement and modeling to evaluate the impact of vegetation barriers and developing recommendation for improved dispersion modeling algorithms based on solid barrier algorithms to be applicable for vegetation barriers. We used the Comprehensive Turbulent Aerosol Dynamics and Gas Chemistry (CTAG) model with Large Eddy Simulation (LES) to simulate the impacts of vegetation barriers on dispersion ultrafine particulates near roadway and evaluated model results against the Chapel Hill field study data (Tong et al., 2016). The results of CTAG with LES model simulations compared well with observations behind the vegetation barrier and the model was able to capture the trend observed in the experiment (Steffens et al., 2012). The results of model evaluation against the Chapel Hill data provided us with the confidence in CTAG with LES to simulate other scenario. Next, we used the model to explore the effects of vegetation barriers on near-road particle concentrations using six common near-road configurations: 1) a no-barrier scenario for comparison with other configurations; 2) a wide vegetation barrier located next to the road; 3) a solid barrier configuration; 4) a “green wall” configuration, which is a combination of solid barrier and vegetation cover; 5) a “vegetation–solid barrier combination” scenario where a tall vegetation barrier is behind a solid wall; 6) configuration where both upwind and downwind vegetation barriers are present. The near-road air quality is primarily driven by two physical mechanisms, i.e., dispersion and deposition, and deposition only occurs in the presence of vegetation. The results of model simulations highlight the removal from vegetation, especially for smaller, ultrafine particles. The modeling suggests two potentially viable design options as a potential mitigation option for near-road particulates: 1) a wide vegetation barrier with high Leaf Area Density, and 2) vegetation–solid barrier combinations, i.e., planting trees next to a solid barrier. However, these recommendations for vegetation barrier designs are based on model simulations for a few generic configurations, and therefore future implementation needs to take into account site-specific characteristics, given the complexity of urban landscapes.

### CALIFORNIA ROADSIDE BARRIER FIELD STUDY

The California Roadside Barrier study was conducted to determine the influence of vegetation barriers on near-road pollutant concentrations. The study was conducted in San Francisco Bay area along Interstate-280 near Woodside, CA. Measurements were conducted near a roadway with varying vegetation types – bush/tree combinations with varying porosity and manicured hedges (Figure 2). The study was conducted for approximately one month, from late August until late September, 2014 for approximately three hours each day during either morning or afternoon time periods. Data collected included traffic counts and speed, meteorology, and air quality for multiple pollutants. Concentrations of NO<sub>2</sub>, CO, ultrafine particles

(UFP), and black carbon (BC) were measured using the Geospatial Monitoring of Air Pollution (GMAP) electric car and fixed sites along two limited-access stretches of highway that contained a section of the vegetation barrier and a section with no noise barrier at-grade with the surrounding terrain.

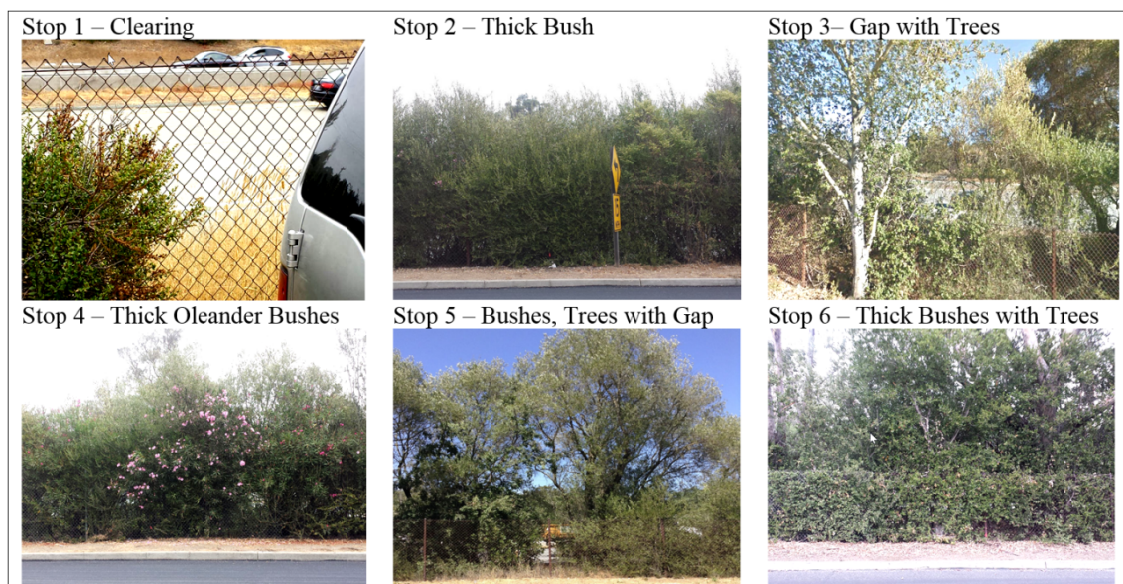


**Figure 2.** Examples of varying near-roadway vegetation types in Woodside, CA

The GMAP measurements were conducted across six locations behind the barrier with different characteristics: Stop 1 – clearing; Stop 2 - behind bushes; Stop 3 - gap with trees; Stop 4 - behind thick oleander bushes; Stop 5 - gap with trees; Stop 6 - behind thick bushes and trees (Figure 3). These measurements and analysis are critical for the development of improved model algorithms capable of simulating pollutant transport and dispersion of near-surface releases in the presence of roadside barriers.

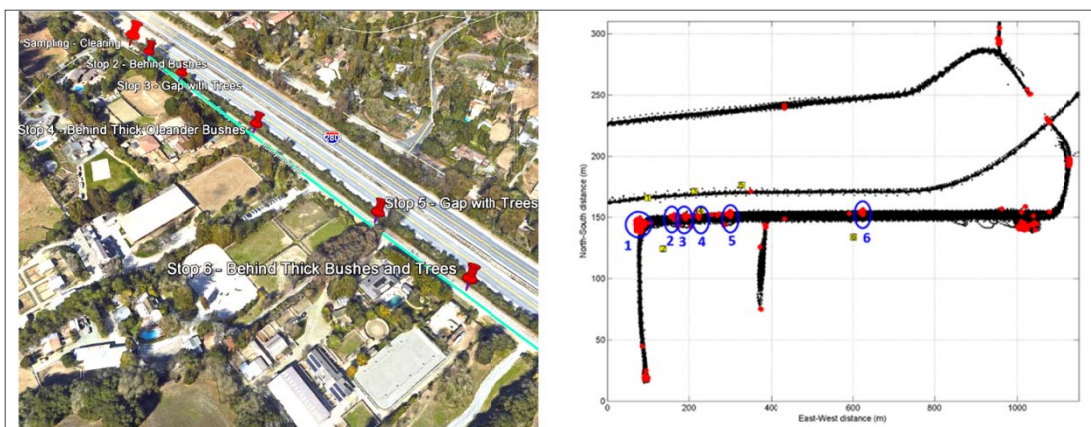


**Figure 3.** Aerial view of the study site in Woodside, CA (left) and a map of mobile measurement locations (right) at selected 6 stops along the vegetation barriers where GMAP measurements were taken.

The results of GMAP measurements at Woodside location for CO and UFP are shown in Figure 4. Distributions of observed concentrations from all 1-second measurements in Woodside are compared across six locations behind the barrier with different characteristics. Each distribution is based on a roughly ten thousand observations during the entire field campaign. This, the distributions represent a longer-term exposure over the range of varying meteorological conditions. The results indicate the reduction in concentrations behind the barrier. The median values of the distribution behind the barrier

with different characteristics (stops 2 and 3 – bushes, stops 5 and 6 –trees) are generally lower than in the clearing. One exception is stop 3, which is a gap in the barrier. This is consistent with the findings from other studies that have shown that spaces and gaps between roadside vegetation can lead to increased pollutant concentrations along and away from the road. Therefore, vegetation must be thick and without gaps to be considered as a potential mitigation option.

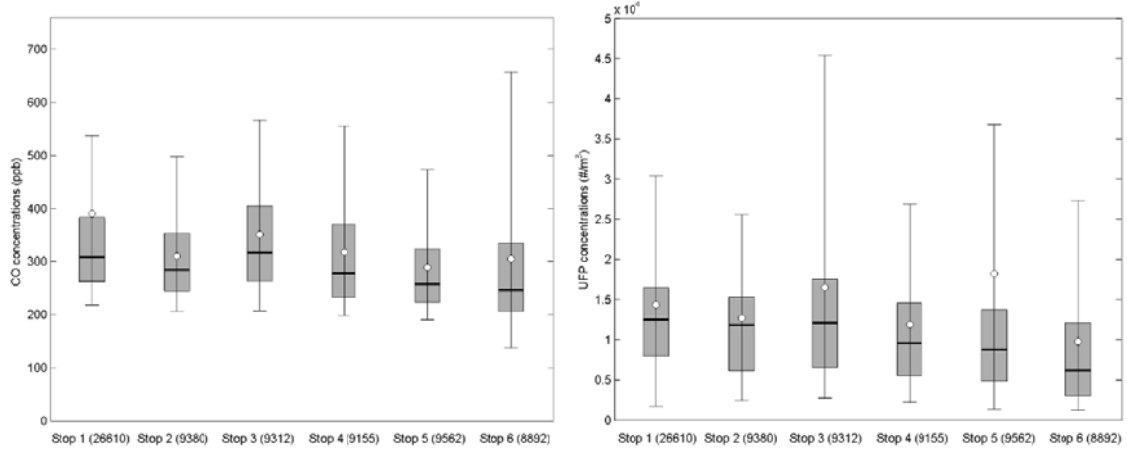


**Figure 4.** Distributions of observed CO (left) and UFP (right) concentrations from all mobile measurements in Woodside. Each distribution is based on  $n$  observations (shown below). The middle line represents the median, the box the 25th and 75th percentiles, and the whiskers the 5th and 95th percentiles. The point represents the mean value of the distribution.

We can quantify the effect of vegetation on reducing near road concentrations by estimating the height of a solid barrier that would result in the same reduction. The primary effect of a solid barrier is to increase vertical dispersion of the pollutants emitted from the road. A simple model of this effect adds the height of the barrier to the vertical dispersion. Then, if we assume that the emissions from the road are distributed over the width of the road,  $W$ , the concentration at a distance,  $d$ , from the edge of the road is given by (Schulte et al., 2014):

$$C = \sqrt{\frac{2}{\pi}} \frac{q}{W \sigma_w} \ln \left( 1 + \frac{W}{d + \frac{HU}{\sigma_w}} \right), \quad (1)$$

where  $q$  is the emission rate per unit length of the road,  $H$  is the height of the barrier,  $\sigma_w$  is the standard deviation of the vertical velocity fluctuations, and  $U$  is the near surface wind speed. If we assume that vehicle induced turbulence enhances the vertical spread by 2 m, we can derive an expression for the solid barrier height that would have resulted in the observed concentration reduction,  $R$ , seen by the vegetative barrier relative to the open section:

$$H = \frac{\sigma_w}{U} \left( \frac{W}{p-1} - 1 \right), \quad (2)$$

where  $p$  is given by

$$p = \left( 1 + \frac{W}{d + \frac{H_0 U}{\sigma_w}} \right)^R, \quad (3)$$

where  $R$  is the ratio of the concentration behind the vegetative barrier to the concentration in the open section, and  $H_0=2$  m corresponds to vehicle induced turbulence in the open section.

Table 1 presents results for the measurements made in Woodside. Here  $R$  refers to the mean of the reductions of the four species at each of the stops. The variables  $\sigma_w$  and  $U$  were derived from the sonic measurements made at a 3m height in the open area. All the variables used in deriving averages correspond to the wind direction blowing the emissions towards the measurement stops.

We see that the computed solid barrier heights, in the last column, are consistent with the heights of the vegetation and their coverage. This suggests that it might be possible to estimate the equivalent height of a barrier using the actual height of the vegetative barrier and its porosity. In principle, this would allow us to compute the effect of a vegetative barrier under different meteorological conditions using more established models for dispersion behind a solid barrier (Schulte et al., 2014).

**Table 1.** Effect of Vegetative Barriers on Concentrations

Stop Number	Height of Vegetation (m)	Description	Reduction	Equivalent Barrier Height (m)
1	0	Clear	1	2.0
2	3-4	vegetation buffer ~6-7m with approx. 75% coverage	0.77	3.5
3	3-4	Wide gap (>4m) with highly porous mix of trees and thin bushes (~6-7m with approx. 50% coverage)	1	2.0
4	3-4	vegetation buffer ~6-7m with approx. 90% coverage	0.73	3.9
5	3-4	trees ~10m, thick vegetation buffer ~7m, and 1m wide gap with little vegetation	0.85	2.8
6	3-4	trees 10-12m, vegetation buffer ~7m with approx. 90% coverage	0.71	4.1

## SUMMARY

The results of the combined monitoring and modeling analysis indicate that roadside vegetation can affect downwind pollutant concentrations in both positive and negative ways. Roadside bushes and hedges can result in improved near-road air quality if designed properly. However, some other configurations such as large gaps in vegetation would not impact the dispersion or could even increase concentrations behind the barrier. Our analysis suggest the following barrier configurations that could help mitigate near-road exposures to traffic pollution: 1) Complete coverage from ground to top; 2) No gaps or dead tree areas (original planting and maintenance of vegetation); 3) Sufficient length for protecting sensitive populations/land uses.

## REFERENCES

- Hagler, G.S.W., E.D. Thoma, R.W. Baldauf, 2010: High-Resolution Mobile Monitoring of Carbon Monoxide and Ultrafine Particle Concentrations in a Near-Road Environment, *J. Air & Waste Manage Assoc.* **60**, 328–336
- Steffens, Y.J. Wang, K.M. Zhang, 2012: Exploration of effects of a vegetation barrier on particle size distributions in a near-road environment. *Atmos. Environ.*, **50**, 120-128
- Tong, Z., R.W. Baldauf, V. Isakov, P. Deshmukh, K.M. Zhang, 2016: Roadside vegetation barrier designs to mitigate near-road air pollution impacts. *Science Tot. Environ.*, **541**, 920-927
- Schulte, N., Snyder, M., Heist, D. and Venkatram, A., 2014: Effects of solid barriers on dispersion of roadway emissions. *Atmos. Environ.* **97**, 286-295.
- Venkatram, A., V. Isakov, P. Deshmukh, R. Baldauf, 2016: Modeling the Impact of Noise Barriers on Near Road Air Quality. *Atmos. Environ.*, (in review)

**17th International Conference on  
Harmonisation within Atmospheric Dispersion Modelling for Regulatory Purposes  
9-12 May 2016, Budapest, Hungary**

---

**A HYBRID APPROACH FOR THE NUMERICAL SIMULATION OF FLOWS IN URBAN ENVIRONMENT**

*Bence Hermann and Miklós Balogh*

Department of Fluid Mechanics, Budapest University of Technology and Economics, Budapest, Hungary

**Abstract:** Observing the nature of the air flows in urban environment is essential in the understanding of processes which have influence on urban climate and air quality. Numerical simulation is one way to achieve this. However, CFD simulations of atmospheric flows in these environments require huge amounts of computational capacity if the whole geometry is fully detailed. There are techniques to reduce this requirement, while still producing acceptable results. One of these is the hybrid method, which uses source terms in the transport equations to model the effects of the buildings implicitly. The geometry is explicitly modelled only around the target area of analysis. This method can drastically reduce the cell number, resulting in a much faster numerical simulation. The aim of this study is to create an OpenFOAM solver which is capable of handling this porosity drag force approach. The parameters of the source terms are calculated by performing a series of CFD calculations with different cuboid-shaped buildings using cyclic boundary conditions. A local drag coefficient can be obtained for each cell level between the ground and the top of the building, for each building geometry. This is the main parameter of the source terms. The final goal was to implement the hybrid model in OpenFOAM with the parametrized implicit approach, and it is compared to the results of explicit CFD simulations.

**Key words:** porous drag-force approach, parametrization, RANS, OpenFOAM, height dependent drag coefficient

## INTRODUCTION

The Reynolds-Averaged Navier-Stokes (RANS) modelling of atmospheric boundary layer flows has always been a widely researched topic as it can assist in the solution of a broad range of engineering problems. In many cases, however, there are various types of roughness elements on the ground. Resolving these details with the mesh vastly increases the computational requirements, so the modelling of the effects of these elements on the flow is advisable. One way to do this is the porous drag-force approach, which utilizes sink terms in the transport equations to avoid explicit modelling of the geometry, reducing the computational cost. This approach has been used to model the effects of roughness elements such as vegetation, trees, crops, forests on the flow, investigated by e.g. Green (1992) and Liu et al. (1996). Yee, Lien (2004-2005), Balogh and Kristóf (2010) among others examined the implicit modelling of building arrays, which is the subject of the current investigation.

In this present study the parametrization of an OpenFOAM solver are performed utilizing a so-called hybrid method based on numerous CFD simulations with explicitly modelled geometries. This method combines the two ways by using the porous drag-force approach in the less important, peripheral regions and modelling the geometry explicitly at the target area of analysis.

## NUMERICAL SIMULATIONS WITH EXPLICIT GEOMETRY

A series of RANS simulations had to be performed to obtain the necessary parameters for the porous drag force approach. In these we examined the vertical distribution of the field variables around a surface-mounted cuboid with cyclic (or in other words periodic) boundary conditions, which models one building of a building array as seen on Figure 1. The cuboids were described using the following two geometric parameters:

- Building density [-]: 
$$\lambda = \frac{L_{dx} L_{dy}}{L_x L_y}$$

- Building height [m]:  $H$

We looked to obtain a local drag coefficient which depends on these two geometric parameters and the distance from the ground. The base cross section of the buildings was assumed to be a square.

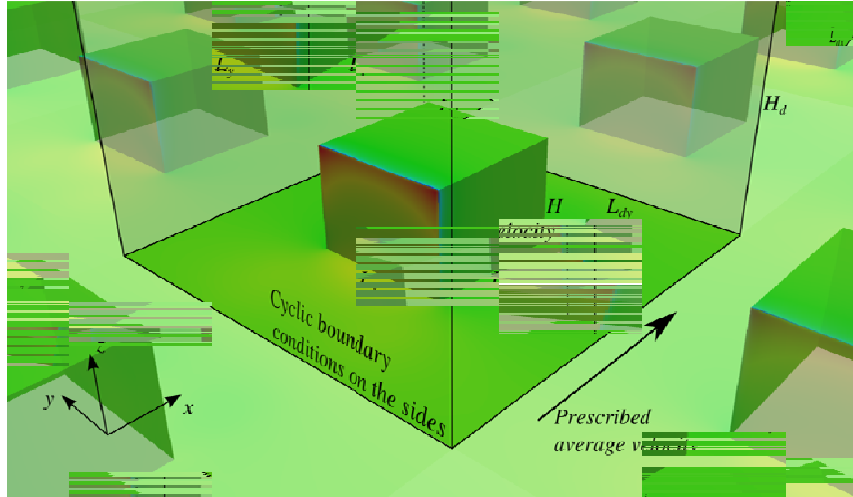


**Figure 1.** Computational domain and geometric dimensions

We used the blockMesh utility of OpenFOAM to create a structured mesh around the building model. To improve the solution quality and convergence, cells with high aspect ratios such as those near the solid surfaces could not be allowed to appear at the cyclic boundaries of the domain, as seen below on Figure 2.

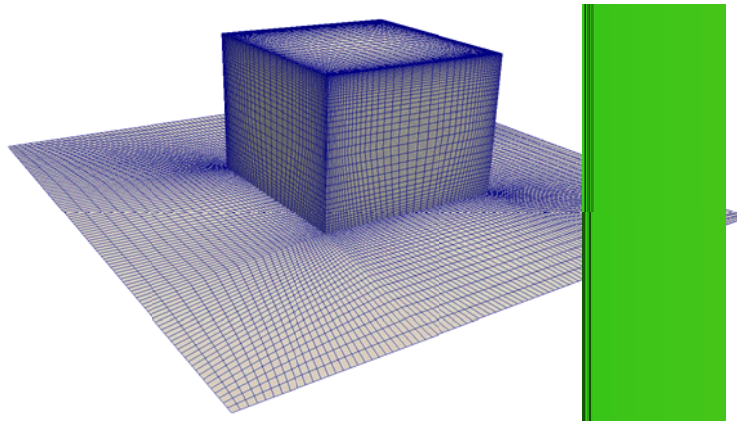


**Figure 2.** Surface mesh on the building walls and ground surfaces

The flow was assumed to be incompressible and steady-state, which greatly reduced computational time. Since the boundary conditions are cyclic on all sides of the domain, an explicit pressure gradient source term was implemented in the momentum equation to allow a steady-state solution. This source term was automatically adjusted to keep a prescribed average velocity constant in the domain, which is the initial condition for the calculations in all cells. The prescribed value is calculated by averaging the velocity profile introduced by Richards and Hoxey (1993) for 2D incompressible steady-state modelling of the atmospheric boundary layer using  $k - \epsilon$  turbulence model:

$$U(z) = \frac{u_\epsilon}{\kappa} \ln\left(\frac{z + z_0}{z_0}\right) \quad (1)$$

With a given reference velocity of  $U_{ref} = 3 \text{ ms}^{-1}$  at the reference height of  $z_{ref} = 10 \text{ m}$  and the known ground surface roughness  $z_0$ , the friction velocity could be calculated, fully defining the profile. The direction of this prescribed velocity was parallel with the x-axis for our current investigation. The cuboid can be considered a bluff body, which means that the Reynolds number dependence of the drag coefficient should be negligible. Therefore the averaged velocity was kept constant throughout all calculations.

The turbulence model used in the simulations was a modified version of the standard  $k - \varepsilon$  model, where a source term used by Parente and Benocci (2010) was added to the dissipation rate transport equation. At the ground and the building walls the rough wall functions proposed by Balogh (2014) were used. The  $k$  and  $\varepsilon$  values were also initialized using the profiles proposed by Richards and Hoxey (1993):

$$k(z) = \frac{u_\tau^2}{\sqrt{C_\mu}} \quad (2)$$

$$\varepsilon(z) = \frac{u_\tau^3}{\kappa(z + z_0)} \quad (3)$$

The numerical simulations took 4-5 days each on a single processor core, which is a very long time for a RANS simulation with a relatively small cell count (1-1.5 million cells). The reason for this was the cyclic boundaries, which vastly increased the number of iterations.

#### PARAMETRIZATION OF THE DISTRIBUTED DRAG FORCE APPROACH

The next step was to extract the vertical distribution of the field variables from the converged solutions, which was realized by averaging the values at the cyclic boundaries in each horizontal cell layer of the structured mesh. All field variables depend on  $\lambda$ ,  $H$ , and the vertical ground distance. For our goals it was necessary to fit analytical expressions to the obtained curves, which was performed in three steps. First, an individual profile was fit in each case for the different  $\lambda$ ,  $H$  pairs. Then, the  $\lambda$  dependence of the parameters of these expressions was described with second-order polynomials. Finally, the building height dependence of the parameters of these polynomials was approximated with another second-order expression. The final two steps are equivalent to fitting a second-order surface to each parameter of the individual expressions. These operations were performed with the built-in Levenberg-Marquardt nonlinear least-squares fitting algorithm in the optim package for Octave ("leasqr" function).

The velocity profile could be approximated with a sum of a tangent and a linear function below the building height, and a logarithmic function above it, which have six parameters altogether:

$$U(\tilde{z}) = \begin{cases} A_{U1} \cdot \tan(A_{U2}(\tilde{z} - A_{U3})) + A_{U4} + A_{U5}\tilde{z} = f_{U1}(\tilde{z}) \\ A_{U5} \cdot \ln(\tilde{z}) + f_{U1}(1) = f_{U2}(\tilde{z}) \end{cases} \quad \text{where } \tilde{z} = \frac{z}{H} \quad (4)$$

The problem with this approximation is that it does not ensure the continuity of the derivative of  $U(z)$ . For this reason a blending function was introduced in the following way to avoid using conditional expressions:

$$U(\tilde{z}) = (1 - f_{blend}(\tilde{z})) \cdot f_{U1}(\tilde{z}) + f_{blend}(\tilde{z}) \cdot f_{U2}(\tilde{z}) \quad , \text{ where } f_{blend}(\tilde{z}) = \frac{\tanh(B \cdot (\tilde{z} - 1)) + 1}{2} \quad (5)$$

This is basically a "derivable" Heaviside step function if the B parameter is a high value. It is also important to note that the points at the very top of the domain were neglected for the curve fitting, because the zero gradient boundary condition "straightened" out the logarithmic velocity profile, which was unphysical.

The turbulent kinetic energy and its dissipation were approximated with the two expressions below:

$$k(\tilde{z}) = A_{k1}e^{-A_{k2}(\tilde{z}-1)} - A_{k3}e^{A_{k4}(-\tilde{z}-A_{k5})} \quad (6)$$

$$\varepsilon(\tilde{z}) = (1 - f_{blend}(\tilde{z})) \cdot \left( \frac{A_{\varepsilon1}}{\tilde{z}} - \frac{A_{\varepsilon2}}{\tilde{z}-1} + A_{\varepsilon3}\tilde{z} + A_{\varepsilon4} \right) + f_{blend}(\tilde{z}) \cdot \frac{A_{\varepsilon5}}{\tilde{z} - A_{\varepsilon6}} \quad (7)$$

For each  $A_{fv,j}$  (the  $j$ -th parameter of the field variable  $fv$ ) a two-step surface fitting was performed. First, for each  $H$ , the  $\lambda$  dependence of the  $A_{fv,j}$  parameters was estimated with a second-order polynomial, then the building height dependence of the  $A_{\lambda i}$  parameters was approximated with a quadratic expression as well:

$$A_{fv,j} = A_{\lambda1} \cdot \lambda^2 + A_{\lambda2} \cdot \lambda + A_{\lambda3} \quad (8)$$

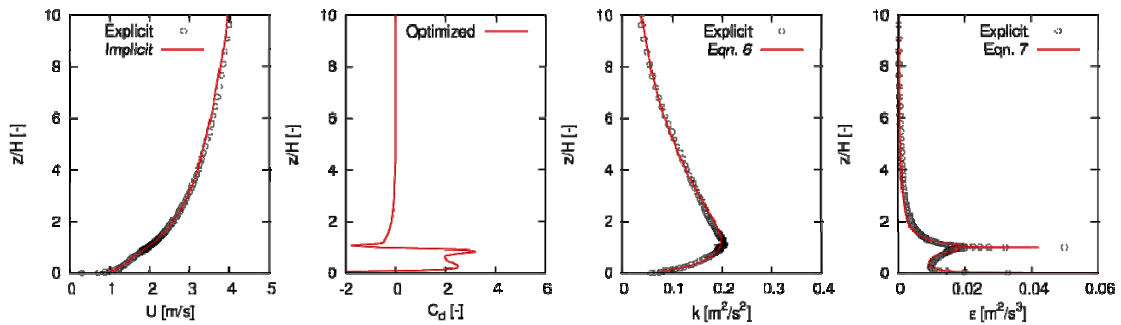
$$A_{\lambda,i} = A_{H1} \cdot H^2 + A_{H2} \cdot H + A_{H3} \quad (9)$$

An example for function parameter fitting can be seen on Figure 3 for  $H = 6.5$  meter and  $\lambda = 0.075$ . The empty circles are the values from the explicit CFD simulations, while the continuous red curves are the fitted analytical expressions.

Based on the results of the simulations with the explicit approach, we could move on to the programming of the OpenFOAM solver. To implement the building resistance implicitly into the solver, we added the following source term into the momentum equation in the desired regions:

$$S_i(z) = \frac{\rho}{2} C_D(z) A_f U(z) u_i(z) \quad (10)$$

$A_f$  is the cross-section area of the building per unit volume,  $U$  is the velocity magnitude and  $u_i$  is the velocity component in the  $i$ -th direction. The vertical distribution of the drag coefficient was obtained by a solver written for this purpose. We ran simulations with a 2D domain with cyclic boundary conditions, basically a slice of the domain seen on Figure 1 in the  $x$ - $z$  plane without the building. The value of  $C_d$  at height  $z$  was continuously modified throughout the iterations according to the difference between the actual and desired velocity distributions, which were calculated according to equation (5).



**Figures 3.** Vertical profiles for velocity, turbulent properties and sectional drag coefficient.

## RESULTS AND DISCUSSION

On Figure 3 it can be observed that the velocity distribution results with the implicit method provide a good approximation of the explicit case, and the necessary local drag coefficient distribution to obtain this can be seen next to it. It can be seen that in order to precisely achieve the desired vertical velocity distribution it is not enough to utilize the source term in the region below the building height, but a value different from zero should be prescribed above it. Simply calculating the sectional drag coefficients from the wall forces would give a significant error mainly because of this.

The implemented hybrid solver is able to handle arbitrary amount of implicit and explicit regions, making it viable for numerous urban atmospheric CFD problems. This mainly includes providing realistic boundary conditions for the target area of analysis, e.g. calculating the forces acting on a certain building, pollutant dispersion in urban areas or planning of the location of wind turbines.

#### SUMMARY AND OUTLOOK

A novel hybrid solver is developed for the simulation of urban flows and it is parameterized based on a series of explicit CFD simulations. Additionally, analytical profiles are fitted for  $U$ ,  $k$  and  $\varepsilon$  based on the explicit results. These profiles could serve as boundary conditions in CFD simulations, where the domain is limited to a bounded region of a city. The implicit parametrization scheme of the hybrid method ensures good agreement between the explicit and implicit volume fluxes with the height dependent drag coefficient values imposed in each cell.

In order to extend the generality of the parametrization, varying building side ratios should be investigated with various flow directions. The implementation of source terms for the turbulent kinetic energy and its dissipation is also planned to ensure pronounced matching between the explicit and implicit turbulent properties. These source terms can be calculated from the analytical profiles in equations (6) and (7) and the previously obtained  $C_d$  profiles, and implemented similarly to Green et al. (1995) and Balogh and Kristóf (2010). The solver can then be validated against the MUST (Mock Urban Setting Trial) experimental data, similarly to Balogh (2014).

#### ACKNOWLEDGEMENTS

The support of the project K 108936 “Flow and dispersion phenomena in urban environment” of the Hungarian Scientific Research Fund is gratefully acknowledged.

#### REFERENCES

- P.J. Richards and R.P. Hoxey, 1993: Appropriate boundary conditions for computational wind engineering models using the k- $\varepsilon$  turbulence model. *Journal of Wind Engineering and Industrial Aerodynamics*, **46 & 47**, 145-153.
- E. Yee and F. Lien, 2004: Numerical Modelling of the Turbulent Flow Developing Within and Over a 3D Building Array, Part I: A High Resolution Reynolds-averaged Navier-Stokes Approach. *Boundary-Layer Meteorology*, **112**, 427-466.
- E. Yee and F. Lien, 2005: Numerical Modelling of the Turbulent Flow Developing Within and Over a 3D Building Array, Part II: A Mathematical Foundation for a Distributed Drag Force Approach. *Boundary-Layer Meteorology*, **114**, 245-285.
- E. Yee and F. Lien, 2005: Numerical Modelling of the Turbulent Flow Developing Within and Over a 3D Building Array, Part III: A Distributed Drag Force Approach, Its Implementation and Application. *Boundary-Layer Meteorology*, **114**, 287-313.
- E. Yee and F. Lien, 2004: A Distributed Drag Force Approach for the Numerical Simulation of Urban Flows. *DRDC Suffield TR 2004-169*
- M. Balogh, 2014: Numerical simulation of atmospheric flows using general purpose CFD solvers. *PhD thesis*
- M. Balogh and G. Kristóf, 2010: Fine scale simulation of turbulent flows in urban canopy layers. *Időjárás, Quarterly Journal of the Hungarian Meteorological Service*, **114**, 135-148.
- S.R. Green, 1992: Modelling turbulent air flow in a stand of widely-spaced trees. *Journal of Computational Fluid Dynamics and Its Applications*, **23**, 294-312.
- S.R. Green, J. Grace, and N.J. Hutchings, 1995: Observations of turbulent air flow in three stands of widely spaced sitka spruce. *Agricultural and Forest Meteorology*, **74**, 205-225.
- J. Liu, J.M. Chen, T.A. Black, and M.D. Novak, 1996: E- $\varepsilon$  Modelling of Turbulent Air Flow Downwind of a Model Forest Edge. *Boundary-Layer Meteorology*, **77**, 21-44.
- A. Parente and C. Benocci, 2010: On the RANS simulation of neutral ABL flows. The Fifth International Symposium on Computational Wind Engineering (CWE2010)

**17th International Conference on  
Harmonisation within Atmospheric Dispersion Modelling for Regulatory Purposes  
9-12 May 2016, Budapest, Hungary**

---

**REDUCED-FORM AIR QUALITY MODELING FOR COMMUNITY-SCALE APPLICATIONS**

*Vlad Isakov<sup>1</sup>, Timothy Barzyk<sup>1</sup>, Saravanan Arunachalam<sup>2</sup>*

<sup>1</sup>U.S. EPA, Office of Research and Development, National Exposure Research Laboratory,  
Computational Exposure Division, Research Triangle Park, North Carolina, USA

<sup>2</sup>Institute for the Environment, University of North Carolina, Chapel Hill, North Carolina, USA

**Abstract:** Transportation plays an important role in modern society, but its impact on air quality has been shown to have significant adverse effects on public health. Numerous reviews (HEI, CDC, WHO) summarizing findings of hundreds of studies conducted mainly in the last decade, conclude that exposures to traffic emissions near roads are a public health concern. The Community LINE Source Model (C-LINE) is a web-based model designed to inform the community user of local air quality impacts due to roadway vehicles in their region of interest using a simplified modeling approach. Reduced-form air quality modeling is a useful tool for examining what-if scenarios of changes in emissions, such as those due to changes in traffic volume, fleet mix, or vehicle speed. Examining various scenarios of air quality impacts in this way can identify potentially at-risk populations located near roadways, and the effects that a change in traffic activity may have on them. C-LINE computes dispersion of primary mobile source pollutants using meteorological conditions for the region of interest and computes air-quality concentrations corresponding to these selected conditions. C-LINE functionality has been expanded to model emissions from port-related activities (e.g. ships, trucks, cranes, etc.) in a reduced-form modeling system for local-scale near-port air quality analysis. This presentation describes the Community modeling tools C-LINE and C-PORT that are intended to be used by local government, city planners and community groups.

*Key words:* Air pollution, Dispersion Modeling, Emissions, Exposure

## **INTRODUCTION**

Transportation plays an important role in modern society, but its impact on air quality has been shown to have significant adverse effects on public health. Numerous reviews (HEI, CDC, WHO) summarizing findings of hundreds of studies conducted mainly in the last decade, conclude that exposures to traffic emissions near roads are a public health concern. Health effects have been associated with near-road exposures and proximity to large emission sources, so characterizing emission sources is important for understanding potential health effects. Community groups are becoming increasingly active in local initiatives that seek to mitigate potentially harmful environmental conditions. However, there is a lack of tools that can be applied to study near-source pollution in an easy manner, and explore the benefits of improvements to air quality and exposures – either due to voluntary or mandatory programs. To address this need, US EPA is developing tools to help community groups to assess air quality impacts from roadway traffic and other sources potentially affecting the community. The modeling tools are designed for a quick assessment and they require limited technical expertise. Such web-based, easy-to-use models can provide valuable insights for the community and can also assist with the decision-making process.

## **REDUCED-FORM MODELS FOR COMMUNITY-SCALE APPLICATIONS**

Reduced-form models provide an opportunity to examine how changes in input parameters can affect results. The power of such tools is to be able to make these assessments in a fairly quick time, and to assess what-if scenarios. These scenarios are created by changing input parameters related to activity, emissions or even meteorological parameters and understanding changes in associated air quality at community scales (that typically range from 10 to 100 square kilometers). The targeted user-community is expected to be non-technical and less sophisticated with modeling expertise, and hence the web-based approach to keep things more intuitive and easy to use.

We are developing a series of community tools (e.g. C-LINE and C-PORT) to study local air quality due to various sources. Each community tool is a modeling and visualization system that accesses inputs, performs calculations, visualizes results, provides options to manipulate input variables, and performs basic data analysis all through an easy-to-use web-based interface. These reduced-form models are intended to support local communities and planners to get an initial assessment of near-source air quality impacts of transportation-related sources (roads, ships, terminal activities, etc.) using national-scale input databases, and reduced-form modeling approaches. These reduced-form models use standard dispersion algorithms and have been evaluated against other regulatory dispersion models, access publicly available emissions, traffic and meteorological datasets, and are optimized to use in community-sized areas (100-1,000 km<sup>2</sup>). The user is not required to provide input data, but can provide their own if desired.

#### **Community-LINE Source Model (C-LINE)**

The Community **LINE** Source Model (C-LINE) is intended to inform the community user of local air quality impacts due to mobile sources in their region of interest (Barzyk et al., 2015). C-LINE is a web-based model that estimates emissions and dispersion of toxic air pollutants for roadways in the U.S. This reduced-form air quality model can examine what-if scenarios for changes in emissions, such as traffic volume, fleet mix and vehicle speed. C-LINE accesses inputs, performs atmospheric dispersion calculations, visualizes results, provides options to manipulate input variables, and performs basic data analysis to present model results in an interpretable manner (Fig 1). C-LINE can identify potentially at-risk populations located near roadways and effects that changes in traffic activity may have on those populations. Currently, C-LINE is capable of modeling any region of the U.S. and can be applied to a number of community-scale applications such as assessing air quality by schools located near busy highways. C-LINE is intended to support local communities and planners to get an initial assessment of near-source air quality impacts of transportation-related sources using national-scale input databases, and reduced-form modeling approaches. C-LINE computes air quality concentrations of primary mobile source pollutants using an analytical version of the R-LINE dispersion model. Specific emissions for each road link are calculated by combining national database information on traffic volume and fleet mix with emissions factors from EPA's MOTO Vehicle Emission Simulator (MOVES) modeling system. Users can modify emissions for each road link by changing traffic composition, speed and/or volume. C-LINE is currently capable of modeling any region of the United States. C-LINE 2.0 can be downloaded from the Community Modeling and Analysis System (CMAS). The CMAS is currently operated under contract by the University of North Carolina at Chapel Hill's Institute for the Environment (<https://www.cmascenter.org/c-tools/>)

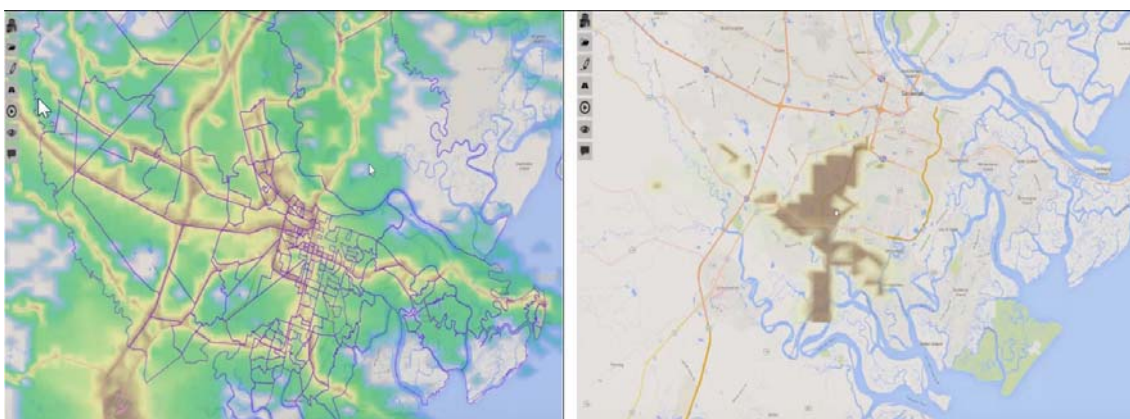


**Figure 1.** Example screen shot from C-LINE showing modelled near-road pollutant gradients (left) as well as the change in PM<sub>2.5</sub> concentrations resulting from emissions changes (right).

#### **Community modeling system for near-port air quality analysis (C-PORT)**

The Community modeling system for near-**PORT** (C-PORT) Tool is intended to inform the community user of localized air quality due to port-related activities in their region of interest using a simplified modeling approach. C-PORT provides a platform for air quality modeling and visualization that can

inform community users about ways that emissions from commercial ports can impact local air quality. The model allows users to visualize and evaluate different planning scenarios under consideration, helping them identify the impacts of varying development alternatives to help make better long-term decisions that protect community health and promote sustainability. Using C-PORT, for example, communities can model the impact of proposed or potential development scenarios, such as increased transport, alternative trucking routes, or alternative energy sources (Fig. 2). In addition, C-PORT can help community leaders identify local hotspots and estimate relative contributions from different source sectors, focus on specific nearby populations and locations, and incorporate input from citizen science and data collection activities, as available, thereby identifying where additional mitigation (e.g. tree buffers) might further reduce potential impacts. The web-based, and easy-to-use interface currently includes data from 20 coastal ports (Seattle, WA; Baltimore, MD; New York/New Jersey; Hampton Roads, VA; Morehead City, NC; Wilmington, NC; Charleston, SC; Savannah, GA; Brunswick, GA; Jacksonville, FL; Port Canaveral; Palm Beach, FL; Everglades, FL; Miami, FL; Tampa, FL; Panama City, FL; Pensacola, FL; Mobile, AL; Gulfport, MS; Pascagoula, MS), and has a map-based interface similar to the widely used Google Earth. The tool has been developed for visualizing changes in air quality due to changing development scenarios, and is not intended to support or replace any regulatory models or programs.

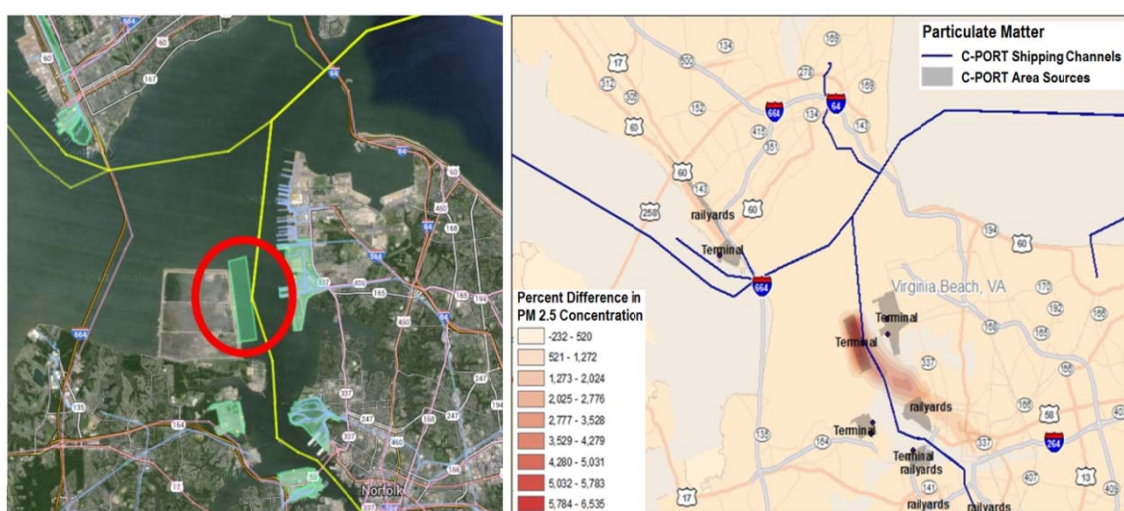


**Figure 2.** Example screen shot from C-PORT showing planned construction of Craney Island to increase container volumes at Panama Canal (left) as well as the change in PM<sub>2.5</sub> concentrations (%) resulting from the proposed expansion (right)

## REFERENCES

- Arunachalam, S., H. Brantley, T. Barzyk, G. Hagler, V. Isakov, S. Kimbrough, B. Naess, N. Rice, M. Snyder, K. Talgo, A. Venkatram. 2016: Assessment of port-related air quality impacts: geographic analysis of population. *International Journal of Environment and Pollution* (in press)
- Barzyk, T., V. Isakov, S. Arunachalam, A. Venkatram, R. Cook, B. Naess. A Near-Road Modeling System for Community-Scale Assessments of Mobile-Source Air Toxics: The Community Line Source (C-Line) Modeling System. *Environmental Modelling & Software*, **66**, 46-56

**MODELLING THE RECIRCULATION ZONE IN STREET CANYONS WITH DIFFERENT  
ASPECT RATIOS, USING CFD SIMULATION**

*Arsenios Chatzimichailidis<sup>1</sup>, Marc Assael<sup>1</sup>, Matthias Ketzel<sup>2</sup> and Konstantinos E Kakosimos<sup>3</sup>*

<sup>1</sup>Department of Chemical Engineering, Aristotle University of Thessaloniki, Thessaloniki, Greece

<sup>2</sup>Department of Environmental Science, Aarhus University, Roskilde, Denmark

<sup>3</sup>Chemical Engineering Department & Mary Kay 'O Connor Process Safety Center, Texas A&M  
University at Qatar, Doha, Qatar

**Abstract:** Poor air quality in cities was indicated as the cause of seven million deaths, one out of eight globally, only in 2012. Urban streets are the epicentre of the problem, as high concentrations are frequently measured, caused mainly by the traffic and secondly by the general urban background pollution. The flow inside street canyons has some specific characteristics that tend to obstruct the removal of pollutants from the city level. The small scale models that are used to study pollution in streets have to consider about these flow patterns, which many times are referred with the collective term recirculation zone. Our main hypothesis is, that the flow regime in a street canyon governs the recirculation zone and consequently the dispersion. Thus, a quasi-universal expression for the recirculation zone could expand the applicability of these simple models in cases of higher complexity. To understand better the recirculation zone, CFD simulations are validated and used. We use vortex detection methods, namely vorticity, streamlines and the  $\lambda_2$  and Q criteria, to visualize the vortex structures. The final results are rather inconclusive, although the combined use of the above methods certainly give some insights to the flow structure. In any case more exploratory analysis is necessary in order to validate the further develop the hypothesis of this work.

**Key words:** *street canyon, recirculation zone, air quality models, Large Eddy Simulation, vortex detection*

## **INTRODUCTION**

Urban streets are a main concern for air quality in cities, as high concentrations are frequently measured, attributed mainly to traffic sources inside the street and secondly to the general urban background pollution. A simple, fast and economical way to study the air pollution is the use of the parameterized air quality models (AQMs), which calculate concentrations of pollutants, using empirical formulations. AQMs have to consider the complexity of the flow inside the streets, as the wind impacts on buildings and creates recirculating vortices, which drastically affect the dispersion of the pollutants inside and above the streets.

The simplest case of flow is the perpendicular, to the building face, wind direction that develops two main vortices, adjacent to the building and the ground (Hanna *et al.*, 1982). Depending on the height to width ratio of the street canyon (aspect ratio), the two vortices inside the canyon intertwine with each other, creating three flow regimes. They have been described (Oke, 1988) as: a) isolated roughness, when the two vortices do not interact, b) wake interference, when the wake behind the leeward building is disturbed by the recirculation created in front of the windward building and c) skimming flow, when the aspect ratio is equal to the unity and one main vortex is formed. Most street canyons are formed by buildings with unequal height and the flow regime for these cases differ significantly (Addepalli and Pardyjak, 2014). Another issue is the solar radiation, as heated facets have been presented to modify the flow and even favour ventilation (Allegrini *et al.*, 2013). Other aspects, such as the roof shape (Kastner-Klein *et al.*, 2004) and the existence of trees at the road sides (Gromke and Ruck, 2009), were indicated to lower the wind speed, reducing the ventilation. Finally, the non-perpendicular wind direction changes the entire flow regime, creating spiral flows (Balogun *et al.*, 2010), which transfer the pollution from one road segment to the other.

Current models haven't incorporated these characteristics yet and rely on empirical parameterizations extensively validated against experiments in real streets. One of the first models, the STREET-SR (Johnson *et al.*, 1973) implicitly defines one single vortex, that covers the width of the canyon and is controlled by the roof level wind velocity. The Canyon Plume Box Model (Yamartino and Wiegand, 1986) uses a single vortex sub-model, for the calculation of the dispersion parameters, the outgoing and incoming fluxes. The Operational Street Pollution Model (Berkowicz *et al.*, 1997), introduced an explicit definition for the recirculation zone as a trapeze, the dimensions of which depend on the upwind building height. On the other hand, SIRANE (Soulhac *et al.*, 2011) assumes that perpendicular wind is a rare situation and most of the time, street canyon segments will be a well-mixed volume with uniform pollutants' concentrations. The fact that these models incorporate the recirculation zone aspect is an advantage for flow regimes that have been defined, but an issue for the rest. On the other hand, the existence of a quasi-universal expression for the recirculation zone could expand the applicability of the typical street canyon models.

Provided that there is convection, the flow regime drives and rules the pollutant concentration levels. In this context, we aim to examine the hypothesis that the recirculation zone can be defined as function of the flow field rather than the geometry. For this reason and to understand better the structure of the recirculation zone, we employ a series of vortex detection methods in various street canyon geometries. These methods analyze the velocity gradient tensor  $\nabla u$ , giving information on the existence of coherent structures. CFD simulations are used to obtain the flow field and apply the detection methods. The next paragraphs discuss the CFD setup and validation, the vortex detection criteria theory and our preliminary results.

## METHODOLOGY

### Configuration setup

Computational Fluid Dynamics (CFD) simulations were carried out using the open-source CFD toolbox OpenFOAM v2.3.1. The used CFD method is the Large Eddy Simulation (LES), the advantage of which is the transient numerical solution of the Navier-Stokes equations, allowing the user to observe the real-time advance of the phenomena. LES use the filtered Navier-Stokes equations, which practically means that the vortices larger than the mesh cells are resolved and the small scale turbulence is modelled. The continuity and momentum equations for incompressible flow are solved by the PISO solver (Issa, 1986). The standard Smagorinsky model (Smagorinsky, 1963) is used for the subgrid turbulence. The model's constant  $C_s$  is set to 0.1 and the van Driest dumping function is applied for the cells along the wall boundaries, as the common suggestions from the papers in this field.

The setup of our simulations is a modified version of the strategy, employed with success initially by (Li, 2008) and later by more researchers such as (Bright *et al.*, 2013). According to the best practices in LES (Franke and Baklanov, 2007), the boundary at the inflow patch has to be time dependent. In our case it is achieved, by recycling the velocity from the outlet patch to the inlet patch (mapped boundary conditions in OpenFOAM 2.3.1). The pressure and turbulent viscosity are solved in each time step. The spanwise boundaries were set to periodic (cyclic in OpenFOAM), as a neutral boundary that doesn't affect the flow. At the top of the computational domain the slip wall or symmetry boundary condition was used, following again the common practice. This setup implies that the studied domain is a street canyon in an infinite array of street canyons with the same aspect ratio. The street canyon area is discretized with 100 cells for the constant height of the buildings and the proportional quantities were assigned to the other acmes, while the width of the mesh was set to 50 cells. The typical computational domain's structure is shown in Figure 1. The results were validated against experimental data from (Li, 2008) for aspect ratios (H/W) 1, 1/2 and 2 and the agreement varied from fair to excellent. The comparisons for aspect ratio 1/2, are shown in Figure 2 and the agreement is fair.

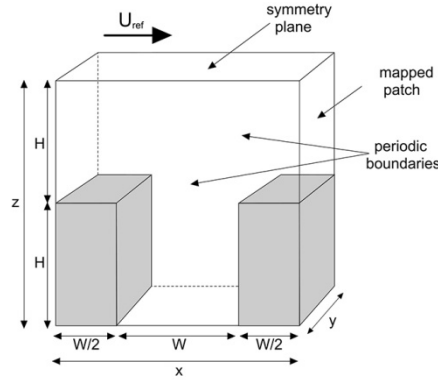


**Figure 1.** The general geometry, computational domain and patches of the simulations

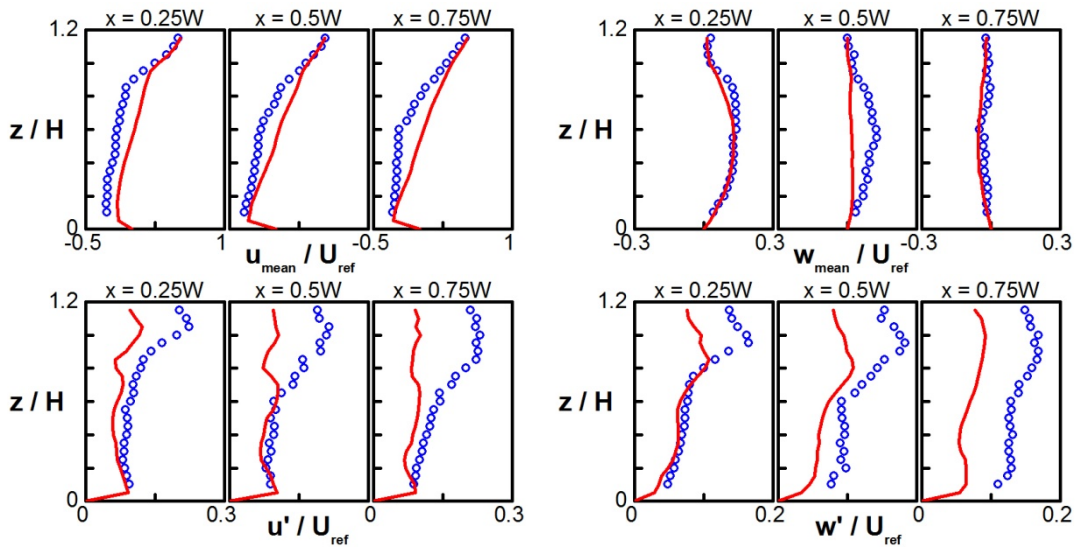


**Figure 2.** Comparison between averages (top) and fluctuations (bottom) of the velocity components for aspect ratio 1. Current simulations (red line) and experiments from (Li, 2008)

### Recirculation zone structure

Any visualization of the instantaneous velocity field is a chaotic picture of vortices. In the case of the average velocity field, the picture becomes clearer, but it is still difficult to distinguish the structure and size of vortices. While there is a lack of a formal and absolute definition of a vortex (Jiang *et al.*, 2005), there are methods – criteria that help to identify and visualize vortices, e.g. vorticity, enstrophy and the Q and  $\lambda_2$  criteria. They are characterized as local, because they apply a point by point mathematical analysis to the gradient velocity tensor  $\nabla \mathbf{u}$  and based on the result, it is decided whether the point is part of the vortex or not (Chakraborty *et al.*, 2005). On the other hand, the velocity streamlines represent the direction of the velocity in the whole studied area and are characterized as a global method, because they examine many cells instead of one. The  $\lambda_2$  criterion (Jeong and Hussain, 1995) has been described as one of the most effective methods.  $\lambda_2$  is the second largest of the three eigenvalues of the gradient velocity tensor  $\nabla \mathbf{u} = \mathbf{S}^2 + \mathbf{\Omega}^2$ , where  $\mathbf{S}$  and  $\mathbf{\Omega}$  are the rate-of-strain and vorticity tensors, respectively. Negative  $\lambda_2$  values indicate that the point belongs to a vortex area, although in practice, such values appear also in areas with highly rotational flow. The Q criterion (Hunt *et al.*, 1988) defines that a vortex exists in the area where  $Q = \frac{1}{2} [|\mathbf{\Omega}|^2 - |\mathbf{S}|^2] > 0$ . Vorticity is a typical but rather vaguely defined meter of the local spinning motion of the flow, described by the vector  $\vec{\omega} \equiv \nabla \times \vec{u}$ , while the streamlines are a number of curves that are tangent to the velocity vector.

## RESULTS

Figure 3 presents the application of some of the vortex detection methods to the average flow field of street canyons with aspect ratio 1/3.

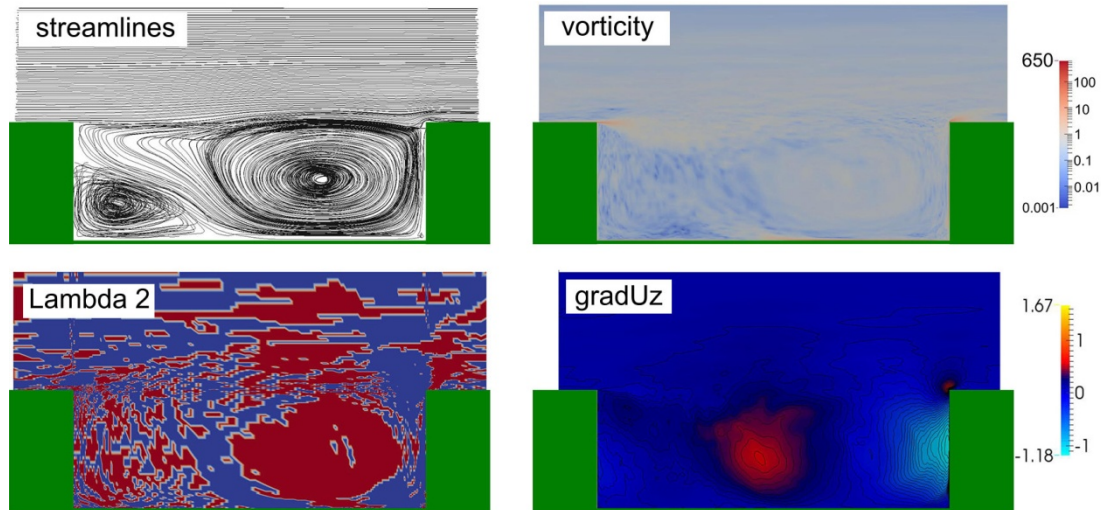


**Figure 3.** Application of vortex detection methods on the average velocity field of a street canyon with  $H/W = 1/3$

Streamlines capture the formation of the biggest vortex in the downwind side of the street canyon, which is backed up by the large area of negative  $\lambda_2$  values (red color) in the same area. The picture for the smaller vortex in the upwind side of the road isn't clear in any of the two methods. A drawback of the local vortex detection methods is noticed, that they tend to show results that indicate the existence of vortices in areas with high turbulence. This is caused because the detection criteria are a measure of the rotation of the flow, which is one of the characteristics of turbulent flow. For this reason, the local methods have to be used in conjunction with global methods. The vorticity field has its largest values in the shear layer, just after the upwind building and it proves more sensitive to the small swirls of the flow. This sustains vorticity unsuitable for the detection of big vortices. Finally, the gradient of the vertical velocity component has zero to positive values in the upwind side, indicating a stagnation area, proving the notion of the recirculation zone, that in this part of the street canyon, the removal of pollutants is obstructed. The big values at the centre of the street canyon, show the ending of this area and the negative values at the downwind side show the influx of fresh air, which has been reported by other researchers.

## CONCLUSIONS

Main hypothesis of this work is that the flow regime in a street canyon governs the recirculation zone and consequently the dispersion. Thus, a quasi-universal expression for the recirculation zone could expand the applicability of these simple models in cases of higher complexity. To understand better the recirculation zone, CFD simulations were validated and used. We used standard vortex detection methods, namely vorticity, streamlines and the  $\lambda_2$  and Q criteria, to visualize the vortex structures. The final results are rather inconclusive, although the combined use of the above methods certainly gives an insight to the flow structure. In any case more exploratory analysis is necessary in order to validate the further develop the hypothesis of this work.

## ACKNOWLEDGEMENTS

This publication was made possible by a NPRP award [NPRP 7-674-2-252] from the Qatar National Research Fund (a member of The Qatar Foundation). The statements made herein are solely the responsibility of the authors.

## REFERENCES

Addepalli, B. and E. Pardyjak, 2014: A study of flow fields in step-down street canyons. *Environ Fluid Mech.* **14**, 1-43.

- Allegrini, J., V. Dorer and J. Carmeliet, 2013: Wind tunnel measurements of buoyant flows in street canyons. *Building and Environment*, **59**:315-326.
- Balogun, A., A. Tomlin, C. Wood, J. Barlow, S. Belcher, R. Smalley, *et al.*, 2010: In-Street Wind Direction Variability in the Vicinity of a Busy Intersection in Central London. *Boundary-Layer Meteorol*, **136**:489-513.
- Berkowicz, R., O. Hertel, S. E. Larsen, N. N. Sorensen and M. Nielsen, 1997. Modelling Traffic Pollution in Streets. National Environmental Research Institute Roskilde, Denmark.
- Bright, V. B., W. J. Bloss and X. Cai, 2013: Urban street canyons: Coupling dynamics, chemistry and within-canyon chemical processing of emissions. *Atmospheric Environment*, **68**:127-142.
- Chakraborty, P., S. Balachandar and R. J. Adrian, 2005: On the relationships between local vortex identification schemes. *Journal of Fluid Mechanics*, **535**:189-214.
- Franke, J. and A. Baklanov, 2007: Best practice guideline for the CFD simulation of flows in the urban environment: COST action 732 quality assurance and improvement of microscale meteorological models. Meteorological Inst.
- Gromke, C. and B. Ruck, 2009: On the Impact of Trees on Dispersion Processes of Traffic Emissions in Street Canyons. *Boundary-Layer Meteorol*, **131**:19-34.
- Hanna, S. R., G. A. Briggs and R. P. J. Hosker, 1982. Handbook on atmospheric diffusion (No. DOE/TIC-11223; Other: ON: DE82002045 United States10.2172/5591108Other: ON: DE82002045Thu Feb 07 00:13:37 EST 2008NTIS, PC A06/MF A01.TIC; NTS-82-008222; ERA-07-038976; EDB-82-097032English).
- Hunt, J. C., A. Wray and P. Moin, 1988: Eddies, streams, and convergence zones in turbulent flows.
- Issa, R. I., 1986: Solution of the implicitly discretised fluid flow equations by operator-splitting. *J. Comput. Phys.*, **62**:40-65.
- Jeong, J. and F. Hussain, 1995: On the identification of a vortex. *Journal of Fluid Mechanics*, **285**:69-94.
- Jiang, M., R. Machiraju and D. Thompson, 2005. Detection and visualization of vortices. In: *Visualization Handbook* (pp. 295-309).
- Johnson, W. B., F. L. Ludwig, W. F. Dabberdt and R. J. Allen, 1973: An Urban Diffusion Simulation Model For Carbon Monoxide. *Journal of the Air Pollution Control Association*, **23**:490-498.
- Kastner-Klein, P., R. Berkowicz and R. Britter, 2004: The influence of street architecture on flow and dispersion in street canyons. *Meteorol Atmos Phys*, **87**:121-131.
- Li, X., 2008. Large-eddy simulation of wind flow and air pollutant transport inside urban street canyons of different aspect ratios. The University of Hong Kong (Pokfulam, Hong Kong).
- Oke, T. R., 1988: Street design and urban canopy layer climate. *Energy and Buildings*, **11**:103-113.
- Smagorinsky, J., 1963: General circulation experiments with the primitive equations: I. the basic experiment\*. *Monthly weather review*, **91**:99-164.
- Soulhac, L., P. Salizzoni, F. X. Cierco and R. Perkins, 2011: The model SIRANE for atmospheric urban pollutant dispersion; part I, presentation of the model. *Atmospheric Environment*, **45**:7379-7395.
- Yamartino, R. J. and G. Wiegand, 1986: Development and evaluation of simple models for the flow, turbulence and pollutant concentration fields within an urban street canyon. *Atmospheric Environment (1967)*, **20**:2137-2156.

**17th International Conference on  
Harmonisation within Atmospheric Dispersion Modelling for Regulatory Purposes  
9-12 May 2016, Budapest, Hungary**

---

**WATER CHANNEL INVESTIGATION OF FLOW AND DISPERSION IN STREET CANYONS**

*Annalisa Di Bernardino<sup>1</sup>, Paolo Monti<sup>1</sup>, Giovanni Leuzzi<sup>1</sup> and Giorgio Querzoli<sup>2</sup>*

<sup>1</sup>Dipartimento di Ingegneria Civile Edile e Ambientale, Università di Roma “La Sapienza”, Roma, Italy

<sup>2</sup>Dipartimento di Ingegneria del Territorio, Università di Cagliari, Cagliari, Italy.

**Abstract:** This paper describes experiments conducted in the water channel for studying the turbulent dispersion of a passive pollutant emitted by a line source located at the bottom of a street canyon. Velocity and pollutant concentration fields have been measured simultaneously in correspondence of an arrangement of two-dimensional obstacles that simulate a street canyon with aspect ratio unity. From the instantaneous values of the pollutant concentration, high-spatial resolution maps of mean, standard deviation and skewness factor of the concentration field have been determined both within and outside the canyon.

**Key words:** *Street Canyon, Concentration fluctuations, Water channel, Line source, Concentration peaks*

## **INTRODUCTION**

Numerous studies have been performed during the last decades in order to improve our understanding on wind flow and pollutant dispersion in urban environments. Vehicular traffic is the major source of pollutants in cities and their concentration depends also on the shape of the buildings surrounding the street. It is therefore of great interest to analyse pollutant dispersion in the street canyon, which can be considered as the simpler entity representing real situations. A number of laboratory experiments have been dedicated to this issue, both for two-dimensional (see for example Caton et al., 2003; Salizzoni et al., 2011; Di Bernardino et al., 2015) and three-dimensional configurations (Takimoto et al., 2011, among others). These studies have shown the role played by the interface layer forming between the flow within the canyon and the outer flow and, at the same time, how its dynamics govern exchanges of mass and momentum, which play a central role in pollutant exchange rates in street canyons (Liu et al., 2005).

An important goal in pollutant dispersion studies is the knowledge of concentration fluctuations. They are useful, for example, to determine the range of the expected values of concentration for microscale dispersion and to better simulate chemical reactions, which depend on the instantaneous concentration, rather than the mean (for recent developments on this issue see for example Amicarelli et al., 2001 and 2012). One of the main problems encountered in flow and dispersion studies conducted by means of laboratory (as well as field) experiments is how to measure flow velocity and concentration simultaneously, being the latter an essential issue in determining important quantities such as the turbulent concentration flux and eddy diffusivity of mass. Besides, given the strong spatial inhomogeneity of street canyon flows, experimental campaigns based on single point measurements rarely allow an exhaustive description of the phenomena. This is the main motivation of this work, which reports some preliminary results on measurements of concentrations of a pollutant emitted at surface level from a line source located within a two-dimensional street canyon with aspect ratio  $H/W=1$ . The experiments, conducted by using a water channel, show the capability of the apparatus in determining spatial inhomogeneities of the mean, the standard deviation and skewness of the pollutant concentration both within and outside the canyon.

## **EXPERIMENTAL SETUP**

The experiments are performed using a closed-loop water channel facility (Figure 1; details on the experimental apparatus can be found in Di Bernardino et al., 2015). The channel is 35 cm high, 25 cm wide, 740 cm long, and a constant head reservoir feeds the flume. A floodgate allows regulating the water

depth and, therefore, the water velocity. A series of parallelepipeds (made by PVC) of square section  $B=H=2$  cm and length ( $L$ ) equal to the channel width are glued onto the channel bottom (Figure 2). Preliminary experiments showed that  $L$  is long enough to ensure that the flow in the central section of the channel is two-dimensional and that the influence of the vertical walls is negligible. The test section is located nearly 500 cm downstream of the inlet, where the boundary layer is fully developed. The water depth is 16 cm and the free stream velocity is  $34 \text{ cm s}^{-1}$ . The Reynolds number of the flow is nearly 50000. A line source of dye (rhodamine) is located at the bottom of the cavity in correspondence of the canyon centre (Figure 2). The tracer reaches the source through a thin silicone tube, connected to a constant head reservoir that guarantees the discharge of the tracer with a constant rate.

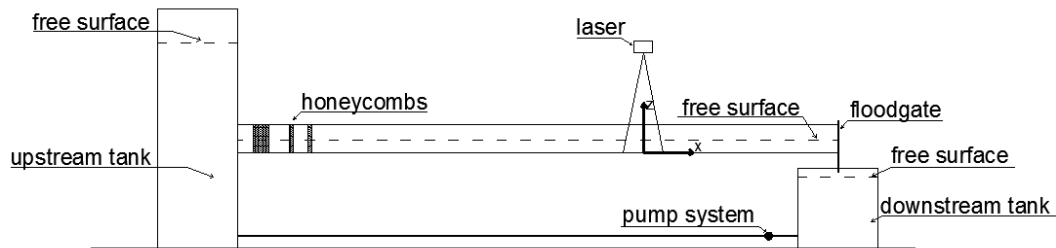


**Figure 1.** Side view of the experimental apparatus. The x-axis refers to the longitudinal axis of the channel, while the z-axis is parallel to the vertical

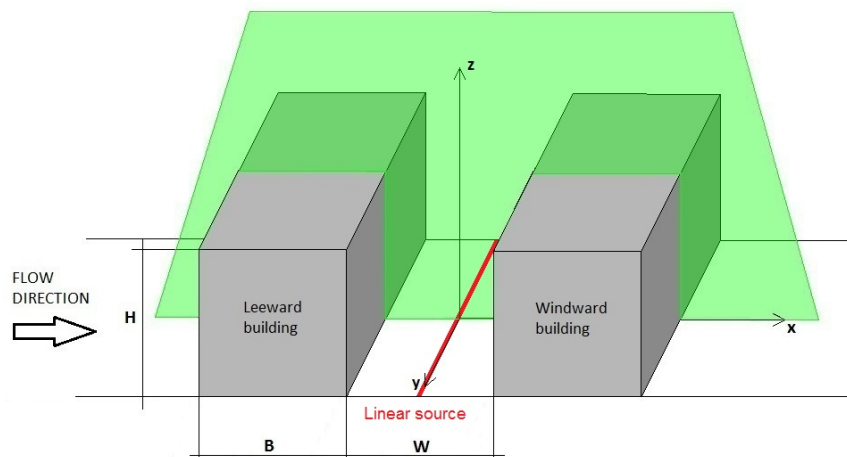


**Figure 2.** Sketch of the modelled street canyon. The vertical plane in green represents the laser beam.

Velocity and concentration fields are measured simultaneously using an image acquisition system consisting of two (synchronized) cameras: the first one permits the velocity field to be evaluated by a feature-tracking algorithm based on image analysis (see for details Di Bernardino et al., 2015), while the second camera is used for the concentration measurements via laser-induced fluorescence (LIF). The cameras ( $1280 \times 1024$  pixels resolution) acquire at 250 frames per second, and a thin laser light sheet (wavelength: 532 nm) illuminates the test section. The two cameras are aligned vertically, to frame the area of interest (i.e. the canyon) and to reduce as much as possible image distortion. The rhodamine is a non-reactive fluorescent dye that, excited at 532 nm (green), emits at 587 nm (red). The light emitted by the rhodamine is captured by the camera equipped with a filter tuned to 587 nm to allow only the fluorescence and not the laser light to pass. The dye concentration at a given pixel (directly proportional to the fractional volume of the dyed fluid) is assumed proportional to the measured luminosity. An affine transformation that best maps the features viewed from one camera on those recognized by the second camera is used to map the concentration field onto the velocity field. For details on this procedure, see Monti et al. (2007). The framed area is rectangular (85 mm long and 74 mm high), lying in the vertical mid-plane of the channel. The velocities measured in each time instant with the feature-tracking algorithm are interpolated on a regular grid by Gaussian averaging. The resulting spatial resolution is 1 mm; the one

of the concentration field is nearly 0.1 mm. The experiments last 80 s and, therefore, 20000 velocity and concentration fields, taken simultaneously, are used to calculate the statistical moments.

## RESULTS

Before proceeding with the analysis of the statistical moments of the pollutant concentration, it is useful to examine some of the main features of the flow. Figure 3 shows the instantaneous velocity (arrows) and the normalized concentration fields (colours) taken in correspondence of the canyon in a phase of the flow when most of the pollutant emitted by the line source is contained within the canyon. The normalized concentration,  $C^*(x,z,t)$ , refers to the ratio between the actual concentration and the (constant) value of the concentration at the source. It is apparent the presence of two main flows, i.e. the external boundary layer and the recirculating eddy inside the canyon (for a detailed description of the flow occurring for the same geometrical arrangement see Di Bernardino et al., 2015). Pollutants remain trapped within the canyon and tend to recirculate several times, carried by the main eddy. The time needed by a fluid particle to travel the whole eddy is 3-4 s, while the time needed by a fluid particle to cross the canyon top is nearly 0.2 s. The interface between the inner and the outer regions, i.e. the shear layer, is characterized by large velocity gradients that give rise to Kelvin-Helmholtz type instabilities governing exchange of mass and momentum between the inner and the outer flow. These play an important role in determining the characteristics of the overlying roughness sublayer, including vertical profiles of wind and temperature (Pelliccioni et al., 2012).

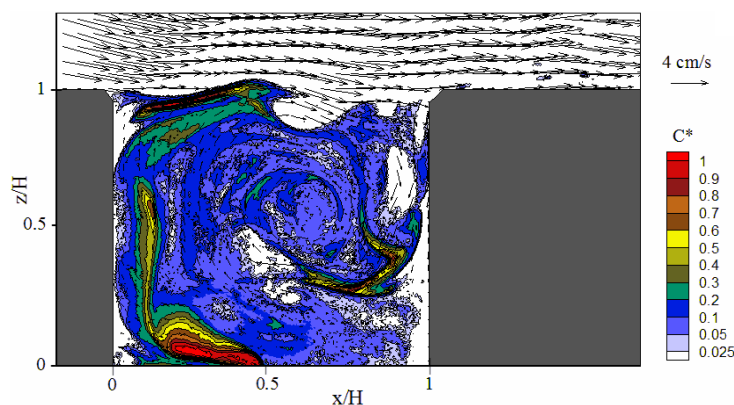


**Figure 3.** Map of the instantaneous velocity (vectors) and concentration (colours) fields in a phase when the recirculating eddy inside the canyon captures all the pollutant.

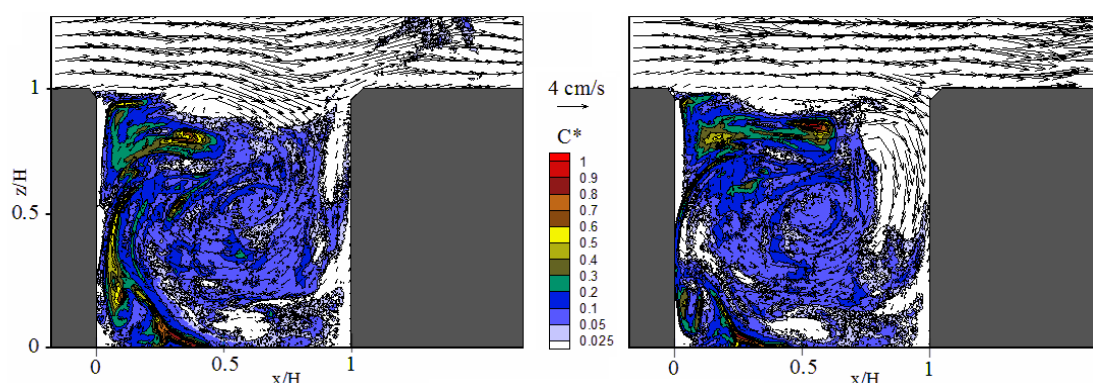


**Figure 4.** Maps of the instantaneous velocity (vectors) and concentration (colours) fields during the sweep mode. The right panel refers to the flow present 0.1 s later than that shown in the left panel.

Figure 4 shows examples of the so-called sweep mode (see for example Takimoto et al., 2011), responsible of intrusion of fresh fluid from the outer layer into the canyon (the two pictures refer to instants of time nearly 0.1 s away). Examples of the counterpart of the previous feature, i.e. the ejection mode, are depicted in Figure 5, where is evident the expulsion of pollutants from the right part of the

canyon top. Both these modes are related to the shear layer flapping and appear with periodicity of nearly 0.5 s. The temporally averaged mean concentration field is plotted in Figure 6, which evidences how the region next to the wall of the windward building is characterized by lower concentration values. This contrast with the findings of Caton et al. (2003), who found a fairly uniform concentration field inside the cavity. The region of nil concentration that appears in the upper part of the leeward building is a signature of the secondary vortex that forms there.

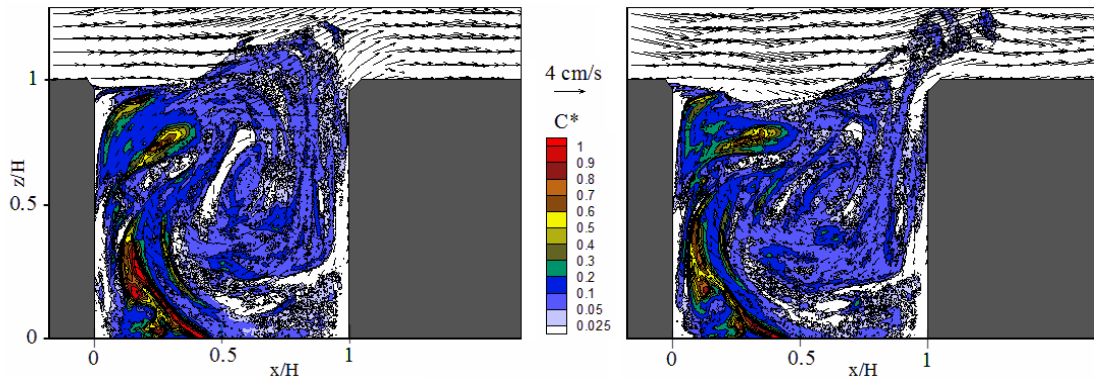


Figure 5. As in Fig. 4, but for the ejection mode.

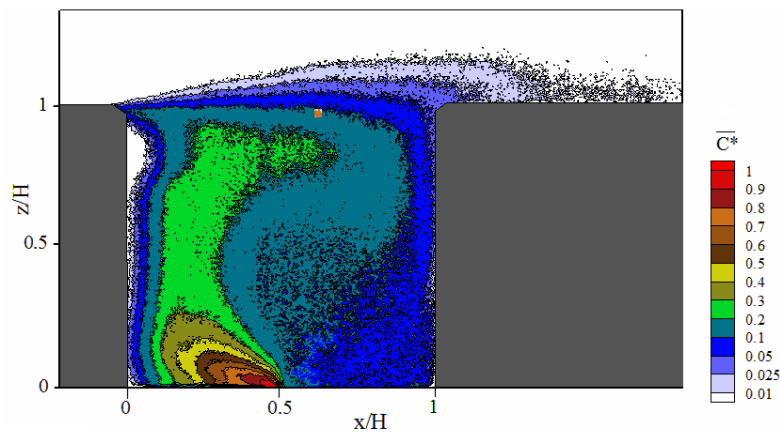


Figure 6. Map of the normalized mean concentration.

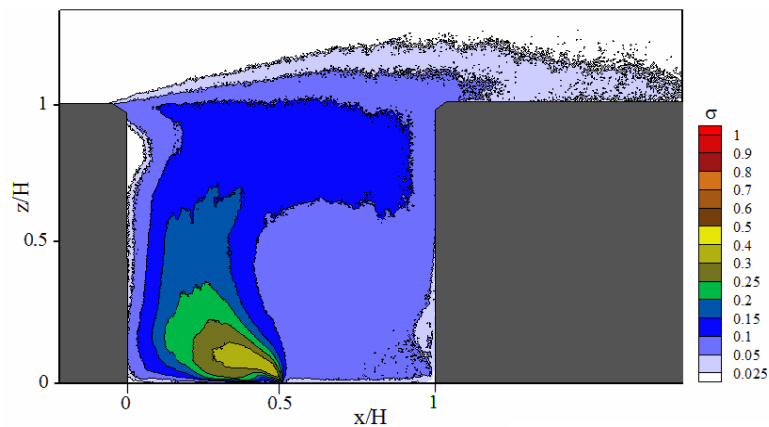
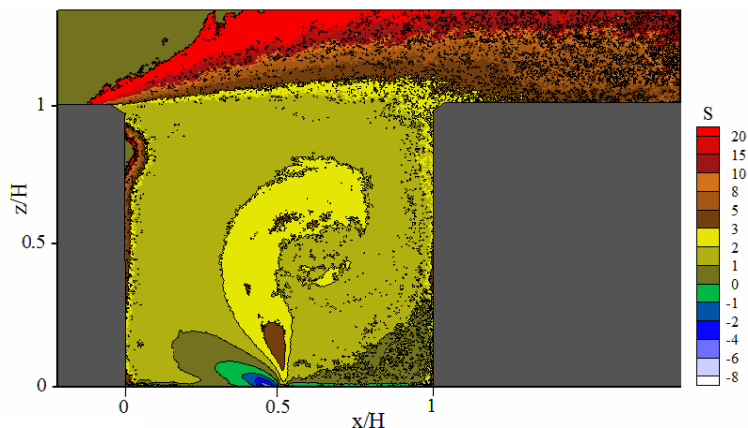


Figure 7. Map of the standard deviation of the normalized concentration.

Figure 7 depicts the map of the standard deviation of the normalized concentration. It behaves similarly to the average, showing larger values close to the source and in the left region of the canyon. Finally, the

skewness factor (Figure 8) shows both positive and negative values, the latter being concentrated close to the source, where the plume oscillation produces a non-negligible asymmetry of the probability density function of the concentration. Note the large, positive values outside the canyon, which are ascribable mainly to the small values of the standard deviation present in the outer layer.



**Figure 8.** Map of the concentration skewness.

## CONCLUSIONS

Simultaneous, whole field measurements of velocity and concentration have been employed to investigate experimentally a vertical plane in the mixing of a passive pollutant emitted from a line source simulating vehicular traffic. Some stages of the flow field, such as the sweep and ejection modes, have been visualized and discussed. We also provided high-resolution measurements of the average concentration field, as well as standard deviation and skewness of the concentration. The method seems to be well suited to acquire important flow variables such as the turbulent concentration flux.

## REFERENCES

- Amicarella, A., G. Leuzzi, P. Monti and D. J. Thomson, 2011: A comparison between IECM and IEM Lagrangian models. *Int. J. Environ. Pollut.*, **44**, 324-331.
- Amicarella, A., P. Salizzoni, G. Leuzzi, P. Monti, L. Soulhac, F.-X. Cierco and F. Leboeuf, 2012: Sensitivity analysis of a concentration fluctuation model to dissipation rate estimates. *Int. J. Environ. Pollut.*, **48**, 164-173.
- Brevis, W., M. Garcia-Villalba and Y. Niño, 2014: Experimental and large eddy simulation study of the flow developed by a sequence of lateral obstacles. *Environ. Fluid. Mech.*, **14**, 873-893.
- Caton, F., R. E. Britter and S. Dalziel, 2003: Dispersion mechanisms in a street canyon. *Atmos. Environ.*, **37**, 693-702.
- Di Bernardino, A., P. Monti, G. Leuzzi and G. Querzoli, 2015: A laboratory investigation of flow and turbulence over a two-dimensional urban canopy. *Boundary-Layer Meteorol.*, **155**, 73-85.
- Liu, C.-H, D. Y. C. Leung and M. C. Barth, 2005: On the prediction of air and pollutant exchange rates in street canyons of different aspect ratios using large-eddy simulation. *Atmos. Environ.*, **39**, 1567-1574.
- Monti, P., G. Querzoli, A. Cenedese and S. Piccinini, 2007: Mixing properties of a stably stratified parallel shear layer. *Phys. Fluids.*, **19**:085104 (1-9). DOI: 10.1063/1.2756580.
- Pelliccioni, A., P. Monti, C. Gariazzo and G. Leuzzi, 2012: Some characteristics of the urban boundary layer above Rome, Italy, and applicability of the Monin-Obukhov similarity. *Environ. Fluid Mech.*, **12**, 405-428.
- Takimoto, H., A. Sato, J. F. Barlow, R. Moriwaki, A. Inagaki, S. Onomura and M. Kanda, 2011: Particle image velocimetry measurements of turbulent flow in outdoor and indoor urban scale models and flushing motions in urban canopy layers. *Boundary-Layer Meteorol.*, **140**, 295-314.
- Salizzoni, P., M. Marro, L. Soulhac, N. Grosjean and R. J. Perkins, 2011: Turbulent transfer between street canyons and the overlying atmospheric boundary layer. *Boundary-Layer Meteorol.*, **141**, 393-414.

**17th International Conference on  
Harmonisation within Atmospheric Dispersion Modelling for Regulatory Purposes  
9-12 May 2016, Budapest, Hungary**

---

**IMPACTS OF GLOBAL CLIMATE SCENARIOS OVER THREE EUROPEAN CITIES USING  
MESOSCALE AND CFD SIMULATIONS WITH VERY HIGH RESOLUTION**

*Roberto San José<sup>1</sup>, Juan L. Pérez<sup>1</sup>, Libia Pérez<sup>1</sup>, Julia Pecci<sup>2</sup>, Antonio Garzón<sup>2</sup> and Marino Palacios<sup>2</sup>*

<sup>1</sup>Environmental Software and Modelling Group, Computer Science School, Technical University of Madrid (UPM), Madrid, Spain

<sup>2</sup> Indra S.A., C/ Mar Egeo, 4, Pol. Industrial 1, 28830 San Fernando de Henares, Madrid (Spain)

**Abstract:** This contribution presents the results of a climate and air pollution dynamical downscaling process from global climate simulations to urban scale with 10-50 m spatial resolution. The final objective is to show how urban meteorological and air pollution respond to different global climatic conditions and how human health could be affected by changes induced by global warming emissions. We have used the mesoscale model WRF-Chem (NOAA, US) to produce information covering all Europe with 25 km spatial resolution and two nested domains with 5 km and 1 km of spatial resolution over Madrid, London and Milan. Finally a detailed simulations using MICROSYS-CFD model are implemented to take into account the buildings of the city. The energy fluxes are calculated with the NOAH land surface model and the UCM (Urban Canopy Model), considering the shadows and reflections of the buildings. Year 2011 is used as reference year and 2030, 2050 and 2100 for future under two RCP scenarios of the IPCC, 4.5 (peak around 2040, then decline) and 8.5 (emissions continue to rise throughout the 21st century). Boundary conditions are taken from the global climate model CCSM with a frequency of six hours. For evaluation we make a comparison between results of a simulation for present situation (2011, with reanalysis data as boundary and initial conditions) and observations showing acceptable agreement with measurements. The results are analyzed with climate indicator and health indicators for mortality and morbidity, using epidemiological studies to fix the exposure-response functions. The purpose is to highlight areas with elevated vulnerability to prepare plans and implement adaptations to reduce human health effect of climate change.

**Key words:** *Dynamical downscaling, Climate, Health, CFD*

## **INTRODUCTION**

Urban areas are the zones where the local response to the global change is more pronounced (Oleson et al. 2010.), recent studies have suggested that global climate change will have a significant impact on both local weather and urban air quality (Mickley et al., 2004). We propose a climate and air pollution dynamical downscaling methodology that combines state-of-the-art of different meteorological and air quality models which objective is the transformation of global model outputs into high spatial resolution products. To downscale a global model in a dynamical way, we need a Regional Climate Model (RCM) forced by the global fields at the initial and boundaries conditions (Giorgi et al., 2009). Atmospheric flow and microclimate over urban areas are influenced by urban features, and they enhance atmospheric turbulence, and modify turbulent transport, dispersion, and deposition of atmospheric pollutants (Piringer et al. 2007). We propose to use a Computational Fluid Dynamic (CFD) model to produce detailed simulations of the wind flow and turbulence in the urban canopy. We start from IPCC (Intergovernmental Panel on Climate Change) scenarios based on the Fifth Assessment Report (AR5) and on the Representative Concentration Pathways (RCP). The IPCC report (IPCC, 2013) identifies up to four climate scenarios, from very strong mitigation scenarios (non-realistic) (RCP2.6) to a business-as-usual scenario (RCP8.5). The choice of the worst-case scenario (8.5) and the best-realistic-case scenario (4.5) was motivated by the goal of displaying extreme changes that can be forecasted at city scale to allow implementing mitigation and adaptation strategies. The 8.5 pathway arises from little effort to reduce emissions and represents a failure to curb warming by 2100. It is characterized by increasing greenhouse gas emissions over time and represents scenarios in the literature leading to high greenhouse gas concentration levels (Riahi et al., 2008). RCP 4.5 is similar to the lowest-emission scenarios (B1)

assessed in the IPCC AR4. It is a stabilization scenario where total radiative forcing is stabilized around 2050 by employment of a range of technologies and strategies for reducing greenhouse gas emissions. This can be considered as a weak climate change mitigation scenario (Smith et al., 2010). This work is part of FP-7 EU DECUMANUS project.

## METHODOLOGY

We use a model chain consists of outputs from the Community Earth System Model (CESM) is input to the Weather Research and Forecasting Chemical model (WRF/Chem) which uses a sophisticated urban canopy model (UCM) scheme to represent near-surface processes. The WRF/Chem outputs are coupled with the Computational Fluid Dynamics (CFD) model called the MICROSYS running at high spatial resolution (meters). This downscaling procedure was performed by using boundary and initial condition data. WRF/Chem dynamically downscales CESM outputs at 50 km resolution to 1 km, it moves across the spatial scales using a nesting approach (50, 5, 1 km). WRF/Chem with UCM (Masson 2000) model outputs at 1 km resolution was fed (offline) into MICROSYS to initialize simulations and to supply boundary conditions. For the regional and urban scale we use the meteorological-chemistry transport model WRF-Chem (Grell et al., 2005). It includes the RADM2 gas phase mechanics, the MADE inorganic aerosol scheme, and the SORGAM aerosol module for secondary organic aerosols (SOA). Model configurations follow the next physical parameterizations, namely the Noah Land Surface Model (Solomon et al., 2007), Morrison double-moment microphysics scheme (Morrison et al., 2009), RRTMG long-wave and shortwave radiation schemes (Rapid Radiative Transfer Model for Global), Grell 3D ensemble cumulus parameterization (Grell et al., 2005), Yonsei University Planetary Boundary Layer (YSU; Hong et al., 1996) and Monin-Obukov surface layer. Emissions are produced by EMIMO (UPM) (EMission Model) (San José et al., 2008) model for 2011. MICROSYS is based into the MIMO CFD model, which takes into account buildings obstacles. The model includes steady three-dimensional system of Reynolds equations, k-ε model of turbulence and the ‘advection-diffusion’ equation to simulate pollution transport on-line coupled with a simple chemistry mechanism for O<sub>3</sub>-NO<sub>x</sub> relationships. The methodology to estimate percentages of climate/pollution-related deaths and hospital admissions due to global climate are based on epidemiologic analysis of weather/air pollution and health data to characterize and quantify mortality/morbidity associations. The exposure-response relationships estimated from the epidemiological studies were applied to projections of climate. The short-term relationship between the daily number of deaths/hospital admissions and day-to-day fluctuations in exposure variables (temperature, heat waves, ozone and particles) for many cities are published in different scientific papers. The relationship between the exposure variable and its effect on health is defined with a log-linear regression (Poisson) and is called exposure-response function (ER). If we derive this function we obtain the equation (1) which calculates the change in mortality or morbidity by a change in the exposure variable.

$$\Delta y = y_0 (e^{\beta \Delta C} - 1) \quad (1)$$

where  $y_0$  is the baseline incidence rate of the studied health effect,  $\beta$  is a parameter which define the mortality effect estimation from epidemiological studies,  $\Delta C$  is the change of the exposure variable (future minus present). (US, EPA, 2010).

## EXPERIMENT

The modelling system described in the last section was used to assess the impacts of projected global climate conditions in three European urban areas: Madrid, Milan and London, assuming no changes in urban landuses and emissions. These three cities have a variety of building sizes and land cover types. The first level with 50 km covers the covers the whole of Europe, 1 km domains cover all the cities (Madrid, London and Milan) and the CFD domains cover a part of the city: Madrid 12 by 12 km, Milan 10 by 10 km and London 6.0 by 5.3 km with different spatial resolutions: Madrid 10 m, London 25 m, and Milan 50 m, although the results will be presented with the same resolution of 50 meters by requirements of the DECUMANUS project. The use of the system is showed conducting yearly simulations for present (2011) and future (2030, 2050 and 2100) climate conditions. The modelling system was used using 2011 emissions as control run, because we want to investigate the effects on the global climate on the actual (2011) cities. Also, one simulation (NNRP) with a real-present scenario (reanalysis data) has been run for the year 2011. This simulation will be used as evaluation simulation of the modelling system.

## RESULTS

Milan and London air quality stations were used to evaluate the modelling system outputs for near-surface SO<sub>2</sub>, NO<sub>2</sub>, CO, O<sub>3</sub> and PM<sub>10</sub> (Table 1). For evaluation we have compared the hourly model outputs for present conditions (2011) following reanalysis scenario (NNRP) to hourly observations. Normalized Mean Bias (NMB), Root Mean Standard Error (RMSE) and the correlation coefficient (R<sup>2</sup>) metrics were used as statistical performance measures. The results of the comparison between the modelled data and the observed data show that the simulated concentrations are within the ranges of measured data. The simulated concentrations regarding the observed concentrations are better in Milan than London. In Milan we have more detailed information about traffic flows and the micro scale emissions are more precise than in case of London. The average simulated levels are within the inter-annual variability of the measured since most of the R<sup>2</sup> values exceed the value of 0.5, except SO<sub>2</sub> but SO<sub>2</sub> concentrations are very low in the cities. The statistical evaluation shows significant evidence that high resolution downscaling procedure could achieve reasonably good performance, particularly for BIAS and R<sup>2</sup> statistics.

**Table 1.** Results of the evaluation of the results of the modelling system

Air quality Monitoring Station (Avg stations)	NMB (%)	RMSE (ug/m3)	R <sup>2</sup>	
<b>Milan</b>	PM10	-1.72	30.77	0.58
	SO <sub>2</sub>	5.0	3.66	0.2
	NO <sub>2</sub>	-1.96	37.92	0.51
	CO	-1.51	57.4	0.66
	O <sub>3</sub>	1.2	20.74	0.84
<b>London</b>	PM10	34.57	18.13	0.47
	SO <sub>2</sub>	-0.72	2.58	0.19
	NO <sub>2</sub>	45.88	48.47	0.34
	CO	-0.47	141.95	0.32
	O <sub>3</sub>	-56.85	31.99	0.63

Spatial differences (high resolution 50m.) of a climatic parameter, health outcome and air quality directive changes between future and 2011 (present) for RCP 4.5 and RCP 8.5 in the three European cities calculated from the WRF/Chem-MICROSYS modelling system are showed. Madrid is in the Figure 1, Milan Figure 2 and London (Kensington and Chelsea area) Figure 3.

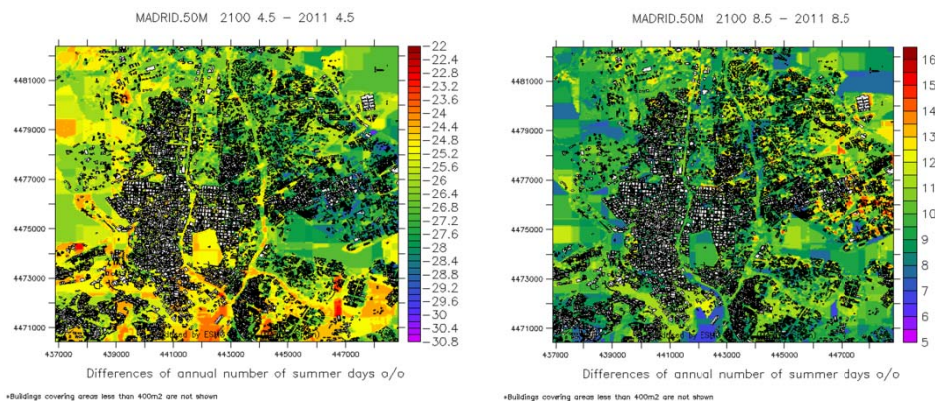


**Figure 1.** Spatial distribution of the differences (%) in annual number of summer days (daily maximum temperature > 25°) for 2100 respect to 2011 following RCP 4.5 (left) and RCP 8.5 (right) scenarios with WRF-Chem-MICROSYS over Madrid with 50 m. spatial resolution.

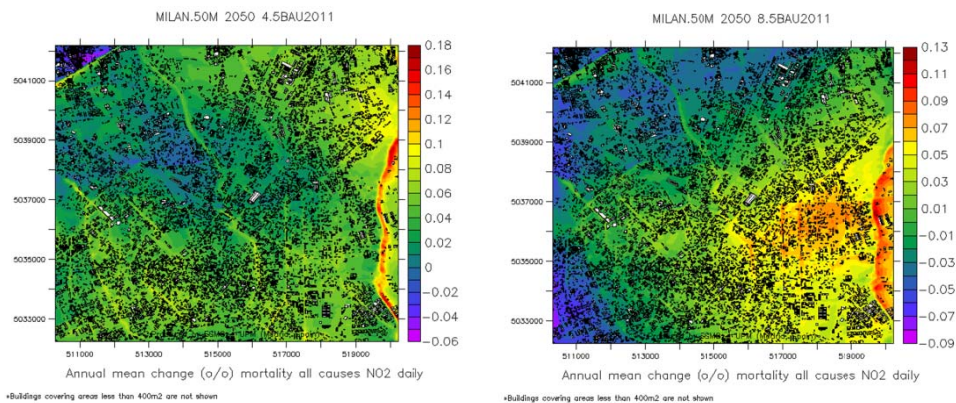


**Figure 2.** Yearly average of spatial distribution of the differences (%) mortality for natural causes due to NO<sub>2</sub> daily concentrations for 2050 respect to 2011 following RCP 4.5 (left) and RCP 8.5 (right) scenarios with WRF-Chem-MICROSYS over Milan with 50 m. spatial resolution.

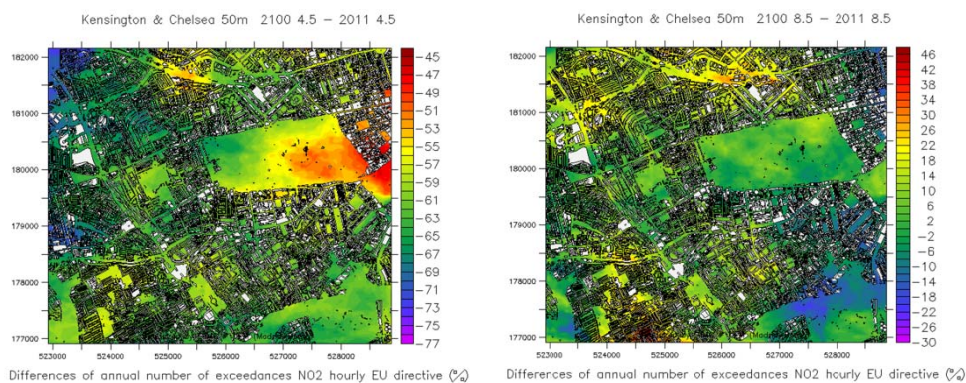


**Figure 3.** Spatial distribution of the differences (%) in annual number of hourly exceedances (>200 ug/m<sup>3</sup>) for 2100 respect to 2011 following RCP 4.5 (left) and RCP 8.5 (right) scenarios with WRF-Chem-MICROSYS over Kensington-Chelsea (London) with 50 m. spatial resolution.

In Madrid, we can clearly see how an increase in summer days (daily maximum temperature > 25°) by 2100 under the RCP 8.5 scenario is expected while RCP 4.5 has reduced summer days by lower temperature. We recall that RCP 4.5 is a scenario where measures for reducing greenhouse gases are taken. The area around the city center of Madrid is the area where the most important effects of the global climate are localized. In Milan, the mortality due to NO<sub>2</sub> concentrations will decrease in some areas and will increase in others under the two climate scenarios by 2050. The major impacts are located close to the roads, especially in the east of the city where a busy motorway is located. In London, decreases of the number of hourly exceedances of the EU directive for 2100 are expected under RCP 4.5 because this is a scenario where precipitation will increase. In RCP 8.5, the zone with higher traffic has an increase in exceedances up to 46% and decreases are located over park or low traffic areas.

## CONCLUSIONS

A nesting procedure was used to assess the effects of climate change on three urban areas: Madrid, Milan and London with very high spatial resolution under two IPCC RCP possible scenarios, 4.5 and 8.5. The model chain included a global climate model (CESM), as well as mesoscale-urban (nested WRF/Chem with UCM spanning from 50 to 1 km resolution) and microscale (MICROSYS) models. The microscale air pollution results were evaluated, respectively, using observations from existing air quality stations. The evaluation of WRF-Chem and MICROSYS coupling showed the utility of the modelling system. To improve the simulation tool, further validation studies are required by comparing simulation results with field measurements. The nested modeling approach proposed and used is portable to other cities, requiring only the adjustment of model parameters and inputs to suit the locality. In the high resolution

simulations we have observed that the building influence is very important to detect hot spots or sensible areas to be affected by the climate change. The information can be used for local decision makers and stakeholders in order to developing strategies to reduce these impacts.

#### ACKNOWLEDGMENTS

The UPM authors acknowledge the computer resources and technical assistance provided by the Centro de Supercomputación y Visualización de Madrid (CeSViMa). The UPM authors thankfully acknowledge the computer resources, technical expertise and assistance provided by the Red Española de Supercomputación. We acknowledge the DECUMANUS EU project from EU Space Call FP7-SPACE-2013-1 at SPA.20131.1-06

#### REFERENCES

- Giorgi, F., C. Jones, and G. R. Asrar, 2009: Addressing climate information needs at the regional level: The CORDEX framework, *WMO Bull.*, **58**(3), 175–183.
- Grell GA, SE Peckham, R Schmitz, and SA McKeen, G Frost, WC Skamarock, and B Eder, 2005: Fully coupled 'online' chemistry in the WRF model. *Atmos. Environ.*, **39**, 6957-6976.
- Hong, S.Y., Pan, H.L., 1996: Nonlocal boundary layer vertical diffusion in a medium-range forecast model. *Monthly Weather Review*, **124**(10), 2322–2339.
- IPCC. Climate Change, 2013: The Physical Science Basis; Cambridge University Press: Cambridge, UK; New York, NY, USA, 2013
- Masson V, 2000: A physically-based scheme for the urban energy budget in atmospheric models. *Boundary Layer Meteorol.* **94**, 357-397.
- Mickley, L. J., Jacob, D. J., Field, B. D., and Rind, D., 2004: Effects of future climate change on regional air pollution episodes in the United States, *Geophys. Res. Lett.*, **31**, L24103.
- Morrison, H., Thompson, G., Tatarskii, V., 2009: Impact of cloud microphysics on the development of trailing stratiform precipitation in a simulated squall line: Comparison of one and two-moment schemes. *Monthly Weather Review*, **137**, 991-1006.
- Oleson, K. W., A. Monaghan, O. Wilhelm, M. Barlage, N. Brunell, J. Feddema, L. Hu, and D. F. Steinhoff, 2010: Interactions between urbanization, heat stress, and climate change. *Climatic Change*, **129**, 525-541, doi:10.1007/s10584-013-0936-8.
- Riahi, Steven Rose, Paul Runci, Ron Stouffer, Detlef van Vuuren, John Weyant, Tom Wilbanks, Jean Pascal van Ypersele, and Monika Zurek., 2008: Towards New Scenarios for Analysis of Emissions, Climate Change, Impacts, and Response Strategies. Intergovernmental Panel on Climate Change, Geneva, 132 pp.
- San Jose R, Juan L. Perez, Jose L. Morant, Rosa M. Gonzalez, 2007: European operational air quality forecasting system by using MM5-CMAQ-EMIMO tool, Simulation Modelling Practice and Theory, Volume 16, Issue 10, The Analysis of Complex Systems, November 2008, Pages 1534-1540
- Smith, Ronald J. Stouffer, Allison M. Thomson, John P. Weyant & Thomas J. Wilbanks, 2010: The next generation of scenarios for climate change research and assessment. *Nature*, **463**, 747-756. doi:10.1038/nature08823
- Solomon S, Qin D, Manning M, Chen Z, Marquis M, Averyt K, Tignor M, Miller H (eds), 2007: Climate change 2007: the physical science basis. Contribution of working group I to the fourth assessment report of the intergovernmental panel on climate change. Cambridge University Press, Cambridge, 996 pp
- Piringer M., Petz E., Groehn I., Schauburger G., 2007: A sensitivity study of separation distances calculated with the Austrian Odour Dispersion Model (AODM), *Atmospheric Environment*, **41**, 725-1735.
- U.S. EPA (U.S. Environmental Protection Agency), 2010: BenMap: Environmental Benefits Mapping and Analysis Program User's Manual, Appendix, Research Triangle Park, NC:U.S. EPA, Office of Air Quality Planning and Standards

**17th International Conference on  
Harmonisation within Atmospheric Dispersion Modelling for Regulatory Purposes  
9-12 May 2016, Budapest, Hungary**

---

**DEVELOPMENT OF THE PARALLEL VERSION OF A CFD – RANS FLOW MODEL  
ADAPTED TO THE FAST RESPONSE IN BUILT-UP ENVIRONMENTS**

*O. Oldrini<sup>1</sup>, M. Nibart<sup>2</sup>, P. Armand<sup>3</sup>, J. Moussafir<sup>2</sup> and C. Duchenne<sup>3</sup>*

<sup>1</sup>MOKILI, F-75014 Paris, France

<sup>2</sup>ARIA Technologies, F-92100 Boulogne-Billancourt, France

<sup>3</sup>CEA, DAM, DIF, F-91297 Arpajon, France

**Abstract:**

Momentum SWIFT is a fast RANS flow model derived from Micro SWIFT. It uses artificial compressibility to solve steady state momentum equations. Rapidity of the momentum solver relies on simplified turbulence closure and regularity of the horizontal mesh. To be able to gain more speed and be able to handle larger size domains, the momentum solver has been parallelized.

Parallelization has been achieved using Message Passing Interface (MPI). Computation can be parallelized either in time, running multiple time frames on different cores, or in space, a large domain can be divided into multiple tiles and distributed to cores. Time and space parallelization schemes can be used at the same time. Momentum SWIFT can be used either on computer ranging from multi core laptop to large cluster. Space parallelization allows Momentum SWIFT to handle very large domains.

Validation has been performed against scalar version on multiple test cases. Test cases are ranging from academic isolated cube to complex city centers, like Michelstadt wind tunnel experiment, or Joint Urban 03 experiment on Oklahoma City. The latest has also been used in Udinee exercise. CPU performances of the model have also been derived both on multi core laptop and cluster.

**Key words:** *SWIFT, Micro-SWIFT, CFD RANS, parallel modelling.*

**INTRODUCTION**

SWIFT (Oldrini et al., 2013) is a very fast mass consistent wind model. It produces mass consistent 3D wind fields from a set of sparse wind measurements or larger scale model outputs. Its range of application has been extended to local scale build-up areas using Röckle type parameterisation for buildings. SWIFT is referred as Micro-SWIFT (Moussafir et al. 2004) for such applications. Micro-SWIFT interpolates available meteorological data in 3D and creates analytical zones attached to various buildings, such as displacement, cavity, wake or skimming. Mass consistency is finally applied to obtain a divergence free wind field. Micro-SWIFT can be used in conjunction with the Lagrangian Particle Dispersion model SPRAY (Tinarelli et al., 2013, Tinarelli et al, 94). The modelling system is called MSS, Micro-SWIFT-SPRAY (Moussafir et al., 2004, Tinarelli et al., 2007), and is designed to model transport and dispersion of pollutants at local scale in build-up environment, ranging from industrial facilities to city centres..

SWIFT / Micro-SWIFT can also use momentum conservation (Oldrini et al. 2014). Simplified turbulence modelling and artificial compressibility scheme allow for fast calculation of steady state wind flow solutions. This capability can be used at the finer scale of a downscaling computation over a large city like Paris, around specific buildings of interest to compute infiltration of dangerous contaminants. Quality of wind field tends to be very similar to more general CFD codes, with very short computational time.

Parallelization scheme has been introduced into Momentum-SWIFT to allow for even faster calculations and also to extend the size of domain. After presenting the parallel implementation, results of parallel calculation are compared to scalar version and performances are evaluated.

## PARALLEL SCHEME

### Overview

The parallel scheme has been introduced consistently with the methodology described in Oldrini et al., 2011. Both weak and strong scaling have been implemented into Momentum-SWIFT:

- Weak scaling allows the code to handle arbitrary large problem by using domain decomposition (DD),
- Strong scaling is obtained by using the diagnostic property of the code: each time frame can be handled independently. This mode is referred later on as TFP (time frame parallelization).

DD can be used also to do strong scaling, but the communications are more numerous than in TFP, and the efficiency is hence less.

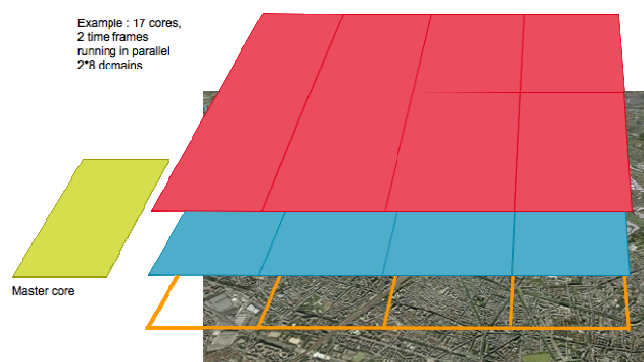


**Figure 1.** Example of TFP + DD for 17 cores, the domain being divided into 8 tiles, two time frames being computed in parallel

To be able to use the parallel scheme both on a laptop but also on a large cluster, Message Passing Interface (MPI) technology has been chosen.

The algorithm uses a master core that drives the computation and split the workload. The master core uses the number of cores available to distribute the workload to do DD, TFP or both. The master core accesses then all the input data, like topography or buildings, and is in charge to distribute them if DD is active. It also reads the meteorological data and distributes them if TFP is active: once a group of cores has finished computing a time frame, the master core sends them a new one.

TFP consists only in workload distribution on groups of cores by the core master: once the meteorological information is distributed, no additional communications are needed. Domain decomposition is more complex.

### Domain decomposition

Using domain decomposition algorithm, the domain is divided in fixed size tiles. The user provides this size, chosen to fit in the memory of each single core.

When using DD, communications are obviously necessary at the code top level. The master core handles the input data: topography, land use, roughness, buildings, etc. The master core splits this information and distributes it to each core according to the tile he is working on.

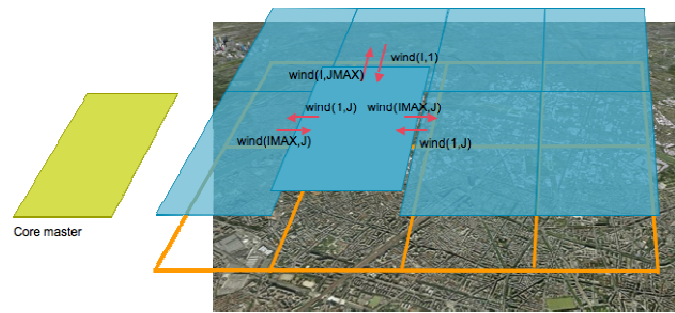


**Figure 2.** Boundary exchanges for wind field calculation in case of domain decomposition in 8 tiles

Then, at the solver level, communications are also necessary for the artificial compressibility scheme that solves mass and momentum equations. Derivatives are computed to solve the equations, and for grid points at tile boundaries, information is needed from neighbouring tiles. The figure 2 displays wind information exchanges needed during each artificial compressibility step. In the same way, pressure is also exchanged but at each algorithm sub step (pressure projection).

### COMPARISON WITH THE SCALAR VERSION OF THE CODE

Parallel-Momentum-SWIFT has been tested against the scalar version.

The test cases chosen are:

- Academic cube,
- JU2003,
- Michelstadt.

The academic cube is a 20m cubic obstacle inside a 190 x 160m domain, with a metric resolution. The vertical grid has 13 nodes going up to 90m.

JU2003 (Allwine et al., 2004) is a field experiment conducted in Oklahoma City (OKC). Our test case is focusing on downtown measurements. The domain has 251 x 251 x 26 grid points and is covering 1km x 1km x 400m in OKC city centre.

Michelstadt (Leitl et al., 2014) is a wind tunnel experiment performed at Hamburg wind tunnel. It reproduced an idealized European city centre. The domain has 533 x 311 x 26 grid points and is covering 1.6km x 930m x 200m.

The following pictures are displaying a slice of the wind field produced by the scalar version and the parallel version seen from above, and with a domain split in four tiles (Cube / JU2003) and 6 tiles (Michelstadt).

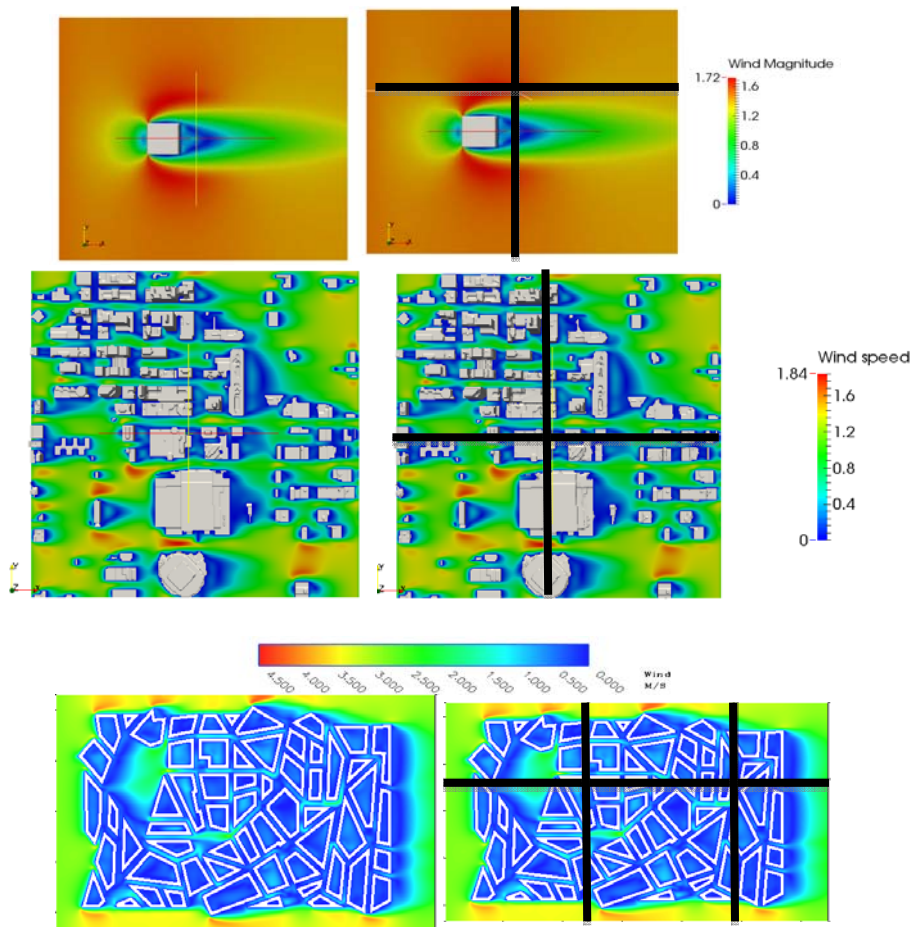


**Figure 3.** Top view of wind intensity. The scalar version is on the left side, the parallel version on the right side. The top picture is the academic cube (slice at 10m above ground), the one in the middle is JU2003 (slice at 1m above ground) and the bottom one is Michelstadt (slice at 6m above ground)

The differences for the wind field are below 5% between the scalar version and the parallel one.

### EFFICIENCY OF DOMAIN DECOMPOSITION

The speedup  $S_n$  is calculated as the ratio of the duration of the calculation using a single core,  $T_1$ , divided by the duration of the calculation on  $n$  cores,  $T_n$ .

$$S_n = T_1 / T_n$$

$S_n$  is ideal when  $S_n = n$ , which means that the calculation is  $n$  time faster when using  $n$  cores. The speedup is limited due to cost of communications, but also due to the fraction of the model that has been parallelized (Amdahl's law).

Preliminary tests on efficiency have been performed on the previous validation test cases.

The academic cube and the OKC grids are small grids and speedup has been evaluated on a multicore laptop. DD with four tiles has been compared to single tile calculation.

The laptop used is a dual core (two processors) but with hyper threading technology, which should increase the physical processors to 4 logical processors.

**Table 1.** Speedup obtained on small test cases (cube and JU2003)

Test case	Academic cube	JU2003
Number of cores	2 physical cores, 4 using hyper threading	
Speedup	1.5	2
Ideal speedup	2-4	2-4

The speedup is acceptable, especially considering the grid size: the test cases are small and DD leads to less than 100 x 100 x 23 grid points for each tile. The workload is small and the parallel fraction of the code is hence limited.

When testing DD on Michelstadt test case, the performances have been evaluated on two nodes of a cluster, each node consisting in 12 processors. The DD uses 6, 9 and 16 tiles and the speedup obtained is presented in table below.

**Table 2.** speedup obtained on Michelstadt case using DD

Test case	Michelstadt		
Number of cores	6	9	16
Speedup	2	4	6
Ideal speedup	6	9	16

The efficiency, defined as the ratio of the actual speedup to the ideal speedup, is around 30-40%. This efficiency is quite common when doing parallel computing and is compatible with the primal objective of DD: DD was implemented for weak scaling, i.e. being able to compute very large domains, too large to fit in the memory of a single computer. Nonetheless overall performances in a strong scaling view are satisfying.

## CONCLUSION

Parallel algorithms have been introduced into Momentum-SWIFT. These algorithms, domain decomposition and time frame parallelization, make it possible to increase the rapidity of the code (strong scaling), but also to compute very large domains (weak scaling).

Comparison on several tests cases, academic, wind tunnel and field experiment, are good. Scalar calculations and parallel calculations are presenting differences below 5% for wind field.

Regarding parallel performances, preliminary DD tests have been performed on the same test cases. DD efficiency is satisfying, even for small domains. More tests are being realized on more intensive test cases, like very large domains.

## REFERENCES

- Allwine, K. J., Leach, M. J., Stockham, L. W., Shinn, J. S., Hosker, R. P., Bowers, J. F., & Pace, J. C. , 2004. Overview of Joint Urban 2003—an atmospheric dispersion study in Oklahoma City. In Preprints, Symp. on Planning, Nowcasting and Forecasting in the Urban Zone, Seattle, WA, Amer. Meteor. Soc., CD-ROM J (Vol. 7).
- Archambeau, F., Mechtoua, N., Sakiz, M., 2004: Code Saturne: a finite volume method for the computation of turbulent incompressible flows, *International Journal of Finite Volumes*.
- Gowardhan A. A., E. R. Pardyjak, I. Senocak, M. J. Brown, 2011: A CFD-based wind solver for urban response transport and dispersion model, *Env. Fluid Mech.*, 11:439-464
- Leitl, B., Castelli, S. T., Baumann-Stanzer, K., Reisin, T. G., Barmpas, P., Balczo, M., ... & Milliez, M., 2014. Evaluation of Air Pollution Models for Their Use in Emergency Response Tools in Built Environments: The ‘Michelstadt’ Case Study in COST ES1006 ACTION. In Air Pollution Modeling and its Application XXIII (pp. 395-399). Springer International Publishing.

- Moussafir J., C. Olry, M. Nibart, A. Albergel, P. Armand, C. Duchenne, F. Mahe, L. Thobois and O. Oldrini, 2013: Aircity, a very High-resolution 3D Atmospheric Dispersion Modeling System for Paris. 15th Int. Conf. on Harmonisation within Atmospheric Dispersion Modelling for Regulatory Purposes
- Moussafir J., Oldrini O., Tinarelli G, Sontowski J, Dougherty C., 2004: A new operational approach to deal with dispersion around obstacles: the MSS (Micro-Swift-Spray) software suite. Proc. 9th Int. Conf. on Harmonisation within Atmospheric Dispersion Modelling for Regulatory Purposes, vol. 2, 114-118
- Napoly A., 2013, Simulation numérique 3D de la dispersion de rejets atmosphériques accidentels. Comparaison d'une approche détaillée et simplifiée de modélisation, Training report.
- Nibart M., Armand P., Olry C., Duchenne C. and Albergel A., 2011, The indoor / outdoor pollutant transfer of a hazardous release: application to a parisian railway station, proc. 14th int. Conf. on Harmonisation within Atmospheric Dispersion Modelling for Regulatory Purposes
- Oldrini, O., Nibart, M., Armand, P., Olry, C., Moussafir, J., & Albergel, A., Introduction of Momentum Equations in Micro-SWIFT, 16th International Conference of Harmonization within Atmospheric Dispersion Modeling for Regulatory Purposes. September 2014, Varna
- Oldrini, O., Nibart, M., Armand, P., Olry, C., Moussafir, J., & Albergel, A., Multi Scale Built-up Area Integration in Parallel SWIFT, 15th International Conference on Harmonization within Atmospheric Dispersion Modeling for Regulatory Purposes. May 2013, Madrid
- Oldrini O., C. Olry, J. Moussafir, P. Armand and C. Duchenne, 2011: Development of PMSS, the Parallel Version of Micro SWIFT SPRAY. Proc. 14th Int. Conf. on Harmonisation within Atmospheric Dispersion Modelling for Regulatory Purposes, 443-447
- Tinarelli G., Mortarini L., Castelli S.T., Carlino G., Moussafir J., Olry C., Armand P., Anfossi D., 2013: Review and validation of MicroSpray, a lagrangian particle model of turbulent dispersion, *Journal of Geophysical Research*, **200**, 311-327.
- Tinarelli G., G. Brusasca, O. Oldrini, D. Anfossi, S. Trini Castelli, J. Moussafir, 2007: "Micro-Swift-Spray (MSS) a new modelling system for the simulation of dispersion at microscale. General description and validation". Air Pollution Modelling and its Applications XVII, C. Borrego and A.N. Norman eds., Springer, 449-458

**17th International Conference on  
Harmonisation within Atmospheric Dispersion Modelling for Regulatory Purposes  
9-12 May 2016, Budapest, Hungary**

---

**MICROSCALE SIMULATION OF ROAD TRAFFIC EMISSIONS FROM VEHICULAR FLOW  
AUTOMATIC SURVEYS AND COMPARISON WITH MEASURED CONCENTRATION DATA**

*Grazia Ghermandi, Sara Fabbi, Alessandro Bigi, Sergio Teggi<sup>1</sup> and Luca Torreggiani<sup>2</sup>*

<sup>1</sup>Department of Engineering “Enzo Ferrari”, University of Modena and Reggio Emilia, Modena, Italy

<sup>2</sup>ARPAE Reggio Emilia, Environmental System Services, Reggio Emilia, Italy

**Abstract:** In order to assess the impact of road traffic on local air quality, a microscale simulation of pollutant concentration fields due to vehicular traffic emissions have been performed. The investigated area is in downtown Reggio Emilia, a city in central Po valley, Italy, and focused on a crossing within the inner ring road, where an air quality monitoring station is present and where traffic is expected to be the main local source of atmospheric pollutants. A microscale simulation approach is suitable to face dispersion within an urban area, where buildings may lead to local peaks in pollutant concentration. The simulation has been performed by the micro-scale model suite Micro-Swift-Spray (Aria Technologies) a Lagrangian particle dispersion model directly derived from the SPRAY code, able to account for obstacles. Simulated pollutants are NO<sub>x</sub> and CO, as main tracers of combustion emissions. Direct measurement of traffic flow have been collected by radar traffic counter for 12 days and used for the hourly modulation of vehicular emissions. Emission factors were calculated according to the EMEP/EEA guidelines for air pollutant emission inventory. Specific emission factors were used depending on vehicle type, fuel type, speed and EURO category. Simulated concentration fields were investigated over the period with availability of traffic counts (13-24 January 2014). Results were compared to local air quality measurements next to the investigated road and within the simulated domain. The simulated NO<sub>x</sub> hourly concentrations highlighted the role of local traffic emissions in occasional exceedances of air quality limit. Simulated CO hourly concentrations result always well below limits. Simulated and observed concentrations show a large agreement for NO<sub>x</sub> and a fair agreement for CO.

**Key words:** MICROSPRAY, traffic emission, radar traffic counter, NO<sub>x</sub>, CO.

## **INTRODUCTION**

Road traffic is notoriously a significant source of air pollution. The pollutants emitted by vehicles are among the main causes of the degradation of air quality in urban areas, even away from busy streets and mainly in regions where meteorological condition are unfavourable to pollutant dispersion in the atmosphere. The atmospheric monitoring of NO<sub>x</sub> and CO, main tracers of combustion emissions, provided by the Environmental Agencies with fixed-site monitoring stations, clearly shows the impact of the daily traffic trend both at kerbside sites on main urban streets and also in urban background sites, with concentration peak during rush hours. The urban background concentrations can be in fact attributed to all sources in the whole agglomeration, among which motor vehicle exhaust emissions give a relevant contribution. At the kerbside sites (traffic stations) the local influence of traffic on the adjacent street is superimposed on the urban background (P. Lenschow et al. 2001), producing higher NO<sub>x</sub> and CO concentration values.

Within the same rationale, the regional background concentration can be attributed to all sources outside the agglomeration, i.e. natural sources and long range transport at local and global scale, with negligible influence of the sources within the agglomeration. Nevertheless, in the Central Po Valley (Northern Italy), whose meteorology is mostly characterised by recurrent wind calm episodes and high-pressure conditions, long-lasting high concentrations might occur at remote rural sites, not due to a direct influence by the large metropolitan and industrial areas of the Valley.

The comparison of the atmospheric concentration measurements at regional and urban background sites and at traffic stations, support source apportionment for main pollutants in urban areas. The investigation of the various contributions to urban air pollution due to different emission sources is one of main applications of air quality models, supporting environmental impact assessment studies, and policy

strategies for urban air pollution control. The evaluation of the direct impact of road traffic on air quality may be effectively performed by microscale simulation of pollutant concentration fields due to motor vehicle exhaust emissions.

In a previous work (Ghermandi et al., 2014) the  $\text{NO}_x$  and CO emissions from an urban crossroad in Modena (Central Po Valley, Italy) was simulated by means of the lagrangian particle dispersion model Micro-Swift-Spray, (Aria Technologies, 2010), a newer release of the Spray code (Arianet, 2010) which has been developed specifically for micro-scale applications in urban environments (Tinarelli et al., 2004). In that study hourly modulation patterns of traffic fluxes taken from literature were used. In the present case we performed a microscale simulation of the concentration fields due to traffic emissions in the vicinity of a crossing within the inner ring road in Reggio Emilia, a 170 000 inhabitants city in the central Po Valley, about 30 km West of Modena. Direct measurements of traffic flow have been collected by the local Environmental Agency (ARPAE) with a radar traffic counter from 13 to 24 January 2014; these data provided the hourly modulation of vehicular emissions for the duration of the measurement campaign (12 days). Hourly concentration of atmospheric  $\text{NO}$ ,  $\text{NO}_2$  and CO at this same street were provided by an ARPAE air quality monitoring station placed at kerbside (Figure 1 (a)).

The simulation results were compared to local air quality measurements of the traffic station next to the investigated road and with the measurements collected at urban background site of Reggio Emilia and at a rural background site of the region. The simulated  $\text{NO}_x$  hourly concentrations show a very large agreement with observed concentrations, allowing to estimate the role of traffic emissions to the observed atmospheric concentrations at the traffic site. The study outlines the importance of direct hourly measurement of traffic flows and of accurate determination of the emission factors in order to optimize the simulation results.

## EXPERIMENTAL AND METHODS

Direct measurements of traffic flows were collected in downtown Reggio Emilia, Northern Italy, by a 2 channel radar traffic counter for 12 days, from 13 to 24 January 2014. The radar was placed in the vicinity of a crossing within the inner ring road, as shown in Figure 1 (a).

The radar traffic counter recorded the time, the length and the speed of each passing vehicle, for all lanes of the adjacent road. The vehicles were divided in three groups depending on the length  $L$ : motorcycles ( $1 \text{ m} \leq L \leq 2.5 \text{ m}$ ), passenger cars ( $2.6 \text{ m} \leq L \leq 6 \text{ m}$ ) and light vehicles ( $6 \text{ m} \leq L \leq 8 \text{ m}$ ). Heavy duty vehicles (HDV) were omitted, having a negligible count during the measurement campaign. Recorded vehicle speed was divided in classes according to type: 12 for motorcycles, 14 for passenger cars and 10 for light duty vehicles (LDV). The speed value distribution into each class was estimated, with the median value taken as representative of the corresponding class. Class medians were used to obtain emission factors (EF) for  $\text{NO}_x$  and CO as a function of vehicle speed, following the European guidelines EMEP/EEA (EMEP/EEA, 2013). The EF for each pollutant vary also depending on the EURO emission standard of the vehicle and on the type of fuel.

Therefore, EF values were mathematically weighted to obtain a single EF for each group of vehicles and for each pollutant (Table 1); the accuracy of the calculation of the weighted EF values depends on the availability of supporting data. The calculation was most accurate for passenger cars (corresponding to about 80% of all recorded vehicles), given the availability of detailed vehicle fleet composition data for the year 2013 in Reggio Emilia provided by Italian Automobile Club (ACI, 2013), including also fuel type and emission standards. For motorcycles and LDV, the average value of EF for the different EURO categories and for the fuel type (mainly diesel for LDV (ACI, 2013)) were evaluated. For mopeds (motorcycles with engine capacity  $< 50 \text{ cm}^3$ ) the guidelines directly provides the EFs.

**Table 1.** Emission Factors (g/km) weighted values

	Passenger cars	Motorcycles	Light vehicles
$\text{NO}_x$	0.277	0.108	0.692
CO	0.191	5.971	0.387

Coupling the hourly radar records with the EF value for each counted vehicle, the hourly mass flows of CO and NO<sub>x</sub> emitted for the whole road length were estimated: the modulated traffic emissions according to the hourly variation of traffic fluxes has been thus obtained for each day of the measurement campaign. The traffic counter, positioned as shown in Figure 1(a) for the entire campaign, directly monitored the lanes on the street side next to the radar; the traffic flows for the other two main roads of the crossing (red lines in Figure 1 (a)) derive from modeled data provided by the Municipality of Reggio Emilia.

### MODEL SETUP AND METEOROLOGICAL DATA SET

The Micro Swift Spray (MSS) simulation domain is 500 m x 500 m large (Figure 1 (a)) with grid step of 2 m (square cells). The vertical grid consists of 5 layers, 2 m deep each, with the domain top of 10 m high above ground level, and the first layer for concentration computing is 2 m high above ground. Building volumes and road geometry were outlined from a high resolution 3D vectorial cartography (UVL\_GPG) of the studied domain (E. R., 2013) (Figure 1 (c)). Following the model by Hertel and Berkowicz (1989), for the studied case the traffic induced turbulence height ranges between 6 - 8 meters above ground level and the traffic induced turbulence width ranges between 14 -21 m around the road axis; these values has been used for MSS simulation. The simulation period spans from 13 to 24 January 2014.

The simulation was ran at hourly time step, consistently with the meteorological data. The hourly meteorological data, mixing height values and turbulence parameters (i.e. friction velocity, convective velocity scale and Monin-Obukhov length) used, were derived from CALMET model simulations by ARPAE (Deserti *et al.*, 2001).

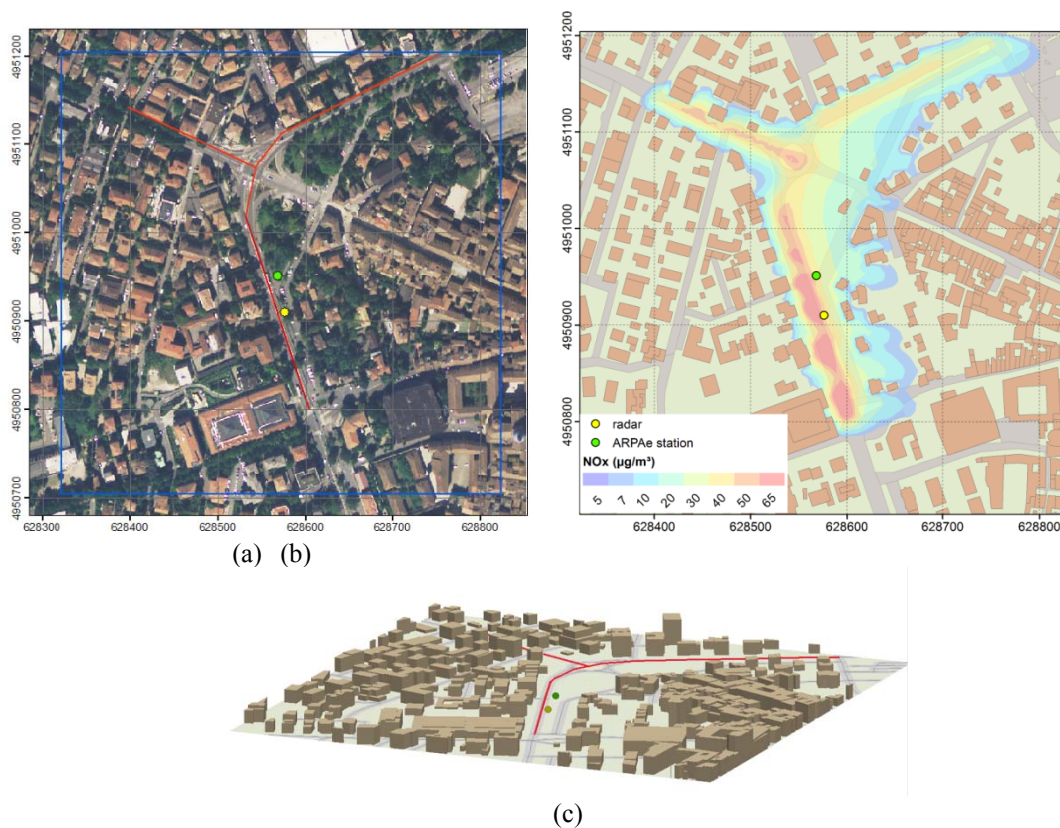


**Figure 1.** Map of the investigation domain (UTM32-WGS84), with corner S-O (628 322, 4 950 704)m (blue square); traffic counter site (yellow point) (628 574, 4 950 910)m; ARPae station (green point) (628 568, 4 950 950)m; road sections (red lines) considered in the simulation as linear emission sources (a).

Average hourly NO<sub>x</sub> concentration (µg/m<sup>3</sup>) in the first atmospheric layer, 2 m above ground level, for 17 January 2014 (b). Block-shaped structures in Micro Swift Spray simulation (c).

During the simulation period unusual weather conditions for the winter period in the Central Po Valley occurred, with heavy storm rainfall on 18 and 19 January, better suitable for spring time. This atypical

weather condition also affected air quality. Mean wind speed during the simulation period is lower than  $1 \text{ m}\cdot\text{s}^{-1}$ , the daily average air temperature ranges from 3 to 10 °C, with higher daytime excursion (up to 9 °C) over the last four days of the period.

## RESULTS AND DISCUSSION

MSS simulation provided hourly  $\text{NO}_x$  and CO concentration fields in the first atmospheric layer, from which average daily concentration maps (i.e. average values over 24 hours) are obtained: in Figure 1 (b) the concentration map for  $\text{NO}_x$  generated by traffic emissions for 17 January 2014, as an example, is presented.

Moreover, the time series of hourly simulated concentrations, from 13 to 24 January 2014, may be compared with measured concentration values collected at ARPAAE air quality monitoring stations. The simulated concentration were evaluated at 4 m above ground level, i.e. the same height of the inlet of air quality monitoring instruments by ARPAAE. The time series of hourly  $\text{NO}_x$  concentrations measured at the ARPAAE traffic station at kerbside on the monitored street from 13 to 24 January 2014, are presented in Figure 2, along with the hourly  $\text{NO}_x$  concentration valued simulated by MSS. The measured concentration results from local traffic emissions and from the sources in the whole agglomeration, that correspond to the urban background. The MSS simulated concentrations represent only the contribution by traffic emission to atmospheric  $\text{NO}_x$ .

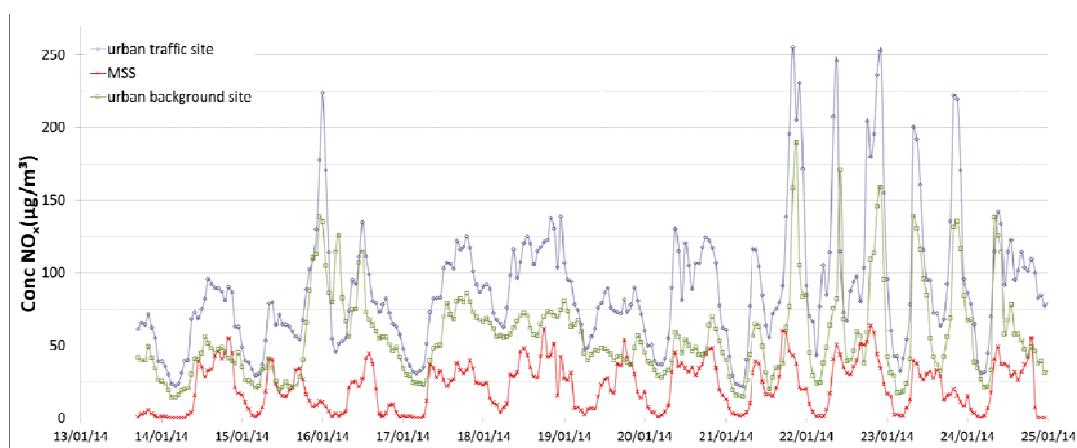


**Figure 2.** Hourly  $\text{NO}_x$  concentration measured at ARPAAE urban traffic station (blue curve), measured at ARPAAE urban background station (green curve) and simulated by MSS (red curve) from 13 to 24 January 2014.

The simulated concentrations remain constantly lower than the measured concentration both at the urban traffic and urban background stations. The pattern of the three series shows a good agreement, the measured concentration peak on 16/01/2014 (at 01:00) a part: that unusually high  $\text{NO}_x$  value measured both in traffic and urban background in Reggio Emilia was also measured at the same time in urban background and traffic ARPAAE stations in the nearby city of Modena; also the CO concentrations measured both in Reggio Emilia and Modena traffic stations (CO measurements are not collected at urban background sites) had a high peak at that time. This may be due to a meteorological event constricting low and polluted air masses towards the ground, as for the local evolution of a cold air front (Li et al., 2015).

The  $\text{NO}_x$  traffic and urban background measured concentrations show a very similar pattern; this mostly depends on the Po Valley meteorological regime, mainly influenced by the valley morphological conformation and characterised by recurrent wind calm episodes, occurring also during the measurement campaign. This condition determinates accumulation and persistence of the pollutant load, therefore also at the urban background site the air quality is clearly affected by the diurnal variability of the main pollutant source. The differences of  $\text{NO}_x$  between the traffic station and the urban background station can be attributed to the local influence of traffic, and this has been here estimated by MSS simulation. In

Figure 3 the hourly NO<sub>x</sub> concentrations measured at the ARPAE traffic station are compared with the sum of NO<sub>x</sub> hourly simulated concentrations and corresponding urban background measured values. The two time series result highly correlated (Pearson coefficient  $r = 0.86$ ).

The traffic emission contribution to air quality at the traffic site, as evaluated by MMS simulation in the present study, corresponds to ~24% of the NO<sub>x</sub> atmospheric concentrations, while about 56% is given by regional background contribution. The remaining 20% corresponds to agglomeration sources emissions (e.g. domestic heating).

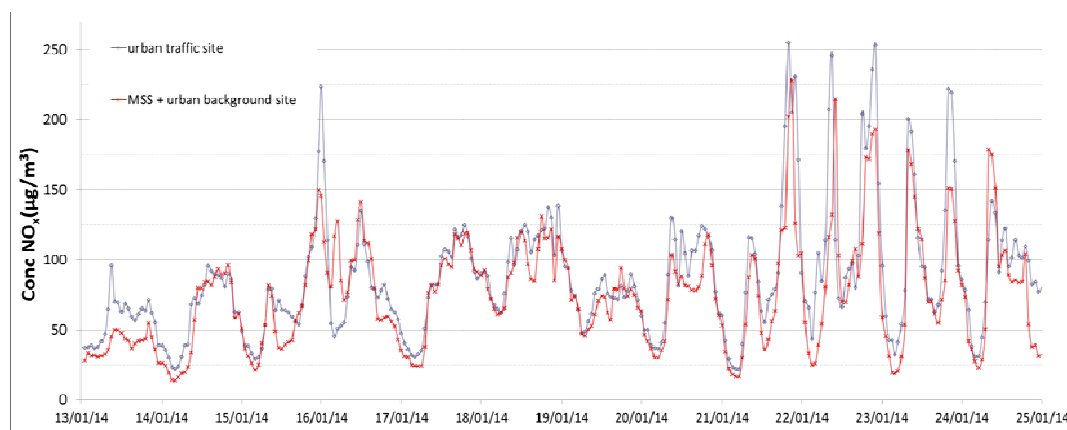


**Figure 3** Hourly NO<sub>x</sub> concentration measured at ARPAE urban traffic station (blue curve) and MMS simulated plus urban background site concentrations (red curve) from 13 to 24 January 2014. The red curve in this figure corresponds to the sum of red and green curve as reported in Figure 2

For the town of Reggio Emilia the traffic contribution to NO<sub>x</sub> emissions had been estimated (E.R., 2013) in about 54.5 %, consequently traffic emissions have a relevant impact both on urban and on regional background NO<sub>x</sub>. CO monitoring is performed only at traffic site, therefore no CO data is available from urban background. The correlation between measured and simulated CO is quite large ( $r = 0.42$ ). The low sensitivity of the CO monitoring instrument has also to be considered, since it prevents to successfully repeat the data processing as done in this work for NO<sub>x</sub>.

## REFERENCES

- ACI, 2013: <http://www.aci.it/> and <http://www.ucer.camcom.it/studi-ricerche/banche-dati/bd/appendice-dati-comunali/trasporti-stradali.-consistenza-dei-veicoli/?searchterm=veicom>
- Arianet, 2010: SPRAY5 - General Description and User's Guide, ARIANET R2010.08.
- Aria Technologies, 2010: SWIFT Wind Field Model, General Design Manual.
- Deserti, M., E. Savoia, C. Cacciamani, M. Golinelli, A. Kerschbaumer, G. Leoncini, A. Selvini, T. Paccagnella, S. Tibaldi, 2001: Operational meteorological pre-processing at Emilia Romagna ARPA Meteorological Service as a part of a decision support system for Air Quality Management. *International Journal of Environment and Pollution*, **16**, 571-582.
- EMEP/EEA, 2013 : air pollutant emission inventory guidebook <http://www.eea.europa.eu/publications/emep-eea-guidebook-2013/part-b-sectoral-guidance-chapters/1-energy/1-a-combustion/1-a-3-b-road-transport/view>
- E. R., 2013: Geoportale Emilia-Romagna (Database topografico 2013): <https://geoportale.regione.emilia-romagna.it/it/download/databasetopografico>
- E. R., 2013: PAIR 2020 QUADRO CONOSCITIVO: <http://ambiente.regione.emilia-romagna.it/aria-rumore-elettrosmog/temi/pair2020>
- Ghermandi, G., S. Fabbri, M. Zaccanti M. M., A. Bigi A., S. Teggi, 2014: Urban micro-scale investigation of NO<sub>x</sub> and CO emissions from vehicular traffic and comparison with air quality data, Proc. of 16<sup>th</sup> International Conference on Harmonisation within Atmospheric Dispersion Modelling for Regulatory Purposes, 8-11 September 2014, Varna, Bulgaria, 380-385.
- Hertel, O., R. Berkowicz, 1989: Operational Street Pollution Model (OSPM). Evaluation of the model on data from St. Olavs street in Oslo, *DMU Luft A-135*.

- Lenschow, P., H.J. Abraham, K. Kutzner, M. Lutz, J.D. Preuß & W. Reichenbacher, 2001: Some ideas about the sources of PM10. *Atmospheric Environment*, **35**, 23-33.
- Li, X., X. Xia, L. Wang, R. Cai, L. Zhao, Z. Feng, Q. Ren, and K. Zhao 2015: The role of foehn in the formation of heavy pollution events in Urumqi, China. *J Geophys. Res. Atmos.*, **120**, 5371-5384.
- Tinarelli, G., G. Brusasca, O. Oldrini, D. Anfossi, S. Trini Castelli, J. Moussafir, 2004: Micro-Swift-Spray (MSS) a new modelling system for the simulation of dispersion at microscale, general description and validation, Proc. of the 27<sup>th</sup> CCMS-NATO meeting, Banff (Canada), 25-29 Oct 2004.

**17th International Conference on  
Harmonisation within Atmospheric Dispersion Modelling for Regulatory Purposes  
9-12 May 2016, Budapest, Hungary**

---

**NEW INFLOW BOUNDARY CONDITIONS FOR HOMOGENEOUS ATMOSPHERIC  
BOUNDARY LAYER UNDER THE POWER LAW FOR STREET SCALE MODELLING**

*Vasilis Akylas<sup>1</sup>, Fotios Barmpas<sup>1</sup>, Nicolas Moussiopoulos<sup>1,2</sup>, and George Tsegas<sup>1</sup>*

<sup>1</sup> Laboratory of Heat Transfer and Environmental Engineering, Department of Mechanical Engineering,  
Aristotle University of Thessaloniki, Greece

<sup>2</sup> International Hellenic University

**Abstract:** Street scale numerical simulations of air pollutant dispersion in urban hotspots normally consider physical processes in the lowest part of the Atmospheric Boundary Layer (ABL). The vertical profiles of the mean wind speed and the turbulent fluxes are obtained either from in-situ measurements or from numerical simulations from larger scale weather models. In street scale numerical simulations utilizing Computational Fluid Dynamics (CFD) models, normally the inlet flow should preserve the horizontal homogeneity upstream and downstream of the resolved obstacle. Hence, the vertical profile of the mean wind speed and turbulent profiles must be in equilibrium with the roughness characteristics of the ground surface. Horizontally homogenous boundary conditions do not normally agree with field measurements while at the same time the profiles obtained by measurements do not preserve the homogeneity of the flow. As a result, in recent years alternative sets of boundary conditions have been proposed in order to bridge the gap between real life vertical ABL profiles and those applied as input boundary conditions for modelling purposes. In the present study the homogeneity of the boundary conditions is addressed by applying the power law for the vertical distribution of horizontal mean wind speed to obtain the appropriate vertical profiles. The purpose of this approach is to establish a new set of turbulence profiles which follow the power law towards increasing the accuracy of modelling predictions for air pollutant dispersion problems in urban areas. In order to validate the new set of inflow boundary conditions a series of numerical simulations were performed. The simulations were conducted for the cases of neutral boundary layer over flat terrain and around a single surface-mounted cube. To this end, the CFD code MIMO was utilized under different sets of boundary conditions. The modelling results were compared with wind-tunnel data and are presented along with other published results. The overall outcome is that the new inflow boundary conditions are improving the simulation of turbulence for street scale applications.

## INTRODUCTION

A proper and accurate description of the lower part of the Atmospheric Boundary Layer (ABL) is necessary for a wide range of environmental flow and air pollutant dispersion studies. Focusing on numerical simulations at the street scale, over the last two decades Computational Fluid Dynamics (CFD) have been recognised as a valuable numerical tool able to offer significantly higher accuracy compared to the most commonly used empirical and semi-empirical models. In order to realize a dispersion study in the microscale it is important to rely on an accurate prediction of the wind properties at the area of interest. The latter requires a precise solution using CFD methods to describe the lower part of the ABL at the inflow side of the computational domain.

Over the past two decades, a consensus has formed among the scientific community that in applying CFD models for dispersion problems in urban areas, the computational domain size must be large enough to ensure that all perturbations of the flow induced by the resolved buildings like the upstream stagnation pressure, are included in the numerical solution (Tominaga et al. 2008). In the long fetch of the computational domain upstream of the obstacles, the approaching ABL flow is similar to the flow of air over roughness elements which are parametrically resolved. The integration of this technique in the numerical solution requires that the vertical profile of the ABL maintains a horizontal homogeneity in order to minimize the generation of disturbances (Richards and Hoxey 1993). This phenomenon normally occurs when streamwise gradients of the wind velocity and the turbulent quantities are zeroed in areas upstream and downstream of the obstacles area. In the case when the standard  $k$ - $\epsilon$  turbulence model is employed, this results to a conservation of the local equilibrium of the local production rates of the main turbulent quantities paired in space and time. To address this problem, the fully developed profiles of the mean velocity, the turbulent kinetic energy and the dissipation rate proposed by Richards and Hoxey

(1993) are normally used to prescribe inflow boundary conditions. However, in these cases, the vertical TKE profile is not necessarily always in agreement with field measurements (Yang et al. 2009). In view of these findings, within the frame of the current study a new set of boundary conditions is proposed which are based on the power law for the description of the mean velocity while the vertical profiles of  $k$  and  $\varepsilon$  are extracted as the solution of the turbulence model and preserve the horizontal homogeneity.

## METHODOLOGY

As stated above, a new set of inflow conditions is considered in this paper. The vertical profile of the mean velocity  $u$ , the turbulent kinetic energy  $k$  and the dissipation rate  $\varepsilon$  are described by the following equations:

$$u(z) = u_s \left( \frac{z}{z_s} \right)^\alpha \quad (1)$$

$$k(z) = \sqrt{D_1 \cdot z^\alpha + D_2} \quad (2)$$

$$\varepsilon(z) = \sqrt{C_\mu} \cdot k(z) \cdot \frac{u_s}{z_s} \cdot a \cdot \left( \frac{z}{z_s} \right)^{(\alpha-1)} \quad (3)$$

where  $u_s$  is the velocity measured at the reference height,  $z_s$ ,  $\alpha$  is the power law exponent,  $D_1$  and  $D_2$  are constants determined by profile fitting based on the available measurements and  $C_\mu$  is a wall constant of the turbulence model, equal to 0.09 for the standard  $k$ - $\varepsilon$  turbulence model. All results produced by these new inflow boundary conditions are denoted as power law conditions (PL).

The performance of the proposed inflow boundary conditions is demonstrated on the basis of comparison between numerical results and wind tunnel measurements for the test case CEDVAL A1-1 (Leitl and Schatzmann 1998), during which the atmospheric flow properties around a surface mounted cube under a scale of 1:200 were measured. The evaluation procedure for the needs of the current study took place in three stages. During the first stage and prior to the numerical simulations, the production of the vertical profile of the approaching wind under different boundary conditions was thoroughly documented. At the second stage, the case of the atmospheric flow over a rough terrain was investigated. For this purpose, a series of two dimensional simulations were performed in order to quantify the correlation of the ABL at the inflow and outflow surfaces and assess the ability of the model to maintain horizontal homogeneity over a rough terrain. In the third stage the complete flow around a surface-mounted cube approximating a single building was considered.

The vertical profile of the ABL was produced using wind tunnel measurements. In particular, the friction velocity was found to be  $u^*=0.377 \text{ ms}^{-1}$ , the roughness length  $z_0=0.007 \text{ m}$ , the reference velocity  $u_s=6 \text{ ms}^{-1}$  at a reference height  $z_s=0.5 \text{ m}$  with a zero displacement height and the power law exponent  $\alpha=0.21$ . The numerical simulations were conducted using the microscale model MIMO (Ehrhard et al., 2000). For the two dimensional case, a structured mesh which comprised of a total of  $150 \times 57$  cells was used with minimum cell size of 0.01 m and 0.0125 m and expansion factors of 1.04 and 1.05 along the longitudinal and vertical axes of the domain respectively. For the three dimensional case, a total of  $150 \times 57 \times 54$  cells were employed with minimum cell sizes of 0.01 m, 0.0125 m and 0.0125 m with expansion factors of 1.04, 1.05 and 1.05 along the longitudinal, vertical and horizontal axes respectively. At the top and at the outflow planes of the domain homogeneous Neumann boundary conditions were applied. At all other face boundaries Dirichlet conditions were applied. At all solid surfaces like the ground and the building's walls the standard wall functions were used.

The results of the numerical simulations with the proposed inflow conditions were compared with results from simulations under the ones proposed both by Richards and Hoxey (1993), denoted hereby as RH and those by Tominaga et al. (2008), denoted as AIJ. The RH conditions employ the log law for the mean velocity in contrast to the AIJ conditions which employ the power law for the mean velocity and the dissipation rates. The TKE profile is generated based on the estimated boundary layer height  $z_G$  in accordance with the roughness class of the terrain. For the needs of the comparison between the calculated vertical profiles, the statistical indices of the normalized mean square error (*NMSE*) and the correlation coefficient  $R$  were used. Furthermore, in order to quantify the agreement between measurements and numerical simulations the hit rate  $q$  is employed in accordance with equation (4):

$$q = \frac{N}{n} = \frac{1}{n} \sum_{i=1}^n N_i, \text{ where } N_i = \begin{cases} 1 & \text{for } \left| \frac{P_i - O_i}{O_i} \right| \leq D \text{ or } |P_i - O_i| \leq W \\ 0 & \text{else} \end{cases} \quad (4)$$

Where  $P_i$  are the model results,  $O_i$  the observation data,  $D$  the relative deviation which is set to 25% and  $W$  the absolute deviation or threshold. This threshold signifies the acceptable degree up the measurement uncertainty of the observation. The value of  $W$  is set to 0.012 for the velocity results and  $0.0316 \cdot (k \cdot u_s^2)^{0.518}$  for the turbulent kinetic energy.

## RESULTS AND DISCUSSION

The first stage results for the vertical profiles of the velocity and TKE at the inlet are presented in Figure 1. It should be clarified that during this specific wind tunnel test, only the lowest part of the ABL up to a height of 90 m was simulated. The estimated values of the *NMSE* for the log and power law cases were 0.09 and 0.037 respectively, with the *R* standing at 0.995% for both cases. A comparison of the results for the velocity illustrated in Figure 1a, reveals that while the power law performs better closer to the ground, the power law proves more accurate at higher locations. A similar comparison for TKE demonstrates that the accurate reproduction of the vertical profile of the TKE is highly uncertain and very difficult to achieve. In any case however, the results for the selected statistical metrics presented in Table 1 show that the application of the proposed flexible conditions leads to relatively more accurate results.

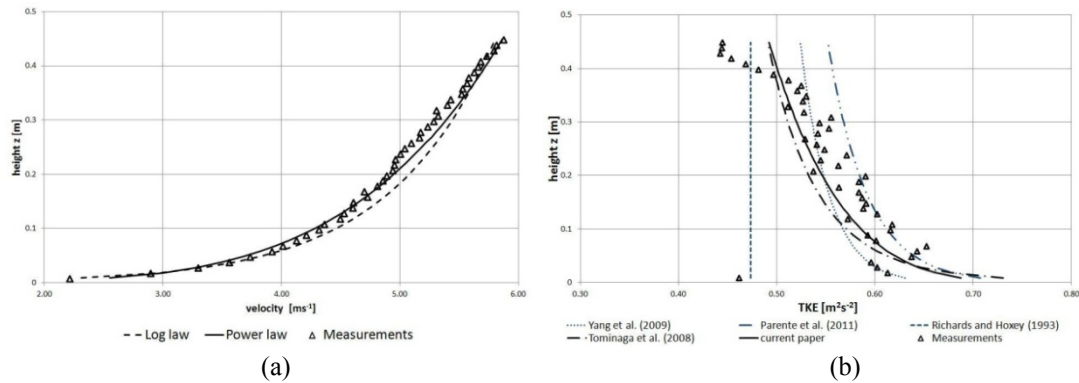


**Figure 1.** Comparison of physical and numerical simulations results for the vertical profile of ABL for (a) the mean wind speed and (b) the TKE

**Table 1.** *NMSE* and *R* for the vertical profile of TKE reproduced under different boundary conditions

	PL	Yang et al. (2009)	Parente et al. (2011)	RH	AIJ
<i>NMSE</i>	0.63	0.66	1.10	3.41	0.95
<i>R</i>	64.1%	58.2%	56.2%	0.0%	51.0%

The second stage results for the correlation between the inlet and the outlet profiles are presented in Figure 2. In this case, only the ability of the model to preserve the vertical profile of the inflow over rough terrain is tested and the correlation between the inlet boundary condition and the vertical profile of the approaching ABL in the wind tunnel is not considered. For moderate values of the approaching wind speed PL and AIJ conditions do not perform as well as the RH. On the other hand in the case of TKE, PL conditions perform much better than AIJ and RH especially at lower heights close to the ground. Overall, the correlation between the inflow and outflow profiles presented in Table 2, is satisfactory in all boundary condition cases, with RH performing better for velocity and PL better in the case of TKE.

For the third stage, the dimensionless simulation results of velocity and TKE are presented in Figure 3. The measurement points were located at a vertical and at a horizontal plane at the middle cross and mid-height sections of the building respectively and were clustered according to their relative position with respect to it. Comparison of results from the simulations with the log and power laws boundary conditions shows larger deviation between the two on the vertical plane and close agreement on the

horizontal plane. In the case of the vertical plane, the utilization of the RH conditions leads to over predictions for the TKE in contrast to AIJ which leads mainly to under predictions. As a result the deviation of the results for TKE between the RH and the AIJ conditions are much larger compared to the ones on the horizontal plane.

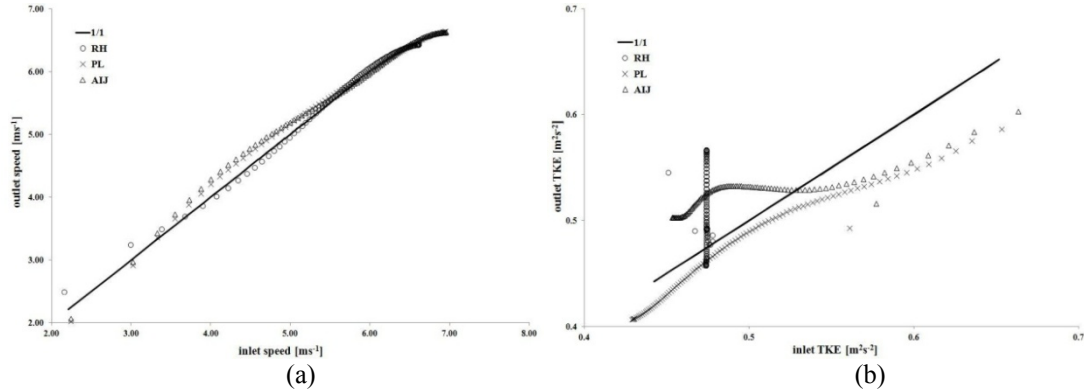


**Figure 2.** Correlation between (a) mean wind speed and (b) TKE at the inflow and outflow boundaries

**Table 2.** Correlation coefficient for velocity and TKE profiles for stage two

	RH	PL	AIJ
Velocity	98.7%	98.3%	98.3%
TKE	91.7%	97.3%	87.4%

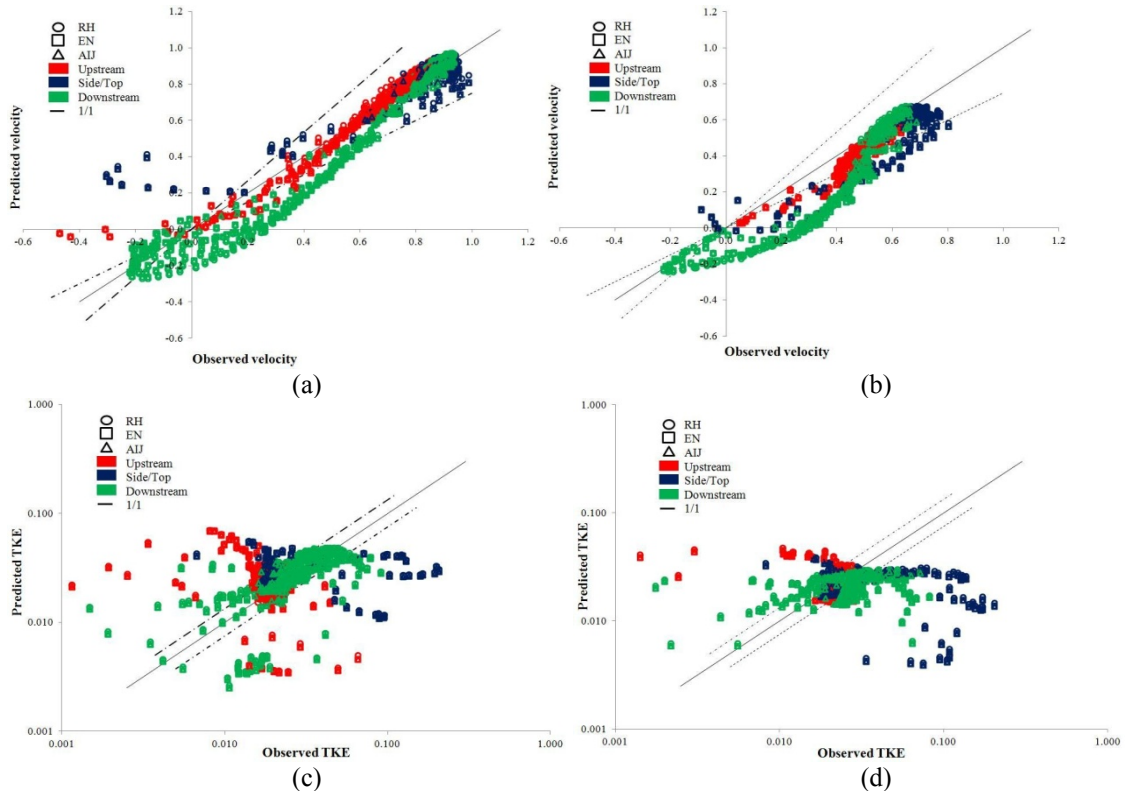


**Figure 3.** Correlation of numerical results and wind tunnel measurements for velocity and TKE at a vertical and a horizontal plane at various areas relative to the building

Results for the hit rate  $q$  for the dimensionless velocity and TKE are presented in Tables 3 and 4 which were estimated utilizing numerical results from simulations with MIMO and Parente et al. (2008) with the commercial software ANSYS Fluent. MIMO predictions for velocity are slightly less accurate compared

to those by Parente et al. (2008). However, it performs much better in predicting TKE, especially upstream of the building area. Further comparison of MIMO results between the different boundary condition cases shows only minor differences. In particular, the application of power law conditions compared to AIJ and the RH resulted in slightly reduced accuracy of the velocity prediction. On the other hand, compared to the cases of the AIJ and RH conditions the use of the PL conditions overall led to better predictions for TKE.

**Table 3.** Velocity hit rate  $q$  for MIMO simulations and other published results

$uu_s^{-1}$	MIMO RH	MIMO PL	MIMO AIJ	Gorle RH	Gorle mod	Parente PS2
Upstream	0.82	0.81	0.81	0.9	0.87	0.9
Side/Top	0.74	0.73	0.73	0.75	0.81	0.79
Downstream	0.47	0.46	0.46	0.49	0.59	0.58
All	0.63	0.61	0.61	0.66	0.71	0.71

**Table 4.** TKE hit rate  $q$  for MIMO simulations and other published results

$ku_s^{-2}$	MIMO RH	MIMO PL	MIMO AIJ	Gorle RH	Gorle mod	Parente PS2
Upstream	0.53	0.52	0.45	0.36	0.51	0.58
Side/Top	0.37	0.33	0.33	0.51	0.31	0.54
Downstream	0.54	0.57	0.54	0.59	0.49	0.62
All	0.50	0.51	0.48	0.51	0.47	0.59

## CONCLUSIONS

In the present study a new set of boundary conditions for the vertical profile of the ABL were proposed with the aim to improve the accuracy of numerical predictions, for dispersion problems in urban areas with the use of traditional CFD codes. These conditions provide a vertical profile of the mean wind speed in the ABL at the inflow face of the computational domain in accordance with the power law and the needs of the  $k - \varepsilon$  turbulence closure model. Simulation results were evaluated over three stages based on through comparisons a wind tunnel simulation of ABL around an isolated building. Overall, under the new conditions simulation results were improved for the flow over rough terrain, especially for TKE. In the case of the surface-mounted obstacle the results were improved for the prediction of TKE especially downstream and in the wake region of the building. To this end, when appropriate, the new inflow boundary conditions should be used instead of the standard ones, especially in cases during which the impact of the complex interactions between the building wakes and the turbulent fluxes on atmospheric dispersion have to be considered.

## REFERENCES

- Ehrhard, J., I.A. Khatib, C. Winkler, R. Kunz, N. Moussiopoulos, and G. Ernst, 2000: The microscale model MIMO: Development and assessment, *Journal of Wind Engineering and Industrial Aerodynamics* **85**,163-176.
- Leitl, B., and M. Schatzmann, 1998: Compilation of experimental data for validation purposes, CEDVAL, Meteorology Institute, U-H, Germany, <http://www.mi.zmaw.de/index.php?id=433>.
- Parente, A., C. Gorlé, J. van Beeck, and C. Benocci, 2011: Improved  $k-\varepsilon$  model and wall function formulation for the RANS simulation of ABL flows, *Journal of Wind Engineering and Industrial Aerodynamics*, **99**, 267-278.
- Richards, P.J , and R.P Hoxey, 1993: Appropriate boundary conditions for computational wind engineering models using the  $k-\varepsilon$  turbulence model, *Journal of Wind Engineering and Industrial Aerodynamics*, **46-47**, 145-153.
- Tominaga, Y., A. Mochida, R. Yoshie, H. Kataoka, T. Nozu., M. Yoshikawa, and T. Shirasawa, 2008: AIJ guidelines for practical applications of CFD to pedestrian wind environment around buildings, *Journal of Wind Engineering and Industrial Aerodynamics*, **96**, 1749-1761.
- Yang, Y., M. Gu, S. Chen, and X. Jin, 2009: New inflow boundary conditions for modelling the neutral equilibrium atmospheric boundary layer in computational wind engineering, *Journal of Wind Engineering and Industrial Aerodynamics*, **97**, 88-95.

**17th International Conference on  
Harmonisation within Atmospheric Dispersion Modelling for Regulatory Purposes  
9-12 May 2016, Budapest, Hungary**

---

**THE AIR QUALITY IN TWO-DIMENSIONAL URBAN CANYONS WITH GABLE ROOF  
BUILDINGS: A NUMERICAL AND LABORATORY INVESTIGATION**

*Simone Ferrari, Maria Grazia Badas, Michela Garau, Alessandro Seoni and Giorgio Querzoli*

DICAAR - Dipartimento di Ingegneria Civile, Ambientale e Architettura, University of Cagliari, Italy

**Abstract:** in this work we compare two typical methods (numerical simulation and laboratory experiment) of modelling air flows at the urban scale to assess air quality in street canyons. We have investigated, both via numerical simulations and laboratory experiments, the effect of gable roofs, on the air quality in urban canyons with different aspect ratios. In particular, we have focused on the flow regimes, turbulence characteristics and air exchanges between the urban canyon and the outer flow. Results highlight how the choice of the roof shape can be meaningful for building design, planning strategies and regulatory purposes.

**Key words:** *Urban boundary layer, natural ventilation, two-dimensional street canyons, gable roof, CFD, RANS simulation, laboratory simulation*

## **INTRODUCTION**

Though some authors have demonstrated the decisive impact of roof slope on wind flow (e.g. Huang et al., 2009; Yassin, 2011), this topic has not been investigated systematically, even if the gable roof building is a widespread typology in many regions all round the world. We have consequently investigated the effect of gable roofs on the air flow and quality in urban canyons with different aspect ratios  $W/H$  ( $W$  is the canyon width and  $H$  is the canyon height). In particular, we have focused on the flow regimes, turbulence characteristics and air exchanges between the urban canyon and the outer flow. The experiments were performed both via numerical and laboratory simulations.

## **MATERIALS AND METHODS**

Both in laboratory and numerical simulations, we have investigated the flows in urban canyons, formed by identical buildings with symmetrical dual-pitched roofs and a constant flow perpendicular to the canyon axis. The roof pitches varied from  $0^\circ$  (flat roof) to  $45^\circ$  and the canyon aspect ratios  $W/H$  from 1 to 4: a wide range of real building configurations has been therefore covered, including most of the values indicated by Grimmond and Oke (1999) for real cities.

### **Laboratory simulations**

Laboratory experiments have been performed in a closed-loop water-channel. The channel is 50 cm high, 40 cm wide and 800 cm long. The canyon array consists in 20 identical buildings: 2 cm high and wide parallelepipeds were chosen, in order to have an obstruction factor close to 3% (Blocken, 2015). The test section is located at around 650 cm downstream of the channel inlet, where the neutral boundary layer can be considered fully-developed. Small pebbles, with an equivalent diameter of 0.5 cm were displaced over the channel bottom for 300 cm upstream the canyon array, in order to increase the roughness of the bottom and to reproduce a logarithmic velocity profile. As flow velocities have been measured by means of a non-intrusive image analysis technique, namely Feature Tracking Velocimetry (FTV), the fluid was seeded with non-buoyant particles, the test section was lighted by a green laser sheet and images were recorded by a high-speed camera at the resolution of 2240 x 1760 px and 200 Hz. FTV has proved to be less sensitive to the appearance and disappearance of particles, and to high velocity gradients than classical Particle Image Velocimetry (PIV). More details on FTV can be found in Besalduch et al. (2013). The Reynolds number  $Re$ , based on the canyon height, is about 5,000, largely higher than the minimum value of 3,400 suggested by Hoydysh (1974) for the flow to be independent on  $Re$ .

### Numerical simulations

Numerical simulations have been performed by means of the open source CFD library OpenFOAM 2.3 (Weller et al. 1998). A Reynolds Averaged Navier-Stokes model (RANS) with two equation  $k-\epsilon$  closure (Launder and Spalding, 1974) was set up; simpleFoam (Patankar and Spalding, 1972), a steady state solver for incompressible turbulent flows, and a second order schemes for discretization were employed. A fully-developed steady turbulent flow was generated. A uniform, indefinite succession of buildings was simulated by imposing periodic boundary conditions in the streamwise direction. The simulation domain is three canyons long in the streamwise direction, and  $15 H$  high, in order to fulfil the condition reported for flow simulation around buildings in the best practice guidelines of Franke et al. (2011).  $Re$ , based on the canyon height, is about 43,000, largely higher than the minimum value of 15,000 suggested by Snyder (1981) for the flow to be independent on  $Re$ . Cyclic boundary conditions were imposed at the inlet and outlet for all the variables, except for pressure, whose gradient is adjusted to obtain the required mean velocity. The upper boundary of the computational domain was considered a symmetry plane. At ground and building surfaces no-slip conditions were imposed for velocity, while Neumann zero gradient conditions were imposed for pressure and turbulent quantities (kinetic energy, energy dissipation rate and turbulent viscosity). OpenFOAM has been already extensively and successfully used to perform wind RANS simulation in urban environment (e.g. Hertwig et al. 2012); moreover, Takano and Moonen (2013) proved that a similar OpenFOAM configuration was able to properly reproduce a two-dimensional periodic array of flat roof buildings.

### RESULTS

In all the figures from 1 to 5 the flow moves from right to left. Fig.1 shows a comparison between the non-dimensional mean velocity field  $u/U$  (i.e. the mean velocity magnitude  $u$  non-dimensionalised by the mean free stream velocity  $U$ ) measured with numerical (left side) and laboratory (right side) simulations, with some streamlines as well, in the case of flat roof and  $W/H = 1$ . The stable single vortex, typical of the skimming flow regime, is well reproduced, as well as the velocity magnitude and the streamlines. The same considerations apply to Fig.2 ( $u/U$  fields from numerical and laboratory simulations for pitched roof and  $W/H = 1$ ) and Fig.3 ( $u/U$  fields from numerical and laboratory simulations for pitched roof and  $W/H = 2$ ), even if in those cases the effect of the pitched roofs in reducing the velocity outside the canyon is slightly overestimated by the numerical simulations. In case of flat roof (Fig.1), the outer stream is almost unperturbed, with a steep increase of the velocity with  $Z$ ; the free stream velocity  $U$  is already attained at  $Z/H = 3$ . From the comparison of Fig.1 with Fig.2 we can see that the pitched roof determines a perturbation that propagates significantly above the roof, with wavy streamlines also above the ridge of the roof and a zone of reduced velocity that extends upwards that is larger than in the flat roof case.

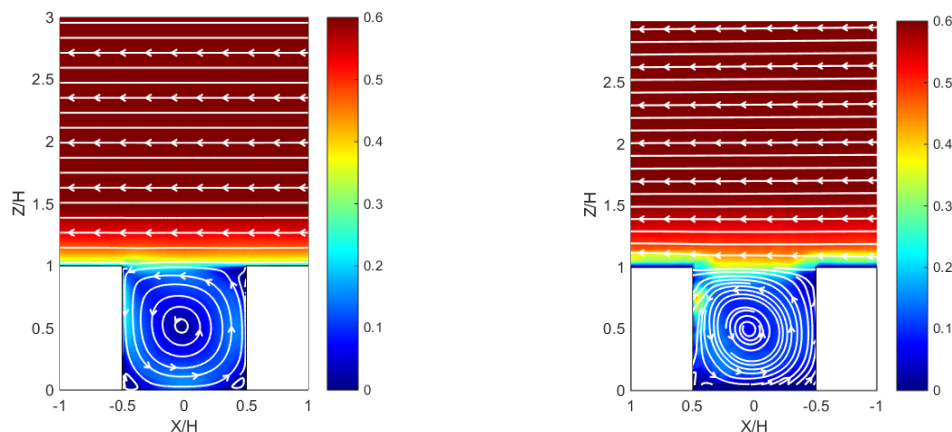


**Figure 1.** Non-dimensional mean velocity  $u/U$  fields (color map) with streamlines (white lines) from numerical (left side) and laboratory (right side) simulations, for flat roof and  $W/H = 1$ .

The left and central panel of Fig 4 ( $W/H = 1$ ) and 5 ( $W/H = 2$ ) show the non-dimensional Turbulent Kinetic Energy  $TKE/U^2$  in the case of pitched roof; the right panel of Fig.4 shows the same quantity in the case of flat roof and  $W/H = 1$ . TKE is lower within the urban canyon than above it. The numerical simulation is able to correctly reproduce the features of the TKE fields, even if it tends to overestimate

their values. From Fig.4 we can state that the pitched roofs determine much higher values of TKE in the outer flow stream than the flat ones. Moreover, the TKE generated on the upstream roof building tends, in the pitched roof case, to propagate down to the eave height of the downstream building, promoting turbulent mixing inside the canyon as well. This phenomenon is stronger in the  $W/H = 2$  case (Fig.5).

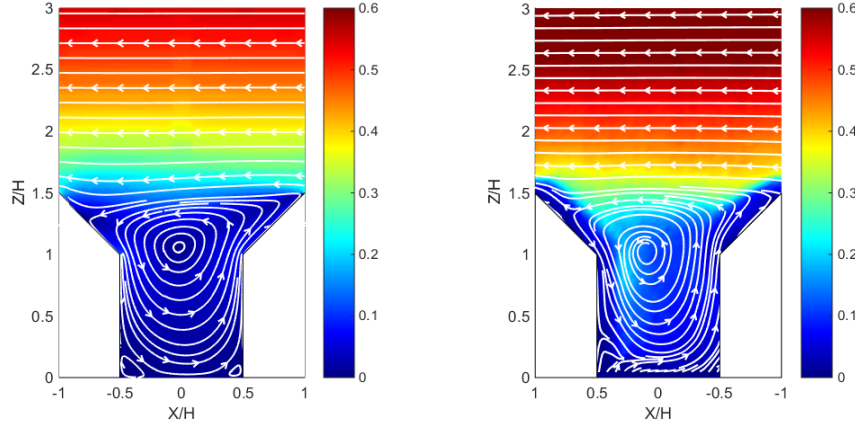


**Figure 2.** Non-dimensional mean velocity  $u/U$  fields (color map) with streamlines (white lines) from numerical (left side) and laboratory (right side) simulations, for pitched roof and  $W/H = 1$ .

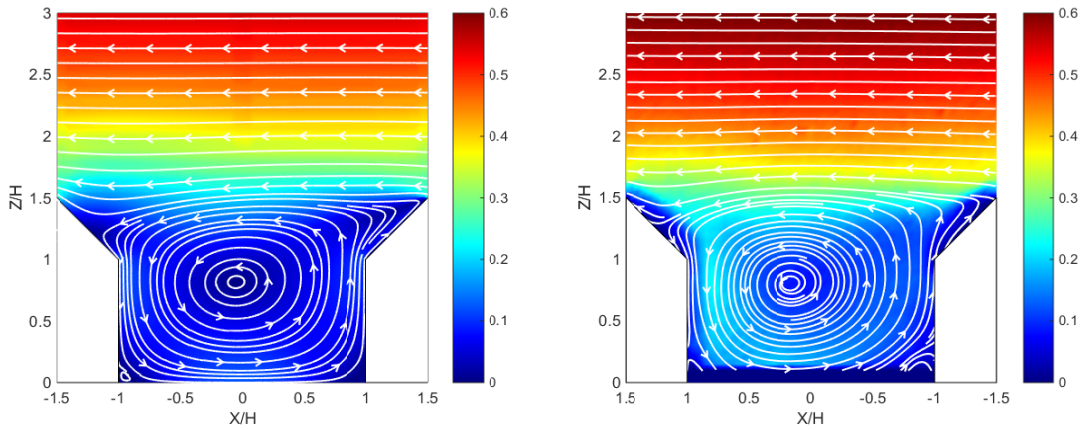


**Figure 3.** Non-dimensional mean velocity  $u/U$  fields (color map) with streamlines (white lines) from numerical (left side) and laboratory (right side) simulations, for pitched roof and  $W/H = 2$ .

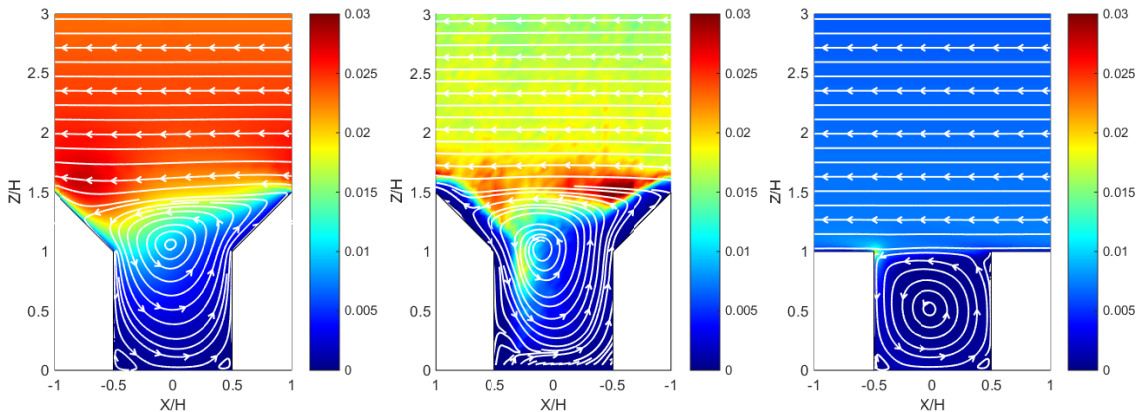


**Figure 4.** Non-dimensional mean Turbulent Kinetic Energy ( $TKE/U^2$ ) fields (color map) with streamlines (white lines) for  $W/H = 1$ : numerical (left side) and laboratory (center) simulations, for pitched roof, numerical simulations for flat roof (right side).

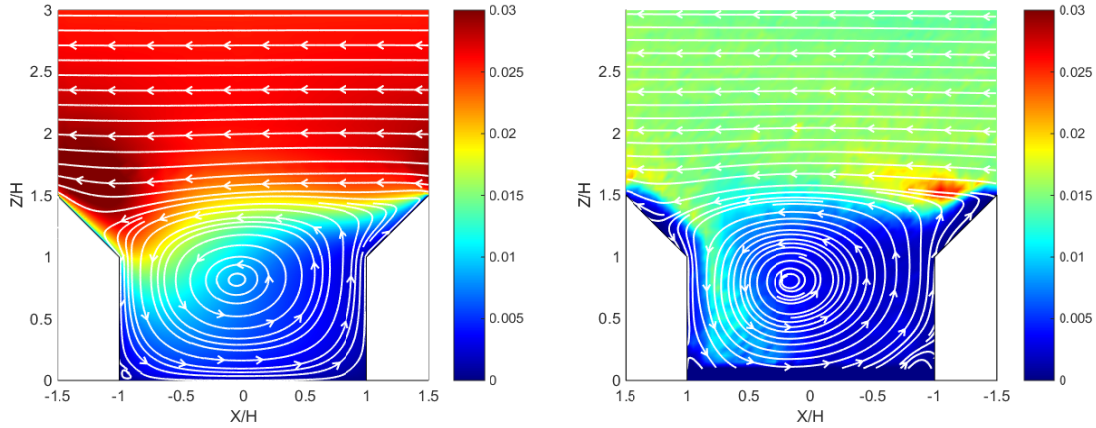


**Figure 5.** Non-dimensional mean Turbulent Kinetic Energy ( $TKE/U^2$ ) fields(color map) with streamlines (white lines) from numerical (left side) and laboratory (right side) simulations, for pitched roof and  $W/H = 2$ .

From the analysis of the  $u/U$  and  $TKE/U^2$  fields we can state that numerical code here employed is able to properly simulate the flow in urban canyons and that the pitched roof strongly modifies the flow.

The air quality and the comfort in an urban canyon depend essentially on the air exchanges between the canyon and the overlying boundary layer. We have so investigated the air-exchange rate, ACH (Ho et al., 2015), which is an integral parameter measuring the rate of air removal from a street canyon, depending on the mean and turbulent flow ( $\langle ACH \rangle$  and  $ACH'$ , respectively):

$$ACH = \langle ACH \rangle + ACH' = \int_b \langle w_+ \rangle dx + \frac{1}{2} \int_b \sqrt{\langle w'^2 \rangle} dx \quad (1)$$

where  $\langle w_+ \rangle$  is the mean upward velocity, at the roof ridge height,  $b$  is the line connecting two consecutive ridges and  $\langle w'^2 \rangle$  is estimated, under the assumption of isotropic turbulence, as:

$$\overline{w'^2} = -2\nu_t \left( \frac{\partial \bar{w}}{\partial z} \right) + \frac{2}{3} k \quad (2)$$

Figure 6 shows the ACH (non-dimensionalised by  $U \cdot b$ ) and its components versus  $W/H$ , for flat and pitched roof. Both ACH values and trends from numerical simulations are very similar to the ones measured in the laboratory. The ACH values for pitched roof are higher than the flat roof ones, showing that pitched roofs tend to enhance the natural ventilation inside the canyon

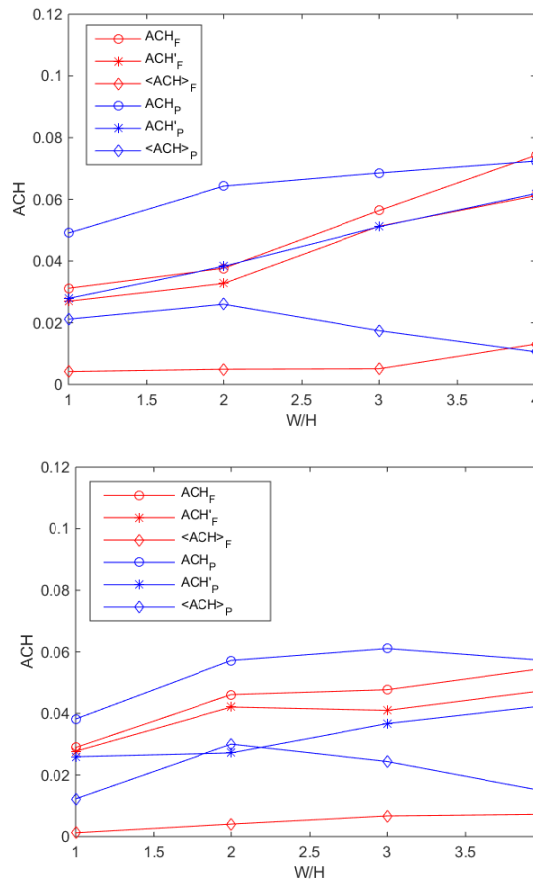


**Figure 6.** ACH versus W/H from numerical (left side) and laboratory (right side) simulations; flat roof values are plotted with red lines, pitched roof values with blue lines; total ACH is plotted with circles, mean ACH component with asterisks and turbulent ACH component with rhombi.

## CONCLUSIONS

We have investigated, both via numerical and laboratory simulations, the effect of gable roofs, on the air quality in urban canyons with different aspect ratios. The numerical code applied here has shown to be able to properly reproduce laboratory investigations. An integral parameter, the air exchange rate ACH, has been used to summarize the results: both numerical and laboratory investigations have highlighted the meaningful role of the roof pitch in enhancing turbulence, which increases the air exchange rate between the street canyon and the outer flow, thus promoting pollutant and heat dispersion. As a consequence, we can state that using a gable roof is a way to increase the air quality. The present results could have an immediate practical impact on the building design and on planning strategies, as the roof shape can be a useful tool to enhance natural ventilation and pollutant or heat dispersion, i.e. the air quality in urban areas.

## REFERENCES

- Bealduch L.A., Badas M.G., Ferrari S. and Querzoli G., 2013: Experimental Studies for the characterization of the mixing processes in negative buoyant jets. *Eur Phys J WoC*, **45**, 01012.
- Blocken B., 2015: Computational fluid dynamics for urban physics: importance, scales, possibilities, limitations and ten tips tricks toward accurate and reliable simulations. *Build Envir*, **91**, 1-27.
- Franke J., Hellsten A., Schlunzen K.H. and Carissimo B., 2011: The COST 732 Best Practice Guideline for CFD simulation of flows in the urban environment: a summary. *Int J Environ Pollut*, **44**, 419.
- Grimmond C.S.B. and Oke T.R., 1999: Aerodynamic properties of urban areas derived from analysis of surface form. *J Appl Meteor*, **38**, 1262-92.
- Hertwig D., Efthimiou G.C., Bartzis J.G. and Leitl B., 2012: CFD-RANS model validation of turbulent flow in a semi-idealized urban canopy. *J Wind Eng Ind Aerodyn*, **111**, 61-72.

- Hoydysh W.G., Griffiths R.A. and Owaga Y.A., 1974: Scale Model Study of the Dispersion of Pollution in Street Canyons, Proceedings of the 67th Annual Meeting of the Air Pollution Control Assn., Denver, Colorado (USA), June 9-13.
- Ho Y.K., Liu C.H. and Wong M.S., 2015: Preliminary study of the parameterisation of street-level ventilation in idealised two-dimensional simulations. *Build Environ*, **89**:345–55.
- Huang Y., Hu X. and Zeng N., 2009: Impact of wedge-shaped roofs on airflow and pollutant dispersion inside urban street canyons. *Build Environ.*, **44**, 2335–47.
- Launder B.E. and Spalding D.B., 1974: The numerical computation of turbulent flows. *Comput Methods Appl Mech Eng* 1974;3:269–89. doi:10.1016/0045-7825(74)90029-2.
- Patankar S. and Spalding D., 1972: A calculation procedure for heat, mass and momentum transfer in three-dimensional parabolic flows. *Int J Heat Mass Transf*, **15**, 1787–806.
- Snyder W.H., 1981: Guideline for fluid modeling of atmospheric diffusion. vol. 81. Environmental Sciences Research Laboratory, Office of Research and Development, US EPA.
- Takano Y. and Moonen P., 2013: On the influence of roof shape on flow and dispersion in an urban street canyon. *J Wind Eng Ind Aerodyn*, **123**, Part A:107–20.
- Weller H.G., Tabor G., Jasak H. and Fureby C., 1998: A tensorial approach to computational continuum mechanics using object-oriented techniques. *Comput Phys*, **12**, 620–31.
- Yassin MF., 2011: Impact of height and shape of building roof on air quality in urban street canyons. *Atmos Environ*, **45**, 5220–9.

**17th International Conference on  
Harmonisation within Atmospheric Dispersion Modelling for Regulatory Purposes  
9-12 May 2016, Budapest, Hungary**

---

**LES STUDY OF UNSTEADY FLOW PHENOMENA IN AN URBAN GEOMETRY – THE NEED  
FOR SPECIAL EVALUATION METHODS**

*Nektarios Koutsourakis<sup>1,2</sup>, John G. Bartzis<sup>1</sup>, George C. Efthimiou<sup>2</sup>, Alexandros G. Venetsanos<sup>2</sup>, Ilias C. Tolias<sup>2,3</sup>, Nicolas C. Markatos<sup>3,4</sup>, Denise Hertwig<sup>5</sup> and Bernd Leitl<sup>6</sup>*

<sup>1</sup>Department of Mechanical Engineering, University of Western Macedonia, Kozani, Greece

<sup>2</sup>Environmental Research Laboratory, NCSR “Demokritos”, Aghia Paraskevi, Greece

<sup>3</sup>School of Chemical Engineering, National Technical University of Athens, Athens, Greece

<sup>4</sup>Department of Chemical Engineering, Texas A&M University, Doha, Qatar

<sup>5</sup>Department of Meteorology, University of Reading, Reading, United Kingdom

<sup>6</sup>Meteorological Institute, KlimaCampus, University of Hamburg, Hamburg, Germany

**Abstract:** Large Eddy Simulation (LES) is performed in the semi-idealized “Michel-Stadt” urban geometry. LES results are successfully compared with detailed experimental data from the CEDVAL-LES wind-tunnel database. Examination of the time-evolution of flow and vorticity fields reveals interesting turbulent phenomena like gusts, unsteady vortices, non-Gaussian velocity distributions and the creation of coherent structures. This study contributes to the need of investigating ways of analyzing the LES results.

**Key words:** CFD, Large Eddy Simulation, validation, turbulent urban flow, coherent structures, wind tunnel, ADREA

## INTRODUCTION

Computational Fluid Dynamics (CFD) is one of the most valuable and versatile approaches for urban pollution and air quality studies. The LES methodology, even if it is currently not widely used for regulatory purposes due to its high computational cost, is expected to play a major role in atmospheric dispersion modelling. Compared to the more widespread Reynolds Averaged Navier-Stokes (RANS) approach, LES partially resolves turbulence and can provide concurrent time series of the desired variables at all points of the flow field and not just average values like RANS. With LES we can examine the unsteady dynamics of the flow and contribute to a deeper understanding of driving physical mechanisms and of fundamental turbulent flow regimes. The amount of simulation data from an LES can be huge and needs additional and different methods to be evaluated and analyzed.

A further issue is the comparison of LES with experimental data. The availability of time series makes the calculation of statistics, high order moments and correlations possible, providing additional information for evaluation (Hertwig, 2013). Thus there is a need for specifically designed and well documented experimental datasets that can significantly help in validating and improving LES models, like those of the CEDVAL-LES wind-tunnel database of the University of Hamburg. In the current study, the semi-idealized city “Michel-Stadt” was chosen, which mimics typical central-European cities at a scale of 1:225 (Figure 1). The geometry is composed of 60 differently shaped building blocks with courtyards and various roof heights of 15, 18 and 24 m, covering an area of 1320 m x 830 m at full scale. The atmospheric boundary layer of the approach flow is characterised by a roughness length  $z_0 = 1.53$  m and a power law profile with exponent  $\alpha = 0.27$  for a reference velocity of 6.1 m/s at 100 m height. Thousands of Laser Doppler Anemometry (LDA) measurements are available at 40 vertical profiles and at 5 horizontal levels in the central part of the city (at heights of 2, 9, 18, 27 and 30 m).

## METHODOLOGY

The LES model of the ADREA-HF code is used for the simulations. The equations solved and an evaluation of the implemented methodology are discussed in Koutsourakis et al. (2010, 2012).

A domain of 1670 m x 900 m x 147 m in x, y, z directions is used, discretized with a mesh of 419 x 238 x 30 cells. The resolution of 3 x 3 x 3 meters that is achieved in most parts of the city is not very high, but is considered adequate for performing urban LES (Tominaga et al., 2008). Rough wall functions are used with a roughness length of 0.0625 m inside the city (for ground and buildings) and 1.5 m upwind (ground). The domain is laterally bounded by smooth walls. At the inlet and top a Langevin-type boundary condition for the velocity  $U$  is applied, fixing  $U_{mean}$ , variance  $\sigma_U$  and autocorrelation time scale  $T_U$  to the experimental values. The Smagorinsky model with constant  $C_s = 0.1$  and a van Driest-type damping near the wall is used for the sub-grid scale modelling. The bounded central differences numerical scheme is chosen for the discretization of the convective terms and for the time advancement the second-order accurate Crank-Nicolson method is used. The time step is limited to 0.2 s. A total of 10000 s is simulated, of which the first 900 s are not considered for the statistical analysis. 8844 “sensors” that provide time-series are placed at various locations. The current simulation is significantly improved compared to that of Koutsourakis et al. (2012), having a finer grid and using a different numerical scheme. The computational time is about 39 days on a quad-core personal computer. More information about the simulations can be found in Koutsourakis (2014).

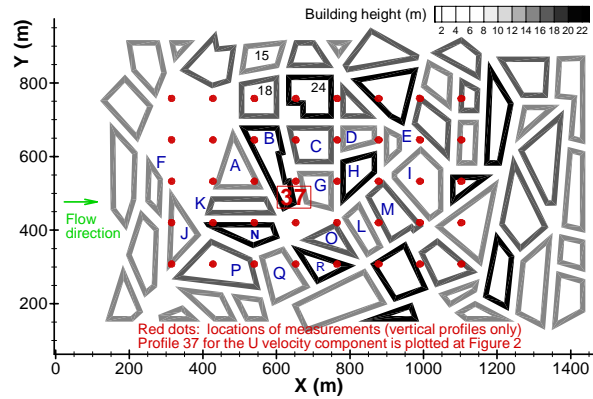


Figure 11. The Michel-Stadt city with building heights

## RESULTS AND DISCUSSION

### Mean flow comparison with experimental data

The scatter plot of experimental vs. simulated results for the mean velocity component  $U_{mean}$  at all 2158 measurement locations and an indicative vertical  $U_{mean}$  profile are presented in Figure 2.

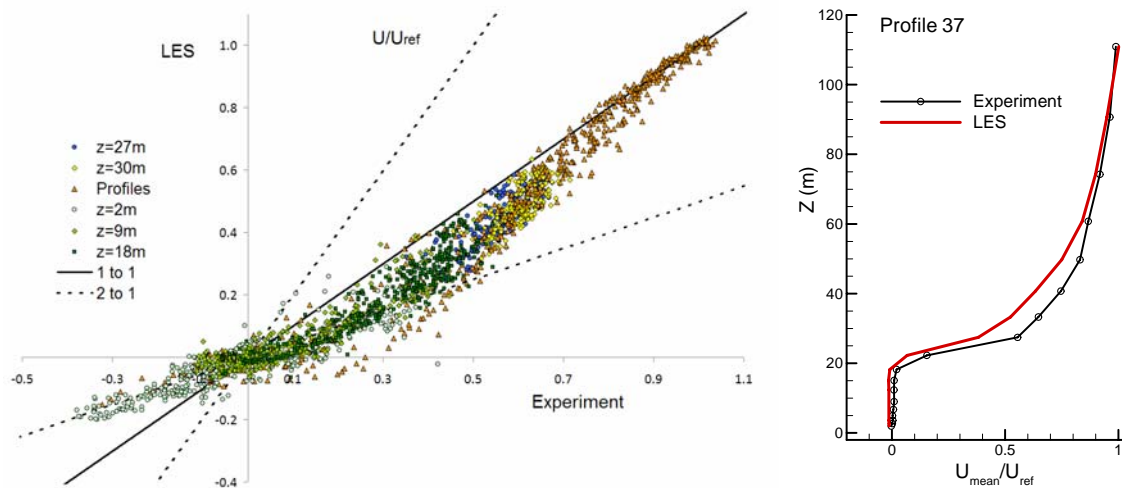


Figure 2. Left: Comparison of experimental and LES values of mean velocity  $U_{mean}$  at all measurement points. Right: Vertical velocity profiles of experiment and LES at point 37, between buildings B and G (Figure 1)

Qualitatively, the average flow results are good, since most of the points fall well within the dotted lines that indicate a 1-to-2 and 2-to-1 relation and the calculated profiles follow closely the experimental ones. An easily observed underestimation of the mean velocity at medium heights is due to the much higher underestimation of the stresses at those heights. Another issue is the lower velocities of LES very close to the ground that can be seen at the scatter plot. It is noted that preliminary results with a finer grid show significant improvement. As a first attempt to quantify that, statistical indexes (validation metrics) can be

used. Table 1 presents FAC2 and HR as defined in Hertwig et al. (2012) for the vertical profiles (that represent the overall quality of the LES) and two horizontal planes at 2 m and 30 m for 3 meshes. Even though the statistical indexes can be misleading and should not be interpreted without inspection of the flow field, the tendency of improvement is unambiguous as the grids get denser.

**Table 1.** Validation metrics for  $U_{mean}/U_{ref}$  &  $V_{mean}/U_{ref}$  for 3 meshes: coarse of 0.74 million cells (minimum horizontal resolution of 6.6 meters)/ **current** (3 million cells, 3 m resolution)/ finer (7 million cells, 2 m resolution)

Mesh	\Variable:	Vertical profiles		$z = 2 \text{ m}$		$z = 30 \text{ m}$	
		$U_{mean}/U_{ref}$	$V_{mean}/U_{ref}$	$U_{mean}/U_{ref}$	$V_{mean}/U_{ref}$	$U_{mean}/U_{ref}$	$V_{mean}/U_{ref}$
Coarse (FAC2 - HR)		0.74 - 0.61	0.63 - 0.62	0.16 - 0.08	0.31 - 0.21	1.00 - 0.47	0.71 - 0.75
<b>Current (FAC2 - HR)</b>		0.77 - 0.66	0.66 - 0.66	0.44 - 0.16	0.45 - 0.25	1.00 - 0.75	0.79 - 0.85
Finer (FAC2 - HR)		0.85 - 0.71	0.74 - 0.74	0.62 - 0.30	0.54 - 0.31	1.00 - 0.96	0.87 - 0.91

### Unsteady turbulent phenomena and coherent structures

With LES successive instantaneous flow snapshots can be studied, revealing turbulent features known from the experiments, like unsteady flow characteristics and non-Gaussian velocity distributions. Figure 3 presents two snapshots of the horizontal velocity vectors at the sensors' positions in the  $z = 2 \text{ m}$  plane.

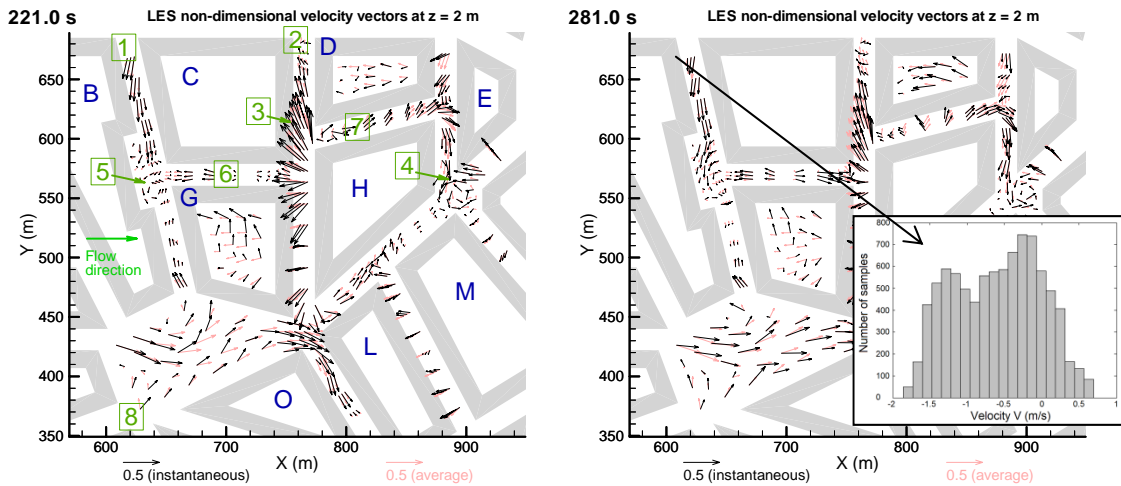


**Figure 3.** Two frames of a 9000 s video showing the LES instantaneous velocity vectors at  $z = 2 \text{ m}$ . In the inset the probability density function of the  $V$  velocity at point 1 is plotted, which shows bimodal behaviour

The observation of the video can lead to numerous remarks. At point 1 a recirculation with unsteady limit exists as the flow turns into the canyon passing around the corner of building B. The leftmost vector at point 1 is either inside the recirculation, having a very low velocity, or outside of it, having a significantly higher velocity. The velocity distribution of the  $V$  component can be seen in the inset of Figure 3 and is bimodal. The two physically possible flow states are represented from the peaks, while the mean value does not really have a physical meaning. In this case neither a RANS simulation nor the use of validation metrics like FAC2 and HR are rigidly correct. With the use of LES, other ways of comparison should also be chosen, like the instantaneous flow events or the distributions of the variables. The ability of LES to calculate non-Gaussian behaviour is crucial for the correct prediction of the flow, as mentioned in a previous study (Hertwig et al., 2012).

At points 2 and 3 gusts can be frequently observed. At point 4 a persistent vortex that slightly shifts at high frequency around a central position of the crossroads is present in both the CFD and the experiment. Around this vortex there are (both in the wind tunnel and the LES) a lot of points featuring skewed or bimodal behaviour for the velocity distributions. The occasional vortex at point 5, however, is very unstable and much weaker. Around point 6 an oscillatory moving end of the recirculation behind the building B exists. Even if the general flow characteristics are captured by the LES in this case, both FAC2 and HR in this area are very low, most probably due to the slightly different position of the recirculation end compared to the experiment. At point 7 LES also predicts a recirculation (easily seen in 3-D plots of

stream traces), which could not be identified in the experiment in this case. Despite this, FAC2 for the  $V$  component is very high in this area. In the cases of points 6 and 7 the validation metrics are misleading. Very high frequency changes of flow direction and a strong velocity variability can be noticed in the yards of buildings D and G in both the LES and the experiment. At point 8, the *average* vectors of LES and experiment have significantly different directions. This could lead to the conclusion that the simulation completely failed here. However, studying the instantaneous flow fields reveals that occasionally the direction changes to that of the experiment. Unfortunately no experimental values exist below that point, in order to help in investigating reasons for the different behaviour. The analysis made clear that more measurement points around the main-interest area would have been helpful in order to have a better understanding of the flow features. It is obvious that a cooperation of experimental and LES research teams both before and after the experiments is of benefit for all parties.

The study of coherent structures that can be identified from the LES is very revealing when it comes to a more fundamental understanding of flow dynamics. In Figure 4 the  $0.33 \text{ s}^{-1}$  vorticity isosurfaces are presented at the central part of the city, colour-coded by the z-axis height. Instantaneous low-momentum (of negative velocity fluctuation  $u'$ ) areas are also plotted as black isosurfaces (Bk) and high-momentum as white (W). We can determine for example structures like in-canyon cylindrical vortices (cv), vorticity sheets (vs) that usually shed-off the building roofs, worm-like vortices (wv) that are usually one of the two legs of hairpin vortices (V), which in turn correlate with low-momentum areas.

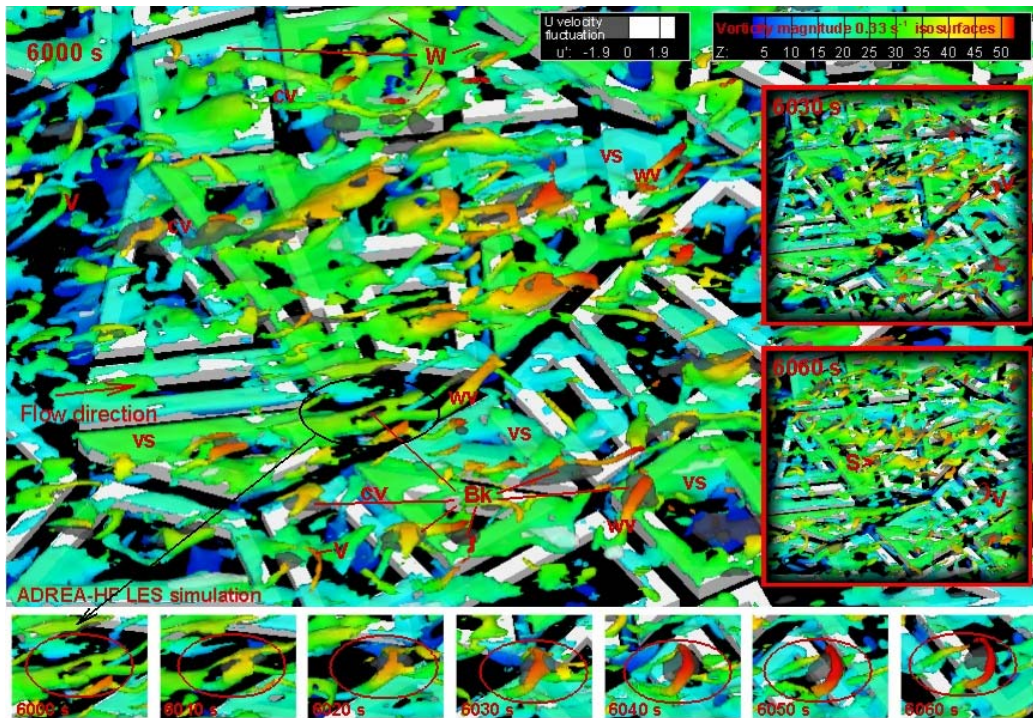


**Figure 4.** Snapshots of vorticity and velocity-fluctuation isosurfaces revealing coherent structures.

By studying the time-evolution of the structures (top part of Figure 4 presents the same area at 3 different times), conclusions about their dynamic behaviour can be drawn. As an example, the bottom part of Figure 4 shows the creation of a hairpin vortex: At first, the vorticity sheet is perforated by an upward-moving low-momentum fluid area which occurred just below it (6000 s). This creates two longitudinal vortices at the sides of the hole (6000-6010 s). The vortices are transported by the flow in parallel to their mutual lifting and joining (6020-6030 s). This leads to their characteristic hairpin shape (6040-6060 s). By studying the relevant video, many such events can be identified. At the video the creation of a hairpin vortex from another one can also be seen, when the low-momentum area below it elongates and breaks, like in point S. Similar events are reported in the literature (e.g. Adrian, 2007). It is known that low-momentum areas have a correlation with pollutant removal events (Coceal et al., 2007). High-momentum (white) isosurfaces are seen to correlate with vorticity sheets and also with the hairpins.

Ways to account for the time-dependent nature of LES in validation studies are discussed by Hertwig (2013). The application of more sophisticated measures of simulation quality not only helps to understand the physical accuracy of the simulation, but can also be of guidance to disentangle errors and sources of uncertainty in the modelling. Apart from comparisons based on higher order statistics and frequency distributions, eddy statistics (e.g. in terms of auto- or two-point correlations, integral length scales or spectral properties of the flow) and conditional averaging should also be consulted to gain further insight into the simulation quality. Depending on the spatial-temporal resolution of the reference experiment, other advanced analysis methods like proper orthogonal decomposition, stochastic estimation or wavelet transform methods can be used comparatively as well (e.g. Hertwig et al., 2011; Kellnerova et al., 2011; Hertwig, 2013). A close collaboration between LES and experimental communities, will help in that objective.

## CONCLUSIONS

LES has a strong potential and can not only provide a general picture of fluid motion in complex geometries, but also supply information about unsteady flow dynamics. With appropriate post-processing, like the time-dependent flow visualizations presented here, LES contributes to a more fundamental understanding of turbulent flow phenomena. This work also makes clear that there is a need to identify and standardize methods to analyze LES results and to compare them with reference data, since classic ways can be misleading. Such methods could include processing the time-series, observing the time-evolution of vectors or isosurfaces and investigating the position, strength and frequency of particular flow events. This study also reveals the need of parallel work of experimentalists and modellers, in both the design of the experiments and the interpretation of the model results. The hope is that in the future, along with the modelling guidelines and the LES-oriented post-processing practices, more sophisticated quality assurance methodologies particularly suitable for turbulence-resolving simulations will emerge.

## ACKNOWLEDGEMENTS

This work was supported by the Greek Scholarships Foundation, by the Municipality of Aghia Varvara Attikis of Greece and by IKYDA, in the framework of the “MODEX” project.

## REFERENCES

- Adrian, R.J., 2007: Hairpin vortex organization in wall turbulence. *Phys. Fluids*, **19**, 041301.
- Coccal, O., A. Dobre and T.G. Thomas, 2007: Unsteady dynamics and organized structures from DNS over an idealized building canopy. *Int. J. Climatol.*, **27**, 1943-1953.
- Hertwig, D., 2013: On aspects of large-eddy simulation validation for near-surface atmospheric flows. PhD thesis, University of Hamburg, Germany.
- Hertwig, D., B. Leidl and M. Schatzmann, 2011: Organized turbulent structures—Link between experimental data and LES. *J. Wind Eng. Ind. Aerodyn.*, **99**, 296-307.
- Hertwig, D., G.C. Efthimiou, J.G. Bartzis and B. Leidl, 2012: CFD-RANS model validation of turbulent flow in a semi-idealized urban canopy. *J. Wind Eng. Ind. Aerodyn.*, **111**, 61-72.
- Kellnerova, R., L. Kukacka, K. Jurcakova, V. Uruba and Z. Janour, 2011: Comparison of wavelet analysis with velocity derivatives for detection of shear layer and vortices inside a turbulent boundary layer. *J. Phys.: Conf. Series*, **318**, 062012.
- Koutsourakis, N., 2014: Turbulent flow and pollutant dispersion in the urban environment. PhD thesis, University of Western Macedonia, Kozani, Greece.
- Koutsourakis, N., A.G. Venetsanos, J.G. Bartzis and I.C. Talias, 2010: Presentation of new LES capability of ADREA-HF CFD code. Proc. 13th Int. Conf. on Harmonisation within Atmos. Disper. Model. for Regul. Purposes, 1-4 June 2010, Paris, France, 662-666.
- Koutsourakis, N., D. Hertwig, G.C. Efthimiou, A.G. Venetsanos, J.G. Bartzis and B. Leidl, 2012: Evaluation of the ADREA-HF LES code for urban air quality assessment, using the CEDVAL-LES wind tunnel database. Proc. 8th Int. Conf. on Air Qual. – Sci. and Appl., 19-23 March 2012, Athens, Greece, paper No. 593.
- Tominaga, Y., A. Mochida, R. Yoshie, H. Kataoka, T. Nozu, M. Yoshikawa and T. Shirasawa, 2008: AIJ guidelines for practical applications of CFD to pedestrian wind environment around buildings. *J. Wind Eng. Ind. Aerodyn.*, **96**, 1749-1761.

**17th International Conference on  
Harmonisation within Atmospheric Dispersion Modelling for Regulatory Purposes  
9-12 May 2016, Budapest, Hungary**

---

**STREET-LEVEL MODELLING OF THE EFFECT OF CLIMATE ADAPTATION MEASURES  
ON AIR QUALITY**

*Jaroslav Resler<sup>1,2,3</sup>, Pavel Krč<sup>1,2,3</sup>, Michal Belda<sup>1,2,3</sup>, Pavel Juruš<sup>1,2</sup>, Kryštof Eben<sup>1,2</sup>, Nina Benešová<sup>1,4</sup>,  
Daša Srbová<sup>1,4</sup>, Přemysl Derbek<sup>1</sup>, Pavel Hrubeš<sup>1</sup>, Jan Lopata<sup>1,4</sup>, Ondřej Vlček<sup>1,4</sup>, Jana Blumelová<sup>1</sup>,  
Mária Kazmuková<sup>5</sup>, Petra Bauerová<sup>1,4</sup>*

<sup>1</sup>Faculty of Transportation Sciences, Czech Technical University in Prague, Czech Republic

<sup>2</sup>Institute of Computer Science, Czech Academy of Sciences, Czech Republic

<sup>3</sup>Czech Institute of Informatics, Robotics and Cybernetics, Czech Technical University in Prague,  
Czech Republic

<sup>4</sup>Czech Hydrometeorological Institute, Prague, Czech Republic

<sup>5</sup>Prague Institute for Planning and Development, Czech Republic

**Abstract:** Cities play an important role regarding potential climate change impacts. Urban areas are often vulnerable and poorly prepared to respond to climate change impacts, such as heat waves. Within UrbanAdapt project we aim to perform high-resolution street-level modelling to evaluate different adaptation measures which are orientated to lower the temperature in the streets during hot summer days. The heterogeneity of urbanized land surface leads to a need for a very fine resolution when modelling air flows and temperature near to the surface. We have chosen the atmospheric model PALM as a tool for our simulations. PALM is a LES model which includes parametrizations of many atmospheric processes (e.g. land surface, plant canopy, solar radiation and convective processes) and also enables to involve pollutant dispersion. On the other hand, the parametrization of building surface energy balance is not included in the model. To account for the realistic implementation of urban canopy processes in complex urban geometry we enhanced PALM model including some of the most important urban canopy mechanisms. In order to evaluate the new module, we performed a field experiment, during which temperature of building facades and road surface on Prague crossroad were measured with infrared camera, during a summer heat wave episode. Newly developed module will be used to estimate the effects of different adaptation measures (planting tree alleys, changing wall paint colors), on air quality and thermal comfort of city inhabitants.

**Key words:** *Large Eddy Simulation, micro-scale modelling, climate change adaptation measures*

## INTRODUCTION

Highly populated cities can be significantly affected by the climate change impacts. We expect that as a result of climate change, extreme events such as heat waves, droughts or floods will become more frequent. Nevertheless urban areas are often vulnerable and poorly prepared to respond to such episodes – particularly the extreme temperatures waves are even more pronounced in cities due to the effect of urban heat island (UHI). The project UrbanAdapt aims to start the process of preparation of cities adaptation strategies, develop adaptation scenarios and test their effects and benefits in the three pilot cities in the Czech Republic. The goal of our group in scope of the UrbanAdapt project is to perform modelling on street-level scale, assess suitable adaptation measures and evaluate their impact on thermal comfort of inhabitants and air pollution.

Urban surfaces pose a serious challenge for weather and climate modelling with the current generation of numerical models. Several approaches can be applied from purely statistical to highly complex dynamical models, each with its own advantages and disadvantages (eg. Mirzaei and Haghghat, 2010). Computational fluid dynamics (CFD) models are numerical models computing fluid flows and the interaction with surfaces. For larger scale applications their subclass, Large Eddy Simulations (LES) models, are usually applied. These use an explicit solution of the dynamic equations limited to a certain resolution combined with a parameterization of sub-scale processes. Based on preliminary testing, we have chosen LES model PALM (Raasch and Schröter, 2001; Maronga et al., 2015) for our application.

## METHODOLOGY

### PALM model

Developed primarily at Leibniz University in Hannover in cooperation with other institutes, the PALM model is a LES model focused on atmospheric modelling. Besides the general LES routines, it incorporates several meteorological modules dealing with processes such as radiation, atmosphere-land surface interaction, humidity and clouds or plant canopy. The model can be used in parallel mode thus allowing it to be run on clusters and supercomputers scaling up to tens of thousands of cores. One of the limitations of the current PALM model for the simulations of urban canopy processes is the fact that in the radiation model, land-surface scheme and plant canopy model, only flat topography is implemented. These modules are however crucial for our application and it was necessary to extend the model with urban surface model (USM) to account for complex urban geometry. The module is designed from scratch but it tries to conform to PALM design and utilizes some approaches of the original PALM land surface model. The calculation of the aerodynamic resistance for walls has been inspired by the approach used in the TUF-3D model (Krayenhoff and Voogt, 2007).

### Urban surface model

The urban surface model extension of the PALM model consists of these submodules:

1. Physical properties of real urban surfaces (ground, walls and roofs) as well as virtual surfaces (top and lateral boundaries of the urban layer). The crucial challenge of this part is an effective and scalable design of the computation and data storage parallelization.
2. Calculation of *shape view factors* (SVF) and *plant canopy sink factors* (PSF). SVFs define the portion of reflected and radiated energy from one surface received by other surface. PSFs define the portion of energy absorbed by vegetation present in the gridbox.
3. Radiation model of urban surfaces. At the top boundary, USM receives radiation from the standard PALM radiation module and adds a description of radiation processes in the urban canopy layer where multiple reflections are considered.
4. Absorption of radiation by vegetation (trees and shrubs). The portion of radiative energy absorbed by vegetation in a gridbox is calculated. This produces a heat flux from the vegetation.
5. Energy balance of the *surface skin layer*. Energy balance equation is expressed in the standard form

$$C_0 \frac{dT_0}{dt} = R_n - H - G , \quad (1)$$

where  $C_0$  is the heat capacity of the surface skin layer,  $T_0$  is the temperature at surface,  $R_n$  is the net radiation,  $H$  is the heat transfer between the surface layer and the air and  $G$  is the heat transfer between surface and the material of soil, wall or roof.

6. Heat transfer between surface and material. The transfer is calculated from temperature gradient and heat conductivity between land surface and air.
7. Heat transfer between surface layer and air. Heat transfer  $H$  is calculated based on aerodynamic resistance coefficient. This coefficient is parameterized according to Krayenhoff and Voogt (2007) for vertical surfaces (walls) while for horizontal surfaces it follows the approach used in the original LSM module of the PALM model.
8. Anthropogenic heat from transportation is modelled with real spatial distribution and daily profile of car density. The heat is incorporated into the surface heat flow.
9. Boundary conditions for the atmospheric component are cyclic at the lateral boundary. Large-scale wind, pressure and temperature are prescribed in configuration for idealized simulations while they are derived from simulations provided by the meso-scale model (WRF) for real case simulations.

### TEST CASE

The implementation of urban surface module was tested both in idealized and real test cases. For real test case we chose an intersection of streets in Prague, Dělnická and Komunardů (Figure 1). For this purpose we prepared an extensive database of geospatial data and surface parameters. This database includes

building heights to describe the domain topography, different surface and material parameters and also the position, height and leaf area density of existing trees.



**Figure 1.** Test case domain. Left: area of interest - intersection of streets Dělnická and Komunardů in Prague (source: IPR Prague). Right: 3D view of the modelled area (source: Google Earth).

The test case domain covered the horizontal area of c. 375 m x 225 m with vertical extent of 187 m; spatial resolution was 2 m x 2 m x 2 m. The time span of our simulation was 24 hours.

To collect data for the verification of our urban surface module we carried out an onsite measurement campaign where we measured the surface temperatures of walls and ground on the Dělnická and Komunardů intersection using the infrared (IR) camera. This measurements took place from July 2, 2015 15h CET to July 3, 2015 18h CET during the hot sunny day (maximum air temperatures were c. 33 °C). Example images taken during this campaign are in Figure 2.



**Figure 2.** Onsite measurement campaign. Left: east facing wall in visible spectrum with reference points. Right: east facing wall in infrared spectrum (8:11 CET).

We compared the results from the measurements to the model results. Figure 3 shows the comparison for the east facing wall (the same as in Figure 2). The agreement is good - the model is able to predict the maximum and minimum temperatures as well as time behaviour reasonably well.

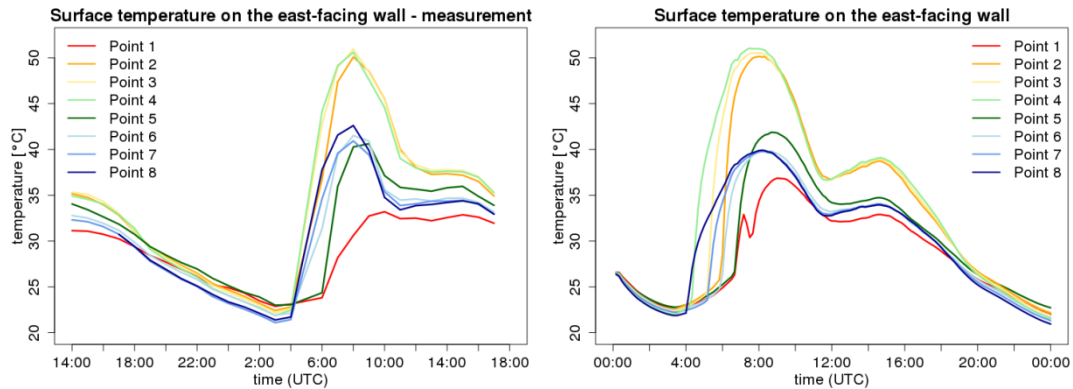


**Figure 3.** The comparison of the surface temperatures of east facing wall from measurement (left) and model (right). For coloring scheme of reference points see Figure 2.

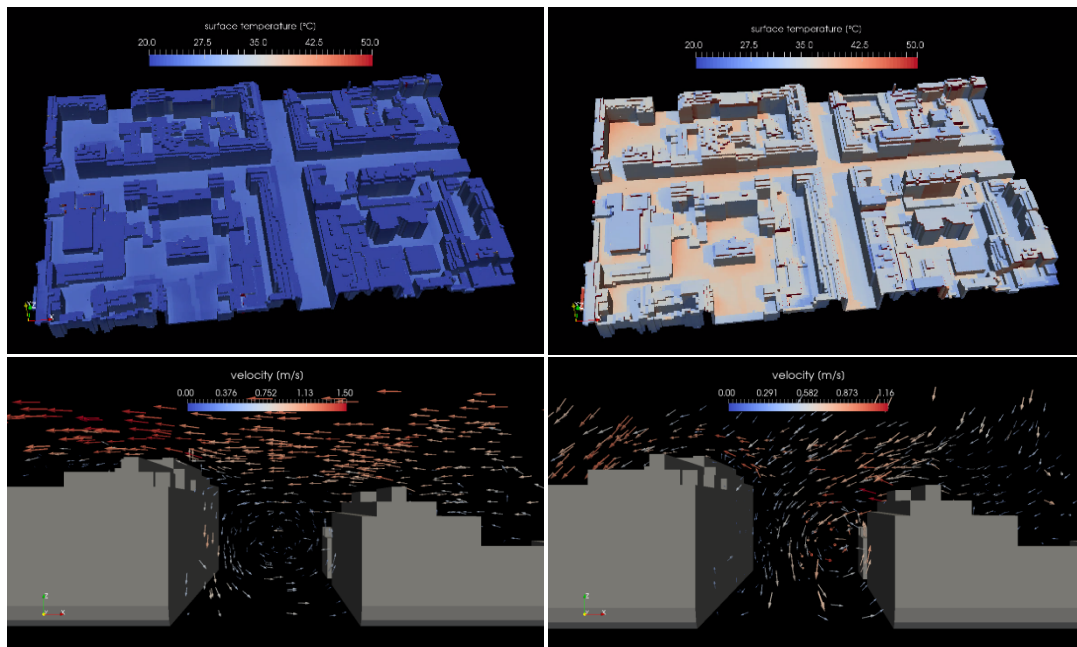


**Figure 4.** The comparison of surface temperatures (upper row) and flow field (bottom row) in two time instants - 23:00 CET (left column) and 7:30 CET (right column).

Figure 4 shows the dependency of the flow in the street on sun radiation. We chose two time instants - in the evening when the temperature gradients of walls are only mild contrary to the situation at the morning where the east wall is irradiated by sun. In the evening we can observe typical street flow pattern with one eddy (bottom left). On the other hand when the east wall heats up it influences the flow pattern in the street and two independent eddies are created. This is important observation as it shows the importance of correct implementation of urban surfaces as they can considerably influence the flow character and thus have impact on air pollution dispersion in the street.

## CONCLUSIONS

We have developed a new urban surface model and incorporated it into LES model PALM. The model has been tested against IR camera measurements with reasonable agreement. Our current work covers the

evaluation of different mitigation scenarios and estimation of their impact on thermal comfort of the inhabitants by means of mean radiant temperature. The scenarios include changes of urban surfaces (material of walls, replacement of ground asphalt with pavement), different scenarios of tree alleys (different tree species and locations) and other urbanistic changes (development plans). Further we will perform air quality simulations to assess the dispersion from local traffic sources under the conditions of assumed scenarios.

#### **ACKNOWLEDGEMENT**

This work was supported by the Iceland, Liechtenstein and Norway grants under the project name UrbanAdapt (EHP-CZ02-0V-I-036-2015).

#### **REFERENCES**

- Krayenhoff, E. S. and J. A. Voogt, 2007: A microscale three-dimensional urban energy balance model for studying surface temperatures. *Boundary-Layer Meteorol*, **123**, 433-461.
- Maronga, B. et al., 2015: The Parallelized Large-Eddy Simulation Model (PALM) version 4.0 for atmospheric and oceanic flows: model formulation, recent developments, and future perspectives. *Geosci. Model Dev.*, **8**, 2515-2551.
- Mirzaei, P. A. and F. Haghighat, 2010: Approaches to study Urban Heat Island – Abilities and limitations. *Build Environ*, **45**, 2192-2201.
- Raasch, S. and M. Schröter, 2001: PALM – A large-eddy simulation model performing on massively parallel computers. *Meteorol. Z.*, **10**(5), 363-372.

**17th International Conference on  
Harmonisation within Atmospheric Dispersion Modelling for Regulatory Purposes  
9-12 May 2016, Budapest, Hungary**

---

**AIR POLLUTION MODELING IN URBAN ENVIRONMENT USING WRF-CHEM MODEL**

*Attila Kovács<sup>1</sup>, Róbert Mészáros<sup>1</sup>, Ádám Leelőssy<sup>1</sup>, István Lagzi<sup>2</sup>*

<sup>1</sup>Eötvös Loránd University, Department of Meteorology, Hungary

<sup>2</sup>Budapest University of Technology and Economics, Department of Physics, Hungary

**Abstract:** Our main goal is to simulate the transport and spatial distribution of atmospheric pollutants in an urban environment in order to make air quality forecasts for the city of Budapest. For this task, we use the WRF-ARW meteorological model (*The Weather Research & Forecasting Model - Advanced Research WRF*, v3.6, 2014.) coupled with a chemistry transport model (WRF-Chem, v3.6, 2014.). The coupling between the meteorology and chemistry is online, which means that the model simulates the transport and chemical transformation of trace gases and aerosols simultaneously with the meteorology in each model time step (*Grell et al.*, 2005). This allows the model system to take account of chemistry feedbacks on the meteorology (e.g., direct and indirect effects of aerosols). Our simulations run on a triple-nested domain with the 30 km horizontal resolution mother domain over Central Europe. The first nested domain with a horizontal resolution of 10 km over Hungary, and the finest resolution domain representing the area of the city of Budapest with 2 km grid spacing. The WRF-Chem model is capable of simulating the emission and transport of gases and aerosols from anthropogenic and biogenic sources depending on the choice of the chemical mechanism package. The steps of the model adaptation, a sensitivity analysis of the model, and some case studies are presented in this study.

**Key words:** *WRF-Chem, air quality modelling, numerical weather forecast*

## INTRODUCTION

Air quality of cities depends on various factors such as meteorological conditions, types and rates of emission sources. However, the most affecting factor is the weather situation. For example, in case of weak winds, the emitted air pollutants can usually accumulate in the boundary layer, so their harmful effects on human health can be significant. In order to predict the air quality, one approach is to use a numerical weather forecast model coupled to a chemistry model. The WRF (*Weather Research and Forecasting*) model uses the meteorological output fields of a global weather forecast model (GFS, *Global Forecast System*) to downscale them to mesoscale meteorological fields. We used the WRF-Chem model to simulation the transport, emissions, chemical reactions, turbulent diffusion and deposition of air pollutants (*Grell et al.*, 2012).

Our main goal is to provide air quality forecasts for Budapest with the WRF-Chem model. The coupling is parallel, which means that not only the effect of meteorology on chemistry is taken into account, but also the direct (e.g., scattering of radiation) and indirect (e.g., becoming cloud condensation nuclei) effects of aerosols on meteorology. The WRF-Chem model is widely used for estimating air quality and making weather forecasts, volcanic ash transport modelling and other research projects, with the developer community providing new physical and chemical options or revising old ones for the model (*Baklanov et al.*, 2014). In the past decade, many studies have been provided on simulating concentration changes of air pollutants. Wang et al. (2010) developed fine temporal and vertical resolution anthropogenic emission distributions for the TRACE-P database and studied their influence on Eastern Asian air quality forecasts for July, 2001 with the WRF-Chem model. Tuccella et al. (2012) integrated the anthropogenic emission database from the European Monitoring and Evaluation Programme (EMEP) into the WRF's pre-processing system (WPS). In their study they modelled transport and chemical transformation of gases and aerosols over Europe for 2007. Obtained model data were validated with the surface measurements.

## METHOD

The WRF-Chem model requires meteorological, static terrain and emission input data. For the meteorological data, we used 3 hour temporal resolution output data from the GFS model ( $0.5^\circ \times 0.5^\circ$  horizontal resolution prior to 2015, and  $0.25^\circ \times 0.25^\circ$  horizontal resolution after 2015). The static terrain data was added to the WRF model. The simulations centred on the transport of Saharan dust used the fraction of erodible surface for each grid cell as emission data. The hourly resolution dust concentration fields from the model output were compared against surface measurement data from the Hungarian Air Quality Network, to validate the arrival passing time of the dust over for big cities of Hungary and districts of Budapest.

## CASE STUDIES

We studied the transport of Saharan desert dust through Europe for the 21<sup>th</sup> of June, 2012 on three nested domains: the mother domain representing North Africa and Europe with 30 km horizontal grid spacing, the first nested domain corresponding to Central Europe with 10 km horizontal grid resolution and the second nested domain representing Budapest with 2 km horizontal grid spacing. The simulations were started from 14 and 7 days prior the mentioned date, where we could study the amount of dust depending on the time allowed for transport processes. The modelled dust concentration was compared against measurement data at Gilice square monitoring station, Budapest.

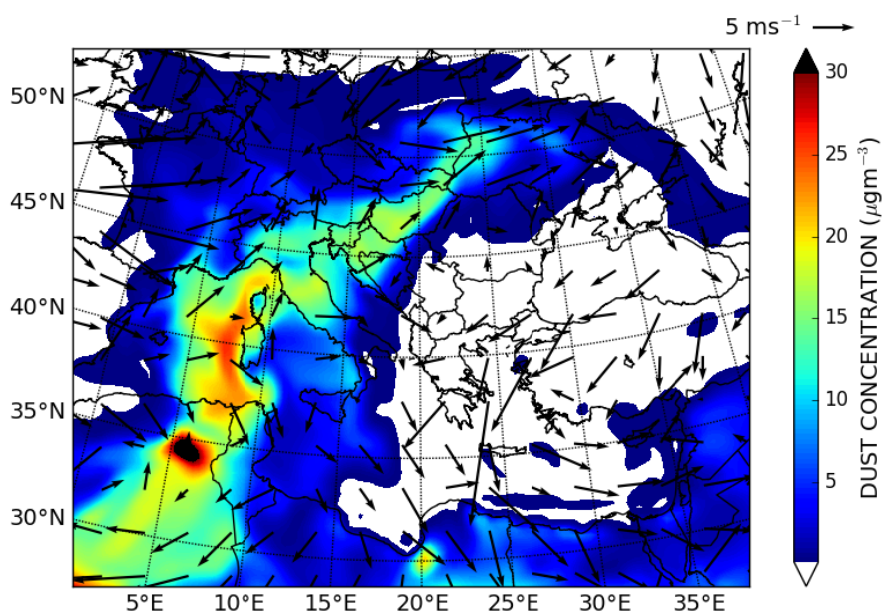


**Figure 1.** Dust ( $2.4 \mu\text{m}$  effective radius) concentration ( $\mu\text{g m}^{-3}$ ) and 10 m wind field ( $\text{m s}^{-1}$ ) on the 21<sup>th</sup> of June, 2012 at 12 UTC for the mother domain.

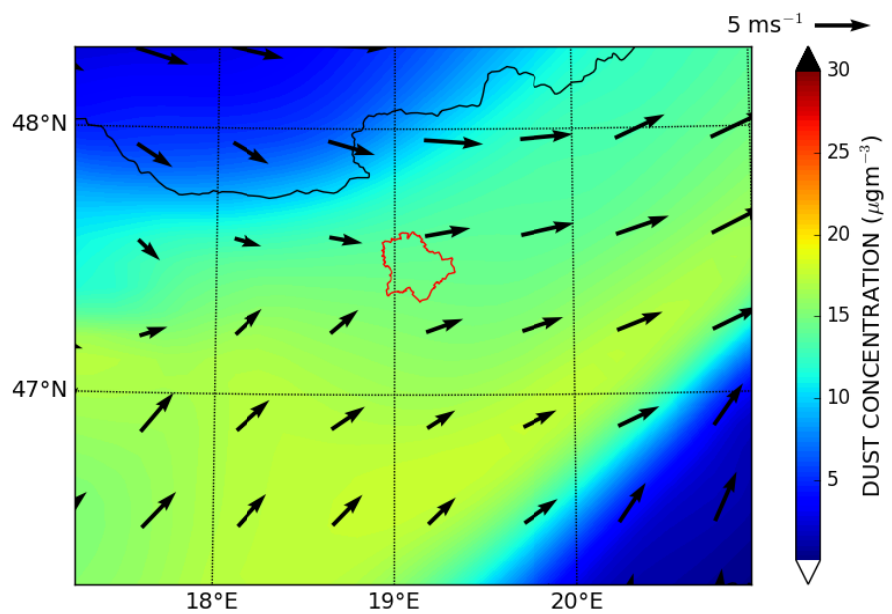


**Figure 2.** Dust (2.4  $\mu\text{m}$  effective radius) concentration ( $\mu\text{g m}^{-3}$ ) and 10 m wind field ( $\text{m s}^{-1}$ ) on the 21<sup>th</sup> of June, 2012 at 12 UTC for the first nested domain.

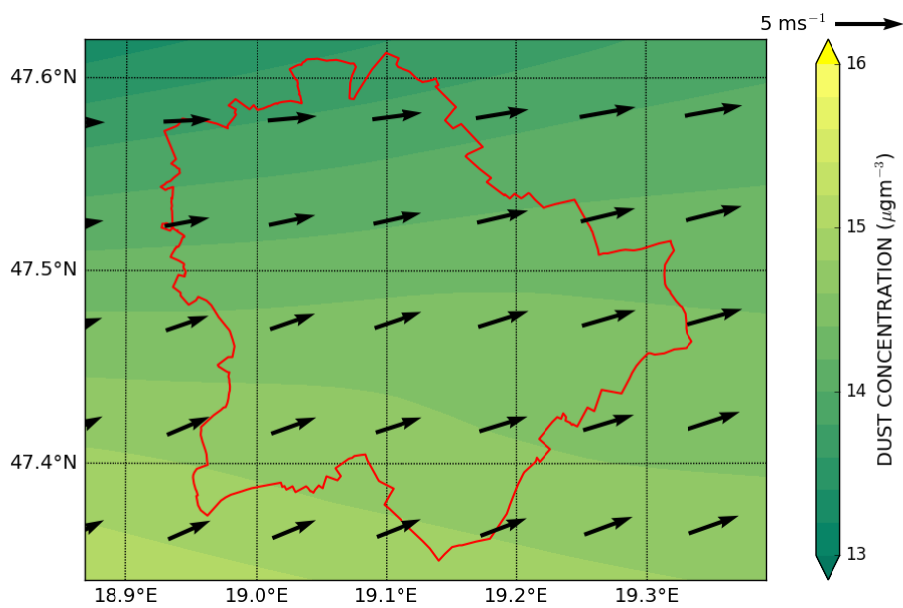


**Figure 3.** Dust (2.4  $\mu\text{m}$  effective radius) concentration ( $\mu\text{g m}^{-3}$ ) and 10 m wind field ( $\text{m s}^{-1}$ ) on the 21<sup>th</sup> of June, 2012 at 12 UTC for the second nested domain.

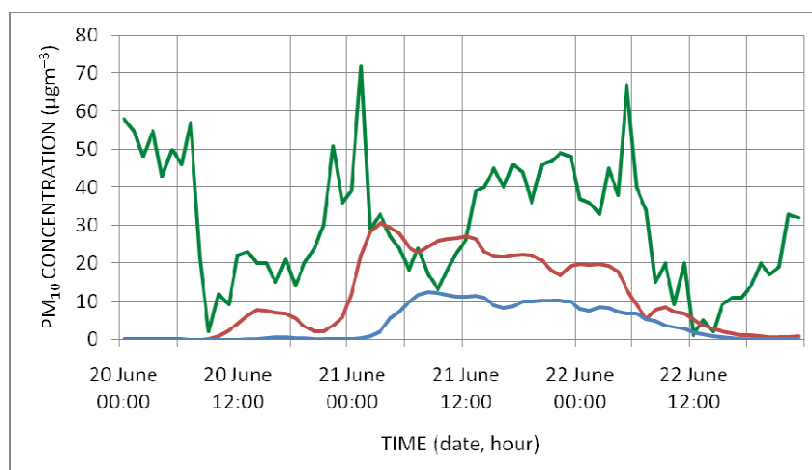


**Figure 4.** Measured concentration of the particulate matter (PM<sub>10</sub>) (Gilice square, Budapest – green) compared against 14 and 7 day simulation time model output data (14 – red, 7 – blue) ( $\mu\text{g m}^{-3}$ ) between the 20<sup>th</sup> and the 23<sup>rd</sup> of June, 2012.

## CONCLUSION

The WRF-Chem model is capable of modelling meteorological and chemistry processes in parallel fashion. Biogenic and anthropogenic emissions, as well as wildfires, deserts and volcanoes can be incorporated as sources of aerosols. Our study shows that the WRF-Chem model can model the transport of Saharan dust on the continental scale. Therefore, WRF-Chem is an efficient tool to simulate the contribution of long-range dust transport to urban air pollution. In the future, we continue our work with taking into account urban anthropogenic emissions such as industrial, traffic and domestic heating sources.

## REFERENCES

- Baklanov, A., Schlünzen, K., Suppan, P., Baldasano, J., Brunner, D., Aksoyoglu, S., ... & Zhang, Y., 2014: Online coupled regional meteorology chemistry models in Europe: current status and prospects. *Atmospheric Chemistry and Physics*, **14**, 317–398.
- Grell, G. A., Peckham, S. E., Schmitz, R., McKeen, S. A., Frost, G., Skamarock, W. C., & Eder, B., 2005: Fully coupled “online” chemistry within the WRF model. *Atmospheric Environment*, **39**, 6957–6975.
- Grell, G. A., McKeen, S. A., Barth, M., Pfister, G., Wiedinmyer, C., Fast, J. D., ... & Easter, R. C., 2012: WRF/Chem Version 3.3 User's Guide. US Department of Commerce, National Oceanic and Atmospheric Administration, Oceanic and Atmospheric Research Laboratories, Global Systems Division.
- Tuccella, P., Curci, G., Visconti, G., Bessagnet, B., Menut, L., & Park, R. J., 2012: Modeling of gas and aerosol with WRF/Chem over Europe: Evaluation and sensitivity study. *Journal of Geophysical Research: Atmospheres (1984–2012)*, **117**(D3).
- Wang, X., Liang, X. Z., Jiang, W., Tao, Z., Wang, J. X., Liu, H., ... & Peckham, S. E., 2010: WRF-Chem simulation of East Asian air quality: Sensitivity to temporal and vertical emissions distributions. *Atmospheric Environment*, **44**, 660–669.

**17th International Conference on  
Harmonisation within Atmospheric Dispersion Modelling for Regulatory Purposes  
9-12 May 2016, Budapest, Hungary**

---

**SIMULATIONS OF TRAFFIC RELATED POLLUTANTS IN A MAIN STREET OF RIO DE JANEIRO CITY (BRAZIL) USING COMPUTATIONAL FLUID DYNAMICS MODELLING**

*Roseane A.S. Albani<sup>1</sup> Beatrice Pulvirenti<sup>2</sup> and Silvana di Sabatino<sup>1</sup>*

<sup>1</sup>Dipartimento di Fisica e Astronomia ,Università degli Studi di Bologna, Bologna, Italy

<sup>2</sup>Dipartimento di Ingegneria Energetica, Università degli Studi di Bologna, Bologna, Italy

**Abstract:** In this work we study atmospheric pollutant dispersion associated to traffic emissions in a main street of down town Rio de Janeiro (Brazil) using Computational Fluid Dynamic (CFD) modelling. Our study area considers the "Presidente Vargas" Avenue, one of the most important artery in down town Rio de Janeiro, having a traffic count of about two hundred thousand vehicles every day. This artery forms in some part a street canyon in a classical sense while the remaining is embedded in more complex urban structures. The study area is a region nearby "Central do Brasil", which is a terminal railway station from where approximately six hundred thousand people make their way daily. The performance of CFD methodologies based on both Reynolds-averaged Navier-Stokes (RANS) and a large-eddy (LES) simulations for carbon monoxide (CO) dispersion is investigated. Numerical results are compared with real concentration data from one monitoring station to highlight the differences between RANS and LES approaches.

*Key words:* Computational Fluid Dynamics, Atmospheric Dispersion, urban areas

## **INTRODUCTION**

Atmospheric dispersion continues to be an active research topic given its relevance in the assessment of air pollution impact on people's health. Traffic emissions are the main source of pollution in urban areas, usually located among or around buildings. Pollutant sources are immersed in the very complicated flow patterns generated by the interaction between airflow and buildings leading to a high complex concentration field whose prediction remains challenging for most current numerical models.

Details of the flow around buildings can be investigated using computational fluid dynamics (CFD) approaches, which has been extensively used in simulations of dispersion phenomena in urban areas during this last decade as largely documented by Anand et al. (2016), Santiago et al. (2010), Di Sabatino et al. (2008) and many others. Despite the several advantages, CFD models have large computational costs still restricting its range of application to small domains (few hundreds to 1 km). In addition, CFD models needs to be thoroughly set up and evaluated case by case, given the large number of parameters to be adjusted to be successful in real scenarios. New simulations requiring different set up to account for real urban geometries as well as specific environmental physical conditions, still depend upon careful evaluation against concentration and meteorological data measured at the site.

The aim of this work is to investigate the atmospheric dispersion considering the complex scenario of Rio de Janeiro down town, which has a highly heterogeneous distribution of the buildings, besides being influenced by the Guanabara bay breeze (on the North direction), just as the sea Breeze (in the South direction) in the morning and afternoon-night periods, respectively. Although many studies focus on evaluating pollutant concentration in rather idealized street canyons here we focus on real scenarios using both Reynolds averaged Navier-Stokes (RANS) and Large-Eddy (LES) simulations to document their performance.

## **DESCRIPTION OF THE STUDY SITE**

The region of study encompass part of the President Vargas avenue, one of the main streets of Rio de Janeiro. The selected built area covers a surface of ~ 657000 m<sup>2</sup>, which includes a very complex

geometry, with asymmetric buildings of different heights, ranging from 10 to 80m and different spacing among them. Trees of different species are spread out over the whole site. The area is bounded from north/east by the Guanabara bay (~1200 m), and from the south by the Atlantic ocean (~7500 m). Near surface wind is influenced by both bay and sea breezes as reported by Pimentel et al. (2014). Figure 1 (right) shows the computational domain (inside the yellow line) where the air quality station is located. The meteorological data for the inlet conditions were obtained in the Santos Dumont airport (left).

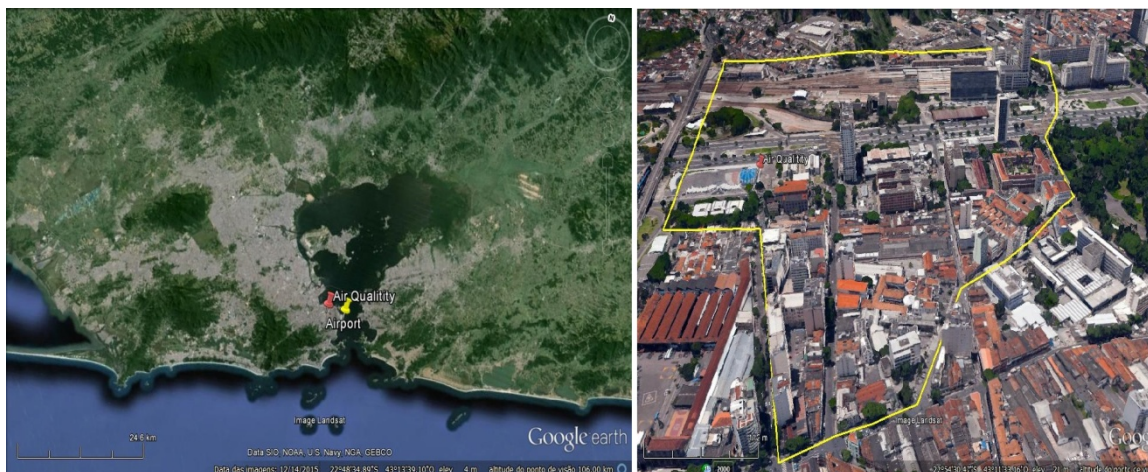


Figure 1. The site of studying encircled by the yellow line. Source: Google earth.

## METHODOLOGY

We used meteorological and air quality data provided by the INEA (Instituto Estadual do Ambiente do Rio de Janeiro) and METAR data obtained from the Santos Dumont Airport (<http://www.redemet.aer.mil.br>). The meteorological and concentration data were taken considering the day 23/07/2013 at 6 PM, where neutral conditions could be found. To estimate the emissions, we used the curve of the volume of vehicles along a day, considering streets around the President Vargas avenue, as shown in Figure 2.

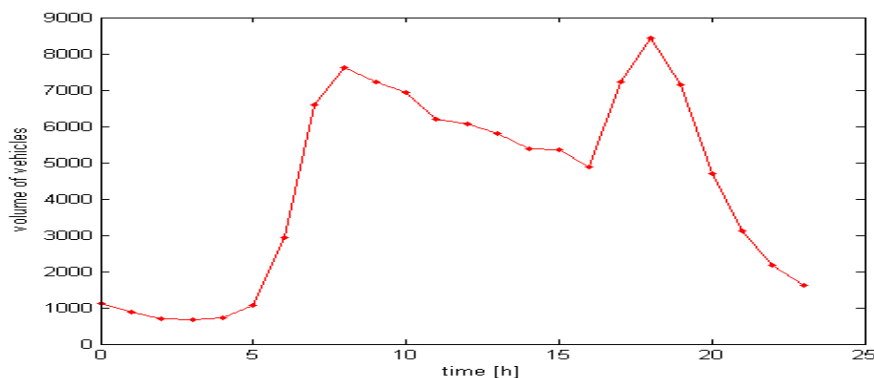


Figure 2. Volume of vehicles along the day 23/07/2013 nearby the air quality station.

Detailed information about the number of vehicles used in this study were publicly available (<http://www.denatran.gov.br/frota2013.htm>) while estimate of hourly emissions were obtained by using the EMIT software kindly made available by CERC Lts according to vehicle category and typical traffic speed.

## SET UP AND CFD SIMULATIONS

Simulations of pollutant dispersion under neutral conditions were performed by means of Fluent ANSYS 17.0. Both RANS (Reynolds Averaged Navier-Stokes equations) and LES (Large Eddy Simulations) methodologies were employed to simulate dispersion of carbon monoxide (CO) in Rio de Janeiro down

town. A description of the set of equations of the RANS and LES models can be found for example in Santiago et al. (2010). The urban boundary layer height was estimated as  $\delta = 5H$ , where  $H$  is the average building height while the usual equilibrium profiles of wind speed, turbulent kinetic energy (TKE) and dissipation rate were used as inlet conditions (see e.g. Di Sabatino et al. 2008). The friction velocity was estimated via the log-law expression with wind speed measured at 10 m height at the airport Santos Dumont (outside the domain). The computational domain, shown in Figure 3, is a volume of  $3L \times 9L$  with a height of  $3L$ , with  $L$  the dimension of the area of interest considered in Figure 1. We used symmetry boundary conditions at the top of the domain and pressure-outlet conditions in the outflow.

### MESH CONSTRUCTION

Mesh building was a rather important and challenging phase especially for such complex structures as in our case. In general terms, the entire domain used for simulations is larger than the volume of interest. Such strategy is employed to ensure that some constraints, imposed by the boundary conditions will not affect excessively the solution in the built area.

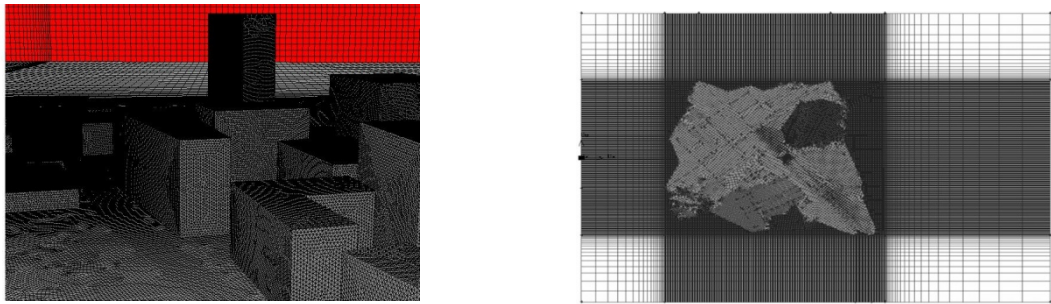


**Figure 3.** Structure of the computational domain in the built area (left) and the whole domain (right).

The whole domain was split into several sub domains of different sizes in order to control the mesh building process. A combination of structured and unstructured meshes composed by hexahedral and tetrahedral elements was designed since it allows a greater flexibility, accuracy and computational efficiency, compared to a purely structured or unstructured mesh. In the free stream region a structured mesh was created, since in such region the flow is predictable and stable. On the other hand, an unstructured mesh was generated for the build region, where the flow pattern is unknown. The grid is built by sweeping a surface ground mesh three times resulting in three different resolution layers. In the first layer near the ground level, a finer mesh is employed to obtain a better description of the flow and concentration at pedestrian level. Considering the second layer, a lower resolution is required compared to the ground level layer, since into this part of the domain large flow structures are expected. The third is the roughest layer, since no high resolution is required there. The mesh was constructed with 2-4-9 million of elements. The finer resolution of the element in the  $x$ ,  $y$  and  $z$  direction was 0.5 m, based on convergence analysis.

### RESULTS AND DISCUSSION

Two different models have been compared: k-epsilon and LES. For the k-epsilon model, standard wall functions and constants have been used, with a standard choice of the turbulent parameters. For the LES model, a fixed time step of 0.1 s was chosen, with a second order implicit discretization. The flow field obtained with the two turbulence models shows channeling and vortices with the same shape and dimensions, as shown in Figure 4.

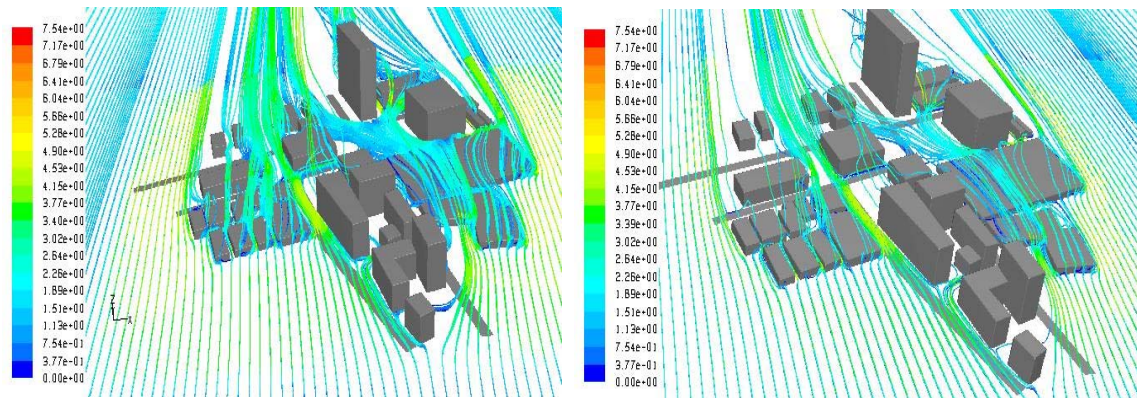


**Figure 4.** Comparison of the streamlines obtained over the built area with the k-epsilon model (left) and LES (right).

The flow channels mainly in the two roads: “Rua de Santana” (shown in figure 5) and “Rua General Caldwell”, as their direction is aligned with the direction of the flow. Then, vortices are observed in many areas near the streets, where large buildings confine the secondary flows. Figure 5 shows that the main vortices obtained by the two turbulence models are similar. However, small vortices are captured only by the LES model.

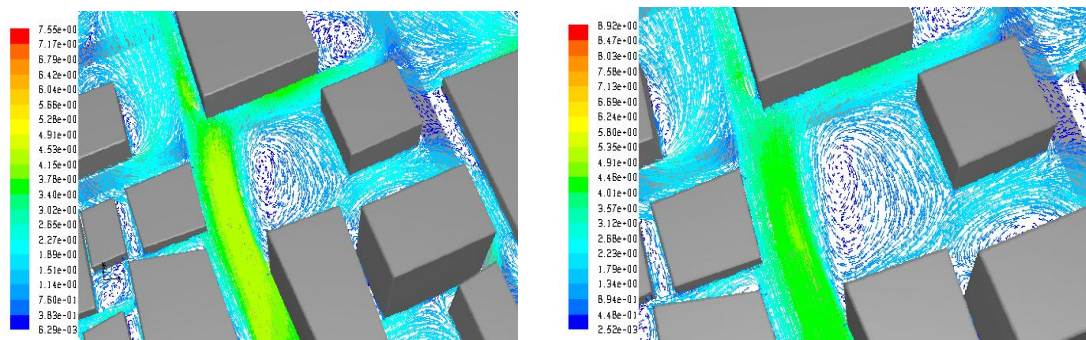


**Figure 5.** The vectors field in the area.

Concentration of CO does not show high values in such recirculation zones, as the main streams carry most of the pollutant and in these areas CO is diluted. The validation has been obtained by a comparison with concentration data obtained from the air quality station positioned in the point remarked by a yellow triangle in the Figure 6 (left). Figure 7 shows CO concentration as a function of vertical direction, in the point where the station is located (yellow triangle).

The red line represents simulation result with the k-epsilon model, while the blue line corresponds to the results obtained with the LES model. The measured value in  $z = 0$  m is  $300\text{mg}/\text{m}^3$ . Figure 7 shows that both numerical results are lower than the CO measured data, with the results obtained by RANS model closer to the measurements than the ones obtained by LES. The reason of the under prediction could be related to the fact that the measured data are averaged over the whole day, while numerical results are instantaneous and related to the case of wind coming from South.

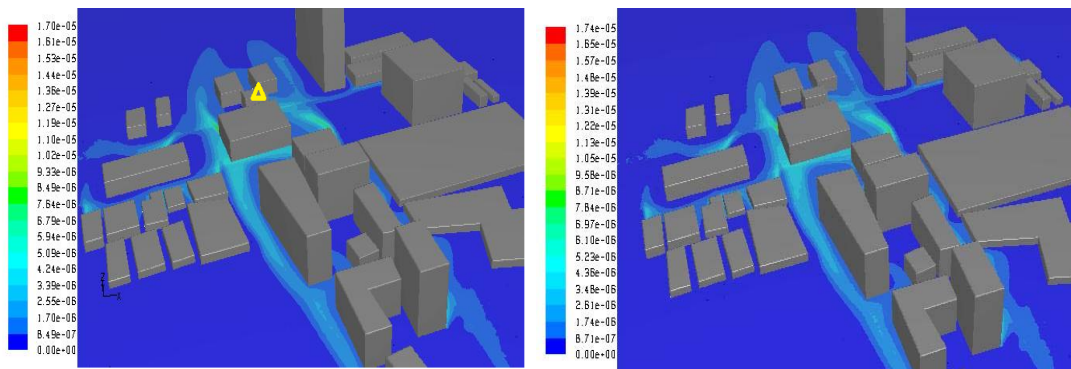


Figure 6. CO concentrations at a plane at  $z=2$  m, for the case with k-epsilon model (left) and LES (right).

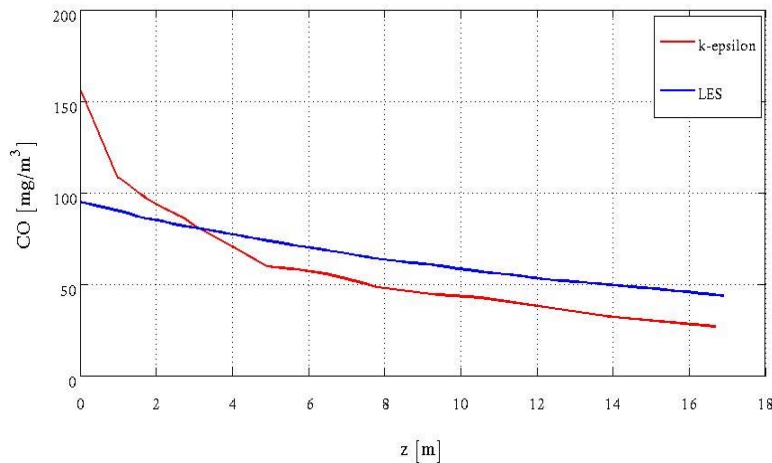


Figure 7. CO concentration along the vertical line, in correspondence of the measuring point.

## CONCLUSIONS

The main characteristics of the flows (vortices and channelling) in the problem of CO diffusion within the real city of Rio de Janeiro are captured by both the RANS and the LES turbulence models, while small vortices are captured only by LES. The CO distributions obtained by both models are lower than the measured CO on ground level, but a longer sequence of measured data in a day is needed for a better comparison.

## REFERENCES

- Anand Y., Gupta, A., Tyagi, S.K., Anand, S. 2016: Computational fluid dynamics, a building simulation tool for achieving sustainable buildings: *Renewable and Sustainable Energy Reviews*, **57**, 1174-1185.
- Di Sabatino, S., Buccolieri, R., Pulvirenti, B., Britter, R. E. 2008: Flow and Pollutant Dispersion in Street Canyons using FLUENT and ADMS-Urban: *Environ Model Assess*, **13**, 369-381.
- Pimentel, L.C.G., Marton, E., Silva Soares, M., Jourdan, P. 2014: Characterization of surface wind regime in the Metropolitan Area of Rio de Janeiro. *Eng Sanit Ambient*, **19**, 121-132.
- Santiago, J. L., Dejoan, A., Martilli, A., Martin, F., Pinelli, A. 2010: Comparison Between Large-Eddy Simulation and Reynolds-Averaged Navier–Stokes Computations for the MUST Field Experiment. Part I: Study of the Flow for an Incident Wind Directed Perpendicularly to the Front Array of Containers. *Boundary-Layer Meteorol.* **135**, 109-132.

**17th International Conference on  
Harmonisation within Atmospheric Dispersion Modelling for Regulatory Purposes  
9-12 May 2016, Budapest, Hungary**

---

**MODELLING NO<sub>x</sub> AND NO<sub>2</sub> IN TWO STREET CANYONS IN COPENHAGEN USING AN  
IMPROVED VERSION OF OSPM**

*Thor-Bjørn Ottosen<sup>1,2</sup>, Matthias Ketzel<sup>3</sup>, Ole Hertel<sup>3</sup>, Jørgen Brandt<sup>3</sup>, Henrik Skov<sup>1,3</sup>, and Konstantinos  
E. Kakosimos<sup>2</sup>*

<sup>1</sup>Department of Chemical Engineering, Biotechnology, and Environmental Technology, University of  
Southern Denmark, Odense, Denmark

<sup>2</sup>Department Chemical Engineering, Texas A&M University at Qatar, Doha, Qatar

<sup>3</sup>Department of Environmental Science, Aarhus University, Roskilde, Denmark

**Abstract:** Simultaneously modelling the measured NO<sub>x</sub> and NO<sub>2</sub> concentrations is a challenge for many atmospheric dispersion models including the Operational Street Pollution Model (OSPM<sup>®</sup>). In the present study two streets in Copenhagen, Denmark are modelled using an improved version of OSPM. The improved model contains a new parametrization for the roof-level wind speed with the aim of better representing the NO<sub>x</sub> concentrations. It is moreover the aim to update the reaction rates for the NO-NO<sub>2</sub>-O<sub>3</sub> chemistry in the street canyons. This is still work-in-progress and thus not presented here. The results show a significantly altered wind direction dependency of the average wind speed for one street canyon and less impact on the other street canyon. The improved wind speed model does however not lead to direct improvements in the street level concentrations.

**Key words:** *OSPM, street canyon modelling, NO<sub>x</sub>-chemistry, wind speed*

#### **INTRODUCTION AND STUDY AREA**

The Operational Street Pollution Model (OSPM<sup>®</sup>) has been applied in a large number of studies in many countries around the globe over the last 25 years. Despite the model's great success, a number of shortcomings have been identified (Kakosimos et al., 2010). One of the model shortcomings is that the model is not reproducing the NO<sub>x</sub> and NO<sub>2</sub> concentrations simultaneously (Ketzel et al., 2012).

Ottosen et al. (2016b) showed that the roof-level wind speed was one of the most sensitive parameters in the model. Moreover, unpublished measurements of the street level wind speed performed at H. C. Andersens Boulevard, Copenhagen, Denmark and Hornsgatan, Stockholm, Sweden showed that the model significantly underestimated this model element. A new model for this was therefore developed and validated against wind speed data in Ottosen et al. (2016a). It is therefore the aim of the present study to analyse the impact of the new parametrization on the NO<sub>x</sub> concentrations. Since the NO<sub>2</sub> concentrations in OSPM are calculated from the NO<sub>x</sub> concentrations, accurate modelling of the NO<sub>x</sub> concentrations becomes important.

Moreover, studies performed after the development of OSPM have analysed the reaction rates for the NO-NO<sub>2</sub>-O<sub>3</sub> reaction, and it is thus a subsequent aim of the present study to analyse the impact of updating these rates.

The present study will validate the updated parametrizations against measurements from the stations at Jagtvej and H. C. Andersens Boulevard (HCAB) both in Copenhagen, Denmark. NO<sub>x</sub> and NO<sub>2</sub> measurements have been performed at these streets for hourly values for the years 1994-2014, and have been the subject of several previous investigations. Detailed information about these streets can be found in (Ottosen et al., 2016b).

## PRESENT MODEL

OSPM is a model for pollutant concentrations in a street canyon, where the measured concentrations are modelled as a sum of a direct contribution and a recirculating contribution, as illustrated in Figure 1 (Berkowicz et al., 1997; Hertel and Berkowicz, 1989a; Ottosen et al., 2015).

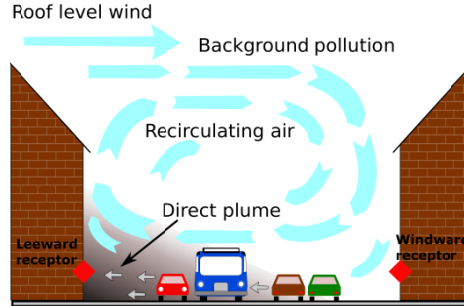


**Figure 1.** Schematic illustration of the direct and recirculating component of the concentration in OSPM. Figure modified from (Silver et al., 2013).

The specific characteristics of the model are:

- The direct contribution is modelled as a Gaussian plume model using a top hat distribution for the vertical diffusion and assuming that horizontal diffusion can be neglected.
- The recirculating contribution is modelled as a trapezium shaped box model with the fundamental assumption that the inflow of pollutants equals the outflow of pollutants. This is justified based on the temporal resolution of the model of one hour.
- Moreover, the model contains expressions for traffic produced turbulence and a numerical averaging procedure to account for wind direction meandering especially pronounced for low wind speeds (Hertel and Berkowicz, 1989c).
- The emissions are modelled using the COPERT IV emission model (EEA, 2009).

The roof level wind speed is assumed to be proportional to the input wind speed coming from an urban mast, a nearby model, or a numerical weather prediction model. The constant of proportionality currently equals 0.4.

The model contains an algebraic expression for the conversion of NO to NO<sub>2</sub> in the presence of O<sub>3</sub> (Hertel and Berkowicz, 1989b; Ottosen, 2016). The reactions are modelled as a box model under the assumption of steady state for the individual hour. The reaction rate (k) for NO reacting with O<sub>3</sub> to form NO<sub>2</sub> and O<sub>2</sub> is from (Seinfeld, 1986):

$$k = 5.38 \cdot 10^{-2} e^{\frac{1430}{T}} \text{ s}^{-1} \text{ ppb}^{-1}. \quad (1)$$

where T is the temperature in Kelvin. The photolysis rate (J) is calculated from the global radiation (Q) fitted to experimental data from the Netherlands:

$$J = 0.8 \cdot 10^{-3} e^{-\frac{10}{Q}} + 7.4 \cdot 10^{-6} Q \text{ s}^{-1} \quad (2)$$

The NO<sub>2</sub> concentration can subsequently be calculated algebraically from the NO<sub>x</sub> concentration.

## NEW WIND SPEED MODEL

A model for the calculation of the roof-level wind speed from an urban mast or a nearby airport was developed in (Ottosen et al., 2016a), and the details can be found therein. Only the main elements of the model are therefore summarized in this section.

To extrapolate the wind speed from one location to another the model goes through three steps following (Wieringa, 1986):

1. The geostrophic wind ( $U_g$ ) (the wind above the boundary layer) is calculated from a measured wind speed using a logarithmic wind profile.

2. The geostrophic wind speed and direction is assumed to be constant. This is a reasonable assumption due to the nearness of the points being extrapolated; a fact also supported by measurements of the wind direction.
3. The roof-level wind speed is calculated from the geostrophic wind using a logarithmic profile again.

### UPDATED REACTION RATES

The reaction rate for the conversion of NO to NO<sub>2</sub> in the presence of Ozone is taken from Sander et al. (2011):

$$k = 22.02 \frac{1}{T} e^{\frac{1500}{T}} \text{ s}^{-1} \text{ ppb}^{-1} \quad (3)$$

Where the dependency of the pre-exponential factor on temperature is taken into account. The relationship between the global radiation and the NO<sub>2</sub> photolysis rate has been studied empirically by Trebs et al. (2009). They found the following relationship:

$$J = (1 + \alpha) \cdot (1.47 \cdot 10^{-5} Q - 4.84 \cdot 10^{-9} Q^2) \text{ s}^{-1} \quad (4)$$

### RESULTS

Updating the NO-NO<sub>2</sub>-O<sub>3</sub> reaction rates is still work in progress. Therefore only results for the new parametrization of the wind speed are shown.

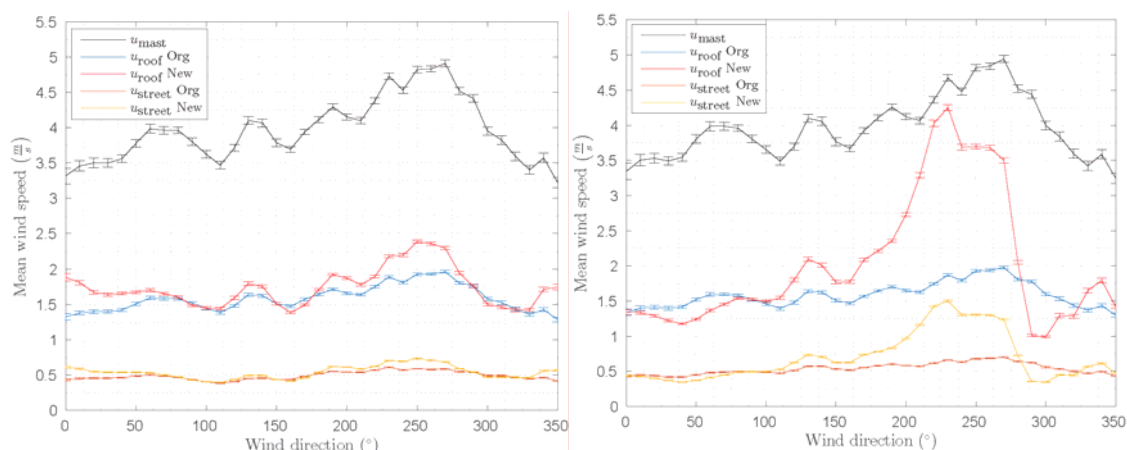


**Figure 2.** Measured wind speed at an urban mast (black), original model roof-level wind speed (blue), new model roof-level wind speed (red), original model street level wind speed (orange), and new model street level wind speed (yellow). The figures are for Jagtvej (left) and HCAB (right).

The difference in wind speed between the original model and the new model is shown in Figure 2. As can be seen, the new model confirms the constant of 0.4 as the ratio between the mast level wind speed and the roof level wind speed for large wind direction intervals. However, the new model also predicts a larger mean wind speed compared to the original model for significant wind direction intervals. The effect is most clearly seen at HCAB where the amusement park located upwind of the street for western and southwestern wind directions gives rise to very large roof-level wind speeds. The difference between the original and the new model is also larger at HCAB due to the longer distance between the urban mast and the street (approximately 500 m at Jagtvej and 3 km at HCAB).

As can also be seen, the increased roof-level wind speed for certain wind directions is transferred to the street-level wind speed, thus contributing twice to reduced concentrations. The impact of the wind speed increase is smaller at the street level; especially at Jagtvej, where the absolute wind speed increase is very small. The relative increase in wind speed at street level is however significant.

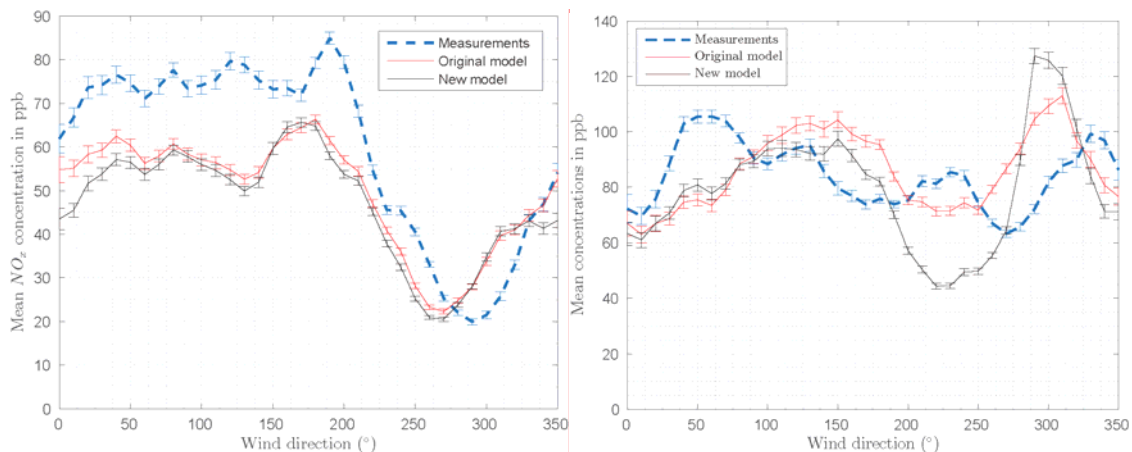


**Figure 3** Mean concentrations of NOx as a function of wind direction for respectively Jagtvej (left) and HCAB (right).

The mean concentration of NOx for the two street canyons is shown in Figure 3. As can be seen, the difference between the old and the new parametrization is smaller at Jagtvej than at HCAB. The performance of the new wind speed parametrization at Jagtvej is slightly worse than the original parametrization. However, it is difficult to assess since both parametrizations generally underestimate the concentrations.

For HCAB the wind direction plot has changed significantly from the original model to the new model; most noticeably for southwestern wind directions where the model now significantly underestimates the concentrations and around 300° where the model significantly overestimates the concentrations. The validation of the model in Ottosen et al. (2016a) showed that the model performed reasonably for southwestern wind directions, so it is possible that this underestimation is caused by another bias in the model. It is also possible that the street level wind direction has an influence on the shape of the wind direction plot.

## CONCLUSION

Implementing the wind speed model developed in Ottosen et al. (2016a) in OSPM significantly alters the mean roof level wind speed with respect to wind direction. This does however not directly lead to improved model performance. Some of the variation can be caused by biases in the wind speed model and other variation can be caused by biases in other parts of the model.

## REFERENCES

- Berkowicz, R., Hertel, O., Larsen, S. E., Sørensen, N. N., and Nielsen, M.: Modelling traffic pollution in streets, Ministry of Environment and Energy, National Environmental Research Institute, 1997.
- EEA: EMEP/CORINAIR Atmospheric Emissions Inventory Guidebook, Chapter on Exhaust Emissions from Road Transport. Methodology for COPERT 4., European Environmental Agency, 2009.
- Hertel, O. and Berkowicz, R.: Modelling Pollution from Traffic in a Street Canyon. Evaluation of Data and Model Development., National Environmental Research Institute, 1989a.
- Hertel, O. and Berkowicz, R.: Modelling NO<sub>2</sub> Concentrations in a Street Canyon, 1989b.
- Hertel, O. and Berkowicz, R.: Operational Street Pollution Model (OSPM) Evaluation of the Model on Data from St. Olavs Street in Oslo, National Environmental Research Institute, 1989c.
- Kakosimos, K. E., Hertel, O., Ketzel, M., and Berkowicz, R.: Operational Street Pollution Model (OSPM) - a review of performed application and validation studies, and future prospects, *Environmental Chemistry*, **7**, 485-503, 2010.
- Ketzel, M., Jensen, S. S., Brandt, J., Ellermann, T., Olesen, H. R., Berkowicz, R., and Hertel, O.: Evaluation of the Street Pollution Model OSPM for Measurements at 12 Streets Stations Using a Newly Developed and Freely Available Evaluation Tool, *Journal of Civil & Environmental Engineering*, **S:1**, 2012.

- Ottosen, T.-B.: Improved Local Air Quality Modelling for Complex Urban Landscapes, Ph.D., Department of Chemical Engineering, Biotechnology, and Environmental Technology, University of Southern Denmark, Submitted, 149 pp., 2016.
- Ottosen, T.-B., Kakosimos, K. E., Johansson, C., Hertel, O., Brandt, J., Skov, H., Berkowicz, R., Ellermann, T., Jensen, S. S., and Ketzel, M.: Analysis of the impact of inhomogeneous emissions in the Operational Street Pollution Model (OSPM), *Geoscientific Model Development*, **8**, 3231-3245, 2015.
- Ottosen, T.-B., Ketzel, M., Hertel, O., Brandt, J., Skov, H., Gryning, S.-E., and Kakosimos, K. E.: Model development and validation for the relationship between urban and non-urban near-surface wind speed, *Boundary-Layer Meteorology*, Submitted, 2016a.
- Ottosen, T.-B., Ketzel, M., Skov, H., Hertel, O., Brandt, J., and Kakosimos, K.: A Parameter Estimation and Identifiability Analysis Methodology Applied to a Street Canyon Air Pollution Model, *Environmental Modelling & Software*, Submitted, 2016b.
- Sander, S. P., Abbatt, J., Barker, J. R., Burkholder, J. B., Friedl, R. R., Golden, D. M., Huie, R. E., Kolb, C. E., Kurylo, M. J., Moortgat, G. K., Orkin, V. L., and Wine, P. H.: Chemical Kinetics and Photochemical Data for Use in Atmospheric Studies, Evaluation No. 17., Jet Propulsion Laboratory, Pasadena, 2011.
- Seinfeld, J. H.: Atmospheric Chemistry and Physics of Air Pollution, California Institute of Technology, 1986.
- Silver, J. D., Ketzel, M., and Brandt, J.: Dynamic parameter estimation for a street canyon air quality model, *Environmental Modelling & Software*, **47**, 235-252, 2013.
- Trebs, I., Bohn, B., Ammann, C., Rummel, U., Blumthaler, M., Königstedt, R., Meixner, F. X., Fan, S., and Andreae, M. O.: Relationship between the NO<sub>2</sub> photolysis frequency and the solar global irradiance, *Atmos. Meas. Tech.*, **2**, 725-739, 2009.
- Wieringa, J.: Roughness-dependent geographical interpolation of surface wind speed averages, *Quarterly Journal of the Royal Meteorological Society*, **112**, 867-889, 1986.

**17th International Conference on  
Harmonisation within Atmospheric Dispersion Modelling for Regulatory Purposes  
9-12 May 2016, Budapest, Hungary**

---

**DRY DEPOSITION ONTO VERTICAL SURFACES IN THE URBAN ENVIRONMENT**

*Patrick Conry<sup>1</sup>, Silvana Di Sabatino<sup>2</sup>, Francesca Di Nicola<sup>3</sup>, Maria Lisa Vincenti<sup>3</sup>, Riccardo Buccolieri<sup>3</sup>,  
Pierina Ielpo<sup>4</sup>, Livia Giotta<sup>3</sup>, Alessandra Genga<sup>3</sup>, Ludovico Valli<sup>3</sup>, Gennaro Rispoli<sup>3</sup>  
and H. J. S. Fernando<sup>1</sup>*

<sup>1</sup>Environmental Fluid Dynamics Laboratories, University of Notre Dame, Notre Dame, IN, USA

<sup>2</sup>Department of Physics and Astronomy, University of Bologna, Bologna, Italy

<sup>3</sup>Department of Biological and Environmental Science and Technologies, University of Salento,  
Lecce, Italy

<sup>4</sup>ISAC-CNR, Lecce, Italy

**Abstract:** A field experiment was performed at the University of Salento, Lecce (Italy) by a team of scientists to investigate dry deposition mechanisms on vertical surfaces in an urban-like setting. Submicronic fluorescein aerosols were used as the tracer during four test releases, and turbulence and thermal conditions in the flow and wall boundary layer were measured simultaneously using an array of meteorological instruments. Flow and turbulence measurements during the fluorescein test releases are presented and discussed. Chemical analysis of material samples exposed during each test produced estimates for the deposition velocity, a key parameter for modelling deposition. The dry deposition depends on many environmental factors, which were represented using a framework of dimensionless parameters, with Reynolds and Grashof (Gr) numbers being among dominant governing parameters. The results indicate that, at high Reynolds ( $10^6$ ) and Grashof ( $10^{12}$ ) numbers, the thermophoresis has a significant impact on deposition velocity. When the vertical surface was heated relative to background air, the deposition velocity may become approximately constant, independent on Gr and even surface material properties. The results were also compared to those of a separate past experiment on the topic.

**Key words:** *dry deposition, urban fluid mechanics, field measurements, dimensional analysis*

## INTRODUCTION

The fate of solid particles suspended in the atmosphere is of key interest for predicative air quality modelling. A significant portion of aerosols in the atmosphere are eventually deposited upon solid surfaces, and therefore deposition processes represent a key sink within the aerosol budget, ultimately impacting the local pollutant concentrations. Vertical surfaces prevalent in urban environments are particularly important to account for in urban dispersion modelling. The built environment undergoes costly dirtying and damage, caused by the deposition of urban aerosols (Sabbioni, 2003), so urban planners, regulators, and cultural heritage managers have been motivated to address this issue, with guidance from dispersion modellers, to improve urban air quality and building aesthetics.

The dry deposition is typically represented using the deposition velocity, which quantifies the transfer of particles from the atmosphere to adhesion to a solid surface. The deposition velocity ( $v_d$ ) is defined as

$$v_d = -\frac{J}{C_\infty}, \quad (1)$$

where  $J$  is the mass flux ( $\text{kg m}^{-2} \text{s}^{-1}$ ) of aerosol onto the surface and  $C_\infty$  is the background concentration ( $\text{kg m}^{-3}$ ) of airborne aerosols near the surface; it is essentially a normalised mass transfer coefficient. This coefficient provides a method to calculate, based on a concentration from a dispersion model for instance, the aerosol mass flux out of the atmosphere and onto a surface. Numerous factors can affect the deposition velocity, including particle size, surface roughness, turbulent diffusivity, gravitational forces, thermophoretic forces, and Brownian motions. Given that deposition velocity can vary from

approximately  $10^{-5}$  to  $10^{-1}$   $\text{m s}^{-1}$  (Guha, 2008), knowledge of an accurate deposition velocity as a function of background environmental conditions is necessary in modelling and design.

This paper focuses on a semi-controlled field experiment performed at the University of Salento (Italy) to study dry deposition in an urban environment. These observations add to the relatively small number of deposition observations from short-term experiments where urban micrometeorological conditions impacting deposition processes have been well-documented (Pesava *et al.*, 1999; Maro *et al.*, 2014). Such experimental studies are imperative to aid urban modelling efforts that seek to better account for micro-scale variability in dry deposition.

### EXPERIMENTAL SET-UP

An experiment was conducted on the campus of the University of Salento on 25-27 October, 2014. The experiment was designed to have many similarities with the short-term “Salissure de Facade” (SaliFa) experiments performed by French researchers in 2005 and 2006 (Maro *et al.*, 2014). Two academic buildings formed an “urban canyon” of sorts, within which a meteorological (“meteo”) station was deployed for long term analysis of local flow conditions. A small wall situated in between these buildings and parallel to the canyon’s axis was selected as the focus area of the experiment. Meteorological instruments were set up to measure the turbulent flow as it passed by this wall, as shown in Figure 1 below. Instrumentation included five sonic anemometers (3 Gill Instruments R3-50’s, 1 Gill Instruments WindMaster, and 1 Campbell Scientific CSAT3), two temperature probes, and an infrared camera. One sonic was placed upstream of the wall to capture incoming turbulent flow conditions, based on the anticipated northerly wind direction. The other four sonics were located near the wall to measure flow adjustments in and away from the wall boundary layer but to avoid interfering with flow past the area of interest for deposition measurements. All sonics were operated at 20 Hz measurement rate.

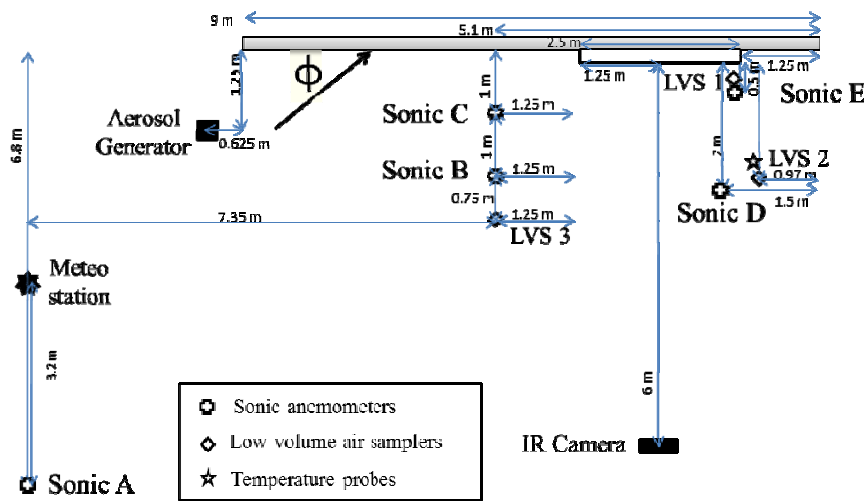


Figure 1. Scaled plan view of experimental set-up with positions of key instruments with respect to panel and wall

Four one-hour aerosol emissions (“Tests”) were performed during the experimental period, and, during each Test, a panel was attached to the wall with the material samples being studied. These materials included auto-cleaning glass and standard glass, which were identical to materials used in SaliFa, as well as marble, Lecce stone, and ceramic, which were selected due to their special application to cultural heritage preservation. Twelve samples ( $10 \times 10$  cm) of each material were affixed to a single panel constructed so that the panel’s face was as even as possible (within approximately  $\pm 2$  mm) to minimize flow separation and internal boundary layers. Such modified flows regimes can have a major impact on local dry deposition (Pesava *et al.*, 1999), and thus our set-up aimed to achieve situation in which roughness of the material would be dominant factor influencing flow and turbulence very near the samples rather than localised effects originating from panel defects. An atomic force microscope was used to obtain estimates of roughness based on few small samples of marble and ceramic. Both consistently had a mean roughness height of  $0.8 \mu\text{m}$ . Additional details about and images of the panels

with material samples can be found in Di Nicola *et al.* (2016), along with measurements of surface temperatures from an infrared camera and air temperatures very near the samples from thermocouples. The surface temperature results could be used to calculate the difference in temperature between panel and background air, hereafter referred to as  $\Delta T_{panel}$ .

For the duration of each emission period, aerosols were released from a pneumatic generator of sodium fluorescein, rented from TechSystemes, at a calibrated average rate of 33.9 mg h<sup>-1</sup>. The calibrated mean diameter of fluorescein aerosols was 0.138 μm. This diameter was within key range relevant for the soiling of urban building facades (Horvath *et al.*, 1996); it was also close to the median diameter of 0.24 μm from Maro *et al.* (2014). Emitted aerosols were collected on the material samples (for post-analysis) as well as on filters (Nuclepore) of three low volume air samplers (LVSS) operated by pumps (Aquaria CF20e) with volume flow rates of ~2.3 m<sup>3</sup> h<sup>-1</sup>. The LVSSs were used to determine the fluorescein concentration around the panel at locations shown in Figure 1.

## RESULTS

### Micrometeorology

The data collected by the sonic anemometers were analysed to determine characteristics of flow and turbulence during the four emissions, which are presented in Table 1. Parameters included the mean wind speed, turbulent root mean square (rms) velocity, vector-averaged wind direction, and integral length scale of turbulence. The integral length scale,  $L_0$ , was calculated using the spatial autocorrelation function for one minute of streamline velocity data;  $L_0$  for each minute was estimated to be where autocorrelation function became zero and then averaged.

**Table 1.** Flow and turbulence measured by the sonic anemometers and temperature difference between panel and air

Test #	Parameter	Sonic A	Sonic B	Sonic C	Sonic D	Sonic E
1	Wind speed (m s <sup>-1</sup> )	2.29	3.01	2.84	3.10	2.90
	Wind angle* (°)	9.1	9.4	10.1	■	8.2
	rms velocity (m s <sup>-1</sup> )	1.91	1.74	1.66	1.67	1.40
	Integral length scale (m)	20.7	27.7	26.9	24.9	15.7
	$\Delta T_{panel}$ (°C)					-1.28
2	Wind speed (m s <sup>-1</sup> )	2.22	2.83	2.64	2.92	2.70
	Wind angle* (°)	15.8	13.1	12.9	■	9.5
	rms velocity (m s <sup>-1</sup> )	1.91	1.79	1.70	1.76	1.51
	Integral length scale (m)	16.9	22.9	22.3	25.5	19.7
	$\Delta T_{panel}$ (°C)					3.86
3	Wind speed (m s <sup>-1</sup> )	1.17	1.52	1.49	1.52	1.46
	Wind angle* (°)	-6.1	2.6	5.4	■	6.0
	rms velocity (m s <sup>-1</sup> )	0.92	0.85	0.84	0.80	0.72
	Integral length scale (m)	11.5	13.5	12.2	11.8	6.8
	$\Delta T_{panel}$ (°C)					8.32
4	Wind speed (m s <sup>-1</sup> )	1.60	1.79	1.62	1.77	1.62
	Wind angle* (°)	23.7	17.7	16.8	■	11.4
	rms velocity (m s <sup>-1</sup> )	1.48	1.36	1.27	1.38	1.15
	Integral length scale (m)	14.2	20.0	18.1	19.2	15.2
	$\Delta T_{panel}$ (°C)					4.06

\*Wind angle is the angle of incidence of wind with respect to wall and is same as  $\phi$  in Figure 1 and  $\phi$  in future sections.

The results from Table 1, when viewed with consideration of the positions of the sonic anemometer (Fig. 1), demonstrated the similarity of flow patterns during Tests 1, 2, and 4. Incoming flows at Sonic A were slightly incident to the wall, but flow channelized along wall, becoming closer to parallel near the wall. Wind speed increased near the wall, but rms velocity decreased. The wall therefore acts as a local sink of turbulent kinetic energy within the highly turbulent urban canopy layer, which was also reported by Maro *et al.* (2014) during Salifa experiments.  $L_0$  adjustments near the wall demonstrated the tendency of

turbulent eddies to stretch in the wall-parallel direction as they shrink in the wall-normal direction. Test 3 was noticeably different from the others in terms of the turbulence level and, more importantly, the incoming wind direction, suggesting a completely different near-wall flow regime.

### Deposition velocity

The results from chemical analysis via spectrofluorometric technique provided the total mass of fluorescein deposited on each sample and the LVSs' filters. The mass on each sample's surface was integrated over sample's area and the emission duration to calculate the mass flux onto the sample, which is the term in the numerator of Eq. 1. The mean concentration at LVS 1 was obtained by dividing the deposited mass on the filter by the total volume sampled based on pump's flow rate. Eq. 1 was then used to calculate the deposition velocity for each material and emission interval. The average deposition velocities are presented in Table 2 for all Tests and materials, except Leccese stone which failed analysis possibly due to its porosity. Results indicate that deposition velocity can have great variability, spanning nearly three orders of magnitude in our studied conditions.

**Table 2.** Average deposition velocities ( $\text{m s}^{-1}$ )

	Auto-cleaning glass	Standard glass	Marble	Ceramic
<i>Test 1</i>	$8.17 \times 10^{-3}$	$7.53 \times 10^{-3}$	$1.05 \times 10^{-3}$	$1.03 \times 10^{-3}$
<i>Test 2</i>	$5.27 \times 10^{-4}$	$6.71 \times 10^{-4}$	$6.56 \times 10^{-4}$	$2.94 \times 10^{-4}$
<i>Test 3</i>	$1.75 \times 10^{-4}$	$2.18 \times 10^{-4}$	$2.07 \times 10^{-4}$	$7.1 \times 10^{-5}$
<i>Test 4</i>	$4.16 \times 10^{-4}$	$5.11 \times 10^{-4}$	$2.44 \times 10^{-4}$	$2.49 \times 10^{-4}$
<i>SaliFa2: Test 3</i>	$\sim 1.65 \times 10^{-5}$	$\sim 2.05 \times 10^{-5}$	■	■

### Governing dimensionless parameters

Given the large variability in deposition velocities ( $v_d$ ), it was important to discover what environmental parameters were influencing the differences in the observed  $v_d$ . Dimensional analysis reduced the problem to a few governing dimensionless parameters. On physical grounds, important dimensional parameters would include the characteristics of incoming flow, such as speed ( $U$ ) and direction of mean flow ( $\phi$ ) as well as velocity and length scales for the turbulent eddies ( $\sigma_{rms}$  and  $L_0$ ). Buoyancy in the area near the panel could also impact aerosol transport in the wall boundary layer so  $\Delta T_{panel}$  was used to account for buoyancy effects. The kinematic viscosity ( $\nu$ ) and thermal diffusivity ( $\alpha$ ) of air must also be included. The contributions to  $v_d$  coming from material characteristics of surface and aerosols, such as roughness and thermal conductivity, were encapsulated in a single dimensionless variable,  $\zeta_{mat}$ , to simplify the analysis. Thus, one can write

$$v_d = F\{U, \phi, \sigma_{rms}, L_0, g\beta\Delta T_{panel}, \nu, \alpha, \zeta_{mat}\}, \quad (2)$$

where  $g$  is the gravitational acceleration and  $\beta$  is the coefficient of thermal expansion. Any parameters not included here were either relatively constant between the Tests or assumed to have negligible influence on  $v_d$ . Since there are two basic dimensions and eight parameters, Eq. 2 can be reduced by Buckingham Pi theorem to an expression involving six dimensionless parameters. The relevant parameters are given by

$$\frac{v_d}{\sigma_{rms}} = F\left\{\phi, \zeta_{mat}, \frac{UL_0}{\nu}, \frac{L_0^3 g\beta\Delta T_{panel}}{\nu^2}, \frac{\nu}{\alpha}\right\}, \quad (3)$$

where the final three terms on the right-hand side are Reynolds (Re), Grashof (Gr), and Prandtl (Pr) numbers. A reduction was made by observing that Pr will be nearly constant across a range of urban micrometeorological scenarios. In Tests 1, 2, and 4,  $\phi$  remained in the same quadrant and within range of  $15^\circ$ , so approximately constant as well. Therefore, besides material characteristics, Reynolds and Grashof number were governing parameters of consequence for the present case.

This approach, making use of dimensionless parameters, permitted comparisons of Tests 1, 2, and 4 as well as SaliFa results gleaned from Maro *et al.* (2014) in a sensible way. The approach flow in SaliFa2 was also nearly parallel to wall and the same exact glass materials were used as in our experiment (i.e.  $\phi$  and  $\zeta_{mat}$  were constant). The only required parameter not presented in Maro *et al.* (2014) was  $L_0$ , which was remedied by assuming the same energy dissipation, given by  $\sigma_{rms}^3 L_0^{-1}$ , between SaliFa2 Test 3 and our similar Test 4. Figure 2a below shows plot of deposition velocity (normalised by rms velocity) for

auto-cleaning and standard glass related to  $Gr$ .  $v_d$  was also normalised by  $Re$  to achieve better collapse of data and because  $v_d$  was positively correlated with  $Re$  so possibly a function of combined  $Re$  and  $Gr$ . Differences in plotted data in this figure should be dominated by the material characteristics. Figure 2b is similar to Fig. 2a but with SaliFa2 data points removed and, instead, with the ceramic and marble results plotted.

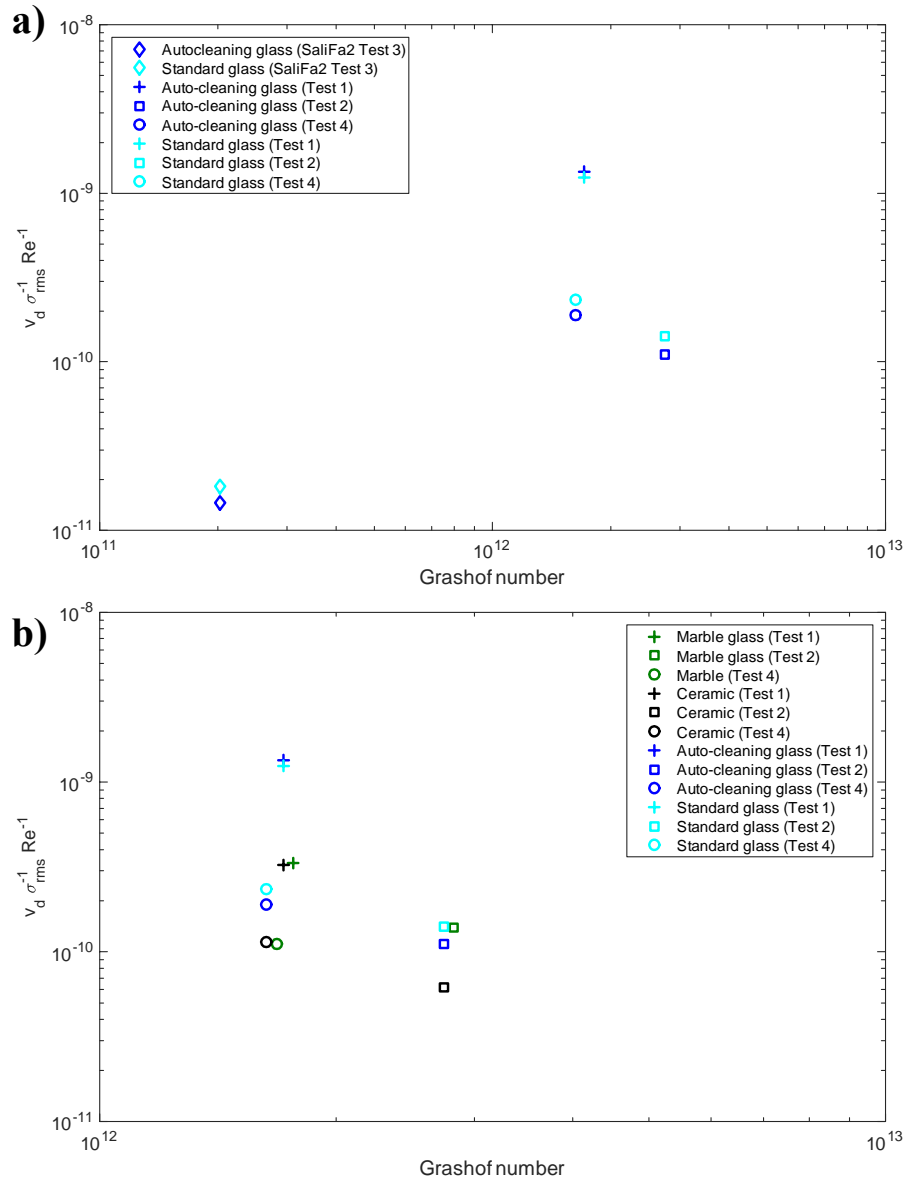


**Figure 2.** Normalised deposition velocities divided by Reynolds number plotted as a function of Grashof number. (a) Results for glass materials from Tests 1, 2, and 4 are shown along with results extracted from a single test during SaliFa. (b) Results for marble and ceramic from Tests 1, 2, and 4 plotted along with glass material data from (a). Marble data points have been shifted along x-axis slightly so visible.

## DISCUSSION

Comparisons with SaliFa results revealed an order of magnitude difference on the y-axis (see also Table 2). The reason for such a disparity cannot be attributed to the  $\zeta_{mat}$  term because same materials from same manufacturer were used, but the order of magnitude difference in  $Gr$  should be noted. Stronger motions perpendicular to the surface, which accompany higher  $Gr$ , could result in stronger diffusivity and more efficient transport of aerosols through concentration boundary layer. A determination of whether  $Gr$  was

responsible for such large differences would require more measurements at intermediate Gr. Some differences in the experimental conditions not evident in Maro *et al.* (2014), or not included in the governing parameters, must not be disregarded as possible sources of the divergence in experimental results.

The higher deposition velocities during Test 1, even though Gr value were comparable to Test 4 (and even Test 2), could be related to thermophoresis (Di Nicola *et al.*, 2016). Even though Gr was similar when absolute value of  $\Delta T_{panel}$  was considered,  $\Delta T_{panel}$  was negative only for Test 1. Therefore the different behaviour of materials during either negative or positive thermophoresis caused the enhanced values in Test 1. A difference in relationship between standard glass and auto-cleaning glass between Test 1 and all other experiments was also noticed. Auto-cleaning glass was consistently lower than standard glass for Tests 2-4 and SaliFa2 (Fig. 2, Table 2), when the panel was heated due to more solar irradiance. This might be attributed to mechanism of the auto-cleaning glass samples' titanium dioxide coats, which relied on sunlight to unlock their self-cleaning properties (Parkin and Palgrave, 2005).

Marble and ceramic behaved similarly to glass materials as shown in Figure 2b, with Test 1 at highest position on y-axis, albeit substantially lower than glass materials. The rough materials, with the exception of marble in Test 2, had lower  $v_d$  than corresponding glass samples, which was counter to general trend of surface roughness, which causes increased dry deposition from turbulent impaction and interception (Guha, 2008). This finding suggests that in high Reynolds and Grashof number flows, surface roughness – at least on the order of  $<1 \mu\text{m}$  as in our case – has negligible impact on deposition as compared to other material characteristics, such as thermal properties. The differences between results from Tests 2 and 4 were relatively small; therefore in high Gr ( $> 10^{12}$ ) situations with positive buoyancy,  $v_d$  may become independent on Gr. Additionally, in these situations,  $\zeta_{mat}$  may have only minor influence as evidenced by the small, though fairly consistent except for marble, separation of different materials on the y-axis in Figure 2b.

## CONCLUSIONS

A field experiment was conducted in an urban-like environment to investigate the dry deposition of submicronic aerosols onto building materials, which has rarely been studied in real urban environments. Results indicated that buoyancy near the wall and intensity of incoming turbulence influenced the mixing and transport of aerosols in the wall boundary layer. The Grashof and Reynolds numbers were selected as governing dimensionless parameters. At high Gr for the channelized, wall-parallel flow of Tests 1, 2, and 4, the deposition velocity was either on order  $10^{-3}$  or  $10^{-4} \text{ m s}^{-1}$ , depending primarily on whether positive or negative buoyancy conditions existed near the panel, and thereby a predominance of negative or positive thermophoretic velocities, respectively. Material properties played a larger role during Test 1 with cooled panel. When the panel was heated, deposition velocity became relatively constant at high Gr, and  $v_d$  may even become approximately independent on material type so that, for deposition modelling purposes, the materials studied here may be treated the same in high Gr and Re scenarios with positive buoyancy.

The differences between results presented here and Maro *et al.* (2014) illustrated the need for more experiments to draw firmer conclusions on functional relationships between non-dimensional  $v_d$  and Re and Gr. Some of the assumptions made on SaliFa may need to be revisited in future work, and more information from the limited number of experiments performed should be extracted to guide interpretation of the results. Conduct of urban aerosol deposition experiments must become standardized for ease of comparisons while expanding to cover a larger variety of geometrical and micrometeorological cases than Maro *et al.* (2014) and this experiment. An approach with dimensionless parameters, as presented here, enabled comparison of different experiments. While laboratory experiments, as in Rounsard *et al.* (2013), can be advantageous, they are unlikely to achieve the high Reynolds numbers required to fully address some key questions on dry deposition in the urban environment. An advantage of the governing dimensionless parameters selected here were that they do not require direct modelling of turbulence very near the wall, a challenging region for many computational fluid dynamics models. Instead, they do require wall temperature, suggestive of the importance of modelling solar-radiative effects for accurate dry deposition predictions.

## ACKNOWLEDGEMENTS

This research was supported by RESEAUX, a spin-off of the University of Salento ([www.reseaux.it](http://www.reseaux.it)). Patrick Conry was supported by the US Department of Defense (DoD) through the National Science & Engineering Graduate Fellowship (NDSEG) Program. A Notebaert Professional Development Award from the University of Notre Dame partly supported Patrick Conry's participation in this research.

## REFERENCES

- Di Nicola, F., M. L. Vincenti, P. Conry, R. Buccolieri, P. Ielpo, A. Genga, L. Giotta, H. J. S. Fernando and S. Di Sabatino: The role of surface building materials in air quality applications. 17<sup>th</sup> International Conference on Harmonisation within Atmospheric Dispersion Modelling for Regulatory Purposes, Budapest, Hungary, European Association for the Sciences of Air Pollution, 9-12 May 2016.
- Guha, A., 2008: Transport and Deposition of Particles in Turbulent and Laminar Flow. *Annu. Rev. Fluid Mech.*, **40**, pp. 311-341.
- Horvath, H., M. Kasahara and P. Pesava, 1996: The size distribution and composition of atmospheric aerosol at a rural and nearby urban location. *J. Aerosol Sci.*, **37**, pp. 417-435.
- Maro, D., O. Connan, J. P. Flori, D. Hébert, P. Mestayer, F. Olive, J. M. Rosant, M. Rozet, J. F. Sini and L. Solier, 2014: Aerosol dry deposition in the urban environment: Assessment of deposition velocity on building facades. *J. Aerosol Sci.*, **69**, 113-131.
- Parkin, I. P. and R. G. Palgrave, 2005: Self-cleaning coatings. *J. Mater. Chem.*, **15**, 1689-1695.
- Pesava, P., R. Aksu, S. Toprak, H. Horvath and S. Seidl, 1999: Dry deposition of particles to building surfaces and soiling. *Sci. Tot. Environ.*, **235**, pp. 25-35.
- Roupsard, P., M. Amielh, D. Maro, A. Coppalle, H. Branger O. Connan, P. Laguionie, D. Hébert and M. Talbaut, 2013: Measurement in a wind tunnel of dry deposition velocities of submicron aerosol with associated turbulence onto rough and smooth urban surfaces. *J. Aerosol Sci.*, **55**, pp. 12-24.
- Sabbioni, C., 2003: Mechanisms of Air Pollution Damage to Stone. The Effects of Air Pollution on the Built Environment, Imperial College Press, USA, pp. 63-106.

**THE ROLE OF SURFACE BUILDING MATERIALS IN AIR QUALITY APPLICATIONS**

*Francesca Di Nicola<sup>1</sup>, Maria Lisa Vincenti<sup>1</sup>, Patrick Conry<sup>2</sup>, Riccardo Buccolieri<sup>1</sup>, Piera Ielpo<sup>3</sup>,  
Alessandra Genga<sup>1</sup>, Livia Giotta<sup>1</sup>, Harindra J. S. Fernando<sup>2</sup>, Silvana Di Sabatino<sup>4</sup>*

<sup>1</sup>University of Salento, Dipartimento di Scienze e Tecnologie Biologiche ed Ambientali, Lecce, Italy

<sup>2</sup>University of Notre Dame, Environmental Fluid Dynamics Laboratories, Notre Dame, IN, USA

<sup>3</sup>Institute of Atmospheric sciences and Climate, National Research Council, Lecce, Italy

<sup>4</sup>University of Bologna, Department of Physics and Astronomy, Bologna, Italy

**Abstract:** In the general context of air quality modelling, the role of surface building materials is investigated through the analysis of near surface thermal flow characteristics. The consequences for dry deposition on vertical surfaces are analysed using data from a series of controlled releases of fluorescein made in October 2014 at the University of Salento (Lecce, Italy) in an urban-like environment. Data were obtained from a total of 4 one-hour long releases in proximity to a vertical wall on which a panel made of different materials (i.e. glass, marble, ceramic and pietra leccese) was hung while recording. Detailed atmospheric conditions were measured simultaneously and are reported in a companion paper (Conry et al., 2016). Here we focus on the analysis of near-surface thermal flow characteristics and evaluate thermophoretic forces which occur when a strong temperature gradient exists between the surfaces and the environment. Specifically, high-frequency 2D surface temperature data from videos at 10Hz using an infrared thermo-camera were used. Surface temperature data so obtained were combined with air temperature measured by thermocouples positioned close to each material, and one thermo-hygrometer which recorded environmental temperature and humidity conditions, to estimate thermophoretic forces. Computational Fluid Dynamics simulations were used to aid data interpretation.

**Key words:** *building material, thermographic measurements, thermophoretic velocity, CFD*

## INTRODUCTION

Air quality predictions in urban areas are usually done by models which includes the specific modelling of dry deposition via the parameterization of the deposition velocity  $v_d$  which in turn depends upon particle physical properties, characteristics of air flow and surface properties (Piskunov, 2009). In the presence of a spatial gradient of particle concentration, Brownian diffusion moves particles from high concentration towards low concentration areas. This mechanism is predominant for particles smaller than  $0.2\mu\text{m}$  (Hussein et al., 2012). In addition, the movement of particles from a hot surface to colder air is due to the so-called thermophoretic force, and it occurs in the presence of a spatial temperature gradient (Baron et al., 2011). Several studies have dealt with this phenomenon: Nazaroff and Cos (1987) found that the deposition velocity depends on the combination of drift, thermophoretic and Brownian motion; Tsai et al. (1999) found that even for small temperature gradients thermophoresis plays an important role for particles less than  $0.1\mu\text{m}$ .

In urban areas significant temperature gradients at surface-air interface are present, mostly due to the presence of different building materials able to store and release the absorbed heat at different time scales. This influences dry deposition on buildings. Detailed surface temperature fields can be obtained via high-frequency thermographic techniques. In this work we describe the methodology for obtaining high frequency temperature data and use them to evaluate thermal-related forces acting relevant for dry deposition on vertical surfaces. Those data were gathered during a field experiment performed in October 2014 at the University of Salento (Lecce, Italy). The experiment consisted in the emission of an aerosol following the 'fluorescein release technique' presented in Maro et al. (2014). The experiment was followed by the measurement of concentration data of aerosol deposited on different building materials samples (for more details see Conry et al., 2016). We used thermography to highlight the thermal

behaviour of materials commonly employed in building construction and its effect on aerosol deposition, the latter evaluated via Computational Fluid Dynamics (CFD) simulations.

## METHODOLOGY

### Experimental set-up

The experiment followed the method by Maro et al. (2014) and was based on the simultaneous emission of an aerosol consisting of fluorescein and Sulphur hexafluoride (SF<sub>6</sub>) as tracer gas, used to track the plume in the environment close to the wall. The scheme of instrumentation shown in Figure 1a was employed to acquire data on aerosol concentration, temperature, and wind speed and direction at high frequency (20 Hz).

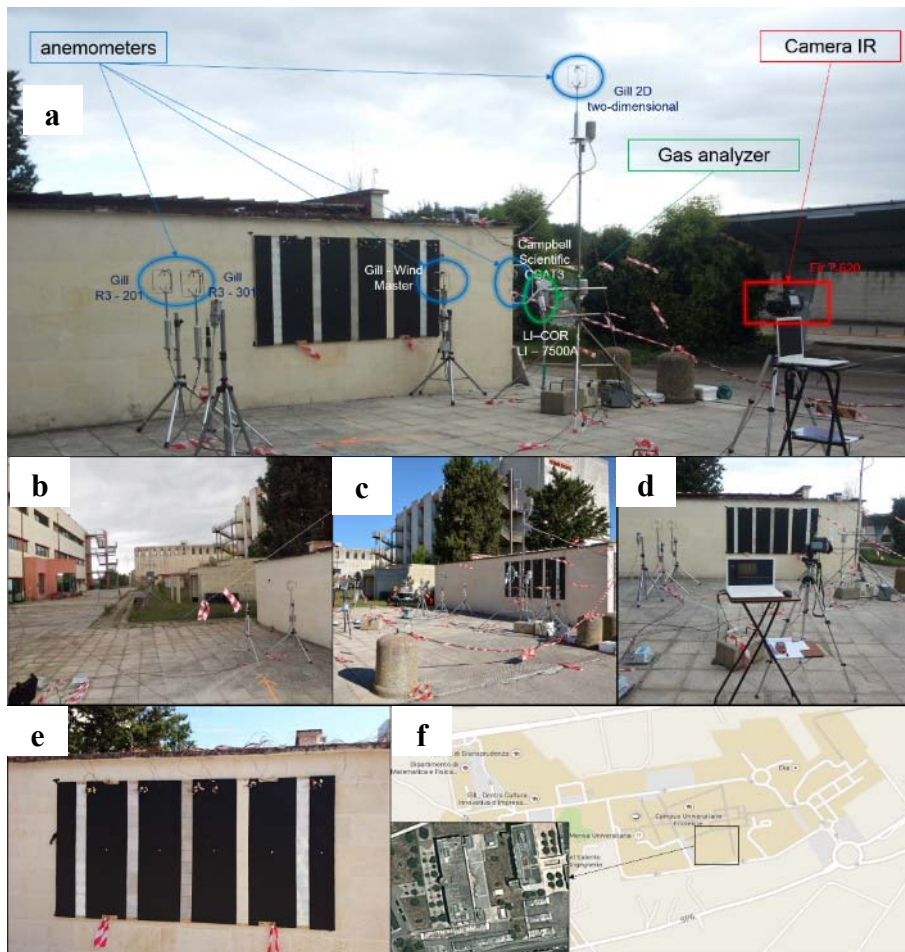


**Figure 1.** a) Experimental set-up; South (b), South-West (c) and West (d) view; e) panel with material; f) aerial view

A wooden panel (OSB3, sizes: 2.50m x 1.25m) was hung up on the façade of a wall facing west and located between two buildings, which formed a wide “street canyon” in the Ecotekne Campus of the University of Salento (Lecce, Italy) (Figure 1b,c,d). The whole experiment was carried out during three days (25 to 27 October 2014). In total, four 1h Tests (Test 1, Test 2, Test 3 and Test 4 hereinafter) were performed. Samples of five different materials were attached to the panel (Figure 1e): standard glass (SG), auto-cleaning glass (AG), marble (M), ceramic (C) and Lecce stone (L) (from left to right in the figure). Each sample was 10cm x 10cm square, with a thickness ranging from 4mm to 1cm. Insulating material (polystyrene) was used to cover the underlying surface of the panel to make uniform the surface and avoid interspaces that could disturb the flow. Further, the insulating material was painted black to

reduce the albedo. The aerosol generator (source) was positioned 6m away from the samples (see Figure 1 of Conry et al. 2016).

The deposition rate was evaluated as (Maro et al., 2014):  $v_d = -J / C_\infty$ , where  $J$  is the mass flux ( $\text{kg m}^{-2} \text{s}^{-1}$ ) of fluorescein aerosol on the wall and  $C_\infty$  is the fluorescein concentration in the air. Chemical spectrofluorometric techniques were used to evaluate concentration of fluorescein deposited on the various samples. Wind speed and direction were also obtained from two sonic anemometers and a wind master placed close to the wall (sonic A, B, and E, respectively, in Figure 1 of Conry et al. 2016). Data from a micrometeorological station placed upstream to the site were used to characterize incoming flow conditions for CFD modelling.

### Temperature data and thermophoretic velocity

Wall temperatures were detected using an infrared (IR) camera, while the boundary layer temperature was detected using thermocouples. High performance FLIR T620 camera IR has been used, with uncooled micro-bolometer 640 x 480 pixels resolution and an image acquisition frequency of 50/60Hz. The camera was mounted on a tripod at a height of 1,32m above the ground and at a distance of 6m from the panel. The camera video mode was employed via the ResearchIR 4.0 software to obtain 2D surface temperature data at 10Hz. For each test, four 15min videos were acquired to cover the entire time of experiment (1h). In post-processing, a specific emissivity was assigned to each pixel to get the temperature and then, for each material, pixel temperatures averages were done to obtain a surface temperature representative of the material itself. For each material, the temperature was also measured by employing two thermocouples (OMEGA Engineering) type K (Chromel/Alumel) which were placed at different distances from surface (Table 1). One thermocouple was also located in the centre of the panel (TC10). A calibration was performed to determine the offset. Air temperature ( $T_{AIR}$ ) was measured using a PT100 resistance thermometer.

The determination of the reflex temperature and the emissivity values of the five materials was done by following a standard procedure (FLIR, 2010): (1) fixing a piece of electrical tape with known emissivity (0.97) on each sample, heat up the sample to a temperature of 10°C degrees higher than the ambient temperature; (2) set the emissivity value of the tape and draw two rectangles, one comprising the tape and the other the sample; (3) change the emissivity value so that the temperature of the sample is the same as that of the tape. The procedure was performed under controlled conditions, i.e. in a closed environment with a single diffuse light source, and with ambient temperature of about 22°C. The samples were fixed on a panel at 1m from the IR camera and three IR images were taken for each material. The emissivity value of the specific material used in post processing was finally obtained as the average of the data obtained from the three IR images for each material.

To assess the contribution of the thermal field on the deposition, the thermophoretic velocity ( $V_{th}$ ) of each material was calculated by using Talbot et al. (1980) equation:

$$V_{th} = -k v \nabla T / T \quad (1)$$

where  $\nabla T$  is temperature gradient,  $T$  is some reference temperature,  $v$  is fluid kinematic viscosity and  $k$  is thermophoretic coefficient which was assumed equal to 0.55, a reasonable value for particles less than 1 $\mu\text{m}$  (Hinds, 1982).  $\nabla T$  was calculated as  $\nabla T = (T_{TC} - T_{IR}) / x$  where  $T_{TC}$  is the boundary layer temperature measured by the thermocouple,  $T_{IR}$  is the averaged surface temperature of material detected by the IR camera and  $x$  is the distance of the thermocouple from the panel.

**Table 1.** Distance of thermocouples and PT100 from the panel and height

	PT100	TC10	FAR					NEAR				
			AG	M	C	L	SG	AG	M	C	L	SG
<b>Test 1 - Distance (mm)</b>	500	138	8	7	11	12	11	1.5	3	4	2	5
<b>Test 4 - Distance (mm)</b>	500	128	9	8.5	10.5	9	9.5	2	2	2	2	1
<b>Height (mm)</b>	1400	1950										

### CFD modelling set-up

3D steady-state CFD simulations were performed by ANSYS Fluent to support field measurements in identifying the influence of near surface temperature gradients on pollutant dispersion and deposition. As a preliminary analysis, we simulated dispersion of a tracer gas (SF6) from a source located at the same position as in the experiment. We considered Test 1 and Test 4 which are characterized by similar meteorological conditions, but different deposition velocities (see Conry et al., 2016). Meteorological conditions used as boundary conditions were those recorded during the experiments (Table 2). Wind velocity was calculated as the mean hourly value, wind direction as the mode of wind direction in the hour. Numerical simulations were performed by employing the standard  $k-\varepsilon$  model (Launder and Spalding, 1979), together with the Fourier equation for temperature. The Boussinesq approximation has been assumed (density and other physical parameters do not change, except for the density in the buoyancy forces term), using thermal expansion coefficient  $\beta=0.0033\text{K}^{-1}$ . The inlet wind velocity, turbulent kinetic energy  $TKE$  and dissipation rate  $\varepsilon$  profiles were specified as follows:

$$U(z) = \frac{u_*}{\kappa} \ln\left(\frac{z+z_0}{z_0}\right) \quad TKE = \frac{u_*^2}{\sqrt{C_\mu}} \left(1 - \frac{z}{\delta}\right) \quad \varepsilon = \frac{u_*^3}{\kappa z} \left(1 - \frac{z}{\delta}\right) \quad (2)$$

where  $z_0=0.08\text{m}$  is the roughness length,  $\kappa$  the von Kàrmàn constant (0.40),  $\delta=13.5\text{m}$  is the computational domain height and  $C_\mu=0.09$ . Symmetry boundary condition was specified at the top and lateral sides of the domain. At the boundary downwind of the obstacles a pressure-outlet boundary condition was used. No-slip wall boundary conditions were used at all solid surfaces. The computational domain was built using about one million elements, with a finer resolution close to the panel (smallest dimension of the elements was 0.025m) (Figure 4a).

**Table 2.** Wind velocity, direction, friction velocity and temperatures of surface used in CFD simulations

Test	Wind velocity at 1.5m (m/s)	Wind Direction	Friction velocity $u_*$ (m/s)	Surface temperature $T_{IR}$ (K)						
				AG	M	C	L	SG	Panel	Wall
1	2.70	330°	0.36	287	287	287	287	287	288	288
4	1.90	330°	0.25	290	291	292	291	292	295	288

The deposition velocity was estimated the model of Lai and Nazaroff (2000) as follows:

$$\frac{v_d}{u_*} = \left[3.64Sc_p^{2/3}(a-b) + 39\right]^{-1} \quad (3)$$

where  $a$  and  $b$  are empirical functions of the particle Schmidt number  $Sc_p$  and Reynolds number  $r+$ . This model has been successfully tested in conditions of building interior smooth wall and low friction velocity. The procedure followed here is the same by Maro et al. (2014), using  $u_*$  in the range 0.23-0.36 m/s as calculated from numerical simulations at a distance of 0.5m from each sample (corresponding to the distance of LVS1, see Conry et al., 2016).

### RESULTS AND DISCUSSION

We considered Test 1 and Test 4 which were characterized by similar meteorological conditions, but different concentration values, i.e. concentrations were much higher in Test 1 (not shown here). We studied the thermal field as lunge to identify its contribution in concentration, by comparing  $T_{IR}$ ,  $T_{TC}$  and  $T_{AIR}$ . For  $T_{IR}$  and  $T_{TC}$  an algorithm was used to remove spikes, and temperature temporal variations were averaged (Figure 2). Averages surface temperature are also summarized in Table 2.

The analysis shows that glasses did not adsorb heat as the ceramic did, while both materials easily lost internal heat. Marble and ceramic were the materials which absorbed and released heat more slowly. As for the different tests, major differences were found between Test 2 and Test 4 which were performed in the morning (Test 1 and Test 3 were instead carried out in the afternoon). The presence of a temperature gradient may have played a dominant role in the different deposition of fluorescein found in Tests 1 and 4. The different thermophoretic force was in fact responsible for moving particles with  $V_{th}$  (Figure 3) depending on the temperature gradient and directed opposite to the gradient itself. In particular,  $V_{th}$  in Test 1 was constantly negative being the material samples colder (about 2°, see Figure 2) than the air close to the sample and with the surrounding air. In Test 4, the thermophoretic velocity was affected by

fluctuations and in some cases (ceramic) also showed positive values. The material temperature was still lower than air close to the sample as in Test 1, but the difference was smaller (about 1°). More important, the surrounding air was in some cases colder than the sample.

By combining experimental data with CFD results we have attempted to evaluate the effect of surface-air temperature gradients on pollutant dispersion. The concentration pattern indicates that the plume was mostly parallel to the wall along the wind direction (Figure 4b). Table 3 summarizes deposition velocities estimated from equation 3 and those estimated by measurements (see Conry et al., 2016). Similar to the experiments, higher deposition velocities during Test 1 were found, confirmed by an increase of gas concentrations obtained in Test 1 (not shown here) when temperature gradients were the largest. However, calculated velocities, although consistent with results by Maro et al. (2014) using the same deposition model, are about two-three orders of magnitude lower than experiments and, further, the velocity diminishes as the distance of the sample from the source increases, thus not capturing higher concentrations at SG (Conry et al., 2016). Further investigations are ongoing to assess these discrepancies which may be due to limitations of the CFD modelling approach as well as the simplicity of the employed deposition model of equation 3. The latter, in fact, takes into account only turbulent transport through the particle concentration boundary layer near smooth surfaces, neglecting other transport mechanisms, such as thermophoresis which, in our case, has been proven to play an important role on particle deposition (Conry et al., 2016).

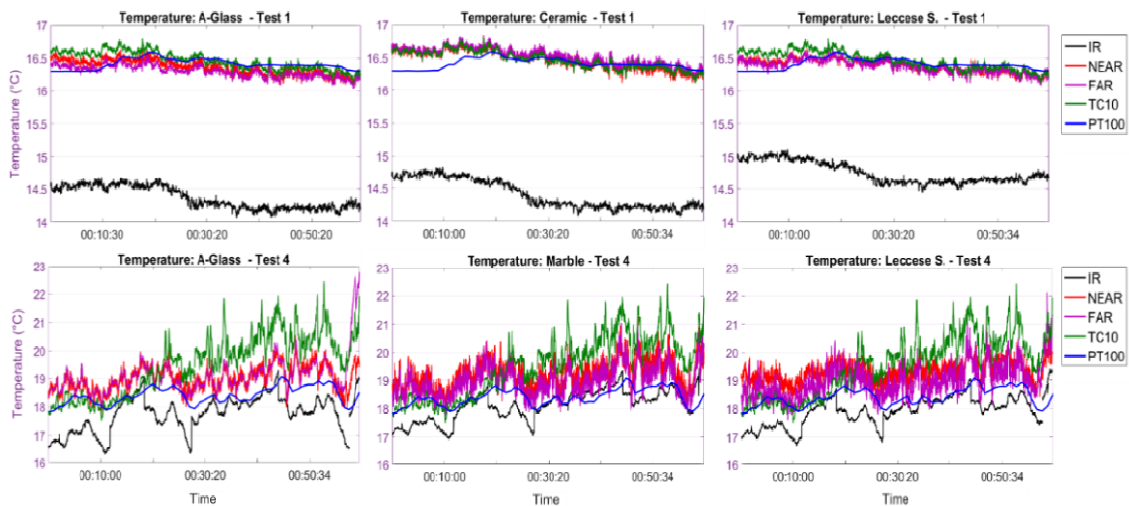


Figure 2. Time series of averages surface temperatures estimated for each material in Tests 1 and 4

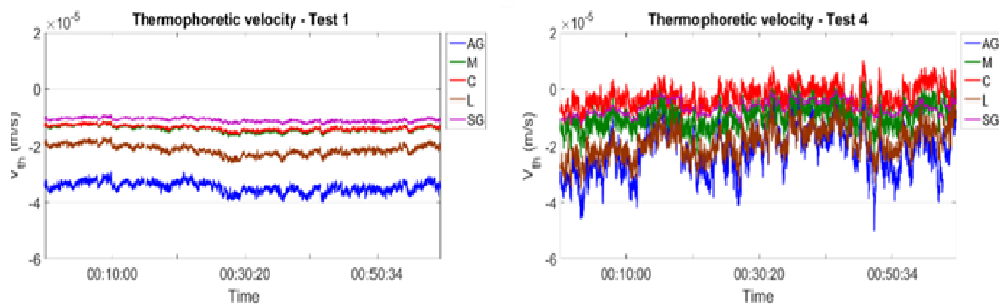
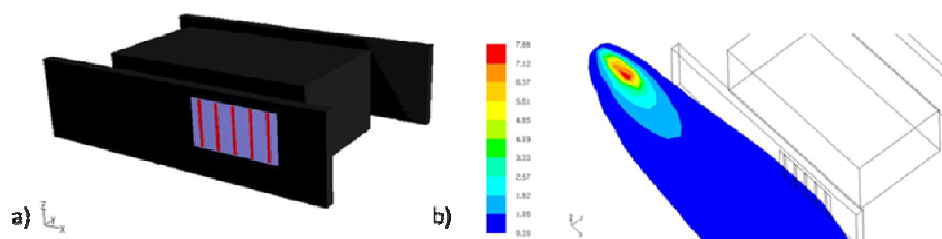


Figure 3. Time series of the thermophoretic velocity estimated in Tests 1 and 4



**Figure 4.** a) Sketch of geometry used in CFD simulations. Violet: panel; red: samples; b) Plume ( $C^*$ ) at source height in Test 4.  $C^*=CH^2U_{ref}/Q$ , where  $C$  is the calculated concentration,  $H$  the building façade height (2.25m),  $U_{ref}$  the reference velocity and  $Q$  the emission rate

**Table 3.** Deposition velocities: model vs. experimental

Test	CFD					Experimental				
	AG	M	C	L	SG	AG	M	C	L	SG
Test 1	$1.44 \times 10^{-5}$	$1.41 \times 10^{-5}$	$1.39 \times 10^{-5}$	$1.36 \times 10^{-5}$	$1.34 \times 10^{-5}$	$8.17 \times 10^{-3}$	$1.05 \times 10^{-3}$	$1.03 \times 10^{-3}$	N/A	$7.53 \times 10^{-3}$
Test 4	$1.00 \times 10^{-5}$	$9.82 \times 10^{-6}$	$9.64 \times 10^{-6}$	$9.46 \times 10^{-6}$	$9.30 \times 10^{-6}$	$4.16 \times 10^{-4}$	$2.44 \times 10^{-4}$	$2.49 \times 10^{-4}$	N/A	$5.11 \times 10^{-4}$

## CONCLUSIONS

A field experiment was performed to investigate the dry deposition of aerosols onto building materials. High-frequency thermographic techniques were employed during the experiment to quantify the thermal behaviour of materials commonly employed in building construction and its effect on aerosol deposition. The aerosol deposition via Computational Fluid Dynamics (CFD) simulations was also evaluated. The use thermographic techniques allow the evaluation of temperature differences between different materials at a frequency close to atmospheric turbulence. It is suitable to study the combined effect of near-surface atmospheric turbulence and buoyancy. The analysis showed the presence of a temperature gradient in Test 1 and 4 and thermophoretic velocity suggests that thermophoresis acted in a decisive way in Test 1 by increasing the deposition of fluorescein greatly. This effect was not captured entirely by CFD simulations, highlighting the need for further development of a deposition model and refinement of wall-parameterizations when temperature gradients are present which can be derived from controlled field and laboratory experiments.

## REFERENCES

- Baron, P.A., P. Kulkarni and K. Willeke, 2011: Aerosol measurement: principles, techniques, and applications, John Wiley & Sons, Inc., Hoboken, New Jersey — 3rd Edition.
- Conry, P., S. Di Sabatino, F. Di Nicola, M.L. Vincenti, R. Buccolieri, P. Ielpo, L. Giotta, A. Genga, L. Valli, G. Rispoli and H.J.S. Fernando: Dry Deposition onto Vertical Surfaces in the Urban Environment, 17<sup>th</sup> International Conference on Harmonization within Atmospheric Dispersion Modelling for Regulatory Purposes, Budapest, Hungary, European Association for the Sciences of Air Pollution, 9-12 May 2016.
- FLIR, 2010: User's manual. Flir reporter professional edition 8.5.
- Hinds, W.C., 1999, "Aerosol Technology: Properties, Behavior, and Measurement of Airborne Particles", John Wiley & Sons, Inc., 2nd Edition.
- Hussein, T., J. Smolik, V.M. Kerminen and M. Kulmala, 2012: Modeling Dry Deposition of Aerosol Particles onto Rough Surfaces, *Aer. Sci. Tech.*, **46**, 44-59.
- Lauder, B.E., D.B. Spalding, 1974: The numerical computation of turbulent flows, *Comput. Methods in Appl. Mech. Eng.*, **3**, 269-289.
- Lai, A.C.K., W.W. Nazaroff, 2000: Modeling indoor particle deposition from turbulent flow onto smooth surfaces. *J. Aerosol Sci.*, **31**, 463-476.
- Maro, D., O. Connan, J.P. Flori, D. Hébert, P. Mestayer, F. Olive, J.M. Rosant, M. Rozet, J.F. Sini, L. Solier, 2014: Aerosol dry deposition in the urban environment: Assessment of deposition velocity on building facades, *J. Aerosol Sci.*, **69**, 113-131.

- Nazaroff WW, Cass GR., 1987: Particle deposition from a natural convection flow onto a vertical isothermal flat plate, *Journal of Aerosol Science*, **18**, 445–55.
- Piskunov, V.N., 2009: Parameterization of Aerosol Dry Deposition Velocities onto Smooth and Rough Surfaces, *J. Aerosol Sci.*, **40**, 664–679.
- Talbot, L., R.K. Cheng, A.W. Schefer, D.R. Wills, 1980: Thermophoresis of particle in a heated boundary layer, *J. Fluid Mech.*, **101**, 737–758.
- Tsai R, Lin ZY., 1999: An approach for evaluating aerosol particle deposition from a natural convection flow onto a vertical flat plate, *Journal of Hazardous Materials*, **B69**, 217–227

**VEHICLE INDUCED TURBULENCE AS KEY FACTOR INFLUENCING POLLUTANT  
DISPERSION IN CLOSE VICINITY OF TRAFFIC PATHS**

*Jiri Pospisil and Miroslav Jicha*

Brno University of Technology, Faculty of Mechanical Engineering, Technicka 2,  
61669 Brno, Czech Republic

**Abstract:** This paper presents an assessment of an influence of turbulence intensity in a vicinity of a linear pollution source on the consequent process of air pollutant dispersion in an urban environment. Pollutant dispersion is monitored at a specific segment of an urban area crossed by a straight traffic path. The traffic path represents a studied linear source of pollution. Vehicles' motion along the traffic path has been considered as an input parameter for the consequent quantification of the kinetic energy generation of turbulence above the traffic path. The influence of generation of the kinetic energy of turbulence by a linear source on the concentration of PM10 at various points of a studied area is obtained by using the mathematical modelling method CFD. Assessment of obtained results defines a relation between the PM10 concentration at a ground-level air layer and the kinetic energy generated by a linear source.

**Key words:** *air pollution, modelling, kinetic energy of turbulence*

## **INTRODUCTION**

Air pollution caused by vehicle traffic represents a significant health risk for inhabitants of urban areas. Prediction tools of immission concentration are required for minimization the impact of pollution on the inhabitants' health quality in the monitored areas. Health risks caused by air pollution are evaluated on the basis of planar maps of immission concentrations. In order to get an authentic planar map of pollution substance concentration within a large urban area it is convenient to combine local immission concentration measurement output and mathematical modelling of planar concentration maps. A typical feature of urban areas is a complex area geometry. Existing buildings together with a surrounding greenery considerably influence the air flow and form unique velocity fields. Several authors have recently presented varied mathematical models enabling solution of pollutant dispersion in urban areas. A number of these models is based on a finite volume method (Computational Fluid Dynamic). Such software tools are highly elaborate and enable correct solution of general issues from the field of fluid mechanics. Application of CFD represents one of the most valid approaches of solving pollutant dispersion in areas with a highly complex surface geometry.

Pollutant dispersion in urban areas is mostly influenced by wind. Air velocity field in a close vicinity of traffic paths with dense traffic is further influenced by vehicles' motion. Moving vehicles drag a mass of air in the motion direction and generate a large number of turbulent eddies (Sabatino S. Di et al, 2003). These phenomena prove to be a crucial factor in the air pollutant dispersion in a close vicinity of vehicles in motion. The turbulent character of the flow at close vicinity of the pollution source significantly affects the consequent air pollution dispersion into the environment. This study focuses on the assessment of how the intensity of turbulence in a vicinity of a linear pollution source influences the consequent process of air pollutant dispersion in urban areas.

The kinetic energy of turbulence is a parameter quantitatively expressing a turbulent character of an air flow. It expresses the mean kinetic energy per unit mass associated with eddies in turbulent flow. Mathematical expression of the kinetic energy of turbulence builds on the basic precondition that the total velocity of air can be expressed as a sum of a mean air velocity and a fluctuation velocity component.

Ascertaining the fluctuation velocity components in a Cartesian system enables to determine the kinetic energy of turbulence by a relation

$$k = \frac{1}{2} \left( \overline{(u'_1)^2} + \overline{(u'_2)^2} + \overline{(u'_3)^2} \right), \quad (1)$$

where  $k$  is the kinetic energy of turbulence and  $u'_i$  is the fluctuation velocity component in particular axis of a Cartesian system.

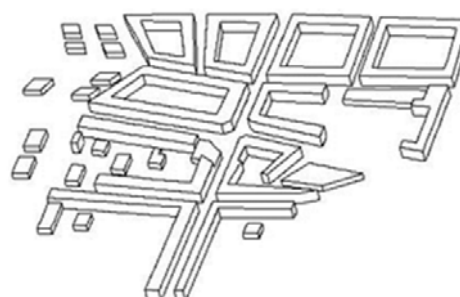
## GEOMETRY OF NUMERICAL MODELS

A characteristic configuration of buildings to be frequently found in urban built-up areas has been selected for a parametric study. In particular, a configuration of adjacent buildings forming a system of perpendicular street canyons has been selected, see Figure 1.

Dimensions of a typical building have been defined for the given configuration. Consequently a field of characteristic buildings organized in a required spatial configuration has been created. Ground plan dimensions of the area with a detailed building geometry are  $0.5 \times 0.5$  km. Gaps between the buildings and the space above the buildings' roofs has been filled by hexagonal control volumes used for determination of air flow. A computational model has been compiled from 30 horizontal control volume layers. Elements of the smallest dimensions have been used at the bottom control volume layer, namely  $0.5 \times 0.5 \times 0.5$  m. Thickness of control volume layer increases with a growing height above the ground surface. The top control volume layer is situated at the height of 200 m above the ground surface and its thickness is 20 m. A band of ground with an assigned parametric roughness has been considered around the area with a detail buildings' geometry.



a) Ground Plan View of Model Area



b) Buildings Included in 3D Model

**Figure 1.** The Studied Configuration of Buildings

A straight band of control volumes above the traffic path has been singled out in a model area. The designated control volumes represent the trajectory of vehicles moving along the studied straight traffic path. The reserved control volumes are used for assignment of a source of kinetic energy of turbulence and a source of a passive scalar substituting the monitored pollutant. Two-way traffic is considered in the tested case.

The numerical modelling based on control volume technique (CFD) represents the only tool capable to take into account detailed geometry of urban areas, detailed position of relevant PM sources and the interaction between vehicles and ambient air (Pospisil et al., 2005). The software package StarCD has been used to perform this study.

## BOUNDARY CONDITIONS

The numerical model represents merely a part of the actual urban area. The limited size of the numerical model emphasises the importance of appropriate boundary conditions which must correctly substitute the influence of an environment and wind conditions. "Slip wall" boundary condition is assigned to the top face of the numerical model. Side boundaries enable setting the actual wind velocity profile created in a canopy layer as a result of the influence of an ambient urban area. Parametric roughness is specified on the ground surface. Buildings and other obstacles located close to the studied traffic path have been modelled with actual geometry since they directly influence the wind flow field in the canyon.

### Wind Conditions

Wind velocity and wind direction have been assigned as a wind velocity profile prescribed at incoming-air faces of the numerical model. This way enables to consider the influence of an environment on the position of boundary faces using the following formula for a wind velocity profile:

$$\frac{u}{u_{ref}} = \left( \frac{z - d_0}{z_{ref} - d_0} \right)^{0.23} . \quad (2)$$

### Simplified Inclusion of Vehicles in Motion

To simulate traffic, a simplified model for two-way traffic roads developed by the authors is used that takes into account traffic density, speed of vehicles and number of traffic lanes. Vehicles in motion are not physically present in the model area. A simplified model uses source terms in balance equations of the kinetic energy of turbulence and a mass balance of a monitored pollutant substance. Source terms quantification is performed using empirical relations that take into account traffic density, speed of vehicles and size of control volumes passed by vehicles.

Source terms are used in control volumes virtually passed by vehicles. With respect to the assumption of a two-way traffic with an equal traffic density in both directions this study does not consider the "piston effect" caused by individual vehicles' motion. This simplification influences the air velocity field in a close vicinity of the traffic path but it has no impact on the pollutant dispersion into a larger distances from a source. Aerodynamic properties of vehicles in motion are taken fully into consideration when quantifying the generated kinetic energy of turbulence. An assumption is applied that the force of aerodynamic resistance acting against the vehicle motion direction is transferred to the source term of generation of kinetic energy of turbulence. This assumption is correct with respect to the law of conservation of energy and it represents a realistic approach in a counter traffic considering the vehicles' motion influence.

The following mathematical description outlines mathematical equation forms valid for force components in the axis oriented in the direction of vehicle motion. Aerodynamic resistance force acting upon a vehicle is given by a relation

$$F_D = \frac{1}{2} \rho_\infty C_D A_{car} |U_\infty - U_{car}| (U_\infty - U_{car}), \quad (3)$$

where  $\rho_\infty$  is the air density,  $C_D$  is the aerodynamic resistance coefficient,  $A_{car}$  is the front view area of the vehicle,  $U_{car}$ ,  $U_\infty$  are the vehicle speed and the ambient air velocity, respectively.

The power of aerodynamic resistance acting upon a single vehicle in the direction of vehicle's motion is defined as

$$P_{FD} = F_D \cdot U_{car} = \frac{1}{2} \rho_\infty C_D A_{car} (U_\infty - U_{car})^2 U_{car} . \quad (4)$$

The power of aerodynamic resistance is consequently transferred into relevant control volumes using a mathematical model as a volumetric source of generation of kinetic energy of turbulence. Specific value of the volumetric source of generation of kinetic energy of turbulence takes into account the traffic density and control volumes' dimensions used for assignment of a volumetric source

$$S_k = \frac{P_{FD} \cdot n_{car}}{A_{cel} \cdot U_{car}}, \quad (5)$$

where  $n_{car}$  is the traffic density [vehicles/s],  $A_{cel}$  is a cross section of control volumes passed by vehicles.

K-ε RNG model of turbulence has been applied in all carried out calculations.

## CALCULATION RESULTS AND COMMENTS

Control volumes passed by vehicles were used for assignment of emission source. The performed study considered a unity emission generation from a linear source. Geometry of the buildings formed a unique velocity field for particular studied areas. Five receptor points were used for identification of immission concentration in the direction of wind from the linear source. All receptor points were located at the height of 1.5 m above the ground surface.

The performed parametric study was focused on relationship between the immission concentration at receptor points and generation of the kinetic energy of turbulence by vehicles in motion. The study considered the wind velocity of 2 m/s at the height of 10 m above the ground surface. The wind direction was perpendicular to the linear road. A parametric study was carried out for traffic density 360, 720, 1440 vehicles/hour at all considered traffic lanes. The aerodynamic drag coefficient of a vehicle was considered to be 0.37 and the vehicle velocity 50 km/h for all calculated situations.

The carried out studies imply that normalized immission concentration generally increases with the increase of turbulence at the traffic path. Normalized immission concentration increases with the increase of traffic density at the traffic path.

Figure 2 presents a graphical expression of obtained normalized concentration of PM10 and the receptor points for various traffic densities at the traffic path.

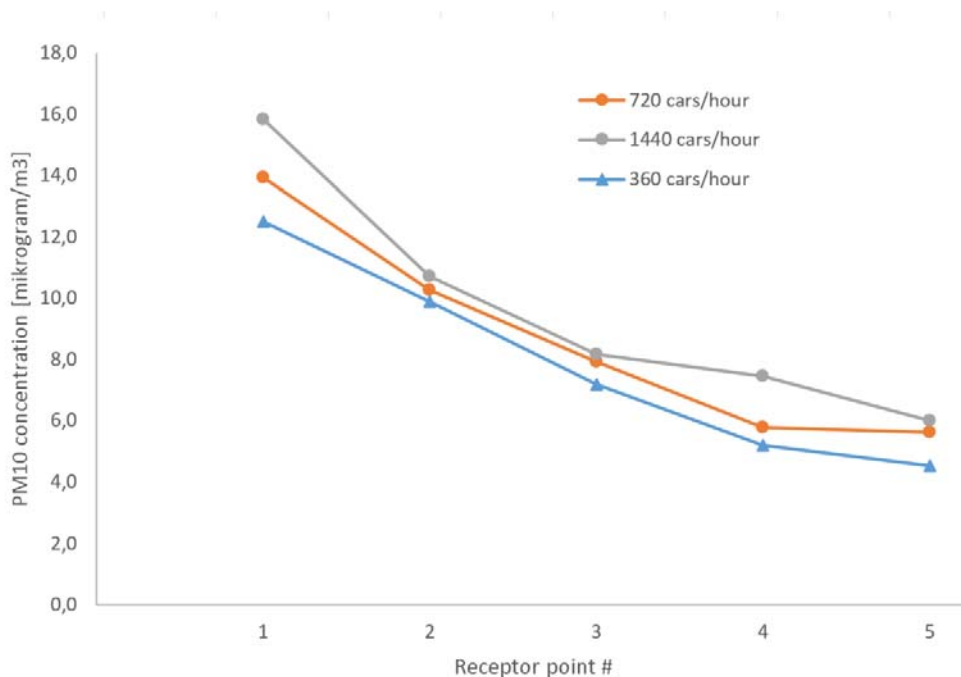


Figure 2. Graphical Expression of Relation between Normalised Concentration and Traffic Density

## CONCLUSION

Turbulent flow structure in a vicinity of vehicles in motion significantly influences the dispersion of air pollutant generated by road traffic into the environment of a traffic path. A higher turbulence intensity results in a greater stir of air. As a result the concentrations of air pollutants in a vicinity of a source are dispersed into larger air volumes. A concentration field in a vicinity of a linear source shows a more uniform pollutant distribution at an increased turbulence rate without significant maximum concentrations. An air pollutant concentration in a vicinity of a traffic path is lower at the human breathing height due to an easier pollutant transfer to higher air layers (above buildings' roofs).

An intense turbulent flow also directly affects the motion of an air mass in street canyons formed by rows of adjacent buildings constructed along a road. Air turbulence is in a direct proportion to a turbulent air viscosity which, along with a physical viscosity, substantially affects the flow interaction with all surface areas included in the numerical model.

The performed study implies that the specific air pollutant concentration in used receptors situated within a model area decreases with an increase of turbulence intensity generated above the surface of a monitored traffic path. Quantification of the turbulence intensity influence on the decrease of pollutant concentration at the human breathing height is dependent on a specific geometry of a model area.

## ACKNOWLEDGEMENT

Presented results were obtained within the project NETME CENTRE PLUS (LO1202), created with financial support from the Ministry of Education, Youth and Sports of the Czech Republic under the „National Sustainability Programme I”.

## REFERENCES

- Sabatino S. Di., Kastner-Klein P., Berkowicz R. Britter R.E. and Fedorovich E., 2003, The Modelling of Turbulence from Traffic in Urban Dispersion Models – Part I: Theoretical Considerations, *Environmental Fluid Mechanics*, **3**, 129–143.
- Pospisil J., Jicha M., Niachou K., Santamouris M., 2005, Computational modelling of airflow in urban street canyon and comparison with measurements, *International Journal of Environment and Pollution*, **25**, 191-200.

**17th International Conference on  
Harmonisation within Atmospheric Dispersion Modelling for Regulatory Purposes  
9-12 May 2016, Budapest, Hungary**

---

**SIMULATING TURBULENT AIR FLOWS IN CENTRAL LONDON AND  
STUDYING EFFECT OF TALL BUILDINGS**

*Elsa Aristodemou<sup>1,2</sup>, Luz Maria Boganegra<sup>1</sup>, Christopher Pain<sup>2</sup>, and Alan Robins<sup>3</sup>*

<sup>1</sup>School of Engineering, London South Bank University, London, UK.

<sup>2</sup>Department of Earth Sciences, Imperial College London, London, UK.

<sup>3</sup>Department of Mechanical Engineering Sciences, University of Surrey, Surrey, UK

**Abstract:** We present work associated with the implementation of a validated street-canyon/neighbourhood model that can help assess the air quality within existing building and neighbourhood designs and suggest modifications & improvements in order to produce sustainable, safer, healthier, and more comfortable urban environments. The work was motivated by both the increasing number of tall buildings in central London (“skyscrapers”) and also the recent plans of placing combined heat and power plants (CHPs) within the urban environment. The Large Eddy Simulation (LES) work was initiated after a series of wind tunnel experiments were carried out at the Enflo wind tunnel (University of Surrey) in order to assess the effect of emissions from Combined and Heat Power plants (CHPs) on top of one of the buildings. A series of scenarios were tested in the wind tunnel and mean concentrations and their fluctuations were measured. The LES models were set-up representing the wind tunnel geometries as well as wind conditions. The novel LES methodology implemented uses an unstructured, adaptive mesh and an anisotropic eddy viscosity tensor for the sub-grid scales (based on the anisotropic mesh). The comparisons of the complex turbulent air flows and concentrations between model results and wind tunnel data show a good correlation – less than 20% error between predictions and measured data. We also looked at the effect of tall buildings on the surrounding complex air flows and dispersion of pollutants, using as prime examples the “Walkie-Talkie” building and the Shard skyscraper in central London, UK. Interesting simulation air flow results and dispersion for the “Walkie-Talkie” building are presented.

**Key words:** *air pollution, urban environment, wind tunnel experiments*

## INTRODUCTION

The need for the development and support of accurate urban dispersion models as well as monitoring air quality is widely recognised worldwide. Efficient, fast, and accurate urban dispersion predictions are necessary to assist with improving air quality within the urban environment through optimisation of critical infrastructure and control of emissions. Correct abatement policies require the understanding of the interaction of pollution from different emission sources at different scales, in a turbulent environment. Appropriate air pollution models involve the solution of non-linear equations (advective transport, chemical reactions, and turbulent diffusion) and require accurate predictions of spatial concentration gradients, as these affect both the reaction rates as well as the transport of the pollutants. To achieve this fine/high-resolution spatial grids are necessary; this has been a major issue in the last four decades, with adaptive grid methodologies appearing in the early 1990s by Benson and McRae (1991) resulting in the development of their Dynamic Solution Adaptive Grid Algorithm (DSAGA) on structured grids whilst Tomlin et al. (1997) and Ghorai et al. (2000) were amongst the first to implement an adaptive grid approach on unstructured grids for pollution problems. High-resolution grids are necessary in determining the correct turbulent characteristics of the flow field and understanding the mixing processes and scalar exchange within and above canyons is also crucial in obtaining accurate predictions of the concentration levels (Zhou and Hanna, 2007; Solazzo and Britter 2007). Turbulent flows in air pollution problems have traditionally been dealt with the Reynolds-Averaged Navier-Stokes methodology (RANS), and the well-established k-epsilon turbulence model. However, studies by Coirier et al. (2005) and Di Sabatino et al. (2008) amongst many showed that the turbulent kinetic energy was usually under-predicted and hence

determining the correct turbulent parameters in the k-epsilon turbulent model was a priority – more so perhaps than grid refinement for obtaining accurate turbulent flow predictions. One of the principle concerns in street canyon pollution studies is the transfer of pollutants from within the canyons to the external shear layer at the top of the canyon. Numerical studies by Baik and Kim (2002) and Caton et al. (2003) showed that both the vertical turbulent velocities and the vertical mean velocities are important. The effect of the turbulent intensity conditions at the inlet on the dispersion of the pollution within the street canyons is also discussed in Kim and Baik (2003), and Milliez and Carisimo (2007). These authors also highlight the importance of the turbulence model parameterisation chosen for their k-epsilon model (RANS) in the simulated mean concentrations and fluctuations and their variance.

An alternative and highly favoured and powerful approach to the well-established RANS models has been gaining momentum fast over the last decade – this being the large eddy simulation (LES) - facilitated by the rapid growth in computing capabilities (Walton and Cheng 2002; Baik and Kim 2002; Baker et al. 2004; ). The strength of LES lies in the fact that, in contrast to both the DNS and the RANS approach, it is able to simulate the unsteadiness of the flow and capture the large-scale turbulent structures explicitly whilst the smaller-scale structures are modelled. Modelling the smaller structures requires some assumptions and parameterisations and the sub-grid scale model has been traditionally based on the well-known Smagorinsky-type eddy viscosity model (Smagorinsky, 1963) with subsequent modification and development of a variety of sub-grid scale models over the past three decades (Germano et al. 1991; Porte-Agel, 2004; Kleissl et al. 2006). Adaptive grids have also been implemented in conjunction with the LES method, with one of the earliest works being those of Ghorai et al. (2000) and Wissink et al. (2005). Fully three-dimensional dynamic grid adaptivity for air quality models is relatively new. Constantinescu et al. (2008) show that high resolution grids are needed both near the emission sources of pollution as well further upwind. Aristodemou et al. (2009) and Boganegra (2016) implemented and validated the adaptive LES method represented in this study using mean flows and fluctuations against wind tunnel data. We continue in this study the exploration of adaptive LES on unstructured grids for urban pollution problems for a new building configuration and investigate the correlation between simulated and measured (wind tunnel) mean concentration levels. We also implemented the LES method in the new area around the Walkie-Talkie building (London, UK) (Bernal-Castro, 2015) in order to study the effect of tall building and also look at the effect of the curved design on the developed flow patterns and effect on the dispersion of pollutants.

## **METHODOLOGY**

Modelling realistic urban flows requires a compromise between the steady-state RANS method and the computationally-intensive direct numerical simulation (DNS) method (Coceal et al. 2007). This is achieved through the gaining popularity large eddy simulation (LES), especially when adaptive-meshes are employed (Pope, 2000). The methodology we implement was initially developed by Bentham (2004), and combines a Smagorinsky-type sub-grid-scale turbulence model, with a fully adaptive unstructured mesh that optimizes the numerical resolution (finite element sizes) throughout the flow. Transport of pollutant concentrations is determined by a high resolution method, which is globally high order accurate in space and time and is designed for use with unstructured finite element meshes (Pain et al., 2001). The advection scheme provides robustness and may even be used as a alternative to traditional LES models (e.g. providing additional dissipation) for the pollutant concentration or momentum fields. The model employs a world-leading anisotropic mesh adaptivity method based on mathematical optimization as described in Pain et al. (2001). This method adapts tetrahedral elements to resolve all flow variables, e.g. velocity, pressure, particle concentration, by producing long-thin (anisotropic) elements with large aspect ratios where the physics dictates, such as in boundary layers. This can achieve great computational efficiency for large transient 3-D fluid flow problems and is fully exploited in the computationally demanding urban flows modelled here. For large problems, a tetrahedral-based parallel adaptive-mesh method described in Gorman et al. (2003) is exploited to achieve highly detailed turbulence model results. With the non-uniform adaptive resolution and use of parallel computing, varying building scales can be resolved. Our methodology has been validated against wind tunnel data (Bentham, 2004; Aristodemou et al. 2009; Boganegra, 2016) as collected in the Enflo wind tunnel (Robins, personal communication). The Enflo wind tunnel has been used successfully in many studies of atmospheric air flows and dispersion

(Carpentieri and Robins, 2015; Belcher et al. 2015) and measurements from one of these experiments is being utilised in the current study.

### The LES equations

The equations used are the three-dimensional filtered Navier Stokes equations for mass continuity and momentum, as follows:

$$(1) \text{ Mass Continuity } \frac{\partial \tilde{u}_i}{\partial x_i} = 0$$

$$(2) \text{ Momentum } \frac{\partial \tilde{u}_i}{\partial t} + \tilde{u}_j \frac{\partial \tilde{u}_i}{\partial x_j} = -\frac{1}{\rho} \frac{\partial \tilde{P}}{\partial x_i} + \frac{\partial}{\partial x_j} \left[ \nu \left( \frac{\partial \tilde{u}_i}{\partial x_j} + \frac{\partial \tilde{u}_j}{\partial x_i} \right) + \tau_{ij} \right]$$

$$(3) \text{ Stress tensor components, } \tau_{ij}, \text{ through: } \frac{\partial \tau_{ij}}{\partial x_j} = \frac{\partial}{\partial x_j} \left[ \nu_{jk} \frac{\partial u_j}{\partial x_k} \right] \quad \text{where}$$

(4) Eddy viscosity mode is given by:  $\nu_{ij} = (C_s \Delta)^2 \tilde{S}_{ij}$  and is dependent on the local filter width  $\Delta$  – associated with the anisotropic adaptive mesh. Hence, a unique anisotropic eddy viscosity model is implemented, with the local strain tensor components being given by:

$$(5) \text{ The local strain rate tensor component : } \tilde{S}_{ij} = \left( \frac{\partial \tilde{u}_i}{\partial x_j} + \frac{\partial \tilde{u}_j}{\partial x_i} \right)$$

### Wind tunnel Experiments

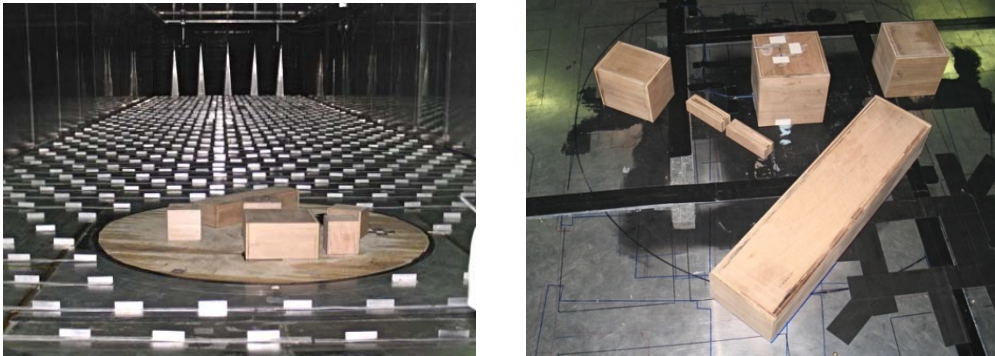


**Figure 1** The complex building configuration in the Enflo wind tunnel, University of Surrey, UK.

The Enflo wind tunnel (University of Surrey) was used to carry out a number of studies with the complex building configuration of interest, as shown in Fig. 1. A total of eight cases were tested representing configurations in which some of the buildings were removed. In the work presented here, the “all-buildings” case was considered. Reference wind velocity was taken to be 2.1 m/s whilst, and mean concentrations and their fluctuations were measured. Four different source locations on top of one of the buildings, were considered (each representing a different tracer), and experiments were also run for four different wind directions.

### COMPARISONS OF LES RESULTS WITH WIND TUNNEL DATA

The LES simulations were carried out on the Dell Precision Tower 7810 computer, with a dual Intel Xeon Processor, until a fully turbulent flow field was produced. The tracer dispersion results are shown in Figs 2 and 3, whilst comparisons with wind tunnel mean concentration values are shown in Fig 4, where a good correlation was found, with less than 20% error in some cases.

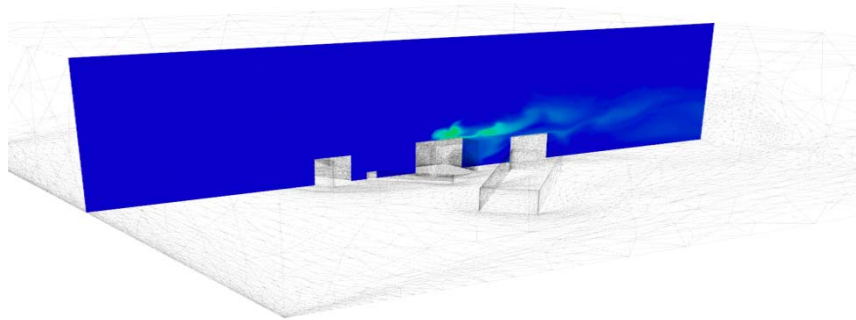
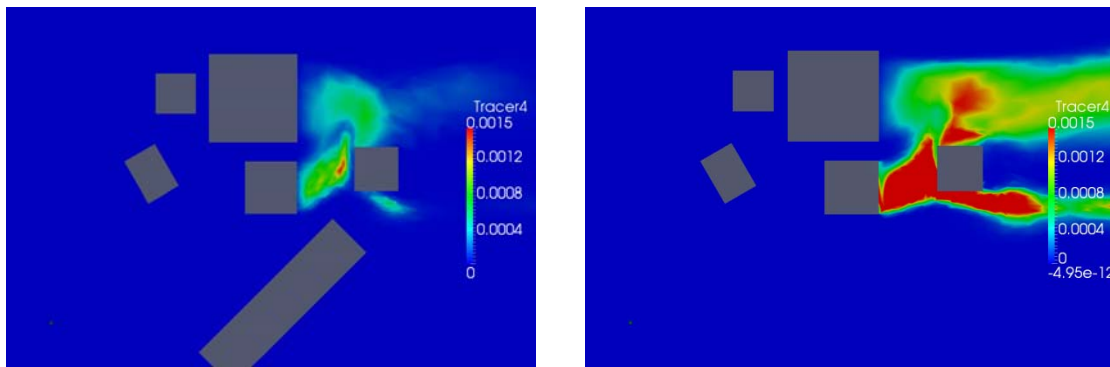


**Figure 2** Vertical Cross-section through centre of computational domain for the dispersion of Tracer 4, with source at top of building.



(a) At Height H=0.05

(b) At height H=1.2

**Figure 3** Case 1: Horizontal views of tracer dispersion (tracer4) at two different heights.

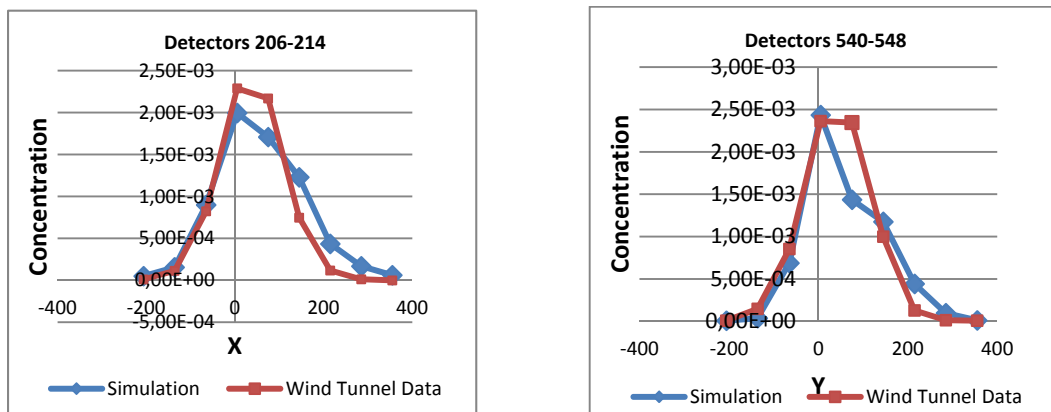
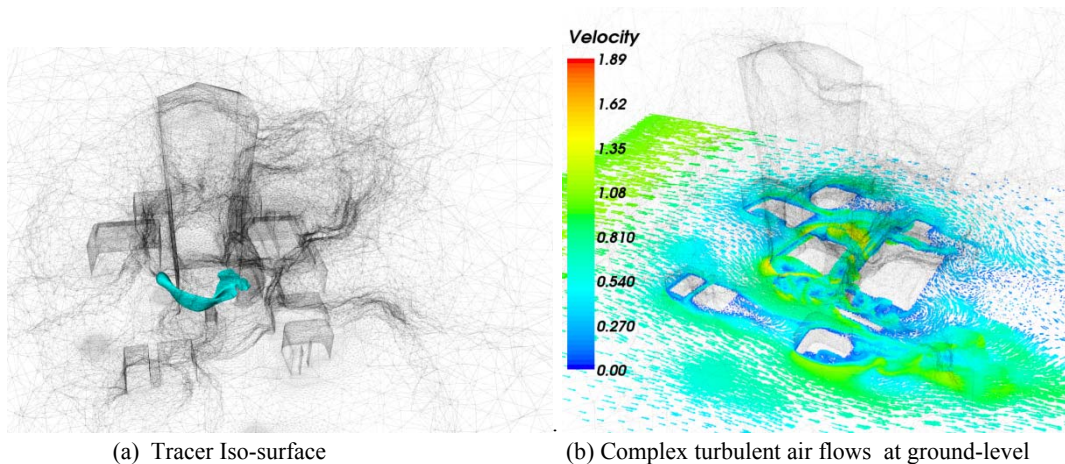


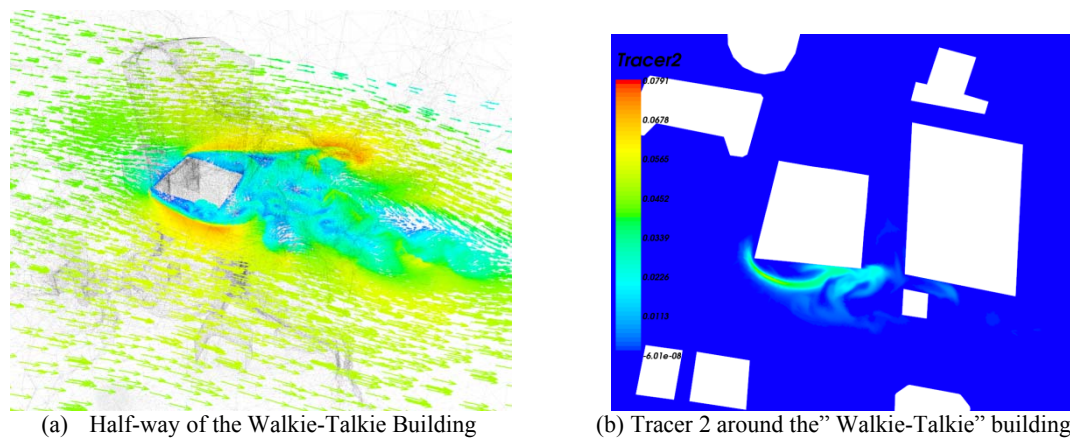
**Figure 4** Comparison of simulated tracer concentrations with wind tunnel measurements from the Enflo wind tunnel.

### EFFECT OF BUILDING DESIGNS ON TURBULENT AIR FLOWS & DISPERSION

The rapidly changing landscape of London has led us to investigate the effect of such tall buildings on the air flow patterns and subsequent dispersal of pollutants. We have chosen to study the effect of the “Walkie-Talkie” building, due to its curved walls and curved roof, as well as its height. A preliminary set of Large Eddy Simulation results are shown in Figures 5 and 6, allowing identification of “dead” zones and demonstrating the effect of the building designs in the surrounding air flow turbulence and subsequent dispersion of pollutants.



(a) Tracer Iso-surface (b) Complex turbulent air flows at ground-level  
**Figure 5** Three-dimensional view of Adaptive mesh-refinement around the “Walkie-Talkie” building area, Central London together with: (a) a tracer isosurface and (b) the complex flow field near ground level.



(a) Half-way of the Walkie-Talkie Building (b) Tracer 2 around the “Walkie-Talkie” building  
**Figure 6** Complex, turbulent flows and dispersion around the “Walkie-Talkie” building area at two different heights.

## CONCLUSIONS

Complex turbulent flows have been accurately captured using an LES approach with a novel anisotropic eddy viscosity model. The LES simulations were compared with wind tunnel data for a particular building configuration, with good correlations between experiments and simulations. The effect of tall buildings and their design on the distribution of “dead” zones has also been investigated, highlighting the importance of detailed modelling in the process of reducing and controlling air pollution within the urban environment.

## ACKNOWLEDGEMENTS

The wind tunnel work was supported by an EPSRC Summer Bursary. The “Walkie-Talkie” building computational geometry was set-up by Carlos Andres Bernal Castro during his Master studies at London South Bank University.

## REFERENCES

- Aristodemou, E., T. Bentham, C. Pain and A. Robins: 2009. *Atmospheric Environment*, **43**, 6238-6253.
- Baik, J. J and J. J. Kim, 2002: On the escape of pollutants from urban street canyons. *Atmospheric Environment*, **36**, 527-536.
- Baker, J., H. L. Walker, X. Cai, 2004: A study of the dispersion and transport of reactive pollutants in and above street canyons – a large eddy simulation. *Atmospheric Environment*, **38**, 6883-6892.
- Belcher, S.E., O. Coceal, E.V. Goulart, A.C. Rudd and A.G. Robins, 2015: Processes controlling atmospheric dispersion through city centres. *Journal of Fluid Mechanics*, **763**, 51-81.

- Benson, R.A. and D. S. McRae, 1991: A solution adaptive mesh algorithm for dynamic/static refinement of two and three dimensional grids: Proceedings of the 3<sup>rd</sup> International Conference on Numerical Grid Generation in Computational Field simulations, Barcelona, Spain, 1991.
- Bentham, T., 2004: PhD thesis, Imperial College, London.
- Bernal Castro, C.A. 2015: Dispersion of air pollutants in central London. Master Thesis, School of Built Environment, London South Bank University, London, UK.
- Boganegra, L. 2016: State of the art modelling of air flows and pollution around a building complex in central London, UK. Master Thesis, School of Built Environment, London South Bank University, UK.
- Carpentieri, M and A.G. Robins, 2015: Influence of urban morphology on air flow over building arrays. *Journal of Wind Engineering and Industrial Aerodynamics*, **145**, 61-74.
- Caton, F. and R. E. Britter and S. Dalziel, 2003: Dispersion mechanisms in a street canyon. *Atmospheric Environment*, **37**: 693-702.
- Coccal, O., A. Dobre, T. Thomas, and S. Belcher, 2007: *Journal of Fluid Mech.*, **589**, 375–409.
- Coirier, W., D. Fricker, M. Furmanczyk, and S. Kim, 2005: A computational fluid dynamics approach for urban area transport and dispersion modeling. *Environmental Fluid Mechanics*, **5**, 443-479.
- Constantinescu, E., A. Sandu and G. Carmichael, 2008: Modelling atmospheric chemistry and transport with dynamic adaptive resolution. *Comput Geosci*, **12**, 133-151.
- Di Sabatino, S., R.B. Buccolieri, B. Pulvirenti and R.E. Britter, 2008: Flow and pollutant dispersion in street canyons using FLUENT and ADMS-Urban. *Environ Model Assess*, **13**, 369-381.
- Germano, M., U. Piomelli, P. Moin and W. H. Cabot, 1991: A dynamic subgrid-scale eddy viscosity model. *Physics of Fluids A*, **3**, 1760.
- Ghorai, S., A. Tomlin and M. Berzins, 2000: Resolution of pollutant concentrations in the boundary layer using a fully 3d adaptive gridding technique. *Atmospheric Environment*, **34**, 2851-2863.
- Gorman, G., C. Pain, C. Oliveira, A. Umpleby, and A. Goddard, 2003: International Conference on Supercomputing in Nuclear Applications.
- Kastner-Klein, P., R. Berkowicz and R.E. Britter, 2004: The influence of street architecture on flow and dispersion in street canyons. *Meteorol Atmos Phys*, **87**,121-131.
- Kim, J.J. and J.J Baik, 2003: Effects of inflow turbulence intensity on how and pollutant dispersion in an urban street canyon. *Journal of Wind Engineering and Industrial Aerodynamics*, **91**, 309-329.
- Kleissl, J., V. Kumar, C. Meneveau, M.B. Parlange, 2006: Numerical study of dynamic Smagorinsky models in large eddy simulation of the atmospheric boundary layer: validation in stable and unstable conditions. *Water Resour Res* **42**, W06D10.
- Milliez, M. and B. Carissimo, 2007: Numerical simulations of pollutant dispersion in an idealized urban area for different meteorological conditions. *Boundary Layer Meteorol.* **122**, 321-342.
- Pavageau, M. and M. Schatzmann, 1999: Wind tunnel measurements of concentration fluctuations in an urban street canyon. *Atmospheric Environment*, **33**, 3961-3971.
- Pain, C., A. Umpleby, C. de Oliveira and A. Goddard, 2001: *Computer Methods in Applied Mechanics and Engineering*, **190**, 3771–96.
- Porte-Agel, F. 2004: A scale-dependent dynamic model for scalar transport in large-eddy simulations of the atmospheric boundary layer. *Boundary-Layer Meteorol* **112**, 81-105.
- Pope, S. 2000: Turbulent flows. Cambridge University Press.
- Solazzo, E. and R. Britter, 2007: Transfer processes in a simulated urban street canyon. *Boundary-Layer Meteorol*, **124**, 43-60.
- Srivastava, R., D. McRae, and M. Odman, 2001a: Simulation of a reacting pollutant puff using an adaptive grid algorithm. *Journal of Geophysical Research*, **106**, 24245-24257.
- Srivastava, R., D. McRae, and M. Odman, 2001b: Simulation of dispersion of a power plant plume using an adaptive grid algorithm. *Atmospheric Environment*, **35**, 4801-4818.
- Walton A., and A.Y.S. Cheng, 2002: Large Eddy simulation of pollution dispersion in an urban street canyon: Part II: idealised canyon simulation.
- Wissink, A., K. Chand, B. Kosovic, S. Chan, M. Berger and F.K. Chow, 2005: Adaptive Urban Dispersion Integrated Model. 86<sup>th</sup> American Meteorological Society Annual Meeting, Atlanta, GA, USA. UCRL-PROC-216813.
- Zhou, Y. and S. Hanna, 2007: Along-wind dispersion of puffs released in a built-up urban area. *Boundary-Layer Meteorol*, **125**, 469-486.

**17th International Conference on  
Harmonisation within Atmospheric Dispersion Modelling for Regulatory Purposes  
9-12 May 2016, Budapest, Hungary**

---

**FLOW AND DISPERSION MODELLING STUDY AT ONE OF DENMARKS  
TRAFFIC HOT-SPOTS**

*Matthias Ketzel<sup>1</sup>, Konstantinos E. Kakosimos<sup>2</sup>, Ulas Im<sup>1</sup>, Thor-Bjørn Ottosen<sup>2,3</sup>, Jørgen Brandt<sup>1</sup>, Steen S. Jensen<sup>1</sup>, Thomas Ellermann<sup>1</sup>, Maria B. Poulsen<sup>1</sup> and Ole Hertel<sup>1</sup>*

<sup>1</sup>Department of Environmental Science, Aarhus University, Roskilde, Denmark

<sup>2</sup>Department Chemical Engineering, Texas A&M University at Qatar, Doha, Qatar

<sup>3</sup>Department of Chemical Engineering, Biotechnology, and Environmental Technology, University of Southern Denmark, Odense, Denmark

**Abstract:** This study aims to investigate in details the pollution situation near one of Denmark's NO<sub>2</sub> hot-spots, the monitoring station at H.C. Andersens Boulevard (HCAB) in Copenhagen. The investigations cover various elements as detailed traffic counts in each of the 7 traffic lanes; wind speed measurements both at a nearby roof station and inside the street canyon and measurements at different locations in the street additional to the main monitoring station. Moreover the study contributes to a further development of the Operational Street Pollution Model (OSPM) that allows handling the inhomogeneous distribution of the emissions over the various lanes and the positioning of the receptor location further away from the buildings. The presentation will give an overview of the study and show the main results and conclusions derived from this comprehensive project.

**Key words:** *Street scale air pollution, OSPM*

## **INTRODUCTION**

HCAB is a street station in the Danish National Monitoring Programme and presently the only monitoring station where the EU limit value for NO<sub>2</sub> is exceeded. This exceedance triggered a lot of interest and research connected with this station. Previously the Danish EPA funded a measuring campaign over several month with a parallel station moved about 3 m further away from the traffic compared to the permanent station (Ellermann et al. 2014). These parallel measurements indicated a relatively large difference of 10 µg/m<sup>3</sup> (18%) between these two locations just 3 m apart.

In order to investigate these small scale air pollution gradients in more details and develop methods to describe these gradients better with OSPM, a new project has been initiated.

The project results help gain a deeper understanding of the complex dispersion situation near HCAB and key findings of the various project elements will be presented. The newly implemented features in OSPM give a much better possibility to describe the measured pollution levels and gradients.

## **METHODOLOGY**

The location of the permanent monitoring station at HCAB close to the 7 traffic lanes is shown in Figure 1. The here-described investigation includes the following experimental elements:

Concentration measurements using passive samplers and small mobile sensors arranged in horizontal profiles along and perpendicular to street orientation to investigate the gradients in NO<sub>2</sub> concentrations (not reported here)

Detailed traffic counts and emission modelling in all 7 driving lanes

Meteorological measurements using sonic anemometers both in the street canon and at the roof top.



**Figure 1.** Map of the location of the measuring station H.C. Andersens Boulevard (read arrow) and the 7 traffic lanes close to it. The cross section for traffic counts and the lane numbering are marked. Lane No.5 is a left exit only lane. The photo on the right side is taken from the roof, close to the red arrow, and shows the traffic lanes but the monitoring station on the right side is hidden.

Based on these experimental inputs as well as previous work conducted by Ottosen et al. (2015) and the suggestions for improvement listed in Kakosimos et al. (2010), this project also includes a further development of OSPM as: the operational implementation of the inhomogeneous distribution of the emissions in-between different driving lanes and enable a variable horizontal positioning of the modelled receptor point between building wall and driving lanes in case of very wide sidewalks or bike lanes as shown in Figure1.

## RESULTS

Some first results from this comprehensive project are given below. Figure1 shows the results from the detailed traffic counts and the estimated NO<sub>x</sub> emissions. The also counted bike/parking lanes are also counted but omitted here due to the negligible NO<sub>x</sub> emissions. The left-turn lane in the middle has as expected lowest emissions traffic and emissions. The outer driving lanes most to the right (No. 2 and 8) are less frequently used by passenger cars and more frequently used by buses and trucks compared to the rest of the lanes. Due to the higher heavy duty share those outer lanes have highest NO<sub>x</sub> emissions.

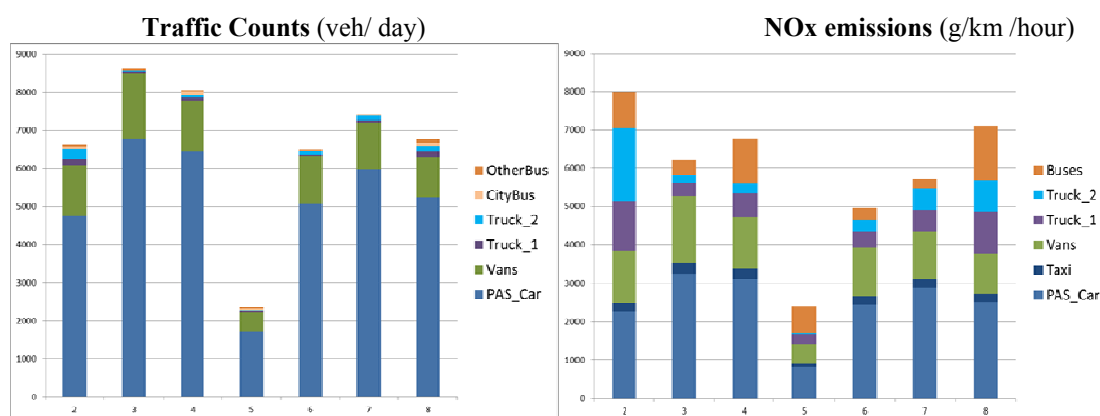


**Figure 2** Left panel: Detailed traffic counts at the 7 driving lanes at HCAB. Lane 2 is closest to the monitoring station; lane 5 is the left-turn lane, see Figure1. Right panel: Average emissions of NOx per lane and vehicle class.

The above mentioned parallel measurements at HCAB in 2014 (Ellermann et al., 2014) have been reanalysed with respect to wind direction. Figure 3 shows the NOx concentration at the two stations with respect to wind direction. This kind of plot has been shown as an important indicator for model evaluation (Ketzler et al. 2012). The relative difference between the concentrations measured at the two stations is larger for the wind directions around 30 compared to 210. For wind direction 30 the stations are located at the so-called leeward side of the buildings along the street and affected by the well-known recirculation vortex. In Figure 2 modelled concentration are plotted as well using the standard OSPM (not taking into account the positioning of the driving lanes and assuming homogenous distribution of the emissions). The results seem to follow much better the measurements from the station2 that was moved 3 m further away from the traffic indicating that especially the elevated concentrations around wind directions 0...90 are underestimated for station1.

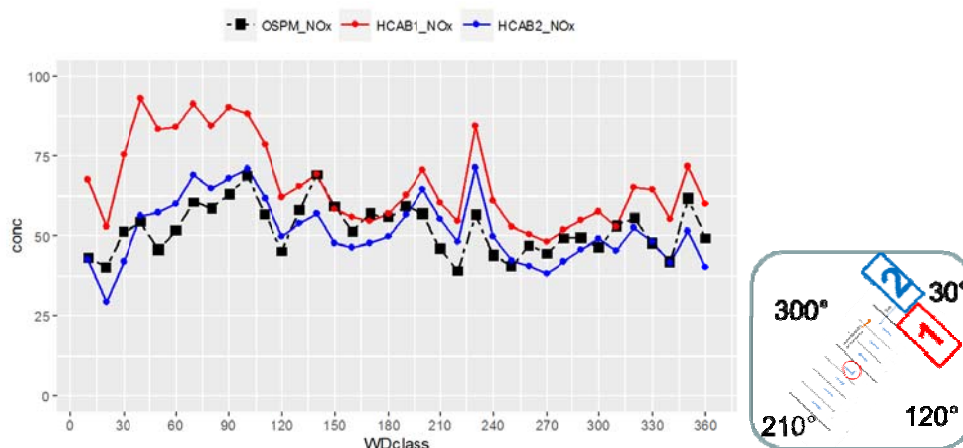


**Figure 3** Mean concentrations of NOx and OSPM model results as a function of wind direction (measured at urban background station) in observation period (8/2 – 23/6 2014) with the two parallel stations at HCAB. The sketch on the right indicates the parallel / perpendicular wind directions with respect to the street orientation of HCAB and the position of the station2 3 meter further away from traffic.

In order to test the new developed OSPM version (Ottosen, 2016) that is able to account for inhomogeneous distribution of the emissions a sensitivity study was performed. The test aims at validating the wind direction dependence of the concentrations under the conditions at HCAB and for the sake of simplicity constant emissions and wind speed is assumed and only wind direction is changed. Results are given in Figure 4 and confirm qualitatively that the model is able to reproduce the increase in concentrations due to a 3 m shift in emissions. The increase in concentrations due to the shift is especially pronounced for wind directions 30...90 replicating a similar behavior as observed in the measurements in Figure 3.

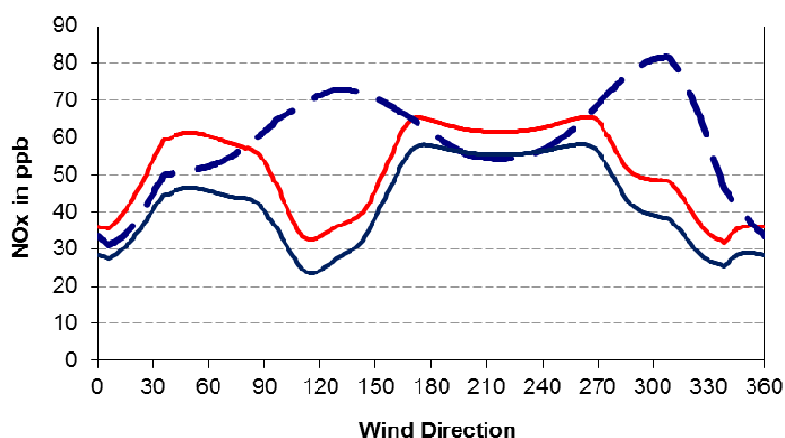


**Figure 4** Sensitivity study using new developed version of OSPM. Dashed line: Standard OSPM with homogeneous emissions. Solid blue line: limit emissions to the seven traffic lanes using correct geometry. Solid red line: Assuming non-homogeneous emissions and moving traffic/emissions 3 m closer to the receptor.

## CONCLUSION

Measurements at HCAB have shown high spatial gradients both in earlier campaigns in 2014. We have gained new insights in the difference measured at two stations by reanalysing the results and plotting against roof wind direction.

For the first time detailed traffic counts and emission estimated per driving lane were obtained. The new OSPM version accounting for in-homogeneous distribution of the emissions is giving a promising first qualitative agreement with the observations.

Future work has to be done implementing a shift of the receptor point (instead emissions) into OSPM.

## ACKNOWLEDGEMENT

This work was supported by DCE-Danish Centre for Environment and Energy at Aarhus University with project funds in fall 2015. The authors are thankful to Copenhagen municipality, especially Åse Boss Henriksen for the good cooperation and performing the detailed traffic counts.

## REFERENCES

- Ellermann, T, Brandt, J, Jensen, SS, Hertel, O, Løfstrøm, P, Ketzel, M, Olesen, HR & Winther, M 2014, Undersøgelse af de forøgede koncentrationer af NO<sub>2</sub> på H.C. Andersens Boulevard. Aarhus University, DCE – Danish Centre for Environment and Energy. Scientific Report from DCE - Danish Centre for Environment and Energy, no. 111
- Kakosimos, K. E., Hertel, O., Ketzel, M., and Berkowicz, R.: Operational Street Pollution Model (OSPM) - a review of performed application and validation studies, and future prospects, *Environmental Chemistry*, **7**, 485-503, 2010
- Ketzel, M., Jensen, S. S., Brandt, J., Ellermann, T., Olesen, H. R., Berkowicz, R., and Hertel, O.: Evaluation of the Street Pollution Model OSPM for Measurements at 12 Streets Stations Using a Newly Developed and Freely Available Evaluation Tool, *Journal of Civil & Environmental Engineering*, **S:1**, 2012
- Ottosen, T-B, Kakosimos, KE, Johansson, C, Hertel, O, Brandt, J, Skov, H, Berkowicz, R, Ellermann, T, Jensen, SS & Ketzel, M, 2015. Analysis of the impact of inhomogeneous emissions in the Operational Street Pollution Model (OSPM). *Geosci. Model Dev.* **8**, 3231-3245
- Ottosen, T.-B.: Improved Local Air Quality Modelling for Complex Urban Landscapes, Ph.D., Department of Chemical Engineering, Biotechnology, and Environmental Technology, University of Southern Denmark, Submitted, 149 pp., 2016

**17th International Conference on  
Harmonisation within Atmospheric Dispersion Modelling for Regulatory Purposes  
9-12 May 2016, Budapest, Hungary**

---

**INTEGRATED URBAN AIR POLLUTION DISPERSION MODELLING FRAMEWORK AND  
APPLICATION IN AIR QUALITY PREDICTION OF THE CITY OF GYŐR**

*Zoltán Horváth<sup>1,2</sup>, Bence Liskai<sup>1,2</sup>, György Istenes<sup>2</sup>, Péter Zsebők<sup>2</sup>, Balázs Szintai<sup>3</sup>, Éva V.P. Rácz<sup>1</sup>,  
László Környei<sup>1</sup> and István Harmati<sup>1</sup>*

<sup>1</sup>Department of Mathematics and Computational Sciences, Széchenyi István University, Győr, Hungary

<sup>2</sup>Research Center for Vehicle Industry, Széchenyi István University, Győr, Hungary

<sup>3</sup>Hungarian Meteorological Services, Budapest, Hungary

**Abstract:** Model accuracy versus model running time - urban air pollution dispersion modellers have to balance between them when selecting models to be implemented. CFD based models seem to be the best candidates for an accurate model that can be validated at urban scale at highest level on the price of a longer running time. In this paper we shall introduce 3DAirQC software framework which addresses a portable and validated CFD model for air quality prediction and control.

**Key words:** *Urban scale modelling, air pollution, CFD, integrated monitoring and modelling.*

## **INTRODUCTION**

Urban citizens are exposed to air pollution at an increased level which causes many premature deaths, see (WHO, 2014). One of the main producer of pollutants in cities is the traffic, which is responsible for emitting more than 40% of relevant contaminants. In order to support policy makers in their job for reducing the risk of health issues computational models have been used for running scenarios for some decades. An overall vision of many stakeholders is the traffic control subject to air quality indicators. The aforementioned computational models can serve as main components in a system integrated with other more traditional tools based on historical and monitoring data and other modelling tools. Although the scientific community has invested significant efforts to develop proper computational models, accurate, fast and easy-to-use models seem to be lacking. The ultimate goal of the research groups of this paper is to fulfil these conditions with developing a portable, modular software framework for urban air quality control called 3DAirQC which is composed of state-of-the-art results and tools of mathematics, scientific computing (including HPC – High Performance Computing) and ICT (in particular cloud computing for providing 3DAirQC as service) as modules of this framework.

In this paper we present the actual state of the software framework, the 3DAirQC, with a demonstration of its application to the city of Győr, Hungary, which is a city of 130.000 inhabitants with strong cross traffic as main emission source. We show validation results as well.

## **THE 3DAIRQC FRAMEWORK AND ITS MODULES**

For the modelling of the dispersion of urban traffic emitted pollutants in particular gases such as NO<sub>x</sub> or O<sub>3</sub>, the Simulation and Optimization Research Group and the Research Centre of Vehicle Industry of the Széchenyi István University, Győr, have developed a software framework, the 3DAirQC. The main goal of this framework is to model air quality indicators of cities capturing real 3D spatial geometry of the towns to be able to compute expositions accurately. Note that for a reliable air quality exposition computation we need high spatial resolution (cell sizes of some metres only) since there is a statistically significant difference of the measured AQ indicators between different points of the street, see e.g. Rácz and Horváth, 2014).

The framework is composed of modules, namely traffic, emission, meteorology, dispersion and the core module, which is either for evaluating assessments or performing optimization or control. An overview of the 3DAirQC workflow can be seen on Figure 1. Note that in this paper we shall confine ourselves to air quality prediction workflow, which is validated and leave the air quality control to a future work when it will be demonstrated and validated.

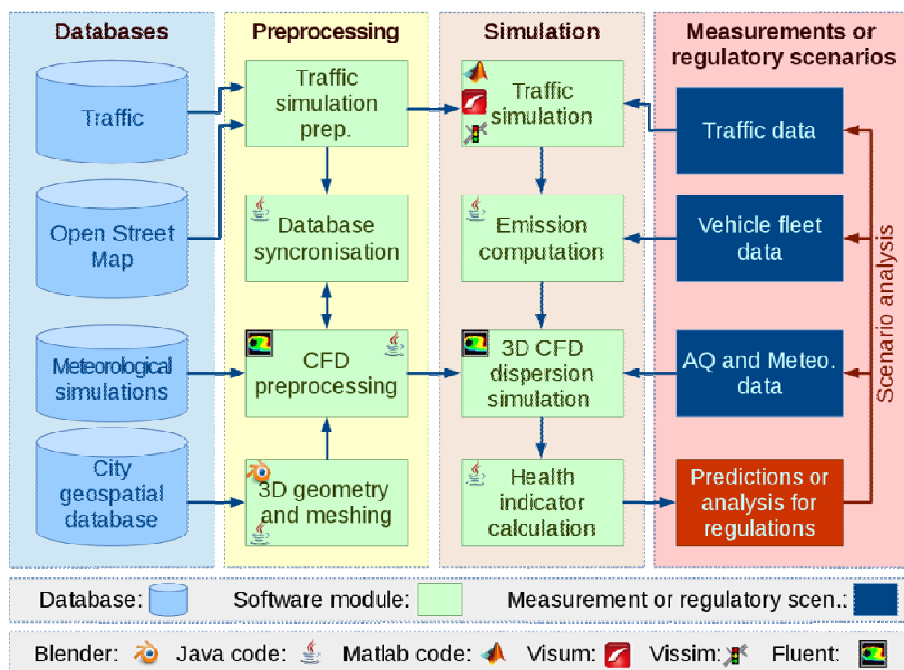


**Figure 1.** An overview of the 3DAirQC workflow for running scenarios for health indicators depending on traffic, fleet and meteorology data or traffic and meteorology measurements and simulations.

### Preprocessing of the data

The preprocessing steps of the simulation modules are based on a toolkit of in-house Java scripts, Blender (see <https://www.blender.org/>) tools for 3D modelling, in-house 3D meshing tools and some commercial tools of ANSYS. All of these steps need normally special and time consuming work, which is done mainly automatically using our tools. For illustration of the tools with geometry preprocessing and meshing see Figure 2 and Figure 3, respectively.

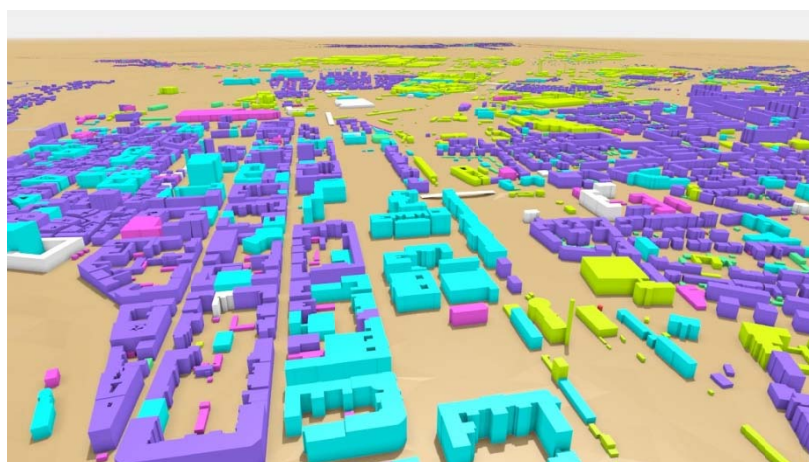


**Figure 2.** CAD geometry of the town resulted from city geoinformatic data base using Blender scripts

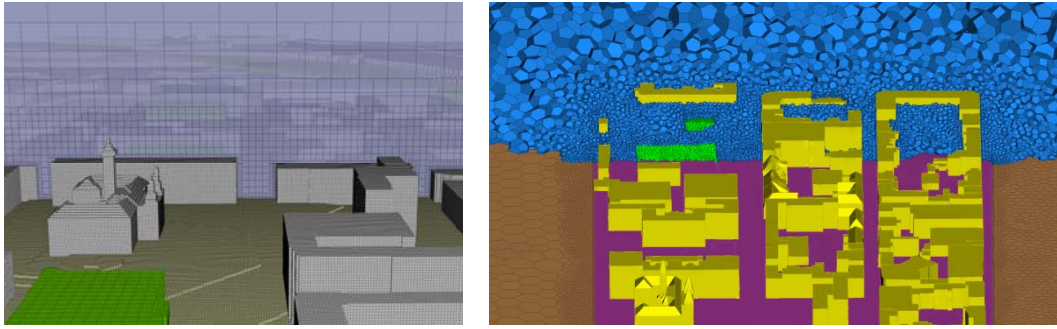


**Figure 3.** An overview of the meshes used in 3DAirQC: octree mesh generated by in-house multi thread Java code (left) and polyhedral mesh resulted from using ANSYS Fluent (right).

### The traffic module

For modelling the urban traffic we have been using macroscopic and microscopic models. These are based on historical traffic count data of a big campaign and monitoring data arising from operational data collected by city and national road authorities. The macroscopic model can be understood as the interpolated result of the operational measured loop data. Since loop data are not available for all road segments, the measurement values are used for calibrating historical data at these segments. In 3DAirQC we have an option to choose PTV VISSIM for microscopic simulation of the traffic as well.



**Figure 4.** An overview of traffic sensor network of the city (on the courtesy of Hungarian National Roads Nonprofit Ltd. -Magyar Közút Nonprofit Zrt).

### The emission module

For modelling the emission of the vehicles in the traffic we use one of the European standard emission model, the COPERT model. Fleet data are adjusted to regional vehicle data. Moreover, in rush hours when in the driving cycles the stop-and-go mode dominates, we used a factor of 1.8 according to the research results in (Fontaras et al., 2014). (Note that in the paper loc. cit. a smaller factor was proposed but that paper tested Euro 5 vehicles and in our case in the bus category Euro 1 and pre-Euro buses are significant.) In a free flow regime, i.e. before and after rush hours, we used the standard COPERT model.

### The meteorology module

For boundary conditions of the dispersion module we used meteorology data from the national official operational data of the Hungarian Meteorology Service (HMS). HMS has been applying the AROME (Application of Research to Operations at Mesoscale) non-hydrostatic numerical weather prediction (NWP) model (Seity et al., 2011) since 2010, see (Szintai et al., 2015) and Figure 5. For the 3DAirQC we interpolated the AROME results at several height to the boundary of the AQ computational domain.

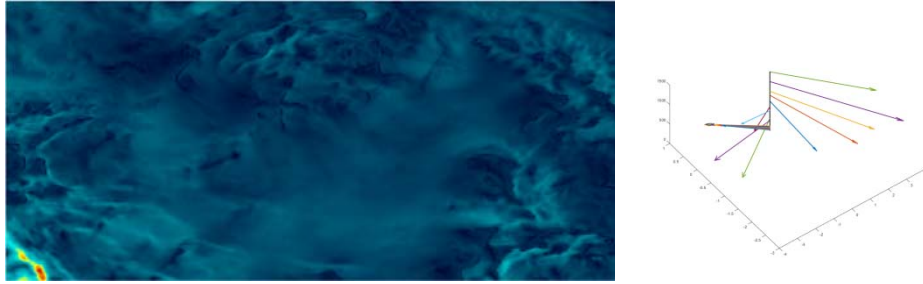


**Figure 5.** AROME simulation data for the Carpathian basin (left) and extracted velocities at several altitudes (right).

### The dispersion module

Dispersion simulation has been done in 3DAirQC with either the commercial state-of-the-art CFD solver ANSYS Fluent or the open source OpenFOAM. There are two options of running these CFD solvers. The first one is the frozen flow field mode where the wind field is precomputed with RANS k-epsilon model and then dispersion of the pollutants with simple advection-diffusion (note that at present only NOx dispersion is computed without reactions). In the second option we compute the wind field and dispersion of the pollutants simultaneously.

The computational time of the full dispersion simulation on a modern laptop with 8 CPU cores takes 4 hours when predicting 4 hours in advance. On clusters, this time is reducible significantly. Note that with the frozen flow field option the advection-diffusion parts, which are repeated many times in optimal control mode of the 3DAirQC takes much shorter, namely just couple of minutes.

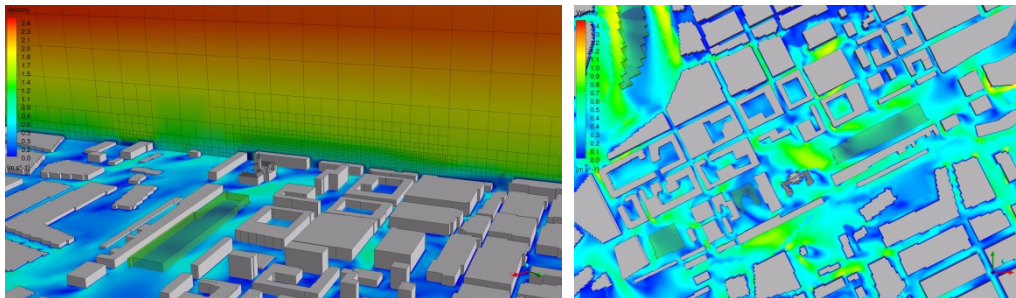


**Figure 6.** Simulation results: wind velocity magnitude.

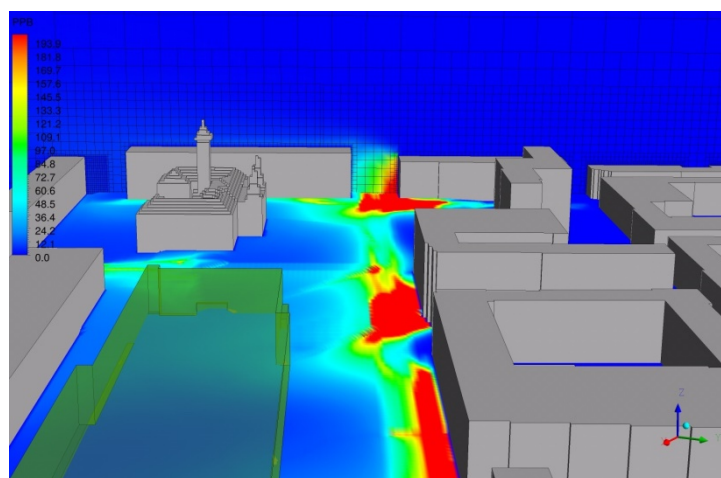


**Figure 7.** NOx concentrations at 1.5m height according to the simulation results.

## VALIDATION OF 3DAIRQC FOR PREDICTION

We applied 3DAirQC to Győr for the time period covering the first rush hours of the day of March 9, 2016. The comparison of measured and simulated data can be seen on Figure 8. The validation of our model is based on high quality measurement data originated from the automata stations of the Hungarian Air Quality Network (HAQN), which is providing official air quality indicators towards the public and EEA. Namely, the validation point is the HAQN station near the junction on Figure 4 (right) and urban background data were taken from the measurement data of the official HAQN point for Győr at Sarród. Comparison of measured and computed data show that 3DAirQC is capable to provide very accurate results before the peak hours and captures pretty well the first maximum near 8am. Concerning the second peak, which seems to be the result of the direction changing of the weak wind (during the validation period the typical wind magnitude was below  $1\text{ms}^{-1}$  and changed direction exactly around 8:10 starting to blow temporary from the polluted region of the street, which could not be captured by CFD on the applied mesh).

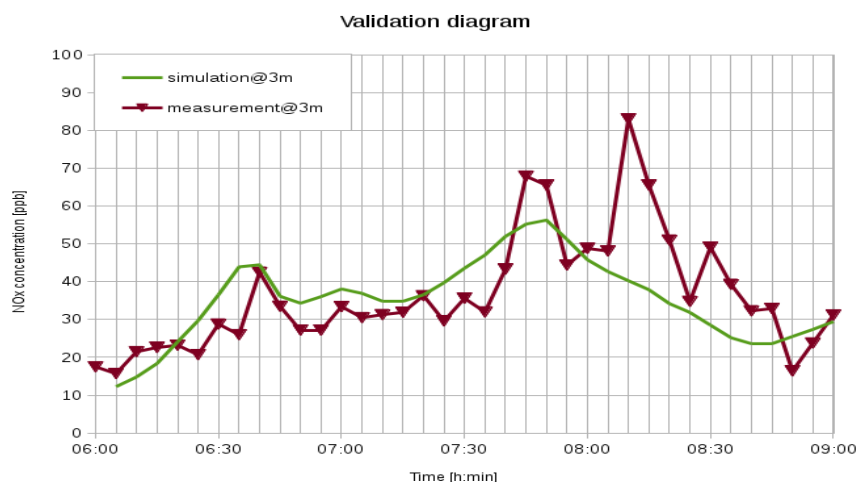


**Figure 8.** Computed and measured NO<sub>x</sub> data at “Győr1” official national air quality measurement container.

## CONCLUSIONS

In this paper we presented the main components and a use case for validation of the 3DAirQC monitoring based model for urban air pollution prediction. More details and steps in the direction of a service, in particular significant improvements of the components are given in the lecture of the conference.

## REFERENCES

- WHO, 2014: Burden of disease from ambient and household air pollution. Report. [http://www.who.int/phe/health\\_topics/outdoorair/databases/en/](http://www.who.int/phe/health_topics/outdoorair/databases/en/)
- Rác, É.V.P. and Z. Horváth, 2014: Small-scale differences of urban NO<sub>x</sub> exposition in field measurement data. *WIT Transactions on Ecology and The Environment: The Sustainable City IX*, 2 **191** 1513-1522.
- Moussafir, J, C. Olry, M. Nibarty, A. Albergel et al., 2013: AIRCITY: A very high resolution 3D atmospheric dispersion modeling system for Paris. Proc. 13th International Conference on Harmonisation within Atmospheric Dispersion Modelling for Regulatory Purposes, 114-118.
- Fontaras, G, V. Franco, P. Dilara, G. Martini and U. Manfredi, 2014: Development and review of Euro 5 passenger car emission factors based on experimental results over various driving cycles. *Science of the Total Environment*. **468–469**, 1034–1042.
- Seity, Y., Brousseau, P., Malardel, S., Hello, G., Bénard, P., Bouttier, F., Lac, C., and Masson, V., 2011: The AROME-France Convective-Scale Operational Model. *Mon. Weather Rev.* **139**, 976–991.
- Szintai B., Szűcs M., Randriamampianina R., Kullmann L. (2015): Application of the AROME non-hydrostatic model at the Hungarian Meteorological Service: physical parametrizations and ensemble forecasting. *Időjárás*, **119**, 241-265.

**GRAMM/GRAL: COMPUTING AIR QUALITY MAPS AT THE URBAN SCALE**

*K. Zink<sup>1</sup>, A. Berchet<sup>1</sup>, D. Brunner<sup>1</sup>, J. Brunner<sup>2</sup> and L. Emmenegger<sup>1</sup>*

<sup>1</sup>Empa, Swiss Federal Laboratories for Materials Science and Technology, Dübendorf, Switzerland

<sup>2</sup>UGZ, Umwelt- und Gesundheitsschutz, Municipality of Zürich, Zürich, Switzerland

**Abstract:** We simulate air pollution at very high resolution at the urban scale for two Swiss cities, Lausanne and Zurich. Combining very detailed emission inventories with high-resolution dispersion simulations, we compute air quality maps at the hourly scale for decade-long periods. Lagrangian dispersion simulations by the model GRAL are forced with high-resolution wind fields computed by the nested system GRAMM/GRAL: the meteorological mesoscale model GRAMM computes large scale wind fields forcing the microscale computations by the CFD model GRAL accounting for buildings and fine scale turbulence. Instead of performing transient simulations for the full period of interest, the temporal dynamics are approximated by an hourly sequence of steady-state solutions. This approach, applied to the modelling system GRAMM/GRAL, proved to accurately reproduce pollutant concentrations at affordable computational costs when compared to observations in different parts of the city and at different time scales.

**Key words:** *city scale, PM10, NO<sub>x</sub>, CFD simulations*

## **INTRODUCTION**

Air pollution is a major issue to be dealt with in urban areas. Air pollutant concentrations vary strongly within cities depending on the proximity to emission sources, meteorology, local dispersion, as well as on the background air pollution. To accurately assess air pollution exposure of citizens it is necessary to provide maps of air quality in different parts of the city at a very high horizontal resolution. Such maps can then be used by policy makers for designing effective mitigation measures, by sensitive persons to reduce their personal exposure, as well as in support to epidemiological long-term studies. However, due to the large spatial and temporal variations of pollutant levels in cities, producing such maps requires either dense observation networks or expensive high resolution dispersion models. To date, models capable of simulating the dispersion of air pollutants are usually one of two types: (1) coarse chemistry transport models where the concentrations are averaged over the city or over parts of it; (2) highly resolved CFD models that are too costly to be run on a regular basis for long time periods.

In the present work, we use an integrated modelling system based on the two models GRAMM and GRAL in order to bridge the gap between the two abovementioned types of models by combining the strengths of each of them. The distributed models have been modified to allow high-resolution long-term simulations with reasonable computational costs. The hourly time series of concentration maps are used in the framework of the Swiss Nano-Tera project OpenSense2, which aims at assessing the impact of air pollution on the health of citizens living and working in urban areas by combining dense sensor networks with high-resolution models to enhance results from epidemiological studies.

In the following, we present the assumptions behind the integrated modelling system and the set-up of the models for simulating NO<sub>x</sub> and PM10 concentration maps at 5 m resolution for two Swiss cities, Lausanne and Zürich. The outputs of the modelling system are evaluated with regard to standard air quality observations existing in most cities. In the present paper, we show results for NO<sub>x</sub> only.

## METHOD AND MATERIALS

### Description of the modelling system

The model system is based on two validated models: the meteorological model GRAMM (Almbauer et al., 2009), and the computational fluid dynamics (CFD) and Lagrangian transport model GRAL (Oetl, 2015). The regional model GRAMM computes high-resolution mesoscale wind fields in a domain covering the city and its surrounding area. It accounts for the effects of the topography and of surface fluxes of heat, momentum, humidity and radiation over different land use types. The boundary conditions in GRAMM are driven by typical profiles of temperature, pressure and wind depending on large scale forcing. Using the GRAMM wind fields as forcing initial and boundary conditions, the Reynolds-Averaged Navier-Stokes (RANS) CFD model GRAL resolves the modification of the air flow at the street and building scale in the area of interest. In GRAL, the computation of the turbulence is solved using a standard  $k - \epsilon$  approach. The modified flow field is then used to compute the dispersion of air pollutants from prescribed emissions for a variety of emission sectors (traffic, industry, heating systems, etc.) based on a Lagrangian approach.

Instead of performing transient simulations of the nested system GRAMM/GRAL, the temporal dynamics are approximated by an hourly sequence of steady-state solutions. Thus, a catalogue of typical steady-state meteorological situations is first computed for a large number of physically possible meteorological situations. These situations are defined by discrete values of wind speed, wind direction and atmospheric stability, adding up to 1008 reference situations in the catalogue. Time series of air pollutant concentrations are then generated by selecting the GRAMM wind fields best matching to in situ wind measurements for each hour of the period of interest and by adding and scaling the corresponding contribution of various emissions sectors according to temporal profiles of emission. In the modelling system, the influence of pollution transported from remote sources to the city of interest is accounted for by adding observations of pollution in the rural environment around the city of interest to the simulated concentration maps.

### Set-up for the city of Zürich and Lausanne, Switzerland

We set up the model system for the two urban areas of Zurich and Lausanne. GRAMM was computed at 100 m resolution on domains of 40 x 40 km<sup>2</sup> around the two cities. GRAMM was forced by topological information from the ASTER GDEM2 data set at 30 m resolution and by land use information from the Corine Land Cover data set at 100 m resolution. GRAL was run at 5 m resolution on domains of 5 x 5 km<sup>2</sup> centred on the densest parts of the two cities. The locations, geometry and heights of individual buildings were provided by the local authorities, as well as the magnitude and location of thousands of individual emission objects. In the emission inventories, streets are described as line sources, heating systems and individual stacks as point sources and sources that are difficult to precisely allocate are reported as area sources. The temporal profiles of emissions are based on either measured proxies of their variability (e.g., traffic count for traffic emissions, outdoor temperature for residential heating), or on aggregated temporal profiles deduced from the TNO-MACC inventory for Europe (Kuenen et al., 2011).

Meteorological observation sites used to select weather situations from the pre-computed catalogue are operated by the Swiss Federal Office of Meteorology and Climatology MeteoSwiss. They are located in open areas and winds are measured at 10 m above ground to guarantee a good representativeness and comparability with the mesoscale model. The GRAL concentration outputs are evaluated with in situ observations of NO<sub>x</sub> and PM10 collected in the vicinity of streets or in the rural background by NABEL, the Swiss air pollution monitoring network. Observations from NABEL outside the city of interest are also used to constrain the background concentrations entering the domain of simulation. Regarding the availability of data, time series of hourly concentration maps were produced for the years 2013 to 2014 in Zürich and from 2005 to 2014 for Lausanne.

In the following, we present evaluation results only for the city of Lausanne.

## EVALUATION OF THE MODEL

### Representation of air flow

After matching weather situations to observations in order to generate the hourly sequence of steady-state solutions, it appears that about 200 out of the 1008 pre-computed reference situations in the catalogue represent more than 80% of the hours of simulation. Thus, air flow around the city is dominated by a limited subset of situations due to the prevalence of characteristic wind patterns related to local and regional processes (e.g., topography-driven winds, land-lake breeze, or downhill drainage of cold air in stable atmospheric conditions). When comparing the time series of simulated winds to observations at specific locations in the domain, these typical patterns seem to be well reproduced by the model, despite a general underestimation of wind speeds. Therefore, the approximated approach with a steady-state sequence appears appropriate for describing air flow around the city of interest in a cost-effective way.

At the building-resolving scale, despite the fact that the complex configuration of buildings is not perfectly represented at 5 m resolution, GRAL computes wind speed and direction in street canyons well, as it is shown in Figure 1 for the observation site LAU (top panel). However, the catalogue of wind fields computed by GRAL only accounts for a given status of construction of the city. New or demolished buildings are not represented in GRAL. In the bottom panel of Figure 1, red buildings were present in the model, but were not already built at the time of the measurements. As a consequence, simulated wind speeds are critically underestimated at this location and the direction of air flow is shifted in the model, which has a strong impact on the dispersion of very local emissions.

As for well-established city centres the configuration of buildings does not change drastically over the years (only a few dozen buildings were built or demolished during the window of simulation in our case), we assume that the overall wind flow in the city is represented in a very satisfactory manner.

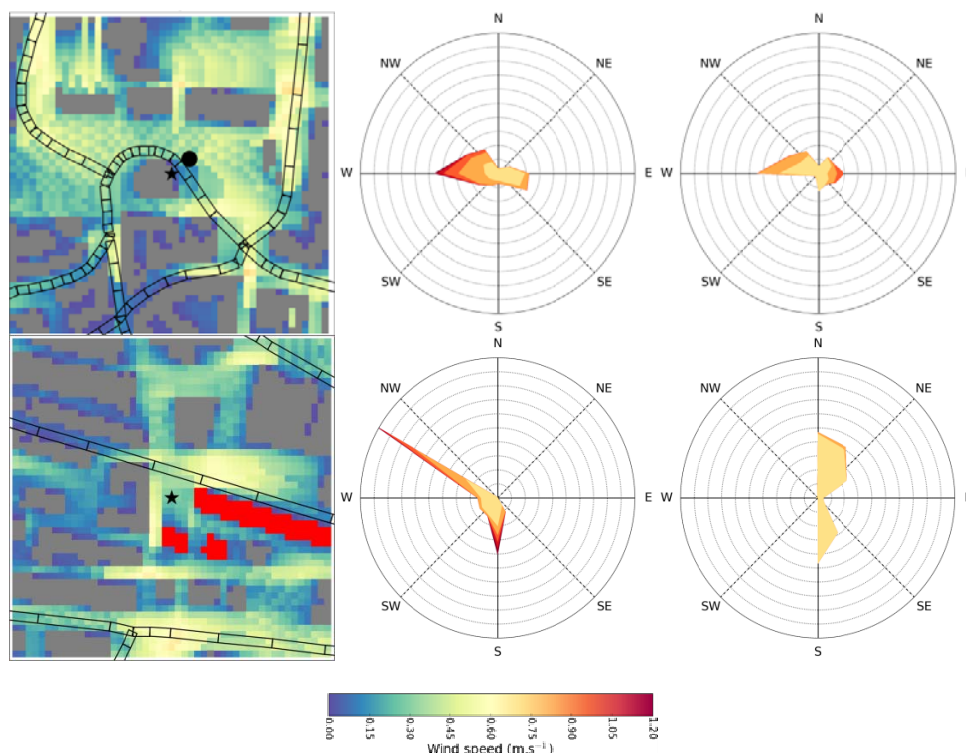


**Figure 1.** Local situation of two observation sites (top: LAU; bottom: DGE07) and observed (left) and simulated (right) wind roses. Observations are located at the black stars. For LAU, the wind measurements (black dot) are slightly shifted compared to the concentration observations (black star).

### Spatial and temporal variability of pollutant concentrations

The time series of concentrations are compared to in situ observations at several different locations in the city (urban background, traffic, city centre). The four sites used for the evaluation of the model in Lausanne are shown in Figure 2, aside quantile-quantile plots. For three of the four sites,  $\text{NO}_x$  concentrations are very well reproduced below  $150 \mu\text{g}\cdot\text{m}^{-3}$ . For these sites, the normalized mean bias is also very low (1%, 2% and 25% for the three sites respectively), proving the capability of the model to reproduce the steep concentration gradients in the vicinity of local emissions and in complex building configurations. As more than 95% of the domain is simulated with concentrations below  $150 \mu\text{g}\cdot\text{m}^{-3}$ , it is expected that the integrated system provides a very reliable spatial distribution of pollutants in the city. The fourth site (blue cross and line in Figure 2) is the same site as in the bottom panel of Figure 1. It confirms that the static catalogue, with no change in the building configuration, can locally diverge from the real situation, and in our case critically underestimate the dispersion of local emissions, leading to overestimated simulated concentrations.

The temporal variability of pollutants is also very well reproduced (no time series shown here). Long-term trends (25% of decrease in observed  $\text{NO}_x$  concentrations in our case) are very well represented when updating the emission inventory according to nationally declared emission trends. The model also manages to represent the year-to-year variability related to changes in meteorological situations between one year and the other. The seasonal cycle of concentrations (winter high related to higher emissions and more stable weather conditions) is also well reproduced, though the timing of the increase (respectively the decrease) of concentrations in autumn (in spring) is generally delayed by a few days to weeks in the model. This is likely related to a hysteresis in the behaviour of citizens when using heating systems, which is not properly reproduced in our system. Synoptic alternation between stagnant and windy situations is very well simulated as well, with a correlation coefficient of 0.8 between simulated and observed daily averages. Thus, the integrated system proves to be very performant for the representation of short-term pollution event. In the case of  $\text{NO}_x$  concentrations, the background deduced from observations in the rural environment around the city plays a marginal role and only at the temporal scales longer than a day. Only a few winter peaks are partially explained by increased background concentrations (associated to large scale stable situations and recirculation of polluted air masses). At the seasonal and yearly scale, the background remains mostly below 10 – 15% of the city signal. Therefore, we can deduce that the steady-state approach is really performant for simulating the short- and long-term variability of pollutant in cities. At the hourly scale, the diurnal cycle of concentrations (mostly related to human activity and emissions) is reasonably well simulated with correlation coefficients of 0.5 – 0.6 depending on the observation site. Nonetheless, at this particular scale, observed concentrations exhibit an already strong correlation to the variability of traffic load (up to 0.5), which mitigates the potential benefits of using a full physics model.

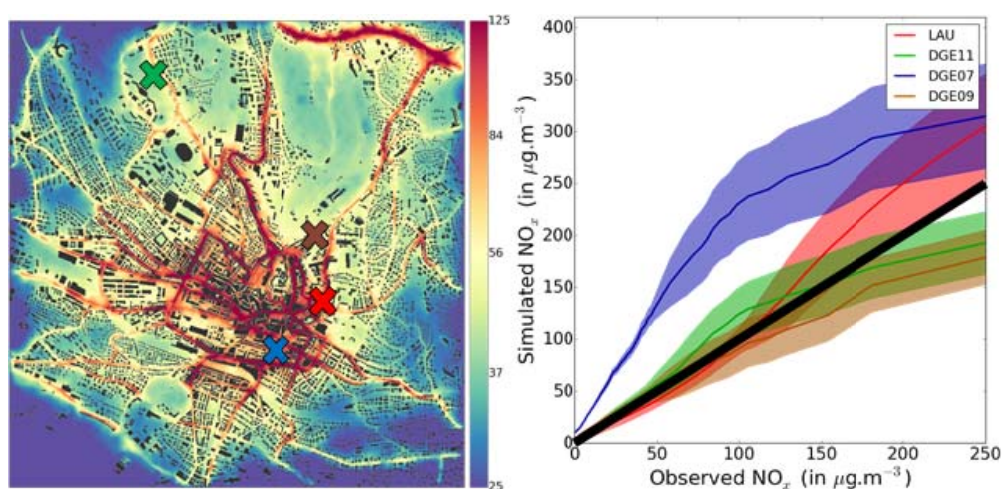


**Figure 2.** Left: yearly average  $\text{NO}_x$  concentrations over the city of Lausanne; location of four evaluation sites. Right: quantile-quantile plot for the four observation sites in Lausanne. The black line is the 1:1 line.

## CONCLUSIONS

We applied a simplified approach for representing the transient evolution of concentration levels at a very fine scale in cities with affordable computational costs. This approach is based on sequencing pre-computed steady-state representative situations. The sequencing is based on in situ observations of winds compared to mesoscale high resolution meteorological simulations. This cost-effective approach proved to be sufficiently accurate when compared to in situ observations of winds and concentrations. The main air flow patterns are represented by the integrated system from the mesoscale to the street level. Thus, the Lagrangian simulations of pollutant dispersion reproduced the spatial distribution of pollutants at a very fine scale and their temporal variability from the hourly scale to the multi-annual trends.

This flexible integrated system can be used for urban planning and pollution abatement measures by policy makers and in support to epidemiological studies for assessing the health impact of pollution on individuals. In this framework, additional active species would be necessary, requiring the development of new modules in our integrated system to simulate the photochemistry and the transformation of particulate matter in a cost-effective way.

## ACKNOWLEDGMENTS

We thank the Direction Générale du Canton de Vaud for providing in situ data in the city of Lausanne and for sharing the CADERO emission inventory for setting our model. We thank the Office de l'Information sur le Territoire du Canton de Vaud (more specifically O. Travaglini) for the 3-dimensional building data set. The office of Environment and Health protection of the city of Zürich provided the emission and building data for the city of Zürich. We thank NABEL network and MeteoSwiss for maintaining permanent measurement sites in the region of Lausanne and freely sharing their data. This work was financed by the Swiss National Fund in the framework of the NanoTera project OpenSense II.

## REFERENCES

- Almbauer, R. A., D., Oettl, M., Bacher, and P. J., Sturm, 2000: Simulation of the air quality during a field study for the city of Graz, *Atmos. Environ.*, **34**, 4581–4594.
- Kuenen, J., H., Denier van der Gon, A., Visschedijk, H., Van der Brugh, and R., Van Gijlswijk, 2011: MACC European emission inventory for the years 2003–2007, TNO-report TNO-060-UT-2011-760-00588, Utrecht.
- Oettl, D., 2015: Quality assurance of the prognostic, microscale wind-field model GRAL 14.8 using wind-tunnel data provided by the German VDI guideline 3783-9, *J. Wind Eng. Ind. Aerod.*, **142**, 104–110.

## **TOPIC 6**

### **USE OF MODELLING IN HEALTH AND EXPOSURE ASSESSMENTS**

**17th International Conference on  
Harmonisation within Atmospheric Dispersion Modelling for Regulatory Purposes  
9-12 May 2016, Budapest, Hungary**

---

**DYNAMIC URBAN POPULATION SIMULATOR**

*Oscar Björnham\* and Håkan Grahn*

Swedish Defence Research Agency

*\* Corresponding author, oscar.bjornham@foi.se*

**Abstract:** Releases of hazardous substances are often investigated using a full chain of models which includes source models followed by atmospheric dispersion models and finally toxicological models that provide the injury outcome for the population in the risk area. A vital component in this chain, that is often neglected or treated on a naïve level, is the exposure model that could be categorized as a part of the toxicological models or positioned after the atmospheric dispersion process. The purpose of an exposure model is to provide the, possible time-dependent, acquired dose for the population. In this work we present an exposure model that treats the synthetic population as dynamically moving individuals in the risk area. A case study is considered where the injury outcome is compared between scenarios utilizing static or dynamic population descriptions.

**Keywords:** *Micro model, Behaviour analysis, Simulation, Modelling, Dispersion, Toxicology.*

## **INTRODUCTION**

In today's society it is of high priority to be prepared for unexpected and sudden events regarding both prevention and ability to handle an ongoing emergency and its aftermath. One situation with possible disastrous result is a release of a hazardous substance in aerosol or gaseous form that is dispersed over a large area in a city. In such a case, the behavior of the population in the area of interest is of most importance to the overall injury outcome. Traditionally, injury assessments in models have been conducted using a static population with a geographical distribution to calculate the exposure dose and thereafter the possible injuries. This method does result in a correct estimate of the total exposure dose of the population but with a distorted exposure distribution on an individual scale. Since the injury outcome for a person often is a highly nonlinear function of the received dose, the total injury outcome of a population is dependent on the exposure distribution and not only the total collective dose.

To improve upon existing scenario tools, we have developed a micro model that allows for simulation of individual movement of the population. The model is called *Dynamic Urban Population Simulator* (DUPS) and is based on a network description of the city. The network captures the geometry, infrastructure, and demography quantitatively which also serve as input data into behavior algorithms that calculate likely paths the population will use depending on the current scenario. The spatial distribution and connectivity of the nodes in the network is a direct reflection of the structure of the city determined from such features as streets, bridges, parks and so on. The citizens, referred to as *agents*, will follow possible paths on this network on an individual level in such a way that the aggregated spatial distribution of the population as well as the distribution over the included types of activities follow user predefined statistics. The idea and mechanisms of DUPS is briefly covered here.

Finally, we present a case study of the Swedish city Norrköping, hosting 23 Seveso-classified companies, using a scenario where a chemical accident causes a hazardous cloud of sulphur dioxide to be transported over the central parts of the city. A comparison over the injury outcome between cases with static or dynamic population models was conducted and is here presented.

## DUPS - AN OVERVIEW

DUPS provides synthetic movement paths for the population in an urban area. The citizens are allocated individual activities that involve being outdoor for a long enough time to possibly be exposed to a hazardous dose of a released substance.

### Purpose and limitations

The task for DUPS is to provide a quantitative description of the movements of the population within an urban area that will serve as a tool for exposure modelling in a scenario including atmospheric dispersion of hazardous substances. This problem is normally restricted to scenarios with distinct spatial and temporal domains. The time span of interest includes the exposure phase of an incident which is assumed to be restricted to a maximum of three hours. The geographical domain is set by the size of a risk area which implies a size of approximately a few hundred square kilometers.

Specifically, DUPS is designed to answer to the following demands and is allowed to hold the following limitations:

- Provide a representative exposure of the population on an individual level after a sudden event.
- Provide the opportunity for agents to interact.
- Provide the opportunity for dynamic behavior alterations of the agents.
  
- Limited to scenario of maximum 3 hours.
- Limited to a geographical domain of a few hundred square kilometers.
- Does not include indoor exposure.

Starting with these demands and limitations, the model DUPS was developed. Structurally, DUPS can be described as a *Time Limited Open Domain Agent Synthesizer*. There are two specifically parts of this description of interest, *Time Limited* and *Open Domain*. The limitation in time refer to the restriction that the model is not expected to be able to handle the population movement for more than three hours which implies that a person that leaves the geographical domain for a time period that is expected to last longer than three hours can be regarded to have left the simulation domain forever. The fact that DUPS is defined using an open domain means that there is no geographical restrictions for the agents. They may enter and leave the resolved region during the simulation.

DUPS includes some additional features that are not discussed in this paper such as walking speeds, breathing frequency, and interactions between agents. For more detailed information regarding DUPS in general as well as the case study the reader is referred to (Björnham, 2013) and (Björnham, 2014).

### PATHBUILDER

DUPS relies on spatial paths on which the agents are dynamically transferred during simulations. A custom made program called *PathBuilder* was constructed to allow the user to set up a spatial network and to insert all other necessary input data.

### Graph theory

A key feature of DUPS is the network (or graph) that describes the urban area. In general, nodes are placed at cross-roads and edges connects the nodes. The idea with this structure is that agents may move between two different nodes following any series of edges that connects the nodes. Any such series of nodes (or edges) is called a *path*. The graph constructed for Norrköping is shown in Figure 1.

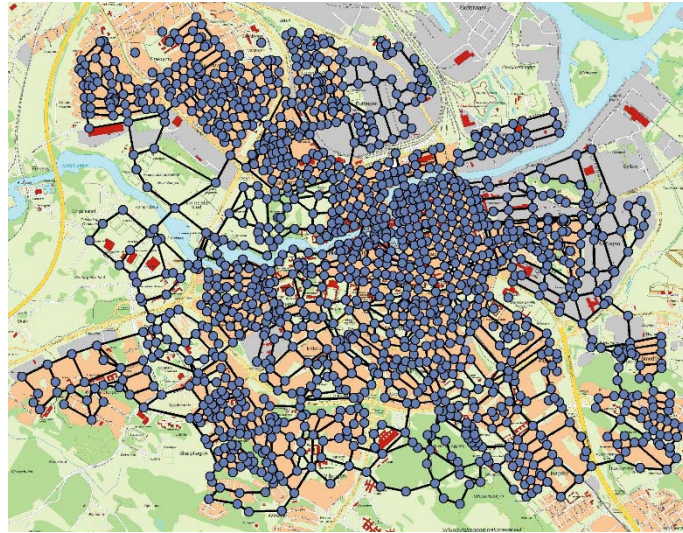


**Figure 1.** The graph over Norrköping contains 1425 nodes (blue circles) and 2110 edges (black lines).

In general there are many possible paths between any two nodes in the graph. It is assumed that people tend to choose one of the shortest paths. There is a commonly used algorithm called A\* to find the shortest path between two nodes in a network. The algorithm uses a distance-plus-cost heuristic function to compare different choices of paths. This is how the algorithm finds the shortest path between a start node and a goal node. All nodes with edges that are directly connected to the start node are compared. The distance to a certain node is the total distance from the start node to that node which in the first step only is the length of the edge. To this distance is a *heuristic estimate* added. This estimate serves as a guide to speed up the search. For this kind of search, the Euclidean distance between the node and the goal node is commonly used as estimate. This implies that edges that geographically leads further away from the goal node are punished. The edge with the smallest distance plus estimate is chosen to be included in the continuing search. In step 2 the same procedure is conducted with the expansion that all nodes connected to the start node or the chosen node are included. For every step the number of chosen nodes grows. This procedure is then repeated until the goal node is reached whereby the shortest path is found. A more detailed description is given by (Hart, Nilsson, & Raphael, 1968). Further on, it is judged unlikely that all people would always choose the exact same path between two nodes if there are several options that only differs marginally in length. To account for this a stochastic element is included in the search algorithm which results in a spread in the distribution of picked paths where the shortest is still the most likely.

### Activities

There are six defined types of activities for the citizens that together span the vast majority of everyday outdoor activities in an urban region, see Table 1.

**Table 1.** There are six different activities in DUPS.

<b>Activity</b>	<b>Description</b>
Walk	A walk with no particular purpose other than the walk itself.
Jogging	A jogging tour.
Shopping	An activity with the purpose of conducting shopping by foot. This activity will mainly be performed in the centrum of the city where most of the shops are located.
To Sink	This activity implies that the agent starts at one node and ends up at another node where it is removed from the simulation. This can typically be the case when the agent are walking from its home to a working place or vice versa.
To Com	The agent is walking to a communication node followed by a certain waiting time to, e.g., enter a bus.
Still	During this activity the agent stays at the same place the entire time. This may typically be used for pupils at a school that are outside for a break.

To conduct an activity equals following a path that has been compiled to represent a likely choice of spatial movement for that particular activity. This means that an agent that is shopping is likely to walk around in the centrum of the city while a person that is out for a walk is most likely to actively choose areas that are generally considered attractive such as parks or riverbanks.

### Creating paths

When an agent is assigned an activity it will follow a representative path that has been constructed for that type of activity. Different nodes are not equally probable to be picked for each type of activity. To take this phenomena into account each node is assigned nine different property values that describe the demography of the region surrounding the node. These properties are *Residences*, *Parks*, *Markets*, *Shops*, *Bicycle Parkings*, *Car Parkings*, *Communications*, *Workplaces*, and *Schools*.

Activities may not be well represented by the shortest path between two nodes. For instance, a walk normally starts and ends at the same node. This is handled by creating a series of subpaths where subpath #2 starts with the same node as subpath #1 ended with. An A\*-search is used to find each subpath and the series of subpaths can thereafter constitute any arbitrary path and still end up at the same node as it started at. A large number of paths was pre-constructed for each activity, see Figure 2. To obtain a likely distribution of path lengths many of them were then discarded and finally six representative sets of paths was stored in a database to be used in simulations.

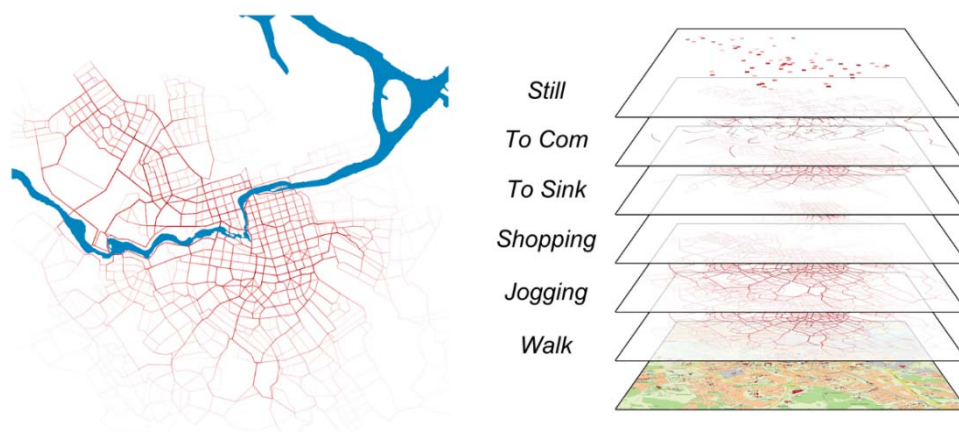


**Figure 2.** A large number of paths for each activity were constructed that together serve as a representation of likely movements for the agents. The paths for the activity Walk is depicted in the left panel where the grade of red represent how commonly the edges are used for this type of activity. The river running through the city is kept in the image to preserve a measure of perspective. The right panel shows the concept that all sets of paths are superimposed on the map to obtain a complete database of possible paths for the simulation.

### SCENARIO

A case study for DUPS was conducted involving a serious accident that lead to the rapid release of one ton of sulphur dioxide. These are the input to the scenario:

- A release of sulphur dioxide takes place in the urban district Sylten southeast of the bridge Hamnbron which is frequently used for transports of dangerous substances in Norrköping.
- The event took place a weekday afternoon at 15.00. It was spring with no extreme weather conditions and no unusual events taking place until the accident.
- Weather: 3 m/s, 12 °C, northeast wind, Pasquill stability class E.
- Release: A 1 cm in radius hole in a tank which creates a leakage that goes on for 4 minutes. The total release amounts to 1000 kg.

When setting up DUPS the user should take into account some scenario input data such as the day of the year, the time of the day and special issues such as possible major events taking place. For instance, people are in general moving from their homes to their workplaces in the mornings and the other way

around at the afternoons. A database consisting of 41.429 paths was constructed for this scenario using the PathBuilder according to the description above. Demographic and infrastructural data were mainly collected from Statistics Sweden and the municipality of Norrköping (Centralbyrån, 2013a, b, c; Quester & Billsjö, 2011). The atmospheric dispersion was treated using the model *LillPello* which is a Lagrangian particle model developed by the Swedish Defence Research Agency.

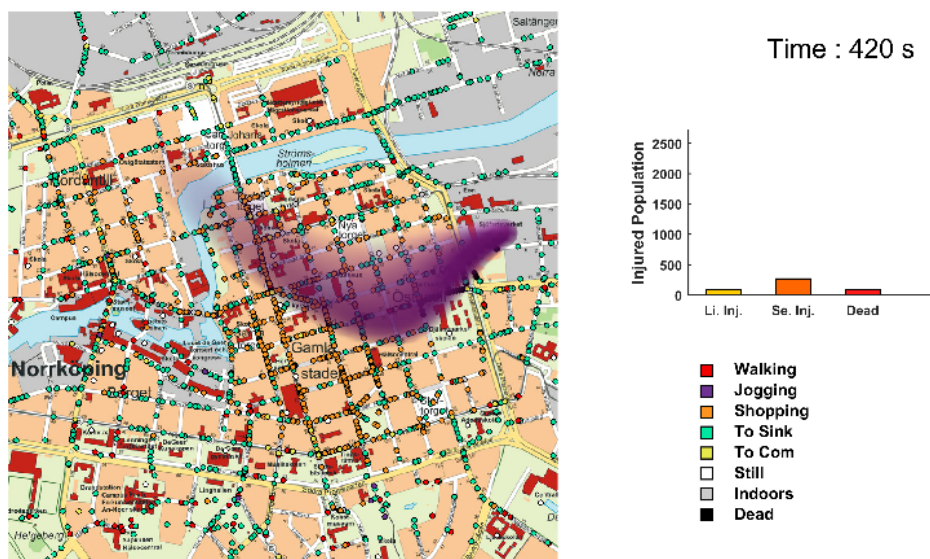


**Figure 3.** Scenario status 420 seconds into the simulation. On the left all agents are depicted as circles that are colour coded according to their activities. The toxic plume is shown as a semitransparent purple cloud. The release has ended at this point in time and the plume is moving along with the wind over the city. As it has passed by some agents has been so heavily exposed that they have died which is shown with a black color on their circles on the map.

Since the time scale of the passing time of the toxic cloud and the movement of the agents are in the same order of magnitude there will be dynamic effects from both on the exposure distribution. There were significantly more injuries with a dynamic population which is explained by the fact that people are moving in and out of the cloud during the scenario, see Table 2.

**Table 2.** The injury outcome of the scenario when static or dynamic population is used.

Injury level	Static	Dynamic
Light injury	283 (29%)	865 (30%)
Serious injury	691 (70%)	2021 (69%)
Dead	11 (1.1%)	24 (0.8%)

This case study showed that DUPS may be implemented in a full chain model and that it has impact on the results. The strong discrepancy between the injury outcomes for two exposure models highlights that the choice of exposure models may be of high importance to the result in these kind of simulations. However, further studies are required before general conclusions may be drawn.

#### ACKNOWLEDGEMENT

This work was conducted with the project *Effect Models* financed by the Swedish Ministry of Defence.

## REFERENCES

- Björnham, O. 2013: Modellering av rörelse-mönster hos en befolkning i en tidsbegränsad öppen domän i urban miljö: Swedish Defence Research Agency.
- Björnham, O. 2014: Parametrisering av DUPS – Fallstudie Norrköping: Swedish Defence Research Agency.
- Centralbyrån, S. 2013a: Arbetstillfällen, delområde, SNI2007, år 2008-2011. In S. centralbyrån (Ed.).
- Centralbyrån, S. 2013b: Befolkning, åldersgrupp, delområde, år 2001-2012. In S. centralbyrån (Ed.).
- Centralbyrån, S. 2013c: Statistiska Centralbyrån. [www.scb.se](http://www.scb.se).
- Hart, P. E., Nilsson, N. J., & Raphael, B. 1968: A Formal Basis for the Heuristic Determination of Minimum Cost Paths. *Systems Science and Cybernetics, IEEE Transactions on*, 4(2): 100-107.
- Qvester, A., & Billsjö, R. 2011: Resvanor i Norrköping 2010.

**17th International Conference on  
Harmonisation within Atmospheric Dispersion Modelling for Regulatory Purposes  
9-12 May 2016, Budapest, Hungary**

---

**EXPLOSION DAMAGE AND INJURY ASSESSMENT MODELLING:  
BALANCING MODEL SOPHISTICATION WITH FINITE RESOURCES**

*Brian Holland<sup>1</sup>, Qiguo Jing<sup>1</sup>, Weiping Dai<sup>1</sup>, Tiffany Stefanescu<sup>2</sup>*

<sup>1</sup>Trinity Consultants Inc., Dallas, Texas, U.S.A.

<sup>2</sup>Trinity Consultants Inc., Charlotte, North Carolina, U.S.A.

**Abstract:** Explosion consequence modelling (ECM) techniques vary significantly in computational complexity. At one end of the spectrum, simple distance-from-blast calculations such as TNT-equivalency and multi-energy methods have utility and are very efficient in terms of computational and labor effort, but have limitations. On the other extreme, computational fluid dynamics (CFD) tools provide a valuable refined modelling capability and are applicable to a wide range of situations, but require a level of resources for a detailed analysis that may be prohibitive for some users.

This paper will present the technological foundations of the BREEZE Explosion Damage Assessment Model (ExDAM), which seeks to fill the “sophistication gap” between purely distance-based simple models and CFD tools. ExDAM builds on a basic empirical phenomenological pressure-impulse vulnerability framework in several ways:

- Explicit estimation of damage and injury effects based on the Physical Vulnerability System (PVS), a phenomenological-based ECM method developed by the DOD after WWII to predict the damage levels of nuclear explosions.
- Accounts for the role of pulse duration in determining the damage incurred by different materials.
- Models the protective shielding effects of structures/individuals on other structures/individuals using finite line doublets from potential theory.
- Able to estimate the secondary fragmentation of materials and resulting injury potential, as well as primary fragmentation from an explosive device.
- Applicable to both vapor cloud and high explosive situations.

Discussion of the model’s capabilities will include the types of situations it is and is not appropriate for, the level of effort required in comparison to other modelling approaches, and the strengths and weaknesses of this approach. Some sample real-world applications of the model will be presented, including both a high explosive and vapor cloud explosion case.

**Key words:** *ExDAM; Explosion Modelling; High Explosive; Vapor Cloud Explosion*

## **INTRODUCTION**

Explosion Consequence Modelling (ECM) techniques vary widely in complexity, from very simple algorithms relying only on distance and explosive type to computational fluid dynamics (CFD) techniques which model the physics of an explosion in great detail. While the most basic pressure-impulse (P-I) curve-based techniques, such as TNT equivalency models, are most appropriate only for explosions of certain materials occurring in flat, open areas, more advanced techniques such as CFD can account for shielding, channeling, reflection, and vapor cloud explosion characteristics such as ignition location, flame speed, and congestion/confinement. However, the time, effort, and expertise required to effectively utilize a model is significantly higher for these more complex modelling approaches. Each type of model is appropriate for certain circumstances. For example, a simple hazard assessment of a chemical stockpile, such as that mandated by the U.S. EPA’s Risk Management Program (RMP) could be conservatively performed using several simple models and does not require the refinement of a CFD analysis. Accurate analysis of a vapor cloud explosion in an offshore platform compartment, on the other hand, requires the consideration of complex geometry that a CFD model can provide.

For some applications, basic modelling approaches are overly simplistic, but a full CFD analysis provides more detail than necessary at a cost that may be prohibitive. The Explosive Damage Assessment Model (ExDAM), originally developed by Dr. Frank Tatom and presently maintained by the BREEZE Software division of Trinity Consultants, takes a high explosive (HE) or vapor cloud explosion (VCE) P-I model as its basis, and adds the ability to model both shielding effects of structures/people and damage and injury to structures/people. As such, ExDAM provides an intermediate ECM tool for predicting incident pressure/impulse that provides more refinement and detail than simple P-I models while requiring less time and specialized expertise than CFD models.

This paper will describe BREEZE ExDAM's HE and VCE models, HExDAM and VExDAM, and discuss application examples with the objective to understand the characteristics, capabilities, and limitations of the model and to demonstrate that the types of scenarios described can be accurately modeled and analyzed using a relatively fast and simple process.

### **ExDAM EXPLOSION MODELS – HISTORY AND COMPUTATIONAL METHODOLOGY**

BREEZE ExDAM provides a phenomenological method to predict damage and injury levels for open-air explosions. Historically, since the mid-1980s, organizations involved in the development of this method include the Strategic Defense Command, U.S. Army Corps of Engineers, Southwest Research Institute, Facility Army System Safety (FASS) Office, the Naval Civil Engineering Laboratory, Engineering Analysis, Inc. (EAI), and BREEZE Software / Trinity Consultants, Inc.

The predecessors to HExDAM, the Nuclear Damage Assessment Model (NDAM) and the Enhanced Nuclear Damage Assessment Model (ENDAM), were originally developed to predict large-scale structure damage for nuclear blasts using the Physical Vulnerability System (PVS) (Defense Intelligence Agency Production Center, 1969). The mathematical and computational aspects of this system are provided in a companion public/unclassified document (Defense Intelligence Agency, 1974). ENDAM evolved into HExDAM when the blast pressure profiles and structure vulnerability data were modified to accommodate conventional high explosives. The overpressure and impulse fields in HExDAM are computed according to Glasstone (Glasstone and Dolan, 1977).

To accommodate the need for modelling vapor cloud explosions (VCEs), VExDAM was developed. VExDAM uses Van den Berg's Multi-Energy Method (Van den Berg, 1985) to generate 3D overpressure and impulse profiles for spherical vapor clouds. Multiple spherical vapor clouds are used to model more complex vapor cloud geometries, and the effects of these sub-clouds are combined to produce cumulative overpressure/impulse fields. Once the initial overpressure and impulse fields are calculated, both HExDAM and VExDAM use the same methodology to compute shielding effects and injury/damage.

For open-air explosions, particularly with conventional high explosives, unshielded peak pressure distributions are well understood. However, damage levels to larger, more complex structure scenarios are increasingly a function of shielding effects. Incident pressures and subsequent damage levels are significantly lower for structures and persons located behind other structures/persons. For this reason, ExDAM's 'shielding algorithm' was developed (Tatom and Norman, 1993). Most generally, the shielding algorithm reduces the peak pressures behind structures based on a dipole-flow-field distribution. Each component of a structure is evaluated separately, such that if an explosion is sufficient to destroy glass windows but not masonry walls, the shielding effect of the walls will be accounted for but little or no shielding will be produced by the window area.

Once an incident pressure/impulse field is calculated, ExDAM computes structure damage based on a Master Structure Data set (Glasstone and Dolan, 1977; Ferritto and Hager, 1988), providing a list of common structures and materials, each with six 'Vulnerability Parameters' (VPs) which directly correlate incident pressures to 'percent' damage. These vulnerability parameters include vulnerability type, which determines whether the material is most sensitive to overpressure, P, or dynamic pressure, Q, and K-factor, which is used to account for the different pressure-time pulse shapes (i.e. pulse duration) of various explosion yields. HExDAM's structure VPs are derived from empirical data.

To allow for the injury potential of an explosion to be quickly evaluated, ExDAM also incorporates model male, female, and child bodies. The ExDAM body models are composed of 28 total body components and 19 different body component types. Like structure materials, empirical vulnerability data was used to develop the body component VPs (Merx, 1989; Evans, 1957; Messerer, 1880).

### **SCALABILITY, APPLICABILITY, AND LIMITATIONS OF ExDAM ANALYSES**

ExDAM can be applied to a wide range of spatial scales, from near-field effects of an explosion on a single nearby structure to effects on a large area with numerous structures. The primary limitation of ExDAM lies in the fact that the model relies on P-I relationships, with modifications to account for shielding effects and to allow damage and injury calculations. ExDAM does not explicitly model flame front or blast wave propagation, and does not account for channeling or reflection (other than interactions with the ground). As with other multi-energy models, some details of a VCE, such as the degree of confinement and congestion and the fuel's characteristic flame speed, can be accounted for by an explosion strength adjustment factor, but fluid flow is not explicitly modeled as in a CFD application. Thus, the model is generally not appropriate for small-scale modelling of internal explosions such as an offshore platform compartment. The model is, however, still suitable for a large variety of applications, and has been used to model situations ranging in spatial scale from a subway car to large petrochemical facilities and entire towns.

### **PROJECT EXAMPLES**

As noted above, while ExDAM is not suitable for every explosion scenario, it can and has been used to model a wide range of HE and VCE cases. Four example case-study projects are listed below, two of which will be presented instead of discussed in this paper due to the extended abstract page restriction:

1. An industrial plant siting analysis involving multiple potential VCE scenarios
2. A large-scale city/residential HE scenario (the West, Texas event)
3. An urban multi-story building external HE scenario
4. A small-scale IED terrorism event (one of the London 7/7 subway bombings), as modeled by researchers at the University of Salzburg.

#### ***Example 1: Industrial Plant Siting Analysis***

Explosion consequence modelling at industrial and military facilities has historically been the most common use of ExDAM. By modelling the worst-case explosion scenarios across the facility, worst-case peak overpressures/impulses and subsequent worst-case damage and injury levels can be estimated across the facility. In the case presented here, modelling was performed for a petrochemical client to determine the potential VCE hazard posed to existing process and office buildings, as well as a safe location for siting of a future portable building (as in API 753).

ExDAM model results predicted broken windows and minor structural damage to exposed faces of several of the permanent structures. Predicted injuries to personnel were slight for personnel in shielded locations, but broken bones and other injuries were predicted for personnel in poorly shielded locations such as near windows. An area for safe placement of portable buildings was defined based on areas with low modeled overpressure. The location of this area was dictated primarily by distance from explosion sources and shielding from permanent structures. A plot plan illustrating some of the shielding effects, structure damage, and occupant injury is shown in Figure 1. Creation and execution of this modelling scenario required approximately two days of time from an experienced user.

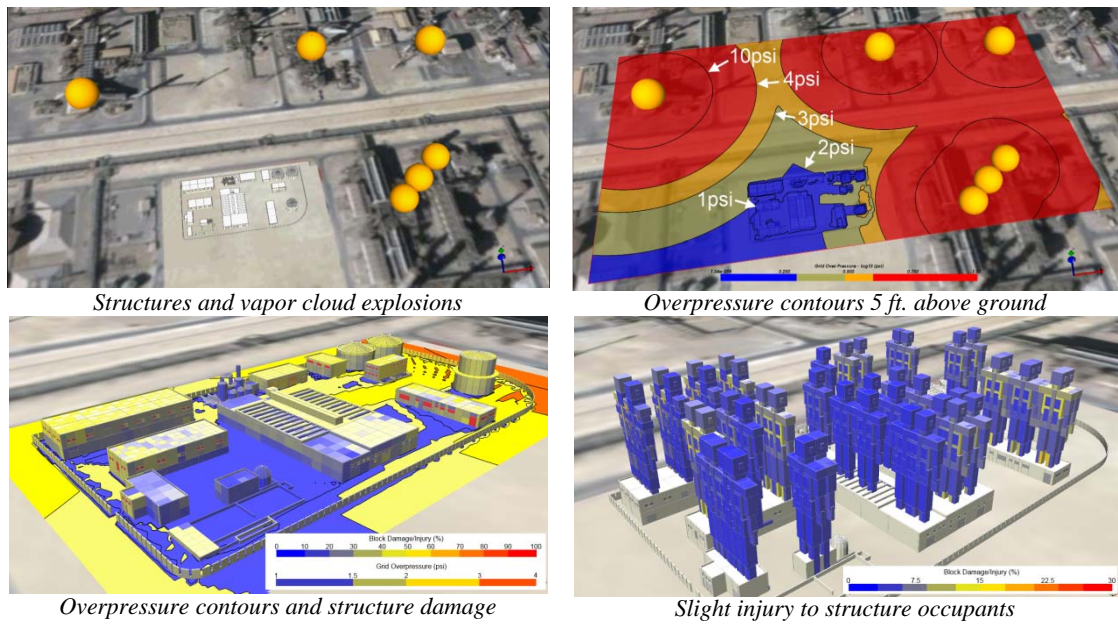


**Figure 1.** Example 1 project results from all possible explosion sources to single building.

**Example 2: City/Residential HE Event (West, Texas)**

ExDAM can also be used for highly macro-scale explosion consequence analyses, such as the effects on a large number of surrounding structures in an urban area. The April 17, 2013 West, Texas fertilizer company explosion is an example of this application. Almost 200 buildings were created in ExDAM based on satellite imagery and street-level photographs. Setup and execution of the model scenario was completed in approximately three days. The model analysis was completed with an assumed TNT-equivalent mass of ammonium nitrate (AN) of 30 tons.

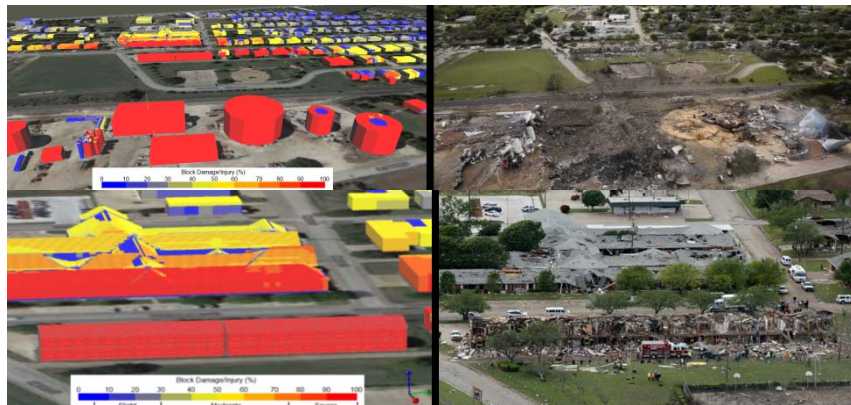


**Figure 2.** Comparison of actual to predicted damage for one portion of the affected area.

**CONCLUSIONS**

The BREEZE ExDAM model provides an intermediate-complexity solution, which is well-suited to modelling explosions of both vapor clouds and high explosives in environments where effects such as reflection and channeling are not expected to have a significant effect, but where shielding caused by structures and people may have an effect.

The model is relatively simple to use and understand in comparison to approaches such as CFD. Thus, while in no way a replacement for applications in which CFD modelling is required, ExDAM is potentially accessible to a wider audience of safety professionals, first responders, etc. than CFD modelling. The ability of the model to correlate predicted overpressure and impulse into predictions of injury and damage adds to the potential utility of the model for these groups – impacts are translated into terms that can be readily understood by those without formal training in interpretation of overpressure and impulse data. However, some expertise is still required to properly use the model, particularly when modelling vapor cloud explosions as these can be more difficult to quantify. Thus, for many persons and applications, a simpler model, and particularly one targeted at non-specialist personnel such as the NOAA ALOHA model, is more appropriate.

## REFERENCES

- Defense Intelligence Agency Production Center, 1969: Vulnerability Handbook -- Nuclear Weapons, AP-55-1-2-69-INT (Confidential)
- Defense Intelligence Agency, 1974: Mathematical Background and Programming Aids for the Physical Vulnerability System for Nuclear Weapons, DI-SSU-27-4.
- Evans, F. G., 1957: Stress and Strain in Bones, Their Relation to Fractures and Osteogenesis, Springfield, Illinois, Charles C. Thomas.
- Ferritto, J. and K. Hager: User's Guide for Conventional Weapon Effects Survivability Computer Programs, Naval Civil Engineering Laboratory, Port Hueneme, California.
- Glasstone S. and P. J. Dolan, Eds., 1977: The Effects of Nuclear Weapons, Third Edition, U.S. DOD and Energy Research and Development Administration.
- Mercx, W.P, 1989: The Consequences of Explosion Effects on Humans. Methods for the Determination of Possible Damage, CPR 16E, Voorburg, The Netherlands, The Director General of Labour, Chapter 3.
- Messerer, O., 1880: Uber Elasticitat Und Festigkeit Der Menschlichen Knochen, Stuttgart: J. G. Cotta'chen.
- Tatom, F. and J. Norman, 1993: Comparison of Measured and Predicted Peak Blast Overpressure Behind a Shielding Wall. SAVIAC 64th Shock and Vibration Symposium, Ft. Walton Beach, Florida.
- Van den Berg, A. 1985: A Framework for Vapour Cloud Explosion Blast Prediction. *Journal of Hazardous Materials*, **12**, 1-10.

**17th International Conference on  
Harmonisation within Atmospheric Dispersion Modelling for Regulatory Purposes  
9-12 May 2016, Budapest, Hungary**

---

**REAL-TIME USE OF A CFD MODELLING SYSTEM IN THE FRAMEWORK  
OF “TOXIC 2014”, A MAJOR CIVILIAN SECURITY EXERCISE  
AT A VERY COMPLEX URBAN SITE IN PARIS**

*Patrick Armand<sup>1</sup>, Christophe Duchenne<sup>1</sup>, Yasmine Benamrane<sup>1</sup>,  
Sébastien Guillaud<sup>2</sup>, Nadège Cabibel<sup>2</sup>, Bertrand Masselin<sup>3</sup>, and Thomas Bineau<sup>4</sup>*

<sup>1</sup>CEA, DAM, DIF, F-91297 Arpajon, France

<sup>2</sup>BSPP, Etat-Major, F-75823 Paris CEDEX 15, France

<sup>3</sup>Defacto, F-92095 Paris La Défense, France

<sup>4</sup>Préfecture des Hauts-de-Seine, SIDPC, F-92013 Nanterre CEDEX, France

**Abstract:** On 22 May 2014, a civilian security exercise named “Toxic 2014” was organized in “La Defense” business district located west of Paris. It was a fictitious massive release of ammonia from a tanker-vehicle (after an accident or a terrorist attack). The French Atomic and alternative Energies Commission (CEA) was involved in “Toxic 2014” to provide in real time the Paris Fire Brigade and the “Prefecture” (local authority) with dispersion and danger zones results taking account of the buildings and the local meteorological conditions. The exercise showed that a modelling and decision-support system like CERES® developed by CEA fosters the understanding and a shared representation of the emergency situation as it facilitates the communication to the authorities. Thus, the exercise illustrated the role of advanced modelling in coordinating a crisis command centre and taking adapted population protection measures.

**Key words:** *advanced modelling, decision support, civilian security, CBRN-E crisis exercise, CERES®.*

## **INTRODUCTION**

Explosions and toxic releases into the atmosphere may originate from accidental situations or malicious emerging threats. The social consequences of such events are increasingly feared and a great attention is paid to the prevention, provision, and managing of what are now called the “CBRN-E threats”.

In the last decades, physical modelling and numerical simulation have experienced parallel considerable improvements (see Benamrane *et al.*, 2013, commenting on the evolution in the use of the models from Chernobyl to Fukushima). This is not only good and important for the scientist and the engineer. It is also an opportunity to change the status of the predictive computations performed in emergency preparedness and response to make them an effective support in the decision-making process. Built environments with, possibly, a complex topography and varying meteorological conditions are definitely the places where CBRN-E events may arise. Advanced modelling is now able to produce 2D and 3D detailed and realistic results directly useable by the civilian security to protect the population in a very limited amount of time (around 15-30 minutes) even for a very large urban simulation domain as shown in Oldrini *et al.* (2013).

The French Atomic and alternative Energies Commission (CEA) is committed to developing a modelling and decision support system called CERES® adapted to CBRN-E threats as illustrated in Armand *et al.* (2013) (2014) and (2015). In this respect, the present paper documents a major civilian security exercise called “Toxic 2014” which was held in “La Defense” district near Paris and implied the fictitious release of a toxic industrial chemical. It is described how the exercise took advantage of CERES® capabilities.

## **THE DESIGN AND SCENARIO OF “TOXIC 2014”**

Since 2012, the CEA has launched a research work aiming at evaluating the adequacy of the modelling and decision-support tools with the actual needs of the emergency players. In this framework, the CEA was associated to the organization of an exercise named “Toxic 2014” held on 22 May 2014 to test the safety procedures plan of “La Defense” business district (located North-West of Paris) in case of a toxic release. The partners were the Paris Fire Brigade, the public body in charge of “La Defense” security, and the “Prefecture” which is the local public authority in France.

The involvement of CEA in “Toxic 2014” exercise included contributions to the preliminary elaboration of the noxious release scenario and to the exercise itself by providing expertise and modelling regarding atmospheric dispersion and health impact assessment. In the following, details are given about these two phases and the simulations that have been produced for preparedness and response.

### Proposal for scenarios

In September 2013, the CEA was asked by the Prefecture to develop realistic scenarios of a hazardous atmospheric dispersion fulfilling of a number of requests: releases should be chemicals as a “dirty bomb” exercise had been carried out the year before; meteorological conditions should be such that a large part of “La Defense” is affected towards Paris; and the danger zones should be quite large in order to simulate a serious event and to train the Fire Brigade first-responders and the Prefecture command centre.

Along with this, the CEA proposed several plausible CBRN-E events corresponding to either accidents or malevolent actions. In order to obtain a large panel of situations, different weather conditions, locations of the release, and toxic chemicals were presented as exemplified in Figure 1. For each possible place of the release, realistic scenarios and operating modes were built up (not reported in this paper).

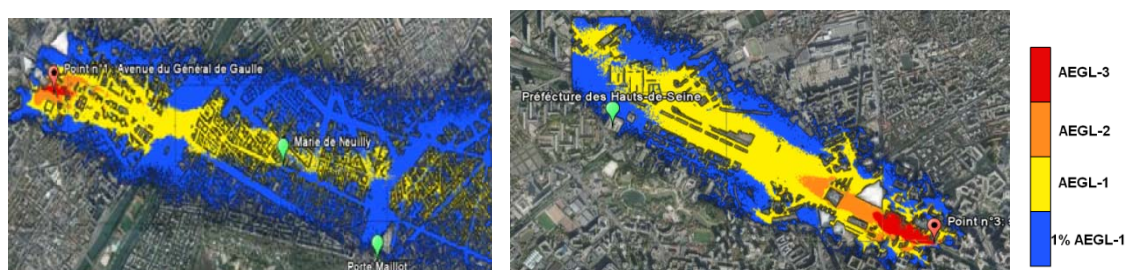


**Figure 1.** Distribution of a toxic chemical released in “La Defense” district (results given for two release locations). The danger zones have warm colours. They were determined using the AEGLs of the US-EPA.

### Choice of the exercise scenario

In December 2013, the CEA presented the modelling results of various fictitious releases and potential consequences on the population to the players implied in the future exercise (Prefecture, municipalities, fire-fighters, police, health service, public transport operators...). Considering the aims of the exercise, the chosen scenario was a hypothetical hazardous material transport accident. More precisely, it was a breach in a tanker-vehicle containing liquefied ammonia. This event was considered as appropriate by the players as ammonia is a usual chemical compared to other proposed species. Moreover, it could be related to both an accidental event and a malevolent action (like a tanker hijacking). The location was taken on the circular boulevard, west of the district, quite aligned with the esplanade of “La Defense”.

The final scenario was featured by CEA choosing it as realistic as possible, respecting the protocols and intervention times of the fire-fighters and making the Prefecture command centre work in anticipation. As a matter of fact, it was decided to have a change in the wind direction during the release, thus a variation of the impacted areas that could be predicted in the course of the exercise.

### Chosen inputs for “Toxic 2014”

In March 2014, the CEA presented the detailed conditions of the scenario (Table 1) to the exercise teams.

**Table 1.** Main features of “Toxic 2014” exercise.

Meteorological conditions	Wind blowing first from northwest then from southwest
Source term	~10 tons of ammonia with 15% instantaneously released and 85% evaporating in 45 min
Mock-up of the district	Includes the topography, the explicit description of the buildings at 1 m resolution and a rugosity length for the small elements (bus shelters, booths...) not described in the obstacles files

### **THE TIME SEQUENCE OF “TOXIC 2014” (IN BRIEF)**

The exercise began on 22 May 2014 at 1 pm. The Prefecture was alerted at 1:15 pm to an accident in “La Defense” implying a tanker-vehicle. The command center and the security procedures plan were activated at 1:25 pm simultaneously with the information about the victims and the plausible chemical risk.

The CEA involvement in the exercise had been predetermined with the Prefecture and Paris Fire Brigade. The CEA was informed at 1:30 pm by the Fire Brigade and received the first input (place of the event and gross estimate of the source term) necessary to begin with a real time simulation of the event. Dispersion results taking account of the buildings were obtained in about 20 minutes and sent by e-mails both to the Fire Brigade operational center in Paris and to the command center of the Prefecture. Meanwhile, a CEA expert was requested to join the command center and arrived there at 2:00 pm.

#### **Phase 1 – Beginning of the exercise**

The question of the population sheltering or evacuation arose very quickly. It was discussed by the Fire Brigade, the medical emergency team, the Prefecture, and the expert using the map views of the complex dispersion pattern (see Figure 2) displayed on the computers terminals of the command center.

At 2:03 pm, the Fire Brigade recommended the skyscrapers confinement rather than their evacuation; as a precaution, the Prefecture decided to confine the whole district waiting for a more accurate assessment.

At 2:23 pm, the CEA debated the plume dispersion simulation with the Fire Brigade. From a video, it was clear that at this time, the release was over and the plume diluted with concentrations below any adverse effects on the human health. Then, the map of the toxic load (presented after the plume crossed all the area) was used to delimitate the health consequences zones (see Figure 3). While the most severe effects were limited to “La Defense” esplanade, it was probable that due to a low olfaction threshold, numerous people may have detected the abnormal presence of the ammonia in many localities at the north of the district. This was considered as a very important information by the Fire Brigade.

#### **Phase 2 – First update of the situation**

At 2:39 pm, the Prefecture cabinet director arrived triggering the first situation update. The Fire Brigade indicated with a map the presence of the rescue teams on the spot and the measures taken to confine the population. The CEA presented the simulation of the plume dispersion on a video and the assessment of the health consequences (cumulated from the beginning of the release). The Fire Brigade explained that at this time, the risk did not evolve anymore and that a confirmation was expected from the field.

The medical emergency team updated the number of casualties and the hospitals taking care of them. It also stressed the saturation problem which could happen if people smelling the ammonia headed to the hospitals (see the olfaction area on Figure 3). Finally, the measures taken in the municipalities at the north of La Defense were further examined. It was noticed that buildings aeration could be advised as the plume had left the sector. Moreover, measurements in the field indicated that the concentration levels were very low consistently with the modelling.

#### **Phase 3 – Second update of the situation**

At 4:00 pm, the Prefect arrived at the command center triggering the second situation update. The nature of the event and the population protection measures were enlightened as the progressive annulment of the confinement measures. To supplement the Fire Brigade and health emergency service reviews, the CEA was requested to present the ammonia dispersion simulation and the consequences assessment. The full termination of the security measures all over “La Defense” district was declared at 4:30 pm.

## NUMERICAL SIMULATIONS IN “TOXIC 2014”

The simulations were performed with PMSS, one of the dispersion solvers set up in CERES® modelling and decision-support tool. PMSS is developed by the CEA, ARIA Technologies, and MOKILI (Tinarelli *et al.*, 2013). It is devoted to research and advanced modelling solutions testing. PMSS is nested in a meso-scale weather forecast system based on WRF and operated routinely by the CEA (resolution of 5 km above France and 1.6 km over the Paris region). Then, PMSS solves the 3D local urban flow and dispersion at a resolution of 1 to 5 meters.

PMSS simulations were carried out on a domain with dimensions 4.2 km x 6.3 km and a horizontal mesh size of 3 meters. This large domain was sub-divided in 24 tiles of 351 x 351 points. The vertical meshing had 37 levels from the ground to a height of 800 m. The flow was run with P-SWIFT on 25 processors and the dispersion with P-SPRAY using a maximum number of 64 processors. All the simulations were carried out in less than 15 minutes (a duration which is consistent with the emergency management).

### Assessment of the toxic loads

The health consequences of the release were evaluated on the basis of the reference toxicological values applicable in France (given by the INERIS for common industrial gases) in case of an accidental acute exposure by inhalation. As the concentration was not time constant, the toxic load was evaluated at each point of the simulation domain and compared to threshold values.

The ammonia sensorial perception (SP) by olfaction was also considered. This is a concentration which is between 3.5 and 35 mg.m<sup>-3</sup> depending on the individuals, does not result in any health effect and it is not associated with a duration. The maximum concentration at each point was compared to the SP to identify the area where the olfaction threshold was exceeded.

### Numerical results

Figures 2-a) to 2-d) illustrate the plume propagation and the volumetric concentration near the ground at successive moments after the beginning of the hypothetical release. The ammonia concentration field is presented with a gradual fading of the same color to avoid any confusion between the concentration and health consequences when providing the Fire Brigade and Prefecture command centers with maps.

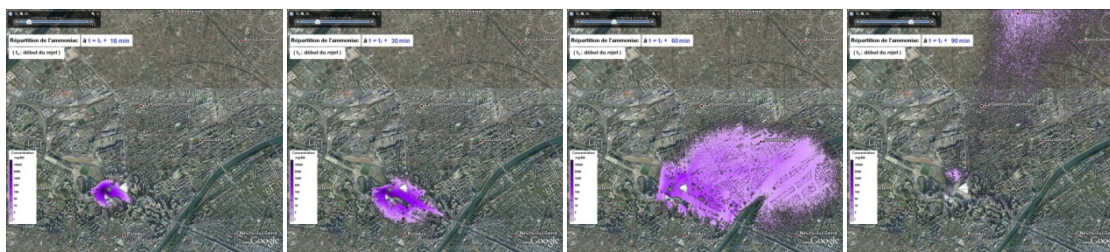


**Figure 2.** Ammonia volumetric concentration distribution at  $t_0 + 15$  min (a), 30 min (b), 60 min (c), and 90 min (d).

Figure 3 presents the danger zones corresponding to the health effects of the toxic plume as the release is over and the plume has crossed the whole simulation domain (90 min after the triggering of the release). The zone of the significant lethal effects (5% of the population) (SELS) is in dark red; the zone of the first lethal effects (1% of the population) (SPEL) is in red; the zone of the irreversible health effects (SEI) is in orange and the zone of the reversible effects (SER) is in yellow. The area in which ammonia smelling may have been detected by the population from the beginning of the release to the considered time frame is colored in blue. It covers an extended area around four municipalities east and north of “La Defense”.

Figure 3 also compares the results issued by CERES® and ALOHA (smooth ellipses) which is the hazard software of the CAMEO modelling system developed by the US-EPA (Jones *et al.* 2013). ALOHA is a Gaussian dispersion model not taking account of the topography and the buildings. It is widespread in the USA with the firemen and also popular in France. Given this model limitations, ALOHA results are quite consistent with PMSS results. The main difference is that the plume progression is contained by the

buildings what can be predicted by PMSS and not by ALOHA. Thirty minutes after the beginning of the release, the wind changes direction with the eastern part of “La Defense” not affected by the plume. This is predicted by PMSS and not foreseen by ALOHA. Finally, due to the complicated meteorological conditions and the air flow in between the buildings, only PMSS can predict contaminated areas upwind.

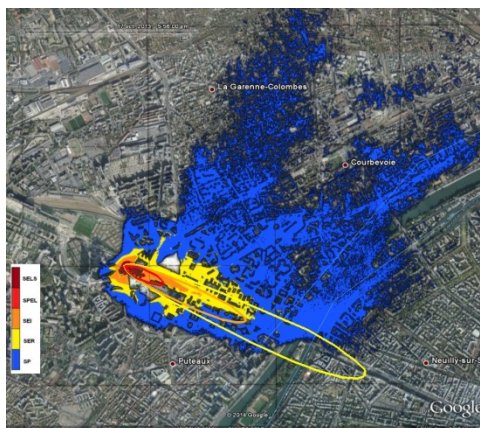


**Figure 3.** Comparison of the danger zones predicted by PMSS and ALOHA.

### **LESSONS LEARNT FROM “TOXIC 2014”**

The toxic release exercise revealed two essential benefits in providing real time modelling expertise:

1. Simulation is relevant to enhance a common understanding of the space-and-time distribution of the chemicals what helps in making decisions and taking adapted measures for the population protection.
2. Simulation may be used to facilitate the communication to the authorities and all players what helps in generating a shared representation of the situation and an optimal coordination of the command center.

The main lesson was the complementarity between the first actions taken by the rescue teams in case of a short or medium duration release and the simulations aiming at diagnosing and anticipating the situation. Even if the performance in real life would be diminished as it is uneasy to determine the source term, the early visualization of the plume dispersion pattern is clearly of interest to support the response first phase.

The integration of modelling activities in the preparation of the exercise had triple benefits:

1. The better mutual knowledge of the scientific tools’ developers and the civilian security services;
2. The full CBRN risk analysis of events targeting “La Defense” with a much better apprehension of the human and organizational impact (to our knowledge, a “premiere” for a business district);
3. The development of a technically more precise than the usual practices, realistic and relevant scenario which allowed the state services to work in-depth the time sequence of the exercise;

The involvement of modelling expertise in the course of the exercise had also triple interests:

1. The effective use of the modelling by the services in charge of the population protection to identify the dispersion processes, adapt the first actions of the rescue teams and anticipate the event follow-up;
2. The static and dynamic presentation of the results (the CEA maps were used all along the exercise for communication purpose and to help in sharing a collective view during the situation updates);
3. For the CEA, the improvement and adaptation of the results provided by the computational tools to better fit the needs and the missions of the civilian security organization.

### **CONCLUSIONS**

The paper addresses the promising capacities of up-to-date dispersion modelling and health consequences assessment applied to CBRN-E emergency preparedness and response. A civilian security exercise hold on 22 May 2014 in “La Defense” business district near Paris, named “Toxic 2014”, was the test bed for CERES® modelling and decision-support system. Flow and dispersion simulation taking account of both the buildings and local meteorological conditions were produced in around 20 minutes at 3 m resolution,

post-processed to deduce the danger zones and transmitted to the Paris Fire Brigade and the “Prefecture”. The modelling was actually utilized by the services in charge of the population protection and contributed to identify the dispersion processes in the built environment, adapt the first actions of the rescue teams and anticipate the event follow-up. Finally, “Toxic 2014” was a good opportunity to work collaboratively with practitioners and make the CEA computational tools better fit their actual needs and missions.

## REFERENCES

- Armand, P., C. Duchenne, Y. Benamrane, C. Libeau, T. Le Nouêne, and F. Brill. Meteorological forecast and dispersion of noxious agents in the urban environment – Application of a modelling chain in real-time to a fictitious event in Paris city. Proceedings of the 15<sup>th</sup> Harmo Conference, May 6-9, 2013, Madrid, Spain, 724-728.
- Armand, P., C. Duchenne, and E. Bouquot. Atmospheric dispersion modelling and health impact assessment in the framework of a CBRN-E exercise in a complex urban configuration. Proceedings of the 16<sup>th</sup> Harmo Conference, Sept. 8-11, 2014, Varna, Bulgaria, 638-643.
- Armand, P., C. Duchenne, and L. Patryl. Is it now possible to use advanced dispersion modelling for emergency response? The example of a CBRN exercise in Paris. ITM 2015, May 4-8 2015, Montpellier, France.
- Benamrane, Y., J.-L. Wybo, and P. Armand. Chernobyl and Fukushima nuclear accidents: what has changed in the use of atmospheric dispersion modeling? *J. of Environmental Radioactivity*, **126** (2013) 239-252.
- Jones, R., W. Lehr, D. Simecek-Beatty, and R. M. Reynolds. ALOHA® (Areal Locations of Hazardous Atmospheres) 5.4.4 Technical Documentation. NOAA Technical Memorandum NOS OR&R 43. November 2013.
- Oldrini, O., M. Nibart, P. Armand, C. Olry, J. Moussafir, and A. Albergel. Multi-scale build-up area integration in Parallel SWIFT. Proceedings of the 15<sup>th</sup> Harmo Conference, May 6-9, 2013, Madrid, Spain, 485-489.
- Tinarelli, G., L. Mortarini, S. Trini-Castelli, G. Carlino, J. Moussafir, C. Olry, P. Armand, and D. Anfossi. Review and validation of Micro-SPRAY, a Lagrangian particle model of turbulent dispersion. Lagrangian Modeling of the Atmosphere, Geophysical Monograph, Volume 200, AGU, pp. 311-327, May 2013.

**17th International Conference on  
Harmonisation within Atmospheric Dispersion Modelling for Regulatory Purposes  
9-12 May 2016, Budapest, Hungary**

---

**THE INFLUENCE OF THE HOLUHRAUN ERUPTION SO<sub>2</sub> EMISSIONS ON THE AUSTRIAN  
AIR QUALITY**

*Christian Maurer<sup>1</sup>, Delia Arnold<sup>1</sup>, Florian Geyer<sup>1</sup>, Claudia Flandorfer<sup>1</sup>, Marcus Hirtl<sup>1</sup>, Sabine Eckhardt<sup>2</sup>, Thomas Krennert<sup>1</sup> and Gerhard Wotawa<sup>1</sup>*

<sup>1</sup>Central Institute for Meteorology and Geodynamics (ZAMG), Vienna, Austria

<sup>2</sup>Norwegian Institute for Air Research (NILU), Kjeller, Norway

**Abstract:** The Holuhraun 2014 eruption released for several months large amounts of SO<sub>2</sub> into the atmosphere. During September 2014, the meteorological conditions favored a fast transport towards Europe which led to increased SO<sub>2</sub> ground-level concentrations in Austria, exceeding national regulatory levels. FLEXPART atmospheric transport calculations were performed with eight emission scenarios. All calculations represent well the transport pathway from Iceland to Austria but the maxima at ground level are often early (1 to 5 hours) with respect to the measurements, especially for the stations at the lee side of the Alps. The run with 6.5 km a.s.l injection height, non-linear vertical mass distribution and 112 kt/day SO<sub>2</sub> flux gives in general the best results. Regions to the north east, the Alpine region and the south-east of Austria are the most affected with modeled and measured concentrations above the Austrian regulatory 200 µg m<sup>-3</sup> threshold for half-hourly values. Exposure of population is fairly low since most of the highly populated regions are outside the path of the plume except for the regions in Styria and Burgenland to the south-east. Daily averages are of no concern in terms of health, even considering the potential prolonged exposure given the 31% frequency of such transport pattern from Iceland to Austria.

**Key words:** *Holuhraun, atmospheric transport, FLEXPART, exposure*

## **INTRODUCTION**

The Holuhraun SO<sub>2</sub> emissions in September 2014 led to increased concentrations at ground level in Austrian regions, especially in those regions at the south-east and on the lee side of the Alps. The Austrian air quality network captured an increase in the SO<sub>2</sub> concentrations, up to two orders of magnitude above the usual anthropogenic originated measurements.

## **DATA**

A climatological study, following strict quality assurance criteria, of the SO<sub>2</sub> measured data has allowed the identification of 56 stations with clear (ratio with respect to the baseline of 10 or more) measurements of SO<sub>2</sub> originating from the Holuhraun eruption both on the upwind and lee sides of the Alps. These stations have been clustered according to the measured concentration time series for the 22nd of September, providing 5 clusters with different behaviour. These clusters have been used to discuss both measurements and model results.

## **METHOD**

Atmospheric transport backtracking and correlation analysis from measurements at two clear sky mountain stations, Jungfraujoch and Sonnblick, shows that the most significant emission period to generate the enhanced ground level concentrations in Austria was that from 16 to 19 September. For this emission period, simulations with the Lagrangian atmospheric dispersion model FLEXPART (Stohl et al., 2005) have been performed, using different emission scenarios with variations in the SO<sub>2</sub> flux quantity and its vertical distribution and injection height. The calculation with an injection height of 6.5 km a.s.l and a non-uniform vertical mass distribution with a peak between 4 and 5 km a.s.l and 112 kt daily emission flux is the one representing best the measurements, whereas the other calculations, with different assumed emission characteristics, do not to represent the measurements that well, with some stations showing zero modeled SO<sub>2</sub> concentrations where measurements would be expected. However,

the statistical metrics per run vary too little to consider the differences between the selected emission scenarios significant.

## RESULTS

The measurements show that the areas at the eastern tip of the Alps and towards the south-east of Austria are the regions with larger ground-level concentrations, with measured exceedances of the national half-hourly threshold level. FLEXPART captures reasonable well the magnitude of the peaks but with a general overestimation partly due to the limitation in the chemical reactions implemented (Figure 1a and b). Correlations largely increase when the lagging between measurements and modeled values is taken into account. The lagged cross-correlations are useful due to a common problem of all the performed FLEXPART simulations: the advancement of the simulated plume with respect to the measurements. The plume arrives too early (mostly between 1 and 3 hours) at the measurement locations. This is especially visible for the stations located at the lee side of the Alps (**Figure 1a**). The effect is due to a non-accurate representation of the flow driven by the ECMWF data and is not a problem that can be tackled without using different meteorological data. We also performed further analyses (not shown) using the high resolution NWP model WRF (the Weather Research and Forecasting Model) driven as well with ECMWF data. This did not improve the problematic time shift, neither was it corrected by using data from the National Centers for Environmental Prediction (NCEP) Global Forecast System (GFS). In addition, the duration of the plume impact is smaller in the FLEXPART calculations, leading to sharper plumes missing the behavior of most of the stations in Styria and Carinthia, with many of them showing a wide (more than 5 hours) observation peak, spanning, station-dependent, from 10:00 to 23:00 UTC September 2014.

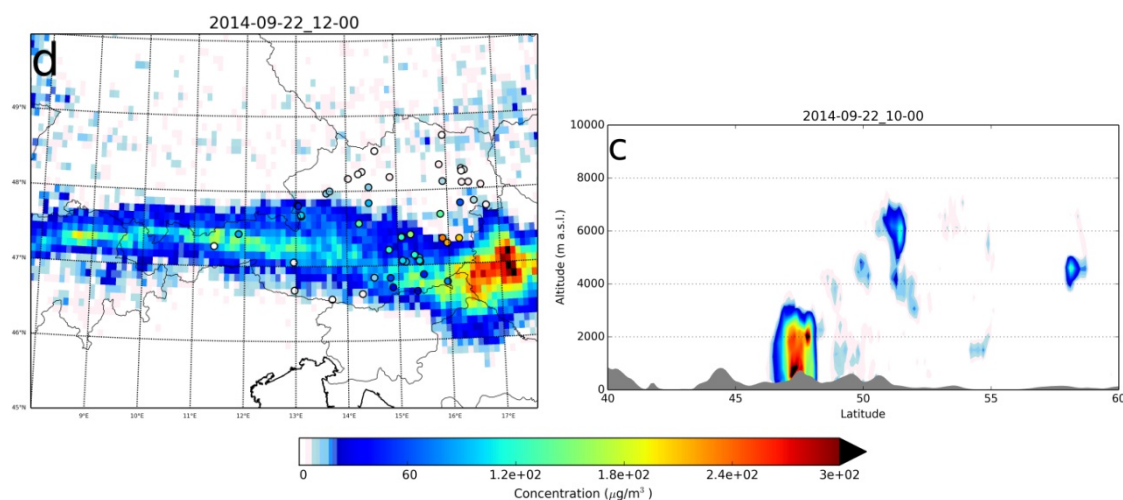


**Figure 1:** a: Modeled and measured (dots) SO<sub>2</sub> concentrations over Austria at 12:00 UTC.  
b: Modeled SO<sub>2</sub> concentrations for a cross section at longitude 16°E at 10:00 UTC.

The cross section of the transport of the plume (**Figure 1b**) shows the areas where the plume is entrained downwards by a combination of post-frontal subsidence, diurnal mixing and, on the lee side of the Alps, a Föhn-like flow. This combination of effects, together with the large but low level emissions of Hohenraun, led to unusually high SO<sub>2</sub> concentrations in Austria. One of the causes of the concentration overestimation may be the lack of aqueous-phase chemistry for SO<sub>2</sub> in the FLEXPART model which, for such low level emissions, with transport within the lower troposphere, may be a significant loss process. Data from the German station Hohenpeissenberg has been used to have a crude estimate of how such a loss process could contribute by looking at SO<sub>2</sub> and H<sub>2</sub>SO<sub>4</sub> measurements, yielding an approximate 20% of the total SO<sub>2</sub> possibly being in the liquid phase.

Although the half-hourly threshold level was exceeded in Austria, with five stations above the 200 μg m<sup>-3</sup>, the annual averages were of no concern. Even extrapolating the effects of the Hohenraun eruption

considering a frequency of occurrence of the same transport pattern of 31% per year, the exposure of the population poses no significant risks, assuming the same flux, according to the current European and Austrian regulations. Nevertheless, the levels could be high enough to yield winter averages above 20  $\mu\text{g m}^{-3}$ ; concentrations that are detrimental to ecosystems.

#### **REFERENCES**

Stohl, A., Forster, C., Frank, A., Seibert, P. and G. Wotawa, 2005: Technical note - The Lagrangian particle dispersion model FLEXPART 6.2. *Atmospheric Chemistry and Physics*, **5**, 2461-2474.

**17th International Conference on  
Harmonisation within Atmospheric Dispersion Modelling for Regulatory Purposes  
9-12 May 2016, Budapest, Hungary**

---

**EVALUATION OF EXPOSURE TO AIR POLLUTION THROUGH MOBILE PHONE DATA IN  
THE CITY OF MADRID (SPAIN)**

*M. Picornell<sup>1</sup>, T. Ruíz<sup>2</sup>, R. Borge<sup>3</sup>, P. García<sup>1</sup>, D. de la Paz<sup>3</sup> and J. Lumberras<sup>3</sup>*

<sup>1</sup>Nommon Solutions and Technologies, Madrid, 28043, Spain;

<sup>2</sup>Universitat Politècnica de València, València, 46022, Spain

<sup>3</sup>Department of Chemical and Environmental Engineering, Technical University of Madrid (UPM),  
Madrid, 28006, Spain

*Presenting author email: miguel.picornell@nommon.es*

**Abstract:** The evaluation of population exposure is essential for accurate impact assessment and intervention planning. Current estimations are typically based on cross-sectional, static data such as census data; that fail to capture the number and profile of the exposed people at different times of the day. The pervasive use of mobile devices in our daily lives opens new opportunities to gather large samples of geolocation data, allowing the estimation of dynamic population distributions along the day. An innovative methodology combining air quality models and dynamic population distributions from mobile phone data has been proposed and tested in the metropolitan area of Madrid (Spain). First results from the analysis performed show the potential of this new methodology to significantly improve population exposure assessments.

**Key words:** *Population exposure, mobile phone data, Call Detail Records, dynamic population distribution*

## **INTRODUCTION**

The evaluation of population exposure is critical for accurate impact assessment and intervention planning. Currently, the estimates of the population exposure to air pollution rely on surveys, census data and other administrative registers that in many cases provide unreliable, scarce or outdated information (Briggs et al., 2007). Additionally, these are typically cross-sectional, static data that fail to capture the number and profile of the exposed people at different times of the day. The pervasive use of mobile devices in our daily lives opens new opportunities to gather large samples of passively collected geolocation data (e.g. mobile phone records, GPS tracks) allowing the construction of dynamic maps of population distribution that can be overlapped with outputs from urban scale air quality models (AQM) to provide more realistic exposure estimates. The main objective of this paper is to explore how the assessment of population exposure can be improved through the estimation of dynamic population distributions based on mobile phone data. This innovative approach is tested in the Madrid (Spain) metropolitan area, calculating the population exposure to NO<sub>2</sub> along the day. The preliminary results obtained with this new approach are presented and compared with the static approach traditionally used for health impact assessment studies (i.a. Boldo et al., 2011). The structure of the paper is as follows: first, the datasets used in this study are described. Secondly, the methodology followed to estimated dynamic population distributions and NO<sub>2</sub> concentrations is shown. In third place, the new methodology proposed is tested in the metropolitan area of Madrid. Finally, the main conclusions of the paper are discussed.

## **DATASETS**

### **Mobile phone data**

The mobile phone data used for this study consist of a set of Call Detail Records (CDRs). CDRs are generated when a mobile phone connected to the network makes or receives a phone call or uses a service. For invoice purposes, the information regarding the time and the Base Transceiver Station (BTS)

tower where the user was located is logged, providing an indication of the geographical position of the user at certain moments. CDRs were collected for the region of Madrid and its surrounding provinces, comprising anonymous information of millions of users. For this first analysis the CDRs cover a period of time from October to November 2014. User's positions were collected from BTS towers around Spain, leading to a location accuracy of few hundreds of meters in urban areas and several kilometers in rural areas due to the different density of towers. In order to preserve privacy, all the information presented was aggregated and original records were encrypted. None of the authors of this study participated in the encryption or extraction of the CDRs.

### **Air quality dataset**

Eulerian mesoscale 3D AQMs can consistently describe the different physical and chemical processes that determine air quality at urban scales. Although model estimates involve uncertainties and errors, unlike observations from air quality monitoring stations, a validated and properly fed model can provide meaningful information of ambient air concentration for a whole city throughout a given period. For this first analysis outputs with 1h temporal resolution and 1 Km<sup>2</sup> spatial resolution were used. The selected pollutant was NO<sub>2</sub> since currently it is the main concern from the air quality point of view in Madrid and the primarily focus of plans and measures. In addition, the modelling system used has been extensively tested and assessed for this pollutant (Borge et al., 2014).

## **METHODOLOGY**

### **Population dynamics from mobile phone data**

CDRs provide information of the location of the user every few minutes or several hours, depending on the usage patterns of each mobile phone user. Therefore, user location information is not longitudinal but discrete, presenting gaps along the day. This poses a problem when trying to estimate dynamic population distributions, leading to underestimations of the total population present in an area since some population may be missing (not user's location information available for specific time periods). In order to overcome this limitation, the mobility model proposed by Picornell et al. (2015) which expands spatio-temporal information present in the CDRs (minimizing the location information gaps) has been used. The sample of users has been properly expanded in order to perform analysis that account for the whole population under study. In this paper, the Spanish 2011 census was used for expansion purposes. From the information provided by the mobility model, it is possible to determine the number of people located in a specific area at a specific period of time.

### **Ambient air NO<sub>2</sub> concentration simulation**

Air quality simulation relies on the WRF (Skamarock and Klemp, 2008) – SMOKE (Institute for the Environment, 2009) – CMAQ (Byun and Schere, 2006) system and a detailed bottom-up emission inventory specifically developed for this area (Borge et al., 2014) to produce reliable ambient air quality estimations.

### **Population exposure indicator**

The population exposure to NO<sub>2</sub> in a specific area has been computed as the product of NO<sub>2</sub> concentration and the number of persons per hour in that zone ( $\mu\text{g}\cdot\text{m}^{-3}\cdot\text{persons}\cdot\text{hour}$ ). From now on, we will refer to that indicator as “exposure indicator”. It should be noted that this index intends to assess general exposure levels since it does not take into account individual exposure patterns or accumulated dose.

## **CASE STUDY**

This new methodology has been tested in the Madrid metropolitan area. The study area (see Figure 1) has been divided in cells of 1Km<sup>2</sup>, covering a total area of 40x44Km accordingly to the AQM model domain and discretization. The analysis has been performed for the 17<sup>th</sup> of November of 2014, which was a standard day in terms of population dynamics and a representative day in terms of NO<sub>2</sub> levels. A model assessment for this particular day shows a satisfactory performance so temporal variation and spatial concentration gradients predicted by the model can be deemed reasonable and fit for purpose. Since a significant number of people trips to Madrid to work from surrounding areas, the population of those

areas (specifically Segovia, Ávila, Toledo, Guadalajara and Cuenca) has also been considered in the analysis.

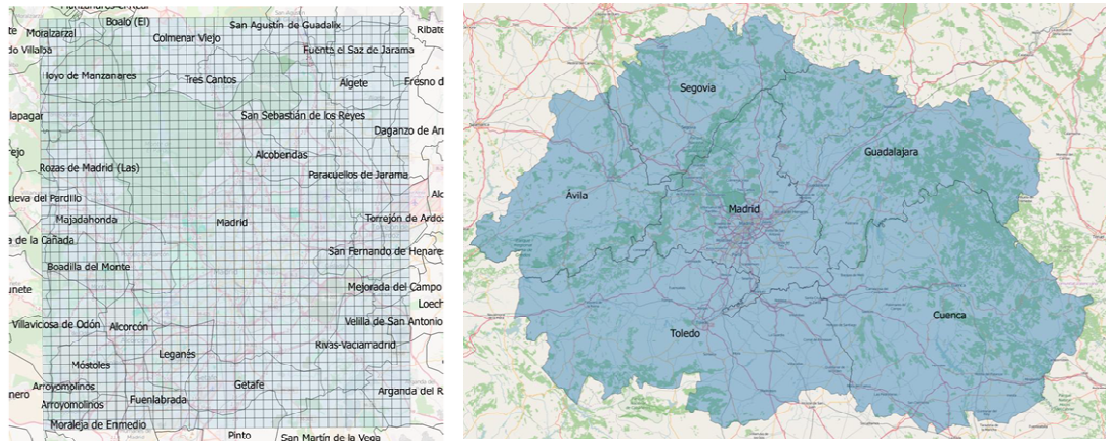


**Figure 1.** Spatial resolution and study area

## RESULTS

Average NO<sub>2</sub> ground level concentration predicted by the modelling system is shown in Figure 2.

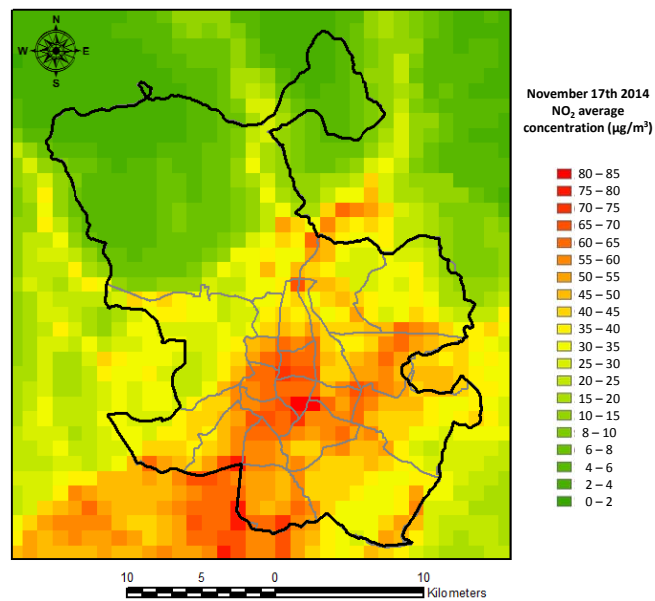


**Figure 2.** NO<sub>2</sub> average 24-h concentration

The exposure indicator has been calculated for the 1760 cells and for each hour of the day. Figure 3 shows the values of the exposure indicator in each cell at different periods of time (04:00, 09:00 and 12:00). At the beginning of the day (04:00), NO<sub>2</sub> levels are lower and Madrid population is located in the residential areas. During the morning peak (09:00), most of the population of Madrid and surrounding provinces trip to the city centre to work. The number of population and the concentration of NO<sub>2</sub> at the city centre significantly increase, leading to higher values of the exposure indicator. At midday, the NO<sub>2</sub> levels decrease and the population remains concentrated in the city centre.

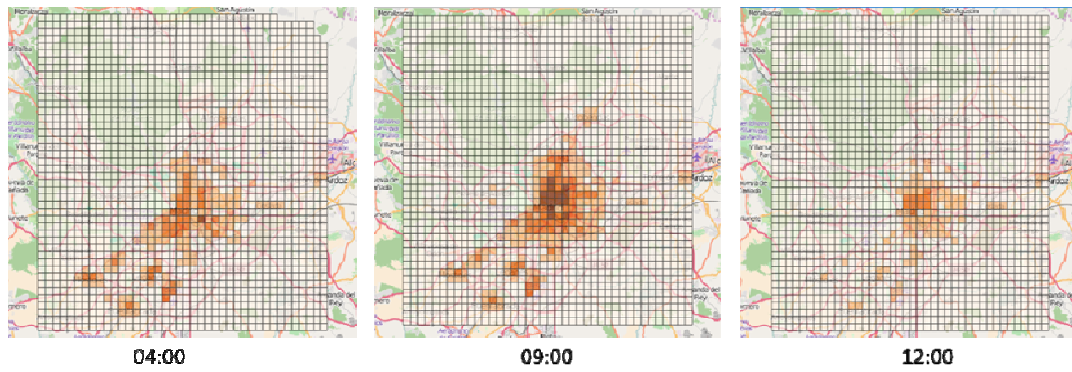


**Figure 3.** Exposure indicator at different periods of time

The comparison of the static conventional approach to assess exposure and the dynamic novel approach developed is illustrated in Figure 4. Although significant differences are found for specific city areas (see Figure 5) it can be seen that total exposure throughout the day for the whole modelling domain is below 4%. The reason for such a small departure is that: first, population fluxes on the boundaries of the area of study are negligible since most of the movements correspond to round trips that start and end inside the modelling domain; and secondly, because most of the trips are performed between areas with similar  $\text{NO}_2$  levels.

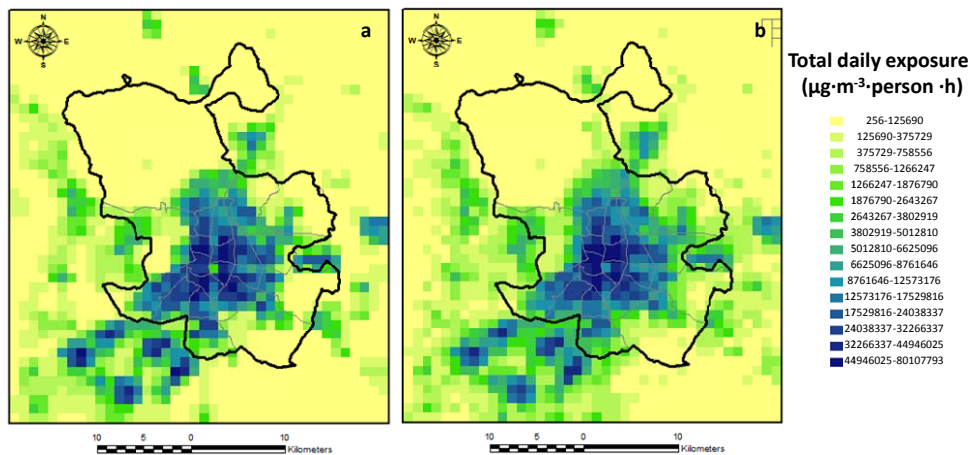


**Figure 4.** Total exposure throughout the day estimates: a) static census-based approach and b) dynamic CDRs-based approach

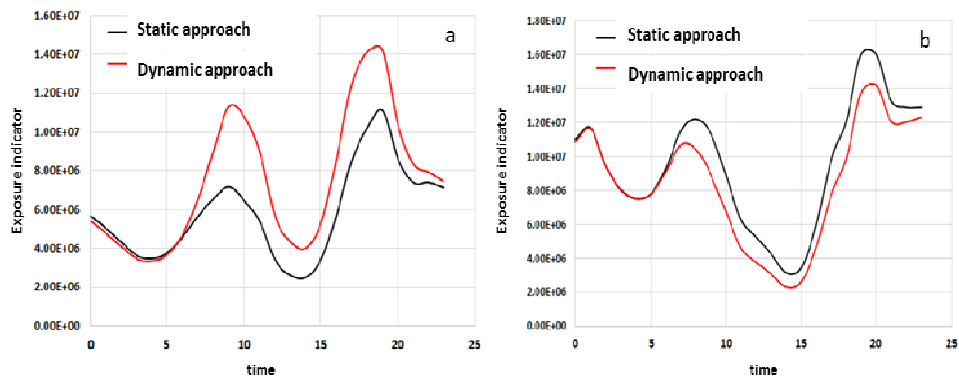


**Figure 5.** Exposure indicator evolution along the day for specific city areas: a) Chamartín district and b) Carabanchel district

## CONCLUSIONS

The combination of air quality models and dynamic population distribution based on mobile phone data opens an opportunity to reliably measure the actual population exposed to pollutants, overcoming the limitations of traditional data sources such as census data. According to the preliminary results of this first analysis, the traditional static approach used for health impact assessment may provide a reasonable estimate of daily average population exposure for mesoscale studies. However, the first results from the analysis performed in the city of Madrid corroborate the potential of this new methodology to significantly improve population exposure assessments, especially considering finer time and spatial resolution

## ACKNOWLEDGEMENTS

This study was supported by the Madrid City Council and the TECNAIRE-CM (innovative technologies for the assessment and improvement of urban air quality) scientific programme funded by the Directorate General for Universities and Research of the Greater Madrid Region (S2013/MAE-2972)

## REFERENCES

- Boldo, E., Linares, C., Lumbreras, J., Borge, R., Narros, A., García-Pérez, J., Fernández-Navarro, P., Pérez-Gómez, B., Aragonés, N., Ramis, R., Pollán, M., Moreno, T., Karanasiou, A., López-Abente, G., 2011. Health impact assessment of a reduction in ambient PM<sub>2.5</sub> levels in Spain. *Environment International*, **37**, 342-348
- Borge, R., Lumbreras, J., Pérez, J., de la Paz, D., Vedrenne, M., de Andrés, J.M., Rodríguez, M.E., 2014. Emission inventories and modeling requirements for the development of air quality plans. Application to Madrid (Spain). *Science of the Total Environment*, **466-467**, 809-819.
- Briggs, D., Fecht, D., & De Hoogh, K. (2007). Census data issues for epidemiology and health risk assessment: experiences from the Small Area Health Statistics Unit. *Journal of the Royal Statistical Society: Series A (Statistics in Society)*, **170**, 355-378.
- Byun, D.W., Schere, K.L., 2006. Review of the governing equations, computational algorithms and other components of the models-3 community multiscale air quality (CMAQ) modeling systems. *Applied Mechanics Review*, **59**, 51-77.
- Institute for the Environment. SMOKE v2.7 user's manual. Chapel Hill, NC: University of North Carolina; [Available online at: <http://www.smoke-model.org/version2.7/html/ch01.html>], 2009.
- Picornell M, Ruiz T, Lenormand M, Ramasco J, Dubernet T, Frias-Martinez E (2015), Exploring the potential of phone call data to characterize the relationship between social network and travel behavior, *Transportation*, **42**, 647-668.
- Skamarock, W. C., and Klemp, J. B.: A time-split nonhydrostatic atmospheric model for weather research and forecasting applications, *Journal of Computational Physics*, **227**, 3465-3485, 2008.

**17th International Conference on  
Harmonisation within Atmospheric Dispersion Modelling for Regulatory Purposes  
9-12 May 2016, Budapest, Hungary**

---

**ARE TOXIC LOAD-BASED TOXICITY MODELS CONSISTENT WITH EXPERIMENTAL  
OBSERVATIONS? INDEPENDENT ANALYSIS OF TIME-VARYING EXPOSURE DATA  
FROM THE 2012–2013 ECBC/NAMRU-D TOXICOLOGICAL EXPERIMENTS**

*Alexander Slawik<sup>1</sup>, James Silva<sup>1,2</sup>, Kevin Axelrod<sup>1,3</sup>, Jeffrey T. Urban<sup>1</sup>, Nathan Platt<sup>1</sup>*

<sup>1</sup>Institute for Defense Analyses, Alexandria, Virginia, USA

<sup>2</sup>Department of Physics, Boston University, Boston, Massachusetts, USA

<sup>3</sup>Graduate Program in Biophysics, Harvard University, Cambridge, Massachusetts, USA

**Abstract:** The U.S. Defense Threat Reduction Agency (DTRA) sponsored a two-year set of experiments, conducted in 2012 and 2013, that were designed and executed through a collaboration between the U.S. Army's Edgewood Chemical and Biological Center (ECBC) and the Naval Medical Research Unit Dayton (NAMRU-D) to explore the effects of time-varying inhalation exposures of hydrogen cyanide (HCN) gas on rats. In this work, we explore the comparison between the observed lethality and the predicted lethality of the "toxic load" model of exposure. Our analysis confirms the conclusion published by the authors of the experiment that the casualties observed for exposures over the experiments' full range of exposures from 2.3 to 30 minutes are not consistent with the predictions of toxic load-based toxicity models. We also conclude that a single set of fitted parameters for the toxic load model (i.e., the toxic load exponent  $n$ , probit slope  $m$ , and median lethal exposure  $TL_{50}$ ) accurately models the single exposure experimental data across the experiments' longer timescales of 10 to 30 minutes. However, we found that none of the toxic load models that we considered appear to fit the experimental data for the novel, time-varying exposures well, with the Average Concentration and Griffiths-Megson models providing the least inaccurate casualty predictions.

**Key words:** *casualty assessment, consequence assessment, Haber's law, toxic load modelling.*

## **INTRODUCTION**

Toxic industrial chemicals and chemical warfare agents present an acute inhalation hazard to civilians and military personnel. An individual exposure to an airborne hazardous material may be highly time-dependent due to the random effects of wind meandering and atmospheric turbulence. Several toxicological models based on the "toxic load" model of exposure have been proposed to predict the casualties arising from time-dependent exposures to airborne hazardous materials, but none were developed using data from toxicological experiments that used time-varying exposure profiles. To explore this experimentally unexplored regime, the U.S. Army's Edgewood Chemical and Biological Center (ECBC) and the Naval Medical Research Unit Dayton (NAMRU-D) performed a two-year set of experiments observing the lethality of time-varying exposures of hydrogen cyanide (HCN) gas on rats.

## **ECBC/NAMRU-D EXPERIMENTAL DATA**

To determine the suitability of toxic load models, the U.S. Army's Edgewood Chemical and Biological Center (ECBC) and the Naval Medical Research Unit Dayton (NAMRU-D) performed a two-year set of experiments. These experiments were designed to observe the lethality of hydrogen cyanide in a healthy population of male Sprague-Dawley rats. A group of ten rats are simultaneously exposed to the airborne toxin using a pressurized, nose-only inhalation apparatus (see Sweeney et al, 2014 for details).

The experimental setup allowed the concentration of the gas to be varied as a function of time; twenty-two separate exposure profiles were tested (eleven for each year or phase of the experiment). These exposure profiles were constructed to approximate square pulses of constant concentration (Sweeney et al, 2014 validates this idealization). The profiles can be grouped into three categories: a single square pulse, two square pulses with no time gap between them, and two square pulses with a

time gap between them when the rat is not exposed to any toxin. All exposure profiles are between 2.3 to 30 minutes long. Each profile was tested a number of times with a unique concentration level, denoted as a trial.

### TOXIC LOAD MODELS

Toxic load models define a quantity  $TL$  (toxic load) which captures the propensity of a population to suffer a physiological effect from exposure to a toxic chemical. For airborne exposures with a single constant exposure, the toxic load is defined as

$$TL = C^n \Delta t, \quad (1)$$

where  $C$  is the air concentration of toxin in the exposure,  $\Delta t$  is the duration of the exposure, and  $n$  is the toxic load exponent, a positive number. The toxic load model holds that the susceptibility of a population, measured in fraction affected, is log-normally distributed with respect to toxic load. The toxic load corresponding to 50% of the population affected is defined as the median toxic load (denoted by  $TL_{50}$ ), and the slope of the cumulative distribution function at  $TL_{50}$  is the probit slope, denoted  $m$ . The following probit model defines the relationship between toxic load and toxic effects,

$$P = \Phi(m \log_{10} TL - m \log_{10} TL_{50}), \quad (2)$$

$$\Phi(z) = \left[ \text{Erf} \left( \frac{z}{\sqrt{2}} \right) + 1 \right] / 2. \quad (3)$$

Here  $P$  corresponds to the percent of a population to exhibit the response of interest (in this case rat lethality),  $\log_{10}$  is the base 10 logarithm,  $\Phi$  is the cumulative distribution function of the standard normal distribution, and Erf is the error function. Figure 1 portrays a generic plot of the toxic load model, with the physical significance of the parameters indicated.

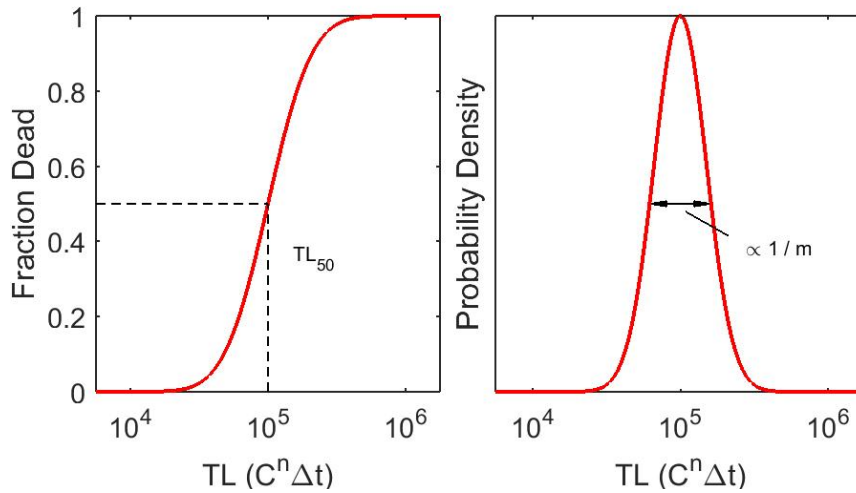


**Figure 1.** The relationship between toxic load and fraction dead (left) and probability density (right) for a population. The toxic load exponent  $n$  parameterizes the x-axis, weighing the relative importance of concentration and exposure time. The median toxic load  $TL_{50}$  captures the overall susceptibility of the population, while the probit slope  $m$  captures the variability of susceptibility in the population.

The toxic load model was originally defined for single square pulse exposures (ten Berge, 1983). However, as the toxic load model is phenomenological, it is unclear how to extend toxic load to a given time varying exposure. Various extensions to the toxic load model have been proposed to capture time dependence: the Ten Berge model (4), the average concentration model (5), the peak concentration model (6), the concentration intensity model (7), and the Griffiths-Megson model (8). These models define the toxic load in terms of the time dependent concentration  $C(t)$  and the toxic load exponent  $n$ :

$$TL = \int C^n(t) dt \quad (\text{Ten Berge}) \quad (4)$$

$$TL = \left( \frac{\int C(t) dt}{\Delta t} \right)^n \Delta t = (\overline{C(t)})^n \Delta t \quad (\text{Average Concentration}) \quad (5)$$

$$TL = \left( \frac{\int C(t) dt}{\sup \{C(t)\}} \right) \sup \{C(t)\}^n \quad (\text{Peak Concentration}) \quad (6)$$

$$TL = \left( \frac{(\int C(t) dt)^{2-n}}{(\int C^2(t) dt)^{1-n}} \right) \quad (\text{Concentration Intensity}) \quad (7)$$

$$TL = \left( \frac{\int C(t) dt}{\Delta t_{C>0}} \right)^n \Delta t_{C>0} \quad (\text{Griffiths-Megson}) \quad (8)$$

The expressions for toxic load are understood to be defined only over the time interval between the onset and termination of chemical exposure. These expressions are well defined given a particular  $C(t)$ , exposure duration  $\Delta t$ , and toxic load exponent  $n$ . The different models generally produce different values of the toxic load and significantly different casualty predictions (Czech 2011). However, in the case of constant exposures ( $C(t) = C$ ), all the extensions are identical to the general toxic load model of Equation (1).

#### **CONSTANT-CONC. EXPOSURES: ESTIMATION OF TOXIC LOAD PARAMETERS**

In order to validate the proposed extensions of the toxic load model (Equations 4 – 8), we first fit the basic toxic load model described in Equation (1). Based upon our assessment of goodness of fit, we find that a toxic load model with parameters  $n = 1.36$ ,  $TL_{50} = 5.41 \times 10^4$ , and  $m = 6.17$  well captures the lethality of HCN in a healthy population of male Sprague-Dawley rats resulting from constant concentration exposures of 10-30 minutes in duration. The details of the model fitting are described in a companion paper (Slawik, et al., 2016). We exclude exposures of shorter duration (2.3 and 5 minutes) because they fit the model poorly.

#### **TIME-VARYING EXPOSURES: VALIDATION OF TOXIC LOAD EXTENSIONS**

All five toxic load model extensions (Equations 4-8) can be shown to fit the 10-30 minute data poorly in plots of predicted versus observed casualties. The Griffiths-Megson and Average Concentration models (equations (8) and (4) respectively, provide the best overall casualty predictions. Figure 1 depicts the accuracy of the Average Concentration model in predicting the 10 and 30 minute time-varying exposure data with and without a time gap.

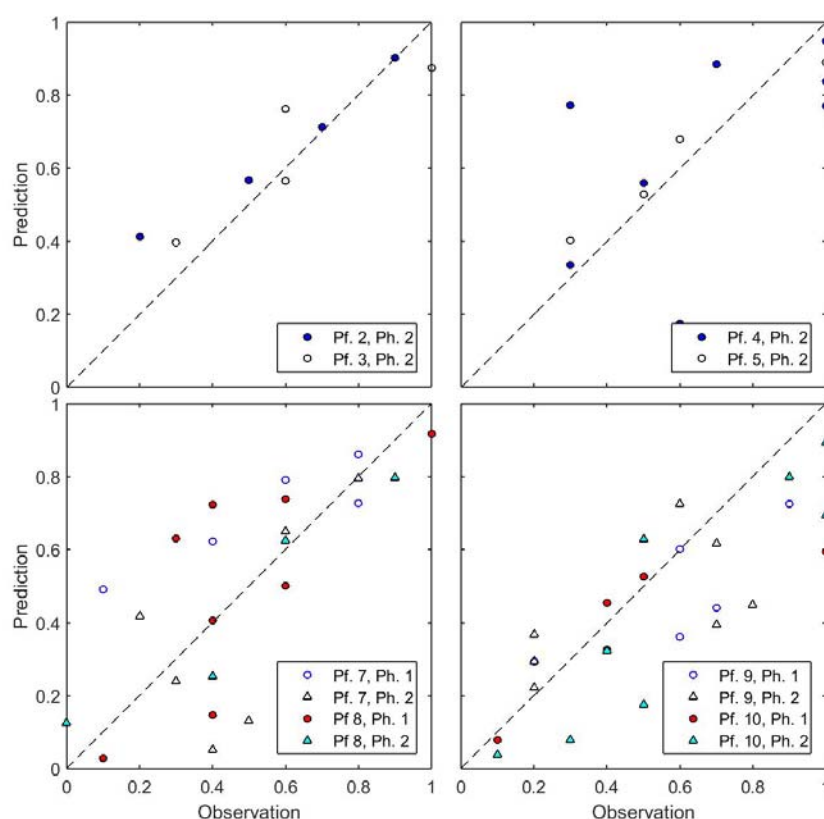


**Figure 2.** Predicted versus observed fractional casualties for time-varying 10 and 30 minute duration profiles using the Average Concentration model, equation (4). The time-constant 10-30 minute duration data are used to fit the toxic load parameters to generate predicted values. Each dot denotes a specific trial (10 rats). Color and shading style denotes each profile (Pf.) and phase or year of experiment (Ph.). For the 10 minute profiles, casualties are slightly over-predicted, and for the 30 minute profiles, there is scatter in the casualty comparisons. For time-varying exposures without a gap (left column), the Griffiths-Megson model, equation (8), is identical to Average Concentration model.

### QUANTIFYING BIAS AND SCATTER

The accuracy of the toxic load model extensions can be assessed by comparing model predictions to observations. Careful inspection of the Average Concentration model's predictions in Figure 2 on a profile by profile basis reveals either over-prediction or under prediction bias for many profiles, and the scatter of the data points is easily visible. The average absolute error in casualty prediction is 1.6 rats, or about 16% of the total sample size. Since only ten rats are exposed for each trial, sampling error can be significant. Taking the predicted casualties as our starting point, we can determine whether the observed difference between the model and the data is larger than that expected to arise by chance alone due to sampling.

We choose the mean square error (MSE) statistic to quantify scatter and the absolute value of mean error (AME) statistic to quantify bias (ie. a tendency to over-predict or under-predict). If the rat population sampled in each trial is assumed to be perfectly described by the toxic load model extension, the observed casualties will be distributed according to a binomial distribution centered at the predicted number of casualties. We can capture the expected distribution of a statistic due to sampling variability alone using Monte Carlo simulations to sample the binomial distribution. If the observed MSE and AME for each profile is uncharacteristically large, then the toxic load model extension in question provides poor predictions. Tables 1 and 2 compare the performance of the five tested toxic load model extensions using the MSE and AME statistics respectively. Performance is measured via the p-value (the probability of obtaining as extreme a value) estimated by Monte Carlo simulation with 10,000 trials. If

the agreement between the model predictions and observations is perfect, the p-values should be evenly distributed between 0 and 1; clustering of p-values near 1 denotes poor predictions. We choose an error in the 90<sup>th</sup> percentile to denote a poor fit. Each combination of exposure profile and toxic load model extension is marked in red or green to denote “bad” or “good” fits respectively.

**Table 1.** Variance of Predictions: p-values of mean squared error statistic

Profile, Year	Profile type	Duration	Griffiths-Megson p-values	Ave. Conc. p-values	Ten-Berge p-values	Conc. Int. p-values	Peak Conc. p-values
Prof. 2, 2013	No gap	10 mins	0.3728	0.3728	0.9723	0.9948	0.9998
Prof. 3, 2013	No gap	10 mins	0.3990	0.3990	0.8206	0.8990	0.9793
Prof. 7, 2012	No gap	30 mins	0.9746	0.9746	0.9918	0.9952	0.9997
Prof. 8, 2012	No gap	30 mins	0.9934	0.9934	0.9938	0.9968	0.9996
Prof. 7, 2013	No gap	30 mins	0.9800	0.9800	0.9993	0.9996	1.0000
Prof. 8, 2013	No gap	30 mins	0.4159	0.4159	0.4871	0.5881	0.8043
Prof. 4, 2013	Gap	10 mins	1.0000	0.9998	1.0000	1.0000	1.0000
Prof. 5, 2013	Gap	10 mins	0.8495	0.1781	0.9964	0.9989	0.9998
Prof. 9, 2012	Gap	30 mins	0.5639	0.8070	0.6333	0.6776	0.8840
Prof. 10, 2012	Gap	30 mins	0.9302	0.9260	0.9997	1.0000	1.0000
Prof. 9, 2013	Gap	30 mins	0.8851	0.9845	0.9647	0.9804	0.9958
Prof. 10, 2013	Gap	30 mins	0.9656	0.9989	0.8944	0.8904	0.9203

**Table 2.** Bias of Predictions: p-values of absolute mean error statistic

Profile, Year	Profile type	Duration	Griffiths-Megson p-values	Ave. Conc. p-values	Ten-Berge p-values	Conc. Int. p-values	Peak Conc. p-values
Prof. 2, 2013	No gap	10 mins	0.6882	0.6882	0.9964	0.9997	1.0000
Prof. 3, 2013	No gap	10 mins	0.4002	0.4002	0.9135	0.9681	0.9964
Prof. 7, 2012	No gap	30 mins	0.9864	0.9864	0.9979	0.9990	1.0000
Prof. 8, 2012	No gap	30 mins	0.9211	0.9211	0.3071	0.5740	0.9791
Prof. 7, 2013	No gap	30 mins	0.5429	0.5429	0.9924	0.9986	0.9999
Prof. 8, 2013	No gap	30 mins	0.4322	0.4322	0.6243	0.7895	0.9328
Prof. 4, 2013	Gap	10 mins	0.9314	0.2194	1.0000	1.0000	1.0000
Prof. 5, 2013	Gap	10 mins	0.9639	0.2483	0.9996	0.9999	1.0000
Prof. 9, 2012	Gap	30 mins	0.4431	0.9009	0.6398	0.7195	0.9513
Prof. 10, 2012	Gap	30 mins	0.8280	0.5758	0.9999	1.0000	1.0000
Prof. 9, 2013	Gap	30 mins	0.0179	0.9852	0.9161	0.9460	0.9972
Prof. 10, 2013	Gap	30 mins	0.9363	1.0000	0.0301	0.2928	0.7334

Table 3 summarizes the results of the Monte Carlo simulations, noting the fraction of profiles without uncommonly large scatter, bias, and scatter or bias. The Griffiths-Megson and Average Concentration model provide the least inaccurate predictions, but their predictions are still poor, failing over half of the profiles tested. The peak concentration model clearly performs poorly, and the commonly used ten-Berge model provides accurate predictions for only a quarter of the profiles.

**Table 3.** Toxic load model extensions’ overall performance in predicting casualties

Metric	Griffiths-Megson	Average Conc.	Ten-Berge	Conc. Intensity	Peak Conc.
# profiles with acceptable scatter	6 of 12	5 of 12	4 of 12	4 of 12	2 of 12
# profiles with acceptable bias	7 of 12	7 of 12	4 of 12	4 of 12	1 of 12
# profiles with acceptable bias and scatter	5 of 12	4 of 12	3 of 12	3 of 12	0 of 12

## CONCLUSIONS

The disagreement between the toxic load model predictions and the 10-30 minuet exposure data is much higher than that expected due to sampling error alone. Systematic experimental error or some physiological process in the rat not described by the models could explain this disagreement. The failure of these models to accurately describe the time-varying exposure data is troubling considering the importance modelling casualties arising from time-varying exposures in real-world airborne hazardous release incidents.

**ACKNOWLEDGEMENTS:** This effort was supported by the US Defense Threat Reduction Agency (through Mr. Richard J. Fry as the project monitor) and the Institute for Defense Analyses' professional development program. The views expressed in this paper are solely those of the authors.

## REFERENCES

- ten Berge, W.F., van Heemst, M.V., 1983: Validity and accuracy of a commonly used toxicity-assessment model in risk analysis, Fourth International Symposium on Loss Prevention and Safety Promotion in Process Industries, Vol. 1, Institute of Chemical Engineers, Rugby, United Kingdom, pp. 11-112.
- Bliss, C. I. (1935). The calculation of the dosage-mortality curve. *Annals of Applied Biology*, 22(1), 134-167.
- Czech, C., Platt, N., Urban, J., Bieringer, P., Bieberbach, G., Wyszogrodzki, A., Weil, J., 2011: A comparison of hazard area predictions based on the ensemble-mean plume versus individual plume realizations using different toxic load models, Paper 2.5 at the Special Symposium on Applications of Air Pollution Meteorology, 91<sup>st</sup> Annual American Meteorological Society Meeting, Seattle, Washington, Jan. 2011.
- Slawik, A.J., Axelrod, K.C., Silva, J.B., Dimitrov, I.K., Urban, J.T., Platt, N., 2016: Are toxic –load-based toxicity models consistent with experimental observations? Independent analysis of steady-exposure data from the 2012–2013 ECBC/NAMRU-D toxicological experiments, Proceedings of the 17th International Conference on Harmonisation within Atmospheric Dispersion Modelling for Regulatory Purposes, 9-12 May 2016, Budapest, Hungary
- Sweeney, L. M., Sommerville, D. R., & Channel, S. R. 2014: Impact of non-constant concentration exposure on lethality of inhaled hydrogen cyanide. *Toxicological Sciences*, **138**(1), 205-216.
- Sweeney, L. M., Sommerville, D. R., Channel, S. R., Sharits, B. C., Gargas, N. M., & Gut, C. P., 2015: Evaluating the validity and applicable domain of the toxic load model: Impact of concentration vs. time profile on inhalation lethality of hydrogen cyanide. *Regulatory Toxicology and Pharmacology*, **71**(3), 571-584.

**17th International Conference on  
Harmonisation within Atmospheric Dispersion Modelling for Regulatory Purposes  
9-12 May 2016, Budapest, Hungary**

---

**ESTIMATING AMBIENT CONCENTRATIONS OF BENZO(A)PYRENE IN EUROPE -  
POPULATION EXPOSURE AND HEALTH EFFECTS**

*Cristina Guerreiro<sup>1</sup>, Jan Horálek<sup>2</sup>, Frank de Leeuw<sup>3</sup>, and Florian Couvidat<sup>4</sup>*

<sup>1</sup>Norwegian Institute for Air Research

<sup>2</sup>Czech Hydrometeorological Institute

<sup>3</sup>National Institute for Public Health and the Environment,

<sup>4</sup>National Institute for Industrial Environment and Risk

**Abstract:** Current ambient background Benzo(a)pyrene (BaP) concentration levels, population exposure and potential health impacts were estimated by combining the results from chemical transport models and observations through the use of spatial interpolation methods. The work was based on the current ETC/ACM mapping methodology, residual kriging, using measured air quality data as a dependent variable and results from a CTM, as well as supplementary data (e.g. altitude and meteorological information), as independent variables. In this study model results from both the EMEP MSC-E and CHIMERE models have been used and analysed. Based on the estimated concentration maps, compliance with the EU TV was assessed. The spatial interpolated concentration fields show quite similar results when comparing the use of EMEP and CHIMERE model results for 2012. Both concentration maps show high 2012 annual mean concentrations of BaP in Eastern Europe, especially Poland and the Czech Republic, as well as in Northern Italy. The analysis of the uncertainties of the interpolated map shows that in large parts of Europe the concentration estimate is quite uncertain, with the relative standard error exceeding the 60%, due to the low density of the measurement network. The population-weighted concentration of BaP averaged over the whole Europe was about 0.9 ng.m<sup>-3</sup> in 2012. About 20 % of the European population was exposed to BaP annual mean concentrations above the target value of 1 ng.m<sup>-3</sup> in 2012 and only about 12 % of the European population live in areas with concentrations under the estimated reference level of 0.12 ng.m<sup>-3</sup>. The estimated population-weighted concentration of BaP is above 1.5 ng.m<sup>-3</sup> in large regions of Eastern Europe, including the Baltic countries. Using the concentration data from both models, the number of lung cancer incidences within the whole model area has been estimated to 550 (95% CI: 180-940) and 600 (95% CI: 200-1030) for the EMEP and CHIMERE model, respectively. About 50% of the incidences occur in Poland and Romania. A brief presentation of the standardisation work on the definition and use of modelling quality objectives for air quality assessment recently started by the CEN group CEN/TC 264/WG 43 will also be given.

**17th International Conference on  
Harmonisation within Atmospheric Dispersion Modelling for Regulatory Purposes  
9-12 May 2016, Budapest, Hungary**

---

**ARE TOXIC LOAD-BASED TOXICITY MODELS CONSISTENT WITH EXPERIMENTAL  
OBSERVATIONS? INDEPENDENT ANALYSIS OF STEADY-EXPOSURE DATA FROM THE  
2012–2013 ECBC/NAMRU-D TOXICOLOGICAL EXPERIMENTS**

*Alexander J. Slawik<sup>1</sup>, Kevin C. Axelrod<sup>1,2</sup>, James B. Silva<sup>1,3</sup>, Ivo K. Dimitrov<sup>1</sup>, Jeffrey T. Urban<sup>1</sup>, and  
Nathan Platt<sup>1</sup>*

<sup>1</sup>Institute for Defense Analyses, Alexandria, Virginia, USA

<sup>2</sup>Graduate Program in Biophysics, Harvard University, Cambridge, Massachusetts, USA

<sup>3</sup>Department of Physics, Boston University, Boston, Massachusetts, USA

**Abstract:** Toxic industrial chemicals and chemical warfare agents present an acute inhalation hazard to civilians and military personnel. An individual exposure to an airborne hazardous material may be highly time-dependent due to the random effects of wind meandering and atmospheric turbulence. Several toxicological models based on the "toxic load" model of exposure have been proposed to predict the casualties arising from time-dependent exposures to airborne hazardous materials, but none were developed using data from toxicological experiments that used time-varying exposure profiles. The US Defense Threat Reduction Agency (DTRA) sponsored a two-year set of experiments, conducted in 2012 and 2013, that were designed and executed through a collaboration between the US Army's Edgewood Chemical and Biological Center (ECBC) and the Naval Medical Research Unit Dayton (NAMRU-D) to explore the effects of time-varying inhalation exposures of hydrogen cyanide (HCN) gas on rats.

Our independent analysis of the data from the ECBC/NAMRU-D toxicological experiments has two components. The first component, which is the subject of this paper, is an analysis of the steady-exposure (square-pulse) data. Since the toxic load model was originally designed with these types of exposures in mind, this analysis is intended to examine whether the basic toxic load model suitably describes the ECBC/NAMRU-D data set. The second component of our analysis, which is described in a separate paper, examines whether several proposed extensions of the basic toxic load model suitably describe the time-varying exposure data from the ECBC/NAMRU-D experiments.

Our analysis of the ECBC/NAMRU-D data indicates that the basic toxic load model is not suitable for describing the steady-exposure data over the full range of the experiments' exposure durations (2.3 minutes to 30 minutes): the model fits the data well only if the short-duration exposures (less than 10 minutes) are dropped from the data set. This is potentially significant since HCN inhalation exposures can be lethal below 10 minutes, so there is a need for toxicological models that can describe toxicity on timescales of not only tens of minutes, but also minutes. Our analysis, however, was unable to determine whether the poor fit was due to systematic experimental error or a failure of the toxic load model to account for the physiological response of the rat across all investigated timescales.

**Key words:** *Toxicology, toxic load, hazardous materials, acute inhalation exposure, consequence assessment, health and exposure assessment, hydrogen cyanide, HCN, rats*

## **INTRODUCTION**

Health assessments based on atmospheric dispersion modelling require a toxicological model to relate the exposures to airborne contaminants predicted by the dispersion models to the likelihood of adverse health effects arising from those exposures. Our previous work examined whether atmospheric dispersion models that predict ensemble-mean plumes can predict casualties and the location of health hazards accurately as well as some of the theoretical differences between different toxic load-based toxicity models (Urban et al., 2011; Urban et al., 2014; Platt et al., 2014). Our present work examines the experimental validation of toxic load-based toxicity models themselves.

Our research focuses on the health effects arising from accidental or intentional releases of toxic industrial chemicals or chemical warfare agents. For these types of scenarios, acute inhalation exposures

may be on the order of tens of minutes or less if the wind transports the hazardous material beyond the affected population quickly enough, or if the affected population is able to take timely action to mitigate the hazard, such as evacuating from the exposed area, seeking shelter, or donning protective equipment. Acute exposures may be longer, on the order of hours, if the hazard is persistent (e.g., a dense gas in low-wind conditions) and effective hazard mitigation is not possible.

The most common statistical model used in the study of acute inhalation toxicology is the dose-probit response model (Finney, 1947; Sommerville et al., 2006). In this model, toxic effects are quantal (dichotomous), and the likelihood of an organism reaching a given toxic endpoint (e.g., death) depends only on the total amount of toxic material (i.e., the total dose of toxicant) that has accumulated in the organism. The dose-probit model, which is purely phenomenological, does not account for variations in the manner in which the dose is administered, such as the time history of the exposure: all combinations of  $C$  and  $T$  that have the same product  $D$  are predicted to have the same toxic effect. The likelihood of a single organism responding to a given exposure (e.g., by dying) is usually equated with the fractional response of a population of identical organisms subjected to identical exposures – the latter quantity can be measured directly in toxicological experiments. The dose-probit model assumes that the fraction of the population responding, when measured on a probit scale, is a lognormal function of the dosage (Equation 1).

$$Y_p = c_0 + m \log_{10}(D) \quad (1)$$

In this equation, the response function  $Y_p$  is measured on a probit scale,  $m$  is a quantity called the probit slope,  $\log_{10}(z)$  is the base-10 logarithm of  $z$ , and the dosage  $D$  is assumed to be proportional to the actual inhaled dose, where  $C$  is the atmospheric concentration of toxicant in the exposure and  $T$  is the exposure duration. The coefficients  $c_0$  and  $m$  depend on the type of toxicant and type of organism. This formulation is valid only for steady exposures where  $C$  is constant over the whole time interval  $T$ . The probit scale linearizes the response function. The actual response function is a sigmoidal function of the logarithm of the dosage  $D$  (Eq. 2).

$$P = \{\text{erf}[(m \log_{10}(D) - m \log_{10}(D_{50})) / \sqrt{2}] + 1\} / 2 \quad (2)$$

Here  $P$  is the fraction of the population that exhibits a given response,  $\text{erf}(z)$  represents the error function of  $z$ , and a new constant has been introduced:  $D_{50}$ , the median effective dosage (i.e., the dosage required to cause a response in 50% of the population). Eqs. 1 and 2 were developed and validated for the case in which  $C$ , the atmospheric concentration of toxicant in the exposure, is constant over the whole exposure duration  $T$ . In this case the dosage is given by Eq. 3.

$$D = C \times T \quad (3)$$

For some toxicants, particularly some of the toxic industrial chemicals (TICs), the dose-probit model yields a poor fit to data from toxicological experiments. Since the dose-probit model does not take into account the time dependence of physiological processes, such as the uptake and clearance of toxicants in the body, a more general phenomenological model has been proposed to account for the fact that a high-intensity but short exposure could have a different toxic effect from a low-intensity but long exposure of equal dosage. This model, called the “toxic load” probit-response model, treats the concentration-dependence and exposure duration-dependence of the physiological response independently. The “toxic load” generalization of Eqs. 1 through 3 is given by Equations 4 through 6 (ten Berge et al., 1986; Sommerville et al., 2006).

$$Y_p = k_0 + k_1 \log_{10}(C) + k_2 \log_{10}(T) \quad (4)$$

$$P = \{\text{erf}[(m \log_{10}(TL) - m \log_{10}(TL_{50})) / \sqrt{2}] + 1\} / 2 \quad (5)$$

$$TL = C^n \times T \quad (6)$$

In the equations the prior measure of exposure, the dosage  $D$ , has been generalized to the “toxic load”  $TL$ , which is no longer proportional to the inhaled dose. The coefficients  $k_0$ ,  $k_1$ , and  $k_2$  in Eq. 4, which depend on the type of toxicant and organism, have been rearranged in Eqs. 5 and 6 as the probit slope  $m$ , the median lethal toxic load  $TL_{50}$ , and the toxic load exponent  $n$ .

The toxic load-probit model (Eqs. 4–6), like the dose-probit model, was formulated only for the case of steady-exposures, which are the exposures that have been accessible to toxicological experiments. Real-world exposures to airborne toxicants, however, may be highly time-dependent due to the random effects of wind meandering and atmospheric turbulence (Wilson, 1995). Various extensions to the toxic load model have been proposed to predict the toxicological effects of time-varying exposures  $C(t)$ , but until recently, little data were available with which to validate these proposed extensions. The toxicological experiments that are the subject of this paper were intended to remedy this deficiency. This paper, however, focuses on the validity of the basic toxic load model rather than its time-dependent extensions.

### **ECBC/NAMRU-D TOXICOLOGICAL EXPERIMENTS**

The US Defense Threat Reduction Agency (DTRA) sponsored a two-year set of experiments, conducted in 2012 and 2013, that were designed and executed through a collaboration between the US Army's Edgewood Chemical and Biological Center (ECBC) and the Naval Medical Research Unit Dayton (NAMRU-D) to explore the toxic effects of time-varying inhalation exposures (Sweeney, et al. 2014; Sweeney, et al., 2015). In these experiments, groups of ten male Sprague-Dawley rats were exposed to HCN gas using a pressurized, nose-only inhalation apparatus that allowed excellent control of the time profile of the exposures. For each exposure, the fraction of the ten rats that did not survive the exposure was recorded.

The ECBC/NAMRU-D experiments investigated three basic types of exposure profile: single steady pulses (i.e., fixed  $C$  and  $T$ ), two unequal-intensity pulses back-to-back, and two unequal-intensity pulses separated by a gap during which there was no exposure to HCN gas. The exposure durations and the ordering of the two-pulse profiles (i.e., high-then-low vs. low-then-high) varied between the 2012 experiments and the 2013 experiments. This paper considers only the steady-pulse data; the two-pulse data are considered in a separate paper. The experiments included 126 trials with ten rats per trial, of which 34 trials featured steady-pulse exposures having various combinations of  $C$  and  $T$ . In 2012 there were 7 trials with  $T = 5$  minutes, 7 trials with  $T = 15$  minutes, and 6 trials with  $T = 30$  minutes. In 2013 there were 7 trials with  $T = 2.3$  minutes, 5 trials with  $T = 10$  minutes, and 2 trials with  $T = 30$  minutes.

### **DATA ANALYSIS**

We evaluated the basic (i.e., steady-exposure) toxic load model by fitting Eq. 5 with the steady-exposure data from the ECBC/NAMRU-D experiments and then examining measures of the goodness-of-fit. We performed the fits by the maximum-likelihood estimation (MLE) method using the Benchmark Dose Software (BMDS) developed by the US Environmental Protection Agency (EPA, 2015). BMDS estimates the three coefficients of the toxic load model by performing a simultaneous 3-parameter fit. BMDS also estimates the coefficients' covariance matrix using the Fischer information matrix and performs parametric tests of the goodness of fit.

#### **Initial analysis**

The BMDS-estimated toxic load model parameters are  $n = 1.35$ ,  $TL_{50} = 5.41 \times 10^4$ , and  $m = 1.68$  using all 34 steady-exposure trials. Figure 1 shows the fit of the sigmoidal response function to the 34 data points and a plot of predicted versus observed response using the fitted coefficients. The latter plot is a measure of the self-consistency of the data. A well-fit model would result in predictions that equal observations (i.e., that lie on the diagonal line in a predictions vs. observations plot).

Note that there is considerable scatter in the data. In particular, the 5-minute exposures generally resulted in more casualties than one would expect from the toxic load model, whereas the 2.3-minute exposures generally resulted in fewer casualties than one would expect.

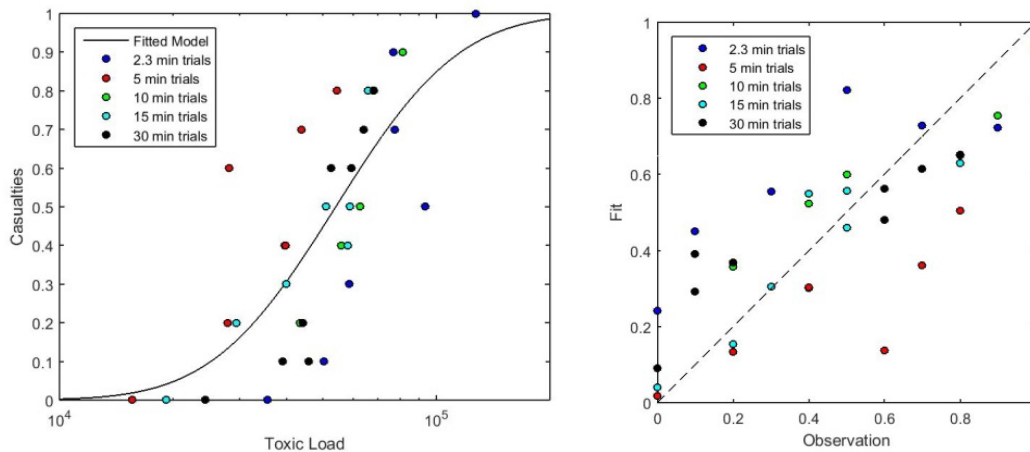


**Figure 1.** Left: Fit of the toxic load model, Eq. 5, to all 34 steady-exposure trials. Fractional casualties (e.g., 4 rats dead out of 10 = 0.4) are plotted as a function of the toxic load for each trial. Each point represents one trial of 10 rats. Right: Predicted vs. observed fractional casualties for all 34 trials using the coefficients from the fit on the left.

### Investigation of the self-consistency of the toxic load model across timescales

Figure 1 indicates that the toxic load model appears not to perform well for the shorter-timescale exposures in the ECBC/NAMRU-D data set. To further explore the performance of the toxic load model at different timescales, we re-fit the model using only subsets of the original 34 trials (e.g., the 20 trials with  $T = 10, 15,$  and 30 minutes) and used the new fitted coefficients to compare predicted vs. observed fractional casualties for the same subset of trials. We also examined measures of goodness of fit. Figure 2 shows an example plot of predicted vs. observed fractional casualties for the subset of 20 trials with  $T = 10, 15,$  and 30 minutes, along with a table showing the fitted model coefficients for different subsets of the data and the associated measures of goodness of fit.

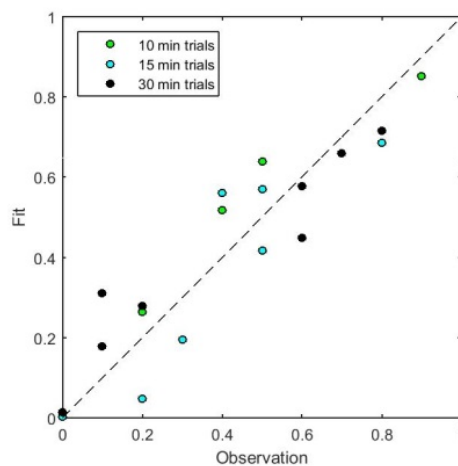


**Figure 2.** Predicted vs. observed fractional casualties for all the subset of 20 steady-exposure trials with  $T = 10, 15,$  and 30 minutes. The predictions used toxic load model coefficients that were fitted using the same subset of data.

**Table 1.** Toxic load model coefficients and goodness-of-fit metrics (root-mean-square error (RMSE) and  $p$ -value) derived from fits to different exposure-duration data subsets. The user manual for the US EPA’s BMDS software, which was used to make the fits, suggests that  $p < 0.1$  indicates a poor fit. Larger RMSE values indicate poorer fits.

Exposure durations (min)	# of trials	$n$	$TL_{50}$	$m$	RMSE	$p$ -value
2.3, 5, 10, 15, 30	34	1.35	$5.41 \times 10^4$	3.87	0.187	0.000337
2.3, 10, 15, 30	27	1.23	$2.71 \times 10^4$	7.04	0.124	0.221
5, 10, 15, 30	27	1.73	$5.20 \times 10^5$	3.71	0.145	0.257
10, 15, 30	20	1.36	$5.62 \times 10^4$	6.15	0.105	0.856
5, 15, 30	20	1.79	$7.06 \times 10^5$	3.85	0.137	0.351
2.3, 5, 10	19	1.12	$1.05 \times 10^4$	4.00	0.209	0.005

Figure 2 indicates that the toxic load model is poorly fit when all 34 trials (i.e., all exposure timescales) of the ECBC/NAMRU-D steady-exposure data set are used. The model fit improves, as does the model predictive performance, when data from some exposure durations are removed. In particular, removing the 5-minute exposure time data results in the largest improvement in the fit, and removing the data for the two shortest exposure times (2.3 minutes and 5 minutes) results in the best fit. This suggests that the toxic load model does not perform well across the full set of exposure durations represented in the ECBC/NAMRU-D steady-exposure data set. The toxic load model cannot predict casualties well at both the shorter (2.3 and 5 minutes) and the longer (10, 15, and 30 minutes) exposure durations using the same set of model coefficients. Since HCN exposure durations of both minutes and tens of minutes can result in a significant likelihood of death if the HCN concentration is high enough, this suggests that there may be an intrinsic problem with the toxic load model – at least for HCN inhalation exposures in rats.

In work not reported here, we also calculated  $p$ -values using an alternative Monte Carlo sampling method since the BMDS-calculated scores from the Pearson’s  $\chi^2$  test (which we converted to  $p$ -values in Table 1) can be inaccurate when sample sizes are small (e.g., 10 rats per trial). Although the Monte Carlo-based  $p$ -values can differ significantly from the BMDS-based ones, our overall findings about which subsets of the data give good fits are not changed appreciably. We further explored the effects of small samples by performing statistical tests to examine whether the scatter in the data could be explained solely by sample size effects. We found that the scatter of the data in the full data set of 34 trials cannot be explained solely by sample size effects, but that the scatter in the  $T = 10, 15,$  and  $30$  minute subset is within the expected scatter. Therefore, we confirm that the 2.3- and 5-minute data are not well-explained by the toxic load model, either due to a systematic experimental error or some physiological process in the rat.

## CONCLUSIONS

Our analysis of the ECBC/NAMRU-D data indicates that the toxic load model is not suitable for describing the steady-exposure data over the full range of the experiments’ exposure durations (2.3 minutes to 30 minutes): the model fits the data well only if the short-duration exposures (less than 10 minutes) are dropped from the data set. Our analysis does not attempt to attribute a physical explanation for these results. We note that a practical toxicology model should be able to describe toxicological effects across the full timescale of interest (i.e., from minutes to tens of minutes or longer).

**Acknowledgements:** This effort was supported by the US Defense Threat Reduction Agency (through Mr. Richard J. Fry as the project monitor) and the Institute for Defense Analyses’ professional development program. The views expressed in this paper are solely those of the authors.

## REFERENCES

- EPA, 2015: Benchmark Dose Software (BMDS) User Manual (BMDS 2.6.0), US Environmental Protection Agency, Washington, DC, USA, 339 pp.
- Finney, D.J., 1947: Probit Analysis: A Statistical Treatment of the Sigmoid Response Curve. Cambridge University Press, Cambridge, UK, 256 pp.

- Platt, N., W.R. Kimball and J.T. Urban, 2014: The use of probabilistic plume predictions for the consequence assessment of atmospheric releases of hazardous materials. *Int. J. of Environment and Pollution*, **55**, 3-12.
- Sommerville, D.R., K.H. Park, M.O. Kierzewski, M.D. Dunkel, M.I. Hutton and N.A. Pinto, 2006: "Toxic Load Modeling" in *Inhalation Toxicity*, 2<sup>nd</sup> ed., eds. H. Salem and S.A. Katz, CRC Press, New York, NY, USA, pp 137-158.
- Sweeney, L.M., D.R. Sommerville and S.R. Channel, 2014: Impact of non-constant concentration exposure on lethality of inhaled hydrogen cyanide. *Toxicol. Sci.*, **138**, 205-216.
- Sweeney, L.M., D.R. Sommerville, S.R. Channel, B.C. Sharits, N.M. Gargas and C.P. Gut Jr., 2015: Evaluating the validity and applicable domain of the toxic load model: Impact of concentration vs. time profile on inhalation lethality of hydrogen cyanide. *Regul. Toxicol. Pharmacol.*, **71**, 571-584.
- ten Berge, W.F., A. Zwart and L.M. Appelman, 1986: Concentration–time mortality response relationship of irritant and systemically acting vapours and gases. *J. Hazard. Mater.*, **13**, 301-309.
- Urban, J.T., M.A. Ambroso, K.J. Galvin, S.M. Nunes, D.F. DeRiggi and N. Platt, 2011: The role of atmospheric dispersion modelling in modern consequence assessment studies. *Proceedings of the 14<sup>th</sup> International Conference on Harmonisation within Atmospheric Dispersion Modelling for Regulatory Purposes*, 713-717.
- Urban, J.T., K.J. Galvin, N. Platt, P.E. Bieringer, G. Bieberbach and A.J. Annunzio, 2014: Comparison of hazard area and casualty predictions of a small-scale chemical attack using various toxic load toxicity models. *Int. J. of Environment and Pollution*, **54**, 222-232.
- Wilson, D.J., 1995: *Concentration Fluctuations and Averaging Time in Vapor Clouds*, Center for Chemical Process Safety of the American Institute of Chemical Engineers, New York, NY, USA, 181 pp.

**17th International Conference on  
Harmonisation within Atmospheric Dispersion Modelling for Regulatory Purposes  
9-12 May 2016, Budapest, Hungary**

---

**BEST PRACTICE GUIDELINES FOR THE USE OF ATMOSPHERIC DISPERSION MODELS  
AT LOCAL SCALE IN CASE OF HAZMAT RELEASES INTO THE AIR**

*Patrick Armand<sup>1</sup>, Kathrin Baumann-Stanzer<sup>2</sup>, E. Bemporad<sup>3</sup>, Claudio Gariazzo<sup>4</sup>, Marko Gerbec<sup>5</sup>,  
Steven Herring<sup>6</sup>, Ari Karpinnen<sup>7</sup>, Bernd Leitl<sup>8</sup>, Tamir G. Reisin<sup>9</sup>,  
Gianni Tinarelli<sup>10</sup>, and Silvia Trini Castelli<sup>11</sup>*

<sup>1</sup>CEA, DAM, DIF, F-91297 Arpajon, France

<sup>2</sup>ZAMG, Hohe Warte 38, A-1190 Vienna, Austria

<sup>3</sup>INAIL DIT, Via Roberto Ferruzzi 38 / 40, 00143 Rome, Italy

<sup>4</sup>INAIL DIMEILA, Via Fontana Candida 1, 00040 Monteporzio Catone, Italy

<sup>5</sup>Jozef Stefan Institute, Jamova 39, 1000 Ljubljana, Slovenia

<sup>6</sup>Dstl, Porton Down, Salisbury, Wiltshire, SP4 0JQ, England

<sup>7</sup>FMI, P.O. Box 503, FI-00101 Helsinki, Finland

<sup>8</sup>University of Hamburg, Meteorological Institute – EWT, Bundesstrasse 55, D-20146 Hamburg, Germany

<sup>9</sup>Israel Atomic Energy Commission, Tel Aviv, Israel

<sup>10</sup>Arianet S.r.l., via Gilino 9, 20128 Milano, Italy

<sup>11</sup>Institute of Atmospheric Sciences and Climate CNR, Corso Fiume 4, I-10133 Torino, Italy

**Abstract:** The last decade witnessed noteworthy progress in both atmospheric dispersion modelling in industrial or urban environments and access to computational power. Although the problem is still challenging, there are now reliable methods for predicting the turbulent flow around the buildings in an uneven terrain and the dispersion and deposition of possibly toxic gases or particles following an accidental or malevolent release. Moreover, some of these Atmospheric Dispersion Models (ADMs) can produce operational information like exposure and dose indexes in a time consistent with crisis management when integrated in Emergency Response Tools (ERTs). However, most practitioners still have reservations about modelling in general or use over-simplified models which are neither accurate, nor systematically conservative. In an important step to bridge the gap between the scientists, model developers and emergency players (plant operators, first responders, public authorities...), COST Action ES1006 undertook the development of Best Practice Guidelines (BPG) for the use of ADMs and ERTs within the framework of emergency preparedness and response. This was deemed essential by experts in the Action for promoting the use of up-to-date models inside ERTs used by the practitioners. This paper presents an overview of the content and main conclusions of the BPG.

**Key words:** *atmospheric dispersion models, emergency preparedness and response, best practice guidance.*

## **INTRODUCTION**

COST Action ES1006 dedicated to the “evaluation, improvement and guidance for the use of local-scale emergency prediction and response tools in case of airborne hazards in built environments” (called “the Action” in this paper) took place between 2011 and 2014. The activities were divided between Working Groups: WG1 aimed to catalogue the threats likely to impact an industrial site or an urban district, and the experiments and models devoted to the local scale atmospheric dispersion; WG2 aimed to benchmark the performance of various models when compared to wind tunnel and real scale experiments; and WG3 was an application oriented sub-project aiming to bridge the gap between model developers and end-users.

A key output from the Action was a document entitled “Best Practice Guidance” (BPG) produced by Working Group 3. These guidelines apply to the usage of Atmospheric Dispersion Models (ADMs) and Emergency Response Tools (ERTs) in support of decision-making in an emergency involving the release of hazardous materials (“hazmat”) into the atmosphere. The following paper strives to (1) exemplify the

differences in modelling the same situation using different types of models, (2) explain and briefly illustrate what can be found in the BPG, and (3) summarize the conclusions drawn by the BPG experts.

### **WHY IS IT CRUCIAL TO USE UP TO DATE DISPERSION MODELS?**

In the framework of the Action, questionnaires were distributed to first responders and stakeholders in several European countries with the objective of identifying their perception of, use of, needs and requirements for ADMs in ERTs. According to some of the responses, the available ADMs are perceived as having low accuracy and significant limitations due to lack of confidence in the input data, lack of modelling of critical phenomena, and lack of standardization in the application of modelling procedures. Several stakeholders did not trust ADM results unless they were presented along with *in-situ* measurements. From these statements, it was clear that there was a huge gap between the stakeholders' perception or state of mind regarding ADMs, the present capabilities of the models, and the efforts of developers to verify and validate model results and adapt ADMs to the practical needs of first responders and decision-makers.

On one side, considerable progress has been made in the last decade on parameterizing physical processes and implementing efficient numerical methods in ADMs. Advanced "4D" models are now available, that enable scientists and engineers to produce realistic and accurate simulations of the air flow and the dispersion. Moreover, the results of these models may be post-processed to provide operational results (danger zones, intervention zones...) when ADMs are integrated in ERTs.

On the other side, most of the first responders and decision makers still use or are provided with the results of simplified models which ignore the local effects of the topography and obstacles such as buildings, and so are not adapted to application in built-up environments. Even when the time constraint is not as stringent as in an emergency, ADMs used by risk assessors and, in general, by stakeholders to establish consequence assessments, emergency planning and management procedures or even urban planning are often over-simplified and do not accurately represent dispersion in complex urban or industrial environments.

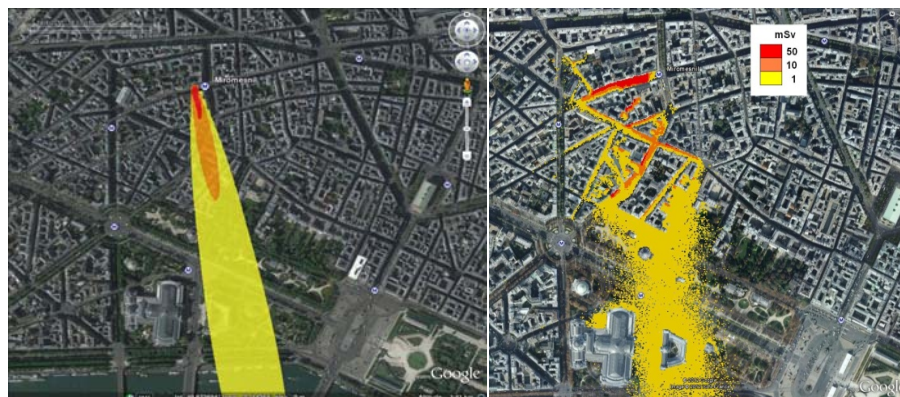
It is indisputable that different models are far from being equivalent as illustrated by the Figures 1-a) and 1-b) which were produced by the French Atomic and alternative energies Commission (Armand et al., 2013) as part of a fictitious "dirty bomb" exercise organised with Paris Fire Brigade. Figures 1-a) and 1-b) show the total effective dose (for an adult) predicted due to the hypothetical dispersion of 10 TBq of cobalt-60 in Paris city centre (8<sup>th</sup> district) following explosion of the dirty bomb. The dose is representative of the radionuclide integrated concentration in a horizontal plane near ground level. The 3D computations were done in real time using dispersion solvers implemented in the CERES® CBRN-E (CEA modelling and decision-support system): a Gaussian puff model Figure (1-a) and a Lagrangian Particle Dispersion Model coupled to a diagnostic flow model (influenced by the buildings) Figure (1-b).

The differences between the model solutions are obvious. The simple Gaussian model which ignores the obstacles predicts a simple dispersion downwind. However, the diagnostic wind field and LPDM model predicts the dispersion to be strongly influenced by the street network, and concentration gradients between the sides of some streets can be seen as the upwind propagation of the contaminant. What is not visible in the figures is that the plume travel time through the domain and its residence time in the streets is also much longer when predicted by the LPDM.

In this fictitious situation developed for emergency preparation training, the results were not of course compared against measurements. However, the LPDM embedded in CERES® CBRN-E was validated in the frame of the Action WG2 (Duchenne et al., 2016). These demonstrate that that the LPDM results are more realistic and relevant than the Gaussian ones. Moreover, they also demonstrated as shown here, that the Gaussian model is not systematically conservative contrary to the widespread belief among first responders.

Finally, the computational time of the LPDM was no more than 10 minutes on an octa-core server, which is an acceptable duration to provide a more accurate and informative prediction of the dispersion and

exposure. This example and many others provide evidence for why first responders and decision makers should use up-to-date flow and dispersion modelling, whether they undertake it themselves or receive it from scientific advisers.



**Figures 1-a) and 1-b).** Total effective dose due to the fictitious release of 10 TBq of  $^{60}\text{Co}$  in Paris city center(emergency response exercise).Prediction by a Gaussian model (a) and by diagnostic flow and LPDM models (b).S is the source location.

### THE JUSTIFICATION AND CONTENT OF THE BPG

Many human beings live in urban industrialized environments where both accidents and emerging threats (like terrorist attacks) may occur which lead to releases of hazardous materials into the air. While fortunately these events are quite seldom, they cannot be ignored. This is the reason why the COST Action ES 1006 focused on the threats to human life posed by hazmat releases in complex built environments. The most severe consequences of such events are likely to occur in the vicinity of the source and up to a few kilometres. At this local scale, it is critical to accurately model the dispersion and deposition of airborne materials in order to reliably assess the health effects on the population and first responders.

This provides the justification for the development and detailed verification and validation of the various kinds of atmospheric dispersion models. However it would be pointless to develop sophisticated dispersion models adapted to complicated environments that are unknown or not used by the people actually facing emergency situations (like the fire fighters, the representatives of public authorities, etc.). Thus, it was considered that to raise awareness the final part of the COST Action ES 1006 should try to establish the BPG for using different ADMs whether they were integrated or not into ERTs.

The BPG strives to organize guidelines with the aim of promoting effective and efficient knowledge transfer from the scientific community to plant operators, first responders, public local and national authorities, and all professionals routinely or occasionally involved in the preparedness and response to potentially hazardous dispersions of Chemical, Biological, or Radiological (CBR) species. The BPG is based on consideration of a range of ADMs and ERTs which have been used for a long time or are at the leading edge of the technology.

In order to establish a common understanding of the fundamental principles, the BPG identifies the key issues linking modelling and emergency preparedness and response. These issues relate to:

- The different types of ADMs, their main features, advantages and drawbacks;
- The position of the ADMs in the chain of assessment in ERTs;
- The estimation of exposure or dose indexes (giving an assessment of the health consequences) produced by post-processing the outputs of ADMs;

- The reference threat scenarios identified by the Action to illustrate the potential use of ADMs and ERTs;
- The people involved in the different phases of the response (risk assessors, experts, emergency responders, decision makers...), their roles and their interest in ADMs and ERTs;
- The results provided by ADMs which can be used in an operational situation and distributed to the emergency responders and / or decision-makers (danger zones, intervention zones...).

As an illustration, Figure 2 presents a simplified organizational diagram applicable to a radiological or chemical emergency involving an accidental or deliberate hazmat release. While national peculiarities might exist in the organization, it appears that as different as an accidental and a terrorist attack are, the organisation of the emergency response is likely to be similar. Figure 2 identifies the points at which the use of ADMs and ERTs may assist during the course of an emergency. For example, at field level, they may support the operational decisions of emergency responders. At local or intermediate level, they may provide information to better understand the situation and anticipate its evolution. At the highest decision making level, the results can be used to better handle the emergency and communicate with the population.

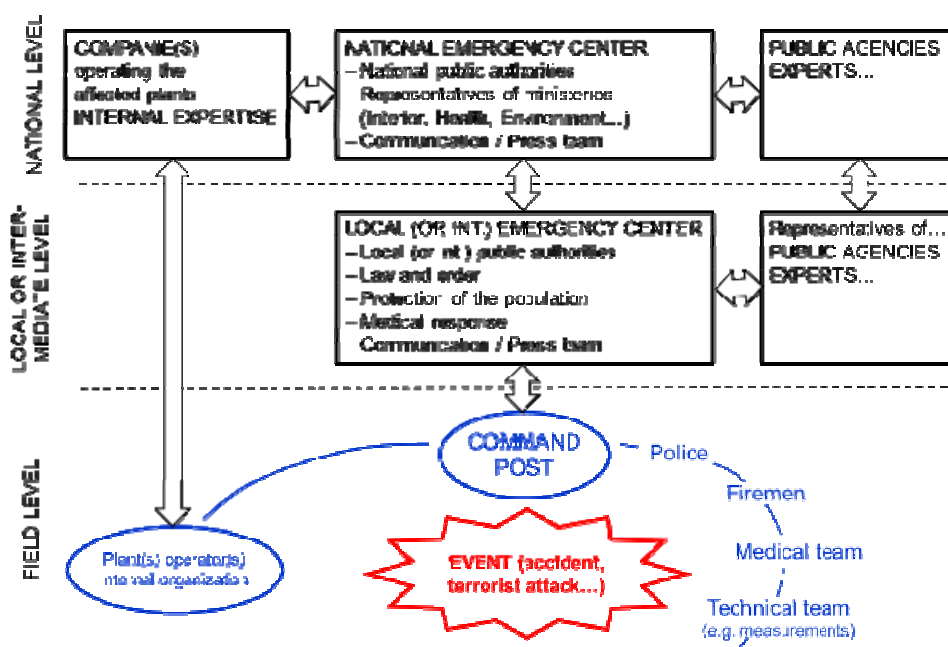


**Figure 2.** General sketch-up of the organization for handling an emergency.

Atmospheric dispersion models require meteorological inputs which may be observations and / or provided by flow models. Flow and dispersion models are connected, and the Action identified the general types of models listed in Table 1 and their typical execution times.

The BPG points out that ADMs and ERTs can provide supporting information whether the releases are long (some hours for continuous releases) or short (some seconds or minutes for puff releases) as, in the latter case, the end of the release is definitely not the end of the crisis.

**Table 1.** The classification by types of flow and dispersion models with their typical execution times (on adapted computational resources, e.g. a basic laptop for type 1 to a large workstation for type 3).

Model type	Flow model	Dispersion model	Execution time
1	No computation of the flow	Gaussian plume / puff model standard or with possible sophistication taking account of buildings	Seconds to minutes
2	Resolution of the flow with simplifications (limited set of equations and / or semi-analytical relations around the buildings...)	In general, Lagrangian particle dispersion model	Minutes to hours
3	Resolution of the flow around the buildings with the complete set of equations (CFD methods such as RANS or LES)	In general, Eulerian transport and dispersion model	Hours to days

Experts commonly agreed that throughout the emergency, a major challenge for the actors is to have the best possible representation of past events and the anticipated evolution of the situation. In this regard, the BPG highlights that even if the nature of the release is not precisely known, a preliminary flow and dispersion computation is instructive. A realistic calculation performed during the early stages of an emergency can provide useful information regarding features of the dispersion that may occur in complex industrial or urban environments that are not intuitive. This information can be valuable to decisions regarding the intervention of rescue teams, even if the exact concentration levels are not yet known.

A new aspect was also to give recommendations on ADMs or ERTs use from different perspectives:

- The first one takes account of the available level of information regarding the complexity of the situation, the environmental data, the release source, the meteorological input and all features of the event. This is related to the available models and computational resources, resulting in a proposal for a harmonized response-practice procedure and flow of actions (see the companion paper Herring *et al.*, 2016).
- The second one considers and separates the successive pre-event, event, and post-event phases of the emergency, the operators of the ADMs or ERTs and the final users of their results with the goal of answering the questions: “what to produce, when, and for whom?”
- The third one makes use of the relevant threat scenarios identified by the Action to give practical guidelines in case of (i) a neutrally buoyant release exemplified by the release of a small amount of chlorine within an urban area, (ii) a positive buoyancy release, as exemplified by a toxic plume produced by a fire in a warehouse, (iii) a dense gas release, exemplified by the leakage of many tonnes of (pressurized) chlorine or LPG, involving the flashing and pooling of material, and (iv) a “dirty bomb” that produces an explosive release of radionuclides.
- The fourth one is based on the results of the three model comparison exercises conducted by the Action, reported in “ES1006 Model Evaluation Case-Studies” (Baumann-Stanzer *et al.*, 2015) and summarized hereafter (see also Trini Castelli *et al.*, 2014; Baumann-Stanzer *et al.*, 2014).

Comparisons between ADM predictions and data from the Michelstadt and CUTE wind tunnel experiments in the Action showed that model performance increased with model complexity (i.e. a higher level of physical description). The improving performance trend was observed qualitatively from scatter plots, quantitatively by comparing the validation metrics, and from examination of scatter plots created for the set of ensembles produced by averaging over all results for a given model type. The type 3 CFD models were in general superior to the type 2 Lagrangian stochastic models and the type 1 Gaussian models (some of which were limited to modelling continuous plume releases).

Computational times are different for each model type as indicated in Table 1. Type 3 models typically involve long computation and preparation times and are not readily applicable during the emergency

phase where a quick simulation is required. Type 2 models are usually significantly faster than type 3 ones and render a satisfying agreement with measurements that suggests they can be used with a reasonable level of confidence. A possible way to reduce the computational time for type 3 models is to provide access to pre-processed meteorological data that is statistically representative of the typical conditions at the site of interest. This would save time in generating the meteorology, and an answer could be obtained quickly because it is only necessary to undertake the dispersion modelling.

Whatever the model, the availability of proper inputs plays a crucial role for obtaining reliable results. As seen from the sensitivity analyses, the more detailed these are, the better the models perform. Nevertheless, the models appeared robust even when dealing with poor driving information, as will be the general case following accidental releases. Thus, they are valid tools to support the handling of emergencies and can be applied with reasonable confidence, even considering the uncertainties when dealing with unexpected situations.

The choice of the modelling approach involves a balance between the model performances, its reliability, and the run-time effort. Different modelling approaches can be used in different phases of the response process: the preparatory phase, the emergency response phase and during a post-accidental analysis. However, another criterion to be considered when making decisions on what modelling tool to adopt is that a fast but inaccurate model output can compromise the effectiveness of a response action.

In its final part, the BPG addresses commonly asked difficult questions such as:

- How to deal with the uncertainties of the input parameters (source term, meteorological data...)?
- How to produce reasonably conservative results?
- How to overcome different results obtained by different models or operators?
- How to reconcile the modelling results and the field measurements?
- How to reconcile the needs and demands of the emergency players? Etc.

The reader is referred to the BPG for the answers to these given by the group of experts.

While it is essential to provide exposure or dose indexes since they are the practical measurement of the risk and cannot be ignored, it was beyond the scope of the Action to study the health and environmental impacts of hazmat releases. There is on-going research work whose aim is to improve the existing methods and the parameterisations associated with them. These topics are not covered by the Action and the BPG does not discuss the methods or parameters used to convert concentrations into exposures or doses.

The aim of the BPG is to provide a comprehensive yet focused document giving essential information for potential users in a straightforward manner. For this reason, the most important aspects of the guidance are summarized, while the reader is referred to other documents prepared in the frame of the Action for in-depth analysis. These include the Background and Justification Document, the Models and Emergency Response Tools Inventory, the Threats and Scenarios Catalogue, the Model Evaluation Protocol for Emergency Response, and the modelling exercises and inter-comparisons conducted by the Action ([www.elizas.eu](http://www.elizas.eu)).

## CONCLUSIONS

A summary of the BPG statements and recommendations built on the consensus among the international experts involved in the COST ES1006 Action is as follows:

- The use of ADMs in an emergency response does not correspond to the state-of-the-science of the 4D dispersion modelling in complex environments and more efforts should be done to promote the use of up-to-date models for emergency preparedness and response.
- Simple Gaussian models are still the models most often used for risk assessment and emergency response. These models do not resolve the detail of local-scale dispersion and without enhancements to predict dispersion in industrial or urban built environments may provide misleading outputs. Moreover, contrary to a common opinion of stakeholders, these models do not always provide conservative results.
- Simple Gaussian models might be advisable only on condition that they take account of buildings in some simplified way and are applied in the configurations for which they have been established.

- Lagrangian models taking account of the buildings may give accurate results in the order of 10-30 minutes with moderate computational resources. Input turbulent flow data models including buildings effects may be provided on-line by diagnostic flow or by CFD RANS models with some approximations, or off-line by pre-computed and tabulated CFD approach (RANS or LES).
- Eulerian models with the same input turbulent flow data as for Lagrangian models may be used when they are able to meet the time constraints of the event phase (although it is more practical to apply them in the pre- or post-event phases than in the emergency phase).

The Action identified the necessity for scientists and modelling experts to be engaged with the stakeholders, as this is a major condition for ensuring that the results from ADMs or ADMs results are trusted, and thus used by emergency responders and decision makers. It means that the development of ADMs in ERTs should not solely respect scientific criteria (like verification and validation), but also meet practical criteria (about the response time, interface, outputs, etc.). R&D in the field of atmospheric dispersion and health impact assessment should not only focus on physical modelling, but also consider the adequacy of the decision-support tools to meet the needs of the user organizations and civilian security missions. It seems to the experts within the Action that this approach is essential to promote the usage of state-of-the-art models inside the operational computational tools used by practitioners.

## REFERENCES

- Armand, P., J. Bartzis, K. Baumann-Stanzer, E. Bemporad, S. Evertz, C. Gariazzo, M. Gerbec, S. Herring, A. Karppinen, J.-M. Lacomme, T. Reisin, R. Tavares, G. Tinarelli, and S. Trini-Castelli. COST ES1006 Best Practice Guidelines for the use of Atmospheric Dispersion Models in Emergency Response Tools at local-scale in case of hazmat releases into the air. COST Action ES1006, April 2015.
- Armand, P., C. Duchenne, Y. Benamrane, C. Libeau, T. Le Nouëne, and F. Brill. Meteorological forecast and dispersion of noxious agents in the urban environment – Application of a modelling chain in real-time to a fictitious event in Paris city. Proceedings of the 15<sup>th</sup> Harmo Conference, May 6-9, 2013, Madrid, Spain, 724-728.
- Armand, P., C. Duchenne, and E. Bouquot. Atmospheric dispersion modelling and health impact assessment in the framework of a CBRN-E exercise in a complex urban configuration. Proceedings of the 16<sup>th</sup> Harmo Conference, Sept. 8-11, 2014, Varna, Bulgaria, 638-643.
- Armand, P., C. Duchenne, and L. Patryl. Is it now possible to use advanced dispersion modelling for emergency response? The example of a CBRN exercise in Paris. ITM 2015, May 4-8 2015, Montpellier, France.
- Baumann-Stanzer, K., S. Andronopoulos, P. Armand, E. Berbekar, G. Efthimiou, V. Fuka, C., Gariazzo, G. Gasparac, F. Harms, A. Hellsten, K. Jurcakova, A. Petrov, A. Rakai, S. Stenzel, R. Tavares, G. Tinarelli, S. Trini Castelli. COST ES1006 Model evaluation case studies: Approach and results. COST Action ES1006, April 2015.
- Baumann-Stanzer K., B. Leitl, S. Trini Castelli, C. M. Milliez, E. Berbekar, A. Rakai, V. Fuka, A. Hellsten, A. Petrov, G. Efthimiou, S. Andronopoulos, G. Tinarelli, R. Tavares, P. Armand, C. Gariazzo, and all COST ES1006 Members. Evaluation of local-scale models for accidental releases in built Environments – Results of the “Michelstadt exercise” in COST Action ES1006. Proceedings of the 16<sup>th</sup> Harmo Conference, Sept. 8-11, 2014, Varna, Bulgaria, 699-703.
- Duchenne, C., P. Armand, M. Nibart, and V. Hergault. Validation of a LPDM against the CUTE experiment of the COST ES1006 Action. Comparison of the results obtained with the diagnostic and RANS version of the model. Proceedings of the 17<sup>th</sup> Harmo Conference, May 9-12, 2016, Budapest, Hungary (to be published).
- Herring, S., P. Armand, and C. Gariazzo. Best practice in applying emergency response tools to local scale hazmat incidents. Proceedings of the 17<sup>th</sup> Harmo Conference, May 9-12, 2016, Budapest, Hungary (to be published).
- Trini Castelli S., B. Leitl, K. Baumann-Stanzer, T. G. Reisin, P. Armand, F. Barmpas, M. Balczo, S. Andronopoulos, K. Jurcakova, and all COST ES1006 Members. Updates on COST Action ES1006 – Evaluation, improvement, and guidance for the use of local-scale emergency prediction and response tools for airborne hazards in built environments. Proceedings of the 16<sup>th</sup> Harmo Conference, Sept. 8-11, 2014, Varna, Bulgaria, 689-693.

**17th International Conference on  
Harmonisation within Atmospheric Dispersion Modelling for Regulatory Purposes  
9-12 May 2016, Budapest, Hungary**

---

**COMBINING METEOROLOGICAL MODELS AND DISPERSION MODELS ON  
LARGESCALE AND MESOSCALE, IMPLEMENTED AS AN AIR QUALITY FORECAST  
MODEL SYSTEM IN IRAN**

*Lorentz, Helmut<sup>1</sup>, Hermann Jakobs<sup>2</sup>, Thomas Flassak<sup>1</sup>, Abbas Ranjbar<sup>3</sup>, Majid Azadi<sup>3</sup>*

<sup>1</sup>Ingenieurbüro Lohmeyer GmbH & Co. KG, Germany

<sup>2</sup>Rhenish Institute for Environmental Research at the University of Cologne, Germany

<sup>3</sup>Iran Atmospheric Science & Metrological Research Centre, Iran

**Abstract:** In many regions of the world air pollution and dust concentrations are so high, that local administrations need forecast systems to warn people or impose short term mitigation measures. In Iran such an Air Quality Forecast System (AQFoS) has been implemented for the entire country and in a higher resolution for the city of Tehran. The requirements for the implemented models comply with different scales and their vertical and horizontal resolutions, the possibilities of the model to describe emissions sources in different detail levels and furthermore interface methods between the models. In Iran the AQFoS has been implemented with special emphasis on dust generation and large range transport using the EURAD Air Quality Prediction System which was developed by the Rhenish Institute for Environmental Research at the University of Cologne (RIU) in a modified version. EURAD consists of three major components: The PennState/NCAR mesoscale model WRF, which predicts the needed meteorological variables, the EURAD Emission Module (EURAD-EEM), which calculates the temporal and spatial distribution of the emissions of the major pollutants and the EURAD Chemistry Transport Model (EURAD-CTM) which predicts the concentrations and deposition of the main atmospheric pollutants. The global emission data base EDGAR (Emissions Database for Global Atmospheric Research) is used as input. Furthermore a dust activation parameterization was implemented within the EURAD system in order to simulate dust emission from arid land areas. The area of Tehran is focused in a higher spatial resolution. For the Tehran area, AQFoS combines the models PROWIMO and LASAT with WRF/EURAD. The AQFoS runs on servers of the Iran National Meteorological Organization (IRIMO) and predicts concentrations of dust, NO<sub>2</sub>, SO<sub>2</sub>, PM<sub>10</sub>, NMVOC, CO and Ozone for 84 hours.

**Key words:** *largescale, mesoscale, Air Quality Forecast System, AQFoS, Iran, dust storm, WRF, EURAD, PROWIMO, LASAT*

## **INTRODUCTION**

In many regions of the world air pollution and dust concentrations are so high, that local administrations need forecast systems to warn people or impose short term mitigation measures. Such an Air Quality Forecast System (AQFoS) with emphasis on dust storms has been implemented by the Rhenish Institute for Environmental Research at the University of Cologne (RIU) and Ingenieurbüro Lohmeyer GmbH & Co. KG (LOH) as contract work for the Iran Atmospheric Science & Metrological Research Centre (ASMERC). The forecast system was implemented for the entire country of Iran and in a higher model resolution for the city of Tehran. The requirements for the implemented models comply with different scales and their vertical and horizontal resolutions, the possibilities of the model to describe emissions sources in different detail levels and furthermore interface methods between the models. AQFoS is a part of the Air Quality Forecast service for the Iran and is running operationally on servers of Iran Meteorological Organization (IRIMO). AQFoS predicts concentrations of dust, NO<sub>2</sub>, SO<sub>2</sub>, PM<sub>10</sub>, NMVOC, CO and Ozone for 84 hours.

## **MODEL COMPONENTS OF THE AIR QUALITY FORECAST SYSTEM AQFOS**

The Air Quality forecast System (AQFoS) comprises of the following meteorological, dispersion and emission models:

- Meteorological model WRF (Weather Research & Forecasting Model, <http://www.wrf-model.org>), which provides the needed meteorological variables within EURAD.
- EURAD (European Air Quality Prediction System, <http://www.eurad.uni-koeln.de>), which is the prediction system at RIU.
- Prognostic mesoscale wind and climate model PROWIMO ([www.lohmeyer.de/en/prowimo](http://www.lohmeyer.de/en/prowimo)), developed by LOH.
- Lagrangian dispersion model LASAT (Lagrange-Simulation Aerosol-Transport, <http://www.janicke.de/en/lasat.html>).

### Domain Configuration of WRF/EURAD and PROWIMO/LASAT

The Air Quality forecast System (AQFoS) of Iran consists of a nesting cascade starting with an initial horizontal domain size of 5 000 x 5 000 km<sup>2</sup> with a 50 km horizontal grid size, which covers major parts of the South West Asian. Within this domain a nested domain with 10 km horizontal grid size is embedded covering Iran (see Figure 1). In a further refinement step, a nested domain with a 1 km horizontal grid size has been implemented for urban region of Tehran. For this nested domain, the models PROWIMO/LASAT are applied. The specification of the domain and the nested grid are given in Table 1. Further nested domains with a 1 km horizontal grid size for other urban regions are possible and are subject to future work in the project.

**Table 1:** Domain and nested grid specifications

Domain	Region	Hor. grid size	Hor. grid points	Wind/Dispersion model
D01	South West Asia	50 km	100 x 100	WRF/EURAD
D02	Iran	10 km	201 x 201	WRF/EURAD
D02.1	Tehran	1 km	50 x 50	PROWIMO/LASAT

This configuration assures that the necessary computing time for the forecast is in an appropriate and acceptable time for the decision makers. A higher horizontal resolution will highly increase the computing time und thus delay the update of the daily forecast.



**Figure 1:** Model domain South West Asia and Iran

### Modelling process

Each daily repeated AQFoS modelling process is started by running WRF. The meteorological results of WRF are passed to EURAD-CTM, which calculates the dispersion of emissions of the global emission data base EDGAR and of dust emissions estimated by the dust storm module.

The following steps are managed by the control software FAQIR. On domain D02.1, PROWIMO is started, which calculates meteorological parameters adopting the results of WRF from the larger D02 domain and provides wind and turbulence fields for LASAT. After that, LASAT is started, which calculates on the D02.1 domain the dispersion of emissions provided by the Tehran municipality. Mainly road traffic emissions are implemented yet. In the next process step, the background concentration calculated by EURAD-CTM and the additional load calculated by LASAT are superimposed.

The superimposed ground level concentration fields are visualized in a WebViewer which is a java based application and can be run with contemporary browsers. The time sequence of the schedule of the different AQFoS modules is shown in Figure 3.

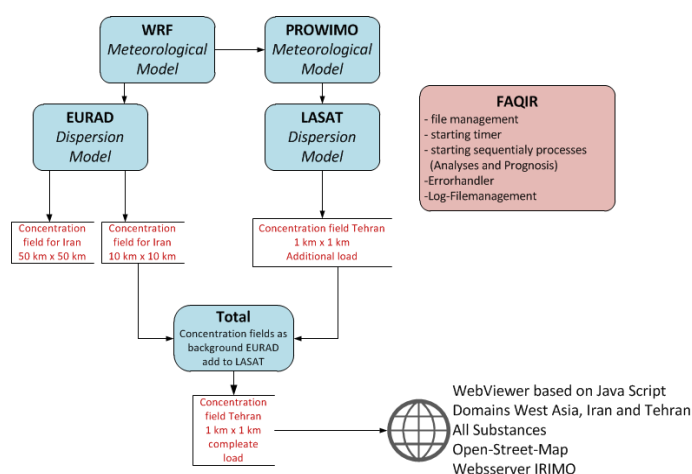


Figure 2. Modelling processes controlled by FAQIR

Procedure	Computing Time	Schedule					
		1	2	3	4	5	6
1 WRF	1.5h	█					
2 EURAD	2h		█				
3 PROWIMO	2.5h			█			
4 LASAT	.5h				█		
5 Superposition	.2h					█	
6 Preparing graphics for WebViewer domain D01 and D02	1.5h				█		
7 Preparing graphics for WebViewer domain D02.1	.5h					█	

Figure 3. Model Schedule

AQFoS starts every day at 20:00 UTC and calculates forecast concentration fields for 84 hours (three and a half days). All results are saved as netcdf-files and image files.

### EURAD

The EURAD Model System is a high sophisticated Chemistry Transport System in order to predict the concentrations of pollutants in the atmosphere. It calculates the transport, chemical transformation and deposition of atmospheric trace gases. The EURAD Model System is used for case studies and especially for the daily operational forecast of air quality over Europe (<http://eurad.uni-koeln.de>). The EURAD Model System is part of many national and international projects. The EURAD model is well described in

numerous case studies (e.g. Hass, 1991, Ackermann et al., 1998, Memmesheimer et al., 2004). It contains also a data assimilation algorithm for analyzing observational data (Strunk, 2006 and Elbern et al., 2007). The system is running on LINUX operational system.

EURAD Model System includes the following submodules:

Emission Module (EURAD-EEM) with the global emission data base EDGAR (<http://edgar.jrc.ec.europa.eu>) as input.

Chemistry Transport Model (EURAD-CTM) which predicts the concentrations and deposition of the main atmospheric pollutants.

A dust activation parameterization module (Chervenkov, Jakobs, 2011), which simulates dust emission from arid land areas due to soil moisture and type of ground substrate.

### THE PROGNOSTIC MESOSCALE MODEL PROWIMO

The model PROWIMO is based on Flassak (1990) and was lately completely recoded and extended at LOH e.g. by the Predicted Mean Vote (PMV) or the "perceived temperature" according to VDI 3787 page 2 (2008) in order to be capable to provide climatological assessments. PROWIMO is suited to simulate the local wind and temperature distribution. The model can be adapted individually to site-specific conditions.

The model PROWIMO is based on the conservation equations for momentum, mass and energy, which are solved numerically in 3D in the flux formulation in terrain following co-ordinates. Prognostic variables are the 3 velocity components  $u$ ,  $v$  and  $w$ , the potential temperature, the humidity, the surface temperature and the surface humidity. The non-hydrostatic pressure is computed by solving an elliptic differential equation. The elliptic solver is based on a Fast Fourier Transformation algorithm in conjunction with a generalized Conjugate Gradient Method. The model applies the anelastic approximation as well as the Boussines approximation. The sub-grid-scaled turbulent fluxes are parametrised with a first order closure. The complete documentation of the model PROWIMO (physical background, approximations, numerical methods, boundary and initial conditions, parametrisations) are given in Flassak (1990).

For the urban regions of Tehran, the PROWIMO simulation domain has a horizontal extent of  $90 \times 90 \text{ km}^2$ . The horizontal grid size within an inner domain of  $50 \times 50 \text{ km}^2$  (Domain D02.1) is 1 km. Outside of that inner domain the horizontal grid size increases with a factor of 1.2. A vertical grid size of 20 m has been chosen from surface up to a height of 120m, above the vertical grid size increases with a factor of 1.2.

An example of the calculated wind and potential temperature distribution at ground level is shown in Figure 4.

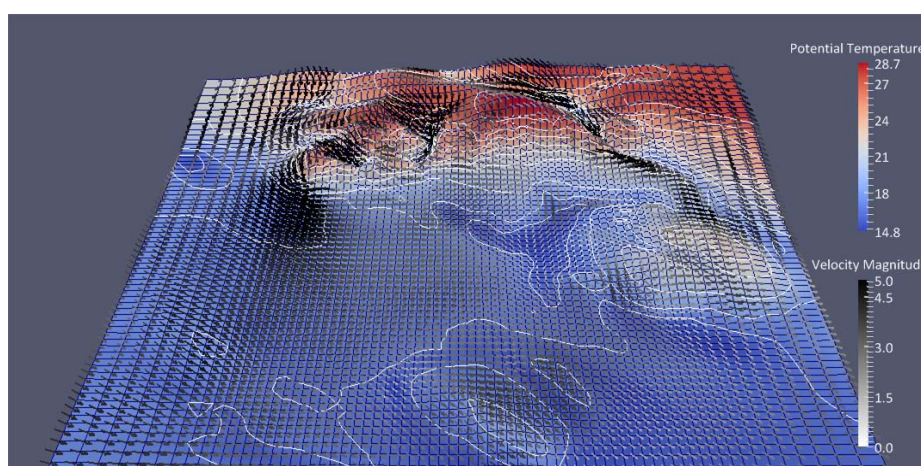


**Figure 4.** PROWIMO simulation results for Tehran on the D02.1 domain: Ground level wind and potential temperature distribution.

## THE LAGRANGIAN DISPERSION MODEL LASAT

The dispersion model LASAT (Lagrangian Simulation of Aerosol-Transport) computes the transport of trace substances in the atmosphere. It simulates the dispersion and the transport of a representative sample of tracer particles utilizing a random walk process (Lagrangian simulation). LASAT conforms to guideline VDI 3945 Part 3. LASAT is able to simulate accidental releases, screening, bio-aerosols, odorants, moving sources. Furthermore LASAT is able to simulate special emitter circumstances like the plum rise of stacks and cooling towers and well traffic induced turbulence. LASAT is able to calculate single meteorological situations and time series as well.

## THE WEBVIEWER ONLINE PRESENTATION

The WebViewer is a java based application and can be run with contemporary browsers. The WebViewer visualises the ground level concentration fields for each domain as an animation on a Open-Street-Map layer (see Figure 5). The WebViewer is able to show concentrations fields for each, domain, substance and forecast hour.

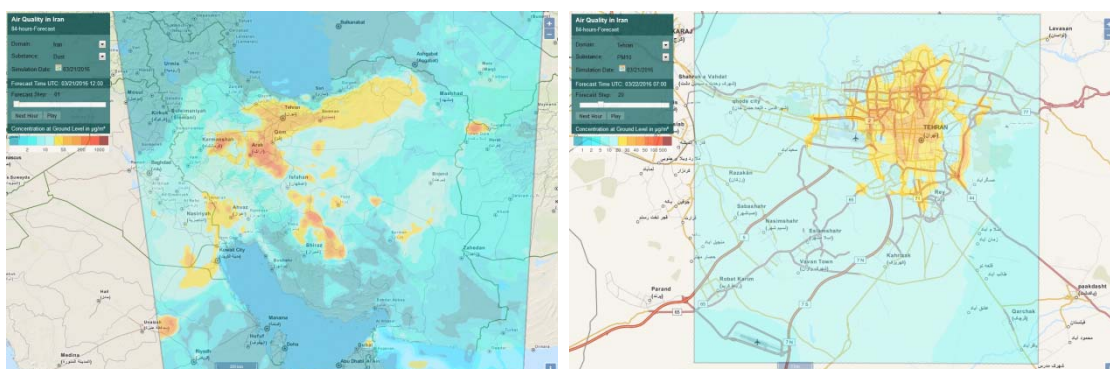


Figure 5. WebViewer screenshot of the PM10 ground level concentration field in Iran and Tehran at forecast hour 70

## REFERENCES

- Ackermann, I.J., H. Hass, M. Memmesheimer, A. Ebel, F.S. Binkowski, and U. Shankar, *Atmos. Environ.*, **32**, 2981-2999, 1998.
- Chervenkov, H. and H.Jakobs, Dust storm simulation with regional air quality model – Problems and results, *Atmospheric Environment* 01/2011; **45**(24):3965-3976, 2011.
- Elbern, H., A. Strunk, H. Schmidt, and O. Talagrand, *Atmos. Chem. Phys.*, **7**, 1-59, 2007.
- Flassak, Th., 1990: Ein nicht-hydrostatisches mesoskaliges Modell zur Beschreibung der Dynamik der planetaren Grenzschicht, Fortschr.Ber. VDI Reihe 15 Nr. 74, VDI-Verlag, Düsseldorf, 203 pp.
- Hass, H., Description of the EURAD Chemistry-Transport-Model version 2 (CTM2), vol 83, Mitteilungen aus dem Institut für Geophysik und Meteorologie der Universität zu Köln, 1991.
- Memmesheimer, M., E. Friese, A. Ebel, H. J. Jakobs, H. Feldmann, C. Kessler and G. Piekorz, *Int. J. Environmental and Pollution*, **22**, (1-2), 108-132, 2004.
- Strunk, A., Tropospheric Chemical State Estimation by Four-Dimensional Variational Data Assimilation on Nested Grids, Ph.D. Thesis, Institut für Geophysik und Meteorologie der Universität zu Köln, 2006.
- VDI 3787 Part 2, 2008: Environmental meteorology, Methods for the human biometeorological evaluation of climate and air quality for urban and regional planning at regional level, Part I: Climate. BeuthVerlag, November 2008.
- VDI 3945 Bart 3, 2000: Environmental meteorology, Atmospheric dispersion models, Particle model, BeuthVerlag, September 2000.

## **TOPIC 7**

# **INVERSE DISPERSION MODELLING AND SOURCE IDENTIFICATION**

**17th International Conference on  
Harmonisation within Atmospheric Dispersion Modelling for Regulatory Purposes  
9-12 May 2016, Budapest, Hungary**

---

**TIME-REVERSIBILITY IN ATMOSPHERIC DISPERSION**

*Tímea Haszpra*

MTA–ELTE Theoretical Physics Research Group, Budapest, Hungary

**Abstract:** Due to the chaotic nature of atmospheric dispersion, small deviations, e.g., numerical errors in dispersion simulations increase rapidly over time. Therefore the accuracy of backward simulations is limited. In the presentation the degree of the fulfillment of time-reversibility over different time periods is investigated by a Lagrangian dispersion model on global scale using pollutant clouds consisting of several particles. The characteristics of the pollutant clouds in the backward simulation are compared to those in the forward simulation. In order to characterize the degree of time-reversibility, Lagrangian quantities such as the proportion of particles which return to the initial volume, and the centre of mass and the standard deviation of the pollutant clouds are determined. Furthermore, the overlap and the Pearson's correlation coefficient between the forward and backward clouds are also investigated. Both a case study and global results are presented. Simulations reveal that the accuracy of time-reversibility decreases generally exponentially in time. We find that after 3 to 4 days the results of the backward tracking become unreliable, any sign of time-reversibility is lost.

**Key words:** *backward tracking, time-reversibility, chaotic advection, Real Particle Lagrangian Trajectory Model, RePLaT.*

## **INTRODUCTION**

Backward calculation of the transport and dispersion in the atmosphere is an essential tool, e.g., to identify the sources of pollutants. Besides simple trajectory computation (see, e.g., Flesch et al., 1995; Onishi et al., 2012), more sophisticated methods are available to estimate the location and distribution of materials at a certain time before the observation. These techniques include inverse modeling using a source-receptor relationship by means of a Lagrangian model and adjoint versions of Eulerian dispersion models.

The paper investigates how precisely a cloud of particles returns to its original position in the atmosphere when after a monitoring over a few days as a forward simulation, time is reversed and the backward simulation runs for the same time period. For the investigation, we use a Lagrangian trajectory model. When only advection is taken into account, particle trajectories are determined utilizing 3D velocity fields of the atmosphere. The trajectories of the particles are deterministic and described by three time-dependent differential equations representing the horizontal and vertical directions. As three-dimensional passive advection has three degrees of freedom, advection dynamics can result in the so-called chaotic behavior, the typical characteristics of which are sensitivity to initial conditions, irregular motion and the appearance of complex formations, like folded, elongated filaments (Ottino, 1989).

The result of chaotic behavior is that the motion of a particle is unpredictable for long times as the trajectories of initially close particles diverge exponentially in time. Small differences in the initial position and numerical approximations applied in the trajectory calculation result in errors growing exponentially in time. In view of the sensitivity to slight deviations, instead of one trajectory, several adjacent particles should be tracked to get a more precise overview of the volume/area covered potentially by the contaminant.

The paper investigates the accuracy of backward trajectory simulations in the context of atmospheric advection as a function of time and, thus, the degree of the fulfillment of time-reversibility in the view of chaotic advection. In order to evaluate the matching of the appropriate backward and forward clouds, statistical parameters are determined. We calculate Lagrangian quantities, which depend solely on the

position of the particles, and Eulerian ones, which require the particles to be projected into grid cells. A case study and global simulations are also presented. As a general rule, the statistical parameters reveal that the accuracy of backward tracking decreases exponentially in time, and usually after a few days or about a week, the results of the backward tracking become unreliable; any sign of time-reversibility is lost. The results of the research are published in Haszpra (2016).

### THE REPLAT DISPERSION MODEL

The RePLaT (Real Particle Lagrangian Trajectory) dispersion model (Haszpra and Tél, 2013), is used to determine the trajectories of particles that compose the pollutant clouds. RePLaT is a Lagrangian model tracking aerosol particles with a realistic radius and density. Ideal tracers and gaseous contaminants correspond to particles with radius  $r = 0$ . RePLaT is applied here in this limiting case. RePLaT calculates particle trajectories due to advection by means of Euler's method, and also reckons with the impact of turbulent diffusion on the particles as a random walk process. However, as the study focuses on the continental and global transport, and in large-scale simulations the effect of turbulent diffusion is much weaker than that of advection, as a first approximation, turbulent diffusion is neglected in the simulations.

### INPUT DATA

The particle trajectories are computed using the 3D reanalysis wind fields of the ERA-Interim database of the European Centre for Medium-Range Weather Forecasts (ECMWF). The meteorological variables utilized in the simulations are given on 32 pressure levels between 1000 and 100 hPa on a horizontal grid of  $1.5^\circ \times 1.5^\circ$  with 6 h of time resolution.

### STATISTICAL PARAMETERS

In order to quantify the accuracy of the backward simulation, the pollutant clouds of the backward and forward simulations at the appropriate time instants are compared using different statistical quantities. The proportion of the particles that returned to the initial volume, the deviation of the center of mass and the difference of the standard deviation of the pollutant clouds (Lagrangian parameters), the figure of merit in space (overlap) and the Pearson's correlation coefficient (Eulerian ones) are determined.

The deviations between the corresponding backward and forward pollutant cloud (abbreviated BWC and FWC from this point, respectively) are considered as a function of the time interval of the backward simulation  $\Delta t_b = t_b - t$ , where  $t_b$  is the initialization time of the backward simulation ( $t_b = 1, 2, \dots, 9$  days) and  $t$  is the time instant of the comparison ( $t = 0, 1, \dots, 8$  days) (Haszpra, 2016).

### CASE STUDY

In order to study the accuracy of time-reversibility in the atmospheric advection, as a first step, a forward simulation of a pollutant cloud for 9 days and the corresponding backward simulations are presented. The particles of the FWC are initiated in a volume of  $1^\circ \times 1^\circ \times 100$  hPa at  $\lambda_0 = 141^\circ\text{E}$ ,  $\varphi_0 = 37.5^\circ\text{N}$ ,  $p_0 = 500$  hPa on 12 March 2011 at 00 UTC. Figure 1 illustrates the FWC (black) and the BWCs (colored) at  $t = 0$  and 8 days after the emission. The folded and extremely stretched shape of the initially compact FWC is the consequence of the chaotic nature of the advection mentioned in the Introduction.

Figure 1 suggests that for  $\Delta t_b = 1-3$  days the backward simulations provide reasonable agreement with the FWCs that are considered here as the “measured” position of the pollutants. See, e.g., the position of the light blue–dark blue dots and the black rectangle in the left panel, and the red and black dots in the right panel. For larger values of  $\Delta t_b$ , the agreement is poor, and a clear breakdown of time-reversibility is found. This is illustrated in the left panel by the extended distribution of the dots with warm colors (especially, by the red dots).

To quantify the differences between the BWCs and FWC, the statistical parameters mentioned before are determined. For illustration, Figure 2 shows the horizontal distance  $\Delta\text{CM}_h$  between the centers of mass and the difference  $\Delta\sigma_h$  between the horizontal standard deviations of the FWC and the corresponding BWC as a function of the time interval of the backward simulation.

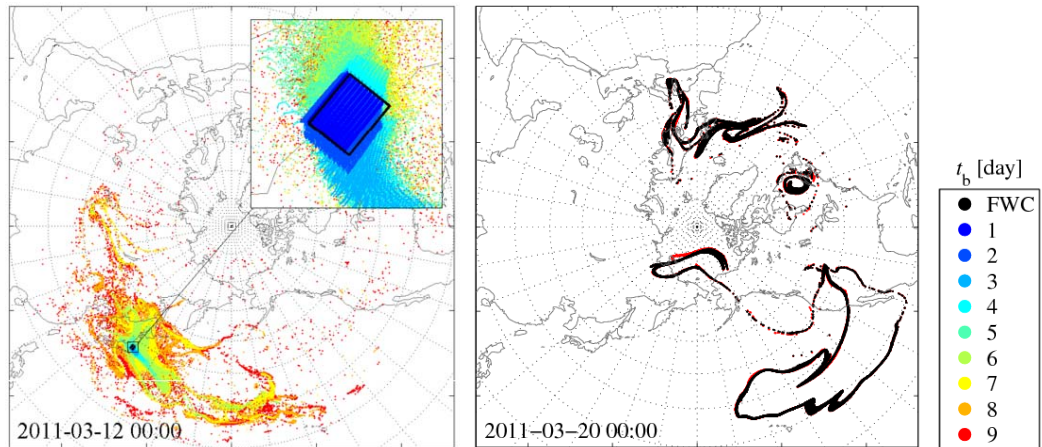


**Figure 1.** FWC (black rectangle and dots, respectively) emitted instantaneously and BWCs (colored) consisting of  $n_0 = 1.25 \times 10^5$  particles at  $t = 0$  and  $t = 8$  days. Colored dots denote the location of the particles backward simulation of which is started at time  $t_b$  [day].

The right panel of Figure 2 reveals that in almost all cases the BWCs extend to a larger area than the corresponding FWC, that is,  $\Delta\sigma_h > 0$ . This is also a sign of the chaotic behavior of the advection of pollutant particles: small deviations grow rapidly over time, and therefore, particles spread to a larger region than where they were at the same time instant in the FWC. An exponential fit to  $\Delta\sigma_h$  over the entire interval seems to be appropriate with an exponent of  $0.467 \text{ day}^{-1}$ . As one can see, the exponent is close to the one for  $\Delta\text{CM}_h$ .

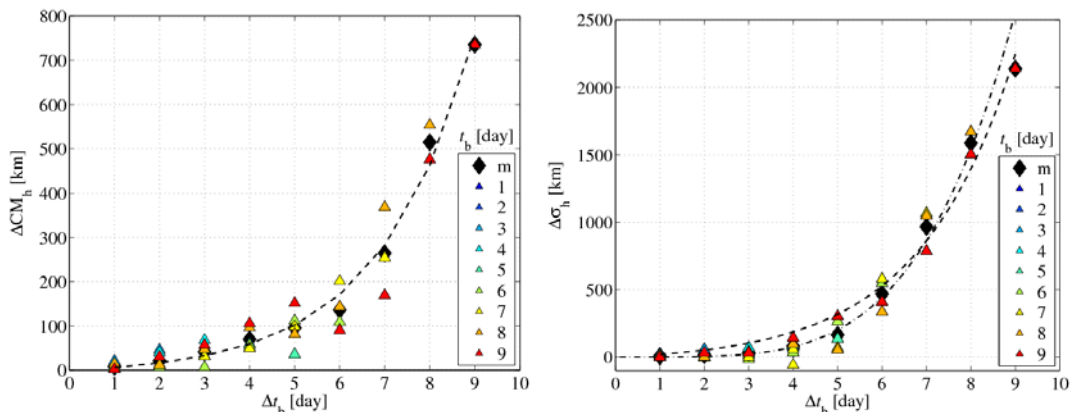


**Figure 2.** The quantity  $\Delta\text{CM}_h$  and  $\Delta\sigma_h$  depending on the time period  $\Delta t_b$  of the backward simulation. Colored triangles indicate the starting time  $t_b$  of the backward simulations, black diamonds are the mean values belonging to a given  $\Delta t_b$  (denoted by “m”). Dashed lines indicate exponential fits to the mean values.

The proportion of the particles that are able to return to the initial volume, the difference of the standard deviation of the pollutant clouds, the figures of merit in space and Pearson's correlation coefficients are found to behave similarly (Haszpra, 2016). As expected from Figure 1, the longer the time period of the backward simulation, the worse the overlap and correlation of the BWCs and FWC. In the case study after  $\Delta t_b \geq 5$  days the BWCs become much more extended than the FWC, and therefore the overlap between the clouds decrease to less than 10%. The possible drift of the BWC from the FWC (which is quantified by the value  $\Delta\text{CM}_h$ ) also contributes to the lack of the coincidence of the two pollutant clouds investigated. A reasonable agreement between the fitted exponents of the above-mentioned quantities is found. The exponents can be considered as specific Lyapunov exponents of the advection and they found to be similar in value to the atmospheric Lyapunov exponents of advection obtained in previous researches (e.g., Pierrehumbert and Yang, 1993; von Hardenberg et al., 2000) for a similar time period of particle tracking.

Although particular values mentioned here might depend on the resolution of meteorological data utilized, on the interpolations applied and on the numerical scheme of the trajectory integration, one feature is independent of these details, namely that the deviation between the appropriate BWC and FWC becomes significant if the integration time exceeds the Lyapunov time of advection (the reciprocal of the Lyapunov exponent of advection) characteristic to the region and to the atmospheric conditions. This is a general property of any kind of chaotic processes and is in harmony with the observation that the Lyapunov time is the characteristic time interval beyond which predictions become unreliable.

### GLOBAL RESULTS

In order to investigate the general behavior of the dependence of the parameters on  $\Delta t_b$  and to gain a global picture, the time evolution of  $12 \times 9$  pollutant clouds uniformly distributed at different geographical locations are monitored. Besides the global distribution of the statistical parameters, the statistics of the tropical region (clouds with initial location  $\varphi_0 = 0^\circ, 20^\circ \text{ N/S}$ ) and that of the mid- and high latitudes (defined as  $\varphi_0 = 40^\circ \text{ N/S}, 60^\circ \text{ N/S}, 80^\circ \text{ N/S}$ ) are also analyzed.

One can ascertain from the left panel of Figure 3 that the  $\Delta \text{CM}_h$  of all three regions defined shows a clear exponential increase over time. In the case of  $\Delta \text{CM}_h$  the positive difference between mean and median values implies to extreme cases when backward simulations give much more inaccurate results than for most of the simulations with the particular  $\Delta t_b$ .

The right panel of Figure 3 shows that for 1 to 3 days of backward tracking  $\Delta \sigma_h$  does not exceed 50 km which implies generally a good agreement in the extension of the BWC and FWC compared to the fact that the average horizontal extension of the FWC (measured by standard deviation of the particles) is about 1100 km. The growth of the difference in the standard deviation of the FWC and BWC can be approximated by an exponential function, similarly to Figure 2. The slower increase in the tropics is due to the differences in the atmospheric circulation of the tropics, and the mid- and high latitudes. In the tropics owing to the less number of cyclones, the weaker shearing in the wind field results in weaker chaoticity of advection. Nonetheless, since pollutant clouds in the tropics can become mixed into the extratropics, and clouds initiated in mid- and high latitudes might get into the tropical region (for illustration, see, e.g. Figure 1 in Haszpra, 2016), the properties of the tropical and extratropical regions can be mixed together as the wide and somewhat overlapping distribution of the TR and M/H bars suggest, e.g. for  $\Delta t_b = 8-9$  days.

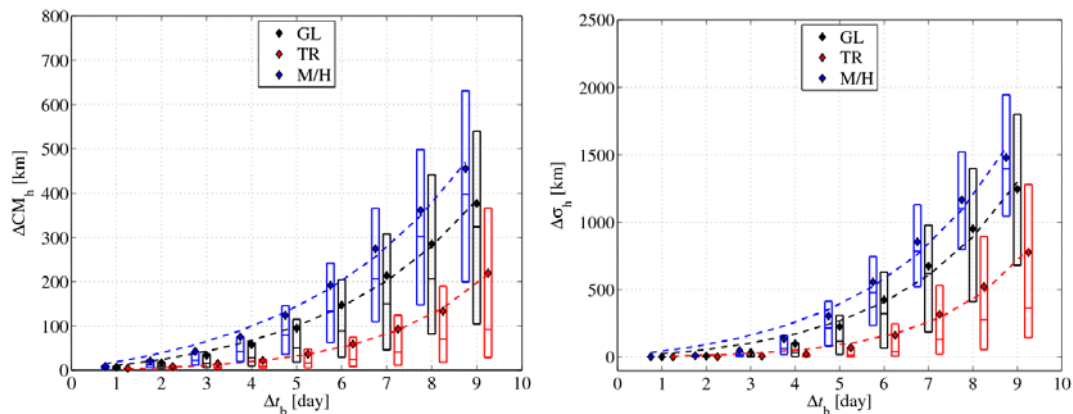


**Figure 3.** The quantity  $\Delta \text{CM}_h$  and  $\Delta \sigma_h$  depending on the time period  $\Delta t_b$  of the backward simulation. The results are shown for the tropical region (TR), for mid- and high latitudes (M/H) and for the globe (GL). Mean values (diamonds), medians and lower and upper quartiles (boxes with horizontal lines) are indicated. Dashed lines indicate exponential fits to the mean values.

As in the case study, the figure of merit in space and the Pearson's correlation coefficient seem to decrease approximately exponentially over time (Haszpra, 2016). The overlap of the BWC and FWC reduces below 50% after 6 days of backward simulation for the tropics and after 3 days for mid- and high

latitudes. The exponents of the fitted exponential functions to the mean data uncover that the time-dependence of the different statistical parameters can be described by similar exponents.

## SUMMARY

In order to study the accuracy of backward trajectory simulations, we carried out a case study to gain a first impression about its characteristics, and several simulations of pollutant clouds distributed all over the globe to investigate the properties in general. Statistical parameters for the backward and the forward pollutant clouds were calculated at the same time instant. Forward pollutant clouds were considered as “real” clouds with which the results of the backward simulation are expected to coincide under full time-reversibility.

The simulations uncover that for about 1 to 3 days of backward tracking, a reasonable coincidence of the backward and forward clouds appear, that is, for such time periods the backward tracking performs reasonably well. This agreement is confirmed by the plots of the backward and forward clouds, and additionally, statistical parameters calculated in the study also verify this statement. The accuracy of backward simulations found to decrease exponentially. A faster decrease characterizes the mid- and high latitudes due to the more intense cyclonic activity compared to the tropical region. It is worth noting that the time interval over which the accuracy of time-reversibility is found to be reasonably good is on the order of magnitude of the predictability time of atmospheric advection (the reciprocal value of the Lyapunov exponent).

Although results in the coincidence of the forward and backward clouds may be improved by applying more sophisticated numerical schemes and meteorological data with finer resolution at the expense of computational cost, it is not expected to basically alter the dynamics of the time-dependence of the quantities investigated, due to the unavoidable exponential degradation of the accuracy of dispersion simulations in our chaotic atmosphere.

## REFERENCES

- Flesch, T. K., J. D. Wilson, E. Yee, 1995: Backward-time Lagrangian stochastic dispersion models and their application to estimate gaseous emissions. *J. Appl. Met.*, **34**, 1320–1332.
- von Hardenberg, J., K. Fraedrich, F. Lunkeit, A. Provenzale, 2000: Transient chaotic mixing during a baroclinic life cycle. *Chaos*, **10**, 122–134.
- Haszpra, T., 2016: Time-reversibility in atmospheric dispersion. *Atmos.*, **7**, 11.
- Haszpra, T., T. Tél, 2013: Escape rate: A Lagrangian measure of particle deposition from the atmosphere. *Nonlin. Proc. Geophys.*, **20**, 867–881.
- Onishi, K., Y. Kurosaki, S. Otani, A. Yoshida, N. Sugimoto, Y. Kurozawa, 2012: Atmospheric transport route determines components of Asian dust and health effects in Japan. *Atmos. Environ.* **49**, 94–102.
- Ottino, J., 1989: *The Kinematics of Mixing: Stretching, Chaos, and Transport*. Cambridge University Press: Cambridge, UK.
- Pierrehumbert, R.T., H. Yang, 1993: Global chaotic mixing on isentropic surfaces. *J. Atmos. Sci.*, **50**, 2462–2480.
- Zemmer, F., F. Karaca, F. Ozkaragoz, 2012: Ragweed pollen observed in Turkey: detection of sources using back trajectory models. *Sci. Tot. Environ.*, **430**, 101–108.

**17th International Conference on  
Harmonisation within Atmospheric Dispersion Modelling for Regulatory Purposes  
9-12 May 2016, Budapest, Hungary**

---

**UNCERTAINTY ESTIMATION IN THE RECONSTRUCTION OF ATMOSPHERIC TRACER  
SOURCE EMISSIONS**

*Sarvesh Kumar Singh, Gregory Turbelin, Pramod Kumar, Raj Rani, Amir-Ali Feiz, Pierre Ngae*

LMEE, Université d'Evry-Val d'Essonne, 40 Rue du Pelvoux, 91020 Evry Cedex

**Abstract:** In an inversion procedure, the interest is not only to obtain an estimate of the unknown parameters but also to determine the uncertainty involved in their estimation. The study proposes advancement within the framework of an inversion technique, called *Renormalization*, to characterize the uncertainties in a point source reconstruction. The novelty stems from the fact that the inherent uncertainties in the retrieved parameters are directly identifiable from the shape and features of the a posteriori source estimate. The uncertainty estimates are illustrated in point source reconstruction using the concentration measurements from field experiments, known as Fusion Field Trials 2007 (FFT07) at Dugway Proving Ground, Utah.

**Key words:** *FFT07, inverse problem, renormalization, source identification, uncertainty.*

## **INTRODUCTION**

Fast growing industrialization and urbanization have posed significant risk towards the human environment and associated ecological systems. Any dispersion event caused intentionally or accidentally may lead fatal mortality in the environment. The notable examples can be seen in the past as, Bhopal gas leakage (December 2, 1984, India), Chernobyl disaster (April 26, 1986, Ukraine), Fukushima nuclear accident (March 11, 2011, Japan) etc. These examples raise the issues regarding the improvement of the emergency preparedness and national security which eventually require fast and preliminary information about the origin and strength of unknown releases caused into the atmosphere. The interest is not only to obtain an estimate but also to determine the uncertainty involved in their estimation.

The study highlights an inversion technique, called "*Renormalization*" (Issartel et al., 2007), recently proposed for the identification of a point release. The technique has been shown efficient in retrieving the origin and strength of a point release requiring minimal a priori information, however, a procedure for determining the uncertainty involved in the parametric estimates has not been developed so far. Thus, the objective here is to propose a methodology for determining the uncertainty involved in the retrieved point release parameters (mainly, location and strength).

Uncertainty estimation is mainly an analysis of the information gained by the measurements over a priori information about the unknown release. The inversion technique lead to a conditional estimate, often called a posteriori, which needs to be inspected in several directions in order to determine the uncertainties associated with this conditional estimate. In a point source reconstruction, maximum of a posteriori provides the location of the point release. Thus, the shape or a distribution of the maxima region may provide an indication of the uncertainties involved. The estimation is said to be well resolved when the source estimate is sharply peaked. These features are explored and quantified in this study and the uncertainty estimation methodology is evaluated with real data taken from Fusion Field Trials 2007 (FFT07) (Storwald, 2007) conducted at Dugway Proving Ground, Utah, USA.

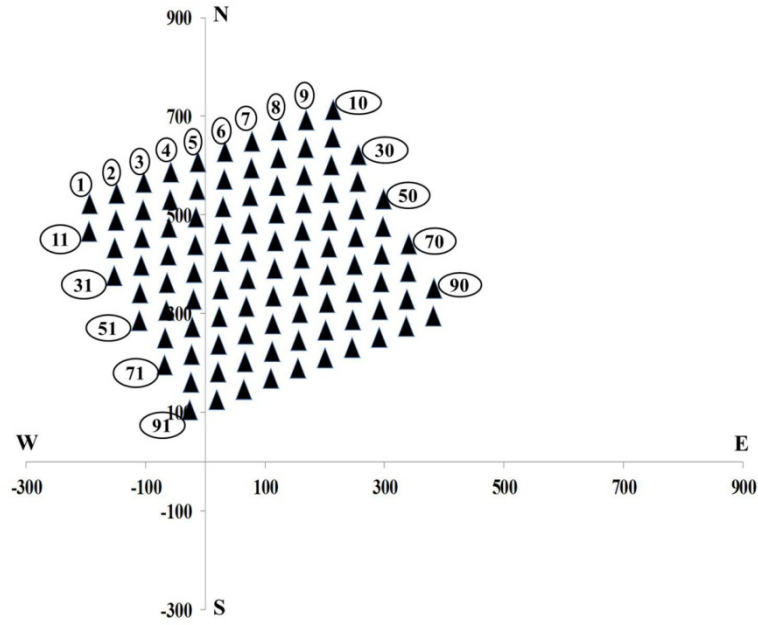


**Figure 1.** Layout of the FFT07 experiment. The triangles denote detectors. Their index number are highlighted in the circles.

The FFT07 experiment consist of 100 digital Photoionization Detectors (digiPID) arranged in a rectangular staggered array (10 rows and 10 columns) in an area  $475 \text{ m} \times 450 \text{ m}$ . The wind flows from south-east to north-west direction. To take an advantage of the prevailing wind direction, the detector's grid was rotated  $25^\circ$  towards west. The spacing between subsequent rows and columns were 50 m. A tracer propylene was released from a height of 2 m continuously for an approximate duration of 10 min. The concentration measurements were collected at a height of 2 m. The release location varies in each trial. The meteorological measurements (wind, temperature, stability etc.,) are taken at 4 m level from a 32 m meteorological tower located at the centre of the grid.

## METHODOLOGY

The inversion technique is described here for point source identification in a least-square framework. For simplicity, the release is assumed continuous and ground level. Accordingly, the identification of a point release refers to the estimation of its location and strength. The source-receptor relationship is described here with the use of an adjoint modelling framework. In discrete notations, a source-receptor relationship is denoted as (Pudykiewicz, 1998),

$$\boldsymbol{\mu} = \mathbf{A}\mathbf{s} + \boldsymbol{\varepsilon} \quad (1)$$

in which  $\boldsymbol{\mu}$  is the measured concentration vector of dimension  $m$ ,  $\mathbf{A} = [\mathbf{a}_1, \mathbf{a}_2, \dots, \mathbf{a}_N]$  is the sensitivity matrix of dimension  $m \times N$ ,  $\mathbf{s}$  is the source vector of dimension  $N$  and  $\boldsymbol{\varepsilon}$  denotes measurement error vector of dimension  $m$ . Assuming a priori that the nature of the release is point type, the source vector  $\mathbf{s}$  is parameterized as  $\mathbf{s} = q\delta(x - x_o)(y - y_o)$  where  $q$  is the release strength and  $\mathbf{x}_o = (x_o, y_o)$  is the ground level release location coordinates. Using the definition of a point source, equation (1) can be reformulated as (Sharan et al., 2009),

$$\boldsymbol{\mu} = q\mathbf{a}(\mathbf{x}_o) + \boldsymbol{\varepsilon} \quad (2)$$

Issartel et al. (2007) have shown that the sensitivity matrix is associated with peaks at the sensitivity vectors coinciding with the cells containing measurements due to the diffusive nature of the transport and strong concentration gradient around the measurement cells. To deal with this, a diagonal weight matrix  $\mathbf{W} = [w_{ij}]$  of dimension  $N \times N$  is proposed (it satisfies properties,  $\text{trace}(\mathbf{W}) = m$  and  $\mathbf{a}_w^T(\mathbf{x})\mathbf{H}_w^{-1}\mathbf{a}_w(\mathbf{x}) = 1$ ) in such a way it normalizes the sensitivity vectors as,  $\mathbf{a}_w(\mathbf{x}_i) = \mathbf{a}(\mathbf{x}_i)/w_{ii}$  (Issartel et al., 2007; Singh et al., 2015). Accordingly, the equation (2) is modified as,

$$\boldsymbol{\mu} = qw(\mathbf{x}_o)\mathbf{a}_w(\mathbf{x}_o) + \boldsymbol{\varepsilon} \quad (3)$$

### Least-squares estimation of release parameters

To estimate the release parameters  $\mathbf{x}_o$  and  $q$ , a least-squares cost function is formulated from equation (3) as  $J = \frac{1}{2}\boldsymbol{\varepsilon}^T \mathbf{H}_w^{-1} \boldsymbol{\varepsilon}$ . In this, matrix  $\mathbf{H}_w = \mathbf{A}_w \mathbf{W} \mathbf{A}_w^T$  is regarded as measurement covariance matrix since it measures for the dispersion in the sensitivity vectors which are linear to the measurements. The minimization of  $J$  is performed, first, with respect to  $q$  and then for  $\mathbf{x}$ . In the first step, minimization of  $J$  with respect to  $q$  leads to a critical estimate by equating  $\partial J / \partial q = 0$  as,

$$\hat{q} = \frac{\mathbf{a}_w^T(\mathbf{x})\mathbf{H}_w^{-1}\boldsymbol{\mu}}{w(\mathbf{x})} \quad (4)$$

From equation (4), the cost function  $J$  is simplified as,  $J = \frac{1}{2}\left(\boldsymbol{\mu}^T \mathbf{H}_w^{-1} \boldsymbol{\mu} - \left(\mathbf{a}_w^T(\mathbf{x})\mathbf{H}_w^{-1}\boldsymbol{\mu}\right)^2\right)$ . Thus, minimization of  $J$  is equivalent to the maximization of  $S'(\mathbf{x}) = \mathbf{a}_w^T(\mathbf{x})\mathbf{H}_w^{-1}\boldsymbol{\mu}$ . By implementing this analogy on a discrete domain, the location of the point source can be identified by searching exhaustively the maximum of the estimate  $S'$  in the domain. Once the release location  $\hat{\mathbf{x}}_o$  is retrieved, its strength  $\hat{q}$  can be derived from equation (4).

### A posteriori estimation of variance in $\hat{q}$ and confidence bounds

A posteriori estimation of variance in  $q$  i.e.,  $\text{var}(\hat{q})$  is based on the fact that  $\mathbf{H}_w$  is proportional to the measurement dispersion matrix. Thus,  $E[\boldsymbol{\mu}\boldsymbol{\mu}^T] = \sigma \mathbf{H}_w$ , where  $\sigma$  is the proportionality constant. Now,  $\text{var}(\hat{q})$  can be given as,

$$\text{var}(\hat{q}) = \text{var}\left(\frac{\mathbf{a}_w^T(\hat{\mathbf{x}}_o)\mathbf{H}_w^{-1}\boldsymbol{\mu}}{w(\hat{\mathbf{x}}_o)}\right) = \frac{\mathbf{a}_w^T(\hat{\mathbf{x}}_o)\mathbf{H}_w^{-1} \text{var}(\boldsymbol{\mu})\mathbf{H}_w^{-1} \mathbf{a}_w(\hat{\mathbf{x}}_o)}{w^2(\hat{\mathbf{x}}_o)} < \frac{\mathbf{a}_w^T(\hat{\mathbf{x}}_o)\mathbf{H}_w^{-1} E[\boldsymbol{\mu}\boldsymbol{\mu}^T] \mathbf{H}_w^{-1} \mathbf{a}_w(\hat{\mathbf{x}}_o)}{w^2(\hat{\mathbf{x}}_o)} \quad (5)$$

$$\text{var}(\hat{q}) < \frac{\sigma}{w^2(\hat{\mathbf{x}}_o)} \quad (6)$$

From equation (6), an upper bound of the  $\text{var}(\hat{q})$  can be determined by estimating the constant  $\sigma$ . An estimate  $\hat{\sigma}$  can be obtained from the residuals since  $E[\hat{\boldsymbol{\varepsilon}}\hat{\boldsymbol{\varepsilon}}^T] = \sigma \mathbf{H}_w [\mathbf{I}_m - \mathbf{a}_w(\hat{\mathbf{x}}_o)\mathbf{a}_w^T(\hat{\mathbf{x}}_o)\mathbf{H}_w^{-1}]$  where  $\hat{\boldsymbol{\varepsilon}} = \boldsymbol{\mu} - \hat{q}w(\hat{\mathbf{x}}_o)\mathbf{a}_w(\hat{\mathbf{x}}_o)$  and  $\mathbf{I}_m$  is  $m \times m$  identity matrix. By using trace operator and simple linear algebra, it is derived as,  $\hat{\sigma} = \frac{\hat{\boldsymbol{\varepsilon}}\mathbf{H}_w^{-1}\hat{\boldsymbol{\varepsilon}}^T}{m-1}$ .

The true variance of the release strength is not known and, under Gaussian assumptions,  $\text{var}(\hat{q})$  can be considered as an approximation to the standard error in  $\hat{q}$ . Hence, an upper bound estimate for  $\text{var}(\hat{q})$  can be utilized to construct the 95% confidence interval for  $\hat{q}$  and  $\hat{\mathbf{x}}_o$  using student t-distribution as,

$$P\left(-t_{m-1, 0.975} < \frac{q - \hat{q}}{\hat{\sigma} / w^2(\hat{\mathbf{x}}_o)} < t_{m-1, 0.975}\right) = 0.95 \quad (7)$$

The 95% confidence region for retrieved point source location can be determined as,

$$P\left(-t_{m-1, 0.975} < \frac{S'(\mathbf{x}) - \hat{S}'(\hat{\mathbf{x}}_o)}{\hat{\sigma}} < t_{m-1, 0.975}\right) = 0.95. \quad (8)$$

## EVALUATION AND RESULTS

The proposed methodology is evaluated using non-zero real measurements of Trial#7 from FFT07 dispersion experiment. For a numerical implementation of the methodology, a domain of size 1200 m × 1200 m is chosen and discretized into 399 × 399 cells (figure 1). The true source location is at cell (200, 200) and true strength was 5.5 g s<sup>-1</sup>. The important step of the inversion algorithm is the computation of sensitivity matrix **A** and weight matrix **W**. The sensitivity elements are derived from the solution of the adjoint dispersion model governing the transport and dispersion of a release tracer from a continuous, non-reactive tracer and ground level source. An analytical dispersion model developed by Sharan et al. (1996) is established in the adjoint mode by inverting the wind direction and replacing the source location by the measurement cell. This is possible since advection and diffusion operators are taken linear, wind is steady and diffusion is self-adjoint. The weight matrix is computed by an algorithm given in Issartel et al. (2007).

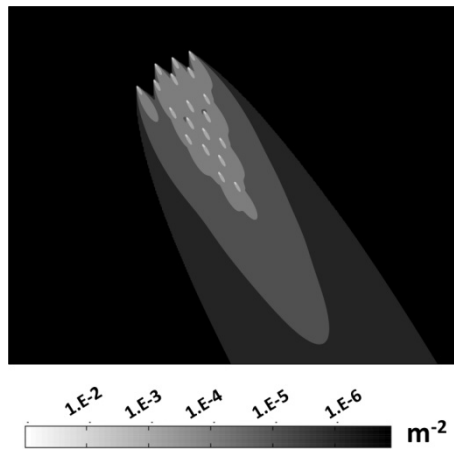


Figure 2. Distribution of weights in the domain.

The distribution of weights (figure 2) describes a priori information about unknown emissions apparent to the monitoring network. The weights are maximum at the measurement cells and decreasing further as one move away in upwind direction of the monitoring network. Figure (3) describes the normalized distribution of retrieved source  $S'(\mathbf{x})$  in which the maxima region is associated with the informative source region.

The maxima region contain an extended branch in the upwind direction which arises mainly due to lack of visibility by the monitoring network in these regions and thus, corresponds to the poor model resolution. From the inversion technique, the maximum of  $S'(\mathbf{x})$  will provide the point release location. With real data, the source location is retrieved very close to the true release location. The location error (Euclidean distance between the true and retrieved release location) is observed as 3 m. The source strength is also retrieved (as 6.98 g s<sup>-1</sup>) within a factor of 1.3. The retrieval errors are mainly due to the model representation errors.

The 95% confidence bounds are derived for the source location and strength and a confidence region for the retrieved source location is highlighted in figure (3). The confidence region is observed similar to an ellipse elongated in the wind direction. The uncertainty in the location error is determined by measuring the length of the major axis. The 95% confidence interval is obtained for the location error (in meters) as [0, 53] m and for strength as [4.9, 9] g s<sup>-1</sup>. This implies that the release parameters are significantly sensitive to the uncertainty in the measurements and model. For a comparison, the confidence estimates are also derived by using a Bootstrap resampling procedure. With bootstrap procedure, the 95% confidence interval for location error is observed as [0, 80] m while for strength, it is [2.2, 14.3] g s<sup>-1</sup>. The present estimates are observed under-predicted (within a factor of 1.5) in comparison to bootstrap which

may not be surprising since  $\mathbf{H}_w$  is only an approximation to the measurement covariance based on overlapping of the sensitivity vectors. It is possible that the cross-correlations between the measurements are not being accounted properly or under/over-predicted which results into such deviations from actual uncertainty. However, figure (3) shows that the confidence region with present methodology is found comparable to the bootstrap estimates.

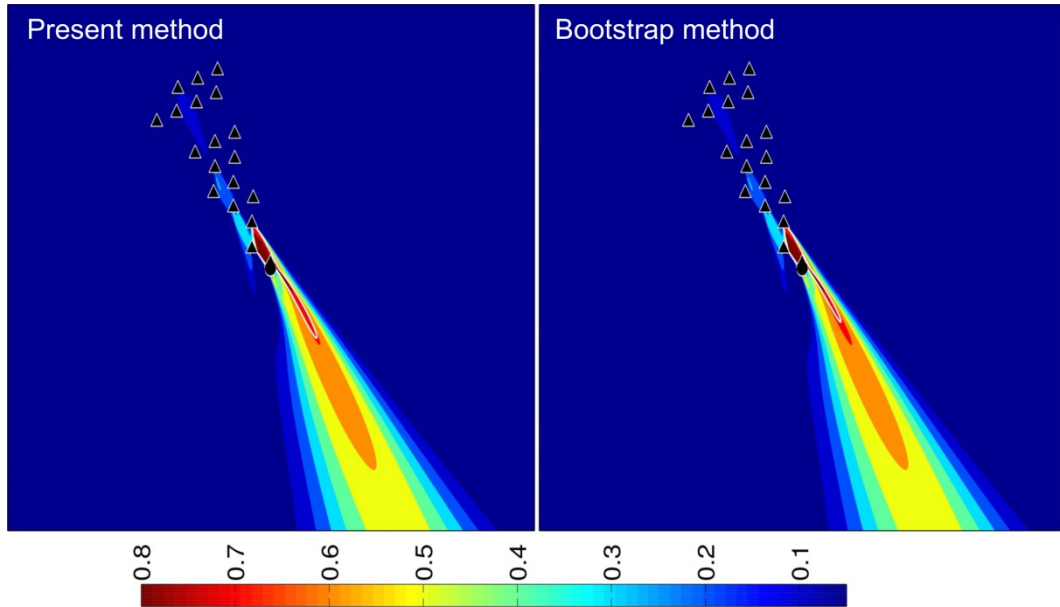


**Figure 3.** Isopleths of  $\frac{S'(\mathbf{x})}{\max(S'(\mathbf{x}))}$ . The black and white circles show true and retrieved source, respectively. The confidence region for point source location is shown by white line.

## CONCLUSION

The study presents an uncertainty estimation methodology for point source reconstruction in the framework of renormalization inversion technique. The methodology is evaluated with real data taken from trial# 7 in FFT07 experiment. It is observed that the release parameters are retrieved close to their true values. In spite of their closeness towards the true parameters, their uncertainty is found to be large. The methodology is computationally efficient in determining uncertainty in comparison to the other methods based on sampling procedure or Hessian since it does not require any sampling or derivative information. However, a further investigation with several datasets is required to highlight the efficiency and accuracy of this methodology.

## REFERENCES

- Pudykiewicz, J., 1998. Application of adjoint tracer transport equations for evaluating source parameters. *Atmospheric Environment* **32**, 3039-3050.
- Issartel, J.-P., M. Sharan, and M. Modani (2007), An inversion technique to retrieve the source of a tracer with an application to synthetic satellite measurements, *Proceeding of Royal Society A*, 463, 2863–2886.
- Sharan, M., A. K. Yadav, M. P. Singh, P. Agarwal, and S. Nigam (1996), A mathematical model for dispersion of air pollutants in low wind conditions, *Atmospheric Environment*, **30**, 1209-1220.
- Sharan, M., J.-P. Issartel, S. K. Singh, and P. Kumar (2009), An inversion technique for the retrieval of single-point emissions from atmospheric concentration measurements, *Proceeding of Royal Society A*, 465, 2069-2088.
- Storwald, D. P. (2007), Detailed test plan for the fusing sensor information from observing networks (Fusion) Field Trial (FFT-07), Tech. Rep. Document No. WDTC-TP-07-078, Meteorology Division, West Desert Test Center, U.S. Army Dugway Proving Ground WDTC, Salt Lake, Utah.

**17th International Conference on  
Harmonisation within Atmospheric Dispersion Modelling for Regulatory Purposes  
9-12 May 2016, Budapest, Hungary**

---

**INVERSE DISPERSION MODELLING FOR IDENTIFICATION OF MULTIPLE-POINT  
SOURCE EMISSIONS IN ATMOSPHERE**

*Raj Rani, Sarvesh Kumar Singh, Gregory Turbelin, Pramod Kumar, Amir-Ali Feiz, Pierre Ngae*

LMEE, Universite d'Evry-Val d'Essonne, 40 Rue du Pelvoux, 91020 Evry Cedex

**Abstract:** The paper deals with a complex situation of dispersion events where multiple releases are simultaneously emitting a common tracer and a merged set of atmospheric concentrations is recorded to identify these releases. The identification, here, refers to the estimation of locations and strengths of a known number of simultaneous point releases. The source-receptor relationship is described in the framework of adjoint modelling by using an analytical Gaussian dispersion model. A least-squares minimization framework, free from an initialization of the release parameters (locations and strengths), is presented to estimate the release parameters. This utilizes the distributed source information observable from the given monitoring design and number of measurements. The technique leads to an exact retrieval of the true release parameters when measurements are noise free and exactly described by the dispersion model. The inversion algorithm is evaluated using the blind data from multiple (two, three and four) releases conducted during Fusion Field Trials in September 2007 at Dugway Proving Ground, Utah. The accuracy of source retrieval is subjected to the retrieved resolution features by the monitoring network.

**Key words:** *Fusion field trials, Inverse dispersion modelling, Least-squares, Multiple source identification*

## **INTRODUCTION**

In the atmospheric dispersion events, fast and accurate identification of unknown releases is one of the major concerns to advance the emergency assessment capabilities and to minimize the threat of exposure to the environment. The dispersion events might involve one or more releases simultaneously emitting the contaminants. In case of simultaneous releases emitting the same contaminant, the field of plumes may overlap significantly and the sampled concentrations may become the mixture of the concentrations originating from all the releases. The other uncertainties may arise as, (i) the sources are seen from the same angle but are located at different distances, (ii) the receptors near to a weak source will report same concentration as the receptors far away from a strong source, etc. In such cases, it is challenging to separate the influence of each source and to correctly identify each source from a set of merged concentration measurements. In local scale dispersion events, the unknown releases are often formulated as point type and their identification is addressed by estimating a fixed set of parameters, for instance, ground level coordinates of the release location, height, strength, etc.,

Fusion Field Trials (FFT07) refer to a series of short range diffusion tests conducted at Dugway Proving Ground, Utah during September 2007 (Storwald, 2007). The dataset corresponds to the instantaneous/continuous single as well as multiple (two, three and four) point releases. The experiment is designed and distributed widely for evaluating the performance and capability of several source estimation algorithms. In this study, an inversion technique is proposed to efficiently address the retrieval of continuous multiple point releases using real measurements from FFT07 datasets. The objective is to highlight the capability and efficiency of the inversion technique in identifying the parameters (mainly, locations and strengths) corresponding to the continuous multiple point releases in a real scenario. The bold symbol denotes vector/matrix and italic denotes scalar.

## **MULTIPLE-POINT SOURCE IDENTIFICATION**

The inversion technique is based on an adjoint source-receptor relationship between measurements  $\mu_i$ ,  $i = 1, 2, \dots, m$  and unknown emissions vector  $\mathbf{s}$  of dimension  $N$  (number of discrete cells in the discretized domain) which is given as (Pudykiewicz, 1998),

$$\boldsymbol{\mu} = \mathbf{A}\mathbf{s} + \boldsymbol{\eta} \quad (1)$$

where  $\boldsymbol{\eta}$  is the residual vector of dimension  $m$  including noise in the measurements and model,  $\mathbf{A} = [\mathbf{a}_1, \mathbf{a}_2, \dots, \mathbf{a}_N]$  is the  $m \times N$  matrix of adjoint elements and  $\mathbf{a}_i$  is a  $m$ -dimension adjoint vector representing sensitivity with respect to  $m$  measurements. Assuming that the measurements are generated from  $k$  point sources such that  $s_i = q_{oi} \delta(\mathbf{x} - \mathbf{x}_{oi})$ ,  $i = 1, 2, \dots, k$  where  $q_{oi}$  and  $\mathbf{x}_{oi}$  are the release strength and location, respectively. Accordingly, the equation (1) is modified as,

$$\boldsymbol{\mu} = \mathbf{K}\mathbf{q}_o + \boldsymbol{\eta} \quad (2)$$

in which  $\mathbf{K}$  is  $m \times k$  matrix expressing sensitivity of  $m$  measurements with respect to  $k$  unknown release locations and  $\mathbf{q}_o = [q_{o1}, \dots, q_{ok}]$  is  $k$ -dimension vector of unknown strength. For the estimation of release locations and strengths, a cost function  $J$  is formulated as  $J = \frac{1}{2} \boldsymbol{\eta}^T \boldsymbol{\eta}$ . First, the function  $J$  is minimized with respect to  $q_{oi}$  which provides a critical estimate as,

$$\hat{\mathbf{q}}_o = (\mathbf{K}^T \mathbf{K})^{-1} \mathbf{K}^T \boldsymbol{\mu} \quad (3)$$

The estimate  $\hat{\mathbf{q}}_o$  is a local minimum of  $J$  provided  $\mathbf{K}^T \mathbf{K}$  is invertible and positive definite. Further using equation (3), function  $\hat{J}$  is simplified as,

$$\hat{J} = \frac{1}{2} \left( \boldsymbol{\mu}^T \boldsymbol{\mu} - \boldsymbol{\mu}^T \mathbf{K} (\mathbf{K}^T \mathbf{K})^{-1} \mathbf{K}^T \boldsymbol{\mu} \right). \quad (4)$$

In equation (4),  $\boldsymbol{\mu}^T \boldsymbol{\mu}$  is constant and minimum of  $\hat{J}$  is equivalent to maximum of  $\omega = \boldsymbol{\mu}^T \mathbf{K} (\mathbf{K}^T \mathbf{K})^{-1} \mathbf{K}^T \boldsymbol{\mu}$ . Accordingly, an algorithm is constructed as showed in figure (1) (Singh and Rani, 2015).

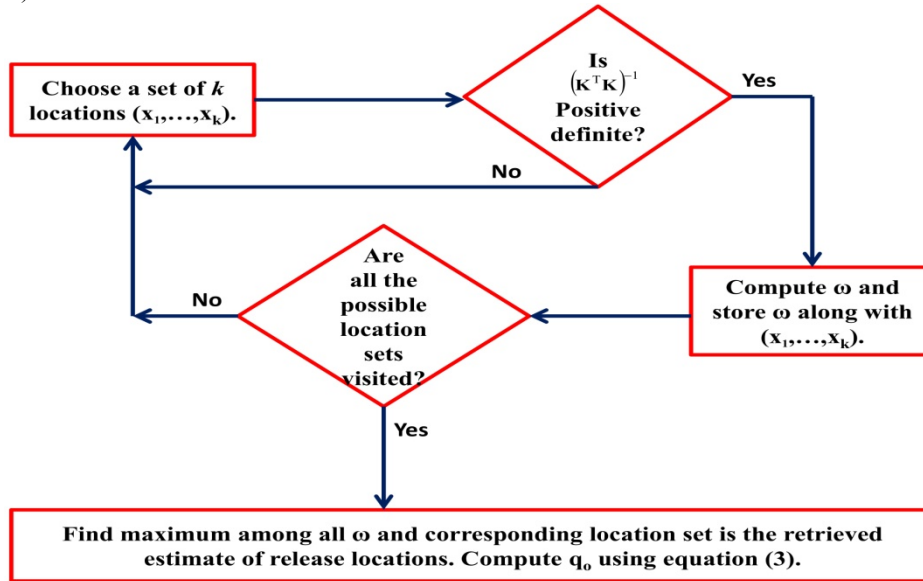
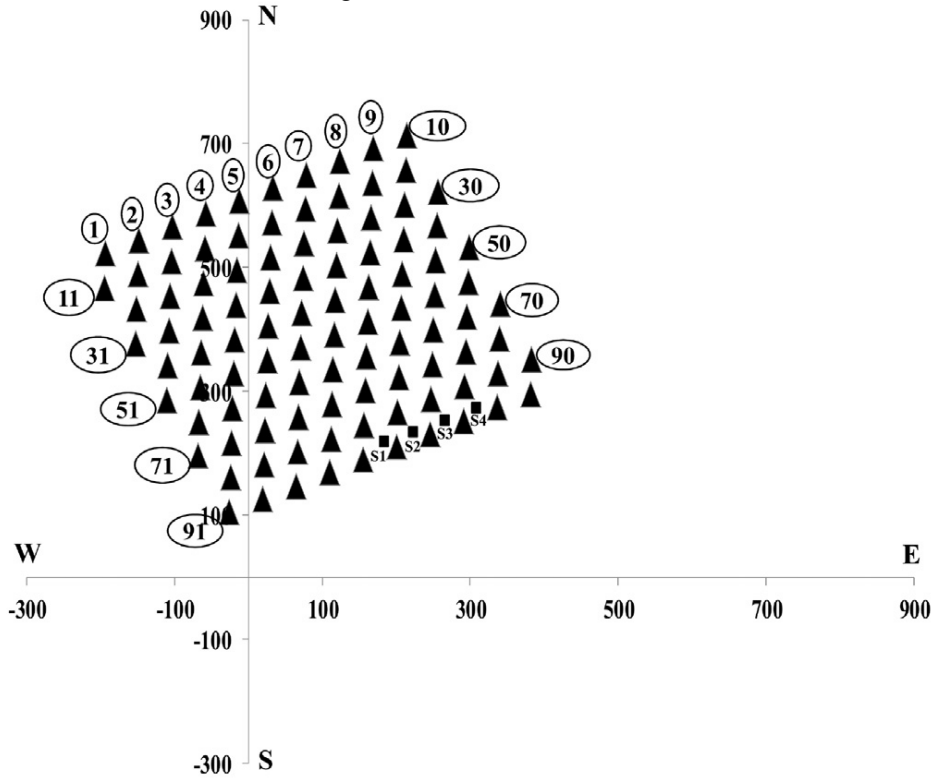


Figure 1. Multiple source identification algorithm.

### FUSION FIELD TRIALS

The inversion methodology is evaluated by using the real data obtained from multiple release trials in FFT07 experiment (Storwald, 2007). The dispersion experiment involved release of a tracer gas propylene ( $C_3H_6$ ) from multiple locations at constant flow rates for approximately 10 min per trial. A total of 100 concentration samplers were arranged in a rectangular staggered grid of area  $475 \text{ m} \times 450 \text{ m}$  at 50 m apart and 2 m above the ground (figure 2). The true releases are located, at the South-East end of the sampling grid, approximately within 30-50 m Euclidean distance from the last line of the receptors (91-100, see figure 2). The height of the releases was 2 m above the ground. In general, the release locations vary in each experimental trial, however, for representation, the release locations (S1, S2, S3 and S4) are

exhibited for four release trials in figure 2. The concentration measurements considered from continuous point releases corresponding to the two, three and four sources. These measurements were mainly based on 4 or 16 samplers and considered as “blind data” distributed during the first phase of the release for the evaluation of several source estimation algorithms.



**Figure 2.** Layout of the computational domain (Singh and Rani, 2015). Black triangles denote position of receptors and their index numbers are mentioned in the circles. Black filled squares denote representative locations of the true releases (S1, S2, S3 and S4) in four release trials.

### NUMERICAL IMPLEMENTATION

An implementation of the inversion algorithm requires a discretized domain. Accordingly, a domain of size  $1200 \text{ m} \times 1200 \text{ m}$ , discretized into  $399 \times 399$  cells, is chosen. The sensitivity matrix (**A**) is computed as plumes originated from receptors backward in space with unit emission rate. For this, an analytical dispersion model by Sharan et al. (1996) is established in the adjoint mode by inverting the wind direction and taking receptor cells as source locations emitting unit amount of tracer per unit time. Further, the inversion algorithm is applied to retrieve the source locations and strengths.

### RESULTS

The distributed source information, given by estimate  $\omega$ , can be utilized to discriminate between the well or poorly resolved source regions (figure 3). In figure (3), the global or local maxima region describes the source information while upwind extensions away from the monitoring network are artifacts (Singh and Rani, 2015).

In two releases trials, all the source locations were retrieved within 200 m of the true source (table 1, figure 3). The average distance and standard deviation are  $55 \pm 61 \text{ m}$ . In trials 19, 40 & 62, both the releases are retrieved far ( $> 100 \text{ m}$ ) from the true releases. The source strengths are retrieved within a factor of five in all the trials. In three releases trials, the average and standard deviation of the location error are obtained as  $121 \pm 71 \text{ m}$ . All the release locations are retrieved within 255 m from the true release locations. The source strength are retrieved within a factor of six to the true release rate. In four releases trials, the average distance from the predicted source to the true source is observed as 146 m, with a standard deviation of 79 m. The source locations are retrieved within 250 m of the true source. In four

release trials, two of the four releases locations are retrieved close to the true releases whereas the other two releases are predicted far upwind/downwind of the true releases. In most of the trials, the source strengths are retrieved within a factor of five to the true release rate. However, the factor increases up to ten (mostly under predicted) when the locations are retrieved upwind of the true releases.

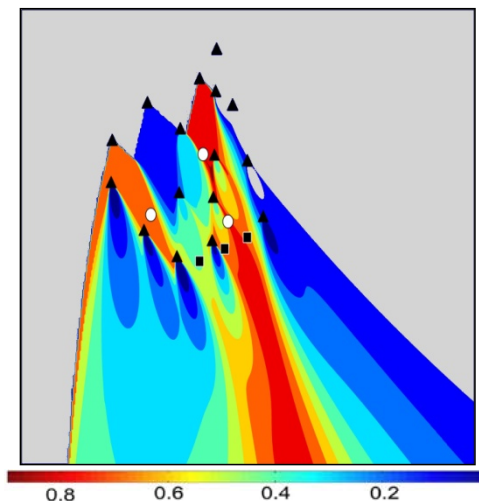


**Figure 3.** The isopleths of  $\omega/\max(\omega)$  in three simultaneous release trial 61. The black filled squares were the true releases whereas the white filled circles are the retrieved release locations.

With blind data, the releases are retrieved both upwind as well as downwind of the true releases subjected to the available source information in the region. In two and four release trials, the release locations are mostly retrieved in the downwind of the true release whereas in three release trials, release locations are retrieved mostly upwind of the monitoring network. With few measurements, inversion technique mostly retrieves the releases downwind of the true releases towards the receptors. When receptors are located only along the plume centerline, the releases are retrieved close to each other or along a line in the upwind direction of the true releases (figure 4). This is interesting to observe in trial 55 that the inversion technique is able to retrieve the four releases with only four measurements, however, the retrieval errors are relatively large (figure 4). The present technique is shown to retrieve the releases within a reasonable accuracy as mentioned in other studies. However, the accuracy in source estimation is also subject to the accurate depiction of the plume features by the utilized dispersion model.

**Table 1.** Source retrieval using blind data. The maximum location error (in meters) and, mean and standard deviation (Std) of the location error, are shown in two, three and four release trials.

	Two releases		Three releases		Four releases	
	Maximum	Mean $\pm$ Std	Maximum	Mean $\pm$ Std	Maximum	Mean $\pm$ Std
<b>Location error</b>	200	55 $\pm$ 61	255	121 $\pm$ 71	250	146 $\pm$ 79

## CONCLUSION

An inversion algorithm is presented here for identifying the release parameters (mainly, locations and strengths) of multiple point releases continuously emitting the same tracer from limited set of merged concentration measurements. The inversion algorithm is free from initial guess of the release parameters and only requires that the number of point releases is known. The inversion algorithm is evaluated with several trials of continuous multiple point releases from FFT07 experiment. It is observed that the inversion algorithm successfully retrieves the release locations within an average Euclidean distance of 150 m from the true release locations. The source strengths are also retrieved mostly within a factor of five. Overall, the retrieval errors are minimized with the addition of measurements.

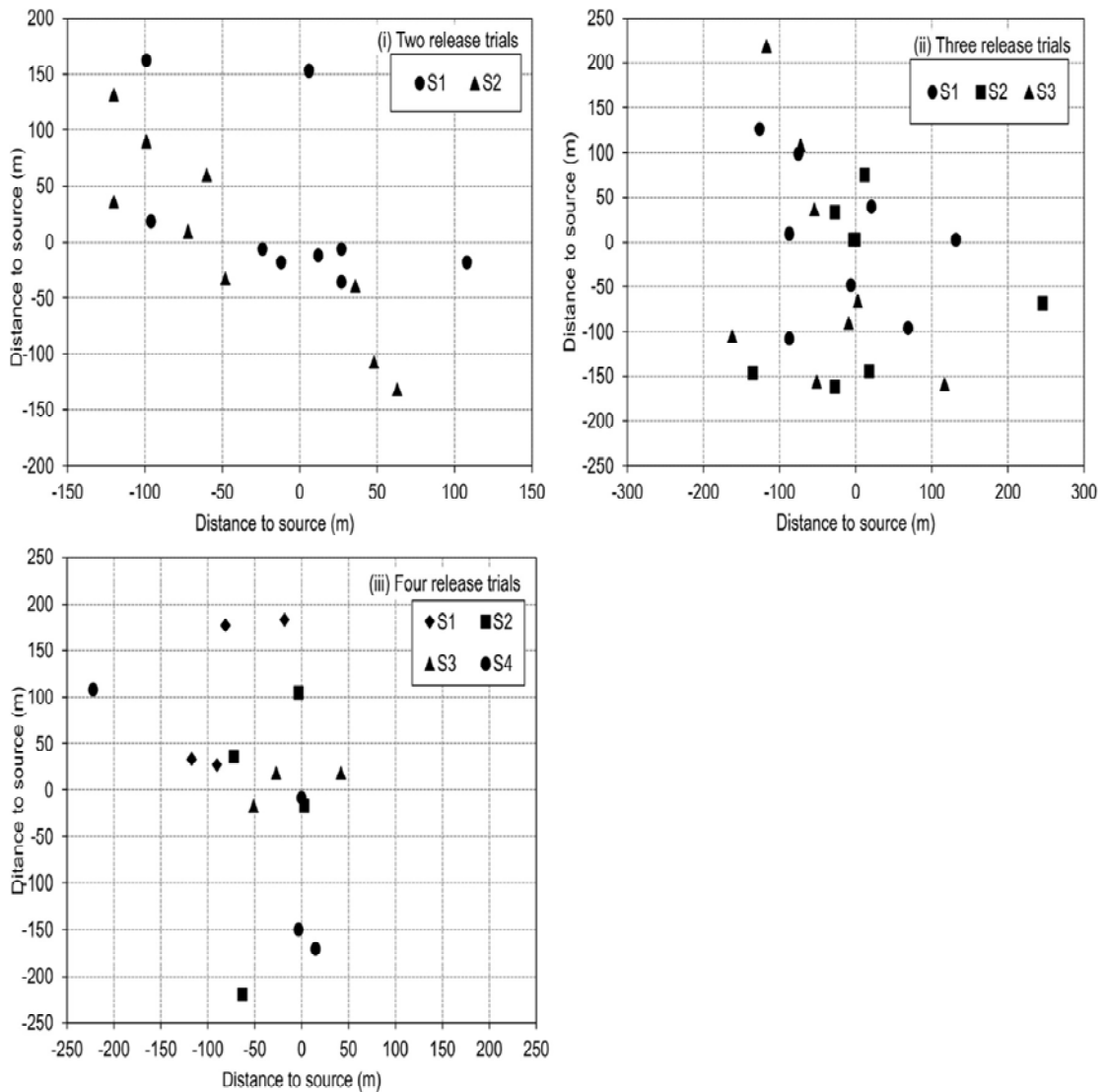


**Figure 4.** Location errors (or Euclidean distance from the corresponding true source) for the source retrieval in two, three and four release trials using blind data. S1, S2, S3 and S4 represent source location. The true source in each case is located at the axes origin and each retrieved source is paired with a true source for the calculation of the location error.

## REFERENCES

- Pudykiewicz, J., 1998. Application of adjoint tracer transport equations for evaluating source parameters. *Atmospheric Environment* **32**, 3039-3050.
- Sharan, M., A. K. Yadav, M. P. Singh, P. Agarwal, and S. Nigam (1996), A mathematical model for dispersion of air pollutants in low wind conditions, *Atmospheric Environment*, **30**, 1209–1220.
- Singh, S. K. and Rani, R., 2015. Assimilation of concentration measurements for retrieving multiple point releases in atmosphere: A least-squares approach to inverse modelling. *Atmospheric Environment* **119**, 402-414.
- Storwald, D.P., 2007: Detailed test plan for the fusing sensor information from observing networks (Fusion) Field Trial (FFT-07), Tech. Rep. Document No. WDTC-TP-07-078, Meteorology Division, West Desert Test Center, U.S. Army Dugway Proving Ground WDTC, Salt Lake, Utah.

**17th International Conference on  
Harmonisation within Atmospheric Dispersion Modelling for Regulatory Purposes  
9-12 May 2016, Budapest, Hungary**

---

**SOURCE RECONSTRUCTION IN URBAN AND NON-URBAN ENVIRONMENTS USING AN  
INVERSION METHODOLOGY COUPLED WITH A CFD APPROACH**

*Pramod Kumar<sup>1</sup>, Amir-Ali Feiz<sup>1</sup>, Sarvesh Kumar Singh<sup>1</sup>, Pierre Ngae<sup>1</sup>, Raj Rani<sup>1</sup>, Emerson Barbosa<sup>1</sup>,  
Grégory Turbelin<sup>1</sup>, Jean-Pierre Issartel<sup>2</sup>, Nadir Bekka<sup>1</sup>*

<sup>1</sup>LMEE, Université d'Evry-Val d'Essonne, 40 Rue du Pelvoux, 91020 Evry, France

<sup>2</sup>NRBC, Centre d'Etudes du Bouchet, 5 Rue Lavoisier, BP 3, 91710 Vert le Petit, France

**Abstract:** Accurate and fast reconstruction of the atmospheric pollutant sources in urban and non-urban regions is essential for emergency regulators to detect the unknown accidental or deliberated releases. This study describes a methodology combining a recently proposed renormalization inversion technique with a building-resolving Computational Fluid Dynamics (CFD) approach for source retrieval in the non-urban and geometrically complex urban regions. The source parameters (i.e. source location, height, and release rate) are reconstructed from a finite set of point measurements of concentration acquired from some sensors and the adjoint functions computed from a CFD model *fluidyn*-PANACHE. Two different experimental datasets (i) Fusion Field Trial-2007 (FFT-07) in flat terrain and (ii) Mock Urban Setting Test (MUST) field experiment in real situations at an urban scale are used for evaluation of the methodology. For both tracer experiments, the inversion results are presented with both synthetic and real measurements in various atmospheric stability conditions. The source locations were retrieved close to their true release locations at urban scale in MUST field experiment and FFT-07 in flat terrain with the real measurements. The study highlights the effectiveness and detection feasibility of the renormalization inversion technique coupled with a CFD modeling system to estimate the unknown source parameters in urban and non-urban regions.

**Key words:** *CFD modeling, Inverse problem, FFT-07, MUST field experiment, Renormalization inversion theory*

## INTRODUCTION

Fast and accurate identification of an unknown atmospheric tracer source in urban and non-urban regions can reduce the extent of subsequent exposure and associated mortality of an accidental or deliberated incident. The source reconstruction provides information about number of sources, their locations, height, and emission rates. A source reconstruction process generally utilizes the concentration measurements of a pollutant observed by a finite number of detectors distributed over a region. However, these concentration measurements, detected over a threshold value of a sensor, alone provide no particular information about the source including its location and release rate. An inversion methodology is required to estimate an unknown contaminant source based on these limited concentration measurements.

Several inversion procedures are described in the literature and recently, Issartel et al. (2007) proposed the renormalization inversion technique for identification of a distributed source in a region. The renormalization inversion technique required the computation of the adjoint functions corresponding to each concentration measurement. Recently, Sharan et al. (2009) extended the renormalization inversion technique to identify a continuous point release. This technique was applied and evaluated to retrieve a point source in flat and homogeneous terrains, where the consideration of a constant flow-field throughout a region is sufficient to compute the adjoint functions by a simple Gaussian model. However, flow-field throughout a complex urban region is generally not constant and diverted into often unexpected directions by the presence of buildings and other obstacles. In a recent study, Kumar et al. (2015) described a methodology based on the renormalization inversion technique and a building-resolving computational fluid dynamics (CFD) approach for reconstruction a continuous point source in the geometrically complex urban regions. The methodology was evaluated with 20 trials from Mock Urban Setting Test (MUST) field experiment in various atmospheric stability conditions. However, the methodology was described and evaluated in a two-dimensional space to retrieve a ground-level source or

the emission sources along a horizontal cross-section area passing through a fixed vertical level. The problem of vertical structure in continuous atmospheric source reconstruction in an urban area in 3-dimensional space is not described. This study addressed this problem of vertical structure in atmospheric source reconstruction. The objective of this study is to estimate the release height, location, and strength of a source in the urban and non-urban regions in 3-dimensional space.

## METHODOLOGY AND MODEL

An inversion technique, based on a concept of the renormalization theory (Issartel et al., 2007; Sharan et al., 2009), is utilized here for reconstruction of a continuous point source in 3-dimensional (3-D) space. It estimates the source parameters, viz. location, height, and intensity of a point release. The renormalization inversion technique returns an emission estimate linear with respect to a finite number  $m$  of concentrations measurements  $\boldsymbol{\mu}$ . It required to compute the adjoint functions  $a_i(\mathbf{x})$ , also known as retroplumes, in a 3-dimensional computational domain  $\mathbf{x} = (x, y, z)$ , corresponding to each concentration measurement at the receptor. The renormalization technique utilises these retroplumes to compute the renormalized weight functions  $w(\mathbf{x})$  in a 3-dimensional domain, and then these weight functions  $w(\mathbf{x})$  along with the concentration measurements  $\boldsymbol{\mu}$  compute a source estimate function  $\mathbf{s}(\mathbf{x})$ . In a case of point release, the maximum value of the source estimate function  $\mathbf{s}(\mathbf{x})$  coincides with a position  $\mathbf{x}_0 = (x_0, y_0, z_0)$  of a point source. Once the location  $\mathbf{x}_0$  is identified in a 3-D domain, the intensity  $q_0$  of the estimated point source is computed by  $q_0 = \mathbf{s}(\mathbf{x}_0) w(\mathbf{x}_0)^{-1}$ . A detailed mathematical description of the renormalization theory for a continuous point source retrieval in 2-D space and various issues and limitations are given in Sharan et al. (2009). However, the inversion methodology is implemented and evaluated here to address the problem of vertical structure in the atmospheric source reconstruction in 3-dimensional domain.

An important step of the inversion technique for source reconstruction is accurately computations of the adjoint functions in urban or non-urban environments. Computation of the adjoint functions by a dispersion or adjoint model required the realistic flow-field in the urban environments. The flow-field in urban regions is complex because the buildings and other obstacles often diverted it into unexpected directions. The CFD models has shown their applicability for computations of the realistic flow-field in urban regions and can be useful to compute the representative adjoint functions. Consideration of the constant flow-field throughout a domain in flat or non-urban terrains is often solve the purpose to compute the adjoint function by a simple Gaussian model. However, recent studies shows that the CFD models can also provide a more realistic flow and dispersion phenomena in homogeneous flat terrains in various atmospheric stability conditions.

This study utilises a CFD model *fluidyn*-PANACHE<sup>®</sup> to compute the flow-field and adjoint functions in urban and non-urban terrains. The *fluidyn*-PANACHE is a 3-dimensional Computational Fluid Dynamics (CFD) diagnostic model for simulating atmospheric processes related to the pollution and hazard in complex geometric environment. It solves the Reynolds Average Navier Stocks (RANS) equation governing air motion using 3-D finite-volume techniques and includes a built-in automatic 3-D mesh generator that can create the finite-volume mesh around obstacles and body-fitting the terrain undulations. To resolve the turbulent structure in computational domain, it includes a modified standard  $k-\epsilon$  3-D prognostic turbulence model. Dispersion of a tracer in the atmosphere is described by the advection-diffusion equation in Eulerian framework in *fluidyn*-PANACHE. To compute the retroplumes at each receptor, the flow-field is reversed by 180° and transport equation is integrated backward in time.

## TRACER FIELD EXPERIMENTS

The source reconstruction methodology coupled with a CFD approach is evaluated with two tracer field experiments, namely, Fusion Field Trial 2007 (FFT-07) experiment in flat terrain and Mock Urban Setting Test (MUST) field experiment in urban like environment. Brief details of these experiments and associated numerical (i.e. CFD) simulation setup to compute the adjoint functions are given as follows.

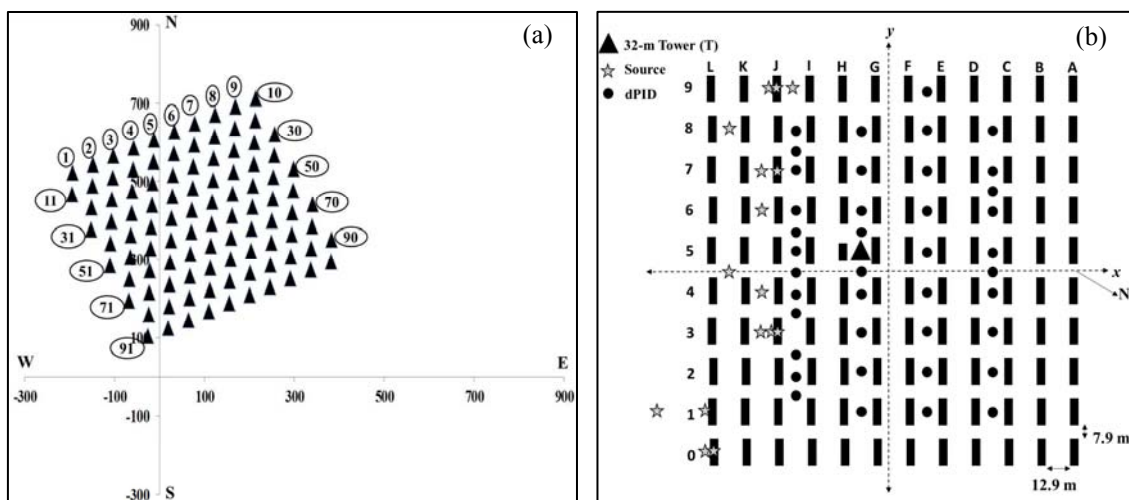


**Figure 1.** Schematic diagrams of (a) Fusion Field Trial (FFT-07) tracer experiment in flat terrain and (b) Mock Urban Setting Test (MUST) field experiment in urban like environment.

### Fusion Field Trial 2007 (FFT-07) experiment

Recently, a short range (~500 m), comprehensive tracer field experiment was conducted in September, 2007 at the U.S. Army's Dugway Proving Ground (DPG), Utah (Storvold, 2007). This highly instrumented test is referred to as Fusing Sensor Information from Observing Networks (FUSION) Field Trial 2007 (FFT-07). This experiment involves various instantaneous, continuous, single as well as multiple point releases in various atmospheric stability conditions varying from neutral to stable, and unstable conditions. In this experiment, a tracer propylene ( $C_3H_6$ ) was released at 2 m height above the ground surface and the concentrations were measured at 100 fast response digital Photo Ionization Detector (digiPID) samplers arranged in a rectangular staggered grid of area  $475 \text{ m} \times 450 \text{ m}$  in 10 rows and 10 columns. The digiPID samplers were also deployed at 2 m height above the ground surface. Figure 1(a) shows a schematic diagram of the FFT-07 experiment.

One trail #30 (Date: 20-09-2007) is selected in present study for the identification of a continuous point source in a flat terrain. In this trial,  $113.6 \text{ l min}^{-1} C_3H_6$  was continuously released in the atmosphere for ~10 min. The study domain for numerical simulations comprises outer and inner domains of width  $\times$  length  $2000 \text{ m} \times 2000 \text{ m}$  and  $1000 \text{ m} \times 1000 \text{ m}$ , respectively. To ensure a smoothly varying wind flow over the boundary of inner domain, outer domain boundary was kept away from the main test site consisting all the sensors and instruments and thus, size of outer computational domain was considered approximately four times of the inner domain. The heights of inner and outer domains were taken as 100 m and 200 m, respectively. The 3-D unstructured mesh in both domains consists 2644149 grid cells.

### Mock Urban Setting Test (MUST) field experiment

For evaluation of the source reconstruction methodology in an urban environment, we have used the observations taken from the MUST field experiment conducted at the U.S. Army Dugway Proving Ground (DPG) Horizontal Grid test site ( $40^\circ 12.606' \text{ N}$ ,  $-113^\circ 10.635' \text{ W}$ ) from 6-27 September 2001 (Biltoft, 2001). The test site was primarily flat with an averaged momentum roughness length of  $0.045 \pm 0.0005 \text{ m}$  (Yee and Biltoft, 2004). The MUST experiment represents an urban geometry by placing 120 shipping containers ( $12.2 \text{ m} \times 2.42 \text{ m} \times 2.54 \text{ m}$ ) arranged in a large array of building-like obstacles in 10 rows and 12 columns (Fig. 1(b)). This experiments was conducted mostly in neutral and stable atmospheric conditions. A detailed description of the meteorological and tracer observations are given in Biltoft (2001) and Yee and Biltoft (2004).

In present study, one trial #2682353 (Date: 25-09-2001) is selected for a continuous point source retrieval in an urban-like environment. In this selected case,  $225 \text{ l min}^{-1} C_3H_6$  was continuously released in the atmosphere for 15 min from a 5.2 m source height and measured at a height of 1.6 m (at 40 receptors) and 1, 2, 4, 6, 8, 10, 12, and 16 m (at 8 receptors in vertical direction on a single point in the domain) above the ground surface. The

mean wind speed and direction during this trial were  $4.49 \text{ ms}^{-1}$  and  $-47^\circ$ , respectively, with stable atmospheric conditions (Obukhov length  $L_{MO} = 120 \text{ m}$ ) (Yee and Biltoft, 2004). The simulation domain comprises outer ( $800 \text{ m} \times 800 \text{ m}$ ) and inner (nested) ( $250 \text{ m} \times 225 \text{ m}$ ) domains. Inner domain contains the urban structure consisting the MUST obstacle array ( $193 \text{ m} \times 171 \text{ m}$ ) and keeping the outer domain boundary away from obstacles ensures a smoothly varying wind flow over the inner domain boundary. The heights of the inner and outer domains were taken as  $100 \text{ m}$  and  $200 \text{ m}$ , respectively. The 3-D unstructured mesh is chosen for both outer and nested domains that consists a total 2849276 grid cells in the embedded mesh. In an ideal run, all the residuals was considered to be equal or less than  $O(10^{-4})$  to ensure a converged solution.

## RESULTS AND DISCUSSIONS

The source reconstructions for both FFT-07 and MUST field experiments are carried out with synthetic and real concentrations measurements. Knowing the location  $\mathbf{x}_0$  and intensity  $q_0$  of a continuous point source, synthetic measurements are simply generated from the computed retroplumes as  $\mu_i^{syn} = q_0 a_i(\mathbf{x}_0)$ . Synthetic measurements are free from any model and instrumental errors and ideal to evaluate a source reconstruction methodology. In case of the synthetic measurements, source parameters (i.e. location, height, intensity) are exactly estimated in flat and urban environments in both the experiments. This affirms the mathematical consistency of the inversion methodology coupled with a CFD approach. The error in retrieved source location is represented by the Euclidian distance of the retrieved location from the true source.

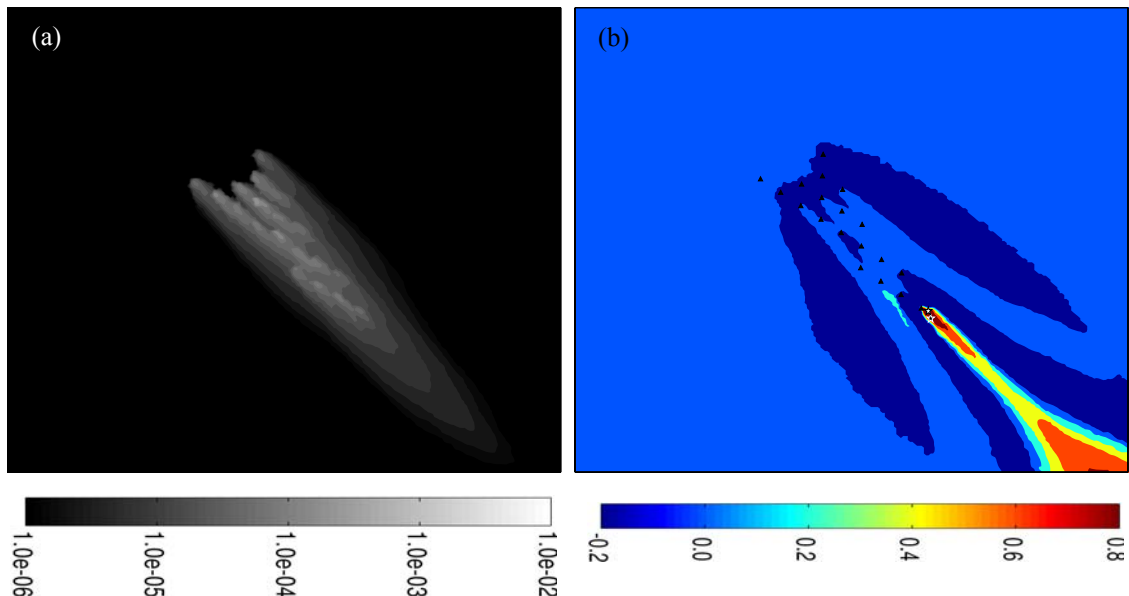


**Figure 2.** Isoleths of (a) weight function  $w(\mathbf{x})$  and (b) normalized source estimates  $\mathbf{s}^n(\mathbf{x}) = \mathbf{s}(\mathbf{x})/\max(\mathbf{s}(\mathbf{x}))$  with real concentration measurements in trial 30 of FFT-07 experiment. The black and white filled circles in Figure (b) show the true and estimated source locations, respectively.

Isolethes of the renormalized weight function in Fig. 2(a) shows the peaked values at the samplers' locations of the non-zero concentrations in trial-30 of FFT-07 experiment. The computed renormalized weight function includes the natural information associated with the sensors and physically interprets the extent of regions seen by the monitoring network. The weight function decreases in upwind direction and shows the lack of visibility for the most distant sources. A distribution of the normalized source estimates is shown in Fig. 2(b) in a horizontal cross-section plane corresponding to the estimated source height. With real concentration measurements, source is retrieved  $20.06 \text{ m}$  upwind from the true location. The release height is retrieved at  $3.125 \text{ m}$  above the ground surface, which is close to the true source height  $2 \text{ m}$ . An overprediction is observed in the retrieved source intensity. The estimated release rate is  $284.7 \text{ l/min}$ , which is  $2.5$  times greater than the true source intensity  $113.6 \text{ l/min}$  in this trial.

Figure 3(a) & (b) show the contour plots of the renormalized weight function and the normalized source

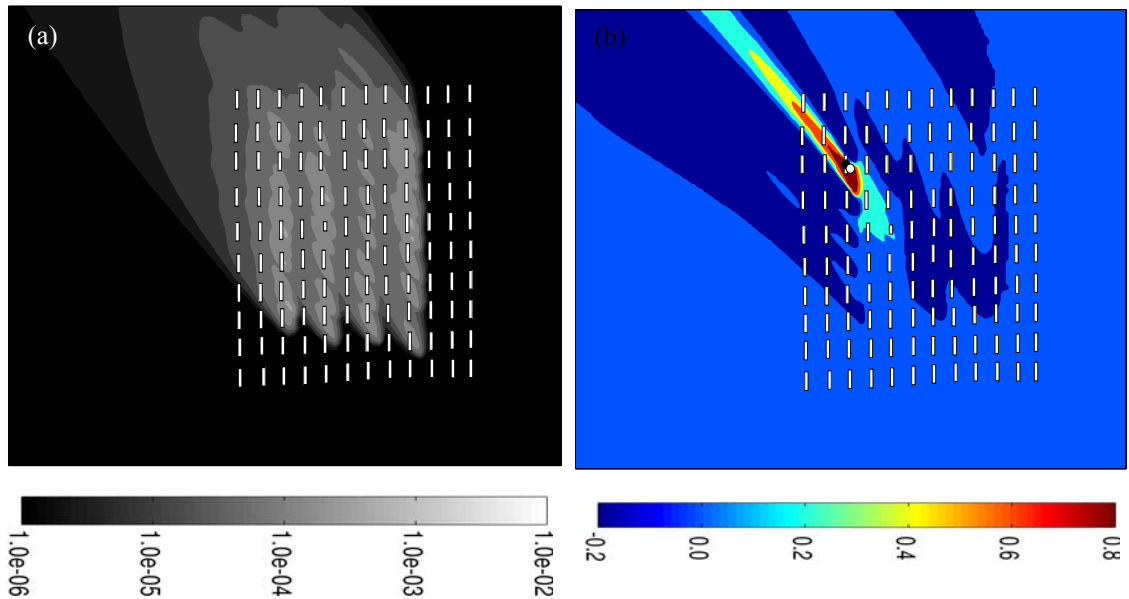


**Figure 3.** Isopleths of (a) weight function  $w(\mathbf{x})$  and (b) normalized source estimates  $\mathbf{s}^n(\mathbf{x}) = \mathbf{s}(\mathbf{x})/\max(\mathbf{s}(\mathbf{x}))$  with real concentration measurements in trial #2682353 of MUST field experiment.

estimates in a horizontal cross-section plane corresponding to the estimated source height in trial #2682353 of MUST experiment. The estimated point source is very close to the true source location (Fig. 3(b)). The Euclidean distance of the estimated source location from the true source is 4.22 m. The release height is estimated at 4.22 m above the ground which is also close to the true source height 5.2 m in this trial. The intensity of the estimated point source is retrieved within a factor of two of the true release rate. The retrieved intensity is 306.12 l/min, which is 1.36 times greater than the true release rate 225 l/min.

## CONCLUSIONS

This study describes a methodology to retrieve a continuous point release in 3-dimensional space in urban and non-urban regions and addresses a problem of vertical structure in atmospheric source reconstruction. The methodology is based on the renormalization inversion technique coupled with a CFD approach. The methodology is evaluated with the FFT-07 and MUST field experiments to retrieve the location, height, and strength of a continuous point release in flat and urban environments, respectively. The source parameters are estimated close to the true source parameters. By estimating the source height along with the other source parameters, this study shows the effectiveness of the renormalization inversion technique coupled with a CFD approach to estimate a continuous point release in urban and non-urban regions.

## REFERENCES

- Biltoft, C. A., 2001: Customer Report for Mock Urban Setting Test, DPG Document No. WDTCFR-01-121, West Desert Test Center, U.S. Army Dugway Proving Ground, Dugway, Utah, 58 pp.
- Fluidyn-PANACHE<sup>®</sup> Version 4.0.7, 2010: User Manual.
- Issartel, J.-P., M. Sharan and M. Modani, 2007: An inversion technique to retrieve the source of a tracer with an application to synthetic satellite measurements. *Proc. Roy. Soc. A*, **463**, 2863-2886.
- Kumar, P., Feiz, A. A., Singh, S. K., Ngae, P. and Turbelin, G. (2015). Reconstruction of an atmospheric tracer source in an urban-like environment. *J. Geophys. Res.: Atmospheres*, **120**, 12589-12604.
- Sharan, M., J.P. Issartel, S. K. Singh, P. Kumar, 2009: An inversion technique for the retrieval of single-point emissions from atmospheric concentration measurements. *Proc. Roy. Soc. A*, **465**, 2069-2088.
- Storwold, D.P, 2007: Detailed test plan for the Fusing Sensor Information from Observing Networks (FUSION) field trial 2007 (FFT 07). West Desert Test Center, U.S. Army Dugway Proving Ground, WDTC Document No. WDTC-TP-07-078.
- Yee, E. and C. A. Biltoft, 2004: Concentration fluctuation measurements in a plume dispersing through a regular array of obstacles. *Boundary-Layer Meteorol.*, **111**, 363-415.

**17th International Conference on  
Harmonisation within Atmospheric Dispersion Modelling for Regulatory Purposes  
9-12 May 2016, Budapest, Hungary**

---

**A BAYESIAN APPROACH OF THE SOURCE TERM ESTIMATE  
COUPLING RETRO-DISPERSION COMPUTATIONS WITH A LAGRANGIAN PARTICLE  
DISPERSION MODEL AND THE ADAPTIVE MULTIPLE IMPORTANCE SAMPLING**

*Harizo Rajaona<sup>1</sup>, François Septier<sup>2,3</sup>, Yves Delignon<sup>2,3</sup>, Patrick Armand<sup>1</sup>,  
Laurent Makke<sup>4</sup>, Christophe Olry<sup>4</sup>, and Armand Alberget<sup>4</sup>*

<sup>1</sup>CEA, DAM, DIF, F-91297 Arpajon, France

<sup>2</sup>Institut Mines-Télécom / Télécom Lille 1, F-59650 Villeneuve d'Ascq, France

<sup>3</sup>CRISTAL UMR CNRS 9189, F-59651 Villeneuve d'Ascq CEDEX, France

<sup>4</sup>ARIA Technologies, F-92100 Boulogne-Billancourt, France

**Abstract:** This paper presents an enhanced version of a STE adaptive algorithm based on probabilistic Bayesian inference (AMIS) that estimates the parameters of an atmospheric pollution source term. After introducing the problem and presenting the initial results obtained with the first version of the algorithm, we describe an efficient way to reduce the computational load in its procedure by shifting the most time-consuming step outside the iterative loop. This is made possible by applying the duality relationship between forward and adjoint advection-diffusion equations, and is proven to work well on a synthetic example using Retro-SPRAY, the backward implementation of SPRAY, the Lagrangian particle dispersion model of the PMSS suite.

**Key words:** *Source Terme Estimate, Bayesian approach, LPDM, retro-dispersion, AMIS.*

## INTRODUCTION

The threat of Chemical, Biological, Radiological, and Nuclear (CBRN) releases in the atmosphere is a key issue. Such incidents may be due to terrorist acts, using non-conventional methods such as dirty bombs in order to create panic. The origin of these events can also be accidental, for example given a leak of hazardous material on an industrial site. Either way, the development of tools to detect the source and assess the parameters of the release is a major concern for the population's safety. Scientifically speaking, the problem of source term estimation (STE) is quite challenging, because obtaining the most accurate estimation within the shortest amount of time is crucial.

There are currently several approaches to solve STE problems, each of them using a specific set of skills. One line of study focuses on adjoint-transport modelling and retro-transport, as further developed in Pudykiewicz (1998) or Issartel and Baverel (2003) where backward simulations are computed using the principle of time-symmetry in atmospheric transport to reconstruct the source. These methods perform well, but most of them do not offer the possibility to properly quantify the uncertainty relative to the given estimation.

Another approach consists in using probabilistic methods. The optimization problem of computing the source term parameters can be treated as a maximum-likelihood estimation scheme (Nehorai, 1995), or by finding the maximum of the posterior distribution of the source parameters given the concentration measurements (Winiarek, 2012). Such methods provide point estimates but are not meant to provide a complete overview of the posterior distribution. To do so, it is possible to use stochastic simulation techniques such as Monte Carlo methods, coupled with Bayesian inference, so that the resulting algorithm delivers a sample of parameters whose distribution aims at approximating the posterior. This kind of method also allows taking into account potential prior information on the source parameters. Several related examples exist in the literature, that use the notorious Markov Chain Monte Carlo (MCMC) algorithm, such as (Delle Monache, 2008), (Chow, 2008), (Keats, 2007) or (Yee, 2014).

Even though MCMC methods are efficient in a number of cases, they are prone to several issues, regarding the inherent *burn-in* time necessary before the convergence, or the choice of how to initialize properly the Markov chain.

In this study, we focus on an alternative Bayesian method called *Adaptive Multiple Importance Sampling (AMIS)*. As presented in (Rajaona, 2015), by adding an advanced adaptive layer to the classical IS scheme, it provides good results for STE problems within a correct amount of time. This paper presents an improvement of the original method, aiming at optimizing the most time-consuming step in the algorithm by using the duality relationship with adjoint models for evaluating concentrations. The enhanced method is illustrated with a synthetic example.

## THE BAYESIAN SOLUTION OF THE STE PROBLEM

The main goal of our work is to use the concentrations measured by a sensor network, resulting from the release of hazardous materials from a source point, in order to characterize the parameters of the latter, namely its position  $\boldsymbol{\theta} = (x_s, y_s)$  and its temporal emission profile  $\mathbf{q} = (q_1, q_2, \dots, q_{T_s})$  over  $T_s$  time-steps. We assume that the source and the sensors are located on the same vertical level. The data model we use assumes the following source-receptor relationship:

$$\mathbf{d} = C(\boldsymbol{\theta})\mathbf{q} + \boldsymbol{\varepsilon} \quad (1)$$

$\mathbf{d} = (d_1, \dots, d_m)$  is the vector of observations, and  $\boldsymbol{\varepsilon}$  is the vector that gathers representativeness, observation and model error in a single term. We assume that  $\boldsymbol{\varepsilon}$  is independent and identically distributed over the sensors, and follows a normal distribution  $N(0, \sigma_{obs}^2)$ , where  $\sigma_{obs}^2$  is the error variance.  $C(\boldsymbol{\theta})$  is a source-receptor matrix of the concentrations obtained at each sensor from a unitary release of a source at potential location  $\boldsymbol{\theta}$ .

Our objective is to compute the posterior probability distribution  $p(\boldsymbol{\theta}, \mathbf{q} | \mathbf{d})$  of the source parameters given the observations. By using Bayesian inference, the posterior can be rewritten as follows, using a marginalization relationship:

$$p(\mathbf{q}, \boldsymbol{\theta} | \mathbf{d}) = p(\mathbf{q} | \boldsymbol{\theta}, \mathbf{d})p(\boldsymbol{\theta} | \mathbf{d}) \quad (2)$$

Since we assume that the observation noise is Gaussian and that the random variables  $\mathbf{q}$  and  $\boldsymbol{\theta}$  are independent, then by making a Gaussian assumption over the prior distribution  $p(\mathbf{q})$  as in (Winiarek et al, 2011), the marginal posterior  $p(\mathbf{q} | \boldsymbol{\theta}, \mathbf{d})$  can be computed analytically, leaving only the posterior distribution of the source location to be estimated numerically. This distribution, denoted by  $\pi(\boldsymbol{\theta})$ , can be expressed up to the normalizing constant  $p(\mathbf{d})$  by the following formula, thanks to Bayes rule:

$$\pi(\boldsymbol{\theta}) = p(\boldsymbol{\theta} | \mathbf{d}) = \frac{p(\mathbf{d} | \boldsymbol{\theta})p(\boldsymbol{\theta})}{p(\mathbf{d})} \propto p(\mathbf{d} | \boldsymbol{\theta})p(\boldsymbol{\theta}) \quad (3)$$

$p(\boldsymbol{\theta})$  is the prior distribution of the source location, and is chosen to be uniform over the domain, implying that the source can be anywhere within the domain boundaries.  $p(\mathbf{d} | \boldsymbol{\theta})$  is the likelihood of having the concentrations  $\mathbf{y}$  given a source located at  $\boldsymbol{\theta}$ .

To estimate the so-called target posterior distribution  $\pi(\boldsymbol{\theta})$ , we resort to the Adaptive Multiple Importance Sampling (AMIS) algorithm (Cornuet, 2012), which iteratively draws sets of samples  $\boldsymbol{\theta} = \theta_1, \dots, \theta_{N_p}$  from a proposal distribution  $\varphi(\boldsymbol{\theta})$ , computes the importance weights  $w = \frac{\pi(\boldsymbol{\theta})}{\varphi(\boldsymbol{\theta})}$ , and adjusts the parameters of  $\varphi$  so that it tends to fit the posterior distribution we try to approximate. The originality of the AMIS lies in the fact that all the importance weights that were previously computed are recycled at each iteration, and reused, in order to accelerate the convergence towards the posterior estimate. A common choice for  $\varphi$  is a mixture of  $D$  multivariate Gaussian distributions (Cappé, 2008) as it is flexible enough to adapt to complex targets, and the update equations for its parameters are analytically available.

In (Rajaona, 2015), the AMIS methodology is applied to the Fusion Fields Trial 2007 (FFT07) experiment, using real concentration data to estimate the source location and emission profile for the trial #7. The AMIS algorithm is coupled with a Gaussian puff dispersion model for the calculation of the source-receptor matrix, and provides good results for locating the source as shown in Figure 1. Regarding the emission rate estimation, despite the fact that the original profile is not completely reconstructed, the estimation provided by the algorithm manages to approximate the start and stop times of the emission, and the estimated release rates remain well within the confidence interval.

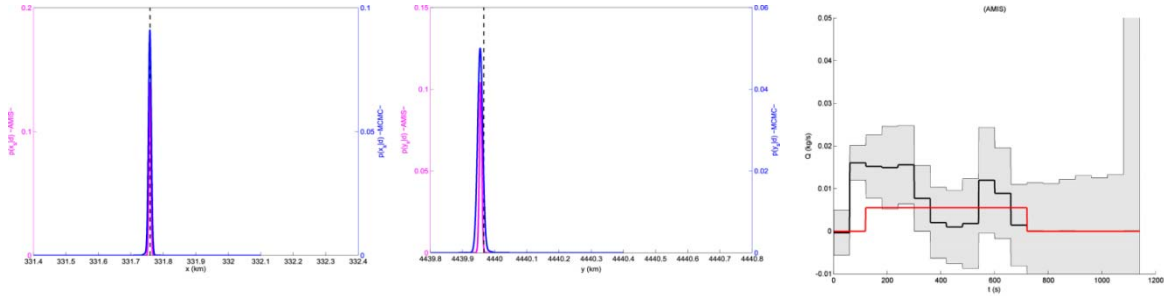


**Figure 1.** Results of the AMIS algorithm for the estimation of FFT07-trial#7's source. Left and middle: estimation of  $p(x_s|d)$  and  $p(y_s|d)$  for AMIS (blue) and MCMC (magenta) compared to the true value (dashed black). Right: estimation of  $p(q|\theta, d)$  (black) and  $\pm 2\sigma$  confidence interval (grey) compared to the true value (red).

## THE ALTERNATIVE SOLUTION FOR COMPUTING THE SOURCE-RECEPTOR RELATIONSHIP

One of the most important feedbacks that emerge from the FFT07 case study was the high number of calls to the dispersion model, which had to be summoned for each sample at each iteration. The Gaussian model we used allowed a reasonable total computational time, but in its original form, the overall algorithmic scheme would certainly scale badly if we were to switch for a more accurate model.

That is why we came up with a more efficient way of optimizing the building of the source-receptor matrix, which is the most costly operation in computation time. In its current version, the source-receptor matrix  $C(\theta)$  is obtained by solving a forward advection-diffusion equation and retrieving its solutions at the sensor locations. However, the duality relationship mentioned in (Keats, 2007) also stipulates that the same values can be obtained by solving the adjoint advection-diffusion equation, provided that the considered release is unitary and instantaneous. In other words, by using a backward dispersion model, it is possible to fill the source-receptor matrix with values of conjugate concentrations to build an operator  $C^*(\theta)$  that can substitute to  $C(\theta)$  in Equation (1).

More precisely, if  $C(R_i, t_j|\theta, t'_n)$  denotes the concentration given by a forward dispersion model at sensor  $R_i$  and observation time  $t_j$ , due to a release at emission time  $t'_n$  of a source located at position  $\theta$ , then the equivalent value in the backward framework is  $C^*(\theta, t'_n|R_i, t_j)$ , which represents the conjugate concentration measured at point  $\theta$  at time  $t'_n$  due to a backward release from the sensor  $R_i$  at time  $t_j$  (Figure 2).

The major improvement resulting from this modification is that there are no more iterative calls to the dispersion model in the iterative scheme of the AMIS as the values of  $C^*$  for each point of the domain are pre-computed and stored in external files. This way, while computing the likelihood during the execution of the AMIS, the algorithm just pulls the  $C^*$  data corresponding to the sampled values of  $\theta$ , rather than launching a forward dispersion calculation as it originally did.

$$C(\theta) = \begin{bmatrix} C(R_1, t_1|\theta, t'_1) & C(R_1, t_1|\theta, t'_2) & \dots & C(R_1, t_1|\theta, t'_{T_s}) \\ C(R_1, t_2|\theta, t'_1) & C(R_1, t_2|\theta, t'_2) & \dots & C(R_1, t_2|\theta, t'_{T_s}) \\ \vdots & \vdots & & \vdots \\ C(R_1, t_{T_c}|\theta, t'_1) & C(R_1, t_{T_c}|\theta, t'_2) & \dots & C(R_1, t_{T_c}|\theta, t'_{T_s}) \\ C(R_2, t_1|\theta, t'_1) & C(R_2, t_1|\theta, t'_2) & \dots & C(R_2, t_1|\theta, t'_{T_s}) \\ C(R_2, t_2|\theta, t'_1) & C(R_2, t_2|\theta, t'_2) & \dots & C(R_2, t_2|\theta, t'_{T_s}) \\ \vdots & \vdots & & \vdots \\ C(R_2, t_{T_c}|\theta, t'_1) & C(R_2, t_{T_c}|\theta, t'_2) & \dots & C(R_2, t_{T_c}|\theta, t'_{T_s}) \\ \vdots & \vdots & & \vdots \\ \vdots & \vdots & & \vdots \\ C(R_{N_c}, t_{T_c}|\theta, t'_1) & C(R_{N_c}, t_{T_c}|\theta, t'_2) & \dots & C(R_{N_c}, t_{T_c}|\theta, t'_{T_s}) \end{bmatrix} \longleftrightarrow C^*(\theta) = \begin{bmatrix} C^*(\theta, t'_1|R_1, t_1) & C^*(\theta, t'_2|R_1, t_1) & \dots & C^*(\theta, t'_{T_s}|R_1, t_1) \\ C^*(\theta, t'_1|R_1, t_2) & C^*(\theta, t'_2|R_1, t_2) & \dots & C^*(\theta, t'_{T_s}|R_1, t_2) \\ \vdots & \vdots & & \vdots \\ C^*(\theta, t'_1|R_1, t_{T_c}) & C^*(\theta, t'_2|R_1, t_{T_c}) & \dots & C^*(\theta, t'_{T_s}|R_1, t_{T_c}) \\ C^*(\theta, t'_1|R_2, t_1) & C^*(\theta, t'_2|R_2, t_1) & \dots & C^*(\theta, t'_{T_s}|R_2, t_1) \\ C^*(\theta, t'_1|R_2, t_2) & C^*(\theta, t'_2|R_2, t_2) & \dots & C^*(\theta, t'_{T_s}|R_2, t_2) \\ \vdots & \vdots & & \vdots \\ C^*(\theta, t'_1|R_2, t_{T_c}) & C^*(\theta, t'_2|R_2, t_{T_c}) & \dots & C^*(\theta, t'_{T_s}|R_2, t_{T_c}) \\ \vdots & \vdots & & \vdots \\ \vdots & \vdots & & \vdots \\ C^*(\theta, t'_1|R_{N_c}, t_{T_c}) & C^*(\theta, t'_2|R_{N_c}, t_{T_c}) & \dots & C^*(\theta, t'_{T_s}|R_{N_c}, t_{T_c}) \end{bmatrix}$$

**Figure 2.** Equivalence relationship between  $C(\theta)$  and  $C^*(\theta)$  over a range of  $N_c$  sensors,  $(1, \dots, T_c)$  observation time steps and  $(1, \dots, T_s)$  emission time steps.

To validate our method, we substituted the Gaussian model with a more elaborate Lagrangian Particle Dispersion Model, namely the Parallel Micro-Swift-Spray (PMSS) suite (Tinarelli et al., 2013). We take advantage of Retro-SPRAY (Armand, 2013), which is the implementation of the backward version of PMSS, in order to prepare the repository of conjugate concentration data. We considered a countryside landscape over a  $6\text{km} \times 6\text{km}$  square domain based on real topographical data for our experiment. A single release is simulated, that emits at a constant rate for one hour, and which resulting concentrations are given by a network of 11 sensors scattered over the domain (Figure 3).

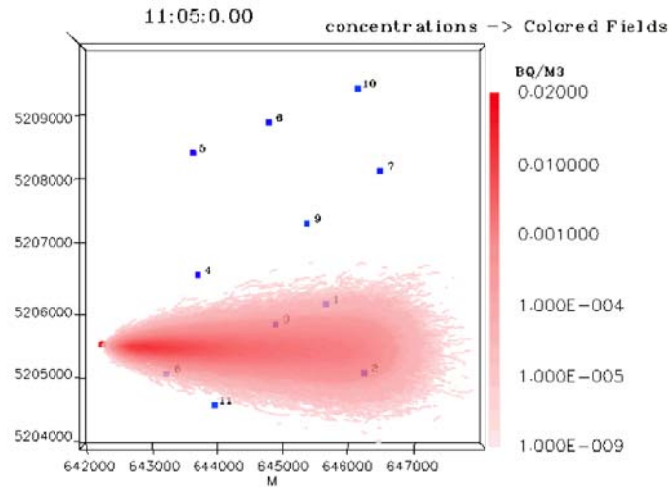


**Figure 3.** Snapshot of the release over the domain, with the location of the source (in red) and the sensors (in blue)

As seen in Figure 4, the results illustrate a good estimation of the source location obtained after 10 iterations of the AMIS algorithm. Furthermore, the total amount of computation time is quite lower than the estimated projection for the forward dispersion configuration in the same use case: it takes around 7.5 seconds to perform an AMIS iteration using backward pre-calculated concentration, whereas an iteration with on-the-fly computation of forward concentrations takes approximately 15 minutes in the same context.

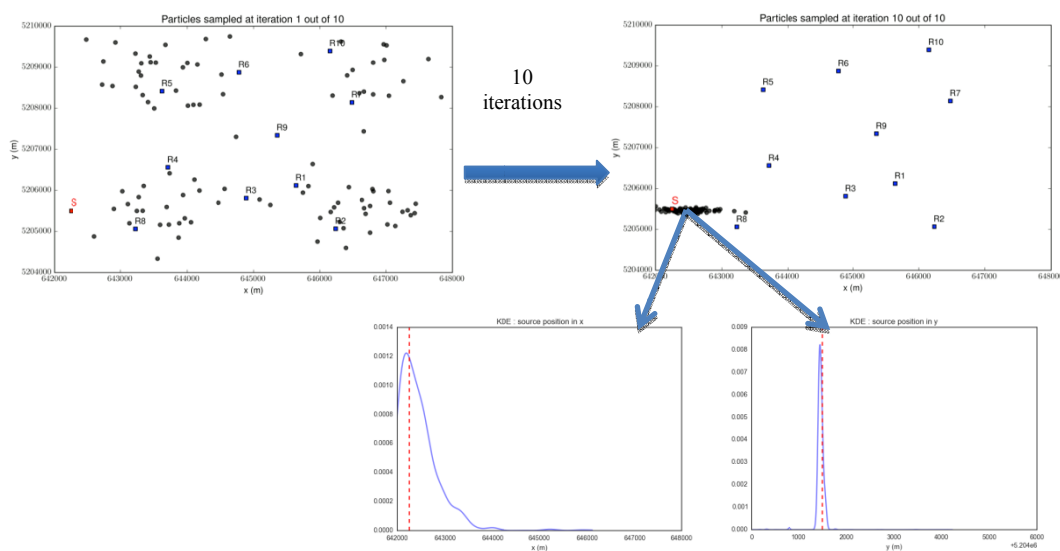


**Figure 4:** Scatterplot of the samples generated by the AMIS algorithm using Retro-SPRAY, with any initial knowledge at the initialization (left), after 10 iterations (right) with the corresponding estimated spatial posterior distributions of the source location (bottom right).

## CONCLUSION

In this paper we have presented an enhanced version of the AMIS algorithm for STE problems. By using the adjoint version of the PMSS model, we demonstrate that it is possible to scale our algorithm by shifting most of the computational load outside the iterative scheme. Provided that a set of conjugate concentrations was pre-calculated, the execution time of our STE algorithm is considerably reduced compared to the initial scheme which resorted to forward dispersion computations.

Even if additional work is still required to ensure the stability of the algorithm, especially on the estimation of the emission profile, such improvements pave the way for future work on more complex situations such as urban scenarios, where applying elaborate models such as PMSS becomes essential.

## REFERENCES

- Armand, P., Olry, C., Albergel, A., Duchenne, C., & Moussafir, J. (2013). Development and application of Retro-spray, a backward atmospheric transport and dispersion model at the regional and urban scale, 15<sup>th</sup> International conference on Harmonisation within Atmospheric dispersion Modelling for Regulatory Purposes, Harmo'15, pp. 789-793.
- Cappé, O., Douc, R., Guillin, A., Marin, J. M., & Robert, C. P. (2008). Adaptive importance sampling in general mixture classes. *Statistics and Computing*, **18**, 447-459.
- Chow, F. K., Kosovic, B., & Chan, S. (2008). Source inversion for contaminant plume dispersion in urban environments using building-resolving simulations. *Journal of applied meteorology and climatology*, **47**, 1553-1572.
- Cornuet, J.M., Mira, A., & Robert, C. P. (2012). Adaptive multiple importance sampling. *Scandinavian Journal of Statistics*, **39**, 798-812.
- Delle Monache, L., Lundquist, J. K., Kosovic, B., Johannesson, G., Dyer, K. M., Aines, R. D., ... & Loosmore, G. A. (2008). Bayesian inference and Markov chain Monte Carlo sampling to reconstruct a contaminant source on a continental scale. *Journal of Applied Meteorology and Climatology*, **47**, 2600-2613.
- Issartel, J. P., & Baverel, J. (2003). Inverse transport for the verification of the Comprehensive Nuclear Test Ban Treaty. *Atmospheric Chemistry and Physics*, **3**, 475-486.
- Keats, A., Yee, E., & Lien, F. S. (2007). Bayesian inference for source determination with applications to a complex urban environment. *Atmospheric environment*, **41**, 465-479.

- Nehorai, A., Porat, B., & Paldi, E. (1995). Detection and localization of vapor-emitting sources. *IEEE Transactions on Signal Processing*, **43**, 243-253.
- Pudykiewicz, J. A. (1998). Application of adjoint tracer transport equations for evaluating source parameters. *Atmospheric Environment*, **32**, 3039-3050.
- Rajaona, H., Septier, F., Armand, P., Delignon, Y., Olry, C., Albergel, A., & Moussafir, J. (2015). An adaptive Bayesian inference algorithm to estimate the parameters of a hazardous atmospheric release. *Atmospheric Environment*, **122**, 748-762.
- Tinarelli, G., Mortarini, L., Trini-Castelli, S., Carlino, G., Moussafir, J., Olry C., Armand, P. and Anfossi D. (2013). Review and validation of Micro-Spray, a Lagrangian particle model of turbulent dispersion. *Lagrangian Modeling of the Atmosphere, Geophysical Monograph*, 200, 311-327
- Winiarek, V., Bocquet, M., Saunier, O., & Mathieu, A. (2012). Estimation of errors in the inverse modeling of accidental release of atmospheric pollutant: Application to the reconstruction of the cesium-137 and iodine-131 source terms from the Fukushima Daiichi power plant. *Journal of Geophysical Research: Atmospheres*, **117**(D5).
- Yee, E., Hoffman, I., & Ungar, K. (2014). Bayesian inference for source reconstruction: A real-world application. *International Scholarly Research Notices*, 2014.

**17th International Conference on  
Harmonisation within Atmospheric Dispersion Modelling for Regulatory Purposes  
9-12 May 2016, Budapest, Hungary**

---

**A CFD MODELING APPROACH FOR A CONTAMINANT RELEASED IN A CITY**

*Nadir Bekka, Pramod Kumar, Amir-Ali Feiz, Sarvesh Singh, Mohamed Sellam, Emerson Barbosa,  
Pierre Ngae, Grégory Turbelin, Amer Chpoun*

Université d'Evry-Val d'Essonne, LMEE, 40 rue du Pelvoux, 91020 Evry, France

**Abstract:** In the context of industrial risk management, occurring at urban scales, decision-making processes remain subject to various sources of uncertainty and required accurate and realistic models to simulate atmospheric pollutant diffusion both in forward and inverse modelling. In the frame of this work, the three-dimensional (3-D) computational fluid dynamic (CFD) model OpenFOAM adapted to the dispersion of toxic and hazardous gases around buildings has been evaluated. In this study, OpenFOAM model is utilized to evaluate the Mock Urban Setting Test (MUST) field tracer experiment that provide a simplified urban-like area. A statistical analysis was performed to compare the concentrations from CFD model simulations with the experimental measurements. A detailed analysis with statistical measures shows that the performance of OpenFOAM model against observations is well within the acceptable bounds of statistical measures for air quality applications. The CFD model predicts 83% of the total concentrations within a factor of two and shows the over-prediction tendency at the receptors near to the source but under-prediction at far away from the source.

**Keywords:** *CFD modeling, MUST experiment, OpenFOAM, Urban dispersion modelling*

## **INTRODUCTION**

Air quality assessment in complex urban terrain with new and existing techniques is imperative to provide the information needed to estimate the population exposure to hazardous airborne matter and to assist regulators, urban planners or emergency authorities to outline the evacuation plans in a case of the natural disasters, accidental or deliberate release. In urban sites, dispersion of toxic gases surrounding the buildings are often predicted with Computational Fluid Dynamic (CFD) codes. A CFD model solves the Navier-Stokes fluid dynamics equations using a small grid size (of the order 1 m or even 12 less) (Hanna et al., 2004) over the complex terrains. Many CFD codes were successfully evaluated against experimental data for various types of releases in diverse geometric environments and atmospheric conditions (Rakai et al., 2014; Labovsky and Jelemensky, 2010; Gromke and Blocken, 2015; Kumar et al., 2015; Efthimiou et al., 2015; etc.). However, to obtain the reliable results for emergency preparedness and air quality analysis, the CFD models are required to be set up, tested, and evaluated correctly with the experimental observations in different geometric environments and atmospheric conditions (Tominaga and Stathopoulos, 2013). Complexities in flow fields and pollutant transport and dispersion in urban region make difficult to assess the contaminant plume concentrations due to local topography, terrain conditions, buildings and other geometrical structures. This study concerns the evaluation of a CFD model OpenFOAM against the Mock Urban Setting Test (MUST) field tracer experiment environments. In order to evaluate the CFD simulations of urban flows and pollutant dispersion, the completeness and the reliability of the experimental data is a necessity. This study utilizes one trial of the MUST field experiment in order to demonstrate the OpenFOAM model's capabilities to simulate the flow and dispersion patterns in the near field but also at larger distances.

## **MOCK URBAN SETTING TEST (MUST) FIELD EXPERIMENT**

In the present study, we have used the observations taken from the MUST field experiment conducted at the U.S. Army Dugway Proving Ground (DPG) Horizontal Grid test site (40°12.606' N, -113°10.635' W) on 6-27 September 2001 (Biltoft, 2001). The test site was primarily flat with an averaged momentum roughness length of  $0.045 \pm 0.0005$  m, and the zero plane displacement height of  $0.37 \pm 0.09$  m (Yee and Biltoft, 2004). The MUST experiment represent an urban roughness geometry by placing 120 shipping containers ordinary arranged in a large array of building-like obstacles. These containers (12.2 m × 2.42 m × 2.54 m) were placed in a regular formation of 10 rows and 12 columns forming an approximately

200 m × 200 m array. Thus the terrain was considered as an idealized urban-like terrain in the computation. The MUST experiments was conducted mostly in neutral and stable atmospheric conditions. A detailed description of the meteorological and tracer observations are given in Biltoft (2001) and Yee and Biltoft (2004) that includes an extensive meteorological observations within and around the test site to characterize flow fields, turbulence, temperature and momentum gradients and fluxes, and atmospheric stability (Biltoft, 2001). One case #2681829 (Date: 25-09-2001, Time: 1830 MDT) is selected in the present study for the dispersion of a Propylene (C<sub>3</sub>H<sub>6</sub>) pollutant. In this selected case, 225 l min<sup>-1</sup> Propylene was continuously released in the atmosphere for 15 min from a 1.8 m source height and measured at 48 receptors points (both horizontal and vertical cross-sections of the dispersing plume) downwind from the source (Figure 1). The concentration measurements were recorded at the height of 1.6 m (at 40 receptor points, in red color in the Figure 1) and 1, 2, 4, 6, 8, 10, 12, and 16 m (at 8 receptors in vertical direction on a single point in the domain, in green color in the Figure 1) above the ground level at the frequency response of 50 Hz. The mean wind speed and direction at South tower upstream the array at 4 m height above the ground surface were 7.93 ms<sup>-1</sup>, and -41° respectively (Yee and Biltoft, 2004). The atmospheric stability was neutral (Obukhov length LMO = 28000 m) during this experimental case (Table 1). By following Yee and Biltoft (2004), 200-s quasi-steady periods within each 15-min plume dispersion experiment was extracted from the selected trial to remove the non-stationary from the data.

**Table 1.** Characteristics of the test case #2681829

$U$ (m s <sup>-1</sup> )	$\alpha$ (deg)	$\sigma_\theta$ (deg)	$k$ (m <sup>2</sup> s <sup>-2</sup> )	$Q$ (L min <sup>-1</sup> )	$z_s$ (m)	$u^*$ (m s <sup>-1</sup> )	$L$ (m)	$\epsilon$ (m <sup>2</sup> s <sup>-3</sup> )
7.93	-41	9.5	1.46	225	1.8	1.1	28000	0.8

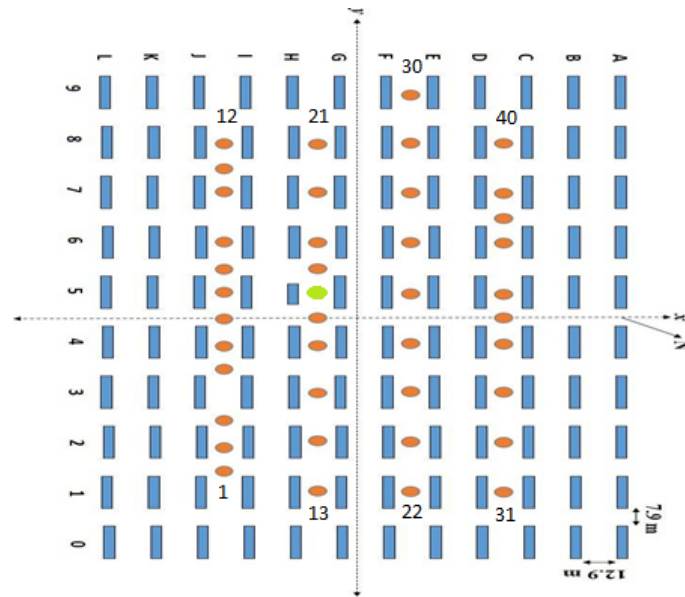


**Figure 1.** Representation of the MUST experiment with the location of measurement sensors

## MODEL AND METHODS

In OpenFOAM, the equation of momentum, mass transfer and the turbulence model (Reynolds Average Navier Stokes (RANS) equation) for homogeneous multiphase flow are supposed to be solved using the finite volume method. Generating mesh using snappyHexMesh tool was used for the geometry. Using embedded meshing techniques, cells are concentrated around each container (Figure 2) in order to capture the detailed shear and entrainment effects at the edge of the gas column. Maximum distance of meshes near the initial plume is 0.5 m. Computational grids consist of 0.83 million cells. The convergence criterion was the residual of root mean square that was considered to be equal to or less than 10<sup>-4</sup>. As

mentioned earlier,  $C_3H_6$  was used in the MUST experiment. Therefore this gas is considered in addition to air in the domain. The experiments were conducted at a neutral atmospheric condition and a standard  $k-\epsilon$  model is used to simulate the turbulence processes. OpenFOAM was modified to estimate the turbulent kinetic energy and dissipation rate based on input Pasquill stability class or input of Monin-Obukhov length  $L$ . For the calculations of transport and dispersion of  $C_3H_6$ , the boundary conditions are usually either (i) no slip solid surfaces, (ii) wind inflow (or outflow), or (iii) a passive outflow condition at ambient pressure.

### NUMERICAL SOLUTION AND DISCUSSION OF THE RESULTS

Figures 3a and 3b represents respectively the 2-D and 3-D contours plot of the steady CFD simulated tracer concentrations at ground level within the site. One can see that the plume disperses mostly in the direction of the mean wind. For a point to point evaluation of the model with observations, Chang and Hanna (2004) suggested to replace all those concentration values which are below detection limit of the samplers to that detection limit. The sampling calibration range of the detectors used in MUST experiment was 0.04-1000 ppmv (Biltoft, 2001).

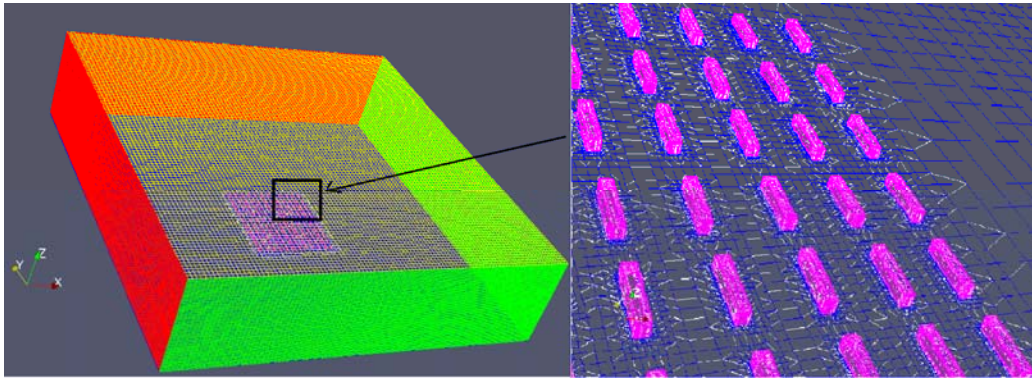


**Figure 2.** Site features and generating mesh using snappyHexMesh in OpenFOAM

By following Donnelly et al. (2009), the lower concentration value from the detection limit in any pair from all the pairs of model and observations is set to the detection limit 0.04 ppmv. If both concentrations in one of the pair are below the detection limit, both have been set to zero and removed from the dataset.

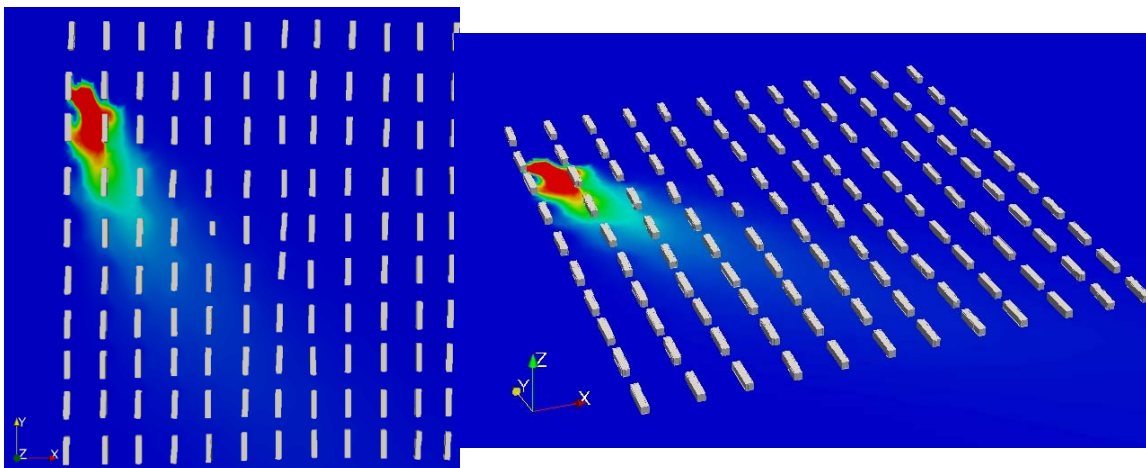


**Figure 3:** Ground level concentration contours (in ppmv) computed from steady CFD solution for the case #2681829 of MUST Experiment ( $\alpha=-41^\circ$ ) (a) 2D view, (b) 3D view. Here, the maximum concentration of  $C_3H_6$  is 5 ppmv (red color on the isopleths).

Experimental measurements indicate in the Figure 4 that detectors n°8 and n°9 (from Figure 1) are the most exposed to the plume (at least 3 ppmv). Four secondary peaks of concentrations are also observed, but their intensity is at least two times lower (between 1 and 1.7 ppmv). It is clear that the OpenFOAM model underestimate the concentrations obtained experimentally. The biggest disagreement is found in the last 8 sensors on the central mast at different heights. It follows that the gas plume does not appear to rise in sea level, and is conditioned by the surface roughness (here the containers). This is one of the characteristics of the flows in a neutral atmosphere. Indeed, the performance of the model is also analysed using the standard statistical performance measures (Chang and Hanna, 2004) such as Normalized Mean Square Error (NMSE), Fractional Bias (FB), Correlation coefficient (COR), Fractional Variance (FS), and Factor of Two (FA2). These measures characterize the agreement between model prediction and observations. The NMSE emphasizes the scattering in a sample and FB indicates an overall over or under-prediction from the observations. A perfect model would have the following idealized values:  $NMSE = FB = FS = 0$  and  $COR = FA2 = 1$  (Chang and Hanna, 2004). The predicted and observed concentrations at all receptors are presented in forms of the scatter plots (Figure 5a) and the Q-Q plots (Figure 5b). In the scatter plots (Figure 5a), it is observed that the simulated concentrations by the CFD model have relatively good agreement with the observations. The simulated higher concentrations at the receptors near to the source are close to one-to-one line; however, comparably more scatter is observed for lower concentrations at far away from the source. This trend of the predicted concentrations is more visible in Q-Q plot in Figure 5b. This Q-Q diagram shows a comparison of the concentration distributions of simulated and observed concentrations. The computed statistical indices are given in Table 2. The computed statistical indices for CFD simulation show that the OpenFOAM is performing good with the observations. The model predicts 83.3% of points within a factor of two. The FB shows that the extent of under- or over-prediction the simulated concentrations from the observations. It shows that similar degree of a slightly under-prediction ( $FB = 0.11$ ) was observed. Good one-to-one correlations can be observed by the higher values of correlation coefficient ( $COR=0.87$ ). The values of  $MG (=0.97)$  and  $VG (=1.33)$  show a small scatter and it is also visible from the scatter and Q-Q plots in Figures 5a-5b. Hence, the statistical evaluation results show an overall good performance of the CFD model in such complex environment. The CFD model OpenFOAM used in this study is well suited for the air pollution and emergency planning in urban area.

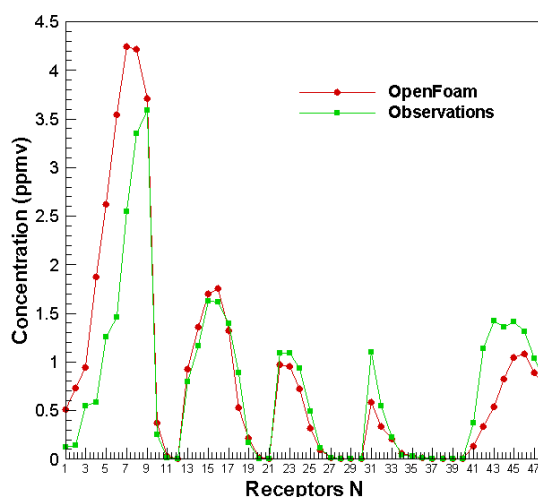
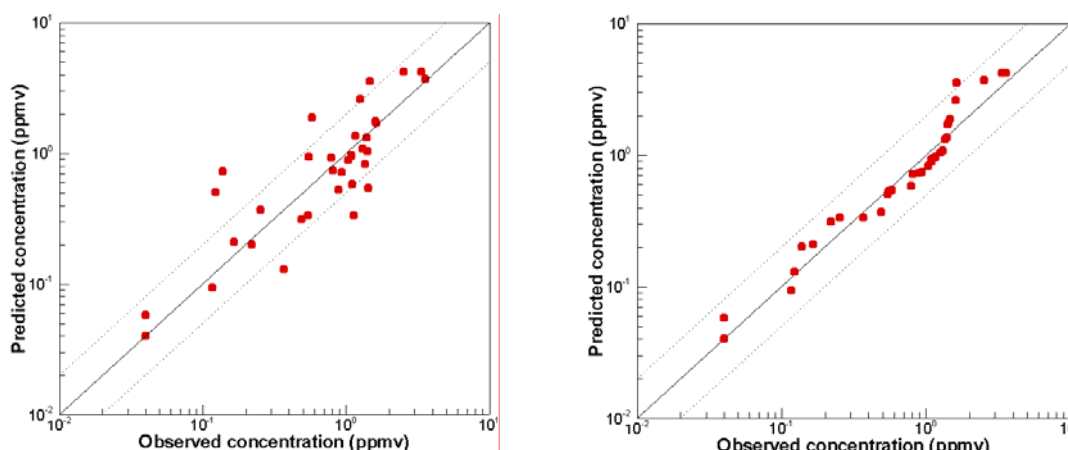


Figure 4.  $C_3H_6$  concentration (in ppmv) at each sensor



**Figure 5.** (a) Scatter and (b) quantile-quantile (Q-Q) plots between the predicted and observed average concentrations. The middle solid line is one-to-one line between observed and simulated concentrations whereas the dotted lines correspond to factor of two.

**Table 2.** Statistical indicators of model quality

$\langle C_o \rangle$	$\langle C_p \rangle$	NMSE	MAE	RMSE	COR	FB	FS	FAC2	MB	VAR	INDEX	MG	VG
0.76	0.85	0.47	0.30	0.55	0.87	0.11	-0.54	83.3	0.09	0.55	0.91	0.97	1.33

## CONCLUSIONS

This study presents the three-dimensional CFD simulations for near-field dispersion of pollutant near buildings. A CFD model OpenFOAM is evaluated with the concentrations measurements obtained from a trial of the MUST field experiment in an urban-like environment. The model is simulating well with the observations for the selected trial in a complex terrain and predicts ~83% concentrations within a factor of two. The modelled concentrations are slightly over-predicting with the observations and have relatively good correlation (COR = 0.87) between them. This first comparison shows an adequate agreement between the modelled values and the measured concentrations. Further, the model has been coupled in inverse mode, based on renormalization theory, for identifying a point source release in an urban like environment of MUST field experiment. The study is underway to highlight the detection feasibility of unknown releases in an urban-like environment with a use of more sophisticated model like OpenFOAM. The study will show the effectiveness of the renormalization inversion technique to estimate the source parameters in an urban area. Estimating the source height along with the other source parameters may further improve the retrieval results and it need to be verified with the available observations in other trials of the MUST field experiment.

## REFERENCES

- Biltoft, C. A., 2001: Customer Report for Mock Urban Setting Test, DPG Document No. WDTCFR- 01-121, West Desert Test Center, U.S. Army Dugway Proving Ground, Dugway, Utah, 58 pp.
- Chang, J. C. and S. R. Hanna, 2004: Air quality model performance evaluation. *Meteorol. Atmos. Phys.* **87**, 167-196.
- Donnelly, R. P., T. J. Lyons and T. Flassak, 2009. Evaluation of results of a numerical simulation of dispersion in an idealized urban area for emergency response modelling. *Atmospheric Environment* **43**, 4416-4423.
- Efthimiou, G. C., Berbekar, E., Harms, F., Bartzis, J. G., Leitl, B., 2015. Prediction of high concentrations and concentration distribution of a continuous point source release in a semi-idealized urban canopy using CFD-RANS modeling. *Atmospheric Environment* **100**, 48–56.
- Gromke, C., Blocken, B., 2015. Influence of avenue-trees on air quality at the urban neighborhood scale. Part I: Quality assurance studies and turbulent Schmidt number analysis for RANS CFD simulations. *Environmental Pollution* **196**, 214–223.

- Hanna, S. R., Hansen, O. R., Dharmavaram, S., 2004. FLACS CFD air quality model performance evaluation with kit fox, must, prairie grass, and EMU observations. *Atmospheric Environment* **38** (28), 4675-4687.
- Kumar, P., Feiz, A.-A., Ngae, P., Singh, S. K., Issartel, J.-P., 2015. CFD simulation of short-range plume dispersion from a point release in an urban like environment. *Atmospheric Environment* **122**, 645-656.
- Labovsky, J., Jelemensky, L., 2010. CFD simulations of ammonia dispersion using dynamic boundary conditions. *Process Safety and Environmental Protection* **88** (4), 243 – 252.
- Rakai A., Berbekar E., Franke J., 2014. RANS Passive Scalar Transport Modelling in a Complex Urban Area—Effect of Source Location on the Results, 6th International Symposium on Computational Wind Engineering, 116-117.
- Tominaga, Y., Stathopoulos, T., 2013. CFD simulation of near-field pollutant dispersion in the urban environment: A review of current modeling techniques. *Atmospheric Environment* **79** (0), 716-730.
- Yee, E. and C. A. Biltoft, 2004: Concentration fluctuation measurements in a plume dispersing through a regular array of obstacles. *Boundary-Layer Meteorol.*, **111**, 363-415.

**17th International Conference on  
Harmonisation within Atmospheric Dispersion Modelling for Regulatory Purposes  
9-12 May 2016, Budapest, Hungary**

---

**MODIFICATION AND VALIDATION OF A METHOD FOR ESTIMATING THE LOCATION  
OF A POINT STATIONARY SOURCE OF PASSIVE NON-REACTIVE POLLUTANT IN AN  
URBAN ENVIRONMENT**

*George C. Efthimiou<sup>1</sup>, Spyros Andronopoulos<sup>1</sup>, Alexandros Venetsanos<sup>1</sup>, Ivan V. Kovalets<sup>2</sup>, Konstantinos Kakosimos<sup>3</sup> and Christos D. Argyropoulos<sup>3</sup>*

<sup>1</sup>Environmental Research Laboratory, INRASTES, NCSR Demokritos, Patriarchou Grigoriou & Neapoleos Str., 15310, Aghia Paraskevi, Greece

<sup>2</sup>Department of Environmental Modelling, Institute of Mathematical Machine and System Problems, National Academy of Sciences of Ukraine, Kiev, Ukraine

<sup>3</sup>Chemical Engineering Department & Mary Kay 'O Connor Processes Safety Center, Texas A&M University at Qatar

**Abstract:** In Kovalets et al. (2011), a method was developed to estimate the location and rate of an unknown point stationary source of passive atmospheric pollutant in a complex urban geometry. The algorithm was implemented in the ADREA-HF Computational Fluid Dynamics code and was applied in a complex urban geometry (the MUST wind tunnel experiment). This approach has also been evaluated for the Michelstadt experiment (Tsiouri et al., 2014). In the present paper, a major change in the data assimilation code includes the implementation of a two-step approach: At first only the source coordinates are analysed using a correlation function of measured and calculated concentrations. In the second step the source rate is identified by minimizing a quadratic cost function. The validation of the new algorithm is performed for the source location by simulating a wind tunnel experiment on atmospheric dispersion among buildings of a real urban environment. Good results of source location estimation are obtained. Special attention is given on the grid influence regarding the obtained results.

**Key words:** *CFD; Data assimilation; Atmospheric dispersion; Inverse problem; Source identification*

## **INTRODUCTION**

The characterization of an unknown atmospheric pollutant's source following a release is a special case of inverse atmospheric dispersion problem. Such kind of inverse problems are to be solved in a variety of application areas such as emergency response and indoor air quality (Kovalets et al., 2011; Koracin et al., 2011; Matsuo et al., 2015; Sharan et al., 2012; Singh et al., 2013).

In the urban or industrial scale, few studies have applied Computational Fluid Dynamics (CFD) combined with different source estimation techniques (Chow et al., 2008; Keats et al., 2007; Libre et al., 2012; Bady et al., 2009). Kovalets et al. (2011) developed an effective variational algorithm of source inversion combined with an urban-scale CFD model. The performance of the algorithm was evaluated against measurements obtained in MUST wind tunnel experiment and with the Michelstadt wind tunnel dataset (Tsiouri et al., 2014). The medium performance of the algorithm in the second case created second thoughts about the calculation of the source location and rate as well as the effect of various numerical parameters (e.g. grid resolution and numerical schemes). The purpose of the present study is to modify the cost function of the source inversion algorithm of Kovalets et al. (2011) for the non-simultaneous calculation of the source location and rate. The effects of the grid resolution used for the numerical simulations on the obtained results are also investigated. The evaluation and demonstration of the proposed methodology is performed on a new experiment called CUTE, the description of which is given below.

## **MODIFICATION OF THE COST FUNCTION OF THE SOURCE INVERSION ALGORITHM**

The use of the Source Inversion (SI) algorithm (Kovalets et al., 2011) for the Michelstadt experiment (Tsiouri et al., 2014) produced unsatisfactory results regarding the distance between the true and the

estimated source location and the true to estimated source rate ratio. The former was in the order to 300 m, while the latter was in the order of 10. The cause of the discrepancy between the results and the measurements was the ‘overfitting’ effect. According to this effect, the calculation errors which are introduced by the wrong source location and led to significant underestimation of the concentration were compensated by the overestimated source rate. Thus, the resulting quadratic cost function reached minimum for the wrong combined solution (source location and source rate). This problem is typical for non-linear least squares fitting. In context of data assimilation this problem is especially important when the number of measurements is insufficiently small. For example, in Kovalets et al. (2009) the cost function was minimized with respect to both wind field and source rate. It was found that for too coarse resolution of the monitoring network the Normalized Mean Squared Error of the concentration field (closely related to the value of cost function) decreased in the data assimilation process while the error of the wind field (being part of the solution vector) increased (Kovalets et al. (2009), p. 3519, par. 1).

A proposed solution to the above mentioned problem is the separation of SI algorithm into the following two steps: Step 1: The source coordinates are analysed; Step 2: Only source rate is analysed.

The aforementioned idea is not new and was also expressed by the authors of the paper Brown and Robins (2010) in private discussion with Ivan Kovalets. They developed a method which allows the source coordinates-only estimation, while unknown source rate was not considered. However, it is not clear how they deal with the issue of unknown source rate in calculating posterior probabilities of the concentrations. Furthermore, it is known that Bayesian inference is under certain assumptions equivalent to least squares approach of source term estimation (see Tarantola, 2005, and more details can be found in Kovalets et al., 2013, Sec. 2.1). However from the implementation point of view the methodology in Brown and Robins (2010) is very different from that in Kovalets et al. (2011).

In the present study, we propose a modified version of the SI algorithm (Kovalets et al., 2011) by using, instead of cost function  $J$  defined by formula (7) (in Kovalets et al., 2011), a correlation coefficient of measured and calculated concentrations:

$$J = \frac{\langle (c^c - \langle c^c \rangle)(c^o - \langle c^o \rangle) \rangle}{\sqrt{\langle (c^c - \langle c^c \rangle)^2 \rangle} \sqrt{\langle (c^o - \langle c^o \rangle)^2 \rangle}} \rightarrow \min \quad (1)$$

where  $\langle \rangle$  denotes arithmetic averaging over all measurements while minimum is sought over all possible source locations. Other notation in (1) as well as everywhere below (until otherwise is stated) is similar to that in Kovalets et al. (2011).

Equation (1) is minimized with respect to source coordinates only, while arbitrary source rate,  $q^s$ , is used for the minimization procedure. The justification for this exclusion of source rate from the control vector is that  $J$  does not depend on  $q^s$ . Indeed, let us consider two calculated concentration fields  $c_1^c$  and  $c_2^c$  obtained with different source rates:  $q_1^s$  and  $q_2^s$ . Since equation of concentration transport is linear with respect to  $q^s$ , then the following relationship holds:

$$c_2^c = c_1^c \cdot \left( \frac{q_2^s}{q_1^s} \right) = c_1^c \cdot \alpha \quad (2)$$

From equation (2), it is obvious that the calculated values of  $J_1$  and  $J_2$  for  $c_1^c$  and  $c_2^c$  will be the same. Thus,  $J$  does not depend on source rate provided that it is constant. For non-constant source rates,  $q_1^s(t)$  and  $q_2^s(t)$ , the values of  $J_1$  and  $J_2$  generally speaking will be different. Only if  $q_1^s(t)$  and  $q_2^s(t)$  are similar, i.e. if  $q_2^s(t) / q_1^s(t) = \alpha = const$ , then again  $J_1$  and  $J_2$  will be the same.

Therefore, the usage of correlation coefficient as a cost function (equation (1)) solves the problem of separate identification of source coordinates and source rate. An arbitrary value of ‘first-guess’ source rate  $q_0^s$  could be used for calculating the correlation coefficient since it will not influence the solution. However, the drawback of the present approach is that prior information can not be used by applying regularization terms.

Therefore, in step 1 of the present approach, the source coordinates are identified using the algorithm of Kovalets et al. (2011) but with the cost function defined above (equation 1) instead of the cost function of Kovalets et al. (2011). In this algorithm, the source location is assumed to coincide with one of the grid nodes. The location of the corresponding grid node  $k^s$  for which minimum of the correlation coefficient (equation (1)) is reached is considered as the analysed source location.

As a second step, the source rate can be identified by minimizing the quadratic cost function with respect to  $q^s$ :

$$J = \sum_{n=1}^K (c_n^c - c_n^o)^2 \rightarrow \min \quad (3)$$

By using a Source Receptor Function (SRF), similarly applied as in Kovalets et al. (2011) for the node  $k^s$  (being the solution found in Step 1), equation (3) can be expressed as (cf. formula (15) from Kovalets et al., 2011):

$$J = \sum_{n=1}^K (q^s c_{n,k^s}^* - c_n^o)^2 \xrightarrow{q^s} \min \quad (4)$$

The solution of problem (4) can obviously be obtained analytically by equating to zero the derivative of  $J$  with respect to  $q^s$ :

$$\frac{\partial J}{\partial q^s} = \sum_{n=1}^K (q^s c_{n,k^s}^* - c_n^o)^2 = \sum_{n=1}^K 2c_{n,k^s}^* (q^s c_{n,k^s}^* - c_n^o) = 0 \quad (5)$$

The solution of (5) is obviously:

$$q^s = \frac{\sum_{n=1}^K c_{n,k^s}^* c_n^o}{\sum_{n=1}^K (c_{n,k^s}^*)^2} \quad (6)$$

### THE COMPLEX URBAN TERRAIN EXPERIMENT (CUTE)

The CUTE (Complex Urban Test Experiment) data set includes results from field and wind tunnel measurements. The data set is dedicated to test Emergency Response Tools/Atmospheric Dispersion Models predicting dispersion processes in urban areas. The second part of the CUTE dataset (CUTE cases 2 to 4) consists of wind tunnel data measured in the model of the European city centre, where the CUTE field test was carried out.

The test was done in the downtown area of a typical Central European city. The area of interest is densely built-up with building heights between 25 m and 35 m. There is no significant elevation and no major urban greenery in the modelled area.

The CUTE wind tunnel dataset consists of concentration data only. Concentration time series of tracer gas from continuous releases were measured at pedestrian level. Concentration measurements are available for three cases. Each case represents a different source location. However, only one case (case 3) was used during the evaluation of the model.

The chosen source is located between houses near the river on the opposite side of the harbour. Case 3 was selected because here the source is at a different location than the release during the field test, representing a different concentration field and therefore a different test case for model evaluation. For

case 4, the release was at the downwind side of river, resulting in fewer measurement points and short travel times of released material. More information about the experiment can be found in [http://www.elizas.eu/images/Documents/Model%20Evaluation%20Case%20Studies\\_web.pdf](http://www.elizas.eu/images/Documents/Model%20Evaluation%20Case%20Studies_web.pdf).

### THE SIMULATIONS OF THE INVERSE PROBLEM

The computational domain for simulating the developing flow and dispersion within and above the three-dimensional obstacle array extended in the streamwise direction from  $x = -540$  m to 2105.02 m, with the upstream wall of the first obstacle at  $x = 0$  m. The simulations were conducted with a domain height of  $6H_{max}$  ( $H_{max}$  is the maximum building height equal to 108 m), which was sufficiently deep to ensure that the flow changes near the surface (within and above the obstacles) were not being moulded (or influenced) by the boundary conditions imposed at the top of the computational domain. In the spanwise (or  $y$ ) direction, the computational domain spanned  $-540 \text{ m} \leq y \leq 1755.02 \text{ m}$ . The vertical  $x$ - $z$  centre plane at  $y \approx 300$  m contained the ground-level source.

Sensitivity analysis of the solution to the discretization of the computational domain is performed in the present paper. A medium and a fine grid have been selected. The number of the control volumes for the medium grid is 891,132 while for the fine grid is 1,372,800. The grid was equidistant between the buildings and increases logarithmically outside the urban area. For the medium grid the minimum cell size in horizontal direction is 12.52 m while for the fine grid it is 9.969 m. Both grids have the same vertical resolution with a minimum cell size close to the ground equal to 1.0 m.

The boundary conditions of the 3D domain are the same for the forward and the inverse problems. In order to solve the adjoint equation (8) in Kovalets et al. (2011) the inverse problem uses the flow results of the forward problem i.e. the mean velocities  $u$ ,  $v$ ,  $w$ , the turbulent kinetic energy  $k$  and the dissipation rate  $\varepsilon$ .

The non-stationary adjoint equation has been integrated in backward direction through the same time interval as the forward problem (1000 s) to achieve established distributions of adjoint variables. The time step was kept constant and equal to 1 s.

### THE RESULTS OF THE INVERSE PROBLEM

Based on the solution of the adjoint equation, the adjoint variables have been pre-calculated for all sensors in the whole computational domain and then stored in binary files.

The performance of the modified algorithm of source estimation was evaluated by two parameters: horizontal  $\left( r_H = \sqrt{(x^s - x_t^s)^2 + (y^s - y_t^s)^2} \right)$  and vertical  $\left( r_V = |z^s - z_t^s| \right)$  distances between the estimated and the true source locations. The results are presented in Table 1. The medium grid presents a rather high discrepancy from the true source location. On the other hand the fine grid predicted perfectly the source. These results indicate that even for a small number of sensors (32 in this experiment) the grid plays a major role for the performance of the methodology.

**Table 1.** Horizontal and vertical distances of the estimated source location from the true source location.

	$r_H$ (m)	$r_V$ (m)
Medium grid	43.33	14.74
Fine grid	0	0

### CONCLUSIONS

In the present work an existing method for estimating the location and rate of a stationary point source of passive nonreactive pollutant in an urban environment was modified and evaluated. A major change in the data assimilation code included the implementation of a two-step approach: At first only the source

coordinates were analysed using a correlation function of measured and calculated concentrations. In the second step, the source rate was identified by minimizing a quadratic cost function. The validation of the new algorithm was performed for the source location by simulating a wind tunnel experiment on atmospheric dispersion among buildings of a real urban environment. Good results of source location estimation have been achieved when all available measurements (32) were used to solve the inverse problem. It was found that the grid resolution plays an important role for the inverse problem.

#### ACKNOWLEDGMENTS

This publication was made possible by a NPRP award [NPRP 7-674-2-252] from the Qatar National Research Fund (a member of The Qatar Foundation). The statements made herein are solely the responsibility of the authors.

#### REFERENCES

- Bady M., S. Kato and H. Huang, 2009: Identification of pollution sources in urban areas using reverse simulation with reversed time marching method. *Journal of Asian Architecture and Building Engineering*, **8**, 275-282.
- Brown G. and P. Robins, 2010: Source term estimation for rapid hazard assessment. HARMO13, Paris, France, 924-928.
- Chow F.K., B. Kosovic and S. Chan, 2008: Source inversion for contaminant plume dispersion in urban environments using building-resolving simulations. *Journal of applied meteorology and climatology*, **47**, 1553-1572.
- Keats A., E. Yee and F.-S. Lien, 2007: Bayesian inference for source determination with applications to a complex urban environment. *Atmospheric Environment*, **41**, 465-479.
- Koracin D., R. Vellore, D.H. Lowenthal, J.G. Watson, J. Koracin, T. McCord, D.W. DuBois, L.-W.A. Chen, N. Kumar, E.M. Knipping, N.J.M. Wheeler, K. Craig and S. Reid, 2011: Regional source identification using lagrangian stochastic particle dispersion and HYSPLIT backward-trajectory models. *Journal of the Air & Waste Management Association*, **61**, 660-672.
- Kovalets I.V., S. Andronopoulos, A. Venetsanos and J.G. Bartzis, 2011: Identification of strength and location of stationary point source of atmospheric pollutant in urban conditions using computational fluid dynamics model. *Mathematics and Computers in Simulation*, **82**, 244-257.
- Kovalets I., R. Hofman, P. Seibert and S. Andronopoulos, 2013: Review of existing approaches of source inversion to be integrated in real-time nuclear emergency response system JRODOS. Report of the EU FP7 PREPARE Project No. PREPARE(WP4)-(14)-01.
- Kovalets I.V., V. Tsiouri, S. Andronopoulos and J.G. Bartzis, 2009: Improvement of source and wind field input of atmospheric dispersion model by assimilation of concentration measurements: Method and applications in idealized settings. *Applied Mathematical Modelling*, **33**, 3511-3521.
- Libre J.-M., S. Guérin, A. Castellari, A. Tripathi, M. Leguellec, T. Mailliard and C. Souprayen, 2012: Source determination in congested environment through Bayesian inference. *Int. J. Environment and Pollution*, **48**, 174-184.
- Matsuo T., A. Kondo, H. Shimadera, T. Kyuno and Y. Inoue, 2015: Estimation of indoor contamination source location by using variational continuous assimilation method. *Build. Simul.*, **8**, 443-452.
- Sharan M., S.K. Singh and J.P. Issartel, 2012: Least square data assimilation for identification of the point source emissions. *Pure Appl. Geophys.*, **169**, 483-497.
- Singh S.K., M. Sharan and J.-P. Issartel, 2013: Inverse modelling for identification of multiple-point releases from atmospheric concentration measurements. *Boundary-Layer Meteorol*, **146**, 277-295.
- Tarantola A., 2005: Inverse problem theory and methods for parameter estimation. SIAM, Philadelphia, USA.
- Tsiouri V., I. Kovalets, K.E. Kakosimos, S. Andronopoulos and J.G. Bartzis, 2014: Evaluation of advanced emergency response methodologies to estimate the unknown source characteristics of the hazardous material within urban environments. HARMO16, Varna, Bulgaria.

**17th International Conference on  
Harmonisation within Atmospheric Dispersion Modelling for Regulatory Purposes  
9-12 May 2016, Budapest, Hungary**

---

**AEROSOL TRANSPORT MODELLING OVER DEBRECEN, HUNGARY**

*Zsófia Török<sup>1</sup>, Zoltán Szoboszlai<sup>1</sup>, Enikő Furu<sup>1</sup>, Anikó Angyal<sup>1</sup>, Rostislav Kouznetsov<sup>2</sup>, Mikhail Sofiev<sup>2</sup>,  
Zsófia Kertész<sup>1</sup>*

<sup>1</sup>Institute for Nuclear Research, Hungarian Academy of Sciences,  
H-4026 Debrecen, Bem tér 18/c, Hungary

<sup>2</sup>Finnish Meteorological Institute, Erik Palménin aukio 1, 00560 Helsinki, Finland

**Abstract:** Backward trajectory modelling (NOAA HYSPLIT) together with statistical techniques like Positive Matrix Factorization (EPA PMF) can be used to determine the relative contributions of local and distant sources of aerosol pollution. These methods were completed with the observational footprints computed with System for Integrated modelLing of Atmospheric coMposition (SILAM). In addition, the variations of emission from different areas in Europe were followed with seasonal- and yearly- averaged footprints, whereas the distribution of aerosol pollution were determined with daily average footprints.

**Key words:** *source identification, long range transport*

## **INTRODUCTION**

Aerosol pollution is a major environmental problem in urban areas due to negative impact of PM on health and on the built environment. In cities, aerosol particles can originate from local (e.g. biomass burning for residential heating, local industrial emissions or traffic) or from distant sources (e.g. sea salt, desert dust or regional industrial emissions). Sometimes local emissions alone cannot explain high air pollution episodes at a receptor site, i.e. long-range transport processes of natural and anthropogenic aerosols can have a significant influence on the local PM concentration levels. In order to get a picture about the geographical distribution of main pollution sources affecting a specific place, receptor modelling combined with backward trajectory calculation is applied (Borbély-Kiss et al., 1999). However, backward trajectory usually indicates only the main directions of the transport and the subjective analysis of the paths is not always conclusive. A more comprehensive methodology for quantitative analysis of the observed footprints is adjoint dispersion modelling.

In the present work, distant source areas have been determined for a Hungarian city, Debrecen. At an urban background station, concentration and elemental composition of PM<sub>10</sub> and PM<sub>2.5</sub> have been monitored regularly twice a week during 24 hours for more than 20 years (Borbély-Kiss et al., 1996). NOAA-HYSPLIT backward trajectory model was used to define the movement of air masses, which reached Debrecen. Correlation analysis (Spearman's correlation) and a receptor model (PMF) were applied to identify elemental fingerprints. This research was completed with source identification via footprints using the SILAM dispersion model, which provided integrated map of distant sources affecting the observation site in each particular day.

## **MATERIALS AND METHODS**

### **Sampling and analysing**

The samples were collected in the garden of Institute for Nuclear Research regularly in two size fractions: PM<sub>10</sub>-PM<sub>2.5</sub> (particles with aerodynamic diameter between 2.5 and 10 µm) and PM<sub>2.5</sub> (particles with aerodynamic diameter < 2.5µm) using a Gent type stacked filter unit since 1993. The aerosol concentration is measured by gravimetry and the elemental composition (for Z >13) is determined by

Proton Induced X-ray Emission (PIXE) method at the macro-PIXE chamber in the IBA Laboratory of Atomki (Borbély-Kiss et al., 1985).

### **Modelling tools**

#### **Positive Matrix Factorization (EPA PMF)**

Source apportionment was carried out with the positive matrix factorisation receptor model developed for aerosol source characterization, provided by US EPA (Paatero and Tappert, 1994). Mass of species apportioned to factor, percentage of species apportioned to factors and contributions associated with factors were determined for the coarse and fine fractions separately. Variability of source contributions by year, season, working day/weekend and hours of the day were also studied as well as the dependence on meteorological parameters, such as wind directions. The source types are identified by comparing them to measured profiles. Source contributions are used to determine how much each source contributed to a sample.

#### **Backward trajectory model (NOAA HYSPLIT)**

HYSPLIT (Hybrid Single Particle Lagrangian Integrated Trajectory) model developed by NOAA's Air Resources Laboratory (ARL) (Draxler et al., 2012) was used to determine the movement of air masses which reached Debrecen. The trajectories were calculated for 72 h periods at three different heights (200, 500 and 1000 m a.g.l.). The meteorological data were obtained from NCEP/NCAR Reanalysis project (Kalnay et al., 1996). The global data are on a latitude-longitude grid (2.5 degree) from 1948 through the end of the previous year. Model vertical velocity was used for simulations, which use the vertical velocity field from the meteorological data.

#### **Dispersion model (SILAM)**

In this study SILAM (System for Integrated modelLing of Atmospheric coMposition) dispersion modelling by the Finnish Meteorological Institute was used with Eulerian transport algorithm (Sofiev et al., 2015). The meteorological data were obtained from ECMWF (European Centre for Medium-Range Weather Forecast) with 3-h time interval. The model included 10 vertical layers up to height of 10.225 Km, the near-surface layer being 25 m thick. The investigated period ranged from 1993 to 2013 with 5 elements chosen for the analysis: S, Si, Pb, Zn and Cr. These species were considered to be fingerprints of four different source types. A model time step was 15 min, horizontal resolution was 0.15 x 0.15 degree and output averaged to 1 h.

## **RESULTS**

The investigated period (1993-2013) contains more than 1400 sampling days and ~ 65.000 concentration data. Four elements were chosen for the footprint analysis: Si – tracer for soil/dust, Pb and Zn – may originate from incineration and industry, Cr – comes from traffic, S - tracer for industry and present in the aerosols in the form of sulphate. As described Viana et al. (Viana, 2008), sulphate possess a high complicity, and although it was grouped in a single category but separated as two individual sources. The first combination: SO<sub>4</sub>, V and Ni and the second: SO<sub>4</sub>, NO<sub>3</sub> and NH<sub>4</sub>. The V/Ni/SO<sub>4</sub> source was occasionally found in combination with trace elements such as Pb or Cu (interpreted as regional-scale pollution), OC and K, or Zn and Pb (long-range transport or anthropogenic pollution). On the other hand, the second combination was interpreted as secondary aerosols, regional background or long-range transport. Debrecen has no heavy industry and the residence time of SO<sub>4</sub> in the atmosphere is a few days, therefore it is associated with long range transport.

Receptor model (PMF) were applied to identify the PM sources in Debrecen. This way we could separate local (e.g. road dust, biomass burning, soil, heavy oil combustion) and remote sources (e.g. Saharan dust, metallurgy from Southern Europe). PMF is resulted some factors with S and other elements: S/V/Ni, S/Cu and S/Cr.

For the present study two years were chosen in order to compared the sources of sulphate: 2000 was a “dirty” year while 2011 was “clear”. The PM<sub>2.5</sub> concentrations can be seen on Figure1 for this two years. The average PM<sub>2.5</sub> concentration in 2000 was 19.2 µg/m<sup>3</sup> and in 2011 was 15.3 µg/m<sup>3</sup>.

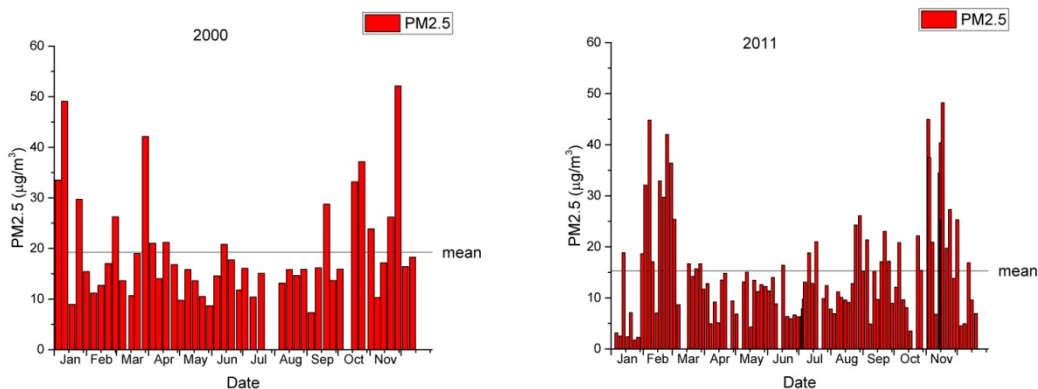


**Figure 1.** The PM<sub>2.5</sub> concentrations of 2000 and 2011. 2011 was more clear in spring and autumn.

The average S concentration was higher in 2011 ( $1288 \pm 998 \text{ ng/m}^3$ ) namely characteristically in winter (november and december:  $2137 \pm 1347 \text{ ng/m}^3$ ). In 2000 the average concentration was  $1103 \pm 618 \text{ ng/m}^3$  and it topped from january to march ( $1235 \pm 942 \text{ ng/m}^3$ ). The results of SILAM (Fig.2) present the potential sources of sulphate for these periods: in 2000 it can be originated from regional-scale pollution, while in 2011 from long-range transport pollution. The main emission source was Romania.

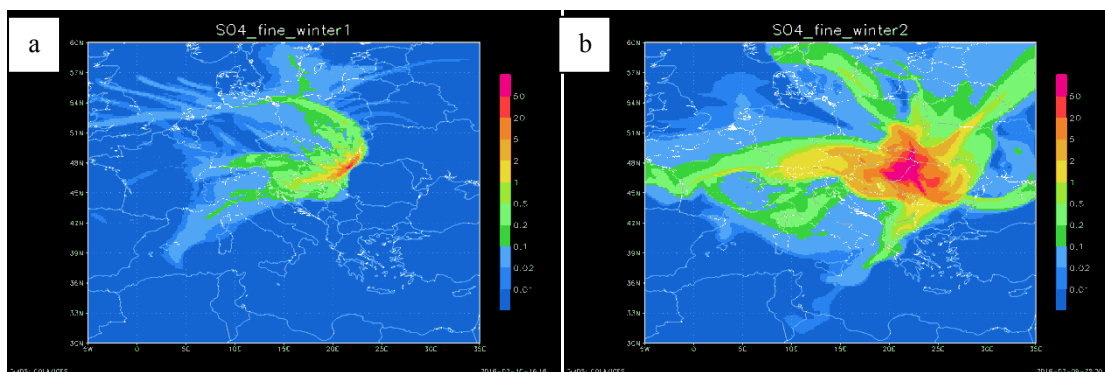


**Figure 2.** Seasonal source apportionment of sulphate using SILAM model. In 2000 (a) sulphate had regional and in 2011(b) had long-range transport source.

In the investigated period there were some days when the PM<sub>2.5</sub> concentration was more than  $50 \mu\text{g/m}^3$  and the elemental concentration of S was higher than  $4000 \text{ ng/m}^3$ ; like in 01.11.1993 when air masses arrived from East and Northeast Europe. The backward trajectories can be seen on Figure 3.

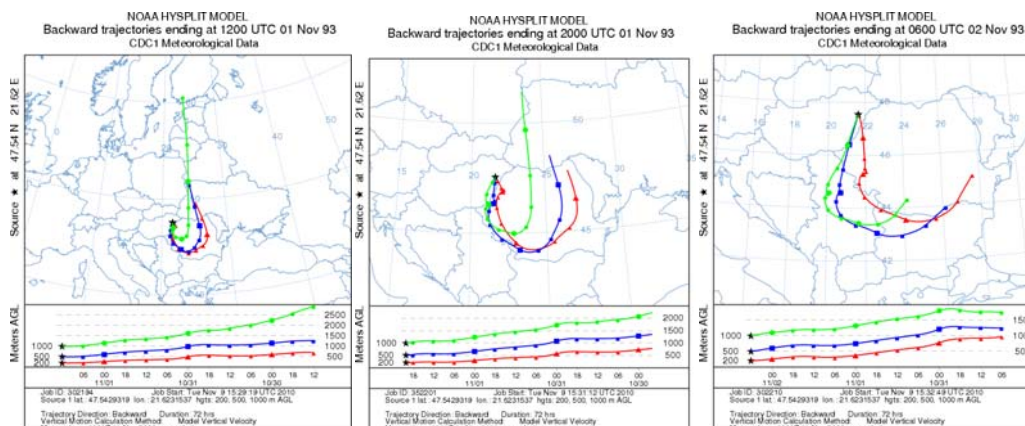


**Figure 3.** Backward trajectories for 01.11.1993 calculated for three different heights and three times. The source areas were East and Northeast Europe.

The SILAM model validated the source apportionment of this pollution episode. On Figure 4 the powerful contribution of Romania can be clearly seen. The computed periods were 5 days for PM<sub>2.5</sub> (a) and 3 days for SO<sub>4</sub> (b).

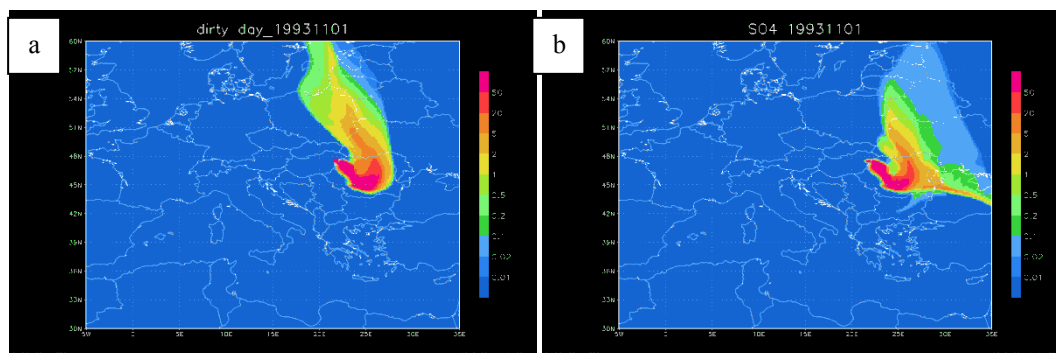


**Figure 4.** Results of SILAM model. The footprints of PM<sub>2.5</sub> (a) and SO<sub>4</sub> (b) calculated 5 and 3 days back.

## CONCLUSIONS

The present study demonstrated source apportionment using two models: HYSPLIT in combination with PMF and SILAM. Our huge database can be helpful to identify regional and long range transport aerosols. The applied statistical techniques (Spearman correlation and positive matrix factorization) can determine the type of sources (soil, traffic, industry, etc.) and then the applied dispersion models can define the origin of air pollution over the observation site.

Over Debrecen the aerosol pollution arrives mainly from Eastern and Southern Europe. The heavy industry in the surrounding countries emitted S, Ni, V, Cu, Zn and Pb which could be measured sometimes in high concentrations at our receptor site.

## ACKNOWLEDGEMENT

The research presented in this paper was supported by the János Bolyai Research Scholarship of the Hungarian Academy of Sciences and by the International Atomic Energy Agency under the Technical Cooperation Project no. HUN0008.

## REFERENCES

- Borbély-Kiss, I., Koltay, E., László, S., Szabó, Gy., Zolnai, L., 1985: Experimental and theoretical calibration of a PIXE setup for K and L X-rays, *Nucl. Instr. Meth. B*, **12**, 496-504
- Borbély-Kiss, I., Koltay, E., Szabó, Gy., 1996: Elemental composition of urban aerosol collected in Debrecen, Hungary, *Nucl. Instr. Meth. B*, **109/110**, 445-449
- Borbély-Kiss, I., Koltay, E., Szabó, Gy., Bozó, L., Tar, K., 1999: Composition and sources of urban and rural atmospheric aerosol in Eastern Hungary. *Journal of Aerosol Science*, **30**, 369-391.
- Draxler, R. R., Stunder, B., Rolph, G., Stein, A., Taylor, A., 2012: HYSPLIT\_4. User's Guide, via NOAA ARL. [http://www.arl.noaa.gov/documents/reports/HYSPLIT\\_user\\_guide.pdf](http://www.arl.noaa.gov/documents/reports/HYSPLIT_user_guide.pdf). NOAA Air Resources Laboratory, Silver Spring, MD, Dec., 1997 revised March, 2012.
- Kalnay, E., Kanamitsu, M., Kistler, R., Collins, W., Deaven, D., Gandin, L., Iredell, M., Saha, S., White, G., Woollen, J., Zhu, Y., Chelliah, M., Ebisuzaki, W., Higgins, W., Janowiak, J., Mo, K. C., Ropelewski, C., Wang, J., Leetmaa, A., Reynolds, R., Jenne, R., Joseph, D., 1996: The NCEP/NCAR 40-Year Reanalysis Project., *Bull. Amer. Meteor. Soc.* **77**, 437-471.
- Paatero, P., Tappert, U., 1994: Positive matrix factorization: a non-negative factor model with optimal utilization of error estimates of data values, *Environmetrics*, **5**, 111-126.
- Sofiev, M., Vira, J., Kouznetsov, R., Prank, M., Soares, J., Genikhovich, E., 2015: Construction of the SILAM Eulerian atmospheric dispersion model based on the advection algorithm of Michael Galperin, *Geosci. Model Dev.*, **8**, 3497-3522.
- Viana, M., Kuhlbusch, T.A.J., Querol, X., Alastuey, A., Harrison, R.M., Hopke, P.K., Winiwarter, W., Vallius, M., Szidat, S., Prévôt, A.S.H., Hueglin, C., Bloemen, H., Wählin, P., Vecchi, R., Miranda, A.I., Kasper-Giebl, A., Maenhaut, W., Hitzenberger, R., 2008: Source apportionment of particulate matter in Europe: A review of methods and results, *Aerosol Science*, **39**, 827-849.

**17th International Conference on  
Harmonisation within Atmospheric Dispersion Modelling for Regulatory Purposes  
9-12 May 2016, Budapest, Hungary**

---

**METEOROLOGICAL ANALYSIS OF SAHARAN DUST TRANSPORT TO SONNBLICK**

*Kathrin Baumann-Stanzer,<sup>1</sup> Sirma Stenzel<sup>1</sup>, Claudia Flandorfer<sup>1</sup>, Gerhard Schauer<sup>1</sup>, Anne Kasper-Giebl<sup>2</sup>*

<sup>1</sup>Central Institute for Meteorology and Geodynamic (ZAMG), Vienna, Austria

<sup>2</sup>Institute of Chemical Technologies and Analytics, Vienna University of Technology, Vienna, Austria

**Abstract:** In cases with dominating long-range transport, several methodologies are available to investigate the source regions of aerosol concentrations measured at high altitude stations. The influence of Saharan dust is reflected by the negative values of the single scattering exponent, as well as by the marked increase of the contribution of coarse particles. In the presented study, back trajectory calculations and backward simulations with a Lagrangian particle dispersion model FLEXPART are used to analyse an event of Sahara dust transport to the Eastern Alpine Area. The air parcels can change their height on the way to Austria; they can sink or lift up. In the backward mode, particles are released from a receptor location (e.g., a measurement point) and a four-dimensional response function (sensitivity) to emission input is calculated. Additionally, satellite images as well as aerosol forecast modelling with the on-line coupled model WRF-Chem are also applied in order to investigate the Sahara dust transport to the Sonnblick at 3106m altitude.

**Key words:** *Saharan dust, Sonnblick, back trajectories, source-receptor sensitivity, WRF-Chem.*

## INTRODUCTION

Mineral dust from the Saharan desert is transported across the Mediterranean Sea towards the Alpine region several times a year. Back trajectory calculations, backward simulations with the Lagrangian particle dispersion model FLEXPART as well as aerosol forecast modeling with the on-line coupled model WRF-Chem are used to analyze events of Saharan dust transport to the Eastern Alpine Area. Figure 1 shows a view to the high Alpine Sonnblick Observatory, where various meteorological and chemical measurements are conducted (<http://www.sonnblick.net/>). The Sonnblick Observatory is situated at the summit of the mountain Sonnblick at 3.106m asl in the Austrian Alps surrounded by the National Park area “Hohe Tauern”.



**Figure 1.** The Sonnblick Observatory (12°57'E, 47°03'N, 3106m asl.)

The probable occurrence of Saharan dust is operationally detected from Nephelometer and Aethalometer measurements by an increase of coarse particle number concentration and a negative exponent of the single scattering albedo (SSA) wavelength dependence (see example in Figure 2). The chemical composition of the mineral aerosol differs between individual dust events according to characteristics of the source areas where dust storms transported particle matter into the atmosphere. Additionally, the dust plume may also be chemically altered during its transport to the deposition site (Sodemann et al., 2006). Increased aerosol concentrations in general may be caused by many factors, by natural sources as dust

storms, forest fires (Schauer et al., 2016) as well by anthropogenic emissions from industry, domestic heating etc. Transport model results help to clarify whether the detected measurements really are due to Saharan dust transport, indicate the most likely source areas and reveal the main course of the air flow. This paper focuses on the first episode (A) indicated in the measured time-series shown in Figure 2. A distinct first signal of possible Saharan dust arrival was observed in the early morning of March 29<sup>th</sup>, 2014, with a sudden increase of aerosol concentrations accompanied by an immediate increase of particle numbers of PM<sub>2.5</sub>, reaching peak values of nearly 30  $\mu\text{g}/\text{m}^3$  (30min averages) in the second half of the day. The measurements repeatedly indicated Saharan dust influence on the two following days, interrupted by hours with air samples of obviously different composition. Most of April 1<sup>st</sup>, 2014, the aerosol measurements once more indicate the arrival of Saharan dust at Sonnblick Observatory.

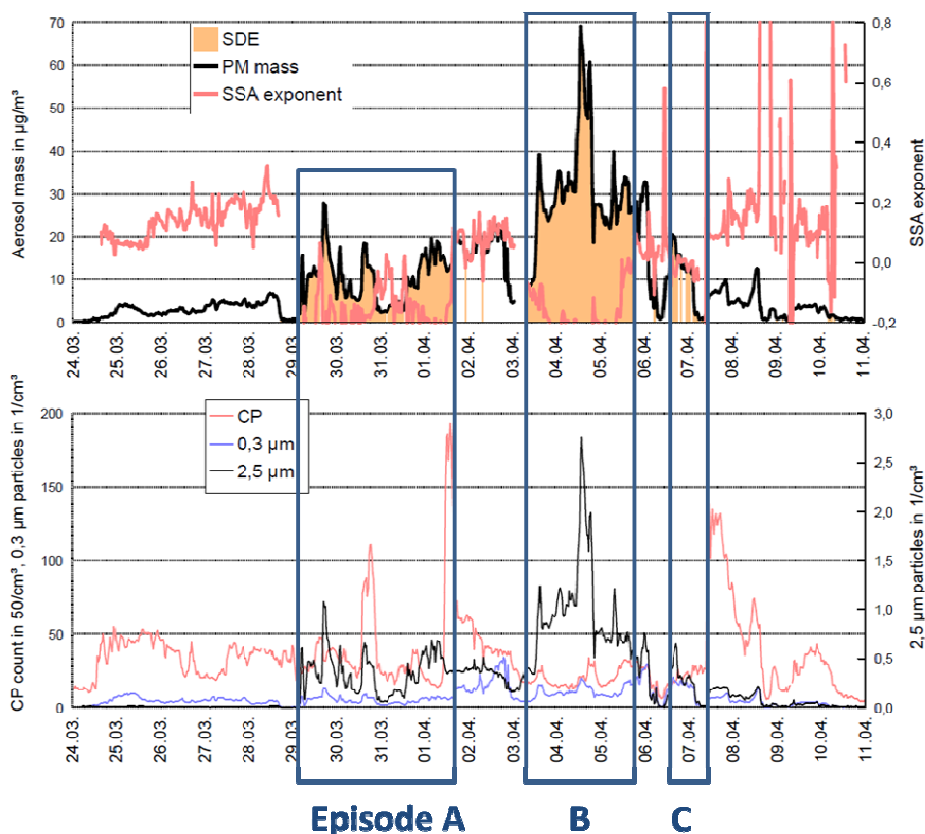


**Figure 2.** Time-series of particle matter measurements. Three episodes with high aerosol concentrations and negative values of the SSA exponent, indicating a high probability of Sahara dust arrival are highlighted with blue boxes.

### BACK TRAJECTORY ANALYSIS

Eight four-days-back trajectories a day are simulated operationally for Sonnblick with the FLEXTRA trajectory model (Stohl et al., 1995; Stohl and Seibert, 1998) based on the operational forecast data from the European Centre for Medium-Range Weather Forecasts (ECMWF) ([https://www.zamg.ac.at/cms/de/umwelt/umwelt-aktuell/sonnblick\\_trajektorien](https://www.zamg.ac.at/cms/de/umwelt/umwelt-aktuell/sonnblick_trajektorien)).

The three-dimensional back trajectories for the first two days of the Saharan dust event indicated as episode A in Figure 2 are depicted in Figure 3. Although back trajectories are an oversimplification of the atmospheric transport as dispersion is not accounted for, the back trajectories for March 29<sup>th</sup>, 2014 (Figure 3, left) indicate well that the air masses arriving in the second half of the day at mountain Sonnblick originate from below 1000m asl above the north parts of Africa. On the other hand, no clear indication of the air mass origin can be derived from the 4 days back trajectories for April 1<sup>st</sup>, 2014 (Figure 3, right). All eight trajectories calculated for this day descend from altitudes higher than 2000m asl in the northern Mediterranean region.

As seen from the weather map in Figure 4 four days before the trajectories reached the mountain Sonnblick, a low-pressure system over the Adriatic Sea dominated the transport ways of these air masses. In the following days, the low-pressure system got weak and the high-pressure system over Scandinavia intensified.

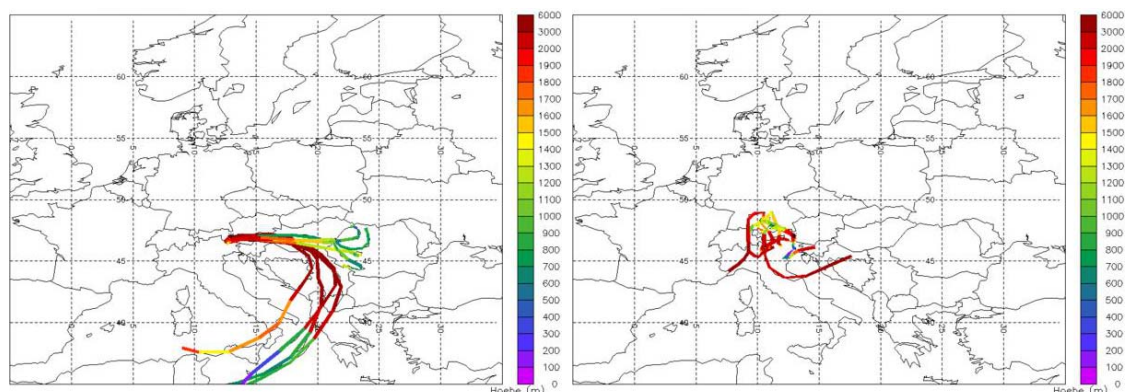


**Figure 3.** 96 hours three-dimensional back trajectories starting from mountain Sonnblick in three hourly intervals on 29.03.2014 (left) and 1.04.2014 (right). Trajectory heights in m asl are indicated in colours.

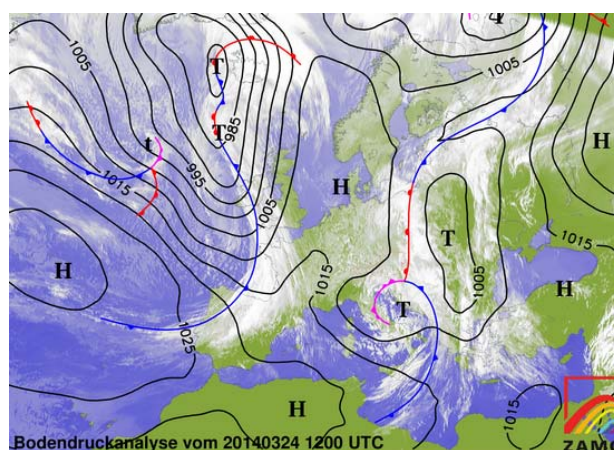


**Figure 4.** Weather map and satellite picture for the 29.03.2014.

### BACKWARD PARTICLE DISPERSION SIMULATIONS

The Lagrangian particle model FLEXPART compute trajectories of a large number of the so-called particles in order to describe the transport and the diffusion of tracers in the atmosphere. In the backward mode, particles are released from a receptor location and a four-dimensional response function (source-receptor sensitivity) to the emission input is calculated (Seibert and Frank 2004; Stohl, 2005). As the particle dispersion model considers turbulence and convection by parametrization and as the partitioning of the sampling volume by large-scale advection is accounted for, the backward FLEXPART simulations are more accurate than back trajectories and are therefore preferred for air mass origin studies (e.g. Williams et al., 2007). The simulations for this analysis were based on operational ECMWF forecast data with a horizontal resolution of  $1^\circ$ , 60 vertical levels, and a temporal resolution of 3 hours. The model results in Figure 5 depict for a selected 3 hourly arrival time window at mountain Sonnblick, April 1<sup>st</sup>, 2014, 0 UTC to 3 UTC, the source-receptor sensitivity in the lowest model level (0 to 500 m gnd) summarized over the previous 5 days (left) and 8 days (right), respectively. The maximum values of the simulated source-receptor matrices within the lowest model level summarized over the previous five days indicate that the main contributions in this case originated from areas in the northwestern vicinity of mountain Sonnblick. In this case, industrial sources as well as from domestic heating in southern

Germany and the eastern Alpine valleys partly might have contributed to the measurements at Sonnblick Observatory if there was significant transport of boundary layer air to the mountain station. As the back trajectories depicted in the right picture of Figure 3 indicate long-range transport from higher altitudes, source-receptor matrices summarized over a longer time-period, 8 days back are shown in the right picture of Figure 5. The maximum values found over the northern African edge in this model result indicate that in this case, indeed some uptake of Saharan dust might have taken place six to eight days before and might have contributed to the noticeable particle matter measurements at Sonnblick on April 1<sup>st</sup>, 2014.

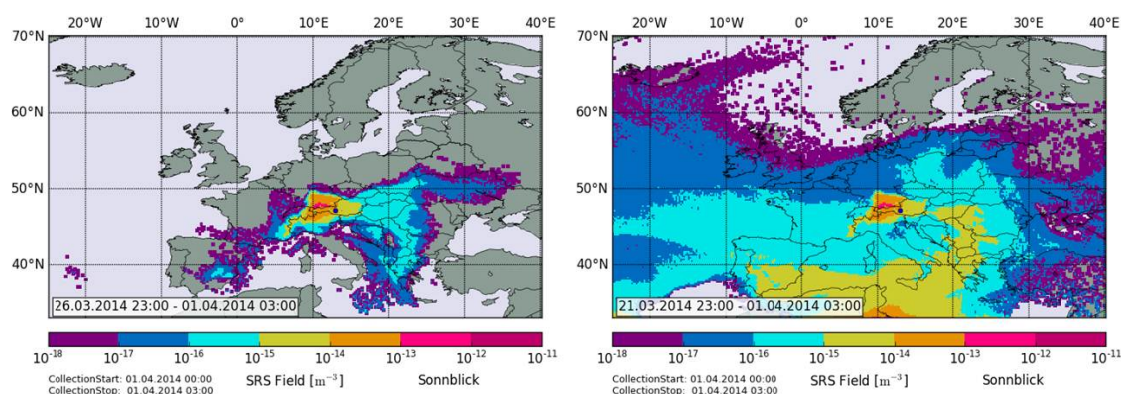


**Figure 5.** Source-receptor sensitivity for air masses arriving at mountain Sonnblick on April 1<sup>st</sup>, 2014, 0 UTC to 3 UTC, summarized over the previous 5 days (left) and 8 day (right), respectively.

#### ATMOSPHERIC TRANSPORT MODELLING

The on-line coupled WRF-Chem incorporates the weather forecast model WRF and a chemistry module that simultaneously simulates the emission, turbulent mixing, transport and chemical transformation, of trace gases and aerosols (Peckham, 2011). The dust scheme used in the WRF-Chem simulations simulates natural dust emission as a function of surface wind speed and surface erodibility and surface wetness (Cavazos-Guerra and Todd, 2012).

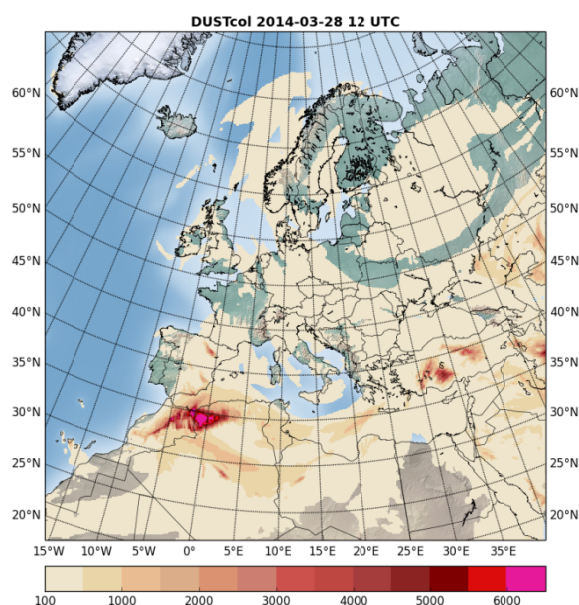


**Figure 6.** Dust column in  $\mu\text{g}/\text{m}^2$  simulated with WRF-Chem for 28.03.2014 12 UTC.

Figure 6 depicts the dust column in  $\mu\text{g}/\text{m}^2$  calculated with WRF-Chem for March 28th, 2014. The model forecast for this day reveals that with high possibility dust outbreaks (visible in the dust column) in the Atlas mountain ridge as well as in the Western Sahara contributed to the dust event observed at Sonnblick.

## CONCLUSIONS

Source areas and transport ways of Saharan dust identified by chemical measurements at mountain Sonnblick are investigated by means of back FLEXTRA trajectory calculations, backward simulations with the particle dispersion model FLEXPART and aerosol forecast modeling with the on-line coupled chemical weather model WRF-Chem. Increased aerosol concentration may be caused by natural sources as well as anthropogenic emissions. Between March 24<sup>th</sup>, 2014 and April, 11<sup>th</sup>, 2014 three periods with remarkable increased aerosol concentrations were observed at Sonnblick Observatory. The model results give clear evidence that Saharan dust outbreaks contributed to the noticeable aerosol increase observed at mountain Sonnblick. Results of the air mass transport analysis for episode A as well as of episodes B and C are shown in a poster presentation at the conference. The use of model forecasts, backward modelling and indicators based on aerosol measurements for the identification of Sahara dust transport to the Alps is subject to further research.

## REFERENCES

- Cavazos-Guerra, C., M. C. Todd, 2012: Model Simulations of Complex Dust Emissions over the Sahara during the West African Monsoon Onset. *Advances in Meteorology*, Volume 2012, Article ID 351731, 17 pages, doi:10.1155/2012/351731
- Peckham, S., G. A. Grell, S. A. McKeen, M. Barth, G. Pfister, C. Wiedinmyer, J. D. Fast, W. I. Gustafson, R. Zaveri, R. C. Easter, J. Barnard, E. Chapman, M. Hewson, R. Schmitz, M. Salzmann, S. Freitas, 2011: WRF/Chem Version 3.3 User's Guide. NOAA Technical Memo., 98 pp.
- Schauer, G., A. Kasper-Giebl, G. Mocnik, 2016: Increased PM Concentrations during a Combined Wildfire and Saharan Dust Event Observed at High-Altitude Sonnblick Observatory, Austria. *Aerosol and Air Quality Research*, **16**, 542–554
- Seibert, P., and A. Frank, 2004: Source-receptor matrix calculation with a Lagrangian particle dispersion model in backward mode, *Atmos. Chem. Phys.*, **4**, 51–63.
- Sodemann, H., A.S. Palmer, C. Schwierz, M. Schwikowski, H. Wernli, 2006: The transport history of two Saharan dust events archived in an Alpine ice core. *Atmos. Chem. Phys.*, **6**, 667–688
- Stohl, A., G. Wotawa, P. Seibert, H. Kromp-Kolb, 1995: Interpolation errors in wind fields as a function of spatial and temporal resolution and their impact on different types of kinematic trajectories. *J. Appl. Meteor.* **34**, 2149-2165.
- Stohl, A., and P. Seibert, 1998: Accuracy of trajectories as determined from the conservation of meteorological tracers. *Q. J. Roy. Met. Soc.* **124**, 1465-1484.
- Stohl, A., Forster, C., Frank, A., Seibert, P., G. Wotawa. 2005: Technical note: The Lagrangian particle dispersion model FLEXPART version 6.2, *Atmos. Chem. Phys.*, **5**, 2461-2474, doi:10.5194/acp-5-2461-2005.
- Williams, J., V. Gros, E. Atlas, K. Maciejczyk, A. Batsaikhan, H. F. Schöler, C. Forster, B. Quack, N. Yassaa, R. Sander, R. Van Dingenen, 2007: Possible evidence for a connection between methyl iodide emissions and Saharan dust. *J. Geophys. Res.*, **112**, D07302, doi:10.1029/2005JD006702

**17th International Conference on  
Harmonisation within Atmospheric Dispersion Modelling for Regulatory Purposes  
9-12 May 2016, Budapest, Hungary**

---

**IMPROVEMENTS TO AN OPERATIONAL INVERSION METHOD FOR ESTIMATING  
VOLCANIC ASH SOURCE PARAMETERS USING SATELLITE RETRIEVALS**

*Helen N. Webster, David J. Thomson, Michael C. Cooke and Rachel E. Pelley*

Met Office, FitzRoy Road, Exeter, EX1 3PB, UK

**Abstract:** Uncertain eruption source parameters can lead to large errors in ash cloud predictions from atmospheric dispersion models. An inversion method, which uses satellite observations to better inform the source term, has recently undergone improvements allowing better use of (potentially few) observations and a significant speed up in run-time. Here we demonstrate the performance of the method using recent volcanic eruptions as test cases and show that the determined source term results in an improved ash cloud forecast.

**Key words:** *volcanic ash, inversion technique, satellite observations, atmospheric dispersion, NAME*

## **INTRODUCTION**

The London Volcanic Ash Advisory Centre (VAAC), hosted by the Met Office, is responsible for issuing advisories on the transport of volcanic ash clouds in the North-East Atlantic region. These forecasts are produced using the atmospheric dispersion model NAME (Jones et al., 2007) and source term parameters based on the observed eruption height. Errors and uncertainties in the estimated source term have a large influence on the accuracy of the ash cloud forecasts.

Following the prolonged eruption of the Icelandic volcano Eyjafjallajökull in 2010, an inversion technique was developed employing satellite observations to better inform the source parameters. The technique uses satellite retrievals of ash column loadings and of regions of clear sky and a probabilistic approach which considers both the uncertainty in the initial best-guess source parameters (the *a priori*) and the uncertainty in the satellite retrievals. The process yields the source term parameters (the *a posteriori*) which optimally fit the predicted ash cloud to the satellite observations within their uncertainty, whilst simultaneously fitting the emissions to the *a priori* estimate of the emissions, again within their uncertainty.

Improvements to the run-time of the inversion technique have recently been made, enabling inversion calculations for prolonged eruptions and large numbers of observations to be run efficiently in an emergency response situation. This speed up has enabled us to consider an increase in the resolution (both vertically and in time) of the source term profile. In addition it has allowed the scheme to undergo further development to include correlations in the errors in the *a priori* source term profile. These correlations between the *a priori* source term components may be induced by variations in the plume rise height (from the observed value used in the *a priori*), variations in the mass release rate for a given plume rise height (from the assumed relationship between these two quantities) and variations in the vertical distribution of ash (from the assumed uniform profile). Including these correlations allows a satellite observation to influence surrounding source term components (both vertically and in time) and enables the inversion method to make better use of information from satellite observations. This is particularly important in the initial stages of an eruption when a limited number of observations are available.

## **THE INVERSION SCHEME**

For a given vector of  $n$  source terms,  $\mathbf{e}$ , an atmospheric dispersion model, such as NAME, can be used to give a vector of model predictions,  $\mathbf{o}_m$ , for  $k$  observations of ash column loading,

$$\mathbf{M}\mathbf{e} = \mathbf{o}_m$$

where  $\mathbf{M}$  is the transport matrix relating the source term to the observations. The inversion technique uses a probabilistic approach to find the time and height varying source term,  $\mathbf{e}$ , which optimally fits both dispersion model ash cloud predictions to the satellite observations,  $\mathbf{o}_a$ , and the emission source term to the *a priori* estimate of the emissions. Bayes theorem states

$$P(\mathbf{e} | \mathbf{o}_a) \propto P(\mathbf{o}_a | \mathbf{e}) P(\mathbf{e})$$

where  $P(\mathbf{o}_a | \mathbf{e})$  is the probability density of obtaining the satellite observations given a source term  $\mathbf{e}$ ,  $P(\mathbf{e})$  is the probability density of the *a priori* source term and  $P(\mathbf{e} | \mathbf{o}_a)$  is the probability density of the source term given the observations. The probability distributions for the satellite retrievals and the *a priori* source are assumed to be Gaussian:

$$P(\mathbf{o}_a | \mathbf{e}) \propto \exp \left[ -\frac{1}{2} (\mathbf{M}\mathbf{e} - \mathbf{o}_a)^T \mathbf{R}^{-1} (\mathbf{M}\mathbf{e} - \mathbf{o}_a) \right]$$

$$P(\mathbf{e}) \propto \exp \left[ -\frac{1}{2} (\mathbf{e} - \mathbf{e}_{ap})^T \mathbf{B}^{-1} (\mathbf{e} - \mathbf{e}_{ap}) \right]$$

where  $\mathbf{e}_{ap}$  is the mean of the *a priori* probability distribution,  $\mathbf{R}$  is the error covariance matrix for the satellite retrievals and  $\mathbf{B}$  is the error covariance matrix for the *a priori* source.  $\mathbf{R}$  is assumed to be a diagonal matrix and errors in the transport model are not considered. The *a posteriori* source which maximises  $P(\mathbf{e} | \mathbf{o}_a)$  is obtained by finding the minimum of the cost function

$$J(\mathbf{e}) = (\mathbf{M}\mathbf{e} - \mathbf{o}_a)^T \mathbf{R}^{-1} (\mathbf{M}\mathbf{e} - \mathbf{o}_a) + (\mathbf{e} - \mathbf{e}_{ap})^T \mathbf{B}^{-1} (\mathbf{e} - \mathbf{e}_{ap})$$

subject to a non-negative constraint. The imposition of the non-negative constraint is a pragmatic choice necessary due to Gaussian assumptions. An alternative, but more complex, option would be to build the non-negativity constraint directly into the probabilistic assumptions (i.e., to assume a non-Gaussian distribution which is, by definition, constrained to be non-negative).

The cost function minimum is now obtained using the non-negative least squares (*NNLS*) solver (Lawson and Hanson, 1974) which has been found to give a substantial speed up in the inversion code.

### The *a priori* emissions

The inversion scheme uses an initial best guess (an *a priori*,  $\mathbf{e}_{ap}$ ) for the source term, together with an estimate of the uncertainty in the *a priori*,  $\mathbf{B}$ . The *a priori* is determined from observations of the eruptive plume heights (e.g., from radar and web cameras), an empirical relationship relating mass eruption rate to the eruptive plume height (Mastin et al., 2009) and a uniform vertical distribution assumption. The fraction of the erupted mass which survives near-source fall-out processes is assumed to be 5%. The *a priori* provides a guide to finding a more realistic solution and prevents over-fitting to uncertain satellite observations. Following recent developments, the uncertainty in the *a priori* is now estimated from errors in the plume rise height, errors in the Mastin et al. relationship or in the distal fine ash fraction, and assumptions about fluctuations in the shape of the emission profile. These errors lead naturally to correlations between the individual source terms and result in a non-diagonal  $\mathbf{B}$  matrix.

### Satellite observations

Data from the Spinning Enhanced Visible and Infrared Imager (SEVIRI) on-board the geostationary Meteosat Second Generation (MSG) satellite are used to retrieve volcanic ash physical properties using a 1-dimensional variational (1D-Var) analysis methodology (Francis et al., 2012). The retrieved properties include ash column loadings ( $\mathbf{o}_a$  in  $\text{g m}^{-2}$ ) together with an estimate of their uncertainties ( $\mathbf{R}$ ). In addition, clear sky observations, which are free from both ash and meteorological cloud, can be used in the inversion scheme.

## RESULTS

The inversion method has been used to study the recent eruptions of two Icelandic eruptions: Grímsvötn in 2011 and Eyjafjallajökull in 2010. Here we present the results from the Eyjafjallajökull eruption in 2010 and briefly discuss results from the 2011 Grímsvötn eruption.

The eruption of Eyjafjallajökull (63.63° N, 19.62° W) started at approximately 09:00 UTC on 14/04/2010 and continued for nearly 40 days. Reports of the eruption plume height, based on radar observations, were obtained throughout the event from the Icelandic Meteorological Office (IMO). Satellite retrievals of ash column loadings and clear sky regions from SEVIRI data provide observations from the start of the eruption until 23:00 UTC on 29/05/2010, thereby allowing observations of ash remaining in the atmosphere past the end of the eruption to be included in the inversion. The observations are processed to select those which coincide (in time and in space) with the model predicted plume and which provide useful information to the inversion system. After processing, a total of 40047 observations of volcanic ash column loadings are available. Including clear sky increases the total number of column load observations to 689492. Following the recent improvements, the inversion calculation of the entire Eyjafjallajökull eruption takes just over 5 minutes using ash only observations and just over 13 minutes using both ash and clear sky observations. Figure 1 compares the *a priori* source term profile with the *a posteriori* source term profiles determined using ash-only observations and both ash and clear sky observations. All source term profiles show only the distal fine ash fraction which survives near-source fall-out processes. The use of clear sky observations removes more ash from the *a posteriori* source.

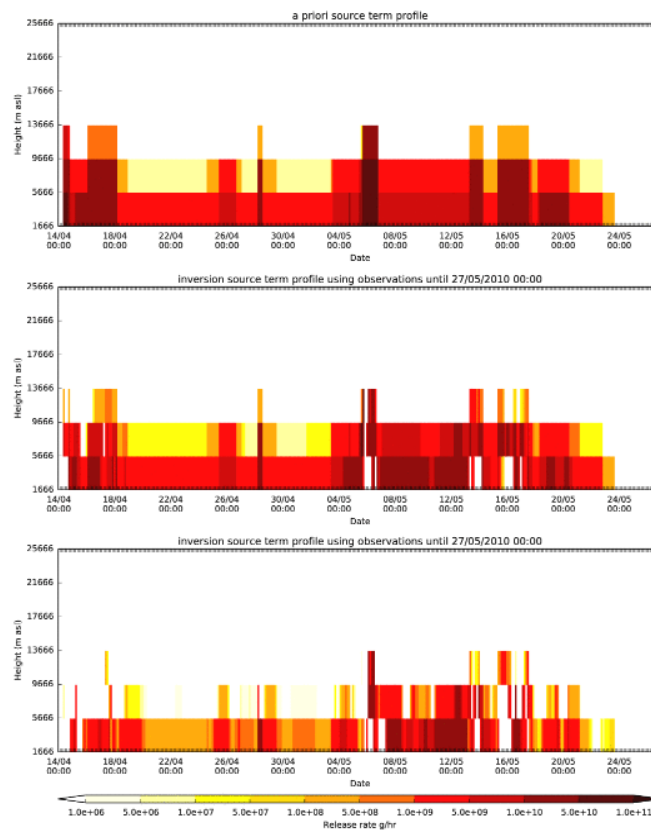


**Figure 1.** The distal fine ash source term profiles for the 2010 eruption of Eyjafjallajökull: the *a priori* (top), the *a posteriori* determined using ash only observations (middle) and the *a posteriori* determined using both ash and clear sky observations (bottom). All source term profiles have a height resolution of 4 km (y axis) and a time resolution of 3 hours (x axis).

Figure 2 shows the column loadings observed by satellite and predicted by NAME between 17:00 and 18:00 UTC on 06/05/2010. In comparison to the *a priori* ash cloud, the *a posteriori* ash clouds have a reduction of ash within the cloud which agrees better with the observed ash cloud. Using clear sky observations removes the small region of ash at approximately 54°N, 20°W seen in the ash-only *a posteriori* cloud.

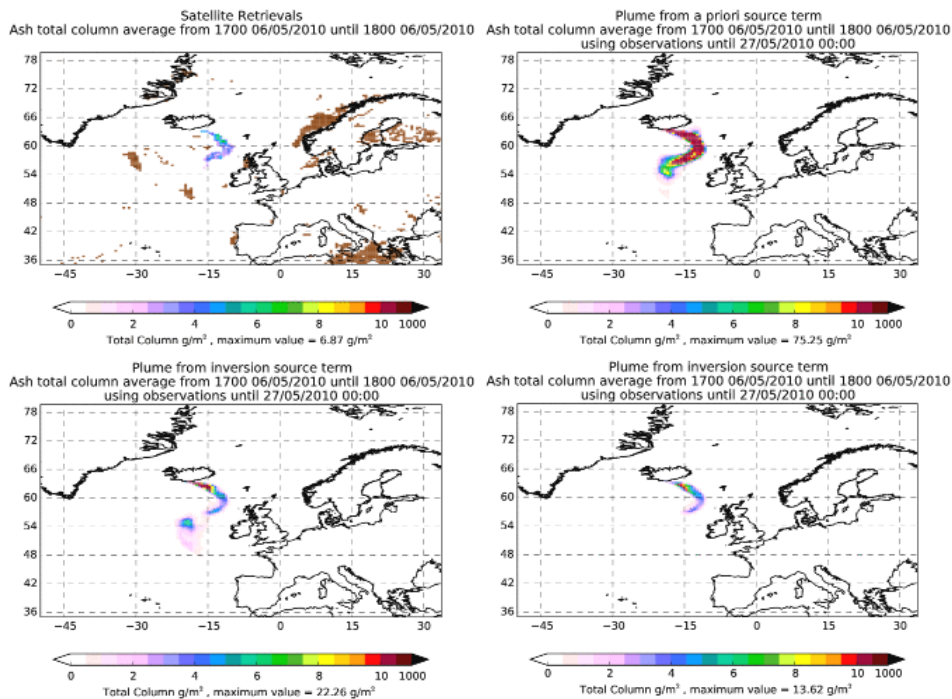


**Figure 2.** The distal ash cloud between 17:00 and 18:00 UTC on 06/05/2010 observed by satellite (ash and clear sky, with clear sky shown in brown) (top left) and predicted by NAME using the *a priori* source term (top right), using the *a posteriori* source term derived using ash only observations (bottom left) and using the *a posteriori* source term derived using both ash and clear sky observations (bottom right).

The eruption of Grímsvötn ( $64.42^{\circ}$  N,  $17.33^{\circ}$  W) at 19:13 UTC on 21/05/2011 was a much shorter eruption, lasting for approximately four days. A total of 3293 useful observations of volcanic ash column load are available from SEVIRI for employing with the inversion system. Including clear sky increases the total number of observations of volcanic ash column load to 88791. The inversion calculation of the Grímsvötn eruption takes less than 13 seconds using ash-only observations and just over 1 minute using both ash and clear sky observations. The erupted mass of fine ash is considerably less in the *a posteriori* source than in the *a priori* source, and is in line with the view held at the time of the eruption that the actual ash cloud contained less ash downwind than the modelling suggested.

## VALIDATION

Webster et al. (2012) validated a scheme for forecasting peak ash concentrations against both ground-based observations and measurements from instrumentation onboard research aircraft from the 2010 eruption of Eyjafjallajökull. Table 1 compares model predictions of peak ash concentrations against these observations for both a simple uniform source term profile based on the observed eruption height (Webster et al., 2012) and the *a posteriori* source terms obtained from the inversion scheme using ash-only observations and both ash and clear sky observations. The model predicts mean ash concentrations over large volumes and time periods and hence a peak-to-mean factor is applied to estimate peak ash concentrations. In line with Webster et al. (2012) a peak-to-mean factor of 10 is used with model predicted mean ash concentrations over 25FL layers. In the comparison of modelled and observed peak ash concentrations, an uncertainty in the observations of a factor of 2 is assumed. Agreement is assessed both with and without consideration of uncertainty in the modelled peak ash concentrations. This model uncertainty is due to slight positional errors in the predicted ash cloud and is accounted for by assessing the variability in the modelled concentrations over neighbouring model output grid-boxes.

The ash cloud predictions obtained from the *a posteriori* source terms show better agreement with the independent observations than the model predictions obtained using a simple uniform source term, particularly when errors in the model predictions are not considered in the comparison. Using clear sky

observations with the inversion scheme reduces the ash in the resulting *a posteriori* source term and the model then has a tendency to under-predict peak concentrations within the ash cloud. This needs further investigation but may be caused by errors in the transport matrix **M** (which are not currently considered in the inversion scheme) resulting in the incorrect removal of ash when deriving the *a posteriori* source term.

**Table 1.** A statistical comparison of modelled and observed peak ash concentrations using different source terms and the high resolution 25FL peak ash concentration scheme (see Webster et al. (2012) for details). Agreement is assessed both with and without consideration of uncertainty in the model predictions due to positional errors in the ash cloud. Uncertainty in the observations is included in both assessments.

Source term	No model uncertainty			With model uncertainty		
	% in agreement	% of over-predictions	% of under-predictions	% in agreement	% of over-predictions	% of under-predictions
Uniform based on eruption height	30	23	48	75	3	22
<i>a posteriori</i> (ash-only observations)	43	25	32	79	3	18
<i>a posteriori</i> (ash and clear sky observations)	36	7	57	61	1	38

## CONCLUSIONS

This inversion technique uses available observations and reported details of the eruption to determine the optimal source (the *a posteriori*) within the uncertainty of the satellite observations and of the *a priori*. The *a posteriori* source can then be used as input to the transport model to give an improved forecast of the ash cloud. The recent improvements have resulted in a significant speed up, enabling the technique to be run quickly in an operational setting. Furthermore the scheme has been extended to include cross correlations in the errors in the *a priori* source term profile which enables better use to be made of the observations, which may be few in number. Two test cases have been studied in detail: the eruption of Eyjafjallajökull in 2010 and the eruption of Grímsvötn in 2011. The *a posteriori* source gives a predicted ash cloud which is in better agreement with the observations. The use of clear sky observations can reduce further the quantity of ash within the *a posteriori* source term and this may lead to an under-estimation of ash within the predicted plume. Further investigation is required here to fully understand the reasons for this.

## REFERENCES

- Francis, P. N., M. C. Cooke and R. W. Saunders, 2012: Retrieval of physical properties of volcanic ash using Meteosat: A case study from the 2010 Eyjafjallajökull eruption. *J. Geophys. Res.*, **117**, D00U09, doi:10.1029/2011JD016788.
- Jones, A. R., D. J. Thomson, M. Hort and B. Devenish, 2007: The U.K. Met Office's next-generation atmospheric dispersion model, NAME III, in Borrego C. and A.-L. Norman (Eds) Air Pollution Modeling and its Application XVII (Proceedings of the 27th NATO/CCMS International Technical Meeting on Air Pollution Modelling and its Application), Springer, 580-589.
- Lawson, C. L. and R. J. Hanson, 1974: Solving least squares problems, Prentice-Hall, 340 pp.
- Mastin, L. G. et al., 2009: A multidisciplinary effort to assign realistic source parameters to models of volcanic ash-cloud transport and dispersion during eruptions. *J. Volcanol. Geotherm. Res.*, **186**, 10-21.
- Pelley, R. E., M. C. Cooke, A. J. Manning, D. J. Thomson, C. S. Witham and M. C. Hort, 2015: Initial Implementation of an Inversion Technique for Estimating Volcanic Ash Source Parameters in Near Real time using Satellite Retrievals, *Forecasting Research Technical Report 604*, Met Office, UK.
- Webster, H. N. et al., 2012: Operational prediction of ash concentrations in the distal volcanic cloud from the 2010 Eyjafjallajökull eruption, *J. Geophys. Res.*, **117**, D00U08, doi:10.1029/2011JD016790.

**17th International Conference on  
Harmonisation within Atmospheric Dispersion Modelling for Regulatory Purposes  
9-12 May 2016, Budapest, Hungary**

---

**ON THE EXPLOITATION OF DOSE-RESPONSE INFORMATION  
FOR THE SOURCE-RECONSTRUCTION  
IN THE CASE OF ATMOSPHERIC HAZARDOUS MATERIAL RELEASES**

*Samar Elkhalfa<sup>1</sup>, Christos D. Argyropoulos<sup>1</sup>, George C. Efthimiou<sup>2</sup>, Spyros Andronopoulos<sup>2</sup>, Alexandros G. Venetsanos<sup>2</sup>, Ivan V. Kovalets<sup>3</sup> and Konstantinos E. Kakosimos<sup>1</sup>*

<sup>1</sup>Department of Chemical Engineering and Mary Kay ‘O Connor Processes Safety Center, Texas A&M University at Qatar, Qatar

<sup>2</sup>National Centre for Scientific Research “Demokritos”, Institute of Nuclear and Radiological Sciences and Technology, Energy and Safety, Environmental Research Laboratory, Athens, Greece

<sup>3</sup>Department of Environmental Modelling, Institute of Mathematical Machine and System Problems, National Academy of Sciences of Ukraine, Kiev, Ukraine

**Abstract:** The atmospheric release of hazardous materials in urban or industrial environments can be the result of an accident, with potential consequences on local or regional scale, or can be an intentional act of violence. In such cases, the highest uncertainty is associated with the location of the release and the quantity of the released substance. So far, all related studies focus on the use of air concentrations as prior information and the development of sophisticated inverse modelling methods. However, in a real case, this information is probably not available to the required extent or at all. The present study examines the hypothesis of using health observations (symptoms like coughing, headaches, asthma attacks and deaths) to derive dosages and air concentration levels of the released hazardous substances.

**Key words:** *source reconstruction; inverse modelling; emergency response; atmospheric dispersion*

## **INTRODUCTION**

The release of hazardous materials (HazMat), whether intentional or accidental, poses great threats to the public, especially in densely populated areas. The Sarin gas terrorist attacks in Matsumoto City in 1994 and Tokyo in 1995, and the famous Bhopal incident in India in 1984 are examples of such release incidents and their severe consequences. In an accidental or malevolent release of a HazMat, the characteristics the source incorporate the highest uncertainty among all other factors like meteorology and model errors (Korsakissok *et al.*, 2013). For example, the assumed emission rate referred as “source term”, can differ from the true one by a factor of 10 or more (US\_Nuclear\_Regulatory\_Commission, 1990) among all other uncertainties like the uncertainties in the meteorological information or the numerical methods. For this reason, the determination of the source term and location is of primary importance in emergency response and preparedness.

The source characterisation of an atmospheric contaminant is approached by solving the inverse problem, in which one has to infer the source characteristics of the released HazMat from concentration or deposition measurements (Lushi and Stockie, 2010). Multiple mathematical approaches have been applied to the inverse problem such as adjoint equations (Le Dimet, 1986) and Kalman filtering (Segers, 2002) together with Gaussian (Drews M, 2005), Lagrangian (Zheng, 2007) and advanced (Chow *et al.*, 2008) computational dispersion models. To reduce the computational demands, many studies employ simple probabilistic methods (Kovalets *et al.*, 2011) and Monte-Carlo sampling (Keats *et al.*, 2007). In any case, the greater the number of available concentration measurements, the closer the guessed/estimated source rate will be to reality, and consequently more reliable and faster dispersion forecast can be achieved. On the other hand, clinical field health observations provided by the emergency response personnel, such as coughing, asthma, gastrointestinal problems, coma and deaths, are of the first information available after such unanticipated events. Since these health symptoms are the outcome of the exposure to the released material, it seems that there is a possibility to exploit the health observations as

input data to reconstruct the release information. Surprisingly, there have been relatively few prior studies that aim to exploit the observed health symptoms. Moreover, in all of them, the objective was to estimate exposure by using again clinical tests and not the symptoms themselves. Georgopoulos *et al.* (2008) used a conceptual/computational framework for exposure reconstruction from biomarker data, employing physiologically based toxicokinetic (PBTk) modelling in conjunction with numerical “inversion” techniques. More recently, Christensen *et al.* (2015) also demonstrated the use of PBTk models in estimating potential exposures to chemical agents through the interpretation of human biomarker data.

Herein, we present a preliminary analysis of the framework to achieve the source reconstruction starting from health observations. To our best knowledge, there is no similar methodology or system reported yet (Heinala *et al.*, 2013). For the sake of simplicity and to focus on the hypothesis, rather than the mathematical background of the inverse problem, we study a simple but realistic HazMat release scenario. We deploy a forward modelling scheme using a semi-empirical dispersion model and a source reconstruction algorithm based on Monte Carlo sampling. Finally, we assess the capability of the proposed method to reconstruct the source over some scenarios that prove the validity of the hypothesis, while at the same time stress its limits.

## METHODS

We consider the realistic release of natural gas from a feed pipeline with a rate of around  $100 \text{ kg s}^{-1}$  and a duration of few seconds, assuming the formation of a horizontal jet at  $45^\circ$  angle. The gas contains 4%  $\text{H}_2\text{S}$ , a well-studied toxic agent with adverse health effects even at sub-ppm concentrations. The area surrounding the facility is flat, and the prevailing wind velocity is set to  $5 \text{ m s}^{-1}$  while the atmospheric stability is neutral. The atmospheric dispersion of the hazardous agent was modelled using the U.S. Environmental Protection Agency’s (USEPA) SLAB model (Ermak, 1990) for the case of a horizontal jet source release. This model has been used in several studies involving denser-than-air atmospheric releases and (Dehankar, 2015) widely employed in some applications involving accidental releases). The results produced by the SLAB model are based on the solution of the one-dimensional equations of momentum, conservation of mass and energy, as well as the equation of state. For a specific release, the model provides an equation and its parameters to calculate the concentration at a given location, relative to the source, and time. This equation is introduced in MatLab, and SLAB predictions are automatically retrieved.

The impact (response) of the exposure at a concentration for a given duration (dose) on the human health is estimated using probit formulations and fixed exposure levels like the Acute Exposure Guideline Levels (AEGLS). These are available for some chemical agents and facilitate the prediction of the onset of adverse health effects in a general population. However, in an actual release, inhalation exposures may vary with durations, which makes it a challenge to estimate the onset of the health effects using the fixed values provided. To surpass this, Boris and Patnaik (2014) developed an approach that calculates the progressive exposure based on the time evolved concentration. When this exposure exceeds a value of one, then the respective AEGL criteria have been reached. Using this approach, we calculated the onset of each of the AEGL criteria either as a continuous toxic load (i.e. TL) or as discrete health effects (i.e. HE; discrete values of AEGL 3, AEGL 2, AEGL 1, and nothing) for every available concentration profile.

Initially, we execute SLAB for the actual source rate and location to form the measurements dataset (synthetic dataset). A random noise of less than  $\pm 20\%$  has been added to represent the expected uncertainty of real measurements and modelling input variability. The source is reconstructed at two different and independent stages: one for the source rate and the other for its location. An optimal estimate of the source rate,  $Q_s$ , is obtained by minimizing the Normalized Mean Square Error (NMSE). The iterative calculation was processed via the “fminbnd” built-in function of Matlab r2014a; an algorithm based on golden section search and parabolic interpolation. To obtain the best estimate of the release location, we employ a cost function method based on the Pearson correlation coefficient  $J$ :

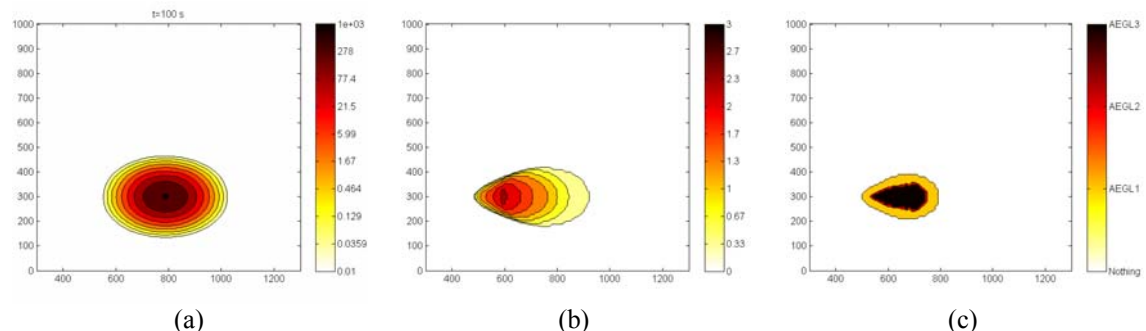
$$J = \frac{1}{N-1} \sum_{i=1}^N \left( \frac{C_{O,i} - \langle C_O \rangle}{\sigma_O} \right) \left( \frac{C_{M,i} - \langle C_M \rangle}{\sigma_M} \right) \quad (2)$$

where  $C$  is the concentration and subscripts O and M denote the observed and modelled values respectively, and  $\sigma$  is the standard deviation.  $J$  approaches a value of unit for two perfectly correlated sets

of observations and modelling results. It should be noted that since the source rate does not directly participate in the correlation coefficient, the solution obtained is independent of the choice of the source rate. In this study, the source coordinates are assumed to coincide with one of the grid nodes. The location of the corresponding grid node for which the correlation coefficient is closest to the unit is considered to be the identified source location.

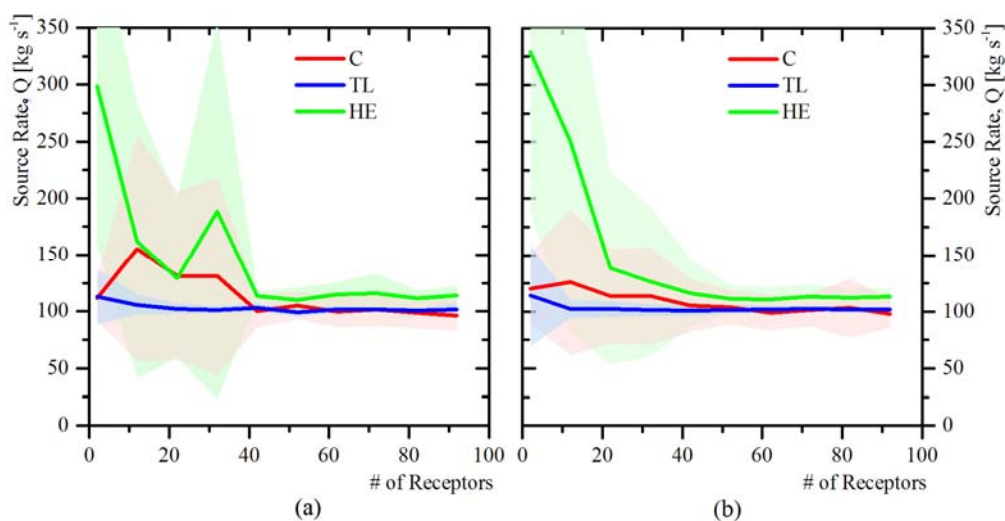
## RESULTS AND DISCUSSION

Figure 1 presents an example of the forward modelling results for the concentration at 100 s as it is directly calculated using SLAB. We also observe the corresponding toxic load (TL) up to this time and the expected health effects (HE). All following calculations assume these results as the measurements/observations dataset.



**Figure 1.** An example of the forward (dispersion) modelling at 100s for a) concentration (ppmv), b) toxic load for AEGL 1, and c) health impact according to AEGL levels. The source is located at (500 m, 300 m).

A computational grid of  $25 \times 25 \text{ m}^2$  is selected for the forward modelling, and the same is used for the source reconstruction. This creates a set of more than 2,000 possible receptors to be used. To reduce extent calculations, we incorporate only the receptors with a non-zero concentration value, which brings the total number of receptors to less than 300 in the specific case of Figure 1. If all receptors are being used then there is one single observations' dataset. However, if a smaller number of receptors is selected then the possibilities are increased following the appropriate combinatorics (e.g.  $n$  choose  $k$ ). A representative conclusion can be reached by repeating the calculations for multiple random sets of receptors or use of Bayesian inference. Figure 2 presents the estimated source rate as the size of the receptors set increases and for a different number of random sets (iterations). In either case (10 or 100 iterations), the estimated source rate is very close to the actual one ( $\sim 100 \text{ kg s}^{-1}$ ) when the observations dataset is based on concentrations (C; solid red line).



**Figure 2.** Source rate estimation for a variable number of receptors: 10 (a) and 100 (b) random sets (iterations) used of Concentration, Toxic Load & Health Effect. The shaded area represents the  $2\sigma$  range.

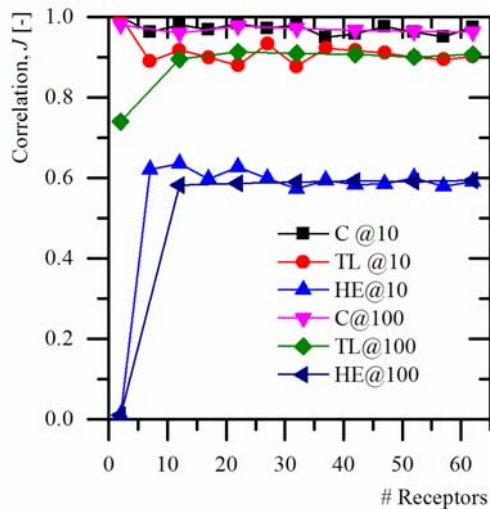


**Figure 3.** Correlation factor dependence over the number of receptors used for 10 and 100 random sets (iterations) of Concentration, Toxic Load & Health Effect values.

that no value for the source rate is needed. However, the correlation coefficient does not exceed 0.6 in the case of HE. This does not improve even for more iterations.

The actual source rate is estimated even faster when the observations dataset is based on the toxic load (TL; solid blue line). The scatter of the results (as expressed by the shaded area) is also smaller in the case of TL compared to C. This is attributed to the fact that TL represents the integrated impact of C over time and thus includes a “larger” amount of information. On the other hand, the actual source rate is approached slower and with a larger scattering when health effects are used as the observations dataset (HE; solid green line). Although HE also reflects the time integrated impact of C, most of the information included in TL is lost since HE receives only discrete values between 0 and 3 (from nothing to AEGL 3). In the case of HE, the actual source rate could be approached with around 20% accuracy when 40 or more receptors are used. A smaller number of receptors might still be adequate if all of them are better located. This is depicted in Figure 3, from which we observe high values of the correlation coefficient even for less than ten receptors. It should be noted

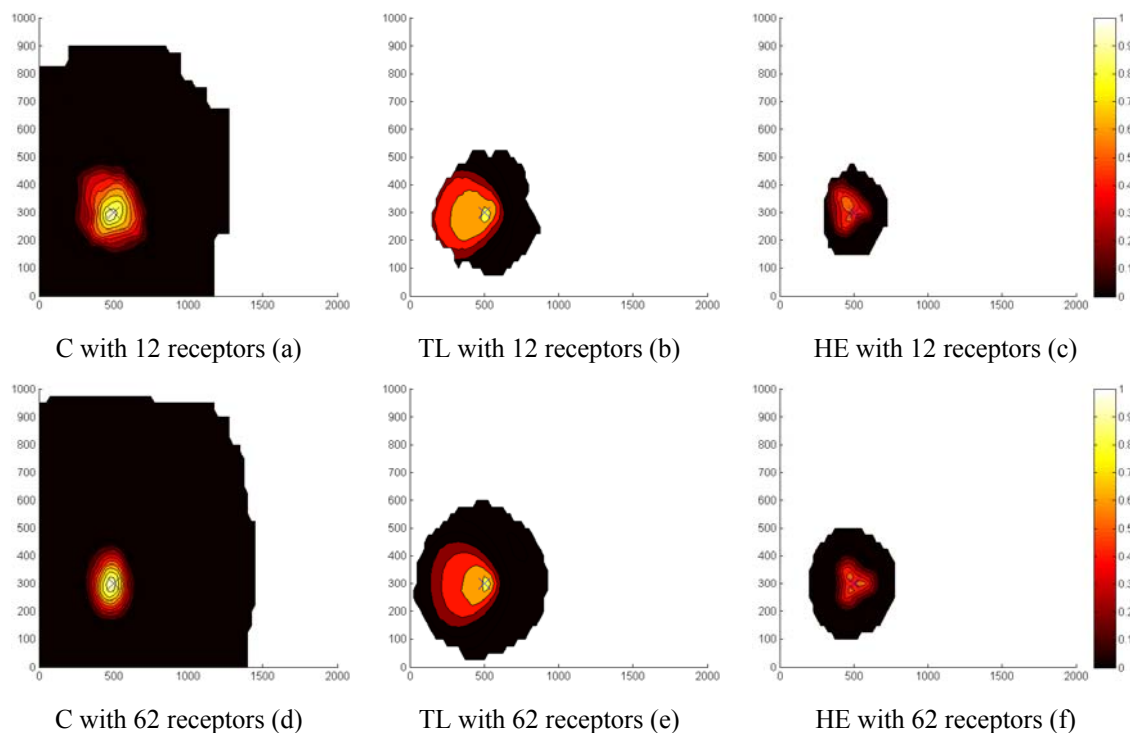


**Figure 4.** Spatial distribution of the correlation factor,  $J$ , for 12 (a-c) and 62 (d-f) receptors used for values of Concentration (a, d), Toxic Load (b, e) & Health Effect (c, f). A black cross denotes the actual source location.

On the contrary, if we study the spatial distribution of the correlation coefficient (Figure 4) the area of the source location is well identified, in all cases, regardless of the low correlation values for HE. This is an important outcome, which demonstrates the advantages of the correlation coefficient compared to the NMSE for the source rate estimation. One could interpret the findings of Figure 4 as such: Source location is identified with high accuracy when C or TL are available, and high probability when HE is used.

## CONCLUSIONS

This study demonstrated the use of health effects or symptoms for the use of source reconstruction (release rate and location). Regardless of the expected uncertainty when such prior information is used there are still three unique advantages: a) health observations will be available in any case, contrary to concentration measurements, b) there are already advanced atmospheric dispersion algorithms that estimate dosages or dosage distributions directly, and c) multiple dosages can be estimated even from a single location (i.e. receptor) based on the different exposures and responses, which leads to concentration time series. The last is expected to improve the performance of the presented approach significantly.

## ACKNOWLEDGEMENTS

This publication was made possible by a NPRP award [NPRP 7-674-2-252] from the Qatar National Research Fund (a member of The Qatar Foundation). The statements made herein are solely the responsibility of the authors.

## REFERENCES

- Boris, J. P. and G. Patnaik, 2014. Acute Exposure Guideline Levels (AEGs) for Time Varying Toxic Plumes. DTIC Document.
- Chow, F. K., B. Kosović and S. Chan, 2008: Source Inversion for Contaminant Plume Dispersion in Urban Environments Using Building-Resolving Simulations. *J. Appl. Meteorol. Clim.*, **47**:1553-1572.
- Christensen, K. L. Y., M. Lorber, X. Ye and A. M. Calafat, 2015: Reconstruction of bisphenol A intake using a simple pharmacokinetic model. *J Expos Sci Environ Epidemiol*, **25**:240-248.
- Dehankar, P. B., 2015: Study of the accidental releases heavy gas dispersion comparing SLAB and SCREEN-3. *Internation Journal of Engineering Sciences & Research Technology*, **4**:765-769.
- Drews M, L. B., Madsen H., 2005: Analysis of a Kalman filter based method for on-line estimation of atmospheric dispersion parameters using radiation monitoring data. *Radiat. Prot. Dosim.*, **113**:75-89.
- Ermak, D. L., 1990. User's manual for SLAB: An atmospheric dispersion model for denser-than-air-releases (No. UCRL-MA-105607; Other: ON: DE91008443 United States Other: ON: DE91008443 Thu Feb 07 19:26:03 EST 2008 OSTI; NTIS; GPO Dep. LLNL; EDB-91-041035; NTS-91-011228; ERA-16-013447 English).
- Georgopoulos, P. G., A. F. Sasso, S. S. Isukapalli, P. J. Lioy, D. A. Vallero, M. Okino, *et al.*, 2008: Reconstructing population exposures to environmental chemicals from biomarkers: Challenges and opportunities. *J Expos Sci Environ Epidemiol*, **19**:149-171.
- Heinala, M., U. Gundert-Remy, M. H. Wood, M. Ruijten, P. M. Bos, A. Zitting, *et al.*, 2013: Survey on methodologies in the risk assessment of chemical exposures in emergency response situations in Europe. *J Hazard Mater*, **244-245**:545-554.
- Keats, A., E. Yee and F.-S. Lien, 2007: Bayesian inference for source determination with applications to a complex urban environment. *Atmos. Environ.*, **41**:465-479.
- Korsakissok, I., A. Mathieu and D. Didier, 2013: Atmospheric dispersion and ground deposition induced by the Fukushima Nuclear Power Plant accident: A local-scale simulation and sensitivity study. *Atmos. Environ.*, **70**:267-279.
- Kovalets, I. V., S. Andronopoulos, A. G. Venetsanos and J. G. Bartzis, 2011: Identification of strength and location of stationary point source of atmospheric pollutant in urban conditions using computational fluid dynamics model. *Mathematics and Computers in Simulation*, **82**:244-257.
- Le Dimet, F. X. a. T., O., 1986: Variational algorithms for analyses and assimilation of meteorological observations: theoretical aspects. *Tellus B*, **38A**:97-110.
- Lushi, E. and J. M. Stockie, 2010: An inverse Gaussian plume approach for estimating atmospheric pollutant emissions from multiple point sources. *Atmos. Environ.*, **44**:1097-1107.
- Segers, A., 2002. Data Assimilation in Atmospheric Chemistry Models using Kalman Filtering. Delft University, DUP Science.
- US\_Nuclear\_Regulatory\_Commission, 1990. Analysis of CDF from internal events: expert judgment. (No. NUREG/CR-4550).
- Zheng, D. Q., 2007. Evaluation and development of data assimilation in atmospheric dispersion models for use in nuclear emergencies. Hong Kong University.

**17th International Conference on  
Harmonisation within Atmospheric Dispersion Modelling for Regulatory Purposes  
9-12 May 2016, Budapest, Hungary**

---

**A NEW PERSPECTIVE ON THE FUKUSHIMA RELEASES BROUGHT BY NEWLY  
AVAILABLE <sup>137</sup>Cs AIR CONCENTRATION OBSERVATIONS AND RELIABLE  
METEOROLOGICAL FIELDS**

*O. Saunier<sup>1</sup>, A. Mathieu<sup>1</sup>, T. Sekiyama<sup>2</sup>, M. Kajino<sup>2</sup>, K. Adachi<sup>2</sup>, M. Bocquet<sup>3</sup>, Y. Igarashi<sup>2</sup>,  
T. Maki<sup>2</sup>, D. Didier<sup>1</sup>*

<sup>1</sup> IRSN - Institute of Radiation Protection and Nuclear Safety, Fontenay-aux-roses, France.

<sup>2</sup>MRI, Meteorological Research Institute, Tsukuba, Japan.

<sup>3</sup>CEREA, Joint Laboratory École des Ponts ParisTech and EDF R&D, Champs-sur-Marne, France.

**Abstract:**

Five years after the Fukushima accident, many estimates of the source term (ST) have been published. In this study, the relevance of several ST is examined by performing a sensitivity analysis using several meteorological fields. The simulations prove that the MRI meteorological fields with higher spatial and temporal resolution give better scores. However, the uncertainties on the meteorological fields and ST remain high since several contamination events remain difficult to reproduce.

In addition, the inverse modeling method developed by IRSN is applied to evaluate new ST using MRI meteorological fields, Tsuruta <sup>137</sup>Cs air concentration and gamma dose rate measurements. Simulations forced by these new inverted ST improve the agreement between model and observations in comparison with previous simulations especially between March 20 and March 22. A better reconstruction of the most of contamination events is also obtained.

**Key words:** *Inverse modelling, source reconstruction, Fukushima accident, atmospheric dispersion model*

**INTRODUCTION**

The disaster at the Fukushima Dai-ichi nuclear power plant (FD-NPP) was the most serious nuclear accident since Chernobyl in 1986. A common feature between these two nuclear accidents is the difficulties encountered to assess the atmospheric releases of radioactive materials. The ST including the time evolution of the release rate to the atmosphere and its distribution between radioisotopes remains one of the key uncertainties in the understanding of the accident consequences.

Five years after the Fukushima accident, many estimations of the ST have been assessed by combination between environmental observations and atmospheric dispersion models. Simple methods for source estimation (Chino et al. 2011, Mathieu et al. 2012, Terada et al. 2012, Katata et al. 2015) and inverse methods have been applied (Stohl et al. 2011, Winiarek et al. 2014, Saunier et al. 2013). The ST estimation methods inherit many uncertainties arising from the number and the type of measurements used, the quality of the meteorological data and the quality of atmospheric dispersion model. That is why the estimates can differ considerably in terms of temporal evolution of the release rates, illustrating how difficult it is to reconstruct.

In this paper, a sensitivity analysis to meteorological fields is made by using several published ST. Then, after some reminders about the inverse modeling method developed by IRSN, new inverted ST based on Tsuruta air concentrations (Tsuruta et al. 2014, Oura et al. 2015) and gamma dose rate measurements are assessed. Forward simulations are performed with the new inverted ST to investigate the relevance of our estimations. Comparisons between several types of measurements and simulations are provided.

**SENSITIVITY TO METEOROLOGICAL DATA**

**Meteorology and model set-up**

In the study, forward simulations have been carried out in order to investigate the relevance of several published ST. Four ST (Saunier et al, 2013, Terada et al., 2012, Winiarek et al. 2014 and Katata et al.

2015) are compared. The Eulerian model IdX is used to simulate the radionuclide dispersion. This model is part of IRSN's (French Institute for Radiation protection and Nuclear Safety) C<sup>3</sup>X operational platform. It is based on the Polair3D chemistry transport model (Boutahar et al., 2004) and has been validated on nuclear accidents (Quelo et al., 2007). IdX takes into account dry and wet deposition as well as radioactive decay and fission. Dry deposition is modeled by simple scheme with a constant deposition velocity:  $v_{\text{dep}} = 2.10^{-3}$  m/s. For wet scavenging, the parameterization used is the form  $\Lambda_s = \Lambda_0 p_0$ , where  $\Lambda_0 = 5.10^{-5}$  h/(mm.s) and  $p_0$  the rainfall intensity in millimeters per hour (Baklanov and Sørensen 2001).

The simulations have been subjected to variation in the meteorological fields (Table 1). Meteorological Research Institute (MRI) of Japan Meteorological Agency (JMA) designed meteorological fields with higher spatial resolution MRI (Sekiyama et al. 2013) to improve the simulation of the atmospheric dispersion from the Fukushima accident. They have been used in the framework of the SAKURA project, collaboration between MRI and IRSN. Meteorological data from ECMWF (European Center for Medium-Range) and JMA (Japan Meteorological Agency) are also used for comparison.

**Table 1.** Meteorological data used in this study.

<b>Origin of meteorological fields</b>	<b>Spatial resolution</b>	<b>Temporal resolution</b>
ECMWF	12 km	3h
JMA	5 km	3 h
MRI	3 km	1 h

### Model to data comparison

New <sup>137</sup>Cs atmospheric concentration obtained from the sampling tapes of the Suspended Particle Matter (SPM) monitoring network by the method of Tsuruta et al. (2014) are available. These data are very useful since several plumes, unknown until now, could be identified in addition with the two major plumes on March 15 and March 21. In Tsuruta et al. (2014), nine major plumes are identified between March 12 and March 23. Besides, the Tsuruta <sup>137</sup>Cs activity concentration measurements are not used to estimate the Saunier et al. ST, Terada et al. ST, Winiarek et al. ST and the Katata et al. ST. As a result, comparing the simulations with these observations is an excellent way of validating the ST. To quantify the comparison between the simulated and observed <sup>137</sup>Cs atmospheric concentration, two statistical indicators are computed:

- Fractional bias, which indicates the degree of any over or underestimate of the values. Negative values mean an underestimate and positive values indicate an overestimate.
- Percent within a factor 5 and 10. Factor 5 (resp. 10) represents the proportion of the simulated activity concentrations that is within a factor of 5 (resp. 10) of the observed values.

The values of the individual statistics are provided in Table 2 for every simulation.

**Table 2.** Values of the statistics indicators for every simulation

<b>Model</b>	<b>FB</b>	<b>FA5</b>	<b>FA10</b>
Terada + CEP	-1.13	32.2	44.0
Saunier + CEP	<b>-0.75</b>	38.3	51.4
Winiarek + CEP	-1.32	23.7	34.3
Katata + CEP	-1.31	27.0	37.9
Terada + JMA	-1.36	25.8	35.7
Saunier + JMA	-1.32	24.7	39.0
Winiarek + JMA	-1.40	22.9	29.8
Katata + JMA	-1.32	28.2	38.3
Terada + MRI	-1.15	33.7	47.6
Saunier + MRI	-0.86	<b>40.0</b>	<b>56.2</b>
Winiarek + MRI	-0.84	36.6	54.0
Katata + MRI	-1.11	33.7	49.5

The best values for every statistic indicator are highlighted in bold text. It shows that the simulations using MRI meteorological fields reproduced  $^{137}\text{Cs}$  air concentrations observations with a higher factor 5 and factor 10 than those using ECMWF and JMA data. A higher temporal and spatial resolution of the MRI meteorological fields can explain this better agreement. The fractional bias shows that all the simulations overestimate the observations. The statistics remain weak although the use of MRI meteorological fields allows the improvement of the scores. The simulations prove that the uncertainties on the meteorological fields and the ST remain high.

#### ASSESSMENT OF NEW INVERTED ST

MRI meteorological fields are more suited to reproduce Tsuruta  $^{137}\text{Cs}$  air concentrations observations. To our knowledge, there is no assessment of the ST using  $^{137}\text{Cs}$  Tsuruta air concentration measurements. Therefore, MRI meteorological fields are used to assess two ST by inverse modeling:

- A  $^{137}\text{Cs}$  ST computed by using 99 Tsuruta air concentrations stations (Oura et al. 2015).
- A ST based on the dose rate measurements. For this computation, 66 dose rate stations are considered.

#### Inverse modelling methodology

The method is based on a variational approach consisting in the minimization of a cost function which measures the differences between the model predictions  $H\sigma$  and the real measurements  $\mu$  (air concentration or dose rate measurement). The cost function also includes a background term which adds the differences between a priori emissions  $\sigma_b$  and the updated estimation  $\sigma$ :

$$J(\sigma) = (\mu - H\sigma)^T R^{-1} (\mu - H\sigma) + (\sigma - \sigma_b)^T B^{-1} (\sigma - \sigma_b)$$

The matrix H is the Jacobian matrix computed under the approach proposed by Winiarek et al. (2011). Each column of H represents the dispersion model's response to a unitary release emitted for one radionuclide whose release rate is to be estimated.  $R = E[\varepsilon\varepsilon^T]$  is the error covariance matrix related to the measurements and model. The vector  $\varepsilon$  is the observation error aggregating instrumental and modeling errors and  $B = E[(\sigma - \sigma_b)(\sigma - \sigma_b)^T]$  is the background error covariance matrix. Simple parametrization for B and R matrixes are used. It is assumed that they are diagonal and the error variance is the same for all diagonal elements of each matrix (homoscedasticity property):

$$B = m^2 I, m > 0 \text{ and } R = k^2 I, k > 0$$

The parameter  $\lambda = \frac{k}{m}$  determines the scale of the fluctuations in the ST. We choose,  $\sigma_b = 0$ . Therefore, the cost function takes the form:

$$J(\sigma) = \|\mu - H\sigma\|^2 + \lambda^2 \|\sigma\|^2 \quad (1)$$

#### Inversion using air Tsuruta activity concentrations observations

In the case of inversion with Tsuruta  $^{137}\text{Cs}$  air concentration measurements the releases rates are assessed between March 11 and March 24. The cost function (1) is directly minimized by using the L-BFGS-B limited-memory quasi-Newton algorithm (Liu and Nocedal, 1989).

#### Inversion using dose rate observations

The method is described in details in Saunier et al. (2013). It has been applied to the Fukushima accident using ECMWF meteorological fields. The gamma dose rate assessment at each element of H matrix is computed from the activity concentrations and surface activities simulated by IdX model. This is done with the C<sup>3</sup>X platform's ConsX model.

Gamma dose rate measurements sum the direct contribution of the plume (plume radiation) and the gamma radiation emitted by radionuclides that fell to the ground (deposited radiation) through dry and wet deposition processes. The data interpretation is complex since the signal provides no information about isotopic composition or the respective contributions of the plume and deposition. Consequently, the minimization of cost function (1) does not lead to a unique solution because the inverse problem is not sufficiently constrained. To reduce the number of unknown parameters to assess, the inverse problem to solve is divided into two steps. In the first step, the cost function (1) is adapted and minimized to identify the periods during which releases may have occurred. It is assumed that the release is composed of one

single radionuclide which acts like a passive tracer. Only the plume component of the dose rate signal is taken into account in the inversion to assess the potential releases periods. An automatic algorithm is used to analyze the slope in the dose rate signal and the peaks corresponding to the detection of the passage of the plume are extracted.

In a second step, it is assumed that most of the dose rate signal is due to 8 radionuclides. The releases rates in  $^{134}\text{Cs}$ ,  $^{136}\text{Cs}$ ,  $^{137}\text{Cs}$ ,  $^{137\text{m}}\text{Ba}$ ,  $^{131}\text{I}$ ,  $^{132}\text{I}$ ,  $^{132}\text{Te}$  and  $^{133}\text{Xe}$  are computed during the periods identified during the first step. Moreover, the elements of the  $^{137\text{m}}\text{Ba}/^{137}\text{Cs}$  and  $^{132}\text{Te}/^{132}\text{I}$  pairs are in secular equilibrium in accordance with the following isotopic ratio:

$$\frac{\sigma_{137\text{mBa}}}{\sigma_{137\text{Cs}}} = 0.946; \frac{\sigma_{132\text{Te}}}{\sigma_{132\text{I}}} = 1.03$$

An analysis of the activity concentration measurements for the whole of Japan has shown that the ratio between the  $^{137}\text{Cs}$  and the  $^{134}\text{Cs}$  was constant over the time. The following isotopic ratio was therefore used:

$$\frac{\sigma_{137\text{Cs}}}{\sigma_{134\text{Cs}}} = 0.94$$

Finally, flexible constraints are added in the cost function (1) by imposing that the radionuclides be released in realistic proportions. The bounded of the isotopic ratios are assessed by analyzing the environmental observations and the knowledge of the core inventory of the FD-NPP:

$$1.67 < \frac{\sigma_{132\text{Te}}}{\sigma_{134\text{Cs}}} < 16; 2 < \frac{\sigma_{131\text{I}}}{\sigma_{134\text{Cs}}} < 100; 0.1 < \frac{\sigma_{133\text{Xe}}}{\sigma_{134\text{Cs}}} < 10000; 0.1 < \frac{\sigma_{136\text{Cs}}}{\sigma_{134\text{Cs}}} < 0.5 \quad (2)$$

Consequently, the cost function to minimize becomes:

$$J(\sigma) = \|\mu - H\sigma\|^2 + \lambda^2 \|\sigma\|^2 + \sum_{j=1}^4 r_j(\sigma) \quad (3)$$

with:

$$r_j(\sigma) = \exp\left(\frac{\sigma_j}{\sigma_{134\text{Cs}}} - a_j\right) + \exp\left(\frac{\sigma_{134\text{Cs}}}{\sigma_j} - b_j\right)$$

and  $a_j$  and  $b_j$  are the nuclide ratios defined in (2). In similar fashion to inversion using  $^{137}\text{Cs}$  Tsuruta air concentration observations, L-BFGS-B algorithm is used to minimize the cost function (3).

## RESULTS AND DISCUSSION

The ST computed by inversion using  $^{137}\text{Cs}$  Tsuruta air concentrations (ST-1) and dose rate observations (ST-2) are plotted in Figure 1. The retrieved ST-1 and ST-2's total emissions in  $^{137}\text{Cs}$  are 7.8 PBq and 6.2 PBq, respectively, which is consistent with the other estimates. The release periods retrieved by inverse modelling are similar but the retrieved ST-1 shows additional release peaks from March 12 to March 14 compared to the ST-2 estimate.

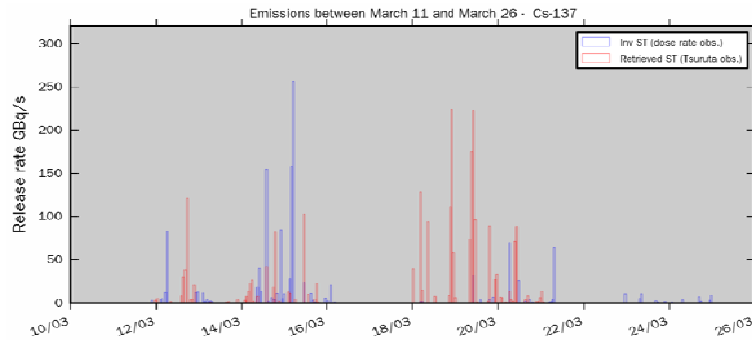


**Figure 1.**  $^{137}\text{Cs}$  release rate according to the estimated retrieved ST using dose rate observations (ST-2 in blue) and Tsuruta air concentrations (ST-1 in red).

Besides, the magnitude of several peaks is sometimes very different. Releases rates occurred between March 19 and March 21 are more significant when Tsuruta air concentrations are used in the inversion. During this period, the dose rate measured at some monitoring stations in the west of Fukushima prefecture did not increase even when a plume flowed over the stations. The value of dose rate was

already too high to detect a new plume, due to the ground shine caused by the deposition of a large amount of radionuclides on the ground by precipitation. That is can be an explanation of the underestimation of the inverted releases assessed using dose rates between March 19 and March 20.

### Comparison with dose rate measurements

Figure 2 shows comparison of the observed and simulated dose rates for monitoring stations located at Iitate and Hirono. At Iitate station, a significant increases of the dose rate occurred in March 15.

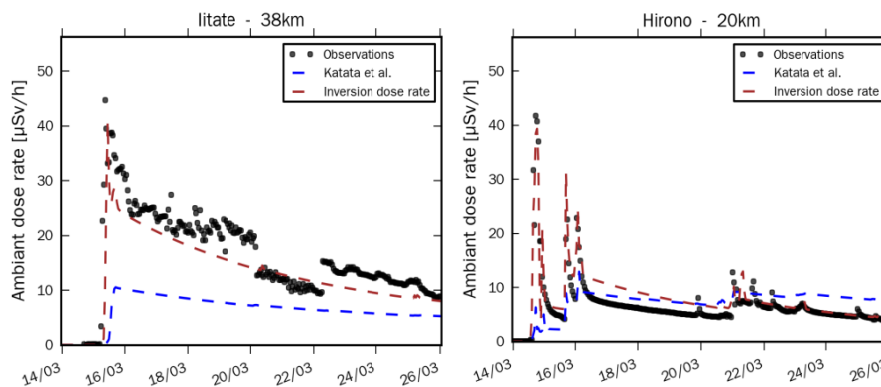


**Figure 2.** Comparisons of the dose rate observations (black dots) with the simulated dose rate computed with the retrieved ST (brown) and with the Katata et al. (2012) ST (blue).

When the plume is passed over the station, precipitations were observed and had led to the deposition of a large amount of radionuclides on the ground. This event is accurately reproduced by the simulation performed with the inverted ST-2 even if a slight delay of two hours is observed on the arrival time of the plume. At Hirono station, located to 20 km in the south of the FD-NPP, three increases of the dose rate occurred between March 14<sup>th</sup> and March 16<sup>th</sup>. Observed values and simulated values are very consistent. In the period of March 20-21, several increases of the dose rate signal occurred but they are not very well reproduced by the simulations. On average, the simulations performed with the retrieved ST are in good agreement with the observations. For 71% of the measurements, observed and modeled values agreed within a factor of 2. The factor 2 of the simulations performed with inverted ST-2 (71%) is higher than the factor 2 of simulations performed with Katata ST (64%). That makes sense because observations and atmospheric transport model used to construct the Katata ST are different from those taken into account in our inversion.

### Comparison with the atmospheric activity concentrations

Figure 3 provides an example of a comparison obtained with the Tanakura measurements in the Fukushima prefecture, a town located 72 km south-west of the power plant.

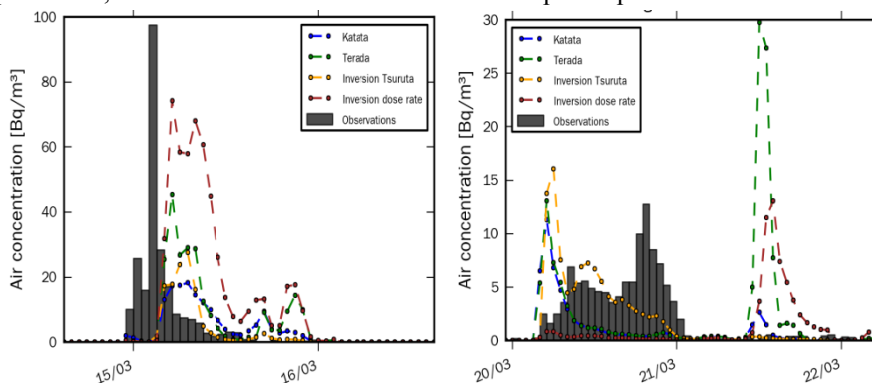


**Figure 3.** Measured activity concentrations (grey rectangles), and activity concentrations simulated with the Katata et al. ST (blue), Terada et al. ST (green), inverted ST assessed using dose rate (brown) and Tsuruta observations (orange) in Tanakura, for  $^{137}\text{Cs}$

As shown in the figure, the maximum concentration of  $98 \text{ Bq/m}^3$  is detected at 3:00 on March 15. It seems that the plume was transported from the power plant to Tanakura area by a north-easterly wind. The simulations are not able to reproduce accurately the main peak since there is always a few hours delay in the forecast plume arrival times.

In the period of March 20-21, significant values of  $^{137}\text{Cs}$  concentration have been detected for several hours. Simulation performed using inverted ST-1 gives a more accurate estimate of the contamination episode but the simulated concentrations are overestimated on the early morning of March 20 and the maximum concentration of  $13 \text{ Bq/m}^3$  at 20:00 on March 20 is underestimated. As expected, simulation forced by inverted ST-1 gives a better performance for the factor 5 and factor 10 values. The factor 10 values computed for 99 stations are 64.7% for the simulation performed with inverted ST-1 and 50.1 % for the simulation performed with inverted ST-2.

### Surface activity concentrations

Simulation results are compared with the observations of  $^{137}\text{Cs}$  deposition provided by Ministry of Education, Culture, Sports, Science and Technology (MEXT). Figure 4 shows that the deposition area to the north-west is well represented using the two retrieved ST, but it is too extensive and too far north compared with the observations when dose rate measurements are used to compute inverted ST.

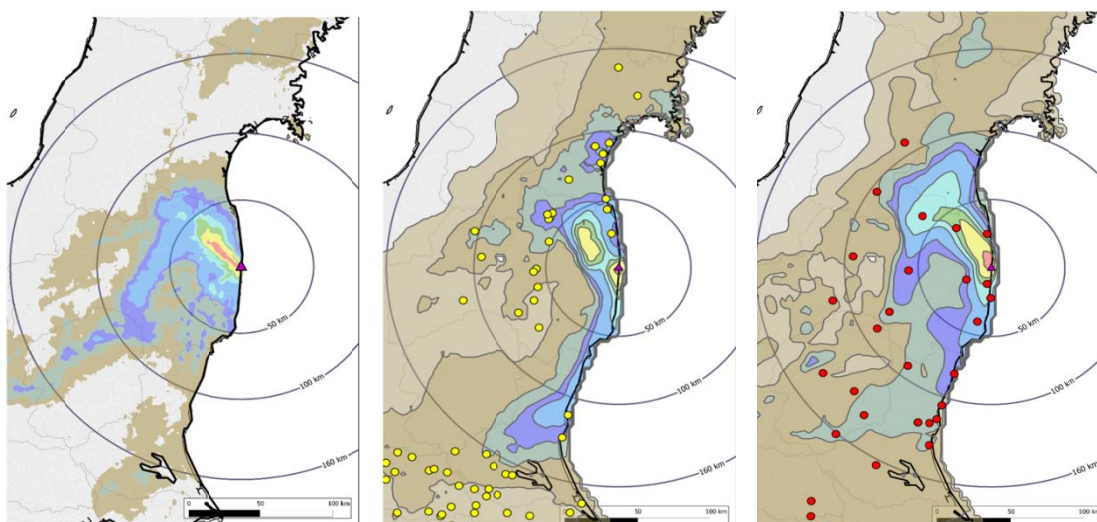


**Figure 4.** Map of cumulated Cs-137 surface deposition observed on April 1, 2011 (left). Comparison of the cumulative  $^{137}\text{Cs}$  ground deposition from simulations forced with inverted ST-1: (middle) and ST-2 (right). Circles represent the location of the stations used in the inversion. Red circles are dose rate observations and yellow circles are Tsuruta  $^{137}\text{Cs}$  air concentrations observations. Values are given in  $\text{Bq/m}^2$ .

To the south (Ibaraki prefecture), the simulation performed with the two inverted ST result in the total deposition amount being considerably overestimated. Another deposition area can be observed in the west and in the south of the Fukushima prefecture, bordering the Tochigi prefecture. These depositions resulting from the releases on March 15 are better reproduced when simulations are forced with the inverted ST-2. The agreement between observed and simulated dose rate is satisfactory in the valley located in the west of Fukushima prefecture. This explains why this deposition area is better reproduced but simulated  $^{137}\text{Cs}$  activity concentrations are strongly overestimated (Figure 3). This result illustrates clearly that uncertainties on vertical distribution of the plume and deposition process remain significant.

### CONCLUSION

In this study, the relevance of several ST has been studied for different types of meteorological input. The comparison between observed and simulated Tsuruta  $^{137}\text{Cs}$  air concentrations measurements shows that the model performs better with MRI fields than with ECMWF and JMA fields.

The assessment of new ST based on the MRI meteorological fields gives a better agreement between model and observations. However, more work needs to be done to improve the realism of the simulations since several contamination events occurred in March 15 are not always satisfactorily simulated. In the future, we plan to use a more realistic deposition model and to take into account simultaneously different types of observations (activity concentrations, gamma dose rate and surface activity concentration) in the inversion process.

## REFERENCES

- Baklanov, B. and Sørensen, J.H., 2001: Parameterisation of radionuclides deposition in atmospheric long-range transport modelling. *Physics and Chemistry of the Earth*, **B26**, 787-799.
- Boutahar, J., Lacour, S., Mallet, V., Quelo, D., Roustan, Y. and Sportisse, B., 2004: Development and validation of a fully modular platform for numerical modelling of air pollution: POLAIR, *International Journal of Environment and Pollution*, **22**, 1-2, 17-28.
- Chino, M., Nakayama, H., Nagai, H., Terada, H., Katata, G. and Yamazawa, H., 2011: Preliminary estimation of release amounts of  $^{131}\text{I}$  and  $^{137}\text{Cs}$  accidentally discharged from the Fukushima Daiichi Nuclear power plant into atmosphere, *J.Nucl.Sci. Technol.*, **48**, 1129-1134.
- Liu, D.C. and Nocedal, J., 1989: On the limited memory method for large scale optimization, *Math. Program. B.*, **45** (3), 503-528.
- Mathieu, A., Korsakissok, I., Quelo, D., Groell, J., Tombette, M., Didier, D., Quentric, E., Saunier, O., Benoit, J.-P. and Isnard, O., 2012: Atmospheric dispersion and deposition of radionuclides from the Fukushima Daiichi nuclear power plant accident, *Elements*, **8**, 195-200.
- Y. Oura, M. Ebihara, H. Tsuruta, T. Nakajima, T. Ohara, M. Ishimoto, H. Sawahata, Y. Katsumura and W. Nitta, 2015: A Database of Hourly Atmospheric Concentrations of Radiocesium ( $^{134}\text{Cs}$  and  $^{137}\text{Cs}$ ) in Suspended Particulate Matter Collected in March 2011 at 99 Air Pollution Monitoring Stations in Eastern Japan, *Journal of Nuclear and Radiochemical Sciences*, **15-2**, 1-12.
- Quelo, D., Krysta, M., Bocquet, M., Isnard, O., Minier, Y. and Sportisse, B., 2007: Validation of the Polyphemus platform on the ETEX, Chernobyl and Algeciras cases, *Atmospheric Environment*, **41**, 5300-5315.
- Querel, A., Quelo, D., Roustan, Y., Mathieu, A., Kajino, M., Sekiyama, T., Adachi, K., Igarashi, Y., Maki, T. and Didier D., 2016: Comparison of  $^{137}\text{Cs}$  deposit simulated on the Fukushima case to the observed deposit, by using several wet deposition schemes in LdX, HARMO 16: proceedings of the 16<sup>th</sup> International Conference on Harmonisation within Atmospheric Dispersion Modelling for Regulatory Purposes, 9-12 May 2016, Budapest, Hungary.
- Saunier, O., Mathieu, A., Didier, D., Tombette, M., Quélo, D., Winiarek, V., and Bocquet, M., 2013: An inverse modeling method to assess the source term of the Fukushima Nuclear Power Plant accident using gamma dose rate observations, *Atmos. Chem. Phys.*, **13**, 11403-11421, doi:10.5194/acp-13-11403-2013.
- Sekiyama, T., Kajino, M. and Masaru, K., 2013: Ensemble simulation of the atmospheric radionuclides discharged by the Fukushima nuclear accident, EGU General Assembly, Vienna, Austria, 7-12 April 2013.
- Stohl, A., Seibert, P., Wotawa, G., Arnold, D., Burkhart, J.F., Eckhardt, S., Tapia, C., Vargas, A. and Yasunari, T.J., 2012: Xenon-133 and caesium-137 releases into the atmosphere from the Fukushima Dai-ichi nuclear power plant: determination of the ST, atmospheric dispersion, and deposition, *Atmos. Chem. Phys.*, **12**, 2313-2343.
- Terada, H., Katata, G., Chino, M. and Nagai, H., 2012: Atmospheric discharge and dispersion of radionuclides during the Fukushima Dai-ichi Nuclear Power plant accident. Part II: verification of the ST and analysis of regional-scale atmospheric dispersion, *J. Environ. Radioact.*, **112**, 141-154.
- Tsuruta, H., Oura, Y., Ebihara, M., Ohara, T. and Nakajima T., 2014: First retrieval of hourly atmospheric radionuclides just after the Fukushima accident by analyzing filter-tapes of operational air pollution monitoring stations, *Sci. Rep.* **4**, 6717.
- Winiarek, V., Vira, J., Bocquet, M., Sofiev, M. and Saunier, O., 2011: Towards the operational estimation of a radiological plume using data assimilation after a radiological accidental atmospheric release, *Atmos. Env.*, **45**, 2944-2955.

- Winiarek V., Bocquet M., Saunier O. and Mathieu A., 2012: Estimation of errors in the inverse modeling of accidental release of atmospheric pollutant: Application to the reconstruction of the cesium-137 and iodine-131 STs from the Fukushima Daiichi power plant. *J. Geophys. Res.*, **117**, D05122.
- Winiarek, V., Bocquet, M., Duhanyan, N., Roustan, Y., Saunier, O., and Mathieu, A., 2014: Estimation of the caesium-137 source term from the Fukushima Daiichi nuclear power plant using a consistent joint assimilation of air concentration and deposition observations, *Atmos. Environ.*, **82**, 268–279.

**17th International Conference on  
Harmonisation within Atmospheric Dispersion Modelling for Regulatory Purposes  
9-12 May 2016, Budapest, Hungary**

---

**APPLICATION OF INVERSE DISPERSION MODELLING FOR THE DETERMINATION OF  
PM EMISSION FACTORS FROM FUGITIVE DUST SOURCES IN OPEN-PIT LIGNITE  
MINES**

*Athanasios Triantafyllou<sup>1,2</sup>, Nicolas Moussiopoulos<sup>3</sup>, Athina Krestou<sup>1,2</sup>, George Tsegas<sup>3</sup>,  
and Melina Andreadou<sup>4</sup>*

<sup>1</sup> LAPEP – Laboratory of Atmospheric Pollution and Environmental Physics, TEI of Western Macedonia,  
50100 Kozani, Greece

<sup>2</sup> TRC – Technological Research Centre, 50100 Kozani,

<sup>3</sup> LHTEE – Laboratory of Heat Transfer and Environmental Engineering, Aristotle University of  
Thessaloniki, 54124 Thessaloniki

<sup>4</sup> PPC, Western Macedonia lignite Centre

**Abstract:** The operation of large open-pit lignite mines represents a significant source of fugitive dust emissions connected to energy production. As part of the preparation of the European pollutant release and transfer register, mining enterprises are obliged to quantify the pollutant emissions from their fugitive sources in relation to various mining activities. PM emission inventories for open-pit mines are typically developed on the basis of activity data provided by the mine operator and emission factors obtained either from official databases or determined for each specific site. These inventories can then be used as input data in dispersion simulation tools or air quality management systems in order to provide operational estimates of the total dust burden in the surrounding areas attributable to mining operations. In this work, a methodology based on the inverse dispersion modelling approach combining two different dispersion models is used for determining PM emission factors for a variety of activities within the four large open-pit lignite mines of Kozani in Western Makedonia, Greece. A series of field measurement experiments, extending over a period of 3 years, provide the necessary meteorological data as well as upwind - downwind concentration levels in the area of each activity. A comparison of calculated emission rates provided by the two dispersion models indicates a very good agreement, while the normalised concentration timeseries downwind of each activity are accurately reproduced. Based on detailed activity information obtained both from on-site observations and data provided by the mine operator, PM emission factors are calculated for each experiment and activity type and empirical relations are developed for the calculation of the fugitive dust emissions from the four mines.

**Key words:** *Inverse Dispersion Modelling, fugitive dust sources, emission factors, open pit mines*

## **INTRODUCTION**

A key element for the environmental protection in areas where open pit mines operate is the mitigation of air pollution caused by the dust emitted from the various mining operations. The reliable quantification of the fugitive dust emissions, an obligation of the mining enterprises according to the Regulation 166 (2006), with a special emphasis in the contribution of each mining activity is the first step in applying corresponding countermeasures.

The selection of the proper emissions quantification methodology is case-specific. For example, in the case of diffuse dust sources, as in the open pit mines of the Western Macedonia Lignite Centre (WMLC), the most applicable methodology is the one using emission factors. These factors relate the quantity of a pollutant emitted in the atmosphere with the associated activity and are expressed as mass of emitted pollutant per a mass, volume, distance or duration unit that quantifies the corresponding activity. Due to the strong dependency of emission factors on the mining method and equipment, as well as the meteorological characteristics of each area, the use of standard emissions factors available in the literature could lead to results with large uncertainties for the diverse activities of the WMLC. As a result,

derivation of emission factors compatible with the area and the activities under study is necessary for a reliable calculation of fugitive dust emissions.

The current work presents the methodology of such a calculation regarding the estimation of emissions of Particulate Matter with aerodynamic diameter up to 10µm (PM<sub>10</sub>) from open mines as the sum of emissions from each fugitive dust source, and the standardisation of the resulting emission factors into empirical relations. The whole study was conducted in the framework of the program “THEOFRASTOS”, with field campaigns carried out in the WMLC open mines over a three-year period.

## METHODOLOGY

In the present study, emission factors for fugitive dust are estimated using the Inverse Dispersion Modelling (IDM) method. Two different dispersion models are applied in order to obtain emission estimates on the basis of detailed measurements of PM concentrations near specific activity locations.

### Field measurements

The method applied in the current study for determining emission rates followed the “upwind – downwind approach (EPA-454/R-93-037, 1993), where PM<sub>10</sub> concentrations measurements are performed upwind and downwind the fugitive dust source combined with an IDM calculation (BS EN 15445:2008). Prior to the commencement of each field measurement, the prevailing wind direction in the area under study was determined.

Field measurements were conducted around all the main fugitive dust sources (excavation – transportation – deposition for barren, lignite and ash) in the four open mines of the WMLC, namely South Sector (SS), Kardias (K), Mavropigi (M) and Amyntaio (A) during the hot (May to October) and the cold (November to April) periods. Five PM<sub>10</sub> concentration analysers with parallel meteorological parameters measurement were installed for each experiment. Critical parameters for the calculation of emission rates were recorded, along with the meteorological conditions during the experiments, the materials characteristics (e.g. silt content, humidity), the control measures that are applied by the mining operators for the reduction of the emitted dust (e.g. wetting) and the activity capacity (e.g. quantity and type of material handled, unloading height, vehicle speed).

Additionally, material sampling was performed in every experiment with the samples matching the material handled by the activity under study. These samples were analysed in the laboratory in terms of their humidity and silt content, according to standard method (ASTM-C-136; Krestou et al, 2011). In a total, 74 sets of field measurements were conducted, out of which 63 were considered adequate for further analysis.

### Inverse dispersion modelling

The Inverse Dispersion Modelling approach provides an estimate of the mean emission rate of each source by a statistical analysis of a) the upwind-downwind PM<sub>10</sub> concentrations measured in appropriately selected points, and b) the corresponding calculated dispersion rates,  $\alpha$ , in order to solve equation (1):

$$c_{rd}(t) = \sum_i c_{ird}(t) = \sum_i \alpha_{ird} e_{id} \quad (1)$$

where  $c_{rd}$  is the measured downwind – upwind concentration increment,  $c_{ird}$  is the concentration of particles with aerodynamic diameter  $d$  that are emitted from the source  $i$  in the sampling location  $r$ ,  $\alpha_{ird}$  is the dispersion rate of particles with aerodynamic diameter  $d$  between the source  $i$  and the sampling area, and  $e_{id}$  is the (unknown) emission rate of particles with aerodynamic diameter  $d$  emitted from the source  $i$ , to be estimated.

The dispersion of the fugitive matter depends on the location and geometry of the source, the topography of the area and the aerodynamic diameter of the fugitive particles. Using the proper source geometry and dispersion model, and applying a fixed emission rate  $e_{id}^l = 1 \text{ gs}^{-1}$ , dispersion rate  $\alpha$  can be calculated in

various locations around the considered source. The contribution of other sources can be isolated by parallel sampling in multiple points and the estimation of the correlation coefficient  $R_\alpha$  among the corresponding dispersion rates  $\alpha$ .

In this work, dispersion calculations were performed using the AERMOD V 8.0.5 and AUSTAL 2000 models. AERMOD is a Gaussian model recommended amongst others by USEPA for the State Implementation Plan in current sources, for New Source Review and for the development of Prevention of Significant Deterioration programs. AUSTAL 2000 (Janicke and Janicke, 2003) is a Lagrangian particle model developed for the German Federal Environment Agency in accordance with German benchmark VDI 3945. The calculations take into account the influence of local topography in determining the local flow field and thus the dispersion patterns of emitted pollutants.

### Empirical relations and dispersion calculations

The application of the IDM methodology provided a set of emission rates ( $e_{id}$ ) and emission factors ( $e_{f,id}$ ) for each individual experiment. These site-specific factors were then correlated with activity data in a regression calculation in order to obtain empirical formulas for the calculation of the per-activity type emission factors  $E_{f,i}$ . The obtained empirical relations relate each per-activity emission factor to several independent variables corresponding to measured parameters, such as the silt content (%) and humidity (%) of the materials handled, the wind speed ( $ms^{-1}$ ) etc. Calculated per-activity type emission rates can be further used as input in a dispersion model in order to determine the PM<sub>10</sub> contribution of each dust source ( $C_{ij}$ ) at selected receptor points as well as to apportion the contribution of each separate mine ( $C_x$ ,  $x=SS, K, M, \text{ or } A$ ) on the total measured PM<sub>10</sub>. Equation (2) (USEPA, 2009) provides the mass of fugitive dust generated from activity  $i$  during one day as,

$$E_i = A_i \times E_{f,i} \prod (1 - n_j) \quad (2)$$

where,  $E_i$  is the PM<sub>10</sub> mass emitted from activity  $i$ ,  $A_i$  is the capacity of activity (usually proportional to the mass of material handled),  $E_{f,i}$  is the emission factor of the activity expressed in mass of fugitive dust per mass of materials handled and  $n_j$  is the effectiveness of emission control measures (if any), applicable to the activity  $i$ . The emission factor of each activity,  $E_{f,i}$ , is expressed by equation (3) (Cowherd, 2001).

$$\text{Emission Factor, } E_f = \frac{\text{emission Rate, } E_r}{\text{activity per time unit}} \quad (3)$$

The total mass of PM<sub>10</sub> emitted from one mine is equal to the sum of PM<sub>10</sub> mass emitted from every activity type in the mine.

### EXAMPLE APPLICATION

In the following sections, an example of the application of the methodology is given for a case of a specific activity, namely open-pit deposition of assorted material (barren and ash) from a boom conveyor.

#### Field measurements

During the cold period, three field tests concerning the measurement of PM<sub>10</sub> emissions from assorted unloading using a boom conveyor were conducted in the open pit mines of SS, K, M on 12/02/2011 (13:00 - 19:00 local time), 15/11/2011(13:00-16:00 local time) and 15/03/2012 (11:00-19:00 local time), respectively. As far as the A open pit mine is concerned, heavy weather conditions generating high risks in reaching the place of the certain activity in the mine as well as operational problems of the unloading equipment, made the field measurements impossible to perform.

During the hot period, field tests were conducted in all four open pit mines SS, K, M and A on 22/07/2011(12:00 - 18:00 local time), 07/09/2012 (12:00 - 17:00 local time), 01/07/2014 (12:00 - 19:00 local time) and 16/07/2013 (11:00 - 17:00 local time), respectively.

Material moisture- and silt content varied from 12.24% to 45% and 0.8% to 9.23%, respectively, during the cold period, while the average wind speed for the same period was  $4.0 \text{ ms}^{-1}$ . Corresponding values for the hot period were 10.95% - 29.89% for moisture content, 1.33% - 18.42% for silt content while the average wind speed was equal to  $3.5 \text{ ms}^{-1}$ .

### Inverse dispersion modelling

In total 65  $\text{PM}_{10}$  hourly concentration measurements (34 during the cold and 31 during the hot period) were collected for the calculation of the  $\text{PM}_{10}$  emission rate from the activity under study by means of the IDM method. For each one of these concentration measurements, the hourly downwind – upwind concentration increment ( $\Delta C$ ) was calculated and plotted versus the dispersion rate ( $\alpha_{\text{irad}}$ ) calculated by means of the AERMOD and AUSTAL 2000 models, the slope of the resulting linear graph corresponding to the mean emission rate ( $\text{gs}^{-1}$ ) of the fugitive source under study. The average discrepancy between emission rates for this activity, as calculated separately by AUSTAL 2000 and AERMOD was 22%, with the former model systematically providing lower values, corresponding to an overestimation of concentrations. This effect could be attributed to the different algorithms in the two models for estimating atmospheric stability on a hourly basis, which in the case of AUSTAL is based on the Turner’s empirical scheme, potentially leading to an over-prediction of stable conditions. Nevertheless, concentrations calculated from both models exhibited good correlation with measurements. A linear regression was performed over the combined set of concentrations provided by the two models, rejecting all values giving unusual residuals until correlation coefficient  $R$  became higher than 0.8. Following this procedure, the mean  $\text{PM}_{10}$  emission rate from open-pit deposition of barren and ash from a boom conveyor was estimated equal to  $4.2452 \text{ gs}^{-1}$ .

In Figure 1, an example of average surface area  $\text{PM}_{10}$  concentrations is presented, attributed to an unloading activity in the South Sector mine during the cold period, as resulted from AUSTAL 2000 calculations with and without the influence of topography. As shown in this figure, with the incorporation of the real topography the  $\text{PM}_{10}$  dispersion is further restricted in the Southwest area of the mine while it is enhanced towards the prevailing south-eastern wind direction. Further sensitivity analysis of  $\text{PM}$  dispersion for various mining activities indicated that the topography of the terrain around the activities needs to be considered in the dispersion calculations.

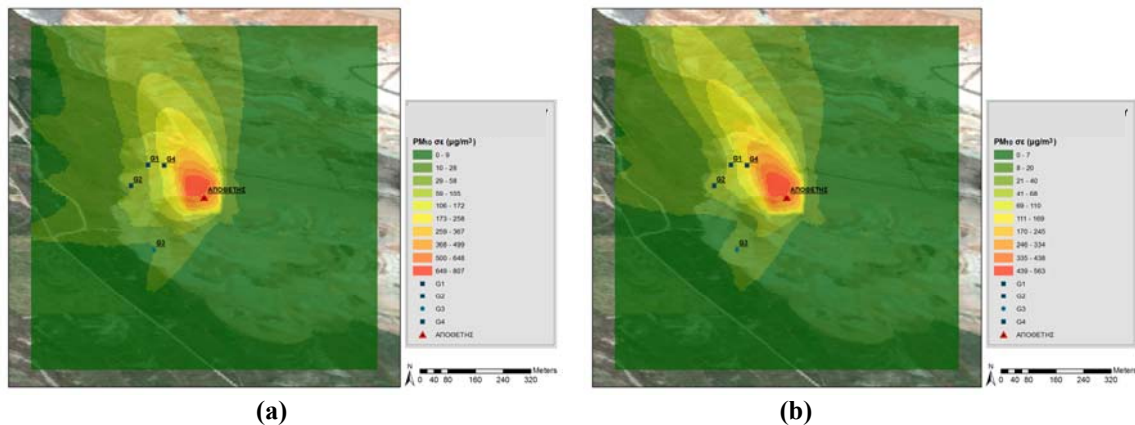


**Figure 1.** Average surface concentrations of  $\text{PM}_{10}$ , calculated for a) flat and b) complex (actual) topography.

### Empirical relations

The Multiple Linear Regression (MLR) method from the STATGRAPHICS software was used for the development of the corresponding empirical mean emission factor. The first step was to determine the variables (moisture content, silt content, wind speed) that influence the value of the emission factor of interest. These variables together with the corresponding per-site emission factors (calculated for the certain time period the variables refer to) were tabulated for all mines and for both periods (in total 20 couples of emission – variables were tabulated). Linear regression for the logarithm of the emission – variables data points was performed and the significance  $P$  of each variable was evaluated in terms of

participating in the empirical equation. Following this procedure, moisture content ( $M$ ) and wind speed ( $u$ ) were decided to be included in the empirical equation since their  $P$  value was lower than 0.05.

Using as dependent variable the natural logarithm of emission factor over a specific period and as independent variables the corresponding  $\ln M$  and  $\ln u$  values, the MLR was repeated four times rejecting each time outlier values until  $P < 0.05$  and  $R > 0.8$  was achieved. A total of 5 outliers were rejected, therefore 15 out of 20 data points were used for the development of the final relation representing the emission factor of open-pit deposition of assorted (barren and ash) from a boom conveyor, shown below:

$$E_f = 0.285 \times \frac{u^{3.627}}{M^{2.924}} \quad (R^2=89.28\%) \quad (4)$$

Each such empirical relation is provided to the end user with specified ranges of validity for the independent variables. In the case of equation (4), its recommended range of application is  $11\% < M < 42\%$  and  $1.6 \text{ ms}^{-1} < u < 8.2 \text{ ms}^{-1}$ .

## CONCLUSIONS

The quantification of dust emissions from open pit mines is imposed by the EC under the European registry of pollutant release and transfer. This obligation, together with the necessity for an air quality monitoring plan to be developed in areas with intensive industrial activity, as is the area of Western Macedonia, has led to the implementation of the project "THEOFRASTOS" aiming to a) quantify the  $\text{PM}_{10}$  emissions from each activity taking place in open lignite mines in Western Macedonia, b) quantify total  $\text{PM}_{10}$  emissions for every open lignite mine, and c) develop proper empirical formulas for the calculation of the aforementioned emissions from the current and future activities of WMLC. The goal of the project was achieved by conducting field measurements through the cold and hot periods of a 3-year period in each mine and applying the Inverse Dispersion Modelling method for determining per-site emission rates. Results using two different dispersion models have shown good correlation with measurements but AUSTAL 2000 appears to systematically overestimate concentrations around activity spots. Model results were then introduced in a multiple linear regression calculation in order to obtain per-activity emission rates as well as a set of robust empirical relations that can be applied over a variety of conditions to estimate total emissions from mining activities.

**Acknowledgements:** Authors would like to thank the WMLC for the financial support of the project, and its employees for their help during the field experiments.

## REFERENCES

- ASTM-C-136, Standard test method for Sieve Analysis of Fine and Coarse Aggregates, 2001.
- BS EN 15445:2008, "Fugitive and diffuse emissions of common concern to industry sectors. Qualification of fugitive dust sources by reverse dispersion modeling", September 2008.
- Cowherd C., JR (2001), "Fugitive dust emissions", Aerosol measurement: Principles, Techniques and Applications, (eds. Paul A. Baron and Klaus Willeke), Wiley-InterScience, Inc, 2001, Second Edition pp. 845-856.
- EPA - 454/R-93-037, 1993 "A Review of Methods for Measuring Fugitive  $\text{PM}_{10}$  Emission Rates".
- IIASA, IR-02-06, Modelling Particulate Emissions in Europe
- Janicke, L. and U. Janicke, 2003: A modelling system for licensing industrial facilities. Entwicklung eines modellgestützten Beurteilungssystems für den anlagenbezogenen Immissionschutz, UFOPLAN 200 43 256, on behalf of the German Federal Environmental Agency (UBA).
- Krestou A., A. Triantafyllou, A. Garas, C. Diamantopoulos and F. Pavloudakis, 2011: First experimental results of particulate matter emission sources characteristic parameters. 4<sup>th</sup> Environmental Conference of Macedonia, Thessaloniki, March 2011.
- Regulation (EC) No 166/2006 of the European Parliament and of the Council of 18 January 2006 concerning the establishment of a European Pollutant Release and Transfer Register and amending Council Directives 91/689/EEC and 96/61/EC
- USEPA (2009) Emission factors & AP 42. <http://www.epa.gov/ttnchie1/ap42/>. Accessed 13 July 2009

**17th International Conference on  
Harmonisation within Atmospheric Dispersion Modelling for Regulatory Purposes  
9-12 May 2016, Budapest, Hungary**

---

**OPTIMIZING INITIAL VALUES AND EMISSION FACTORS ON MESOSCALE AIR  
QUALITY MODELLING USING 4D-VAR DATA ASSIMILATION**

*Isabel Ribeiro<sup>1</sup>, Zoi Paschalidi<sup>1</sup> and Hendrik Elbern<sup>1,2</sup>*

<sup>1</sup> Rhenish Institute for Environmental Research (RIU-EURAD) at the University of Cologne, Germany.

<sup>2</sup> Research Centre of Jülich, Institute for Energy and Climate Change – Troposphere (IEK-8), Germany.

**Abstract:** The use of models to analyse the complex atmospheric physical and chemical processes deals with significant uncertainties of key parameters and input information, most prominently emission rates and chemical background information. In this frame, the four-dimensional variational (4D-var) data assimilation scheme for gas-phase and aerosols, encoded in the EUROpean Air pollution Dispersion – Inverse Model (EURAD-IM), was used to improve concentrations predictions of gaseous and aerosol species in the troposphere through corrections on emission rates jointly with initial values. The Po valley region was defined as a case study due to the availability of PEGASOS campaign observational data measured by the Zeppelin NT instruments. Observed data from the campaign, ground stations and satellite retrievals were assimilated by the EURAD-IM system, resulting in a model performance improvement not only at the surface level but also in height within the planetary boundary layer (PBL).

**Key words:** Data assimilation, inverse modelling, initial values and emission factors optimization

## **INTRODUCTION**

The complexity of atmospheric models has been rising with the increase of computational power and scientific knowledge, leading to higher spatial and temporal resolutions as well as more sophisticated physical and chemical processes. However, to obtain a good prediction it is also needed to start from reasonable initial values estimation. The provision of a set of optimum initial values (IV) by employing as much observational data as possible is the classical goal of data assimilation, combining observations with physical and chemical knowledge of atmospheric processes encoded in the numerical models (Kalnay, 2003).

Besides the initial values, the application of space-time-dimensional variational data assimilation (4D-var DA) also allows the estimation of emission factors (EF) due to the comprised inverse modelling technique (Elbern et al., 2007). The 4D-var DA algorithm propagates the model forward and backward in time fitting the model simulation to the set of observations, distributed in a predefined time interval (assimilation window). By this way, the model is able to calculate the system state that lays in the minimum distance between model and observations: the analysis state. The consistency of this system state is guaranteed by the inverse (or adjoint) simulation of the emitted species and their products. The sophisticated 4D-var DA scheme for gas-phase and aerosols included in the EURAD-IM (Elbern et al., 2007), is used to define an optimized set up to apply 4D-var assimilation of ground based measurements and satellite retrievals data. The optimal 4D-var application is the key to quantitatively estimate anthropogenic and biogenic pollutant concentration patterns, as well as to understand their interactions at a given air-shed, by the provision of improved IV and EF of gas-phase and aerosol species.

The EURAD-IM is an Eulerian mesoscale chemical transport model (CTM) that includes the Modal Aerosol Dynamics Model for Europe (MADE, Ackermann et al., 1998) to simulate the aerosol dynamics. The meteorological driver that is applied in the EURAD-IM is the Weather Research and Forecasting Model (WRF, Skamarock et al., 2008). For this work, the Po valley region was defined as a case study due to its high density of anthropogenic emissions and frequent occurrence of stagnant meteorological conditions that promote recurrent episodes of high air pollutant concentrations. The optimized model set up was used to assimilate data measured by the Zeppelin NT borne instruments of the PEGASOS

campaign over the same region, during 10-12.07.2012 (Li et al., 2014). The added value from the combination of PEGASOS campaign data by the 4D-var DA scheme is the provision of improved model results in the boundary layer. The corrections provided by the observed data to the numerical modelling system are explored in this work.

#### 4D-VAR DATA ASSIMILATION TECHNIQUE

Data assimilation methods use all the available information about the system to provide an as accurate as possible and consistent image of a system's state at a given time (the optimal guess). Within 4D-var DA the analysis problem is formulated as a minimisation problem using variational calculus. The definition of a cost function ( $J$ , Eq. 1) is necessary, aiming the calculation of the distance between the model simulation and the observations, during a predefined time interval (assimilation window) (Kalnay, 2003).  $J$  is derived from the properties of the mapping between the model space and the observational space (the forward model  $H$ ) and from the prognostic model  $M$  itself. Due to the fact that 4D-var algorithm propagates information forward and backward in time, it is regarded a smoother, fitting a model simulation to a set of observations distributed in a predefined assimilation window.

$$J(x_0, e_0) = J_{iv} + J_{obs} + J_{ef} \quad (1)$$

$$= \frac{1}{2} \left( [x_0 - x_b]^T \mathbf{B}^{-1} [x_0 - x_b] + \sum_{i=0}^N ([HM_i x_0 - y_i] R^{-1} [HM_i x_0 - y_i]) + [e_0 - e_b]^T K^{-1} [e_0 - e_b] \right)$$

Encoded on the EURAD-IM modelling system, the 4D-var DA scheme is able to optimize IV and EF benefiting from their individual impact on the model evolution (Elbern et al., 2007). The IV play an important role in the beginning of the assimilation window, while the EF optimization represents an influence through all the assimilation window. Consequently, an optimal result is given by joint optimisation of both parameters. In this sense, the total cost ( $J$ ) results from the sum of three individual costs: the background cost of the initial state of the chemical constituents ( $J_{iv}$ ), the observational costs ( $J_{obs}$ ) and the cost of the emission inventory, expressed as EF ( $J_{ef}$ ).  $J_{iv}$  and  $J_{ef}$  are, respectively, calculated taking into account the error covariance matrixes of the initial state of the chemical constituents ( $\mathbf{B}$ ), the emissions ( $\mathbf{K}$ ) and the observations ( $\mathbf{R}$ ).

#### METHODOLOGY AND CASE STUDY DESCRIPTION

The 4D-var DA algorithm described in the previous section is applied over the Po valley region, during the Pan-European Gas-AesoSOs Climate Interaction Study (PEGASOS) flight campaign, on 10-12 July 2012. This case study is partly motivated by the necessity to evaluate the 4D-var data assimilation analysis performance in a highly resolved grid over polluted areas, such as Po valley, as well as the new opportunities provided by the airborne data to the model in terms of: distinguishing emission patterns, investigating the vertical distribution of trace gases and the PBL dynamics. To this end, the current study applied the 4D-var data assimilation method by EURAD-IM. For that, a sequence of three domains (Figure 1) is used starting with the coarse grid covering Europe, followed by the central Europe and finally the Po valley area, with 15×15, 5×5 and 1×1 km<sup>2</sup> of horizontal resolution, respectively. Further, the optimisation of EF in nested grids of 1×1 km<sup>2</sup> resolution is studied, addressing the issue of the

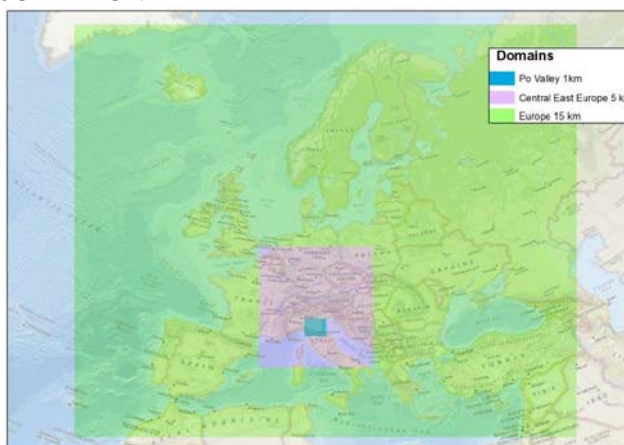


**Figure 16.** The sequence of nests in EURAD-IM. The coarse grid is Europe with 15×15 km<sup>2</sup> resolution which includes two nest domains: the central Europe and the area of Po Valley in Italy with 5×5 km<sup>2</sup> and 1×1 km<sup>2</sup> resolution, respectively.

Further, the optimisation of EF in nested grids of 1×1 km<sup>2</sup> resolution is studied, addressing the issue of the

representatively of observations such as NO<sub>2</sub>. Taking advantage of the high quality airship campaign measurements, special focus is given on the analysis of the vertical mixing in the PBL with EURAD-IM.

The set of observations used here consists of ground based and satellite measurements as well as PEGASOS campaign data. AirBase measurements of NO<sub>2</sub>, O<sub>3</sub>, NO, SO<sub>2</sub> and CO were combined with the O<sub>3</sub> and CO observations from MOPITT and NO<sub>2</sub> tropospheric columns of GOME-2. The vertical profiles of NO<sub>2</sub>, O<sub>3</sub> and CO from the flight campaign over the rural supersite of San Pietro Capofiume (SPC) were also used.

For aerosols, the 4-Dvar scheme included in the EURAD-IM modelling system is at an earlier stage of development than for the gas-phase. Currently, it only includes the IV optimization, the EF optimization being in a development stage. The study here presented is focused on the European domain (15x15 km<sup>2</sup>) and comprehends assimilation of above-mentioned species plus PM10, PM2.5 and NH<sub>3</sub> from the AirBase network as well as aerosol optical depth (AOD) retrievals from MODIS satellite. Based on this case study, the performance of the EURAD-IM 4D-var data assimilation scheme with joint optimisation of IV and EF for gas-phase, and the IV optimization for aerosols, is assessed in the following section.

### CASE STUDY ANALYSIS

The accuracy of the EURAD-IM 4D-var data assimilation scheme is assessed by highly resolving grids, together with the joint optimisation of IV and EF for gas-phase. Figure 2 underlines the benefit from the joint optimisation, illustrating the differences between the analysis result and the model's first guess in case of NO<sub>2</sub> concentrations and the NO<sub>x</sub> emission factors correction, during the first day of assimilation (10.07.2012). The increased optimization of NO<sub>x</sub> emission factors, up to a factor of 4, correct the general underestimation of the model for the NO<sub>2</sub> concentration. Moreover, as the domain is 1 km grid spacing, emission patterns can be resolved and the problem of the representatively of NO<sub>2</sub> observations is diminished in comparison with less resolved grids (not shown here).

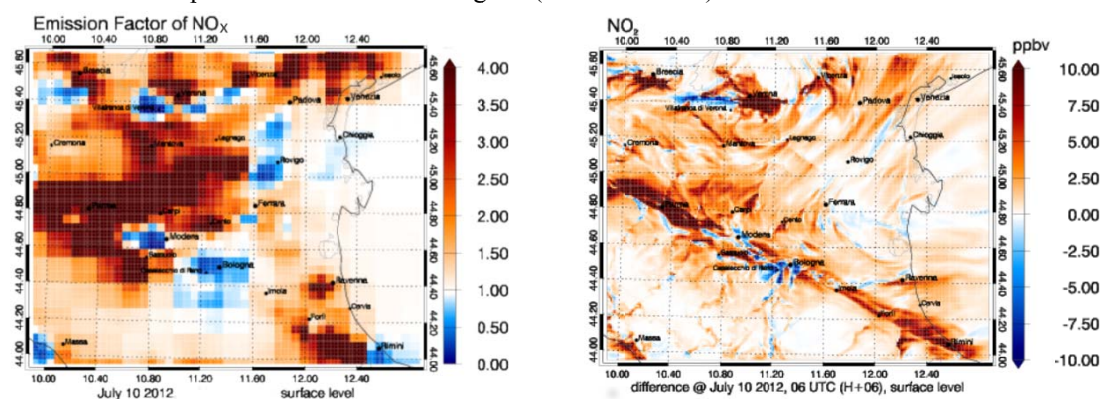


**Figure 2.** Differences between the analysis and the background for NO<sub>2</sub> during morning rush hour (06:00 UTC) over Europe (left panel) and over the Po valley area (right panel), on 10.07.2012.

Validating the analysis output for each resolution, a comparison with independent observations took place. Figure 3 depicts the timeseries of NO<sub>2</sub> and O<sub>3</sub> concentrations for the analysis result of the three different domains against measurements of two stations in Italy that are not included into the assimilation procedure. For both the emitted NO<sub>2</sub> and its product O<sub>3</sub>, the optimisation is more efficient for the finest nest grid (blue curve). The good representativeness of NO<sub>2</sub> observations for the 1 km resolved grid is obvious, fact that also influences the analysis of O<sub>3</sub>, since the system maintains its chemical consistency. The afternoon peak of NO<sub>2</sub> analysed concentrations in case of the second nest (blue curve) presumably comes from the assimilation of observations from other stations over areas with higher traffic activity, fact that is not possible to recognised in case of the less resolved grid.

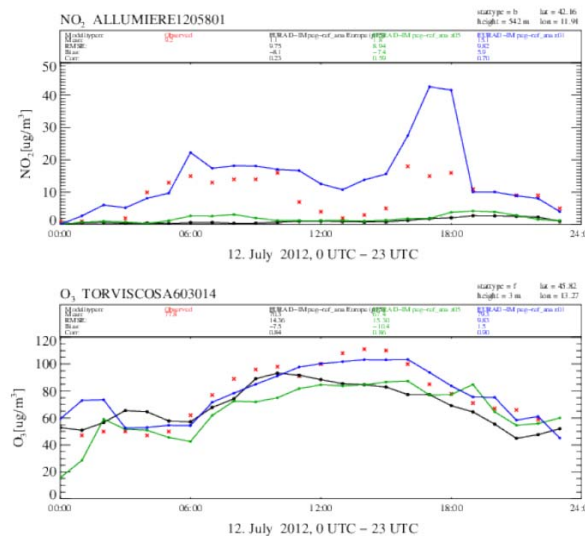


**Figure 18.** Timeseries of NO<sub>2</sub> (upper panel) and O<sub>3</sub> (lower panel) concentrations regarding the three domains, for two ground stations non-assimilated observations (Allumiere and Troviscosa, in Italy). Observations are given in red; the analysis are given in black for the European domain, in green and blue for central Europe and Po valley, respectively.

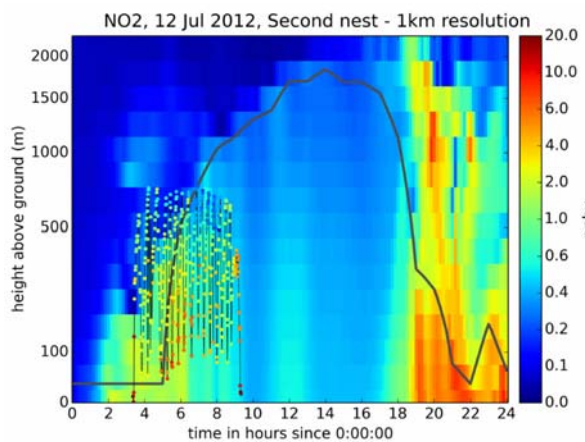


**Figure 19.** Hovmöller plot. Timeseries of PBL and the vertical NO<sub>2</sub> concentrations at SPC: observations from the flight campaign (dots) and model results from concerning the Po valley domain (background).

Figure 4 depicts the Hovmöller plot for the assimilation of the PEGASOS airborne observations, on 12.07.2017, over the SPC supersite, taking into account the finest nest ( $1 \times 1 \text{ km}^2$  of spatial and 25 seconds of temporal resolution). Compared with the analysed concentrations (background colour), there is a match with them and the airborne data in upper altitudes (500-700m) from the beginning of the flight until around 8:00, as well as at close to 300 m until 6:00. On the other hand, in the model's mixed layer, the observed NO<sub>2</sub> concentrations are higher than the analysed ones, up to 300-400 m. The Zeppelin's observations capture clearly the layered structure of the PBL (see also Li et al., 2014), however differently than the model. In other words, the campaign data underline that the model calculates a higher PBL than it is measured. Although there is a correction of the analysed concentrations towards the observations, this does not influence the calculation of the PBL by the model. Thus, during the model analysis the mixing takes place in higher altitudes.

Regarding the aerosols, the optimal dimension of the assimilation window was tested, taking into account only IV optimization for both gas-phase and aerosols. In other words, how many hours of observations are needed to provide improved model information with as less computing time consumption as possible? Two ranges of assimilation windows were tested: 12h and 6h which allowed to verify that the shortest assimilation window provides better analysis reducing the root mean square error in 8%. Nevertheless, the better analysis achieved was still far of the observations (observed mean value is  $19.5 \mu\text{g}\cdot\text{m}^{-3}$  while for analysis (6h) it is  $6.7 \mu\text{g}\cdot\text{m}^{-3}$ ). As aerosols formation is highly dependent of gas-phase, the previous best analysis (6h assimilation window) was compared against the analysis from 24h of assimilation window with optimization of IV (gas-phase and aerosols) and EF from gas-phase. Combining gas-phase with aerosol optimisation improved the analysis in 22% (Figure 5).

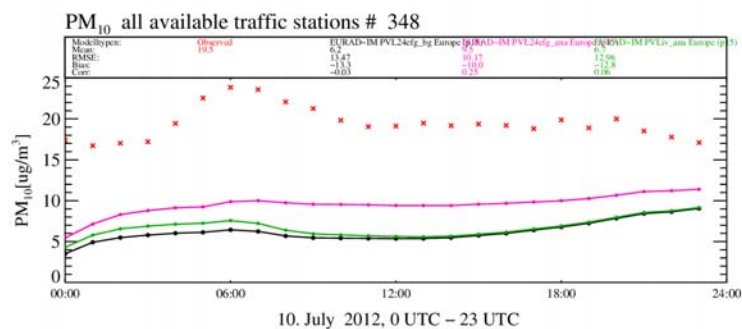


**Figure 5.** Timeseries for PM<sub>10</sub> concerning the average of all AirBase station with traffic influence over the European domain. Observations are given in red, background in black; analyses with 6h of assimilation window in green and with joint optimization of aerosol and gas-phase are in pink.

## CONCLUSIONS

The joint optimisation of IV of the chemical constituents and EF has been successfully employed for a 24 hours assimilation window, letting the better-known diurnal emission profiles be considered as strong constraint. The high resolution nesting technique is shown to face the representativity of NO<sub>2</sub> observations in the finest grid, being able to identify traffic emissions and more accurate emission patterns. Beyond that, it was verified that rich campaign measurements have been essential to the model analysis as they give a more detailed insight than the routine data to the horizontal and vertical dispersion of the emissions in polluted areas. Regarding aerosols, the IV optimisation has shown as effective, the joint EF optimisation is crucial to an accurate prediction, however.

## ACKNOWLEDGEMENTS

The authors gratefully acknowledge the computing time granted by the John von Neumann Institute for Computing (NIC) and provided on the supercomputer JURECA at Jülich Supercomputing Centre (JSC).

## REFERENCES

- Ackermann, I.J., Hass, H., Memmesheimer, M., Ebel, A., Binkowski, F.S., Shankar, U., 1998. Modal aerosol dynamics model for Europe. *Atmos. Environ.* **32**, 2981–2999. doi:10.1016/S1352-2310(98)00006-5
- Elbern, H., Strunk, A., Schmidt, H., Talagrand, O., 2007. Emission rate and chemical state estimation by 4-dimensional variational inversion. *Atmos. Chem. Phys.* **7**, 3749–3769. doi:10.5194/acp-7-3749-2007
- Kalnay, E., 2003. Atmospheric modeling, data assimilation, and predictability, *Annals of Physics*. doi:10.1256/00359000360683511
- Li, X., Rohrer, F., Hofzumahaus, A., Brauers, T., Häseler, R., Bohn, B., Broch, S., Fuchs, H., Gomm, S., Holland, F., Jäger, J., Kaiser, J., Keutsch, F.N., Lohse, I., Lu, K., Tillmann, R., Wegener, R., Wolfe, G.M., Mentel, T.F., Kiendler-Scharr, A., Wahner, A., 2014. Missing gas-phase source of HONO inferred from Zeppelin measurements in the troposphere. *Science* **344**, 292–6. doi:10.1126/science.1248999
- Skamarock, W.C., Klemp, J.B., Dudhia, J., Gill, D.O., Barker, D.M., Huang, X.Y., Wang, W., Powers, J.G., 2008. A Description of the Advanced Research WRF Version 3.

**17th International Conference on  
Harmonisation within Atmospheric Dispersion Modelling for Regulatory Purposes  
9-12 May 2016, Budapest, Hungary**

---

**SOURCE REGIONS OF BIOGENIC AEROSOLS IN WROCLAW (POLAND) AND THE  
INFLUENCE OF METEOROLOGICAL DATA ON THE HYSPLIT MODEL RESULTS**

*Daria Bilińska<sup>1\*</sup>, Carsten Ambelas Skjøth<sup>1,2</sup>, Małgorzata Werner<sup>1</sup>, Maciej Kryza<sup>1</sup>, Małgorzata Malkiewicz<sup>3</sup>, Justyna Krynicka<sup>1</sup>, Anetta Drzeniecka-Osiadacz<sup>1</sup>*

<sup>1</sup> Department of Climatology and Atmosphere Protection, University of Wrocław, Poland

<sup>2</sup> National Pollen and Aerobiology Research Unit, Institute of Science and the Environment,  
University of Worcester, Henwick Grove, WR2 6AJ, Worcester, UK

<sup>3</sup> Institute of Geological Sciences, University of Wrocław, Poland

**Abstract:** We have investigated the relationship between the inflow of air masses and the ragweed and birch pollen concentration in SW Poland (Wrocław) for a 10-year period of 2005-2014. The HYSPLIT model was used to calculate trajectories for high pollen concentrations and for the entire pollen season for both species. The results show that the episodes of high pollen ragweed concentration (above 20 pm<sup>-3</sup>) represent a great part of total recorded ragweed pollen in Wrocław. The high pollen episodes are connected with air masses coming from south and south-west Europe, which confirms the existence of known ragweed centres but showed that other centres for SW Poland are not present. The footprint areas for birch suggest that the source of the pollen grains are mainly local trees but appear to be augmented by remote sources.

**Key words:** *Ambrosia artemisiifolia*, *Betula*, HYSPLIT, bioaerosols

## INTRODUCTION

*Ambrosia artemisiifolia* (ragweed) is an invasive species for Europe. It was accidentally introduced in Europe through agricultural products from the USA (Chauvel et al. 2006) and since the 2nd World War ragweed has established in abundance at several locations with the main centres on the Pannonian Plain, northern Italy, France and Ukraine (e.g. Smith et al. 2013). Regarding *Betula* (birch), Poland has been identified as an area with large amounts of birch pollen from both forest and small woodlands (Skjøth et al. 2013).

Both ragweed and birch are very troublesome plants because their pollen is very allergenic (Burbach et al. 2009, van Ree et al. 1999). The study on patients visiting specialist centres within the Global Asthma and Allergy European Network has shown standard sensitization rates to birch pollen of 24% and 28%, respectively for Europe and Poland.

In the case of ragweed, very low concentrations, such as 5–10 pm<sup>-3</sup> can cause allergic reactions in sensitized patients (Tamarcaz et al. 2005) and the symptoms include rhino-conjunctivitis and more rarely contact dermatitis or urticaria (Tamarcaz et al. 2005), while concentrations such as 10-20 pm<sup>-3</sup> nearly always cause allergic symptoms in these patients (Bergmann et al. 2008).

It should be noted, almost 30% of Wrocław's population suffer because of allergies. Exposure to air pollution may account for this increased prevalence. Air pollutants not only have a direct or indirect effect on the health, but also might exert important actions upon aeroallergens. Pollen in heavily polluted zones can express a larger amount of proteins described as being allergenic. It seems necessary to air pollution may exaggerate the effects of aeroallergens. Therefore in order to improve human health, it seems very important to carry out simultaneous studies on the variability of allergenic pollen of anemophilous plants and air pollution concentration.

Numerical models are useful tools to analyse atmospheric transport and to determine the source areas of bioaerosols. One of the most applied models in aerobiology is HYSPLIT that has been used to study atmospheric transport of a number of species such as *Olea* pollen in southern Iberian Peninsula

(Fernandez-Rodriguez et al. 2014; Hernandez-Ceballos et al. 2014), ragweed pollen in several European countries (Smith et al. 2013), birch pollen in central and northern European countries (e.g. Skjøth et al. 2007; Veriankaite et al. 2010).

The main aim of our study is to investigate the relationship between the inflow of air masses and the concentration of ragweed and birch pollen in south-west Poland (Wroclaw) for a 10-year period of 2005-2014. We investigate if high concentrations of ragweed and birch can be attributed to regions outside of the main known centres in Europe.

## DATA AND METHODS

### Pollen data

The daily pollen concentration data cover a 10-year period of 2005-2014. The measurements were carried out at the Wroclaw station in south-west Poland (51.1164N, 17.0278E) using a Burkard 7-day volumetric pollen trap. The sampler (borrowed from the Centre for Research on Environmental Allergens in Poland) is placed in the city centre, on the roof of the building at a height of 20 m above ground level. In the immediate vicinity of the sampling site, there are a dense urban built-up areas and scanty patches of greenery. From the south, the building is surrounded by an alley of plane trees, while several horse-chestnut trees and small birches grow to the north of the building (Malkiewicz et al. 2014).

For ragweed, we analysed two months (August and September) of each year during the 2005-2014 period, which cover the blooming season of *Ambrosia artemisiifolia* (e.g. Makra et al. 2005; Šikoparija et al. 2009). For birch, we analysed the period between day of start and end of birch season of each year. Periods lasted from 25 to 38 days (on average 30 days).

The data were divided into two groups of low (<20 pm<sup>-3</sup>) and high (>20 pm<sup>-3</sup>) concentration, which is a method that has been used in previous studies, e.g. in Stach et al. (2007), Šikoparija et al. (2009), Kasprzyk et al. (2011).

### Backward trajectories with HYSPLIT

The HYSPLIT (HYbrid Single-Particle Lagrangian Integrated Trajectory) model was used to analyse the entire observational record (2005-2014) with the meteorological data obtained from the Global Data Assimilation System (GDAS) with a 1° × 1° degree spatial resolution and 3 h temporal resolution. We used 96 hours backward trajectories with 2 hours intervals and with three different altitudes: 500, 1000 and 1500 meters above ground level (agl) as this is the standard methodology in many aerobiological studies (e.g. Fernández-Rodríguez 2014, Hernandez-Ceballos et al. 2014 and references therein). These parameters were taken in order to observe relationships between different inflowing air masses and concentration of ragweed and birch pollen. Trajectories were calculated for Wroclaw (51°06'N 17°05'E) and matched with the corresponding records with measured ragweed and birch concentrations. The trajectories were then sorted into two groups of low and high concentrations of pollen according to Stach et al (2007). Each day is represented by 36 trajectories, which reduces the uncertainty associated with individual trajectories (Stach et al. 2007) and also takes into account the variation in air flow pattern during the day. Using the HYSPLIT trajectories, foot print maps were created using the two main groups as in Skjøth et al. (2014). The analysis was done for the entire period (sum of trajectory points) and individually for each year of the period. Due to the page limit, the trajectories have been presented in the figure only for a high concentrations group and for four selected years.

## RESULTS

### Trajectories with HYSPLIT for the period of 2005-2014

The number of trajectories on days with high *Ambrosia* pollen concentrations is 756 (Figure 1). The dominant flow on those days was from south and south-eastern directions. It suggests that the air masses crossed the Pannonian Plain (e.g. Czech Republic, Slovakia, Hungary) and Ukraine on the high days.

The results for birch show that the dominant flow of air masses, during the high *Betula* season, was from west and south-west to east. The air masses crossed Germany, Czech Republic, Slovakia, Hungary, Netherlands, northern France and Belgium

#### **Foot print area with GDAS-HYSPLIT for individual years during 2005-14.**

##### **Ragweed**

There is a dominating western and north-western flow in August-September of each individual year of the period 2005-2014. For some years there is a second source areas of trajectories - southern or south-eastern direction for years 2006, 2007, 2011, 2014 and eastern direction for 2005, 2008 and 2012 (not shown in the figure). High pollen concentrations are mainly related to the flow either from the west or from the south or from both these directions (Figure 1). A special situation occurred in 2014, when high concentrations appear during the eastern flow. For the western and north-western flow (e.g. years 2009, 2011), the foot print area of trajectories covers Germany, northern and central France and the UK. During the southern flow (e.g. 2005, 2006, 2007, 2009, 2011), the foot print area covers mainly Northern and Central Italy and Pannonian Plain (Hungary, the Czech Republic, Romania, Slovakia). The main trajectory centre for the eastern flow is Ukraine.

##### **Birch**

The annual results for birch show that prevailing flow of air masses during the high days in the period 2005-2014 was from west and south-west directions (Figure 1). For 2005, 2006, 2007, 2010, 2011, 2014 the foot print area of trajectories covers Germany and the Benelux countries. For 2008, 2009 and 2012 the main trajectory source was south-west part of Europe (including Germany, Czech Republic, Slovakia and Hungary). The foot print area of trajectory does not appear to include Russia, Belarus, Scandinavia and the Baltic region. This is surprising because these areas have been previously identified as major source regions for birch pollen (Sofiev et al. 2006, Mahura et al. 2007). This situation could be caused because of general air flow pattern in investigated period - these source areas of birch pollen were not crossed by flowing air masses in investigated period.

#### **SUMMARY**

Our results show that ragweed pollen during 2005-2014 is not common in Wroclaw because its concentration is generally low during the flowering season. The exceptions are high pollen episodes, which are connected with flow of air masses from south (years: 2005, 2006, 2007, 2009 and 2011) or west Europe (years: 2009, 2011). For 2014 a high pollen episode is related to the eastern flow. The study confirms the existence of known ragweed centres but has also shown that other ragweed centres for south-west Poland are not present. High episodes are observed almost every year.

Poland is identified as areas with large amount of birch pollen (Skjøth et al. 2013). Low days in birch season represent only small part of sum of pollen in season. Our investigations show, that to these big amounts of birch pollen in Poland contribute also other source areas of birch pollen like Germany and the Benelux countries.

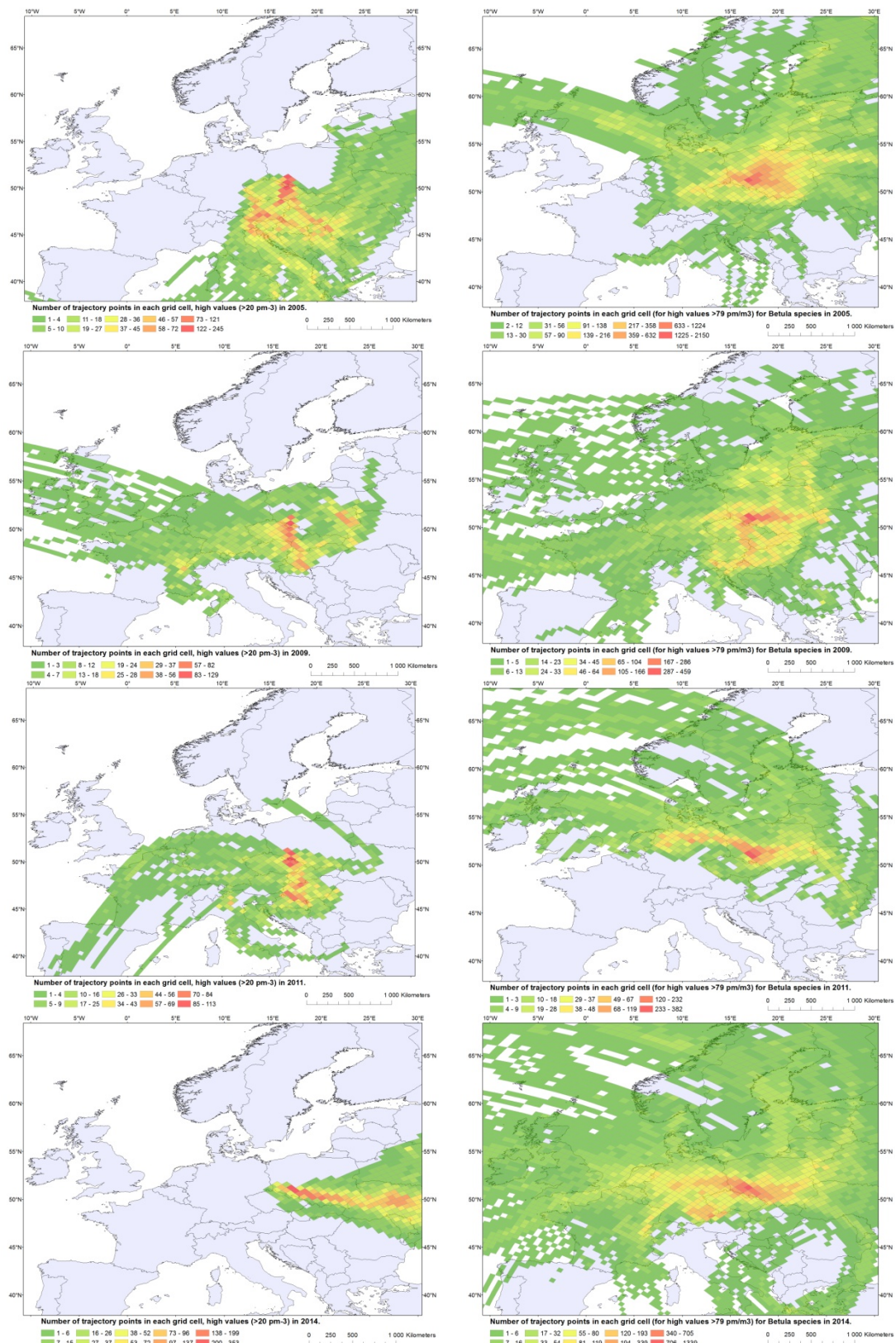


**Figure 1.** Number of trajectory points in each grid cell for high values of ragweed (left) and birch (right) concentrations for 2005, 2009, 2011, 2014 year. Calculations are based on HYSPLIT using GDAS data and 96 h backtrajectories for Wrocław at 500 m, 1000 m, 1500 m.

## ACKNOWLEDGEMENTS

The project was partially financed by European Union and co-financed by NFOSiGW within LIFE+ Program, Project: LIFE-APIS/PL - Air Pollution and biometeorological forecast and Information System. LIFE12 ENV/PL/000056

## REFERENCES

- Bergmann, K. C., D. Werchan and M. M. Zuberbier, 2008: The threshold value of *Ambrosia* pollen inducing acute nasal reactions is very low, *Allergo*, **17**, 375-376.
- Burbach, G. J., L. M. Heinzerling, C. Rohnelt, K. C. Bergmann, H. Behrendt and Zuberbier, 2009: T. Ragweed sensitization in Europe — GA(2)LEN study suggests increasing prevalence, *Allergy*, **64**, 664–5.
- Chauvel, B., F. Dessaint, C. Cardinal-Legrand and F. Bretagnolle, 2006: The historical spread of *Ambrosia artemisiifolia* L. in France from herbarium records, *J Biogeogr*, **33**, 665–73.
- Fernández-Rodríguez, S., C. A. Skjøth, R. Tormo-Molina, R. Brandao, E. Caeiro, I. Silva-Palacios, Á. Gonzalo-Garijo and M. Smith, 2014: Identification of potential sources of airborne *Olea* pollen in the Southwest Iberian Peninsula, *Int. J. Biometeorol*, **58**, Iss 3, 337-348.
- Hernández-Ceballos, M. A., C. A. Skjøth, H. García-Mozo, J. P. Bolívar and C. Galán, 2014: Improvement in the accuracy of backtrajectories using WRF to identify pollen sources in southern Iberian Peninsula *Int. J. Biometeorol*, **58**, 2031-204.
- Kasprzyk, I., D. Myszkowska, Ł. Grewling, A. Stach, B. Šikoparija, C. A. Skjøth and M. Smith, 2011: The occurrence of *Ambrosia* pollen in Rzeszów, Kraków and Poznań, Poland: investigation of trends and possible transport of *Ambrosia* pollen from Ukraine. *Int J Biometeorol*, **55**:633–44.
- Mahura A., U. Korsholm, A. Baklanov and A. Rasmussen, 2007: Elevated birch pollen episodes in Denmark: contributions from remote sources, *Aerobiologia*, **23**, 171–179, [doi.org/10.1007/s10453-007-9061-3](https://doi.org/10.1007/s10453-007-9061-3)
- Makra L., M. Juhász, R. Béczi and E. Borsos, 2005: The history and impacts of airborne *Ambrosia* (*Asteraceae*) pollen in Hungary, *Grana*, **44**, 57–64.
- Malkiewicz M., K. Klaczak, A. Drzeniecka-Osiadacz, J. Krynicka and K. Migala, 2014: Types of *Artemisia* pollen season depending on the weather conditions in Wrocław (Poland), 2002–2011, *Aerobiologia*, **30**, 13-23.
- van Ree R., W. A. van Leeuwen, J. H. Akkerdaas and R. C. Aalberse, 1999: How far can we simplify in vitro diagnostics for Fagales tree pollen allergy? A study with three whole pollen extracts and purified natural and recombinant allergens. *Clin Exp Allergy*, **29**, 848–855. <http://dx.doi.org/10.1046/j.1365-2222.1999.00521.x>
- Šikoparija B., M. Smith, C. A. Skjøth, P. Radišić, S. Milkovska, S. Šimić and J. Brandt, 2009: The Pannonian Plain as a source of *Ambrosia* pollen in the Balkans, *Int J Biometeorol*, **53**, 263–72.
- Skjøth C. A., P. Baker, M. Sadys and B. Adams-Groom, 2014: Pollen from alder (*Alnus sp.*), birch (*Betula sp.*) and oak (*Quercus sp.*) in the UK originate from small woodlands. Article in press
- Skjøth C. A., J. Sommer, A. Stach, M. Smith and J. Brandt, 2007: The long range transport of birch (*Betula*) pollen from Poland and Germany causes significant pre-season concentrations in Denmark, *Clinical and Experimental Allergy*, DOI: 10.1111/j.1365-2222.2007.02771.x
- Skjøth, C. A., B. Šikoparija and S. Jeger, 2013: Pollen Sources in Sofiev M, Bergmann KC, editors. Allergenic Pollen, Springer, [http://dx.doi.org/10.1007/978-94-007-4881-1\\_2](http://dx.doi.org/10.1007/978-94-007-4881-1_2), 9-27.
- Smith M., L. Cecchi, C. A. Skjøth, G. Karrer and B. Šikoparija, 2013: Common ragweed: a threat to environmental health in Europe. *Environ. Int*, **61**, 115–126.
- Sofiev M., P. Siljamo, H. Ranta and A. Rantio-Lehtimäki, 2006: Towards numerical forecasting of long-range air transport of birch pollen: theoretical considerations and a feasibility study. *Int J Biometeorol.*, **50**, 392–402. <http://dx.doi.org/10.1007/s00484-006-0027-x>
- Stach A., M. Smith, C. A. Skjøth and J. Brandt, 2007: Examining *Ambrosia* pollen episodes at Poznań (Poland) using back-trajectory analysis. *Int J Biometeorol*, **51**, 275–86.
- Taramarcaz P., C. Lambelet, B. Clot, C. Keimer and C. Hauser, 2005: Ragweed (*Ambrosia*) progression and its health risks: will Switzerland resist this invasion? *Swiss Med Wkly*, **135**, 538-548
- Veriankaite L., P. Siljamo, M. Sofiev, I. Sauliene and J. Kukkonen, 2010: Modelling analysis of source regions of long-range transported birch pollen that influences allergenic seasons in Lithuania. *Aerobiologia*, **26**, 47–62. <http://dx.doi.org/10.1007/s10453-009-9142-6>

**17th International Conference on  
Harmonisation within Atmospheric Dispersion Modelling for Regulatory Purposes  
9-12 May 2016, Budapest, Hungary**

---

**PRELIMINARY ANALYSIS OF OBSERVATIONS FROM THE JACK RABBIT II–2015 FIELD  
EXPERIMENT ON DENSE GAS DISPERSION IN A BUILT ENVIRONMENT**

*Steven Hanna<sup>1</sup>, Joseph Chang<sup>2</sup>, Thomas Spicer<sup>3</sup>, Michael D. Sohn<sup>4</sup>, Shannon Fox<sup>5</sup>, Mark Whitmire<sup>6</sup>,  
Leo Stockham<sup>7</sup>, Damon Nicholson<sup>8</sup>, Thomas Mazzola<sup>9</sup>*

<sup>1</sup>Hanna Consultants, Kennebunkport, ME;

<sup>2</sup>Homeland Security Studies and Analysis Institute, Falls Church, VA;

<sup>3</sup>Univ Arkansas, Fayetteville, AR;

<sup>4</sup>LBNL, Berkeley, CA;

<sup>5</sup>DHS S&T Chemical Security and Analysis Center (CSAC),  
Aberdeen Proving Ground, MD;

<sup>6</sup>Noblis, Falls Church, VA;

<sup>7</sup>Leidos, Albuquerque, NM;

<sup>8</sup>Dugway Proving Ground, UT;

<sup>9</sup>Engility, Lorton, VA, USA

**Abstract:** The Jack Rabbit II field experiment, carried out in August and September 2015 at Dugway Proving Ground, Utah, USA, involved five releases of 4.5 to 8.3 tons of pressurized liquefied chlorine within a “mock urban” environment of about 80 CONEX shipping containers set up on a staggered grid in a packed gravel area 122 m square. In addition, trailers and a two-wide by three-high CONEX stack were placed about 70 m downwind of the source, to study the transport and dispersion of dense gas around and inside urban structures. Chlorine was released at the center of a 25 m diameter concrete pad as a downward-directed two-phase momentum jet in about one minute from a horizontal tank with a 15 cm opening at about 1.0 m agl. The concrete pad’s center was positioned 31 m from the upwind edge of the mock urban area. Wind speeds at a height of 2 m ranged from 2 to 5 m/s during the five trials. Concentrations and winds were measured within the obstacle array and on 90° arcs at distances of 0.2, 0.5, 1, 2, 5, and 11 km. The initial jet formed a broad and shallow dense wall jet that rapidly spread in all directions to a distance of about 50 to 75 m, before moving with the wind across the urban array and over the desert surface downwind. When encountering obstacles, the wall jet mixed up and around them. Limited liquid pooling was observed on the concrete pad. Quantitative observations, photos, and videos have passed QA/QC, and this paper describes some results of preliminary analysis. For example, the decrease of concentration is seen to follow basic dense gas similarity relations.

**Key words:** *dense gas dispersion, chlorine releases, dispersion in urban built environment*

## **INTRODUCTION**

As has been known for many years, chlorine gas is very toxic (Marshall 1989). There has been much recent concern about the possible effects of pressurized liquid chlorine released from storage tanks and transportation vessels. Hanna et al. (2008) reviewed three railcar accidents involving chlorine, and compare predictions of six widely used dense gas models. It appears that, at these sites, there were fewer observed casualties than would be expected from the model predictions. Consequently, the U.S. Department of Homeland Security (DHS) initiated a research program to study the source emissions characteristics, transport and dispersion, and deposition of large releases of pressurized liquefied chlorine. Several other sponsors and collaborators also contributed resources. The research program is centered on the Jack Rabbit (JR) field experiments. JR I, which took place at Dugway Proving Ground (DPG) in the U.S. in 2010, used one and two ton releases from a tank mounted about 1 m above ground, with the initial jet pointed downward. The tank was in the center of a depression of depth 2 m and diameter 50 m dug into the flat desert surface. There were five releases of chlorine and five of

anhydrous ammonia, with about one to two tons released in each trial. Videos during the JR I chlorine experiments clearly show the two phase chlorine momentum jet striking the ground and deflecting into a donut-shaped dense wall jet (Hanna et al., 2012; Bauer, 2013). The characteristics of the releases conform to general models of mass flux, flashing, and velocities of jets from pressurized liquefied tanks (see Britter et al., 2011). Concentrations were measured from the edge of the depression to a distance of about 500 m, although samplers were sparse at that distance. It was found that the gas was “held-up” for several minutes in the depression at lighter wind speeds (< about 2 m/s), but was transported downwind for a wind speed of 6 m/s. The variation of arc-maximum 1-min-avg concentration with distance during JR I was found to follow basic dimensional relations suggested by Britter and McQuaid (1988) and Hanna et al. (1996) as shown in Figure 1 from Hanna et al. (2016).

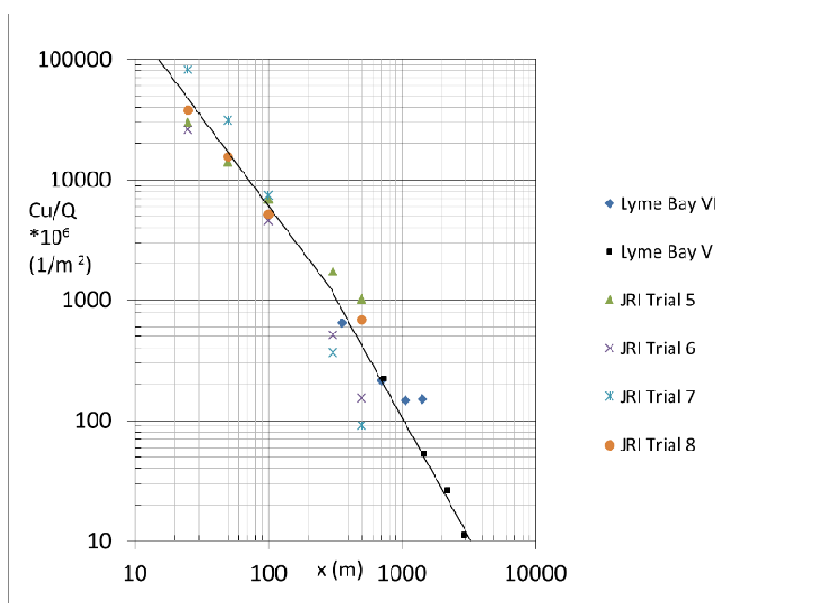


**Figure 1.** Lyme Bay and JR I observed  $\ln C_u/Q_c$  versus  $\ln x$  (from Hanna et al., 2016).  $C$  is one-min avg arc max,  $u$  is wind speed, and  $Q_c$  is mass emission rate.

However, several of the stakeholders in the Jack Rabbit study pointed out that the one and two ton releases during JR I in 2010 were significantly less than the 20 to 60 tons that can be released from a railcar. Therefore, the JR II experiments were planned for 2015 and 2016, where 10 to 20 tons of chlorine would be released from larger tanks. In addition, JR II includes indoor measurements. The 2015 JR II experiments took place at DPG with the source location within a “mock urban” environment of about 80 CONEX shipping containers (2.3 by 2.6 by 6.1 or 12.2 m) set up on a staggered grid in a packed gravel area 122 m square. In addition, trailers and a two wide by three high CONEX stack were placed about 70 m downwind of the source, to study the transport and dispersion of dense gas around and inside urban structures. Chlorine was released at the center of a 25 m diameter concrete pad as a downward-directed two-phase momentum jet in about 30 to 60 seconds from a horizontal tank with a 15 cm opening at about 1.0 m agl (Spicer et al., 2016). The concrete pad’s center was positioned 31 m from the upwind edge of the mock urban area. Figure 2 provides a view of the experiment setup. Concentrations and winds were measured within the obstacle array and on 90° arcs at distances of 0.2, 0.5, 1, 2, 5, and 11 km. Figure 3 shows the sensor placements on the 2, 5, and 11 km arcs. The 11 km experimental domain is within a relatively flat salt playa at DPG, although there were 1000 m mountain ranges about 40 km to either side of the playa. The JR II domain is about 10 km west of the JR I domain. The JR II site was chosen because winds are known to be steady from the south at dawn most of the time during the summer.

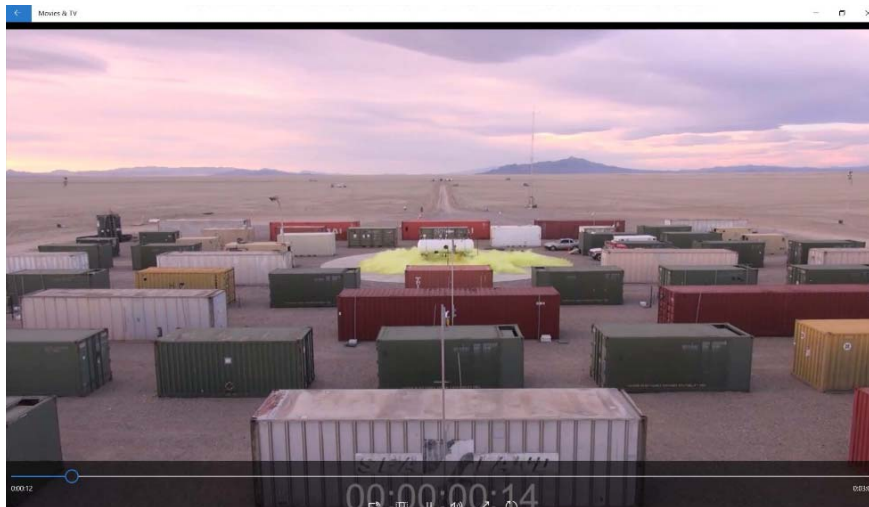


**Figure 2.** JR II 2015 Trial 5, looking towards south (upwind), 0.5 sec after release. Note tank and yellow chlorine cloud.

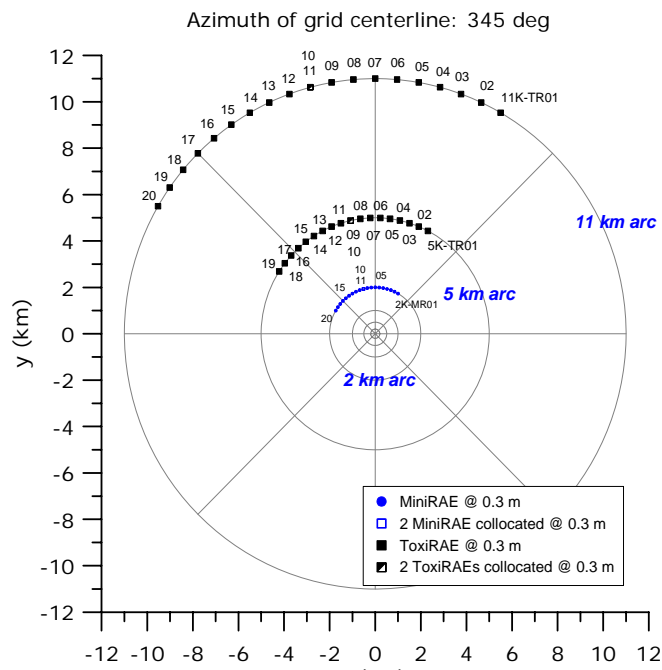


**Figure 3.** JR II 2015 sampler grid for 2, 5, and 11 km arcs.

For large releases of pressurized liquefied chlorine, the resulting initial cloud is characterized by a strong momentum jet consisting of about 20 % gas, and 80% liquid (by mass) in the form of aerosol (drops) with a broad size range but a mass median diameter of about 20 to 100  $\mu\text{m}$  (Britter et al., 2011). Several attempts were made to measure the chlorine aerosol in 2015 but with limited success. It is uncertain whether an observed drop consists of chlorine, ambient water, natural particles, or a combination.

All JR II experiments have extensive observations of winds, as well as surface energy budget and turbulence. The releases took place only if the average on-site wind speeds were roughly in the range from 2 to 6 m/s, and wind directions were within the 90° sampling arcs.

The JR II experiment planned for 2016 will be at the same location as the 2015 experiment but most of the mock urban obstacles will be removed. One obstacle will be retained for an indoor experiment. Ten to twenty tons of chlorine are planned to be released in seven trials, with different jet orientations: upwards, horizontal downwind, 45 degrees downwards and downwind, and directly downwards. There will be deposition measurements taken.

The current paper describes some general characteristics of the JR II 2015 field experiment. The data have recently passed QA/QC and are being distributed to JR II participants. However, these data are all “raw” in the sense that they have not been corrected for known biases. For example, a correction curve is available for each MiniRae concentration sampler, based on laboratory calibrations carried out after the field experiment, but has not been applied to the raw data in the data archive.

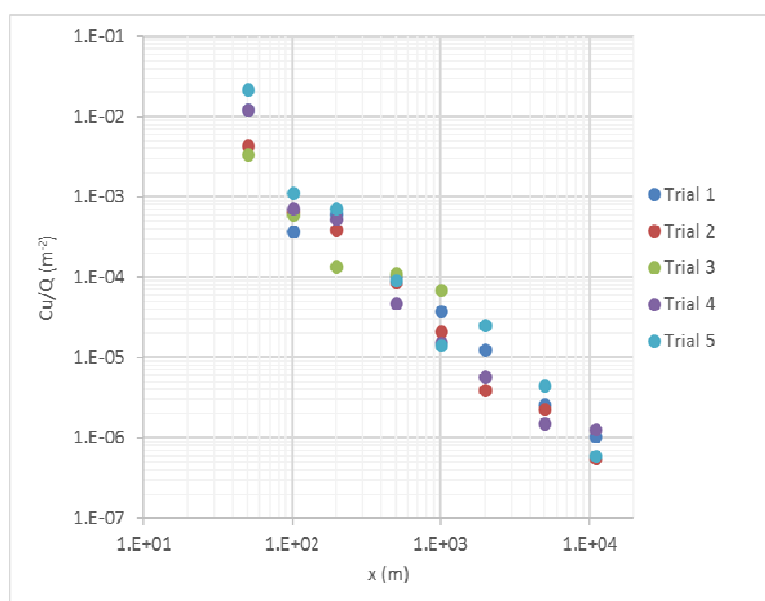
## OVERVIEW OF JR II 2015

Table 1 lists the characteristics of the five JR II chlorine release trials during 2015, where the mass released ranged from 4518 to 8321 kg. The details of the tank and the pressurized releases from the 6” (15.2 cm) hole are described by Spicer et al. (2016). The duration of the two-phase release was about 30 to 60 sec. All experiments were conducted in early morning. Videos showed that rain-out (liquid pooling) was relatively small (less than 10 % of the total mass), and most of the small pool evaporated within a few minutes. The strong downward pointing dense momentum jet spread out in all directions for about 50 to 75 m, and the videos showed the material “splashing” upwards to the above the tops of the obstacles when it encountered the CONEX obstacles in the near field. This broad spread was able to be simulated by several models that were run prior to the experiments. After the initial jet and outwards cloud motion ceased, the cloud settled down and began being transported downwind as a “normal” shallow dense cloud. As concentrations dropped below about 1000 ppm at the 200 to 500 m arcs, the cloud density effects gradually became insignificant and the cloud behaves as a neutral passive cloud. Many samplers recorded significant chlorine concentrations with resolution of about 1 sec and the duration of time for cloud passage across a sampler at the larger ranges was on the order of five to ten minutes.

**Table 1.** Summary of JR II 2015. Note that MDT = GMT-6. PWIDS are aerovanes on short towers at heights of about 2 m. There were 34 PWIDS placed over the JR II domain.

Trial		1	2	3	4	5
Release (MDT, = UTC-6)	Date	8/24/2015	8/28/2015	8/29/2015	9/1/2015	9/3/2015
	Start Time	7:35:45	9:24:21	7:56:55	8:38:50	7:28:19
	Duration (sec)	30	60	30	45	60
Release Amount (kg)		4,518	8,168	4,521	6,985	8,321
AVG PWIDS Wind Direction (deg)		147	158	170	184	183
AVG PWIDS Wind Speed (m/s)		1.9	4.3	4.0	2.3	2.8
AVG PWIDS Temperature (C)		17.7	22.7	22.6	22.6	22.2

Although the data have just recently passed QA/QC, preliminary analysis shows good consistency among the five trials and agreement with results of previous analyses with JR I and other dense gas data (such as shown above in Figure 1 for JR I and Lyme Bay). Figure 4 contains the observed JR II 2015 Cu/Q values versus  $x$ , for the five trials and for downwind distances,  $x$ , from 50 m to 11 km.  $C(g/m^3)$  is the arc max 1 sec average concentration,  $u(m/s)$  is the average wind speed, and  $Q(g/s)$  is the source mass emission rate. The data from the five trials all follow an approximate  $-5/3$  power law, as found at other locations and in approximate agreement with suggested relations by Britter and McQuaid (1988). At any given distance, the range of the five data points is about a factor of plus and minus three about a best-fit line.



**Figure 4.** Observed JR II 2015 arc max 1 sec avg Cu/Q ( $\text{m}^{-2}$ ) vs x (m).

Figures 1 and 4 both have Cu/Q plotted versus x, although 1-min concentration averages are used in Figure 1 and 1 sec averages in Figure 4. The units of the y-axis are different by  $10^6$ . If the same y-axis units were used, the JR II points are slightly below (about a factor of two on average) the JR I and Lyme Bay points. We note that a major difference is that the JR II release duration is much smaller than the JR I and Lyme Bay release durations, causing the JR II cloud to be effectively a puff (not a continuous plume) over nearly all of its range (all  $x > 50$  m). However, the overall agreement is fairly good.

Much more analysis will be carried out and the data archive and video footage are being made accessible to stakeholders upon request to DHS S&T CASAC ([JackRabbit@st.dhs.gov](mailto:JackRabbit@st.dhs.gov)) pending successful approval of access to the HSIN web site.

**ACKNOWLEDGEMENTS** - The research has been sponsored primarily by the U.S. Department of Homeland Security (DHS) and the U.S. Defense Threat Reduction Agency (DTRA)

## REFERENCES

- Bauer, T.J., 2013: Comparison of chlorine and ammonia concentration field trial data with calculated results from a Gaussian atmospheric transport and dispersion model. *J. Haz. Mat.*, **254-255**, 325-335.
- Briggs, G.A., Britter, R.E., Hanna, S.R., Havens, J.A., Robins, A.G., Snyder, W.H., 2001: Dense gas vertical diffusion over rough surfaces: results of wind-tunnel studies. *Atmos. Environ.*, **35**, 2265-2284.
- Britter, R.E., McQuaid, J., 1988. Workbook on the Dispersion of Dense Gases. HSE Contract Research Report No. 17/1988, Health and Safety Executive, Sheffield, UK, 158 pp.
- Hanna, S.R., Britter, R.E., Chang, J., Argenta, E., 2012: The Jack Rabbit chlorine release experiments: Implications of dense gas removal from a depression and downwind concentrations. *J. Haz. Mat.*, **213-214**, 406-412.
- Hanna, S.R., Chang, J., Huq, P., 2016: Observed chlorine concentrations during Jack Rabbit I and Lyme Bay field experiments. *Atm. Environ.*, **125**, 252-256.
- Hanna, S.R., Dharmavaram, S., Zhang, J., Sykes, I., Witlox, H., Khajehnajafi, S., Koslan, K., 2008. Comparison of six widely-used dense gas dispersion models for three recent chlorine railcar accidents. *Proc. Safety Prog.* **27**, 248-259.

- Hanna, S.R., Drivas, P.J., Chang, J.C., 1996. Guidelines for Use of Vapor Cloud Dispersion Models. AIChE/CCPS, 345 East 47th St., New York, NY, 285 pp + CD.
- Hearn, J.D., Weber, R., Nichols, R., Henley, M., Fox, S., 2013: Deposition of Cl<sub>2</sub> on soils during outdoor releases. *J. Haz. Mat.*, **252-253**, 107-114.
- Marshall, V.C., 1989. The predictions of human mortality from chemical accidents with especial reference to the lethal toxicity of chlorine. *J. Haz. Mat.* **22**, 13-56.
- Spicer, T., Wallace, S., Tabara, C.E, Sun, S., 2016. Transient Large-Scale Chlorine Releases in the Jack Rabbit II Field Tests: Near Source Release Data and Preliminary Analysis, Am. Inst. Chem. Eng. 2016 Spring Meeting, 12th Global Congress on Process Safety, Houston, Texas, April 11-13.

## **TOPIC 8**

# **MODELLING AIR DISPERSION AND EXPOSURE TO ACCIDENTAL RELEASES**

**17th International Conference on  
Harmonisation within Atmospheric Dispersion Modelling for Regulatory Purposes  
9-12 May 2016, Budapest, Hungary**

---

**RADON-BASED ASSESSMENT OF STABILITY EFFECTS ON POTENTIAL  
RADIOLOGICAL RELEASES**

*Scott Chambers<sup>1</sup>, Alastair Williams<sup>1</sup>, Dan Galeriu<sup>2</sup>, Anca Melintescu<sup>2</sup> and Marin Duma<sup>2</sup>*

<sup>1</sup> Institute for Environmental Research (ANSTO), Lucas Heights, NSW, Australia

<sup>2</sup> “Horia Hulubei” National Institute for Physics & Nuclear Engineering, Bucharest-Magurele, Romania

**Abstract:** Eight months of climatology and <sup>222</sup>Rn observations from a 60 m tower at a nuclear research facility in Romania are analysed. Heterogeneous surface roughness conditions in the site’s 1 km radius exclusion zone hinder accurate characterisation of atmospheric stability using meteorological techniques, so a radon-based scheme is trialled. When the nocturnal boundary layer is very stable, the Pasquill-Gifford “radiation” scheme overestimates the atmosphere’s capacity to dilute pollutants with near-surface sources (such as tritiated water vapour) by 20% compared to the radon-based scheme. Under these conditions, near-surface wind speeds drop below 1 ms<sup>-1</sup> and nocturnal mixing depths vary from ~25 m to less than 10 m above ground level (agl.). Daytime mixing depths at this flat inland site range from 1100 to 1800 m agl. in summer, and 500 to 900 m in winter. Using tower observations to constrain the nocturnal radon-derived effective mixing depth, we were able to estimate the seasonal range in the Bucharest regional radon flux as: 12 mBq m<sup>-2</sup> s<sup>-1</sup> in winter to 14 mBq m<sup>-2</sup> s<sup>-1</sup> in summer.

**Key words:** <sup>222</sup>Rn; nocturnal stability; stable nocturnal boundary layer; urban pollution; mixing height.

Near-surface concentrations of air-borne pollutants are primarily a function of source strength and mixing depth. Nuclear facilities are required to monitor their emissions and local meteorology to gauge the environmental impacts of routine or accidental releases (Galeriu et al., 2014). Here, plume dispersion modelling is usually employed in lieu of a dense monitoring network to assess regional impacts, with the accuracy of forecasts closely related to how well meteorological observations can be used to characterise the atmospheric mixing state (“stability”). Historically, categorical techniques such as the Pasquill-Gifford schemes (e.g. Pasquill and Smith, 1983) have been used for stability classification rather than techniques based on similarity theory. Here we demonstrate a recently-developed radon-based technique for stability classification (Chambers et al., 2015a,b) that can be easily implemented in models for regulatory reporting. Radon is an ideal atmospheric tracer; it is unreactive, poorly soluble, has a relatively consistent terrestrial source, and is approximately conservative over the course of a single night ( $t_{0.5} \sim 3.8$  days). Consequently, near-surface radon concentrations represent a direct measure of the intensity and vertical extent of nocturnal atmospheric mixing, and perform better than meteorological proxies in characterising the outcomes of vertical mixing on surface-emitted passive scalar quantities (Williams et al. 2013).

Horia Hulubei National Institute for Research and Development in Physics and Nuclear Engineering is situated 10 km SSW of Bucharest, Romania, in a mixed urban-rural landscape. Since operations at this facility ceased in 1997 radioactive emissions from its 40 m stack have been minor. Hourly meteorological monitoring is routinely conducted from a nearby tower at 30 and 60 m agl. to assess the fate of emitted radioactive gases and aerosols. Observations from this tower have served as a real-time data provider for the RODOS (Real-time On-line DecisiOn Support) decision support system for nuclear emergencies (Galeriu et al., 2011). In addition to the tower observations, 10m radon concentrations were recorded hourly (AlphaGUARD, PQ200 PRO), and daytime mixing depths were provided by a CHM 15k Nimbus ceilometer.

In the vicinity of the tower surface roughness elements (including trees and buildings) reach 10-15 m agl., which has made nocturnal stability classification by conventional meteorological approaches problematic. Here we use 8 months of hourly radon and meteorological observations in 2012 to develop a versatile classification scheme for the atmospheric mixing state, characterise the behaviour of key meteorological quantities within the defined mixing states, compare the efficacy and consistency of the Pasquill-Gifford and radon-based approaches for stability classification, and characterise seasonal changes in mixing depth across the diurnal cycle for a range of atmospheric stabilities.

Unlike the Pasquill-Gifford or bulk Richardson number techniques, which can provide stability classifications on an hourly basis, the radon-based approach assigns stability classifications to whole nights, based on observations within a 10-hour nocturnal window. Stability classification of the following daytime period is then inferred, with a high success rate, based on atmospheric “persistence”.

A radon time-series (Figure 1a) represents variability on both long ( $>$  diurnal) and short ( $\leq$  diurnal) timescales. While long timescale variability is mostly related to air mass fetch effects, diurnal variability is mostly related to changes in the atmospheric mixing state (or “atmospheric stability”).

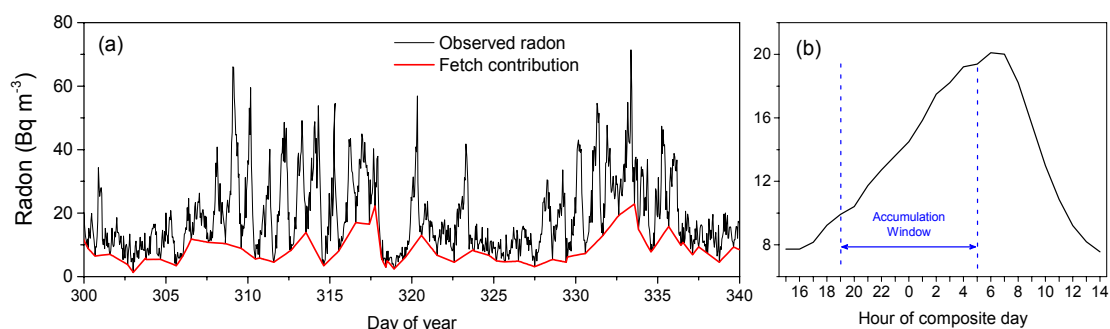


**Figure 1.** (a) Hourly radon time series with fetch-related component shown in red, and (b) composite diurnal cycle of radon at 10m agl., with 10-hour nocturnal accumulation window indicated.

Once the diurnal component has been isolated (i.e. by subtracting the fetch contribution from the observed concentrations), the mean nocturnal radon accumulation from 1900h – 0500h (Figure 1b) can be calculated each night and related to the mean atmospheric mixing state (e.g. Williams et al. 2016). After plotting the cumulative frequency histogram of nocturnal radon accumulation values (Figure 2a) thresholds (such as quartile ranges) can be assigned to define stability categories which are applied to 24-hour periods. Diurnal composites of radon for days assigned to one of the 4 stability categories (Figure 2b) show that “stable nights” result in the greatest diurnal amplitude of radon, whereas near-neutral (well mixed) nights result in the lowest amplitude changes. Since stable nights are usually associated with the clearest sky conditions and calmest winds, corresponding daytimes are usually the most unstable, and vice versa.

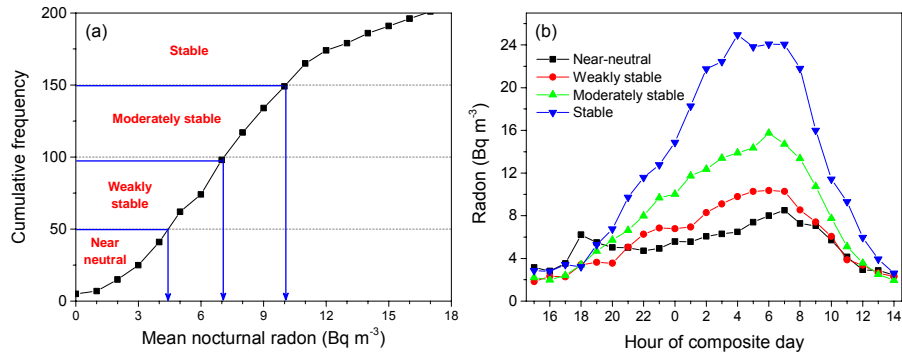


**Figure 2.** Cumulative frequency plot of nocturnal radon accumulation with assigned stability categories, and (b) diurnal composite radon concentration in each stability category.

As a “sanity check” of the radon-based scheme, we performed an hourly stability classification of the entire dataset using the Pasquill-Gifford radiation scheme (PGR), and bulk Richardson number ( $Ri_B$ ) approach. We then formed diurnal composites (Figure 3) of the hourly PGR and  $Ri_B$  stability classifications according to the 4 daily radon-based stability categories. Most clearly seen in the seasonal  $Ri_B$  composites (Figure 3c,d), despite being defined for 24-hour periods based on only 10-hours of observations, the radon-based scheme reliably assigns hourly  $Ri_B$  estimates across the entire diurnal cycle (large positive values for stable nights, and increasingly large negative values for daytime instability); near neutral and weakly stable cases even fall either side of the “critical” Richardson number ( $Ri_C=0.25$ ).

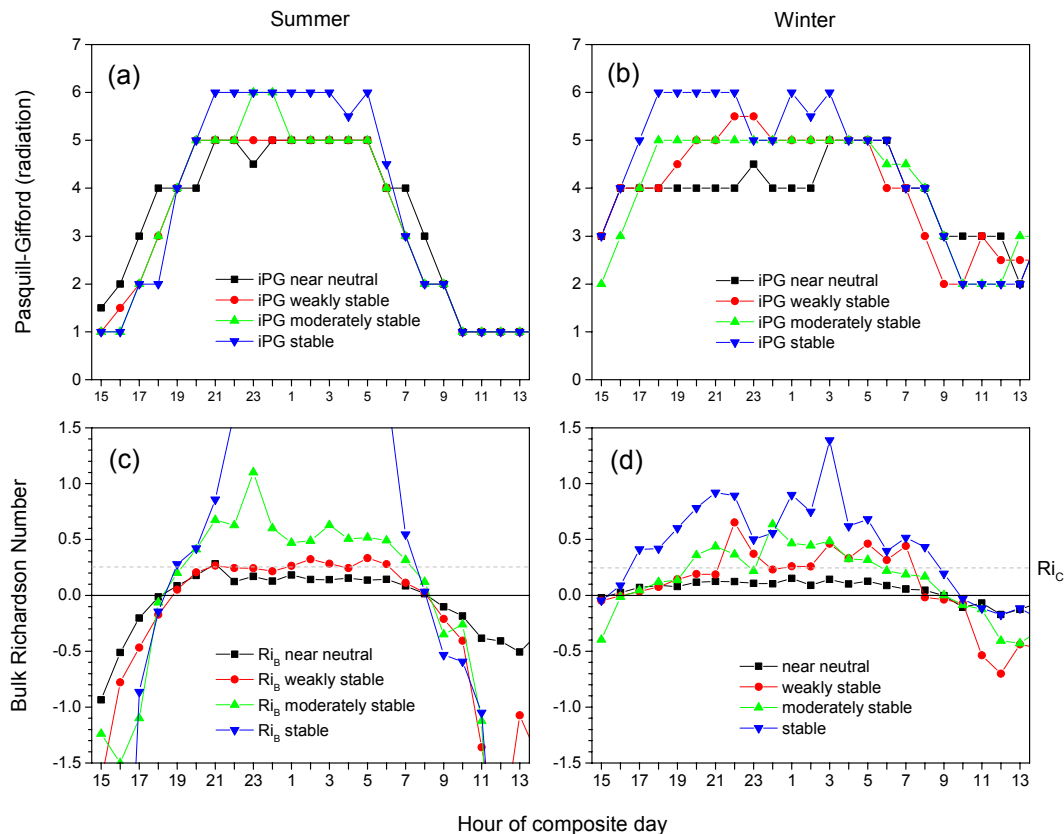


**Figure 3.** Composite PGR and  $Ri_B$  stability classifications for each radon-based stability category (PGR: 1 – unstable; 4 – neutral; 6 – stable).

Looking at hourly distributions of diurnal composite plots of evenings classified as stable by the radon-based and PGR schemes (Figure 4), the radon-based scheme yields median diurnal amplitudes ~20% greater than that of the PGR scheme. Since the behaviour of radon is representative of the behaviour of tritiated water vapour (or other gaseous pollutants with sources beneath the nocturnal inversion layer), it is evident that the choice of stability classification technique can have serious implications for exposure estimates in the event of a release from the facility.

When climatological observations are grouped by radon-based stability categories clear and consistent differences are apparent (Figure 5). Near-neutral conditions were associated with stronger winds and more cloud cover and small near-surface temperature gradients, whereas “stable” nocturnal conditions were associated with near-calm conditions, clear skies and strong near-surface temperature gradients.

Average daytime mixing depths reported by the ceilometer ranged from 600m in winter to 1200m in summer. Nocturnal mixing depths estimated from the 10m radon observations and a box model (Griffiths et al., 2013) varied from <10m on stable nights to ~60m on weakly stable nights. By constraining radon box model estimates of nocturnal effective mixing depth with tower observations we were able to well-constrain the seasonal variability in the Bucharest regional radon flux: 12 mBq m<sup>-2</sup> s<sup>-1</sup> in winter to 14 mBq m<sup>-2</sup> s<sup>-1</sup> in summer; values which were in close agreement with recently published European radon flux maps (e.g. Karstens et al., 2015).

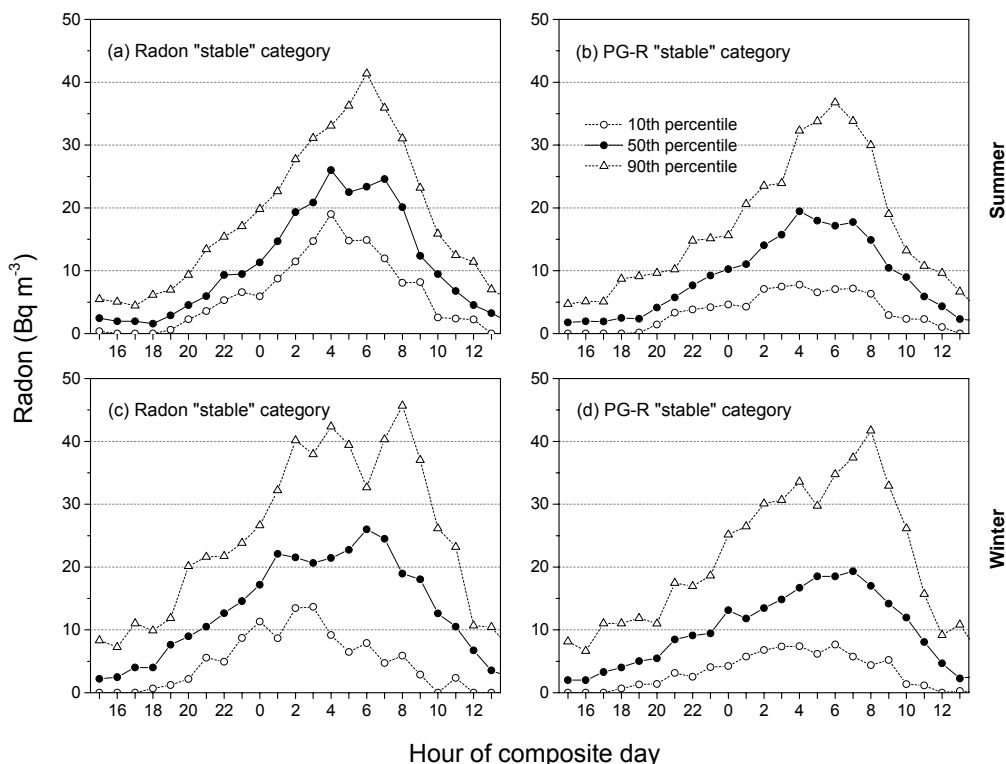


**Figure 4.** Comparison of extreme pollution events (stable nocturnal conditions) in summer and winter as predicted by the (a,c) radon-based scheme, and (b,d) PGR scheme.

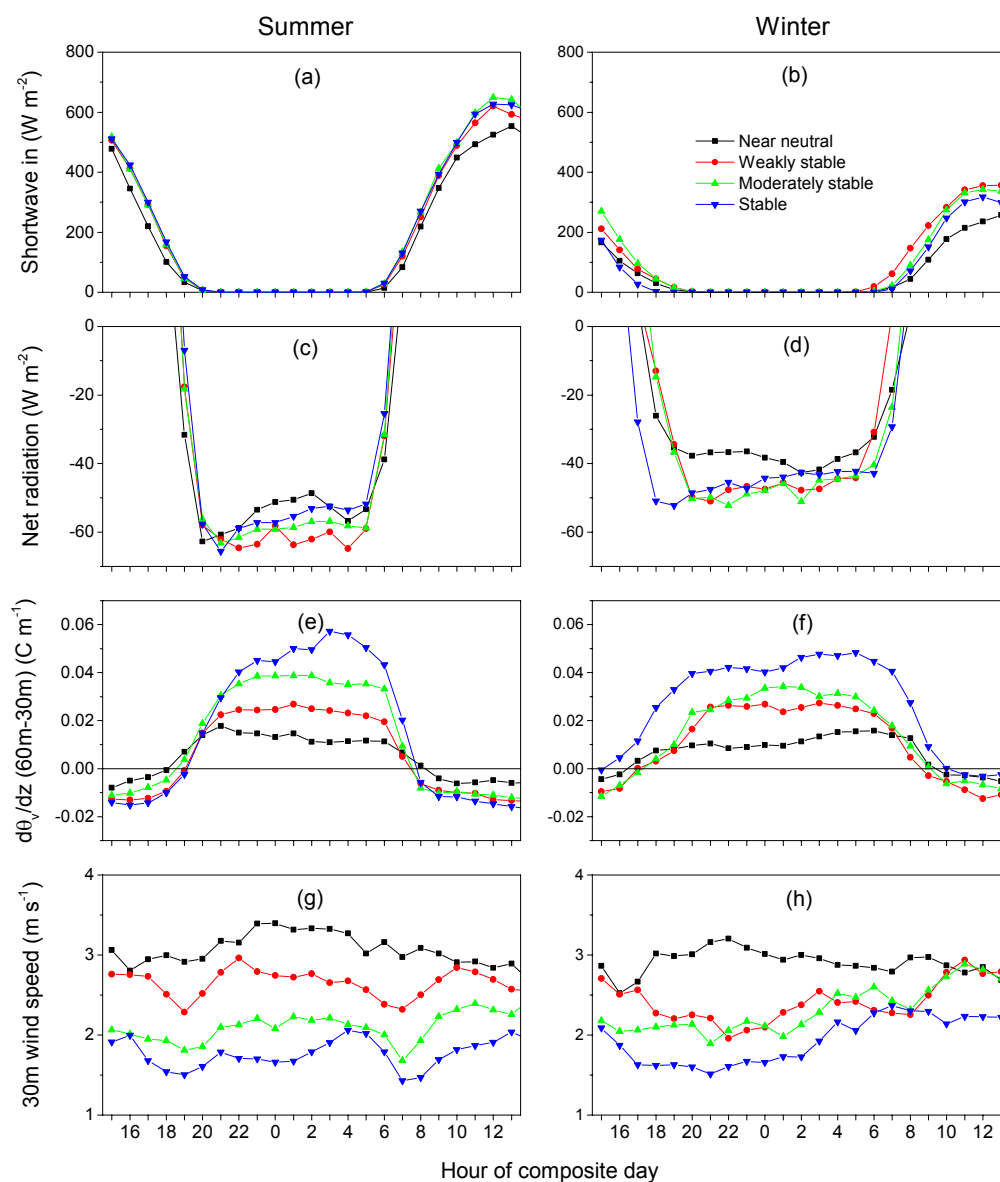


**Figure 5.** Diurnal composites of climatological parameters by season and radon-based stability category.

### ACKNOWLEDGMENTS

This study is part of the project EXPLORATORY IDEAS 65/2011 financed by the Romanian Authority for Scientific Research.

### REFERENCES

- Chambers, S.D., A.G. Williams, J. Crawford, and A.D. Griffiths, 2015a: On the use of radon for quantifying the effects of atmospheric stability on urban emissions. *Atmos. Chem. Phys.*, **15**, 1175-1190.
- Chambers, S.D., F. Wang, A.G. Williams, D. Xiaodong, H. Zhang, G. Lonati, J. Crawford, A.D. Griffiths, A. and Ianniello, I., 2015b: Quantifying the influences of atmospheric stability on air pollution in Lanzhou, China, using a radon-based stability monitor. *Atmos. Environ.*, **107**, 233-243.

- Galeriu, D., and A. Melintescu, 2011: Research and development of environmental tritium modelling. *Fusion Sci. Technol.*, 60 (4), 1232 – 1237.
- Galeriu, D., A. Melintescu, M. Duma, B. Zorila, A. Gheorghiu, 2014: Nuclear meteorology at IFIN-HH. *Romanian Journal of Physics*, 59(9–10), 999–1011.
- Griffiths, A.D., S.D. Parkes, S.D., Chambers, M.F. McCabe, and A.G. Williams, A.G., 2013: Improved mixing height monitoring through a combination of lidar and radon measurements. *Atmos. Meas. Tech.*, 6, 207–218.
- Karstens, U., C. Schwingshackl, D. Schmithüsen, and I. Levin, 2015: A process-based  $^{222}\text{Rn}$  flux map for Europe and its comparison to long-term observations. *Atmos. Chem. Phys. Discuss.*, 15, 17397-17448, doi:10.5194/acpd-15-17397-2015.
- Pasquill, F., and F.B. Smith, 1983: *Atmospheric Diffusion*, 3<sup>rd</sup> Edition, Ellis Horwood Ltd., John Wiley & Sons, Chichester, 437 pp.
- Williams, A.G., S.D. Chambers, F. Conen, S. Reimann, M. Hill, A.D. Griffiths and J. Crawford, 2016: Radon as a tracer of atmospheric influences on traffic-related air pollution in a small inland city. *Tellus B*, submitted January 2016.
- Williams, A. G., S.D. Chambers and A.D. Griffiths, 2013: Bulk Mixing and Decoupling of the Nocturnal Stable Boundary Layer Characterized Using a Ubiquitous Natural Tracer. *Bound.-Lay. Meteorol.*, 149, 381–402.

**17th International Conference on  
Harmonisation within Atmospheric Dispersion Modelling for Regulatory Purposes  
9-12 May 2016, Budapest, Hungary**

---

**NAME-EPS: DEVELOPING A DISPERSION MODELLING CAPABILITY UTILISING  
ENSEMBLE WEATHER FORECASTS FOR EMERGENCY-RESPONSE APPLICATIONS**

*Andrew R. Jones, Ayoë B. Hansen and Susan J. Leadbetter*

Met Office, FitzRoy Road, Exeter, EX1 3PB, United Kingdom

**Abstract:** The poster demonstrates some initial work from a project at the UK Met Office aimed at enhancing operational capabilities for emergency-response dispersion modelling by improving how uncertainties are represented when assessing accidental releases of harmful materials into the atmosphere. The early focus of this work is on the representation of meteorological uncertainty in the dispersion modelling and explores developing the use of forecasts from an ensemble weather prediction system to generate an ensemble of dispersion model predictions. A demonstration of the application of this system is presented. It is equally acknowledged that other aspects of uncertainty, especially in the description of source terms, are often highly significant and future work will be needed to consider suitable methods to represent and interpret these wider uncertainties in an operational context.

**Key words:** *meteorological uncertainty, ensemble weather prediction, radiological dispersion modelling*

## **INTRODUCTION**

Awareness of uncertainties in radiological dispersion modelling has grown over recent years, as has the need to better understand and quantify these uncertainties. One approach that has been adopted for operational response is to consider a ‘best estimate’ and a ‘reasonable worst case’ for an event. More advanced approaches might consider wider assessment of the sensitivities to model inputs, including use of ensemble-based techniques, but the requirement for a rapid and unambiguous response is paramount.

While various research and demonstration systems based on ensemble approaches have been developed over the last decade or two, it is only recently that computing power has evolved to a stage where many of these earlier research activities are now becoming tractable for real-time operational prediction capability. Such developments are now happening at various centres around Europe and beyond. However significant challenges (both at a technical and a conceptual level) still remain concerning the efficient generation of ensemble dispersion products and their effective presentation and communication.

## **UNCERTAINTIES IN ATMOSPHERIC MODELLING**

Emergency-response modelling of radiological incidents needs to examine a wide range of uncertainties (Haywood, 2008), from the description of the source term (which is often highly uncertain), the transport of material by the atmosphere and deposition of radionuclides to the ground surface, through to the representation of the health (and other) impacts and their consequences in terms of countermeasures, etc. The focus of this poster is on one link in this chain, viz. uncertainties in the large-scale atmospheric transport, and will examine how we can use an ensemble weather prediction to represent this uncertainty.

NWP ensemble systems are designed specifically to sample a range of possible future weather states by representing both the *analysis errors* in the initial model state and the *forecast errors* that arise due to model limitations and deficiencies. Uncertainties in the NWP modelling system and in the observations are both accounted for. Ensembles are useful not only in providing possible forecast outcomes (including potential high-impact weather events) but also in giving a means to estimate the confidence in a forecast. The ensemble approach operates by simulating many different realisations to sample the effect of initial analysis errors and forecast errors – each ensemble member starts from a ‘perturbed’ initial state and uses modified physics schemes in the model integration.

## MODELLING SYSTEM COMPONENTS

The poster demonstrates initial results achieved by coupling output from the Met Office's global ensemble forecasting system, MOGREPS-G, with the atmospheric dispersion model, NAME.

### The NAME atmospheric dispersion model

The *Numerical Atmospheric-dispersion Modelling Environment*, NAME, is the Met Office's Lagrangian atmospheric dispersion model (Jones et al., 2007). It is designed to predict the atmospheric transport and deposition to the ground surface of airborne material and is able to handle both gaseous and particulate substances. As a Lagrangian model, NAME uses Monte Carlo random-walk techniques to represent the turbulent transport of pollutants in the atmosphere. Processes such as dry and wet deposition, gravitational settling and radiological decay can be represented within the model. NAME is typically driven using three-dimensional gridded meteorological fields supplied by the Met Office's numerical weather prediction model, the Unified Model (MetUM), which provides a real-time dispersion modelling capability ranging from the global scale to kilometre-scale over the United Kingdom.

NAME was originally developed as a nuclear accident model in response to the Chernobyl disaster in 1986, and it continues to have an important operational role within UK and international frameworks for responding to radiological incidents. For instance, the Met Office is a Regional Specialized Meteorological Centre (RSMC) under the WMO's Emergency Response Activities programme, providing specialized dispersion products for the European and African regions. The radiological capabilities of NAME include a simple half-life decay scheme for the activity of individual radionuclides (including that of deposited material) as well as more advanced options such as decay-chain modelling and cloud gamma dose calculations. NAME has also evolved in a much broader sense as a general-purpose atmospheric dispersion model and is today used for a wide variety of emergency-response and research applications, including modelling of airborne volcanic ash and the spread of animal diseases and plant pathogens.

### MOGREPS-G global ensemble forecasting system

The *Met Office Global and Regional Ensemble Prediction System*, MOGREPS, is the operational ensemble forecasting system developed at the Met Office (Tennant and Beare, 2014). A global ensemble (MOGREPS-G) is used to provide lateral boundary conditions and initial-condition perturbations for a high-resolution regional ensemble (MOGREPS-UK) over the UK area. The MOGREPS system is primarily intended for short-range weather prediction (1 to 2 days ahead), especially in relation to high-impact severe weather events such as windstorms and extreme rainfall. Only the global component of the system is used for dispersion modelling with NAME in the present study, but future work will aim to extend this to high-resolution prediction over the UK.

Global ensemble forecasts from MOGREPS-G are produced operationally four times per day at 00, 06, 12 and 18 UTC. Initial conditions are obtained from the global deterministic 4D-Var data assimilation, while perturbations are generated using the Ensemble Transform Kalman Filter (ETKF) approach, which is a computationally-efficient form of the ensemble Kalman filter. Model uncertainties are represented using stochastic physics schemes to target structural and sub-grid scale sources of model error. The current configuration of MOGREPS-G is shown in Table 1.

**Table 1.** Operational configuration of the MOGREPS-G global ensemble forecasting system

Domain	Ensemble size	Forecast range	Horizontal resolution	Vertical levels
Global	Control + 11 perturbed members	7 days (T+168)	33 km (mid latitudes)	70 levels with model top at 80 km

### DEMONSTRATION STUDY

NAME has the capability to handle multiple meteorological forecast realisations (such as those supplied by an ensemble NWP system) and to derive statistical output products (e.g., the ensemble median) from them. An example will be presented here illustrating use in NAME of an ensemble weather forecast from the MOGREPS global ensemble forecasting system. While it is acknowledged that it is difficult to draw any conclusions from a single case study, it does nonetheless provide some useful insight into the potential benefits of an ensemble-based approach over the conventional deterministic one.

### Scenario details

The modelling system is demonstrated for a hypothetical accident scenario at the (now closed) Barsebäck nuclear power plant (12.92° E, 55.74° N) in Sweden. An RSMC-type source term is used, in which 1 TBq (=  $10^{12}$  Bq) of radioactivity is released at a constant rate over a 6 hour time period starting at 09 UTC on 08/03/2016 and ending at 15 UTC on 08/03/2016. The material is released into the atmosphere uniformly between the ground level and an elevation of 500 metres. The modelled radionuclide is Cs-137, which is subject to dry and wet deposition. Model simulations are run for 63 hours to generate output fields valid at 00 UTC on 11/03/2016. Meteorological forecasts from the 00 UTC forecast cycle on 08/03/2016 are used for the study, so as to simulate a real-time response that would occur for a real event.

### Results

Results of the NAME simulations are shown for the total deposition of Cs-137 at 00 UTC on 11/03/2016. Figure 1 shows an estimated deposition field produced by NAME retrospectively using ‘analysed’ global meteorological fields. This will be adopted as a benchmark against which the other predictions can be compared. The deposition pattern extends north-eastwards from the power plant across southern parts of Sweden and the Baltic Sea into Finland and northern Russia.

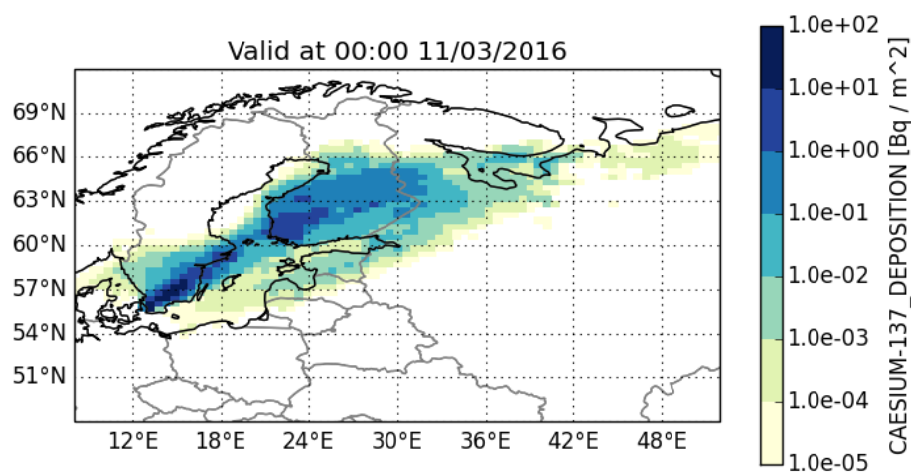


**Figure 1.** Estimated Cs-137 deposition at 00 UTC on 11/03/2016 based on a post-event NAME simulation using ‘analysed’ global meteorological data.

The predicted deposition from the NAME simulation using the real-time operational global forecast is shown in Figure 2. There is clearly very good agreement with the simulation based on the analysed met fields, indicating that model forecast errors are small on this occasion. However, the extent and nature of these forecast errors would be unknown when the forecast was first prepared, and decision makers might be concerned with the proximity of the plume to Stockholm or the scope for impacts in other Baltic states. Differences can be observed (mostly at low-to-moderate deposition values) to the north of the main plume over Sweden and the extent of the ‘tail’ extending from St Petersburg back towards Latvia.

The *postage stamp* plot in Figure 3 depicts the modelled deposition based on the 12 members of the MOGREPS-G ensemble forecast with the same base time as the operational global forecast in Figure 2. There is good agreement for the deposition pattern across the ensemble. There are small variations in the plume orientation over Sweden but magnitudes of deposits are broadly consistent. It is interesting that no ensemble member captures the greater northward extent of the low-to-moderate deposition values here. However there is a signal for some variability in the extent of the ‘tail’ over Latvia.

While there are some benefits to viewing the separate ensemble members individually, it can be difficult to analyse and interpret the information in a usable way. Statistical processing can assist in identifying the main signals contained within the ensemble. For instance, percentiles calculated over the ensemble are shown in Figure 4. The *median* forecast (50-th percentile) is often adopted as a central measure of the ensemble forecast and would be a reasonable choice in this instance, though the 75-th percentile appears

to give a better indication of deposition values over Finland and highlights better the presence of the ‘tail’. The 100-th percentile can be viewed as a ‘worst case scenario’ *at any location* (noting that a ‘worst case’ could not occur at all locations together) and would be useful to decision makers in giving an indication about the maximum extent of the area that could be affected and where remediation measures might need to be considered. The level of agreement for exceeding particular thresholds (not shown here) is also a useful method of assessing agreement between the ensemble members, though the choice of suitable thresholds needs careful consideration.

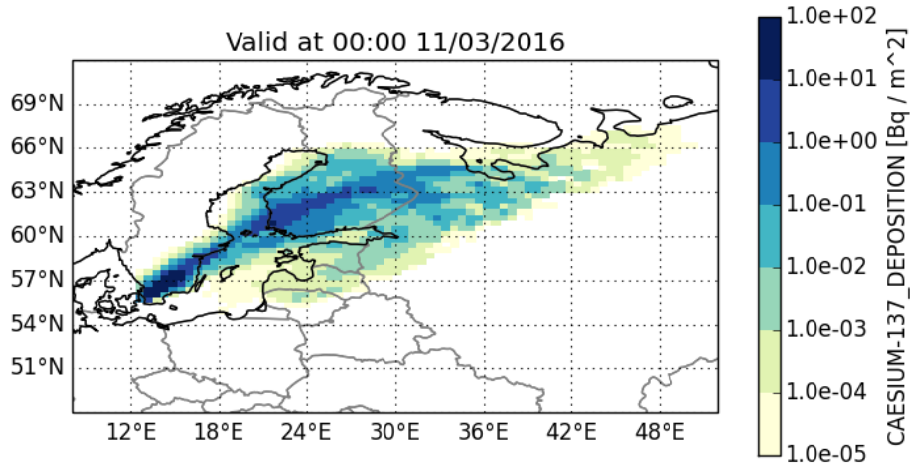


**Figure 2.** Predicted Cs-137 deposition at 00 UTC on 11/03/2016 based on the NAME simulation using the 00 UTC (on 08/03/2016) forecast cycle of the (deterministic) operational global forecast model.

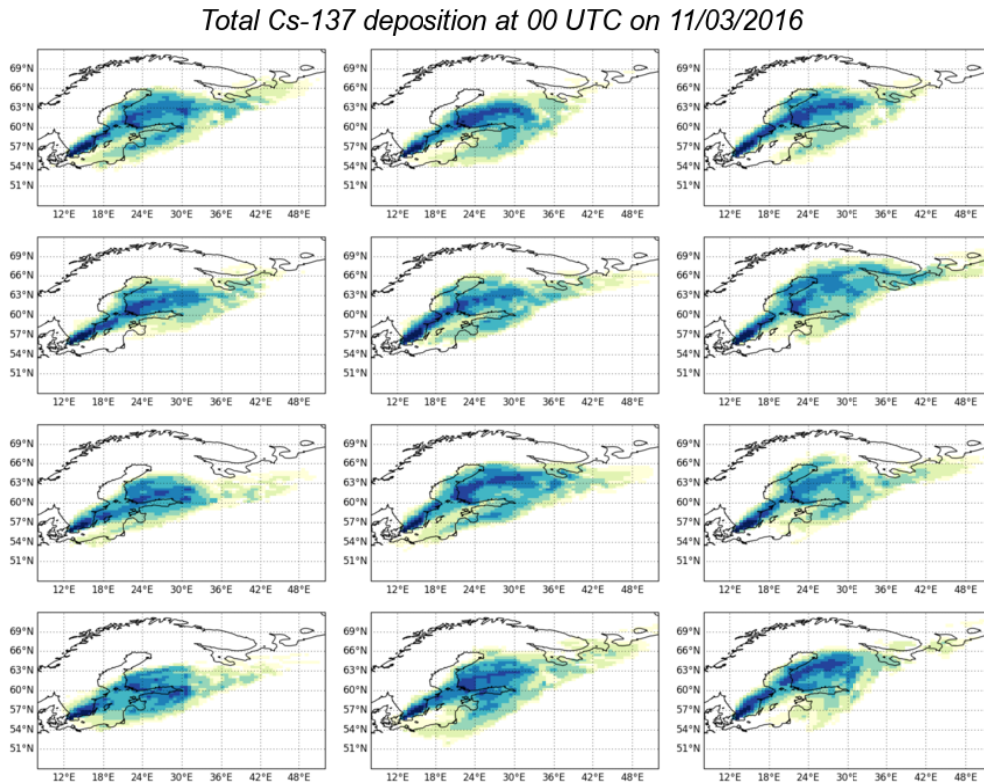


**Figure 3.** Predicted Cs-137 deposition at 00 UTC on 11/03/2016 using each ensemble member from the 00 UTC MOGREPS-G forecast on 08/03/2016.

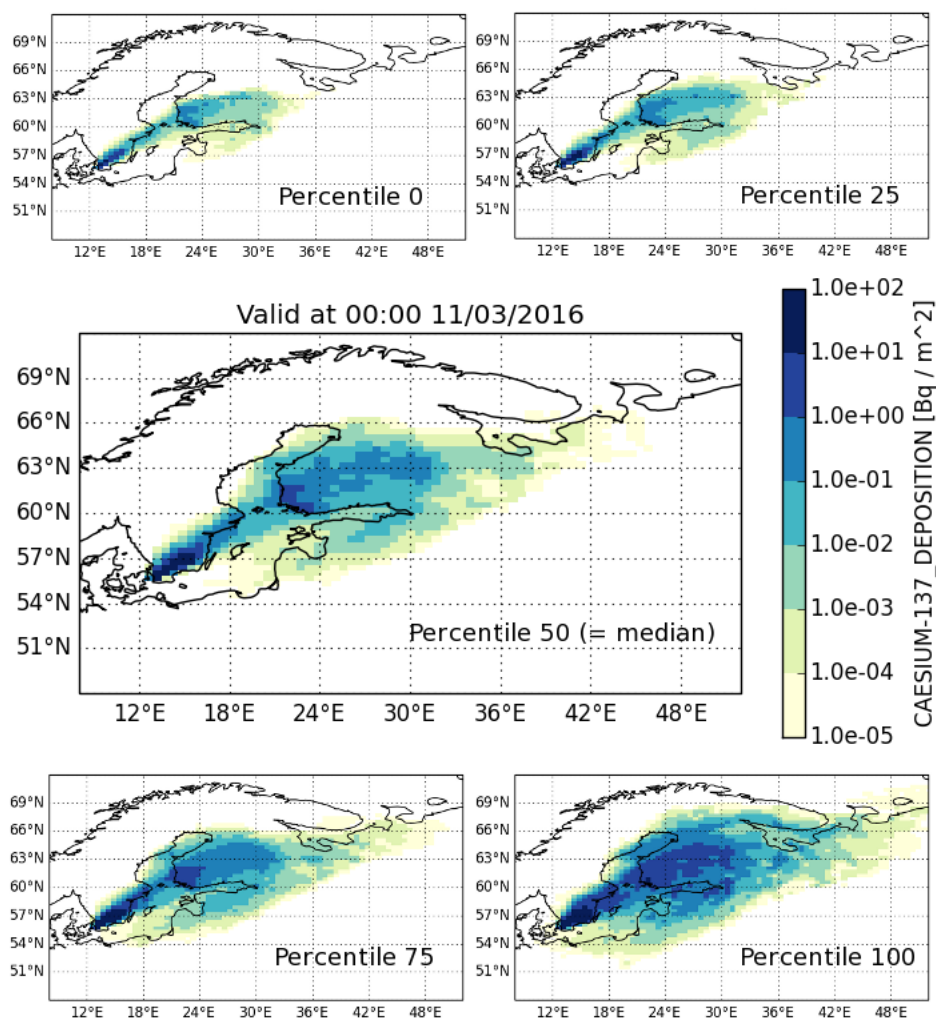


**Figure 4.** Percentile plots of Cs-137 deposition at 00 UTC on 11/03/2016 calculated over the 12 ensemble members shown in Figure 3.

## FUTURE WORK

Further cases will be examined to establish the extent to which results seen in this initial demonstration case are more generally applicable. Further planned work includes investigating the use of *clustering techniques* for the computationally efficient production of ensemble-based dispersion results, and examining how to represent uncertainty in the meteorological ‘*analysis*’ state. Further work will also consider development of appropriate methods to represent other types of uncertainty (e.g., source term sensitivities) and the design of application-specific uncertainty products that *communicate* uncertainties effectively with end users. Engagement with users and decision makers is viewed as a crucial aspect of this work to ensure that products are not just scientifically robust but also helpful for informing decisions.

## REFERENCES

- Haywood, S.M., 2008: Key sources of imprecision in radiological emergency response assessments, *J. Rad. Protection*, **28**, 169-183.
- Jones, A.R., D.J. Thomson, M. Hort and B. Devenish, 2007: The U.K. Met Office’s next-generation atmospheric dispersion model, NAME III, in Borrego, C. and Norman, A.-L. (Eds) *Air Pollution Modeling and its Application XVII (Proceedings of the 27th NATO/CCMS International Technical Meeting on Air Pollution Modelling and its Application)*, Springer, pp. 580-589.
- Tennant, W. and S. Beare, 2014: New schemes to perturb sea-surface temperature and soil moisture content in MOGREPS. *Q.J.R. Meteorol. Soc.*, **140**, 1150-1160. doi: 10.1002/qj.2202

**17th International Conference on  
Harmonisation within Atmospheric Dispersion Modelling for Regulatory Purposes  
9-12 May 2016, Budapest, Hungary**

---

**SIMULATION OF EXPLOSIVE EVENTS IN THE URBAN ENVIRONMENT  
COUPLING A FAST DYNAMICS CFD MODEL WITH LOW MACH NUMBER  
DISPERSION SOLVERS IN CERES® CBRN-E**

*Luc Patryl<sup>1</sup>, Emmanuel Lapébie<sup>2</sup>, and Patrick Armand<sup>1</sup>*

<sup>1</sup>CEA, DAM, DIF, F-91297 Arpajon, France

<sup>2</sup>CEA, DAM, F-46500 Gramat, France

**Abstract:** CBRN-E threats are a major concern of the public authorities, relayed by the people and sadly rekindled by recent events, notably in Paris, France. In case of hazardous atmospheric releases, preceded or not by an explosion, first responders in particular, and all decision makers in general, wish to gain as quick as possible the most accurate and reliable representation of the situation in order to foster the crisis management and return to normalcy. This is precisely the role that a modelling and decision-support computational tool could play in the emergency preparedness and response process. Consistently, this is also the objective of CERES® which is entirely developed by the Atomic and alternative Energies Commission (CEA) in France. In this framework, our paper is intended (1) to recall the main principles and characteristics of CERES® placing an emphasis on the ability to carry out explosion and dispersion simulations in the same tool, then (2) to comment on recent advances of experimental and modelling activities in the field of the detonations, and finally (3) to describe the coupling between explosion and dispersion modules with the announcement of computations related to realistic scenarios in large urban domains to be presented in the conference.

**Key words:** *Explosion, dispersion, low Mach, high Mach, D2R2, HI2LO, CERES® CBRN-E.*

## **INTRODUCTION**

CBRN-E threats may have various expressions including possibly deleterious atmospheric releases and / or explosions originating from industrial accidents or terror events. In such cases, a rapid assessment of the situation is of high-stake for both rescue teams and stakeholders (facilities operators, local or national authorities...). It can even constitute a strong element of differentiation between the emergency handling strategies to efficiently control the situation and return to normal, a fact exemplified through examples of CBRN-E emergency exercises in Armand *et al.* (2013) (a), (2014), and (2015).

Since 2005, CEA has been mandated to coordinate and run the inter-ministerial R&D program dedicated to CBRN-E threats in France. Modelling and simulation contribute to the cross feeding of topics included in this program such as prevention, detection, alert, intervention, and / or mitigation. In this framework, CERES® CBRN-E (shortened as CERES® in the paper) is a recent operational modelling and decision-support system which is being developed in collaboration between services of the Atomic and alternative Energies Commission (CEA) in France. The software has been specifically designed to evaluate the short term and the long term health consequences of chemicals, radionuclides or biological pathogenic agents, accidentally or maliciously emitted into the air. CERES® is committed to provide numerical results in a limited amount of time (less than 15 minutes in most cases), thus to be applicable in an emergency.

The present paper is divided in three main parts, including (1) a quick recall of the principal development guidelines and features of CERES®, (2) an insight on experiments and models related to the detonations, recently achieved in connection with the software, and (3) the presentation of the coupled explosion and dispersion modelling system with near future applications to simulations in very large urban domains. As a matter of fact, CERES® modelling edge is to tackle explosions, dispersions or the combination of both.

## **CERES® MODELLING SYSTEM IN CASE OF CBRN-E EVENTS**

The specifications of CERES® software are to be a modelling and decision-support tool able to deal with several types of threats and scenarios and give the possibility to run flow and dispersion models adapted to complex built-up (industrial and urban) environments (Armand *et al.*, 2013 (b)). Moreover, the 2D / 3D

simulation results have to be produced within a fairly short time consistent with the “hot phase” of an emergency. Finally, the results must be provided as a mapping of danger zones (health consequences) or counter-measures zones (sheltering-in-place or evacuation) to be directly useable by the civilian security.

The major features of CERES® are reported hereafter.

- The software deals with 3D dispersion at local and regional scale in both natural and complex built-up environments (industrial sites or urban areas).
- It handles various categories of threat agents (radionuclides, chemicals or biological pathogens); thus, it has endpoint health impact models specifically devoted to these kinds of releases.
- It is equipped with a large panel of scenarios (leakage from a tank or a pipe, evaporation from a pool, fire, explosion...) and associated simplified or more advanced “source term” models.
- Depending on the skill and computational resources of the user, it gives the choice between three dispersion models: Gaussian puff, sophisticated urbanized Gaussian and, more farsighted and R&D oriented, a Lagrangian Particle Dispersion Model (LPDM) using a 3D flow field.
- It can use a range of meteorological data: measurements at one or more stations, vertical profiles, and / or meso-scale numerical weather forecasting.

CERES® encompasses not only physical models, but also numerous data bases with the terrain elevation, land-use, building data, physicochemical properties of stable or radioactive elements, transfer coefficients in the soil and the biota, radiological dose conversion coefficients, toxicological reference values, etc.

Along with the transport and dispersion, the fate of the gases or particles released in the air is considered according to their nature (radioactive decay chains, chemical reactions, or bio-agents degradation).

CERES® input data are recorded and CERES® output results are disseminated through a tried and tested ergonomic graphical user interface. All kinds of maps are exportable to Graphical Information Systems (GIS), like e.g. ArcGIS®, as a support to the intervention and decision-making processes.

All models implemented in CERES® have been rigorously validated using experimental wind tunnel or in-field data (see validation cases in a mock-up and full-scale city centre in Duchenne *et al.*, 2016).

On-going developments include source term estimation and data assimilation. As the computational time is reduced, CERES® simulations can be performed repeatedly using all the present available information. In an emergency, the first aim is to quickly provide atmospheric dispersion and health impact assessment, afterward to improve gradually the initial evaluation using more and more complete and reliable data.

Finally, the software motto is to be modular and flexible as versions can be instantly generated with the one and only software components the user is interested in. As modules are plug-ins, it is easy to derive a version for instance devoted to the chemical risk with the *ad hoc* data bases, source term, dispersion and chemical dose models.

While CERES® is aimed at the CEA own safety needs and missions, its interest for more users has been also clearly identified. Thus, CERES® has been licensed for more than five years to the French nuclear and non-nuclear industry and distributed to civilian security services for experimentation and feedback.

### **HIGH-MACH SOURCE TERMS**

While most of the atmospheric transport and dispersion models use the assumption of incompressibility, a special attention has to be paid to highly transient source terms like those generated by energetic events. As a matter of fact, incompressible flows are limited to flows with a local Mach number less than 0.1. (The Mach number,  $Ma$ , is defined as  $u_s/a_s$ ,  $u_s$  being the particle velocity and  $a_s$  the sound speed.  $Ma = 0.1$  corresponds to a particle velocity of  $35 \text{ m}\cdot\text{s}^{-1}$  or a density increase of 11%, thus a reasonable limit for the incompressible flow hypothesis. See Patryl *et al.* (2014) for more details.)

However, there are several source terms beginning with high Mach flows, for instance in the accidental releases from pressurized containers or in the events involving high explosives (dirty bombs, Biological / Chemical – Improvised Explosive Devices), etc. As it would not be mathematically and physically correct to connect such source terms to incompressible models, ways to overcome this issue have been studied and graduated simplified or full CFD strategies have been implemented in CERES®:

- First of all, source terms with no interaction with obstacles may be described analytically up to the extent where the flow is nearly at rest. For instance, this is the case for Improvised Explosive Devices using the D2R2 model (see more below) or for stratified clouds models after explosive releases such as TESATEX in CERES® (Armand *et al.*, 2008) or HOTSPOT (Homann, 2010).
- Another method for more complex events is to describe the mass, impulse, and energy flow rates through a given surface. For instance, this is the case of an indoor detonation and dissemination in a single- or multi-room building followed by an outdoor flow through windows and doors. As the resulting flow may be a high-Mach one, it is computed as a boundary condition by the 3D compressible solver HI2LO (Hank *et al.*, 2012). Then, HI2LO results may be further computed by the LPDM dispersion solver in CERES® with a time coupling of the two models.
- In the most complex cases, it might be necessary to use 3D multiphase computations from the beginning. Once again, the results can be remapped in HI2LO and, step by step, when reaching a low-Mach state, also remapped in CERES® and its low-Mach dispersion solvers.

The following paragraphs give some more details about the experimental validation and application of the D2R2 and HI2LO models.

#### **Analytical model for Improvised Explosive Devices**

Several explosive dissemination experiments have been conducted at CEA with liquids and powders. The reference setup is a cylindrical plastic shell (external diameter of around 10 cm) with an inner cylinder of high explosive of variable diameter. This setup allows the mass ratio between the explosive and the inert material to vary. For experiments with water, the  $M_{\text{inert}} / M_{\text{TNT}}$  ratio ranged from 1.6 to 12.8.

From the analysis of experiments, two regimes can be identified as illustrated in Figure 1. The first one is a highly structured regime with the formation of characteristic “finger” instabilities. After a transitional break-up process, the second one forms cloudy shapes soon followed by the end of the expansion.

The D2R2 (Rapid Releases Dynamical Dispersion) model describes these two regimes correctly as shown for example in Figure 2. One can notice that the predicted external cloud radius compares quite well with the experimental values for three different  $M_{\text{inert}} / M_{\text{TNT}}$  ratios. D2R2 has been successfully applied to the CEA experiments and also to literature results such as Apparao *et al.* (2013) or Zabelka *et al.* (1969).

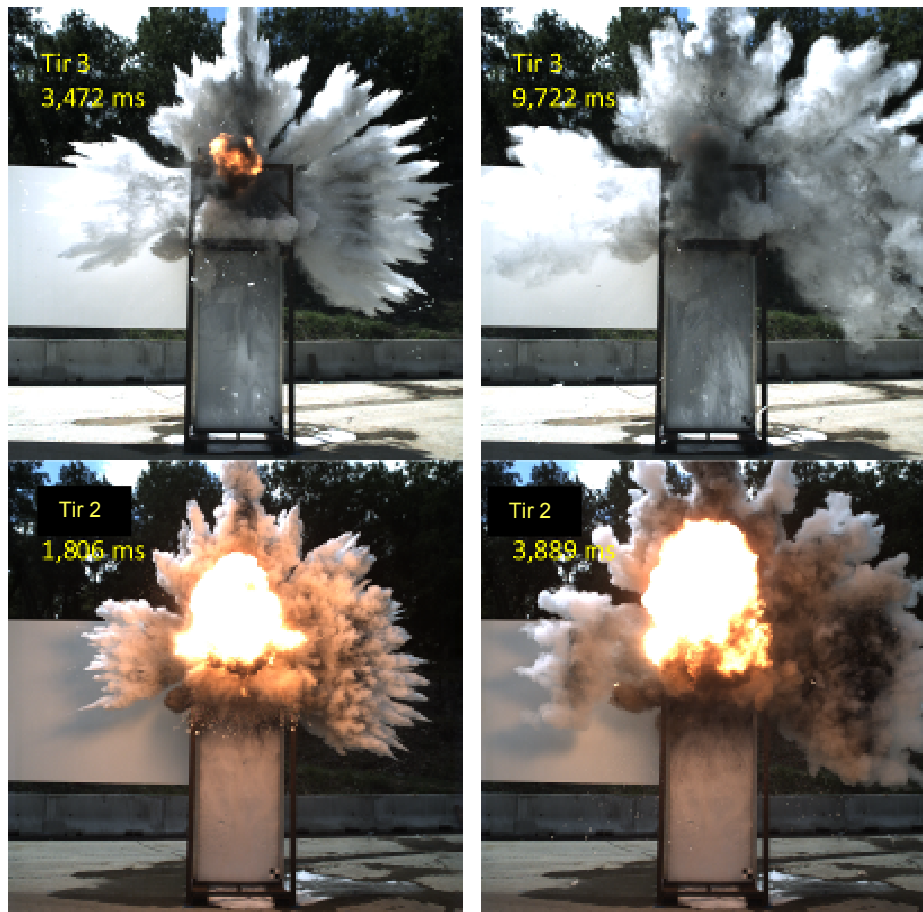


**Figure 1.** Change of morphology for two mass ratios (from top to bottom: 4.8 and 1.6).  
Left: fingers structures – Right: cloudy shapes.

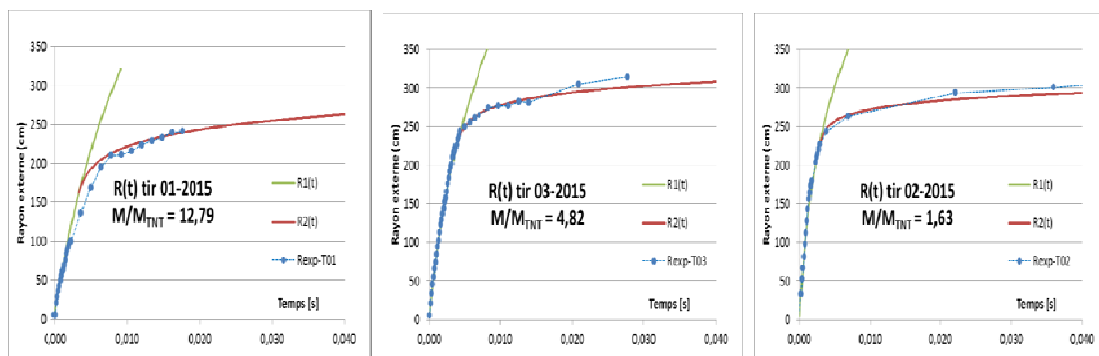


**Figure 2.** D2R2 results compared to CEA experiments (time evolution of the external radius).  
Blue: experiments – Green: D2R2 first regime – Red: D2R2 second regime.

### Source term as a boundary condition in a high-Mach 3D solver

HI2LO is the CEA reference model for 3D high-Mach to low-Mach transition computations. Albeit not a fully multiphase model, HI2LO is able to remap results obtained with the other models of the multiphase CHYMERE suite developed for CEA by the RS2N company ([www.rs2n.eu](http://www.rs2n.eu)).

HI2LO is able to use complex boundary conditions as well as in-cell obstacles which may also serve as a source for boundary conditions. For instance, one can declare a subsonic, sonic or supersonic injection in a computational cell as if the cell was connected to a pressurized tank. Many other options are available, and it is also the way chosen to branch some of the analytical source term models (which may also spread on more than one cell).

Figure 3 shows the result of a HI2LO simulation involving such an “internal” source term. A reservoir boundary condition (internal pressure 3.67 bar and temperature 991 K) is defined inside a computational cell and the release is allowed to take place during 0.02 second. The domain size is 3.2 m x 0.8 m x 0.8 m and the release is located at (3.1 m, 0.4 m, 0.4 m) and is directed towards “-X”. Strong turbulent mixing with ambient air is accounted for through a simple model. At the end of the simulation, the local Mach number is everywhere lower than 0.06, so the incompressible approximation is valid.

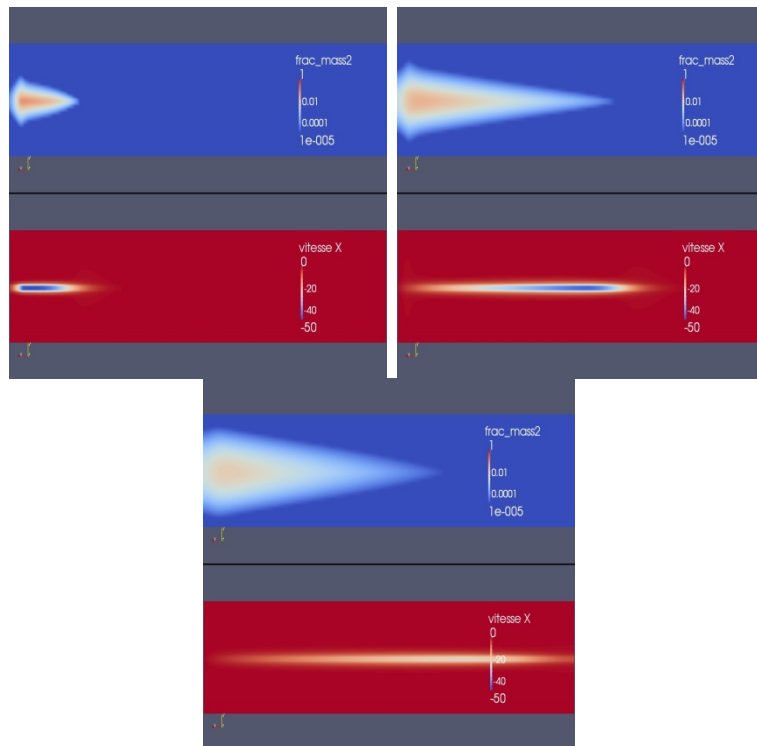


**Figure 3.** Pollutant mass fraction (top) and axial velocity (bottom).  
Times from left to right: 5 ms, 25 ms and 45 ms (X axis flipped for clarity).

### COUPLING EXPLOSION AND DISPERSION IN A REAL URBAN DISTRICT

As mentioned before, graduated strategies have been developed to take account of either open air or more or less confined explosions and, possibly, the coupled dispersion of noxious species. Models consisting in analytical relations like D2R2 are integrated in CERES® while the CFD model called HI2LO is coupled to the Lagrangian dispersion solver in CERES®.

HI2LO and CERES® share the ability to import topographies (DEM: Digital Elevation Maps) and urban geometries from GIS (Geographic Information System) data, especially from the widely used “shapefile” format. To make HI2LO and CERES® compatible, the same urban geometries are used in both models and a pre-processor has been developed to convert shapefile into 3D extruded obstacles (see Figure 4).

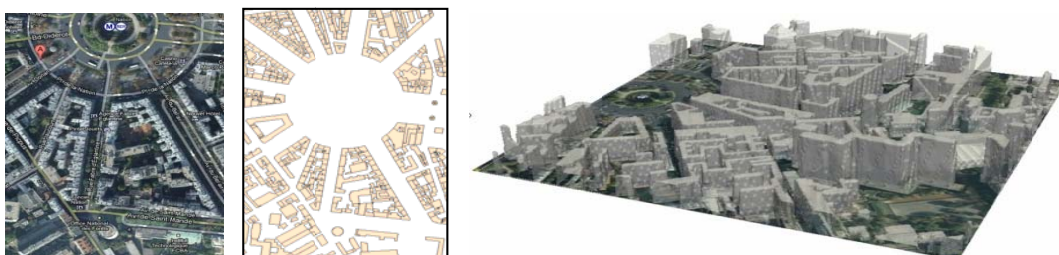


**Figure 4.** From left to right: Google Maps® view, BD TOPO shapefile, and HI2LO geometry after processing.

HI2LO simulations of explosive disseminations have been performed in this geometry and other ones. In such complex environments, the high-Mach flow strongly interacts with the ground as the buildings. The plume outer boundary and internal distribution of the species may be obtained when the maximum Mach number of the flow is under the threshold value of 0.1. It gives the appropriate input state for the LPDM model in CERES® where the HI2LO data are imported to continue the simulation for longer timescales. Such computations in some Paris districts are under way and will be presented during the conference.

## CONCLUSION

Explosions may happen as a consequence of accidents or terror events with dramatic consequences on the human health and the infrastructure. Moreover, explosions may generate the dissemination of hazardous species in more or less confined spaces, from open air spaces to semi-confined built-up industrial sites or urban districts, or even initially confined buildings or underground networks. Explosion modelling is thus a complicated task for many reasons and, in the same time, intuited to be very useful in an emergency.

CERES® is the fast-response modelling and decision-support computational tool developed by the CEA. It is equipped with both explosion and dispersion models adopting a graduated range of strategies to deal with more or less complicated environments and threat scenarios. One ambitious approach which may be necessary in the case of industrial sites or urban districts is the direct time-coupling between the transient results of the HI2LO (high- to low-) Mach number CFD model with the Lagrangian dispersion solver in CERES® taking account of both the explosion characteristics and the obstacles influence. This approach will be soon applied to districts in Paris in order to simulate the flow and the dispersion pattern and assess the overpressure and the toxicity consequences in case of hypothetical explosive noxious releases.

## REFERENCES

- Apparao A. et al. Studies on Formation of Unconfined Detonable Vapor Cloud Using Explosive Means. *Journal of Hazardous Materials*. **254–255** (2013) 214–220.
- Armand, P., C. Olry, A. Albergel, and C. Duchenne. 3D simulation of the dispersion in the urban environment in case of an explosion using TESATEX pre-processor and Micro-SWIFT-SPRAY modelling system. Proceedings of the 12<sup>th</sup> Harmo Conference, October 6-9, 2008, Cavtat, Croatia, 199-203.
- Armand, P., C. Duchenne, Y. Benamrane, C. Libeau, T. Le Nouëne, and F. Brill. Meteorological forecast and dispersion of noxious agents in the urban environment – Application of a modelling chain in real-time to a fictitious event in Paris city. Proceedings of the 15<sup>th</sup> Harmo Conference, May 6-9, 2013, Madrid, Spain, 724-728 (a).
- Armand, P., L. Patryl, G. Lamaison, L. Soulhac, L. Deguillaume, and N. Chaumerliac. CERES® CBRN – A unified modelling and decision support system to assess the dispersal and health impact of hazardous releases in urban or open-field environments. Proceedings of the 15<sup>th</sup> Harmo Conference, May 6-9, 2013, Madrid, Spain, (b).
- Armand, P., C. Duchenne, and E. Bouquot. Atmospheric dispersion modelling and health impact assessment in the framework of a CBRN-E exercise in a complex urban configuration. Proceedings of the 16<sup>th</sup> Harmo Conference, Sept. 8-11, 2014, Varna, Bulgaria, 638-643.
- Armand, P., C. Duchenne, and L. Patryl. Is it now possible to use advanced dispersion modelling for emergency response? The example of a CBRN exercise in Paris. Proceedings of the International Technical Meeting on Air Pollution Modelling and its Application, May 4-8 2015, Montpellier, France.
- Bloom S. G. Models for Close-In Atmospheric Dispersion, Explosive Releases, and Particle Deposition. Rapport Oak Ridge National Laboratory, ORNL/TM-12452, 1993.
- Duchenne C., P. Armand, M. Nibart, and V. Hergault. Validation of a LPDM against the CUTE experiments of the COST ES1006 Action – Comparison of the results obtained with the

- diagnostic and RANS versions of the flow model. Proceedings of the 15<sup>th</sup> Harmo Conference, May 6-9, 2013, Madrid, Spain, to be published.
- Hank S., O. Le Métayer, R. Saurel, and E. Lapébie. HI2LO: A 3D unsteady code for the numerical simulation of shock wave propagation and dispersion phenomena in large scale heterogeneous media. 43<sup>rd</sup> European Safety, Reliability and Data Acquisition Seminar, 2012, Rouen, France.
- Homann, S. G. HotSpot 2.07.1 NARAC, Lawrence Livermore National Laboratory, 2010.  
<https://narac.llnl.gov/HotSpot/HotSpot.html>
- Patryl, L., E. Lapébie, S. Hank, and P. Armand. New capabilities of CERES® CBRN-E decision-support tool in the fields of explosion modelling and source term estimation. Proceedings of the Harmo'16 conference, Sept. 8-11, 2014, Varna, Bulgaria, 644-649.
- Zabelka R. J. et al. Explosively Dispersed Liquids. Part I: Dispersion Model. Rapport NWC TP 4702 (AD 863268), 1969.

**PROBABILISTIC ASSESSMENT OF DANGER ZONES ASSOCIATED  
WITH A HYPOTHETICAL ACCIDENT IN A MAJOR FRENCH PORT  
USING A SURROGATE MODEL OF CFD SIMULATIONS**

*Felipe Aguirre Martinez<sup>1</sup>, Yann Caniou<sup>1</sup>, Christophe Duchenne<sup>2</sup>, Patrick Armand<sup>2</sup>, and Thierry Yalamas<sup>1</sup>*

<sup>1</sup>PHIMECA Engineering, F-75012 Paris, France

<sup>2</sup>CEA, DAM, DIF, F-91297 Arpajon, France

**Abstract:** This paper presents a probabilistic framework used to assess the risk of exceeding health thresholds after an accidental release of a pollutant. Probabilistic risk maps are produced that highlight the 95% confidence interval of the boundary of the danger zone. The methodology is applied to an accidental release of ammoniac simulated with PMSS. Uncertain release and atmospheric conditions are propagated through the model using a Monte-Carlo approach. Gaussian predictors are used to replace the long running PMSS model. It is shown that taking uncertainty into account prevents us from neglecting potential danger zones not identified by a simple deterministic approach.

**Key words:** *Probabilistic risk assessment, dispersion, Gaussian process predictors, Monte-Carlo simulations.*

## **INTRODUCTION**

Risk assessment studies are an invaluable support in the framework of emergency preparedness and response. They are of special importance when dealing with toxic industrial chemicals releases in complex built environments. Simulations on this kind of sites require 3D physical models capable of integrating the influence of the topography and buildings on the flow field and pollutant dispersion. The 3D simulations are most often carried out using a deterministic set of parameters describing the release and meteorological conditions (location, release height and rate, wind speed and direction, stability...). However, these parameters are highly variable or partially unknown. To tackle this, the inherent uncertainty can be propagated through the models using probabilistic methods. The interpretation of the danger zones gets associated to a probability of exceeding a critical dose conditioned by the uncertain parameters. However, this approach is very time consuming for large dimensions and high-resolution domains. An alternative method that reduces the computational cost is to resort to a surrogate model of the flow and dispersion models. Such a methodology has already been developed and tested on a local scale (Armand *et al.* 2014; Dubourg *et al.* 2013). This paper proposes the application of the methodology on a bigger scale, a fictitious accidental release on an industrial site in a French port. Gaussian process predictors are used in combination with a dimension reduction based on Principal Component Analysis. The results are validated by making use of the crude Monte-Carlo uncertainty propagation. Results are presented as probabilistic danger zones maps with a confidence interval of 95% and compared with the “deterministic” result obtained by simulation of the original models on the mode values of the input parameters. Finally, the interest in taking the uncertainties into account is commented on as well as the computational resources needed by the method.

## **CASE STUDY: FICTITIOUS ACCIDENTAL RELEASE OF AMMONIAC**

The proposed method was applied to a fictitious situation of an accidental release on an industrial site in a French port. Following an accident in the port, ammoniac is released for a period of 45 minutes. The meteorological flows and atmospheric dispersion are simulated using the Parallel-Micro-SWIFT-SPRAY (PMSS) modelling system from the CEA and ARIA Technologies. The simulation extends for 75 mins after the release (120 mins in total), the time that the pollutant exits the domain of interest. Meteorological conditions fluctuate within two main wind directions impacting the lower and upper parts of the town (cf. Figure 1). The parameters that describe the release and meteorological conditions are considered to be

uncertain. Table 1 summarizes these parameters as probability distributions whose parameters are based on expert judgement. The 9 km x 12 km domain is divided in 63 tiles (9 columns and 7 rows) with a horizontal mesh resolution of 3 meters. The cliffs relief and all buildings details are taken into account in the flow and dispersion models and their surrogate. The computational time is of approximately 1 hour and 40 minutes over 128 CPUS.

**Table 1** - Probability model of the uncertain release and meteorological conditions

Variable	Distribution
Wind speed 1 (°)	$N(170, \sigma_1 = 10)$
Wind speed 1 (m/s)	$N(3, 0.3)$
Wind direction 2 (°)	$N(120, \sigma_2 = 10)$
Wind direction 2 (m/s)	$N(4, 0.4)$
Temperature gradient (°C/100 m)	$LN(\mu = -0.1, \sigma = 0.7, \gamma = -2)$
Rejection height (m)	$U[0,20]$
Amount of pollutant (kg/m <sup>3</sup> /s)	$LN(\mu = 7.65 E9, \sigma = 5.1 E9, \gamma = 0)$

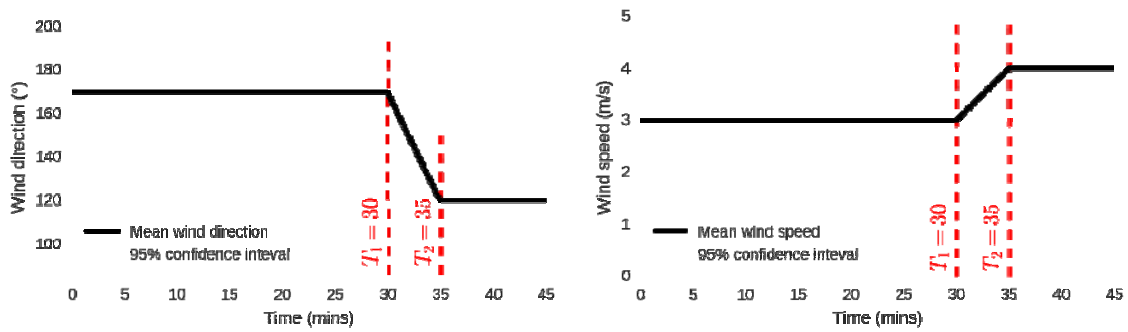


**Figure 1.** Wind conditions

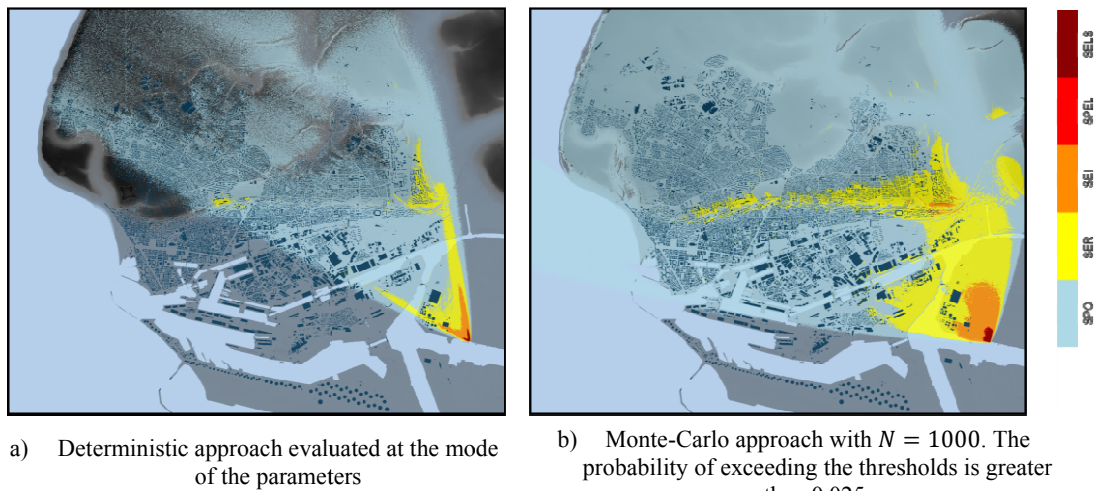


**Figure 2.** Comparison of risk maps obtained with deterministic and probabilistic approach.

The objective is to quantify the health risk through time and space following the accidental release of ammoniac. Figure 2.a shows the risk map of the proposed case study when applying a deterministic workflow using the mode of the uncertain parameters. This risk map is the reference upon which the probabilistic approach is compared. Five safety thresholds are depicted:

- SER: Reversible effects threshold
- SEI: Irreversible effects threshold
- SPEL: First lethal effects threshold
- SELS Significant lethal effects threshold

The SPO odor threshold is also considered.

### DISPERSION MODELING

PMSS is the parallel version of the MSS modelling system integrating the diagnostic mass-consistent model MicroSwift with MicroSpray Lagrangian particle dispersion model. MicroSwift (Oldrini et al. 2013) interpolates the input wind data, coming from outputs of a larger scale model, from a dispersed meteorological network or both of them, on the simulation 3D domain through an objective analysis based on the mass conservation equation. Temperature and humidity can also be interpolated, such as some 2D parameters like the friction velocity or the mixing layer height, if these data are available. In MSS the total turbulence is obtained summing the local one, produced by the flow distortion around the obstacles, plus a background level obtained by standard boundary-layer parameterizations. The local turbulence is estimated on the basis of a mixing-length closure, with the mixing length being a function of the distance to the obstacle or the ground. MicroSpray (Tinarelli et al. 2013) is able to take into account the presence of obstacles. The dispersion of an airborne pollutant is simulated following the motion of a large number of fictitious particles. The mean (“transport”) component of the particle velocity is provided by the meteorological driver. The stochastic (“turbulent”) component of the particle motion is obtained by solving a 3-D form of the Langevin equation for the random velocity. The parallelization of MSS is based on the MPI message-passing system in order to deal with huge computation domains. Parallelization is implemented in ParallelMicroSwift both for splitting geographically huge domains, and for gaining speed-up based on code specific properties. ParallelMicroSpray has an elaborated load balancing to provide sub domains containing numerous particles with maximum core power, and is able to transition particles between sub domains.

### UNCERTAINTY PROPAGATION FOR RISK ASSESSMENT

Risk is quantified as the probability that the ammoniac dose perceived by an individual in a given point of the city for a given period of time exceeds the critical health thresholds. Intuitively, this probability can be quantified with Monte-Carlo sampling. For example, the probability of exceeding the irreversible effects threshold dose *SEI* in a given point *p*, within a period of time *t* is estimated as follows:

$$P[D(X; p, t) > SEI] \approx \frac{1}{N} \sum_{i=1}^N \mathbf{1}_{D(p,t) > SEI}(x^{(i)}) \quad (1)$$

where  $D(X; p, t)$  corresponds to the computational chain associated to the case study and evaluated for  $X$ , the random vector of the uncertain parameters.  $\mathbf{1}_{D(p,t) > SEI}$  is the indicator function that is equal to one if the SEI threshold is exceeded for a given realization  $x^{(i)}$  of  $X$  and zero otherwise.  $N$  is the size of the Monte-Carlo experiment.

As a rule of thumb, a confident estimate of a probability of the order  $10^{-k}$  requires at least a Monte-Carlo experiment of size  $10^{k+2}$ . For this study, the attention is focused on a 0.025 probability level; we then need a Monte-Carlo experiment of at least 3900 PMSS simulations in order to correctly estimate the risk map. Such an experiment would require 9 months on a sequential machine, which is incompatible with the urgency related to a potential real scenario. Moreover, each PMSS simulation produces ~10 GB of data, which means that ~39TB of available storage space are needed for such a design of experiments. To overcome this, we use the methodology introduced by (Armand *et al.* 2014). PMSS is replaced with vectorial Gaussian process predictors in combination with a dimension reduction based on Principal Component Analysis. Besides the fact that the scenario, the pollutant and the parameters taken into account have changed, the novelty of this study lies on the following factors:

- The models are implemented using the PMSS modelling system.
- The methodology was adapted so that it can be applied on a much larger scale with a division of the domain in tiles. The simulations are distributed on a High Performance Computing (HPC) cluster over 128cpus for each simulation.
- A change on the wind direction during the rejection period is considered.

## RESULTS

In order to validate the methodology, a reference probabilistic risk map was constructed with a Sobol design of experiments of size 1000. The Sobol design of experiments has the advantage that it is space-filling and guarantees that any of its sub-sequences is also space-filling (Santner et al. 2003). Thanks to this property, subsequences of the design of experiments can be used to fit the Gaussian process predictors without the need to run additional simulations. The simulations were distributed over an HPC cluster and obtained in 19 days. Due to storage limits, it was impossible to constitute the 3900 points. The predictors are then used to obtain the 3900 simulations needed to correctly estimate the risk maps. Figure 2.b shows the probabilistic risk map constructed from the 1000 simulations. The enclosed zones correspond to the upper bound (conservative stand) of the 95% confidence interval of the location of the boundary of the risk zones. For a closer comparison with the deterministic approach, Figure 3.a shows the 95% confidence interval of the location of the SEI boundary with the deterministic risk zone superposed on black. The orange zone (the 95% confidence interval) can be seen as the uncertainty of the location of the real boundary of the risk zone due to the uncertainty about the release and atmospheric conditions. The location of the boundary is highly dependent on the wind conditions, which explains why the confidence interval is so wide compared to the deterministic approach. Only near the source (red zone) it can be concluded with great certainty (probability greater than 0.975) that the SEI threshold is exceeded. The more we go further from the source, the more the risk will depend on the wind direction and speed. To the point where the yellow zone has a probability lower than 0.025 of exceeding the SEI threshold.

Vectorial Gaussian process predictors are used to predict the 3900 simulations needed to correctly estimate the 95% confidence interval. One predictor is fitted for each tile of the domain. For demonstration purposes, only the SEI threshold is considered. Due to memory limitations, some extra steps are required:

- Only the tiles / points of interest are taken into account in the Gaussian process predictors. A point is considered of interest if for the risk map in Figure 2.b it exceeds the safety threshold. A tile is considered of interest if it has at least one point of interest.
- For each tile of interest, a vectorial Gaussian process is fitted only over the points of interest.
- Tiles that have more than 10000 points of interest had to be divided further in sub-tiles.

One of the advantages of Gaussian process predictors is that they yield a response in the form of a probability distribution whose mean is the most probable prediction and whose standard deviation depends on an auto-evaluation of the prediction error (Santner et al. 2003). This information is used to compute confidence intervals of the predictions. In a conservative stand, we take into account the upper bound of such an interval for the dose predictions.

The methodology was tested with a learning design of experiments of 100, 200, 300 and 400 simulations. It was concluded that starting at 300 simulations the results were satisfactory. Below this number, there are not enough points to represent the whole range of the phenomena over the spatial grid, mostly due to the fact that the wind direction is uncertain. The Gaussian predictors fitted with 400 simulations managed to better predict low probability zones. The fitting time was of 40 minutes with a prediction time of 5 minutes for the 3900 simulations. The predictors were validated using the leave-one-out method to estimate the coefficient of determination  $R^2$  (Santner *et al.* 2003). Only three tiles had an  $R^2$  below 0.75, but they are far from the source and have low impact. Figure 3.b shows the risk map constructed with the Gaussian predictors approach. For the sake of comparison, the Monte-Carlo reference is superposed in black. It can be seen that the 0.025 probability boundaries are tightly closed together, which is the target from a conservative stand.

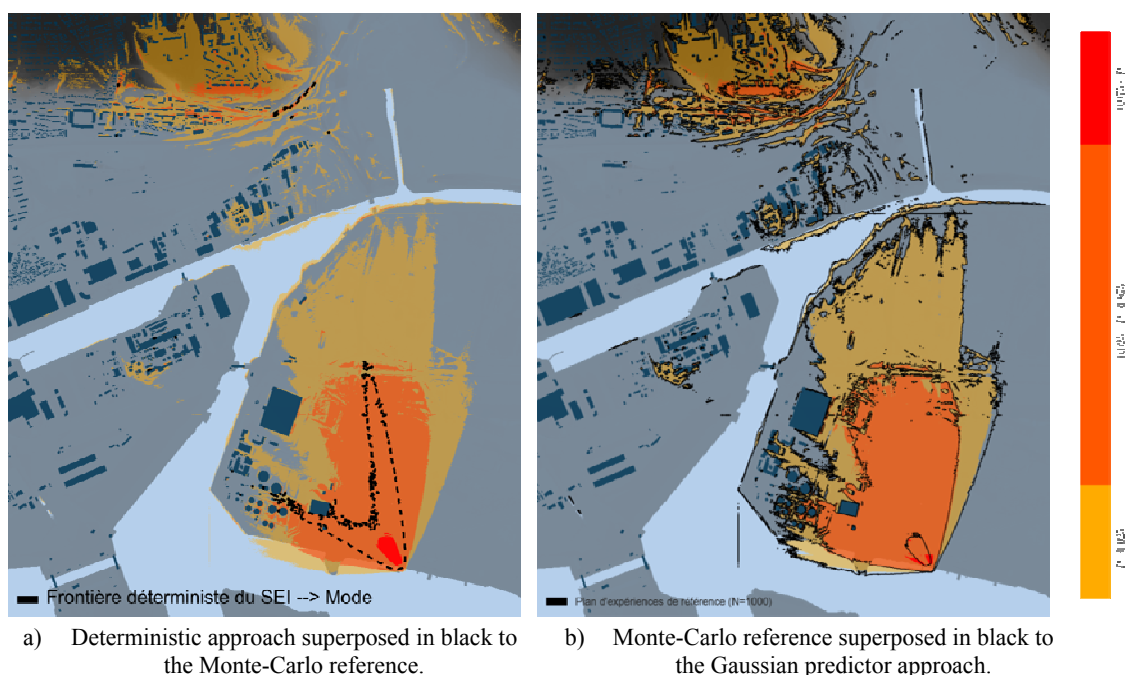


**Figure 3.** 95% confidence interval of the boundary of the risk zone for the SEI threshold.

## CONCLUSIONS

This study constitutes an improvement of the probabilistic risk assessment approach previously introduced by (Armand et al. 2014). It allowed the extension of the methodology to a larger scale divided in tiles and to the case where the wind conditions are considered uncertain and vary along the release period. It was concluded that the wind conditions have a great impact on the position of the boundary of the risk zone, which is why the 95% confidence interval is considerably wide. Taking uncertainty into account also revealed danger zones that are not identified by the deterministic approach (near the top at the level of a cliff). This reinforces the need to take into account uncertainty in this type of studies. Even when applying a worst-case-scenario deterministic approach, it is impossible to obtain a conservative risk map that reflects the uncertainty about the wind conditions and some potential danger zones may be neglected.

## REFERENCES

- Armand, P. et al., 2014. Probabilistic safety analysis for urgent situations following the accidental release of a pollutant in the atmosphere. *Atmospheric Environment*, **96**, .1–10. Available at: <http://linkinghub.elsevier.com/retrieve/pii/S1352231014005433>.
- Dubourg, V. et al., 2013. Uncertainty treatment in dispersion modelling of accidental releases. In *15th International Conference on Harmonisation within Atmospheric Dispersion Modelling for Regulatory Purposes*. Madrid, Spain.
- Santner, T.J., Williams, B.J. & Notz, W., 2003. *The design and analysis of computer experiments*, Springer.
- Tinarelli, G., L. Mortarini, S. Trini-Castelli, G. Carlino, J. Moussafir, C. Olry, P. Armand, and D. Anfossi. 2013. Review and validation of Micro-SPRAY, a Lagrangian particle model of turbulent dispersion. *Lagrangian Modeling of the Atmosphere, Geophysical Monograph*, Volume 200, AGU, 311-327.

**17th International Conference on  
Harmonisation within Atmospheric Dispersion Modelling for Regulatory Purposes  
9-12 May 2016, Budapest, Hungary**

---

**CFD-RANS PREDICTION OF INDIVIDUAL EXPOSURE FROM CONTINUOUS RELEASE OF  
HAZARDOUS AIRBORNE MATERIALS**

*George C. Efthimiou<sup>1</sup>, Spyros Andronopoulos<sup>1</sup>, John G. Bartzis<sup>2</sup>*

<sup>1</sup>Environmental Research Laboratory, INRASTES, NCSR Demokritos, Patriarchou Grigoriou &  
Neapoleos Str., 15310, Aghia Paraskevi, Greece

<sup>2</sup>University of Western Macedonia, Dept. of Mechanical Engineering, Sialvera & Bakola Str., 50100,  
Kozani, Greece

**Abstract:** One of the key issues of recent research on the dispersion inside complex urban environments is the ability to predict individual exposure of an airborne material which is released continuously from a point source. The present work addresses the question whether the Computational Fluid Dynamics (CFD) – Unsteady Reynolds Averaged Navier Stokes (URANS) methodology can be used to predict individual exposure for various exposure times. The whole effort is focused on the prediction of individual exposure inside a complex real urban area. Sensitivity analysis for the turbulence closure modeling is also performed. The capabilities of the proposed methodology are validated against wind tunnel data. The reference data set was compiled by members of COST Action ES1006. The provision of reference data is gratefully acknowledged.

**17th International Conference on  
Harmonisation within Atmospheric Dispersion Modelling for Regulatory Purposes  
9-12 May 2016, Budapest, Hungary**

---

**CFD MODELLING OF DISPERSION IN NEUTRAL AND STABLE ATMOSPHERIC  
BOUNDARY LAYERS: RESULTS FOR PRAIRIE GRASS AND THORNEY ISLAND**

*Rachel Batt<sup>1</sup>, Simon Gant<sup>1</sup>, Jean-Marc Lacome<sup>2</sup>, Benjamin Truchot<sup>2</sup> and Harvey Tucker<sup>1</sup>*

<sup>1</sup>Health and Safety Executive, Buxton, UK

<sup>2</sup>INERIS, Verneuil-en-Halatte, France

© British Crown Copyright (2016)

**Abstract:** The purpose of this paper is to assess the impact on dispersion model predictions of errors introduced by Computational Fluid Dynamic (CFD) models of Atmospheric Boundary Layers (ABLs). It is a known problem that CFD models using the standard  $k-\varepsilon$  turbulence model struggle to maintain the correct ABL profiles along the length of a flat, unobstructed computational domain. Appropriate ABL profiles may be imposed at the inlet but they are often progressively modified downwind by the CFD model until they no longer represent the specified stability class and/or wind speed. Various solutions have been proposed in the literature to address this issue, although many of them are complex and difficult to implement in commercial CFD software. Also, little is known about the impact of the ABL profiles on dispersion model predictions.

To examine this issue, CFD simulations are presented for two sets of field scale experiments: Prairie Grass and Thorney Island. The Prairie Grass cases considered involve continuous releases of a passive tracer in both neutral and stable ABLs. One of the reasons for studying these experiments is to compare dispersion predictions from a standard CFD solution to results obtained from fixing the ABL with prescribed profiles throughout the flow domain. This approach is only possible for passive releases, where the flow field is unaffected by the presence of the tracer gas. Simulations are then presented for a Thorney Island experiment which involved a continuous release of dense gas in a stable ABL.

The results show that the modified ABL profiles produced by the CFD models affect the predicted concentrations in most cases. The maximum differences range from 50% to a factor-of-two in the two Prairie Grass cases, although the differences are minimised in the neutral ABL by using a short upwind fetch in the CFD model. For the Thorney Island case, attempts were made to use a modified  $k-\varepsilon$  turbulence model to maintain the correct stable ABL profiles but the solution was numerically unstable and it failed to produce results. Results are presented for the standard  $k-\varepsilon$  turbulence model with two different roughness lengths, which produce different results. The inherent difficulties in resolving dense-gas flows over rough surfaces using CFD models are discussed.

**Key words:** *CFD, atmospheric boundary layers, passive gas, dense gas, dispersion, Prairie Grass, Thorney Island*

## **INTRODUCTION**

There is growing interest in the use of CFD to assess the risks posed by atmospheric releases of toxic and flammable gases from industrial sites. However, there are a number of challenges to overcome in modelling these flows. A central problem is that CFD models with the standard  $k-\varepsilon$  turbulence model are unable to preserve the correct ABL profiles throughout the flow domain. The problem is particularly acute in modelling stable ABLs, which are of primary interest to industrial risk assessments, since they often produce the largest hazard distances.

A companion paper by Batt *et al.* (2016) explores different treatments for CFD boundary conditions and adjustments to the standard  $k-\varepsilon$  turbulence model to overcome the problems in sustaining the correct ABL profiles throughout the domain. The work shows that improvements can be obtained by using the modified  $k-\varepsilon$  turbulence model of Alinot and Masson (2005) with consistent boundary conditions, but the ABL profiles still change along the length of a 2 km long domain. The Batt *et al.* (2016) work focuses solely on the ABL profiles themselves and does not consider gas dispersion. The present work extends

that work to consider passive and dense-gas dispersion. Two Prairie Grass experiments (Barad, 1958) in neutral (PG33) and stable (PG36) conditions and one Thorney Island trial (TI47, McQuaid and Roebuck, 1985) in stable conditions are simulated. These three cases do not provide a full picture of the CFD model's abilities: to do so would require simulations of many more experiments and a statistical assessment of the model's performance. The aim therefore is not to develop a validated model but to illustrate how changes in the ABL profiles affect dispersion results, with the experimental data providing a useful comparison measure.

### CFD MODEL CONFIGURATION

The simulations were all performed using the ANSYS-CFX v15 commercial CFD code with grids constructed from prism-shaped cells and grid-refinement near the ground. Conditions for each of the simulations are summarised in Table 1. In all of the simulations, the wind speed and direction were modelled as constant, i.e. wind-meandering was not modelled. Two values are shown in Table 1 for the roughness length,  $z_0$ : one for the ABL inlet profiles and one for the ground surface boundary condition within the CFD model. The reason these two values are different in the Thorney Island case is that the wall functions employed in ANSYS-CFX for the  $k-\varepsilon$  model (which are similar to those present in most CFD codes) have a limit on the maximum roughness length: the equivalent sand-grain roughness (which is approximately 30 times the value of  $z_0$ ), must be less than half the height of the near-wall grid cell. For fine grids it is therefore necessary to use a smoother wall than is present in reality. In the Thorney Island case, the dense gas cloud was less than 1 m deep and therefore a fine grid was used with a near-wall cell height of 0.05 m, which necessitated a smoother wall in the CFD model with a  $z_0$  of 0.0008 m, as compared to the experimental value of 0.01 m.

**Table 1** Conditions for the three test cases

<b>Trial</b>	<b>PG33</b>	<b>PG36</b>	<b>TI47</b>
<b>Atmos. stability (Pasquill class)</b>	Neutral (D)	Stable (F)	Stable (F)
<b>Source temperature (K)</b>	302.15	293.15	287.45
<b>Source elevation (m)</b>	0.45	0.45	0
<b>Source diameter (m)</b>	-	-	2
<b>Spill rate (kgs<sup>-1</sup>)</b>	0.0947	0.04	10.22
<b>Wind speed (ms<sup>-1</sup>)</b>	8.5	1.9	1.5
<b>Wind reference height (m)</b>	2	2	10
<b>Roughness length, <math>z_0</math> (m) – ABL</b>	0.006	0.006	0.01
<b>Roughness length, <math>z_0</math> (m) – Wall</b>	0.006	0.006	0.0008 and smooth*
<b>Friction velocity (ms<sup>-1</sup>)</b>	0.585	0.107	0.0378
<b>Domain size (m × m × m)</b>	2000 × 100 × 30	2000 × 100 × 30	1000 × 800 × 10
<b>Total grid nodes (millions)</b>	1.6	1.6	2.9
<b>Near-wall cell height (m)</b>	0.4	0.4	0.05
<b>Turbulence model</b>	Standard $k-\varepsilon$	Standard $k-\varepsilon$	Standard $k-\varepsilon$ and A-M

Standard  $k-\varepsilon$  = default ANSYS-CFX version of  $k-\varepsilon$  using coefficients from Jones and Launder (1974)

A-M = Alinot and Masson (2005)

\* The standard  $k-\varepsilon$  model used either  $z_0 = 0.0008$  m or  $z_0 = 0$  m and the Alinot and Masson (2005) used  $z_0 = 0.0008$  m.

The ABL inlet profiles for the mean velocity and turbulence parameters ( $U$ ,  $k$  and  $\varepsilon$ ) were specified using the French Working Group profiles (Lacome and Truchot, 2013) and for the stable cases (PG36 and TI47) the temperature ( $T$ ) profile was given by Alinot and Masson (2005).

An additional test was performed for TI47 with the inlet ABL profiles for  $U$ ,  $k$ ,  $\varepsilon$  and  $T$  all taken from Alinot and Masson (2005) with their modified  $k$ - $\varepsilon$  model. The reason for this extra case was that previous work (Batt *et al.*, 2016) showed that the model worked best with consistent inlet profiles. Other boundary conditions at the top, sides and outlet to the flow domain are the same as those used by Batt *et al.* (2016).

For the two Prairie Grass cases, the sulphur dioxide tracer gas was modelled as a passive scalar, i.e. the presence of the gas had no influence on the calculated flow field. To investigate the influence of the developing ABL profile on the results, two sets of simulations were performed: one denoted “fixed” where the ABL profiles were fixed throughout the domain to be the correct inlet profiles (i.e. the CFD model did not solve for  $U$ ,  $k$ ,  $\varepsilon$  and  $T$ , only the passive scalar) and another where the CFD model calculated the  $U$ ,  $k$ ,  $\varepsilon$  and  $T$  profiles (by solving the transport equations for  $U$ ,  $k$ ,  $\varepsilon$ ,  $T$  and the passive scalar). In the latter simulations, to investigate how the distance upstream of the source influenced the results, two separate passive scalars were injected at different locations in the CFD domain: one at 10 m downstream from the inlet boundary and another at 1000 m downstream. The results from these two scalars at 10 m and 1000 m are denoted “Full G1” and “Full G2”, respectively

In the Thorney Island simulations, the source of dense gas composed of 32% freon and 68% nitrogen, (with a density of about twice that of air) was released at a downstream distance of 250 m through a disc-shaped opening 2 m in diameter with a 2 m diameter capping disc 0.5 m above the opening. Simulations were also performed with no dense gas to assess how the ABL profiles changed along the length of the domain.

## RESULTS

### Prairie Grass

The results for the neutral Prairie Grass PG33 case, presented in Figure 1, show that the ABL profiles are well maintained, except for the turbulence kinetic energy which decreases downwind from the inlet. The predicted concentrations from the scalar released near the inlet (Full G1) are practically identical to those produced using the fixed ABL profiles. However, the results from the scalar released 1000 m downstream of the inlet are up to 50% higher, which demonstrates that minor changes in the ABL profiles along the length of the domain have an impact on the dispersion behaviour. All of the results predict concentrations between 3 and 30 times larger than the experiments, which suggest that mixing is globally underestimated.

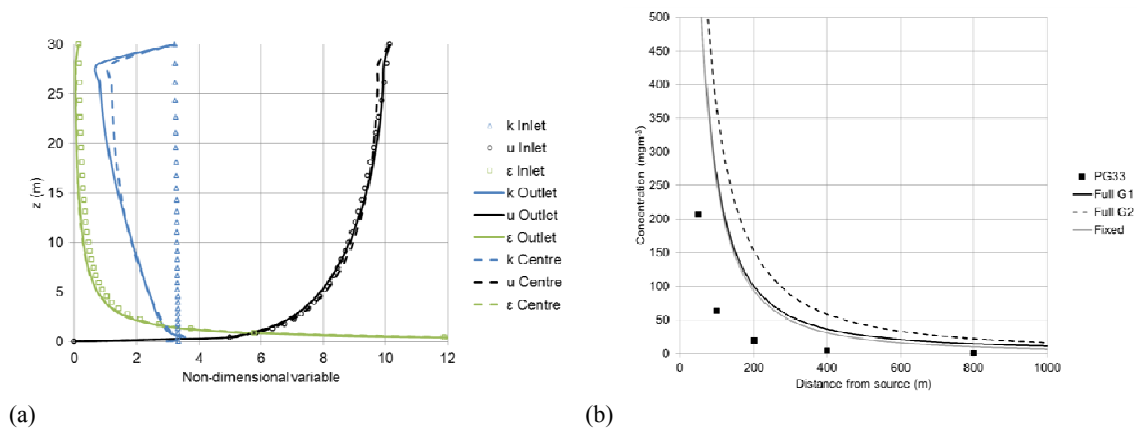
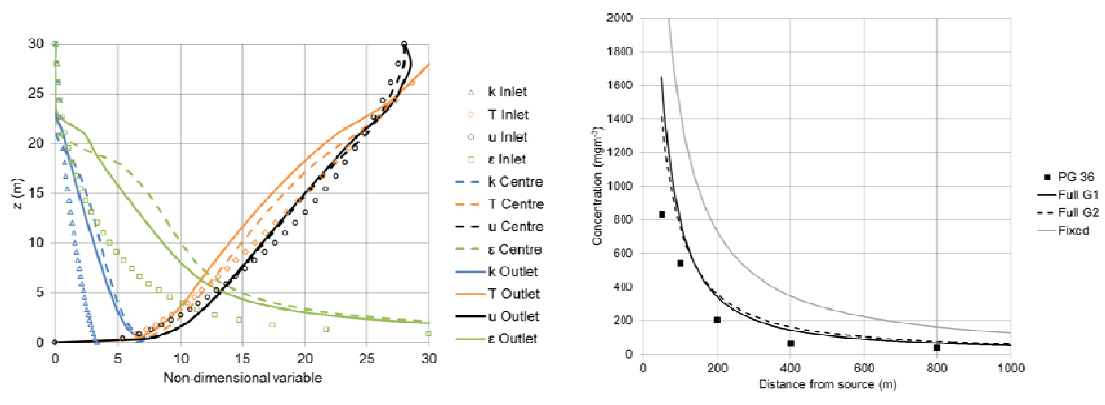


**Figure 1** Predicted results for Prairie Grass PG33 (a) Dimensionless ABL profiles at the inlet, centre and outlet of the domain (b) Concentrations downwind of the source along the centreline at a height of 1.5 m



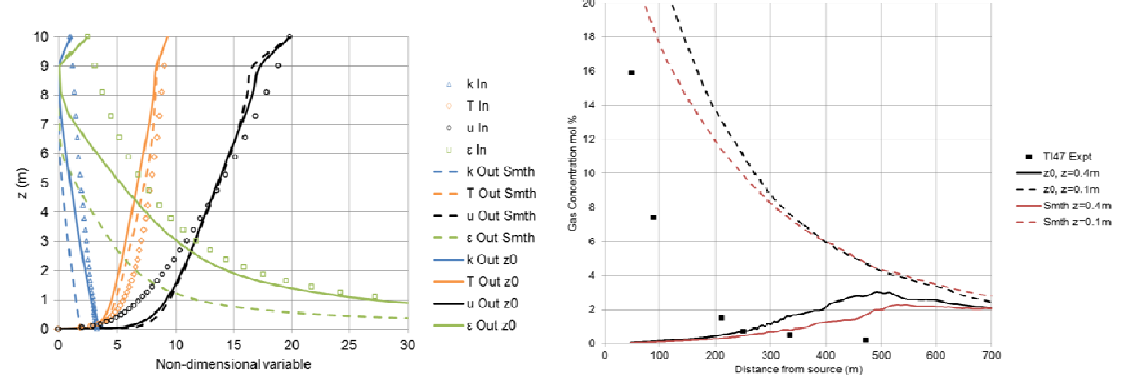
(a) (b)  
**Figure 2** Predicted results for Prairie Grass PG36 (a) Dimensionless ABL profiles at the inlet, centre and outlet of the domain (b) Concentrations downwind of the source along the centreline at a height of 1.5 m

For the stable Prairie Grass PG36 case, Figure 2 shows that the velocity and temperature profiles change along the domain: both of them increasing near the ground and decreasing above a height of around 6 m. The concentrations from the two tracer releases near the inlet and 1000 m downstream are practically identical (Cases Full G1 and Full G2) but both are around a factor of two lower than the result obtained with the fixed ABL profiles. Again, all of the model predictions are higher than the measurements, which may be due to several factors, such as the assumed constant wind speed and direction.

Sensitivity tests were performed with finer meshes and lower roughness lengths for the two Prairie Grass cases (not presented here) which showed that the results were insensitive to the grid resolution but they were affected by the roughness value (a 7 - 15% increase in concentration along the plume centreline for a release from 1000 m when the roughness was reduced from 0.006 m to 0.003 m).

**Thorney Island**

Attempts were made to model the Thorney Island TI47 case using the Alinot and Masson (2005) turbulence model in order to maintain the correct ABL profiles along the length of the domain. However, the solution was numerically unstable and it did not produce results. This was probably due to the Alinot and Masson (2005) model's use of tuning factors that produce unrealistically large source terms in the *k* and  $\epsilon$  transport equations in the regions of the flow where the dense gas produces strong density gradients. The model was developed for stable ABLs without the presence of any dense gas. Future work could consider modifying the model equations or using a zonal approach.



(a) (b)  
**Figure 3** Predicted results for Thorney Island TI47 (a) Dimensionless ABL profiles at the inlet of the domain and at the outlet, using standard *k-ε* with a rough wall and a smooth wall (b) Concentration (mol %) downwind of the source along the centreline at  $z = 0.4$  m and  $z = 0.1$  m for the model with roughness ( $z_0$ ) and with a smooth wall (Smth). The experimental measurements (TI47 Expt) were at height  $z = 0.4$  m

Results are presented for Thorney Island TI47 in Figure 3 using the standard  $k-\varepsilon$  model and two different roughness lengths (see Table 1 for details). Figure 3 (a) shows that the profiles are not maintained along the domain in either the rough or the smooth case with the smooth case showing significantly reduced turbulence levels, as might be expected. The predicted concentrations are shown in Figure 3 (b) at 0.4 m, the height at which the concentrations were measured in the experiments, and the arbitrary height of 0.1 m to show the strong vertical gradient in concentration. The results show that the roughness length has a modest effect on the predicted concentrations, with a maximum difference of a factor of two. In both cases, the predicted concentrations at 0.4 m are considerably lower than the measurements in the near-field, up to a distance of around 250 m downwind from the source, and further downwind the models significantly over-predict the measurements. The predicted plume is very shallow in the near-field with insufficient vertical mixing, which may be responsible for concentrations being over-predicted further downstream. This behaviour may be due to the model using a roughness length that was lower than the experimental value. However, the correct roughness length could not be used in the CFD model since to do so would have required grid cells to be at least 0.6 m high (due to the wall-function limits), which would not have resolved such a shallow layer of dense gas. A further complication of the relatively fine grid used was that the length-to-height ratio of the grid cells near the wall was large (up to a hundred). These high aspect ratio cells may be partly responsible for the small undulations shown in the concentration profiles in Figure 3 (b).

## CONCLUSIONS

The results presented here have demonstrated that CFD simulations using the standard  $k-\varepsilon$  turbulence model produce changes to the ABL profiles along the length of a CFD domain which affect the predicted gas concentrations. In the neutral Prairie Grass PG33 case, these changes were minimal if the gas was released near to the inlet to the domain. However, if the gas was released further downstream, the predicted concentrations differed by up to 50% as compared to the reference case with “correct” ABL profiles. In the stable PG36 Prairie Grass experiment, the predicted concentrations differed by up to a factor-of-two from the reference case, irrespective of whether the gas was released close to the orifice or further downwind.

The Thorney Island test case showed that CFD models face several challenges in modelling dense-gas dispersion over long distances in the atmosphere. It was not possible to produce a reference case with correct ABL profiles since the Alinot and Masson (2005) model was found to be numerically unstable and failed to produce results. CFD results from the standard  $k-\varepsilon$  turbulence model were in poor agreement with the measurements. This may have been due to the model using a smoother ground surface than was present in the experiments. Tests showed that the roughness length affected the predicted concentrations but it was not possible to use the correct roughness value from the experiments due to the limitations of the CFD wall functions and the need to use a fine near-wall grid. Future work could examine the use of a porosity/distributed resistance model to overcome this problem.

The results are in line with previous studies which pointed towards inherent limitations of CFD models based on  $k-\varepsilon$  turbulence models for modelling atmospheric dispersion of passive and dense gases. It is important that risk assessments using CFD results take into account the uncertainties introduced by the limitations of the  $k-\varepsilon$  turbulence model and issues relating to surface roughness and grid resolution.

## DISCLAIMER

The contributions made to this publication by Rachel Batt, Simon Gant and Harvey Tucker were funded by the Health and Safety Executive (HSE). The contents of the publication, including any opinions and/or conclusions expressed, are those of the authors alone and do not necessarily reflect HSE policy.

## REFERENCES

- Alinot C. and C. Masson, 2005:  $k-\varepsilon$  model for the atmospheric boundary layer under various thermal stratifications, *J. Solar Energy Engineer.*, **127**, 438-443.
- Barad, M.L, 1958: Project Prairie Grass, a field program in diffusion, Vol. 1–3, Geophysical Research Papers No. 59, Rep. AFCRC-TR-58-235, U.S. Air Force Cambridge Research Center, Bedford, Massachusetts.

- Batt, R. S.E. Gant, J.-M. Lacomme and B. Truchot, 2016: Modelling of stably-stratified atmospheric boundary layers with commercial CFD software for use in risk assessment, 15<sup>th</sup> International Symposium on Loss Prevention and Safety Promotion in the Process Industries, Freiburg, Germany, 5-8 June 2016.
- Jones W.P. Launder B.E., 1974: The numerical computation of turbulent flows, *Comput. Methods Appl. Mech. Eng.*, **3**, 269-289.
- Lacomme J.-M. and B. Truchot, 2013: Harmonization of practices for atmospheric dispersion modelling within the framework of risk assessment, 15th conference on “Harmonisation within Atmospheric Dispersion Modelling for Regulatory Purposes”, Madrid, Spain, 6-9 May 2013.
- McQuaid J and Roebuck B, 1985: Large scale field trials on dense vapour dispersion, Commission of the European communities indirect action programme “Safety of thermal water reactors”, 1979-83, Final report on contracts 029SRUK and 036SRUK with the Health and Safety Executive, EUR10029en, Commission of the European Community, Brussels.

**17th International Conference on  
Harmonisation within Atmospheric Dispersion Modelling for Regulatory Purposes  
9-12 May 2016, Budapest, Hungary**

---

**CONCLUSIONS AND REFLECTIONS FROM COST ACTION ES1006 ACTIVITY: WHAT DO WE MISS FOR THE APPLICATIONS OF MODELS IN LOCAL-SCALE EMERGENCY RESPONSE IN BUILT ENVIRONMENTS?**

*Trini Castelli S.<sup>1</sup>, Leitl B.<sup>2</sup>, Baumann-Stanzer K<sup>3</sup>., Reisin T.G.<sup>4</sup>, Armand P.<sup>5</sup>, Andronopoulos S.<sup>6</sup>,  
and all COST ES1006 Members<sup>7</sup>*

<sup>1</sup>Institute of Atmospheric Sciences and Climate, National Research Council, Torino, Italy

<sup>2</sup>Meteorological Institute, University of Hamburg, Hamburg, Germany

<sup>3</sup>Central Institute for Meteorology and Geodynamics, Vienna, Austria

<sup>4</sup>SOREQ NRC, Yavne, Israel

<sup>5</sup>CEA, DAM, DIF, Arpajon, France

<sup>6</sup>National Centre for Scientific Research "Demokritos", Institute of Nuclear and Radiological Sciences and Technology, Energy and Safety, Aghia Paraskevi, Greece

<sup>7</sup>[http://www.cost.eu/domains\\_actions/essem/Actions/ES1006](http://www.cost.eu/domains_actions/essem/Actions/ES1006), <http://www.elizas.eu/>

**Abstract:** The main focus of the COST ES1006 Action has been the evaluation of the airborne pollutant dispersion models applied to accidental or intentional releases in complex built environments, urban or industrial, in the emergency response framework. The results of the three modelling exercises performed during the Action research activity are summarized and discussed, referring to the related model evaluation protocol and the connected best-practice guidelines elaborated during the Action.

**Key words:** emergency response, accidental releases, model evaluation

## **INTRODUCTION**

A main research task of COST Action ES1006 was to evaluate the available local-scale models in built environments, by model inter-comparison, as well as by comparison against test data from qualified field and laboratory experiments. Assuming that a typical atmospheric dispersion model has already been validated with regard to local-scale dispersion simulation, the existing model evaluation and validation strategies were extended towards task- and application-specific measures for accidental release scenarios in emergency response conditions. Thus, additional quantities, such as extreme value prediction and exposure assessment, have been considered for the evaluation of the model performances. Both continuous and puff releases were taken into account in three modelling exercises carried out during the Action. The model evaluation focuses on the output obtained by the different model categories considered. On the basis of the results, and for supporting their analysis, a model evaluation protocol was established with an application-oriented approach and recommendations for its adoption in emergency response were proposed. The comprehensive analysis was then finalized issuing best-practice guidelines for consolidating the use of atmospheric dispersion models into emergency response tools, with a particular attention to the needs of model users and stakeholders.

The main results of the Action are summarized and the main issues still open are discussed. In the context of the conference, we like to propose an interactive discussion on what has been learnt, what are the limitations found in applying up-to-date air pollution models in emergency response, and, in particular, what the scientific community needs still to do in order to address and support the use of atmospheric dispersion models in such context

## **THE MODELLING EXERCISES**

Three case studies were considered as benchmarks for the modelling evaluation exercises (Baumann-Stanzer et al., 2015): (1) the Michelstadt case, based on flow and dispersion data gathered in a wind-

tunnel experiment carried out at the Environmental Wind Tunnel Laboratory (Hamburg University), where an idealized urban environment was modelled and both continuous and puff releases were reproduced; (2) a real-field campaign with continuous and puff releases conducted in a European harbour, named as CUTE 1 case, which was also reproduced in the wind tunnel, named as CUTE 3; (3) a real industrial accident occurred in a European Country, named as AGREE case.

In the experimental cases, the hazardous releases occurred in different locations in the built-up area: in open squares, small or wide streets, perpendicular or parallel to the prevailing large-scale flow or in court yards. After a preliminary non-blind test in one Michelstadt case, in all other cases the exercises were performed as ‘blind tests’, that is only the minimum information on the flow was provided to the modellers, while no information on the measured concentrations were available.

Different modelling tools were applied, from Gaussian type, to Lagrangian and advanced Eulerian CFD and LES. Given the varying airborne hazards flow and dispersion modelling approaches that were used, models were classified as three main types, according to their flow and dispersion approach characteristics, as reported in Table 1.

**Table 1.** Classification of the types of models applied in the COST ES1006 Action modelling exercises

Model type	Modelling approach: Flow	Dispersion
<b>Type I</b>	models that do not resolve the flow between buildings	Gaussian
<b>Type II</b>	models resolving the flow diagnostically or empirically	Lagrangian
<b>Type III</b>	models that resolve the flow between buildings	Eulerian

In case of continuous releases, steady-state concentrations, and the area affected by values above a relevant threshold are usually the information expected from an emergency response model. In case of puff releases, the dosage, the arrival time of the puff at given locations, the duration of the puff passage and the peak concentration values are of interest. In Figures 1 and 2 examples of the results based on scatter plots are shown.

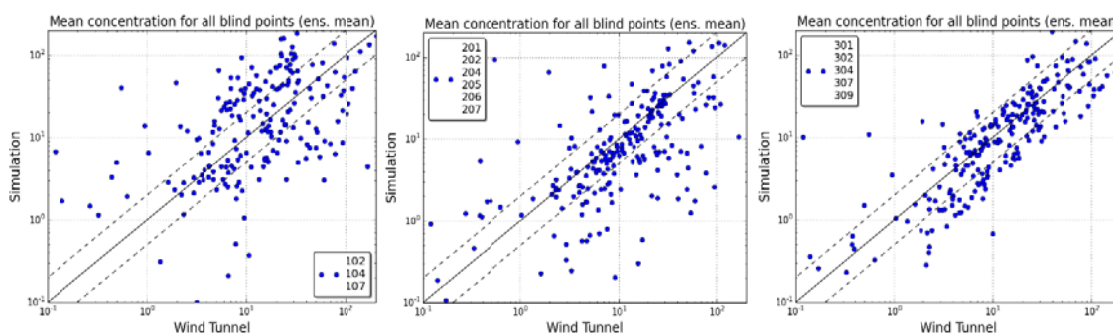


**Figure 1.** Michelstadt test-case. Scatter-plots of measured versus ensemble averaged modelled mean concentration values at all receptors for all blind continuous releases for model Type I (left), Type II (centre) and Type III (right).

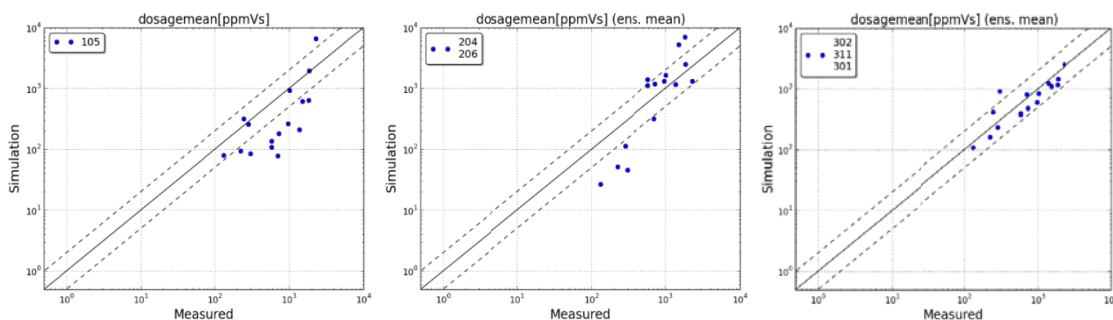


**Figure 2.** CUTE 3 test-case. Scatter-plots of measured versus ensemble averaged modelled mean dosage values at all receptors for all blind puff releases for model Type I (left), Type II (centre) and Type III (right).

To provide an overall view on the different test cases, a statistical analysis was applied to Michelstadt and CUTE experiments. Summarizing the results, it was found:

for continuous releases, (i) the metrics are generally better for the non-blind case, where more detailed meteorological information for the model input was available; (ii) the metrics show a better performance and agreement with the observations under controlled conditions (wind tunnel data); (iii) Type II and Type III models are generally superior to Type I ones, in particular for the FAC2 and the correlation coefficient R; (iv) some specific metrics, MG and VG, hardly get good values, since they are strongly influenced by extremely low values and are undefined for zero values: this type of problems are discussed in the Model Evaluation Protocol document (see next section);

for puff releases, (i) Type II and Type III statistics are often comparable, with some better performances for Type III models; (ii) the metrics do not differ substantially with respect to the continuous case, even if in some cases they are a bit worse: (iii) the metrics are not always better for the non-blind case with respect to the blind one.

The comparison of the statistics between the continuous and puff releases confirms the robustness of the models even in simulating short and transient events and suggests that, since the main difficulty here is the correct reproduction of transient events, the ‘blindness’ of the test play a secondary role.

In general, despite of the trend to improving performances with a higher complexity in modelling, the accuracy of the results produced by the most advanced models is still not guaranteed to be always and fully satisfying. The availability of proper inputs was proved once more to play a fundamental role for obtaining reliable results, based on sensitivity analyses. Yet, the models showed to be robust enough even when dealing with poor driving information, as it generally happens in case of accidental releases. Models showed to represent a valid tool to support handling emergency situations and can be applied with a certain confidence, all uncertainties considered when dealing with unexpected situations. It was established that to drive the choice of the kind of modelling approach, a balance between the model performances, thus its reliability, and the run-time effort, given that a fast answer is required, has to be considered. Different modelling approaches can be used in the different phases of the response process: preparatory, emergency and post-analysis. However, a fast but inaccurate model output can compromise the effectiveness of a response action, and this is another criterion to consider when taking decisions on what modelling tool to adopt.

#### **MODEL EVALUATION PROTOCOL AND BEST PRACTICE GUIDELINES**

The pertinence and applicability of the standard evaluation protocols and, specifically, of the commonly used statistical figures for the evaluation of the model performances in the emergency response context was a main subject matter for discussion. Recommendations based on the experiences gained through the course of COST Action ES1006 and, specifically, from the modelling exercises, are detailed in the Model Evaluation Protocol (MEP) document (Andronopoulos et al., 2015). The Best Practice Guidelines (BPG) document (Armand et al., 2015) integrates the results obtained and the analysis performed in the course of the Action, to organize information and guidelines based on state-of-the-art atmospheric dispersion models (ADM), at the same time tailoring them to the needs of the emergency responders, decision makers and/or stakeholders.

In applying ADM for accidental or deliberate hazardous releases in built areas, it is necessary to address both general and specific requirements for each of the three distinct phases of emergency response and preparedness: (1) pre-accidental analysis and planning (a priori predictions); (2) predictions during an actual emergency; (3) post-accidental analysis (a posteriori simulations). The final objective is to propose guidance for using ADM integrated (or not) in Emergency Response Tools (ERT, Figure 3), dedicated to decision-support in case of releases of hazardous materials into the atmosphere

The basic structure of the MEP adopted in the Action assumes to provide the following: (i) model description; (ii) description of the database used for the validation; (iii) scientific assessment of the model; (iv) user-oriented assessment of the model; (v) code verification (software errors); (vi) validation (or corroboration) of the model by comparing model predictions with observations; (vii) sensitivity and uncertainty analyses. It was then established that using ADM for emergency response, in application to

releases of airborne hazardous materials in urban areas, needs specific important requirements: (i) computation of dispersion from transient-in-time releases, (ii) computation of flow and dispersion in built up (urban or industrial) environment, (iii) computation of affected areas based on a defined threshold of a quantity of interest, (iv) modelling of special relevant physico-chemical phenomena, (v) addressing the required computing resources (computing time and hardware).

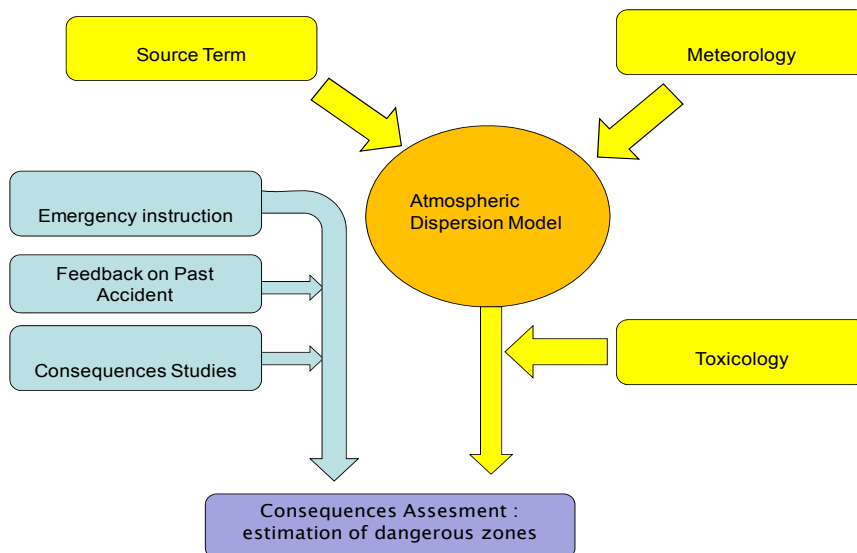


**Figure 3.** General sketch-up of an Emergency Response Tool (ERT).

The use of standard statistical metrics provides a usual platform for the validation of any ADM. In addition to these, within the context of emergency response and releases in urban areas, an important indicator of a model's fitness for purpose is the correct prediction of spatial and temporal extension of risk zones or affected areas. As stated in the BPG document, this evaluation should be based on exposure values depending on specific threat scenarios, which define the interval of concentrations that lie in the specific hazard zone. The affected areas can be defined through different quantities, but for emergency response cases, it is recommended to define them through Levels of Concern (LOC) values, such as AEGs (Acute Exposure Guideline Levels) or IDLH (Immediate Danger to Life or Health).

A fundamental aspect is that the evaluation process should reflect a consensus among the various parties involved: the model developer, the model user and the stakeholder who undertakes the task of decision making. The improvement of the model has to be guided by the user and stakeholder requirements, and supported by the provision of guidance for its application within the context of emergency response: this topic is thoroughly addressed in the BPG document. The interaction between the different parties is thus highly recommended. Since the simulation results contain uncertainties due to the model formulation, to the input data and to the inherent variability of the physical system, it is also recommended to communicate to the stakeholders in a transparent and understandable manner the quantified uncertainties of the numerical outcomes. The BPG document is also devoted to highlight the supporting information which can be provided to first responders by ADM and ERT in an emergency.

### CONCLUSIONS AND OPEN ISSUES

From the experience gained, in the context of emergency response, it is highly recommended to validate an ADM against several sets or test cases of observational data. These sets should include both dedicated boundary layer wind tunnel measurements as well as dedicated field trials. Experiments should be designed as application-oriented, so that the observed data reflect the difficulties associated with the specific type of the problem, which is accidental or deliberate release in real urban areas. Test cases should treat many different release scenarios: varying source release rates, different source locations and even simultaneous releases from different sources in a city. This implies the need for a close collaboration of experts in the fields of observational techniques and modelling as well as first responders and key

policy and decision makers. Each test case dataset has to be easily accessible and well documented. When it gets difficult to locate experimental data sets descriptive of conditions of interest for validation of models for emergency response, it is suggested to consider also inter-comparisons among the results from different models in real cases. Model to model validation needs to be treated with care, and more systematic work is needed to come up with clear rules on this subject. In particular, each reference model data set that is used for the comparison needs to have its uncertainty adequately quantified. These requirements need to be more precisely defined with additional research work and sufficient application experience.

Several open issues need further investigation and a concerted and harmonized approach to address them. Among them, here we briefly list some main items to open a discussion in the scientific community.

In a real emergency situation, the required input information to ADM is not always available: *how to deal with incomplete information of source term and meteorological data and their uncertainties?* The source term is the most difficult information to retrieve. Meteorological input data should not be an issue in principle, but their access needs to be facilitated. *How to systematically take into account and communicate stochastic and epistemic uncertainties*, on model physics and input data, is a very complicated matter and still a topic for scientific research. In emergency response, it is crucial not to under-estimate the actual consequences of a noxious dispersion event: *how to produce reasonably conservative results?* Conservative results should be in a range that enables to adopt actions for which the benefits are greater than their drawbacks, with the need of being realistic in the dispersion computation and the distribution of the noxious agent. Related to this, it is important to establish *how to overcome different results obtained by different models or operators*: consistency has to be found between models in the same or in neighbouring categories. Moreover, even if and ADM is verified and validated, it cannot give results that correspond exactly to the field measurements: an effort and an agreed approach are needed to establish *how to reconcile the modelling results and the field measurements*. This is an important issue especially when supporting decision makers, responding at the same time to the question on *how to reconcile the needs and demands of the people involved*, whom in the end take care of the actions to face the emergency. The final question, on which consensus needs to be built, is: *how to choose the appropriate ADM and ERT?* The choice should take into consideration a series of conditions and parameters, such as the topography and morphological characteristics of the area, the climatology of the area, the scenario of the release, the expertise of operators, the computational and operative resources available, the emergency phase and the time restrictions.

The COST ES1006 Action succeeded in addressing these items and in proposing possible solutions to some open issues, based on an international debate in the frame of the Action activity. We like to promote further the discussion inside the ADM community, in order to establish a harmonized approach to the problem of applying models for emergency response scenarios in complex, built environments.

## REFERENCES

- Andronopoulos S., Barmpas F., Bartzis J.G., Baumann-Stanzer K., Berberkar E., Efthimiou G., Gariazzo C., Harms F., Hellsten A., Herring S., Jurcakova K., Leidl B., Trini Castelli S., 2015. COST ES1006 - Model evaluation protocol, Publisher: University of Hamburg, ISBN: 987-3-9817334-1-9  
[http://www.elizas.eu/images/Documents/Model%20Evaluation%20Protocol\\_web.pdf](http://www.elizas.eu/images/Documents/Model%20Evaluation%20Protocol_web.pdf)
- Armand, P., J. Bartzis, K. Baumann-Stanzer, E. Bemporad, S. Evertz, C. Gariazzo, M. Gerbec, S. Herring, A. Karppinen, J.-M. Lacomme, T. Reisin, R. Tavares, G. Tinarelli, and S. Trini Castelli, 2015 COST ES1006 Best Practice Guidelines. COST Action ES1006, April 2015. Publisher: University of Hamburg, 987-3-9817334-0-2 [http://elizas.eu/images/Documents/Best%20Practice%20Guidelines\\_web.pdf](http://elizas.eu/images/Documents/Best%20Practice%20Guidelines_web.pdf)
- Baumann-Stanzer, K., S. Andronopoulos, P. Armand, E. Berberkar, G. Efthimiou, V. Fuka, C., Gariazzo, G. Gasparac, F. Harms, A. Hellsten, K. Jurcakova, A. Petrov, A. Rakai, S. Stenzel, R. Tavares, G. Tinarelli, S. Trini Castelli, 2015. COST ES1006 Model evaluation case studies: Approach and results. COST Action ES1006, April 2015. Publisher: University of Hamburg, 987-3-9817334-2-6  
[http://elizas.eu/images/Documents/Model%20Evaluation%20Case%20Studies\\_web.pdf](http://elizas.eu/images/Documents/Model%20Evaluation%20Case%20Studies_web.pdf)

**17th International Conference on  
Harmonisation within Atmospheric Dispersion Modelling for Regulatory Purposes  
9-12 May 2016, Budapest, Hungary**

---

**EFFECTS FROM URBAN STRUCTURES TO ATMOSPHERIC DISPERSION MODELS IN  
DECISION SUPPORT SYSTEMS FOR NUCLEAR EMERGENCIES**

*Hartmut Walter and Gerhard Heinrich*

Federal Office for Radiation Protection, Munich, Germany

**Abstract:** In present times, even no more than in the past, there is a fear that terrorists might threaten population or a state to enforce illegal demands. An often-discussed possibility is to disperse explosive material combined with radioactive substances somewhere in public areas (dirty bomb- or RDD- (radiological dispersive device) scenario). These public areas consist generally of urban structures, from smaller buildings like housing areas to complex buildings like areas in the centre of big cities.

A decision support model (LASAIR) has been developed to assist in such a case providing quick and basic information on the radiation exposure. The paper gives an overview of the model and especially on the influence of simple urban structures to the dispersion of radioactive substances and related radiation exposure.

**Key words:** *Urban structures, malevolent attacks, dirty bomb, Lagrangian- Particle-Model, decision support.*

## **INTRODUCTION**

In present times there still is a fear that terrorists might aim with an act of violence against population in an urban environment to enforce illegal demands. An often-discussed possibility is to disperse explosive material combined with radioactive substances somewhere in public areas. This is called a dirty bomb- or RDD- (Radiological Dispersive Device) scenario.

In such a case, it is essential to get as quickly as possible a clear picture of the potential threat. This means that the possible radioactive concentration in surrounding areas and the contribution to the pathways that lead to the exposure of the population are assessed and counter measures are recommended.

## **THE DECISION SUPPORT SYSTEM LASAIR**

An existing system program LASAT, (Janicke, L., 1983, 1985) based on Lagrangian particle simulation has been adapted to meet the requirements of a dirty bomb scenario. Conducted by the German Federal Office for Radiation Protection (BfS) and under the direction of the German Federal Ministry for Environment, Nature Preservation, Building and Reactor Safety (BMUB) the program LASAIR (Walter, H. and G. Heinrich, 2011, Walter, H. and G. Heinrich, 2014)) has been developed which is able to give a first and rapid overview of atmospheric dispersion, ground activity, deposition and different exposition pathways (inhalation, ground- and cloud shine) after an instantaneous release of radioactive material.

The program can be used by radiation emergency authorities that are responsible for emergencies within the different German Federal States (Bundesländer). The program was developed in the year 2000 and has been continuously upgraded since then.

The model LASAIR (Lagrangian Simulation of the Dispersion and Inhalation of Radionuclides) in its latest version is able to simulate an explosion of an RDD with additional radioactive material and computes the dispersion in the planetary boundary layer. In order to assess the dose to the population, the inhalation, ground- and cloud shine doses to individuals can be computed. The model has been introduced as a rapid decision support system within the Federal Office for Radiation Protection and authorities in Federal States in Germany. LASAIR has been used within model comparisons for dispersion models especially used for radioactive substances and herein proved its ability (von Arx et al., 2016, Thiessen et al 2011).

## **FEATURES OF THE DECISION SUPPORT SYSTEM LASAIR**

Special attention has been directed to the usage of the program in emergency cases. The program can be run on a laptop, is extremely easy to handle and allows the user only a strictly straight forward step by step usage in order to grant a maximum security feeding the program with input data.

To model just needs basic necessary meteorological input as

- wind speed and wind direction
- stability class,
- precipitation
- roughness length
- source term (single point, area, volume, with momentum)
- amount of explosives
- radionuclide and activity

Outputs of the model are activity concentration, deposition, ground shine, cloud shine, inhalation dose and time dependant information (activity, dose) in different scales.

The latest version of LASAIR (Version 4.0.5, April 2014) includes the following features additionally:

- actual turbulence parameterisation (harmonized in Germany),
- verification according to radioactive dispersion experiments with Tc-99m,
- worldwide orography and individual topography,
- rapid online integration of urban structures,
- use of Open Street Maps for EU or worldwide operation.

## **ACTUAL TURBULENCE PARAMETERISATION (HARMONIZED IN GERMANY)**

Investigating literature one will find a huge amount of different atmospheric dispersion models. They have been developed according to different demands and applications. It is one aim of the HARMO-Organisation to provide harmonisation for the dispersion models in such a way that the application of different models e.g. in an emergency, will lead to similar results.

In Germany, the VDI (Verein Deutscher Ingenieure, Association of German Engineers) supports strongly the idea of harmonisation in different aspects. One of it is to develop state of the art standards for the turbulence parameterisation in mesoscale dispersion models. In the course of 2014 the basic work for a new turbulence parameterisation based on measurements at a weather mast close to the city of Hamburg in the northern part of Germany will be completed. This parameterisation will end in a guideline that is applicable for all modelers (VDI 3783, Blatt 8; 2014 Gründruck/ 2016 Weißdruck) and shall set a standard in Germany but as well in other countries.

The new turbulence parameterisation will be implemented in LASAT and therefore in LASAIR making sure that the scientific improvement will be available for the model users.

## **USAGE OF LASAIR WITHIN URBAN STRUCTURES**

The application of LASAIR especially for dirty bomb scenarios requires the consideration of urban structures. Special windfield models therefore have been examined to be implemented in Decision Support Systems. Complex wind field models are available however require detailed input information that is not available in general during a real emergency. Alternatively less complex windfield models based on a diagnostic approach have been taken into account.

Following the development of the windfield model TALDia (Janicke, U. and L. Janicke, 2004) it was demonstrated, that for long term dispersion calculations and ground based releases the differences between complex (nonhydrostatic) windfield models and TALDia is less than 30 %. This level might be higher for short term or instantaneous releases. However as the computation time for complex windfield models is significantly higher than that for diagnostic windfield modes it was judged that the advantages are on the diagnostic windfield side and therefore a combination of the basic dispersion model (LASAT) and the diagnostic windfield model similar to TALDia (Lprwnd, three dimensional, divergence free windfield model) was implemented in LASAIR.

To demonstrate the abilities of Lprwnd several dispersion calculations with different urban structures from very simple to complex has been conducted.

Description of the urban scenarios that have been investigated:

- simple building, basic dimensions 30 m x 20 m x 20 m
- building block with courtyard, basic dimensions 110 m x 80 m x 20 m (see Figure 1)
- several building blocks, basic dimensions 350 m x 80 m x 20 m (see Figure 2)
- simple building, dimensions see above, building is upwind of the source
- simple building, dimensions see above, building is downwind to the source
- simple building, dimensions see above, building is upwind to the source
- two simple buildings, dimensions see above, source is between the buildings

Some results for wind fields (Lprwnd) and exposition from LASAIR are depicted in the following figures:



**Figure 1.** a, b, c, d. Scenario building block. Figures show 2 d- and 3 d- sight (top left, top right), windfield (wind direction 270°) and inhalation dose for an arbitrary radionuclide and activity (bottom left, bottom right).

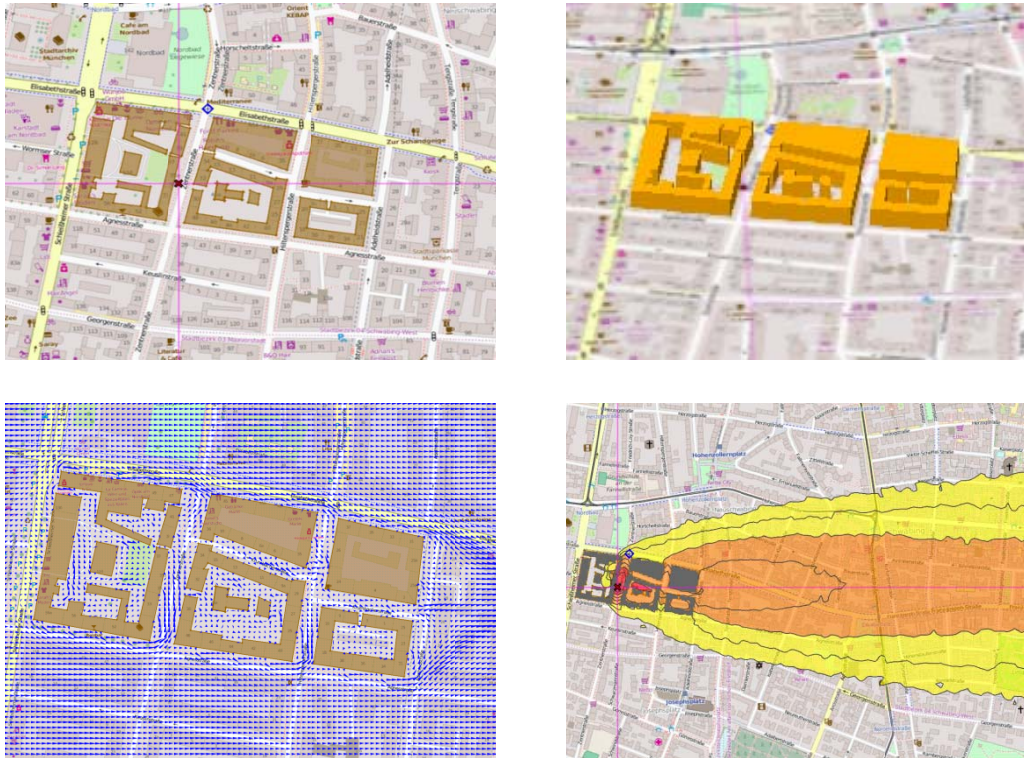


**Figure 2.** a, b, c, d. Scenario several building blocks. Figures show 2 d- and 3 d- sight (top left, top right), windfield (wind direction 270°) and inhalation dose for an arbitrary radionuclide and activity (bottom left, bottom right).

The following Figure 3 shows the inhalation dose [mSv] of an arbitrary radionuclide and activity in six different building scenarios compared to the flat scenario (without buildings). It can be seen, that the building effects reach a distance downwind of minimum 200 m from the source. From these scenarios it can be assumed, that for a realistic urban scenario the downwind distance will significantly exceed the distance as shown here.

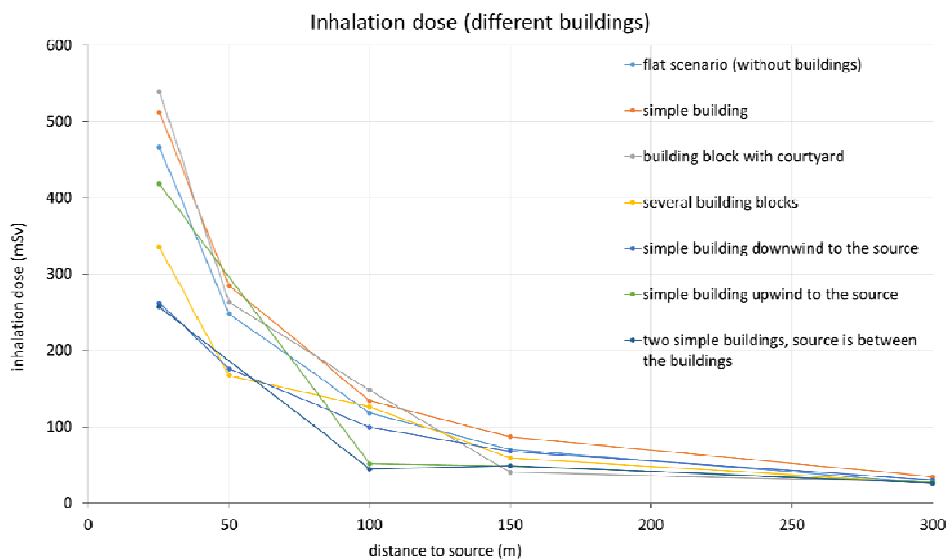


**Figure 3.** Overview for the inhalation dose [mSv] of an arbitrary radionuclide and activity in six different building scenarios compared to the flat scenario (without buildings).

## SUMMARY

The Decision Support Model LASAIR has proven to be a quick and easy to handle tool for operational use within microscale nuclear emergency scenarios and has been applied successfully within exercises and model intercomparisons.

A special feature of LASAIR is the consideration of building effects within a city based on a simple mass consistent flow model Lprwnd. It can be seen from cases studies that depending on the kind of building scenario the inhalation dose can be higher or lower according to either the mechanical induced turbulence or due to downwind turbulent wake effects. As for this, it seems obvious that the building wake effects should be taken into account if ever possible in such an emergency situation. The downwind distance of the effects from buildings in this study reaches up to 200 m away from the end of the building and might reach even further as the buildings dimensions used in this study had only a limited range. Further studies (not listed here due to constraints of page number) showed that the influence of building blocks perpendicular or with an angle close to 90° is able to shift significantly the main dispersion lateral and downwind.

The Decision Support Models used in such situations therefor should have the possibility to consider buildings and implement the building situation as quick as possible into the model in order not to spend too much time during the emergency itself. LASAIR provides the possibility to define the actual buildings within a few minutes. However this feature will be improved in future as there is a chance to load building scenarios at least for main cities automatically via the internet into the program.

## REFERENCES

- von Arx, C., Glaab, H., Grimm, Chr., Martens, R., Päsler-Sauer, J., Scheuermann, W., Schnadt, H. , Schumacher, P., Torchiani, S., Walter, H., Wilbois, T.: Vergleich aktuell eingesetzter Modelle zur Beschreibung der atmosphärischen Ausbreitung radioaktiver Stoffe. Abschlussbericht zum Arbeitspaket AP5500 im Projekt A510 der Strahlenschutzkommission, Bundesamt für Strahlenschutz (BfS), BfS-SCHR-58/16, 2016.
- Janicke, L., 1983: Particle Simulation of Inhomogeneous Turbulent Diffusion. Air Pollution Modelling and its Application, (ed. Weber). Plenum Press, N.Y., 527-535.
- Janicke, L., 1985: Particle simulation of Dust Transport and Deposition and Comparison with Conventional Models. Air Pollution Modelling and its Application, IV, (ed. C. de Wispelaere). Plenum Press, N.Y., 759-769.
- Janicke, U, Janicke, L., Weiterentwicklung eines diagnostischen Windfeldmodells für den anlagenbezogenen Immissionsschutz (TA Luft), Umweltforschungsplan des Bundesministeriums für Umwelt, Naturschutz und Reaktorsicherheit, Anlagenbezogener Immissionsschutz, Förderkennzeichen (UFOPLAN) 203 43 256, Oktober 2004
- Prouza, Z.; V. Beckova, I. Cespirova, J. Helebrant, J. Hulka, P. Kuca, V. Michalek, P. Rulik, J. Skrkal and J. Hovorka, 2010: Field Tests using radioactive matter, Radiation Protection Dosimetry (2010), pp. 1–13.
- VDI-Richtlinie 3783, Blatt 8, 2014: Umweltmeteorologie, Messwertgestützte Turbulenzparametrisierung für Ausbreitungsmodelle, Environmental meteorology – Turbulence parameters for dispersion models supported by measurement data, 15. Vorentwurf, 2014-06-03, to be published in 2016..
- Thiessen, K.M., K.G. Andersson, V. Berkovskyy, T.W. Charnock, S.L. Chouhan, G. de With6, J. Dúran, V. Fuka, J. Helebrant, J. Hůlka, W.T. Hwang, P. Kuča, F. Mancini, E. Navarro, R. Periañez, Z. Prouza, G. Sdouz, J. Tomás, D. Trifunović, L. Urso, and H. Walter: Assessing emergency situations and their aftermath in urban areas: The EMRAS II Urban Areas Working Group International Conference on Radioecology & Environmental Radioactivity (ICRER 2011), Hamilton , Canada.
- Walter, H. and G. Heinrich, 2014: The Decision Support System LASAIR: New features for evaluating Dirty Bomb scenarios in: Proceedings of the 16th International Conference on Harmonisation within Atmospheric Dispersion Modelling for Regulatory Purposes, Varna, Bulgaria, 8th – 11th September 2014.
- Walter H. and, G. Heinrich, 2011: Quick and clean: Dirty bomb scenarios evaluated with the decision support system LASAIR. ICRER 2011, Hamilton, Canada.

**17th International Conference on  
Harmonisation within Atmospheric Dispersion Modelling for Regulatory Purposes  
9-12 May 2016, Budapest, Hungary**

---

**IMPACT OF CHANGING THE WET DEPOSITION SCHEMES IN LDX ON 137-CS  
ATMOSPHERIC DEPOSITS AFTER THE FUKUSHIMA ACCIDENT**

*Arnaud Quérel<sup>1</sup>, Denis Quélo<sup>1</sup>, Yelva Roustan<sup>2</sup>, Anne Mathieu<sup>1</sup>, Mizuo Kajino<sup>3</sup>, Thomas Sekiyama<sup>3</sup>,  
Kouji Adachi<sup>3</sup>, Damien Didier<sup>1</sup>, Yasuhito Igarashi<sup>3</sup>, Takashi Maki<sup>3</sup>*

<sup>1</sup>IRSN, PRP-CRI, SESUC, BMCA, Fontenay-aux-Roses, France

<sup>2</sup>CEREA, ENPC/EDF R&D, Champs-sur-Marne, France

<sup>3</sup>MRI, Japan Meteorological Agency, Tsukuba, Japan

**Abstract:** The Fukushima-Daiichi release of radioactivity is a relevant event to study the atmospheric dispersion modelling of radionuclides. Actually, the atmospheric deposition onto the ground may be studied through the map of measured Cs-137 established consecutively to the accident. The limits of detection were low enough to make the measurements possible as far as 250km from the nuclear power plant. This large scale deposition has been modelled with the Eulerian model IdX. However, several weeks of emissions in multiple weather conditions make it a real challenge. Besides, these measurements are accumulated deposition of Cs-137 over the whole period and do not inform of deposition mechanisms involved: in-cloud, below-cloud, dry deposition.

In a previous study (Quérel et al., 2016), a comprehensive sensitivity analysis was performed in order to understand wet deposition mechanisms. It has been shown that the choice of the wet deposition scheme has a strong impact on assessment of deposition patterns. Nevertheless, a “best” scheme could not be highlighted as it depends on the selected criteria: the ranking differs according to the statistical indicators considered (correlation, figure of merit in space and factor 2). A possibility to explain the difficulty to discriminate between several schemes was the uncertainties in the modelling, resulting from the meteorological data for instance. Since the move of the plume is not properly modelled, the deposition processes are applied with an inaccurate activity concentration in the air. In the framework of the SAKURA project, an MRI-IRSN collaboration, new meteorological fields at higher resolution (Sekiyama et al., 2013) were provided and allow to reconsider the previous study.

An update including these new meteorology data is presented. In addition, the focus is put on the deposition schemes commonly used in nuclear emergency context.

**Key words:** *Fukushima; sensitivity analysis; wet deposition, atmospheric dispersion model*

## **INTRODUCTION**

Wet deposition processes are a crucial component of radionuclide atmospheric transport and soil contamination models. Within atmospheric dispersion model these processes are represented by coefficients that quantify the proportion of scavenged radionuclides per unit of time. Radionuclides are captured by hydrometeors (droplets, snowflakes, etc...) and brought to the Earth's surface by precipitations (rain, snow, etc...). If the capture occurs when the condensed water is aloft in the atmosphere, the phenomenon is called rainout (or in-cloud scavenging). If it occurs during the precipitations, it is called washout (or below-cloud scavenging). These processes are physically separated and can be distinctly represented with their own scavenging coefficients. A wide range of parametrizations are proposed in the scientific literature to determine these coefficients (Duhanyan and Roustan, 2011), and currently no scientific consensus allows to discriminate between them.

Furthermore, the Fukushima case shows significant episodes of wet deposition, making it particularly well suited to study the wet deposition modelling. The release of long-lived species 137-Cs, bound to atmospheric particles, is simulated with the Eulerian long-range dispersion model from the IRSN, IdX (Groëll et al., 2014).

In a previous step, a sensitivity analysis, relying on an ensemble-type approach, was performed in an attempt to discriminate between the various wet deposition schemes proposed in the literature (Quérel et al., 2016). The results of this analysis confirm the strong sensitivity of the simulated deposits to the choice of deposition schemes, both in terms of magnitude and spatial patterns and similar results were shown in Leadbetter et al. (2015). However it was not possible to identify a particular scheme which lead to an overall improvement in modelling performance and call for caution regarding the results obtained. This could be partly attributed to the uncertainties remaining in the meteorological fields and in the source terms used to drive the atmospheric dispersion model. To go further, finer meteorological data and more up-to-date source terms are now considered. Moreover, since IdX aims at nuclear emergency response, it is suitable to have at our disposal in our modelling framework other parameterizations for wet deposition, like the ones used in similar operational atmospheric dispersion models.

## WET DEPOSITION SCHEMES

In addition to the IRSN ones, other wet deposition schemes are considered: those documented in the WMO Task Team report investigating the impact of meteorology on the dispersion of radioactive material from Fukushima-Daiichi Nuclear Power Plant (Draxler et al., 2012). They are issued from the following atmospheric dispersion models: **CMC-MLDP0** (D'Amours et al., 2010), **HYSPLIT** (Draxler and Hess, 1997), **NAME** (Jones et al., 2007), **RATM** (Shimbori et al., 2010) and **FLEXPART** (Stohl et al., 2010). The description of deposition schemes are reported in Table 1.

**Table 1:** Deposition schemes used by models involved in the WMO Task Team.

<b>Atmospheric transport modelling</b>	<b>Below-cloud scheme</b>	<b>In-cloud scheme</b>
CMC-MLDP0	$\Lambda = 0$	$\Lambda = 3 \times 10^{-5}$
FLEXPART	$\Lambda = 10^{-5} I^{0.8}$	Hertel et al. (1995)
HYSPLIT	$\Lambda = 10^{-6}$	Hertel et al. (1995) with $S = 4 \times 10^4$
IRSN	$\Lambda = 5 \times 10^{-5} I$	$\Lambda = 5 \times 10^{-5} I$
NAME	$\Lambda = 8.4 \times 10^{-5} I^{0.79}$	$A = 3.36 \times 10^{-4} I^{0.79}$
RATM	$\Lambda = 2.78 \times 10^{-5} I^{0.75}$	Hertel et al. (1995) with LWC model

## METHODOLOGY AND INPUT DATA

In this study, washout and rainout parameterizations are not considered independently in our ensemble-type approach. Then, model configurations look through a pair of deposition schemes (listed in table1), in addition to meteorological data, precipitation field and source terms. Input data considered are listed below:

- Meteorological data: number 1 and number 8 of Sekiyama's ensemble (Sekiyama et al., 2013).
- Precipitations: issued from the meteorological simulation or radar rainfall data corrected by rain-gauges observations (Saito et al., 2015).
- Source term: Katata (2015), Saunier (2013) and Terada (2012).

All simulations are performed using the long-range transport model IdX with common settings except for the wet scavenging schemes. Clouds vary between fixed altitudes of 800 m and 5000 m. Dry deposition is modelled through a constant deposition velocity of  $2 \times 10^{-3} \text{ m.s}^{-1}$ . Horizontal grid comes from the meteorological data whose resolution is  $0.03^\circ$  and vertical resolution follows a non-linear scale ranging from 0 to 5546 m (0, 40, 85, 141, ... 5546 m).

Simulations are compared to a data set of 137-Cs deposit observations which comprises airborne measurements made by the US Department of Energy as well as ground measurements collected by the Ministry of Education, Culture, Sports, Science and Technology of Japan. This data are averaged onto the Model grid (see Figure 1, a).

## DATA EXPLOITATION

Three statistical indicators are used to evaluate the performance of simulations to reproduce the deposits:

- Pearson correlation, used to quantify the linear relationship between observations and simulations.
- Factor 2, used to obtain an overall measure of the magnitude of discrepancies between observations and simulations, with equal weighting of low and high values.
- Figure of Merit in Space (FMS), used to compare simulated and observed deposition patterns.

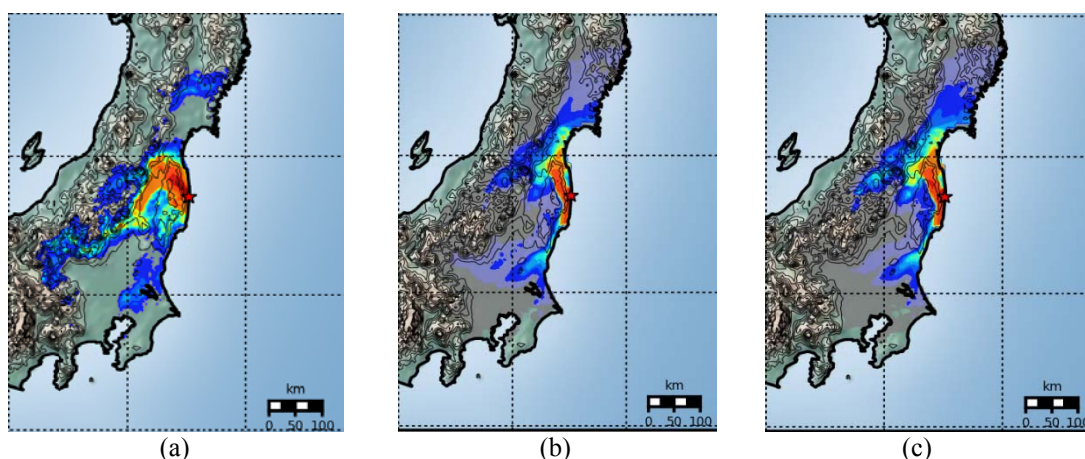
A minimum value of  $10\text{kBq}\cdot\text{m}^{-2}$  is applied for observed deposits.

Influence of a specific scheme rather than others is investigated within this ensemble type of simulations. Issues considered are: How many simulations are improved by this given choice? Is it a significant improvement? In order to estimate this impact, each simulation performed with the chosen deposition schemes is compared to simulations sharing the same configuration. This comparison is made for each statistical indicator is a distribution of discrepancies for each choice of deposition schemes.

These obtained distributions are then drawn with the help of whisker box.

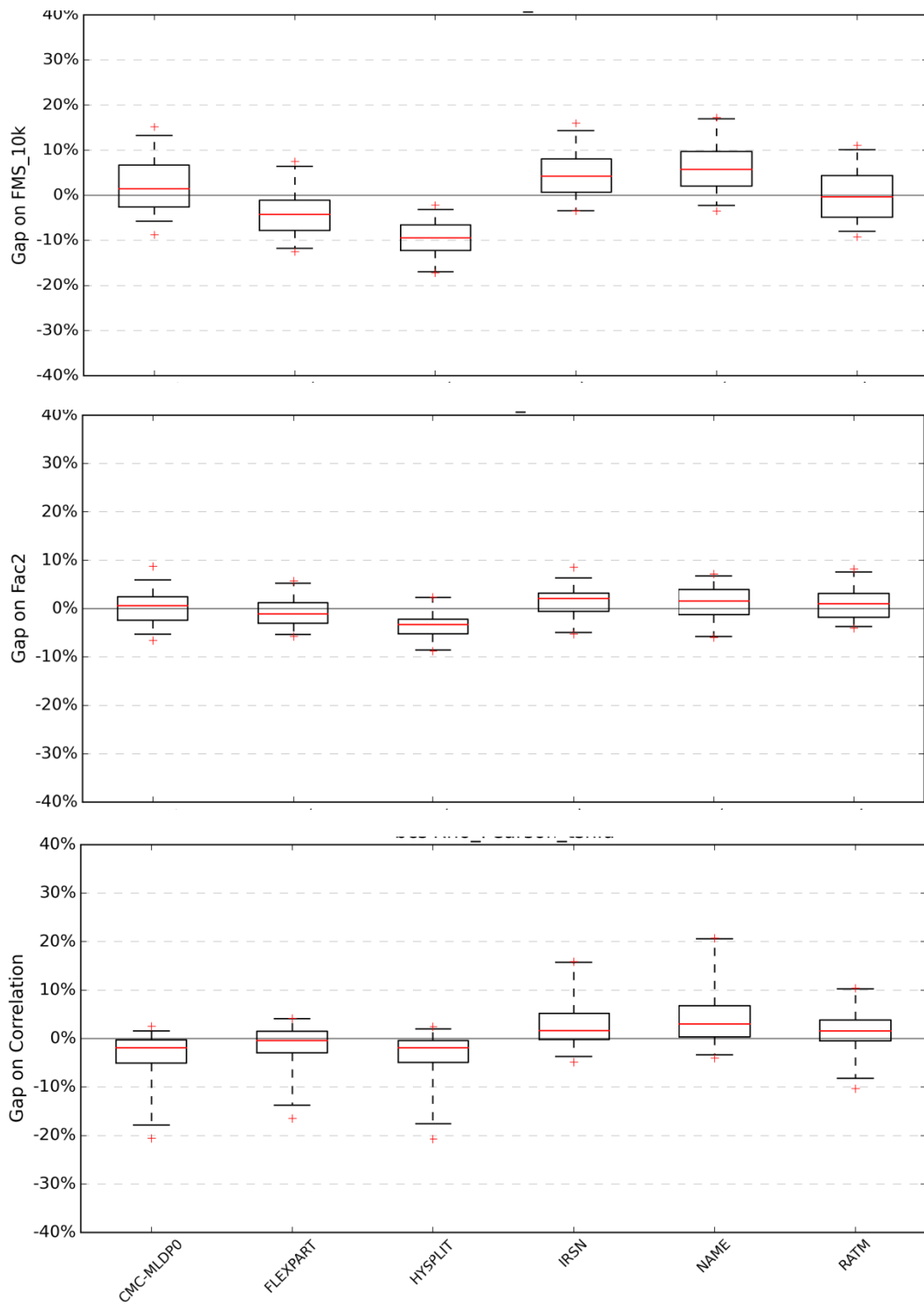
## RESULTS

Figure 1 shows maps of deposits considering different wet deposition schemes. In this example, NAME schemes lead to a greater deposit than IRSN's one.



**Figure 1:** Deposit (a) Observed; (b) simulated using IRSN deposition schemes; (c) simulated using NAME deposition schemes. Both simulations are performed with Katata source term, Sekiyama n°8 meteorological data and radar rainfall data.

Figure 2 shows an example of the impact on statistical indicators using the possible options for wet deposition. A sensitivity of a given choice is observed on all the indicators. Some wet deposition schemes appear to give better results than others and one can wonder if it is specific to this case study or to the input data (meteorological fields and source terms) included in this ensemble-type approach. These preliminary results need to be consolidated.



**Figure 2:** Impact of wet deposition schemes on FMS, factor 2 and correlation.

## REFERENCES

- Brandt, J., Christensen, J.H., Frohn, L.M., 2002. Modelling transport and deposition of caesium and iodine from the Chernobyl accident using the DREAM model. *Atmospheric Chem. Phys.* **2**, 397–417.
- D'Amours, R., Malo, A., Servranckx, R., Bensimon, D., Trudel, S., Gauthier-Bilodeau, J.-P., 2010. Application of the atmospheric Lagrangian particle dispersion model MLDP0 to the 2008 eruptions of Okmok and Kasatochi volcanoes. *J. Geophys. Res.* **115**, 1–11. doi:10.1029/2009JD013602
- Draxler, R.R., Arnold, D., Galmarini, S., Hort, M.C., Jones, A.R., Leadbetter, S.J., Malo, A., Maurer, C., Rolph, G., Saito, K., Servranckx, R., Shimbori, T., Solazzo, E., Wotawa, G., 2012. Third meeting of WMO task team on meteorological analyses for Fukushima-Daiichi nuclear power plant accident.
- Draxler, R.R., Hess, G.D., 1997. Description of the HYSPLIT\_4 modelling system (Technical Report No. ERL ARL-224). NOAA.
- Duhanyan, N., Roustan, Y., 2011. Below-cloud scavenging by rain of atmospheric gases and particulates. *Atmos. Environ.* **45**, 7201–7217. doi:10.1016/j.atmosenv.2011.09.002
- Groëll, J., Quélo, D., Mathieu, A., 2014. Sensitivity analysis of the modelled deposition of Cs-137 on the Japanese land following the Fukushima accident. *Int. J. Environ. Pollut.* **55**, 67–76.
- Hertel, O., Christensen, J.H., Runge, E.H., Asman, W.A.H., Berkowicz, R., Hovmand Mads F., 1995. Development and testing of a new variable scale air pollution model - ACDEP. *Atmos. Environ.* **29**, 1267–1290. doi:10.1016/1352-2310(95)00067-9
- Jones, A.R., Thomson, D., Hort, M.C., Devenish, B., 2007. The UK Met Office's next-generation atmospheric dispersion model, NAME III, in: *Air Pollution and Its Applications XVII*. Presented at the 27th NATO/CCMS International Technical Meeting on Air Pollution Modelling and its Application, Carlos Borrego, Ann-Lise Norman, Portugal.
- Katata, G., Chino, M., Kobayashi, T., Terada, H., Ota, M., Nagai, H., Kajimo, M., Draxler, R., Hort, M.C., Malo, A., Torii, T., Sanada, Y., 2015. Detailed source term estimation of the atmospheric release for the Fukushima Daiichi Nuclear Power Station accident by coupling simulations of atmospheric dispersion model with improved deposition scheme and oceanic dispersion model. *Atmospheric Chem. Phys.* **15**, 1029–1070. doi:10.5194/acp-15-1029-2015
- Leadbetter, S.J., Hort, M.C., Jones, A.R., Webster, H.N., Draxler, R.R., 2015. Sensitivity of the modelled deposition of Caesium-137 from the Fukushima Dai-ichi nuclear power plant to the wet deposition parameterisation in NAME. *J. Environ. Radioact.* **139**, 200–211. doi:http://dx.doi.org/10.1016/j.jenvrad.2014.03.018
- Quérel, A., Roustan, Y., Quélo, D., Benoit, J.-P., 2016. Hints to discriminate the choice of wet deposition models applied to an accidental radioactive release. *Int. J. Environ. Pollut.* in press.
- Saito, K., Shimbori, T., Draxler, R., 2015. JMA's regional atmospheric transport model calculations for the WMO technical task team on meteorological analyses for Fukushima Daiichi Nuclear Power Plant accident. *J. Environ. Radioact.* **139**, 185–199. doi:10.1016/j.jenvrad.2014.02.007
- Saunier, O., Mathieu, A., Didier, D., Tombette, M., Quélo, D., Winiarek, V., Bocquet, M., 2013. An inverse modelling method to assess the source term of the Fukushima Nuclear Power Plant accident using gamma dose rate observations. *Atmospheric Chem. Phys.* **13**, 11403–11421. doi:10.5194/acp-13-11403-2013
- Sekiyama, T., Kajino, M., Kunii, M., 2013. Ensemble simulation of the atmospheric radionuclides discharged by the Fukushima nuclear accident. Presented at the EGU, p. 1695.
- Shimbori, T., Aikawa, Y., Fukui, K., Hashimoto, A., Seino, N., Yamasato, H., 2010. Quantitative tephra fall prediction with the JMA mesoscale tracer transport model for volcanic ash: A case study of the eruption at Asama volcano in 2009. *Pap. Meteorol. Geophys.* **61**, 13–29. doi:http://doi.org/10.2467/mripapers.61.13
- Stohl, A., Sodemann, H., Eckhardt, S., Frank, A., Seibert, P., Wotawa, G., 2010. The Lagrangian particle dispersion model FLEXPART version 8.2.
- Terada, H., Katata, G., Chino, M., Nagai, H., 2012. Atmospheric discharge and dispersion of radionuclides during the Fukushima Dai-ichi Nuclear Power Plant accident. Part II: verification of the source term and analysis of regional-scale atmospheric dispersion. *J. Environ. Radioact.* **112**, 141–154.

**17th International Conference on  
Harmonisation within Atmospheric Dispersion Modelling for Regulatory Purposes  
9-12 May 2016, Budapest, Hungary**

---

**PROJECT SAGEBRUSH: A NEW LOOK AT PLUME DISPERSION**

*Kirk L. Clawson, Richard M. Eckman, Dennis D. Finn*

National Oceanic and Atmospheric Administration (NOAA), Air Resources Laboratory,  
Field Research Division, Idaho Falls, Idaho USA

**Abstract:** Project Sagebrush (PSB) is a multi-year tracer dispersion field experiment based roughly on the venerable Project Prairie Grass (PPG) conducted in 1956. PSB builds on and expands the results of PPG and other early dispersion tests through the use of modern 3-d sonic anemometers to directly measure atmospheric turbulence and through the use of fast-response analyzers for measuring tracer concentration fluctuations. The first phase of Project Sagebrush (PSB1) was conducted in October 2013. A total of 5 tests were completed resulting in 60 separate sample periods. One hundred-fifty bag samplers were used to obtain ten-minute average concentrations while six real-time analyzers simultaneously sampled tracer concentration fluctuations. A bevy of meteorological instruments was also utilized. Examination of cross-wind concentration fields showed that PSB2 plumes were generally more spread out and much less Gaussian in shape than plumes from PPG. The data from PSB1 are openly available for further scientific scrutiny and model testing. A follow-on study dubbed PSB Phase 2 will be conducted in 2016 with a focus on light wind speed conditions.

**Key words:** *Atmospheric tracer dispersion, field studies, atmospheric stability, atmospheric turbulence, Project Prairie Grass*

## **INTRODUCTION**

The benchmark tracer dispersion studies of the 1950s and 1960s are still the basis for modern dispersion model development and validation [e.g., AERMOD (Cimorelli et al. 2004), RLINE (Snyder et al. 2013), and ADMS (Carruthers et al. 1994)]. Those early dispersion studies were carefully designed to take advantage of the latest meteorological and tracer measurement technology available at the time. Project Prairie Grass (Barad, 1958), conducted in 1956 in the state of Nebraska, USA, is perhaps the best known of these classic experiments. Project Prairie Grass (PPG) was focused on short-range dispersion from a near-surface source over flat terrain.

Although PPG remains one of the most used dispersion studies in flat terrain, many users are unaware of its limitations. For example, sulphur dioxide (SO<sub>2</sub>) was used as the tracer gas in PPG; it is both reactive and depositing, and these characteristics may affect the interpretation of the results. Furthermore, estimates of atmospheric boundary layer stability and surface fluxes were derived from mean wind and air temperature profiles because the ability to measure fluxes directly was severely limited. Information on vertical dispersion came from a single set of towers 100 m downwind of the source, with a maximum tracer measurement height of 17.5 m AGL.

Over the course of the last half century, there has been considerable improvement in both meteorological and tracer measurement technologies. Now it is possible to measure three-dimensional atmospheric turbulence directly with high fidelity—a capability that did not exist when PPG was conducted. Likewise, tracer concentration fluctuations can now be measured. The arrival of these new technologies has led some experts to recommend that the early dispersion experiments be reinvestigated using the new tools that are now available. Further impetus for new tracer studies comes from a 2008 tracer experiment conducted at the Idaho National Laboratory (Finn et al., 2010). This experiment focused on the effects of roadside sound barriers on vehicle pollution, but a subset of the data was compared to PPG results and showed interesting deviations (Venkatram, 2011, personal communication).

Because of these developments, the Field Research Division (FRD) of the National Oceanic and Atmospheric Administration Air Resources Laboratory (NOAA ARL) has begun a new series of tracer experiments using modern turbulence instrumentation and tracer technology. The experiments are collectively called Project Sagebrush (PSB) in a nod to its predecessor, Project Prairie Grass. PSB is a multi-year dispersion study that is being based loosely on PPG with a continued focus on short-range dispersion in open terrain.

### **NOAA GRID 3 TRACER DISPERSION TEST BED**

Project Sagebrush is being conducted at the NOAA Grid 3 tracer dispersion test bed (Grid 3) on the Idaho National Laboratory (INL), a U.S. Department of Energy facility in southeast Idaho, USA. The INL covers approximately 2,300 km<sup>2</sup> and is located in a broad, relatively flat plain on the western edge of the Eastern Snake River Plain (ESRP). The average elevation across the INL is approximately 1500 m MSL. Several parallel mountain chains with peaks exceeding 3000 m MSL dominate the western edge of the ESRP. These chains are separated by a series of tributary valleys that feed into the ESRP. The base of the closest mountain peak is approximately 15 km from the Grid 3 facility.

Grid 3 was first used in the late 1950s or early 1960s for tracer dispersion studies. Sampling arcs have been surveyed at 25, 50, 100, 200, 400, 800, 1600, and 3200 m. Conducting PSB at Grid 3 allows ARLFRD scientists to use valuable knowledge gained from previous work [e.g., Start, et al. (1984), Sagendorf and Dickson (1974), Garodz and Clawson (1991, 1993), and Finn et al. (2010)]. Grid 3 is well-positioned near the middle of an existing 34-station mesonet that was designed for the very purpose of collecting high fidelity wind data required for emergency dispersion modelling to support the safe operation of INL research nuclear reactors and associated activities (Clawson et al. 2007; Rich et al. 2016).

An important feature of Grid 3 is a 62 m tower (designated GRI) that provides vertical profiles of wind and air temperature. Soil moisture and temperature are also measured at 5 depths at GRI. A 924 MHz wind profiling radar with RASS and a mini-SoDAR are also permanently installed at Grid 3. The radar measures wind profiles in 100 m increments up to 2.9 km and virtual temperature profiles up to 1.0 km AGL. The SoDAR measures winds in 10 m increments up to 200 m AGL. An Eddy covariance surface flux system has been in operation at Grid 3 since 2000 for the measurement of sensible heat, latent heat, soil heat, and momentum fluxes and for the measurement of the complete energy balance.

Grid 3 offers relatively uniform aerodynamic characteristics across the study area. The canopy is mostly sagebrush and grass. The near-surface wind usually blows parallel to the axis of the ESRP, with southwest winds common during the day and northeast winds at night (Clawson et al. 2007). The median roughness length ( $z_0$ ) has been determined to be 3-4 cm. The displacement height ( $d$ ) estimate was not significantly different from 0. The orientation of the prevailing winds means that the tracer facility has a relatively flat, uniform fetch extending many tens of kilometers in the prevailing upwind direction.

### **PHASE 1 EXPERIMENTAL DESIGN**

Phase 1 of Project Sagebrush (PSB1) utilized all of the meteorological equipment described above, and added a suite of additional atmospheric turbulence measurements to fully describe and identify the meteorological factors controlling tracer dispersion. An array of tracer sampling equipment was also deployed that included real-time analyzers as well as bag samplers. Full details of the experiment can be found in the data report by Finn et al. (2015).

### **Additional Meteorological Equipment**

The following broad array of meteorological instrumentation was deployed at Grid3 in addition to the existing instrumentation:

- 62 m tower (GRI): 3-d sonic anemometers at 7 levels; 2-d sonic anemometers at 6 levels; air temperature and relative humidity at 14 levels; fast response infrared gas analyzers at 4 levels; solar radiation, barometric pressure at 3 levels; net radiometer at 2 levels; infrared thermometer, soil heat flux at 2 levels.
- Three 3-d sonic anemometers arrayed along the 3200 m arc (R2, R3, R4).

- 10 m meteorological tower at 3200 m (TOW): cup and vane anemometers at 2 levels.
- 30 m Command Center (COC) meteorological tower: cup and vane anemometers at 3 levels.
- 1 additional SoDAR at 3200 m arc (wind profiles from 30-200 m).
- Radiosonde launches before and after each test.

### Tracer Sampling Strategy

Six fast response SF<sub>6</sub> analyzers were deployed to measure concentration fluctuations. Five of these were mounted in vehicles and co-located with a bag sampler on the sampling arcs. One analyzer was mounted in an airplane provided by the University of Tennessee Space Institute during tests 1, 2, and 3. During tests 4 and 5 the airplane was not available, so this analyzer was re-located to a site on the sampling arcs.

Tracer releases were restricted to the daytime when prevailing winds were from the southwest. Therefore, the study domain was located on the northeast quadrant of the Grid 3 dispersion test bed. Twenty-eight bag samplers were placed at 3° intervals from 4° azimuth to 85° azimuth along each of the 4 circular arcs designated for a test. These were either the 200, 400, 800, and 1600 m arcs or the 400, 800, 1600, and 3200 m arcs, depending upon the forecast atmospheric stability and the planned release rate. Each bag sampler was mounted at 1 m AGL and contained 12 bags. The 12 bags collected samples sequentially with each bag covering a 10-minute interval, so concentration averaging times between 10 minutes and 2 hours are available at each location.

Three towers were available for vertical tracer sampling to the northeast of the source. Four samplers were mounted on a 15 m tower (1, 5, 10, and 15 m AGL) located at the intersection between the 55° azimuth radial road and the 200 m arc. Five samplers were mounted on a 21 m tower (1, 5, 10, 15, and 20 m AGL) located at the intersection of the radial road and the 400 m arc. Seven samplers were mounted on a 30 m tower (1, 5, 10, 15, 20, 25, and 30 m AGL) located 499 m from the source at about 60° azimuth. This tower served the dual purpose as the meteorological tower for the nearby command center (COC). A total of 150 bag samplers, including those used for quality control, were employed during each test.

### Tracer Release Strategy

Five sulfur hexafluoride (SF<sub>6</sub>) tracer releases took place from 02 October to 18 October, 2013. SF<sub>6</sub> has several advantages over SO<sub>2</sub> (the tracer used in PPG) because it is non-depositing, non-reacting, and non-toxic. It is also odorless, and invisible. SF<sub>6</sub> tracer was released continuously at a constant rate from a point source at 1.5 m AGL at the center of the dispersion array for each test. The releases began one-half hour prior to the start of sampling on the dispersion array to establish a quasi-steady state SF<sub>6</sub> plume across all of the arcs. The release then continued for the two-hour sampling duration in each test. Release rates were set based upon preliminary estimates of concentrations at different heights and distances, the anticipated atmospheric stability conditions, and whether the aircraft would be making tracer measurements.

## RESULTS AND DISCUSSION

A brief summary of test dates and times, tracer release rates, general meteorological conditions, and atmospheric stability is listed in Table 1. Since all tests were conducted in the afternoon, atmospheric stability ranged from unstable to neutral. A total of 60 unique tracer sample periods were collected.

Table 1. PSB1 test summary.  $\sigma_\theta$  is the standard deviation of the wind direction.

Test	Date	Start Time (MST)	Release Rate (g s <sup>-1</sup> )	Meteorological Summary	Atmospheric Stability
1	02 Oct 2013	1430	10.177	Mostly sunny with cirrostratus haze. Wind speeds 1-2 m s <sup>-1</sup> ; $\sigma_\theta$ 18-67 deg.	Unstable
2	05 Oct 2013	1300	9.986	Mostly sunny. Wind speeds 2.4-4.8 m s <sup>-1</sup> ; $\sigma_\theta$ 10-64 deg.	Unstable
3	07 Oct 2013	1300	9.930	Mostly sunny. Wind speeds 7.3-10.0 m s <sup>-1</sup> ; $\sigma_\theta$ 8-11.5 deg.	Neutral
4	11 Oct 2013	1400	1.043	Mostly sunny. Wind speeds 4.3-5.9 m s <sup>-1</sup> ; $\sigma_\theta$ 9.5-20 deg.	Weakly Unstable
5	18 Oct 2013	1300	1.030	Mostly sunny. Wind speeds 3.6-5.0 m s <sup>-1</sup> ; $\sigma_\theta$ 11-22 deg.	Weakly Unstable

For the initial analysis, lateral tracer plume spread obtained during PSB1 was first compared with PPG (Aarhus University, 2016). Example graphs are shown in Figure 1. PSB1 plume cross-sections tended to exhibit more complex internal structure and greater variability than PPG cross-sections. With few exceptions, cross-sections deviated significantly from an idealized Gaussian form, mainly during the near-neutral conditions of test 3. Individual cross-sections commonly exhibited irregular concentration variations, outlier peaks, and skewed asymmetry of concentrations around the peak concentration. Furthermore, some of the cross-sections exhibited truncated profiles at the edge of the sampling array. It can also be seen that the PPG plumes exhibited much narrower arcs than the PSB1 plumes for comparable wind speeds and downwind distances.

The plume spread parameter  $\sigma_y$  calculations obtained from PSB1 were compared with  $\sigma_y$  predictions of AERMOD (Cimorelli et al., 2004), a model that uses recent PBL theory to estimate turbulence levels. The values of the empirical constants used in AERMOD are based on fits to PPG data. The comparisons are shown in Figure 2. It is clear the AERMOD predictions do not fit the PSB1 results. These results indicate the need for additional tracer dispersion datasets such as PSB and raise questions about the parameterization and validation of any model that is based upon classical field studies such as PPG.

### PROJECT SAGEBRUSH PHASE 2

Project Sagebrush Phase Two (PSB2) will be a follow-on experiment to PSB1 and will focus on light wind speeds ( $\leq 2 \text{ m s}^{-1}$ ) under both stable and unstable atmospheric conditions. Very few data sets with a focus on light winds are currently available for analysis. There were no tests conducted during PPG in light wind conditions, for example. Detailed meteorological measurements similar to those obtained in PSB1 are planned. PSB2 is scheduled to occur this year in two test windows from 25 July to 10 August

2016 and 12 October through 28 October 2016. The first series of tests will be conducted in the afternoon hours and will concentrate on unstable atmospheric conditions. The second set of tests will be conducted in the early morning hours before sunrise and will concentrate on stable atmospheric conditions. Four tracer release periods are planned during each test window, which will result in a total of 96 ten-minute sample periods being available for analysis.

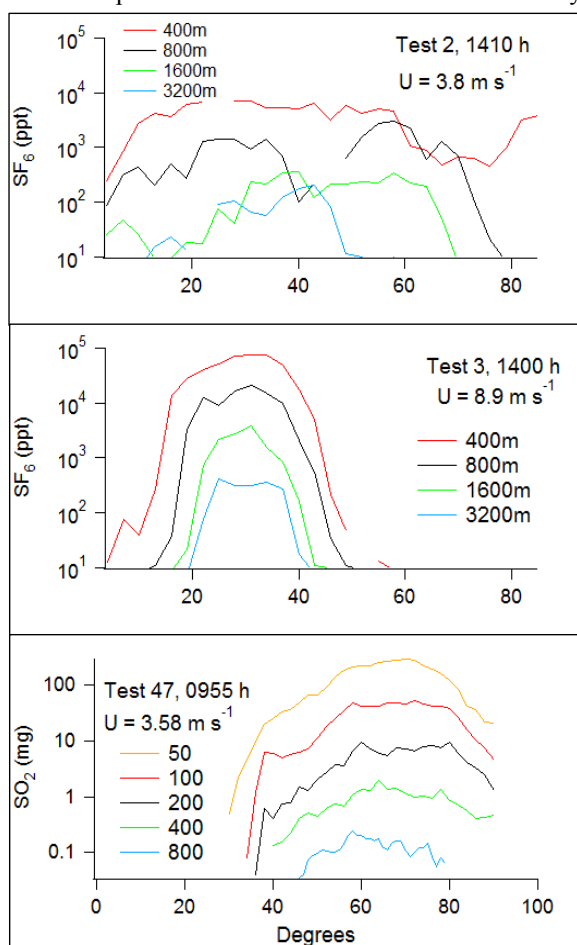


**Figure 12.** Tracer concentration plume cross-sections from PSB1 Tests 2 and 3 and PPG Test 47.

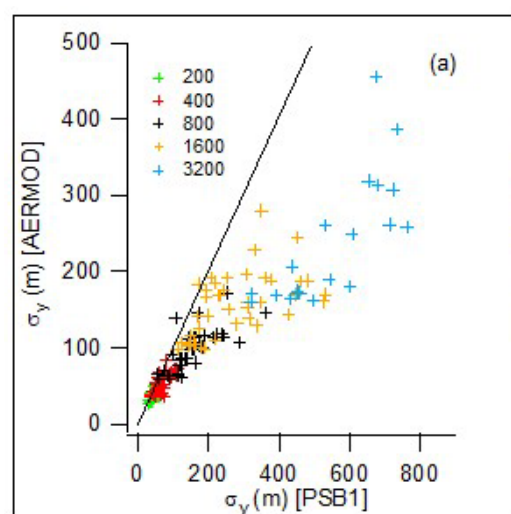


**Figure 11.** Plots of 10-minute period  $\sigma_y$  predicted by AERMOD versus those estimated from PSB1. The black line is the 1:1 reference.

## ACKNOWLEDGEMENTS

We thank Dr. Steve Brooks and the University of Tennessee Space Institute for providing the aircraft. We also thank Dr. Heping Liu, and Messrs. Eric Russell and Zhongming Gao at Washington State University for providing the Eddy correlation equipment and the bulk of the instrumentation on the GRI tower. We are grateful for the entire staff at NOAA ARLFRD and Cherie Clawson for their untiring help with the field work. This work was funded primarily by NOAA annual appropriations.

## REFERENCES

- Aarhus University, Dept. of Environmental Science, 2015. <http://envs.au.dk/en/knowledge/air/models/background/omlprairie/excelprairie/> (accessed 22 Feb 2016)
- Barad, M. L. (Ed.), 1958: Project Prairie Grass, a Field Program in Diffusion, Volume I-II of Geophysical Research Papers No. 59. Air Force Cambridge Research Center, AFCRC-TR-58-235, USAF, Bedford, MA, USA.
- Carruthers, D. J., R. J. Holroyd, and others, 1994: UK-ADMS: A new approach to modelling dispersion in the earth's atmospheric boundary layer. *J. Wind Eng. Ind. Aerodyn.*, **53**, 139–153.
- Cimorelli, A.J., S.G. Perry, A. Venkatram, J.C. Weil, R.J. Paine, R.B. Wilson, R.F. Lee, W.D. Peters, R.W. Brode, and J.O. Paumier, 2004: AERMOD: Description of model formulation. U.S. Environmental Protection Agency, EPA-454/R-03-004, 91 pp.
- Clawson, K.L., R.M. Eckman, N.F. Hukari, J.D. Rich, and N.R. Ricks, 2007: Climatology of the Idaho National Laboratory, 3<sup>rd</sup> edition. NOAA Tech. Memo OAR ARL-259, Air Resources Laboratory, Idaho Falls, ID, USA.
- Finn, D., K. L. Clawson, R. G. Carter, J. D. Rich, R. M. Eckman, S. G. Perry, V. Isakov, and D. K. Heist, 2010: Tracer studies to characterize the effects of roadside noise barriers on near-road pollutant dispersion under varying atmospheric stability conditions. *Atmos. Environ.*, **44**, 204–214.
- Finn, D., K.L. Clawson, R.M. Eckman, R.G. Carter, J.D. Rich, T.W. Strong, S.A. Beard, B.R. Reese, D. Davis, H. Liu, E. Russell, Z. Gao, S. Brooks, 2015: Project Sagebrush Phase 1. NOAA Tech. Memo OAR ARL-268, NOAA Air Resources Laboratory, Idaho Falls, ID, USA, 338 pp. doi:10.7289/V5VX0DHV
- Garodz, L. J., and K. L. Clawson, 1991: Vortex Characteristics of C5A/B, C141B, and C130E aircraft applicable to ATC terminal flight operations, tower fly-by data. NOAA/ERL/ARLFRD, Idaho Falls, ID, USA, 250 pp.
- Garodz, L. J., and K. L. Clawson, 1993: Volume 1, Vortex Wake Characteristics of B757-200 and B767-200 Aircraft Using the Tower Fly-By Technique. Volume 2, Appendices. NOAA/ERL/ARLFRD, Idaho Falls, ID, USA.
- Rich, J.D., R.G. Carter, K.L. Clawson, D. Finn, 2016: An Overview of the NOAA/INL Mesoscale Meteorological Monitoring Network. Submitted to *Journal of Idaho Academy of Sciences*.
- Sagendorf, J. F. and C. R. Dickson, 1974. Diffusion under low windspeed, inversion conditions. NOAA Tech. Memo ERL ARL-52, Air Resources Laboratory, Idaho Falls, ID, USA.
- Snyder, M.G., A. Venkatram, D.K. Heist, S.G. Perry, W.B. Petersen, and V. Isakov, 2013: RLINE: A line source dispersion model for near-surface releases. *Atmos. Environ.*, **77**, 748-756.
- Start, G. E., J. F. Sagendorf, G. R. Ackermann, J. H. Cate, N. F. Hukari, and C. R. Dickson. 1984. Idaho Field Experiment 1981, Volume II: Measurement data. NUREG/CR-3488 Vol 2, U.S. Nuclear Regulatory Commission.

**17th International Conference on  
Harmonisation within Atmospheric Dispersion Modelling for Regulatory Purposes  
9-12 May 2016, Budapest, Hungary**

---

**FLOW AND DISPERSION MODELLING IN A COMPLEX URBAN DISTRICT TAKING  
ACCOUNT OF THE UNDERGROUND ROADS CONNECTIONS**

*Maxime Nibart<sup>1</sup>, Patrick Armand<sup>2</sup>, Christophe Duchenne<sup>2</sup>, Christophe Olry<sup>1</sup>, Armand Albergel<sup>1</sup>,  
Jacques Moussafir<sup>1</sup>, Olivier Oldrini<sup>3</sup>*

<sup>1</sup>Aria Technologies, F-92100 Boulogne-Billancourt, France

<sup>2</sup>CEA, DAM, DIF, F-91297 Arpajon, France

<sup>3</sup>MOKILI, F-75014 Paris, France

**Abstract:** In the study of accidental or intentional releases of hazardous materials, dispersion modelling based on computational methods is increasingly used. The spatial resolution which can be reached is about one to a few meters with a system like PMSS, Parallel-Micro-SWIFT-SPRAY. At the local scale, explicitly taking account of the flow and dispersion of pollutants within the underground roadways and the tunnels may be very important. As a matter of fact, modern districts like “La Defense” (in the Western part of Paris) have so complex road connections that it may be influential on the propagation of plumes.

A new feature in PMSS dealing with underground tunnels have been implemented, tested and applied on the “La Defense” area.

**Key words:** *underground roadway, tunnel, PSWIFT, PSPRAY, urban environment*

## **INTRODUCTION**

PMSS, Parallel-Micro-SWIFT-SPRAY (Oldrini et al., 2011), is a fast transport and dispersion modelling system. It is designed for local scale and takes buildings into account. The parallel version can be run on multi-core computers or large parallel clusters. PMSS consists of PSWIFT and PSPRAY used in urban mode (Micro SWIFT, Micro Spray).

SWIFT / Micro-SWIFT (Tinarelli et al., 2007) is an analytically modified mass consistent interpolator over complex terrain. Given topography, meteorological data and buildings, a mass consistent 3D wind field is generated. It is also able to derive diagnostic turbulence parameters to be used by SPRAY / Micro-SPRAY. Micro-SPRAY (Tinarelli et al., 2013) is a LPDM (Lagrangian Particle Dispersion Model) able to take the presence of obstacles into account. It derives from the SPRAY code and is based on a 3D form of the Langevin equation for the random velocity.

In urban applications, the spatial resolution is usually between 1 to 5 meters. The buildings that are taken into account are typically defined through geographic information system (GIS) databases such as BD TOPO® from IGN in France where each building, or block of buildings, is described by its footprint and a vertical extrusion height from the ground level. In the framework of what is often referred as “geo-design” which is a digital description of urban environment, setting together the features of both computer-aided design (CAD) and GIS, this footprint and extrusion type of description is called Level of Detail (LoD) 1. More realistic, the LoD 2, 3 and 4 include more information such as roof shape, windows locations and dimensions or even indoor description.

The LoD 1 digital models are widely available, making the setup of geometry for urban dispersion modelling at small scale quite easy. But with a spatial resolution of 1 - 5 m, the buildings are not the only geometrical objects that can be explicitly described and have a significant influence on the dispersion. The underground road tunnels are quite widespread in cities (for example, in Paris, “La Defense” area, tunnel under the forecourt of “Gare de Lyon” rail station, tunnels along the Seine river banks). However, they are quite seldom considered in urban numerical dispersion modelling. For air quality studies near

tunnel portals, CFD calculations are performed, but they are limited to the evaluation of the pollutant transfer from the tunnel to the outdoor. Then, the inside of the tunnel is not explicitly modelled.

We propose here a new feature of PMSS that allows the underground tunnels and the transfer of material from tunnel to outdoor and from outdoor to tunnel to be taken into account. In the framework of accidental or malicious release in urban area, for emission near tunnel portal, this new capability could lead to more realistic prediction of material transport and thus of danger zones.

A brief description of tunnel modelling state of the art, the technical description of the implementation into PMSS and an application on “La Defense” area are presented in the next sections.

## **UNDERGROUND TUNNEL MODELING**

### **Underground road tunnel**

The present study is focused on underground tunnels and road connections that have a spatial scale that is compatible with the spatial resolutions typically used in PMSS (1 to 5 meters).

Besides its geometry and its mono- or bi-directional property, such tunnels are characterized by their ventilation system. The basic one is the natural ventilation. In this case, air movement relies on piston effects from vehicles motion, temperature and pressure differences at portals and outdoor wind velocity and direction. The phenomenon can also be increased by the addition of vertical shafts taking benefits of chimney effects. Natural ventilation is mainly applied to short tunnel (a few hundred of meters).

Mechanical ventilation systems can be split into two categories: the longitudinal systems and the transversal systems. In the first type, a longitudinal flow is generated by a limited number of fans at the ceiling (“jet fans”) or horizontal air injection near portal (*Saccardo* system). In the second type, a uniform supply and extraction of air is used along the tunnel length. This requires two related duct networks. If only extraction or supply is used, the system is called semi-transversal.

### **Modelling techniques**

Dispersion in tunnel modelling is commonly used for fire safety design. Examples of 1D models are MFIRE (U.S. Bureau of Mines), SES (U.S. Department of Transportation), ROADTUN (UK), SPRINT (Switzerland), Express’Air (SETEC) or New Vendis (INERIS) . They allow a complete and compact description of complex networks (main tunnels and ventilation ducts) but with the approximation of homogeneity in cross sections. Coupling between this kind of model and outdoor dispersion models does not seem to be proposed yet.

CFD models are also applied as engineering tools for tunnel fire safety (Collela, 2010). Their computational cost limits their use to simple networks or parts of tunnel. Momentum effect of jet fans or thermal effect of fire for example can be modelled using this approach.

Hybrid methods, coupling 1D and CFD models have also been developed more recently (Collela, 2010) but they are still focused on the inside of the networks.

Material transfers from the inside to the outside of tunnel portal are also computed with CFD models (Lacour et al. 2004) for air quality purposes. Here, only the tunnel part that is close to the portal needs to be included in the calculation domain.

At larger scale, for traffic pollution study, the pollution near tunnel portal can be computed by moving the mass rate, emitted inside tunnel, to additional releases located in front of the portal.

In all these existing methods, the focus is clearly not set on the two-way material transfer. The approach described in this paper proposes a solution to fill this gap with an operational objective.

### **Description formats**

As mentioned in the introduction, urban numerical databases are available for many cities in standard GIS formats such as shape file (ESRI). It makes the operational / automatic setup of micro-scale urban modelling possible. For urban objects, such as underground road tunnels, the availability and the format standardisation are much less mature.

In urban digital modelling new formats, based on a hierarchical structure, named LoD, are rising: CityGML or LandXML are the main ones.

In the CityGML framework, Bormann et al. (2014) have recently proposed a structure dedicated to underground tunnels where LoD1 is limited to simple polylines for mapping and where LoD5 can include the description of traffic lights or walkway, to give an example.

Some dataset samples are available (<http://www.citygml.org/?id=1539>) and can be visualized thanks to a tool developed by the Karlsruhe Institute of Technology. In some of them, a specific layer is devoted to underground tunnels. It is interesting also to note the holes in the topography layer, corresponding to the portals of the tunnels. Such interfaces between ground and tunnel do not exist in standard Digital Elevation Model like SRTM (CGIAR) or BDALTI® (IGN).

The detailed definition structure of underground tunnel for urban modelling is available inside the CityGML format, but the databases are not available. In the implementation proposed here, the tunnels geometry is designed in a similar fashion as building using footprints and vertical dimensions saved in the shape file format. More details are given in next section.

## PMSS UPGRADE

### Dealing with underground volume

To include underground tunnels into PMSS, several methods have been considered. Knowing that the nesting and tiling capabilities of PMSS rely on the use of spatial sub-domains management, the underground sections can be seen as additional and independent nest or tile structures. The other considered method consists in extending the vertical grid to negative heights from ground surface. This second method has been selected, mainly to avoid complex interface management at tunnels portals between separated sub-domains that would have been required in the first method.

PMSS grids are structured, regular in horizontal and based on a terrain following transformation for the vertical dimension (see equation (1), where  $H$  is the top of the domain,  $z$  the current altitude,  $z_g$  the ground surface altitude) as illustrated on Figure 1 (left). The vertical grid has been extended to negative value of  $z^*$ , using the same transformation as for positive value (Figure 1 (right)). In the future, a dedicated transformation for negative value could be implemented because the underground volume should not be terrain-following.

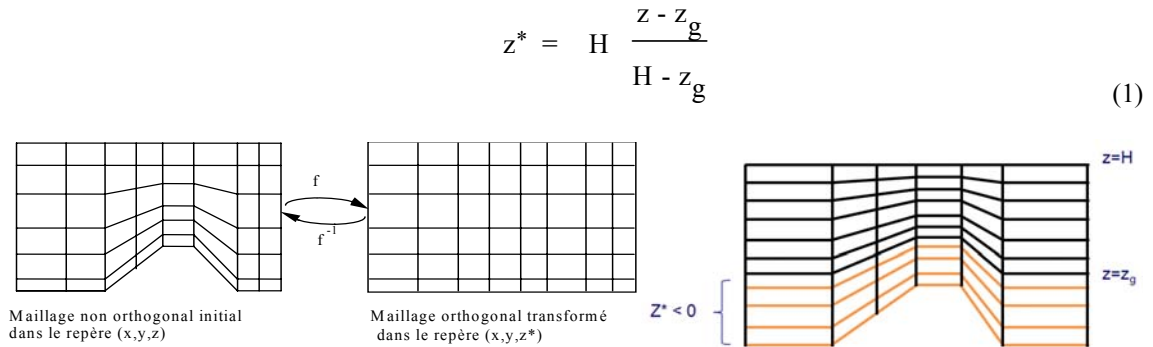


**Figure 1.** Left: Terrain following transformation of PMSS vertical grid –  
Right : Extension of the vertical grid to negative value of  $z^*$

PMSS has been updated to be able to distinguish the first level of the vertical grid and the ground surface which are not the same anymore. PSWIFT has also been modified to set specific velocity profile in the underground tunnels (Poiseuille law for the moment as it is used for aerial tunnels in PMSS).

### Input files and pre-processing

In order to have a friendly-user definition of tunnels geometry and to be consistent with the others obstacle types that can be set as input to PMSS, a LoD1 type solution based on shape file format has been implemented. The obstacles pre-processor, named Shaft, have been generalized and can load different

layers in this GIS format, before extracting and translating them into the native format of PMSS. Buildings, canyon zones and now underground tunnels can be handled. In the future, others types like trees could be added. The tunnels geometry is defined by their footprint (polygon) and two attributes for each polygon corresponding to bottom and top limit height from ground surface (negative values).

**Test cases**

Different test cases have been set up before applying the new feature to a realistic case. Figure 2 shows one of these tests. It consists in a tunnel limited to the entering portal. The axis of the tunnel is aligned with the direction of the wind. The academic wind profile is stationary and a punctual release of tracer has been placed in the portal zone, at an altitude close to 0 meter. The results are satisfying: the flow field has a logarithmic shape above ground, a Poiseuille shape in the tunnel and a transition at the portal. The plume is split with one part above ground and one part confined into the tunnel.

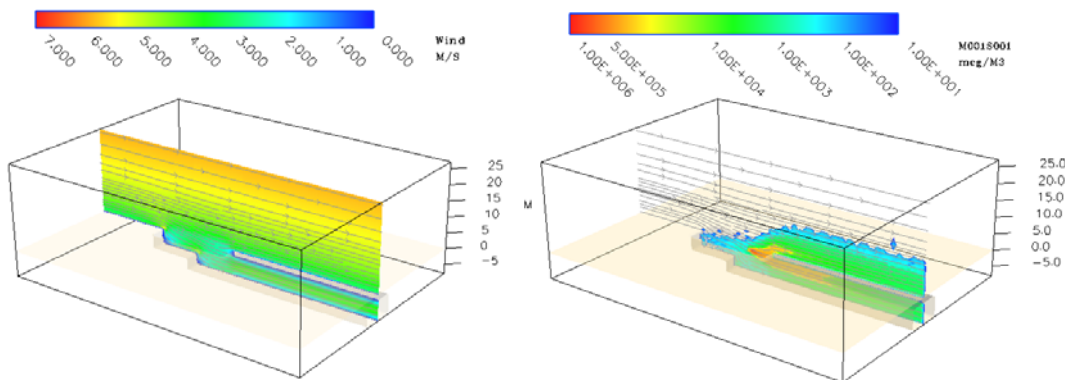


**Figure 2.** Simple underground tunnel test case – 3D interface surface between solid and fluid is displayed with transparency. On a vertical slice along the wind direction: Velocity magnitude and streamlines (left), concentrations and streamlines (right)

**APPLICATION CASE**

“La Defense” area is a complex urban domain. It is well known for its skyscrapers but also for its numerous tunnels. The BD TOPO® (IGN) has been used to define the buildings. This database has been modified to take into account aerial tunnels that are shown in orange on Figure 3 (left). The underground tunnels layer has been created from maps data and observations. The underground road tunnels considered in the calculation are displayed on Figure 3 (right).

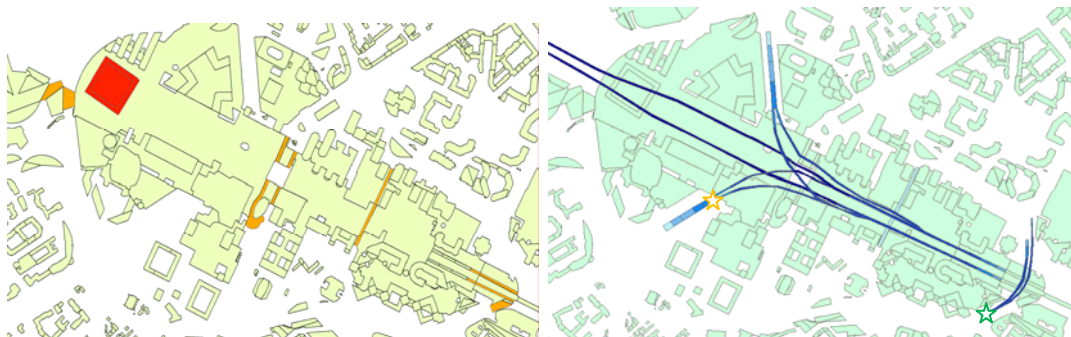


**Figure 3.** Left: Buildings footprints from BD TOPO® (IGN) in green and applied modifications to take into account arch structure (red) and aerial tunnels (orange). Right: Underground road tunnels in blue – Blue scale in giving the deepness of the tunnels floor – Orange and green stars show the location of considered hypothetical releases

The meteorology is driven by the extraction of 4 vertical profiles from a meso-scale model, following the operational configuration where a downscaling from WRF model to PMSS model is performed. The wind is here blowing mainly from the West. Two hypothetical releases have been considered (see Figure 3 for their locations). They are both punctual continuous releases with duration of 1 minute and a total emitted mass of 5 kg. The results are illustrated on figure 4. For both releases, the main part of material is transported and diffused above the ground but a significant amount is also confined into the closest tunnel. These amounts are then advected through the tunnels to the exit portals and back to the outdoor domain with a significant time delay.

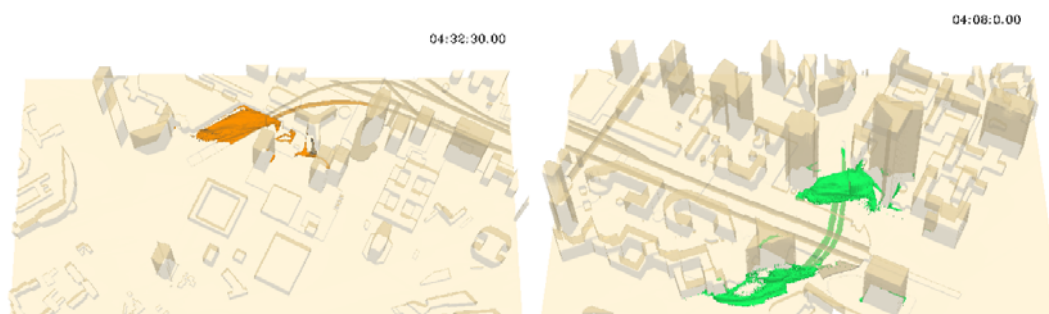


**Figure 4.** Left: South-West part of the calculation domain – Buildings and underground tunnels with opacity – Plume from orange release, time is 2’30’’ after the beginning of the emission – 3D iso-surface at 10 mg/m<sup>3</sup> in orange - Right: South-East part of the calculation domain – Buildings and underground tunnels with transparency – Plume from green release, time is 8’00’’ after the beginning of the emission – 3D isosurface at 2 mg/m<sup>3</sup> in green

## CONCLUSIONS

While the underground tunnel databases are not available, the CityGML format has been recently used to develop the numerical description of these tunnels. PMSS model is not able to use this format yet but it will surely have to in the future. In the meantime and keeping an operational objective, the underground tunnels have been added in the panel of the objects that PMSS can explicitly model using a simple footprint and vertical extrusion definition. This first implementation has been applied on a complex domain such as “La Defense”, and gives satisfying results and improves the realism of concentration field.

## REFERENCES

- Bormann A., Kolbe T. H., Donaubaue A., Steuer H., Jubierre J.R., Flurl M., (2014) Multi-scale geometric-semantic modeling of shield tunnels for GIS and BIM applications. *Computer-aided Civil and Infrastructure Engineering*
- Colella F. (2010) Multiscale modelling of tunnel ventilation flows and fires – PhD thesis
- Lacour S., Carissimo B., Foudhil H., Musson-Genon L., Dupont E., Milliez M., Albriet B., Demael E. , (2004) Estimation de ratios moyens de NO<sub>2</sub>/NO<sub>x</sub> au voisinage du débouché d’un tunnel en tranchée en milieu urbain – Collaboration CERE/CETU
- Oldrini O., C. Olry, J. Moussafir, P. Armand and C. Duchenne, (2011) Development of PMSS, the Parallel Version of Micro SWIFT SPRAY. Proc. 14th Int. Conf. on Harmonisation within Atmospheric Dispersion Modelling for Regulatory Purposes, 443-447
- Tinarelli G., G. Brusasca, O. Oldrini, D. Anfossi, S. Trini Castelli, J. Moussafir (2007) “Micro-Swift-Spray (MSS) a new modelling system for the simulation of dispersion at microscale. General description and validation”. Air Pollution Modelling and its Applications XVII, C. Borrego and A.N. Norman eds., Springer, 449-458
- Tinarelli G., L. Mortarini, S. Trini-Castelli, G. Carlino, J. Moussafir, C. Olry, P. Armand, and D. Anfossi. Review and validation of Micro-SPRAY, a Lagrangian particle model of turbulent dispersion. Lagrangian Modeling of the Atmosphere, *Geophysical Monograph*, Volume 200, AGU, pp. 311-327, May 2013.

**17th International Conference on  
Harmonisation within Atmospheric Dispersion Modelling for Regulatory Purposes  
9-12 May 2016, Budapest, Hungary**

---

**EMERGENCIES – A MODELING AND DECISION-SUPPORT PROJECT FOR THE GREAT  
PARIS IN CASE OF AN ACCIDENTAL OR MALICIOUS CBRN-E DISPERSION**

*O. Oldrini<sup>1</sup>, S. Perdriel<sup>2</sup>, M. Nibart<sup>3</sup>, P. Armand<sup>4</sup>, C. Duchenne<sup>4</sup> and J. Moussafir<sup>3</sup>*

<sup>1</sup>MOKILI, F-75014 Paris, France

<sup>2</sup>CAIRN Development, F-92380 Garches, France

<sup>3</sup>ARIA Technologies, F-92100 Boulogne-Billancourt, France

<sup>4</sup>CEA, DAM, DIF, F-91297 Arpajon, France

**Abstract:** EMERGENCIES aims to demonstrate the feasibility of real time tracking of toxic atmospheric releases, be they accidental or intentional, in a large city and its buildings through numerical simulation. Our modelling domain covers Greater Paris, and extends to the airports of Orly and Roissy Charles de Gaulle. This geographic area is under the authority of la Brigade des Sapeurs-Pompiers de Paris (BSPP), the Paris Fire Brigade. The domain forms a giant square measuring 40 km by 40 km, and consists in a 3D grid with a horizontal resolution of 3 meters. It features sub-grids with a resolution of 1 meter, describing the interior and vicinity of public-access buildings. EMERGENCIES is a world première in very high resolution atmospheric simulations and was tested for the first time in Greater Paris. This model can be transposed to every metropolis in the world.

**Key words:** CBRN-E dispersion, PMSS, Code *SATURNE*, high performance computing, very large domain, parallel modeling, nested simulations.

## INTRODUCTION

PMSS (Parallel-Micro-SWIFT-SPRAY), (Oldrini et al., 2011) allows modelling of atmospheric transport and dispersion on large areas, like the whole city of Paris, at high metric resolution. PMSS consists of SWIFT (Oldrini et al., 2014, Moussafir et al., 2004), a 3D wind field model, and SPRAY (Tinarelli et al., 2013), a Lagrangian particle dispersion model. Parallelization allows PMSS to model large areas compatible in size with responsibility areas of emergency response units.

Project EMERGENCIES was a modelling exercise of the transport and dispersion of fictitious CBRN-E releases on a gigantic area. The project was done to demonstrate the capacity of modelling as a support tool for crisis management. Domain chosen for the exercise is the Great Paris area. This domain is the responsibility area of Paris Fire Brigade. The size of modelling domain is 40 by 40km with a resolution of 3m. Calculations were performed on CCRT (*Centre de Calcul Recherche et Technologie*), CEA intensive cluster, using from 1,000 to 30,000 computational cores. Project EMERGENCIES was labelled “Grand Challenge” by the CEA.

Modelling was realized considering three hypothetical CBRN-E releases near, or inside, public buildings in Paris centre area: a museum, a train station and an administrative building. Three nested domains were defined around these buildings, modelling both the inside and the outside at 1m resolution. The 40 by 40km grid has a 3m resolution and is split in 1,088 sub domains, computed in parallel. Meteorology is computed on a 24h basis.

Visualization of simulations was also a challenge, due to the generated volume of data. Tools were developed to handle large quantity of data and allow a smooth visualization through web browser using online geographical information system. These tools allow operational exploration of data in a time compatible with crisis management.

## SCENARIO OF THE FICTITIOUS ATMOSPHERIC RELEASES

The case chosen to demonstrate our purpose is a hypothetical scenario of accidental or intentional toxic atmospheric release of NRBC-E substances, in the vicinity or within the confines of a rail station, a museum, or a major public administration.

The first emission occurs at 10 o'clock within the museum, and propagates outside of the building. The second emission occurs one hour later in the courtyard of the administration building and propagate inside and around the building. The third and last emission, at noon, is located in front of the train station and propagates inside and around the building. All releases are 10mn long.

Meteorology and turbulence are computed starting from WRF meso-scale forecasts operated routinely at CEA over France. The domain is 40 by 40km and meshed at a resolution of 3m, consisting of roughly 12 500 x 13 300 nodes. Vertically, it extends up to 1000m using 39 grid points. The domain contains more than 6 billion nodes. It is divided in 1088 tiles, computed in parallel. Each tile has a size of 401 x 401 x 39 nodes.



**Figure 13.** View of the 1088 computing tiles over the 40 by 40km domain

The domain contains 1.15 millions buildings. Its size is 1Go.

Three very-high-resolution nests are defined around the buildings of interests. The meshes have a resolution of 1m and count 2.6, 4.6 and 5.6 million nodes. They describe both the inside and outside of buildings.

Massively parallel clusters simulate:

- Turbulent airflows in and around public-access buildings at ultra high resolution (1 meter). Simulations over Greater Paris are produced at high resolution (3 meters) and feature explicit modelling for all buildings.
- Toxic dispersion at the same scales, transfers between the interior and the exterior of public-access buildings, and plume tracking at a larger distance through the street network.

## PHYSICAL AND NUMERICAL MODELLING

EMERGENCIES enables coupling of the following models:

- PMSS (Parallel-Micro-SWIFT-SPRAY, see Oldrini et al., 2011), which was jointly developed by ARIA Technologies, MOKILI, ARIAnet and the French Atomic and alternative Energies Commission (CEA). This model incorporates the PSWIFT simplified wind and atmospheric turbulence model, and PSPRAY, a Lagrangien Particle Dispersion Model.
- Code\_SATURNE (Archambeaul et al., 2004) developed by Electricité de France Research and Development, another Computational Fluid Dynamics model that enables flow computations of public-access building interiors.

PMSS is used on the 40x40km domain, while Code\_SATURNE is handling the three very-high-resolution nests. SPRAY is used both on the gigantic domain and the three nests, using the nested capability (Nibart et al., 2011). 40 000 particles are emitted every 5 seconds, leading to a global emission of 14.4 million particles.

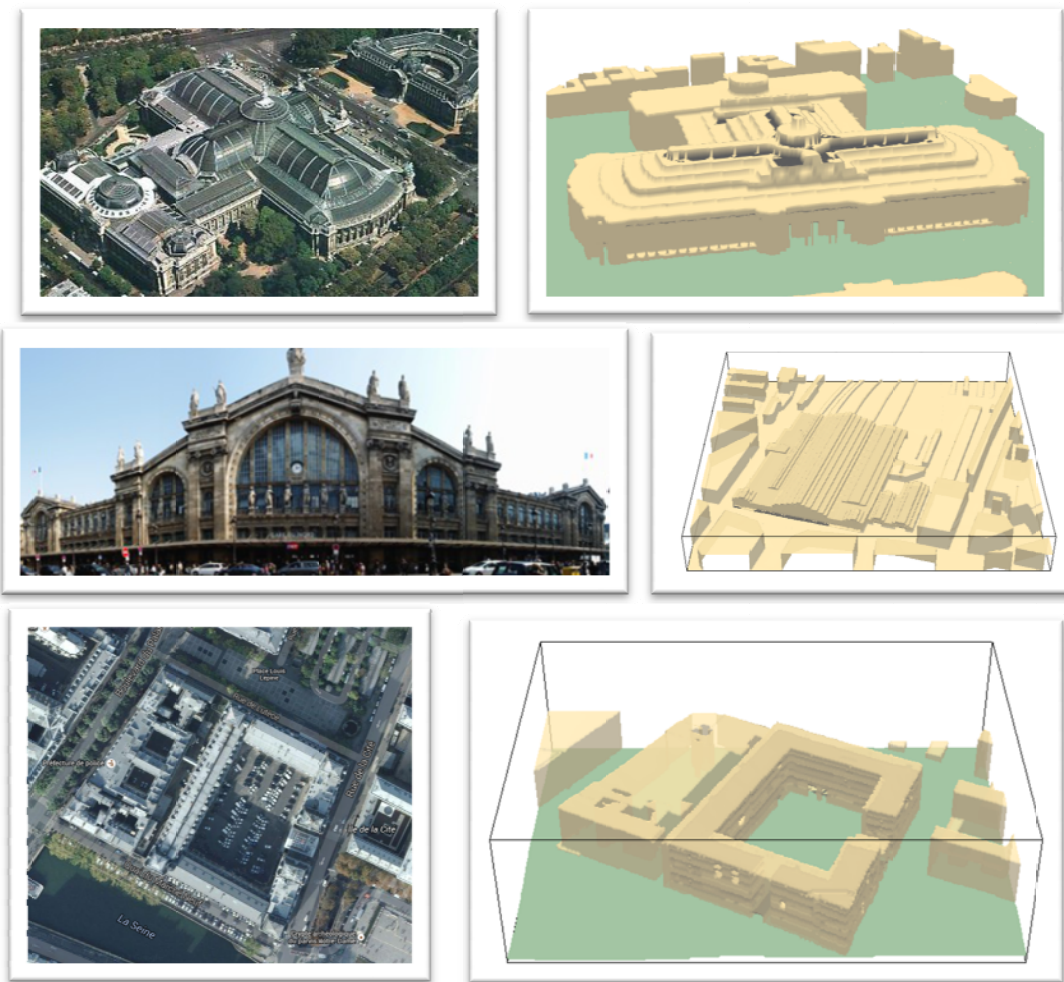


**Figure 2.** Picture of the building next to the release point, and their 3D numerical models (right side)

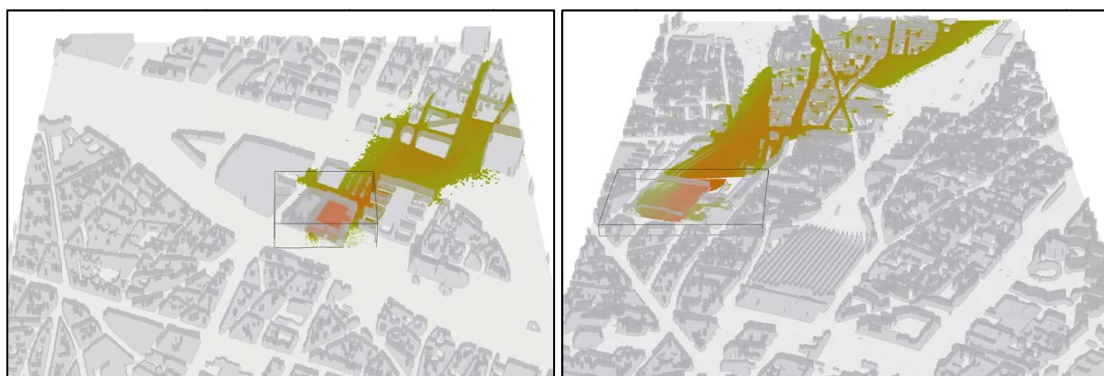


**Figure 3.** Close view of ground concentration in the vicinity of the administrative building and the train station, 20mn after the release

## PERFORMANCE

3D simulation of local-scale air flow, hour by hour and over an entire day, is obtained through mesoscale weather forecasts, kindly provided by the CEA (WRF model).

EMERGENCIES produces local forecasts for the following day:

- Two hours are required for greater Paris, covering a gigantic domain measuring 40 km by 40 km, which is divided into 1 088 tiles using 2177 cores,
- Two additional hours, using 5000 cores, are required to produce sub-grids encompassing indoor and outdoor domain around public-access buildings, measuring 300 meters by 300 meters.

Dispersion simulations for the urban domain and public-access buildings are obtained in one and a half hours and produce a five-hour simulation, using 500 cores.

The 3D viewing of this huge volume of data (about 100 terabytes) requires a massively parallel reader and a software library, kindly provided by AmpliSIM. This allows almost instantaneous viewing of simulations through the major Geographic Information Systems (GIS).

Tests have been realised using from 1 000 (the minimum) up to 25 000 cores.



**Figure 16.** Close-up 3D view of the plume remaining trapped by topography and buildings near the *Buttes Chaumont* park on the left side of the picture



**Figure 5.** Web geographical information system view of the plumes 1h50mn after the first release

## CONCLUSION

EMERGENCIES project demonstrated the feasibility of high-end simulations integrating:

- Meteorological forecasts at metric resolution on a very large 40 by 40km domain encompassing Paris and the neighboring districts,
- Coupling of simulations between the very large domain and several nested domains describing the interior of chosen public-access buildings,
- Visualisation of the huge amount of data.

Atmospheric hazard have been simulated in and around the public-access buildings, including the transport and dispersion inside the gigantic urban domain. Nested domain and parallel computing made it possible to:

- Handle the propagation inside out or outside in of the selected buildings, the release point being inside or outside,
- Follow the propagation up to several tenths of kilometers downwind, with a very fine resolution, and thus permitting to see the entrapment of airborne contaminant in street canyons and the influence of the topography even very far from the source.

EMERGENCIES is a collaborative work between small and medium businesses (MOKILI, CAIRN and ARIA) and a large research institute (CEA). It was awarded the Great Challenge Label for exceptional value. Through this recognition, EMERGENCIES gained access to the resources of the CEA Research and Technology Computing Centre.

EMERGENCIES would not have been possible without the calculation resources, and the support of the CCRT team at the CEA.

## REFERENCES

- Archambeau, F., Mechtoua, N., Sakiz, M., 2004: Code Saturne: a finite volume method for the computation of turbulent incompressible flows, *International Journal of Finite Volumes*.
- Gowardhan A. A., E. R. Pardyjak, I. Senocak, M. J. Brown, 2011: A CFD-based wind solver for urban response transport and dispersion model, *Env. Fluid Mech.*, 11:439-464
- Moussafir J., C. Olry, M. Nibart, A. Albergel, P. Armand, C. Duchenne, F. Mahe, L. Thobois and O. Oldrini, 2013: AIRCITY, a very High-resolution 3D Atmospheric Dispersion Modeling System for Paris. 15th Int. Conf. on Harmonisation within Atmospheric Dispersion Modelling for Regulatory Purposes
- Moussafir J., Oldrini O., Tinarelli G, Sontowski J, Dougherty C., 2004: A new operational approach to deal with dispersion around obstacles: the MSS (Micro-Swift-Spray) software suite. Proc. 9th Int. Conf. on Harmonisation within Atmospheric Dispersion Modelling for Regulatory Purposes, vol. 2, 114-118
- Nibart M., Armand P., Olry C., Duchenne C. and Albergel A., 2011, The indoor / outdoor pollutant transfer of a hazardous release: application to a parisian railway station, proc. 14th int. Conf. on Harmonisation within Atmospheric Dispersion Modelling for Regulatory Purposes
- Oldrini, O., Nibart, M., Armand, P., Olry, C., Moussafir, J., & Albergel, A., Introduction of Momentum Equations in Micro-SWIFT, 16th International Conference of Harmonization within Atmospheric Dispersion Modeling for Regulatory Purposes. September 2014, Varna
- Oldrini, O., Nibart, M., Armand, P., Olry, C., Moussafir, J., & Albergel, A., Multi Scale Built-up Area Integration in Parallel SWIFT, 15th International Conference on Harmonization within Atmospheric Dispersion Modeling for Regulatory Purposes. May 2013, Madrid
- Oldrini O., C. Olry, J. Moussafir, P. Armand and C. Duchenne, 2011: Development of PMSS, the Parallel Version of Micro SWIFT SPRAY. Proc. 14th Int. Conf. on Harmonisation within Atmospheric Dispersion Modelling for Regulatory Purposes, 443-447
- Tinarelli G., Mortarini L., Castelli S.T., Carlino G., Moussafir J., Olry C., Armand P., Anfossi D., 2013: Review and validation of MicroSpray, a lagrangian particle model of turbulent dispersion, *Journal of Geophysical Research*, **200**, 311-327.
- Tinarelli G., G. Brusasca, O. Oldrini, D. Anfossi, S. Trini Castelli, J. Moussafir, 2007: "Micro-Swift-Spray (MSS) a new modelling system for the simulation of dispersion at microscale. General description and validation". Air Pollution Modelling and its Applications XVII, C. Borrego and A.N. Norman eds., Springer, 449-458

**17th International Conference on  
Harmonisation within Atmospheric Dispersion Modelling for Regulatory Purposes  
9-12 May 2016, Budapest, Hungary**

---

**BEST PRACTICE IN APPLYING EMERGENCY RESPONSE TOOLS TO LOCAL-SCALE  
HAZMAT INCIDENTS**

*Steven Herring<sup>1</sup>, Patrick Armand<sup>2</sup> and Claudio Gariazzo<sup>3</sup>*

<sup>1</sup>CBR Advice Group, Defence Science and Technology Laboratory, Porton Down, Salisbury, England

<sup>2</sup>CEA, Centre DAM-Ile de France, Bruyeres-le-Chatel, France

<sup>3</sup>INAIL Research Center, Monteporzio catone (RM), Italy

**Abstract:** A great range of hazardous materials are produced, transported and stored within our society and their accidental or malicious release may pose significant threats to human health, the environment and infrastructure. If such an event occurs, first responders and higher level decision makers require an understanding of the scale of the incident and risks it poses. Dispersion modelling within an Emergency Response Tool (ERT) can provide an effective means of providing the necessary situational awareness. However, providing accurate local-scale predictions within urban or industrial areas is a challenging problem due to the complex nature of the dispersion induced by local wind flows. In addition, the problem of estimating a source's emission characteristics introduces further uncertainties in the final evaluation of impacts.

There are now a large number of ERTs based on methods ranging from simple Gaussian plume calculations to complex computational fluid dynamics (CFD) predictions. Although sophisticated CFD methods should provide the most accurate predictions, they require much more input information and computational effort than Gaussian approaches. Given that first responders need information as rapidly as possible, there is a trade-off in accuracy of solution and execution time. However, a minimum level of accuracy is required to enable the correct decisions to be made and maintain the credibility of the ERT. This implies that the accuracy and processing requirements of models in ERTs, and the situations to which they may be applied with confidence need to be understood.

This question has been addressed by COST Action ES1006 through examining the performance of different modelling approaches, the range of hazmat incidents that may occur and the requirements of the various decision makers and actors involved. This has resulted in the development of a Best Practice Guidance Document. An important finding was that first responders often use only the simplest models, which may be subject to large errors when applied in the unsteady wind conditions associated with local-scale urban problems, although opportunities exist to use more sophisticated methods. The guidance therefore recommends that the choice of modelling method is based on the availability of information and time constraints, and that there is a need for greater engagement between scientists and practitioners to exploit state-of-the-art modelling more effectively.

*Key words: dispersion modelling, emergency response*

## **INTRODUCTION**

The aim of the European Union Cooperation in Science and Technology (COST) Action ES1006 was to address 'Evaluation, improvement and guidance for the use of local-scale emergency prediction and response tools for airborne hazards in built environments'. The Action focused on complex urban areas as these are the environments in which releases of hazardous materials are likely to have the greatest impact, and the most difficult in which to provide accurate hazard predictions to support emergency responders.

A great range of hazardous chemical, biological and radiological materials are produced, transported and stored within urban areas. If these are released, either accidentally or maliciously, they may pose significant threats to human health, the environment and infrastructure. If such an event occurs, then in addition to personal protection equipment and first aid interventions, emergency responders and higher level decision makers ideally require, Emergency Response Tools (ERTs) that can provide them with the situational awareness necessary to make the appropriate decisions to best protect people and minimise environmental effects.

A wide range of ERTs are now available, ranging from simple stand-alone dispersion models to complex tools that provide a complete incident management system, able to receive inputs from a range of sensors and track assets, as well as perform the dispersion and consequence modelling. No matter how sophisticated the ERT is, though, its value to the emergency responder is entirely governed by the accuracy of its hazard predictions.

The dispersion models used to predict hazard areas in ERTs range from simple analytic Gaussian plume models to predictions generated using sophisticated computational fluid dynamics (CFD) codes. The complexity of local-scale atmospheric transport and dispersion processes in urban environments means that CFD methods should provide the most accurate hazard predictions, but they require substantially more input information and computational effort than those based on Gaussian assumptions. Given that first responders need information as rapidly as possible, there is a trade-off in time and solution accuracy. However, a minimum level of accuracy is required to enable the correct decisions to be made and to maintain the credibility of the ERT. This implies that emergency responders and decision makers need to understand the accuracy and processing requirements of the models used in ERTs, and the situations to which they may be applied with confidence. This leads to the need for a Best Practice Guidance (BPG) document as produced by COST Action ES1006.

### **COST ACTION ES1006 BEST PRACTICE GUIDANCE**

In order for a BPG document to be useful to emergency responders, it has to be applicable to the full range of situations that they may encounter, and to the actors at a number of decision making levels. In addition, such guidance has been written for the emergency responder and not for the ERT developer. This means that it should be clear, succinct and avoid technical details, and these were considerations in developing the COST ES1006 BPG document (Armand *et al.* 2015).

The diversity of possible releases means that it is impractical to provide detailed guidance for handling every type. The approach adopted in ES1006 was therefore to assess databases of real accidents to identify a representative sub-set of likely hazard scenarios (Turner and Lacomme 2014). The BPG was then related to four example scenarios in which local-scale effects were important and imposed different requirements on the ERT. These four scenarios consisted of:

- A neutrally buoyant release (i.e. a release in which density effects are negligible), as exemplified by the release of a small amount of chlorine within an urban area;
- A positive buoyancy release, as exemplified by a toxic plume produced by a warehouse fire;
- A dense gas release, as exemplified by a leakage of many tonnes of chlorine or LPG, involving the flashing and pooling of material;
- A dirty bomb that produces an explosive release of radionuclides.

The major activity undertaken by COST Action ES1006 was to conduct a series of four exercises in which the predictive performances of a range of dispersion models were compared. The different dispersion models were divided into the three categories defined in Table 1.

**Table 1.** Model types.

<b>Model type</b>	<b>Description</b>	<b>Execution time</b>
1	Models that do not resolve the dispersion around buildings. Typically semi empirical Gaussian plume/puff methods of varying complexity and sophistication.	Seconds to minutes
2	Models that resolve the dispersion around building by coupling rapid flow field calculation methods and Lagrangian Particle dispersion models.	Minutes to hours
3	Models that resolve the dispersion around and within buildings by adopting Eulerian CFD based approaches, such as RANS and LES modelling.	Hours to days

The principal reason for conducting the performance comparisons was that it was believed first responders often used only the simplest Type 1 models. This belief was confirmed through a survey of emergency responders and through information gained from first responders who participated in the four workshops run by the Action. There were two concerns associated with this, firstly that although simple models may be easy to use and provide quick answers, they may be subject to large errors when applied to local-scale urban problems, and secondly that responders were not taking advantage of the more sophisticated approaches that could be used.

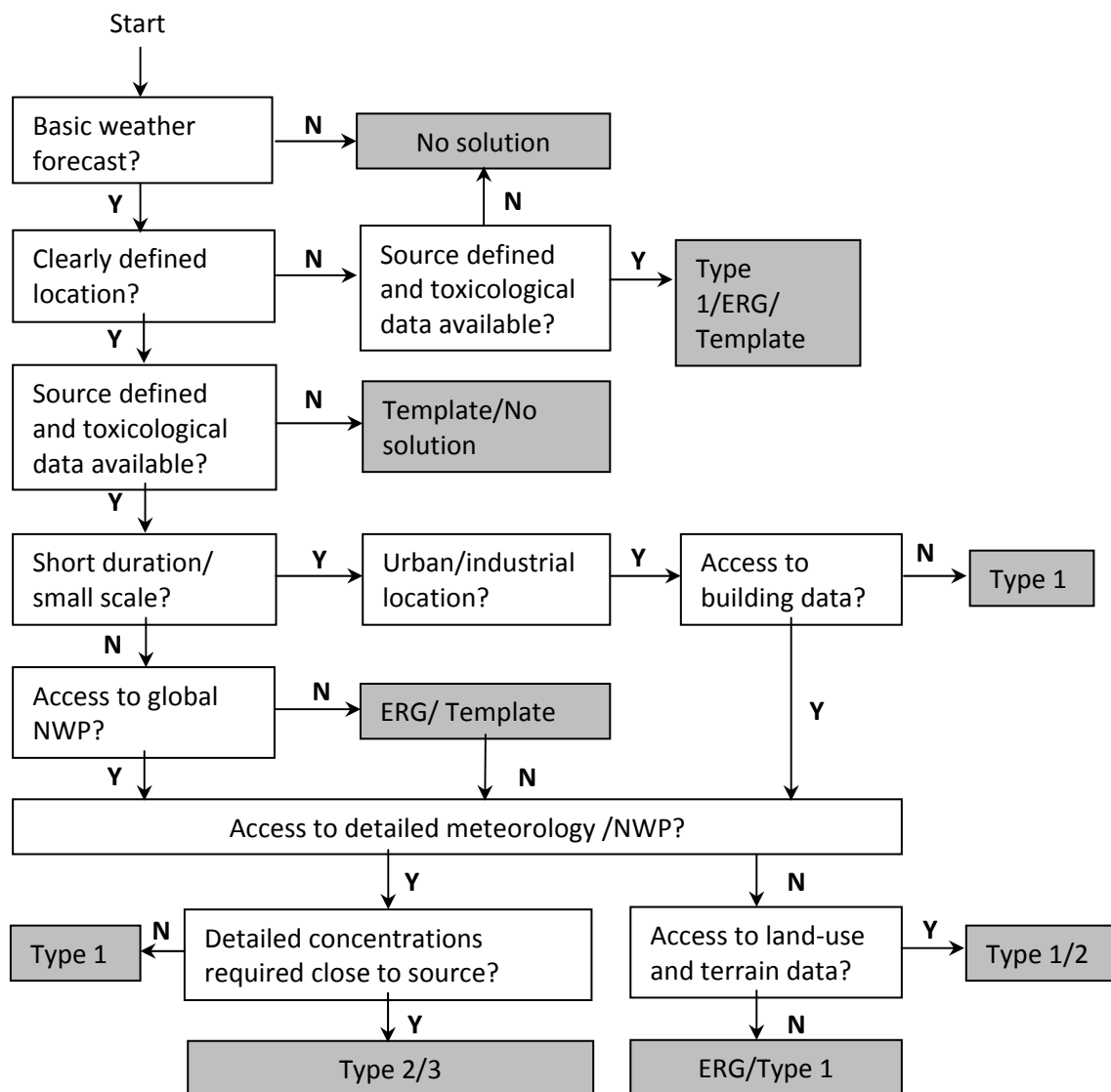


**Figure 1.** Emergency response modelling selection flowchart.

The four comparison exercises compared model predictions from some 20 models against dispersion data from wind tunnel experiments, an urban field experiment and from an actual incident. The wind tunnel comparisons showed that increasing model sophistication led to increasing model performance when the scenario was well defined. However, the performance differences reduced when the data was from the field rather than a wind tunnel, and as knowledge of the input conditions, such as the emission rate and meteorology, became more limited. These results led to the conclusion that emergency response modelling should be based on using the most sophisticated modelling approach possible, based on the input information and time available. This was reduced to the flowchart shown in Figure 1, which guides

the user to an appropriate modelling response, or in the most information poor cases a simple Emergency Response Guidebook (ERG) (Transport Canada, 2012) solution or template, such as incorporated in the NATO Chemical, Biological, Radiological and Nuclear Warning and Reporting procedures (NATO, 2014).

Examination of Figure 1 highlights the importance of the quality of the input information on the modelling that can be undertaken and, implicitly the quality of the hazard predictions that are likely to be obtained. What is not evident in Figure 1, is that when considering local-scale emergency response scenarios, that Type 2/3 models may be able to capture features of the dispersion that cannot be predicted by the simplest models and provide a substantially enhanced level of situational awareness to aid decision makers, in addition to a basic hazard area prediction. This might, for example, be through identifying localised areas of high concentration (and hence increased exposure), such as in courtyards, or transport down side-streets, that simple models cannot resolve.

While the BPG developed by the participants of COST ES1006 focusses on guiding the emergency responder to the type of dispersion model to be used, it also identifies other factors that must be considered when using ERTs, such as the fact that there may be discrepancies between models and the need for the users to have appropriate training and experience.

### **TOWARDS IMPROVING EMERGENCY RESPONSE MODELLING**

The work undertaken by COST ES1006 showed that a range of modelling options exist to support emergency responders and that different models may be required to handle different types of release. Furthermore, given sufficient input data and computational resources, it is possible to provide high fidelity local-scale hazard predictions. It has also suggested, however, that because of time and information constraints that the emergency response modeller should have a suite of modelling options at his disposal from the simplest Type 1 models to the more sophisticated Type 2 and 3 models,. The user might then rapidly produce an initial solution using a Type 1 model, but then refine the prediction by using Type 2 and Type 3 models as their solutions and more information become available to him.

It is implicit in the above that the modeller is remote from the emergency responder in order to have access to the data and computing resources required. Nevertheless, current developments in connectivity should enable this barrier to be broken down. The critical requirement is for the emergency responders and decision makers to have confidence in the modelling supporting him. This means ensuring that the models are adequately verified and validated for the situation in which they are being applied, and that the modeller has access to all the data (topographical, meteorological, etc.) required at an appropriate level of accuracy. It can be seen that this means that the goal is no longer to produce an ERT, but rather to produce an integrated emergency response system comprising the emergency responder, the communications system, the ERT and the modeller. In order to realise this, it is evident that greater engagement is required between scientists and practitioners, to exploit the state-of-the-art more effectively.

### **CONCLUSIONS**

The work of COST Action ES1006 led to the production of a BPG document for emergency response practitioners. This provided an overview of the state-of-the-art in dispersion modelling, and divided the models into three categories depending upon their level of sophistication. Based on the results from model performance comparison studies conducted within ES1006, it was concluded that emergency response modelling should be based on using validated models of a specified level of accuracy, using the most sophisticated approach available that can be supported by the input information and time available. However, in order to progress from the current position in which many first responders use only simplest models, to one in which they use more sophisticated methods that can provide substantial improvements in accuracy and situational awareness, it is evident that scientists and practitioners need to work collaboratively to establish confidence in the ERTs and implement the level of connectivity required to ensure that the modelling can be performed as part of an integrated emergency response system.

## REFERENCES

- Armand P., J. Bartzis, K. Baumann-Stanzer, E. Bemporad, S. Evertz, C. Gariazzo, M. Gerbec, S. Herring, A. Karppinen, J-M Lacomme, T. Reisin, R. Tavares, G. Tinarelli and S. Trini-Castelli 2015: COST ES1006 – Best Practice Guidelines, COST Action ES1006, ISBN: 987-3-9817334-0-2.
- Baumann-Stanzer, K. and S. Andronopoulos, P Armand, E. Berbekar, G. Efthimiou, V. Fuka, C. Gariazzo, G. Gasparac, F. Harms, A. Hellsten, K. Jurcakova, A. Petrov, A. TRakai, S. Stenzel, R. Tavares, G. Tinarelli, S. Trini-Castelli 2015: COST ES1006- Model evaluation case studies: approach and results. COST Action ES1006, ISBN 987-3-9817334-2-6.
- NATO 2014: Warning and Reporting and Hazard Prediction of Chemical, Biological, Radiological and Nuclear Incidents (Operators Manual) Allied Technical Publication ATP-45 Edition E, version 1.0, NATO Standardization Agency.
- Transport Canada, 2012 Emergency Response Guidebook (ERG2012).
- Turner M. and Lacomme J-M. 2014: COST ES1006 – STSM 2: Developing Scenarios for Testing Atmospheric Dispersion Models in Urban Areas.

Content includes material subject to © Crown copyright (2016), Dstl. This material is licensed under the terms of the Open Government Licence except where otherwise stated. To view this licence, visit <http://www.nationalarchives.gov.uk/doc/open-government-licence/version/3> or write to the Information Policy Team, The National Archives, Kew, London TW9 4DU, or email: [psi@nationalarchives.gsi.gov.uk](mailto:psi@nationalarchives.gsi.gov.uk).

**17th International Conference on  
Harmonisation within Atmospheric Dispersion Modelling for Regulatory Purposes  
9-12 May 2016, Budapest, Hungary**

---

**VALIDATION OF THE GAMMA SUBMERSION CALCULATION OF THE REMOTE POWER  
PLANT MONITORING SYSTEM OF THE FEDERAL STATE OF BADEN-WÜRTTEMBERG**

*Janis Lapins<sup>1</sup>, Wolfgang Bernnat<sup>2</sup>, Walter Scheuermann<sup>2</sup>*

<sup>1</sup>Institute of Nuclear Technology and Energy Systems, Pfaffenwaldring 31, University of Stuttgart,  
Stuttgart, Germany

<sup>2</sup>KE-Technologie GmbH, Stuttgart, Germany

**Abstract:** The radioactive dispersion model used in the framework of the remote nuclear power plant monitoring system of the federal state of Baden-Württemberg applies the method of adjoint fluxes to calculate the sky shine from gamma rays with a regarded gamma energy spectrum for nuclides released. The spectrum is represented by 30 energy groups of the released nuclides. A procedure has been developed to calculate the dose distribution on the ground in case of an accident with a release of radioactivity. For validation purposes, the results produced with the adjoint method in the dispersion code ABR are compared to results produced by forward calculations with Monte Carlo methods using the Los Alamos Code MCNP6.

**Key words:** *adjoint method, MCNP, validation, gamma submersion*

**THE MODULAR DISPERSION TOOL “ABR”**

The federal state of Baden-Württemberg, Germany, operates a remote power plant monitoring system that has an online access to the main safety relevant parameter of the power plant as well as the meteorological data provided by the German weather forecast service (DWD). The data are sent to a server system that is operated for the Ministry of Environment of the federal state. The radioactive dispersion tool “ABR” is an integral part of this system and is used for calculation of radiological consequences in case of an accident, or to prepare and to perform emergency exercises for the civil protection. For a dispersion calculation, the ABR has to account for the following:

- Interpolation of forecasted or measured precipitation to grid (precipitation module)
- Calculation of the wind field from forecast or measurement on grid (terrain-following wind field module)
- Release of the amount of radioactivity to the environment accounting for decay time of nuclides between shutdown of the reactor and the time of emission (release module)
- Transport of radioactivity with wind, also washout and fallout due to deposition or rain, respectively (Lagrange particle transport module)
- Sky shine to a detector 1 m above the ground (sky shine module)
- Calculation of the doses from various exposure paths (gamma submersion, beta submersion, inhalation and ground shine) and for 25 organs and one effective dose (dose module)

All of this is performed by the different modules of the programme system mentioned above. However, this paper will focus on the validation of the sky shine module in conjunction with the dose module which calculates the gamma submersion by the method of adjoint fluxes [1]. For validation, the reference code system MCNP6 [2] is used. Results produced with ABR are benchmarked against it.

**METHOD OF CALCULATION**

The dose calculation is performed applying the method of adjoint fluxes to calculate the gamma cloud radiation with a regarded gamma ray energy spectrum for nuclides released comprising 30 energy groups. This procedure enables an efficient algorithm to calculate the dose rates or integrated doses in case of an accident with a release of radioactivity. The system is part of the emergency preparedness and response and is in online operational service. The adjoint fluxes were produced by results from MCNP6 [2].

For validation purposes, the results produced with the adjoint method in the dispersion code ABR are compared to results produced by forward calculations with Monte Carlo methods using MCNP6. The

computational procedure comprises the following steps: From a point or a volume source, respectively, photons are started isotropically for average energies of the 30 energy groups or distinctive gamma spectrum for single nuclides. Travelling through space, these photons collide with nuclides present in air or the ground and are scattered until they reach the detector. With the help of point detectors, the flux density spectrum can be estimated, and, by making use of a dose-flux-relation, the resulting gamma submersion dose on the ground can be determined.

The backward method in the ABR uses the adjoint fluxes to evaluate the influence of a certain nuclide (spectrum) in the cloud at a certain distance from a detector point on the ground. To obtain these adjoint fluxes, a large number of calculations has been performed to determine the adjoint flux for all energy groups and distances (radii). The radii for which the fluxes were produced are support points. Radii between support points are interpolated. Depending on the energy of the group under consideration there are different exponential fitting functions that account for both energy and distance. The energy deposited within human tissue is accounted for by age classes and by use dose factors from the German Radiation Protection Ordinance that provide dose factors for organs and effective dose [5].

### SOLUTION OF THE TRANSPORT EQUATION

The transport equation in operator notation is

$$M\Phi = Q \quad (1)$$

with

$$M = \vec{\Omega}grad + \Sigma_T(E) + \iint_{\vec{\Omega}', E'} \Sigma_s(\vec{\Omega}' \rightarrow \vec{\Omega}, E' \rightarrow E) dE' d\Omega' \quad (2)$$

In equation (1) above  $Q(\vec{r}, \vec{\Omega}, E)$  represents the source vector and  $\Phi(\vec{r}, \vec{\Omega}, E)$  represents the flux density vector which both depend on the location  $\vec{r}$ , the direction  $\vec{\Omega}$ , and the Energy  $E$ . In equation (2) the first term represents the leakage term,  $\Sigma_T(E)$  represents the collision, and the integral represents the scattering from any direction  $\vec{\Omega}'$  and energy  $E'$  into the direction  $\vec{\Omega}$  and energy  $E$  of interest.

After solution of the transport equation reaction rates, e.g. dose rates  $\bar{D}$  can be calculated with the help of a response function  $R(\vec{r}, E)$  such that the condition

$$\bar{D} = \langle \Phi R \rangle = \int_V \int_E \Phi(\vec{r}, E) R(\vec{r}, E) dr dE \quad (3)$$

is valid. The adjoint equation to the equation (1) is

$$M^+ \Phi^+ = R \quad (4)$$

The adjoint equation has to be defined in a way that the condition

$$\langle \Phi^+ M \Phi \rangle = \langle \Phi M^+ \Phi^+ \rangle \quad (5)$$

holds. If this is the case, the following is also valid:

$$\bar{D} = \langle \Phi^+ M \Phi \rangle = \langle \Phi^+ Q \rangle = \langle \Phi M^+ \Phi^+ \rangle = \langle \Phi R \rangle = \bar{D} \quad (6)$$

I.e. instead of eq. (1), the adjoint function eq. (4) can be solved and the reaction rates are determined by eq. (3). The solution of the adjoint transport equation provides a relation between photon emission of a certain energy/energy range of a point/volume regarded and the dose at a computational point.

### CALCULATION OF ADJOINT FLUXES WITH MCNP

The calculation of the gamma submersion as a consequence of radioactive nuclides in the radioactive cloud can be achieved if the spatial and energy distribution of the gamma sources in relation to certain computational points at the ground are known, together with the composition of air and soil. The computation necessitates the solution of the photon transport equation with respect to the energy dependence of the possible reactions of photons with atoms in air or soil (photo-electrical effect, Compton effect, pair production effect etc.). The solution of the transport equation yields photon spectra for computational points that enable dose calculations. Relevant dose/flux relations are defined by ICRP, [3]. For photons ICRP 74 can be applied. The dose/flux relation is presented in Figure 2. With Monte Carlo codes with their continuous energy dependence of the cross sections, a direct solution of the adjoint transport equation is not possible. Nevertheless, these codes can be used to estimate the contribution of a source point/volume to the dose at a computational point, see Figure 1. To do this, the source

point/volume a sufficiently great number of photon trajectories have to be simulated and their contribution to the dose is calculated. Computing the dose rates at a computational point of interest, the relevant contributions from all source points/volumes of the whole emission field have to be summed up such that the dose at the computational point  $(x, y, z)$  can be estimated with

$$D(x, y, z) = \sum_q \sum_g \Phi_g^+(r_q, z_q - z) \cdot Q(x_q, y_q, z_q) \cdot V_q \quad (7)$$

with

$$r_q = \sqrt{(x_q - x)^2 + (y_q - y)^2} \quad (8)$$

$\Phi_g^+$  as the adjoint flux depending on the radius and the height,  $Q_g$  as specific source concentration and  $V_q$  as the volume that contains the concentration.

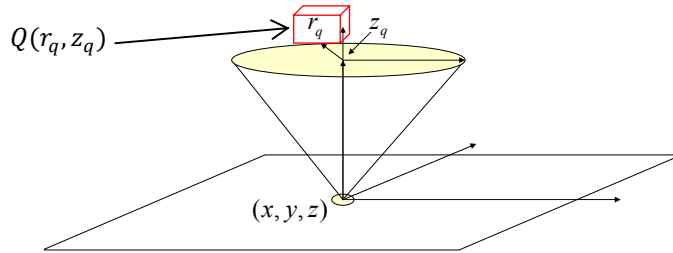


**Figure 1.** Source point/volume  $Q(r_q, z_q)$  and computational point of interest  $P(x, y, z)$  in dose calculations

The index  $q$  corresponds to the source; the index  $g$  corresponds to the energy group or the gamma line of the source of the photon emission energy. The coordinates  $x, y, z$  correspond to the computational point of interest. The coordinates  $x_q, y_q$  (resp.  $r_q$ ),  $z_q$  correspond to the centre point of the source volume  $V_q$ , see Figure 1.

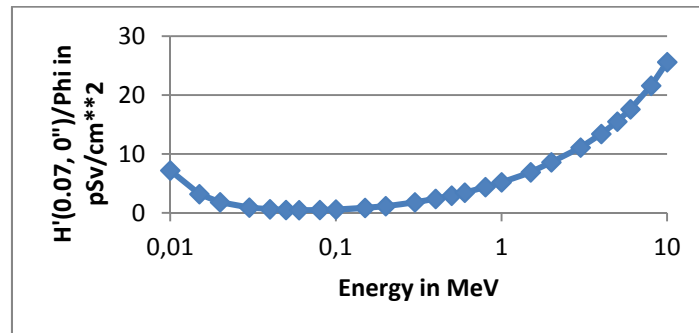


**Figure 2.** Dose/flux relation for gamma energies from 0.01 – 10 MeV in 0.07 cm depth of the body according to ICRP 74 [3]

## 2 SCENARIOS FOR DOSE COMPARISONS: A HOMOGENEOUS AND A NON-HOMOGENEOUS RADIOACTIVE CLOUD OF REFERENCE NUCLIDES

For comparison of the results of the gamma submersion dose rates, two scenarios have been defined. The base scenario assumes a homogeneous concentration distribution of three reference nuclides Xe-133, Cs-137 and I-131 with a flat topography both for the ABR and MCNP, respectively. There is no use of the dispersion module of the ABR, but the concentrations are artificially input into the sky shine and dose modules of the ABR. The computational domain and the boundary conditions for this scenario are presented in Table 1. A sketch of the scenario is shown in Figure 5.

An advanced scenario with a 3-D cloud is also presented. For this scenario, a realistic concentration distribution has been generated with the ABR, i.e. the release height of 150 metres with a wind speed of 4 m/s at 10 m height and increasing wind speed with the height for diffusion category D (neutral conditions). The released activity is transported with the wind. After one time step the doses are compared. Since the MCNP cannot simulate the transport of radioactive particles with the wind, the distribution of concentration of the isotope regarded is imported to MCNP via an interface. The results for the dose calculation are also compared. The radioactive cloud together with the wind speed is presented in

Figure 6. For this paper, the shape of the cloud is regarded as given as the dose rates are subject to comparison and not the cloud shape. The boundary conditions and general assumptions for this case is given in Table 2

The gamma lines of the reference nuclides are shown in Figure 3 and Figure 4, [4]. These gamma emissions are accounted for in the 30 group spectrum of the ABR with their respective intensity. For the MCNP calculation, the gamma energies and their respective intensity are directly input.

**Table 1.** Simulation set-up for homogeneous cloud from 120 – 160 m

Constant source	ABR	MCNP6
Computational area (x, y, z)	20 km x 20 km x 1 km	20 km x 20 km x 1 km
Mesh number (x, y, z)	100 x 100 x 25	-
Mesh size in x, y, z - direction	200 m , 200 m, 40 m	-
Cloud height	120 – 160 m	120 – 160 m
Activity in cloud [Bqm <sup>-3</sup> ]		
Cs-137	6.0E+04	6.0E+04
Xe-133	2.0E+10	2.0E+10
I-131	1.0E+06	1.0E+06

**Table 2.** Simulation set-up for a non-homogeneous cloud

Realistic source	ABR	MCNP6
Computational area (x, y, z)	20 km x 20 km x 1 km	20 km x 20 km x 1 km
Mesh number (x, y, z)	100 x 100 x 25	100 x 100 x 25
Mesh size in x, y, z - direction	200 m , 200 m, 40 m	200 m , 200 m, 40 m
Emission height	150 m	150 m
Total activity released [Bq]		Activity imported via interface
Cs-137	6.0E+09	6.0E+09
Xe-133	2.0E+17	2.0E+17
I-131	1.0E+10	1.0E+10
Wind speed in 10 m height	4 m/s	-
Diffusion category	D	-
Emission duration	1 hour	-

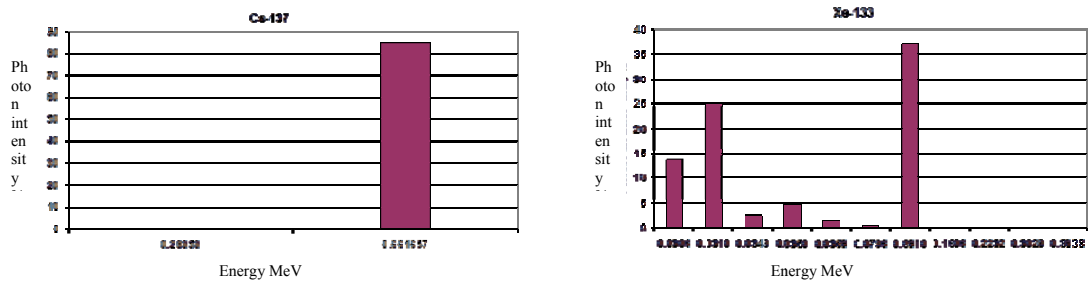


**Figure 3.** Gamma lines and intensities of Cs-137 and Xe-133 (NUDAT 2.6) [4]

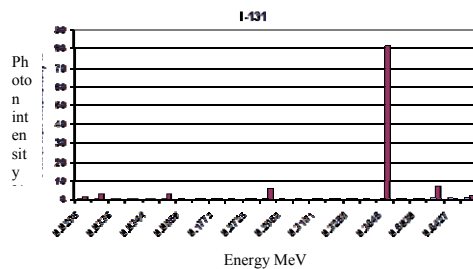


**Figure 4.** Gamma lines of I-131 (NUDAT 2.6) [4]

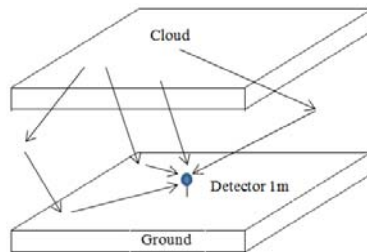


**Figure 5.** Sketch of the scenario with homogeneous emission layer and exemplary paths from the cloud to the detector (direct, indirect via air and ground reflection, or both)

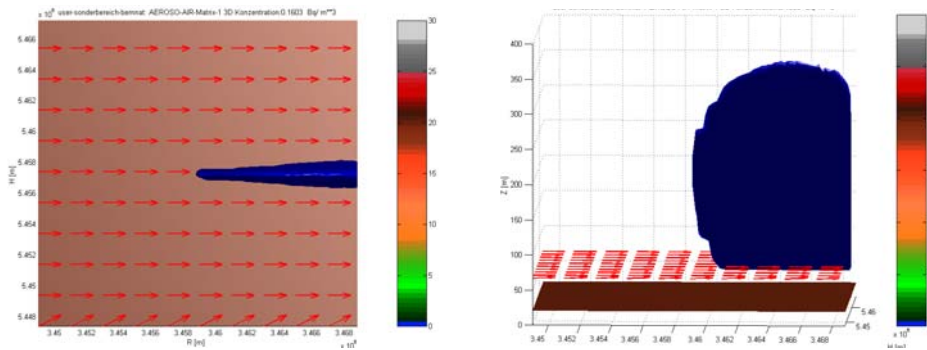


**Figure 6.** Non-homogeneous distribution of aerosoles after 1 hour with a wind speed of 4 m/s at a height of 10 m simulated with the ABR. The concentration is exported to MCNP

## RESULTS OF COMPARISON

The results of the comparison are presented in the tables below. One can see that the results are in good agreement for the three reference nuclides.

**Table 3.** Results for the base case with homogeneous cloud

Nuclide	MCNP6 [Sv/h]	ABR [Sv/h]	Ratio ABR/MCNP6
Cs-137	9.31E-07	8.33E-07	0.89
Xe-133	1.36E-02	1.30E-02	0.96
I-131	1.01E-05	1.03E-05	1.02

**Table 4.** Results for the advanced case with non-homogenous cloud

Nuclide	MCNP6 [Sv/h]	ABR [Sv/h]	Ratio ABR/MCNP6
Cs-137	1.42E-10	1.36E-10	0.96
Xe-133	4.49E-04	4.9E-04	1.09
I-131	1.49E-10	1.57E-10	1.05

## CONCLUSION

The results for the comparison of gamma submersion dose rates show that there is good agreement between the ABR and MCNP6 for the cases analysed. It could be shown that for all three reference nuclides the maximum deviation for the dose rate of Cs-137 is -11% for the base case.

For the non-homogenous distribution of the concentration for the reference nuclides the agreement is better than 10%. Keeping in mind that for a real dispersion calculation there are a multitude of uncertainties, e.g. emitted nuclide vector, meteorological prediction, transport of cloud, this agreement presented for the comparison of the dose rates for the reference nuclide each can be regarded as excellent.

## REFERENCES

- [1] Sohn, G. Pfister, W. Bernat, G. Hehn: Dose, ein neuer Dosismodul zur Berechnung der effektiven Dosis von 21 Organdosen für die Dosispfade Submersion, Inhalation und Bodenstrahlung, IKE 6 UM 3, Nov. 1994.
- [2] D. B. Pelowitz: MCNP6™ User's Manual Version 1.0 LA-CP-13-00634, Rev. 0 (2013)
- [3] ICRP, 1996: Conversion Coefficients for use in Radiological Protection against External Radiation. ICRP Publication 74, Ann. ICRP 26 (3-4).
- [4] NUDAT 2.6, National Nuclear Data Centre, Brookhaven National Laboratory.
- [5] Entwurf zur AVV zu §47 Strahlenschutzverordnung, Anhang 3 (German: General Administrative Regulation for §47 of the German Radiation Protection Ordinance, Appendix 3), (2005).

**SPATIAL AND TEMPORAL CONCENTRATION DISTRIBUTIONS IN URBAN AREAS**

*Eva Berbekar, Frank Harms, Bernd Leitl*

Meteorological Institute, University of Hamburg, Germany

**Abstract:** Mathematical models are frequently applied to predict the concentration field in urban environments. In emergency situations involving airborne hazardous materials, first responders often rely on models based on distribution functions (such as the Gaussian models) to define the danger zone and support the rescue. Above flat open terrain and homogeneous roughness, distribution functions are applied successfully to describe the spatial concentration distributions. However, due to turbulence caused by the city structure, it is not straight forward that the approximating functions applied for flat open terrain and homogeneous roughness give a reasonable estimation of the concentration distribution in an urban area. Results of boundary-layer wind tunnel measurements from the COST Action ES1006 were investigated. The dataset contains two different urban setups: a semi-idealized urban structure (Michelstadt) and the model of an existing city centre (CUTE). The lateral and longitudinal profiles of mean concentrations are approximated by the Gaussian dispersion equation. The results help to improve and identify the strengths and weaknesses of predicting the concentration field based on distribution functions in urban areas. The parametrised Gaussian dispersion equation fits well on the mean concentration profiles, however the maximum concentration is not aligned with the source parallel to the main wind direction.

**Key words:** *Gaussian distribution, urban dispersion, wind tunnel*

## INTRODUCTION

Due to urbanisation, accidental releases inside cities affect more and more people. First responders often rely on results from numerical models to predict the dispersion of hazardous materials. Due to its instantaneous results and simplicity, the Gaussian plume model is often used for this purpose.

According to Hanna et al. (1982), the Gaussian model originates from Sutton (1932), Pasquill (1961, 1974) and Gifford (1961). The generalized Gaussian dispersion equation for a continuous point-source plume (not considering vertical dispersion reflection due to inversion) has the form

$$C(x, y, z) = \frac{Q}{u} \frac{1}{2\Pi\sigma_y\sigma_z} \exp\left(\frac{-y^2}{2\sigma_y^2}\right) \left[ \exp\left(\frac{-(z-H)^2}{2\sigma_z^2}\right) + \exp\left(\frac{-(z+H)^2}{2\sigma_z^2}\right) \right], \quad (1)$$

where  $C$  is the concentration,  $x$  is the coordinate parallel to the direction of the approach flow,  $y$  is the horizontal coordinate perpendicular to the direction of the approach flow and  $z$  is the vertical coordinate (Beychok, 1994). The coordinates of the source are  $(0,0,H)$ .  $Q$  stands for the release flow rate,  $U$  is the mean wind velocity component parallel to the main wind direction of the approach flow at  $H$  height,  $\sigma_y$  is the horizontal dispersion coefficient and  $\sigma_z$  is the vertical dispersion coefficient. In case of ground-level point sources ( $H=0$ ), equation (1) can be simplified to

$$C(x, y, z) = \frac{Q}{u} \frac{1}{\Pi\sigma_y\sigma_z} \exp\left(\frac{-y^2}{2\sigma_y^2}\right) \exp\left(\frac{-z^2}{2\sigma_z^2}\right). \quad (2)$$

Among other limitations, the Gaussian dispersion equation applies only if the turbulence is homogeneous throughout the plume (Beychok, 1994). However, when an airborne pollutant is released in a built-up

area, the city geometry causes inhomogeneity in the turbulence, therefore the applicability of the Gaussian dispersion equation is not straightforward.

To investigate the dispersion characteristics in an urban environment, wind tunnel measurements were carried out. The dataset contains two different urban setups: a semi-idealized urban structure (Michelstadt) and the Complex Urban Terrain Experiment (CUTE). The measurements serve as validation test cases used in the frame of the COST Action ES1006 to evaluate and improve local-scale emergency response tools (Baumann-Stanzer et al., 2015). Based on the datasets, the concentration profiles parallel and perpendicular to the approach flow direction were investigated.

### EXPERIMENTAL SETUP

The wind tunnel measurements were carried out in the “WOTAN” boundary-layer wind tunnel located in the Environmental Wind Tunnel Laboratory in Hamburg. The tunnel has an 18 m long and 4 m wide test section. The height is adjustable between 2.75 and 3.25 m. The boundary layer is generated by turbulence generators and roughness elements placed upwind of the test section.

Results of two wind tunnel measurement campaigns are evaluated to investigate urban dispersion. Michelstadt (Figure 1) is a 1:225 model of a semi-idealized urban geometry (Hertwig et al., 2012). The model has aspect ratios, building heights and street widths typical for many Central-European cities (Di Sabatino et al., 2010). The CUTE measurements (Figure 2) were carried out within the 1:350 model of the downtown area of a typical Central European city (Baumann-Stanzer et al., 2015).

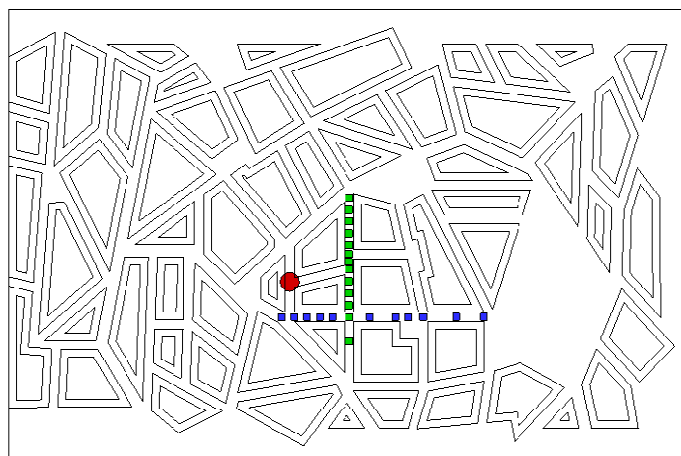


**Figure 1.** Model of Michelstadt with the selected measurement profiles. The source is indicated with a red circle and the measurement locations are marked with blue and green squares.

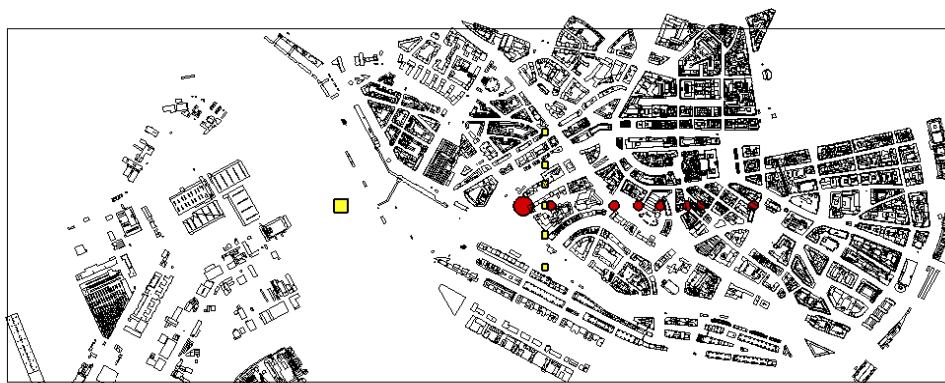


**Figure 2.** Model of the CUTE test case. The sources are indicated with large symbols, and the corresponding measurement locations are marked with smaller squares and circles.

To model urban dispersion, ethane tracer gas was released from ground-level point sources represented by fast solenoid micro-valves. The concentration was recorded with high temporal resolution by a fast-Flame Ionisation Detector. The uncertainty of the results was determined based on repetitive measurements. The results are converted to dimensionless concentration values using the formula

$$C^* = \frac{CU_{ref}L_{ref}^2}{Q}, \quad (3)$$

where  $C^*$  is the dimensionless concentration,  $C$  is the measured concentration,  $U_{ref}$  is mean reference wind speed,  $L_{ref}$  is the reference length and  $Q$  is the flow rate of the release.

The measurement results form a dataset to evaluate numerical models in the frame of the COST Action ES1006 (Baumann-Stanzer et al., 2015). The main purpose of the measurements was to provide a high-quality dataset optimal for the validation of emergency response tools applied during an accidental release in an urban area. For this paper, the data is evaluated to investigate dispersion characteristics relevant for urban areas. The concentration distribution is investigated based on the mean concentration field of continuous release dispersion.

## RESULTS

Four concentration profiles were selected for this paper, a lateral (constant- $y$ ) and a longitudinal (constant- $x$ ) profile for each dataset. The selected measurements were carried out at pedestrian-level height.

Parametrised Gaussian equations were fitted on the measured mean dimensionless concentration profiles. For lateral profiles equation (4) and for longitudinal profiles equation (5) were fitted. The parameters  $a$ ,  $b$ ,  $c$ ,  $d$  and  $e$  were approximated using nonlinear least squares method. The fitted functions are plotted in Figure 3.

$$C^*(x) = \frac{a}{\Pi bx^c dx^e} \quad (4)$$

$$C^*(y) = \frac{a}{\Pi bc} \exp\left(\frac{-(y-d)^2}{2b^2}\right) \exp\left(\frac{-(z)^2}{2c^2}\right) \quad (5)$$

While deriving equation (4) and (5), additional assumptions were considered to those already applying to the Gaussian dispersion equation (Beychok, 1994). For equation (4) the shape of mean dimensionless concentration profile is expected to be similar throughout the  $y$  axis and the height of the measurement points is neglected. The horizontal and vertical dispersion coefficients ( $\sigma_y = bx^c$  and  $\sigma_z = dx^e$  in equation 4) are modelled as power functions of the distance from the source as suggested originally by Smith (1968). For equation (5), an extra degree of freedom is introduced with the  $d$  parameter, allowing the profile to take its maximum independently from the source location. Whereas the Gaussian dispersion equation assumes that the plume centreline is aligned with the source parallel to the main wind direction.

The Gaussian distribution fits well to the lateral and longitudinal concentration profiles for both test cases (Figure 3). However, the approximated maximum concentrations of the lateral profiles are not aligned with the source locations due to the influence of the city geometry.

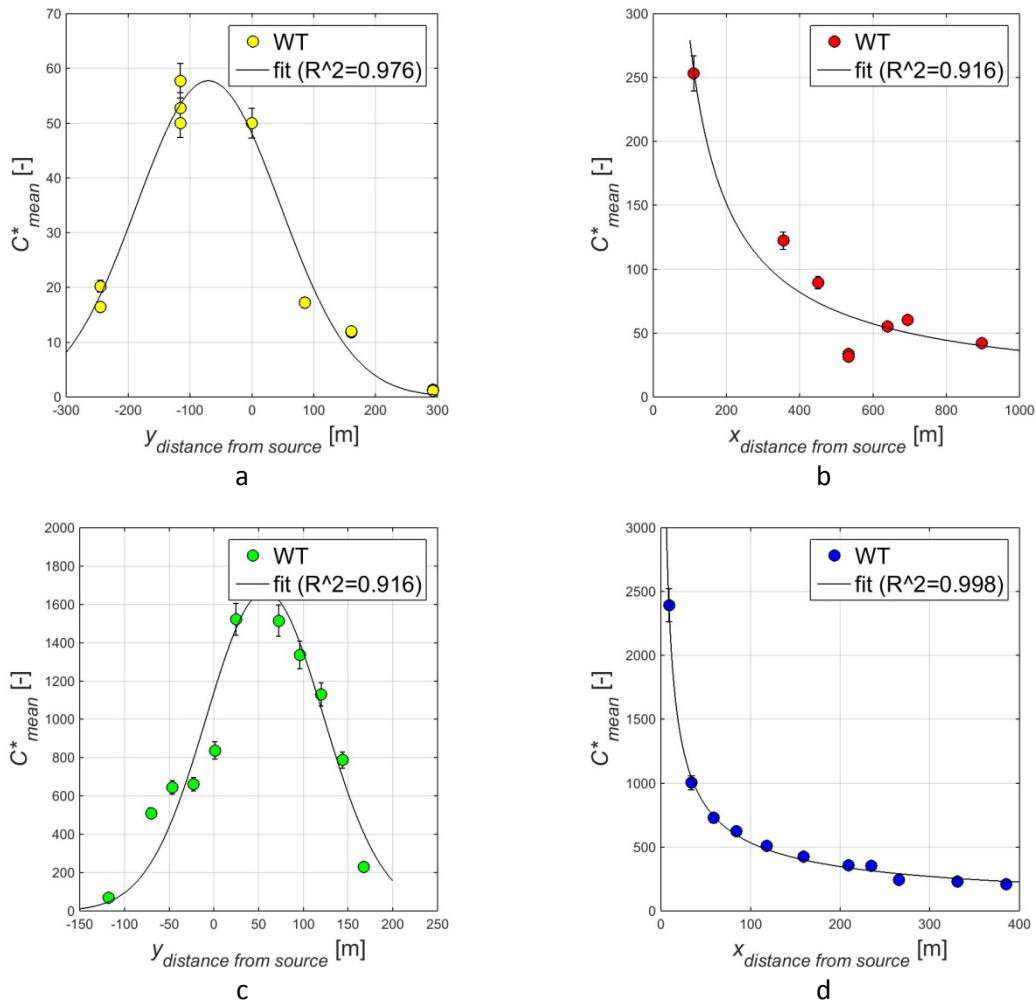


**Figure 3.** Concentration profiles measured in Michelstadt (a and b) and CUTE (c and d). Equation 4 is fitted on the lateral profiles (a and c) and equation (5) is fitted on the longitudinal profiles (b and d). The goodness of the fit is indicated by the  $R^2$  measure, WT stands for wind tunnel results.

## CONCLUSIONS

During emergency situations involving accidental releases, first responders often rely on models based on distribution functions (such as the Gaussian model) to support the rescue. When the turbulence is homogeneous, the distribution functions are applied successfully to describe the mean concentration field. However, due to inhomogeneous turbulence caused by the city structure, it is not straight forward that the Gaussian dispersion equation applied for flat open terrain or above homogeneous roughness gives a reasonable estimation of the concentration distribution in an urban area.

Results of boundary-layer wind tunnel measurements from the COST Action ES1006 were investigated. Concentration profiles of two datasets were studied: a semi-idealized urban structure (Michelstadt) and the model of an existing city centre (CUTE). The lateral and longitudinal profiles of mean concentrations are approximated by the Gaussian dispersion equation. The results show that the parametrised Gaussian dispersion equation fits well on the lateral and longitudinal mean concentration profiles. However, the maximum concentration is not aligned with the source parallel to the main wind direction due to the influence of the urban structure.

The results show that the distributions described by equations (4) and (5) fit well to the selected measurement profiles. However, this does not necessary imply that a Gaussian model would give such a

good fit to the measurements. The parameters of equations (4) and (5) were approximated by non-linear regression analysis to fit to the results. Whereas the Gaussian model calculates the concentration profiles using only the boundary conditions of the measurements.

#### **ACKNOWLEDGEMENT**

The financial support of the *Behörde für Inneres und Sport* in Hamburg is gratefully acknowledged. The valuable guidance by COST Action ES1006 members during the measurements and data processing is very much appreciated.

#### **REFERENCES**

- Baumann-Stanzer and the members of the COST Action ES1006, 2015: COST ES1006 Model evaluation case studies: approach and results. Hamburg University, Germany.
- Beychok, M. R., 1994: Fundamentals Of Stack Gas Dispersion, 3<sup>rd</sup> Edition, author-published. USA.
- Di Sabatino, S., L. S. Leo, R., Cataldo, C. Ratti, R. E. Britter, 2010: Construction of Digital elevation models for a southern European city and a comparative Morphological analysis with respect to northern European and North American cities. *Journal of Applied Meteorology and Climatology* **49**, 1377–1396.
- Gifford, F. A. 1961: Use- of Routine Meteorological Observations for Estimating Atmospheric Dispersion, *Nucl. Saf.*, **2**, 47-57.
- Hanna, S. R., G. A. Briggs, R. P. Hosker, 1982: Handbook on Atmospheric Diffusion. U.S. Department of Energy, Technical Information Center
- Hertwig, D., G. C. Efthimiou, J. G. Bartzis, and B. Leitl, 2012: „CFD-RANS model validation of turbulent flow in a semi-idealized urban canopy. *Journal of Wind Engineering and Industrial Aerodynamics*, **111**, 61–72.
- Pasquill, F., 1961: The Estimation of the Dispersion of Windborne Material. *Meteorol. Mag.*, **90**, 33-49.
- Pasquill, F., 1974, Atmospheric Diffusion, 2<sup>nd</sup> Edition, John Wiley & Sons, New York.
- Smith, M. E., 1968: Recommended Guide for the Prediction of the Dispersion of Airborne Effluents, 1<sup>st</sup> Edition, American Society of Mechanical Engineers, New York
- Sutton, O. G., 1932: A Theory of Eddy Diffusion in the Atmosphere. Proc. R. SOC. (London), Ser. A, 135: 143.

**17th International Conference on  
Harmonisation within Atmospheric Dispersion Modelling for Regulatory Purposes  
9-12 May 2016, Budapest, Hungary**

---

**HARMONIZATION IN CFD APPROACHES TO ASSESS TOXIC CONSEQUENCES OF  
AMMONIA RELEASES**

*Guillaume Leroy, Jean-Marc Lacome, Benjamin Truchot, Lauris Joubert*

INERIS, Parc Technologique ALATA, BP2, Verneuil en Halatte 60550, (France)

*Corresponding author: Guillaume Leroy, [Guillaume.Leroy@ineris.fr](mailto:Guillaume.Leroy@ineris.fr)*

**Abstract:** In the framework of land use planning, massive releases have to be modelled considering they generate important toxic effect distances. The common way to deal with such scenarios is currently based on Gaussian models or, more recently, CFD codes based on a RANS turbulence model. While the first does not enable taking account of the environment with a high level of precision, the second are not suitable for accounting for Atmospheric Boundary Layers (ABLs) anisotropy. Using LES CFD approaches then appears nowadays as promising to overcome those difficulties. However it is necessary to perform the best input parametrization among a large variety of method (recycling method, synthetic method, forcing method) to generate appropriate inflow boundary conditions. The objective of this paper is to present results obtained with the open source LES CFD code FDS by using synthetic eddy method. Parameterizations to generate inlet conditions were tested and compared to large scale INERIS ammonia releases. Comparison with the RANS CFD model *Code\_Saturne* and the shallow layer SLAB model are also presented and discussed.

**Key words:** *CFD LES modelling, experimental data, inlet CFD modelling, ammonia release*

## **INTRODUCTION**

Several models are used in the framework of land use planning, based on a large variety of nature and complexity. For an identical accidental release in the atmospheric, within the context of a regulatory study, discrepancies could appear in terms of computed distances, this means major differences in impacted zones. Those variations can be observed either between atmospheric CFD model results or with conventional approaches as Gaussian or shallow layer approach models. Reasons that can explain these discrepancies are numerous and have various origin. A major issue for risk assessments is the harmonisation of input data for the flow modelling between widely-used approach and CFD (RANS or LES) approaches which using is continuously increasing. These latter can be an improvement for being more predictive specifically when natural or anthropogenic obstructions are located in the vicinity of the release. RANS approaches appear as the simplest way but some limitations can appear considering the specific turbulence intermittency and anisotropy of the flow of the ABLs. LES modelling appears then as relevant because of its ability to consider unsteady and anisotropic turbulence and its consequences on the cloud dispersion.

This paper focuses on the ability of the shallow layer SLAB, the RANS code (*Code\_Saturne*) and the LES code (FDS) to model an ammonia release experiment and the work required to harmonize input data for predictive atmospheric model. Large scale INERIS ammonia releases were used in this paper because it corresponds to a free field jet release that can be compared to atmospheric dispersion model to check the ability of these tools in predicting the consequences of toxic industrial chemicals (TIC s) atmospheric dispersion following an accident. Comparisons between modeling results from these three approaches and experimental measurement are presented and analyzed.

## **EXPERIMENTAL TEST DESCRIPTION**

Ammonia dispersion field tests performed by INERIS were presented in a previous paper (Bouet, 2005). INERIS conducted real-scale releases of ammonia on the 950 ha flat testing site of CEA-CESTA (Centre of Scientific and Technical Studies of Aquitaine). During experiments, the atmospheric conditions were

analyzed using a meteorological mast. This mast was 10 m high and was equipped with 3 cup anemometers located at 1.5, 4 and 7 m above the ground, a wind vane at 7 m and an ultrasonic anemometer at 10 m. A weather station was also installed near the testing site. It allowed recording the ambient temperature, the relative humidity and the solar flux 1.5 m above the ground. Sensors were located in 7 arc shapes centered on the release point. Several release test cases were achieved with mass flow rate up to 4.2 kg/s. For the scope of the present study the trial case 4 is considered (release duration time: 10 min) which corresponds to a free field jet release. As expected, the ammonia cloud behaved like a heavy gas. A description of this experimental trial and a modeling study have already been presented in a previous paper (Lacome et al., 2014). In this present paper an enhanced wind flow analysis is carried out to take into account additional measurements provided by ultrasonic anemometer (see Table 1).

**Table 1.** Ultrasonic anemometer (10 Hz) measurements (over first 5 mins of the release) for trial case 4

Ambient temperature	LMO (-)	$u_*$ (m/s)	wind speed (m/s) at 10 m
14.82°C	-166	0.36	3.24

### GOVERNING EQUATIONS FOR THE 3 MODELLING APPROACHES

The widely-used dense gas dispersion SLAB has been used to simulate the trial case. It is available for free thanks to the Environmental Protection Agency (EPA). The RANS CFD simulations were performed with *Code\_Saturne* (CFD freely available code), which has been previously tested on flat terrain (E. Demael and B. Carissimo, 2008) and obstructed environment (M. Milliez and B. Carissimo, 2007). The LES CFD runs were achieved with FDS a freely available CFD code provided by the NIST (McGrattan, 2005) and initially dedicated to fires and smoke propagations modelling. The main features of the 3 modelling approaches are briefly summarized in the following part.

#### SLAB

The model can handle horizontal jets (Ermak, 1990); in the far field a shallow-layer approach is widely used to disperse a dense gas (Hanna et al., 2008) according to the observed behavior of the release.

#### RANS

The governing equations are solved under Boussinesq's hypothesis. Simulations were run with an adapted  $k - \varepsilon$  turbulence model for atmospheric flows (Wei, 2016). The transport equations for the turbulent kinetic energy  $k$  and the scalar dissipation rate,  $\varepsilon$ , take into account the wind shear and buoyance effect on production or dissipation of  $k$ . This latter term is formulated by means of potential temperature gradient. Indeed, transport equation for the potential temperature,  $\theta$ , profile is solved along the domain. The models constants for  $k - \varepsilon$  turbulence model take the values modified for atmospheric flows following (Detering, 1985) where  $C_\mu = 0.03$  according to the work of Duynkerke (Duynkerke, 1988) and the value of  $C_{\varepsilon 3}$  is taken after (Violet, 1988):  $C_{\varepsilon 3} = 0$  for a stably stratified atmosphere and  $C_{\varepsilon 3} = 1$  for an unstably stratified atmosphere corresponding to the present studied case.

#### LES

Turbulence model is based on the Large Eddy Simulations (LES) approach. The fundamental idea of LES is the segregation between large scales, that are explicitly solved, and small ones, that are modelled. Because the anisotropy is governed by the large scale and considering small scales are dissipative ones, this consequently enables solving the whole characteristics of turbulence in the ABLs. The key issue then consists in prescribing relevant velocity profile in terms of instantaneous velocity. In the last version of FDS, v6.1.2, was introduced the SEM methods as developed by Jarin (Jarin et al. 2008).

### ADAPTATION OF AN EXPERIMENTAL SIGNAL FOR THE CODES INFLOW

#### SLAB

The model was run with the optimum source release terms knowing the experimental mass flow rate and that experimental observations showed very little rainout deposition on the ground. The flow input is set by choosing a stability Pasquill class of type C, according to the sonic anemometer measurements, and a

roughness value of  $z_0 = 0.03$  m was selected according to the land cover of the experimental site ground (prairie grass). An enhanced study, based on a statically wider wind study of the site, would be necessary to assess this value that is generally sensitive for atmospheric dispersion modelling.

#### RANS

The atmospheric stability class is represented by the inflow boundary condition for the velocity, the turbulent kinetic energy  $k$ , dissipation of turbulent kinetic energy  $\varepsilon$  and temperature profile. The inlet and the top boundary are specified by the Dirichlet condition. The outlet is a free outflow condition. The lateral boundaries are symmetry condition. The wind velocity and direction were modelled as constant, i.e. wind-meandering was not modelled. Previous CFD flow simulations (Milliez and Carissimo, 2007) with RANS approach show that better results could be obtained by fitting the inlet conditions to measurements for both the mean velocity profile and the turbulence intensity. According to these previous results, a power law velocity, according to the stability class reported by Barrat (Barrat, 2001), i.e.,  $n = 0.16$  (stability class C), is used to build the velocity profile (see Figure 1). The turbulent kinetic energy and the dissipation of turbulent energy profiles are built using the similarity functions proposed by Dyer (1974) for unstable condition which main inputs, i.e. the friction velocity ( $u_*$ ) and the Monin-Obukohv length, were measured by anemometer sonic (see Table 1). The scalar dissipation rate profile is based on the hypothesis that viscous dissipation balances shear production and buoyancy. The profiles of  $k$ ,  $\varepsilon$  and the turbulent viscosity,  $K_m$  are specified as follows:

$$k(z) = \frac{u_*^2}{\sqrt{C_\mu}} \sqrt{1 - \frac{z}{L}} \quad \varepsilon(z) = \frac{u_*^3}{\kappa} \left(1 - \frac{16z}{L}\right)^{-1/4} \left(1 - \frac{z}{L}\right) \quad K_m(z) = C_\mu \frac{k^2(z)}{\varepsilon(z)} \quad (1)$$

#### LES

When using LES, defining a representative turbulent flow field as inflow boundary condition is required. This flow should satisfy prescribed spatial correlations and turbulence characteristics. The method used here is the synthetic eddy method (SEM) (Jarrin and al, 2014). The SEM approach involves the generation and superposition of a large number of random eddies, with some control on their statistical properties and using the following predefined shape function for the velocity fluctuation:

$$u'(x) = \frac{1}{\sqrt{N}} \sum_{k=1}^N a_{ij} \varepsilon_j^k f_\sigma(x - x^k) \quad (2)$$

These eddies are then transported through a 800 m long rectangular cross-section domain. The resultant, time-dependent, flow field taken from a cross-section of this domain can be extracted and imposed as an inlet condition for LES. This method allows the desired Reynolds stress field to be prescribed. Inflow boundaries for synthetic method available in FDS consists of data given by following experimental results:  $U_{\text{mean}}$  mean velocity,  $\text{RMS}_x$  Root Mean Square velocity in x-direction matching with mean wind direction,  $L_x$  integral scale in x-direction. Inflow mean velocity profile follows an exponential law. Integral length scale may be defined by assuming the advection of turbulent structures by the averaged wind such as:  $L_x = U_{\text{mean}} T_x$  with  $T_x$  : observed integral time scale in x-direction. The atmospheric data used as inflow boundary conditions for LES approach are presented in Table 2.

**Table 2.** Atmospheric input data for LES approach

<b>Anemometer altitude (m)</b>	<b>Mean velocity <math>U_{\text{mean}}</math> (m/s)</b>	<b>Integral time scale <math>T_x</math> (s)</b>	<b>Integral length scale <math>L_x</math> (m)</b>	<b><math>\text{RMS}_x</math></b>
1.5	2.59	12	31.0	0.72
4	2.94	14	41.1	0.68
7	3.18	20	63.6	0.64
10	3.24	-	-	0.9

RMS velocity fluctuation set up at inlet is isotropic. In other words, diagonal components of the Reynolds stress are identical and all others are set to 0. The outlet is a free outflow condition. The lateral boundaries are symmetry condition. No temperature profile is set up at the inlet.

The Table 3 summarizes the data used as inflow boundary condition for the three approaches.

**Table 3.** Harmonized input data for the SLAB model, RANS and LES approach

Code	Dispersion model	Common input flow Data	Specific input flow data	Source term modelling
SLAB	Shallow layer		Pasquill Stability class	Orifice release conditions: NH <sub>3</sub> Mass flow rate of 4.2 kg/s, 0.6 liquid fraction
<i>Code_Saturne</i>	RANS	Mean velocity profile Ground roughness of 0.03 m	Turbulent kinetic energy and dissipation and temperature profile (not shown) based on experimental friction velocity, LMO and heat flux	Equivalent gas source term located at 6m from orifice NH <sub>3</sub> mass flow rate of 4.2 kg/s Total mass flow rate of 37.5 kg/s Surface area of 1 m <sup>2</sup>
FDS	LES		Isotropic integral time, length scale and RMS <sub>x</sub> based on experimental data	

**SOURCE TERM**

FDS and *Code\_Saturne* cannot directly deal with high speed multi-phase releases. Then in order to bypass this limitation, an equivalent source term (see Table 3) was implemented at a distance from orifice, thus leading to moderate velocity and a weak liquid fraction which can be readily handled by CFD codes (see Lacome and al., 2014).

**MESH**

The modelling area used is 1300 m x 600 m x 60 m in the x, y and z directions, respectively for RANS and 800 m x 400 m x 40 m for LES. The computational grid consists of approximately 1.2 million of hexahedral volume elements for RANS (expanded grid with an expansion ratio lower than 1.2) and 6.5 hexahedral volume elements for LES. The minimal space length is 0.5 m corresponding to cells located close to the ground, it allows implementing the source term with 4 cells.

**FLOW ANALYSIS FOR DIFFERENT APPROACHES**

The first step in the whole simulation task consists in checking whether the wind flow is correctly modelled or not in order to demonstrate that a homogeneous ABL is obtained along the whole domain. For the RANS approach, the results show that the ABL profiles are well sustained, except for the turbulent kinetic energy which decreases downwind from the inlet. Difficulties faced of in the present atmospheric condition (slightly unstable) were expected and this issue is addressed by previous works (Gorlé, 2009; Batt *et al.* 2016). However, it turns out that turbulent viscosity profile (see Figure 1) are eventually quite well sustained along the domain close to the ground (z < 5 m). Consequently, it is assumed that the difference between ABL profiles at inlet and at outlet generates a weak impact on dispersion predictions. Moreover, the theoretical profile used to build the input turbulence slightly overestimates the value measured by sonic anemometer at 10 m height (see Figure 1) such the level of turbulence modelled by *Code\_Saturne* could be deemed close to the one observed during the test.

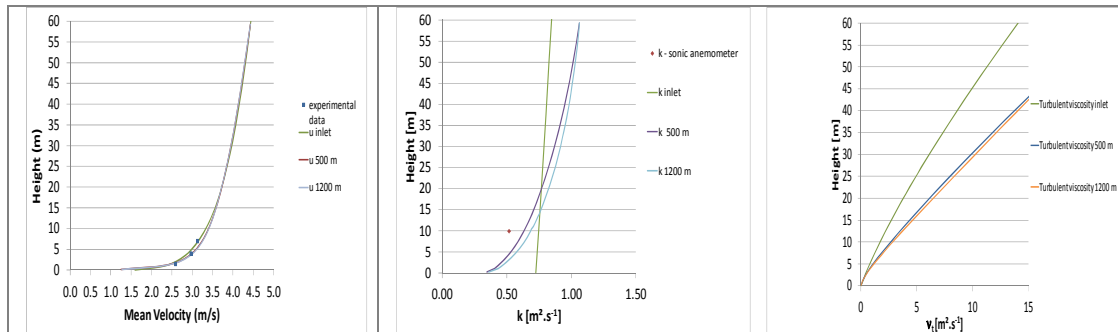


**Figure 1.** Predicted results for the flow ABL profiles at the inlet (x=-100m), centre and outlet of the domain with RANS CFD code

In Figure 2 flow characteristics obtained with LES approach at different x-positions are compared against inflow conditions and experimental data.

Mean velocity is well maintained in the domain. However, turbulence decreases rapidly in the first part of the domain but RMS profiles are sustained in a steady way. This turbulence decrease was expected (Hanna, 2002) and explained the underestimation of friction velocity when compared to experimental data. A foreseeable solution would consist in stabilizing the flow as a preliminary step in a given domain.

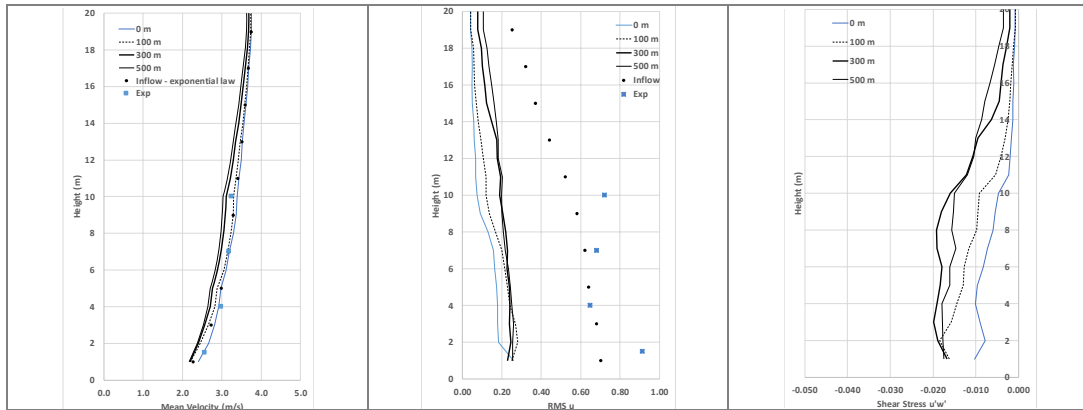


Figure 2. Flow characteristics against inflow conditions ( $x=-100m$ ) and experimental data - LES approach

### ANALYSIS OF THE ATMOSPHERIC DISPERSION RESULTS

Figure 3 and Figure 4 shows comparison between experimental and predicted mean concentrations obtained with the three codes.

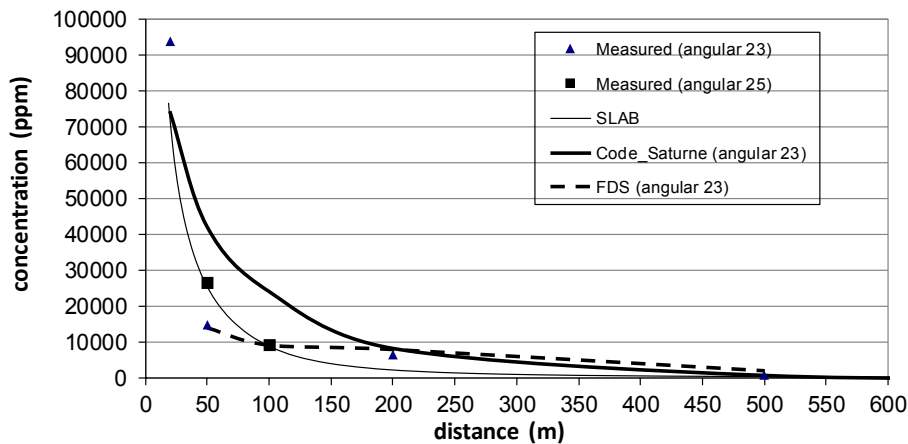
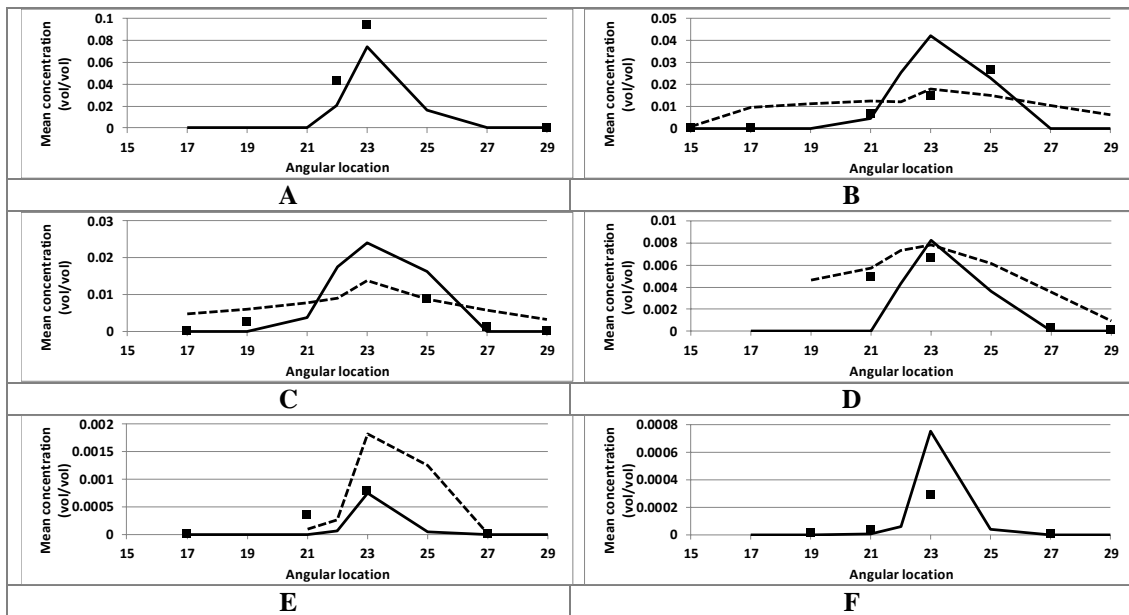


Figure 3: Comparison between simulation results and experimental concentration data along the axis (angular 23 and 25) downwind of the source which are closest to the mean direction of the wind

It can be noticed that numerical results are in good agreement with sensor measurements, although meandering effect has not been taken into account. Previous work (Lacome, 2014) has considered this effect. For RANS and LES approach these results are promising regarding the complexity to describe both the release in the near field and the far field. However, the model slightly over-predicts the measurements respectively in the near field ( $50 m < x < 200 m$ ) for the RANS model and in the far-field ( $x > 200 m$ ) for the LES model. An explanation could be the insufficient level of mixing due to the atmospheric flow. Indeed, previous studies (Demaël, E. and B. Carissimo, 2008; Hanna, 2002) demonstrated this possible  $k-\epsilon$  and LES turbulence model's weakness. Bearing in mind the use of an optimum source term, it can be noticed the good accordance between the concentrations decrease, along the lean wind axis, modelled by SLAB and the observations.



**Figure 4.** Comparison between simulation results (FDS: dotted line; *Code\_Saturne* : continuous line) and experimental concentration for each arc (A=20 m, B=50m, C=100m, D=200m, E=500m, F=800m) of receptors.

## CONCLUSION

Several dispersion models of different nature (shallow-layer, RANS, LES) have been used to model a large scale experimental ammonia release. Based on experimental observations analysis, flow input data and source term of different level of complexity have been set up for each approach. While LES code (FDS) need the most advanced input analysis, mean velocity and ground roughness form the common input parameter to the three approaches. The same equivalent gas source term located has been set for LES and RANS approaches in order to harmonize practices. Expected difficulties to maintain the turbulence level along the flat domain have been encountered for CFD approaches. Taking into account the inherent complexity to model and simulate the atmospheric turbulence, predicted concentration is in good agreement with experimental data for both RANS and LES approach.

## ACKNOWLEDGEMENTS

Authors would like to thank the French Ministry of Environment which financially supports this project.

## REFERENCES

- Barratt, R., 2001: Atmospheric Dispersion Modelling: A Practical Introduction. (Business & Environmental Practitioner).
- Batt, R. S.E. Gant, J.-M. Lacombe and B. Truchot, 2016: Modelling of stably-stratified atmospheric boundary layers with commercial CFD software for use in risk assessment, 15<sup>th</sup> International Symposium on Loss Prevention and Safety Promotion in the Process Industries, Freiburg, Germany, 5-8 June 2016.
- Bouet R., Duplantier S. and Salvi O., 2005: "Ammonia large scale atmospheric dispersion experiments in industrial configurations", *Journal of Loss Prevention in the Process Industries*, **18**, 512-519.
- Demael, E., and B. Carissimo. "Comparative Evaluation of an Eulerian CFD and Gaussian Plume Models Based on Prairie Grass Dispersion Experiment." *Journal of Applied Meteorology and Climatology* **47**, (2008): 888–900.
- Detering, H. and Etling, D. (1985). Application of the turbulence model to the atmospheric boundary layer. *Boundary-Layer Meteorology*, **33**:113–133.
- Duynkerke, P. (1988). Application of the k-ε turbulence closure model to the neutral and stable atmospheric boundary layer. *Journal of the Atmospheric Sciences*, **45**, 865–880.
- D.L. Ermak, Users Manual for SLAB: An Atmospheric Dispersion Model for Denser-than-Air Releases, UCRL-MA-105607, Lawrence Livermore Nat Lab, Livermore, CA, 1990.

- Gorlé, C., J. van Beeck, P. Rambaud, and G. Van Tendeloo. “CFD Modelling of Small Particle Dispersion: The Influence of the Turbulence Kinetic Energy in the Atmospheric Boundary Layer.” *Atmospheric Environment* **43**, (2009): 673–81.
- Hanna, S. R., S. Tehranian, B. Carissimo, R. W. Macdonald, and R. Lohner. “Comparisons of Model Simulations with Observations of Mean Flow and Turbulence within Simple Obstacle Arrays.” *Atmospheric Environment* **36**, (2002): 5067–79.
- Hanna, Steven, Seshu Dharmavaram, John Zhang, Ian Sykes, Henk Witlox, Shah Khajehnajafi, and Kay Koslan. “Comparison of Six Widely-Used Dense Gas Dispersion Models for Three Recent Chlorine Railcar Accidents.” *Process Safety Progress* **27**, (September 2008): 248–59. doi:10.1002/prs.10257.
- Jarrin, N., Synthetic Inflow Boundary Conditions for the Numerical Simulation of Turbulence, PhD Thesis (2008).
- Lacome J.M., Truchot B.. « Harmonisation of practices for atmospheric dispersion modelling within the framework of risk assessment » 15th International Conference on Harmonisation within Atmospheric Dispersion Modelling for Regulatory Purposes (HARMO 15), Madrid (Espagne).
- Lacome J.M., Leroy G., Truchot B., Joubert L., Wei X, Dupont E., Gilbert E., Bertrand Carissimo. Large-eddy simulation of wind flows and comparisons with very-near field campaign data. 16th International Conference on Harmonisation within Atmospheric Dispersion Modelling for Regulatory Purposes (HARMO 16), Varna (Bulgarie), 2014.
- McGrattan, K. B. (2005). Fire Dynamics Simulator (Version 4). Technical Reference Guide NIST Special Publication 1018.
- Milliez, Maya, and Bertrand Carissimo. “Numerical Simulations of Pollutant Dispersion in an Idealized Urban Area, for Different Meteorological Conditions.” *Boundary-Layer Meteorology* **122**, (January 29, 2007): 321–42. doi:10.1007/s10546-006-9110-4.
- Van Ulden, A.P., 1974: On the spreading of heavy gas released near the ground. Proceedings Int. Loss Prevention Symp., pp 221-226, C.H. Buschman ed., Elsevier, Amsterdam.
- Xiao Wei. Experimental and numerical study of atmospheric turbulence and dispersion in stable conditions and in near field at a complex site. , PhD Thesis. 2016.

**17th International Conference on  
Harmonisation within Atmospheric Dispersion Modelling for Regulatory Purposes  
9-12 May 2016, Budapest, Hungary**

---

**A SENSITIVITY ANALYSIS FOR A LAGRANGIAN PARTICLE DISPERSION MODEL IN  
EMERGENCY-RESPONSE TEST CASES**

*Gianni Tinarelli<sup>1</sup>, Maxime Nibart<sup>2</sup>, Patrick Armand<sup>3</sup>, Silvia Trini Castelli<sup>4</sup>*

<sup>1</sup>Arianet Srl, Milano, Italy

<sup>2</sup>ARIA Technologies, Paris, France

<sup>3</sup>CEA, DAM, DIF, F-91297 Arpajon, France

<sup>4</sup>Institute of Atmospheric Sciences and Climate ISAC – CNR, Torino, Italy

**Abstract:** Different setups of the modelling system MSS (MicroSwiftSpray) have been tested and analysed in application to flow and dispersion in built environments. Case studies from the COST Action ES1006 have been considered, with the aim of assessing the modelling tools in the emergency response context. Examples from the sensitivity analysis are here proposed, to evaluate the effects of different configurations of the models and different initial conditions.

**Key words:** *flow and dispersion modelling, built environment, emergency response.*

## **INTRODUCTION**

In the frame of the modelling exercises carried out in COST Action ES1006 (Baumann-Stanzer et al., 2015), considering accidental releases in urban environments, a sensitivity analysis was performed for MicroSpray Lagrangian particle model (Tinarelli et al., 2007 and 2012). Different groups have been using the same model but applied in different configurations. MicroSpray model is integrated with the mass consistent diagnostic flow model MicroSwift in a modelling system, and it was run (1) in a standalone configuration, named as MSS, (2) in the parallel version for a standalone configuration, named PMSS, and (3) in its version inserted in a modelling suite providing advanced GIS-embedded software for modelling air quality in cities, named ARIA City.

The simulations were run in a standard setup and here we show results related to releases for the Michelstadt and CUTE test cases, where flow and dispersion data were collected. In Michelstadt wind-tunnel test case, a typical European urban site is reproduced, designed to characterise the neighbourhood-scale urban areas across Europe. Several continuous and puff releases in different locations were reproduced and both non-blind and blind tests were performed. CUTE test case refers to a real-field campaign, then reproduced also in the wind tunnel, with continuous and puff releases in a European city with a harbour. CUTE exercise was run in a blind way.

## **THE MSS MODELLING SYSTEM**

MSS, and its parallel version PMSS, is a modelling system integrating the diagnostic mass-consistent model MicroSwift with MicroSpray Lagrangian particle dispersion model. MicroSwift interpolates the input wind profile on the simulation 3D domain through an objective analysis based on the mass conservation equation. In MSS the total turbulence is obtained summing the local one, produced by the flow distortion around the obstacles, plus a background level obtained by standard boundary-layer parameterizations. The local turbulence is estimated on the basis of a mixing-length closure, with the mixing length being a function of the distance to the obstacle or the ground. MicroSpray is able to take into account the presence of obstacles. The dispersion of an airborne pollutant is simulated following the motion of a large number of fictitious particles. The mean (“transport”) component of the particle velocity is provided by the meteorological driver. The stochastic (“turbulent”) component of the particle motion is obtained by solving a 3-D form of the Langevin equation for the random velocity.

## MICHELSTADT TEST CASE

The **Michelstadt** modelling exercise is based on data gathered in a flow and dispersion experiment performed in the atmospheric boundary layer wind tunnel at the Environmental Wind Tunnel Laboratory in Hamburg. The measurements were carried out in an idealized Central-European urban environment model. Five point sources were used non-simultaneously in continuous and short-term release mode, and two wind directions were investigated. For the modelling exercise, both non-blind and blind tests were performed.

Here we discuss the results obtained, when MSS model is applied by different users in different configurations: the Lagrangian particle model is integrated with the mass consistent diagnostic flow model in a modelling system, hereafter named as MC&L (CONF\_2). This system can be run in its parallel version (PMC&L hereafter), in a standalone configuration (CONF\_1) or in a modelling suite providing advanced GIS-embedded software for modelling air quality in cities (CONF\_3). In Table 1 we report the details of the model configurations as applied in three different setups. The simulations were run in a standard setup and here we show results related to the non-blind continuous release for different emission locations.

**Table 1.** Details on the configurations of the three different runs

	CONF_1	CONF_2	CONF_3
Model	PMC&L stand alone	MC&L standalone	PMC&L in modelling suite
Scale	Full		
Buildings	Shape file derived from dxf file available in COST ES1006 Action		
Wind velocity	Power law fitting experimental profile	Logarithmic law extrapolation below 9.9 m (with experimental friction velocity $u_*$ and roughness length $z_0=1.53$ m) Experimental profile above 9.9 m	MC automatic logarithmic extrapolation below 99.9 m using roughness length $z_0=1$ m  6 m/s at 99.9 m and power law above 99.9 m
Background turbulence	Fitted to experimental : Urms=1.2m/s, Vrms=1.2m/s, Wrms=0.86m/s	$z_0$ and $u_*$ imposed to fit experimental Urms and Vrms profile between <b>1m/s and 1.5m/s</b> , Wrms profile between <b>0.8m/s and 1.2m/s</b>	« Urban » landuse type in the modelling suite $z_0 = 1$ m. Leading to Urms and Vrms <b>~1m/s and Wrms~0.8m/s</b>
Horizontal resolution	1.5 m	2 m	3 m
Vertical grid	1 m below 27m, top = 200m; 40 points	1m below 12m, top=200m 21 points	2 m from the first level to the top=200m; 21 points
Emission time step	1 s	3 s	1 s
N particles/dt	1275	1000	100
Averaging period	2700s(+900s for steady state)	3600s (+1200s)	3600s(+1200s)
CPU time	15 minutes	1 hour	2 minutes
Hardware	8 cores (3.2GHz)	1 core Intel i7 2.67 Ghz	7 cores Intel Xeon 2.8 GHz

In Figure 1 the differences among the inlet wind speed profiles as used in the three setups can be appreciated and are compared to the experimental data. In Figure 2 the contours of concentration data are plotted for the three setups. In general, the agreement with the observed values (squares) is fair for all cases. We notice that downwind the source, the area with highest concentrations inside the longitudinal and diagonal canyons extends further for CONF\_1 simulations than for the others. The tracer distribution

is generally well captured in the longitudinal canyon, while in the diagonal one the predicted concentrations are higher than the observed. The area with medium concentration values has a larger downwind extension for CONF\_2 and CONF\_3, thus far from the source, in the cross section at street-level, the concentrations are lower for CONF\_1 than for CONF\_2 and CONF\_3. We note that in CONF\_1 a very fine vertical meshing is used, allowing to better detail the flow inside and at the top of the canopy level, at the same time detecting larger vertical wind velocity gradients. The vertical transfer at the top level may become strong and, consequently, part of the tracer is trapped in the street canyons near the source while another part is pushed above the buildings by a quick airflow. The vertical mesh of CONF\_2 has the same resolution but for shallower layer, while CONF\_3 vertical mesh is coarser. Thus the vertical velocity gradients are smoother and lead to a weaker transfer from the canopy towards the inertial atmospheric sublayer above it. The area of smallest concentration values is more extended for CONF\_1 at the boundary of the plume - this might be linked to the higher number of particles used in CONF\_1 run, increasing the statistics of the particle dispersion. In Figure 3 we compare the concentrations predicted with the three different setups for three continuous releases, named as S2, S4 and S5, through scatter plots. A larger spread occurs between CONF\_1 and CONF\_2, especially in case of S4 source, while the agreement looks slightly better in the other cases.

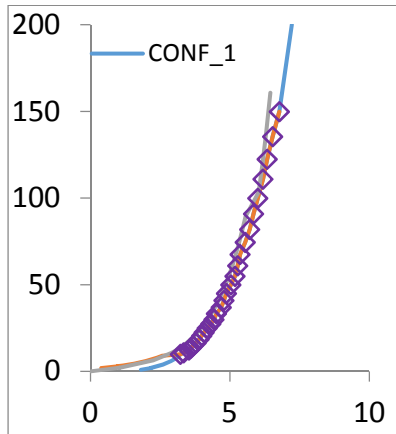


**Figure 1.** Michelstadt case. Inlet wind speed profile as used in the three different configurations (solid lines, blue for ‘CONF\_1’, dark red for ‘CONF\_2’ and green for ‘CONF\_3’) and experimental data (diamonds).

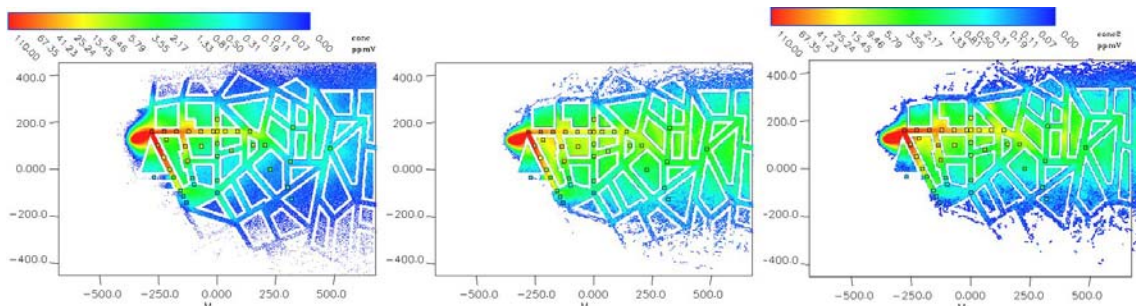


**Figure 2.** Concentration contours in the simulation domain for CONF\_1, CONF\_2 and CONF\_3 (from left to right) The coloured squares represent the observations in the same colour scale as for the simulations.

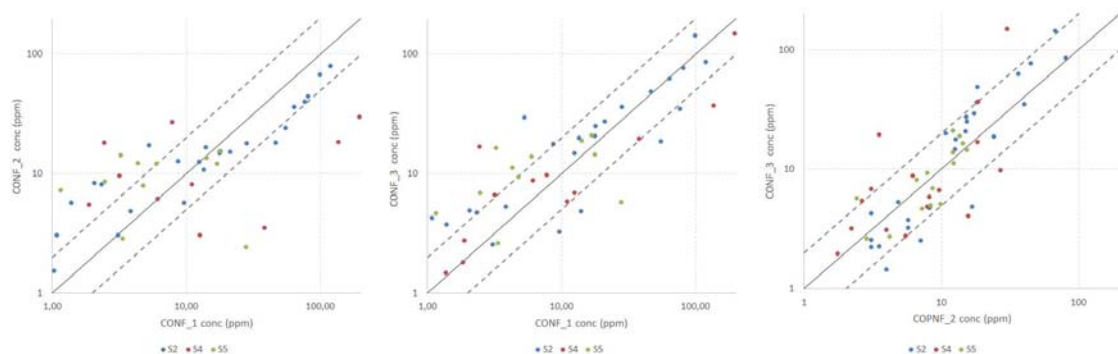


**Figure 3.** Scatter plots (logarithmic scale) of the different setups predicted concentration values at the measuring locations for the release at sources S2 (blue points), S4 (red points) and S5 (green points)

### CUTE TEST CASE

In CUTE test case data from both a field experiment in a real city and its reproduction in the EWTL wind tunnel were gathered. Continuous and puff releases from a boat towards a harbour area were carried out. Concentrations were detected by 20 measurement stations located at different positions in the field experiment, while more than 30 recording stations were used in the wind tunnel.

For CUTE case a sensitivity analysis on the initial conditions is proposed to address the problem of their uncertainty, which is particularly high in case of accidental release and which may strongly influences the model results. Test simulations were run for both the field and wind tunnel experiments, continuous release, in neutral conditions. Alternative wind velocity and turbulence input settings were considered to verify the variability of model outputs to different driving meteorological data. For the wind, two different simulations were run, in the first one (W#1) a vertical wind profile was calculated starting from the only measurement at 175m provided to all modellers in COSTES1006 Action exercise, keeping the direction homogenous in vertical. In the second one (W#2) all data available at the weather mast were used to build a wind profile having directions that vary in the vertical following the available measurements. In Figure 4 the effect of the different wind direction in input is clear, the plume deviates in slightly different directions and the affected areas are thus different, having an impact on the possible response. The performance of the run W#2 were found to be better than for W#1 initialization.

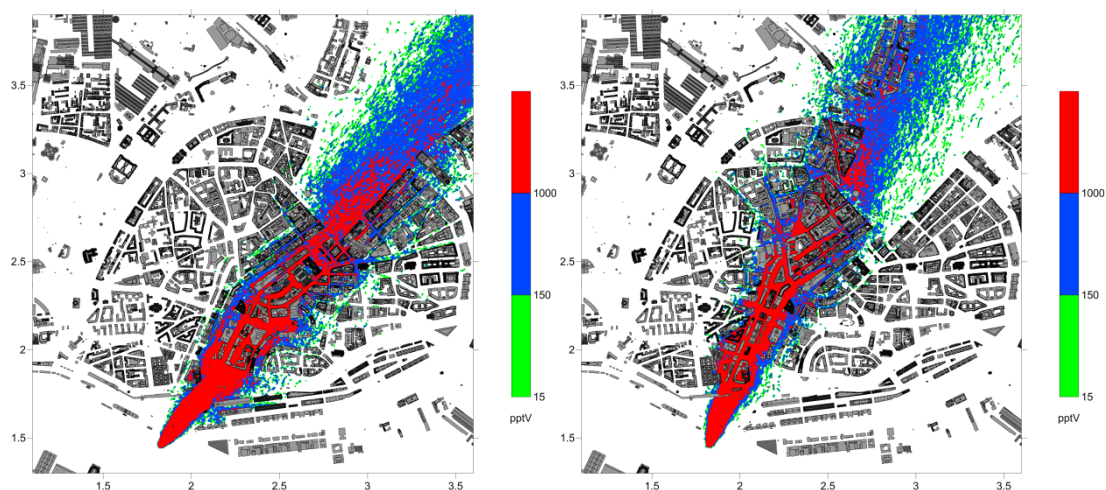


**Figure 4.** CUTE case, field experiment. Comparison of concentration field with two wind inlet profiles, W#1 on the left and W#2 on the right.

The turbulence input was estimated with an analytical formulation, for neutral atmosphere using two roughness values, so that T#1 corresponds to a stronger turbulence than the one determined in T#2:

T#1:  $z_0=1\text{m}$ ; in the field case  $u_*=1.31\text{m/s}$  ;  $\text{TKE}(z=10\text{m})=6.4\text{m}^2/\text{s}^2$ ; in the wind tunnel case  $u_*=1.26\text{m/s}$  and  $\text{TKE}(z=10\text{m})=5.9\text{m}^2/\text{s}^2$

T#2:  $z_0=0.1\text{m}$ ; in the field case  $u_*=0.33\text{m/s}$  ;  $\text{TKE}(z=10\text{m})=0.4\text{m}^2/\text{s}^2$ ; in the wind tunnel case  $u_*=0.31\text{m/s}$ ;  $\text{TKE}(z=10\text{m})=0.39\text{m}^2/\text{s}^2$

The resulting concentrations fields, plotted in Figure 5 for the field experiment, highlight the impact of the different turbulence, where a stronger turbulence spreads and dilutes more the plume so that the zones with high concentration extend less far downwind the source.

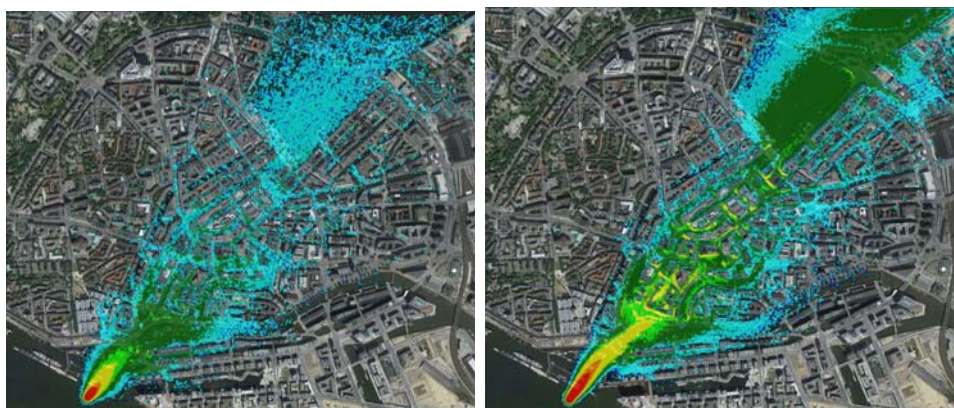


**Figure 5.** CUTE case, field experiment. Comparison of concentration field with two turbulence inlet profiles, T#1 on the left, T#2 on the right.

## CONCLUSIONS

The sensitivity tests allowed confirming the robustness of the dispersion model, since even in different configurations, with different input conditions and turbulence parameterizations, and using it in different modelling systems or suites, the quality of the results is comparable and the simulations provide reliable outputs. The analysis also highlighted that, besides the physical quantities, there are key quantities handled by the users that can help improving the performances, such as the number of particles and the horizontal and vertical grid resolution. We notice that the possibility to run the model in a parallel configuration allows largely reducing the computational time, which however keeps being small also when using the model on a single CPU.

The sensitivity test on the initial conditions proved the importance of having appropriate local measurements, possibly characterizing also the vertical variability, to achieve more reliable simulations of an accidental release. While in general it is not easy to have such kind of observed data available, in case of known sensitive sites, where for instance industrial plants are located, a proper planning of the net of sensors becomes fundamental to support emergency response tools.

## REFERENCES

- Baumann-Stanzer K., B. Leidl, S. Trini Castelli, C. M. Milliez, E. Berbekar, A. Rakai, V. Fuka, A. Hellsten, A. Petrov, G. Efthimiou, S. Andronopoulos, G. Tinarelli, R. Tavares, P. Armand, C. Gariazzo, all COST ES1006 Members, 2014. Evaluation of local-scale models for accidental releases in built Environments – results of the “Michelstadt exercise” in COST Action ES1006. Proceedings of the 16th Conference on Harmonisation within Atmospheric Dispersion Modelling for Regulatory Purposes, 699-703.

- Baumann-Stanzer, S. Trini-Castelli, S. Stenzel (Eds), 2015. COST ES1006 Model evaluation case studies: Approach and results. Publisher: University of Hamburg, ISBN: 987-3-9817334-2-6
- Tinarelli G., Mortarini L., Trini Castelli S., Carlino G., Moussafir J., Olry C., Armand P. and Anfossi D., 2012. Review and Validation of MicroSpray, a Lagrangian Particle Model of Turbulent. In: Dispersion Lagrangian Modeling of the Atmosphere, AGU Geophysical Monograph, Lin J.C., D. Brunner, C. Gerbig, A. Stohl, A. Luhar, and P. Webley Eds., vol. 200, 311-327. ISBN: 978-0-87590-490-0;
- Tinarelli G., Brusasca G., Oldrini O., Moussafir J., Anfossi D., Trini Castelli S., 2007. Micro Swift-Spray (MSS), a new modelling system for the simulation of dispersion at microscale. Air Pollution Modelling and its Applications XVII, Borrego C. and Norman A.L. Eds., Springer Publishers, 449-458. ISBN: 978-0-387-28255-8

## **TOPIC 9**

# **MATHEMATICAL PROBLEMS IN AIR QUALITY MODELLING**

**17th International Conference on  
Harmonisation within Atmospheric Dispersion Modelling for Regulatory Purposes  
9-12 May 2016, Budapest, Hungary**

---

**ANALYSIS OF SIMULATION RESULTS ISSUED BY A LATTICE BOLTZMANN METHOD  
IN COMPLEX URBAN ENVIRONMENTS – APPLICATIONS TO PARIS AND HAMBURG**

*Fabrice Boisseranc<sup>1</sup>, Patrick Armand<sup>2</sup>, Christophe Duchenne<sup>2</sup>, and Guillaume Douarre<sup>1</sup>*

<sup>1</sup>Exa Corporation, Le Madeleine, 76 Route de la Demi-Lune, 92057 Paris La Défense, France

<sup>2</sup>CEA, DAM, DIF, F-91297 Arpajon, France

**Abstract:** This paper presents the summary of a 3D numerical simulation in an urban environment. The city centre of Hamburg has been chosen to realize this simulation, and a Lattice-Boltzmann CFD solver is used to compute both the flow field of the wind, as well as the plume propagation in the street network after the release of a tracer in the air.

**Key words:** *CFD, Lattice-Boltzmann, simulation, flow, passive scalar, urban environment, concentration.*

## **INTRODUCTION**

In general, advanced flow simulations in built-up (urban or industrial) environment are carried out using “conventional” CFD codes, most of them based on RANS solvers (Reynolds-Averaged Navier-Stokes) or LES solvers (Large Eddy Simulation). Alternative methods presented in the companion paper Duchenne *et al.* (2016) are less time consuming as they rely on a simplified 3D diagnostic or RANS flow modelling coupled to a Lagrangian Particle Dispersion Model (LPDM).

This study is dedicated to the presentation of an approach that is still not much used in the environmental CFD. It is based on a Lattice-Boltzmann solver for modelling of both the fluid flow and the tracer (gas or fine particles) dispersion. This approach has several characteristics that significantly differ from classical CFD methods. One main difference is the unsteadiness of the Lattice-Boltzmann solver which notably enables to capture the transient behaviour of the flow, thus of the plume propagation. References to this method can be found in Chen *et al.* (2004), Chen *et al.* (2003), Chen *et al.* (1992) and Teixeira (1998).

The software used in this study is PowerFLOW which has been developed by Exa Corporation for twenty years. PowerFLOW is extensively used in the transportation industry, especially the automotive one. In the field of environment, some large scale simulations have been performed in the past (e.g. to study wind forces on buildings for architectural purposes), but they are not the core application of PowerFLOW.

Since March 2014, PowerFLOW has been equipped with a module adapted to the computation of passive scalar variables in the flow field. The dispersion of a tracer represented by a passive scalar is computed in parallel with the flow variables (pressure, velocity, etc.) using PDE (Partial Differential Equations). The passive scalars may be gases or fine aerosol particles associated to chemical pollutants, radionuclides or pathogenic agents, etc.

In the study, the Lattice-Boltzmann approach has been applied to a fictitious dispersion in two large urban simulation domains: “La Defense” business district located west of Paris), and Hamburg city centre. The present paper describes the case of Hamburg with some details while the case of “La Defense” will not be developed as the simulations are not completed at this point.

In the case of Hamburg, we discuss how the environmental conditions are taken into account, and how the simulation is set-up. Then, a physical analysis of the results is performed to help in understanding how the simulation can give some insights about the complex flow phenomenon in urban environments.

### PRESENTATION OF THE “HAMBURG CASE”

In the framework of the COST ES1006 Action, the CUTE trials (Complex Urban Terrain Experience) have been conducted for both reduced scale, in the Hamburg University wind tunnel, and real scale in Hamburg city centre. These experiments implied the release of tracer gases in the environment. Hereafter, we consider the continuous release conducted downtown Hamburg. The purpose of the numerical study is to model this trial using PowerFLOW Lattice-Boltzmann code with its passive scalar module.

#### Simulation set-up

The simulation takes into account the complex geometry (see Figure 1) of the buildings and of the terrain and land-use (ground elevation, river, etc.).

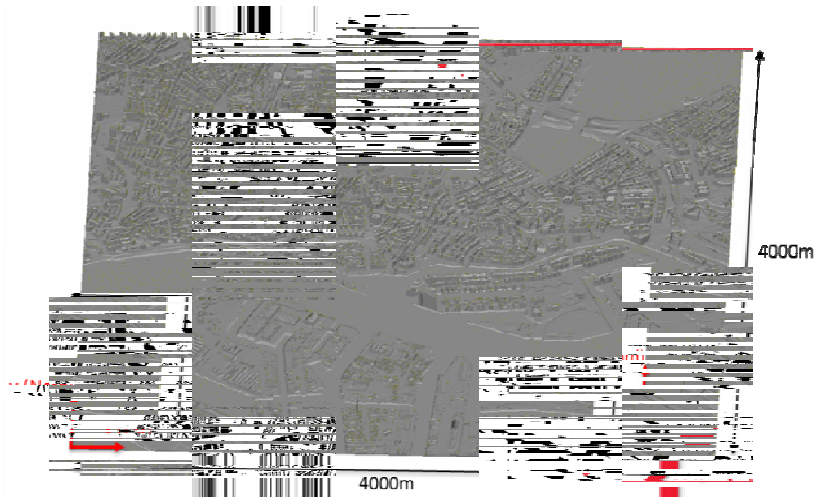


Figure 1. Geometry of Hamburg downtown.

During the whole experiment and simulation, the meteorological conditions are considered as constant. The direction of the wind is 219° (wind from south-west). The speed of the wind varies with the height above the ground to represent a typical atmospheric boundary layer profile. This wind profile has been recreated considering the velocity at 175 m (equal to 8.9 m.s<sup>-1</sup>) and a neutral atmosphere.

The gas source is located on a boat on the river (location is shown in Figure 2). It releases the tracer gas during 45 minutes at a constant mass rate of 2 g.s<sup>-1</sup>. The gas used in the experiment was SF<sub>6</sub> which has a diffusion coefficient  $D = 1.5 \cdot 10^{-5} \text{ m}^2.\text{s}^{-1}$ .

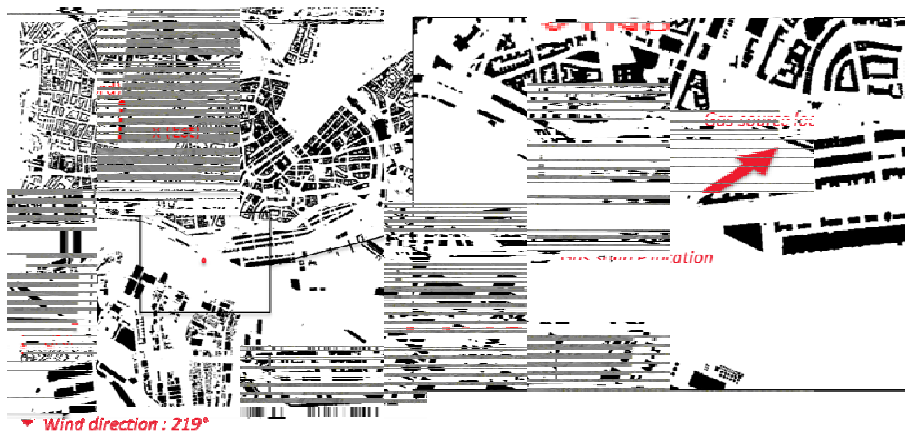


Figure 2. Wind direction and tracer gas source location.

Regarding the numerical resolution, the smallest fluid element size is 0.5 m close to the source of the gas. Except from the source area, the rest of the domain is meshed with a smallest cell size of 2 m. The size of the elements increases gradually away from the geometrical obstacles to optimize the computational cost while the boundary layers as well as the flow phenomena are correctly modelled. The largest cell size reaches 64 m far away from any building.

Concerning the computation duration, the flow field is simulated during 75 minutes, from  $t_0 - 15$  min to  $t_0 + 60$  min,  $t_0$  being the time at which the tracer starts to be released. The simulation is started 15 minutes before the tracer is released in order to reach a stabilized flow field.

### Simulation computational cost

The simulation completed in 23 hours using a total of 280 processors. It means that the CPU cost for such a simulation is 6,432 CPUh (hours multiplied by CPUs).

### RESULTS AND ANALYSIS OF THE “HAMBURG CASE”

Figure 3 shows the time-averaged velocity field using streamlines at 10 m above the ground level. Several areas can be distinguished (see the right side of Figure 3) and commented:

- As the city centre is densely built-up, the velocities in this area are low (blockage effect).
- Areas with no building or sparsely built-up have higher velocities (over the river and the lake).
- Some local accelerations of the wind (“Venturi effects”) are due to narrowing between buildings.
- “Wind corridors” are present around the city centre.

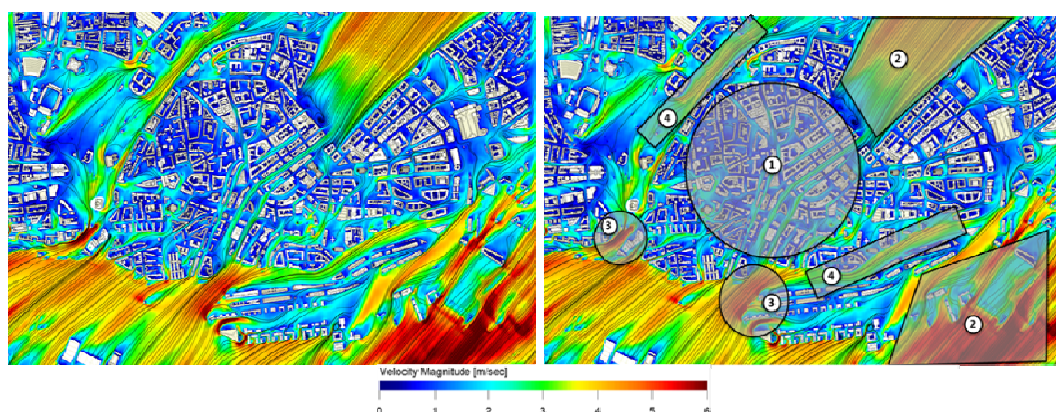


Figure 3. Time-averaged velocity at 10 m above the ground level.

Figure 4 shows the averaged concentration field (10 minutes average) presented at 2 m above the ground level with a logarithmic scale. This enables to visualize the propagation of the tracer along with the wind.

Figure 5 highlights an interesting local phenomenon that can be seen in Figure 4: On the east side of the source, the tracer gas is going upstream the flow field.

This phenomenon can be explained with the Figure 6. The left part of this figure shows the velocity field where a separation of the flow can be noticed. The right part of the figure illustrates the pressure in the same area (pressure difference with the reference level of the atmospheric pressure). The recirculation (1) creates a low pressure zone in the wake of the building (2) leading to an adverse pressure gradient (3). This adverse pressure gradient associated with low velocities brings the tracer in this area.

The iso-surfaces of the gas concentration are a useful post-processing method to help in defining the risk regions. As an example, Figure 7 shows the propagation of the plume in the domain during the first 20 minutes of the simulation (transient period). In this particular case, the iso-surfaces are drawn for  $C = 1 \text{ mg.m}^{-3}$ .

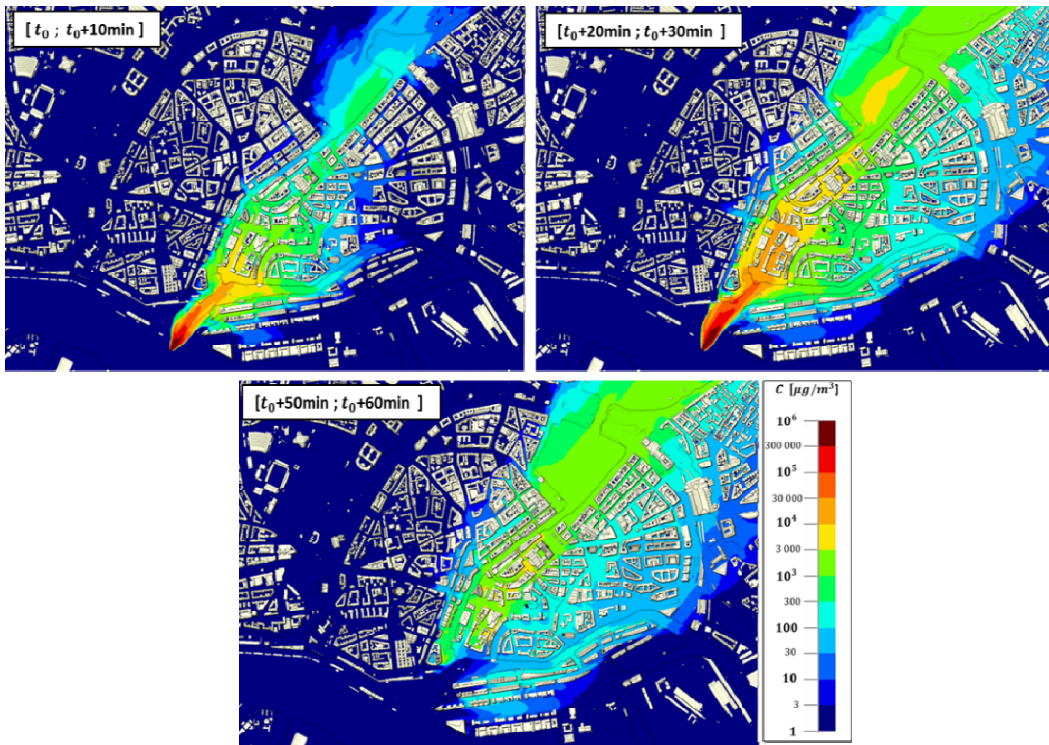


Figure 4. Time-averaged concentration field at 2 m above the ground level.

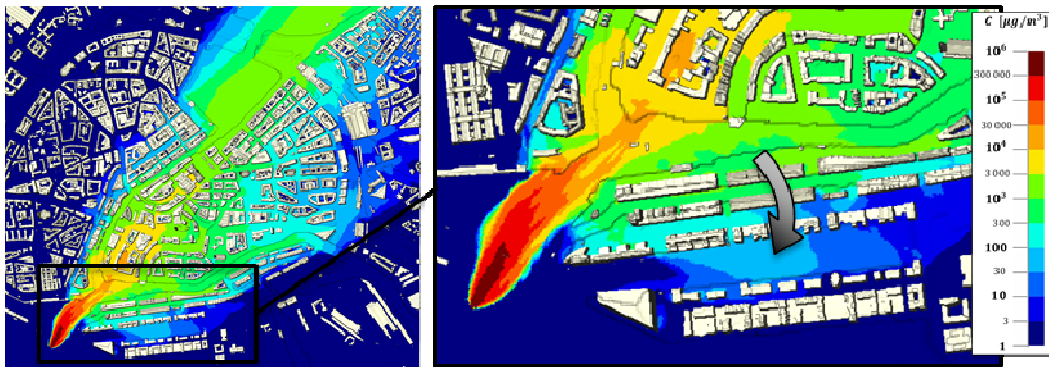


Figure 5. Direction of the plume propagation opposite to the main flow direction.

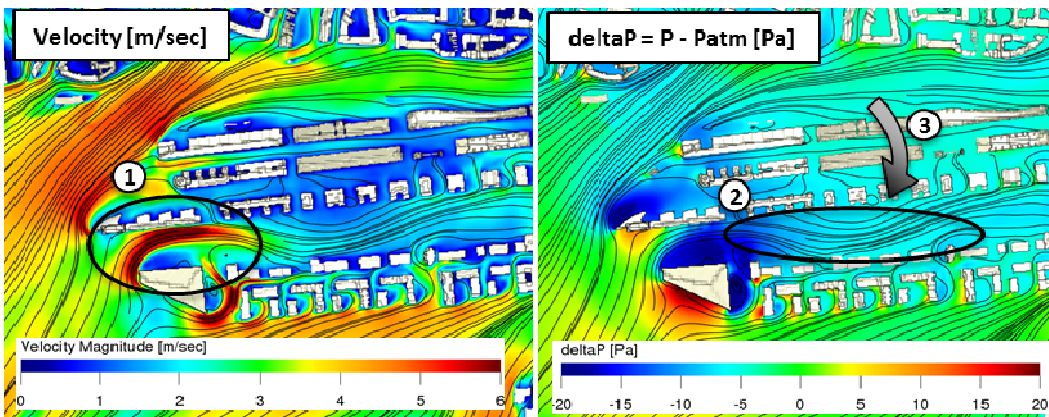
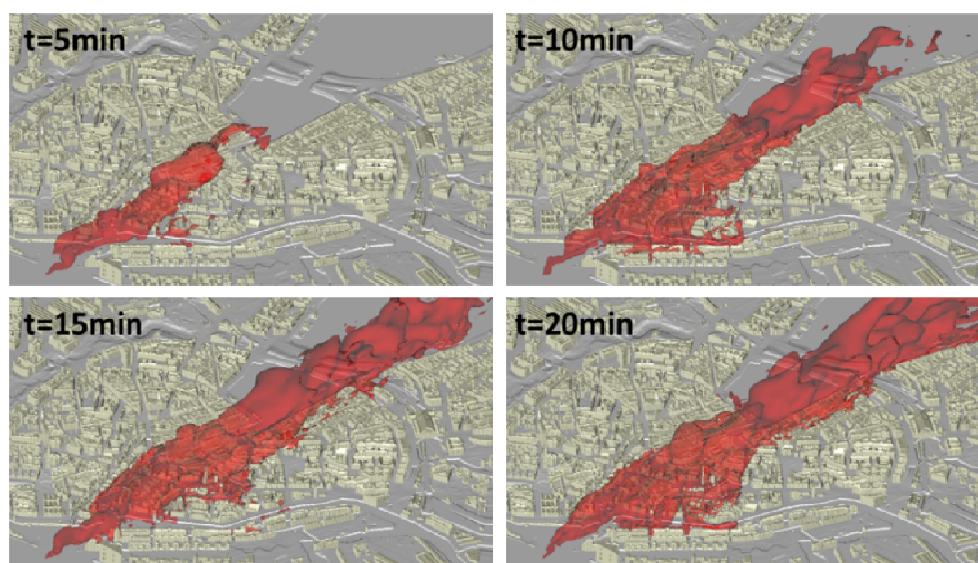


Figure 6. Velocity magnitude and relative pressure on the east side of the source.



**Figure 7.** Iso-surfaces corresponding to  $C = 1 \text{ mg.m}^{-3}$  during the transient period (first 20 minutes of the simulation).

## CONCLUSIONS

CFD simulations in complex urban environments can bring insights into the flow complexity and the associated dispersion phenomena, something that is a much more difficult to achieve either via a simpler modeling approach or an experimental approach. To illustrate this, the Lattice-Boltzmann simulation has identified a hazardous region on the east side of the source, even though this area is not located in the main flow direction.

To leverage the full benefits of the transient simulation, much more analysis and validation will have to be performed. In the near future, we will carry out a full transient analysis and determine the radiological / chemical doses considering diverse radionuclides / chemicals in order to assess the health consequences of accidental or malevolent scenarios.

In the Hamburg city example, a constant atmospheric boundary layer was used as an inlet condition. However, a natural extension of the Lattice-Boltzmann Method is to leverage the unsteady nature of the solver by applying more representative meteorological conditions, something that will be applied for the study of “La Defense”.

This study was performed on a relatively small cluster which allowed for a 24 hour turnaround time for a single simulation. As the solver has a good scalability, a larger cluster could be used in the case of an emergency to allow for a quick response. In addition, these simulations can be used for building databases or response surfaces to qualify in advance multiple scenarios that could be then interrogated in such an event.

## REFERENCES

- Duchenne, C., P. Armand, M. Nibart, and V. Hergault. Validation of a LPDM against the CUTE experiment of the COST ES1006 Action. Comparison of the results obtained with the diagnostic and RANS version of the model. Proceedings of the 17<sup>th</sup> Harmo Conference, May 9-12, 2016, Budapest, Hungary (to be published).
- Chen, H., S. Chen, W. H. Matthaeus. Recovery of the Navier–Stokes equations using a lattice-gas Boltzmann method. *Phys. Rev. A* 45, R5339, 1992.
- Chen, H., S. Kandasamy, S. Orszag, R. Shock, S. Succi, and V. Yakhot. Extended Boltzmann kinetic equation for turbulent flows. *Science*, **301**, 2003, 633–636.
- Chen, H., S. Orszag, I. Staroselsky, and S. Succi. Expanded analogy between Boltzmann kinetic theory of fluid and turbulence. *Journal of Fluid Mechanics*, **519**, 2004, 307–314.
- Teixeira, C. M. Incorporating turbulence models into the Lattice-Boltzmann Method. *International Journal of Modern Physics C*, **9**, 1998, 1159–1175.

**17th International Conference on  
Harmonisation within Atmospheric Dispersion Modelling for Regulatory Purposes  
9-12 May 2016, Budapest, Hungary**

---

**IMPROVEMENT OF ATMOSPHERIC DISPERSION SIMULATIONS IN CASE OF AN  
ACCIDENT OR A MALEVOLENT ACTION USING DATA ASSIMILATION METHODS IN  
CERES® CBRN-E**

*Robin Locatelli<sup>1</sup>, Vivien Mallet<sup>2</sup> and Patrick Armand<sup>3</sup>*

<sup>1</sup>Strathom Energie, Paris, France

<sup>2</sup>INRIA, Paris, France

<sup>3</sup>CEA DAM Ile-De-France, Bruyères-le-Chatel, France

**Abstract:** Developed at CEA since 2008, CERES® CBRN-E is a computational tool designed for crisis management in case of accidental, malevolent or terrorist releases of hazardous radiological, chemical or biological materials. CERES® CBRN-E computes atmospheric dispersion in complex environments including buildings (industrial sites or urban areas), assesses the health consequences of the toxic releases on the population and first responders, and delivers operational results to rescue teams and decision makers. This paper aims to present a recent development, which could be implemented in CERES® with the final goal to reduce discrepancies between modeled and measured concentrations. This development is based on data assimilation techniques (combination of a state estimation algorithm with an ensemble approach) in order to improve the atmospheric simulation of a dispersion model by incorporating different sources of information (observations, simulation results, error statistics). The results obtained in a synthetic experiment show that this method is very encouraging to derive surface concentrations consistent with observations. Indeed, mean concentration levels and strong spatial and temporal variations are well represented after optimization. Before implementing this approach into CERES® CBRN-E, the next step is to analyze the behavior in real cases.

**Key words:** *data assimilation, ensemble methods, atmospheric dispersion*

## **INTRODUCTION**

In the case of an accident or a malevolent action implying a release of gases or fines particles in the atmosphere, dispersion models are used to identify impacted areas with the final aim to protect population. However, discrepancies between modeled and measured concentrations may be large due to uncertainties in the representation of atmospheric transport, ignorance on the characteristics of the source term, errors related to measurement instruments, etc. Consequently, these different sources of uncertainties limit the trust in dispersion and impact assessment models for the decision-makers in an emergency. Thus, there is a strong interest in using all available information together (measurements, simulated concentrations, error statistics) in the course of the crisis in order to strongly reduce the uncertainties. Data assimilation methods are able to combine all these sources of information in order to improve the representation of atmospheric concentrations. Data assimilation is used operationally since the eighties in atmospheric sciences with objectives such as to improve the initial conditions of the operational meteorological forecasts, to identify uncertain parameters by inverse modelling, or to compute a field as close as possible to the “true” state of a dynamic system as it can be the case in air quality issues. In this study, we set up data assimilation techniques into the CERES® CBRN-E software, which is a fast-response modeling and decision-support tool, for improving simulations aiming to evaluate as accurately as possible the consequences of toxic dispersions and/or explosions.

Firstly, we detail the theory of data assimilation with a special focus on the algorithm implemented into this system for optimizing concentrations consistent both with observations and outputs from the PMSS model. The different characteristics of this method (definition of the *prior*, the observation operator, observational error covariance matrix, etc.) are detailed. Secondly, we expose the strategy set up in this study to evaluate the improvements and the drawbacks of the implementation of the data assimilation

techniques. Thirdly, we present the main results of a synthetic experiment. Finally, we give some indications for future works in order to apply this method in decision-support systems.

#### DATA ASSIMILATION METHOD

Data assimilation is a powerful tool which is used in different fields of geosciences (hydrology, seismology, weather forecasting...). Data assimilation refers to the process by which models and measurements are combined to produce an optimal representation of the state of the studied system. In atmospheric sciences, data assimilation techniques could be applied with different objectives: to produce an analysis, in other words to compute a field as close as possible to the “true” state; to improve the initial conditions in order to improve the forecasts; or to identify uncertain parameters, such as the emission fluxes. Here, we use data assimilation to improve atmospheric concentration simulations in order to bring valuable information for decision makers in emergency situations. There are many existing approaches to data assimilation: they include nudging methods, statistical methods, variational methods (e.g., 3-dimensional (3D-Var) and 4-dimensional variational (4D-Var)), and sequential methods (e.g., optimal interpolation and Kalman filters).

Here, we have chosen to compute the so-called best linear unbiased estimator (BLUE) in regard of the static nature of the model and the constraints related to the context of emergency situations. Indeed, the CERES® CBRN-E decision support tool has to deliver operational results (e.g., danger zones, intervention zones...) in less than 15 minutes to rescue teams and decision makers. Computing BLUE has several advantages: it does not require high computational resources and is yet efficient. It is also quite easy to implement. Consequently, this method presents several advantages in agreement with the constraints imposed by the management of crisis situations.

BLUE allows to find some best compromise between a set of observations and *prior* (or background) information on the system state. The observational data set is stored in the  $\mathbf{y}_o$  vector, and the state vector is represented by  $\mathbf{x}$ . The observation operator  $\mathbf{H}$  links the observation vector with the state vector:

$$\mathbf{y}_o = \mathbf{H}\mathbf{x}^t + \boldsymbol{\varepsilon}^o. \quad (1)$$

$\boldsymbol{\varepsilon}^o$  is called the “observational error” vector gathering all sources contributing to the gap between the observations and the representation of the “true” state,  $\mathbf{x}^t$ , in the observation space. In our case, the main contributor to observational errors is the instrumental error. A background (or *prior*) information is also taken into account in this method. It is represented by the vector  $\mathbf{x}^b$ ,

$$\mathbf{x}^b = \mathbf{x}^t + \boldsymbol{\varepsilon}^b. \quad (2)$$

We give a confidence level to this information through the  $\boldsymbol{\varepsilon}^b$  vector, which gathers the different errors contributing to a gap between the *prior* state and the “true” state of the system. Then, we define the *prior* errors and the observational errors covariance matrices,  $\mathbf{B}$  and  $\mathbf{R}$ , according to the equations (3).  $E[\ ]$  is the expectation operator.

$$\mathbf{B} = E[(\boldsymbol{\varepsilon}^b - E[\boldsymbol{\varepsilon}^b])(\boldsymbol{\varepsilon}^b - E[\boldsymbol{\varepsilon}^b])^t]; \quad \mathbf{R} = E[(\boldsymbol{\varepsilon}^o - E[\boldsymbol{\varepsilon}^o])(\boldsymbol{\varepsilon}^o - E[\boldsymbol{\varepsilon}^o])^t] \quad (3)$$

We are looking for the best linear unbiased estimator,  $\mathbf{x}^a$ . It is defined by:  $\mathbf{x}^a = \mathbf{x}^t + \boldsymbol{\varepsilon}^a$ , where  $\boldsymbol{\varepsilon}^a$  is the optimized state error. To find the best linear unbiased estimator, we make few assumptions. We assume that background and observational errors have zero mean:  $E[\boldsymbol{\varepsilon}^o] = 0$  and  $E[\boldsymbol{\varepsilon}^b] = 0$ . We also assume they are uncorrelated:  $E[\boldsymbol{\varepsilon}^b(\boldsymbol{\varepsilon}^o)^t] = 0$ . Then, we are looking for the expression of  $\mathbf{x}^a$ , whose the error  $\boldsymbol{\varepsilon}^a$  has zero mean and has a minimum total variance (i.e., the trace of the matrix  $E[\boldsymbol{\varepsilon}^a(\boldsymbol{\varepsilon}^a)^t]$  is minimal). Then,  $\mathbf{x}^a$  is given by:

$$\mathbf{x}^a = \mathbf{x}^b + \mathbf{B}\mathbf{H}^t(\mathbf{H}\mathbf{B}\mathbf{H}^t + \mathbf{R})^{-1}(\mathbf{y}_o - \mathbf{H}\mathbf{x}^b) \quad (4)$$

### MODELING OF THE ERROR COVARIANCE MATRICES

The observational error covariance matrix  $\mathbf{R}$  and the *prior* error covariance matrix  $\mathbf{B}$  are essential in data assimilation. Indeed, these matrices determine the respective weights given to each piece of information in the analysis. However, the correct specification of those statistics remains a major challenge in data assimilation systems. The structure of background error correlations is particularly important, as it determines how the observed information is filtered and propagated spatially.

The observational error covariance matrix is taken diagonal, hence assuming no correlation between the observational errors at two different monitoring stations. The expression of the observational error covariance matrix is therefore  $\mathbf{R} = \nu_o \mathbf{I}$ , where  $\nu_o$  is the observational error variance and  $\mathbf{I}$  is the identity matrix.  $\nu_o$  is mainly determined thanks to our knowledge on instrumental errors.

The definition of the  $\mathbf{B}$  matrix is more complex and more crucial for the optimization. Indeed, a good specification of the  $\mathbf{B}$  matrix is necessary to take correctly into account the spatial information brought by the model. For data assimilation at large scale, the *prior* error covariance is sometimes parameterized as a function of the geographical distance, e.g., with a decreasing exponential. At regional or local scales, the *prior* error covariances do not only depend on the distance, but also on different other parameters (distance to the source, wind speed, wind direction, turbulence...). Consequently, at regional or urban scales, it can be more complex to diagnose a satisfactory formulation for the  $\mathbf{B}$  matrix. We have tested three different analytical formulations based on the works of Balgovind et al. (1983), Frydendall et al. (2009) and some variants of these. The results found with these approaches are not detailed in this paper because they suffer from limitations. Moreover, the analytical formulations of the  $\mathbf{B}$  matrix are largely dependent on the configuration of the domain (size of the domain, localization of the source, wind direction...). Consequently, it does not seem reasonable in an emergency situation to take time for finding the best formulations for  $\mathbf{B}$ . We need to be able to quickly propose a correct configuration for the simulations of the gas dispersion. Consequently, it has been decided to use another way to define  $\mathbf{B}$ . Indeed, we can define  $\mathbf{B}$  by using a Monte Carlo approach: with an ensemble of  $N$  “perturbed” simulations, we are able to sample the *prior* error. From  $N$  different simulations based on different perturbations in the inputs, the elements of  $\mathbf{B}$  as

$$B(i, j) = \frac{1}{N-1} \sum_{k=1}^N (x_i^k - \bar{x}_i)(x_j^k - \bar{x}_j) \quad ; \quad \bar{x} = \frac{1}{N} \sum_{k=1}^N x^k \quad (6)$$

The  $N$  different simulations are created using different perturbations on the meteorological conditions, the characteristics of the gas source and the choice of numerical schemes for dispersion computations.

### SYNTHETIC EXPERIMENT

We analyze the capabilities of the system in a study case using synthetic observations. The domain size of the study is 17x35 kilometers with a regular grid-space of 100 meters (171x351 points). A total tracer amount of  $1.2 \times 10^5$  Becquerel is emitted during 1 hour. Outputs are available every 300 seconds (5 minutes). We describe on the Figure 1 the method used here to evaluate the assimilation results on the simulation of atmospheric concentrations in this specific case.



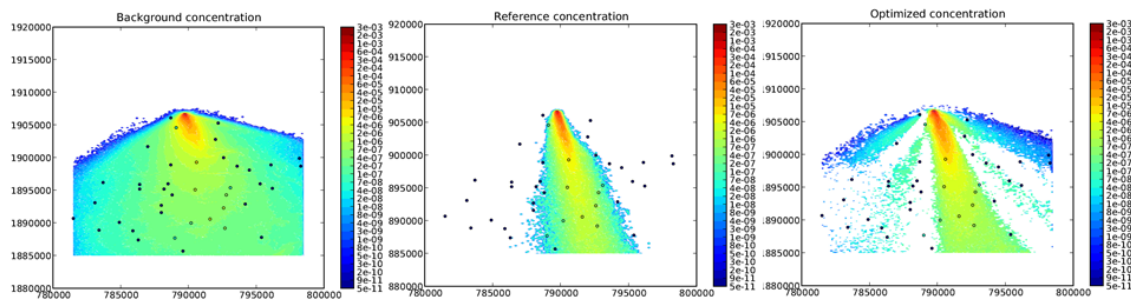


**Figure 2.** Spatial distribution of the *prior* (left), reference (middle) and optimized (right) concentrations (at the final time step) based on a configuration of the assimilation system using 60 members and 40 observation sites. The points represent the localization of the observation sites.

The *prior* concentration map (left plot of the Figure 2) is computed as the mean of the 60 concentration maps simulated by the 60 members of the ensemble. The aim is to reproduce the reference concentration map (center plot of the Figure 2) after the assimilation process. Here, we show that we are able to reproduce the main characteristics of the plume (shape, direction, size, etc.). Moreover, the magnitude of the optimized concentrations looks very similar to the reference concentrations. However, some low concentrations are located at the edges of the *prior* plume coming from an inadequate specification of the **B** matrix in these areas.

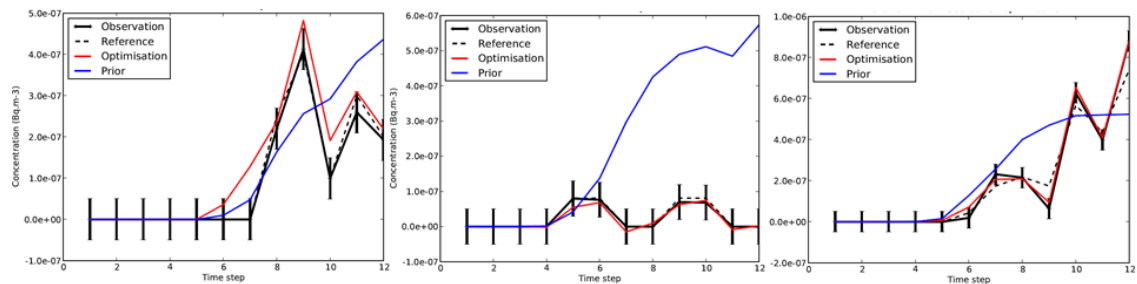


**Figure 3.** Time series of the *prior*, reference and optimized concentrations at three sites. The observations “measured” at these sites are used in the assimilation process, which explains the close proximity of the optimized concentrations. The observations have been created as a deviation from the reference simulation using a Gaussian distribution. The errors bars represent the observational errors.

On the Figure 3, it is found that the optimized concentrations (in red) fit very well the observations (in black with the errors bars). The system is able to reproduce the fast variations in the concentrations, while the *prior* was only able to reproduce the magnitude of the concentrations (left and right plots). Moreover, when the *prior* concentrations are very far from the observations, the system is also able to strongly move from the *prior* to derive optimized concentrations fitting the observations (center plot). These results are of course explained by the fact that these observations are assimilated.

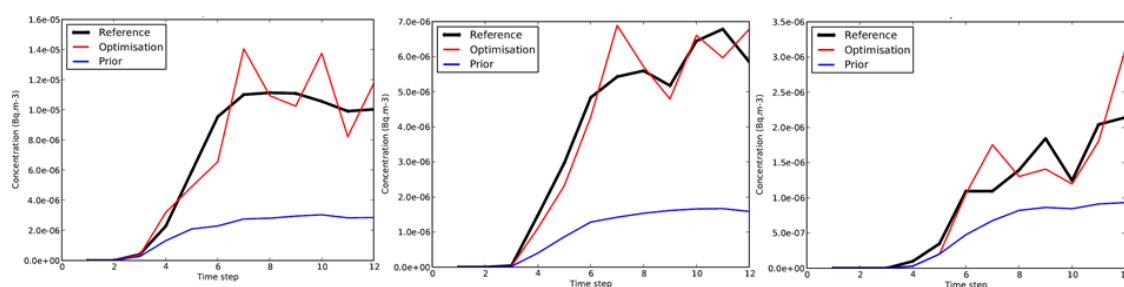


**Figure 4.** Time series of *prior*, reference and optimized concentrations at 3 different independent stations. *Independent* means here that observations used in the assimilation process are not coming from these independent stations.

Hence, these results only mean that the assimilation system works properly, but they do not give much information on the quality of the assimilation outside areas surrounding the observations. One way to evaluate the quality of the optimization is to compare the time series of optimized and reference concentrations at independent stations (which are not included in the assimilation process). The Figure 4 presents these time series at 3 different independent stations. We show here that the optimized concentrations perform much better than the *prior* concentrations at these stations, even if some variations are too strong in the optimized concentrations. Statistically, the scores confirm that the optimization works well in the areas far from the observations assimilated: the normalized bias, correlation and normalized root mean square error shift before and after optimization from -0.62 to 0.1, from 0.81 to 0.92 and from 1.9 to 0.3 respectively.

## CONCLUSION

In this paper, we present a data assimilation system based on the BLUE in order to improve the representation of atmospheric dispersion at regional or local scales in the CERES® CBRN-E system. The definition of the variance/covariance matrix  $\mathbf{B}$  is a fundamental point of this method: a good specification of this matrix is needed to spread the information given by the observations. Here, we compute the  $\mathbf{B}$  matrix by using an ensemble of simulations based on different perturbation of the inputs, what gives indications on the covariances of simulation errors.

The analysis of the system in the context of a synthetic experiment shows that the system developed here is able to correctly assimilate the synthetic observations in order to produce an optimized state close to the reference state. Indeed, the statistical scores of the optimized concentrations are much better than those obtained with the *prior* concentrations. Moreover, the temporal variations of the concentrations show that the system is able to reproduce the main characteristics contained in the observations. On-going and future work will apply this method to real cases and experimental cases in wind tunnels with more or less complex situations (considerations of buildings, complex topography, etc.).

## REFERENCES

- Balgovind, R., A. Dalcher, M. Ghil and E. Kalnay, 1983: A Stochastic-Dynamic Model for the Spatial Structure of Forecast Error Statistics, *Monthly Weather Review*, 111, 701-722.
- Frydendall, J., J. Brandt and J.H. Christensen, 2009: Implementation and testing of a simple data assimilation algorithm in the regional air pollution forecast model, DEOM. *Atmospheric Chemistry and Physics*, 9, 5475-5488.
- Tinarelli, B., S. Trini-Castelli, G. Carlino, J. Moussafir, C. Olry, P. Armand and D. Anfossi, 2013: Review and validation of Micro-SPRAY, a Lagrangian particle model of turbulent dispersion. *In Lagrangian Modeling of the Atmosphere*, Volume 200, AGU, doi: 10.1029/2012GM001242.

**17th International Conference on  
Harmonisation within Atmospheric Dispersion Modelling for Regulatory Purposes  
9-12 May 2016, Budapest, Hungary**

---

**EFFICIENT NUMERICAL METHODS IN AIR POLLUTION TRANSPORT MODELLING:  
OPERATOR SPLITTING AND RICHARDSON EXTRAPOLATION**

*Ágnes Havasi<sup>1</sup>, István Faragó<sup>1</sup> and Zahari Zlatev<sup>2</sup>*

<sup>1</sup>Department of Applied Analysis and Computational Mathematics, Eötvös Loránd University and  
MTA-ELTE Numerical Analysis and Large Networks Research Group, Budapest, Hungary

<sup>2</sup>Department of Environmental Science, Aarhus University, Roskilde, Denmark

**Abstract:** The mathematical modelling of air pollution processes is usually based on a system of nonlinear partial differential equations called transport-chemistry system. The numerical integration of this system is a rather difficult computational task, especially in large-scale and global models, where the number of grid-points can range from a few thousand to a few hundred thousand, and the number of chemical species is typically between 20 and 200. We present two robust techniques that can significantly enhance the efficiency of the numerical solution and the computer realization. During operator splitting the different sub-processes of the described phenomenon are treated separately, by coupling the corresponding mathematical problems through their initial conditions. Richardson extrapolation is based on a combination of two numerical solutions obtained by different discretization parameters. We present the basics of these methods and illustrate their benefits in different environmental models.

**Key words:** *Transport-chemistry system, Danish Eulerian Model, splitting methods, passive and active Richardson extrapolation*

## INTRODUCTION

The spatial and temporal changes of pollutant concentrations in the atmosphere are typically described by a system of nonlinear partial differential equations called transport-chemistry system. This system is rather complex in its original form, since the right-hand sides of the equations contain several terms with different mathematical properties. These terms describe advection, diffusion, deposition, chemical reactions and emissions in the general case. Due to the complicated structure and the large size, the solution of this system imposes a very challenging task for environmental modellers.

In this contribution we introduce the general form of the transport-chemistry system and outline the problems of its numerical solution. Then we present two approaches that – applied separately or together – can provide a sufficiently accurate numerical solution of the transport-chemistry system within reasonable computational time: operator splitting and Richardson extrapolation. The achievable efficiency is illustrated by numerical experiments.

## THE TRANSPORT-CHEMISTRY SYSTEM

In the centre of deterministic air pollution models one finds the system of partial differential equations

$$\frac{\partial c_i}{\partial t} = -\nabla(u c_i) + \nabla(K \nabla c_i) - \sigma_i c_i + R_i(c_1, \dots, c_m) + E_i(x, t), \quad i = 1, 2, \dots, m \quad (1)$$

called transport-chemistry system (Zlatev, 1995). Here  $m$  denotes the number of chemical species,  $c_i = c_i(x, t)$  denotes the concentration of the  $i$ -th species,  $u$  is the three-dimensional wind field,  $K$  is the turbulent diffusion matrix,  $\sigma_i$  denotes the (dry and/or wet) deposition velocity,  $R_i$  describes the chemical reactions and radioactive decay (in case of radionuclides), while  $E_i$  involves the emission sources.

The direct numerical treatment of this system is rather difficult for the following reasons.

- Due the term  $R_i$ , we have a coupled system of nonlinear partial differential equations.
- The direct discretisation of this system would result in a large nonlinear system of algebraic equations, where in case of  $M$  grid points for each time layer  $mM$  unknown values are to be computed.
- The numerical method is expected to satisfy certain properties, such as consistency, stability, convergence and other qualitative properties. However, if some off-the-shelf numerical method is applied directly to such a complicated system, these properties cannot be guaranteed.

In the following we present two powerful techniques which make the above system tractable for numerical integration.

### OPERATOR SPLITTING

During this procedure the right-hand side of the system to be solved is divided into a few simpler terms, and the corresponding sub-systems – which are connected to each other through the initial conditions – are solved one after the other in each time step of the numerical integration. In this manner, we replace the original model with one in which the different sub-processes take place successively in time. For example, in the Danish Eulerian Model the five sub-systems describe 1) the horizontal advection, 2) the horizontal diffusion, 3) the chemical reactions to which also emissions are added, 4) the deposition and 5) the vertical exchange (Zlatev, 1995). Assume that some approximation to the concentration vector  $(c_1, \dots, c_m)$  at the beginning of the time step has been found. The first system is solved by using this vector as a starting vector. The obtained solution will serve as the initial vector in the treatment of the second system and so on. The solution of the fifth system is accepted as an approximation to the concentration vector at the end of the time step. So, this so-called DEM splitting is based on a separation of the different physical processes of the air pollution transport and a separation of the vertical and horizontal directions for advection and diffusion. The distinction of the vertical and horizontal directions is natural in shallow atmospheres, and makes it easier to switch on to the 2-D version of the model. An alternative of the DEM splitting is the so-called physical splitting, where the sub-operators belong to the five basic air pollution processes, and there is no directional separation.

The application of any of the above splitting methods has the following advantages:

- The original problem is decomposed into several simpler problems.
- Apart from the reaction problem, we obtain independent linear scalar equations for the different species. Therefore, instead of a complicated problem with  $mM$  unknowns in each time step, we practically obtain discrete models with only  $M$  unknowns.
- When operator splitting is applied, each sub-problem is solved by using a numerical method that is tailored to the given sub-problem, and so the sub-problems can be treated in a mathematically correct way.

Operator splitting has the disadvantage that even if the sub-problems are solved exactly, the application of splitting gives rise to the local splitting error, defined as the difference of the exact model and the split model by assuming exact solution of the sub-problems after one splitting time step. There are certain splitting techniques which have smaller local splitting error, but these are more costly (Strang-Marchuk splitting (Strang, 1968 and Marchuk, 1968), symmetrically weighted sequential (SWS) splitting (Strang, 1963, Csomós et al., 2005). The treatment of the boundary conditions (in case they exist) are not trivial, either, when operator splitting is applied.

### RICHARDSON EXTRAPOLATION

It can be shown that if the local splitting error has order  $p$  and each sub-problem is solved by a  $p$ -th order numerical method, then the whole numerical method will also have order  $p$ . When the order of the local splitting error and the order of the applied numerical methods are different, the whole approximation will be determined by the lowest error order. This means that it is not worth using higher order methods for the sub-problems, unless the splitting method is also of higher order. However, the application of a higher order splitting method and higher order numerical methods for the sub-problems would often be too expensive. So the question arises how we can enhance the accuracy in a cost-effective way. A possible approach to this problem is Richardson extrapolation.

The Richardson extrapolation can be applied for the increase of the order of convergence (and so efficiency) of any convergent time integration method (Richardson, 1911 and Richardson, 1927). The key to this procedure is to apply the same  $p$ -th order method by two different choices of the time-step size, and combine the two solutions by appropriately chosen weights as follows.

Assume that we apply a numerical method of order  $p$  for the solution of a system of ordinary differential equations, and denote the numerical solution at time layer  $t_{n-1}$  by  $y_{n-1}$ . Then we calculate the approximation  $y_n$  in three steps:

1. Perform one time step of size  $\tau$  to calculate the approximation  $z_n$  of  $y(t_n)$ .
2. Perform two small time steps with step-size  $\tau/2$  to calculate another approximation  $w_n$  of  $y(t_n)$ .
3. Calculate an improved approximation  $y_n$  by applying the formula

$$y_n = \frac{2^p w_n - z_n}{2^p - 1} \quad (2)$$

The order of accuracy of the improved approximation  $y_n$  given by (2) is  $p+1$ .

The Richardson Extrapolation can be implemented in two different ways. One can apply the improved approximation  $y_n$  in step  $n+1$  to  $z_{n+1}$  and  $w_{n+1}$  or one can alternatively use the approximations  $z_n$  and  $w_n$  in the calculation of  $z_{n+1}$  and  $w_{n+1}$ , respectively. The first implementation is called active, while the name passive is used for the second one.

Assume that the computations have been performed with the larger time-step  $\tau$ , and denote by  $N$  the number of time-steps. Obviously, during the computation with the halved time-step  $\tau/2$ ,  $2N$  time-steps are to be taken. It is easy to see that both the passive and active Richardson extrapolations require approximately 1.5 times more computations than the integration with the underlying method in  $2N$  time-steps. Moreover, if the computation has been performed with the time step  $\tau$  (which means  $N$  steps), then applying the passive Richardson extrapolation hardly requires more computations than performing  $2N$  steps with the underlying method. In case parallel computers are available, then even applying the active Richardson extrapolation does not require significantly more computational time than performing  $2N$  steps with the underlying method. This clearly shows the efficiency of the Richardson extrapolation.

The implementation of the Richardson Extrapolation is relatively simple. It is nearly obvious that the stability properties of the combined method obtained when the passive implementation is used are the same as those of the underlying numerical method. However, the requirement for stability of the computational process may cause serious difficulties when the active Richardson extrapolation is used. Through the investigation of the stability function of the combined method separately in each case the following results have been obtained (Zlatev et al., 2010):

- The combination of the trapezoidal rule and the active Richardson extrapolation is not A-stable.
- The combination of backward Euler method and the active Richardson extrapolation is L-stable.
- The combination of the general  $\theta$ -method and the active Richardson extrapolation is A-stable for  $\theta \in [2/3, 1]$ .
- In case of two implicit Runge-Kutta methods (three-stage fifth-order fully implicit Runge-Kutta method and two-stage third-order diagonally implicit Runge-Kutta method) we could not prove A-stability, strong A-stability and L-stability, but found very large stability regions (Zlatev et al. 2015).

## NUMERICAL EXPERIMENTS

We successfully applied Richardson extrapolation in some simplified environmental models, see Brajnovits, 2010 and Mona et al., 2015. Here we will show some results that have been obtained when we applied passive and active Richardson extrapolation in the chemistry module of UNI-DEM. This module is based on the chemical scheme of the EMEP model with 56 chemical species. The computations were performed on the computers of the Centre for Scientific Computing at the Technical University of Denmark (<http://www.hpc.dtu.dk>) and at the Department of Environmental Science at the Aarhus University. The equations describing the chemical transformations between these species form a nonlinear system of ordinary differential equations. Due to the fact that the reaction rates have very different magnitudes, some species transform slowly, while others very rapidly, which results in a

strongly stiff system. During the experiments the time interval of the computations was 24 hours long (from noon to the noon of the next day). The reference solution was computed by a four-step, fifth-order L-stable implicit Runge-Kutta method. The errors were measured in the maximum norm.

**Table 1.** Errors obtained by the backward Euler method and the combinations of the backward Euler method with passive/active Richardson extrapolation (RE) in the chemical module of UNI-DEM.  $N$  denotes the number of time-steps that were taken during the time integration. The numbers in parentheses give the ratio of the given error and the error obtained by using the previous time-step size.

<b>N</b>	<b>Backward Euler</b>	<b>Backward Euler + active RE</b>	<b>Backward Euler + passive RE</b>
1344	3.063e-1	7.708e-3	6.727e-3
2688	1.516e-1 (2.02)	1.960e-3 (3.93)	1.739e-3 (3.87)
5376	7.536e-2 (2.01)	5.453e-4 (3.59)	4.417e-4 (3.94)
10752	3.757e-2 (2.01)	1.455e-4 (3.75)	1.113e-4 (3.97)
21504	1.876e-2 (2.00)	3.765e-5 (3.86)	2.793e-5 (3.98)
43008	9.371e-3 (2.00)	9.583e-6 (3.93)	6.997e-6 (3.99)
86016	4.684e-3 (2.00)	2.418e-6 (3.96)	1.751e-6 (4.00)
172032	2.341e-3 (2.00)	6.072e-7 (3.98)	4.379e-7 (4.00)
344064	1.171e-3 (2.00)	1.522e-7 (3.99)	1.095e-7 (4.00)

The backward Euler method is a first-order numerical method, which is reflected by the fact that the errors are roughly halved when the time-step size is halved during the direct implementation of this method. Both Richardson extrapolations increase the order to 2, which is shown by error ratios around 4. Note that for the achievement of the same accuracy much fewer time-steps are needed when the Richardson extrapolation is used. This is even clearer from Table 2, which shows how many time integration steps were needed in order to achieve some given accuracy. One can see that the Richardson extrapolation considerably enhances the efficiency.

**Table 2.** CPU times in seconds and numbers of time-steps needed for the global errors to fall into given intervals. The results are the same for both the active and passive Richardson extrapolations.

<b>Global error</b>	<b>Backward Euler</b>		<b>Backward Euler + RE</b>	
	<b>CPU time / Number of time-steps</b>		<b>CPU time / Number of time-steps</b>	
[1e-2,1e-1]	274	5376	304	672
[1e-3,1e-2]	862	43008	374	1344
[1e-4,1e-3]	7144	688128	661	5376
[1e-5,1e-4]	42384	5505024	1428	21504
[1e-6,1e-5]	265421	44040192	2240	43008

**Table 3.** Errors obtained when the chemical scheme of UNI-DEM was solved by sequential splitting and the combination of sequential splitting and Richardson extrapolation. The sub-problems were solved by the backward Euler method.  $N$  denotes the number of time-steps that were taken during the time integration. The numbers in parentheses give the ratio of the given error and the error obtained by using the previous time-step size.

<b>N</b>	<b>Sequential splitting</b>	<b>Sequential splitting + RE</b>
1344	2.154e-1	1.799e-2
2688	1.093e-1 (1.97)	5.862e-3 (3.07)
5376	5.509e-2 (1.99)	1.698e-3 (3.45)
10752	2.764e-2 (1.99)	4.598e-4 (3.69)
21504	1.384e-3 (2.00)	1.199e-4 (3.84)
43008	6.926e-3 (2.00)	3.062e-5 (3.92)
86016	3.464e-3 (2.00)	7.740e-6 (3.96)
172032	1.733e-3 (2.00)	1.946e-6 (3.98)

Finally we illustrate that the Richardson extrapolation can be successfully applied in combination with operator splitting as well. The above chemical scheme was split into two parts: The first part contained mainly the chemical reactions in which ozone participates. The second part contained all the other chemical reactions. The backward Euler method was run in combination with (a) only the sequential splitting procedure and (b) both the sequential splitting procedure and Richardson Extrapolation. Results are given in Table 3. It is clearly seen that the application of Richardson Extrapolation together with the backward Euler method and the sequential splitting procedure results in a second-order numerical method and, thus, in significantly more accurate results. For more details see Zlatev et al., 2012.

## REFERENCES

- Brajnovits, B., 2010: Mathematical investigation of the Richardson extrapolation and its application in a simplified CO<sub>2</sub> model (in Hungarian), MSc diploma work, Eötvös Loránd University, Budapest.
- Csomós, P., Á. Havasi, I. Faragó, 2005: Weighted sequential splittings and their analysis, *Comp. Math. Appl.* **50**, 1017-1031.
- Marchuk, G. I., 1968: Some application of splitting-up methods to the solution of mathematical physics problem. *Aplik. Mat.* **13**, 103-132.
- Mona, T., I. Lagzi and Á. Havasi, 2015: Solving Reaction-Diffusion and Advection Problems with Richardson Extrapolation, *J. Chemistry* **2015**, DOI: <http://dx.doi.org/10.1155/2015/350362>
- Richardson, L. F., 1911: The Approximate Arithmetical Solution by Finite Differences of Physical Problems Including Differential Equations, with an Application to the Stresses in a masonry dam, *Philosophical Transactions of the Royal Society of London, Series A*, **210**, 307–357.
- Richardson, L. F., 1927: The Deferred Approach to the Limit, I—Single Lattice, *Philosophical Transactions of the Royal Society of London, Series A* **226**, 299–349.
- Strang, G., 1963: Accurate partial difference methods I: Linear Cauchy problems. *Archive for Rational Mechanics and Analysis* **12**, 392-402.
- Strang, G., 1968: On the construction and comparison of difference schemes. *SIAM Journal of Numerical Analysis* **5**, 506-517.
- Zlatev, Z., 1995: Computer Treatment of Large Air Pollution Models, Kluwer Academic Publishers, Dordrecht, Boston, London (now distributed by Springer-Verlag, Berlin).
- Zlatev, Z., I. Faragó and Á. Havasi, 2010: Stability of the Richardson Extrapolation together with the  $\theta$ -method, *Journal of Computational and Applied Mathematics* **235**, 507-520.
- Zlatev, Z., I. Faragó and Á. Havasi, 2012: Richardson extrapolation combined with the sequential splitting procedure and the theta-method, *Central European Journal of Mathematics* **10** (2012), 159-172.
- Zlatev, Z., K. Georgiev and I. Dimov, 2014: Studying absolute stability properties of the Richardson Extrapolation combined with explicit Runge-Kutta methods, *Computers and Mathematics with Applications* **67**, No. 12, 2294-2307.
- Zlatev, Z., I. Dimov, I. Faragó, K. Georgiev and Á. Havasi, 2015: Stability of the Richardson Extrapolation combined with some implicit Runge-Kutta methods, *Journal of Computational and Applied Mathematics*, submitted.

**17th International Conference on  
Harmonisation within Atmospheric Dispersion Modelling for Regulatory Purposes  
9-12 May 2016, Budapest, Hungary**

---

**AN APPLICATION OF THE SCHAAKE SHUFFLE TECHNIQUE TO GENERATE SPACE-TIME CONSISTENT AQ PREDICTIONS**

*S. Alessandrini<sup>1</sup>, L. Delle Monache<sup>1</sup>, Irina Djalalova<sup>2</sup>, Jim Wilczak<sup>2</sup>*

<sup>1</sup>National Center for Atmospheric Research, Boulder, Colorado, USA

<sup>2</sup>National Oceanic and Atmospheric Administration, Boulder, Colorado, USA

**Abstract:** Several statistical methods used to generate ensemble forecast of air pollutants or different meteorological variables do not represent accurately the covariance between neighbouring stations or temporal correlation between subsequent lead times. Probabilistic predictions of O<sub>3</sub> and PM<sub>2.5</sub> surface concentrations over the U.S. are generated with the analog ensemble (AnEn) technique. The ensemble members provided by AnEn are statistically indistinguishable and they are generated without space-time correlation. We apply the Schaake Shuffle technique to reorder the ensemble members and recover space-time variability of PM<sub>2.5</sub> and O<sub>3</sub> forecast time-series.

**Key words:** *Analog Ensemble, Schaake Shuffle, air quality ensemble forecasting*

## **INTRODUCTION**

Several statistical methods used to generate ensemble forecast of air pollutants or different meteorological variables do not represent accurately the covariance between neighbouring stations or temporal correlation between subsequent lead times. This is an important issue for air quality ensemble forecast when generating, for example, two-dimensional maps of the concentration of a given pollutant, or when trying to predict the risk of consecutive days/hours with hazardous concentrations. Probabilistic predictions of O<sub>3</sub> and PM<sub>2.5</sub> surface concentrations over the U.S. are generated with the analog ensemble (AnEn) technique. The ensemble members provided by AnEn are statistically indistinguishable and they are generated without space-time correlation. We apply the Schaake Shuffle technique, widely used for hydrological application, to reorder the ensemble members and recover space-time variability of PM<sub>2.5</sub> and O<sub>3</sub> forecast time-series. With this technique, the ensemble members for a given forecast lead-time are ranked and matched with the rank of PM<sub>2.5</sub> or O<sub>3</sub> past observations at the same hours appropriately selected across the historical record. The ensembles are then reordered to match the original order of the selected historical data. Using this technique, the observed inter-station correlation and the observed temporal auto-correlation are almost completely recovered.

## **METHODOLOGY AND RESULTS**

The AnEn technique (Delle Monache et al. 2011, 2013) has been extensively tested for the probabilistic prediction of both meteorological variables and renewable energy (Alessandrini et al., 2015).

The AnEn is built from a historical set of deterministic predictions and observations of the quantity to be predicted. For each forecast lead time and location, the ensemble prediction of a given variable is constituted by a set of measurements of the past (i.e., 1-hour averages of PM<sub>2.5</sub> and O<sub>3</sub> concentrations). These measurements are those concurrent to past deterministic predictions for the same lead time and location, chosen based on their similarity to the current forecast. The forecasted variables used to identify the past forecast similar to the current one are called analog predictors. In this application we use as predictors, among others meteorological variables, the O<sub>3</sub> and PM<sub>2.5</sub> concentrations forecasts over the continental US generated by the U.S. EPA CMAQ CTM (Byun and Schere, 2006) model. The forecasts are issued at 12 UTC with a 24 hours frequency for lead times between 0-48 hours ahead over the period 01 July 2014-31 July 2015. The AnEn forecasts are issued for all the 564 stations of the AIRNow EPA network whose locations is depicted in Figure 1. The first 6 months of this period are used for training

purposes while the remaining part for the verification. The AnEn provides reliable, sharp, and statistical consistent probabilistic AQ predictions, at a fraction of the real-time computational cost of traditional ensemble methods.

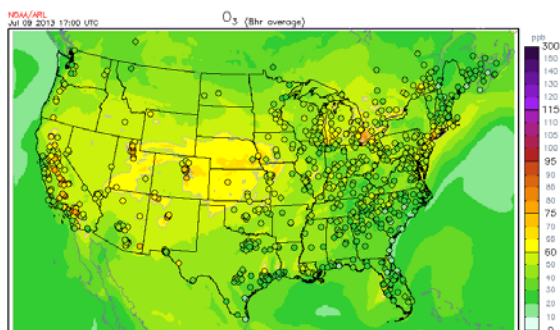


**Figure 1.** Maximum daily 8-hour average surface  $O_3$  on July 9 2013. Shown are the model prediction (shading) from CMAQ, and measurement (filled solid circle) from the AIRNow EPA network.

The ensemble members provided by AnEn are statistically indistinguishable and they are generated without space-time correlation. We apply the Schaake Shuffle (ScS) technique (Clark et al., 2004), widely used for hydrological application, to reorder the ensemble members and recover space-time variability of  $PM_{2.5}$  and  $O_3$  forecast time-series. With this technique, the ensemble members for a given forecast lead-time are ranked and matched with the rank of  $PM_{2.5}$  or  $O_3$  past observations at the same hours appropriately selected across the historical record. The ensembles are then reordered to match the original order of the selected historical data. Using this technique, the observed inter-station correlation and the observed temporal auto-correlation are almost completely recovered.

In Figure 2 the autocorrelation function of  $PM_{2.5}$  concentrations is plotted for all the 20 members (red line) generated by the AnEn and the measurements (black line) for one station. On the left, the autocorrelations are computed for the AnEn members not yet reordered by the ScS technique which has been instead applied to plot the chart on the right. The observed temporal auto-correlation is significantly underestimated by all the 20 members when computed without the ScS reordering. When ScS is applied, the observed auto-correlation is better reproduced by all AnEn members.

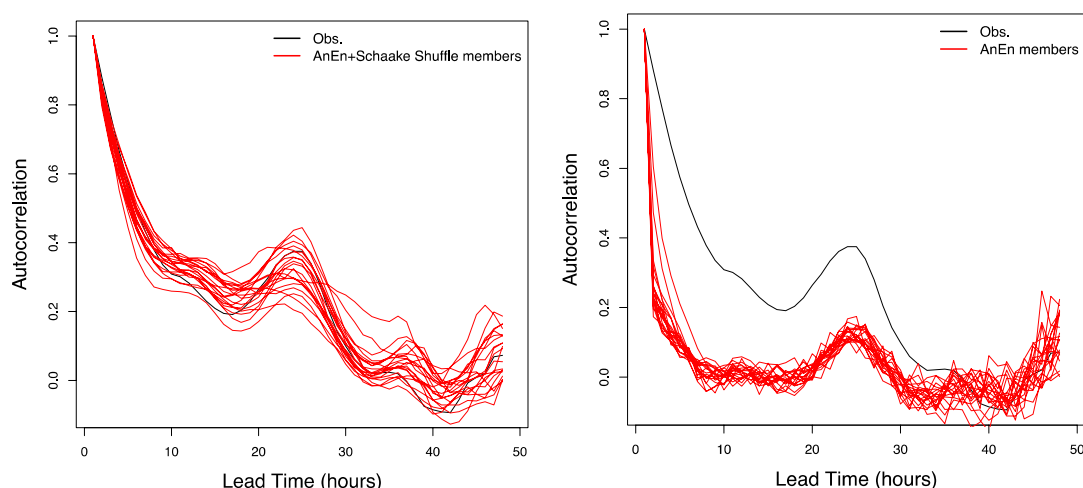


**Figure 2.** The autocorrelation function of  $PM_{2.5}$  concentrations is plotted for all the 20 members (red line) generated by the AnEn and the measurements (black line) for one station. On the left the autocorrelations are computed for the AnEn members not yet reordered by the Schaake Shuffle (ScS) technique. The ScS technique has been instead applied to plot the chart on the right.

## CONCLUSION

We have applied the Schaake Shuffle (ScS) to recover the observed temporal auto-correlation of the PM<sub>2.5</sub> ensemble forecast generated by the analog ensemble (AnEn) technique. Preliminary results show that the ScS can recover the observed temporal auto-correlation of PM<sub>2.5</sub> hourly concentrations. Future work will extend the ScS application to O<sub>3</sub> concentration forecasts and to verify the ScS ability to recover the observed inter-station correlation.

## REFERENCES

- Alessandrini, S., Delle Monache, L., Sperati, S., & Nissen, J. N. (2015). A novel application of an analog ensemble for short-term wind power forecasting. *Renewable Energy*, **76**, 768-781.
- Byun D. W., and K. L. Schere (2006), Description of the Models-3 Community Multiscale Air Quality (CMAQ) Model: System overview, governing equations, and science algorithms, *Appl. Mech. Rev.*, **59**, 51-77.
- Clark, M., Gangopadhyay, S., Hay, L., Rajagopalan, B., & Wilby, R. (2004). The Schaake shuffle: A method for reconstructing space-time variability in forecasted precipitation and temperature fields. *Journal of Hydrometeorology*, **5**(1), 243-262.
- Delle Monache, L., T. Nipen, Y. Liu, G. Roux, and R. Stull (2011), Kalman filter and analog schemes to post-process numerical weather predictions, *Mon. Wea. Rev.*, **139**, 3554–3570.
- Delle Monache, L., T. Eckel, D. Rife, B. Nagarajan, K. Searight (2013), Probabilistic weather predictions with an analog ensemble, *Mon. Wea. Rev.*, **141**, 3498-3516.

**MODITIC**

**MODELLING THE DISPERSION OF  
TOXIC INDUSTRIAL CHEMICALS**

**17th International Conference on  
Harmonisation within Atmospheric Dispersion Modelling for Regulatory Purposes  
9-12 May 2016, Budapest, Hungary**

---

**MODITIC - MODELLING THE DISPERSION OF TOXIC INDUSTRIAL CHEMICALS  
IN URBAN ENVIRONMENTS**

*Monica Endregard<sup>1</sup>, Stephane Burkhardt<sup>2</sup>, Jan Burman<sup>3</sup>, Olivier Gentilhomme<sup>4</sup>, Alan Robins<sup>5</sup>,  
Emma M. M. Wingstedt<sup>1</sup>, B. Anders Pettersson Reij<sup>6</sup>, Leif Persson<sup>3</sup>, Niklas Brännström<sup>3</sup>,  
Oskar Parmhed<sup>7</sup>, Oscar Björnham<sup>3</sup>, Guillaume Leroy<sup>4</sup>, Daniel Eriksson<sup>1,3</sup>, Thomas Vik<sup>1</sup>,  
John Aa. Tørnes<sup>1</sup> and Jean-Pierre Issarte<sup>2</sup>*

<sup>1</sup>Norwegian Defence Research Establishment (FFI), Kjeller, Norway

<sup>2</sup>Direction Générale de l'Armement (DGA) CBRN Defence, Vert-le-Petit, France

<sup>3</sup>Swedish Defence Research Agency (FOI), Umeå, Sweden

<sup>4</sup>Institut National de l'Environnement Industriel et des Risques (INERIS), Verneuil-en-Halatte, France

<sup>5</sup>University of Surrey, Guildford, United Kingdom

<sup>6</sup>The University Graduate Center (UNIK), Kjeller, Norway

<sup>7</sup>Swedish Defence Research Agency (FOI), Grindsjön, Sweden

**Abstract:** The main objective of the MODITIC project is to enhance our fundamental understanding of modelling the dispersion of non-neutral gasses in built-up environments. The project goal is to lay the ground for future improvements of dispersion models used in emergency situations by military personnel as well as civilian emergency services, thereby improving emergency preparedness and response. Atmospheric wind tunnel experiments have been systematically applied and novel experimental data sets for a number of carefully chosen dispersion scenarios have been provided. The same set of configurations has also been subject to computational modelling efforts using both advanced Computational Fluid Dynamics (CFD) and simpler Gaussian models. Experimental data for the release of toxic chemicals from pressurized vessels in order to provide realistic source characterisations in the case of an event have also been made available to the project. Accompanying computations using the conditions of the release experiments has been conducted in order to validate computational models. The project has generated a large database comprising experimental and numerical results for release and dispersion of neutral and dense gasses in configurations ranging from simple to complex geometries. This database will be a valuable addition to the body of reference data needed to advance the fundamental understanding of dispersion in urban environments and its modelling. The database may be used for development, improvement and validation of dispersion models for hazardous materials in urban environments.

**Key words:** *MODITIC, dense gas dispersion, urban environments, wind tunnel experiments, Computational Fluid Dynamics, RANS, Large Eddy Simulations, linear inverse modelling*

## **INTRODUCTION**

Toxic industrial chemicals are produced, transported and stored in relatively large quantities. The possible consequences of accidental or intentional release of such compounds are of concern both to military and civilian authorities. The main objective of the European Defence Agency (EDA) Project "Modelling the dispersion of toxic industrial chemicals in urban environments" (MODITIC) is to enhance our fundamental understanding of modelling the dispersion of heavier-than-air gasses in built-up environments. The project goal is to lay the ground for future improvements of dispersion models used in emergency situations by military personnel as well as civilian emergency services, thereby improving emergency preparedness and response.

The project work encompasses atmospheric wind tunnel experiments on neutral and dense gas dispersion for a selection of geometries with increasing complexity. Selected geometries were subject to computational modelling efforts using both advanced Computational Fluid Dynamics (CFD) and simpler Gaussian models to investigate performance of various numerical methods. In addition, special data sets

were compiled to examine inverse modelling capabilities. The project also made use of available experimental data for outdoor and indoor ammonia releases from pressurized vessels in order to test modelling strategies to realistically characterise the release characteristics.

The MODITIC project results is summarised below under six headings corresponding to the various activities. Further details are available in the accompanying papers.

### **ATMOSPHERIC WIND TUNNEL EXPERIMENTS**

Atmospheric wind tunnel experiments at the University of Surrey (Robins *et al.*, 2016) have been systematically applied and detailed experimental data sets for a number of carefully chosen dispersion scenarios have been provided. Project planning identified six categories of increasing complexity, the aim being to ensure gradual progress in complexity that, in turn, would lead to progress in understanding and capability for both forward and inverse modelling, namely:

1. A flat surface
2. A two-dimensional hill
3. A two-dimensional back-step
4. A simple array of obstacles
5. A complex array of obstacles
6. An urban area (central Paris).

Each of these categories was further sub-divided by wind direction, emission conditions (continuous and finite duration), and data requirements. In support of the overall project aims, an extensive series of experiments was conducted in the EnFlo ‘meteorological’ wind tunnel at the University of Surrey (UK) to generate data both to evaluate dispersion models and to aid understanding of underlying physical processes. Two component laser-Doppler anemometer (LDA) and fast flame ionisation detector (FFID) instrumentation were used to measure the flow and concentration fields in categories 2 to 6 (suitable data were already available for category 1) for a range of source locations and emission conditions (non-buoyant and dense gas) in a simulated neutrally stable atmospheric boundary layer. The overall strategy was to use operating conditions that were consistent with good quality flow in the wind tunnel but produced significant dense gas effects in the carbon dioxide plumes; e.g. as exemplified by upwind and enhanced lateral spread. The data are contained in a collection of text and Excel files with supporting meta-data, comprising in total a very extensive and detailed data-base of dispersion in complex environments. Included in the data-base is a collection of long, simultaneous data series from four FFIDs that can be used in investigating inverse modelling capabilities.

### **SOURCE TERM EXPERIMENTS AND COMPUTATIONS**

Large scale ammonia release experimental data have been made available and used for comparison with simulation results using Gaussian models. Experimental data for the release of toxic chemicals from pressurized vessels have also been made available to the project in order to provide realistic source characterisations in the case of such an event. Accompanying computations using the conditions of the release experiments have been conducted in order to validate computational models.

Toxic industrial chemicals are often stored as pressurized liquefied gas. A vessel failure or rupture induces a violent two-phase release of liquid and gas (thermodynamic flash), that current CFD models used by the MODITIC project partners are not able to deal with in all its complexity. Interaction with an obstacle close to the release adds further complexity of the behaviour of the multi-phase turbulent jet. The impact on an obstacle and the subsequent drainage to the ground of a liquid fraction remains to be studied. On the other hand, it is currently possible to integrate part of the source term as an empirical term in complex CFD models, by specifying the form and content of liquid and gas mass fractions, and rates, energetic contents at the end of the expansion phase, and to compute the following dispersion and air entrainment. Finally, in order to handle a CFD source term such as a dense gas released from a ruptured vessel in an urban area, a decoupled approach is recommended between rapid phenomena (flashing and expansion) that need empirical descriptions, and slow phenomena (gas dispersion and entrainment) that can be computed using CFD.

## OPERATIONAL MODELS

Referring to COST action ES1006 (COST ES1006 (1), COST ES1006 (2)) on the use of atmospheric dispersion models (ADM) in emergency response tools (ERT), we confirm a number of statements (Björnham *et al.*, 2016):

- The different expertise levels needed to use operational tools differing by model complexity levels (ARGOS, PUMA: Gaussian puffs-QUIC, PMSS: Lagrangian)
- The type of response to give to decision makers depends on the end-user needs: danger zones corresponding to concentrations/dosage above toxicological thresholds, confidence intervals or percentiles to be in such limits; we have seen that FACn statistical measures to give confidence in our outputs will depend strongly on the lowest levels considered (ARGOS or PMSS results).
- These models are usually conservative, and overestimate the concentration levels close to the source (ARGOS on Paris scenario).

Regarding **dense gas** in operational tools, QUIC software (Los Alamos National Laboratory, 2016) seems to compare well with INERIS data (Gentilhomme, 2013) using the included dense gas sub-model, and PUMA also gives promising results. These last developments on PUMA have been tested within the scope of this project, dealing with dense puff interaction, in a semi-linearized way to keep the response fast enough. ARGOS (PDC-ARGOS, 2016) heavy puff model works well on INERIS ammonia (NH<sub>3</sub>) release, but cannot handle obstacles at the same time.

Regarding **obstacles**, ARGOS Urban Dispersion Model (URD) necessitates to scale up small obstacles (INERIS case with wall) and is more suited to a densely built urban-like area (PARIS case, with source surrounded by buildings). The URD model can handle passive gas only, so no dense gas-obstacle interaction could be tested and validated. On the PARIS case, tendency to overestimate by a factor of 3 to 5 close to the source, and underestimate by such in far field was observed and explanations were proposed. PUMA is not able to include obstacles and is therefore not suitable for complex geometry cases. PMSS (ARIA VIEW, 2016) was tested against DEMI-COMPLEX ARRAY and PARIS cases (Robins *et al.*, 2016) for passive gas only, and behaved reasonably well. Overestimations of concentrations behind buildings and underestimations in main streets were usually observed. QUIC software is currently able to handle both obstacles and dense gas. In the study with ARGOS, a “real” case with hydrogen cyanide (HCN) was considered by scaling up the wind tunnel flow conditions.

Finally, these tools are not push-button tools and require expert skills. The advantage against CFD is their cheap computing cost, but they still need relatively large set-up times compared to the run-time.

## RANS SIMULATIONS

RANS-models have a number of applications where they produce good results, but the models are not general and cannot be used for all types of problems. Thus it is important to evaluate different types of RANS-models for a range of scenarios to make clear what the range of usefulness is. The results show that both models capture the main features of the flow: turbulence levels and flow directions are mainly in line with the findings from the experiment (Burkhart and Burman, 2016). The comparison of the neutral release shows for both models that they can capture the turbulent transport. The heavy gas release though, indicates that the buoyant effects are only partially captured. A possible improvement would consist in using low-Reynolds models such as  $k\omega$ -sst and more refined meshes in stratified regions to better capture the boundary layer and the dense plume edge gradients. It would be also worth investigate algebraic flux models to better capture anisotropic turbulent viscosity, or damping factors in isotropic turbulent viscosity as a function of local Ri number.

## INVERSE MODELLING

Linear inverse dispersion modelling, in particular from a single point source, is a maturing field where least square optimisation methods as well as Bayesian approaches have been adapted to solve the problem. In many studies, however, the setting is both oversimplified (flat terrain, Gaussian plume dispersion models) and the detector data generated synthetically. In MODITIC we have brought linear inverse modelling to an urban environment (there are up to 14 buildings in the town studied) and we use

detector signals from MODITIC wind tunnel experiments of the same configuration. Two different methods, renormalisation (Issartel *et al.*, 2012) and a Bayesian framework (see e.g. (Stuart, 2010)), have been used to solve the resulting inverse problem. Both methods rely on having adjoint functions for computational efficiency. In this case the adjoint fields are RANS CFD-fields. Preliminary studies, as well as the literature, indicate that for flat terrain the location of the reconstructed source will have a good accuracy in the cross wind direction while the uncertainty is much larger in the wind direction. As a knock on effect the release rate will also be associated with the corresponding uncertainty: a source located further away will have to release more mass per time unit to render the detection readings in the correct range. Comparison of the two inverse solving methods for the built up environment for neutral releases show that the results keep within expectations: since there is no change in the prevailing wind direction there is little uncertainty in the source location in the cross wind direction, but significantly more in the direction along the wind direction.

We therefore conclude that the inverse methods work acceptably well in the urban setting with neutral releases: the challenge lies in generating adjoint plumes capturing the dispersion process (Brännström *et al.*, 2016). An even greater challenge is the treatment of dense gas emissions.

### **LARGE EDDY SIMULATIONS**

Large Eddy Simulations (LES) represent the current state-of-the-art method in applied turbulence research. In this project, the LES methodology has been applied to model dispersion of neutrally buoyant and dense gas in the geometries tested in the wind tunnel (Wingstedt *et al.*, 2016). Different methods of providing inflow conditions have been utilized as well as descriptions of the dense gas. The changes the dense gas exerts on the average wind field are validated against experimental results with good agreement as well as the concentration fields, Reynold stresses and turbulent mass fluxes. Interesting characteristics of the dense gas dispersion are the upstream spread and the wider and shallower plume. Obstacles affect the dense gas to a higher degree compared to a neutral release because the dense gas remains within the street network.

The conclusion is that the LES methodology used within the MODITIC project is suitable to predict both dense and neutrally buoyant releases of gas within an urban environment. One of the major findings is that care should be taken concerning the inflow conditions with regard to the spatial and temporal resolution of the incoming boundary layer.

### **MAIN RESULTS AND CONCLUSIONS**

The project has generated a large database comprising experimental and numerical results for release and dispersion of neutral and dense gasses in complex geometries. The experimental data cover a range of realistic scenarios of increasing complexity, from a flat, open surface to the centre of Paris. This database will be a valuable addition to the body of reference data needed to advance the fundamental understanding of dispersion in urban environments and its modelling. The database may be used for development, improvement and validation of dispersion models for hazardous materials in urban environments.

### **FUTURE WORK**

One of the primary scientific objectives of MODITIC has been to study the interactions between a dense gas and the wind field in the vicinity of the source. These are very complex dynamical interactions that pose particular challenges for a modeller. A similar, and an oftentimes occurring situation, is the dispersion of gasses and aerosols in a stably stratified atmospheric background. One obvious follow-on study to MODITIC would be to benefit from the experiences and lessons learned in the application of a wide range of models with different complexity and repeat the work in stable boundary layers. Similar work could also be carried out in unstable boundary layers, including the study of bouyant sources (e.g. fires). Topics that deserve further and deeper study include the relation between upwind and lateral spread near the source and the emission properties and the adaptation of street network dispersion models to dense gas emissions.

The project partners will continue analysing and exploiting the MODITIC data to fill knowledge gaps related to dense gas dispersion. This includes the development of an inverse model for dense gas dispersion in urban environments. A systematic study of the dynamic interaction between a dense gas cloud and the wind field in the vicinity of the source in a massively separated boundary layer will be investigated using MODITIC experimental data and LES. The data from both experiments and LES computations will also be put to good use in the development of improved models based on the RANS method. The practical experiences with dense gas releases in a wind tunnel environment will be beneficial in future studies.

The project partners are planning a new European Defence Agency (EDA) project entitled “CR MODelling of Sources and Agent FatE” (MODISAFE) aimed to start 1 January 2017, which builds on and supplements MODITIC. Processes such as evaporation, deposition fractions on environmental surfaces such as the ground, buildings and vegetation, as well as suspension and re-suspension of particles greatly influence the resulting hazardous concentrations of various threat agents, thus should be properly dealt with in modelling and simulation approaches and hazard prediction tools. The project will perform both experimental and numerical work and contribute to improved scientific knowledge and to advance the state-of-the-art operational models used for emergency response.

#### ACKNOWLEDGEMENTS

This work was conducted within the European Defence Agency (EDA) project B-1097-ESM4-GP “Modelling the dispersion of toxic industrial chemicals in urban environments” (MODITIC).

#### REFERENCES

- ARIA View, 2016: ARIA Technologies, <http://www.aria.fr>.
- Björnham, O., Gousseff, A., Tørnes, J. and Burkhart, S., 2016. MODITIC operational models. Proc. HARMO17, Budapest, May 9-12, 2016.
- Brännström, N., Brännvall, T., Burkhart, S., Burman, J., Busch, X., Issartel, J.-P. and Persson, L.Å., 2016. MODITIC inverse modelling in urban environments. Proc. HARMO17, Budapest, May 9-12, 2016.
- Burkhart, S. and Burman, J., 2016. MODITIC wind tunnel experiments neutral and heavy gas simulation using RANS. Proc. HARMO17, Budapest, May 9-12, 2016.
- Burkhart, S., Gousseff, A., Tørnes, J., and Björnham, O., 2016. MODITIC - Simulation Report on Operational Urban Dispersion Modelling.
- COST ES1006 (1), Best Practice Guidelines for the use of Atmospheric Dispersion Models in Emergency Response Tools at local-scale in case of hazmat releases into the air, COST European Cooperation in Science and Technology, April 2015.
- COST ES1006 (2), Model evaluation case studies: Approach and results, COST European Cooperation in Science and Technology, April 2015.
- Gentilhomme, O., 2013. MODITIC project: Agent characterisation and source modelling, INERIS.
- Los Alamos National Laboratory, 2016: QUIC Atmospheric Dispersion Modeling System, <http://www.lanl.gov/projects/quic/index.shtml>.
- Issartel, J.-P., M. Sharan and S. K. Singh, 2012: Identification of a Point of Release by Use of Optimally Weighted Least Squares. *Pure and Applied Geophysics*, **169**, 467-482.
- Osnes, A., Eriksson, D. and Reif, B.A.P., 2016. MODITIC – on the generation of inflow boundary conditions for dispersion simulations using Large Eddy simulations. Proc. HARMO17, Budapest, May 9-12, 2016.
- PDC-ARGOS, 2016: CBRN Crisis Management, <http://www.pdc-argos.com>.
- Robins, A. G., Carpentieri, M., Hayden, P., Batten, J., Benson, J and Nunn, A, 2016. MODITIC wind tunnel experiments. Proc. HARMO17, Budapest, May 9-12, 2016.
- Stuart, A. M., 2010: Inverse problems: a Bayesian perspective, *Acta Numerica*, **19**.
- Wingstedt, E.M.M., Eriksson, D., Parmhed, O., Leroy, G., Osnes, A.N., Reif, B.A.P. and Burman, J., 2016. MODITIC – Large Eddy simulations of dispersion of neutral and non-neutral scalar fields in complex urban-like geometries. Proc. HARMO17, Budapest, May 9-12, 2016.

**17th International Conference on  
Harmonisation within Atmospheric Dispersion Modelling for Regulatory Purposes  
9-12 May 2016, Budapest, Hungary**

---

**MODITIC WIND TUNNEL EXPERIMENTS**

*Alan Robins, Matteo Carpentieri, Paul Hayden, Joseph Batten, Jack Benson and Ashley Nunn*

EnFlo, Mechanical Engineering Sciences, FEPS, University of Surrey, Guildford, UK

**Abstract:** An extensive series of experiments was conducted in the EnFlo wind tunnel to investigate the behaviour of dense gas emissions in complex flows and provide data for evaluating dispersion models capable of handling gravitational effects. The reference points were passive and dense gas dispersion on level terrain, for which ample data already existed. Increasingly complex scenarios were studied, commencing with a two-dimensional hill, then a simple array of 4 identical obstacles, a more complex, irregular array of 14 obstacles and finally an urban area (central Paris at 1:350 scale). The research treated continuous and finite duration emissions of either air, carbon dioxide or a mixture of the two into a neutrally stable simulated atmospheric boundary layer.

**Key words:** *MODITIC, dense gas dispersion, wind tunnel modelling*

## **INTRODUCTION**

The objective of the MODITIC project was to conduct a systematic study of the transport of neutral and heavier-than-air gaseous chemicals in complex urban environments. In support of this overall aim an extensive series of experiments was conducted in the EnFlo ‘meteorological’ wind tunnel at the University of Surrey (UK) to generate data for evaluating dispersion models and to aid understanding of the underlying physical processes.

Project planning identified six scenarios, the aim being to ensure gradual progress in complexity that, in turn, would lead to progress in understanding and computational capability, namely:

1. A flat surface
2. A two-dimensional hill
3. A two-dimensional back-step
4. A simple array of obstacles
5. A complex array of obstacles
6. An urban area (central Paris).

Each of these categories was further sub-divided by wind direction, source conditions and measurement requirements. Use was also made of relevant previous EnFlo work, including the PERF project that studied dense gas dispersion in neutral and stable boundary layers (Robins et al., 2001a & b), the DAPPLE studies of dispersion in central London (e.g. Wood et al., 2009) and the DYCE project that investigated inverse modelling for identifying source strength and location (Rudd et al., 2012).

This paper describes the methods use in the wind tunnel simulations, the scaling criteria, the overall strategy, the experiments undertaken, and hence the content of the resulting data-base. Some results are presented and discussed from the simulations of dispersion in central Paris - other examples are to be found in the accompanying MODITIC papers, to which this and the overview paper act as an introduction.

## **EXPERIMENTAL METHODS**

### **The wind tunnel**

The EnFlo wind tunnel was designed specifically to simulate flow and dispersion processes in the atmospheric boundary layer, in particular where density differences are a key factor, either in emissions

or the background flow. It is an open circuit wind tunnel with a 20m long working section, 3.5 by 1.5m in cross-section, the capability to heat and cool the flow and the tunnel surfaces, and the ability to operate at low flow speeds of order  $1\text{ms}^{-1}$ . Reference flow conditions are measured by two ultrasonic anemometers, one held at a fixed reference location and the other positioned as required. Temperature conditions are recorded by thermistor rakes in the flow and individual thermistors in each tunnel wall, roof and floor panel. Flow conditions through the inlet are also monitored, primarily to indicate the state of the inlet screens. The wind tunnel and all associated experimental equipment and instrumentation operate under full computer control, which allows un-manned and remote operation of the control software. All data collected, including a wide range of environmental and operational information, metadata and web-cam outputs are automatically archived.

### Procedures

All velocity and turbulence measurements were made using a two-component Dantec laser-Doppler anemometer (LDA) system with a FibreFlow probe. Data collection durations were selected to control the standard error in the results; achieving a typical standard error in the longitudinal mean velocity of about 2%, and in the turbulence normal stresses between 5 and 10%. Plume concentrations were measured with Combustion Fast Flame Ionisation Detectors (FFIDs), which respond to hydrocarbon concentrations and have a frequency response of order 200Hz. Small proportions of propane (of order 1%) were added to emissions and acted as the plume tracer. FFIDs were calibrated at regular intervals against standard mixtures of tracer-in-air. Data collection times were again selected to control the standard error in the results, achieving a typical standard error of about 2% in the mean concentration data with a 4 minute averaging time with the tunnel reference velocity at  $1\text{ms}^{-1}$ . Positional accuracy was generally  $\pm 2\text{mm}$ , but considerably better following reset of the traverse position.

A standard source diameter of 100mm was used, the source installation extending to approximately 300mm below the tunnel floor and being packed with 3mm diameter beads and covered with a mesh in order to achieve uniform emission conditions; similar arrangements were used in the PERF dense gas dispersion studies (Robins et al., 2001a). In the majority of cases, emissions were either air or carbon dioxide with a trace amount of propane added, as discussed above. Mixtures of air and carbon dioxide were used in some experiments with the Paris model to obtain intermediate densities. A thermal mass-flowmeter and flow-control system was used to regulate emission rates.

### Similarity conditions

Neutral boundary layer simulation does not impose any relationships between the wind speeds in the tunnel and at full scale, all that is required is that certain Reynolds number constraints are satisfied to ensure that the surface is fully rough and the flow around buildings Reynolds number independent. These conditions were indeed met. However, scaling of buoyant plume dynamics implies similarity of three parameters (a density ratio, a velocity ratio and a Richardson number; Obasaju et al., 1998) and this leads to an explicit relation between wind speeds at model and full scale (suffices m and fs):

$$\varepsilon_u = \frac{u_{fs}^*}{u_m^*} = \frac{U_{ref-fs}}{U_{ref-m}} = \left(\frac{h_{fs}}{h_m}\right)^{1/2} = \varepsilon^{1/2} \quad (1)$$

where  $\varepsilon_u$  is the velocity ratio,  $u^*$  the friction velocity,  $U_{ref}$  a reference wind speed,  $h$  and length scale (e.g. the mean block height) and  $\varepsilon$  the geometrical scale ratio. The time scale ratio,  $\varepsilon_T$ , is:

$$\varepsilon_T = \frac{t_1}{t_2} = \frac{H_1 U_{ref2}}{H_2 U_{ref1}} = \varepsilon \varepsilon_u^{-1} = \varepsilon^{1/2} \quad (2)$$

It is sometimes assumed that the density ratio of itself is not a significant parameter away from the immediate vicinity of the source and similarity can be based on just two parameters, the dimensionless buoyancy and momentum fluxes from the source. That approach could be, but has not been, used here.

### Strategy

The scenarios of interest were based on emissions that might occur, for example, in the catastrophic failure of a large tank of chlorine in an urban area. However, what could be simulated in the wind tunnel work was tempered by the constraints of the simulation criteria summarised above, which are particularly severe in the case of dense gas dispersion modelling where carbon dioxide is really the only gas that can

be used at model scale. The wind tunnel work therefore adopted a strategy that used experimental conditions, controlled by the tunnel speed and the emission rate of carbon dioxide, that produced clear dense gas effects but, at the same time, led to plumes that remained well clear of the wind tunnel side walls. Results obtained in this manner could be used to test models that operate satisfactorily at model scale, in particular CFD-based approaches. However, some operational models only function at full scale and for these the similarity conditions described above were used to convert results from model to full scale. This generally led to emission conditions that were far out of range for the applicability of such models (emissions being far too great to be plausible). Some additional experiments were therefore carried out with considerably reduced emission rates to provide data for more realistic full scale conditions, accepting that dense gas effects would be reduced (but not absent) in such circumstances.

### **THE DATA-BASE**

Existing results from the PERF (Robins et al., 2001) and DYCE (Rudd et al., 2010) projects were used to fill Scenario 1 data requirements, respectively for forward and inverse modelling. For the remaining scenarios, an extensive series of experiments was conducted in the EnFlo wind tunnel to provide data that, again, was suitable for assessing forward and inverse dispersion modelling capability. All the work discussed below made use of the same, neutrally stable boundary layer inflow.

#### **The inflow**

The inflow boundary layer was generated in a standard manner using vorticity generators (Irwin spires) and surface roughness. The details and resulting profiles of the mean inflow velocity, turbulent stresses and associated length scales are included in the data-base and summarised here: boundary layer depth,  $H = 1$  m; friction velocity,  $u^* = 0.055U_{ref}$ ; surface roughness length,  $z_o = 0.088$  mm.

#### **The two-dimensional hill**

The hill shape was scaled from the WALLTURB ‘bump’, which itself was designed to generate a small separation bubble on the downwind face and for which high quality LES flow simulations already existed within the MODITIC group. Two source positions were used, one on the upwind face and the other on the downwind face, and initial experiments settled on  $U_{ref} = 1\text{ms}^{-1}$ ,  $Q_{(\text{CO}_2)} = 100\text{litre}\cdot\text{min}^{-1}$  as the operating conditions; the same emission rate being used for the neutral density (air) cases. Extensive, simultaneous LDA and FFID measurements made in all four cases (2 sources, 2 gases). Buoyancy effects in the dense gas plumes led to local flow deceleration near the upwind source and acceleration near the downwind source. The associated plume showed significant upwind spread and greatly enhanced lateral spread (relative to the neutral density cases).

#### **The two-dimensional back-step**

The back-step was formed by removing the downwind section of the hill model, separating the two parts at the crest. This gave a step aspect ratio (width,  $W$ , to height,  $h$ ) of just 10, which was clearly too small as it implied that the length of the recirculation region,  $L_R$ , formed downwind of the step was similar in magnitude to step width (3m). The floor level downwind of the step was therefore built-up to reduce the step height to 0.1m, increasing  $W/h$  to 30 and implying that  $W/L_R \sim 5$ . The source was located with its centre 0.1m from the step. Experiments were conducted with the floor downwind of the step either smooth or covered in the roughness elements that were used to simulate the approach flow boundary layer. The reference speed and emission rate were kept at the values used with the hill model. The most dramatic results were seen in the mean concentration field. In comparison with the neutral density plume, the heavier than air plume was much shallower, as expected, but essentially two-dimensional, spreading across the full extent of the recirculation region. Vertical turbulence intensities were greatly reduced and associated vertical mass fluxes much smaller, in keeping with the reduced rate of vertical spread. Differences between results over the smooth and rough wall were very small. Variants on the basic experiments with the back-step saw two-dimensional arrays of obstacles installed on the downstream surface. These comprised three rows of 0.11m cubes, separated laterally and longitudinally by 0.11m. In the first case, the obstacle array commenced at 0.8m from the step and downstream of the recirculation region; in the second at 0.36m and well within the recirculation region.

### **The simple array of obstacles**

The small array comprised four  $h = 110\text{mm}$  cubes in an aligned  $2 \times 2$  array, with a separation of  $110\text{mm}$ . Experiments were carried out with the array either aligned normal to the approach flow, defined as  $0^\circ$ , or at  $45^\circ$ . Sources were located upwind, on the centre line, or upwind and to one side ( $y = 1.5h$ ). Initial tests with the array at  $0^\circ$  examined the effect of carbon dioxide emission rate on the plume width around and downwind of the array. The concentration field was judged to be too wide relative to the tunnel cross-section with  $Q = 100\text{litre}\cdot\text{min}^{-1}$ ,  $U_{ref} = 1\text{ms}^{-1}$ , as in the hill experiments, and a lower emission rate of  $50\text{litre}\cdot\text{min}^{-1}$  was therefore adopted in this work and also that with the complex array. Measurements were made both upwind and downwind of the array. The most obvious difference between the air and carbon dioxide plumes was that the former passed through the array whilst the latter were deflected around it.

### **The complex array of obstacles**

This model comprised fourteen rectangular blocks of differing sizes arranged in an irregular manner, all constructed from  $110\text{mm}$  cubes. 'Tree' simulators were used in some of the experiments to study their impact on dispersion behaviour. The array was aligned either normal to the approach flow, defined as  $0^\circ$ , or at  $45^\circ$ . Sources were located within the array, upwind on the centre line, and upwind to one side at  $y = 3h$ ; the emission rate were again  $50\text{litre}\cdot\text{min}^{-1}$  with  $U_{ref} = 1\text{ms}^{-1}$ . Measurements were made within the array and downwind from it.

### **Data for inverse modelling studies**

Four FFIDS were operated simultaneously to generate long concentration time series that could be used in inverse modelling studies. Experiments ran for 16 minutes, with the emission initially off, then on and, finally, off again so that concentrations fell to background levels by the end of the whole period, providing a period of approximately 13 minutes of steady emission. Both the raw data, sampled at 400 Hz, and equivalent full scale data were made available to test the ability of inverse modelling systems to detect the location of the source, the emission rate and the emission profile. A geometrical scale of 1:200 was assumed in converting the results to full scale, the data being first down-sampled to 100 Hz.

### **The urban area (central Paris).**

By far the greatest effort was devoted to simulations with the Paris model. A geometrical scale of 1:350 was selected in order to encompass a sufficient area of central Paris, from the Arc de Triomphe, along Avenue des Champs Elysees to the Grand Palais, and an equivalent distance on either side. The model comprised almost a hundred blocks, each with a flat roof, a great simplification of the real topography but one judged to be fit for purpose, given that whatever was used in the wind tunnel work had to be reproduced in the numerical modelling. The 1:350 scale implied that the ratio of full scale and model wind speeds was  $\sqrt{350} = 18.7$ , so that the standard  $1\text{ms}^{-1}$  wind tunnel reference speed used in the bulk of MODITIC wind tunnel work was equivalent to  $18.7\text{ms}^{-1}$ , or more usefully  $9\text{ms}^{-1}$  at  $10\text{m}$  height and  $11.6\text{ms}^{-1}$  at the average building block height of  $27\text{m}$ . and very large emission rates are required at this full-scale wind speed to ensure significant dense gas effects. Both the reference and emission velocities scale by 18.7 and the basic experimental conditions ( $Q = 50\text{litre}\cdot\text{min}^{-1}$ ,  $U_{ref} = 1\text{ms}^{-1}$ ) were unrealistic when scaled. Additional experiments were carried out with reduced emission rates and lower tunnel speeds to provide data for more realistic full scale conditions - dense gas effects were much reduced but not absent in these cases. Experiments were conducted with both continuous and short duration emissions.

Three source locations and associated wind directions were identified: one in the Avenue des Champs Elysees (S1) and two in the narrow side streets on either side (S2, S3). A wind direction was associated with each:  $300^\circ$  for S1,  $220^\circ$  for S2 and  $40^\circ$  for S3. Three types of concentration measurements were made: in-street at  $z = 10\text{mm}$ , lateral profiles (cross-wind) above roof level, at  $z = 120\text{mm}$ , vertical profiles from street level. In contrast to the other scenarios, wide ranges of emission rates (1 to  $50\text{litre}\cdot\text{min}^{-1}$ ), emission density ratios relative to air (1 to 1.52) and reference flow speeds ( $0.6$  to  $2.0\text{ms}^{-1}$ ) were examined. Dense gas effects were found to be very strong with the carbon dioxide plume almost entirely confined to the street network, with significant upwind and lateral spread apparent. In all the cases studied, the downwind carbon dioxide plume was much shallower than the equivalent air plume (Figure 1a), though upwind spread ceased at sufficiently low emission rates. The runs with air at different emission rates produced concentration results that scaled with emission rate, as expected of a passive

plume (Figure 1b). Passive gas dispersion from S2 and S3 followed the empirical relation between maximum round level concentration and separation found in the DAPPLE work (Woods et al., 2009) but the confinement of the Av. Champs Elysees led to a slower decay rate for S1, a rate that reduced even further as density effects became more pronounced (i.e. with increasing source Richardson No.).

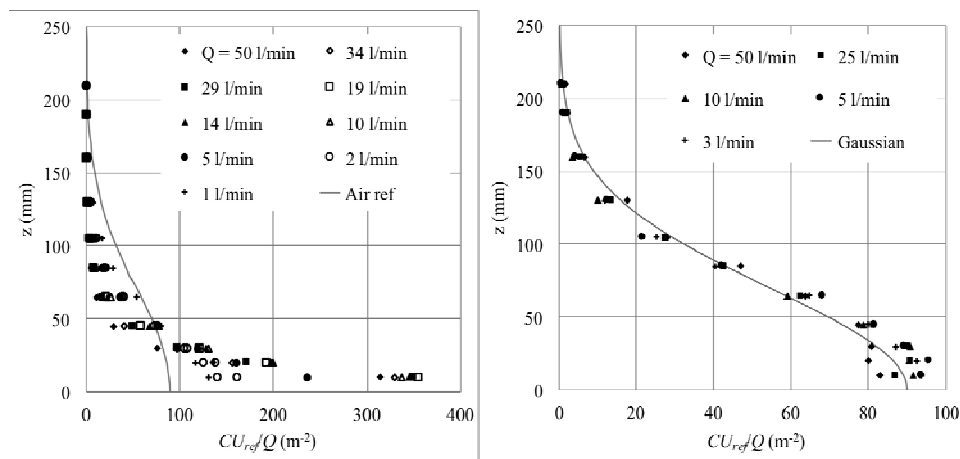


**Figure 1.** Vertical profiles of normalised mean concentration measured at 1000mm downwind (in Av. Champs Elysees) from source S1. 1a, left: Results for a range of emission rates compared with the results for an air plume; 1b, right: Results for air emissions fitted by a Gaussian profile. The reference speed was  $1\text{ms}^{-1}$  in all cases.

## CONCLUSIONS

A detailed and comprehensive data-base has been prepared from wind tunnel simulations of non-buoyant and dense gas dispersion in conditions of increasing geometrical complexity. Data were compiled as a set of text and Excel files, together with accompanying meta-data. The prime use of this data within the MODITIC project was to examine the performance of a range of forward and inverse dispersion models, though the results also provided insight into dense gas dispersion behaviour. Future research could most usefully: repeat the present work in stable and unstable boundary layers; study the relation between upwind and lateral spread near the source and the emission properties (geometry, Richardson number and velocity ratio); the adaptation of street network dispersion models to dense gas emissions through a Richardson number dependent entrainment velocity.

## ACKNOWLEDGEMENT

This work was conducted within the European Defence Agency (EDA) project B-1097-ESM4-GP “Modelling the dispersion of toxic industrial chemicals in urban environments” (MODITIC).

## REFERENCES

- Obasaju, ED & Robins, AG, 1998. Simulation of pollution dispersion using small scale physical models - assessment of scaling options. *Environmental Monitoring and Assessment*, **52**, 239-254.
- Robins, AG, Castro, IP, Hayden, P, Steggel, N, Contini, D, & Heist, D, 2001. A wind tunnel study of dense gas dispersion in a neutral boundary layer over a rough surface. *Atmos. Environ.*, **35**, 2243-2252.
- Robins, AG, Castro, IP, Hayden, P, Steggel, N, Contini, D, Heist, D & Taylor, TJ, 2001. A wind tunnel study of dense gas dispersion in a stable boundary layer over a rough surface. *Atmos. Environ.*, **35**, 2253-2264.
- Rudd, AC, Belcher, SE, Robins, AG, & Lepley, JJ, 2012. An Inverse Method for Determining Source Characteristics for Emergency Response Applications. *Boundary-Layer Meteorology*, **144**, 1-20.
- Wood, CR, Arnold, SJ, Balogun, AA, Barlow, JF, Belcher, SE, Britter, RE, Cheng, H, Dobre, A, Lingard, JJN, Martin, D, Neophytou, MK, Petersson, FK, Robins, AG, Shallcross, DE, Smalley, RJ, Tate, JE, Tomlin, AS & White, IR, 2009. Dispersion Experiments in Central London: The 2007 DAPPLE project. *Bull. Amer. Meteor. Soc.*, **90**, 955-969.

**17th International Conference on  
Harmonisation within Atmospheric Dispersion Modelling for Regulatory Purposes  
9-12 May 2016, Budapest, Hungary**

---

**MODITIC WIND TUNNEL EXPERIMENTS  
NEUTRAL AND HEAVY GAS SIMULATION USING RANS**

*Stéphane Burkhart<sup>1</sup> Jan Burman<sup>2</sup>*

<sup>1</sup>DGA Maitrise NRBC France

<sup>2</sup>FOI, Swedish Defence Research Agency, Sweden

**Abstract:** Wind tunnel experiments with heavy gas release in the vicinity of an urban like complex geometry is modelled and simulated with two different codes and turbulence models. The results are compared to the MODITIC wind tunnel data. The results show that both models capture the main features of the flow: turbulence levels and flow directions are mainly in line with the findings from the experiment. The comparison of the neutral release shows for both models that they can capture the turbulent transport. The heavy gas release though, indicates that the buoyant effects are only partially captured.

**Key words:** *RANS, Saturne, PHOENICS, neutral gas release, heavy gas release*

## **INTRODUCTION**

Wind tunnel experiments with heavy gas release in the vicinity of an urban like complex geometry gives a well-defined scenario and well established data with statistical confidence. This can be used for validation and comparison of models aiming to mimic the flow within such geometries. Though the dataset holds several scenarios with neutral and heavy gas release, with and without simulated trees, here only a few of these are used.

The building scenario (Robins et al, 2016) can be described as a market square surrounded by buildings and beyond that a line of buildings in two directions. Two alleys are also part of the scenario. Three source locations are used: the market square and upwind on two locations laterally displaced. The source is either neutrally buoyant or buoyant with a relative density to the ambient with 1.5.

Two different RANS models with different solvers are used. RANS1 is the code Saturne v4.0 developed by EDF. It uses a *kH17-MODITIC* linear model together with an atmospheric module developed at EDF.

RANS2 is PHOENICS, which was developed by CHAM and uses the MMK-model.

In addition to concentration plots, the comparison between experiment and model results also uses a user-oriented measure of effectiveness (MOE) and statistical parameters such as fraction of prediction within a factor of 2 (FAC2) (see Warner et al ).

The results show that both models capture the main features of the flow: turbulence levels and flow directions are mainly in line with the findings from the experiment. The comparison of the neutral release shows for both models that they can capture the turbulent transport.

The heavy gas release though, indicates that the buoyant effects are only partially captured.

An improvement would consist in using low-Reynolds models such as  $k\omega$ -sst and more refined meshes in stratified regions to better capture the boundary layer and the dense plume edge gradients.

It would be also worth investigate algebraic flux models to better capture anisotropic turbulent viscosity, or damping factors in isotropic turbulent viscosity as a function of local Ri number.

## RANS MODELLING

### Code Saturne:

The atmospheric module in Code Saturne with dry atmosphere was activated. It uses a high Reynolds  $k-\epsilon$  turbulent model with linear production (corrects the known flaw of the standard  $k-\epsilon$  model which overestimates the turbulence level in case of strong velocity gradients) and an adapted rough wall law to atmospheric MO theory. It relies on works by Musson-Genon [1] and Geylen [2] to reconstruct turbulent fluxes and mean profiles from two-points vertical measurements (taken from the inlet profile) to be used as boundary layer profiles. The meteorological profile is read from a met file with the possibility to vary in time (one entry per date/time). It contains mean velocity, turbulent kinetic energy and dissipation rate, temperature and humidity as a function of altitude  $z$ . This module can a priori handle neutral, slightly stable and unstable atmospheres dry or wet (adiabatic profile modified). The turbulent production gravity term is included in the  $k-\epsilon$  equations ( $G=1/\rho(\mu_t/\sigma_t) \nabla \rho \cdot g$ ). A “scalable wall law” instead of a log law is used in well meshed cases ( $y^+ < 10$ ).

### Code PHOENICS.

PHOENICS is a general purpose CFD-code that allows for easy implementation of boundary conditions and grid generation for this case. Boundary conditions are set according to the measured values from the wind tunnel for wind speed and turbulence for the approaching flow. The MMK model differs from the standard high Reynolds  $k-\epsilon$  turbulent model in that the eddy viscosity coefficient is limited in strong shear by multiplication with the ratio of the vorticity and strain parameters [3]. The same turbulent production gravity term as in Saturne is included.

## HEAVY GAS RELEASE FLAT SURFACE

The flat surface dispersion case is limiting for dense gas release as it is always encountered in the other more complex cases upstream of the building area.

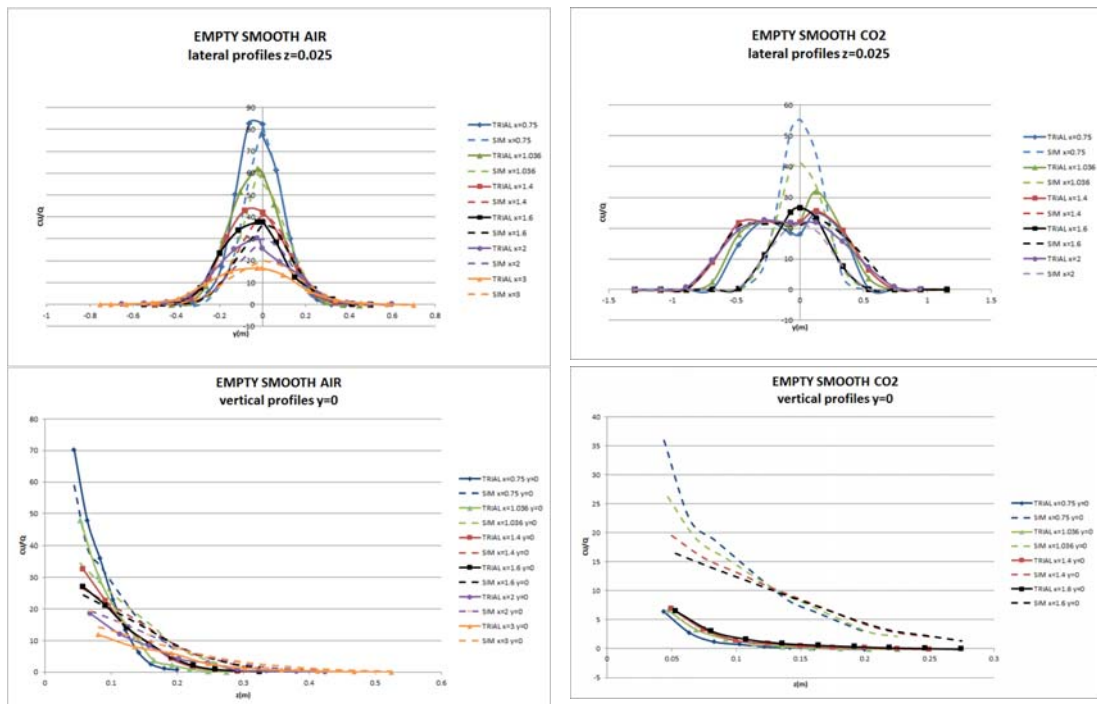


**Figure 1.** Normalized concentration for AIR (left) and CO2 (right) on Flat Surface with Code Saturne

On flat surface, Air release (passive gas, left Figure 1) normalized concentrations close to the floor are rather well reproduced, whether CO<sub>2</sub> (dense gas, right Figure 1) release concentrations are clearly overestimated with a factor 2 in magnitude and half width. The 2 peaks feature is missed. The neutral case is similar with RANS2 but the dense gas release in the smooth case is seen in Figure 2.

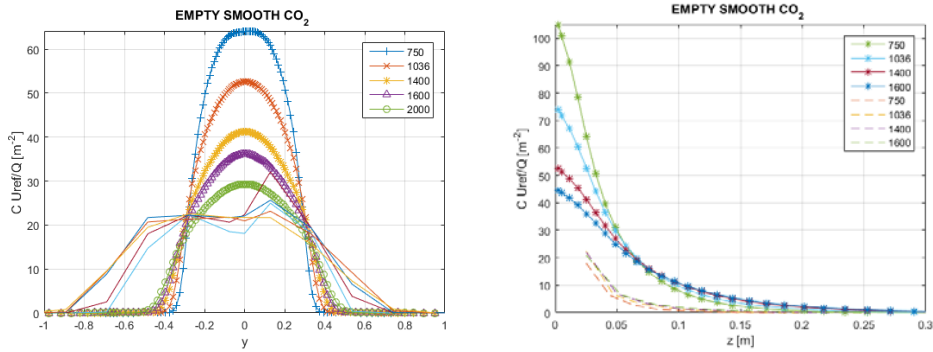


**Figure 2.** RANS2 using the MMK model cannot resolve the broadening of the plume in the way the experiment elucidates (left pane), but the right pane show that the gas is vertically dispersed in a way the experiment do not show. It is not clear if the concentration close to the floor was higher than the simulation but it is likely to assume that. Thus the density also is higher and maintained close to the surface.

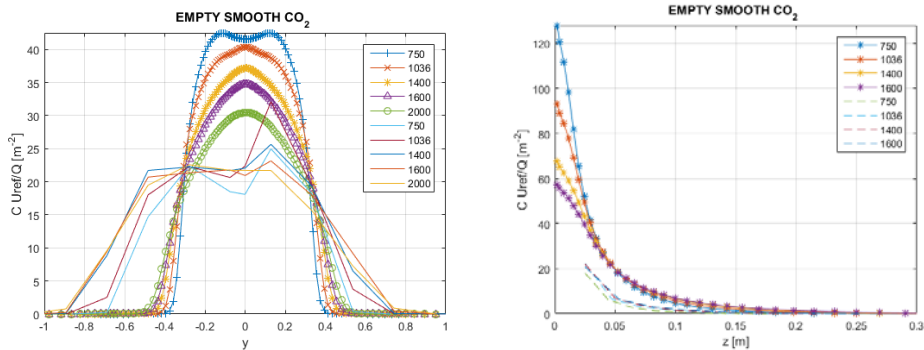


**Figure 3.** A minor correction of the MMK model is investigated in RANS2. By changing the Prandtl number in the GB formulation from unity to 0.714 a minor improvement is seen. The effect of the density gradient is increased. Still the left pane show unaltered broadening but a decrease of concentration levels and a double peak has emerged. The right panel indicate higher concentration close to the surface but the concentration levels are a factor of from the measured values.

In Figures 1, 2 and 3 the behaviour of the different turbulence models is seen. The AIR case for RANS2 is similar to RANS and is not reproduced. Figure 3 show that an increase in the production term from buoyancy will improve the concentration profile but does not change the broadening to a visual degree.

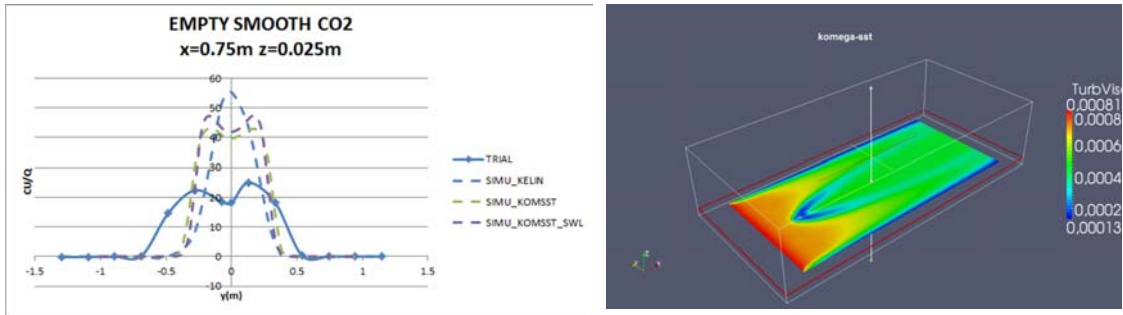


**Figure 4.** Normalized concentration close to the ground, effect of turbulence model. The left pane show the same pattern as Figure 3 that a modified turbulence model will improve the concentration profile but still cannot simulate the broadening of the plume.

One reason appears to be the use of a high Re turbulence model: we see a slight improvement going from  $k-\epsilon$ -linear (Left pane in Figure 2, dashed blue) to  $k\omega$ -sst models (dashed purple and green), capturing the peaks and lowering the magnitude. The effect of the sharp density gradient is not well resolved by the RANS models studied and does not allow the slumping motion from the dense gas to develop. Further improvement is to be sought in anisotropic viscosity model (Figure 3, right) and mesh refinement in density gradient region.

#### HEAVY GAS RELEASE COMPLEX ARRAY

This semi-complex idealized urban area increases the flow patterns and the turbulent field complexity, hence the following dispersion.

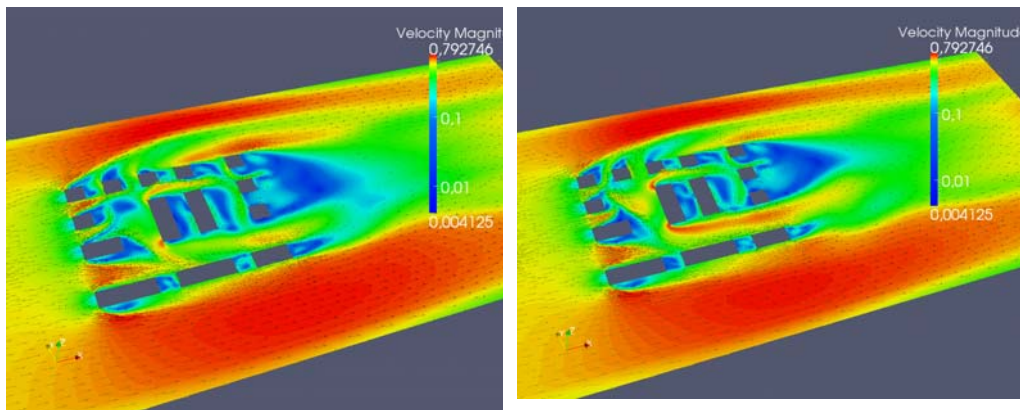


**Figure 5.** Velocity contours for AIR (left) and CO2 (right) for complex array case with Code Saturne

We see a rather strong effect of the vertical dense gas release in the source vicinity, with a stronger wind speed in the lower street canyon (Figure 5).

Sensors are placed after the array on cross lines at  $x=0.8m, 1.0m, 1.5m, 3.0m, 3.0m$

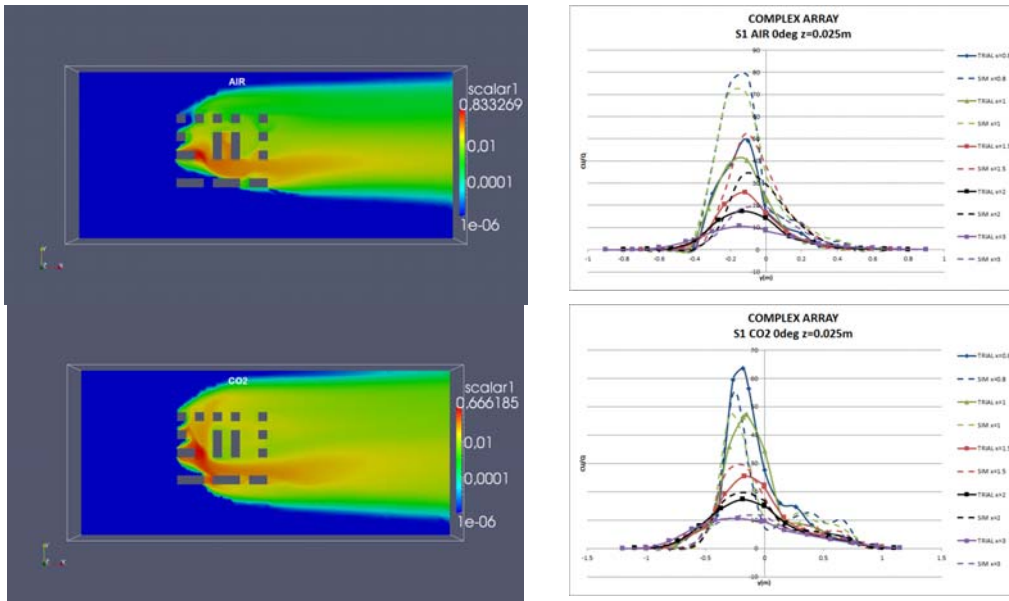


**Figure 6.** Mass Fraction contours for AIR (top) and CO<sub>2</sub> (bottom) and cross wind profiles close to the ground for the 0° orientated array

The Air release results (mass fraction here in Figure 6, top) close to the ground show an overestimation, indicating that the non-stationary mixing turbulent process is under-rated. A slight orientation shift between simulation and experiment may also explain part of the difference. CO<sub>2</sub> simulation results (Figure 6, bottom) are this time very close to the observations. Gravitational effects are less critical where strong mixing within building mixing layers occurs.

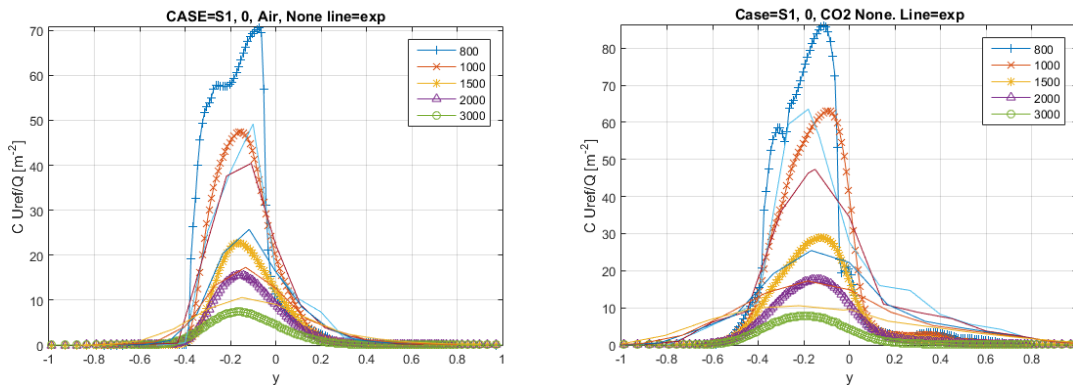


**Figure 7.** Measurements in the wind tunnel is compared with simulations with the RANS2 model. The lines with symbols are simulations, and the solid lines wind tunnel measurements. In the left pane the release is a neutrally buoyant gas and in the right pane the release is with heavy gas, (CO<sub>2</sub>). The left pane (Air) shows an overprediction of concentration closer to the array but an under prediction farther away. The right pane (CO<sub>2</sub>) show the same pattern in concentration but misses also to explain the broadening of the plume caused by the heavy gas effects.

## CONCLUSIONS

As long as the source is surrounded by buildings, AIR as well as CO<sub>2</sub> (dense) gas release are well reproduced by RANS and RANS2 models tested here in terms of wind speed and concentration (see Figures 5 to 7). This is confirmed in the Paris Case RANS results (not shown here), see (Robins et al, 2016) for reference. The RANS  $k$ - $\epsilon$ -linear does perform a bit better for the complex array case than the MMK-model used in RANS2. The CO<sub>2</sub> flat case is more problematic since it reveals the shortcomings of RANS models in this context: high Re turbulence models overestimate the turbulent viscosity, the gravity terms in the  $k\epsilon$  equations is probably not sufficiently resolved by too rough a mesh at the plume edge (where high density gradients happen). Finally the dependence of turbulent viscosity with plume Ri number to further reduce it would be worth to study.

## ACKNOWLEDGEMENT

This work was conducted within the European Defence Agency (EDA) project B-1097-ESM4-GP “Modelling the dispersion of toxic industrial chemicals in urban environments” (MODITIC). A special thanks to those performing the experiments.

## REFERENCES

- L.Musson-Genon et al., 2007: Reconstruction of the surface-layer vertical structure from measurements of wind, temperature and humidity at two levels”, *Boundary-layer Meteorol.*, **124**, 235-250
- J.-F. Geleyn, 1988: Interpolation of wind, temperature and humidity values from model levels to the height of measurement, *Tellus*, **40A**, 347-351 Edition, Cambridge University Press, UK
- M. Tsuchiya, Murakami,S.,Mochida, A., Kondo,K.,Ishida, Y., Development of a new k-e model for flow and pressure fields around bluff body, *J.Wind Engineering & Industrial Aerodynamics*, **67,68** (1997) 169-182.
- A. Robins, M. Carpentieri, P. Hayden, J. Batten, J. Benson and A. Nunn, 2016, MODITIC WIND TUNNEL EXPERIMENTS, FFI Report (in preparation), see also HARMO17 extended abstract with same title.

**17th International Conference on  
Harmonisation within Atmospheric Dispersion Modelling for Regulatory Purposes  
9-12 May 2016, Budapest, Hungary**

---

**MODITIC INVERSE MODELLING IN URBAN ENVIRONMENTS**

*Niklas Brännström<sup>1</sup>, Tobias Brännvall<sup>1</sup>, Stéphane Burkhardt<sup>2</sup>, Jan Burman<sup>1</sup>, Xavier Busch<sup>2</sup>, Jean-Pierre Issartel<sup>2</sup>, Leif Å. Persson<sup>1</sup>*

<sup>1</sup>The Swedish Defence Research Agency, Sweden

<sup>2</sup>DGA CBRN Defence, France

**Abstract:** Linear inverse dispersion modelling, in particular from a single point source, is a maturing field where least square optimisation methods as well as Bayesian approaches have been adapted to solve the problem. In many studies, however, the setting is both oversimplified (flat terrain, Gaussian plume dispersion models) and the detector data generated synthetically. In the present study we bring linear inverse modelling to an urban environment (there are up to 14 buildings in the town studied) and we use detector signals from MODITIC wind tunnel experiments of the same configuration. We employ two different methods, renormalisation (Issartel et al, 2012) and a Bayesian framework, to solve the resulting inverse problem. We compare and contrast the two different methods and their results. Both methods rely on having adjoint functions for computational efficiency. In this case the adjoint fields are RANS CFD-fields.

**Key words:** *Inverse modelling, urban environment, linear atmospheric dispersion, Bayesian, Renormalisation*

## **INTRODUCTION**

Over the years atmospheric dispersion models have been developed and refined to be able to cope with dispersal problems of varying, or rather increasing, complexity: the original problems were usually involving a hazardous substance that was dispersed linearly by a given meteorology over flat terrain while today the state-of-the-art cases, like those studied in the MODITIC project, handle nonlinear dispersal in built up environments. Being able to predict where a known release of a hazardous substance is carried by the wind field in order to calculate risk areas, estimate casualties and devising mitigating actions is important. These are questions that typically arise before an event has taken place, or, possibly during an event if the source of the release is known. Often the source is unknown, indeed networks of sensors are employed around critical infrastructure or soft targets to give an early warning of a developing event. That raises the natural question: can the knowledge of how a hazardous substance disperse through the atmosphere combined with the information given by the detectors allow us to deduce where the hazardous substance was released, i.e. determine the source. Enter inverse dispersion modelling. In this talk we will use two different inverse modelling techniques and apply them to a linear inverse problem set in a built up environment. We verify the methods for synthetic sensor data, showing what accuracy we can expect from the methods, and then apply the methods to sensor data generated in wind tunnel experiments.

## **EXPERIMENTAL SET-UP**

We study two urban environments of increasing complexity: the simple array with 4 equal sized buildings, and a complex array with 14 buildings of varying sizes.

### **Simple array**

The dimensions of the simple array, with the positions of the synchronized detectors we use for backtracking is shown in Figure 1.

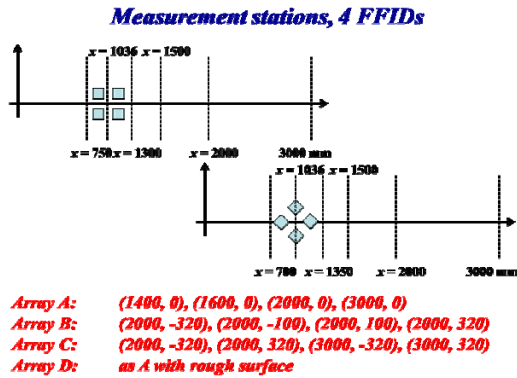


**Figure 1.** Sensors network (A, B, C arrangement) for the simple array cases. In each scenario 4 synchronized detectors are used to measure the concentration of the released gas. The detectors are located at the positions stated under A, B and C respectively.

The wind direction in the wind tunnel experiments is aligned with the x-axis in Figure 1, and as shown in the figure the simple array may be aligned at two different angles: we denote the alignment in the upper pane as “0 degrees” and the alignment in the lower pane as “45 degrees”. In each scenario four synchronized detectors were used, hence the reference 4 FFID in Figure 1, and we chose three different sets of locations for these detectors: we refer to these as case A, B and C. In addition to this two different source locations were available: these we denote S1 and S2, both S1 and S2 (at the origin) are located at 8H upwind (= 0.88m) in the x direction, but S1 is shifted off the x-axis by 1.5H (=0.165m) in the +y direction. The location of S2 was chosen to be the origin of the coordinate system. The diameter of the sources is 0.1m (to be compared to building height and sides of H=0.11m). A constant release rate of 50l/min=8.33e-4 m<sup>3</sup>/s was used in all scenarios.

### Complex array

In the complex array there are more buildings present and there is less symmetry. The configuration also opens up for a larger number of sensible detector locations, however, still only 4 synchronized detectors were used in these scenarios. For the complex array we chose five different sets of detector configurations: these are denoted case A through to E, and these are shown together with the geometry of the complex array in Figure 2. Note that some detectors are located on the roof tops (cases A and C) and others are inside the street canyons (cases B, D and E).

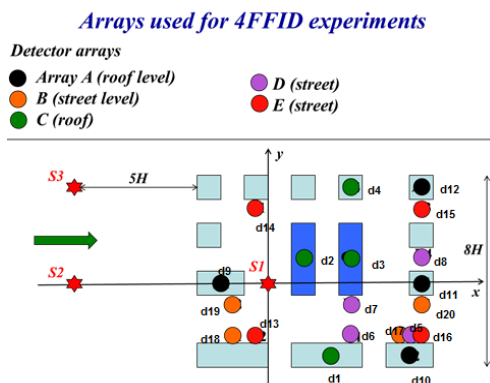


**Figure 2.** Configuration of the complex array. In each scenario, denoted case A through to E, 4 synchronized detectors were used to measure the concentration of the released gas. Note that some detectors are located at the roof of the buildings. Two different source locations were used, denoted S1 and S2. (There is a third source S3 indicated in the figure, but it was not used for inverse modelling).

Two different source locations were used S1 and S2. The diameter of the sources is 0.1m. The source S1 is defined to be at the origin (see Figure 2) while S2 is located upwind at x=-8H=-0.88m and y=0. S1 and

S2 are both located on the ground. As for the empty and complex array the source strength is  $50\text{l/min}=8.33\text{e-}4\text{m}^3/\text{s}$ .

For full details on the wind tunnel experiments that were conducted we refer to (Robins et al, 2016).

## INVERSE MODELLING METHODS

There are many inverse modelling techniques for atmospheric dispersion problems, but in general there are two main classes of such methods in use: in the first one the inverse problem is considered to be a probabilistic problem and Bayes theorem is used to deduce information about the source, in the second one the problem is viewed as a deterministic problem and the source is solved for by using some optimality principle (e.g. least squares). Common for both of these classes of methods is that they rely on being able to link a hypothetical source to its sensor response (a source-sensor relationship). This source-sensor relationship is readily given by the atmospheric dispersion model if it was not for the problem of computational cost. For each hypothetical source the atmospheric dispersion model must be used to establish the desired source-sensor relationship, for a Gaussian model on flat terrain this could be doable, but in the case of complex geometry and CFD-models it is not feasible. Thus a method called adjoint plumes is used. This method initially requires a more involved mathematical derivation, but once the adjoint model is found and it only have to be solved once for each detector to establish the source-sensor relationship. As part of the MODITIC project it was shown that neutral gas release for the simple and complex array are self-adjoint (Brännvall, 2015).

### Bayesian method

In the Bayesian approach to the inverse problem the source is estimated from the a posteriori probability distribution function which is obtained by calculating a likelihood function and weighing it with any a priori information that one has at hand (see e.g. (Stuart, 2010) for an introduction to general Bayesian inverse problems, and (Franklin, 1970) for an early reference). Let  $u$  be the sought input (the source), and  $y$  the observed sensor data, then the posterior distribution is given by

$$P(u | y) = \frac{P(u)P(y | u)}{P(y)}$$

where  $P(u)$  is the prior distribution,  $P(y | u)$  is the likelihood and  $P(y)$  is the evidence – the latter is only normalising the distribution and is not required for sampling the posterior distribution. This method avoids the pitfalls of ill-conditioning which are often associated with directly inverted problems and adds the benefit of allowing uncertainties in models and measurements to be handled in a tractable fashion.

### Renormalisation

Renormalization theory is a theory for data assimilation that allows reconstructing some estimated sources (Turbelin et al, 2014). It works in linear situations, where the measurements depend linearly on the source that is to be estimated. The estimated source is then a linear function of the measures, and no prior data has to be incorporated to the inputs: the experimenter does not have to guess what could be the source, nor the error of the model that has been used. The only inputs are the measurements  $\mu$  and the adjoint function  $a(x)$  (i.e., the values of the measurements associated to point sources).

To compute these adjoint functions, it is helpful to first compute retro-plumes and to make a post-treatment to eventually add some information: if the source is known to be on the ground, only the ground value of the retro-plumes is the adjoint; if the source is known to be stationary, the mean value (in time) of the retro-plumes is the adjoint.

From these adjoint functions, a visibility function is computed (Turbelin et al, 2014). The estimated source is then a linear combination of the ratios of the adjoint functions over the visibility function. To optimize the choice of visibility function  $\varphi(x)$ , the entropy lost (or information gained) by the action of measuring is maximized. The optimal visibility function obeys the following equation:

$$\varphi^2(x) = a^t(x)H_\varphi^{-1}a(x), H_\varphi(x) = \int \frac{a(z)a^t(z)}{\varphi(z)} dz,$$

where  $a(x)$  is the adjoint function. Amongst the properties of the visibility function, an important one is that when the real source is a single point source, then the estimated source is maximal at the point of the real source. This allows identifying point releases in the presence of detection and model errors (Issartel et al, 2012). To estimate the intensity of the source  $q$  and its position  $(x,y)$ , assuming that the source is a point source in the ground plane, that is the source  $s(x, y, z) \equiv s_0(x, y) = q_0 \delta(x - x_0) \delta(y - y_0)$  is a point source at  $(x_0, y_0)$  of intensity  $q_0$ , we minimize the distance between the given measurements  $\mu$  and the model predicted “measurements”  $(s(x, y, z), a(x, y, z)) = q_0(a_1(x_0, y_0), \dots, a_n(x_0, y_0))$  in the renormalized norm induced by  $H_\varphi(x)$  i.e. we minimize  $\|\mu - q_0(a_1(x_0, y_0), \dots, a_n(x_0, y_0))\|_{H_\varphi}$  over  $q_0, x_0, y_0$ . The consequences of minimizing with respect to the renormalized norm is expanded on in (Issartel et al, 2012).

### RESULTS ON SYNTHETIC SENSOR DATA

In order to verify that the inverse methods are working and to give us an idea of what to expect in terms of uncertainties for the Bayesian method we begin with studying the case where sensor measurements have been generated synthetically: the same dispersion model has been used (in forward mode) to simulate the concentrations at the sensor locations as been used to generate the adjoint plumes for inverse modelling. This approach eliminates the errors that would be induced by the fact that the model is a simplified description of the physics it is modelling. Two representative results are shown in Figure 3. In the figure, apart from the estimated source locations, the location of the sensors and the geometry, a visualisation of the posterior distribution are shown: it is plotted as a highest posterior density region (HPD) where the color scale shows the highest posterior density (HPD) credibility level. For example, a level curve in the yellow region bounds a HPD area containing almost 100% of the posterior probability mass, whereas a level curve in the blue region bounds a HPD area containing nearly 0% of the posterior probability mass. Hence 0% HPD credibility level represents the maximum posterior density, whereas 100% HPD credibility level represents the minimum posterior density.

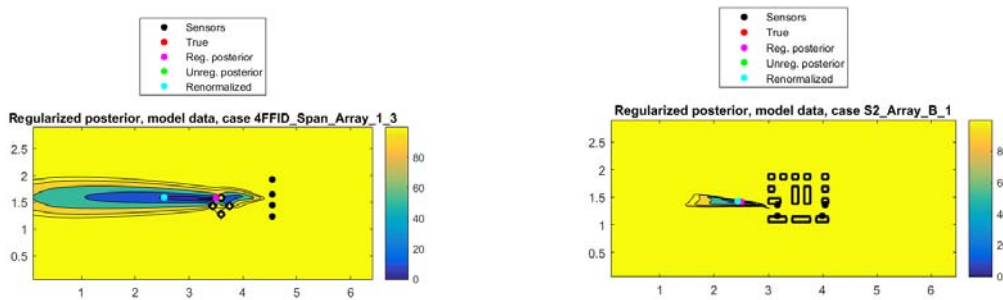


**Figure 3.** Estimated sources using synthetically generated data. In the left pane the simple array at 45° with sensor configuration B (compare Figure 1) is shown, and in the right pane the complex array with sensor configuration B (compare Figure 2) is shown. In both panes the estimated source location using Bayes (regularised), pink dot, and the Renormalisation method, cyan dot, are shown as well as the true source location (red dot) – in both panes however the renormalized estimate coincides with the true source location hiding the red dot.

### RESULTS ON WIND TUNNEL DATA

Having dealt with the case of synthetically generated measurements we now proceed to the case of estimating the source based on actual measurements in the wind tunnel. We stick to the same cases and configurations as shown in Figure 3 for easy comparison. See Figure 4 for the results.

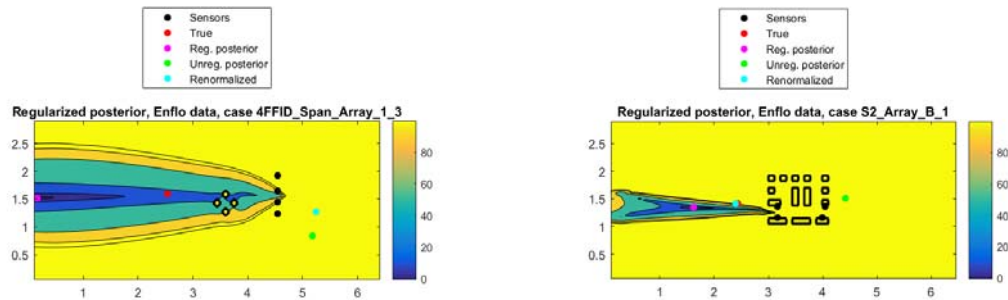


**Figure 4.** Estimated sources using wind tunnel measurements, same cases as in Figure 3. In both panes the estimated source location using Bayes (regularised), pink dot, and the Renormalisation method, cyan dot, are shown as well as the true source location (red dot).

## CONCLUSION

Looking at Figure 3, where we used synthetically generated data and thus eliminated the error that any model/physics discrepancies would have induced, we conclude that the uncertainties for the Bayesian case are much larger in the wind direction (along the x-axis) compared to the resolution in the cross wind direction (y-direction). Studying the geometry of the visibility function  $\varphi(x)$  underpinning the renormalization method we would conclude that the renormalization method suffers from the same feature: the error in source location is larger in the wind direction than in the cross wind direction. We also note that from an inverse modelling point of view the simple array is a harder case. The reason for this is that the source is located relatively far upwind from the buildings, and then the symmetrically positioned buildings scramble the signal that is picked up by a sensor network located far downstream. The Bayesian methods struggles to pinpoint the true source location for wind tunnel measurements as well as synthetic data, even though the true source location is enclosed in the HPD-region with quite high confidence level. The renormalisation method is spot on for synthetic data, but is for some reason disturbed by the wind tunnel measurements. The complex array on the other hand is an easier case, the source is located closer to the buildings (which are not quite symmetric) and the sensors are located within the town. For this complex array case the renormalisation method works beautifully, and the Bayesian method is not far off. Overall we note that when the sensor network has good visibility (in terms of the visibility function  $\varphi(x)$ ) the renormalisation method works well.

## ACKNOWLEDGEMENTS

This work was conducted within the European Defence Agency (EDA) project B-1097-ESM4-GP “Modelling the dispersion of toxic industrial chemicals in urban environments” (MODITIC).

## REFERENCES

- Brännvall, T., 2015: Source Term Estimation in the Atmospheric Boundary Layer :*Using the adjoint of the Reynolds Averaged Scalar Transport equation*, Master Dissertation, University of Umeå.
- Franklin, J. N., 1970: Well-Posed Stochastic Extensions of Ill-Posed Linear Problems. *Journal of mathematical analysis and applications*, **31**, 682-716.
- Issartel, J.-P., M. Sharan and S. K. Singh, 2012: Identification of a Point of Release by Use of Optimally Weighted Least Squares. *Pure and Applied Geophysics*, **169**, 467-482.
- Robins, A., M. Carpentieri, P. Hayden, J. Batten, J. Benson and A. Nunn, 2016: MODITIC WIND TUNNEL EXPERIMENTS, FFI Report (in preparation), see also Harmo17 extended abstract with the same title.
- Stuart, A. M., 2010: Inverse problems: a Bayesian perspective, *Acta Numerica*, **19**.
- Turbelin G., S. K. Singh and J.-P. Issartel, 2014: Reconstructing source terms from atmospheric concentration measurements: Optimality analysis of an inversion technique. *J. of Advances in Modeling Earth Systems*, **6**, 4, 1244-1255.

**17th International Conference on  
Harmonisation within Atmospheric Dispersion Modelling for Regulatory Purposes  
9-12 May 2016, Budapest, Hungary**

---

**MODITIC - LARGE EDDY SIMULATIONS OF DISPERSION OF NEUTRAL AND NON-NEUTRAL SCALAR FIELDS IN COMPLEX URBAN-LIKE GEOMETRIES**

*E. M. M. Wingstedt<sup>1</sup>, D. Eriksson<sup>1,2</sup>, O. Parmhed<sup>2</sup>, G. Leroy<sup>4</sup>, A. N. Osnes<sup>1</sup>, B. A. Pettersson Reif<sup>1</sup>,  
and J. Burman<sup>2</sup>*

<sup>1</sup>Norwegian Defence Research Establishment (FFI), Norway

<sup>2</sup>Swedish Defence Research Agency (FOI), Sweden

<sup>3</sup>The University Graduate Center (UNIK), Norway

<sup>4</sup>Institut National de l'Environnement Industriel et des Risques (INERIS), France

**Abstract:** Release and dispersion of a neutrally buoyant and a dense gas is modelled using the LES approach in two urban-like geometries; an array of four cubes and a part of Paris. The description of the dense gas includes a variable density formulation and a Boussinesq approach, both of which are able to satisfactorily predict the dense gas dispersion. Velocity- and concentration fields are compared to measurements from wind tunnel experiments and show overall good agreement. It is shown that the methodology used in the MODITIC project is well suited in order to model both dense and neutral gas dispersion in urban environments.

**Key words:** MODITIC, Large Eddy Simulations, dispersion modelling, dense gas, neutral gas, urban environment

## **INTRODUCTION**

Release and aerial dispersion of toxic industrial chemicals (TIC) may threaten the lives and health of an urban population. In order to estimate the consequences and to identify most effective countermeasures to limit the impact, responsible authorities need to have reliable predictions of the spatial distributions as well as the time variations of the TIC concentrations. When considering non-neutral TIC, i.e., a denser-than-air or a lighter-than-air gas, the dispersion process poses severe challenges especially in complex urban environments and is an important area of research.

The transport and dispersion of pollutants in the atmosphere are governed by the conservation laws of mass, momentum, and energy. Non-neutral gases will predominantly be transported with the wind field, but the transport may also be significantly affected by e.g. the density differences, heat exchange, and gravitational force. The density difference may severely alter the turbulence field due to the resulting stably or unstably stratified background. The stratification primarily modifies the vertical mixing process of the plume, and therefore also the overall transport process. A neutral gas, i.e. a gas with the same density as air, on the other hand will be transported with the wind field without affecting its dynamics. In both cases it is the wind field that is the most important dynamical process, and in order to model the dispersion successfully, it is crucial to accurately model the wind field.

In the past two decades Computational Fluid Dynamics (CFD) has become a more popular tool for modelling dispersion. There exists a variety of different CFD models but the Large Eddy Simulation methodology seems to be most suitable for dispersion modelling in urban areas (Lateb et al. 2016). LES resolves the inherent unsteadiness of the large scale turbulence irrespectively of the nature of the averaged flow field. Previous studies using the LES approach for modelling the dispersion of neutral gases in urban areas have shown good results (cf. e.g. Boppana et al. 2010, Fossum et al. 2012, Liu et al. 2011).

This paper describes the work conducted using the LES approach to simulate release and dispersion of neutral and dense gas in urban-like geometries. The configurations consist of an array of four cubes and an actual urban area comprising a part of Paris. Three different solvers have been used (FDS, CDP and OpenFOAM) and the description of the dense gas includes both the variable density method and the

Boussinesq approach on incompressible flow. The purpose of the study is to improve the methodology for high fidelity dispersion models and validate the results to wind tunnel data.

### SCENARIO DESCRIPTION

The transport and dispersion of a neutrally buoyant and a dense gas have been studied using both a large wind tunnel and numerical models, for two different urban-like geometries. The first consists of four cubes, with height  $h=0.11$  m, mounted on a flat plate which are to resemble an urban street canyon. The second case is an urban area of parts of Paris in scale 1:350, which in full scale correspond to approximately  $2 \text{ km}^2$ . In the latter case, two different source locations are considered (source 1 and 2) whereas only one is considered in the former (see Figure 1).

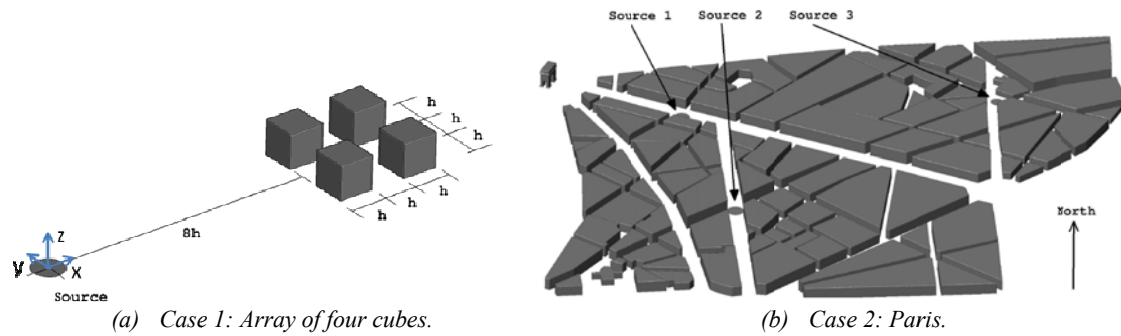


**Figure 1.** Schematics of the two configurations (a) four cubes and (b) Paris.

Flow parameters defining the incoming flow field and the emission can be found in Table 1. The dense gas used in this study is  $\text{CO}_2$ , which is approximately 1.5 times heavier than air.

**Table 1.** Parameters describing the incoming wind field and source characteristics.

Parameter	Emission rate $Q \text{ (dm}^3\text{/min)}$	Source diameter $d \text{ (m)}$	Reference velocity $U_{\text{ref}} \text{ (m/s)}$	Boundary layer height $H \text{ (m)}$	Friction velocity $U^*/U_{\text{ref}}$
Value	50	0.1	1	1	0.055

### MATHEMATICAL MODELLING

In LES, the filtered Navier-Stokes equations are solved numerically and the small scale turbulence is modelled using a sub-grid scale model. There exist a wide range of different sub-grid models and in this study both the dynamic Smagorinsky model (DS) and the localized dynamic kinetic energy model (LDKM) is used. The dynamic process governing the transport of a scalar field is described by a Eulerian convection – diffusion equation. The effect of dense gas is accounted for using either a Boussinesq approach, assuming small density variations, or with a variable density formulation. In Table 2, simulation parameters for the different solvers used are stated.

**Table 2.** Simulation parameters for the different solvers used by the partners in MODITIC.

Solver	Dense gas description	Sub-grid model	Wall functions	Inflow conditions
CDP	Variable density	DS	No	Roughness elements
FDS	Variable density	DS	Yes	Synthetic turbulence
OpenFOAM	Boussinesq	LDKM	No	Roughness elements

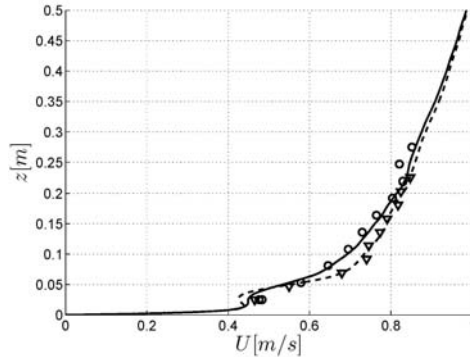
Two methods for generating the inflow boundary layer from the wind tunnel are adopted; synthetic turbulence and roughness elements. Both methods are described in detail in Osnes et al. (2016).

### RESULTS AND DISCUSSION

In the following evaluation, computed flow quantities and concentrations are compared to experimental wind tunnel measurements.

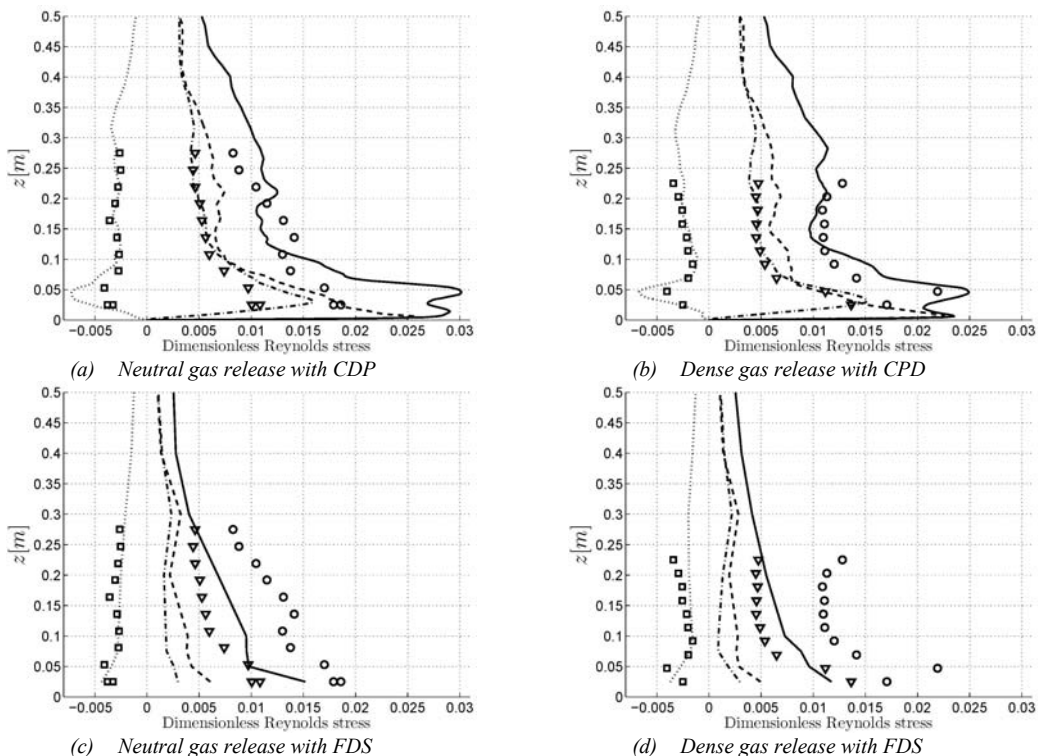
### Case 1: Array of four cubes

Figure 2 displays the vertical variation of the mean streamwise velocity component across the boundary layer for neutral and dense gas release at a position located in between the cubes  $(x,y)=(9.5h,0)$  (cf. Figure 1a) using the CDP solver. Similar profiles are observed with the FDS solver. Comparison with the experimental data shows very good agreement and we are able to predict the effect of the dense gas release on the wind field.



**Figure 2.** Vertical profiles of mean streamwise velocity for neutral and dense gas release at  $(x,y)=(9.5h,0)$ . Symbols denote experimental measures (neutral  $\circ$ , dense  $\nabla$ ) and lines numerical results (neutral —, dense ---) using the CDP solver.

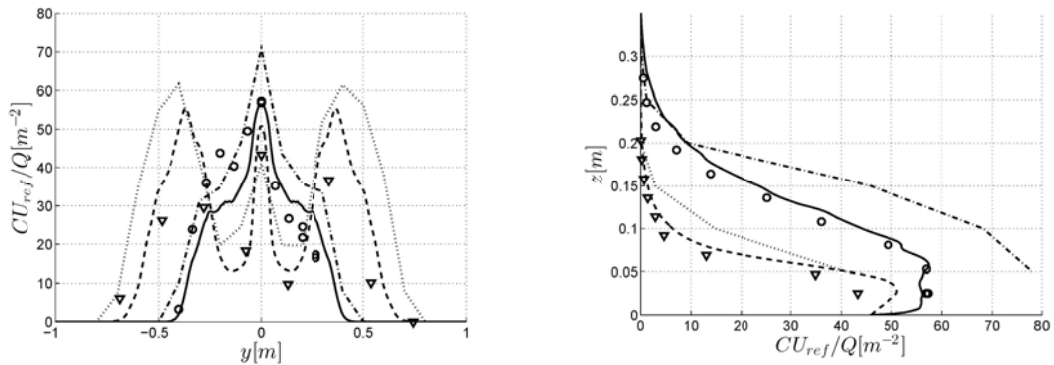
Figure 3 shows the vertical distribution of the dimensionless Reynolds stresses taken in the same position as in Figure 2. The dominating Reynolds stresses are predicted with good results for both the neutrally buoyant (Figure 3a,c) and the dense gas (Figure 3b,d). FDS gives a slight underprediction of the stresses which is most likely due to the synthetic turbulence at the inflow and the grid resolution. The release of dense gas seems to affect the level of turbulence kinetic energy.



**Figure 3.** Vertical variation of Reynolds stresses at  $(x,y)=(9.5h,0)$ . Symbols illustrate experimental measures and lines show numerical result.  $\langle u'u' \rangle$  ( $\circ$ , —),  $\langle v'v' \rangle$  ( $\nabla$ , ---),  $\langle w'w' \rangle$  ( $\nabla$ , -.-) and  $\langle u'w' \rangle$  ( $\square$ , .....).

In Figure 4 the mean concentrations are compared to experimental results. The height and width of the dispersed plumes are predicted with good agreement. The FDS solver yields slightly higher

concentrations which could be due to the reduced mixing stemming from lower turbulence kinetic energy. There is a very different dispersion pattern between the dense and the neutral gas. The dense gas forms a wider and shallower plume which is mostly deflected around the cubes, whereas the neutral gas passes through them.



(a) Lateral concentration profile at  $(x,z)=(9.5h,0.25h)$  (b) Vertical concentration profile at  $(x,y)=(9.5h,0)$   
**Figure 4.** Mean concentrations for neutral (Experiment  $\circ$ , CDP —, FDS -.-) and dense gas (Experiment  $\nabla$ , CDP ---, FDS .....).

### Case 2: Paris

The difference between the dispersion of a neutrally buoyant and dense gas close to the ground in Paris are visible in Figure 5.

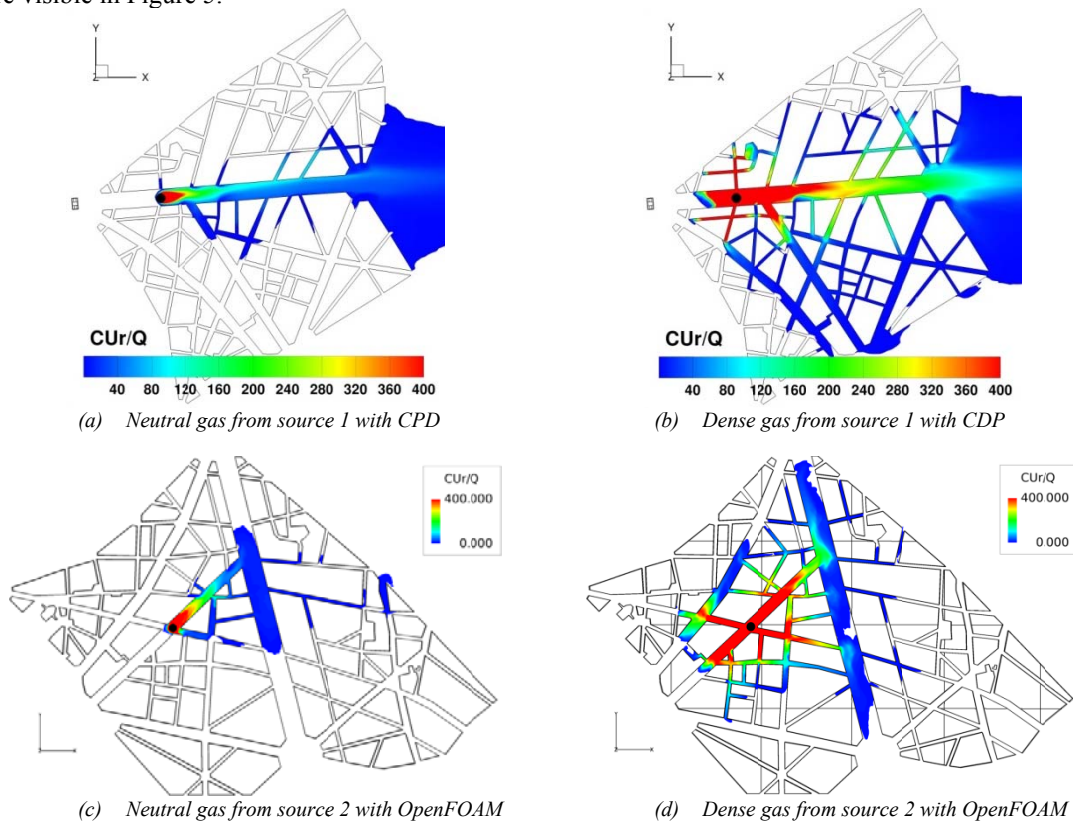


**Figure 5.** Mean concentration contours in a plane parallel to the ground at  $z = 0.01$  m.

The dense gas has a larger spanwise and shallower plume spread, with higher concentrations close to the ground, compared to the neutral gas. Interesting is the upstream transport for the dense gas (see Figures

5b,d). The interaction between the dense gas release and the wind field in the vicinity of the source results in a horse-shoe type vortex that transports the gas upstream. Similar results for source 1 (cf. Figure 5a,b) are observed for the FDS solver. Even if different source locations and dense gas models are used, similar dispersion effects are observed. Hence, the variable density and the Boussinesq approximation, assuming small density variations, seem to capture the dispersion pattern similarly.

In Figure 6, lateral and vertical measurements are compared to experiments using a method called Measure of efficiency (MOE) (Warner et al. 2001). A value of (1,1) corresponds to a perfect agreement with measurements, while a value of (1,<1) indicate that the model overpredicts the concentration at all positions. Similarly, if the MOE gives a value of (<1,1), the model underpredicts the concentration field.

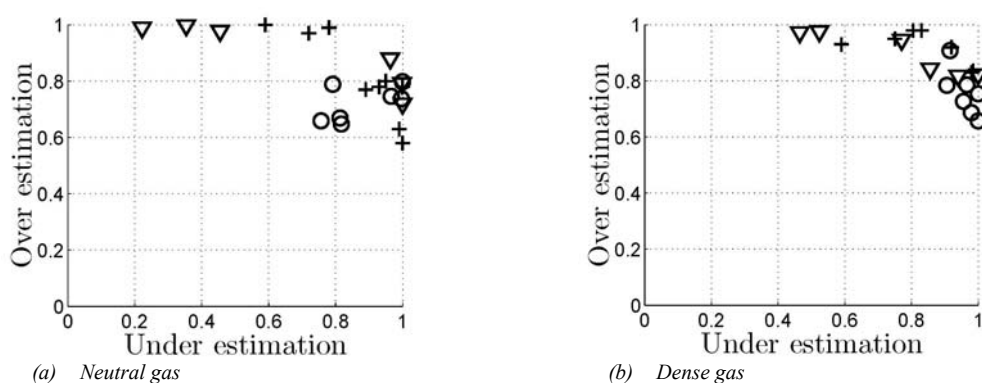


**Figure 6.** Measure Of Efficiency. CDP (○, source 1), FSD (▽, source 1) and OpenFOAM (+, source 2).

The MOE from the dense gas simulations gives slightly better results, especially when using the FSD and OpenFOAM solvers. The CDP code produces fairly consistent results for both neutral and dense gas releases which is very encouraging. It should be noted that most of the dense gas stays within the street network where the wind field is less sensitive for deviations from the experimental incoming boundary layer compared to the neutrally buoyant gas that mostly spreads above roof height.

## CONCLUSION

In this study, dispersion of neutral and dense gas in urban-like geometries has been modelled using LES. The results are compared to wind tunnel experiments and both the velocity- and concentration fields show good agreement. Due to the coupling with the wind field, dense gas is dispersed differently than the neutral gas, with higher concentrations close to the ground, upwind spread, and a wider plume. The neutrally buoyant gas is to a higher degree transported above the building-like structures, where the wind field is more affected by the atmospheric boundary layer. In order to accurately predict the dispersion above building structures it is crucial to have appropriate inflow conditions. Both the variable density method and the Boussinesq approach imbedded within the framework of LES give acceptable results for urban dispersion.

## ACKNOWLEDGEMENTS

This work was conducted within the European Defence Agency (EDA) project B-1097-ESM4-GP “Modelling the dispersion of toxic industrial chemicals in urban environments” (MODITIC).

## REFERENCES

- Boppana, V. B. L., Xie, Z. T., & Castro, I. P. (2010). Large-eddy simulation of dispersion from surface sources in arrays of obstacles. *Boundary-layer meteorology*, 135(3), 433-454.
- Fossum, H. E., Reif, B. P., Tutkun, M., & Gjesdal, T. (2012). On the use of computational fluid dynamics to investigate aerosol dispersion in an industrial environment: a case study. *Boundary-layer meteorology*, 144(1), 21-40.

- Lateb, M., Meroney, R. N., Yataghene, M., Fellouah, H., Saleh, F., & Boufadel, M. C. (2016). On the use of numerical modelling for near-field pollutant dispersion in urban environments– A review. *Environmental Pollution*, 208, 271-283.
- Liu, Y. S., Cui, G. X., Wang, Z. S., & Zhang, Z. S. (2011). Large eddy simulation of wind field and pollutant dispersion in downtown Macao. *Atmospheric environment*, 45(17), 2849-2859.
- Osnes, A. N., Eriksson, D., & Reif, B. A. P. (2016). MODITIC – On the generation of inflow boundary conditions for dispersion simulations using Large Eddy Simulations. *Proc. HARMO17*, 9-12 May 2016, Budapest, Hungary
- Santiago, J. L., Martilli, A., & Martín, F. (2007). CFD simulation of airflow over a regular array of cubes. Part I: Three-dimensional simulation of the flow and validation with wind-tunnel measurements. *Boundary-layer meteorology*, 122(3), 609-634.
- Warner, S., Platt, N., Heagy, J. F., Bradley, S., & Bieberbach, G. (2001). User-oriented measures of effectiveness for the evaluation of transport and dispersion models, IDA Paper P-3554.

**17th International Conference on  
Harmonisation within Atmospheric Dispersion Modelling for Regulatory Purposes  
9-12 May 2016, Budapest, Hungary**

---

**MODITIC- ON THE GENERATION OF INFLOW BOUNDARY CONDITIONS FOR  
DISPERSION SIMULATIONS USING LARGE EDDY SIMULATIONS.**

*Andreas N. Osnes<sup>1</sup>, P. Daniel Eriksson<sup>1,2</sup> and B. Anders Pettersson Reif<sup>3</sup>*

<sup>1</sup>Norwegian Defence Research Establishment (FFI), Norway

<sup>2</sup>Swedish Defence Research Agency (FOI), Sweden

<sup>3</sup>The University Graduate Center at University of Oslo (UNIK), Norway

**Abstract:** Development of realistic inflow conditions is crucial to successful use of Large Eddy Simulations in dispersion simulations. In this paper, three different strategies for the development of inflow conditions are presented, and the resulting turbulent statistics for each method are presented and discussed in relation to wind-tunnel experiments conducted at Laboratoire de Mécanique de Lille, and a set of urban dispersion experiments conducted in the MODITIC project. The POD-LSE method is found to give a realistic high Reynolds number turbulent boundary layer, but is not readily applied to arbitrary geometries. For reproducing the flow-field in the urban dispersion wind tunnel experiments, a precursor simulation with a numerical mesh that included the roughness elements used in the experiments was found to be a suitable method.

**Key words:** *MODITIC, Computational Fluid Dynamics, Large Eddy Simulations, Inflow conditions, Proper Orthogonal Decomposition, Linear Stochastic Estimation*

## **INTRODUCTION**

Computational fluid dynamics methods can be used to accurately describe the dispersion of aerosols and neutral gases in urban environments. The case of urban dispersion of neutrally buoyant gas has been investigated quite extensively in the past, see e.g. Liu et al (2011) and the reviews by Tominaga and Stathopoulos (2013) and Lateb et al. (2016). The case of urban dispersion of a non-neutrally buoyant gas is significantly more difficult, and requires sophisticated models that include the two-way dynamic coupling between the gas-phase and the air flow field. Large Eddy Simulations (LES) are potentially able to accurately account for this two-way coupling, but have the disadvantage of sometimes being overwhelmingly computationally expensive. However, LES can be put to good use by providing detailed data-bases that can serve as a basis for improved understanding of the complex physical processes governing the dispersion of non-neutral gases. These data-bases can also be used in combination with fast operational models for specific geometries, i.e. cities or industrial locations, where the dispersion of gas from a specific location can be predicted rapidly using pre-computed wind-fields from LES, such as e.g. the CT-analyst framework (Boris et al, 2010).

The usefulness of LES can however partly diminish due to unknown or inconsistent inflow boundary conditions. In order to minimize the effect of inappropriate inflow boundary conditions, excessively large computational domains or precursor simulations are often used. These methods significantly increase the computational cost and alternatives are sought. Here, three different approaches for generating inflow conditions for dispersion simulations using LES performed at the Norwegian Defence Research Establishment (FFI) within the MODITIC project (EDA project B-1097-ESM4-GP) are presented and discussed. This project investigated the dispersion of neutral and non-neutral gas in urban environments using both with tunnel experiments and numerical simulations. First a method applying proper orthogonal decomposition (POD) together with linear stochastic estimation (LSE) is presented. In the next section, results obtained with a synthetic turbulence method are presented. This method generates random velocity fluctuations with given statistical properties and these are superimposed onto a known mean flow. Lastly the advantages of using precursor simulations are discussed, and results from two precursor simulations

are presented. Throughout this paper  $u$ ,  $v$ , and  $w$  denote the streamwise, spanwise and wall-normal fluctuating velocity components respectively.

### POD-LSE

Proper orthogonal decomposition is a method which decomposes a given field into a set of orthogonal modes with the property that for any finite number of modes  $N$ , the set of  $N$  modes used is the set that minimizes the difference between the original field and the reconstructed field. The method was first used in turbulence analysis by Lumley (1967) for identifying dynamical structures with finite energy. In the present study, POD was used on particle image velocimetry (PIV) data from a high Reynolds number turbulent boundary layer experiment conducted at LML (Laboratoire de Mécanique de Lille, France). This experiment was conducted in a wind tunnel with a 20 m long test section and a cross-section of 1x2 m. The free-stream velocity was 10 m/s, and the resulting boundary layer had a momentum thickness Reynolds number of 19100. The boundary layer thickness at the measurement position was  $\delta = 30$ . The application of classical POD on a two-dimensional velocity field gives the following formulation:

$$\int_D R_{ij}(y, y', z, z') \phi_j^{(n)}(y', z') = \lambda^{(n)} \phi_i^{(n)}(y, z) \quad (1)$$

where the kernel  $R_{ij}$  is the two-point cross-correlation tensor of the fluctuating velocity field:

$$R_{ij} = \langle u_i(y, z) u_j(y', z') \rangle \quad (2)$$

where  $\langle \rangle$  represents an ensemble average, here defined as the average over the ensemble of PIV-planes measured in the experiment.

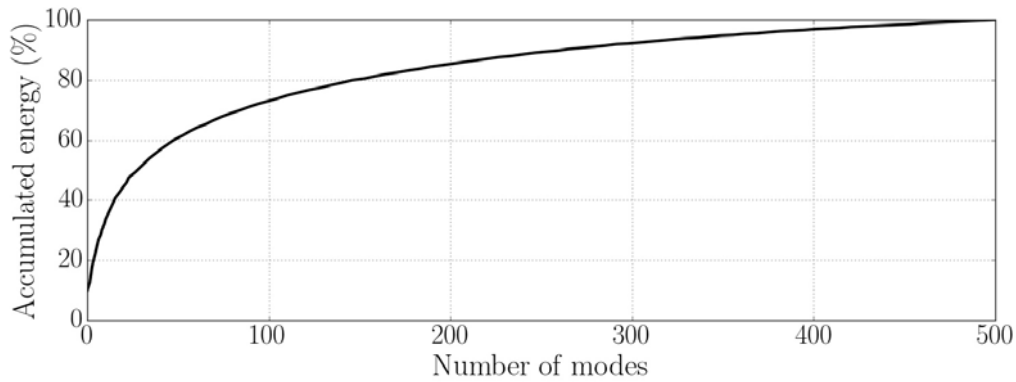


**Figure 1** Accumulative content of energy in the POD modes, in %, as a function of number of modes.

Wingstedt et al. (2013) used linear stochastic estimation in combination with POD to construct a velocity field which was highly resolved in both space and time. The PIV-planes, which were highly resolved in space but poorly resolved in time, was combined with hot-wire data, which were poorly resolved in space but highly resolved in time, and a velocity field was constructed based on these. This method also enables reconstruction of a velocity field based on a smaller number of modes while retaining most of the energy in the flow field. The energy content as a function of number of modes is shown in Figure 1. As can be seen, the accumulative energy rapidly increases for the first modes and then flattens as the number of modes increases.

Using this method for generating the inflow boundary condition, a number of turbulent boundary layer simulations were performed. All simulations discussed here were performed with the node-based finite volume incompressible flow solver "Cliff" from Cascade Technologies Inc. (CTI, 2014). Velocity fields with varying amounts of energy were constructed by varying the number of POD-modes, and for each constructed velocity field, a turbulent boundary layer simulation was performed. The numerical simulations used a domain of size 3x0.6x0.3 m in the streamwise, wall-normal and spanwise directions respectively. The number of cells in each direction were 1000, 150 and 100 and the cells were uniformly distributed in the streamwise and spanwise directions. In the wall-normal direction, geometric stretching of the cells was used to obtain a finer spatial resolution close to the wall. The reconstructed velocity field

did not cover the entire inlet-plane, missing a small area close to the wall and an area above the boundary layer. In these areas the velocity field was extended by interpolating between zero velocity at the wall and the experimental points closest to the wall, and a constant velocity above the boundary layer.

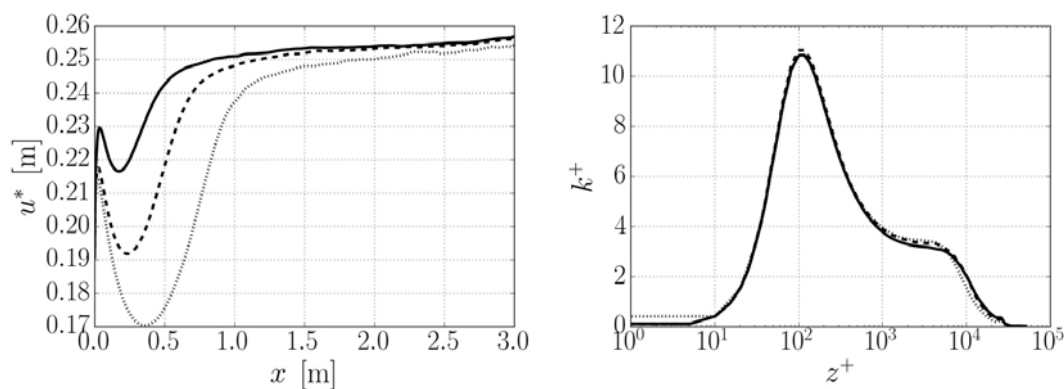


**Figure 2.** Left: Friction velocity throughout the domain. Right: Turbulent kinetic energy for the turbulent boundary layer simulations with varying inflow energy (in wall units). Solid lines: 100% energy, dashed lines: 75% energy, dotted lines: 50% energy.

The friction velocities obtained from these simulations are shown in Figure 2. As can be seen, the friction velocities have a region close to the inlet where they change rapidly as functions of downstream distance  $x$ , but they eventually stabilize to almost the same value for all three configurations. The turbulent kinetic energy at the end of the computational domain is also shown in Figure 2. The resulting peak and plateau structure of the turbulent kinetic energy is characteristic of high Reynolds number turbulent boundary layers. As can be seen, the profiles collapse to almost identical forms when scaled by wall units, indicating that a similar flow field is achieved using all three inflow energies.

#### SYNTETHIC TURBULENCE INFLOW

As the POD-LSE method generates approximated velocity fields based on a given original field, it is not readily applicable to applications where a velocity field is not known both in space and time. The extension to other geometries and scales is also not straightforward. For this reason, it was not applied to the urban dispersion simulations performed at FFI within the MODITIC project. Instead, a turbulent velocity field was approximated by a random-field generation method in which turbulence scales are prescribed and fluctuations are superimposed on a known mean velocity field. This field was subsequently used as the inlet boundary condition for the LES. This method can be applied directly to a dispersion simulation, but can also be used as input to precursor simulations, as discussed below. A problem with this method is that the constructed velocity field is not generally a solution to the LES equations themselves on the specific numerical grid used. Because of this, when the reconstructed velocity field is used as inflow, there is a region between the inlet and some point downstream where the velocity field is adjusting to the mesh, similar to the initial region in Figure 2. This region is typically long, especially if the spectral content is not realistic (Keating, 2004), e.g. if random noise is used for the velocity fluctuations. Because it is preferred that the interesting region in the simulation is located outside the initial adjustment region, the direct use of synthetic turbulence inflow can be very computationally expensive. A simulation was performed, where a synthetic inflow method was applied by prescribing the Reynolds stress profiles along with the mean velocity profiles measured in the wind-tunnel experiments performed at the Environmental Flow Research Centre in Surrey, within the MODITIC project. This simulation used a computational domain of  $10 \times 3.5 \times 1.5$  m with 140, 280, and 101 cells in the streamwise, wall-normal and spanwise directions, respectively. Geometric stretching of cells was used in the wall-normal direction. Figure 3 shows Reynolds stress profiles at the end of the domain and the friction velocity throughout the domain. As can be seen, the Reynolds stresses do not agree very well with the experimental values, and are closer to the profiles that correspond to a flat-plate boundary layer. The friction velocity, also shown in Figure 3, can be seen to stabilise after about 2 m, which is comparable to the length of the adjustment region obtained with the POD-LSE method, when scaled by the boundary layer thickness (here 1.0 m).

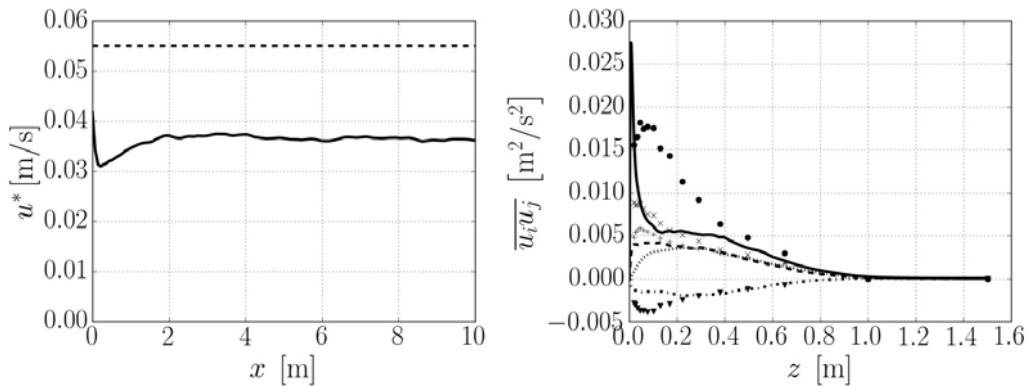


**Figure 3.** Left: friction velocity throughout the domain. Right: Reynolds stress profiles in the flat plate turbulent boundary layer simulation with synthetic turbulence inflow. Solid line:  $uu$ , dashed line:  $vv$ , dotted line:  $ww$ , dash-dotted line:  $uw$ . Symbols indicate the experimental values,  $\bullet$ :  $uu$ ,  $\times$ :  $vv$ ,  $+$ :  $ww$ ,  $\blacktriangledown$ :  $uw$ .

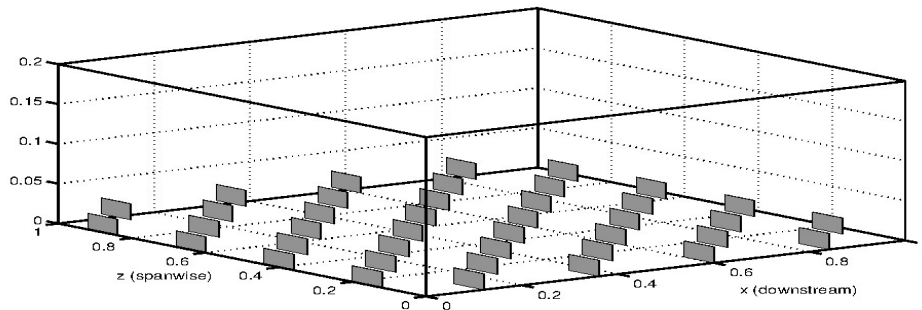


**Figure 4.** Sketch of the roughness elements used in the precursor simulation and their relative configuration.

## USING THE METHOD OF PRECURSOR SIMULATIONS

Using synthetic turbulence as inflow conditions directly to a dispersion simulation significantly increases the computational cost due to the need for an initial and quite large adjustment region that computationally needs to be resolved. A precursor simulation can be suitable, especially when the same inflow can be used for multiple simulations. This was the case in the MODITIC project, where release of neutral and non-neutral gas from different source locations and with different geometries were considered. Most of the wind tunnel experiments used the same upstream turbulent boundary layer and therefore the precursor simulation method was suitable. Two different precursor simulations were performed. One simulation on a flat-plate geometry, as discussed above, and one simulation with roughness elements. The flat-plate precursor simulation was used to obtain the final inflow for simulations of dispersion over the MODITIC hill performed at FFI.

### Precursor simulation with roughness elements

The synthetically generated turbulence inflow conditions considered above did not provide Reynolds stress profiles that corresponded well to the experimental results. For this reason, a precursor simulation was performed, where roughness elements, consisting of thin plates, were placed onto the floor. These roughness elements correspond geometrically to the ones used in the wind tunnel. A sketch of the roughness elements and their configuration is shown in Figure 4. The total number of cells in the computational mesh used here was  $10^7$ . As inflow conditions for the precursor simulation the synthetic turbulence method was used. Figure 5 shows the Reynolds stress profiles obtained just before the last row of roughness elements in this simulation. As can be seen, they are in much better agreement with the experimental results than those obtained with the flat-plate precursor simulation. The velocity field obtained with this method was used as inflow for all the dispersion simulations performed at FFI within the MODITIC project, except those with the hill geometry.

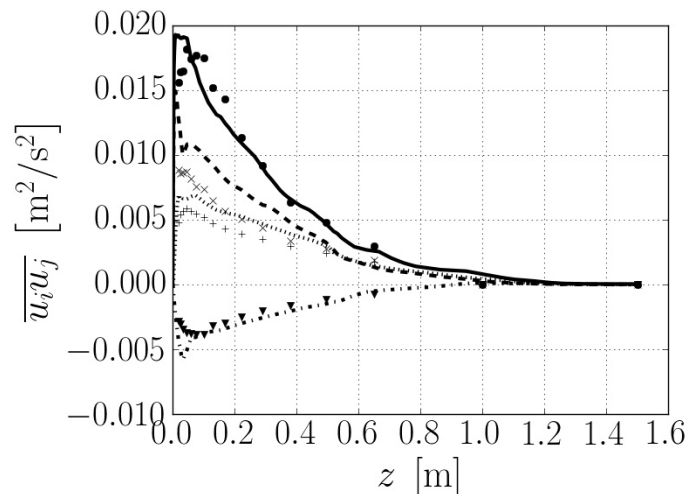


**Figure 5.** Reynolds stress profiles in the roughness boundary layer simulation with synthetic turbulence inflow. Solid line: uu, dashed line: vv, dotted line: ww, dash-dotted line: uw. Symbols indicate the experimental values, • : uu, × : vv, +: ww, ▼ : uw.

## CONCLUSIONS

Three methods for generating time-varying inflow conditions for dispersion simulations using LES have been evaluated. The POD-LSE method was shown to give results that correspond very well to the high Reynolds number turbulent boundary layer upon which the POD field was based, and did not require a long initial adjustment region. However, the method is not readily applicable to arbitrary geometries, and was therefore not used for any dispersion simulations within the MODITIC project. The synthetic inflow method was used for generating inflow for two different precursor simulations, which were subsequently used as inflow for the dispersion simulations performed at FFI. Of the precursor simulations, the roughness element simulation gave results in best agreement with the experimental flow field, and therefore the velocity field from this simulation was used as inflow for most of the dispersion simulations.

## REFERENCES

- Boris, J, G. Patnaik, K. Obenschain, A. Moses, M.-Y. Obenschain, T. Young Jr, J. Delaney, J. Donnelly, 2010: Fast and accurate prediction of windborne contaminant plumes for civil defense in cities, Proceedings of the 5th international symposium, Computational wind engineering conference (CWE'2010), 23–27.
- CTI, 2014, Cascade Technologies Inc. User's & Developer's Manual, Jefferson Release Version 4.1.0.
- Keating, A, U. Piomelli, E. Balaras and H.-J. Kaltenbach, 2004: A priori and a posteriori tests of inflow conditions for large-eddy simulation. *Phys. Fluids* **16**, 4694–4712.
- Lateb, M, R. N. Meroney, M. Yataghene, H. Fellouah, F. Saleh, and M. C. Boufadel, 2016: On the use of numerical modelling for near-field pollutant dispersion in urban environments – A review, *Environmental Pollution* **208**, 271–283.
- Liu, Y.S, G. X. Cui, Z. S. Wang and Z. S. Zhang, 2011: Large eddy simulation of wind field and pollutant dispersion in downtown Macao, *Atmospheric Environment* **45**, 2849–2859.
- Lumley, J. L, 1967: The structure of inhomogeneous turbulent flows. *Atmospheric turbulence and radio wave propagation*, 166–178.
- Tominaga, Yoshihide and T. Stathopoulos, 2013: CFD simulation of near-field pollutant dispersion in the urban environment: A review of current modeling techniques. *Atmospheric Environment* **79**, 716–730.
- Wingstedt, E. M. M, M. Vartdal, A. N. Osnes and M. Tutkun, 2013: Development of LES inflow conditions for turbulent boundary layers, FFI/report 2013/02420.

**17th International Conference on  
Harmonisation within Atmospheric Dispersion Modelling for Regulatory Purposes  
9-12 May 2016, Budapest, Hungary**

---

**MODITIC OPERATIONAL MODELS**

*Oscar Björnham<sup>1</sup>, Arnaud Gousseff<sup>2</sup>, John Tørnes<sup>2</sup> and Stephane Burkhart<sup>3\*</sup>*

<sup>1</sup> Swedish Defence Research Agency

<sup>2</sup> Norwegian Defence Research Establishment

<sup>3</sup> Direction Générale de l'Armement (DGA)

\* Corresponding author, [stephane.burkhart@intradef.gouv.fr](mailto:stephane.burkhart@intradef.gouv.fr)

**Abstract:** Events including toxic substances can be dangerous and difficult for first responders to handle since there is often limited time for decisions regarding evacuation of nearby regions. There are many quick operational models that simulate atmospheric dispersion and thereby provide guidelines for which risk area to expect. A few different models are evaluated in this work against real scale and wind tunnel experiments with the main emphasis on dense gas. The models have different merits and shortcomings with regards to their ability to handle dense gases and complex geometries which are briefly covered here.

**Keywords:** *Atmospheric dispersion, QUIC, PUMA, ARGOS, Lagrangian model.*

## **INTRODUCTION**

Unexpected events involving hazardous substances are of growing concern in today's societies. In the case of an outdoor release, the area of impact is by far the largest if the released substance is in gaseous form. The ambient advection and turbulence of the air will then lead to a dispersion process causing a spread and subsequent dilution of the concentration. Many chemicals are stored as liquefied gas for practical reasons. The rapid decrease of pressure after a sudden release in combination with a limited infusion of heat leads to a dense gas dispersion. This means that the released substance is in gaseous form with high density and will therefore spread close to the ground, which strongly reduces the vertical dilution process resulting in an increased area of potentially dangerous concentration levels. Dense gas modelling has been the main target for the EDA project MODITIC which has treated many aspects of the problem. The project has included large scale field experiments and downscaled wind tunnel experiments. These results have then been used to benchmark different models that simulated the same geometries and scenarios. There are a wide selection of dispersion models that are useful for different situations. Here we discuss a chosen set of operational models, i.e., close to real-time models, which have been tested upon several different cases spanning geometries from open field dispersion to the complex geometry of central Paris.

## **ARGOS**

ARGOS is sold by PDC-ARGOS (Denmark) and is an operational commercial software for crisis analysis involving CBRN agents (PDC-ARGOS, 2016). It deals with scenarios such as gas releases (no liquid discharge), fires, explosions and nuclear accidents. The dispersion sub-model Rimpuff is a local scale puff model taking into account local wind variations and turbulence levels. It can also calculate dry and wet deposition. ARGOS includes models for estimating the releases from containers and pipes as well as evaporation of spills on the ground and has also a special model for dispersion of heavy gasses. Heavy gases behave quite different than normal aerosols or smokes from fires. ARGOS can geo-reference a domain and import user specified meteorological profiles, weather profiles from meteorological towers or numerical weather prediction (NWP) data. A database is included for a number of substances. Based on the properties in the chemical database, ARGOS can calculate suggestions for emergency zones based on the levels of concerns for the substances involved in the incident. Obstacles can be taken into account through the sub-model Urban Dispersion Model (URD) which has been used for the Paris scenario. Since ARGOS cannot use URD for dense gas releases, only the neutral gas release has been modelled in the

Paris scenario. For the INERIS case, the heavy-gas module was used for the release of ammonia without any obstacle present, while neutral gas only was released against the obstacle.

### **QUIC**

QUIC (Quic Urban and Industrial Complex) is developed at LANL laboratory, US, and is specifically designed for treating crisis urban scenarios with TICs, C, B and R agents and a number of source terms (Los Alamos National Laboratory, 2016). A material database is not provided, so users have to enter their own material properties. The wind field is computed from a diagnostic mass preserving model. QUIC-PLUME uses Lagrangian random-walk dispersion model, accounting for building-induced turbulence to reconstruct the chemical concentration field. Buildings are constructed either manually, based on simple available geometrical forms, or automatically from imported shape files. Winds can be provided as academic laws or imported discrete data profiles in multiple points. Multiphase releases are also available in addition to basic source terms.

### **PUMA**

The Swedish Defence Research Agency (FOI) develops a custom made program suit for atmospheric dispersion called FOI Dispersion Engine (DE). Several models are included in DE that together span the entire spectrum of temporal and spatial scales needed when dealing with dispersion issues. The model PUMA is designed to operate in real-time and utilizes Gaussian puffs in a Lagrangian approach. The puffs are semi-symmetrical discrete puffs that collectively represent the entire concentration field from one or several sources. In the case of neutral gas the puffs are independent of each other and evolves due to parameterized turbulence as they are transferred according to the meteorological circumstances. PUMA has been extended to also include dense gas physics. The main phenomena that capture the nonlinear dense gas case have been developed and implemented. The introduction of dense gas implies a transition from independent to dependent puffs. Since the main idea with PUMA is to be as fast as possible, the puffs are still treated individually to a high extent. Basically each puff is first treated separately and independently with the inclusion of dense gas physics. In the next step dependencies between overlapping puffs are treated. The model is still under development and the results here represents the model status at the end of 2015.

### **PMSS**

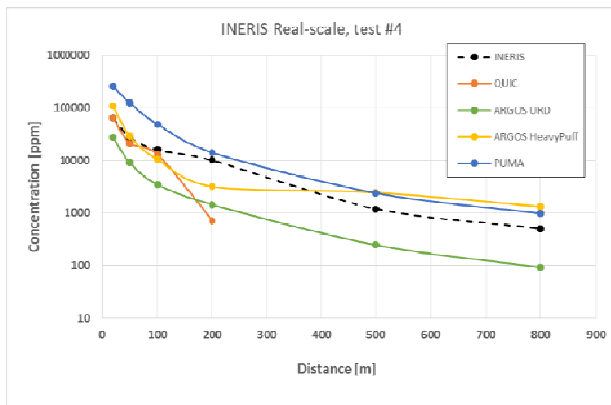
ARIA Technologie is a French company has developed PMSS (Parallel Micro Swift Spray) as a micro-scale version of its own models of wind computation (SWIFT) and agent atmospheric dispersion modelling (SPRAY) (ARIA VIEW, 2016). This version allows for obstacles in a simplified way and performs the dispersion computation in a Lagrangian mode. Obstacles can be isolated or representing a town district. PMSS software is thus constituted by two modules: Micro Swift that computes diagnostic 3D wind field and Micro SPRAY that computes 3D dispersion. It is necessary to pre-process building description files to be readable by PMSS through the translator SHAFT provided by ARIA. A dense gas module exists, but is not at the time available in the version in use at DGA CBRN Defense. It is worth mentioning that PMSS is part of the CERES software (CEA, FR) and also integrated in a HPAC version that is not available in France.

## **REAL SCALE EXPERIMENTS - INERIS**

An outdoor release experiment of ammonia has been conducted at the Centre of Scientific and Technical Studies of Aquitaine (CEA-CESTA) in France. The release site has a radius of approximately two kilometres, is flat and free from any obstacles (Gentilhomme, 2013).

### **Without obstacle, test #4**

Ammonia was released with an average flow rate of 4.2 kg/s through a release device placed on a square (10 m x 10 m) concrete slab, approximately 15 cm thick. The test was a reference case with a horizontal release through a 50.8 mm diameter orifice without any obstacles. The temperature during the test was 12.5 °C, the relative humidity 82% and the wind velocity was 3 m/s at 7 m height. The experiment was simulated using ARGOS, QUIC and PUMA.



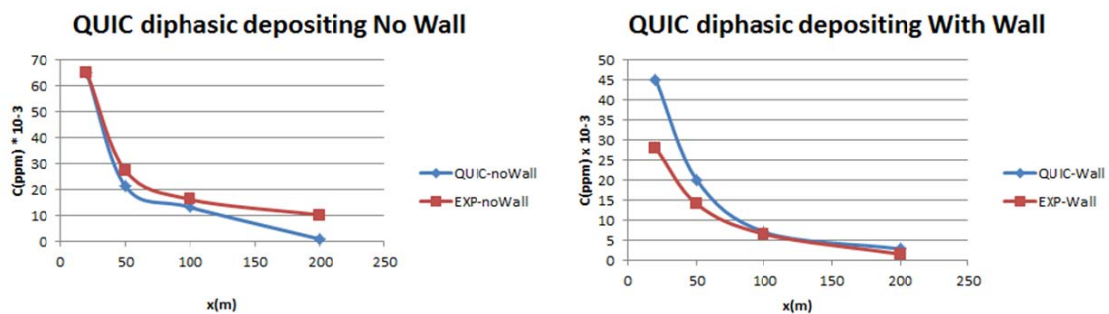
**Figure 1.** Comparison of experimental and simulation results for the plume centerline concentration at 1.0 meters height above the ground.

Figure 1 shows that the results from the HeavyPuff module in ARGOS are much closer to the measurements done at INERIS than the results from ARGOS using the URD module. This is because compressed ammonia act as a heavy gas close to the release site and this is not captured by the URD module. In this case ARGOS uses the HeavyPuff module up to 440 m from the release site, where Rimpuff takes over. PUMA constantly over-predicts the plume centreline concentration. However, the relative concentration change over distance is quite close to that of the experimental data.

QUIC multiphase pick results are shown for the case without obstacle in orange colour in Figure 1 and in the left panel in Figure 2. The jet horizontal direction is well taken into account (not possible for passive release) and leads to a good correlation in close field (distance <100m). In far field, too much deposition imposed to the model leads to a strong underestimation.

**With obstacle, test #5**

In this case the jet is obstructed by a concrete wall of dimension 3x3 meters located 3 meters from the source.



**Figure 2.** QUIC dense gas release without wall (left) and with wall (right)

In the case with obstacle in the close-field (right panel in Figure 2), the correlation between QUIC and the experiment is not as good as in the no-obstacle case. This is caused by the fact that rainout is not considered in the model. Some dilution by the obstacle takes place (compare with the no obstacle case) and a good far-field correlation is retrieved.

**WIND TUNNEL EXPERIMENTS – PARIS**

Extensive down-scaled, geometrically by a factor of 350, experiments were conducted at the EnFlo ‘meteorological’ wind tunnel University of Surrey (Robins et al., 2016). Many different cases were investigated using both neutral and dense gases. The most complex case included the urban region of Paris centred on Champs-Élysées. The same geometry was also utilized in a study of operational models and the results are here compared.

ARGOS has been used in full scale for the calculation of the Paris scenario.

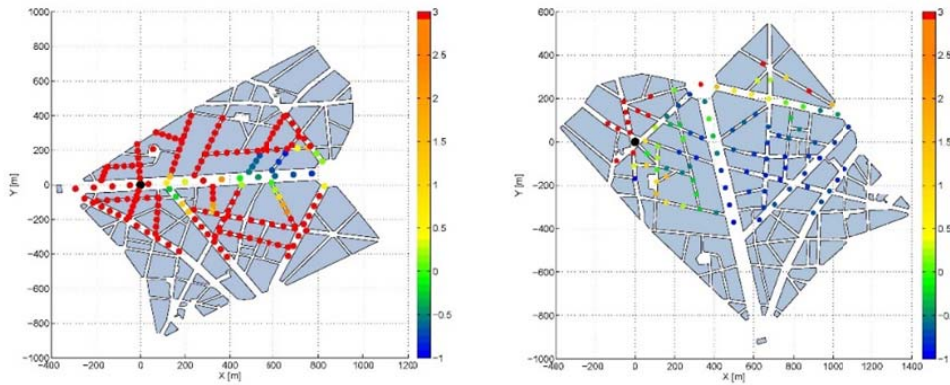


**Figure 3.** Comparison of ARGOS concentrations with wind tunnel measurements (Source position S1 to the left and S3 to the right). Positive values indicate factors of over-prediction and negative values indicate factors of under-prediction. The black dot shows the position of the source. The wind direction is from left to right in the figures.

Since most of the significant concentrations of air in the wind tunnel from source position S1 are not retained as much as from the other source positions, but channeled along Champs-Élysées, a large portion of the predicted ARGOS concentrations outside Champs-Élysées are higher than in the wind tunnel (left panel in Figure 3). However, the overestimation by Argos upstream of S1 is not significant, as they represent very small concentration values. ARGOS also predicts a faster decrease of agent concentration along Champs-Élysées compared to the wind tunnel, resulting of under-prediction of the air concentration at the longest distances from the source. When the source is located in a more enclosed position (S3), where the wind is not channeled along large avenues, ARGOS produces results more similar to wind tunnel measurements (Right panel in Figure 3).

**PMSS** has been used for the Paris cases (presented here for source positions S1 for passive gas release). Results are presented as

- Analysis rates (MOE1=overlapping between experiment and simulation, Occurrence=probability to observe a given concentration)
- MOE2 indicating performances of false positive (FP) against false negative (FN) rates
- FAC2 and FAC10 values for individual concentrations and all concentrations

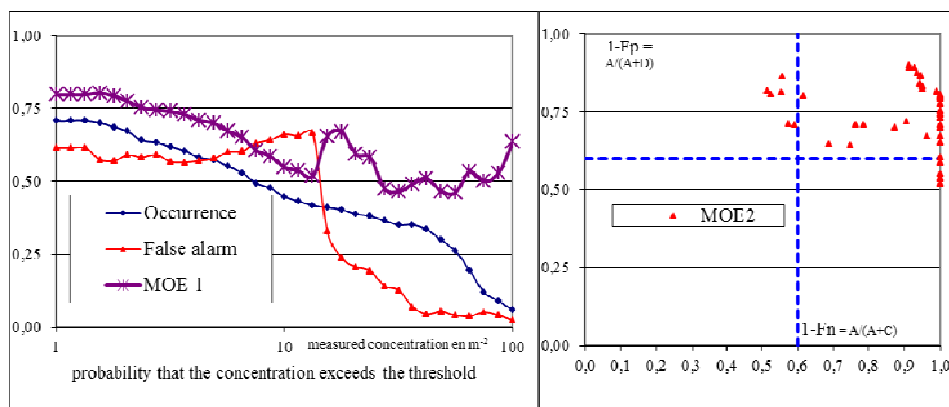


**Figure 4.** Left panel, false alarm represent ~60% for low concentrations  $< 10\text{m}^{-2}$  in streets a few hundred meters from the source. Much better False Alarm rates ( $< 25\%$ ) are obtained if we cut at  $10\text{m}^{-2}$ . MOE1  $> 50\%$  is acceptable for validation purpose. Right panel, points are in general centered in a 60% square. A few false positives and false negatives in far field are probably due to an orientation shift between experiment and simulation.

## GENERAL CONCLUSIONS

In this study, we wanted to assess the capabilities of current national members' in-use operational models to handle complex urban dispersion of dense gas release. Referring to COST action ES1006 (COST ES1006 (1), COST ES1006 (2)) on the use of atmospheric dispersion models in emergency response tools, we confirm a number of statements: 1) The different types of operational tools require different skill or expertise levels. The execution time for the simulations varies from minutes to hours. The most time consuming and demanding part is the setup of the models and to couple them to meteorology and source term descriptions. 2) The type of response to give to decision makers is not straightforward: shall we give risk zones corresponding to concentrations, confidence intervals or percentiles to be in such limits. 3) These models are usually conservative, and overestimate the concentration levels close to the source which may lead to an exaggerated decisions. In addition to these remarks, our current models are not all capable to handle dense gas dispersion, and take into account obstacles or complex geometries.

QUIC software seems to work well using the included dense gas sub-model (compared to INERIS Ammonia release data). The latest developments on PUMA have been tested with promising results in the scope of this project, dealing with dense puff interaction, in a semi-linearized way to keep the response fast enough. PUMA is a real-time model and is not able to treat obstacles and is therefore not suitable for complex geometries. ARGOS heavy puff model also provides good results for dense gas on open field but cannot handle obstacles in combination with dense gas. Regarding obstacles, ARGOS URD model with RIMPUFF puff model is mainly suited to a densely built urban like area but can only handle passive gas. On the PARIS case, tendency to overestimate by a factor of 3 to 5 close to the source, and underestimate by such in far field, was observed and explanations were proposed. PMSS was tested against the PARIS case for passive gas only and behave quite satisfyingly. Overestimations of concentrations behind buildings and underestimations in main streets was usually observed. This semi-operational tools demand some skill to scale and import shape files of the urban area. A dense gas module exists but was not available at the time.

In conclusion, as far as we tested our models, only QUIC has proved able to handle both obstacles and dense gas, PUMA was modified to handle dense gas characteristics but lacks functionalities on urban geometries. PMSS and ARGOS were partially validated with passive gas on urban scenarios, but dense gas module remain to be tested/developed. These models are not push-button tools and require various level of expert skills. The advantage against CFD is their cheap computer cost, but they still need relatively large set-up times compared to the run-time. For a substantially more thorough description of the models and all results we refer to the project report (Burkhart, Gousseff, Tørnes, & Bjørnham, 2016).

## ACKNOWLEDGEMENT

This work was conducted within the European Defence Agency (EDA) project B-1097-ESM4-GP "Modelling the dispersion of toxic industrial chemicals in urban environments" (MODITIC).

## REFERENCES

- ARIA View, 2016: ARIA Technologies, <http://www.aria.fr>.
- Burkhart, S., Gousseff, A., Tørnes, J., & Bjørnham, O. 2016. MODITIC - Simulation Report on Operational Urban Dispersion Modelling
- COST ES1006 (1), April 2015: Best Practice Guidelines for the use of Atmospheric Dispersion Models in Emergency Response Tools at local-scale in case of hazmat releases into the air, COST European Cooperation in Science and Technology
- COST ES1006 (2), April 2015: Model evaluation case studies: Approach and results, COST European Cooperation in Science and Technology
- Gentilhomme, O., 2013. MODITIC project: Agent characterisation and source modelling, INERIS.
- Los Alamos National Laboratory, 2016: QUIC Atmospheric Dispersion Modeling System, <http://www.lanl.gov/projects/quic/index.shtml>
- PDC-ARGOS, 2016: CBRN Crisis Management, <http://www.pdc-argos.com>.
- Robins, A., M. Carpentieri, P. Hayden, J. Batten, J. Benson, A. Nunn. 2016: MODITIC Wind Tunnel Experiments. Proc. HARMO17, Budapest, May 9-12, 2016

## AUTHOR INDEX

Adachi, K.	86, 528, 598	Benešová, N.	117, 362
Adriaenssens, S.	248, 300	Benson, J.	672
Akylas, V.	346	Berbekar, E.	628
Albani, R.A.S.	371	Berchet, A.	415
Albergel, A.	492, 608	Di Bernardino, A.	324
Alessandrini, S.	150, 663	Bernnat, W.	623
Alföldy, B.	7	Bianconi, R.	96
Alpert, P.	208	Bigi, A.	340
Andreadou, M.	536	Bikse Jr., J.	237
Andronopoulos, S.	523, 504, 581, 588	Bikse, J.	237
Anfossi, D.	150	Bilińska, D.	546
Ángeles González, M <sup>a</sup>	135	Bineau, T.	432
Angyal, A.	509	Bisignano, A.	155
Antonacci, G.	160	Björnham, O.	186, 421, 667, 699
Arasa, R.	135, 283	Blumelová, J.	362
Argyropoulos, C.D.	504, 523	Bocquet, M.	528
Aristodemou, E.	400	Boganegra, L.M.	400
Armand, P.	76, 334, 432, 459, 492, 569, 576, 588, 608, 652, 613, 640, 647, 618	Boisseranc, F.	647
Arnold, D.	438	Borge, R.	277, 289, 441
Arunachalam, S.	145, 316	Borrego, C.	180
Assael, M.	319	Božnar, M. Z.	30, 171
Assennato, G.	262	Bozó, L.	166
Attree, M.	71	Brabec, M.	117
Auvinen, M.	242	Brandt, J.	376
Axelrod, K.C.	446, 453	Brandt, J.	406
Azadi, M.	466	Brännström, N.	186, 667, 683
Babinskyy, M.	227	Brännvall, T.	683
Backman, J.	242	Brunner, D.	415
Badas, M.G.	351	Brunner, J.	415
Baldauf, R.	306	Buccolieri, R.	381, 388
Balogh, M.	311	Burkhart, S.	667, 677, 683, 699
Bao, M.	191	Burman, J.	186, 667, 677, 683, 688
Barbosa, E.	498	Busch, X.	683
Barbosa, E.	487	Cabibel, N.	432
Barmpas, F.	346	Caniou, Y.	576
Barnet, J.	117	Carpentieri, M.	672
Bartzis, J.G.	357, 581	Carrera-Chapela, F.	46
Barzyk, T.	316	Carruthers, D.	66, 71
Batt, R.	582	Cartelle, D.	191
Batten, J.	672	Casares, J.J.	81
Bauerová, P.	362	Casas, C.	191
Baumann-Stanzer, K.	459, 513, 588	Castelli, S.T.	459, 588, 640
Baumann-Stanzersen, K.	51	Chambers, S.	558
Bekka, N.	487, 498	Chang, J.	96, 551
Bellasio, R.	96	Chatzimichailidis, A.	319
Belda, M.	362	Chen, L.	13, 20
Bemporad, E.	459	Chpoun, A.	498
Benamrane, Y.	432	Clappier, A.	256, 277
		Clawson, K.L.	603

Codina, B.	283	Galeriu, D.	558
Coldrick, S.	61	Galmarini, S.	96
Connan, O.	91	Gama, C.	180, 256
Conry, P.	381, 388	Gant, S.	61, 582
Contu, M.	91	Garau, M.	351
Cooke, M.C.	518	García, P.	441
Costa, S.	180	Gariazzo, C.	459, 618
Couvidat, F.	452	Garzón A.	329
Dai, W.	26, 427	Geertsema, G.	140
Dale, W.	71	Genga, A.	381, 388
Delignon, Y.	492	Gentilhomme, O.	667
Derbek, P.	362	Gerbec, M.	459
Deshmukh, P.	306	Germán, M.	197
Deutsch, F.	248, 300	Geyer, F.	438
Di Sabatino, S.	294, 371, 381, 388	Ghermandi, G.	340
Dias, D.	267	Gioia, S.	227
Didier, D.	86, 91, 528, 598	Giotta, L.	381, 388
Dimitrov, I.K.	453	Giovannini, L.	160
Djalalova, I.	663	Giua, R.	262
Domingo-Dalmau, A.	283	González, J.A.	46, 81, 191
Douarre, G.	647	González, M.Á.	283
Drzeniecka-Osiadacz, A.	217, 546	Gouillat, S.	432
Duchenne, C.	76, 334, 432, 576, 608, 613, 647	Gounaris, N.	202
Duda, F.P.	294	Gousseff, A.	699
Duma, M.	558	Gradišar, D.	30, 171
Eben, K.	117, 362	Grahn, H.	126, 186, 421
Eckhardt, S.	438	Grašič, B.	30, 171
Eckman, R.M.	603	Groma, V.	7
Efthimiou, G.C.	357, 504, 523, 581	Le Guellec, M.	13
Elbern, H.	541	Guerreiro, C.	452
Elkhalifa, S.	518	Haikin, N.	208
Ellermann, T.	406	Hanna, S.	96, 551
Ellis, A.	71	Hansen, A.B.	564
Emmenegger, L.	415	Harmati, I.	410
Endregard, M.	667	Harms, F.	41, 628
Eriksson, D.	667	Haszpra, T.	472
Eriksson, P.D.	688, 694	Havasi, Á.	658
Fabbi, S.	340	Hayden, P.	672
Falocchi, M.	160	Heinrich, G.	593
Faragó, I.	658	Hergault, V.	76
Feiz, A.-A.	20, 477, 482, 487, 498	Hermann, B.	311
Ferenczi, Z.	7, 166	Hernandez, A.	81
Fernández-Pampillón, J.	197	Hernández-Ceballos, M.A.	96
Fernando, H.J.S.	381, 388	Herring, S.	101, 459, 618
Ferrari, S.	351	Hertel, O.	376, 406
Ferreira, J.	126, 180	Hertwig, D.	41, 357
Ferrero, E.	150, 155	Hirtl, M.	438
Fierens, F.	248, 300	Hnilicová, H.	117
Finn, D.D.	603	Hoi, K.I.	126
Flandorfer, C.	438, 513	Holland, B.	26, 427
Flassak, T.	466	Hooyberghs, H.	248, 300
Fox, S.	551	Horálek, J.	452
Fuglík, V.	117	Horváth, Z.	410
Furu, E.	509	Hrubeš, P.	362
		Huq, P.	101

Ielpo, P.	381, 388	de Leeuw, F.	452
Igarashi, Y.	86, 528, 598	Lefebvre, W.	248, 300
Iglesias, J.D.	197	Leguellec, M.	20
Im, U.	406	Leitl, B.	41, 357, 459, 588, 628
Isakov, V.	306, 316	Leonhartsberger, K.	51
Issartel, J.-P.	487, 667, 683	Leroy, G.	633, 667, 688
Istenes, Gy.	410	Leuzzi, G.	324
Jakobs, H.	466	Lindgren, P.	186
Janssen, S.	272, 300	Liszkai, B.	410
Jareš, R.	117	Locatelli, R.	652
Jensen, S.S.	406	Lopata, J.	362
Jicha, M.	395	Lopes, D.	126
Jing, Q.	26, 427	Lopes, M.	180
Johnson, J.	46	Lorentz, H.	466
Jones, A.R.	564	Lumbreras, J.	277, 441
Joubert, L.	633	Machálek, P.	117
Juruš, P.	117, 362	Mahrer, Y.	208
Kaasik, M.	140	Maki, T.	86, 528, 598
Kadlubiec, R.	117	Makke, L.	492
Kajino, M.	86, 528, 598	Malkiewicz, M.	546
Kakosimos, K.E.	319, 376, 406, 504	Mallet, V.	86, 652
Kangas, L.	242	Markatos, N.C.	357
Karel, J.	117	Martilli, A.	289
Karpinnen, A.	242, 459	Martinez, F.A.	576
Kasper-Gieb, A.	513	Martinovský, J.	117
Kazmuková, M.	362	Masselin, B.	432
Kerr, A.A.F.S.	227	Matejovičová, J.	252
Kertész, Zs.	509	Mathieu, A.	86, 91, 528, 598
Ketzel, M.	319, 376, 406	Maurer, C.	438
Kleperis, J.	237	Mazzeo, N.A.	36
Kocijan, J.	30, 171	Mazzola, T.	96, 551
Kokal, D.	30	Melintescu, A.	558
Konár, O.	117	Mészáros, R.	367
Környei, L.	410	Miranda, A.I.	121, 180, 256
Korsakissok, I.	86, 91	Mlakar, P.	30, 171
Koutsourakis, N.	357	Modlík, M.	117
Kouznetsov, R.	509	Mok, K.M.	126
Kovács, A.	367	Monache, L.D.	663
Kovalets, I.V.	504, 523	Monteiro, A.	180, 256
Krajčovičová, J.	252	Monti, P.	324
Krč, P.	362	Morabito, A.	262
Kremler, M.	252	Mortarini, L.	155
Krennert, T.	438	Moussafir, J.	334, 608, 613
Krestou, A.	536	Moussiopoulos, N.	346, 536
Krynicka, J.	546	Nemček, V.	252
Kryza, M.	130, 217, 546	Ngae, P.	477, 482, 487, 498
Kukkonen, J.	242	Nibart, M.	76, 334, 608, 613, 640
Kumar, P.	20, 477, 482, 487, 498	Nicholson, D.	551
Lacome, J.-M.	582, 633	Di Nicola, F.	381, 388
Lagzi, I.	367	Núñez, L.	197
Lapébie, E.	569	Nunn, A.	672
Lapins, J.	623	Oberle, M.	177
Lazar, D.	110	Oetl, D.	2
Leadbetter, S.J.	564	Oitzl, S.	2
Leelőssy, Á.	367	Ojrzyńska, H.	217

Oldrini, O.	334, 608, 613	Ruiz-Filippi, G.	46
Olesen, H.R.	212	Sá, E.	180
Oliver, A.	135	San José, R.	329
Olry, C.	492, 608	Santiago, J.L.	197
Osán, J.	7	Saunier, O.	528
Osnes, A.N.	688, 694	Schatzmann, M.	41
Ottosen, T.-B.	376, 406	Schauer, G.	513
Pain, C.	400	Scheele, R.	140
Palacios, M.	197, 329	Scheuermann, W.	623
Papadopoulos, A.	202	Schipa, I.	262
Parmhed, O.	667, 688	Seaton, M.	66
Paschalidi, Z.	541	Sekiyama, T.	86, 528, 598
Patryl, L.	569	Sellam, M.	498
de la Paz, D.	289,441	Selvaratnam, V.	56
Pecci, J.	329	Seoni, A.	351
Pelikán, E.	117	Septier, F.	492
Pelley, R.E.	518	Sfetsos, A.	202
Perdriel, S.	613	Sigg, R.	186
Pérez, J.L.	329	Silibello, C.	262
Pérez, L.	329	Silva, J.B.	446, 453
Pérez-Foguet, A.	135	da Silva, L.A.F.	294
Périllat, R.	86	Silveira, C.	180
Persson, L.Å.	186, 667, 683	Singh, S.K.	477, 482, 487,498
Pettersson Reif, B.A.	667, 688, 694	Škarková, P.	117
Picanyol, M.	283, 441	Skjøth, C.A.	130, 546
Pimentel L. C.G.	294	Skov, H.	376
Pineda Rojas, A.L.	36	Skřetowicz, M.	222
Piñón, J.	283	Slawik, A.J.	446, 453
Píša, V.	117	Smith, S.	71
Platt, N.	446, 453	Smith, S.E.	66
Polák, R.	117	Smolová, E.	117
Porras, I.	283	Sofiev, M.	509
Pospisil, J.	395	Sohn, M.D.	551
Poulsen, M.B.	406	Soucacos, P.	145
Pujadas, M.	197	Souza Silva, A.	227
Pulvirenti, B.	371	Spicer, T.	551
Quélo, D.	598	Srbová, D.	117, 362
Quérel, A.	598	Stefanescu, T.	26, 427
Querzoli, G.	324, 351	Steib, R.	7
Rácz, É.V.P.	410	Steinberga, I.	237
Rajaona, H.	492	Stenzel, S.	513
Rani, R.	477, 482	Stenzel, S.	51
Ranjbar, A.	466	Stocker, J.	66, 71
Rau, G.	51	Stockham, L.	551
Reisin, T.G.	459, 588	Szintai, B.	410
Relvas, H.	180	Szoboszlai, Z.	509
Resler, J.	117, 362	Tanzarella, A.	262
Ribeiro, I.	541	Tchepel O.	267
Rispoli, G.	381	Teggi, S.	340
Robins, A.	400, 677, 672	Teixeira, J.P.	180
Rodríguez, A.	191	Teppner, R.	51
Rodríguez, M.E.	277	Thaning, L.	186
Roebeling, P.	180	Thomson, D.	56
Roustan, Y.	598	Thomson, D.J.	518
Ruiz, T.	441	Thunis, P.	256, 272, 277

Tickle, G.	61	Vincenti, M. L.	381, 388
Tinarelli, G.	459, 640	Vlachogiannis, D.	202
Tolias, I.C.	357	Vlček, O.	117, 362
Tomasi, E.	160	von Arx, C.	177
Tørnes, J.	699	von Schoenberg, P.	126, 186
Tørnes, J.Aa.	667	Wałaszek, K.	130, 217
Török, Sz.	7	Walter, H.	593
Török, Zs.	509	Webster, H.N.	56, 518
Torreggiani, L.	340	Weidinger, T.	110
Triantafyllou, A.	536	Weil, J.	145
Trimpeneers, E.	300	Werner, M.	130, 217, 546
Truchot, B.	582, 633	Whitmire, M.	551
Tsegas, G.	346, 536	Wilczak, J.	663
Tucker, H.	582	Williams, A.	558
Tucker, H.	61	Wingstedt, E.M.M.	667, 688
Tunved, P.	126	Wood, C.	242
Turbelin, G.	477, 482, 487, 498	Wotawa, G.	438
Ulke, A.G.	106	Yalamas, T.	576
Urban, J.T.	446, 453	Yarwood, G.	46
Valencia, A.	145	Yuen, K.V.	121
Valiño, D.	191	Zapletal, M.	117
Valli, L.	381	Zardi, D.	160
Varga, Á.	232	Zhang, M.	306
Vedrenne, M.	277	Zink, K.	415
Vellón, J.M.	191	Zlatev, Z.	658
Venetsanos, A.G.	357, 504, 523	Zsebök, P.	410
Venkatram, A.	71, 306	Zwoździak, J.	222
Vik, T.	667		

## HARMO 17 PROGRAMME: ORAL PRESENTATIONS

**17<sup>th</sup> International Conference on  
Harmonisation within Atmospheric Dispersion  
Modelling for Regulatory Purposes  
9-12 May 2016, Budapest, Hungary**

**Sunday, 8 May 2016**

<b>14:00 – 19:30</b>	<b>Registration (Danubius Health Spa Resort Margitsziget)</b>
----------------------	---

**Monday, 9 May 2016**

<b>8:00 - 9:00</b>	<b>Registration (Danubius Health Spa Resort Margitsziget)</b>
--------------------	---

<b>9:00 - 9:30</b>	<i>Opening plenary session: Star Auditorium Chair: Prof. László Bozó</i>
--------------------	--

	Welcome by the organisers, Opening
--	------------------------------------

	Official words from Dr. Kornélia Radics, President of the Hungarian Meteorological Service,
--	---

	Official words from Ministry of Agriculture
--	---

<b>9:30 – 10:40</b>	<i>Plenary session 1, Star Auditorium Chair: Dr. Helge Olesen</i>
---------------------	---

	<b>Introductory lecture by the representative of the Environment Directorate-General</b>
--	--

	<b>Topic 1:</b> Model evaluation and quality assurance – model validation, model intercomparisons, model uncertainties and model sensitivities
--	--

	<b>Topic 8:</b> Modelling air dispersion and exposure to accidental releases
--	--

9:30 – 10:00	<b><u>Philippe Thunis</u></b> : Update on the Clean Air for Europe Programme
--------------	--

10:00 – 10:20	<b>H17-053:</b> Bernd Leitl, Frank Harms, Denise Hertwig, <b><u>Michael Schatzmann</u></b> : Field data versus wind tunnel data: The art of validating urban flow and dispersion models
---------------	---

10:20 – 10:40	<b>H17-096:</b> <b><u>Silvia Trini Castelli</u></b> , Leitl B., Baumann-Stanzer K., Reisin T.G., Armand P., Andronopoulos S., and all COST ES1006 Members: Conclusions and reflections from COST Action ES1006 activity: what do we miss for the applications of models in local-scale emergency response in built environments?
---------------	--

<b>10:40 – 11:10</b>	<b>Coffee/Tea break, Beginning of Poster session: Topic 1, Topic 2, Topic 8 (Magnólia Room)</b>
----------------------	---

<b>11:10 - 12:30</b>	<i>Parallel session 1, Star Auditorium</i> <i>Chair: Prof. John Bartzis</i>	<i>Parallel session 2, Jázmin Room</i> <i>Chair: Dr. Fernando Martín</i>
	<b>Topic 1:</b> Model evaluation and quality assurance – model validation, model intercomparisons, model uncertainties and model sensitivities	<b>Topic 8:</b> Modelling air dispersion and exposure to accidental releases
11:10 – 11:30	<b>H17-006:</b> <u>Dietmar Oettl</u> , Stefan Oitzl: Comparing dispersion modelling and field inspection for odour impact assessment in the vicinity of two animal husbandry farms	<b>H17-001:</b> <u>Scott Chambers</u> , Alastair Williams, Dan Galeriu, Anca Melintescu, Marin Duma: Radon-based assessment of stability effects on potential radiological releases
11:30 – 11:50	<b>H17-062:</b> <u>Vibha Selvaratnam</u> , David Thomson, Helen Webster: Validation of the atmospheric dispersion model NAME against long-range tracer release experiments	<b>H17-059:</b> <u>Rachel Batt</u> , Simon Gant, Jean-Marc Lacome, Benjamin Truchot, Harvey Tucker: CFD modelling of dispersion in neutral and stable atmospheric boundary layers: results for Prairie Grass and Thorney Island
11:50 – 12:10	<b>H17-099:</b> <u>Miguel A. Hernández-Ceballos</u> , Stefano Galmarini, Steven Hanna, Thomas Mazzola, Joseph Chang, Roberto Bianconi, Roberto Bellasio: UDINEE project: international platform to evaluate urban dispersion models' capabilities to simulate Radiological Dispersion Device	<b>H17-104:</b> <u>Kirk L. Clawson</u> , Richard M. Eckman, Dennis D. Finn: Project Sagebrush: A New Look at Plume Dispersion
12:10 – 12:30	<b>H17-155:</b> <u>Albert Oliver</u> , Raúl Arasa, Agustí Pérez-Foguet, M <sup>a</sup> Ángeles González: Simulating large emitters using CMAQ and a local scale finite element model. Analysis in the surroundings of Barcelona	<b>H17-149:</b> <u>Eva Berbekar</u> , Frank Harms, Bernd Leitl: Spatial and temporal concentration distributions in urban areas

<b>12:30 – 14:00</b>	<b>Lunch (Platán Restaurant)</b>	
----------------------	----------------------------------	--

<b>14:00 - 15:40</b>	<i>Parallel session 3: Star Auditorium</i> <i>Chair: Prof. Carlos Borrego</i>	<i>Parallel session 4: Jázmin Room</i> <i>Chair: Dr. Bertrand Carissimo</i>
	<b>Topic 1:</b> Model evaluation and quality assurance – model validation, model intercomparisons, model uncertainties and model sensitivities	<b>Topic 8:</b> Modelling air dispersion and exposure to accidental releases
14:00 – 14:20	<b>H17-014:</b> Liying Chen, Malo Le Guellec, ( <u>Amita Tripathi</u> ): Validation of PANACHE CFD pollution dispersion modelling with dense gas experiments	<b>H17-034:</b> <u>Luc Patryl</u> , Emmanuel Lapébie, Patrick Armand: Simulation of explosive events in the urban environment coupling a fast dynamics CFD model with low Mach number dispersion solvers in CERES® CBRN-E
14:20 – 14:40	<b>H17-080:</b> <u>Cornelis Cuvelier</u> : A harmonised approach to European Air Quality trend analyses over the period 1990-2010	<b>H17-100:</b> <u>Hartmut Walter</u> , Gerhard Heinrich: Effects from urban structures to atmospheric dispersion models in decision support systems for nuclear emergencies
14:40 – 15:00	<b>H17-120:</b> <u>Steven Herring</u> , Pablo Huq: Assessing the performance of atmospheric dispersion models	<b>H17-118:</b> <u>Fotios Barmpas</u> , Claudio Carriazo, Armando Pellicioni, Gianni Tinarelli, Nicolas Moussiopoulos: A novel metric to evaluate model's performance in predicting hazard zones
15:00 – 15:20	<b>H17-171:</b> <u>Enrico Ferrero</u> , Stefano Alessandrini, Domenico Anfossi: Lagrangian simulations of the plume rise in strong capping inversion	<b>H17-168:</b> <u>Guillaume Leroy</u> , Jean-Marc Lacome, Benjamin Truchot, Lauris Joubert: Harmonization in CFD approaches to assess toxic consequences of ammonia releases
15:20 – 15:40	<b>H17-137:</b> <u>Pontus von Schoenberg</u> , Håkan Grahn, Peter Tunved: Evaluation of model performance using new deposition schemes in the random displacement particle model Pello using Fukushima power plant accident data	<b>H17-115:</b> <u>Oliver Oldrini</u> , S. Perdriel, M. Nibart, P. Armand, C. Duchenne, J. Moussafir: EMERGENCIES – A modeling and decision-support project for the Great Paris in case of an accidental or malicious CBRN-E dispersion

<b>15:40 – 16:30</b>	<b>Coffee break, Poster session: Topic 1, Topic 2, Topic 8 (Magnólia Room)</b>	
----------------------	--	--

<b>16:30 – 18:10</b>	<i>Parallel session 5, Star Auditorium</i> <i>Chair: Dr. Amela Jeričević</i>	<i>Parallel session 6, Jázmin Room</i> <i>Chair: Dr. Stijn Janssen</i>
	<b>Topic 1:</b> Model evaluation and quality assurance – model validation, model intercomparisons, model uncertainties and model sensitivities	<b>Topic 8:</b> Modelling air dispersion and exposure to accidental releases
16:30 – 16:50	<b>H17-089:</b> Beatriz Sanchez, Christina Quaassdorff, <b>Jose Luis Santiago</b> , Rafael Borge, , Fernando Martin, David de la Paz, Alberto Martilli, Esther Rivas: Effects of traffic emission resolution on NO <sub>2</sub> concentration obtained by CFD-RANS modeling over a real urban area in Madrid (Spain)	<b>H17-038:</b> <b>Felipe Aguirre Martinez</b> , Yann Caniou, Christophe Duchenne, Patrick Armand, Thierry Yalamas: Probabilistic assessment of danger zones associated with a hypothetical accident in a major French port using a surrogate model of CFD simulations
16:50 – 17:10	<b>H17-176:</b> <b>Andrea Bisignano</b> , Luca Mortarini, Enrico Ferrero: Model chain for buoyant plume dispersion	<b>H17-173:</b> <b>Gianni Tinarelli</b> , Maxime Nibart, Patrick Armand, Silvia Trini Castelli: A sensitivity analysis for a Lagrangian particle dispersion model in emergency-response test cases
17:10 – 17:30	<b>H17-063:</b> <b>Simon Gant</b> , Simon Coldrick, Graham Tickle, Harvey Tucker: Impact of alternative dispersion model validation methods: A case study on the LNG model validation database using DRIFT	<b>H17-101:</b> <b>Arnaud Quérel</b> , Denis Quélo, Yelva Roustan, Anne Mathieu, Mizuo Kajino, Thomas Sekiyama, Kouji Adachi, Damien Didier, Yasuhito Igarashi, Takashi Maki: Impact of changing the wet deposition schemes in IdX on 137-Cs atmospheric deposits after the Fukushima accident
17:30 – 17:50	<b>H17-166:</b> <b>Arunachalam Saravanan</b> , Alejandro Valencia, Philip Soucacos, Jeffrey Weil: Assessing air quality impacts of airport emissions at the Los Angeles International Airport using an integrated modeling and measurement approach	<b>H17-108:</b> <b>Luca Delle Monache</b> , Ryan Cabell, Daniel Steinhoff: Self-organizing maps to generating reduced-size, statistically similar climate datasets for air dispersion applications
17:50 – 18:10	<b>H17-002:</b> Wu Zhangquan, <b>Liu Chun-Ho</b> : Time scale analysis of chemically reactive pollutants over urban roughness in the atmospheric boundary layer	<b>H17-162:</b> <b>Denise Hertwig</b> , Vladimir Fuka, Paul Hayden, Matteo Carpentieri, Elisa Goulart, Glyn Thomas, Ian Castro, Alan Robins, Zheng-Tong Xie, Omduth_Cocean,: A comparison of fast dispersion models for localised releases in a street network
<b>19:00 – 21:00</b>	<b>Icebreaker (Platán Restaurant)</b>	

**Tuesday, 10 May 2016**

<b>9:00 – 10:40</b>	<i>Plenary session 2: Star Auditorium</i> <i>Chair: Prof. Michael Schatzmann</i>
	<p><b>Topic 1:</b> Model evaluation and quality assurance – model validation, model intercomparisons, model uncertainties and model sensitivities</p> <p><b>Topic 2:</b> Environmental impact assessment: Air pollution management and decision support systems</p> <p><b>Topic 10:</b> Highlights of past work. Session devoted to reviews and to prominent scientists and ‘golden papers’ of the past, which have still relevance and should not be forgotten</p>
9:00 – 9:20	<b>H17-180: <u>Marta Garcia Vivanco</u></b> , Bessagnet, B. Cuvelier, C. Tsyro, S. Aulinger, A. Bieser, J. Calori, G. Ciarelli, G. A. Manders Mircea, M. Aksoyoglu, S. Briganti, G. Cappelletti, A. Colette, A. Couvidat, F. D’Isidoro, M. Kranenburg, R. Meleux, F. Menut, L. Pay, M.T. Pirovano, G. Rouil, L. Silibello, C. Theobald, M.R. Thunis, P. Ung, A. Joint analysis of deposition fluxes and atmospheric concentrations predicted by six chemistry transport models in the frame of the EURODELTA III project
9:20 – 9:40	<b>H17-025:</b> Weiping Dai, Qiguo Jing, Tiffany Stefanescu, <b><u>Brian Holland</u></b> : Roadside hot-spot analysis in urban area
9:40 – 10:00	<b>H17-143: <u>Helge R. Olesen</u></b> : Challenges in assessing air pollution from residential wood combustion
10:00 – 10:20	<b>H17-078: <u>Robert Sigg</u></b> , Håkan Grahm, Jan Burman, Niklas Brännström, Oscar Björnham, Petter Lindgren, Leif Å Persson, Pontus Von Schoenberg, Lennart Thaning: Dispersion modeling uncertainties in Dispersion Engine (DE)
10:20 - 10:40	<b>H17-157: <u>Bertrand Carissimo</u></b> : A look back at 25 years of atmospheric CFD and field campaigns: from Thorney-Island to Jack Rabbit II

**10:40 – 11:30**

**Coffee break, Poster session : Topic 1, Topic 2, Topic 8 (Magnolia Room)**

<b>11:30 - 12:30</b>	<i>Parallel session 7: Star Auditorium</i> <i>Chair: Dr. Helen Webster</i>	<i>Parallel session 8: Jázmin Room</i> <i>Chair: Dr. Domenico Anfossi</i>
	<p><b>Topic 1:</b> Model evaluation and quality assurance – model validation, model intercomparisons, model uncertainties and model sensitivities</p>	<p><b>Topic 8:</b> Modelling air dispersion and exposure to accidental releases</p> <p><b>Topic:2:</b> Environmental impact assessment: Air pollution management and decision support systems</p>
11:30 – 11:50	<b>H17-065: <u>Stephen E. Smith</u></b> , Jenny Stocker, Martin Seaton, David Carruthers: A validation study of the ADMS plume chemistry schemes	<b>H17-121: <u>Steven Herring</u></b> , Patrick Armandand, Claudio Gariazzo: Best practice in applying emergency response tools to local-scale hazmat incidents
11:50 – 12:10	<b>H17-093:</b> Raphaël Périllat, <b><u>Irène Korsakissok</u></b> , Vivien Mallet, Anne Mathieu, Thomas Sekiyama, Mizuo Kajino, Kouji Adachi, Yasuhito Igarashi, Takashi Maki, Damien Didier: Using meteorological ensembles for atmospheric dispersion modeling of the Fukushima nuclear accident	<b>H17-028: <u>Marija Zlata Božnar</u></b> , Boštjan Grašič, Primož Mlakar, Dejan Gradišar, Juš Kocijan: Analysis of the daily cycles in the data on air pollution through the use of advanced analytical tools
12:10 – 12:30	<b>H17-164: <u>Goran Gašparac</u></b> , Amela Jeričević, Branko Grisogono: Application and comparison of the air quality modeling systems in statically stable conditions	<b>H17-076: <u>Philippe Thunis</u></b> , Enrico Pisoni, Bart Degraeuwe, Alain Clappie: SHERPA: an approach to explore potential air quality improvements at the regional/local scales

**12:30 – 14:00**

**Lunch (Platán Restaurant)**

<b>14:00 - 15:40</b>	<i>Parallel session 9: Star Auditorium</i> <i>Chair: Dr. Marija Zlata Božnar</i>	<i>Parallel session 10: Jázmin Room</i> <i>Chair: Prof. Roberto San Jose</i>
	<b>Topic 1:</b> Model evaluation and quality assurance – model validation, model intercomparisons, model uncertainties and model sensitivities <b>Topic 5:</b> Urban scale and street canyon modelling: Meteorology and air quality	<b>Topic 2:</b> Environmental impact assessment: Air pollution management and decision support systems
14:00 – 14:20	<b>H17-066:</b> Jenny Stocker, Andrew Ellis, Steve Smith, <b>David Carruthers</b> , Akula Venkatram, William, Dale Mark Attree: A review of dispersion modelling of agricultural and bioaerosol emissions with non-point sources	<b>H17-167:</b> <b>Atenágoras Silva</b> , Américo Kerr, Simone Gioia, Marly Babinski: Investigation of the transport of pollutants from the Metropolitan Area of São Paulo and from the industrial city of Cubatão to nearby areas
14:20 – 14:40	<b>H17-136:</b> <b>Roseane A.S. Albani</b> , Beatrice Pulvirenti, Silvana di Sabatino: Simulations of traffic related pollutants in a main street of Rio de Janeiro city (Brazil) using computational fluid dynamics modelling	<b>H17-184:</b> <b>John Backman</b> , Curtis Wood, Mikko Auvinen, Leena Kangas, Ari Karppinen, Jaakko Kukkonen: Sensitivity analysis of a meteorological pre-processor using algorithmic differentiation
14:40 – 15:00	<b>H17-158:</b> Francesca Di Nicola, Maria Lisa Vincenti, Patrick Conry, Riccardo Buccolieri, Piera Ielpo, Alessandra Genga, Livia Giotta, Harindra J. S. Fernando, <b>Silvana Di Sabatino</b> : The role of surface building materials in air quality applications	<b>H17-070:</b> A.I. Miranda, <b>Joana Ferreira</b> , C. Silveira, H. Relvas, M. Lopes, P. Roebeling, A. Monteiro, E. Sá, C. Gama, S. Costa, J.P. Teixeira, C. Borrego: Improving urban air quality using a cost-efficiency and health benefit approach
15:00 – 15:20	<b>H17-172:</b> <b>Márton Balczó</b> , Tamás Lajos: Investigation of the ventilation and air quality of urban squares	<b>H17-114:</b> <b>Nitsa Haikin</b> , P. Alpert, Y. Mahrer: A Numerical study of air-pollution and atmospheric fine-scale flow over the coastal complex terrain of Mt. Carmel
15:20 – 15:40	<b>H17-183:</b> K. Zink, <b>Antoine Berchet</b> , D. Brunner, J. Brunner, L. Emmenegger: GRAMM/GRAL: Computing air QUALITY maps at the Urban scale	<b>H17-181:</b> <b>Amela Jericevic</b> , Goran Gasparac: Modeling of aviation emissions impact on local air quality
<b>15:40 – 16:30</b>	<b>Coffee break, Poster session : Topic 1, Topic 2, Topic 8 (Magnólia Room)</b>	
<b>16:30 - 17:50</b>	<i>Parallel session 11: Star Auditorium</i> <i>Chair: Prof. Steven Hanna</i>	<i>Parallel session 12 : Jázmin Room</i> <i>Chair: Prof. István Faragó</i>
	<b>Topic 5:</b> Urban scale and street canyon modelling: Meteorology and air quality	<b>Topic 9:</b> Mathematical problems in air quality modelling
16:30 – 16:50	<b>H17-144:</b> <b>Patrick Conry</b> , Silvana Di Sabatino, Francesca Di Nicola, Maria Lisa Vincenti, Riccardo Buccolieri, Pierina Ielpo, Livia Giotta, Alessandra Genga, Ludovico Valli, Gennaro Rispoli, H. J. S. Fernando: Dry deposition onto vertical surfaces in the urban environment	<b>H17-032:</b> <b>Fabrice Boisseranc</b> , Patrick Armand, Christophe Duchenne, Guillaume Douarre: Analysis of simulation results issued by a Lattice Boltzmann Method in complex urban environments – Applications to Paris and Hamburg
16:50 – 17:10	<b>H17-160:</b> <b>Elsa Aristodemou</b> , Luz Maria Boganegra, Christopher Pain, Alan Robins: Simulating turbulent air flows in central London and studying effect of tall buildings	<b>H17-139:</b> <b>Stefano Alessandrini</b> , L. Delle Monache, Irina Djalalova, Jim Wilczak: An application of the Schaake Shuffle technique to generate space-time consistent AQ predictions
17:10 – 17:30	<b>H17-165:</b> <b>Zoltán Horváth</b> , Bence Liszkai, György Istenes, Péter Zsebők , Balázs Szintai, Éva Pestiné Rácz, László Környei: Integrated urban air pollution dispersion modelling framework and application in air quality prediction of the city of Győr	<b>H17-045:</b> <b>Ágnes Havasi</b> , István Faragó, Zahari Zlatev: Efficient numerical methods in air pollution transport modelling: operator splitting and Richardson extrapolation
17:30 – 17:50	<b>H17-140:</b> <b>Thor-Bjørn Ottosen</b> , Matthias Ketzel, Ole Hertel, Jørgen Brandt, Henrik Skov, Konstantinos E. Kakosimos: Modelling NO <sub>x</sub> and NO <sub>2</sub> in two street canyons in Copenhagen using an improved version of OSPM	<b>H17-037:</b> <b>Robin Locatelli</b> , Vivien Mallet, Patrick Armand: Improvement of atmospheric dispersion simulations in case of an accident or a malevolent action using data assimilation METHODS in CERES@ CBRN-E
<b>17:50 – 20:00</b>	<b>End of Poster session: Topic1, Topic2, Topic 8 and</b> <b>Start of Poster Session: Topic 3, Topic 4, Topic 5, Topic 6, Topic 7 (Magnólia Room)</b>	

**Wednesday, 11 May 2016**

<b>9:00 – 10:20</b>	<i>Plenary session 3: Star Auditorium</i> <i>Chair: Prof. László Bozó</i>
	<p><b>Topic 5:</b> Urban scale and street canyon modelling: Meteorology and air quality</p> <p><b>Topic 6:</b> Use of modelling in health and exposure assessments</p> <p><b>Topic 7:</b> Inverse dispersion modelling and source identification</p>
9:00 – 9:20	<b>H17-003: Hans Hooyberghs</b> , Wouter Lefebvre, Felix Deutsch, Sandy Adriaenssens, Elke Trimpeneers, Frans Fierens, Stijn Janssen: Modelling ultrafine particle concentrations at street-level scale for the entire city of Antwerp
9:20 – 9:40	<b>H17-125: Nektarios Koutsourakis, John G. Bartzis</b> , George C. Efthimiou, Alexandros G. Venetsanos, Ilias C. Tolias, Nicolas C. Markatos, Denise Hertwig, Bernd Leitl: LES study of unsteady flow phenomena in an urban geometry – the need for special evaluation methods
9:40 – 10:00	<b>H17-113: Patrick Armand</b> , Kathrin Baumann-Stanzer, E. Bemporad, Claudio Gariazzo, Marko Gerbec, Steven Herring, Ari Karpinnen, Bernd Leitl, Tamir G. Reisin, Gianni Tinarelli, Silvia Trini Castelli: Best practice guidelines for the use of atmospheric dispersion models at local scale in case of hazmat releases into the air
10:00 – 10:20	<b>H17-128: Athanasios Triantafyllou, Nicolas Moussiopoulos</b> , Athina Krestou, George Tsegas, Melina Andreadou: Application of inverse dispersion modelling for the determination of pm emission factors from fugitive dust sources in open-pit lignite mines

<b>10:20 – 11:10</b>	<b>Coffee break, Poster session: Topic 3, Topic 4, Topic 5, Topic 6, Topic 7 (Magnolia Room)</b>
----------------------	--

<b>11:10-12:30</b>	<i>Parallel session 13: Star Auditorium</i> <i>Chair: Dr. Peter Suppan</i>	<i>Parallel session 14: Jazmin Room</i> <i>Chair: Dr. Cristina Guerreiro</i>
	<b>Topic 5:</b> Urban scale and street canyon modelling: Meteorology and air quality	<b>Topic 7:</b> Inverse dispersion modelling and source identification
11:10 – 11:30	<b>H17-163: Matthias Ketzl, Konstantinos E. Kakosimos</b> , Ulas Im, Thor-Bjørn Ottosen, Jørgen Brandt, Steen S. Jensen, Thomas Ellermann, Maria B. Poulsen, Ole Hertel: Flow and dispersion modelling study at one of Denmark's traffic hot-spots	<b>H17-135: Isabel Ribeiro</b> , Zoi Paschalidi, Hendrik Elbern: Optimizing initial values and emission factors on mesoscale air quality modelling using 4D-var data assimilation
11:30 – 11:50	<b>H17-103: Beatriz Sanchez, Jose Luis Santiago</b> , Alberto Martilli, Magdalena Palacios, Manuel Pujadas, Lourdes Nuñez, Monica German, Jaime Fernandez-Pampillon, Jose Daniel Iglesias,: CFD Modeling of Reactive Pollutants Dispersion and Effect of Photocatalytic Pavements in a Real Urban Area	<b>H17-048: George C. Efthimiou</b> , Spyros Andronopoulos, Alexandros Venetsanos, Ivan V. Kovalets, Konstantinos Kakosimos, Christos D. Argyropoulos: Modification and validation of a method for estimating the location of a point stationary source of passive non-reactive pollutant in an urban environment
11:50 – 12:10	<b>H17-098: Roberto San José</b> , Juan L. Pérez, Libia Pérez, Julia Pecci, Antonio Garzón, Marino Palacio: Impacts of global climate scenarios over three European cities using mesoscale and CFD simulations with very high resolution	<b>H17-110: Olivier Saunier</b> , A. Mathieu, T. Sekiyama, M. Kajino, K. Adachi, M. Bocquet, Y. Igarashi, T. Maki, D. Didier: A new perspective on the Fukushima releases brought by newly available <sup>137</sup> Cs air concentration observations and reliable meteorological fields
12:10 – 12:30	<b>H17-064: Arsenios Chatzimichailidis</b> , Marc Assael, Matthias Ketzl Konstantinos E Kakosimos: Modelling the recirculation zone in street canyons with different aspect ratios, using CFD simulation	<b>H17-005: Tímea Haszpra</b> : Time-reversibility in atmospheric dispersion

<b>12:30 – 14:00</b>	<b>Lunch (Platán Restaurant)</b>
----------------------	----------------------------------

<b>14:00 - 15:40</b>	<i>Parallel session 15: Star Auditorium</i> <i>Chair: Dr. Philippe Thunis</i>	<i>Parallel session 16: Meeting Room 2</i> <i>Chair: Dr. Scott Chambers</i>
	<b>Topic 5:</b> Modelling air dispersion and exposure to accidental releases	<b>Topic 7:</b> Inverse dispersion modelling and source identification
14:00 – 14:20	<b>H17-041 Vlad Isakov</b> , Akula Venkatram, Richard Baldauf, Parik Deshmukh, Max Zhang: Evaluation and development of tools to quantify the impacts of roadside vegetation barriers on near-road air quality	<b>H17-007: Sarvesh Kumar Singh</b> , Gregory Turbelin, Pramod Kumar, Raj Rani, Amir-Ali Feiz, Pierre Ngae, Jean-Pierre Issartel: Uncertainty estimation in the reconstruction of atmospheric tracer source emissions
14:20 – 14:40	<b>H17-119: Vasilis Akylas, Fotios Barmpas</b> , Nicolas Moussiopoulos, George Tsegas: New inflow boundary conditions for homogeneous atmospheric boundary layer under the power law for street scale modelling	<b>H17-030: Pramod Kumar</b> , Amir-Ali Feiz, Sarvesh Kumar Singh, Pierre Ngae, Raj Rani, Emerson Barbosa, Grégory Turbelin, Jean-Pierre Issartel, Nadir Bekka: Source reconstruction in urban and non-urban environments using an inversion methodology coupled with a CFD approach
14:40 – 15:00	<b>H17-124 Simone Ferrari</b> , Maria Grazia Badas, Michela Garau, <b>Alessandro Seoni</b> , Giorgio Querzoli: The air quality in two-dimensional urban canyons with gable roof buildings: a numerical and laboratory investigation	<b>H17-033: Harizo Rajaona</b> , François Septier, Yves Delignon, Patrick Armand, Laurent Makke, Christophe Olry, Armand Albergel: A Bayesian approach of the source term estimate coupling retro-dispersion computations with a Lagrangian particle dispersion model and the adaptive multiple importance sampling
15:00 – 15:20	<b>H17-074 Esther Rivas, Jose Luis Santiago</b> , Fernando Martin, Beatriz Sanchez, Alberto Martilli: Estimating the impact of urban vegetation on air quality in a neighborhood: real case vs new vegetation scenarios	<b>H17-109: Samar Elkhalfa</b> , Christos D. Argyropoulos, George C. Efthimiou, Spyros Andronopoulos, Alexandros G. Venetsanos, Ivan V. Kovalets, <b>Konstantinos E. Kakosimos</b> : On the exploitation of dose-response information for the source-reconstruction in the case of atmospheric hazardous material releases
15:20 – 15:40	<b>H17-186: Steven Hanna</b> , Joseph Chang, Thomas Spicer, Michael D. Sohn, Shannon Fox, Mark Whitmire, Leo Stockham, Damon Nicholson, Thomas Mazzola: Preliminary analysis of observations from the Jack Rabbit II-2015 field experiment on dense gas dispersion in a built environment	<b>H17-174: Chi Vuong N'guyen</b> , Lionel Soulhac: Implementation and application of a source apportionment approach in the SIRANE urban air quality model
<b>15:40 – 16:10</b>	<b>Coffee break, Poster session: Topic 3, Topic 4, Topic 5, Topic 6, Topic 7 (Magnolia Room)</b>	
<b>16:10 - 17:30</b>	<i>Parallel session 17: Star Auditorium</i> <i>Chair: Dr. Silvia Trini Castelli</i>	<i>Parallel session 18: Meeting Room 2</i> <i>Chair: Dr. Kees Cuvelier</i>
	<b>Topic 4:</b> Parametrization of physical processes in mesoscale meteorology relevant for air quality modelling <b>Topic 3:</b> Use of modelling in support of EU air quality directives, including FAIRMODE	<b>Topic 6:</b> Use of modelling in health and exposure assessments
16:10 – 16:30	<b>H17-088: David de la Paz, Rafael Borge</b> , Alberto Martilli: Impact of WRF urban parameterizations in the performance of CMAQ on 1 km <sup>2</sup> resolution annual runs in Madrid (Spain)	<b>H17-106: Cristina Guerreiro</b> , Jan Horálek, Frank de Leeuw, Florian Couvidat: Estimating ambient concentrations of benzo(a)pyrene in Europe - population exposure and health effects
16:30 – 16:50	<b>H17-138: Leonardo Aragão Ferreira da Silva</b> , Silvana Di Sabatino, Luiz Claudio Gomes Pimentel, Fernando Pereira Duda: Analysis of the internal boundary layer formation on tropical coastal regions using sodar data in Santa Cruz region of MRRJ	<b>H17-039: Patrick Armand</b> , Christophe Duchenne, Yasmine Benamrane, Sébastien Gouillat, Nadège Cabibel, Bertrand Masselin, Thomas Bineau: Real-time use of a CFD modelling system in the framework of “Toxic 2014”, a major Civilian Security exercise at a very complex urban site in Paris
16:50 – 17:10	<b>H17-079: Alexandra Monteiro</b> , Carla Gama, Alain Clappier, Philippe Thunis, Ana Isabel Miranda: Testing the SHERPA tool to support air quality plans over Portugal	<b>H17-102: Alexander Slawik</b> , James Silva, Kevin Axelrod, <b>Jeffrey T. Urban</b> , Nathan Platt: Are toxic load-based toxicity models consistent with experimental observations? Independent analysis of time-varying exposure data from the 2012–2013 ECBC/NAMRU-D toxicological experiments

17:10 – 17:30	<b>H17-148: <u>Oxana Tchepel</u></b> , Daniela Dias: Urban traffic emission modelling for policy-related applications	<b>H17-091: <u>Miguel Picornell</u></b> , T.Ruíz, R. Borge, P.García, D. de la Paz, J.Lumbreras: Evaluation of exposure to air pollution through mobile phone data in the city of Madrid (Spain)
---------------	---	--

<b>19:30 – 23:00</b>	<b>Conference dinner (Gróf Széchenyi Event Boat)</b>	
----------------------	--	--

<b>Thursday, 12 May 2016</b>		
------------------------------	--	--

<b>9:20 – 10:40</b>	<i>Plenary session 4: Star Auditorium</i> <i>Chair: Prof. David Carruthers</i>	
	<b>Topic 1:</b> Model evaluation and quality assurance – model validation, model intercomparisons, model uncertainties and model sensitivities <b>Topic 3:</b> Use of modelling in support of EU air quality directives, including FAIRMODE <b>Topic 7:</b> Inverse dispersion modelling and source identification <b>MODITIC:</b> MODelling the DIspersion of Toxic Industrial Chemicals in urban environments	
9:20 – 9:40	<b>H17-068: <u>Christophe Duchenne</u></b> , Patrick Armand, Maxime Nibart, Virginie Hergault: Validation of a LPDM against the CUTE experiments of the COST ES1006 Action – comparison of the results obtained with the diagnostic and RANS versions of the models	
9:40 – 10:00	<b>H17-094: <u>Cornelis Cuvelier</u></b> , P. Thunis, L. Tarrason, M. Guevara-Villardell, S. Lopez-Aparicio: A benchmarking tool to screen and compare bottom-up and top-down emission inventories	
10:00 – 10:20	<b>H17-077: <u>Helen N. Webster</u></b> , David J. Thomson, Michael C. Cooke, Rachel E. Pelley: Improvements to an operational inversion method for estimating volcanic ash source parameters using satellite retrievals	
10:20 - 10:40	<b>H17-017: <u>Monica Endregard</u></b> Stephane Burkhart, Jan Burman, Olivier Gentilhomme, Alan Robins, Emma M. M. Wingstedt, B. Anders Petterson Reif, Leif Persson, Niklas Brännström, Oskar Parmhed, Oscar Björnham, Guillaume Leroy, Daniel Eriksson, Thomas Vik, John Aa. Tørnes, Jean-Pierre Issartel: MODelling the DIspersion of Toxic Industrial Chemicals in urban environments	

<b>10:40 – 11:30</b>	<b>Coffee break, Poster session: Topic 3, Topic 4, Topic 5, Topic 6, Topic 7 (Magnólia Room)</b>	
----------------------	--	--

<b>11:30 - 12:30</b>	<i>Parallel session 19: Star Auditorium</i> <i>Chair: Dr. Patrick Armand</i>	<i>Parallel session 20: Jázmin Room</i> <i>Chair: Prof. Alan Robins</i>
	<b>Topic 3:</b> Use of modelling in support of EU air quality directives, including FAIRMODE	<b>MODITIC:</b> MODelling the DIspersion of Toxic Industrial Chemicals in urban environments
11:30 – 11:50	<b>H17-075: <u>Philippe Thunis</u></b> , Bart Degraeuwe, Enrico Pisoni, Alain Clappier, Frederik Meleux: On the efficiency of short-term air quality plans in European cities	<b>H17-018: <u>Alan Robins</u></b> , Matteo Carpentieri, Paul Hayden, Joseph Batten, Jack Benson and Ashley Nunn: MODITIC wind tunnel experiments
11:50 – 12:10	<b>H17-152: <u>Stijn Janssen</u></b> , Philippe Thunis: FAIRMODE's EU Composite Mapping Exercise	<b>H17-019:</b> Stéphane Burkhart, Jan Burman: MODITIC wind tunnel experiments Neutral and heavy gas simulation using RANS
12:10 – 12:30	<b>H17-004: <u>Wouter Lefebvre</u></b> , Hans Hooyberghs, Felix Deutsch, Sandy Adriaenssens, Frans Fierens: Exceeding the European NO <sub>2</sub> -limit value in Belgium: can we solve the problem in a short to medium time frame?	<b>H17-020:</b> Niklas Brännström, Tobias Brännvall, Stéphane Burkhart, Jan Burman, Xavier Busch, Jean-Pierre Issartel, <b><u>Leif Å. Persson</u></b> : MODITIC Inverse modelling in urban environments

12:30 – 14:00	Lunch (Platán Restaurant)
---------------	---------------------------

14:00 - 15:00	<i>Parallel session 21: Star Auditorium</i> <i>Chair: Dr. Stefano Alessandrini</i>	<i>Parallel session 22: Jázmin Room</i> <i>Chair: Prof. Alan Robins</i>
	<b>Topic 3:</b> Use of modelling in support of EU air quality directives, including FAIRMODE	<b>MODITIC:</b> MOdelling the DIspersion of Toxic Industrial Chemicals in urban environments
14:00 – 14:20	<b>H17-052:</b> Bino Maiheu, Laure Malherbe, Ana I. Miranda, Alexandra Monteiro, Claudio Carnevale, <b>Stijn Janssen</b> : Evaluation of a Monte Carlo-based validation technique for data assimilated air quality assessments within FAIRMODE	<b>H17-022:</b> <b>Andreas N. Osnes</b> , D. Eriksson, B. Anders, P. Reif: On the generation of inflow boundary conditions for dispersion simulations using Large Eddy Simulations
14:20 – 14:40	<b>H17-060:</b> <b>Fernando Martin</b> , Jose Luis Santiago, Oliver Kracht, Laura García, Michel Gerboles: Feasibility of an intercomparison exercise of methods for the assessment of the spatial representativeness of monitoring sites	<b>H17-021:</b> <b>Emma Wingstedt</b> , D. Eriksson, O. Parmhed, G. Leroy, A. N. Osnes, B. A. P. Reif, J. Burman: Large Eddy Simulations of dispersion of neutral and non-neutral scalar fields in complex urban-like geometries
14:40 – 15:00	<b>H17-154:</b> Michel Vedrenne, <b>Julio Lumbreras</b> , Rafael Borge, Alain Clappier, Philippe Thunis, María Encarnación Rodríguez: Comparing air quality model performance for planning applications	<b>H17-023</b> <b>Oscar Björnham</b> , Arnaud Gousseff, John Tørnes, Stephane Burkhart: MODITIC Operational Models

15:00 – 15:30	Closing of the conference – Dr. Helge Olesen
---------------	--

# HARMO 17 Programme: POSTER PRESENTATIONS

**17<sup>th</sup> International Conference on  
Harmonisation within Atmospheric Dispersion  
Modelling for Regulatory Purposes  
9-12 May 2016, Budapest, Hungary**

**Monday, 9 May 2016**

<b>Topic 1: Model evaluation and quality assurance – model validation, model intercomparisons, model uncertainties and model sensitivities</b>		
<b>ID number</b>	<b>authors</b>	<b>title</b>
<b>013</b>	Veronika Groma, Zita Ferenczi, Bálint Alföldy, János Osán, Szabina Török, Roland Steib	EDMS model verification considering remarkable changes in airport traffic system
<b>015</b>	Liyang Chen, Pramod Kumar, Malo Leguellec, Amir-Ali Feiz	An Air Quality CFD model performance in complex environment with EMU observations
<b>029</b>	Primož Mlakar, Dragana Kokal, Boštjan Grašič, Marija Zlata Božnar, Dejan Gradiša, Juš Kocijan	Validation of the performance of meteorological forecasts in fine spatial and temporal resolution designed as an input for dispersion models
<b>040</b>	Andrea L. Pineda Rojas, Nicolás A. Mazzeo	Sensitivity of modelled urban background ozone concentrations to uncertainties in the GRS input variables
<b>054</b>	Pierre Ngae, Grégory Turbelin Pramod Kumar, Sarvesh Kumar Singh, Amir-Ali Feiz, Hamza Kouichi, Emerson Barbosa, Amer Chpoun	A Meandering Short Time Average for dispersion characterization under low winds conditions
<b>057</b>	F. Carrera-Chapela, G. Ruiz-Filippi, J.A. González, G. Yarwood, J. Johnson	WRF surface and upper air validation over Central Chile during La Niña-El Niño transition
<b>061</b>	Sirma Stenzel, Kathrin Baumann-Stanzersen, Gabriele Rau, Renate Teppner, Kurt Leonhartsberger	FLow Simulations for the assessment of small wind turbines in urban Areas
<b>083</b>	A. Hernandez, J.A. Gonzalez, J.J. Casares	Effect of the terrain features on the accuracy of CALMET. A complex terrain case study
<b>086</b>	Roberto Giua, Angela Morabito, Ilenia Schipa, Annalisa Tanzarella, Camillo Silibello, Giorgio Assennato	A nested air quality prediction modelling system for urban scale: an application over southern Italy
<b>095</b>	Irène Korsakissok, Mathieu Contu, Olivier Connan, Anne Mathieu and Damien Didier	Validation of the Gaussian puff model pX using near-field krypton-85 measurements around the AREVA NC La Hague reprocessing plant: comparison of dispersion schemes

123	Ana Graciela Ulke	Wind profiles for the atmospheric boundary layer in different stability conditions
126	Dora Lazar, Tamas Weidinger	CMAQ (Community Multi-Scale Air Quality) atmospheric dispersion model adaptation for Hungary
130	Pavel Juruš, Jan Karel, Radek Jareš, Josef Martinovský, Václav Píša, Robert Polák, Eva Smolová, Emil Pelikán, Marek Brabec, Ondřej Konár, Viktor Fuglík, Kryštof Eben, Jaroslav Resler, Ondřej Vlček, Pavel Machálek, Miloslav Modlík, Helena Hnilicová, Nina Benešová, Daša Srbová, Miloš Zapletal, Radek Kadlubiec, Pavla Škarková, Jiří Barnet	Emission processor for Air Quality models utilizing newly available data
133	Diogo Lopes, Joana Ferreira, Ka In Hoi, Kai Meng Mok, Ana I. Miranda and Ka Veng Yuen	WRF-CAMX application to The Pearl river delta region
142	Kinga Wałaszek, Małgorzata Werner, Maciej Kryza, Carsten Ambelas Skjøth	Impact of biogenic emission model and landuse on isoprene and ozone concentrations from a chemical transport model
156	Marko Kaasik , Gertie Geertsema, Rinus Scheele	Validation of Gaussian plume model AEROPOL against Cabauw field experiment
161	Marko Rus, Rahela Žabkar, Jure Cedilnik,	Hindcasting, verification and sensitivity analysis of photochemical dispersion model CAMx for a long time period
182	Amela Jericevic, Darko Koracin, Goran Gasparac	Boundary layer processes and air pollution modelling in coastal areas
185	Elena Tomasi, Lorenzo Giovannini, Marco Falocchi, Dino Zardi, Gianluca Antonacci	Preliminary pollutant dispersion modelling with CALMET and CALPUFF over complex terrain in the Bolzano basin (IT)

**Topic 2: Environmental impact assessment: Air pollution management and decision support systems**

ID number	authors	title
009	Anselmo de Souza Pontes, Luiz Cláudio Gomes Pimentel , Otto Corrêa Rotunno Filho	Impact assessment of emissions from port of activities on air quality in the metropolitan area of Rio de Janeiro
011	Zita Ferenczi, László Bozó	Effect of the long-range transport on the air quality of Budapest
035	Marilyne Tombette, Emmanuel Quentric; Denis Quelo, Anne Mathieu; Irène Korsakissok; Jérôme Groell, Damien Didier	C3X: an environmental platform for nuclear crisis facing the challenge of its improvements
044	Sylvio Freitas, Henrique Balona, Joana Valente, Jorge Amorim, Carlos H.Borrego,	Numerical and physical modelling of the emission and dispersion of petroleum coke from a seaport
049	Markus Oberle, Cyrill von Arx	JRODOS for nuclear emergencies: Implementation in Switzerland and further developments

<b>081</b>	D. Cartelle, J.M. Vellón, A. Rodríguez, D. Valiño, J.A. González, M. Bao, C. Casas	Estimation of short odor events by using chemically reactive odorants atmospheric dispersion modelling around a pulp paper mill
<b>082</b>	Ivan Kovalets, Alexander Khalchenkov, Christian Asker, Tatiana Lavrova, Sergey Todosienko, Christer Persson	Numerical modelling of concentrations in air of radioactive aerosols and radon following emissions from contaminated territories of Pridneprovsky Chemical Plant in Ukraine
<b>090</b>	Manuel Pujadas, Magdalena Palacios, Lourdes Nuñez, Monica German, David Fernandez-Pampillon, Jose Daniel Iglesias, Beatriz Sanchez	Real Scale Demonstration of the Depolluting Capabilities of a Photocatalytic Pavement in a Real Urban Area
<b>111</b>	Diamando Vlachogiannis, Athanasios Sfetsos, Nikolaos Gounaris, Athanasios Papadopoulos	Investigation of atmospheric dispersion of gas compounds from an industrial installation over a realistic topography
<b>147</b>	Małgorzata Werner, Maciej Kryza, Hanna Ojrzyńska, Kinga Wałaszek, Anetta Drzeniecka-Osiadacz	Air quality forecasts for Poland - application of the WRF-Chem model within the LIFE/APIIS project
<b>150</b>	Maria Skrętowicz, Jerzy Zwoździak	Dynamic-statistical odour dispersion model using the CALPUFF model and geostatistical analysis
<b>169</b>	Eliana Pecorari, Elena Innocente Alice Mantovani Davide Bassano Giancarlo Rampazzo Luca Palmeri	Evaluation of taxi times effect on aircraft exhausts emissions and dispersion
<b>170</b>	Árpád Varga	Far-field effect of a tall building on the shear layer above street canyons
<b>177</b>	Iveta Steinberga, Janis Bikse Jr, Janis Kleperis, Janis Bikse	Application of dispersion models for development of atmospheric pollution management zones in Riga agglomeration

#### **Topic 8: Modelling air dispersion and exposure to accidental releases**

<b>ID number</b>	<b>authors</b>	<b>title</b>
<b>031</b>	Andrew R. Jones, Ayoe B. Hansen and Susan J. Leadbetter	NAME-EPS: Developing a dispersion modelling capability utilising ensemble weather forecasts for emergency-response applications
<b>036</b>	Emmanuel Quentric, Jean-Pierre Benoit; Damien Didier; Marilynne Tombette, Denis Quelo; Anne Mathieu, Irène Korsakissok	scenarX : A platform for the simulation and broadcasting of fictitious environmental measurements during emergency exercises
<b>050</b>	George C. Efthimiou, Spyros Andronopoulos, John G. Bartzis	CFD-RANS prediction of individual exposure from continuous release of hazardous airborne materials
<b>107</b>	Maxime Nibart, Patrick Armand, Christophe Duchenne, Christophe Olry, Armand Albergel, Jacques Moussafir, Olivier Oldrini	Flow and dispersion modelling in a complex urban district taking account of the underground roads connections
<b>122</b>	Emese Homolya, Zita Ferenczi, Péter Zagyvai	An analysis of the evolution of radioactive contamination using the FLEXPART model

145	Janis Lapins, Wolfgang Bernnat, Walter Scheuermann	Validation of the gamma submersion calculation of the remote power plant monitoring system of the federal state of Baden-Württemberg
-----	--	--

**Wednesday, 11 May 2016**

<b>Topic 3: Use of modelling in support of EU air quality directives, including FAIRMODE</b>		
<b>ID number</b>	<b>authors</b>	<b>title</b>
043	Jana Krajčovičová, Jana Matejovičová, Martin Kremler, Vladimír Nemček	Air quality modeling of non-attainment areas as a basis for Air quality plans
085	R. Giua, A. Morabito, I. Schipa, A. Tanzarella, C. Silibello, G. Assennato	Application of a photochemical model to the assessment of regional air quality levels in southern Italy: procedures and results
146	Denise Pernigotti, Claudio A. Belis	SPECIATE and SPECIEUROPE source profiles analysis

<b>Topic 4: Parametrization of physical processes in mesoscale meteorology relevant for air quality modelling</b>		
<b>ID number</b>	<b>authors</b>	<b>title</b>
012	M <sup>a</sup> Ángeles González, Raúl Arasa, Anna Domingo-Dalmau, Ignasi Porrás, Miquel Picanyol, Bernat Codina, Jesica Piñón	A sensitivity analysis for determining optimum WRF and CALPUFF configuration for operational air quality forecast: application to a case study in the port of Huelva (Southern Spain)

<b>Topic 5: Urban scale and street canyon modelling: Meteorology and air quality</b>		
<b>ID number</b>	<b>authors</b>	<b>title</b>
055	Bence Hermann, Miklós Balogh	A hybrid approach for the numerical simulation of flows in urban environment
056	Vlad Isakov, Timothy Barzyk, Saravanan Arunachalam	Reduced-form air quality modeling for community-scale applications
058	Ng Chi-To, Liu Chun-Ho	On the ventilation mechanism over idealized street canyons under stably stratified flow environment
087	Annalisa Di Bernardino, Paolo Monti, Giovanni Leuzzi, Giorgio Querzoli	Water channel investigation of flow and dispersion in street canyons
097	Armando Pelliccioni, Paolo Monti, Gianni Leuzzi	Wind-speed profile and Prandtl's mixing length in urban boundary layers
116	O. Oldrini, M. Nibart, P. Armand, J. Moussafir, C. Duchenne	Development of the parallel version of a CFD – RANS flow model adapted to the fast response in built-up environments
117	Grazia Ghermandi, Sara Fabbi, Alessandro Bigi, Sergio Teggi, Luca Torreggiani	Microscale simulation of road traffic emissions from vehicular flow automatic surveys AND comparison with measured concentration data

<b>129</b>	Jaroslav Resler, Pavel Krč, Michal Belda, Pavel Juruš, Kryštof Eben, Nina Benešová, Daša Srbová, Přemysl Derbek, Pavel Hruběš, Jan Lopata, Ondřej Vlček, Jana Blumelová, Mária Kazmuková, Petra Bauerová	Street-level modelling of the effect of climate adaptation measures on air quality
<b>132</b>	Leszek Osrodka, Ewa Krajny	The relationship between PM concentrations and ventilation conditions obtained from SODAR measurements at the example Krakow
<b>134</b>	Attila Kovács, Róbert Mészáros, Ádám Leelőssy, István Lagzi	Air pollution modeling in urban environment using WRF-Chem model
<b>159</b>	Jiri Pospisil, Miroslav Jicha	Vehicle induced turbulence as key factor influencing pollutant dispersion in close vicinity of traffic paths
<b>178</b>	Chi N'Guyen, Lionel Soulhac	Evaluation of data assimilation methods at urban scale with the SIRANE model

#### **Topic 6: Use of modelling in health and exposure assessments**

<b>ID number</b>	<b>authors</b>	<b>title</b>
<b>010</b>	Prashant Kumar, Anju Goel	Characterisation of pedestrian exposure to nanoparticle emissions at traffic intersections
<b>024</b>	Oscar Björnham, Håkan Grahn	Dynamic urban population simulator
<b>026</b>	Brian Holland, Qiguo Jing, Weiping Dai, Tiffany Stefanescu	Explosion damage and injury assessment modelling: balancing model sophistication with finite resources
<b>071</b>	Christian Maurer, Delia Arnold, Florian Geyer, Claudia Flandorfer, Marcus Hirtl, Sabine Eckhardt, Thomas Krennert and Gerhard Wotawa	The influence of the Holuhraun eruption SO <sub>2</sub> emissions on the Austrian air quality
<b>112</b>	Alexander J. Slawik, Kevin C. Axelrod, James B. Silva, Ivo K. Dimitrov, Jeffrey T. Urban, and Nathan Platt	Are toxic load-based toxicity models consistent with experimental observations? Independent analysis of steady-exposure data from the 2012–2013 ECBC/NAMRU-D toxicological experiments
<b>141</b>	Lorentz, Helmut, Hermann Jakobs, Thomas Flassak, Abbas Ranjbar, Majid Azadi	Combining meteorological models and dispersion models on largescale and mesoscale, implemented as an air quality forecast model system in Iran

#### **Topic 7: Inverse dispersion modelling and source identification**

<b>ID number</b>	<b>authors</b>	<b>title</b>
<b>008</b>	Sarvesh Kumar Singh, Raj Rani, Sarvesh Kumar Singh, Gregory Turbelin, Pramod Kumar, Amir-Ali Feiz, Pierre Ngae	Inverse Dispersion Modelling for Identification of Multiple-Point Source Emissions in Atmosphere
<b>047</b>	Nadir Bekka, Pramod Kumar, Amir-Ali Feiz, Sarvesh Singh, Mohamed Sellam, Emerson Barbosa, Pierre Ngae, Grégory Turbelin, Amer Chpoun	A CFD modeling approach for a contaminant released in a city

<b>051</b>	Zsófia Török, Zoltán Szoboszlai, Enikő Furu, Anikó Angyal, Rostislav Kouznetsov, Mikhail Sofiev, Zsófia Kertész	Aerosol transport modelling over Debrecen, Hungary
<b>067</b>	Kathrin Baumann-Stanzer, Sirma Stenzel, Claudia Flandorfer, Gerhard Schauer, Anne Kasper-Giebl	Meteorological analysis of Saharan dust transport to Sonnblick
<b>151</b>	Yelva Roustan, Eva Marie Eriksson, Didier Buty, Christophe Olry, Marc Bocquet	Inverse modelling of methane fugitive emissions from industrial facilities
<b>174</b>	Chi N'Guyen, Lionel Soulhac	Implementation and application of a source apportionment approach in the SIRANE urban air quality model
<b>175</b>	Daria Bilińska, Carsten Ambelas Skjøth, Małgorzata Werner, Maciej Kryza, Małgorzata Malkiewicz, Justyna Krynicka, Anetta Drzeniecka – Osiadacz	Source regions of biogenic aerosols in Wrocław (Poland) and the influence of meteorological data on the HYSPLIT model results